NEOPROTEROZOIC TO PALEOZOIC GEOLOGY OF SOUTHWESTERN MONGOLIA

A dissertation presented

by

Uyanga Bold

to

The Department of Earth and Planetary Sciences

in partial fulfillment of the requirements

for the degree of

Doctor of Philosophy

in subject of

Earth and Planetary Sciences

Harvard University

Cambridge, Massachusetts

April 2016

Dissertation Advisor: Dr. Francis Macdonald Uyanga Bold

NEOPROTEROZOIC TO PALEOZOIC GEOLOGY OF SOUTHWESTERN MONGOLIA

ABSTRACT

The Neoproterozoic and Paleozoic evolution of global climate, tectonics, ocean geochemistry, and biological diversification are recorded in stratigraphic successions globally. The rock record of southwestern Mongolia has potential to reveal additional constraints as it is in the early stages of exploration. It has been known for several years that Cryogenian passive margin sedimentation on the Zavkhan Terrane hosts evidence for Neoproterozoic glaciation, and that overlying early Cambrian strata host rich records of small shelly fossils; however, the geological context for these critical records has been previously lacking.

Although these unknowns can be regarded as local geologic uncertainties, together they hold implications to test existing tectonic and crustal growth models of the Central Asian Orogenic Belt (CAOB), preservation potential of geochemical proxies within carbonate dominated strata, and biologic milestones as recorded in Paleozoic sediments. To understand and interpret the above implications, methods of field geology, litho- and chemo-stratigraphy, geochemistry, petrography, fluid inclusion and clumped isotope thermometries, and U-Pb zircon geochronology were used.

As a result, the tectonic origin and travels of the Zavkhan Terrane during the Neoproterozoic to early Paleozoic is refined and models of apparent crustal growth in the CAOB are re-assessed. Global Cryogenian and Ediacaran carbon and strontium isotope curves are constructed from limestone-dominated successions of the Tsagaan-Olom Group of the Zavkhan Terrane and are integrated with available geochronologic and geochemical data from around the globe. Finally, dolomitization is shown to greatly alter primary geochemical signatures, including carbon isotope values of carbonate rocks.

TABLE OF CONTENT

LIST OF FIGURES

LIST OF TABLES

ACKNOWLEDGMENTS

In my thesis, I would like to acknowledge many of the people that I have collaborated with and learned from throughout my PhD. I was very fortunate to have met many outstanding scientists and fellow graduate students, and completed my research with the best support from my family and friends.

First of all, I have to thank the people who have helped me grow interest in scientific research in geology at School of Geology and Petroleum Engineering at Mongolian University of Science and Technology (MUST). I would like to thank my undergraduate advisor Dr. Bayasgalan Amgalan, masters thesis advisors Dr. Chuluun Minjin and Dr. Bolortsetseg Minjin, and MUST professors Dr. Ochir Gerel, Dr. Chuluun Danzan, Dr. Khishigsuren Sodnom, and Dr. Batkhishig Bayaraa for their continuous support and encouragement throughout my studies. I regret that Dr. Chuluun Minjin is no longer with us, but I hope to continue to spread the knowledge he had passed on for many years to come.

Scientists at Mongolian Academy of Sciences, Dr. Dorjnamjaa Dorj and Dr. Ariunchimeg Yarinpil, have also been helpful and assisted me in having my research discussed among scientists at the Paleontology and Geology Center in Mongolia. I would like to thank Nagoya University Field Research Center at MUST for granting me access to their laboratory facility and especially Dr.Hitoshi Hasegawa for his incredible support and insightful discussions on Mongolian geology.

First and foremost with regards to my PhD, I would like to acknowledge my advisor Dr. Francis Macdonald without whom any of my research would have been possible. He has been my constant challenge, critic, and support at the same time, enabling me to grow as a person and a scientist since the day I started the program. I will always remember the days we have spent in the field, memories shared, adventures experienced, geologic problems discussed, and classes taught during this time. Hopefully, we will keep sharing these moments and exploring Asian tectonics and geology for many years in the future.

I would also like to thank my fellow graduate student and a friend, Dr. Emily Smith, with whom I have spent many months in the field in Mongolia and many years in the same office as graduate students. It

was great to experience how our friendship evolved over time and to notice her becoming a great scientist who finished her PhD while becoming one of my mentors both in my career and personal life. I also need to acknowledge fellow graduate students in our group, Dr. Justin Strauss, Athena Eyster, and Eben Hodgin, and a post-doctorate fellow Dr. Alan Rooney. I thank my friends and other fellow graduate students Eugenia Hyung, Dr. Yingjun Liu, Huan Jin, Kevin Chen, Lizzy Chen, Dr. Kun Wang, Yanpeng Sun, Tamara Pico, and Emma Bertran for always being available and their help in improving every bit of my talks that I needed to prepare as a graduate student. I would also like to thank Dr. Raquel Alonso-Perez, curator at Mineralogical & Geological Museum of Harvard University, for her constant support and valuable discussions on fundamental geologic concepts.

I would like to thank Dr. David Jones, Dr. Jessica Creveling, Dr. Aaron Putnam, Dr. Constance Soja, Dr. Mark van Baalen, and Dr. Claire Bucholz for all of their support and encouragement and for allowing me to participate in great geologic trips where I experienced and learned international collaborations, geologic field techniques, and ways to organize field trips successfully. I also thank the students both at Harvard University and MUST, who have helped me in the field as field assistants. They include Sarah Moon, Tanya Petach, Javzandulam Chuluunbaatar, Munkh-Erdene Delger, Munkh Jugder, Uchral Khuchitbaatar, Otgonbayar Dandar, Ariunsanaa Dorj, and Odbayar Erdenebat.

In order to obtain geochemical and geochronologic data for my research, I have spent many hours in university laboratories. In the process, I have received incredible help from the scientists who have taught me laboratory procedures, with whom I have discussed the data, and expanded collaboration with on projects. I have to thank the laboratory managers in our group, Sasha Breus, Camille Steel, and Sarah Dendy, for always keeping track of all of the stock items I have needed throughout my laboratory work and constant support in the process, as well as Robert Ackert at Archeology Multi-user Laboratory at Harvard University. I would also like to thank my committee members Dr. Daniel Schrag and Dr. David Johnston for allowing me to use their facilities very flexibly; their laboratory managers Dr. Greg Eischeid, Dr. Sarah Goff, and Dr. Erin Beirne, graduate students Andrew Masterson and Dr. Sierra Petersen; and post-doctorate fellows Dr. Ben Gill and Dr. Ben Cowie for teaching me laboratory procedures. I thank Dr.

John Higgins, his laboratory manager Elizabeth Lundstrom, his graduate students Anne-Sofie Cruger Ahm, Alliya Akhtar, and Danielle Santiago Ramos, and his post-doctorate fellow Dr. Clara Blättler for hosting me at Princeton University, Dr. Mark Schmitz and his laboratory manager Dr. James Crowley at Boise State University, Dr. Boswell Wing and his graduate student Dr. André Pellerin at McGill University.

With regards to all of the administrative documentations, I would like to thank Sarah Colgan for always keeping track of my graduate school performance and her endless help, Marissa Reilly for always taking a good care of my field work logistics, and Maryorie Grande and Chenoweth Moffatt for providing necessary stationery items to work as a teaching fellow in the department.

Finally, my thesis would not have come together without constant family support. Balancing life between being a graduate student and a mother was not straightforward at times. I have to thank all of the people who have helped me in the process, but most of all, I would like to thank my mother, Dr. Oyungerel Sambuu, who has sacrificed so much of her life for my well-being and I hope to continuously acknowledge her through my work. I would also like to thank my sister Khulan Bold, my brother-in-law Nasandelger Urtnasan, and my favorite nephew Tomkhangai Nasandelger for taking a good care of my family in the academic year of 2012-2013. Moreover, I would like to acknowledge my friend Dorjkhand Tsogzol and her family for constant support and companionship in the USA throughout these years.

In order to better take care of my child, I have received the Winkler Fellowship from Harvard University since 2014. I would like to thank the Winkler Fund Committee at Financial Services at Harvard University for relieving me from a big stress to send my child to full time daycare centers in Cambridge MA and providing me an opportunity to concentrate on my research full time. I thank Admissions and Financial Aid Officer Tracey Newman for her support and help with the application process.

I would like to highlight my husband, Lkhagva-Ochir Said, for his constant support, sacrifice, and encouragement throughout these years. I would like to thank him for always being there for me wherever he was, making sure all of the problems were taken care of, and in general, being the biggest supporter of

my career. I have to also thank my precious son, Khuslen Lkhagva-Ochir, for his constant entertainment and unintentional support. I thank both of you so much as you fill my life with joy, laughter, and happiness and I hope to enjoy our life together as long as I live.

CHAPTER 1. INTRODUCTION

During the Neoproterozoic Era, the Earth experienced global, low-latitude glaciations (Hoffman et al., 1998; Hoffman and Schrag, 2002; Kirschvink, 1992), the break-up and assembly of supercontinents (Hoffman, 1991; Li et al., 2008), large perturbations to geochemical cycles (Halverson et al., 2010), and the diversification of eukaryotes followed by the rise of metazoans (Cohen and Macdonald, 2015; Erwin et al., 2011; Knoll et al., 2006). These climatic, tectonic, geochemical, and biological aspects shaped the nature of Neoproterozoic geology and understanding their interrelationships is essential and dependent on integration of high quality data from around the world.

The geologic record of southwestern Mongolia includes Precambrian basement (for example Badarch, 1998; Kröner et al., 2010; Ruzhentsev and Burashnikov, 1996; Togtokh, 1995; Tomurtogoo, 2005), Neoproterozoic magmatism and passive margin sedimentation (for example Bold et al., 2016; Macdonald, 2011b), and Paleozoic tectonism and overlap assemblages (Kilian et al., in preparation; Smith et al., 2015). These are situated in the core of the Central Asian Orogenic Belt (CAOB) and hold important records for the models of cratonization and continental crustal growth (e.g. Wilhem et al., 2012). Moreover, carbonate-dominated strata of the Tsagaan-Olom Group of the Zavkhan Terrane have become an ideal target to measure variety of geochemical proxies to explore Neoproterozoic biogeochemistry (for example Brasier et al., 1996b; Johnston et al., 2012) mainly due to the co-existing preservation of organic-rich limestone and dolomitized carbonates (Bold et al., 2016).

Geologically, Mongolia was first explored at the end of the 19th century, mainly by joint Mongolian, Russian, German, Chinese, and Danish research teams (Byamba, 2011). By the end of the 20th century, the 1:200,000 scale geologic mapping projects were completed and preliminary attempts were made to integrate geologic data to composite tectonic evolution models for the formation of Central Asia (for example Mossakovsky et al., 1994; Sengör et al., 1993; Sengor and Natal'in, 1996). The first English descriptions of the geology of southwestern Mongolia appeared in 1996 (Brasier et al., 1996a;

Brasier et al., 1996b; Evans et al., 1996; Goldring and Jensen, 1996; Khomentovsky and Gibsher, 1996; Kruse et al., 1996; Lindsay et al., 1996a; Lindsay et al., 1996b; Ruzhentsev and Burashnikov, 1996) and stimulated much interest within the international community of Precambrian geologists (for example Demoux et al., 2009a; Kröner et al., 2010; Lehmann et al., 2010; Levashova et al., 2010; Macdonald et al., 2009a; Ovchinnikova et al., 2012a; Serezhnikova et al., 2014). As a result, western Mongolian territory was described to be comprised of Proterozoic cratonic fragments that are stitched together by Paleozoic arcs and accretionary zones.

One of these research teams, led by Dr. Francis Macdonald since 2006, has been working primarily on the Zavkhan Terrane of southwestern Mongolia. Consequently, terrane-wide mapping has been completed, stratigraphic complexities have been unraveled, the significance of the Neoproterozoic through Cambrian rock record has been further described, and the tectonic and geologic evolution of the entire region has been interpreted and integrated into a global geologic context (Bold et al., 2013; Bold et al., 2016; Bosak et al., 2011a; Bosak et al., 2011b; Cohen et al., 2015; Macdonald, 2011b; Macdonald and Jones, 2011; Macdonald et al., 2009a; Rooney et al., 2015; Smith et al., 2015).

During my PhD, I have worked on three main projects (Figure 1.1) in southwestern Mongolia. The first project (Figure 1.1A) is on tectonic evolution of the entire region (Bold et al., in review) and its greater implication for the crustal growth in the CAOB. In addition to refining the ages of the Neoproterozoic and Paleozoic lithostratigraphic units of the Zavkhan Terrane, a comparative study was done with the tectonic evolution of neighboring Proterozoic cratonic fragments in Mongolia and nearby stable cratons such as Tarim, North China, southern Siberia, and NE Gondwana. This, coupled with new paleomagnetic constraints (Kilian et al., in preparation), led to 1) re-interpretation of the Neoproterozoic to early Paleozoic tectonic evolution of the Proterozoic cratonic fragments in southwestern Mongolia and 2) a re-assessment of models for apparent crustal growth.

The second project (Figure 1.1B) is on Neoproterozoic stratigraphy of the Zavkhan Terrane, where I report geologic data collected during field seasons from 2011-2014 and interpret Cryogenian and early Ediacaran chemostratigraphic records of the Tsagaan-Olom Group (Bold et al., 2016). Both litho-

and chemo-stratigraphy are accompanied by detailed geologic observations and geochronological data. Composite Cryogenian and Ediacaran carbon and strontium isotope curves are constructed in combination with geochronological and geochemical data sets from around the globe.

The third project (Figure 1.1C) is on the effect of dolomitization on isotopic records from carbonates in the Tsagaan-Olom Group. This project stemmed from inconsistencies and non-reproducibility of carbon isotope values recorded in co-existing limestone and dolomitized carbonates. Unraveling this issue was important because, carbon isotope values from dolomites are widely considered as robust recorders of the carbon cycle in Earth history (Tucker and Wright, 1990) and geochemical records in dolomite successions have played an important role in the interpretation of Neoproterozoic environmental change (e.g. Halverson et al., 2010) and putative large lateral and vertical gradients in the carbon isotope value of paleo-basins (for example Fike et al., 2006; Halverson et al., 2005; Misi and Veizer, 1998; Pokrovskii et al., 2006; Rose et al., 2012; Zhu et al., 2013). Detailed geochemical and petrographic studies reveal that dolomitization was the driver for isotopic variation recorded in the Tsagaan-Olom Group carbonates, which implies extremely high water-rock ratios during diagenesis. In combination with temperature estimates from fluid inclusions and clumped-isotope thermometry, a dolomitization model is proposed (Bold et al., in preparation).

These projects are interrelated and span from regional to local in extent under a broader aim to understand Precambrian to Paleozoic geologic evolution of southwestern Mongolia and its greater significance in the Neoproterozoic to early Paleozoic Earth. Based on the detailed geologic data, I have tested existing models for the crustal growth in the CAOB, refined the stratigraphy of the Cryogenian to early Ediacaran strata of southwestern Mongolia, and assessed effect of dolomitization on geochemical records of the carbonate dominated Tsagaan-Olom Group.

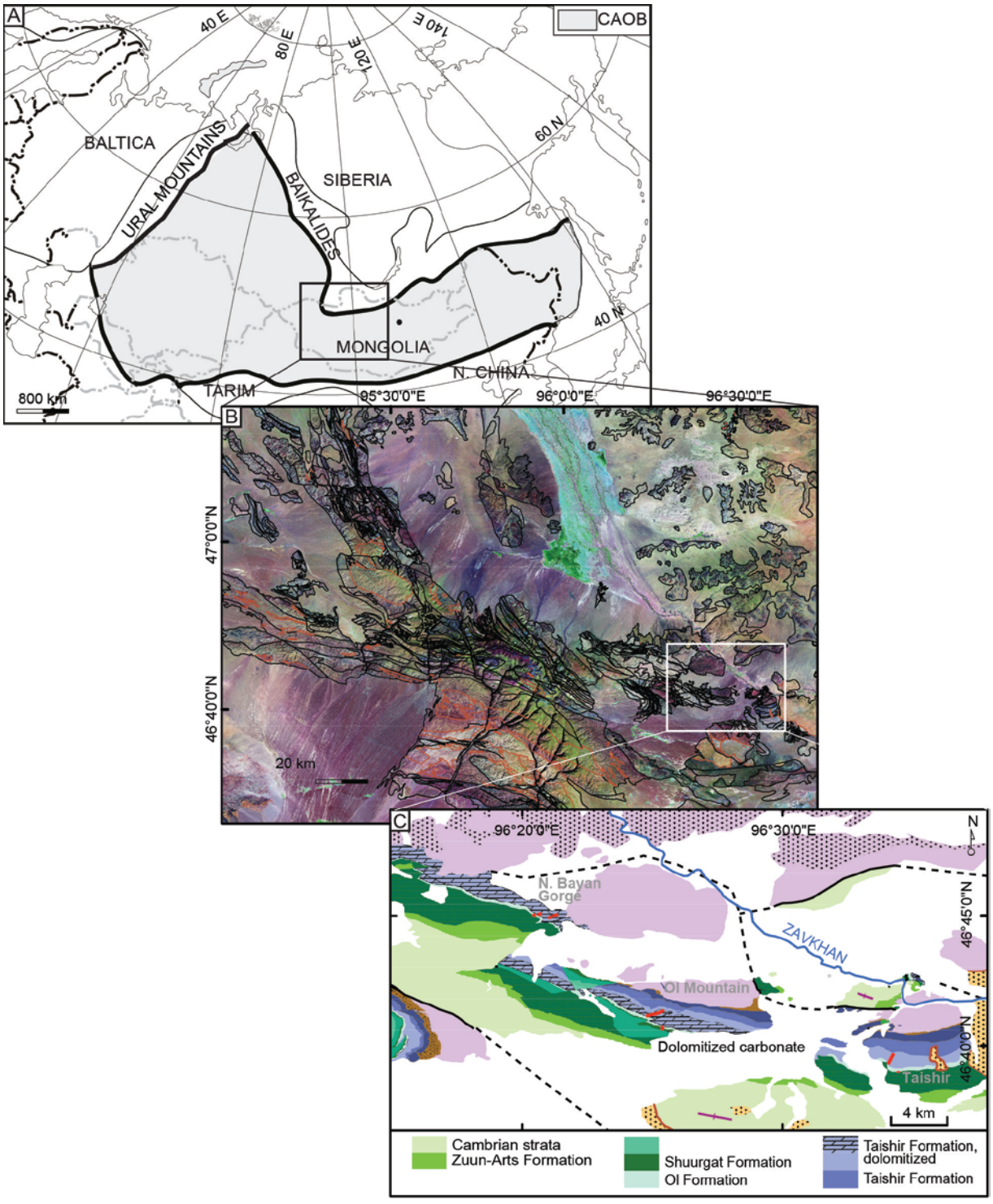

Figure 1.1. Aerial extent and outline of the chapters included in the thesis
A) Chapter 2: Neoproterozoic to early Paleozoic tectonic evolution of the Zavkhan Terrane of Mongolia: Implications for crustal growth in the Central Asian Orogenic Belt; B) Chapter 3: Neoproterozoic stratigraphy of the Zavkhan Terrane – the backbone for Cryogenian and early Ediacaran chemostratigraphic records. Base map: Landsat TM. Geologic boundaries are outlined; C) Chapter 4: Effect of dolomitization on isotopic records from Neoproterozoic carbonates (Tsagaan-Olom Group: Taishir, Ol, and Shuurgat formations) in southwestern Mongolia.

1.1. REFERENCES

Badarch, G., Byamba, J., Mahbadar, Ts., Minjin, Ch., Orolmaa, D., Tomurtogoo, O., and Khosbayar, Ts, 1998, Geological map of Mongolia: Mongolian Academy of Sciences, Mineral Resources Authority of Mongolia.

Bold, U., Crowley, J. L., Smith, E. F., Sambuu, O., and Macdonald, F. A., submitted, Neoproterozoic to early Paleozoic tectonic evolution of the Zavkhan Terrane of Mongolia: Implications for crustal growth in the Central Asian Orogenic Belt: Lithosphere.

Bold, U., Macdonald, F. A., Smith, E. F., Crowly, J. C., Minjin, C., and Dorjnamjaa.D., 2013, Elevating the Neoproterozoic Tsagaan-Olom Formation to a Group: Mongolian Geoscientist, v. 39, p. 5.

Bold, U., Schrag, D. P., Higgins, J. A., Erdenebayar, J., and Macdonald, F. A., in preparation, Effect of dolomitization on isotopic records from Neoproterozoic carbonates in southwestern Mongolia: Geological Society of America Bulletin.

Bold, U., Smith, E. F., Rooney, A. D., Buchwaldt, R., Ramezani, J., Schrag, D. P., and Macdonald, F. A., 2016, Neoproterozoic stratigraphy of the Zavkhan Terrane of Mongolia: The backbone for Cryogenian and Early Ediacaran chemistratigraphic records: American Journal of Science, v. 316, p. 1-63.

Bosak, T., Lahr, D. J. G., Pruss, S. B., Macdonald, F. A., Dalton, L., and Matys, E., 2011a, Agglutinated tests in post-Sturtian cap carbonates of Namibia and Mongolia: Earth and Planetary Science Letters, v. 308, p. 29-40.

Bosak, T., Macdonald, F. A., Lahr, D. J. G., and Matys, E., 2011b, Putative Cryogenian ciliates from Mongolia: Geology, v. 39, no. 12, p. 1123-1126.

Brasier, M. D., Dorjnamjaa, D., and Lindsay, J. F., 1996a, The Neoproterozoic to early Cambrian in southwest Mongolia: an introduction: Geological Magazine, v. 133, no. 4, p. 365-369.

Brasier, M. D., Shields, G., Kuleshov, V. N., and Zhegallo, E. A., 1996b, Integrated chemo- and biostratigraphic calibration of early animal evolution: Neoproterozoic -early Cambrian of southwest Mongolia: Geological Magazine, v. 133, no. 4, p. 445-485.

Byamba, J., 2011, History of geologic study in Mongolia, Ulaanbaatar, Mongolia, Soyombo printing, Stratigraphy.

Cohen, P. A., and Macdonald, F. A., 2015, The proterozoic record of eukaryotes: Paleobiology, v. 41, no. 04, p. 610-632.

Cohen, P. A., Macdonald, F. A., Pruss, S., Matys, E., and Bosak, T., 2015, Fossils of putative marine algae from the Cryogenian glacial interlude of Mongolia: Palaios, v. 30, no. 3, p. 238-247.

Demoux, A., Kroener, A., Badarch, G., Jian, P., Tomurhuu, D., and Wingate, M. T. D., 2009, Zircon ages from the Baydrag block and the Bayankhongor ophiolite zone: Time constraints on late Neoproterozoic to Cambrian subduction- and accretion-related magmatism in central Mongolia: Journal of Geology, v. 117, p. 377-397.

Erwin, D. H., Laflamme, M., Tweedt, S. M., Sperling, E. A., Pisani, D., and Peterson, K. J., 2011, The Cambrian Conundrum: Early Divergence and Later Ecological Success in the Early History of Animals: Science, v. 334, p. 1091-1097.

Evans, D. A. D., Zhuravlev, A. Y., Budney, C. J., and Kirschvink, J. L., 1996, Palaeomagnetism of the Bayan Gol Formation, western Mongolia: Geological Magazine, v. 133, no. 4, p. 487-496.

Fike, D. A., Grotzinger, J. P., Pratt, L. M., and Summons, R. E., 2006, Oxidation of the Ediacaran Ocean: Nature, v. 444, p. 744-747.

Goldring, R., and Jensen, S., 1996, Trace fossils and biofabrics at the Precambrian-Cambrian boundary interval in western Mongolia: Geological Magazine, v. 133, no. 4, p. 403-415.

Halverson, G. P., Hoffman, P. F., Schrag, D. P., Maloof, A. C., and Rice, A. H. N., 2005, Toward a Neoproterozoic composite carbon-isotope record: Geological Society of America Bulletin, v. 117, no. 9-10, p. 1181-1207.

Halverson, G. P., Wade, B. P., Hurtgen, M. T., and Barovich, K. M., 2010, Neoproterozoic Chemostratigraphy: Precambrian Research, v. 182, no. 4, p. 337-350.

Hoffman, P. F., 1991, Did the breakout of Laurentia turn Gondwanaland inside-out?: Science, v. 252, no. 5011, p. 1409-1412.

Hoffman, P. F., Kaufman, A. J., Halverson, G. P., and Schrag, D. P., 1998, A Neoproterozoic Snowball Earth: Science, v. 281, p. 1342-1346.

Hoffman, P. F., and Schrag, D. P., 2002, The snowball Earth hypothesis; testing the limits of global change: Terra Nova, v. 14, no. 3, p. 129-155.

Johnston, D. T., Macdonald, F. A., Gill, B., Hoffman, P. F., and Schrag, D. P., 2012, Uncovering the Neoproterozoic carbon cycle: Nature, v. 483, p. 320-324.

Khomentovsky, V. V., and Gibsher, A. S., 1996, The Neoproterozoic-Lower Cambrian in northern Govi-Altai, western Mongolia: Regional setting, lithostratigraphy and biostratigraphy: Geological Magazine, v. 133, p. 371-390.

Kilian, T. M., Swanson-Hysell, N. L., Macdonald, F. A., Bold, U., and Crowley, J. L., in preparation, Paleomagnetism of Ordovician-Silurian Teel basalts from the Zavkhan Terrane - Paleogeography of Mongolia during the Paleozoic.

Kirschvink, J. L., 1992, Late Proterozoic low-latitude global glaciation: the snowball earth, *in* Schopf, J. W., and Klein, C., eds., The Proterozoic Biosphere: Cambridge, Cambridge University Press, p. 51-52.

Knoll, A. H., Javaux, E., Hewitt, D., and Cohen, P. A., 2006, Eukaryotic organisms in Proterozoic oceans: Philosophical Transactions of the Royal Society of London B: Biological Sciences, v. 361, no. 1470, p. 1023-1038.

Kröner, A., Lehmann, J., Schulmann, K., Demoux, A., Lexa, O., Tomurhuu, D., Štípská, P., Liu, D., and Wingate, M. T., 2010, Lithostratigraphic and geochronological constraints on the evolution of the

Central Asian Orogenic Belt in SW Mongolia: Early Paleozoic rifting followed by late Paleozoic accretion: American Journal of Science, v. 310, no. 7, p. 523-574.

Kruse, P. D., Gandin, A., Debrenne, F., and Wood, R., 1996, Early Cambrian bioconstructions in the Zavkhan Basin of western Mongolia: Geological Magazine, v. 133, no. 4, p. 429-444.

Lehmann, J., Schulmann, K., Lexa, O., Corsini, M., Kröner, A., Štípská, P., Tomurhuu, D., and Otgonbator, D., 2010, Structural constraints on the evolution of the Central Asian Orogenic Belt in SW Mongolia: American Journal of Science, v. 310, no. 7, p. 575-628.

Levashova, N. M., Kalugin, V. M., Gibsher, A. S., Yff, J., Ryabinin, A. B., Meert, J., and Malone, S. J., 2010, The origin of the Baydaric microcontinent, Mongolia: Constraints from paleomagnetism and geochronology: Tectonophysics, v. 485, no. 1-4, p. 306-320.

Li, Z. X., Bogdanova, S. V., Collins, A. S., Davidson, A., De Waele, B., Ernst, R. E., Fitzsimons, I. C. W., Fuck, R. A., Gladkochub, D. P., Jacobs, J., Karlstrom, K. E., Lu, S., Natapov, L. M., Pease, V., Pisarevsky, S. A., Thrane, K., and Vernikovsky, V., 2008, Assembly, configuration, and break-up history of Rodinia: A synthesis: Precambrian Research, v. 160, no. 1-2, p. 179-210.

Lindsay, J. F., Braiser, M. D., Dorjnamjaa, D., Goldring, R., Kruse, P. D., and Wood, R. A., 1996a, Facies and sequence controls on the appearance of the Cambrian biota in southwestern Mongolia: Implications for the Precambrian-Cambrian boundary: Geological Magazine, v. 133, p. 417-428.

Lindsay, J. F., Brasier, M., Shields, G., Khomentovsky, V. V., and Bat-Ireedui, Y. A., 1996b, Glacial facies associations in a Neoproterozoic back-arc setting, Zavkhan Basin, western Mongolia: Geological Magazine, v. 133, no. 4, p. 391-402.

Macdonald, F. A., 2011, The Tsagaan Oloom Formation, southwestern Mongolia: Geological Society, London, Memoirs, v. 36, no. 1, p. 331-337.

Macdonald, F. A., and Jones, D. S., 2011, The Khubsugul Basin, *in* E., A., Halverson, G. P., and Shields, G., eds., The geological record of Neoproterozoic glaciations: London, Geological Society of London.

Macdonald, F. A., Jones, D. S., and Schrag, D. P., 2009a, Stratigraphic and tectonic implications of a new glacial diamictite-cap carbonate couplet in southwestern Mongolia: Geology, v. 37, p. 123-126.

Misi, A., and Veizer, J., 1998, Neoproterozoic carbonate sequences of the Una Group, Irecê Basin, Brazil: chemostratigraphy, age and correlations: Precambrian Research, v. 89, no. 1, p. 87-100.

Mossakovsky, A., Ruzhentsev, S., Samygin, S., and Kheraskova, T., 1994, Central Asian fold belt: geodynamic evolution and formation history: Geotectonics, v. 27, no. 6, p. 445-474.

Ovchinnikova, G., Kuznetsov, A., Vasil'eva, I., Gorokhov, I., Letnikova, E., and Gorokhovskii, B., 2012, U-Pb age and Sr isotope signature of cap limestones from the Neoproterozoic Tsagaan Oloom Formation, Dzabkhan River Basin, Western Mongolia: Stratigraphy and Geological Correlation, v. 20, no. 6, p. 516-527.

Pokrovskii, B. G., Melezhik, V. A., and Bujakaite, M. I., 2006, Carbon, Oxygen, Strontium, and Sulfur Isotopic Compositions in Late Precambrian Rocks of the Patom Complex, Central Siberia:

Communication 1. Results, Isotope Stratigraphy, and Dating Problems: Lithology and Mineral Resources, v. 41, no. 5, p. 450-474.

Rooney, A. D., Strauss, J. V., Brandon, A. D., and Macdonald, F. A., 2015, A Cryogenian chronology: Two long-lasting synchronous Neoproterozoic glaciations: Geology, v. 43, no. 5, p. 459-462.

Rose, C. V., Swanson-Hysell, N. L., Husson, J. M., Poppick, L. N., Cottle, J. M., Schoene, B., and Maloof, A. C., 2012, Constraints on the origin and relative timing of the Trezona δ< sup> 13</sup> C anomaly below the end-Cryogenian glaciation: Earth and Planetary Science Letters, v. 319, p. 241-250.

Ruzhentsev, S. V., and Burashnikov, V. V., 1996, Tectonics of the western Mongolian Salairides: Geotectonics, v. 29, no. 5, p. 379-394.

Sengör, A., Natal'In, B., and Burtman, V., 1993, Evolution of the Altaid tectonic collage and Palaeozoic crustal growth in Eurasia: Nature, v. 364, p. 299-307.

Sengor, A. C., and Natal'in, B. A., 1996, Paleotectonics of Asia: fragments of synthesis, *in* Yin, A., and Harrison, M., eds., The Tectonic Evolution of Asia: Cambridge, Cambridge University Press, p. 486-640.

Serezhnikova, E. A., Ragozina, A. L., Dorjnamjaa, D., and Lyubov'V, Z., 2014, Fossil microbial communities in Neoproterozoic interglacial rocks, Maikhanuul Formation, Zavkhan basin, Western Mongolia: Precambrian Research, v. 245, p. 66-79.

Smith, E. F., Macdonald, F. A., Petach, T. A., Bold, U., and Schrag, D. P., 2015, Integrated stratigraphic, geochemical, and paleontological late Ediacaran to early Cambrian records from southwestern Mongolia: Geological Society of America Bulletin, p. B31248. 31241.

Togtokh, D., Baatarkhuyag, A., and Bayardalai, S., 1995, The report of result of the geological grouppedmapping at scale 1:200000: Ulaanbaatar, Mongolia, p. 1575.

Tomurtogoo, O., 2005, Tectonics and structural evolution of Mongolia: Geodynamics and Metallogeny of Mongolia With a Special Emphasis on Copper and Gold Deposits: IAGOD Guidebook Series, v. 11, p. 5-12.

Tucker, M. E., and Wright, V. P., 1990, Dolomites and dolomitization models: Carbonate sedimentology, p. 365-400.

Wilhem, C., Windley, B. F., and Stampfli, G. M., 2012, The Altaids of Central Asia: A tectonic and evolutionary innovative review: Earth-Science Reviews, v. 113, no. 3, p. 303-341.

Zhu, M., Lu, M., Zhang, J., Zhao, F., Li, G., Aihua, Y., Zhao, X., and Zhao, M., 2013, Carbon isotope chemostratigraphy and sedimentary facies evolution of the Ediacaran Doushantuo Formation in western Hubei, South China: Precambrian Research, v. 225, p. 7-28.

CHAPTER 2. NEOPROTEROZOIC TO EARLY PALEOZOIC TECTONIC EVOLUTION OF THE ZAVKHAN TERRANE OF MONGOLIA: IMPLICATION FOR CRUSTAL GROWTH IN THE CENTRAL ASIAN OROGENIC BELT

This chapter is under review by GSA Journal Lithosphere: ***Bold, U.****, Crowley, J. L., Smith, E. F., Sambuu, O., and Macdonald, F. A., in review, Neoproterozoic to early Paleozoic tectonic evolution of the Zavkhan Terrane of Mongolia: Implications for crustal growth in the Central Asian Orogenic Belt: Lithosphere.*

ABSTRACT

The Zavkhan Terrane is one of several Proterozoic cratonic fragments in southwestern Mongolia that form the core of the Central Asian Orogenic Belt. We provide new geologic and U-Pb zircon geochronologic constraints on the Neoproterozoic and early Paleozoic tectonic evolution of the terrane. Orthogneisses dated at ~ 1967 and ~ 839 Ma form the basement of the Zavkhan Terrane and are intruded and overlain by ~ 811-787 Ma arc-volcanic and volcaniclastic rocks that lack a gneissic fabric, suggestive of a mid-Neoproterozoic metamorphic event. Rifting and formation of the Zavkhan ribbon continent occurred from ~ 770-717 Ma and was followed by passive margin sedimentation of the Tsagaan-Olom Group between 717 and 580 Ma. During the latest Ediacaran to Cambrian, the southern margin of the Zavkhan Terrane was reactivated with the obduction of the Lake Terrane, slab break-off and reversal, and ~ 509-507 Ma syn-orogenic magmatism. These units are cut by undeformed ~ 496 Ma gabbro providing a tight constraint on the age of Cambrian metamorphism. Upper Ordovician to Silurian rifting is marked by bimodal magmatism and deposition in narrow fault bounded basins. Our data suggest that the Zavkhan Terrane travelled alone in the Neoproterozoic, collided with Siberia during Cambrian Series 2-Series 3, and rifted away in the Ordovician as part of a larger ribbon continent. Accretionary growth around the Mongolian terranes occurred during the Ediacaran-Cambrian and late Paleozoic, but the majority of the

apparent crustal growth is due to the trapping and oroclinal bending of ribbon continents between larger cratons.

2.1. INTRODUCTION

The Central Asian Orogenic Belt (CAOB), also known as the Altaids, is located between the East European, Siberian, North China, and Tarim cratons and is considered the largest area of Phanerozoic continental crustal growth (Figure 2.1A; e.g. Windley et al., 2007). Tectonic activity in the CAOB is commonly thought to have started at ~ 1020 Ma (Khain et al., 2002) with the opening of the Paleo-Asian Ocean (Dobretsov et al., 2003) and to have continued until its closure in the latest Permian (Xiao et al., 2003) or Jurassic (Van der Voo et al., 2015). The immense area and timescale of the CAOB point to its formation being generated through multiple orogenic cycles; however, due to the lack of detailed geologic mapping and outdated geochronologic techniques, the nature and precise timing of these tectonic events have not been clearly delineated. Particularly, it is unclear when and over what extent the CAOB was affected by accretionary or collisional processes (e.g. Schulmann and Paterson, 2011). Moreover, due to a dearth of robust U-Pb single zircon ages and paleomagnetic poles, the origin and travels of the CAOB's Proterozoic and early Paleozoic cratonic fragments remain poorly constrained. Precise geochronology, petrology, and paleomagnetic data integrated into new geologic mapping is needed to provide the necessary geologic context to create the next generation of models for crustal growth and assess when, where, and how the CAOB formed.

Mongolia is located in the heart of the CAOB (Figure 2.1A) and its southwestern and northeastern regions constitute the Proterozoic cratonic fragments that are stitched together by Paleozoic arcs and accretionary zones (Figure 2.1B; for example Dobretsov et al., 2003; Khain et al., 2003; Kröner et al., 2010; Lehmann et al., 2010; Wilhem et al., 2012; Windley et al., 2007; Yakubchuk, 2004). Previous studies have assumed a shared Proterozoic through Paleozoic geologic evolution between many of the Mongolian cratonic fragments (Kröner et al., 2011; Lehmann et al., 2010; Levashova et al., 2010; Wilhem et al., 2012; Windley et al., 2007). Although this assumption may be correct for some of the terranes, it

has not been the direct result of detailed geologic observations or geochronologic constraints; there are no specific data that unequivocally support this model. Recently, additional geochronologic data have been reported from several of the cratonic terranes (for example Kozakov et al., 2012b; Kuzmichev et al., 2005a; Salnikova et al., 2001; Yarmolyuk et al., 2008a), but they have not been integrated with geologic mapping and stratigraphy.

Figure 2.1. Location map of the study area
A) Extent of Central Asian Orogenic Belt, illustrated after Sengor and Natal'in (1996) and Bucholz et al. (2014). B) Terrane map of western Mongolia, modified from Badarch et al. (2002). Proterozoic cratonic fragments described in western Mongolia are shaded in light grey and Ediacaran-Terreneuvian arc terrane, the Lake Terrane, is highlighted. The Tuva-Mongolia terranes borders the Zavkhan Terrane to the north and it is comprised of Sangelin, Hug, Darhad, and Gargan terranes and Khuvsgul Terrane (Badarch et al., 2002). Major tectonic structures near the Zavkhan Terrane are highlighted along with estimated ages.

In this study, we present new geochronologic data and geologic mapping from the Zavkhan Terrane. We then integrate these data with existing data from adjacent terranes to develop a new model

for the tectonic evolution of southwestern Mongolia and discuss implications for crustal growth in the CAOB.

2.1.1. Previous models for the Proterozoic and early Paleozoic tectonic evolution of southwestern Mongolia

In Mongolia, the Paleozoic CAOB outlines Proterozoic terranes with crystalline basement (Figure 2.1B). Through most of the 20th century, the cratonic fragments of Mongolia were separated between Tuva-Mongolia terranes (also referred to as the Tuva-Mongolia zone or massif) and Central Mongolia (Ilyin, 1990), which served as the foundation for future geologic interpretation. By the turn of the century, the joint Mongolian and Russian 1:200,000 scale regional mapping projects provided additional relative age constraints on lithostratigraphic units. These data were central to the Kipchak-Tuva-Mongol magmatic arc model of Sengör et al. (1993). In this *peri-Siberian arc model*, crustal growth occurred predominantly around a single Cambrian arc that formed on the margins of Siberia and Baltica, which was oroclinally bent and imbricated during the later Paleozoic. With little attention to the Precambrian geology, these authors assumed that the Mongolian terranes were part of a peri-Siberian arc, floored by Siberian basement. Moreover, with little paleomagnetic evidence, Sengör et al. (1993) kept Mongolia close to Siberia throughout the Paleozoic, as have many subsequent authors (e.g. Wilhem et al., 2012). Paleozoic fauna are commonly cited in referring to Mongolian terranes as "peri-Siberian" (e.g. Cocks and Torsvik, 2007) based on the similarity in trilobite assemblages found in Cambrian sedimentary rocks of some of the terranes north and west of the Zavkhan Terrane with those endemic to Siberia (Atashkin, 1995), along with the Silurian *Tuvaella* brachiopod fauna, which is restricted to terranes in the CAOB but not found on the Siberian Craton (Wang et al., 2011). Thus, direct paleontological ties between the Zavkhan Terrane and the Siberian Craton are equivocal and limited to the early Paleozoic.

Using a different approach, Mossakovsky et al. (1994) compared geologic data from Proterozoic regions of Mongolia, which they called the microcontinents of the southern CAOB with that from North China, Tarim, Tien Shan, Ulutau, and Amur. Based on available stratigraphic sections of the

Neoproterozoic and Cambrian terrigenous-carbonate cover sequences of the Khuvsgul and Zavkhan terranes, they suggested that the Mongolian cratonic terranes originated from eastern Gondwana and collided with Siberia during the Paleozoic. Building on this *peri-Gondwanan collisional model* with additional Paleozoic tectonostratigraphic, geochronologic, and Hf and Nd isotope data, Kröner et al. (2010) invoked repeated magmatic reworking of both proximal and distal passive margins of a composite peri-Gondwanan terrane (Kröner et al., 2014) prior to a final Permian collision with Siberia, Tarim, and North China. A Gondwanan origin of the Mongolian terranes was further supported by detrital zircon provenance data (Rojas-Agramonte et al., 2011); however, this study lumped samples from many regions within Mongolia, and the samples were mostly Paleozoic, yet were compared with mostly Precambrian samples from Tarim, North China, NE Gondwana, and Siberia.

Badarch et al. (2002) used a third approach in which they employed terrane analysis (Jones, 1983) to divide Mongolia into forty-four cratonic, metamorphic, and passive continental margin terranes and proposed an *accretionary growth model* on the Siberian margin with pulses of events in the Neoproterozoic, Cambrian-Ordovician, Devonian, Permian, and Triassic. This *accretionary growth model* (Windley et al., 2007) shares elements of both the *peri-Siberian arc model* and the *peri-Gondwanan collisional model* with the main-Mongolian lineament separating peri-Siberian and peri-Gondwanan terranes.

Sparse paleomagnetic data have been used variously to argue either for or against a Siberian origin for the Mongolian terranes. A paleomagnetic pole on the ~ 800 Ma old Zavkhan Formation (Fm) volcanics (described as the Baydrag microcontinent in the paper) was used by Levashova et al. (2010) to argue for an origin from either India, South China, Tarim, or Australia. Additionally, paleomagnetic data from Terreneuvian strata of the Zavkhan Terrane suggested that it was far north from the equatorial Siberian Craton at this time (Evans et al., 1996). However, another paleomagnetic study from the Neoproterozoic and Cambrian strata on the Zavkhan Terrane suggested that these rocks formed adjacent to Siberia (Kravchinsky et al., 2001). These large inconsistencies in Neoproterozoic and Paleozoic

paleolatitude of the Zavkhan Terrane highlight the need for additional paleomagnetic data and a new synthesis of existing data (Kilian et al., in preparation).

In summary, there are currently three broad classes of models for the Neoproterozoic to Paleozoic tectonic evolution of Mongolia: 1) a *peri-Siberian arc model* (for example Cocks and Torsvik, 2007; Sengör et al., 1993; Tomurtogoo, 2005; Wilhem et al., 2012), 2) a *collisional model of Gondwanan terranes* (for example Kröner et al., 2014; Kröner et al., 2010; Mossakovsky et al., 1994), and 3) *an accretionary growth model* (Badarch et al., 2002; Windley et al., 2007). A key distinction of these models is that both the peri-Siberian arc model and the accretionary model predicts the Zavkhan Terrane has Siberian basement and experienced a similar Paleozoic tectonic history as the southern margin of Siberia. In contrast, the *collisional model* predicts that the Proterozoic and Paleozoic geologic history of Mongolia should be distinct from Siberia.

2.1.2. Tectonic and Geologic setting of the Zavkhan Terrane

The Zavkhan Terrane is divided into two regions, an autochthonous region to the northeast and a para-autochthonous region to the southwest (figures 2.1 and 2.2). The para-autochthonous region was called the Urgamal subzone by Badarch et al. (2002) and the Altai Allochthon by Bucholz et al. (2014) and Bold et al. (2016) due to prevalence of highly metamorphosed rock assemblage, the lack of the late Neoproterozoic to Terreneuvian overlap sequence that is characteristic of the Zavkhan Terrane, and uncertainty of the age of basement. The para-autochthon borders the Lake Terrane (Ediacaran-Cambrian arc terrane, formerly known as Lake Zone) to the west, southwest, and south, and the autochthon borders the Baidrag Terrane to the east, Tarvagatay Terrane to the northeast, and Tuva-Mongolia terranes (particularly the Sangelin Terrane) to the north, separated by the Bulnai Fault (Figure 2.1B; Rizza et al., 2015).

The Zavkhan Terrane has been described as a cratonic terrane (Badarch et al., 2002) or a microcontintent (for example Lehmann et al., 2010; Wilhem et al., 2012) that hosts a gneissic basement as old as 1868 ± 3 Ma (Burashnikov, 1990); however, this date is a U/Pb TIMS age on multi-grain bulk

zircon fractions with metamorphic rims and consequently likely incorporated zircon domains of different ages. Several attempts have been made to better constrain the age of the Zavkhan Terrane basement. Zircon rims from a potash-leucosome within a migmatitic gneiss were dated from the Khavchig Complex at 840 ± 9 Ma (SHRIMP U-Pb zircon) with inherited zircon cores from 2445 to 1440 Ma (Zhao et al., 2006). In Zavkhanmandal soum (local administrative division within province) of the Zavkhan province, an additional granite-gneiss was dated at 856 ± 2 Ma (multi-grain bulk zircon fractions) (Kozakov et al., 2012b), suggesting there were several stages of magmatism and metamorphism in the region.

The para-autochthonous region of the Zavkhan Terrane is composed of amphibolite- to granulite facies para- and ortho-gneisses and greenschist facies metasedimentary and volcanic sequences (figures 2.2, 2.3, and 2.4). The oldest unit of the para-autochthon is the Khavchig Complex (Togtokh, 1995), which is composed of biotite, biotite amphibolite, and garnet gneiss with rare beds of quartzite and marble. It is overlain by the Yesonbulag Fm, which is composed of gneiss, amphibolite, and marble and intruded by gabbro, gabbro-diorite, and diorite of the Dund-Orthocomplex (Ruzhentsev and Burashnikov, 1996). Togtokh (1995) distinguished metasedimentary units of the Yargait and Shandiinnuruu formations (fms) above the Dund-Orthocomplex that are characterized by interbeds of metasediments, rhyolite, and dolerite, which are unconformably overlain by the Zavkhan Fm.

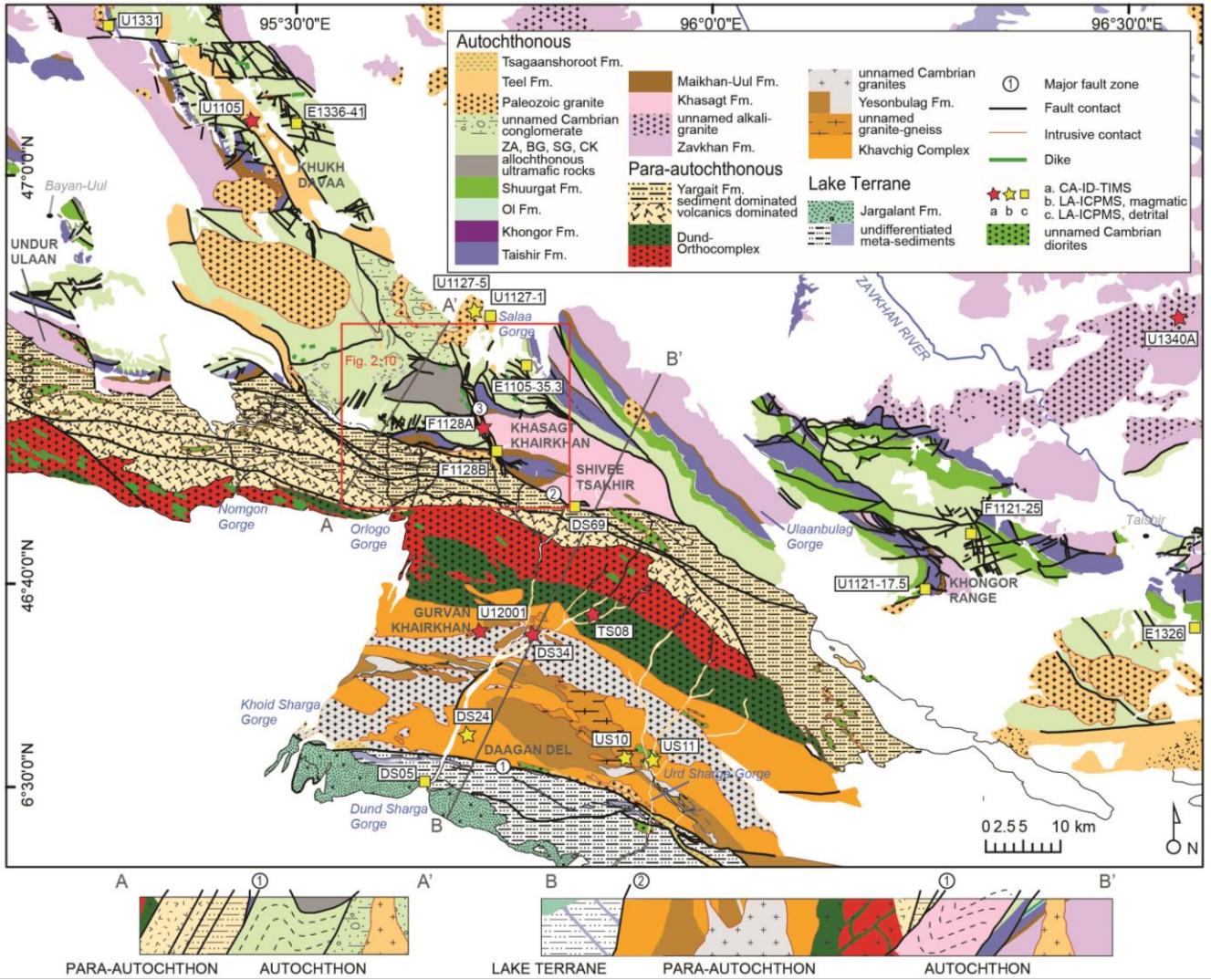

Figure 2.2. Geologic map of the Zavkhan Terrane

As mapped by Macdonald, F.A., Bold, U., and Smith, E.F. Mapping of para-autochthonous region is adapted from Togtokh (1995). Main fault zones are numbered from #1 to #4. Dated samples are labeled except U1519 and U1520 (Yarmolyuk et al., 2008a); see Figure 2.3. Geochronologic results of samples U1105 and U1127-5 are described in Kilian et al. (in preparation).

In the northwestern part of the Zavkhan Terrane, the Zavkhan Fm unconformably overlies the Tsagaankhairkhan Fm, which is a carbonate sequence dominated by stromatolitic dolomite. Unfortunately, this unit is only exposed in western Khukh Davaa (Figure 2.2), with no apparent stratigraphic relationships with other units, and consequently its age relative to other pre-Zavkhan Fm units remains poorly constrained. The overlying Zavkhan Fm can be divided into two sub-units. The lower Zavkhan Fm is dominated by boulder clast conglomerate, whereas rhyolite and minor mafic flows prevail the upper portion. The age of the volcanism of the Zavkhan Fm is constrained by CA-ID-TIMS U-Pb dates on zircon that range from 787.45 ± 0.47 to 802.11 ± 0.45 Ma (Bold et al., 2016). The stratigraphy above the Zavkhan Fm has been revised by Macdonald et al. (2009a), Bold et al. (2013), and Smith et al. (2015) in detail following terrane-wide, member-level mapping. According to the revised stratigraphic nomenclature, the Khasagt Fm unconformably overlies the volcanics of the Zavkhan Fm, which in turn is unconformably overlain by the Tsagaan-Olom Group (Bold et al., 2016).

Lithologically, the Khasagt Fm is composed of siltstone, sandstone, and conglomerate with large lateral changes in thickness. It is best exposed and thickest in the Khasagt Khairkhan Range, thinning towards the Khukh Davaa region, and absent in the north of the Zavkhan Terrane. These thickness changes represent both facies change, fault-controlled deposition in a narrow graben, and erosion beneath 717-660 Ma Sturtian glacial deposits of the overlying Maikhan-Uul Fm (Macdonald et al., 2010; Rooney et al., 2015), which forms the base of the Tsagaan-Olom Group. The Maikhan-Uul Fm is sharply overlain by carbonate strata of the Taishir Fm, which in turn overlain by ~ 635 Ma Marinoan glacial deposits of the Khongor Fm (Macdonald et al., 2009a). Early Ediacaran carbonate of the overlying Ol and Shuurgat fms are > 500 m thick with the top of the Tsagaan-Olom Group defined by a karstic unconformity (Bold et al., 2013). Overlying this unconformity are late Ediacaran phosphorite and carbonate strata of the Zuun-Arts Fm and mixed carbonates and siliciclastic strata of the Terreneuvian Bayangol, Salaagol, and Khairkhan fms (Figure 2.3), which record deposition in a foreland basin (Macdonald et al., 2009a; Smith et al., 2015) .

On the Zavkhan Terrane, the Terreneuvian Khairkhan Fm is overlain by Cambrian to Ordovician chert and cobble conglomerate units, and the Upper Ordovician to Silurian Teel Fm (Kilian et al., in preparation), which is composed of bimodal series of rhyolite and basalt with interbeds of conglomerate, sandstone, and siltstone (Togtokh, 1995). Regionally, red beds of the Teel Fm have been mismapped as the Tsagaanshoroot Fm (Togtokh, 1995), which is composed of interbedded limestone, conglomerate, sandstone, siltstone, and rare beds of basalt in the para-autochthonous region that preserves the Middle Devonian brachiopod *Wilsonella sp.* (Pojeta Jr, 1986) and the progymnosperm *Aneruophyton sp.* (Petrosyan, 1967). The youngest sedimentary rocks in the region are in the Jurassic sedimentary sequence of the Jargalant Fm, which is exposed on the para-autochthonous basement, in the southern opening of the Khoid and Dund Sharga gorges of the Sharga soum of Govi-Altai province (Figure 2.2).

Paleozoic felsic magmatism is abundant in the Zavkhan Terrane, but none of the plutons or volcanic rocks have been dated with the U-Pb zircon method. These intrusions are interpreted to be correlative with the Paleozoic Numrug and Tonkhil complexes based on map relationships. Both of these Paleozoic granites are alkaline but the Tonkhil Complex is characterized by coarse crystalline syenite-porphyry. Based on map relationships the Numrug Complex was previously mapped as Pennsylvanian and the Tonkhil Complex was mapped as Permian (Togtokh, 1995). Below we demonstrate that the Numrug Complex is earliest Silurian in age, and the age of the Permian Tonkhil Complex is refined in Kilian et al. (in preparation).

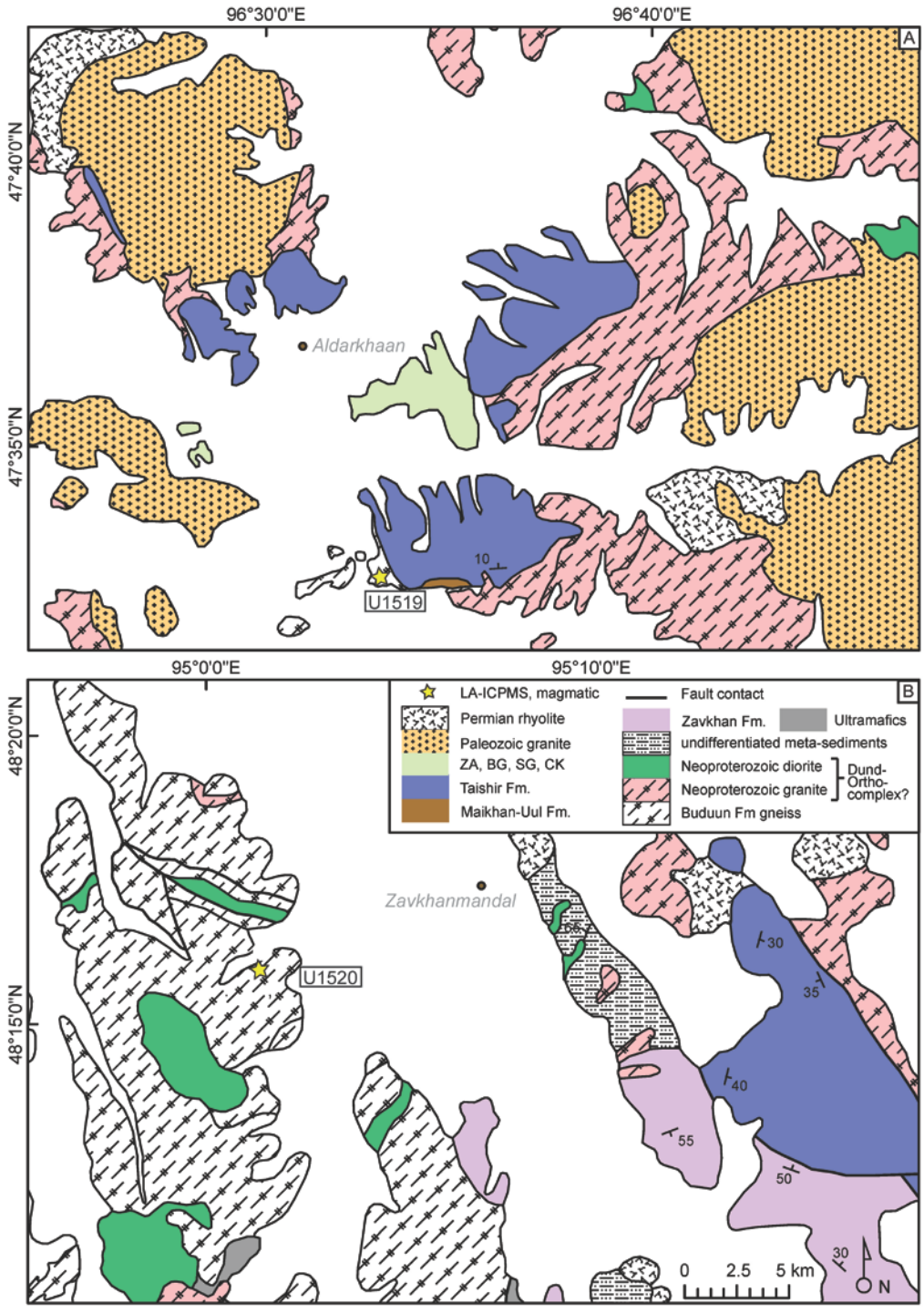

Figure 2.3. Geologic map of the northern Zavkhan Terrane
Modified from 1:200,000 scale regional geologic map by Samozvantsen (1981). A) Geologic map of the Binder Khairkhan Mountain of the Aldarkhaan soum of the Zavkhan province where granite-gneiss sample U1519 was sampled. B) Geologic map of the Zavkhanmandal soum where granite-gneiss sample U1520 was sampled. For detailed lithologic characteristics, see Kozakov et al. (2012b).

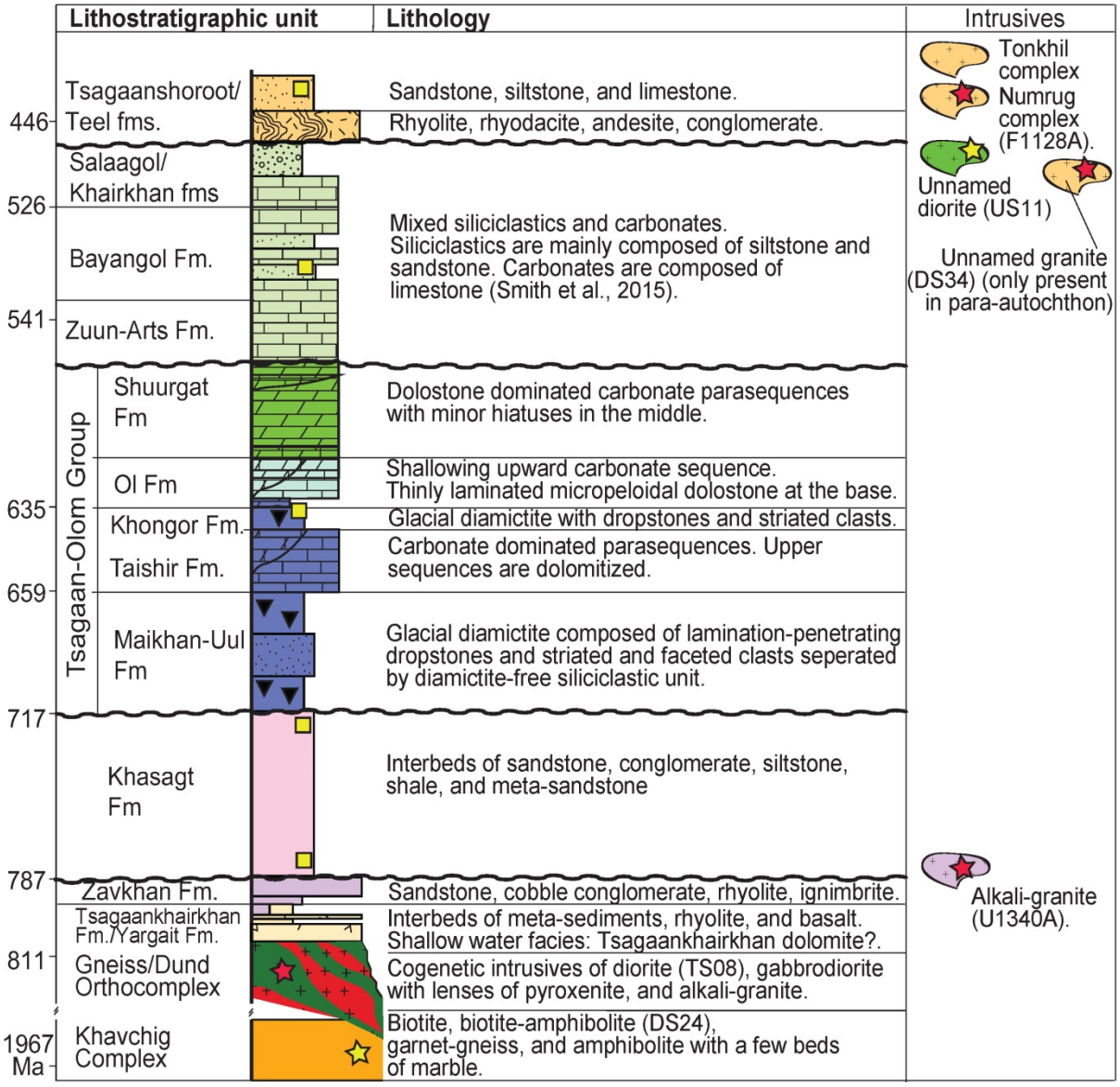

Figure 2.4. Generalized lithostratigraphy of the Zavkhan Terrane
The units are color-coded and labeled following Figure 2.2. The stratigraphic horizons sampled for geochronology are labeled and magmatic sample numbers are included in parenthesis.

2.2. METHODS

2.2.1. Sampling

From 2011-2015, in the course of geological mapping (Figure 2.2), the main lithostratigraphic units were sampled for U-Pb zircon geochronology. In addition, in the Zavkhanmandal (U1520, Figure 2.3B) and Aldarkhaan soums (U1519, Figure 2.3A) of the northern Zavkhan province, granite-gneisses of

the Buduun Fm (Samozvantsen, 1981) were sampled to better constrain the age of the basement of the Zavkhan Terrane. Petrographic thin sections were prepared at Harvard University.

2.2.2. U-Pb Zircon Geochronology

Zircon grains were separated at Harvard University using standard gravitometric methods including crushing, pulverizing, washing, magnetic separation, heavy liquids, hand picking, annealing (at 900^{o}C for 60 hours), and mounting. For detrital zircon, random selection was performed to ensure selection of a variety of zircon sizes and morphologies. Grain mounts were polished and imaged by cathodoluminescence at the Isotope Geology Laboratory at Boise State University. Detailed descriptions of analytical methods of Laser ablation - inductively coupled plasma mass spectrometry (LA-ICPMS) and Chemical abrasion - isotope dilution thermal ionization mass spectrometry (CA-ID-TIMS) are in Macdonald et al. (2014). All samples were first dated by LA-ICPMS U-Pb method and five samples were further analyzed by CA-ID-TIMS (Table 2.1).

Table 2.1. Summary of magmatic and detrital samples dated

Sample number	Age (Ma)	Uncertainty (±)	MSWD*	p.o.f†	Method	Latitude (°N)	Longitude (°E)	Interpretation	Formation/Rock Type
Para-autochthon									
DS24	1967	13	1.3	0.15	ICPMS	46.5451	95.6934	Crystallization	Khavchig Complex/muscovite-biotite gneiss
TS08	811.36	0.24/0.45/0.94	0.6	0.67	TIMS	46.6380	95.8510	Crystallization	Dund-Orthocomplex/hornblende diorite
DS05	558	23	N.A.§	N.A.	ICPMS	46.5010	95.6553	Maximum age	unnamed/sandstone
US10	800	19	0.84	0.5	ICPMS	46.5257	95.9174	Crystallization	unnamed/granite-gneiss
US10	529	22	0.62	0.43	ICPMS	46.5257	95.9174	Metamorphic rim	unnamed/granite-gneiss
DS34	509.56	0.19/0.31/0.61	1.9	0.13	TIMS	46.6288	95.7774	Crystallization	unnamed/granite
DS34	507.07	0.32/0.4/0.66	1.3	0.25	TIMS	46.6288	95.7774	Metamorphic rim	unnamed/granite
U12001	509.3	0.42/0.49/0.72	1.3	0.27	TIMS	46.6272	95.7161	Crystallization	Yesonbulag/granite-gneiss
US11	496	7	1.14	0.25	ICPMS	46.5234	95.9214	Crystallization	unnamed/biotite-hornblende-quartz diorite
Autochthon									
U1519	N.A.	N.A.	N.A.	N.A.	ICPMS	47.5445	96.5492	N.A.	Buduun/granite-gneiss
U1520	839	11	1.2	0.15	ICPMS	48.2713	95.0245	Crystallization	Buduun/granite-gneiss
U1331	778	37	N.A.	N.A.	ICPMS	47.1181	95.2778	Maximum age	Khasagt/sandstone
U1340A	770.31	0.23/0.43/0.89	1.8	0.12	TIMS	46.8842	96.5595	Crystallization	unnamed/alkaline granite
DS69	733	34	N.A.	N.A.	ICPMS	46.7363	95.8335	Maximum age	Khasagt/arkose
U1121-17.5	646	23	N.A.	N.A.	ICPMS	46.6630	96.2554	Maximum age	Khongor/siltstone
F1128B	465	15	N.A.	N.A.	ICPMS	46.7841	95.7332	Maximum age	Teel/conglomerate
F1128A	442.1	0.19/0.28/0.54	1.5	0.18	TIMS	46.7841	95.7332	Crystallization	Numrug Complex/granite
U1127-1	341	40	N.A.	N.A.	ICPMS	46.8878	95.7278	Maximum age	Teel/sandstone
E1105-35.3	533	18	N.A.	N.A.	ICPMS	46.84342	95.77497	Maximum age	Bayangol/siltstone
F1121-25	721	19	N.A.	N.A.	ICPMS	46.7068	96.31077	Maximum age	Bayangol/sandstone
E1326	695	38	N.A.	N.A.	ICPMS	46.62258	96.65673	Maximum age	Bayangol/quartz pebble conglomerate
E1336-41	722	49	N.A.	N.A.	ICPMS	47.0473	95.48747	Maximum age	Khairkhan/conglomerate

*Mean Square of Weighted Deviates.

†Probability of fit.

§N.A. = not applicable.

LA-ICPMS data were collected in 13 experiments from March 2012 until January 2016. For U-Pb and $^{207}Pb/^{206}Pb$ dates, instrumental fractionation of the background-subtracted ratios was corrected and dates were calibrated with respect to interspersed measurements of zircon standards and reference materials. The primary standard Plešovice zircon (Sláma et al., 2008) was used to monitor time-dependent instrumental fractionation based on two analyses for every 10 analyses of unknown zircon. A secondary correction to the $^{206}Pb/^{238}U$ dates was made based on results from the zircon standards Seiland (530 Ma, unpublished data, Boise State University) and (or) Zirconia (327 Ma, unpublished data, Boise State University), which were treated as unknowns and measured once for every 10 analyses of unknown zircon. These results showed a linear age bias of a few percent that is related to the ^{206}Pb count rate. The secondary correction is thought to mitigate matrix-dependent variations due to contrasting compositions and ablation characteristics between the Plešovice zircon and other standards (and unknowns).

Radiogenic isotope ratio and age error propagation for all analyses includes uncertainty contributions from counting statistics and background subtraction. Because the detrital zircon analyses are interpreted individually, uncertainties from the standard calibrations are propagated into the errors on each detrital zircon date. These uncertainties are the local standard deviations of the polynomial fits to the interspersed primary standard measurements versus time for the time-dependent, relatively larger U/Pb fractionation factor, and the standard errors of the means of the consistently time-invariant and smaller $^{207}Pb/^{206}Pb$ fractionation factor. They are 0.5-1.0% (2σ) for $^{206}Pb/^{238}U$ and 0.2-1.0% (2σ) for $^{207}Pb/^{206}Pb$. For groups of analyses that are collectively interpreted from a weighted mean date (i.e., igneous zircon analyses), a weighted mean date is first calculated using Isoplot 4.15 (Ludwig, 2008) using errors on individual dates that do not include a standard calibration uncertainty, and then a standard calibration uncertainty is propagated into the error on the weighted mean date.

Age interpretations are based on $^{207}Pb/^{206}Pb$ dates for analyses with $^{207}Pb/^{206}Pb$ dates > 1000 Ma. Analyses with > 20% positive discordance and > 10% negative discordance are not considered. The $^{206}Pb/^{238}U$ dates are used for analyses with $^{207}Pb/^{206}Pb$ dates < 1000 Ma. Errors on the dates from individual analyses are given at 2σ.

CA-ID-TIMS analysis was done at the Isotope Geology Laboratory at Boise State University. Weighted mean $^{206}Pb/^{238}U$ dates are calculated from equivalent dates and also plotted using Isoplot 4.15 (Ludwig, 2008). Errors on the weighted mean dates are given as ± x / y / z, where x is the internal error based on analytical uncertainties only, including counting statistics, subtraction of tracer solution, and blank and initial common Pb subtraction, y includes the tracer calibration uncertainty propagated in quadrature, and z includes the ^{238}U decay constant uncertainty propagated in quadrature. Internal errors (x) should be considered when comparing our dates with $^{206}Pb/^{238}U$ dates from other laboratories that used the same Boise State University tracer solution or a tracer solution that was cross-calibrated using EARTHTIME gravimetric standards. Errors including the uncertainty in the tracer calibration (y) should be considered when comparing our dates with those derived from other geochronologic methods using the U-Pb decay scheme (e.g. LA-ICPMS). Errors including uncertainties in the tracer calibration and ^{238}U decay constant (z) (Jaffey et al., 1971) should be considered when comparing our dates with those derived from other decay schemes (e.g., $^{40}Ar/^{39}Ar$, ^{187}Re-^{187}Os). Therefore, internal error x is used in the discussion when in comparison with data generated by U-Pb zircon method. Errors for weighted mean dates and dates from individual grains are given at 2σ.

2.3. RESULTS

Geochronologic results from the dated samples of the Zavkhan Terrane are described stratigraphically, from the oldest to the youngest. Petrographic observations (Figure 2.8) are included where available along with chemical compositions of the zircons. Based on these new data, timing of major structures is refined, which is explained in discussion in association with magmatic events.

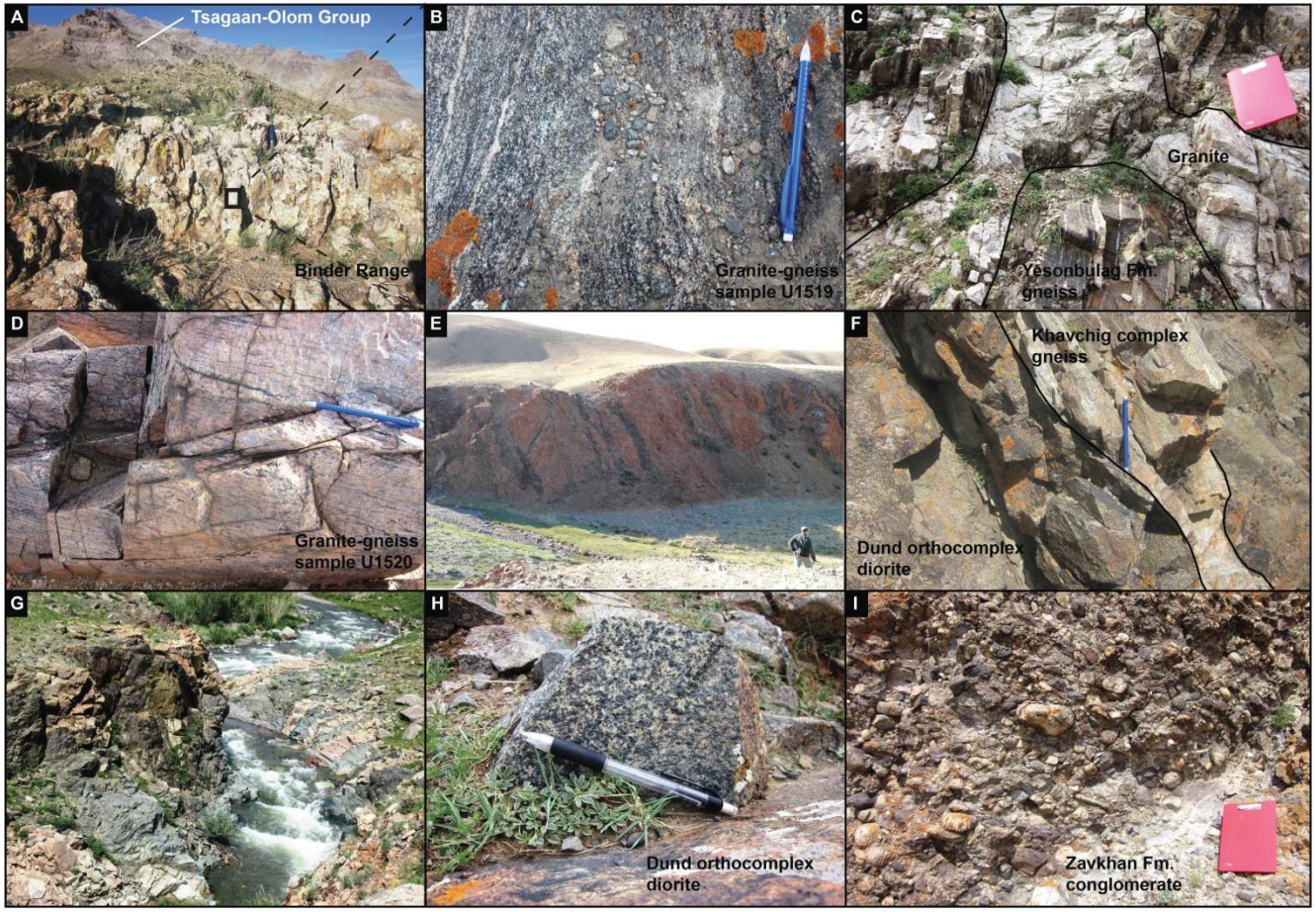

Figure 2.5. Field photographs of representative lithostratigraphic units of the Zavkhan Terrane
A) Granite-gneiss exposed in Binder Khairkhan Mountain in Aldarkhaan soum of Zavkhan province with direct contact with dolomitized Tsagaan-Olom Group carbonates. View to the east. B) Zoomed in view of the granite-gneiss where sample U1519 was taken. C) Granite-gneiss of the Yesonbulag Formation as exposed in Tsagaanchuluut Gorge. Later granite intrusions are highlighted. D) Granite-gneiss previously dated by Kozakov et al. (2012b) in the Zavkhanmandal soum of the Zavkhan province where sample U1520 was sampled. E) The Dund-Orthocomplex as exposed in the mouth of the Orlogo Gorge. View to the southeast. Note the extent of mafic dikes that are prevalent throughout the massive. F) A view in the Urd Sharga Gorge of the Dund-Orthocomplex diorite that intrudes through the Khavchig Complex granite-gneiss. G) The Dund-Orthocomplex diorite along with co-genetic granite as exposed in the Dund Sharga Gorge. H) The Dund-Orthochomplex diorite as exposed in the Dund Sharga Gorge. I) The Zavkhan Formation cobble conglomerate as exposed in the western Khukh Davaa.

DS24 – Micaceous granite-gneiss in the Khavchig Complex: A micaceous granite-gneiss (Figure 2.5F) was sampled in the northern part of the Daagan Del Range in the Dund Sharga Gorge (Figure 2.2). The gneiss is lepido-hetero-granoblastic and poikiloblastic in texture and is composed of plagioclase (35-40%), quartz (25-30%), micas (10-15%), and potassium feldspar – perthite (10-15%). Secondary minerals are represented by sericite, muscovite, chlorite, and epidote-zoisite and accessory minerals by opaque minerals (< 5%), apatite, and zircon (Figure 2.8A). LA-ICPMS dates from 41 zircon cores and magmatic rims are 2469 ± 27 to 1888 ± 25 Ma (Figure 2.A1, Table 2.A2). Dates from 26 grains (excluding dates from cores) are equivalent with a weighted mean of 1967 ± 13 Ma (Mean Square of Weighted Deviates (MSWD) = 1.3, probability of fit = 0.15) (Figure 2.6A).

U1519 – Granite-gneiss in the Buduun Fm: A light green granite-gneiss (figures 2.5A and B) was sampled near the Binder-Khairkhan Mountain (Figure 2.3A) in the Aldarkhaan soum of the Zavkhan province where directly overlain by the Maikhan-Uul Fm diamictite and Tsagaan-Olom Group carbonates. The lepido-hetero-granoblastic gneiss is composed of plagioclase (25-30%), quartz (25-30%), potassium feldspar (25-30%), and biotite (5-10%). Plagioclase is sericitizated, corroded by quartz, and sometimes shows myrmekite intergrowths. Potassium feldspar is partly pelitizated and includes poikiloblastic quartz and sometimes relicts of plagioclase and biotite. Biotite is often replaced by chlorite and rarely by epidote-zoisite. Accessory minerals are represented by apatite, titanite, zircon, and opaque minerals (Figure 2.8B). LA-ICPMS dates from 46 zircon cores and magmatic rims are 2523 ± 31 to 724 ± 15 Ma (Figure 2.A2, Table 2.A2). 4 grains have Paleoproterozoic inherited zircon cores. The rest of the grains are complicated mixtures of metamorphic and magmatic early Neoproterozoic zircons. The youngest four dates of 776 ± 30 to 724 ± 15 Ma are from rims. Because only one rim had a reliable zircon chemical composition, no weighted mean date was calculated for this metamorphic event (Figure 2.6C).

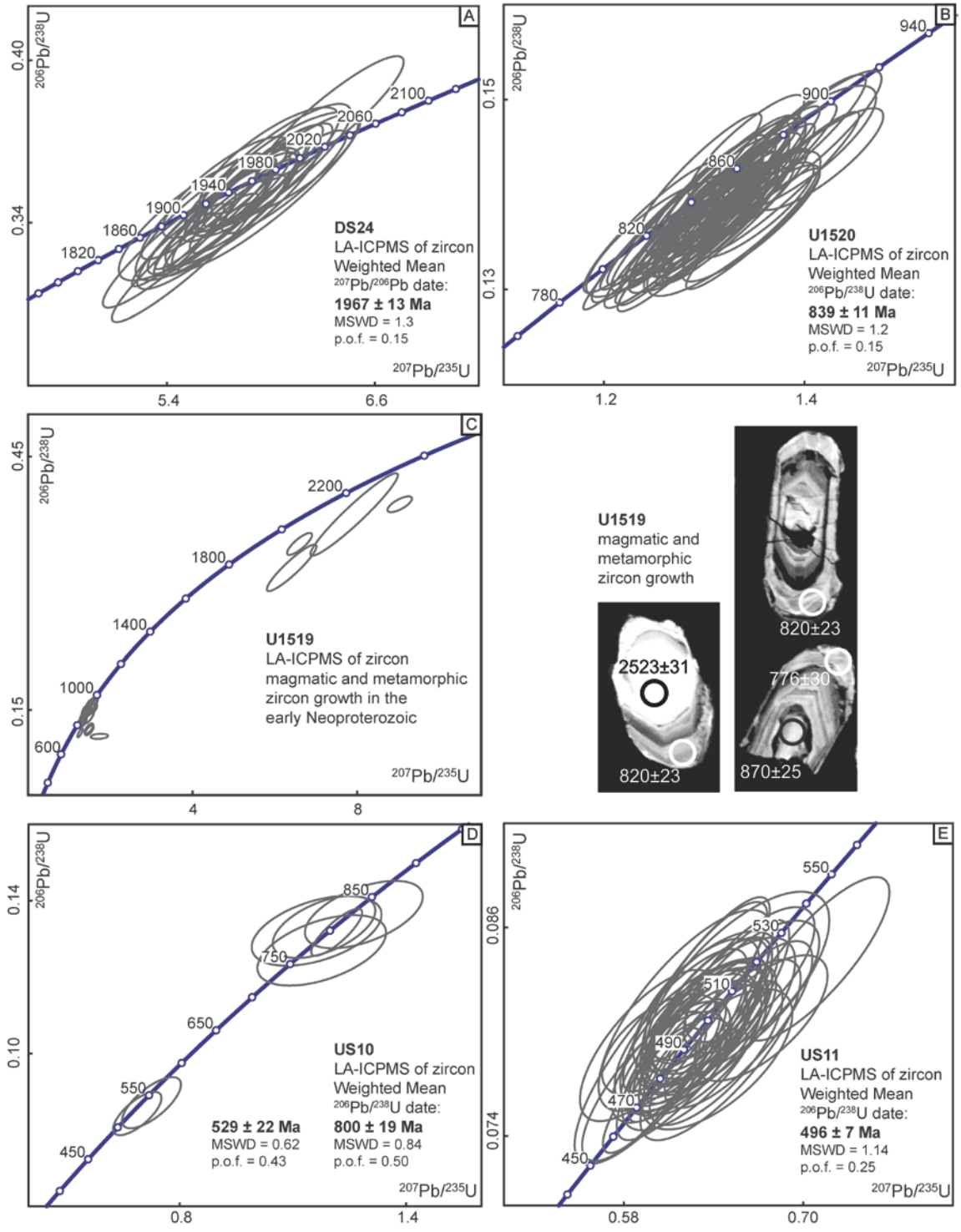

Figure 2.6. Concordia diagrams of the dated samples analyzed by LA-ICPMS

A) A granite-gneiss (U1520) dated in the Zavkhanmandal soum of the Zavkhan province from a previously dated complex by Kozakov et al. (2012b). B) A granite-gneiss (DS24) dated in the Khavchig Complex. C) A biotite-hornblende-quartz diorite (US11) dated in the Urd Sharga Gorge. D) A granite-gneiss (US10) dated in the Urd Sharga Gorge. E) A granite-gneiss (U1519) dated at Khairkhan Mountain in the Aldarkhaan soum of the Zavkhan province. Results yield complicated mixture of metamorphic and magmatic zircon growth in the early Neoproterozoic and hence cathodoluminescence images of representative zircon grains are shown.

U1520 – Granite-gneiss in the Buduun Fm: A pink granite-gneiss (Figure 2.5D) was sampled near Zavkhanmandal soum of the Zavkhan province (Figure 2.3B) from a locality described to be the basement of the Zavkhan Terrane (Samozvantsen, 1981). U1520 was sampled from the same map unit dated by Kozakov et al. (2012b) at 856 ± 2 Ma. The porphyroblastic and lepido-hetero-granoblastic granite-gneiss is composed of microcline-perthite (35-40%), plagioclase (20-25%), biotite (< 5%), and quartz (30-35%). Micropoikiloblastic texture is common, which is represented by quartz included in potassium feldspar. Biotite is often altered to sericite, muscovite and opaque minerals. Recrystallized quartz is also common (Figure 2.8C). LA-ICPMS dates from 61 zircon grains are 886 ± 28 to 795 ± 29 Ma (Figure 2.A3, Table 2.A2). Dates from 54 dates are equivalent with a weighted mean of 839 ± 11 Ma (MSWD = 1.2, probability of fit = 0.15) (Figure 2.6B).

TS08 – Hornblende diorite in the Dund-Orthocomplex: A dark green, coarsely crystalline hornblende diorite (Figure 2.5H) was sampled in the eastern tributary of the Dund Sharga Gorge, the Tsagaanchuluut Gorge (Figure 2.2). It is hypidiomorphic granular in texture and composed of plagioclase (50-55%), hornblende (35-40%), and quartz (< 5%). Secondary minerals are represented by sericite and pelite and accessory minerals by opaque minerals (< 5%). Plagioclase is subhedral and polysynthetically twinned whereas hornblende is euhedral to subhedral (Figure 2.8D). LA-ICPMS dates from 59 zircon grains are 872 ± 35 to 750 ± 31 Ma (Figure 2.A4, Table 2.A2). The 5 oldest of 7 zircon grains analyzed by CA-ID-TIMS yielded equivalent dates with a weighted mean of 811.36 ± 0.24 / 0.45 / 0.94 Ma (MSWD = 0.6, probability of fit = 0.67). 2 other grains yielded dates of 809.91 ± 0.52 and 810.23 ± 0.52 Ma (Figure 2.7A, Table 2.A1).

U1331 – Arenite in the Khasagt Fm: A dark purple, coarse to medium grained arenite was sampled in the Khasagt Fm that directly overlies the Zavkhan Fm rhyolites in the western Khukh Davaa (Figure 2.2). The psammitic arenite is clast dominated (85-90%) and is composed of well-rounded and medium-sorted quartz grains (0.1-1.2 mm; 90-95%) that are cemented by sericite (0.6-1 mm; 6-8%) and opaque minerals (0.2-0.3 mm; 1-2%) (Figure 2.8I). LA-ICPMS dates from 112 detrital zircon grains are

2930 ± 70 to 778 ± 33 Ma (Figure 2.A5, Table 2.A3). Prominent age peaks are at 1000–750 and 1900 – 1780 Ma (Figure 2.9).

U1340A – Alkaline granite that intrudes the Zavkhan Fm: A coarse-grained alkaline granite (Yarmolyuk et al., 2008a) that intrudes the Zavkhan Fm rhyolite was sampled near Tsagaanchuluut soum of Govi-Altai province. This granite was previously dated with two large multi-grain bulk zircon fractions at 755 ± 3 (Yarmolyuk et al., 2008a). The granite is composed of potassium feldspar – perthite (55-60%), quartz (25-30%), plagioclase (5-10%), and biotite (< 5%). Potassium feldspar is subhedral, often pelitizated, and corroded by quartz. Plagioclase is subhedral and lightly sericitizated. Pseudomorphs of biotite and hornblende that are completely altered by chlorite, opaque minerals, and quartz are present. Accessory minerals are apatite, titanite/sphene, and zircon (Figure 2.8E). Micro-fractures within the granite are commonly filled by sericite, quartz, opaque minerals, and hydrous ferric oxides. LA-ICPMS dates from 25 zircon grains are 872 ± 31 to 670 ± 31 Ma (Figure 2.A6, Table 2.A2). CA-ID-TIMS dates from 5 grains are equivalent with a weighted mean of 770.31 ± 0.23 / 0.43 / 0.89 Ma (MSWD = 1.8, probability of fit = 0.12) (Figure 2.7B, Table 2.A1).

DS69 – Lithic sandstone in the Khasagt Fm: A pale grey, coarse grained lithic sandstone was sampled in the Khasagt Fm that directly overlies a local fault bordering with the Yargait Fm in the Dund Sharga Gorge (Figure 2.2). The sandstone is psepho-psammite in texture, clast dominated (85-90%), and is cemented by carbonate, sericite, quartz, and chlorite. Clasts are often angular, poorly sorted, and are mainly composed of rhyolite (1-4.6 mm; 60-65%). LA-ICPMS dates from 60 detrital zircon grains are 1998 ± 25 to 733 ± 34 Ma. Prominent peak in the age spectra occurs at 850-700 Ma (figures 2.9 and 2.A7, Table 2.A3).

U1121-17.5 – Siltstone in the Khongor Fm: A shaly siltstone was sampled in the matrix of the Khongor Fm diamictite in the Khongor Range, 17.5 m above the base. LA-ICPMS dates from 70 detrital zircon grains are 2623 ± 57 to 646 ± 23 Ma. Prominent age peaks are at 900-700 and 2100-2000 Ma (Figure 2.9, Table 2.A3).

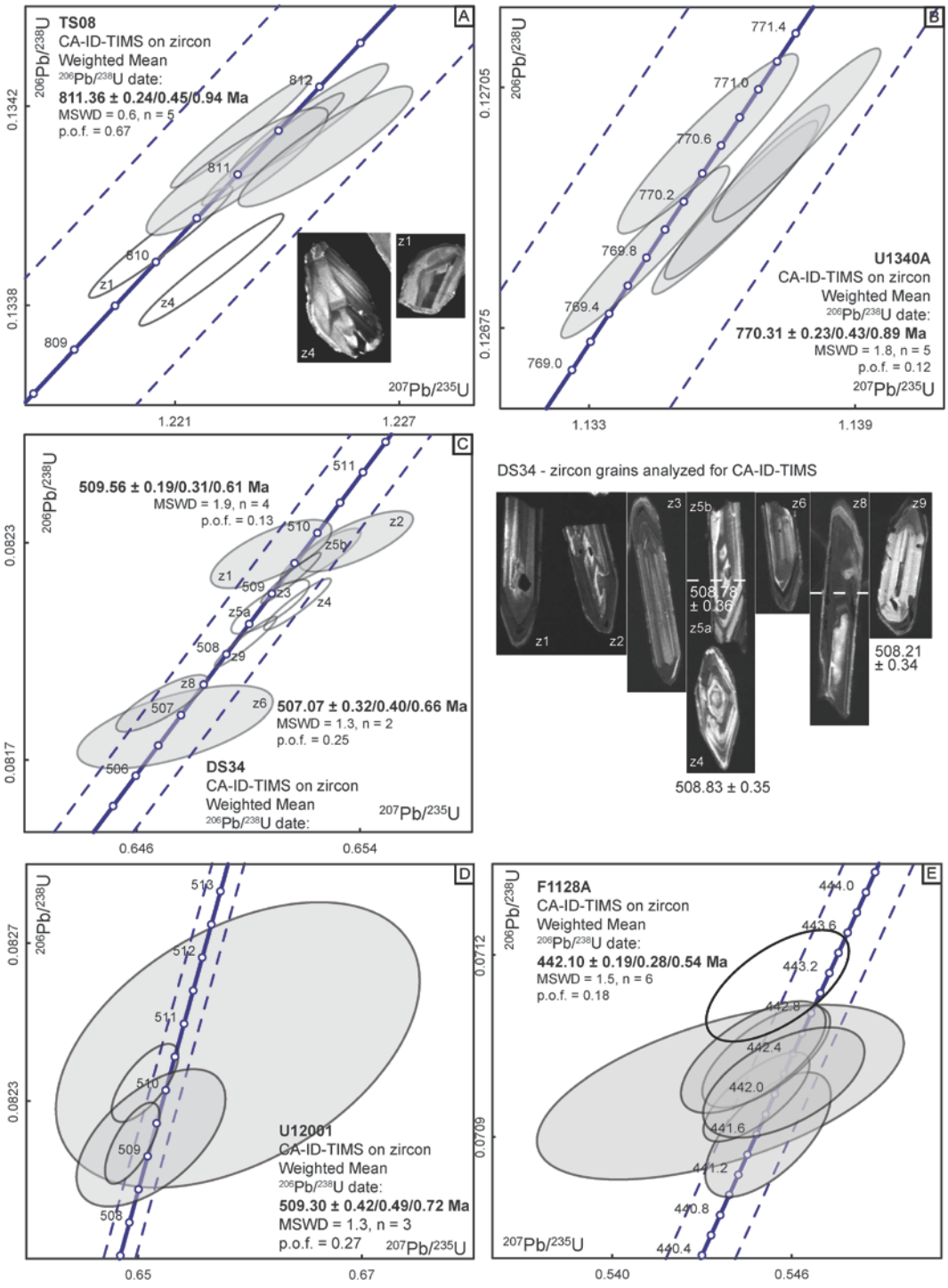

Figure 2.7. Concordia diagrams of the samples analyzed by CA-ID-TIMS
A) A granite (F1128B) taken along a fault zone in Salaa Gorge. B) A granite-gneiss (U12001) taken in the Yesonbulag Formation in the western Dund Sharga Gorge. C) A hornblende diorite (TS08) of the Dund-Orthocomplex sampled in Tsagaanchuluut Gorge. The two zircon grains that yielded younger dates have thin white rims (metamorphic?), which may have affected the final result. D) An alkaline granite (U1340A) sampled in Tsagaanchuluut soum. E) A granite (DS34) sampled in the Dund Sharga Gorge in the para-autochthonous region. Two weighted mean dates were calculated to constrain tectonomagmatic events recorded within the zircon grains. Probability of fit is abbreviated as p.o.f.

E1105-35.3 – Siltstone in the Bayangol Fm: A siltstone was sampled from measured section E1105 of the Bayangol Fm in Salaa Gorge (Figure 2.2). Sample was collected as possibly being an ash, but dates indicate zircon grains are detrital. LA-ICPMS from 31 zircon grains are 2401 ± 25 to 533 ± 18 Ma (Figure 2.A9, Table 2.A3). Age peaks are at 920-760 Ma (Figure 2.9).

F1121-25 – Sandstone in the Bayangol Fm: A ~ 10 cm-thick sandstone from just below pink stromatolite marker beds in Member BG3 of the Bayangol Fm in Bayan Gorge (Figure 2.2). This sample was collected while measuring section F1121 in the Bayan Gorge. LA-ICPMS dates from 29 zircon grains are 2419 ± 55 to 721 ± 19 Ma (Figure 2.A10, Table 2.A3). Age peaks are at 850-750 Ma (Figure 2.9).

E1326 – Conglomerate in the Bayangol Fm: A white to pink quartz pebble conglomerate from the top of Member BG6 of the Bayangol Fm was sampled just below the base of the Salaagol Fm in southern Khukh Davaa (Figure 2.2). LA-ICPMS dates from 69 zircon grains are 2423 ± 56 to 695 ± 38 Ma (Figure 2.A11, Table 2.A3). Age peaks are at 900-720 Ma (Figure 2.9).

E1336-41 – Sandstone in the Khairkhan Fm: A poorly-sorted pebble conglomerate that was collected just above the contact between the Bayangol Fm and the Khairkhan Fm in southern Khukh Davaa (Figure 2.2). This sample was collected in measured section E1339. At this locality, the Salaagol Fm is absent, and the Khairkhan Fm sits directly on the Bayangol Fm. LA-ICPMS dates from 112 zircon grains are 2988 ± 53 to 722 ± 49 Ma (Figure 2.A12, Table 2.A3). Age peaks are at 950-720 Ma (Figure 2.9).

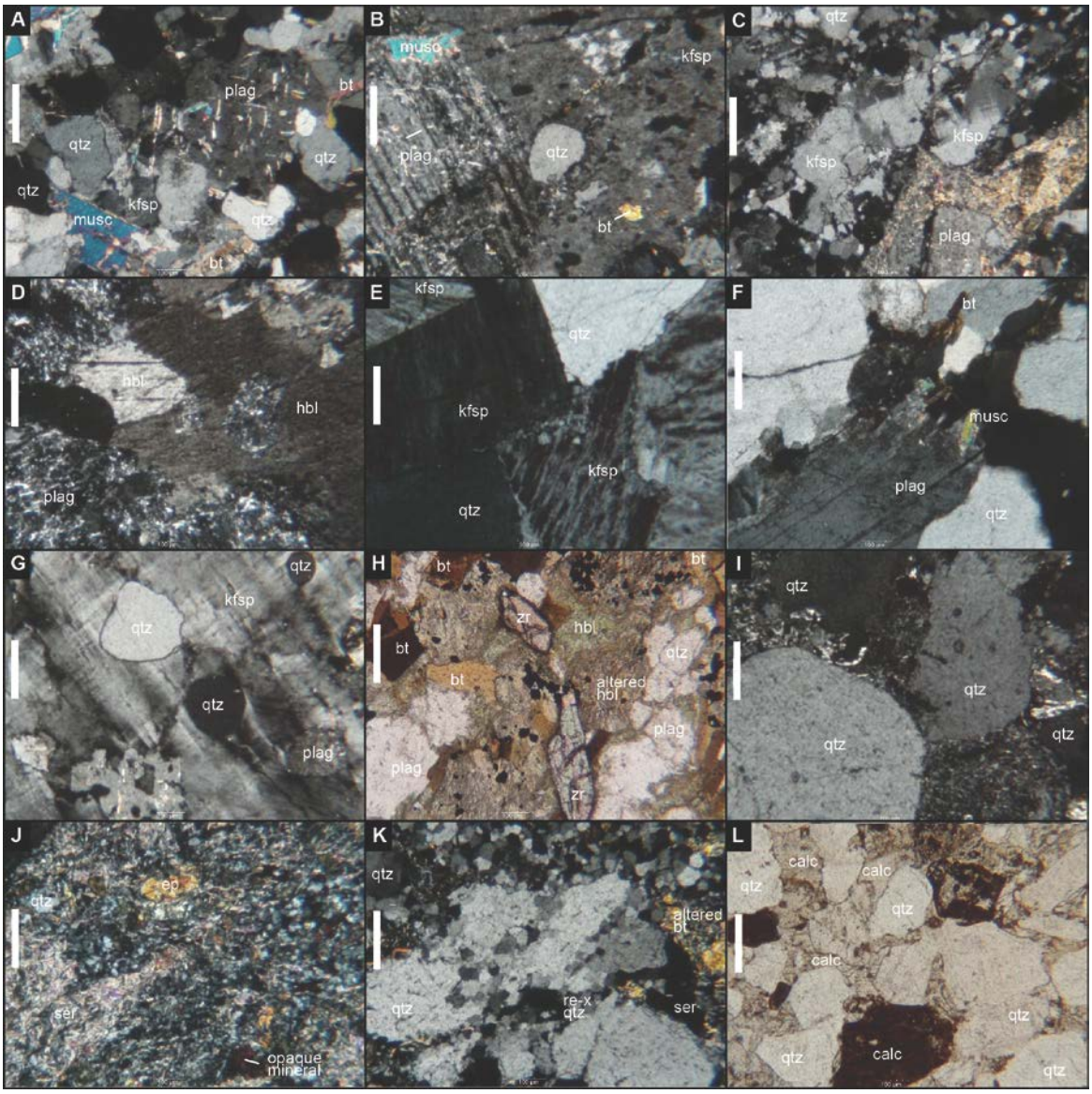

Figure 2.8. Photomicrographs of the representative lithostratigraphic units

A, B, C, D, E, F, G, I, J, and K were taken in crossed polarized light and H and L were taken in plain polarized light. Qtz = quartz, kfsp = potassium feldspar, calc = calcite, plag = plagioclase, musc = muscovite, bt = biotite, ser = sericite, zr = zircon, hbl = hornblende, ep = epidote, and re-x = recrystallized. Scale bar is 200 μm. A) Micaceous granite-gneiss (DS24). Poikiloblastic texture is shown by quartz grain at the boundary between plagioclase and quartz. B) Granite-gneiss (U1519). Poikiloblastic texture is shown by quartz included in plagioclase crystal. C) Granite-gneiss (U1520). Poikiloblastic texture is shown by small quartz crystals. Plagioclase is sericitizated. D) Hornblende diorite (TS08). Abundance of hornblende is represented by large hornblende crystals. E) Coarse crystalline alkaline granite (U1340A). Subhedral to euhedral potassium feldspar crystals are shown with quartz crystals. F) Plagiogranite (US10). Faint polysynthetic twinning of plagioclase crystals is shown. G) Granite-gneiss (U12001). Poikiloblastic texture is represented by quartz grains included in large potassium feldspar crystal. Plagioclase crystals are sericitizated. H) Biotite-hornblende-quartz diorite (US11). Large zircon crystals are shown by high relief and representative crystal habit. I) Arenite (U1331). Quartz grains are well-rounded but poorly sorted. Matrix is composed of sericite and opaque minerals. J and K are photomicrographs of meta-sandstone (DS05). J) Epidotizated, silicified, and sericitizated sandstone. K) Large quartz crystals are shown along with recrystallized quartz and silicified matrix. L) Litho-arenite (U1127-1). Quartz grains are poorly rounded and matrix is composed of mostly carbonate.

DS05 – Meta-sandstone in meta-siliciclastics in undifferentiated unit in the southern Dund Sharga Gorge: A pink grey, epidotizated, sericitizated, and silicified lithic meta-sandstone was sampled in the south of Dund Sharga Gorge (Figure 2.2). The meta-sandstone is blasto-psammitic and schistose in texture and composed of clasts (50-55%) of quartz (< 1 mm; 40-45%), altered color minerals that are characterized by epidote and sericite (~ 0.8; < 5%), feldspar (< 0.1 mm, < 5%), apatite (< 0.15 mm; < 1%), opaque minerals (< 0.15 mm; < 1%), and rhyolite (< 1.8 mm; < 5%). Quartz clasts are partly recrystallized forming micro-granoblastic aggregates. Cements (45-50%) are composed of epidote-zoisite (10-15%), quartz (10-15%), and sericite (15-20%) (figures 2.5J and K). LA-ICPMS dates from 12 zircon grains are 689 ± 71 to 558 ± 23 Ma (Figure 2.A13; Table 2.A3).

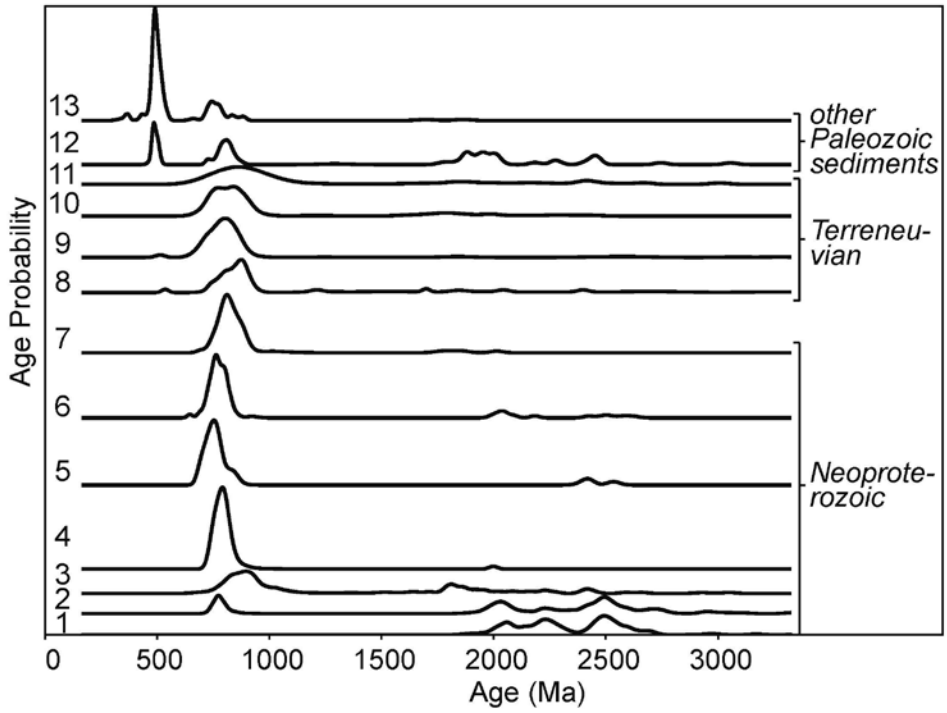

Figure 2.9. Normalized probability plots of U-Pb dates obtained by LA-ICPMS from zircon grains of the detrital samples
The Zavkhan (1, 2), Khasagt (3, 4), Maikhan-Uul (5), Shuurgat (7), Bayangol (8,9,10), Khairkhan (11), and Teel (12, 13) formations of the Zavkhan Terrane. 1 - U1333, 2 - U1214, 3 - U1331, 4 - DS69, 5 - F1203-272.1, 6 – U1121-17.5, 7 - F1206-146.1, 8 - E1105-35, 9 - F1121-25, 10 - E1326, 11 - E1336-41, 12 – F1128B, and 13 - U1127-1. Data of U1333, U1214, F1203-272.1, and F1206-146.1 are published in (Bold et al., 2016).

US10 – Granite-gneiss: A light grey, weakly gneissose granite (mapped as Paleoproterozoic by Togtokh (1995)) was sampled to the west of the Urd Sharga Gorge near where US11 was sampled (Figure

2.2). It is lepido-granoblastic in texture and composed of plagioclase (35-40%), microcline (5-10%), quartz (30-35%), biotite (5-10%), and muscovite (< 5%). Micro-poikiloblastic texture is often shown by small quartz grains included in microcline. Secondary minerals are sericite, chlorite, and hydrous iron oxides. Accessory minerals are represented by opaque minerals (< 1%), apatite (1-2%), titanite (< 1%), zircon (1-2%), and garnet (< 1%) (Figure 2.5F). LA-ICPMS dates from 23 zircon cores and magmatic rims are 2629 ± 51 to 522 ± 28 Ma (Figure 2.A14, Table 2.A2). Excluding the cores, the dates on magmatic rims are equivalent with a weighted mean of 800 ± 19 Ma (MSWD = 0.84, probability of fit = 0.5). Dates from metamorphic rims on 2 grains are equivalent with a weighted mean of 529 ± 22 Ma (MSWD = 0.62, probability of fit = 0.43) (Figure 2.6D).

DS34 – Unnamed granite: A white, coarsely crystalline granite (Figure 2.5C) that intrudes the gneissozed strata of the para-autochthon was sampled in the Dund Sharga Gorge (Figure 2.2). LA-ICPMS dates from 33 zircon cores and magmatic rims are 2900 ± 54 to 461 ± 17 Ma (Table 2.A2). 8 zircon grains were analyzed by CA-ID-TIMS method, with 2 fragments from one of the grains being analyzed. The 2 youngest dates are equivalent with a weighted mean of 507.07 ± 0.32 / 0.40 / 0.66 Ma (MSWD = 1.3, probability of fit = 0.25). Th/U ratios of these grains are < 0.1. The next oldest 3 dates are 508.21 ± 0.34 to 508.83 ± 0.35 Ma. The next oldest 4 dates are equivalent with a weighted mean of 509.56 ± 0.19 / 0.31 / 0.61 Ma (MSWD = 1.9, probability of fit = 0.13) (figures 2.7C and 2.A15; Table 2.A1).

U12001 – Biotite-granite gneiss in the Yesonbulag Fm: A biotite-granite gneiss (Figure 2.5C) was sampled south of the Gurvan Khairkhan Mountain, east of Khoid Sharga Gorge (Figure 2.2). The gneiss is lepido-granoblastic in texture and composed of microcline-perthite (30-35%), plagioclase (20-25%), quartz (25-30%), biotite (5-10%), and muscovite (< 5%). Microcline-perthite is subhedral to anhedral, weakly pelitizated, shows micro-poikiloblastic texture by inclusion of quartz, and hosts micrograins of plagioclase, and biotite. Plagioclase is often subhedral, altered to pelite and sericite, sometimes replaced by potassium feldspar displaying myrmekite texture, corroded by quartz, and includes quartz micro-poikiloblasts. Quartz is recrystallized and biotite is often replaced by muscovite (Figure 2.8G). LA-ICPMS dates from 18 zircon grains (cores and magmatic rims) are 1993 ± 58 to 465 ± 23

(Figure 2.A16, Table 2.A2). 3 of the 4 zircon grains analyzed by CA-ID-TIMS are equivalent with a weighted mean of 509.30 ± 0.42 / 0.49 / 0.72 Ma (MSWD = 1.3, probability of fit = 0.27). The other date is 510.11 ± 0.48 Ma (Figure 2.7D, Table 2.A1).

US11 – Unnamed biotite-hornblende-quartz diorite: A dark green biotite-hornblende-quartz diorite (mapped as middle Paleoproterozoic in age on geologic map by Togtokh (1995)) was sampled in Urd Sharga Gorge (Figure 2.2). It is hypidiomorphic granular in texture and composed of plagioclase (45-50%), hornblende (15-20%), biotite (10-15%), and quartz (10-15%). Plagioclase is subhedral, zonal, polysynthetically twinned, and sometimes deformed. Hornblende is euhedral to subhedral, and often replaced by actinolite, tremolite, chlorite and reddish brown biotite. Accesssory minerals are represented by titanite, apatite, zircon, and opaque minerals (Figure 2.8H). LA-ICPMS dates from 42 zircon grains are 541 ± 20 to 476 ± 18 Ma (Figure 2.A17, Table 2.A2). 39 dates are equivalent with a weighted mean of 496 ± 7 Ma (MSWD = 1.14, probability of fit = 0.25) (Figure 2.6E).

F1128B – Conglomerate in Teel Fm: A conglomerate was sampled along a major fault zone in the Khasagt Khairkhan Range along with sample F1128A (Figure 2.2). LA-ICPMS dates from 56 zircon grains are 3056 ± 28 to 474 ± 30 Ma (Figure 2.A18, Table 2.A3). Age peaks are at 550-450, 1050-800, 2100-1900, and 2550-2450 Ma (Figure 2.9).

F1128A – Unnamed granite: A pink granite was sampled along a major fault zone in the Khasagt Range (Figure 2.2). LA-ICPMS dates from 29 zircon grains are 445 ± 26 Ma and 372 ± 14 Ma. CA-ID-TIMS dates from 7 grains were analyzed (Figure 2.A19, Table 2.A2). The 6 youngest dates are equivalent with a weighted mean of 442.10 ± 0.19 / 0.28 / 0.54 Ma (MSWD = 1.5, probability of fit = 0.18). The other date is 443.07 ± 0.45 Ma (Figure 2.7E, Table 2.A1).

U1127-1 – Litharenite in the Teel Fm: A pale brown litharenite was sampled in the mouth of the Salaa Gorge (Figure 2.2). The sample is psammitic in texture and clast dominated (80-85%) that are composed of quartz (~ 0.5 mm; 75-80%), potassium feldspar (~ 0.4 mm; < 5%), micro-quartzite (5-10%), micas (< 0.3 mm; 1-2%), and limestone (5-10%) and are cemented by mostly carbonate (10-12%) and rarely hydrous ferric oxide and opaque minerals (2-3%) (Figure 2.8L). LA-ICPMS dates from 89 zircon

grains are 1698 ± 81 to 361 ± 20 Ma (Figure 2.A20, Table 2.A3). Only one zircon grain yielded a date younger than 432 ± 18 Ma; this needs to be analyzed by CA-ID-TIMS before giving it any significance. Age peaks are at 650-500 Ma and 900-750 Ma (Figure 2.9).

2.4. DISCUSSION

2.4.1. Tectonic significance of U-Pb zircon geochronology

2.4.1.1. Age constraints on magmatism and metamorphism

The age of the Zavkhan Terrane basement has long been considered to be ~ 1800 Ma from a bulk zircon fraction TIMS $^{207}Pb/^{206}Pb$ date from the Khavchig Complex (Burashnikov, 1990). We suggest that ~ 507 Ma metamorphic rims compromised the previous date and that our LA-ICPMS date of 1967 ± 13 Ma (Figure 2.6A) from zircon rims of Khavchig Complex gneiss is more accurate. This difference is significant because the basement was previously correlated with 1820 ± 27 Ma basement of the Baidrag Terrane (SHRIMP U-Pb zircon; Demoux et al., 2009a), which contributed to the assumption that the two terranes were one (for example Wilhem et al., 2012; Windley et al., 2007).

It was also previously unclear if the Altai Allochthon and the Zavkhan Terrane shared the same Proterozoic basement (Bold et al., 2016; Bucholz et al., 2014; Kozakov et al., 2012b); however, we show that diorite of the Dund-Orthocomplex intruded the Khavchig Complex (Figure 2.5F) and underlies the Yargait and Shandiinnuruu fms, which are depositionally overlain by the Zavkhan Fm. The Dund-Orthocomplex (Ruzhentsev and Burashnikov, 1996) consists of cogenetic massive intrusions of diorite (Figure 2.5H), gabbrodiorite, gabbro, and alkaline granite (Figure 2.5G) that are particularly well-exposed in the Khoid Sharga Gorge (Figure 2.5E) with mutually cross-cutting relationships. The CA-ID-TIMS date of 811.36 ± 0.24 Ma from the diorite (sample TS08, Figure 2.7A) is interpreted to reflect magmatism and crystallization of mingling mafic and felsic end-members of the Dund-Orthocomplex on the Zavkhan Terrane. In the Nomgon, Dund Sharga, and Urd Sharga gorges, the Dund-Orthocomplex directly feeds rhyolite domes and dolerite sills (figures 2.2 and 2.4). The overlying Shandiinnuruu Fm was defined based on more interbeds of volcanic rocks whereas the definition of the Yargait Fm was based on

prevalence of meta-sedimentary rocks (Togtokh, 1995). Recognizing that these units interfinger and represent lateral facies change rather than temporally discrete stratigraphic units, the entire volcanic strata and meta-sedimentary units above the Dund-Orthocomplex are lumped into the Yargait Fm (Figure 2.4). Hence, the autochthon and para-autochthon were conjoined by at least 811.36 ± 0.24 Ma. Detrital zircon data discussed below further demonstrate that overlap assemblages on the autochthon and para-autochthon have the same basement sedimentary sources (Figure 2.9).

On the para-autochthonous basement, two other orthogneiss samples have crystallization ages of 800 ± 19 Ma (sample US10, with a metamorphic zircon rim growth at 529 ± 22 Ma, Figure 2.6D) and 509.30 ± 0.42 Ma (sample U12001, Figure 2.7D). The 800 ± 19 Ma age provides another tie with the autochthon. On the contrary, the Buduun Fm gneiss on the autochthonous Zavkhan Terrane yielded a crystallization age of 839 ± 11 Ma (sample U1520, Figure 2.6B) and is intruded by undeformed granite and gabbroic dikes, potentially correlative with the Dund-Orthocomplex. Both the gneiss and the granite-gabbro intrusions are unconformably overlain by low-grade Cryogenian strata (Figure 2.3). These data suggest a metamorphic event in the northern portion of the Zavkhan Terrane between 839 ± 11 and 811.36 ± 0.24 Ma.

Rhyolites of the Zavkhan Fm have previously been dated between ~ 802–787 Ma (Bold et al., 2016). The tectonic setting of these volcanic rocks has been debated in the literature (Ilyin, 1990; Levashova et al., 2010; Ruzhentsev and Burashnikov, 1996); however, the zircon chemical composition of the Zavkhan Fm samples that we dated are consistent with an arc origin (Yang et al., 2012; Figure 2.A21). North of the Zavkhan River, the Zavkhan Fm is intruded by 770.31 ± 0.23 Ma alkaline granites (sample U1340A, Figure 2.7B), which have been interpreted to be rift-related based on whole-rock geochemistry (Yarmolyuk et al., 2008a). Therefore, we suggest that the 770.31 ± 0.23 Ma alkaline granites mark the beginning of rifting, which was responsible for the fault-bounded deposition of the Khasagt Fm sediments and potentially associated with the few tens of meters thick basaltic flows above the Zavkhan Fm in the Ulaanbulag Gorge (Figure 2.2).

Detrital zircon dates reveal a magmatic gap between ~ 750 and 580 Ma (Figure 2.9), which along with the Cryogenian to Ediacaran stratigraphic architecture (Bold et al., 2016), verify the development of a rifted passive margin. Dates between ~ 581 and 558 Ma, revealed in unnamed meta-sediments (sample DS05) in the south Dund Sharga Gorge, record arc magmatism in the Lake Terrane, whereas the youngest date of 533 ± 18 Ma in the siliciclastics of the Bayangol Fm (sample E1105-35.3) support arrival of the arc. Cambrian plutonism is present on the para-autochthon, where we dated a granite at 509.56 ± 0.19 Ma with a metamorphic zircon rim growth at 507.07 ± 0.32 Ma (sample DS34, Figure 2.7C). This granite intruded not only the 1967 ± 13 Ma Khavchig Complex, but also an 800 ± 19 Ma gneiss with a metamorphic zircon rim growth at 529 ± 22 Ma (sample US10), and a 509.30 ± 0.42 Ma gneiss (sample U12001). Thus, we suggest that ~ 509-507 Ma granites are syn-orogenic. Metamorphic grade decreases rapidly to the north with greenschist metamorphism and tight folding south of the fault (#2, Figure 2.2) separating the Yargait Fm from the weakly folded Tsagaan Olom Group.

In addition to massive diorite and granodiorite plutons of the Dund-Orthocomplex, smaller plugs of diorite are present in the southern portion of the Zavkhan Terrane (Figure 2.2). Previously, these were all mapped as part of the Dund-Orthocomplex; however, we have demonstrated that at least some of these are Cambrian (496 ± 7 Ma (sample US11, Figure 2.6E)). These intrusions lack the gneissic fabric present in the Yesonbulag Fm granite-gneiss and tightly constrain the age of metamorphism in the para-autochthonous region to between 507.07 ± 0.32 and 496 ± 7 Ma.

The age of the Numrug Complex is now constrained at 442.10 ± 0.19 Ma (sample F1128A, Figure 2.7E). This is associated with Upper Ordovician to Silurian extensional tectonism responsible for forming grabens that are filled with bimodal volcanism and sedimentary strata of the Teel Fm (Kilian et al., in preparation).

2.4.1.2. Age constraints on faulting

With better geologic and geochronologic characterization of the main lithostratigraphic units of the Zavkhan Terrane, the major structures can now be discussed in more detail with greater confidence.

The para-autochthonous basement of the Zavkhan Terrane is bound to the south by a large fault (#1, Figure 2.2) that separates Khavchig Complex gneiss to the north with undifferentiated meta-volcano-sedimentary unit (sample DS05) to the south. The few zircon grains retrieved from DS05 yielded dates of ~ 581-558 Ma (Table 2.A3), which are indistinguishable from plagiogranites dated in both the Dariv and Khantaishir ophiolites (Khain et al., 2003) of the Lake Terrane. We suggest these units are distal foreland equivalent to the Terreneuvian foreland on the Zavkhan Terrane, but more dominated by sedimentary sources from the upper plate, whereas the foreland on the autochthon received most of its sediment from the autochthon. To the west of the Urd Sharga Gorge, north of fault #1, a Paleozoic alkaline granite intrudes the Khavchig Complex gneiss. However, a strip of the Middle Devonian Tsagaanshoroot Fm is present along the fault zone, which suggests that although this structure defines a Cambrian suture, it was reactivated sometime after the Middle Devonian.

In the Dund Sharga, Khoid Sharga, and Nomgon gorges, a major fault (#2, Figure 2.2) separates tightly folded metasedimentary and volcanic rocks of the Yargait Fm with broadly folded Cryogenian to Terreneuvian strata and unfolded Silurian Numrug Complex granite. Fold axes are oriented E-W, broadly parallel with this fault and do not appear to affect Ordovician to Silurian units. Thus, we suggest that this fault and the associated folds in the region are Cambrian in age and that this structure was reactivated sometime during or after the Silurian (Figure 2.10). Further to the northwest, in the Undur-Ulaan Mountain area, this fault zone splays into series of faults in older units, and thus does not provide additional age control (Figure 2.2). This fault is broadly aligned with high-angle ESE-WNW structures that locally have sinistral offset.

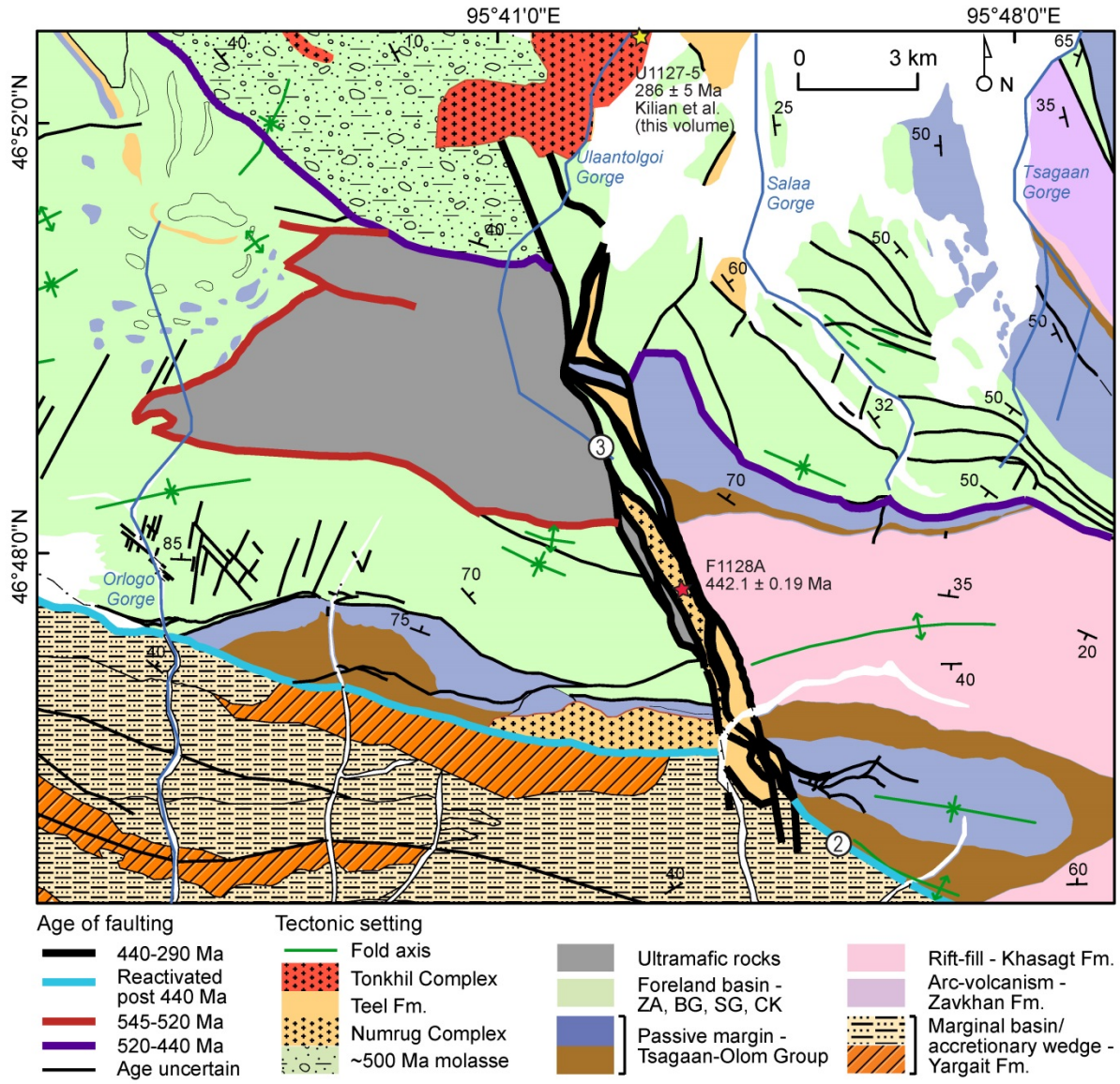

Figure 2.10. Detailed geologic map of central Zavkhan Terrane depicting age of faulting
Tectonic setting of the units is described. Description of lithology is outlined in figures 2.2 and 2.4. ZA – Zuun-Arts, BG – Bayangol, SG – Salaagol, and CK – Khairkhan fms.

An 11 km long and 5 km wide ultramafic nappe is present on top of the Khairkhan Fm to the NW of the Khasagt Khairkhan Range (Figure 2.10). This ophiolite fragment likely originated from Khantaishir-Dariv arc and was overthrusted onto the Zavkhan Terrane (potentially along fault #3) during the accretion of the Lake Terrane (Ruzhentsev and Burashnikov, 1996) in the Terreneuvian. This interpretation is supported by the presence of clasts of ultramafic rocks within the mélange of the Khairkhan Fm (Smith et al., 2015).

ESE-WNW to E-W high angle faults with sinsistral offset are common on the Zavkhan Terrane. In the Khukh Davaa region and SW of Khukh Davaa, these faults are accompanied by a NNW-SSE conjugate set of normal faults, which define narrow transtensional pull-apart basins that accommodate the Teel Fm (Figure 2.2). West of the Khasagt Khairkhan Range and Shivee Tsakhir Mountain a NNW-SSE fault displaces the early Silurian Numrug Complex granite (sample F1128A, Figure 2.7E), Taishir Fm carbonates, serpentinized ultramafic rocks, and red beds of the Teel Fm (#3, figures 2.2 and 2.10). Displacement on this fault is consistent with down to the east transport with a component of sinistral dip-slip movement. To the east of this fault, folds with E-W oriented axes in the Khasagt Fm and Tsagaan-Olom Group are truncated. On the western side of this fault, the Terreneuvian thrust fault at the base of the ultramafic rocks and a Cambrian to Ordovician conglomerate unit are truncated (Figure 2.10). The northwestern continuation of this fault is stitched by the Permian alkaline granite of the Tonkhil Complex exposed in the Ulaantolgoi Gorge that was dated at 286 ± 5 Ma (Kilian et al., in preparation). This map relationship constrains movement on this NNW-SSE fault between ~ 442 and 286 Ma (Figure 2.10), but regionally, the close association of the NNW-SSE structures and deposition of the Teel Fm in en echelon transtensional pull-apart basins suggests these faults were active during the Late Ordovician to Silurian. It is unclear if the ESE-WNW to E-W high angle faults were later reactivated.

2.4.2. Relationship to neighboring Proterozoic cratonic fragments of Mongolia

It has been previously assumed that the Proterozoic terranes of Mongolia originated from the same parent craton. While the Zavkhan Terrane may have similar Proterozoic basement ages and Neoproterozoic overlap assemblages with the Tuva-Mongolia terranes, our data suggest distinct differences between the basement ages of the Baidrag Terrane and other terranes to the south (Figure 2.11).

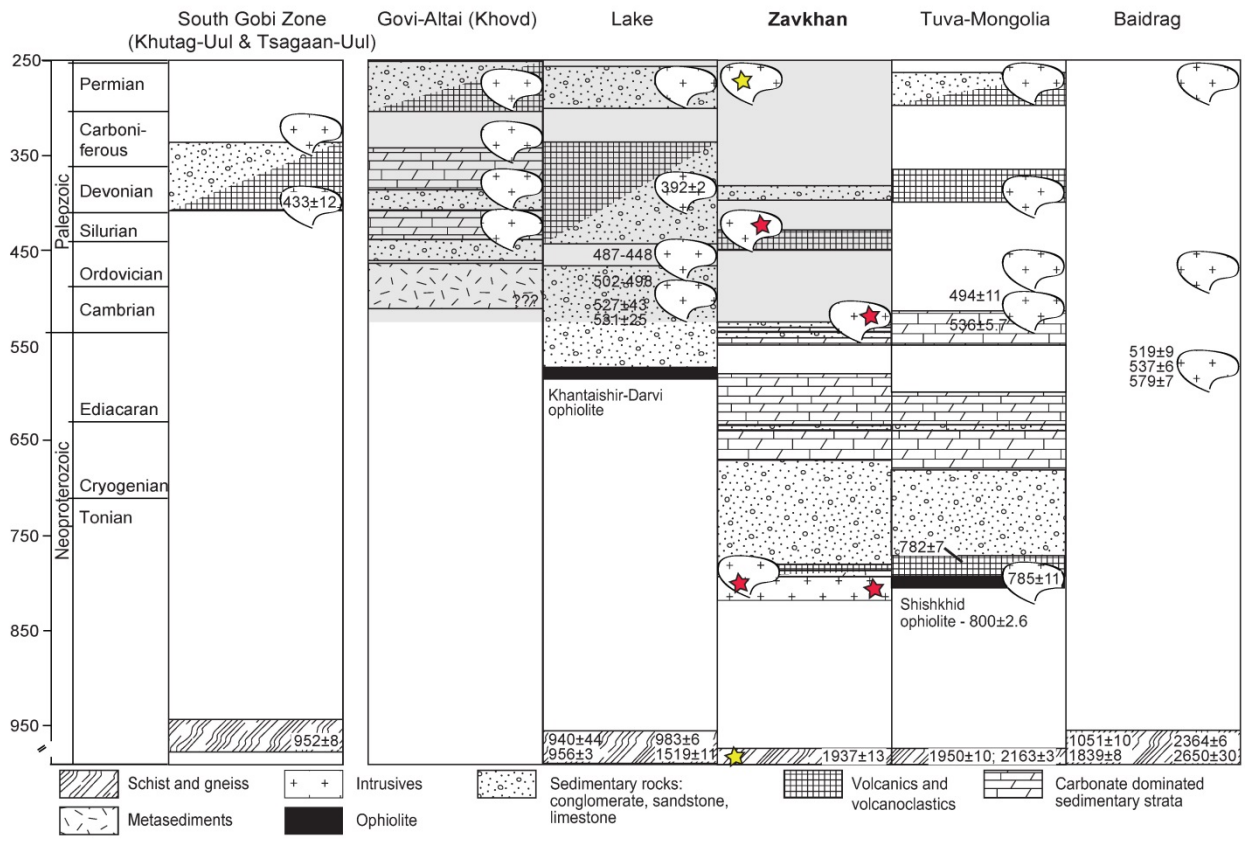

Figure 2.11. Geology of the neighboring terranes of the Zavkhan Terrane in southwestern Mongolia Basic geologic description was after Badarch et al. (2002). Stratigraphic levels of the samples included in this study are labeled after Figure 2.2. Recently published magmatic ages are labeled. South Gobi Zone (Khutag-Uul and Tsagaan-Uul terranes (Badarch et al., 2002)) - Yarmolyuk et al. (2005); Lake Terrane - Demoux et al. (2009c), Soejono et al. (2016), and Yarmolyuk et al. (2011); Zavkhan Terrane – this study; Tuva-Mongolia - Khain et al. (1995), Kuzmichev et al. (2005b), and Kuzmichev and Larionov (2011); Baidrag - Demoux et al. (2009a).

Crystalline basement of the Tuva-Mongolia terranes (Dergunov, 2001), which include the Sangelin, Hug, Darhad, and Gargan terranes of northern Mongolia (Badarch et al., 2002), has been dated in the eastern Sayan Range of Russia with U/Pb TIMS on multi-grain bulk zircon fractions between 2163 ± 3 and 1950 ± 10 by (Khain et al., 1995). The oldest ophiolitic sequence documented in Mongolia, the Shishkhid ophiolite, is also part of this region and is overlain by a rhyolite flow that was dated with U-Pb SHRIMP on zircon at 800 ± 3 Ma (Kuzmichev et al., 2005a). The authors interpreted this ophiolite to have formed in a supra-subduction zone setting and to have collided with Tuva-Mongolian continental crust during the late Neoproterozoic. Magmatism related to obduction of Dunzhugar island arc with the Gargan Terrane was also dated with U/Pb TIMS on multi-grain bulk zircon fractions at 785 ± 11 Ma

(Kuzmichev et al., 2001), and active continental margin volcanism of the Sarkhoi Group was dated with U-Pb SHRIMP on zircon at 782 ± 11 Ma (Kuzmichev and Larionov, 2011). The ~ 800-770 Ma Sarkhoi Group can be correlated with the Zavkhan Fm on the Zavkhan Terrane (Kuzmichev and Larionov, 2011). Moreover, the overlying Cryogenian glacial diamictites and Neoproterozoic to Cambrian carbonate strata and phosphorite deposits on the Khuvsgul Terrane (Figure 2.11) can be correlated almost unit-for-unit with Neoproterozoic strata on the Zavkhan Terrane (Macdonald and Jones, 2011). Neoproterozoic to Cambrian strata on the Khuvsgul Terrane are also intruded by Series 3-Furongian syn- and post-metamorphic felsic magmatic rocks (Kozakov et al., 1999; Salnikova et al., 2001) and middle to late Paleozoic subalkaline granitic plutons (Badarch et al., 2002).

Basement gneisses of the Baidrag Terrane were dated at 2650 ± 30 and 1854 ± 5 Ma (Badarch et al., 2002) and 2364 ± 6, 1839 ± 8, and 1051 ± 10 Ma (Demoux et al., 2009a). It has been suggested that the basement is overlain by Neoproterozoic metasediments (Teraoka et al., 1996), but these are from the Bayankhongor accretionary zone, and no Neoproterozoic overlap assemblage comparable to that on the Zavkhan Terrane has been documented. In addition, Demoux et al. (2009a) and Kozakov et al. (2012a) dated magmatism in the northeastern part of the Baidrag Terrane at ~ 579-537 Ma that is interpreted to have been related to closure and subduction of the Bayankhongor Ocean to the SW (Buchan et al., 2001). Metamorphism and magmatism of this age is absent on the Zavkhan Terrane.

Further south, near the border with China, the South Gobi Zone (Kröner et al., 2010) includes Proterozoic basement of the Tsagaan-Uul and Khutag-Uul terranes (Badarch et al., 2002) and hosts basement gneisses that are dated at 952 ± 8 (Yarmolyuk et al., 2005) and 916 ± 16 Ma (Wang et al., 2001). The gneisses are overlain by Carboniferous and Permian volcano-sedimentary strata and Permian marine sedimentary rocks and are intruded by Carboniferous through Lower Cretaceous magmatic rocks (Badarch et al., 2002). Both the basement ages and overlap assemblages have no counterparts in the Zavkhan Terrane except for Permian magmatic rocks (Figure 2.11). However, the ~ 950 Ma basement ages are similar to those in the Gurvan Bogd Mountains of the Lake Terrane (Demoux et al., 2009c).

2.4.3. Detrital zircon provenance of the Zavkhan Terrane

Detrital zircon provenance of Neoproterozoic strata on the Zavkhan Terrane were reported by Bold et al. (2016), including data from a quartzite clast from the Zavkhan Fm cobble conglomerate and sandstones from middle Zavkhan, Maikhan-Uul, and Shuurgat fms. The comparison did not reveal a perfect match with any of the neighboring terranes such as Siberia, Tarim, North China, and NE Gondwana (Rojas-Agramonte et al., 2011), which suggested that the detrital population of the Zavkhan Terrane is locally derived from the underlying basement and it may have its own distinctive late Neoproterozoic characteristics, consistent with the interpretation that the Zavkhan Terrane was an independent ribbon continent at this time.

Additional detrital zircon data presented here are from the previously under-sampled Paleozoic strata in the Zavkhan Terrane (Figure 2.9). In Figure 2.12, probability density plots from sedimentary successions on the Zavkhan Terrane are compared to data from other terranes with the plots divided into Precambrian and Paleozoic successions to help reduce bias in interpretation resulting from re-sedimentation. The dominant populations in Precambrian samples (Figure 2.12B) are at 2800-2400 Ma (peak of 2500 Ma), 2300-1800 Ma (peak of 2050 Ma), and 900-700 Ma (peak of 800 Ma). An additional population of 550-450 Ma zircon grains (peak of 500 Ma) appears in Paleozoic samples. On the other cratons considered, the 2800-2400 Ma population is present in North China (Rojas-Agramonte et al., 2011; Xia et al., 2006), possibly in Tarim (Han et al., 2015; Rojas-Agramonte et al., 2011; Zhang et al., 2013), and in NE Gondwana (Rojas-Agramonte et al., 2011). The 2300-1800 Ma population is present in all of the cratons (Letnikova et al., 2013; Powerman et al., 2015; Rojas-Agramonte et al., 2011) except in North China. However, the 900-700 Ma population resembles only that the Tarim Craton, which includes the Aksu blueschist terrane that has been interpreted to have formed along an active continental margin (Zhu et al, 2011). Moreover, the Tarim experienced magmatism at ~ 2500 Ma and metamorphism at ~ 1900 Ma age peaks that are also present in the detrital zircon spectra of the Zavkhan Terrane (Figure 2.12B). Although the basement comparison is not perfect, the best fit for the Zavkhan Terrane in the

Precambrian appears to be the Tarim Craton, which can be tested with additional geochronologic and paleomagnetic studies.

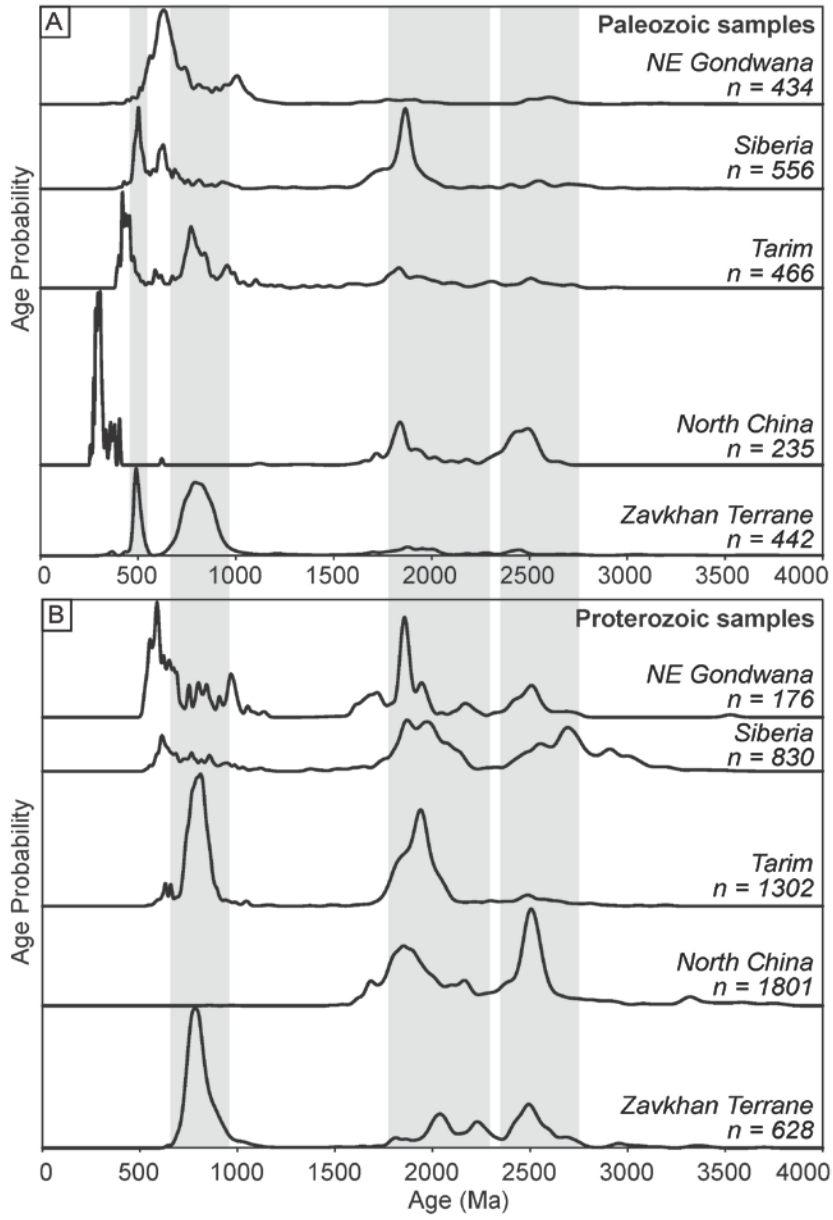

Figure 2.12. Detrital zircon provenance for the Zavkhan Terrane
A) Normalized probability plots of the Paleozoic samples preserved in NE Gondwana (Kolodner et al., 2006), Siberia (Gladkochub et al., 2013; Glorie et al., 2014), Tarim (Han et al., 2015), and North China (Li et al., 2009; Yang et al., 2006). B) Normalized probability plots of the Precambrian successions. The plots were constructed using previous compilations by Rojas-Agramonte et al. (2011) in addition to Powerman et al. (2015) and Letnikova et al. (2013) for Siberia, Han et al. (2015) for Tarim, and Xia et al. (2006) for North China.

For the Paleozoic comparison, recently published detrital zircon data from North China (Li et al., 2009; Yang et al., 2006), Tarim (Han et al., 2015), southern Siberia (Gladkochub et al., 2013; Glorie et

al., 2014), and NE Gondwana (Kolodner et al., 2006), allow for a more robust comparison (Figure 2.12A). A resemblance to the youngest major peak of Mongolia at ~ 500 Ma is present in southern Siberia related to the Kalar and Onkolokit granitoids, which intruded through the suture between the Baikal-Muya Terrane and Siberia (Powerman et al., 2015) and 520-490 Ma collisional magmatism in the Gorny Altai Terrane (Dobretsov et al., 2003). This magmatism and metamorphism occurred in response to Ediacaran and Cambrian collision of microcontinents, including the Tuva-Mongolia terranes, to the southern Siberian margin (Dobretsov and Buslov, 2007). Our detrital zircon data are consistent with this scenario.

2.4.4. Tectonic model

The newly obtained geochronologic constraints and field observations, including those from the para-autochthonous region, have allowed us to propose an updated tectonic model for the Zavkhan Terrane. The model spans the Neoproterozoic through early Paleozoic and is supported by map relationships, U-Pb zircon geochonologic constraints (Figure 2.11), available whole-rock geochemical data on the magmatic samples (Levashova et al., 2010; Yarmolyuk et al., 2008a), and new paleomagnetic constrains (Kilian et al., in preparation).

2.4.4.1. Tonian – Arc magmatism and subduction of a spreading-ridge

Detrital zircon spectra from sedimentary rocks on the Zavkhan Terrane lack grains between ~ 1800 and 850 Ma. In the northern portion of the Zavkhan Terrane, undeformed granite and gabbroic dikes potentially correlative with the Dund-Orthocomplex intrudes 839 ± 11 Ma gneiss of the Buduun Fm. This relationship suggests a metamorphic event in the northern portion of the Zavkhan Terrane between 839 ± 11 and 811.36 ± 0.24 Ma. Although the nature of this metamorphic event remains enigmatic, based on the zircon chemical compositions (Figure 2.A21), we suggest it marks the initiation of continental arc volcanism on the Zavkhan Terrane.

Mixed volcanic and siliciclastic strata of the Yargait Fm were deposited as a marginal basin fill above the 811.36 ± 0.24 Ma core of the Dund magmatic arc (Figure 2.13A-1), either as an intra- or back-

arc basin. The Yargait Fm is potentially correlative with the Oka prism of the Tuva-Mongolia terranes, which has alternatively been interpreted to represent an accretionary wedge related to accretion of the pre-800 ± 3 Ma Shishkhid ophiolite (Kuzmichev et al., 2007). Nonetheless, due to continued subduction to the NE (in present coordinates), arc-related volcanism persisted to at least ~ 787 Ma (the Zavkhan Formation volcanics, Bold et al., 2016). Alkaline granites dated at 770.31 ± 0.23 Ma (Figure 2.13A-2) with geochemistry consistent with an intra-plate setting (Yarmolyuk et al., 2008a) are consistent with rifting at this time. Additionally, terrestrial sedimentary successions of the Khasagt Fm were deposited between ~ 787 and 717 Ma in narrow, fault-bounded basins succeeded by ~ 717-580 Ma rifted passive margin sedimentation of the Tsagaan-Olom Group (Bold et al., 2016). That is, between 787 and 717 Ma, the Zavkhan Terrane was transformed from an active continental arc into a ribbon continent with two passive margins. We propose that the subduction of a spreading-ridge (Cole and Stewart, 2009) can explain ophiolite obduction, Neoproterozoic magmatic and stratigraphic patterns, and the development of a ribbon terrane.

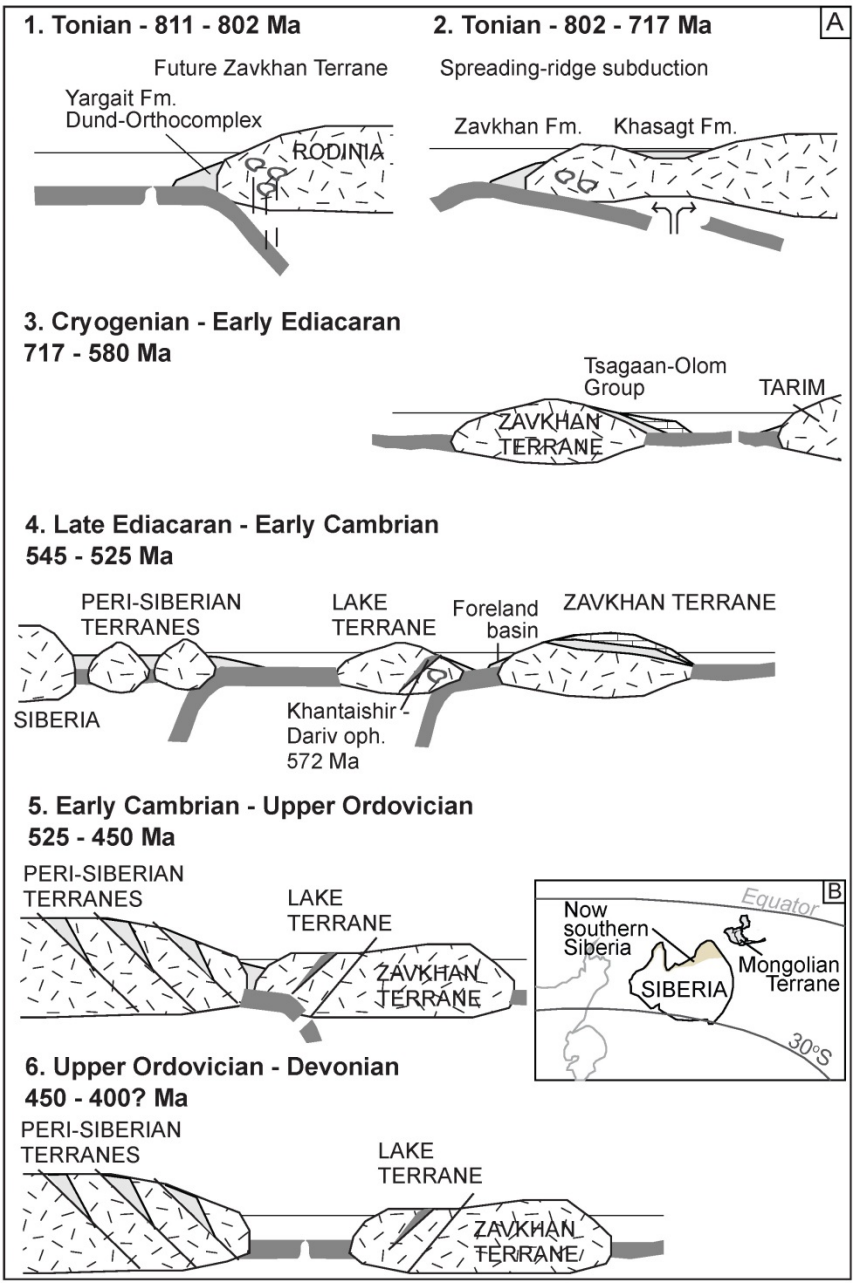

Figure 2.13. Neoproterozoic to early Paleozoic tectonic model of the Zavkhan Terrane
A) Schematic cross-section of the major tectonic events occurred between 811-400? Ma. B) Configuration of the Siberian Craton and the composite Mongolian terrane (Zavkhan and Lake terranes along with the Tuva-Mongolia terranes) in the Terreneuvian, modified from Kravchinsky et al. (2010).

2.4.4.2. Cryogenian to early Ediacaran – Passive margin

Passive margin sedimentation (Figure 2.13A-3) of the Tsagaan-Olom Group hosts deposits from both the Sturtian and Marinoan global Cryogenian glaciations along with their respective cap carbonates

in the Cryogenian Maikhan-Uul, Taishir, and Khongor fms, and the Ediacaran Ol and Shuurgat fms (Figure 2.4; Bold et al., 2016; Macdonald et al., 2009a; Rooney et al., 2015). A gap in sedimentation, evidenced by karsted surface at the top of the Shuurgat Fm that marks an unconformity of ~ 40 Myr, is inferred from geochemical correlations (Bold et al., 2016; Macdonald et al., 2009a). In the neighboring Baidrag Terrane (Figure 2.1B), ~ 579-537 Ma magmatism and metamorphism (Demoux et al., 2009a) has been associated with the Neoproterozoic closure of the Bayankhongor Ocean (Buchan et al., 2001). Magmatism and metamorphism of this age have not been identified on the Zavkhan Terrane, suggesting that the Baidrag and Zavkhan terranes were still separate during the late Ediacaran. Alternatively, the ~ 40 Myr late Ediacaran hiatus on the Zavkhan Terrane may be the result of the collision between the two. In the hinterland, plagiogranite in supra-subduction zone ophiolites of the Dariv and Khantaishir ranges (Khain et al., 2003) in the Lake Terrane were dated at ~ 572 Ma (Khain et al., 2003); however, timing for obduction of this arc is estimated to have occurred by 540-525 Ma (Štípská et al., 2010), which is much later than observed sedimentary hiatus on the Zavkhan Terrane, but correlates well with foreland deposition in the Zuun-Arts, Bayangol, Salaagol, and Khairkhan fms (Macdonald et al., 2009a; Smith et al., 2015).

2.4.4.3. Late Ediacaran to Terreneuvian – Peripheral foreland basin formation and accretion with the Lake Terrane

The next stage of sedimentation on the Zavkhan Terrane is related to late Ediacaran to Terreneuvian foreland basin formation, starting at ~ 545 Ma, that accomodated mixed siliciclastic and carbonate strata of the Zuun-Arts, Bayangol, Salaagol, and Khairkhan fms until ~ 525 Ma (Smith et al., 2015). We propose that these strata were deposited in a peripheral foreland that formed in response to SW-dipping subduction and flexure of the slab as the Zavkhan Terrane collided with the arc and supra-subduction ophiolites of the Lake Terrane (Figure 2.13A-4). In our model, the foreland basin is suggested to have closed by arc obduction at ~ 525 Ma, which is supported by detailed stratigraphic and paleontological constraints (Smith et al., 2015), the youngest detrital zircon date of 533 ± 18 Ma in the

siliciclastics of the Bayangol Fm (sample E1105-35.3), granitoid magmatism dated in Bumbat-Khairkhan area of the Lake Terrane at 551-524 Ma (Rudnev et al., 2012), and ^{40}Ar-^{39}Ar date on a muscovite from eclogite with the accretionary prism of this subduction zone between 548-537 Ma (Štípská et al., 2010). This contrasts with earlier models that called for later obduction until ~ 470 Ma (Dijkstra et al., 2006; Jian et al., 2014; Kovach et al., 2011; Rudnev et al., 2012; Yarmolyuk et al., 2011).

2.4.4.4. Terreneuvian to Upper Ordovician – Accretion to peri-Siberian realm

After the closure of the foreland basin and arrival of the Lake Terrane, 509.56 ± 0.19 and 509.30 ± 0.42 Ma syn-metamorphic magmatic rocks with metamorphic rims of 507.07 ± 0.32 Ma are intruded by and post-deformation 496 ± 7 Ma gabbroic dikes and sills. We suggest that the ~ 509-507 Ma magmatism and metamorphism represents a collisional event that occurred after slab break-off and reversal (Figure 2.13A-5). Similar ages of magmatism and metamorphism were reported from the southern margin of Siberia, and are further supported by our detrital zircon provenance constraints of a major peak at ~ 500 Ma (Figure 2.12A) (Dobretsov and Buslov, 2007; Glorie et al., 2014).

2.4.4.5. Upper Ordovician to Silurian – Separation from Siberia

The bond between the Mongolian terranes and Siberia was not strong and did not last long. Upper Ordovician to Silurian rift-related magmatism and sedimentation in narrow transtensional grabens are consistent with a major extensional event on the Zavkhan Terrane. Moreover, to the south on the Gobi-Altai terrane, a Silurian passive margin sequence developed, consistent with the formation of an open margin and late Paleozoic ocean basin (Kröner et al., 2010; Lehmann et al., 2010).

Yarmolyuk et al. (2011) proposed that 470-440 Ma subalkaline high-Ti basalt, alkaline-ultrabasic complexes, nepheline syenites, alkaline granites, and granosyenites in the Lake Terrane are associated with a large igneous province. Alternatively, Soejono et al. (2016) suggested that 459.1 ± 1.8 Ma gabbrodiorites in the western Lake Terrane are arc related. We document Upper Ordovicain to Silurian deposition on the Zavkhan Terrane in sinistral transtensional pull-apart basins associated with bimodal volcanism (Kilian et al., in preparation), and granite magmatism of Lower Ordovician Numrug Complex

of the Zavkhan Terrane. Kilian et al. (in preparation) also demonstrate that Upper Ordovician volcanics of the Teel Fm of the Zavkhan Terrane were emplaced at a subtropical paleolatitude (19.5º +/- 5.2º). This result is consistent with an association of the terrane with Siberia in the Ordovician; however, a Paleozoic low-latitude overprint suggest subsequent separation given that Siberia continued to travel to north (Cocks and Torsvik, 2007). Thus, it is clear that Upper Ordovician to Silurian magmatism and deposition on the Lake and Zavkhan terranes was related to extension or transtension, but it remains to be seen if this magmatism was driven by back arc extension or intraplate rifting.

Multiple collisions between the Mongolian terranes and Siberia has been previously proposed (Tomurtogoo, 2005; Zorin, 1999), but associated with the opening and closure of the Mongol-Okhotsk Ocean behind a peri-Siberian arc. Dobretsov and Buslov (2007) suggested that northward movement of the Siberian Craton initiated the opening of the Uralian and Mongol-Okhotsk oceans. Instead, *Sengör et al.* (1993) proposed that the western and northern regions of Precambrian basement of Mongolia accreted to Siberia in the early Paleozoic and the eastern and central regions of Mongolia accreted in the middle to late Paleozoic (e.g. Lehmann et al., 2010).

Although many studies link the Mongolian terranes with Siberia based on early Paleozoic paleontological and geological ties (for example Kuzmichev and Larionov, 2011; Sengor and Natal'in, 1996; Tomurtogoo, 2005), early Paleozoic stratigraphic, metamorphic, and magmatic belts are truncated by high-angle faults against the Siberian margin, suggestive of later displacement.

2.4.4.6. Devonian to Carboniferous – Renewal of arc magmatism and accretionary tectonics

During the Devonian, a volcanic arc formed on the southern margin of the composite Mongolian terranes (for example Badarch et al., 2002; Demoux et al., 2009b; Guy et al., 2015; Kröner et al., 2010; Lamb and Badarch, 1997). The tectonic driver that transformed the Silurian passive margin to a Devonian active margin, referred to as the 'Tsakhir event', remains uncertain (Gibson et al., 2013b). Devonian to Carboniferous magmatism and deformation on the Mongolian terranes have been broadly attributed to accretionary processes (for example Kröner et al., 2010; Lamb and Badarch, 2001). Late Paleozoic

accretion is consistent with the southwestern progression of magmatism: Devonian and Permian magmatic rocks are present in the Lake Terrane (e.g. Badarch et al., 2002; Soejono et al., 2016); Carboniferous and Permian magmatic rocks are present in the Gobi-Altai Terrane (including the Khovd Terrane; Figure 2.11) (Kröner et al., 2010; Zacek et al., 2016); and Permian to Lower Cretaceous magmatic rocks are present in the South Gobi Zone (Badarch et al., 2002).

2.4.5. Comparison with previous models, and paleontological and paleomagnetic constraints

As outlined in the introduction, there are currently three broad classes of models for the Neoproterozoic to Paleozoic tectonic evolution of Mongolia: 1) a *peri-Siberian arc model* (for example Cocks and Torsvik, 2007; Sengör et al., 1993; Tomurtogoo, 2005; Wilhem et al., 2012), 2) a *collisional model of Gondwanan terranes* (for example Kröner et al., 2014; Kröner et al., 2010; Mossakovsky et al., 1994; Rojas-Agramonte et al., 2011), and 3) *an accretionary growth model* (for example Badarch et al., 2002; Windley et al., 2007). The data presented here is most consistent with the *collisional model of Gondwanan terranes*; however, there are some key differences with previous tectonic models and intervals in which both a single arc and accretionary tectonics play prominent roles. Particularly, although our data suggest that the Proterozoic basement of the Zavkhan Terrane is exotic to Siberia and perhaps originated from near the Tarim Craton, we propose that the Zavkhan and other terranes amalgamated and formed a composite arc terrane in the Ediacaran and Terreneuvian before colliding with Siberia in the Cambrian Series 2-Series 3, and then rifted away from Siberia in the Ordovician forming a ribbon continent that experienced an independent phase of accretion during the late Paleozoic before colliding with Siberia again during the Mesozoic (Kilian et al., in preparation; Van der Voo et al., 2015).

The scenario outlined above is consistent with recent paleomagnetic data. Particularly, paleomagnetic studies on the Neoproterozic Zavkhan Fm have yielded paleolatitudes more consistent with Gondwanan terranes such as Tarim than Siberia (Levashova et al., 2010). Yet, early Paleozoic paleopoles are consistent with the Zavkhan Terrane being near Siberia (Kilian et al., in preparation;

Kravchinsky et al., 2010), and late Paleozoic data suggest the Zavkhan Terrane was at low-latitude when Siberia was at high latitude (Kilian et al., in preparation).

Paleontological data are also consistent with our tectonic model. Although no trilobites have been described from the Zavkhan Terrane, Terreneuvian trilobites from the Khuvsgul Terrane (Korobov, 1980, 1989) are distinct from Siberian trilobites and those of terranes to the northwest (Álvaro et al., 2013). The presence of Ordovician to Silurian corals and the low diversity Silurian *Tuvaella* brachiopod in Mongolia are consistent with a Furongian to Silurian connection to peri-Siberia (Ulitina et al., 2009); however, although the distinctive *Tuvaella* brachiopod is found throughout southern and northeastern Mongolia and terranes to the northeast, it is not present on the Siberian craton (Wang et al., 2011). Moreover, Ordovician brachiopod assemblages from the Mongolian terranes and Siberia diverge after the Ordovician (Harper et al., 2013). Early and Middle Devonian brachiopods in the Mongolian terranes are different from those occurring in Siberia, North China, and South China (Alekseeva et al., 2001; Blodgett et al., 2002; Hou and Boucot, 1990), and Devonian crinoids in southern Mongolia are most similar to European and North American fauna (Webster and Ariunchimeg, 2004).

2.4.6. Implication for crustal growth in the CAOB

Orogenic belts are commonly distinguished as either accretionary or collisional (e.g. Brown et al., 2011). Collisional orogeny invokes collision of buoyant continents, whereas the accretionary tectonism explains formation of mountain belts above subduction zones (Schulmann and Paterson, 2011). Although we agree that the evolution of the CAOB was complex and it involved both of the above, we suggest that distinct tectonic settings were responsible for episodic crustal growth and recycling.

Crustal growth has been previously attributed to magmatism in both intraplate or convergent margins (Rudnick, 1995). Recently, Hanzl et al. (2016) suggested an alternative model that involves syn-tectonic magmatism through orogen-scale shortening and used this mode to account for extensive Devonian metamorphism in southeast Mongolia. We suggest that accretionary crustal growth occurred around the Mongolian basement terranes during the Ediacaran to Cambrian Series 3 and in late Paleozoic

while they were independent crustal fragments or ribbon continents. These terranes were later trapped and oroclinally duplexed between the Siberian, Tarim, and North China cratons and incorporated into the CAOB. As this region appears to be a prime candidate for future cratonization, we suggest that accretion around continental fragments and ribbon continents and later oroclinal bending and trapping between larger cratons is a viable framework for net crustal growth.

2.5. CONCLUSIONS

The Zavkhan Terrane is one of the Proterozoic cratonic fragments in southwestern Mongolia that make up the core of the CAOB. The Khavchig Complex gneiss, which forms the basement of the Zavkhan Terrane, was dated at 1967 ± 13 Ma with inherited cores as old as 2469 ± 27 Ma. After a magmatic hiatus of over one billion years, the Zavkhan Terrane was intruded by 839 ± 11 Ma granite, which is present as gneiss of the Buduun Fm. Both the Khavchig Complex and the Buduun Fm are intruded by 811.36 ± 0.24 Ma arc-related intrusions of Dund-Orthocomplex that lack a gneissic fabric, suggestive of a Tonian metamorphic event. The Dund-Orthocomplex is overlain by ~ 811-787 Ma arc-volcanic and volcaniclastic rocks of the Yargait and Zavkhan fms. The beginning of rifting is marked by alkaline magmatism dated at 770.31 ± 0.23 Ma, and is followed by sedimentation of the Khasagt Fm in narrow rift grabens from 770 to 717 Ma and passive margin sedimentation of the Tsagaan-Olom Group between 717 and 580 Ma. The southern margin of the Zavkhan Terrane was reactivated with the obduction of the Lake Terrane and the development of a late Ediacaran to Terreneuvian peripheral foreland basin. After this arc-ribbon continent collision, Cambrian slab break-off and reversal led to the renewal of magmatism on the Zavkhan Terrane, which was by this time embedded in a composite Mongolian terrane. Zircon from the Khavchig Complex have metamorphic rims dated at 529 ± 22 Ma and are intruded by 509.30 ± 0.42 Ma granite-gneiss of Yesonbulag Fm and 509.56 ± 0.19 Ma unnamed granite, which has a metamorphic zircon rim growth dated at 507.07 ± 0.32 Ma. The succession of ages and a rapid lateral metamorphic gradient are suggestive of Series 2-Series 3 syn-orogenic magmatism. These units are cut by undeformed 496 ± 7 Ma mafic dikes and sills, providing a tight constraint on the

age of Cambrian metamorphism. An Upper Ordovician to Silurian rifting event is marked by bimodal magmatism and deposition in narrow pull-apart basins, and by alkaline granite intrusions dated at 442.10 ± 0.19 Ma.

In our proposed tectonic model, we suggest that the Zavkhan Terrane travelled alone for much of the Neoproterozoic, collided with Siberia during Cambrian Series 2-Series 3, rifted away during the Ordovician as part of a larger ribbon continent, and became an active margin in the Paleozoic. Much of the crustal growth around the Mongolian terranes occurred during the Ediacaran-Terreneuvian and late Paleozoic, while they were independent crustal fragments or ribbon continents. This is distinct from models of crustal growth in the CAOB that invoke direct accretion on the margin of a large craton, and suggests instead that the trapping of crustal fragments and ribbon continents between larger cratons may be an effective mechanism of cratonization.

2.6. ACKNOWLEDGMENTS

We would like to thank our field assistants Gerelt Sarantuya, Javzandulam Chuluunbaatar, Munkh-Erdene Delger, Munkh Jugder, Uchral Khuchitbaatar, Otgonbayar Dandar, Ariunsanaa Dorj, Odbayar Erdenebat, Dan Bradley, Tanya Petach and Sarah Moon; Nicholas Swanson-Hysell and Taylor Kilian for insightful comments and discussions; and MIT NAI node for support.

2.7. REFERENCES

Alekseeva, R., Afanasjeva, G., and Shishkina, G., 2001, Lower and Middle Devonian brachiopods of the Far East of Russia and Mongolia: strophomenids and chonetids: Trudy Palaeontological Institute, Russian Academy of Sciences, v. 281, p. 1-132.

Álvaro, J. J., Ahlberg, P., Babcock, L. E., Bordonaro, O. L., Choi, D. K., Cooper, R. A., Ergaliev, G. K., Gapp, I. W., Pour, M. G., and Hughes, N. C., 2013, Global Cambrian trilobite palaeobiogeography assessed using parsimony analysis of endemicity: Geological Society, London, Memoirs, v. 38, no. 1, p. 273-296.

Atashkin, V. A., 1995, The Cambrian system of the foldbelts of Russia and Mongolia: correlation chart and explanatory notes, International Union of Geological Sciences, v. 32.

Badarch, G., Cunningham, W. D., and Windley, B., 2002, A new terrane subdivision for Mongolia: implications for the Phanerozoic crustal growth of Central Asia: Journal of Asian Earth Sciences, v. 21, p. 87-110.

Blodgett, R. B., Rohr, D. M., and Boucot, A. J., 2002, Paleozoic links among some Alaskan accreted terranes and Siberia based on megafossils, *in* Miller, E. L., Grantz, A., and Klemperer, S. L., eds., Tectonic Evolution of the Bering Shelf--Chukchi Sea--Arctic Margin and Adjacent Landmasses: Boulder, Colorado, Geological Society of America Special Paper 360, p. 273-290.

Bold, U., Macdonald, F. A., Smith, E. F., Crowly, J. C., Minjin, C., and Dorjnamjaa.D., 2013, Elevating the Neoproterozoic Tsagaan-Olom Formation to a Group: Mongolian Geoscientist, v. 39, p. 5.

Bold, U., Smith, E. F., Rooney, A. D., Buchwaldt, R., Ramezani, J., Schrag, D. P., and Macdonald, F. A., 2016, Neoproterozoic stratigraphy of the Zavkhan Terrane of Mongolia: The backbone for Cryogenian and Early Ediacaran chemistratigraphic records: American Journal of Science, v. 316, p. 1-63.

Brown, D., Ryan, P. D., Afonso, J. C., Boutelier, D., Burg, J., Byrne, T., Calvert, A., Cook, F., DeBari, S., and Dewey, J., 2011, Arc–continent collision: the making of an orogen, Springer.

Buchan, C., Cunningham, D., Windley, B., and Tomurhuu, D., 2001, Structural and lithological characteristics of the Bayankhongor Ophiolite Zone, Central Mongolia: Journal of the Geological Society of London, v. 158, p. 445-460.

Bucholz, C. E., Jagoutz, O., Schmidt, M. W., and Sambuu, O., 2014, Phlogopite-and clinopyroxene-dominated fractional crystallization of an alkaline primitive melt: petrology and mineral chemistry of the Dariv Igneous Complex, Western Mongolia: Contributions to Mineralogy and Petrology, v. 167, no. 4, p. 1-28.

Burashnikov, V. V., 1990, Tectonics of the Urgamal zone, Early Calidonides of western Mongolia [Phd: Russian Academy of Sciences, 25 p.

Cocks, L., and Torsvik, T. H., 2007, Siberia, the wandering northern terrane, and its changing geography through the Paleozoic: Earth Science Reviews, v. 82, no. 1-2, p. 29-74.

Cole, R. B., and Stewart, B. W., 2009, Continental margin volcanism at sites of spreading ridge subduction: examples from southern Alaska and western California: Tectonophysics, v. 464, no. 1, p. 118-136.

Demoux, A., Kroener, A., Badarch, G., Jian, P., Tomurhuu, D., and Wingate, M. T. D., 2009a, Zircon ages from the Baydrag block and the Bayankhongor ophiolite zone: Time constraints on late Neoproterozoic to Cambrian subduction- and accretion-related magmatism in central Mongolia: Journal of Geology, v. 117, p. 377-397.

Demoux, A., Kröner, A., Hegner, E., and Badarch, G., 2009b, Devonian arc-related magmatism in the Tseel terrane of SW Mongolia: chronological and geochemical evidence: Journal of the Geological Society, v. 166, no. 3, p. 459-471.

Demoux, A., Kröner, A., Liu, D., and Badarch, G., 2009c, Precambrian crystalline basement in southern Mongolia as revealed by SHRIMP zircon dating: International Journal of Earth Sciences, v. 98, no. 6, p. 1365-1380.

Dergunov, A. B., 2001, Tectonics, Magmatism, and Metallogeny of Mongolia, Psychology Press.

Dijkstra, A. H., Brouwer, F. M., Cunningham, W. D., Buchan, C., Badarch, G., and Mason, P. R., 2006, Late Neoproterozoic proto-arc ocean crust in the Dariv Range, Western Mongolia: a supra-subduction zone end-member ophiolite: Journal of the Geological Society, v. 163, no. 2, p. 363-373.

Dobretsov, N. L., and Buslov, M., 2007, Late Cambrian-Ordovician tectonics and geodynamics of Central Asia: Russian Geology and Geophysics, v. 48, no. 1, p. 71-82.

Dobretsov, N. L., Buslov, M. M., and Vernikovsky, V. A., 2003, Neoproterozoic to Early Ordovician evolution of the Paleo-Asian Ocean: implications to the break-up of Rodinia: Gondwana Research, v. 6, no. 2, p. 143-159.

Evans, D. A. D., Zhuravlev, A. Y., Budney, C. J., and Kirschvink, J. L., 1996, Palaeomagnetism of the Bayan Gol Formation, western Mongolia: Geological Magazine, v. 133, no. 4, p. 487-496.

Gibson, T., Myrow, P., Macdonald, F. A., Minjin, C., and Gehrels, G., 2013, Depositional history, tectonics, and detrital zircon geochronology of Ordovician and Devonian strata in southwestern Mongolia: Geological Society of America Bulletin, v. 125, no. 5-6, p. 877-893.

Gladkochub, D., Stanevich, A., Mazukabzov, A., Donskaya, T., Pisarevsky, S., Nicoll, G., Motova, Z., and Kornilova, T., 2013, Early evolution of the Paleoasian ocean: LA-ICP-MS dating of detrital zircon from Late Precambrian sequences of the southern margin of the Siberian craton: Russian Geology and Geophysics, v. 54, no. 10, p. 1150-1163.

Glorie, S., De Grave, J., Buslov, M., Zhimulev, F., and Safonova, I. Y., 2014, Detrital zircon provenance of early Palaeozoic sediments at the southwestern margin of the Siberian Craton: Insights from U–Pb geochronology: Journal of Asian Earth Sciences, v. 82, p. 115-123.

Guy, A., Schulmann, K., Janoušek, V., Štípská, P., Armstrong, R., Belousova, E., Dolgopolova, A., Seltmann, R., Lexa, O., and Jiang, Y., 2015, Geophysical and geochemical nature of relaminated arc-derived lower crust underneath oceanic domain in southern Mongolia: Tectonics, v. 34, no. 5, p. 1030-1053.

Han, Y., Zhao, G., Sun, M., Eizenhöfer, P. R., Hou, W., Zhang, X., Liu, D., Wang, B., and Zhang, G., 2015, Paleozoic accretionary orogenesis in the Paleo-Asian Ocean: Insights from detrital zircons from Silurian to Carboniferous strata at the northwestern margin of the Tarim Craton: Tectonics, v. 34, no. 2, p. 334-351.

Hanzl, P., Schulmann, K., Janousek, V., Lexa, O., Hrdlickova, K., Jiang, Y., Burianek, D., Altanbaatar, B., Ganchuluun, T., and Erban, V., 2016, Making continental crust: origin of Devonian orthogneisses from SE Mongolian Altai: Journal of GEOsciences, v. 61, no. 1, p. 25-50.

Harper, D. A., Rasmussen, C. M., Liljeroth, M., Blodgett, R. B., Candela, Y., Jin, J., Percival, I. G., Rong, J.-y., Villas, E., and Zhan, R.-b., 2013, Biodiversity, biogeography and phylogeography of Ordovician rhynchonelliform brachiopods: Geological Society, London, Memoirs, v. 38, no. 1, p. 127-144.

Hou, H. F., and Boucot, A. J., 1990, the Balkhash-Mongolia-Okhotsk region of the Old World realm: Geological Society, London, Memoir, v. 12, p. 297-303.

Ilyin, A. V., 1990, Proterozoic supercontinent, its latest Precambrian rifting, breakup, dispersal into smaller continents, and subsidence of their margins: Evidence from Asia: Geology, v. 18, p. 1231-1234.

Jian, P., Kröner, A., Jahn, B.-m., Windley, B. F., Shi, Y., Zhang, W., Zhang, F., Miao, L., Tomurhuu, D., and Liu, D., 2014, Zircon dating of Neoproterozoic and Cambrian ophiolites in West Mongolia and implications for the timing of orogenic processes in the central part of the Central Asian Orogenic Belt: Earth-Science Reviews, v. 133, p. 62-93.

Jones, D., 1983, Recognition, Character and Analysis of Tectonostratigraphic Terranes In Western North America: Journal of Geological Education, v. 31, no. 4, p. 295-303.

Khain, E. V., Bibikova, E. V., Kröner, A., Zhuravlev, D. Z., Sklyarov, E. V., Fedotova, A. A., and Kravchenko-Berezhnoy, I. R., 2002, The most ancient ophiolite of the Central Asian fold belt: U–Pb and Pb–Pb zircon ages for the Dunzhugur Complex, Eastern Sayan, Siberia, and geodynamic implications: Earth and Planetary Science Letters, v. 199, no. 3, p. 311-325.

Khain, E. V., Bibikova, E. V., Salnikova, E. B., Kroener, A., Gibsher, A. S., Didenko, A. N., Degtyarev, K. E., and Fedotova, A. A., 2003, The Palaeo-Asian ocean in the Neoproterozoic and early Palaeozoic: new geochronologic data and palaeotectonic reconstructions: Precambrian Research, v. 122, p. 329-358.

Khain, E. V., Neymark, L. A., and Amelin, Y. V., ISOTOPIC-GEOCHRONOLOGICAL STUDY OF THE GRANITES AND GRANITE-GNEISSIS OF THE GARDAN BLOCK THE EASTERN SAYAN RANGE IN SIBERIA BY PB-PB AND U-PB METHODS ON ZIRCONS AND SM-ND METHOD, *in* Proceedings DOKLADY AKADEMII NAUK1995, Volume 342, MEZHDUNARODNAYA KNIGA 39 DIMITROVA UL., 113095 MOSCOW, RUSSIA, p. 776-780.

Kilian, T. M., Swanson-Hysell, N. L., Macdonald, F. A., Bold, U., and Crowley, J. L., this volume, Paleomagnetism of Ordovician-Silurian Teel basalts from the Zavkhan Terrane - Paleogeography of Mongolia during the Paleozoic.

Kolodner, K., Avigad, D., McWilliams, M., Wooden, J., Weissbrod, T., and Feinstein, S., 2006, Provenance of north Gondwana Cambrian–Ordovician sandstone: U–Pb SHRIMP dating of detrital zircons from Israel and Jordan: Geological Magazine, v. 143, no. 03, p. 367-391.

Korobov, M., 1980, Biostratigrafiya i miomernye trilobity nizhnego kembriya Mongolii [Biostratigraphy and miomerid trilobites from the Lower Cambrian of Mongolia]. The Joint Soviet-Mongolian Scientific-Research Geological Expedition: The Joint Soviet-Mongolian Scientific-Research Geological Expedition, Transactions, v. 26, p. 5-108.

-, 1989, Lower Cambrian biostratigraphy and polymeroid trilobites of Mongolia: Trans. Joint Soviet–Mongolian Research Expedition [in Russian]. Nauka, Moscow, no. 48, p. 186-192.

Kovach, V., Yarmolyuk, V., Kovalenko, V., Kozlovskyi, A., Kotov, A., and Terent'eva, L., 2011, Composition, sources, and mechanisms of formation of the continental crust of the Lake Zone of the Central Asian Caledonides. II. Geochemical and Nd isotope data: Petrology, v. 19, no. 4, p. 399-425.

Kozakov, I., Kotov, A., Sal'nikova, E., Bibikova, E., Kovach, V., Kirnozova, T., Berezhnaya, N., and Lykhin, D., 1999, Metamorphic age of crystalline complexes of the Tuva-Mongolia Massif: the U-Pb geochronology of granitoids: PETROLOGY C/C OF PETROLOGIIA, v. 7, p. 177-191.

Kozakov, I., Sal'nikova, E., Yarmolyuk, V., Kozlovsky, A., Kovach, V., Azimov, P. Y., Anisimova, I., Lebedev, V., Enjin, G., and Erdenejargal, C., 2012a, Convergent boundaries and related igneous and metamorphic complexes in Caledonides of Central Asia: Geotectonics, v. 46, no. 1, p. 16-36.

Kozakov, I., Yarmolyuk, V., Kovach, V., Bibikova, E., Kirnozova, T., Kozlovskii, A., Plotkina, Y. V., Fugzan, M., Lebedev, V., and Erdenezhargal, C., 2012b, The Early Baikalian crystalline complex in the basement of the Dzabkhan microcontinent of the Early Caledonian orogenic area, Central Asia: Stratigraphy and Geological Correlation, v. 20, no. 3, p. 231-239.

Kravchinsky, V. A., Konstantinov, K. M., and Cogne, J.-P., 2001, Palaeomagnetic study of Vendian and Early Cambrian of South Siberia and Central Mongolia: was the Siberian platform assembled at this time?: Precambrian Research, v. 110, p. 61-92.

Kravchinsky, V. A., Sklyarov, E. V., Gladkochub, D. P., and Harbert, W. P., 2010, Paleomagnetism of the Precambrian Eastern Sayan rocks: implications for the Ediacaran–Early Cambrian paleogeography of the Tuva-Mongolian composite terrane: Tectonophysics, v. 486, no. 1, p. 65-80.

Kröner, A., Demoux, A., Zack, T., Rojas-Agramonte, Y., Jian, P., Tomurhuu, D., and Barth, M., 2011, Zircon ages for a felsic volcanic rock and arc-related early Palaeozoic sediments on the margin of the Baydrag microcontinent, central Asian orogenic belt, Mongolia: Journal of Asian Earth Sciences, v. 42, no. 5, p. 1008-1017.

Kröner, A., Kovach, V., Belousova, E., Hegner, E., Armstrong, R., Dolgopolova, A., Seltmann, R., Alexeiev, D., Hoffmann, J., and Wong, J., 2014, Reassessment of continental growth during the accretionary history of the Central Asian Orogenic Belt: Gondwana Research, v. 25, no. 1, p. 103-125.

Kröner, A., Lehmann, J., Schulmann, K., Demoux, A., Lexa, O., Tomurhuu, D., Štípská, P., Liu, D., and Wingate, M. T., 2010, Lithostratigraphic and geochronological constraints on the evolution of the Central Asian Orogenic Belt in SW Mongolia: Early Paleozoic rifting followed by late Paleozoic accretion: American Journal of Science, v. 310, no. 7, p. 523-574.

Kuzmichev, A., Bibikova, E. V., and Zhuravlev, D. Z., 2001, Neoproterozoic (~800 Ma) orogeny in the Tuva-Mongolia Massif (Siberia): island arc-continent collision at the northeast Rodinia margin: Precambrian Research, v. 110, p. 109-126.

Kuzmichev, A., Kroener, A., Hegner, E., Dunyi, L., and Yusheng, W., 2005a, The Shishkhid ophiolite, nothern Mongolia: A key to the reconstruction of a Neoproterozoic island-arc system in central Asia: Precambrian Research, v. 138, p. 125-150.

Kuzmichev, A., Kröner, A., Hegner, E., Dunyi, L., and Yusheng, W., 2005b, The Shishkhid ophiolite, northern Mongolia: a key to the reconstruction of a Neoproterozoic island-arc system in central Asia: Precambrian Research, v. 138, no. 1, p. 125-150.

Kuzmichev, A., and Larionov, A., 2011, The Sarkhoi Group in East Sayan: Neoproterozoic (~ 770–800 Ma) volcanic belt of the Andean type: Russian Geology and Geophysics, v. 52, no. 7, p. 685-700.

Kuzmichev, A., Sklyarov, E., Postnikov, A., and Bibikova, E., 2007, The Oka Belt (Southern Siberia and Northern Mongolia): A Neoproterozoic analog of the Japanese Shimanto Belt?: Island Arc, v. 16, no. 2, p. 224-242.

Lamb, M. A., and Badarch, G., 1997, Paleozoic sedimentary basins and volcanic-arc systems of Southern Mongolia: new stratigraphic and sedimentologic constraints: International Geology Review, v. 39, no. 6, p. 542-576.

-, 2001, Paleozoic sedimentary basins and volcanic arc systems of southern Mongolia: new geochemical and petrographic constraints: Geological Society of America Memoirs, v. 194, p. 117-149.

Lehmann, J., Schulmann, K., Lexa, O., Corsini, M., Kröner, A., Štípská, P., Tomurhuu, D., and Otgonbator, D., 2010, Structural constraints on the evolution of the Central Asian Orogenic Belt in SW Mongolia: American Journal of Science, v. 310, no. 7, p. 575-628.

Letnikova, E., Kuznetsov, A., Vishnevskaya, I., Veshcheva, S., Proshenkin, A., and Geng, H., 2013, The Vendian passive continental margin in the southern Siberian Craton: geochemical and isotopic (Sr, Sm–Nd) evidence and U–Pb dating of detrital zircons by the LA-ICP-MS method: Russian Geology and Geophysics, v. 54, no. 10, p. 1177-1194.

Levashova, N. M., Kalugin, V. M., Gibsher, A. S., Yff, J., Ryabinin, A. B., Meert, J., and Malone, S. J., 2010, The origin of the Baydaric microcontinent, Mongolia: Constraints from paleomagnetism and geochronology: Tectonophysics, v. 485, no. 1-4, p. 306-320.

Li, H., Xu, Y., Huang, X., He, B., Luo, Z., and Yan, B., 2009, Activation of northern margin of the North China Craton in Late Paleozoic: Evidence from U-Pb dating and Hf isotopes of detrital zircons from the Upper Carboniferous Taiyuan Formation in the Ningwu-Jingle basin: Chinese Science Bulletin, v. 54, no. 4, p. 677-686.

Ludwig, K. R., 2008, User's manual for Isoplot 3.70: A geochronological Toolkit for Microsoft Excel: Berkeley Geochronology Center Special Publication, v. 4.

Macdonald, F. A., and Jones, D. S., 2011, The Khubsugul Basin, *in* E., A., Halverson, G. P., and Shields, G., eds., The geological record of Neoproterozoic glaciations: London, Geological Society of London.

Macdonald, F. A., Jones, D. S., and Schrag, D. P., 2009a, Stratigraphic and tectonic implications of a new glacial diamictite-cap carbonate couplet in southwestern Mongolia: Geology, v. 37, p. 123-126.

Macdonald, F. A., Ryan-Davis, J., Coish, R., Crowley, J., and Karabinos, P., 2014, A newly identified Gondwanan terrane in the northern Appalachian Mountains: Implications for the Taconic orogeny and closure of the Iapetus Ocean: Geology, v. 42, no. 6, p. 539-542.

Macdonald, F. A., Schmitz, M. D., Crowley, J. L., Roots, C. F., Jones, D. S., Maloof, A. C., Strauss, J. V., Cohen, P. A., Johnston, D. T., and Schrag, D. P., 2010, Calibrating the Cryogenian: Science, v. 327, p. 1241-1243.

Mossakovsky, A., Ruzhentsev, S., Samygin, S., and Kheraskova, T., 1994, Central Asian fold belt: geodynamic evolution and formation history: Geotectonics, v. 27, no. 6, p. 445-474.

Petrosyan, N., 1967, Stratigraphic importance of the Devonian flora of the USSR.

Pojeta Jr, J., 1986, Devonian rocks and Lower and Middle Devonian pelecypods of Guangxi, China, and the Traverse Group of Michigan, 2330-7102.

Powerman, V., Shatsillo, A., Chumakov, N., Kapitonov, I., and Hourigan, J., 2015, Interaction between the Central Asian Orogenic Belt (CAOB) and the Siberian craton as recorded by detrital zircon suites from Transbaikalia: Precambrian Research, v. 267, p. 39-71.

Rizza, M., Ritz, J. F., Prentice, C., Vassallo, R., Braucher, R., Larroque, C., Arzhannikova, A., Arzhannikov, S., Mahan, S., and Massault, M., 2015, Earthquake Geology of the Bulnay Fault (Mongolia): Bulletin of the Seismological Society of America, v. 105, no. 1, p. 72-93.

Rojas-Agramonte, Y., Kröner, A., Demoux, A., Xia, X., Wang, W., Donskaya, T., Liu, D., and Sun, M., 2011, Detrital and xenocrystic zircon ages from Neoproterozoic to Palaeozoic arc terranes of Mongolia: significance for the origin of crustal fragments in the Central Asian Orogenic Belt: Gondwana Research, v. 19, no. 3, p. 751-763.

Rooney, A. D., Strauss, J. V., Brandon, A. D., and Macdonald, F. A., 2015, A Cryogenian chronology: Two long-lasting synchronous Neoproterozoic glaciations: Geology, v. 43, no. 5, p. 459-462.

Rudnev, S., Izokh, A., Borisenko, A., Shelepaev, R., Orihashi, Y., Lobanov, K., and Vishnevsky, A., 2012, Early Paleozoic magmatism in the Bumbat-Hairhan area of the Lake Zone in western Mongolia (geological, petrochemical, and geochronological data): Russian Geology and Geophysics, v. 53, no. 5, p. 425-441.

Rudnick, R. L., 1995, Making continental crust: Nature, v. 378, no. 6557, p. 571-577.

Ruzhentsev, S. V., and Burashnikov, V. V., 1996, Tectonics of the western Mongolian Salairides: Geotectonics, v. 29, no. 5, p. 379-394.

Salnikova, E., Kozakov, I., Kotov, A., Kröner, A., Todt, W., Bibikova, E., Nutman, A., Yakovleva, S., and Kovach, V., 2001, Age of Palaeozoic granites and metamorphism in the Tuvino-Mongolian Massif of the Central Asian Mobile Belt: loss of a Precambrian microcontinent: Precambrian Research, v. 110, no. 1, p. 143-164.

Samozvantsen, B. A., Tsukerik, A. B., Golyakov, B. I., 1981, Report of geological mapping work of scale 1: 200 000 in area Great Lakes deppression to western branches of Hangay Highland, v. 3576.

Schulmann, K., and Paterson, S., 2011, Geodynamics: Asian continental growth: Nature Geoscience, v. 4, p. 827-829.

Sengör, A., Natal'In, B., and Burtman, V., 1993, Evolution of the Altaid tectonic collage and Palaeozoic crustal growth in Eurasia: Nature, v. 364, p. 299-307.

Sengor, A. C., and Natal'in, B. A., 1996, Paleotectonics of Asia: fragments of synthesis, *in* Yin, A., and Harrison, M., eds., The Tectonic Evolution of Asia: Cambridge, Cambridge University Press, p. 486-640.

Sláma, J., Košler, J., Condon, D. J., Crowley, J. L., Gerdes, A., Hanchar, J. M., Horstwood, M. S., Morris, G. A., Nasdala, L., and Norberg, N., 2008, Plešovice zircon—a new natural reference material for U–Pb and Hf isotopic microanalysis: Chemical Geology, v. 249, no. 1, p. 1-35.

Smith, E. F., Macdonald, F. A., Petach, T. A., Bold, U., and Schrag, D. P., 2015, Integrated stratigraphic, geochemical, and paleontological late Ediacaran to early Cambrian records from southwestern Mongolia: Geological Society of America Bulletin, p. B31248. 31241.

Soejono, I., Burianek, D., Svojtka, M., Zacek, V., Cap, P., and Janousek, V., 2016, Mid-Ordovician and Late Devonian magmatism in the Togtokhinshil Complex: new insight into the formation and accretionary evolution of the Lake Zone (western Mongolia): Journal of GEOsciences, v. 61, no. 1, p. 5-23.

Štípská, P., Schulmann, K., Lehmann, J., Corsini, M., Lexa, O., and Tomurhuu, D., 2010, Early Cambrian eclogites in SW Mongolia: evidence that the Palaeo-Asian Ocean suture extends further east than expected: Journal of metamorphic Geology, v. 28, no. 9, p. 915-933.

Teraoka, Y., Suzuki, M., Tungalag, F., Ichinnorov, N., and Sakamari, Y., 1996, Tectonic framework of the Bayankhongor area, west Mongolia: BULLETIN-GEOLOGICAL SURVEY JAPAN, v. 47, p. 447-456.

Togtokh, D., Baatarkhuyag, A., and Bayardalai, S., 1995, The report of result of the geological grouppedmapping at scale 1:200000: Ulaanbaatar, Mongolia, p. 1575.

Tomurtogoo, O., 2005, Tectonics and structural evolution of Mongolia: Geodynamics and Metallogeny of Mongolia With a Special Emphasis on Copper and Gold Deposits: IAGOD Guidebook Series, v. 11, p. 5-12.

Ulitina, L., Bondarenko, O., and Minjin, C., 2009, Evolution of the taxonomic diversity of Mongolian Ordovician-Silurian corals: Paleontological Journal, v. 43, no. 5, p. 499-505.

Van der Voo, R., van Hinsbergen, D. J., Domeier, M., Spakman, W., and Torsvik, T. H., 2015, Latest Jurassic–earliest Cretaceous closure of the Mongol-Okhotsk Ocean: A paleomagnetic and seismological-tomographic analysis: Geological Society of America Special Papers, v. 513, p. 589-606.

Wang, C., Li, N., Sun, Y., and Zong, P., 2011, Distribution of Tuvaella brachiopod fauna and its tectonic significance: Journal of Earth Science, v. 22, p. 11-19.

Wang, T., Zheng, Y., Gehrels, G., and Mu, Z., 2001, Geochronological evidence for existence of South Mongolian microcontinent—A zircon U-Pb age of grantoid gneisses from the Yagan-Onch Hayrhan metamorphic core complex: Chinese Science Bulletin, v. 46, no. 23, p. 2005-2008.

Webster, G. D., and Ariunchimeg, Y., 2004, The northern most Emsian crinoids known, a Devonian fauna from the Chuluun Formation, Shine Jinst area, Southern Mongolia: Geobios, v. 37, no. 4, p. 481-487.

Wilhem, C., Windley, B. F., and Stampfli, G. M., 2012, The Altaids of Central Asia: A tectonic and evolutionary innovative review: Earth-Science Reviews, v. 113, no. 3, p. 303-341.

Windley, B. F., Alexeiev, D., Xiao, W., Kroener, A., and Badarch, G., 2007, Tectonic models for accretion of the Central Asian Orogenic Belt: Journal of the Geological Society of London, v. 164, p. 31-47.

Xia, X., Sun, M., Zhao, G., and Luo, Y., 2006, LA-ICP-MS U–Pb geochronology of detrital zircons from the Jining Complex, North China Craton and its tectonic significance: Precambrian Research, v. 144, no. 3, p. 199-212.

Xiao, W., Windley, B. F., Hao, J., and Zhai, M., 2003, Accretion leading to collision and the Permian Solonker suture, Inner Mongolia, China: termination of the central Asian orogenic belt: Tectonics, v. 22, no. 6.

Yakubchuk, A., 2004, Architecture and mineral deposit settings of the Altaid orogenic collage: a revised model: Journal of Asian Earth Sciences, v. 23, no. 5, p. 761-779.

Yang, J.-H., Wu, F.-Y., Shao, J.-A., Wilde, S. A., Xie, L.-W., and Liu, X.-M., 2006, Constraints on the timing of uplift of the Yanshan Fold and Thrust Belt, North China: Earth and Planetary Science Letters, v. 246, no. 3, p. 336-352.

Yang, J., Cawood, P. A., Du, Y., Huang, H., Huang, H., and Tao, P., 2012, Large Igneous Province and magmatic arc sourced Permian–Triassic volcanogenic sediments in China: Sedimentary Geology, v. 261, p. 120-131.

Yarmolyuk, V., Kovach, V., Kovalenko, V., Salnikova, E., Kozlovskii, A., Kotov, A., Yakovleva, S., and Fedoseenko, A., 2011, Composition, sources, and mechanism of continental crust growth in the Lake Zone of the Central Asian Caledonides: I. Geological and geochronological data: Petrology, v. 19, no. 1, p. 55-78.

Yarmolyuk, V., Kovalenko, V., Anisimova, I., Sal'nikova, E., Kovach, V., Kozakov, I., Kozlovsky, A., Kudryashova, E., Kotov, A., and Plotkina, Y. V., Late Riphean alkali granites of the Zabhan microcontinent: evidence for the timing of Rodinia breakup and formation of microcontinents in the Central Asian Fold Belt, *in* Proceedings Doklady Earth Sciences2008, Volume 420, Springer, p. 583-588.

Yarmolyuk, V., Kovalenko, V., Sal'nikova, E., Kozakov, I., Kotov, A., Kovach, V., Vladykin, N., and Yakovleva, S., 2005, U-Pb-Age of sin-and postmetamorphic granitoids from Southern Mongolia-evidence for the presence of grenvilides in the Central Asian Fold Belt.

Zacek, V., Burianek, D., Pecskay, Z., and Skoda, R., 2016, Astrophyllite-alkali amphibole rhyolite, an evidence of early Permian A-type alkaline volcanism in the western Mongolian Altai: Journal of GEOsciences, v. 61, no. 1, p. 93-103.

Zhang, C.-L., Zou, H.-B., Li, H.-K., and Wang, H.-Y., 2013, Tectonic framework and evolution of the Tarim Block in NW China: Gondwana Research, v. 23, no. 4, p. 1306-1315.

Zhao, Y., Song, B., and Zhang, S. H., The Central Mongolian microcontinent: Its Yangtze affinity and tectonic implications, *in* Proceedings Symposium on continental growth and orogeny in Asia, Taipei, Taiwan, 2006, p. 135-136.

Zorin, Y. A., 1999, Geodynamics of the western part of the Mongolia–Okhotsk collisional belt, Trans-Baikal region (Russia) and Mongolia: Tectonophysics, v. 306, no. 1, p. 33-56.

CHAPTER 3. NEOPROTEROZOIC STRATIGRAPHY OF THE ZAVKHAN TERRANE OF MONGOLIA: THE BACKBONE FOR CRYOGENIAN AND EARLY EDIACARAN CHEMOSTRATIGRAPHIC RECORDS

*This chapter is published in **Bold, U**., Smith, E. F., Rooney, A. D., Buchwaldt, R., Ramezani, J., Schrag, D. P., and Macdonald, F. A., 2016, Neoproterozoic stratigraphy of the Zavkhan Terrane of Mongolia: The backbone for Cryogenian and Early Ediacaran chemistratigraphic records: American Journal of Science, v. 316, p. 1-63.*

ABSTRACT

The Neoproterozoic Tsagaan-Olom Group is exposed in the Zavkhan Terrane of southwestern Mongolia and hosts unique geochemical, paleoclimate, and paleontological records that have become central to our understanding of this pivotal interval of Earth history. New sedimentological, stratigraphic, geochronological, and geochemical data provide context for and further develop these records. Detrital zircon provenance indicates that Neoproterozoic strata of the Zavkhan Terrane were derived from basement with age peaks between 1950-2100 and 2400-2600 Ma. At ~ 800 Ma, the Zavkhan Terrane transformed from an active arc and back-arc complex to a rifted ribbon continent with passive margins on both sides. Deposition was accommodated by extension, which is recorded with syn-sedimentary normal faulting and alluvial fan deposition in the Zavkhan and Khasagt formations. Passive margin sedimentation in the overlying Tsagaan-Olom Group begins with the glacigenic Maikhan-Uul Formation, which consists of two massive diamictite units separated by clast-poor graded beds of the middle member. Detrital zircon at the base of the middle member of the Maikhan-Uul Formation were dated with U-Pb chemical abrasion isotope-dilution thermal ionization mass spectrometry and constrained its age to < 729.8 ± 1.4 Ma. This, along with chemostratigraphy and Re/Os geochronological constraints from the overlying Taishir Formation, supports our correlation of the Maikhan-Uul Formation with the ~ 717-660 Ma Sturtian

glaciation. The Taishir Formation was deposited on a carbonate ramp in four large-scale sequence tracts that thin to the southwest. The Taishir Formation preserves a large negative $\delta^{13}C$ excursion referred to as the Taishir excursion that covaries in carbonate and organic carbon isotopes in limestone sections. A dolomitization front at the top of the Taishir Formation also results in depleted $\delta^{13}C$ values, however, these are related to local processes and do not represent a global Trezona excursion. Although $\delta^{13}C$ values in the Ol Formation are highly variable along strike, 0.70756 initial strontium isotope values in limestone of the upper Ol Formation are consistent with earliest Ediacaran values. A sandstone-filled karst surface at the top of the Shuurgat Formation that overlies the Ol Formation defines the top of the Tsagaan-Olom Group and is interpreted to mark a major unconformity. Carbon and strontium isotope values in the uppermost Shuurgat Formation are also consistent with early Ediacaran values and suggest that most of the late Ediacaran Period is missing in the Zavkhan Terrane of Mongolia. Carbon isotope profiles from sections preserved as limestone and dolostone display large differences and indicate that isotopic data from dolomites should be used with caution. With our new data and correlations, we construct composite Cryogenian and Ediacaran carbon and strontium isotope curves from limestone-dominated successions in Mongolia, and then integrate additional geochronological and geochemical data sets from around the globe.

3.1. INTRODUCTION

Neoproterozoic strata record global, low-latitude glaciations (known as Snowball Earth episodes: Hoffman et al., 1998; Hoffman and Schrag, 2002; Kirschvink, 1992), the break-up of the supercontinent Rodinia and assembly of Gondwana (Hoffman, 1991; Li et al., 2008), large perturbations to geochemical cycles (e.g. Halverson et al., 2010), a putative second global oxygenation event termed the Neoproterozoic Oxygenation Event (Och and Shields-Zhou, 2012; Planavsky et al., 2010), and the diversification of eukaryotes followed by the rise of metazoans (Erwin et al., 2011; Knoll et al., 2006). Unravelling the interrelationships between these climatic, tectonic, geochemical, and biological milestones is dependent on integrating high-quality data sets from around the world.

Thick, low-grade Neoproterozoic successions are spectacularly exposed in the Tsagaan-Olom Group in the Zavkhan Terrane of Mongolia (Figure 3.1) (Macdonald, 2011a; Macdonald et al., 2009a). The Mongolian records are important because, along with Namibia (Hoffman, 2011) and Arctic Alaska (Macdonald et al., 2009b), they represent the only carbonate-dominated Cryogenian* successions. Unlike the other two successions, the Tsagaan-Olom Group, particularly the Taishir Formation (Fm), is fossiliferous (Bosak et al., 2011a; Bosak et al., 2012; Bosak et al., 2011b; Cohen et al., 2015) and composed predominantly of limestone, making it ideal for a variety of geochemical proxy studies. These paleontological and lithological features distinguish Mongolia as an ideal locality to explore Cryogenian and early Ediacaran biogeochemical cycles.

* The Cryogenian Period was redefined in 2015 by the International Commission of Stratigraphy at ~ 720-635 Ma.

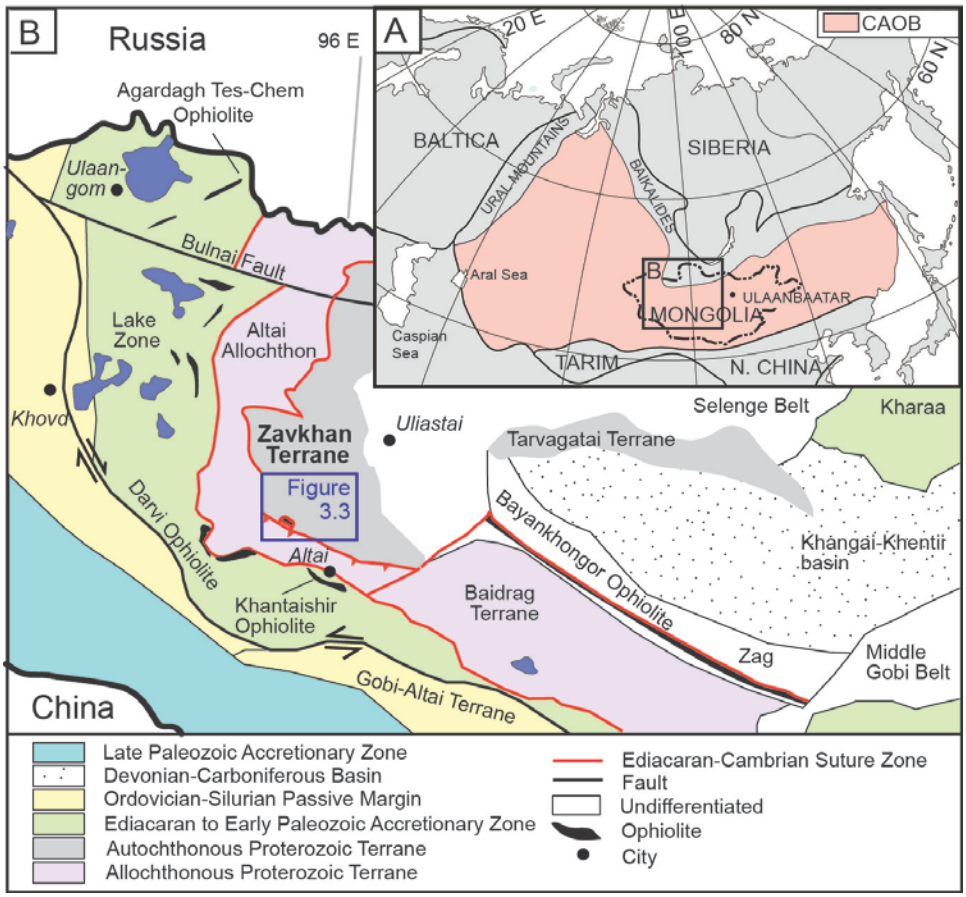

Figure 3.1. Location map of the Zavkhan Terrane of Mongolia
(A) Location map showing extent of the Central Asian Orogenic Belt (CAOB) and its surrounding areas (Sengör et al., 1993). (B) Tectonic map of western Mongolia (after Badarch et al., 2002; Bucholz et al., 2014). Contacts modified from the 1:1,000,000 geological map of Mongolia (Badarch, 1998).

Since the conception of the Snowball Earth hypothesis, the number and duration of Neoproterozoic glacial events has been debated (Rooney et al., 2015). The lack of a robust global age model has made it difficult to integrate geochemical and paleontological data with the glacial record. Recent geochronology coupled with geochemistry has reinforced geochemical correlations and has suggested a long Sturtian glacial epoch from ca. 717 to 660 Ma, and a relatively short Cryogenian nonglacial interlude (Macdonald et al., 2010; Rooney et al., 2014; Rooney et al., 2015). These geochronological constraints, directly linked to carbon and strontium isotope chemostratigraphy, provide a template to more broadly integrated global records.

Previous attempts at integrating Mongolian records into the global database have been limited not only by the lack of robust geochronology, but also by the lack of regional geological mapping and stratigraphic studies. Particularly, disagreement has centered on the number and age range of Cryogenian glacial deposits (see review in Macdonald, 2011). The earliest description of the sedimentology of the Maikhan-Uul Fm, which forms the base of the Tsagaan-Olom Group, was interpreted as evidence of two glacial advances separated by an interglacial period (Lindsay et al., 1996b). This study, however, was from a single locality, Tsagaan Gol (*tr.* 'White Gorge'; here we use 'gorge' in place of 'gol'), and it is unclear if these deposits represent movement in the ice-grounding line or two distinct early Cryogenian glaciations (Macdonald, 2011a). Macdonald and others (2009a) discovered a large negative $\delta^{13}C$ excursion in the Taishir Fm that covaries in organic and carbonate carbon isotopes (Johnston et al., 2012), and a Marinoan age diamictite and basal Ediacaran cap dolostone in overlying strata, which defined the Cryogenian-Ediacaran boundary in Mongolia. Despite these refinements of the age model for the Tsagaan-Olom Group, it has remained uncertain whether the Maikhan-Uul Fm represents a single Sturtian glaciation or multiple Cryogenian glaciations. Moreover, it has also been unclear if the Taishir excursion is correlative with the Cyogenian Trezona excursion in Australia, Namibia, NW Canada and elsewhere (Macdonald et al., 2013; Swanson-Hysell et al., 2010), or if it represents a distinct event that has not been well-documented in records elsewhere. Here we present a comprehensive stratigraphic study of Cryogenian successions from southwest Mongolia that provides sedimentological and tectonic context to these records. We then consider the degree to which these geochemical records are affected by diagenesis and represent global conditions, refine global correlations, and and then discuss how the successions of the Zavkhan Terrane inform our understanding of Cryogenian and early Ediacaran Earth history.

3.2. GEOLOGICAL SETTING

Neoproterozoic strata are exposed in the Mongolian Altaids as crustal fragments embedded within the ~ 5000 km long Central Asian Orogenic Belt (CAOB) (Figure 3.1A). Early studies on the Mongolian Altaids divided the region into two super-units: the Neoproterozoic northern super-unit, or

Mongolian continent, which was consolidated with an early Paleozoic orogeny, and an early Paleozoic southern super-unit that accreted during the late Paleozoic (Zonenshain, 1973). These were later divided into zones, blocks, and terranes (e.g. Ruzhentsev and Pospelov, 1992), culminating with the separation of the Mongolian Altaids into 44 terranes (Badarch et al., 2002) (Figure 1B).

The stratigraphy of the Zavkhan Terrane (Figure 3.2) was first described by Bezzubtsev (1963) who named the Zavkhan, Tsagaan-Olom, and Bayangol formations (fms). After regional scale mapping (1:200,000 scale), Togtokh and others (1995) identified and named the Maikhan-Uul Fm, a unit below the Tsagaan-Olom Fm (Figure 2). The first stratigraphic descriptions in English came in 1996 with the publication of a *Geological Magazine* issue dedicated to the Neoproterozoic-Cambrian stratigraphy of southwestern Mongolia (Brasier et al., 1996a). This publication included the translation of geological maps and measured sections into English (Khomentovsky and Gibsher, 1996), a reconnaissance chemostratigraphic characterization of the Tsagaan-Olom, Bayangol, and Salaagol fms (Brasier et al., 1996b), and a detailed stratigraphic study of the Maikhan-Uul Fm at Tsagaan Gorge (Lindsay et al., 1996b). More recently, this stratigraphic framework was revised by Macdonald and others (2009a) and formalized by Bold and others (2013) (Figure 3.2).

Although distinguished by Badarch and others (2002), the Zavkhan and Baidrag terranes are commonly grouped together and called one or the other (e.g. Levashova et al., 2010), or even grouped with the Lake Zone (e.g. Kröner et al., 2010). We separate the Zavkhan and Baidrag terranes because they lack a shared Neoproterozoic overlap assemblage (Badarch et al., 2002), and it appears unlikely that they were attached until at least the Cambrian. Moreover, in our distinction of terranes, we separate the Altai allochthon from the Lake Zone (also called the Ozernaya Zone, e.g. Khomentovsky and Gibsher, 1996) (Figure 3.1B).

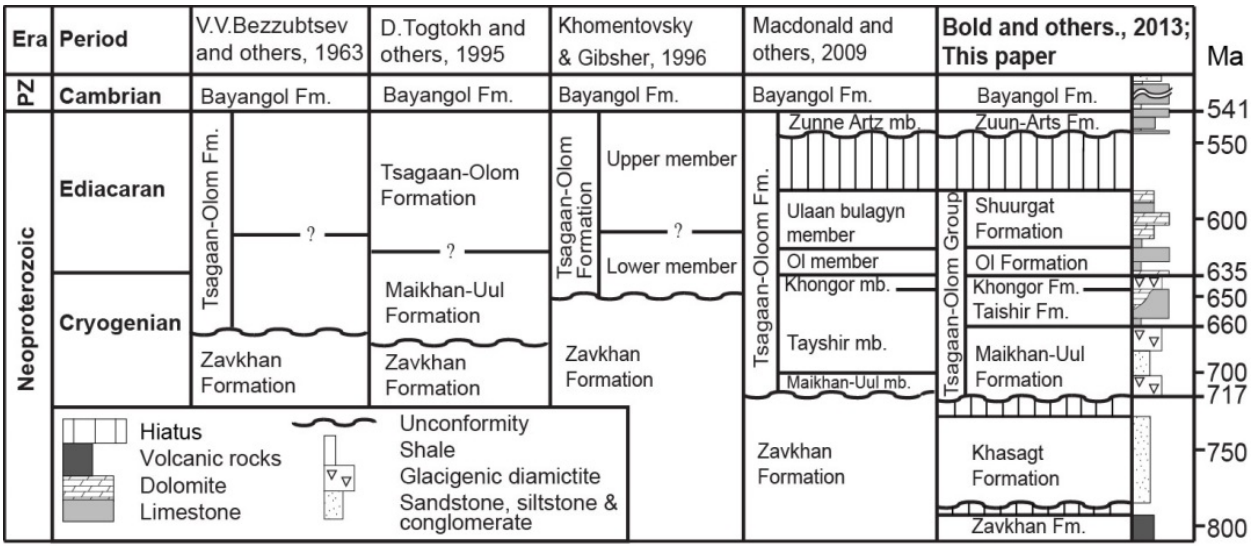

Figure 3.2. Revised stratigraphy of the Tsagaan-Olom Group
The figure is modified from Bold and others (2013).

It is widely cited that the Zavkhan Terrane hosts Archean to Paleoproterozoic crystalline basement (e.g. Yarmolyuk et al., 2008b). This stems in part from the inclusion of the Baidrag Terrane and the Dariv Range with the Zavkhan Terrane (e.g. Lehmann et al., 2010). However, there is no exposed basement on the Zavkhan Terrane older than ~ 850 Ma (Kozakov et al., 2012c). According to our study, the newly discovered Tsagaankhairkhan Fm (figures 3.3 and 3.5), which underlies the Zavkhan Fm, is the oldest sedimentary succession on the Zavkhan Terrane. Further south, the relationship between the Tsagaankhairkhan Fm and undifferentiated Neoproterozoic units that underlie the Zavkhan Fm is unclear (Figure 3.3). The Zavkhan Fm (figures 3.4 and 3.5) is overlain by siliciclastic rocks of the Khasagt Fm and glacial diamictite of the Maikhan-Uul Fm, which is the basal unit of the Tsagaan-Olom Group.

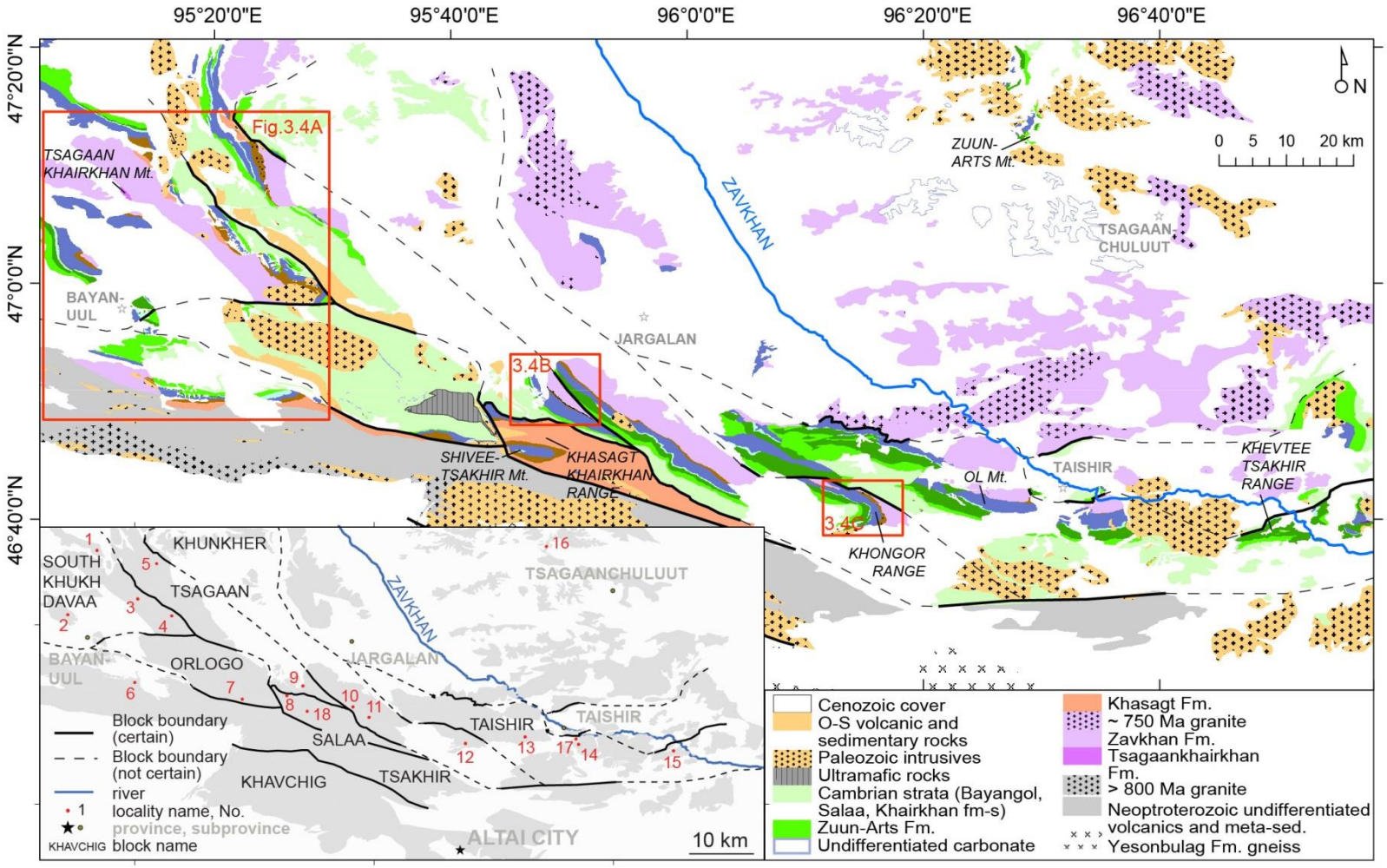

Figure 3.3. Geological map of the Zavkhan Terrane (F. A. Macdonald, U. Bold, and E. F. Smith)
Structural blocks are illustrated in the inset map with their corresponding names. Legend for the Tsagaan-Olom Group is in Figure 3.4. Localities discussed in this study are numbered as follows: (1) Unkheltseg; (2) Ikh Goliin Tsakhir; (3) western Khukh Davaa; (4) southern Khukh Davaa; (5) northeastern Khukh Davaa; (6) Tsakhir Range; (7) Orlogo Gorge; (8) Salaa Gorge; (9) Tsagaan-Gorge; (10) Uliastai Gorge; (11) Khunkher Gorge; (12) Khongor Range; (13) Ol Mountain; (14) eastern Taishir; (15) Khevtee Tsakhir Range (KTN); (16) Zuun-Arts locality; (17) western Taishir; and (18) Shivee Tsakhir.

The Tsagaan-Olom Group (*tr.* 'White bridal strap') was named after the eponymous location near the Khevtee Tsakhir Range (abbreviated as KTN by Khomentovsky and Gibsher, 1996). Unfortunately, the Maikhan-Uul and Taishir fms are largely faulted out at this location, leaving just the early Ediacaran Shuurgat Fm of the Tsagaan-Olom Group exposed. Previous studies have focused on sections exposed at Bayan and Tsagaan gorges (Brasier et al., 1996b; Khomentovsky and Gibsher, 1996) where ~ 200 m of stratigraphy in the middle of the Tsagaan-Olom Group is faulted out and poorly exposed. Recently, the Tsagaan-Olom was elevated to Group status and the informal members (Macdonald et al., 2009a) were elevated to formations (Bold et al., 2013; Dorjnamjaa, 2011). Spelling of Formation names were changed from Russian to Mongolian and the informal Ulaanbulag fm (Macdonald et al., 2009a) was changed to Shuurgat Fm because the former name was already used for other units on regional maps (Bold et al., 2013).

The Tsagaan-Olom Group begins with the Maikhan-Uul Fm, which consists of 3-500 m of glacigenic diamictite and siliciclastic rocks that unconformably overlie the Khasagt and Zavkhan fms (figures 3.2 and 3.5). The Maikhan-Uul Fm is sharply and conformably overlain by 300-600 m of dark-colored limestone of the Taishir Fm, which is composed of four super-sequences that are locally dolomitized towards the top. Rooney et al. (2015) recently dated the base of the Taishir Fm with Re-Os on organic-rich carbonate at 659.0 ± 3.9/4.5[†] Ma (MSWD[‡] = 0.67) , which further supports correlation of the base of the Taishir Fm with Sturtian cap carbonates around the globe. The Taishir Fm is sharply overlain by 0-50 m of glacigenic diamictite of the Khongor Fm and an additional ~ 500 m of early Ediacaran carbonate strata of the Ol and Shuurgat fms (Figure 3.2).

[†] ± Internal uncertainty only/including decay constant uncertainty.
[‡] Mean Square of Weighted Deviates.

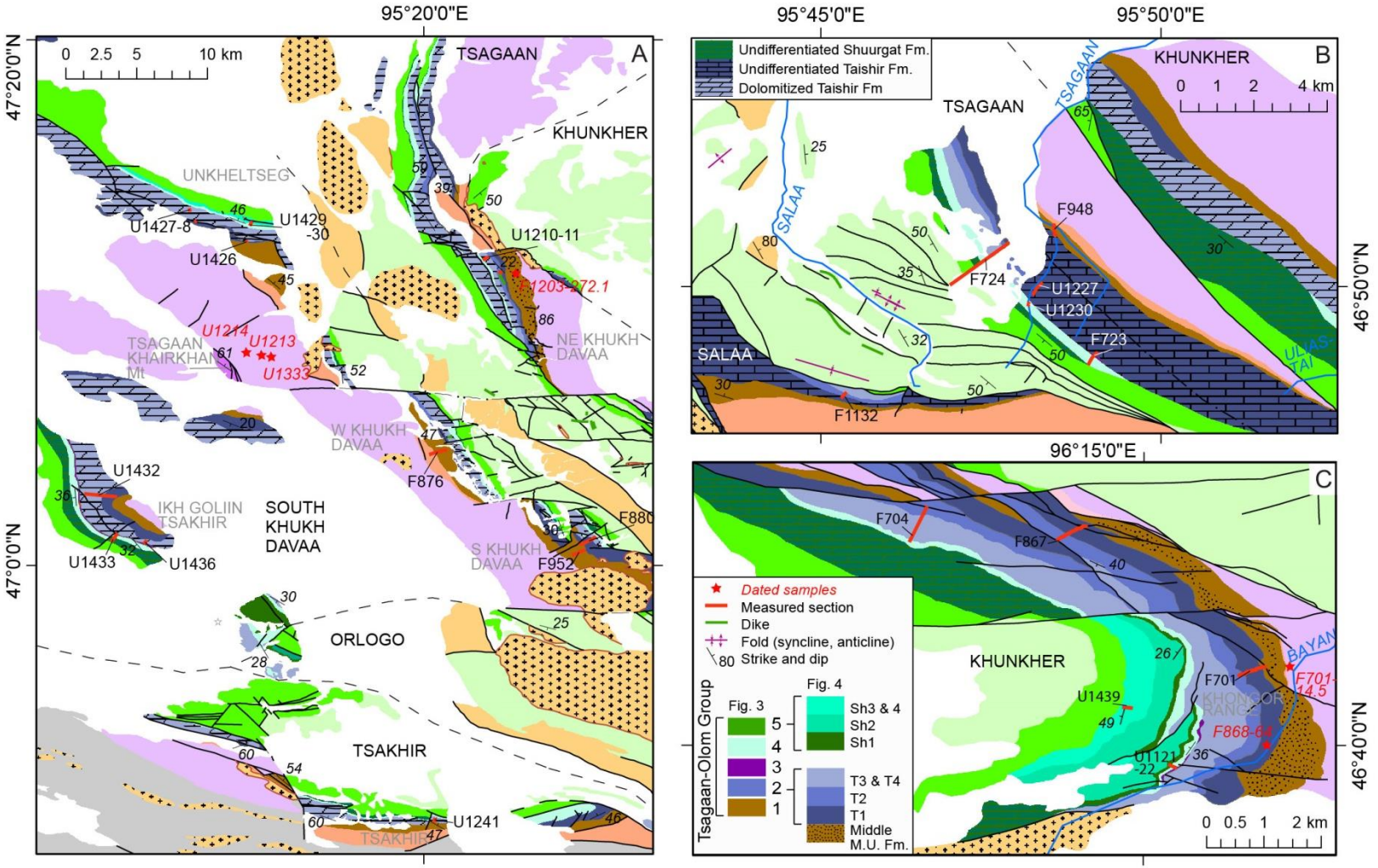

Figure 3.4. Detailed geological maps with samples and sections labeled

(A) Western Zavkhan Terrane, Tsakhir, Orlogo, southern Khukh Davaa, Tsagaan and Khunkher blocks. (B) Salaa, Tsagaan, and Khunkher blocks. (C) Khunkher block. Measured stratigraphic sections included in this study are shown in red with corresponding labels. Key for units except the Tsagaan-Olom Group is the same as in Figure 3.3. Color schemes used in Figure 3.3 (1. Maikhan-Uul Formation; 2. Taishir Formation; 3. Khongor Formation; 4. Ol Formation; 5. Shuurgat Formation) are shown along with detailed color schemes used in Figure 3.4 for members of each formation of the Tsagaan-Olom Group. Location names are labeled in dark gray. Structural blocks are labeled in black in all capitalized letters. Inferred structural block boundaries are illustrated with dashed line.

In the late Ediacaran Period, the passive margin on the southwestern side of the Zavkhan Terrane was transformed into a foreland basin and an active margin with the arrival of the Ediacaran to Paleozoic arc terranes to the south (Macdonald et al., 2009a). Above the karstic unconformity that defines the top of the Shuurgat Fm, simple bed planar trace fossils are present within the Zuun-Arts Fm (*tr.* 'eastern Juniper') (Goldring and Jensen, 1996) as well as a large negative $\delta^{13}C$ excursion (Brasier et al., 1996b; Macdonald et al., 2009a) indicating a latest Ediacaran to early Cambrian age with the Ediacaran-Cambrian boundary in the uppermost Zuun-Arts Fm (Smith et al., 2015). Consequently, the Zuun-Arts Fm (formerly the upper member of the Tsagaan-Olom Fm) was removed from the Tsagaan-Olom Group to reflect its position above a major unconformity and tectonostratigraphic affinity to the Bayangol Fm (Bold et al., 2013).

The Neoproterozoic stratigraphy of the Zavkhan Terrane was buried with ~ 1 km of early Cambrian foreland deposits and then deformed and weakly metamorphosed during multiple Paleozoic orogenic events in the CAOB (Figure 3.1A). After late Ediacaran to Ordovician accretion of arc terranes to the south (Jian et al., 2014; Macdonald et al., 2009a), the late Ordovician to Silurian record of Mongolia is marked by sinistral transtension (Figure 3.3), extensional magmatism and basin formation (Gibson et al., 2013a; Kröner et al., 2010). During this time, the Zavkhan Terrane is interpreted to have been part of a composite ribbon continent that was located between North China and Siberia (Wilhem et al., 2012). From the Devonian to early Permian, the Zavkhan Terrane was oroclinally buckled during the convergence between North China, Tarim, and Siberia (Edel et al., 2014; Lehmann et al., 2010). Locally, in the Zavkhan Terrane, this late Paleozoic collision is manifested in dextral strike-slip wrench structures (Figure 3.1B) and widespread Permian plutonism (Jahn et al., 2009).

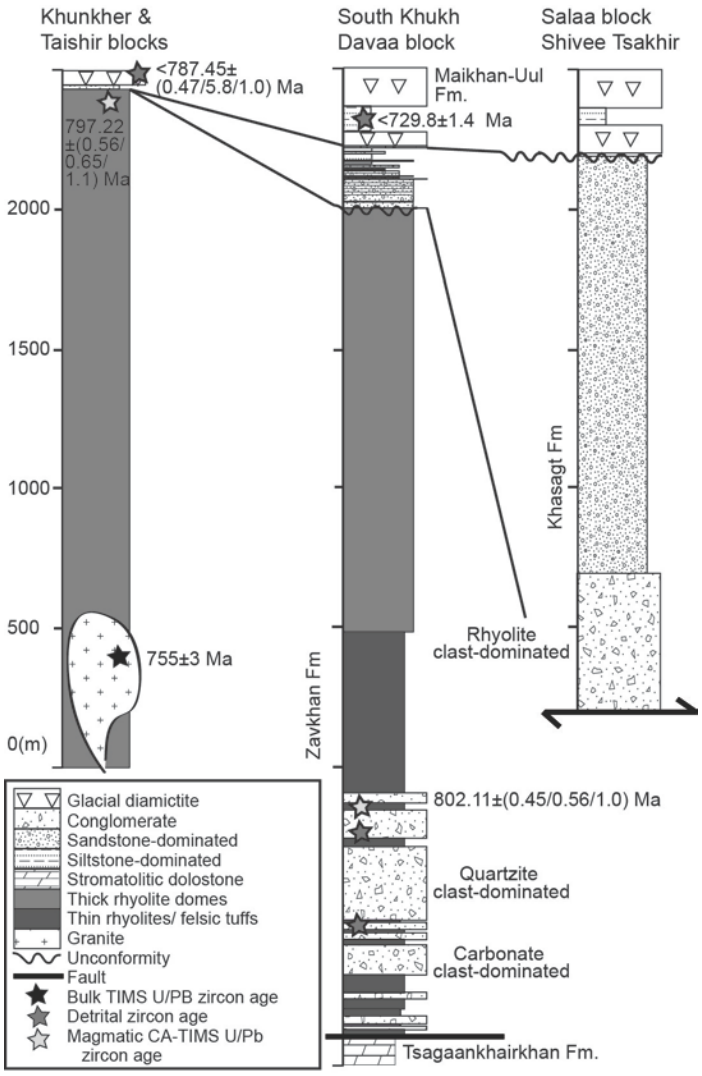

Figure 3.5. Stratigraphy of the Zavkhan and Khasagt formations
Age constraints are discussed in the geochronology section. Bulk TIMS U-Pb zircon age is from Yarmolyuk et al. (2008b).

3.3. STRATIGRAPHY

Here we briefly describe the Zavkhan and Khasagt fms. Then we describe measured stratigraphic sections of the Tsagaan-Olom Group in more detail. The Tsagaan-Olom Group is exposed on the Zavkhan Terrane in eight structural blocks, referred to here as the Taishir, Salaa, Tsakhir, Khavchig, Tsagaan, Orlogo, Khunkher, and South Khukh Davaa blocks, each of which are bound by major faults (Figure 3.3) and characterized by distinct stratigraphy.

3.3.1. Zavkhan and Khasagt formations

The Zavkhan Fm consists of > 1 km of volcanic and volcanoclastic rocks dominated by rhyolite with subsidiary dacitic and basaltic flows that are exposed in the Zavkhan Terrane for > 400 km along strike (Figure 3.3). Rhyolites of the Zavkhan Fm are red to green in color and form massive domes and thin-bedded ignimbrites and lithic tuffs. On the South Khukh Davaa block (Figure 3.4A), the Zavkhan Fm begins with > 1 km of boulder clast conglomerate with interbedded rhyolite flows that structurally overlie the Tsagaankhairkhan Fm (Figure 3.5). Although the contact is locally faulted, the lower few tens of meters of this conglomerate unit are dominated by redeposited clasts of the Tsagaankhairkhan Fm dolostone, which suggests a stratigraphic relationship between the two. Up-section, conglomerate is interbedded with medium-bedded sandstone and the clasts become dominated by sedimentary quartzite of an unknown source that is not exposed on the Zavkhan Terrane. Hence, it is inferred that these clasts preserve an inverted footwall stratigraphy from a syn-sedimentary fault, providing a window into units underlying the Zavkhan and Tsagaankhairkhan fms. This conglomerate unit is topped by > 500 m of thin-bedded rhyolite flows and felsic tuffs, which are overlain by massive rhyolite domes that are > 1 km thick.

On the Taishir, South Khukh Davaa, Tsakhir and Salaa blocks (Figure 3.4B), the Zavkhan Fm is unconformably overlain by conglomerate and sandstone of the Khasagt Fm (named after the Khasagt Khairkhan Range where these rocks are the ridge-former and best exposed). On the Taishir, South Khukh Davaa, and Tsakhir blocks, the Khasagt Fm consists of 0-200 m of red to green, medium-bedded sandstone and siltstone with common large-scale trough cross-stratification, channelization, and minor basalt flows (Figure 3.5). Thickness of the Khasagt Fm increases abruptly across the fault that marks the western margin of the Salaa block. There the Khasagt Fm is composed of > 1 km of red to green graded beds of siltstone, sandstone and conglomerate (Figure 3.5).

3.3.2. Tsagaan-Olom Group

Measured stratigraphic sections of the Maikhan-Uul, Taishir, Khongor, Ol and Shuurgat fms of the Tsagaan-Olom Group are reported in this paper with locations marked on figures 3.3 and 3.4. The stratotype sections are assigned and presented in Bold and others (2013). Carbonate and siliciclastic lithofacies are defined in Table 3.1. We have further distinguished facies assemblages in Table 3.2 for glacigenic facies of the Maikhan-Uul and Khongor fms and for carbonate facies of the Taishir, Ol, and Shuurgat fms.

Maikhan-Uul Formation.—The Maikhan-Uul Fm (*tr.* 'tent mountain') rests on the Khasagt Fm at Tsagaan Gorge, Salaa Gorge, Shivee Tsakhir, and Khukh Davaa, the Zavkhan Fm near Khunkher Gorge, Khongor Range and west of Taishir (Figure 3.6) and on ~ 850 Ma gneiss to the north in the Zavkhanmandal zone (Kozakov et al., 2012c). The Maikhan-Uul Fm progressively thickens to the west-southwest (Figure 3.6), but also displays considerable variability along strike. For mapping purposes, the Maikhan-Uul Fm is separated into informal lower, middle, and upper members. Generally, the lower and upper members are composed of diamictite with clear evidence of a glacial origin including lamination-penetrating dropstones (Figure 3.7A) and striated (Figure 3.7B) and faceted clasts (Lindsay et al., 1996b; Macdonald, 2011a) that are separated by a middle, diamictite-free siliciclastic unit.

In the Maikhan-Uul Fm, we distinguish stratified diamictite from massive diamictite and use other sedimentary features to identify glacitectonic deformation such as soft-sedimentary folding and shear fabrics (Table 3.1). Massive diamictite is distinguished from conglomerate in that diamictite facies are matrix-supported and poorly sorted. In both the upper and lower members of the Maikhan-Uul Fm, the diamictite matrix is composed of shale to sandstone that varies in color from black to green to brown to red (Figure 3.6). Clasts are commonly sub-rounded and faceted and consist predominantly of felsic volcanic rocks from the underlying Zavkhan Fm, siliciclastic rocks from the Khasagt Fm, minor dolostone clasts from the Tsagaankhairkhan Fm, granite, and meta-sediments and meta-volcanics of unknown origin. Clast-size varies from granule to boulder (Macdonald, 2011a). Below we describe the

stratigraphy from northeast to southwest in 11 measured stratigraphic sections (Figure 3.6) of the Maikhan-Uul Fm.

Table 3.1. Carbonate and siliciclastic lithofacies used
Descriptions of lithology, bedding, grains, and sedimentary structures that distinguish these facies are included.

Carbonate Facies

Lithofacies	Bedding	Grains	Sedimentary Structures
Micrite	Flat thin beds	Mud	Grading
Calcisiltite	Flat to nodular	Mud to silt	Ripple cross-lamination and grading
Grainstone (includes wackestone and packestone)	Thin to thickly bedded	Peloids, ooids, and chips of microbialite	Trough cross-bedding and normal grading
Microbialaminite	Crinkly laminated	Boundstone with cement and organic mats	Microbial bounding of grains, cements, dolomitized tops
Breccia	Massive	Carbonate clasts with ubiquitous cement	Teepee structures, void-filling cement and dolomitization
Heterolithic interbeds	Thin to thickly bedded	Angular to sub-rounded clasts and grains	Imbrication and normal grading

Siliciclastic Facies

Lithofacies	Bedding	Grains	Sedimentary Structures
Massive diamictite	Massive to thickly bedded	Shale to sandstone matrix with common boulder- to gravel-sized clasts of underlying units	Shear fabrics, soft-sedimentary folding, concretions, scours
Stratified diamictite	Fine laminated to medium bedded	Shale to sandstone matrix with rare lonestones	Normally graded with lamination penetrating clasts
Conglomerate	Massive to medium bedded	Clasts of carbonate, quartzite, and volcanic rocks	Weakly graded with imbrication
Sandstone	Thin to massive	Fine- to coarse grained volcaniclastic (quartz, feldspar, lithic fragments)	Both normally graded and cross-bedded facies
Siltstone	Thin to medium, commonly graded between shale and fine-sandstone	Volcaniclastic (quartz, feldspar, lithic fragments)	Grading from shale to fine sandstone, ripple cross-lamination
Shale	Thin	Green to black colored	Suspension lamination

In the Khukh Davaa region (stratigraphic sections F1203 and F1204, Figure 3.6) of the Tsagaan block, the Maikhan-Uul Fm is 250-370 m thick. The lower member rests on an erosional unconformity

and consists predominantly of red-green colored, massive diamictite. The contact between the massive diamictite of the lower member and the green shale and siltstone at the base of the middle member is marked by a ~ 20 cm thick bed of concretionary limestone. The middle member coarsens upwards to massive sandstone, which is in turn succeeded by a second succession of recessive, thinly bedded shale and siltstone. Rare lonestones and lamination-penetrating dropstones are present in the upper ~ 20 m of the middle member. The middle member culminates with massive, channelized sandstone bodies that are < 10 m wide with ~ 4 m of local relief on incising margins. These sandstone bodies are succeeded by massive diamictite of the upper member. Striated clasts and carbonate concretions are common. At western Khukh Davaa, the upper member consists of interbedded siltstone, sandstone, conglomerate, and diamictite. Mudcracks are present near the top of the upper member (Figure 3.7E).

Table 3.2. Carbonate and glacial facies assemblages
Descriptions of lithofacies associations and depositional environments are included.

Carbonate Facies Asssemblage

Assemblage	Lithofacies Associations	Depositional environments
Inner ramp	Micrite, calcisiltite, grainstone, microbialaminite, intraclast breccia in m-scale parasequences.	Periodically restricted and sub-aerially exposed intertidal platform with early dolomitization capping parasequences
Mid-ramp	Medium-bedded micrite, calcisiltite, grainstone and heterolithic interbeds.	Near or below wave-base with ooid-grainstone shoals and frequent storm-derived grain- and debris flows
Outer ramp	Flat, graded, thin beds of micrite, calcisiltite, grainstone, and conglomerate interpreted as debris flow with minor slump folding.	Below wave base with gravity deposits on lower ramp to basin

Glacial Facies Asssemblage

Assemblage	Lithofacies Associations	Depositional environments
Subglacial-ice contact	Massive to weakly bedded diamictite with glacio-tectonic deformation, minor sandstone.	Lodgment till and till in a proximal ice-contact fan deposited below an ice sheet grounded to a marine margin
Sub-ice shelf or glacio-laucustrine	Graded beds of shale to sandstone.	Turbidites and shale deposited below an ice shelf or distal to the grounding line without evidence of significant ice-breakup
Proglacial	Pebbly cross-stratified sandstone, and both massive and stratified diamictite	Marine ice contact fan to glacio-fluvial environments

To the southeast on the Salaa block, in Salaa Gorge (stratigraphic sections F950 and F1212, Figure 3.6) and at Shivee Tsakhir (stratigraphic sections F1127 and F1214-1216, Figure 3.6) (Figure 3.3), the lower member of the Maikhan-Uul Fm consists predominantly of massive, green wackestone matrix diamictite with minor siliciclastic strata and common concretionary carbonate. Similar to northeastern and western Khukh Davaa, the lower member is sharply overlain by green shale and siltstone with the contact marked by a < 20 cm thick concretionary limestone bed. The middle member of the Maikhan-Uul Fm is composed of graded beds of sandstone, siltstone and shale. Lonestones have only been observed in the

uppermost ~ 5 m of the middle member, directly below an erosive contact with the upper member that is marked by a concretionary limestone. At both Salaa Gorge and Shivee Tsakhir the upper member is composed of green and red colored massive diamictites composing the lower ~ 150 m and a > 50 m massive diamictite with a black colored wackestone matrix forming the uppermost unit. This upper black diamictite unit is separated from the underlying red and green diamictites by a laterally continuous, ~ 50 cm thick concretionary carbonate bed.

On the Tsagaan block, in Tsagaan Gorge (stratigraphic sections F724 and F948, Figure 3.6), where the Maikhan-Uul Fm measures > 275 m, again two diamictites are separated by a thick sequence of flat bedded, shale, siltstone and sandstone (Lindsay et al., 1996b). There the lower member consists of at least five massive diamictite units separated by carbonate concretions, erosive surfaces, boulder pavements, shear fabrics (Figure 3.7C) and evidence of soft sedimentary deformation. Striated and faceted bullet-shaped clasts are common. The top of the lower member is marked by 20 cm of stratified diamictite and succeeded by shale, and then ~ 50 m of siltstone dominated graded beds with 1-5 m intervals of graded sandstone. The middle member coarsens up from a lower package of graded siltstone to massively bedded very coarse sandstone with weakly developed ~ 50 cm scale tabular cross-beds. This very coarse sandstone is succeeded by green, mm-laminated, varve-like shale and siltstone (Figure 3.7D). Cobble lonestones are present in the upper 50 cm of the middle member. The upper member begins with a massive diamictite unit above an erosive base that is marked with a concretionary carbonate. In total, the upper member at Tsagaan Gorge consists of massive diamictite separated by < 50 cm thick sandstone beds and weakly stratified diamicite. Clasts of felsic volcanic rocks, carbonate, and siliciclastic rocks are present with several siltstone clasts that preserve soft-sedimentary folding. The contact between the Maikhan-Uul Fm and the overlying laminated limestone of the Taishir Fm is not exposed.

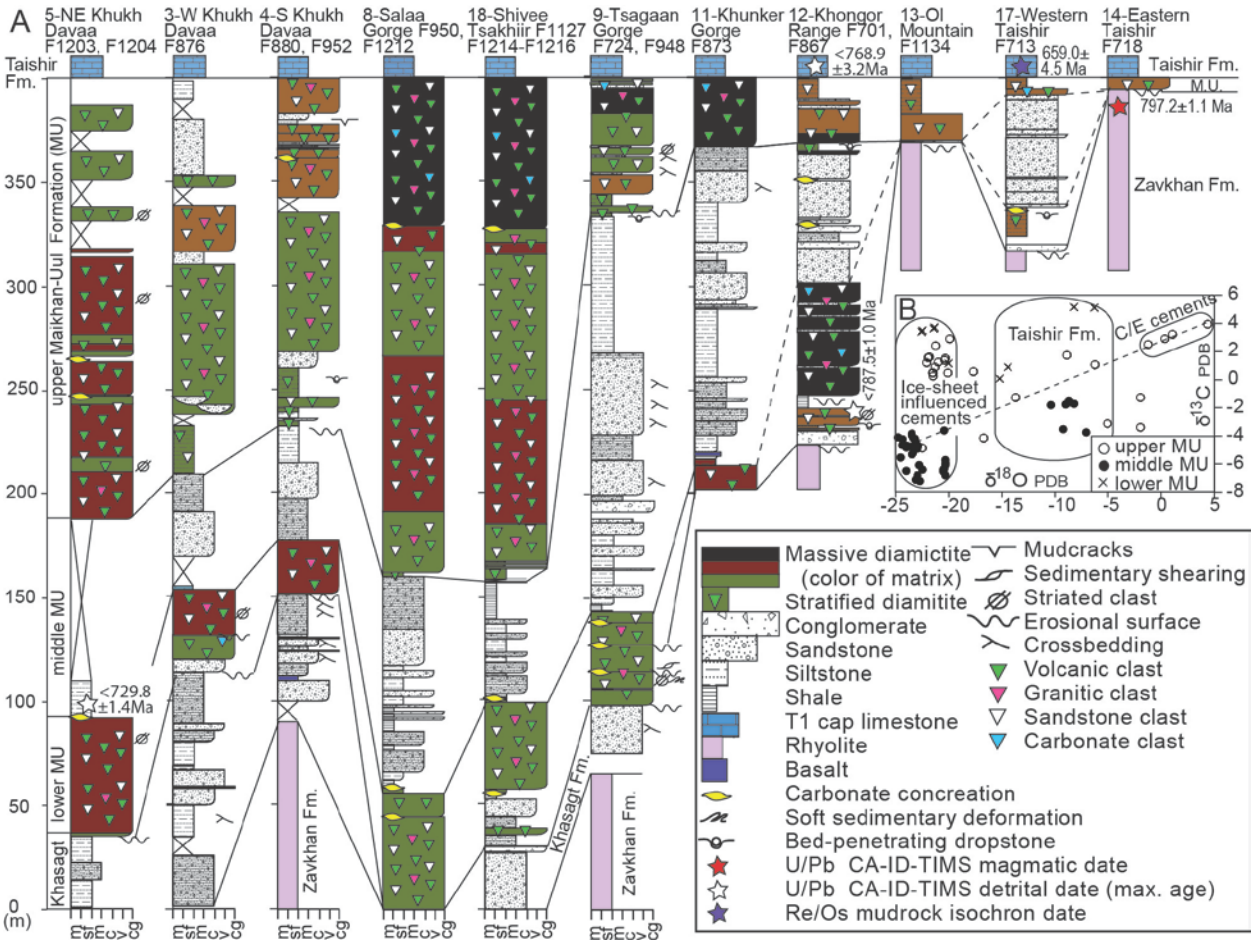

Figure 3.6. The Maikhan-Uul Formation
(A) Stratigraphy of the Maikhan-Uul Formation. Location of sections is shown in Figure 3.3. MU - Maikhan-Uul, m - mudstone, sf - siltstone to fine-grained sandstone, ms - medium-grained sandstone, c - coarse-grained sandstone, cg - conglomerate. (B) Carbon-oxygen isotope cross-plot of cements in the Maikhan-Uul Formation. C/E – clathrate- or evaporation-influenced cement. Dashed line is a mixing line between ice-sheet influenced cements and clathrate- or evaporation-influenced cements. Values of carbon and oxygen isotopes from the Taishir Formation, which includes both cements and micritic groundmass, are also outlined to show range of values from cements that could have precipitated at a later stage.

Farther east, in the Khongor Range (stratigraphic section F701, Figure 3.6) of the Taishir block, the Maikhan-Uul Fm is composed of three distinct massive diamictite intervals separated by siliciclastic strata. The lower diamictite-rich interval begins with a massive, clast-dominated conglomerate, dominated by Zavkhan Fm clasts. This is succeeded by an interval of interbedded massive and stratified diamictite

that contains both bed-penetrating dropstones (Figure 3.7A) and striated clasts (Figure 3.7B). The lower unit is succeeded by graded siltstone and shale beds and then black shale to wackestone matrix, massive diamictite. This second diamictite-rich interval contains clasts of the Zavkhan Fm, the Tsagaankhairkhan Fm dolostone, sandstone and siltstone of the Khasagt Fm, and granite. It is succeeded by siltstone and sandstone with rare cobble lonestones and at least two ~ 20 cm thick bands of concretionary carbonate. The uppermost diamictite-rich interval exposed at Khongor Range has an erosive base and contains both massive and stratified diamictite facies with bed-penetrating dropstones and striated clasts, and minor sandstone beds. A ~ 10 cm thick layer of red clay separates the Maikhan-Uul Fm from the overlying Taishir Fm.

East of the Khongor Range, the Maikhan-Uul Fm rests unconformably on the Zavkhan Fm, with the contact commonly mantled with a boulder pavement. At the easternmost exposures on the Taishir block (stratigraphic section F718, Figure 3.6), the Maikhan-Uul Fm is only ~ 7 m thick and composed predominantly of a massive cobble to boulder clast diamictite, whereas just 1 km to the west (stratigraphic section F713, Figure 3.6) it thickens to ~ 82 m with two diamictite-rich intervals separated by ~ 57 m of massive, medium to very coarse-grained sandstone (Figure 3.6). The lower diamictite-rich interval consists of stratified diamictite with bed-penetrating dropstones. Clast composition is dominated by felsic volcanic rocks, presumably from the Zavkhan Fm. Beds of the overlying middle member of the Maikhan-Uul Fm are commonly graded in cm thick beds, but massive, poorly-sorted, several meter-thick beds with cross-beds and outsized gravel to cobble clasts are also present. The upper diamictite-rich interval begins with massive diamictite with clasts of sandstone and volcanic rocks and culminates with stratified diamictite and a ~ 10 cm thick clay bed that is sharply overlain with laminated limestone of the Taishir Fm (Figure 3.7F).

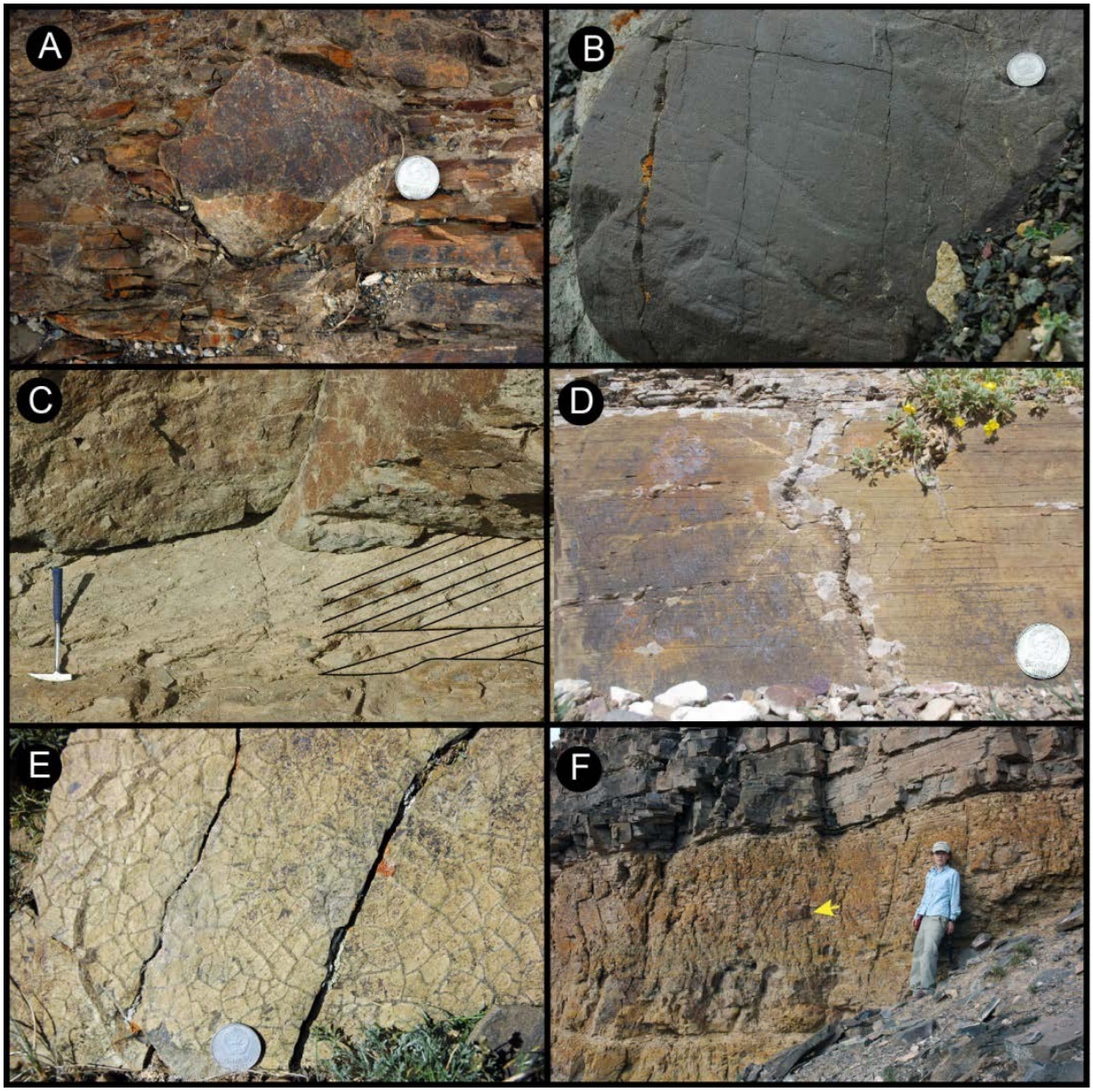

Figure 3.7. Sedimentary features of the Maikhan-Uul Formation
Mongolian coin is 2.25 cm in diameter. (A) Bed-penetrating dropstone in lower member of the Maikhan-Uul Formation at Khongor Range. (B) Striated clast from lower member of the Maikhan-Uul Formation at Khukh Davaa. (C) Top to the right (southwest) shear fabric and concretionary carbonate horizon from the lower member of the Maikhan-Uul Formation at Tsagaan Gorge. Fabric is traced on right side of image. (D) Brown weathered, green when fresh, mm-laminated and varve-like shale, siltstone and sandstone of middle member of the Maikhan-Uul Formation exposed in Tsagaan Gorge. (E) Mud-cracks in the upper member of the Maikhan-Uul Formation at South Khukh Davaa. (F) Orange when weathered, stratified rain-out deposit at the top of the upper member of the Maikhan-Uul Formation at western Taishir, sharply overlain by the Taishir Fm. Arrow points to boulder lonestone.

Taishir Formation.—The Taishir Fm consists of 300-600 m of carbonate that is comprised of four members (T1, T2, T3 and T4), which record four super-sequences (Figure 3.8). Carbonate lithofacies are defined (Table 3.1) and used in the lithostratigraphic descriptions. In the discussion section, carbonate

lithofacies are grouped into facies assemblages (Table 3.2) to interpret evolving depositional environments and distinguish stratigraphic sequences. Sequences described are composed of nested parasequence sets within larger systems tracts (Sarg, 1988).

At all localities, the base of the lower member (T1) rests sharply on the Maikhan-Uul Fm with a 1-10 cm thick claystone layer at the contact (Figure 3.9A). In the Taishir region, the T1 cap carbonate is composed of ~ 0.1-0.5 m graded beds of grainstone and calcisiltite (Figure 3.9A) within background sedimentation of mm-pinstripe laminated micritic limestone (Figure 3.9B). The T1 cap carbonate is tan when weathered, dark gray when fresh. It is succeeded by 10-100 m of pink when weathered and recessive shale, limestone micrite, calcisiltite with minor nodular chert, and carbonate clast breccias interpreted as debris flows. T1 culminates with black lime-grainstone that also contains nodular chert. To the south and west, T1 thins to < 10 m and is composed entirely of mm-laminated micritic limestone (Figure 3.9B).

The second sequence (T2), thins to the south and west and begins with 1-10 m of limestone calcisiltite and thin-bedded micrite with abundant chert nodules, followed by 50-200 m of blue when weathered carbonate in 1-10 m thick carbonate parasequences (Figure 3.9C). The parasequences typically begin with flat- to nodular-bedded calcisiltite and micrite (Table 3.1), succeeded by grainstone and capped either by microbialite or brecciated exposure surfaces. The tops of these parasequences are also commonly partially dolomitized (Figure 3.9D). Giant ooids, < 1 cm in diameter, are common in T2 (Figure 3.4C).

T2 is sharply overlain by an abrupt, recessive flooding surface (Figure 3.9E), marking the base of T3. The third Member, T3, begins with 10-50 m of thin-bedded limestone micrite with interbeds of debris flows with numerous black chert beds and nodules. These beds are succeeded by massive weathering, mm-laminated, dark, fetid thin-bedded limestone micrite with common contortions interpreted as slump folds. The lamination is highlighted by mm-scale lighter bands of calcite (Figure 3.9G), presumably created through remineralization and the *in situ* production of carbonate alkalinity. These massive black mudstone facies were originally interpreted as deepwater microbialaminites (Johnston et al., 2012;

Macdonald et al., 2009a) due to their superficial similarity to massive microbialaminites in the Rasthof Fm (Pruss et al., 2010). However, petrographic examination has revealed micro-grading without strong microbial fabrics (Figure. 3.9G). Consequently, we have reinterpreted these facies as allodapic micritic carbonate deposited below storm wave base and distal to massive grain flows and debris flows. Although microbes may have been involved in remineralization and the creation of the thin bands of light-colored calcite and crinkly lamination, these microbes did not necessarily form mats. This massive unit of black carbonate mudstone is succeeded by thickly bedded grainstone with giant ooids. Unlike other units that generally thin to the south and west, the thickness of T3 is relatively consistent across the platform.

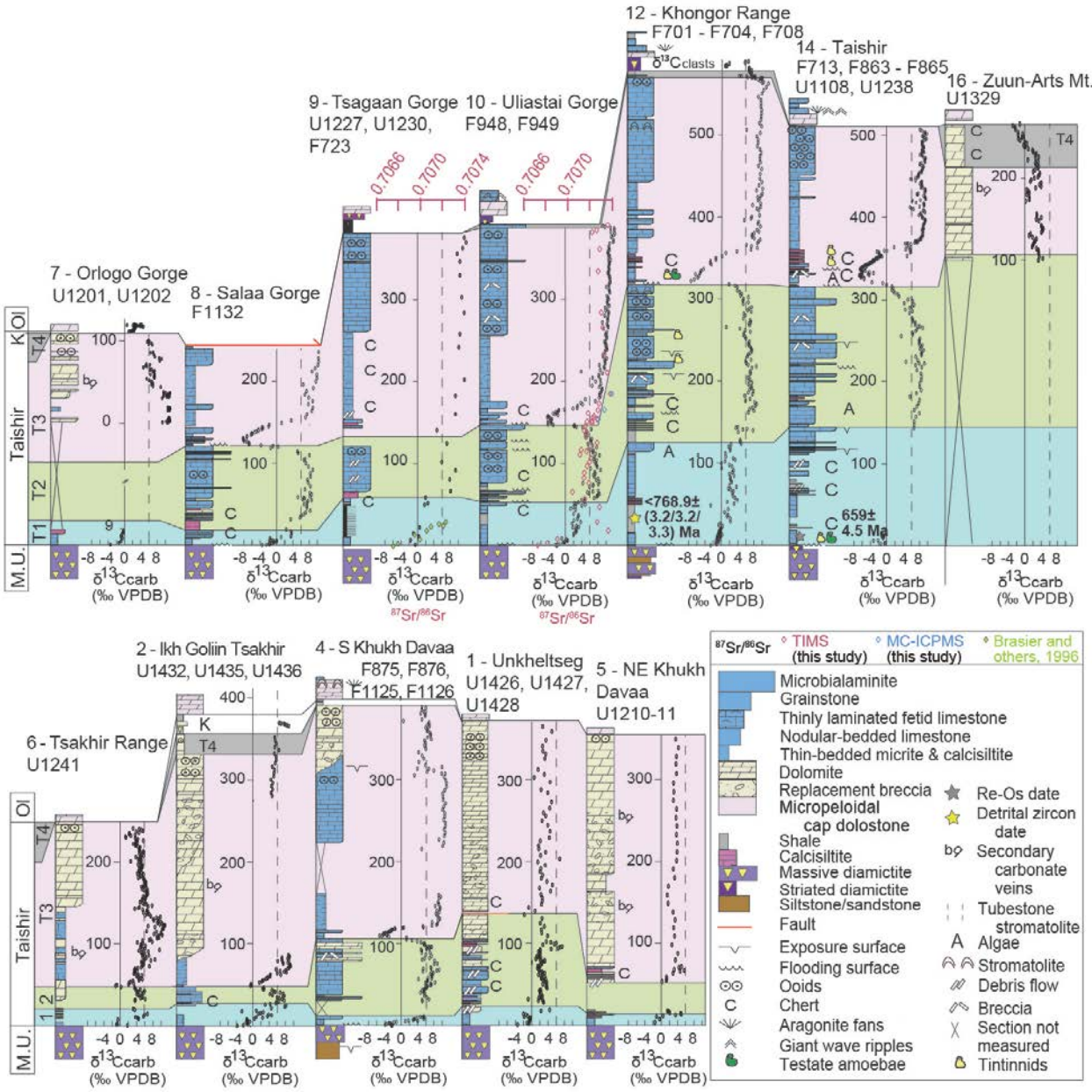

Figure 3.8. Stratigraphy of the Taishir and Khongor formations
Location of sections is depicted in inset outline map. Key for the localities labeled in inset map is the same as in Figure 3.3. Dashed line is drawn to highlight +6‰ $\delta^{13}C$ values. Microfossils, testate amoebae (Bosak et al., 2011a), tintinnids (Bosak et al., 2011b), and algae (Cohen et al., 2015) are shown stratigraphically. $^{206}Pb/^{238}U$ CA-ID-TIMS detrital age on tuffaceous sandstone from Member T1 of the Taishir Fm is shown with the corresponding maximum age. $\delta^{13}C$ values plotted in Tsagaan Gorge section are from Brasier et al. (1996b).

Exposure in the Khongor Range (stratigraphic sections F701-704 and F708, Figure 3.8) is similar to what is exposed in the Taishir Region. Here, T1 culminates with lime-grainstone. T2 begins with shale and calcisiltite, followed by m-scale carbonate parasequences defined by interbeds of thin-bedded

limestone micrite and calcisiltite and blue when weathered, dark gray when fresh grainstone. T2 is ~ 20 m thicker than T2 at the Taishir locality and chert nodules are common in the lower portion, whereas < 1 cm ooids become common towards the top. The base of T3 is also well-exposed and succeeded by thick fetid limestone. Top of T3 is defined by massively bedded lime-grainstone with < 1 cm ooids at the top. Importantly, this unit is overlain by < 10 m of thin-bedded limestone micrite and black shale (T4), which is sharply overlain by the Khongor Fm diamictite.

The Taishir Fm exposure in Uliastai Gorge (stratigraphic sections F948 and F949) of the Khunkher block is comparable and similar to exposures in Tsagaan Gorge (stratigraphic sections U1227, U1230 and F723) of Tsagaan block (Figure 3.8). T1 is thinner but T2 is thicker than Khunkher block section. The direct contact of the Maikhan-Uul Fm and the T1 cap carbonate is not exposed in Tsagaan Gorge although the Maikhan-Uul Fm is well-exposed and preserved. In addition, T1 recessive interval is composed of dominantly black shale with interbeds of thinly-bedded and dark colored carbonate and thin-bedded micrite and nodular-bedded limestone with lenticular chert nodules. T2 is composed of massively bedded lime-grainstone with abundant intraclast breccia and lenticular chert nodules with redeposited clasts and coated grains that become more common up-section. However, in Uliastai Gorge, T2 is dominated by ooid lime-grainstone. The lower T3 that hosts the Taishir excursion is not well-exposed in Tsagaan Gorge compared to Uliastai Gorge but the rest of the T3 including fetid and massively weathered limestone mudstone and ooid lime-grainstone is similarly well-exposed. Although not complete, the Member T4 is preserved in Uliastai Gorge and consists of ~ 2 m of microbialiminite, which is overlain by < 2 m of shale.

In Salaa Gorge (stratigraphic section F1132, Figure 3.8) of the Salaa block, T1 becomes even thinner and is entirely composed of mm-laminated micritic limestone with a few meters of pink calcisiltite on top. At the top of the pink calcisiltite unit, gray when fresh dolostone bed with occasional chert nodules is present and is succeeded by patchily exposed, dark gray when fresh lime-grainstone. The overall thickness of T2 is greater than elsewhere. The T2 flooding surface begins with shale and is succeeded by lime-grainstone with minor interbeds of < 10 m thick thin-bedded limestone micrite with

black chert nodules. The base of T3 and the overlying fetid, thin-bedded limestone micrite and calcisiltite are well-exposed at Salaa Gorge and starts out with interbeds of thin-bedded micrite, nodular-bedded limestone, and grainstone followed by dark gray when fresh, fetid limestone mudstone with an interbed of lime-grainstone. The uppermost part of T3, usually characterized by ooid lime-grainstone, is faulted out at this locality.

In Orlogo Gorge (stratigraphic sections U1201 and U1202, Figure 3.8) of the Orlogo block, the Taishir Fm is patchily preserved compared to elsewhere with some units that are not exposed in the transition between the members. Thin (mm)-laminated micritic limestone of the T1 cap carbonate is overlain by recessive, poorly exposed, pink when weathered calcisiltite. The upper portion of T1, the whole of T2, and the lower portion of T3 were not measured at this locality due to poor exposure. However, T3 starting from the upper part of the fetid, massively weathered, thin-bedded limestone micrite to the Ol Fm carbonate was measured. The upper portion of T3 is dolomitized at this locality and transitions from limestone to partially dolomitized limestone to dolostone are well-preserved. The dolomitized strata of T3 are composed of brown- to yellow-colored ooid dolostone grainstone that is sugary and vuggy with abundant secondary calcite veins. More than a meter of non-exposure separates the Taishir Fm and the overlying Ol Fm, which could be correlated to either T4 or the Khongor Fm.

Similar facies of the Taishir Fm are exposed at the NE Khukh Davaa (stratigraphic sections U1210 and U1211) and Unkheltseg (stratigraphic sections U1426, U1427 and U1428) localities although most of the carbonates are dolomitized (Figure 3.8). T1 is only 10-13 m thick at both localities and composed of thinly laminated micritic limestone at the base that is succeeded by a recessive unit composed of fine- to medium-bedded, gray limestone and pink calcisiltite. Interbeds of black shale are common at Unkheltseg Mountain where the overlying ~ 80 m thick interval of T2 is characterized by carbonate parasequences that are composed of dolomite allochems marked by intraclast breccia with bedded and nodular chert. Although the parasequences are mostly dolostone, the lower ~ 50 m of this sequence are dominated by limestone, and the transition from limestone to dolostone is characterized by alternations of limestone and dolomite breccia up to the shale and calcisiltite at the base of the T3. The

recessive unit is composed of pink calcisiltite and brown to gray, thinly-laminated, dark gray limestone with occasional intraclast breccia and chert nodules succeeded by lime-grainstone. The rest of the T3 is heavily dolomitized and composed of recrystallized, sugary, and vuggy dolo-grainstone.

In the South Khukh Davaa block (stratigraphic sections F875, F876, F1125 and F1126; Figure 3.8), the contact between the Maikhan-Uul and the basal Taishir Fm is well-preserved and exposed. However, the T1 cap carbonate becomes very thin and is composed solely of mm-laminated black limestone. It is overlain by lime-grainstone and a ~ 20 m interval that is not exposed. The base of T2 is characterized by thick limestone microbialite and thin-bedded limestone micrite. It is succeeded by thick lime-grainstone with several interbeds of microbialite towards the top. The base of T3 is well-exposed at this locality and is composed of thin-bedded limestone micrite. Aside from a thick non-exposed interval, the upper portion of T3 is well-exposed with a transition from limestone to dolostone towards the top. Above the non-exposed interval, the upper part of the T3 continues for ~ 170 m with the upper ~ 85 m dolomitized. The dolostone is characterized by sugary and vuggy dolo-grainstone with abundant ooids. Due to silicification, the ooids stand out in relief.

At Ikh Goliin Tsakhir Mountain (stratigraphic sections U1432, U1434 and U1436, Figure 3.8) of the South Khukh Davaa block, the contact between the Maikhan-Uul and Taishir fms is well-exposed, and T1 and T2 are thin. T1 is composed of mostly mm-laminated micritic limestone, which is succeeded by a recessive unit with fine (< 10 cm) interbeds of limestone. A massively-bedded limestone caps the recessive unit. The base of T2 is well-exposed and characterized by a recessive unit, which is composed of interbeds of red and pink shale, calcisiltite and weakly-laminated, light brown when weathered limestone. This light brown limestone is succeeded by medium- to thick-bedded, black gray limestone with bedded to lenticular chert beds, followed by massively weathering, black limestone with occasional beds of intraclast breccia. The lower recessive portion of T3 is composed of < 10 cm bedded, massively weathered orange to brown limestone micrite. It is overlain by fetid thin-bedded limestone micrite and an additional ~ 250 m of dolomitized T3. The dolomitized strata are intensely veined and brecciated. Similar to Unkheltseg, both texture retentive and destructive dolostone are present. The brecciated interval is

succeeded by coarsely recrystallized, vuggy and sugary dolostone with silicified ooids. Above the ooid dolo-grainstone, dolomitized T4 is present (Figure 3.8) and characterized by a ~ 25 m thick, weakly-laminated, blue-gray, recrystallized dolostone that is overlain by the Khongor diamictite.

In the Tsakhir Range (stratigraphic section U1241, Figure 3.8) of the Tsakhir block, the Taishir Fm is relatively thin. At this locality, the contact of the Maikhan-Uul and Taishir fms is well-exposed. Mm-laminated micritic limestone of the T1 cap carbonate is overlain by a poorly exposed recessive unit characterized by subcrop of pink calcisiltite and thinly-bedded black limestone. The upper portions of T1 through the base of T3 are not exposed but subcrop measures to < 50 m. The overlying fetid thin-bedded limestone micrite of the T3 is present but partially dolomitized. Similar to the other localities, the Taishir Fm is preserved as dolostone that is heavily veined and brecciated. Both texture retentive and destructive dolostone are present and are capped by sugary and vuggy, recrystallized ooid dolostone grainstone. In the Tsakhir Range the Ol Fm directly overlies the Taishir Fm.

At Zuun-Arts Mountain (stratigraphic section U1329, Figure 3.8), due to abundant Permian intrusions nearby, T1 and T2 are poorly exposed. Laterally, they crop out and are composed of limestone. However, in section U1329, only the upper T3 and its transition to Ol Fm are captured. Here, the whole T3 is composed of recrystallized, sugary, and vuggy dolo-grainstone. It is succeeded by medium-bedded, light blue gray when weathered, black blue gray when fresh, and recrystallized dolostone that is attributed to T4.

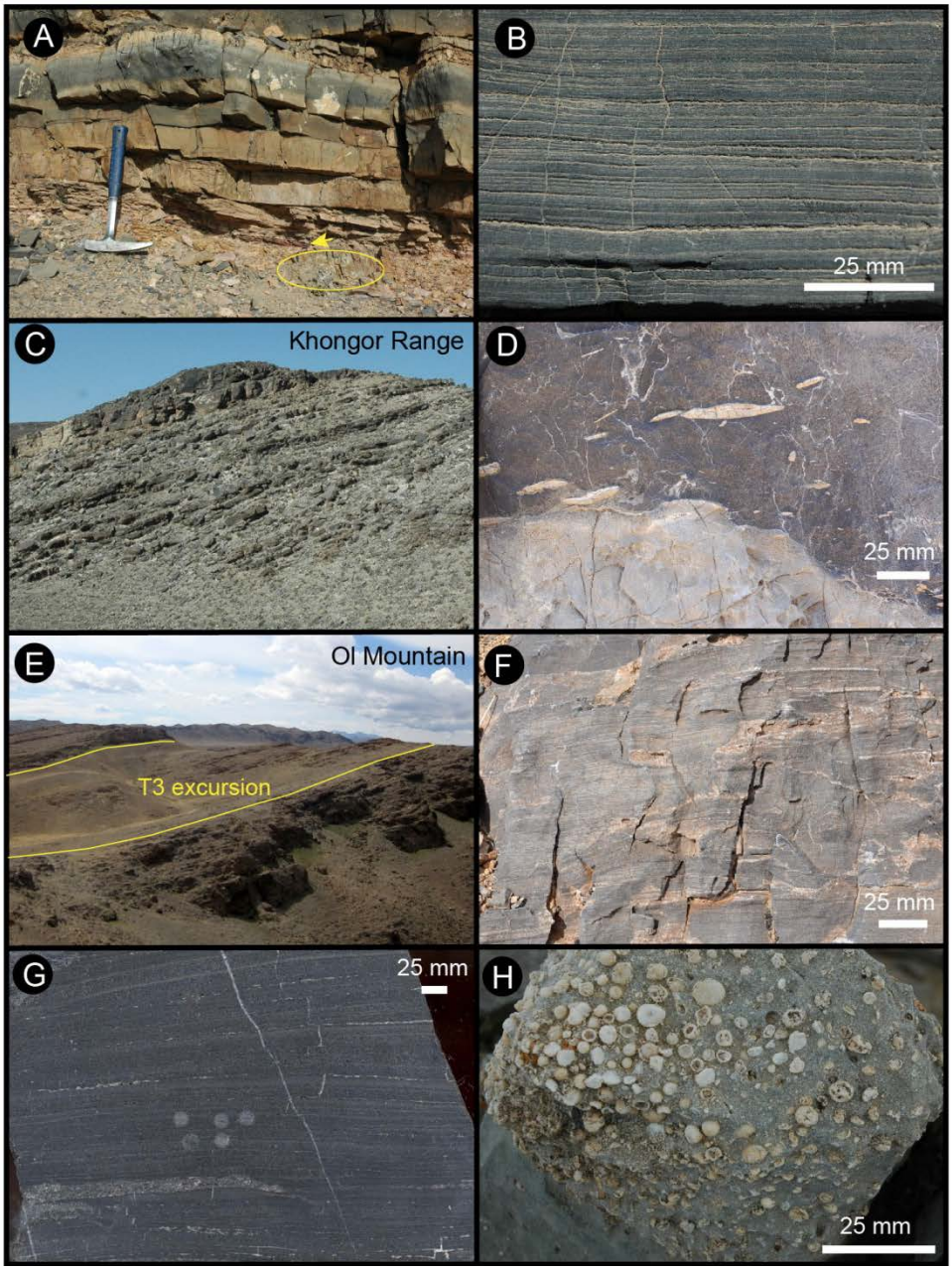

Figure 3.9. Sedimentary textures in the Taishir Formation
(A) Basal contact of Taishir Formation at western Taishir. Rhyolite clast in uppermost Maikhan-Uul Formation is circled. Arrow points to red claystone layer that separates the Maikhan-Uul and Taishir formations. At this locality, the basal Taishir Formation consists of ~ 0.1 m of graded beds of grainstone and calcisiltite in a background of mm-pinstripe laminated micrite. (B) Pinstripe lamination of the basal T1 cap limestone at Shivee Tsakhir. (C) Resistant ledges marking meter-scale parasequences in T2 at Khongor Range. Field of view is ~ 20 m. (D) Partially dolomitized top of parasequence in T2 at Khukh Davaa. Dolomitized parasequence cap is cut by a scour surfaced and filled with a lime-grainstone with chips of the underlying dolomitized unit. (E) Recessive calcisiltite and shale interval marking the onset of T3 and the Taishir excursion at Ol Mountain. Field of view is ~ 35 m. Note how bedding becomes thinner above the recessive interval. (F) Dolomitized T3 of the Taishir Formation exposed in the Unkheltseg Mountain (U1427). (G) Polished slab showing micro-grading and mm-scale bands of remineralization in sulfidic calcisiltite of T3 at Salaa Gorge. Pits are micro-drill holes used to extract carbonate powder for geochemical analyses. (H) Partially dolomitized giant ooids from top of T3 near Ol Mountain.

Khongor Formation.—The Khongor Fm is composed of carbonate clasts in weakly stratified shale, siltstone, or calcisiltite matrix. Clasts range from gravel to boulder in size and are typically sub-angular to sub-rounded (figures 3.8 and 3.10A). The Khongor Fm is thickest and best exposed and preserved in three localities: the eastern tributary of Tsagaan Gorge (stratigraphic section F723), Khongor Range (stratigraphic sections F708 and F949) and Ikh Goliin Tsakhir Mountain (stratigraphic section U1433) (Figure 3.8). However, like the Maikhan-Uul Fm, there are significant facies changes due to channelization.

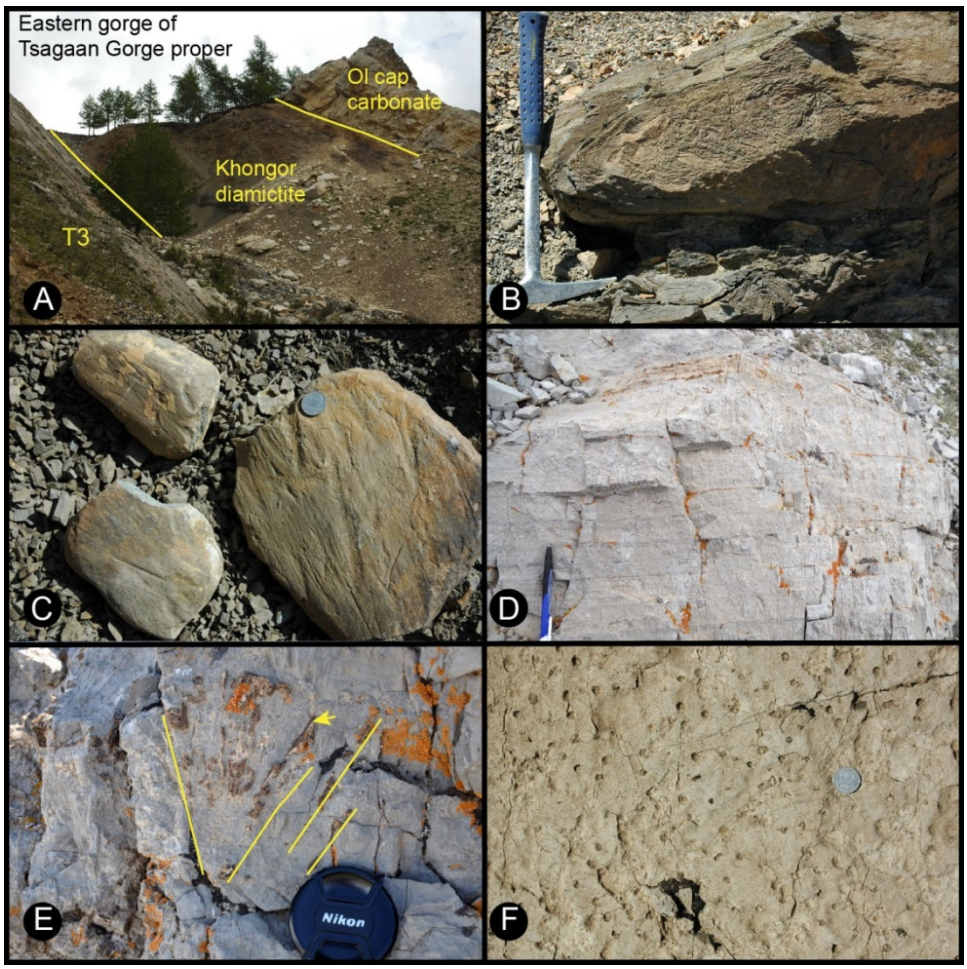

Figure 3.10. Sedimentary textures in the Khongor and Ol formations
Mongolian coin is 2.25 cm in diameter. (A) Khongor diamictite and Ol cap dolostone exposure at Tsagaan Gorge tributary (eastern gorge of Tsagaan gorge proper). Tree in foreground is growing off of the basal contact with T3. Section is 22 m thick. Ol cap dolostone is in top right of frame. (B) Limestone clast with soft-sedimentary, glacitectonic folding from Khongor diamictite. (C) Striated clasts of the Khongor Formation as preserved in the eastern tributary of Tsagaan Gorge. (D) Finely laminated, pale white colored Ol cap dolostone. Photo is taken in South Khukh Davaa block (U1216). Pen is 14 cm in length. (E) Silicified aragonite fan growth in the Ol Formation carbonate (U1217). (F) Plan view of tubestone stromatolites in Ol cap dolostone taken from near Taishir.

In the eastern tributary of Tsagaan Gorge (figures 3.8 and 3.10A), the Khongor Fm diamictite is ~ 25 m thick and is composed of pebble- to boulder-sized clasts of blue-gray limestone from the underlying Taishir Fm in a dark gray wackestone matrix that becomes lighter colored upwards with increasing carbonate content. A glacial origin is demonstrated by the presence of spectacular striated clasts (Macdonald et al., 2009a), and cobble dropstones (Figure 3.10C) that penetrate and deform the bedded, shale matrix. Just 6 km west, the diamictite is nearly absent with only 2 m of recessive siltstone preserved.

The Khongor Fm in the Khongor Range (stratigraphic section F708, Figure 3.8) consists of ~ 16 m of sub-rounded limestone pebbles and cobbles in weakly stratified, gray shale to wackestone matrix. Elsewhere, on the thrust blocks to the northeast, the Khongor Fm is either thin or absent. Although most clasts in the exposure of the Khongor Fm at the eponymous location can be identified as sourced from the Taishir Fm, clasts of carbonate mudstone with intense soft sediment deformation (Figure 3.10B) were not recognized from exposures of the underlying Taishir Fm. Concentrations of boulder clasts ('boulder nests') are present in the Khongor Range exposures (Macdonald, 2011a).

The Ikh Goliin Tsakhir (stratigraphic section U1435, Figure 3.8) is the third locality where the Khongor Fm is preserved as a thick diamictite (Figure 3.12A). At this locality, the basal part of the Khongor Fm is not well-exposed but is characterized by subcrops of shale and siltstone with pebble-sized carbonate clasts. Interestingly, there is < 5 m thick, brown weathered, black to gray fresh, coarsely recrystallized dolostone preserved a few meters above the poorly exposed base of the Khongor Fm. It is succeeded by dark green to gray wackestone matrix diamictite with gravel to cobble clasts. This dolostone could either represent a large clast or could be part of T4.

At the South Khukh Davaa block (stratigraphic section F875, Figure 3.8), the Khongor Fm is also present, albeit poorly exposed. Here the Khongor Fm is 7 m in thickness, including 2 m of unit that is not exposed at the base and overlying subcrops of rounded clasts in a green wackestone matrix.

Ol Formation.—The Ol Fm sharply overlies the Khongor diamictite and marks the beginning of the Ediacaran Period on the Zavkhan Terrane (Macdonald et al., 2009a). The sequence begins with < 40

m of buff-colored, finely-laminated micropeloidal dolostone (Figure 3.10D), which locally contains tubestone stromatolites (Figure 3.10F) and giant wave ripples (Bold et al., 2013; Macdonald, 2011a; Macdonald et al., 2009a). At some localities, the cap dolostone is succeeded by aragonite crystal fans that are pseudomorphed by dolomite and sometimes silicified (pseudomorphed aragonite crystal fans) (Figure 3.10E) present both as individual blades growing upwards into the sediment, similar to the Hayhook Member in the Mackenzie Mountains of Canada (Aitken, 1991), and as crystal fan shrubs that are over 10 cm across, as is seen in northern Namibia (Hoffman and Halverson, 2008). Elsewhere, this limestone is dolomitized to a chocolate brown colored dolostone that co-occurs with disseminated barite, barite breccia (dolomitized pseudomorphed barite breccias, recognized visually by crystal habit), and locally barite fans (Hoffman et al., 2011). For mapping purposes, the first transgressive sequence above the finely laminated micropeloidal dolostone is included in the Ol Fm.

At the Zuun-Arts locality (stratigraphic section U1329, Figure 3.11), the Ol cap dolostone is ~ 6 m thick. It is succeeded by ~ 28 m of light brown when fresh, chocolate brown when weathered, finely-bedded dolostone.

At Ol Mountain (stratigraphic section U1337, Figure 3.11) of the Taishir block, the cap dolostone is ~ 7 m thick and is succeeded by thinly-bedded, chocolate brown colored dolostone with < 50 cm tall wave ripples and disseminated barite. The start of the overlying transgressive sequence is poorly exposed. At Ol Mountain, the top of the Ol Fm consists of ~ 22 m of massively bedded, dark gray dolostone.

In the Khongor Range (stratigraphic sections F708 and F949, Figure 3.11) of the Taishir block, the Ol Fm is very well-exposed and preserved, and it overlies one of the thickest sequences of the Khongor Fm diamictite. There the base of the Ol Fm, the cap dolostone, is ~ 8 m thick and consists of buff-colored micropeloidal dolostone. It is succeeded by blue-gray nodular-bedded limestone and thinly-bedded, dark gray lime-micrite interbedded with shale and calcisiltite. This succession contains abundant chert nodules and is capped by massively bedded lime-grainstone (Figure 3.11).

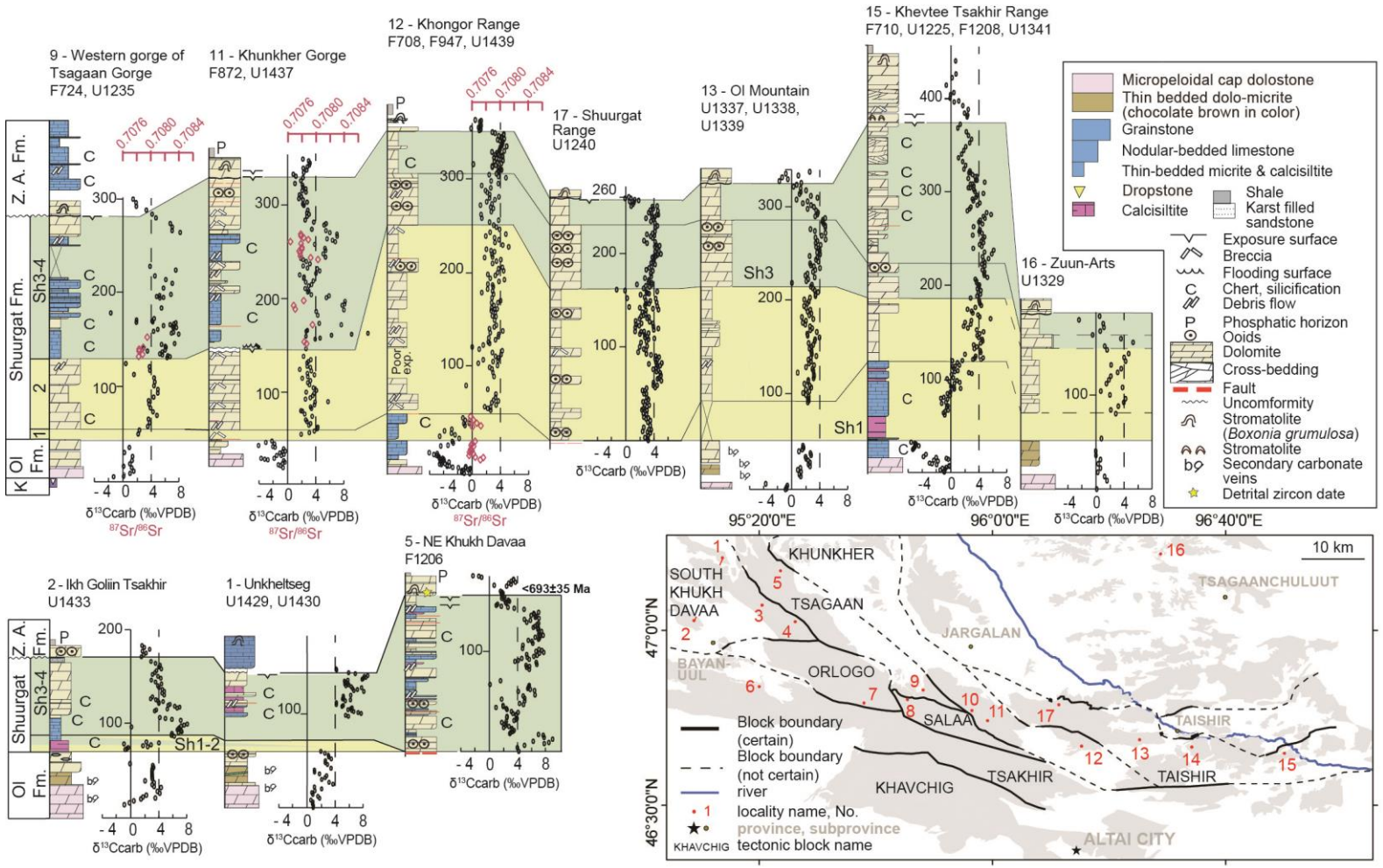

Figure 3.11. Stratigraphy of the Ol and Shuurgat formations

Location of sections is depicted in inset outline map. Key for the localities labeled in inset map is the same as in Figure 3.3. Dashed line is drawn to highlight +4‰ $\delta^{13}C_{carb}$ values. $^{87}Sr/^{86}Sr$ values are co-plotted with $\delta^{13}C$ where measured.

In Khunkher Gorge (stratigraphic sections F872 and U1437, Figure 3.11), the basal Ol cap dolostone is ~ 11 m thick and overlies a ~ 2 m poorly exposed interval above the ooid lime-grainstone of the T3 Member of the Taishir Fm. The cap dolostone is overlain by a recessive unit is composed of interbeds of blue dolostone grainstone and calcisiltite. It is succeeded by recessive unit composed of mostly thin-bedded mircrite and nodular-bedded limestone, interbedded with thin beds of calcisiltite. The uppermost unit of the Ol Fm, which is often massively bedded blue limestone is faulted out and juxtaposed against the second member of the Shuurgat Fm.

In the western tributary of Tsagaan Gorge (stratigraphic sections F724 and U1235, Figure 3.11), the basal contact of the Ol Fm with the underlying Khongor Fm is well-exposed. Although the basal exposure is poor in the main Tsagaan Gorge, the mm-laminated, micropeloidal dolostone of the Ol Fm is well-exposed and is ~ 11 m thick. It is succeeded by light blue dolostone. The overlying recessive unit is not exposed for ~ 4 m. At this locality, the uppermost Ol Fm is composed of blue dolostone with black chert nodules. The contact between the upper Ol Fm and the overlying Shuurgat Fm is poorly exposed.

At the northeastern Khukh Davaa locality (stratigraphic section F1206, Figure 3.11) of the Tsagaan block and in Shuurgat Range of the Taishir block, the Ol Fm is not well-exposed. A series of faults are mapped both below and above the different units of the Ol Fm. At Unkheltseg and Ikh Goliin Tsakhir localities of the South Khukh Davaa block, the Ol Fm is better exposed and appears thicker. At the Unkheltseg locality, a meter of non-exposure is present below the base of the Ol Fm. The buff-colored, finely-laminated micropeloidal dolostone is ~ 23 m thick and is overlain by massively-bedded, dark blue to gray dolostone. It is succeeded by finely-laminated, chocolate brown colored dolostone. The overlying recessive unit is poorly exposed, but all of the interbeds that crop out are massively-bedded dolostone, which culminates with beds of ooid dolo-grainstone. Due to silicification, ooids become prominent and are lithologically indistinguishable from silicified giant ooids at the top of T3.

At Ikh Goliin Tsakhir (stratigraphic sections U1433 and U1435, Figure 3.11), the contact with the underlying Khongor Fm is well exposed. The buff-colored, finely-laminated micropeloidal cap dolostone is comparatively thicker than elsewhere. It is succeeded by ~ 15 m thick, chocolate brown, finely-bedded

dolostone. There is no recessive unit present at this locality. Instead, finely laminated micropeloidal dolostone is overlain by dark gray when fresh, poorly-bedded dolo-grainstone. Above, the exposure becomes poor but where it crops out the dolostone unit is composed of nodular-bedded dolostone with lenses of green siltstone and shale. The micropeloidal dolostone as well as the overlying dolostone contains veins of pseudomorphed calcite and barite. Recessive interbeds of black limestone and pink calcisiltite of the basal Shuurgat Fm overlie the Ol Fm.

Shuurgat Formation.—The Shuurgat Fm (Bold et al., 2013) is composed of 100-500 m of carbonate that comformably overlies the Ol Fm. The Shuurgat Fm is best exposed at Khongor, Shuurgat, Ol Mountain and in the Khevtee Tsakhir Range. For mapping purposes, we have divided the Shuurgat Fm into four members (Sh1, Sh2, Sh3, and Sh4). Broadly, Sh1 is dominated by recessive calcisiltite that shoal upwards into massively weathering dolostones of Sh2. Although these dolomites are massive on the outcrop scale, where primary fabrics are preserved, Sh2 consists predominantly of finely-laminated micrite, with rare ooid grainstone beds, but dolomitization was fabric destructive, leaving a zebra dolostone texture (Vandeginste et al., 2005). Sh1 and Sh2 exhibit large lateral facies changes and vary in thickness from ~ 20-200 m. Sh2 is capped by a karstic erosional surface that is best developed at Khunkher Gorge (Figure 3.12C). The overlying members Sh3 and Sh4 consist of blue colored limestone and dolostone with well-developed parasequences and common chert nodules and beds. Dolomitization is fabric retentive and more common to the northeast. The top contact of the Shuurgat Fm is defined by quartz sandstone-filled grikes (Figure 3.12E) along a karstic unconformity, locally with several meters of relief. Below we describe 10 measured sections of the Shuurgat Fm from representative structural blocks.

At Zuun-Arts (stratigraphic section U1329, Figure. 3.11), the Shuurgat Fm is comparatively thin. The recessive Member Sh1 is poorly-exposed. It is overlain by thinly-bedded, dolo-micrite and nodular-bedded dolostone of Sh2 and dolo-grainstone of Sh3. Sh4 is composed of light blue-gray when fresh, medium-bedded micritic dolostone, which is capped by the uncomformity that defines the top of the Shuurgat Fm.

In Khevtee Tsakhir Range (stratigraphic sections F1208, U1225, and U1341, Figure 3.11) of the Taishir block, all four members are well-defined and exposed. Member Sh1 is composed of interbeds of purple when weathered calcisiltite and dark gray nodular-bedded limestone. The basal ~ 60 m is dominated by calcisiltite, which is overlain by nodular-bedded limestone with abundant chert nodules and beds. The upper ~ 30 m is carbonate-dominated with minor interbeds of calcisiltite and shale. Local folding is apparent at the top of Sh1 with fold axes trending ENE-WSW. The overlying Sh2 is characterized by thinly-bedded dolo-micrite that is variably brecciated. It is succeeded by Sh3 that is recrystallized, sugary and vuggy dolo-grainstone with occasional ooid shoals. Sh4 is ~ 150 m thick (Figure 3.11) and is composed of crossbedded nodular bedded dolostone and dolo-grainstone in ~ 5 meter-scale parasequences that are variably silicified with abundant chert beds and nodules. Multiple karst surfaces are present at the top of Sh4 and are defined by < 0.5 m local relief filled with carbonate breccia. The uppermost karst surface is overlain by dolo-grainstone with both domal and columnar stromatolites of the Zuun-Arts Fm.

At Ol Mountain (stratigraphic sections U1337, U1338, and U1339, Figure 3.11) of the Taishir block, the Shuurgat Fm begins with non-exposed interval above the massively bedded dolostone of the upper Ol Fm. Abundant black chert, red calcisiltite, and pink siltstone of Sh1 are present in the scree. These strata are succeeded by thinly laminated dolostone of Sh2 that is variably brecciated with massively bedded dark gray dolostone in the middle. Sh3 begins with brown to gray, sugary dolo-grainstone with ooids that are variably silicified. It is overlain by Sh4 that is composed of medium-bedded, light-gray when weathered nodular-bedded limestone with silicified vugs towards the top. Here the karsted surface at the top of the Shuurgat Fm is not well-exposed.

In the Shuurgat Range (stratigraphic section U1240, Figure 3.11) of the Taishir block, Sh1 is faulted and the rest of the Shuurgat Fm is very-well exposed. Hence, exposed Sh2 is ~ 160 m thick and composed of alternations of thinly laminated dolo-micrite (Figure 3.12D) that is variably brecciated and occasional massive, dark gray ooid dolo-grainstone. Succeeding Sh3 is composed of light blue-gray

silicified ooid dolo-grainstone and is lithologically similar to that exposed at Ol Mountain. Sh4 at this locality is composed of variably silicified nodular-bedded dolostone.

The Khongor Range (stratigraphic sections F708 and U1439, Figure 3.11) of the Khunkher block is another locality where the Shuurgat Fm is well exposed and thick. Member Sh1 is composed of pink calcisiltite with interbedded black limestone and bedded chert (Figure 3.12B). Sh2 is thickest in the Khongor Range and is composed of primarily thinly laminated dolo-micrite that is variably brecciated and occasional massive-bedded ooid dolo-grainstone. Sh3 is thinner consisting of thinly-bedded, light-gray, variably silificied ooid dolo-grainstone and is succeeded by variably silicified, fine- to medium-bedded, light gray dolo-grainstone that is assigned to Member Sh4.

In Khunkher Gorge of Khunkher block as well as in Tsagaan and South Khukh Davaa blocks, carbonate facies of Sh3 change dramatically from east to west and are composed of thinly laminated micrite and nodular-bedded limestone with abundant chert nodules and lenses (Figure 3.11). At these localities, Sh4 is also dominated by limestone and it is especially prevalent in Khunkher and western tributary of Tsagaan gorges with interbeds of calcisiltite and a few meters thick dolostone. Due to the carbonate facies similarity between Sh3 and Sh4 in these localities, on Figure 3.11, we group these together as Sh3-4 but acknowledge that in other localities, Member Sh3 is easily identifiable as thickly bedded blue-gray dolo-grainstone with ooid shoals.

In Khunkher Gorge (stratigraphic sections F872 and U1437, Figure 3.11), the basal member of the Shuurgat Fm is not exposed. Member Sh2 is faulted against the upper part of the Ol Fm and is composed of massively recrystallized thinly-laminated dolo-micrite and nodular bedded dolostone that are variably brecciated. A sandstone-filled karst with a meter of relief is present at the top of Sh2 (Figure 3.12C). It is succeeded by Sh3 and Sh4 that are composed of fine- to medium-bedded lime-micrite with black chert, calcisiltite and shale with thin interbeds of intraclast breccia. There is a ~ 40 m-thick dolo-micrite and nodular bedded dolostone present in the middle of this limestone dominated succession, and the uppermost ~ 65 m are also composed of dolostone that is characterized by recrystallized, massive-bedded dolo-grainstone with minor ooid shoals developed at the top. Above the unconformity at the top

of the Shuurgat Fm, dolo-grainstone with columnar stromatolites is present with multiple small-scale exposure surfaces that are defined by local relief and secondary silicification.

In the western tributary of Tsagaan Gorge (stratigraphic sections F724 and U1235, Figure 3.11), the whole Shuurgat Fm is patchily exposed. The basal Sh1 recessive unit is poorly exposed and abundant black chert, black limestone and pink when weathered calcisiltite are present in the scree. It is overlain by fine- to medium-bedded dolostone and massive-bedded dolo-grainstone that are variably brecciated of Sh2. Facies-wise, Sh3 is similar to the exposure at Khunkher Gorge and is limestone dominated. The limestone dominated strata of Sh3 and Sh4 at this locality starts out with thin-bedded micritic limestone that is capped by dolo-micrite. The transition from limestone to dolostone is poorly exposed here. Similarly to the Khunkher Gorge, this dolostone succession is succeeded by thin-bedded lime-micrite and nodular-bedded limestone. This limestone dominated strata of Sh4 is capped by massively-recrystallized dolo-grainstone. The uncomformity with the basal Zuun-Arts Fm at the top of the Sh4 is well-exposed at this locality and is defined by a white colored, poorly sorted sandstone that fills a karast surface.

At northeastern Khukh Davaa, Unkheltseg and Ikh Goliin Tsakhir localities, the whole Shuurgat Fm thins dramatically. In NE Khukh Davaa region (stratigraphic section F1206, Figure 3.11) of the Tsagaan block, Sh1 and 2 are faulted against the upper Ol Fm and parts of Sh3 and Sh4 are preserved as limestone. It is composed of ooid dolo-grainstone at the base that is succeeded by carbonate succession dominated by thin-bedded micritic limestone. The rest of the carbonate succession exposed at this locality is distinct by its ~ 30 m thick parasequences composed of alternating beds of thin-bedded micritic limestone, nodular-bedded calcisiltite and grainstone with occasional conglomerates interpreted as debris flows, pink when weathered calcisiltite and dolo-grainstone. Chert nodules and lenses are abundant throughout this succession. At the Unkheltseg locality (stratigraphic sections U1429 and U1430, Figure 3.11), the base of the Shuurgat Fm is not-exposed, and the overlying strata consists of recessive interbeds of < 40 cm micritic nodular-bedded limestone, lime-grainstone, and pink when weathered calcisiltite with abundant chert nodules that are sometimes bedded to lenticular. These are succeeded by massively bedded, light gray when weathered lime-grainstone with occasional 2 by 1 cm chert nodules and are

capped by a significant karst surface filled with quartz arenite. Above this uncomformity, the basal unit of the Zuun-Arts Fm is present and composed of massively bedded lime-grainstone with stromatolites.

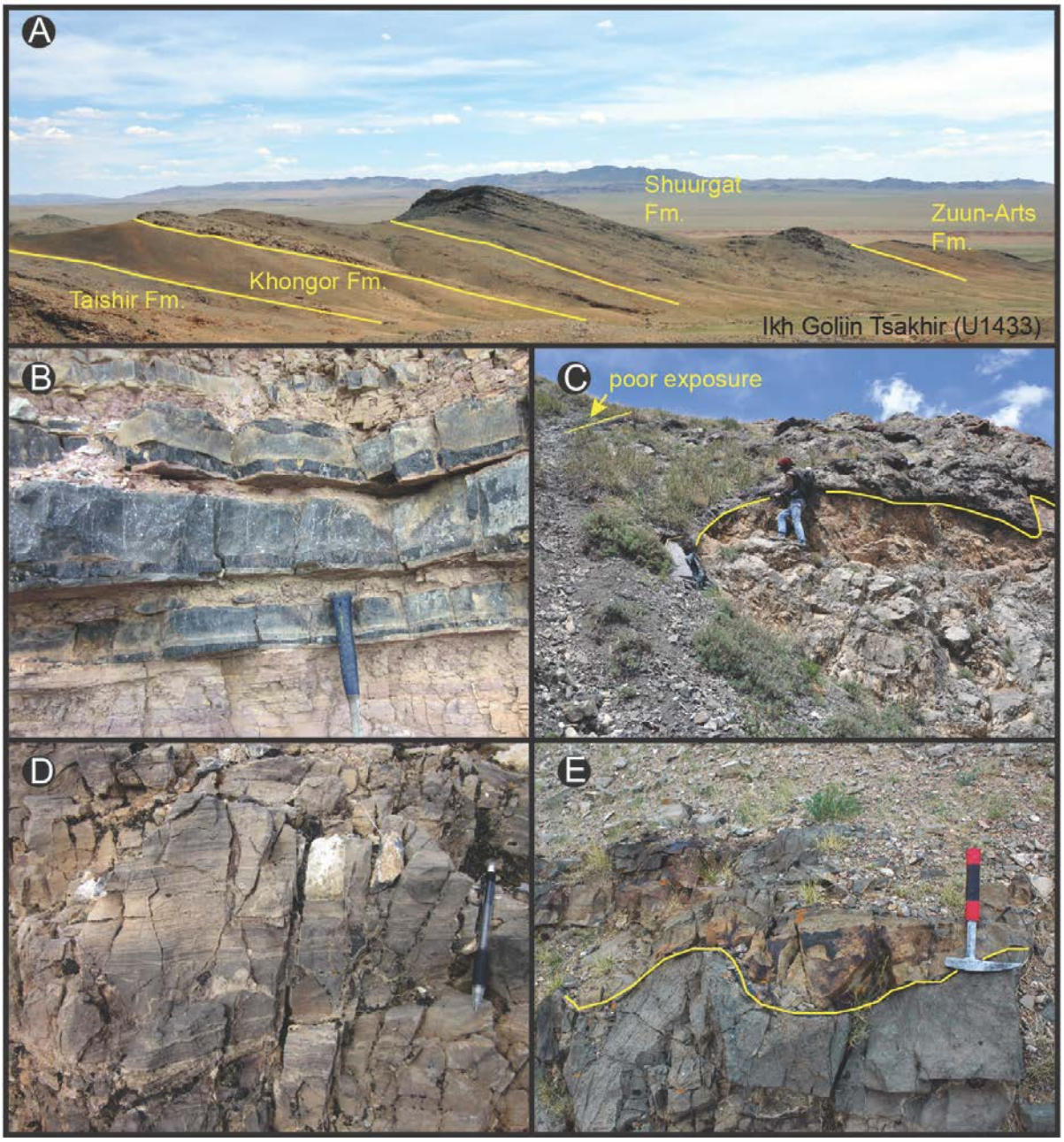

Figure 3.12. The Shuurgat Formation
(A) Complete section of the upper Tsagaan-Olom Group, T3 to the base of Zuun-Arts Formation. Photo is taken in the Ikh Goliin Tsakhir Mountain of the southern Khukh Davaa block. View to the west. (B) Sh1 Member of the Shuurgat Formation characterized by interbedded black limestone, bedded chert and pink calcisiltite. (C) An extensively silicified exposure surface at the top of the Sh2 in Khunkher Gorge (F872 and U1437). Person in scale is 1.8 m tall. (D) Laminated dolo-micrite of Sh2 of the Shuurgat Formation at Ol Mountain (U1337). Quartz-sand filled karst surface present at the top of the Shuurgat Formation in northeastern Khukh Davaa Region of Tsagaan block (F1206).

At Ikh Goliin Tsakhir locality (stratigraphic section U1433, Figure 3.11) (Figure 3.12A), the base of the Shuurgat Fm, Sh1, is well-exposed but thin, which is composed of massive-bedded, black to gray dolo-micrite and purple calcisiltite with interbeds of limestone with intraclast breccia. The succeeding carbonate succession of Sh3 and Sh4 are ~ 85 m thick. The lower ~ 20 m are composed of thin-bedded micritic limestone with interbeds of purple calcisiltite, which is capped by massive-weathering, thin- to medium-bedded and light blue gray dolo-micrite. The uppermost ~ 6 m succession of Sh4 at this locality is characterized by primarily orange green when weathered siltstone with < 2 m thick interbeds of brown gray when fresh dolo-grainstone. The base of the Zuun-Arts Fm that is usually represented by dolo-grainstone with stromatolite that is overlain by phosphatic shale is not present here. Instead, 6 m thick ooid dolo-grainstone is present below the phosphatic shale of the basal Zuun-Arts Fm.

3.4. U-Pb GEOCHRONOLOGY

Zircons were separated from samples of rhyolite, sandstone and a quartzite clast from the Zavkhan Fm and were subjected to U-Pb analyses by the isotope-dilution thermal ionization mass spectrometry (ID-TIMS) and *in situ* laser-ablation inductively coupled plasma mass spectrometry (LA-ICPMS) techniques in order to infer provenance for the Zavkhan Terrane basement and to constrain the age of the Zavkhan Fm volcanism. Zircons were also analyzed from a rhyolite and two tuffaceous sandstones (U-Pb ID-TIMS methods) from the Maikhan-Uul and Taishir fms, as well as sandstone from the Shuurgat Fm (LA-ICPMS methods), in order to establish a chronostratigraphy for the Tsagaan-Olom Group. Analyzed samples are listed in Table 3.3 and the analytical methods are described in the Appendix. Complete U and Pb isotopic data are given in Tables 3.A1 and 3.A2 and plotted in figures 3.5, 3.13, and 3.14. The results are discussed in stratigraphic order below.

3.4.1. Geochronology Results

Sample U1213: Rhyolite in the lower Zavkhan Formation.—A 27.5 meter-thick green rhyolite flow bound by beds of conglomerate (figures 3.4A and 3.5) was sampled on the South Khukh Davaa block (Table 3.3). Thirty six zircon grains were dated by LA-ICPMS (Table 3.A1) from which five

euhedral zircons were selected and pre-treated with the chemical abrasion method and analyzed (CA-ID-TIMS), yielding a statistically coherent cluster of data (Figure 3.13A) with a weighted mean $^{206}Pb/^{238}U$ date of 802.11 ± 0.45/0.56/1.0 Ma (see Appendix for date uncertainty notation) and a MSWD of 0.7. The latter serves as the best estimate for the age of rhyolite eruption.

Table 3.3. Summary of magmatic and detrital samples dated

Sample No.	Member/Formation name	Location	Latitude	Longitude	Elevation, m
U1213	Zavkhan Fm	South Khukh Davaa	47°8.020'N	95°13.667'E	2180
F718	Zavkhan Fm	Taishir	46°41.241'N	96°34.567'E	1725
F701-14.5	Maikhan-Uul Fm	Khongor Range	46°40.801'N	96°16.524'E	2020
U1214	Zavkhan Fm	South Khukh Davaa	47°7.8370'N	95°13.105'E	2175
U1333	Zavkhan Fm	South Khukh Davaa	47°7.887'N	95°13.732'E	2245
F1203-272.1	Maikhan-Uul Fm	Tsagaan Block	47°11.280'N	95°23.580'E	1900
F868-64	Taishir Fm	Khongor Range	46°39.990'N	96°16.250'E	2018
F1206-146.1	Shuurgat Fm	Tsagaan Block	47°5.433'N	95°28.721'E	2070

Sample U1214: Sandstone in the lower Zavkhan Formation.—A dark purple, bedded sandstone was sampled in the conglomerate unit of the lower Zavkhan Fm in South Khukh Davaa block (Table 3.3). Sample U1214 was taken from ~ 250 m below sample U1213 (see above). 162 detrital zircon grains (cores and magmatic rims) were dated by LA-ICPMS (figures 3.4A, 3.14A, and 3.A3; Table 3.A1). Prominent peaks in the age spectra occur at 800 Ma, 2050 Ma, and 2500 Ma. Several (Archean) grains were analyzed, with the oldest having a $^{207}Pb/^{206}Pb$ date of 3699 ± 22 Ma.

Sample U1333: Quartzite clast in the conglomerate unit of the Zavkhan Formation.—A brown quartzite clast was sampled from within the conglomerate unit of the Zavkhan Fm in South Khukh Davaa block, to the NE of the Tsagaankhairkhan Mountain (Table 3.3). 122 zircon grains were dated by LA-ICPMS (figures 3.4A, 3.14A, and 3.A2; Table 3.A1). The dominant peaks are at 2000 - 2350 Ma and 2450 - 2550 Ma, in addition to several Archean age grains with the oldest having a $^{207}Pb/^{206}Pb$ date of 3366 ± 40 Ma.

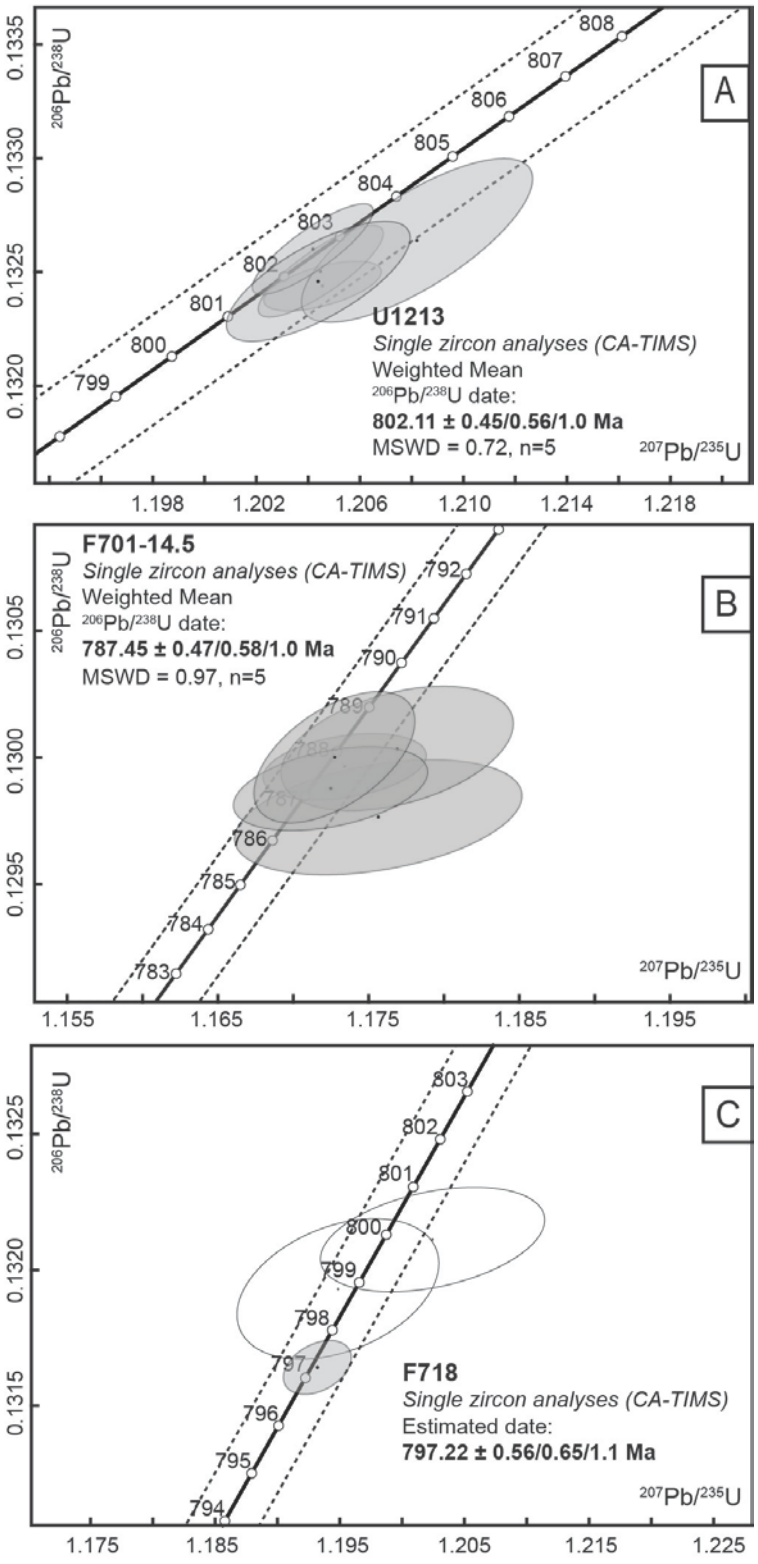

Figure 3.13. Concordia diagrams of zircon 206Pb/238U CA-ID-TIMS dates
(A) U1213 – rhyolite from the Zavkhan Formation. (B) F701-14.5 – rhyolite olistolith near base of the Maikhan-Uul Formation. (C) F718 – rhyolite from the top of the Zavkhan Formation.

Sample F718: Rhyolite from the top of the Zavkhan Formation.—A massive, ~ 5 meter-thick, green rhyolite was sampled at the top of the Zavkhan Fm near the town of Taishir (Table 3.3) and yielded only few quality zircons suitable for analysis. Three grains were analyzed by the CA-ID-TIMS method, producing scattered $^{206}Pb/^{238}U$ dates that range from 799.9 ± 1.1 Ma to 797.22 ± 0.56 Ma (figures 3.5 and 3.13C; Table 3.A2). Because no statistically meaningful weighted mean date can be calculated, the youngest analysis is interpreted as a maximum age for the eruption/deposition of rhyolite.

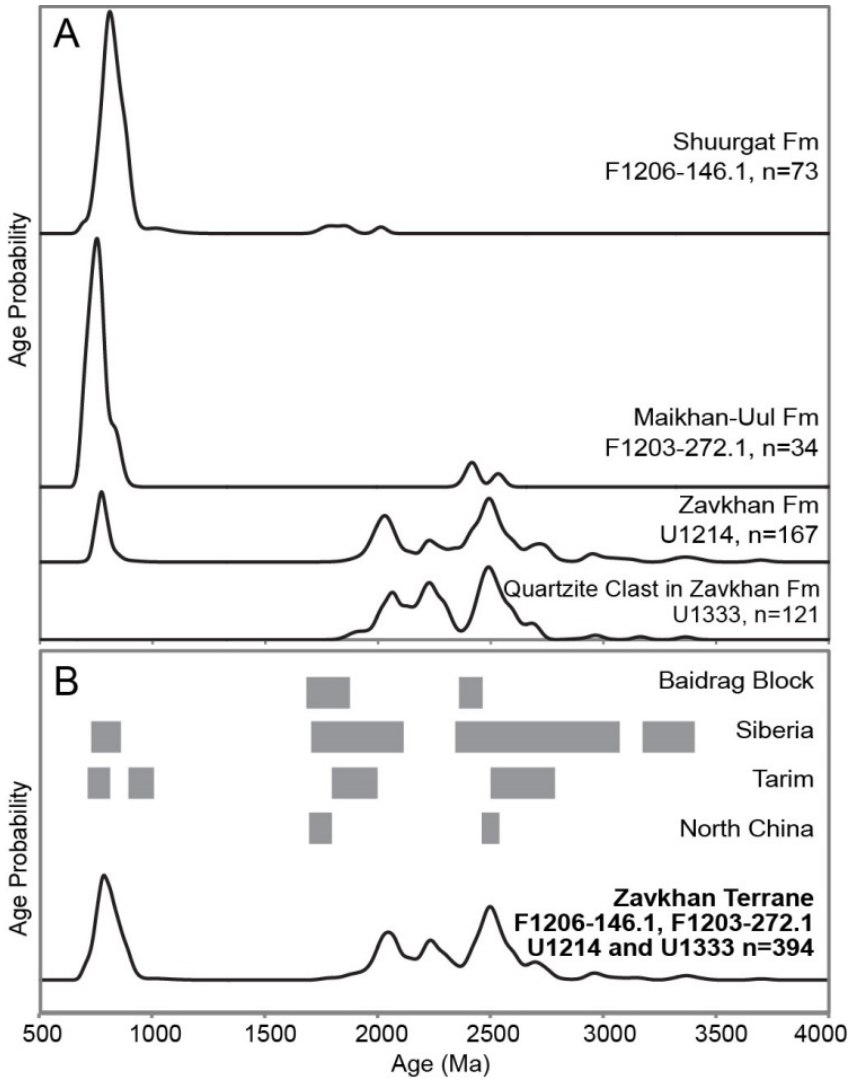

Figure 3.14. Normalized probability plots
(A) Normalized probability plots of U-Pb dates obtained by LA-ICPMS from zircon from samples U1333, U1214, F1203-272.1, and F1206-146.1. (B) Dominant age peaks present in detrital zircon spectra of Precambrian rocks of Siberia, North China, Tarim, and Zavkhan Terrane. Dates used in normalized probability plot of the Zavkhan Terrane are the composite of the detrital zircon spectra in A. Dates used in the plots of Siberia, North China and Tarim are from Rojas-Agramonte et al. (2011), Sun et al. (2012) and Zhang et al (2013).

Sample F701-14.5: Rhyolite olistolith (?) near base of the Maikhan-Uul Formation.—A green rhyolite was sampled 14.5 m above the base of the Maikhan-Uul Fm in the Khongor Range, along the southernmost part of the Bayan Gorge (Table 3.3). It was from ~ 1 m thick rhyolitic welded tuff with eutaxitic texture and was originally interpreted as a bed as it extends laterally for < 10 m, but cannot be followed further and disappears in non-exposure. Hence we interpreted it as a Zavkhan Fm rhyolite olistolith that forms a part of the Maikhan-Uul diamictite. Five overlapping zircon CA-ID-TIMS analyses yield a weighted mean $^{206}Pb/^{238}U$ date of 787.45 ± 0.47/0.58/1.0 Ma (MSWD = 0.97) (figures 3.4C, 3.5 and 3.13B; Table 3.A2) that is interpreted as a maximum depositional age for the basal Maikhan-Uul Fm.

Sample F1203-272.1: Tuffaceous sandstone in the middle Maikhan-Uul Formation.—A green tuffaceous sandstone was sampled at the base of the middle Maikan-Uul Fm, directly above the lower massive diamictite of the Maikhan-Uul Fm, in exposures in the northeastern limb of the Khukh Davaa Range in Tsagaan block (Table 3.3). Thirty four euhedral zircon grains were analyzed with LA-ICPMS (figures 3.4A, 3.14A, and 3.A4; Table 3.A1), yielding a dominant age peak at 700-850 Ma, and three older grains with $^{207}Pb/^{206}Pb$ dates ranging from 2534 ± 55 Ma to 2406 ± 66 Ma. Five additional zircons analyzed by CA-ID-TIMS produced significantly scattered $^{206}Pb/^{238}U$ dates ranging from 792.3 ± 2.1 Ma to 729.8 ± 1.4 Ma (Figure 3.5 and Table 3.A2), with the latter providing a maxium depositional age for the middle Maikhan-Uul Fm.

Sample F868-64: Tuffaceous sandstone in the lower Taishir Formation.—A green tuffaceous sandstone was sampled in the lower Taishir Fm in the Khongor Range (Table 3.3). Six CA-ID-TIMS zircon analyses yielded widely scatterd $^{206}Pb/^{238}U$ dates that range from 1741.4 ± 5.8 Ma to 768.9 ± 3.2 Ma (Figure 3.4C and Table 3.A2). Judging from stratigraphic superposition, all analyzed zircons were detrital and significantly older than the expected depositional age.

Sample F1206-146.1: Sandstone in karst-fill at the top of the Shuurgat Formation. – A brown sandstone was sampled from the karst-fill at the top of the Shuurgat Fm in the northeastern Khukh Davaa of Tsagaan block (Table 3.3). One hundred zircon grains of similar morphology (mostly long and prismatic) were mounted and 71 grains were analyzed with the LA-ICPMS method (figures 3.11, 3.14A,

and 3.A5; Table 3.A1). Data indicate a prominent age peak is at 750-900 Ma, with the remaining 10% of the grains extending in age up to 2000 Ma. The youngest single analysis from this sample yielded a $^{206}Pb/^{238}U$ date of 693 ± 35 Ma, which is interpreted as a maximum depositional age for the upper Shuurgat Fm.

3.5. GEOCHEMISTRY

In addition to sampling volcanic and siliciclastic rocks of the Tsagaan-Olom Group for chronostratigraphic constraints, carbonates were sampled for $\delta^{13}C$, $\delta^{18}O$, and $^{87}Sr/^{86}Sr$ analyses. See appendix for methods used.

3.5.1. Carbonate Carbon and Oxygen Isotope Results

Reconnaissance-scale carbon and oxygen isotopes from the Tsagaan-Olom Group were previously reported by Brasier and others (1990) and Shields and others (1997; 2002), and higher resolution single sections by Macdonald and others (2009a) and Johnston and others (2012). However, in relation to our detailed mapping and stratigraphic work, we report carbonate $\delta^{13}C$ and $\delta^{18}O$ measurements of 3581 samples from multiple parallel vertical sections of the Taishir, Khongor, Ol, and Shuurgat fms (Table 3.A3) from each locality (figures 3.3 and 3.4).

Carbon and oxygen isotope analyses where performed on cements from the Maikhan-Uul Fm to determine the origin of the cements and the isotopic composition of the fluids that these cements precipitated from. Carbon isotope values vary from -7 to +5‰ and $\delta^{18}O$ values vary from -25 to +5‰ with the majority being extremely depleted (Figure 3.6).

Carbon isotope values in the black laminated limestone of the basal Taishir Fm are moderately negative with values increasing up-section through the highstand of T1 to +4‰ (Figure 3.8). $\delta^{13}C$ values increase abruptly at the base of T2 to +8‰ and return to +4‰ at the top of T2. These values plummet abruptly at the transgression at the base of Member T3 reaching a low of -7.5‰. From this nadir (the Taishir excursion), $\delta^{13}C$ values increase smoothly to +10‰ where they remain for the majority of Member T3 before declining again in T4 to +4‰ near the top of the Taishir Fm. Where undolomitized,

these trends can be reproduced for over 100 km across the Zavkhan Terrane through large facies changes and differences in thicknesses of the members (Figure 3.8).

Different carbonate lithologies, however, do affect the $\delta^{13}C$ values of the Taishir Fm. The $\delta^{13}C$ values vary by as much as 8‰ within the upper Taishir Fm between limestone and dolostone strata. For instance, where the dolomitization front cuts down in sections on the South Khukh Davaa, northern Tsagaan, Orlogo, western Taishir and Tsakhir blocks, $\delta^{13}C$ values of the uppermost dolomitized succession of the Taishir Fm are less enriched at ~ +2 to +3.5‰ whereas in undolomitized sections, equivalent horizons yield values of between +10 to +12‰ (Figure 3.8). Specifically, in both the Orlogo Gorge (U1202) and South Khukh Davaa (F875, F876, F1125 and F1126) localities, the $\delta^{13}C$ values of the dolomitized upper T3 decrease from +10 to +12‰ down to ~ +6‰ (Figure 3.8).

In the Taishir Fm, carbonate $\delta^{13}C$ and $\delta^{18}O$ do not covary (Table 3.A3). In members T1, T2, and the lower half of T3, $\delta^{18}O$ varies between -20 and -3‰, in the upper ~ 150 m of the Member T3, $\delta^{18}O$ values get markedly more enriched and vary between -10 and 0‰.

Carbon isotope values of limestone clasts in the Khongor Fm range from +1 to +8‰ (Figure 3.8). The clasts with $\delta^{13}C$ values at +1‰ also contain soft sedimentary folding and are not recognizable Taishir lithologies, suggesting that they were from a bed deposited above the Member T3 that was eroded by the Khongor diamictite. There is a < 4.5 m thick, bedded dolo-grainstone clast that is ~ 10 m in length and not traceable along strike present in the basal part of the Khongor Fm at the Ikh Goliin Tsakhir (U1433 and U1435, Figure 3.8) locality as well. Interestingly, there is no apparent soft sedimentary folding in this clast, and the lithology may be correlated with T3 ooid-grainstone although the weathering color is brown gray and it is coarsely recrystallized. $\delta^{13}C$ values of this bedded dolostone clast range between +6.5‰ to +9.2‰ within individual beds, and the $\delta^{18}O$ values range between -3‰ to -4.9‰ (Table 3.A3).

Overlying the Khongor Fm, in the localities where the Taishir Fm carbonates are preserved as limestone, $\delta^{13}C$ profiles through the Ol Fm form a sigmoidal pattern that reaches a nadir of -6‰ (Macdonald et al., 2009a) (Figure 3.11), similar to basal Ediacaran cap dolostones elsewhere (Hoffman et al., 2007). The $\delta^{13}C$ profiles of the Ol Fm successions that overlie the dolomitized Taishir carbonates

show large lateral variations (Figure 3.11). At the Ikh Goliin Tsakhir, NE Khukh Davaa and Unkheltseg localities, the $\delta^{13}C$ values of the Ol Fm become enriched. Rather than recording negative values, the Ol Fm reaches values as high as ~ +4‰. In the western tributary of Tsagaan Gorge (F724) and at Zuun-Arts (U1329), the $\delta^{13}C$ values reach +2‰. However, the Ol Fm in the Tsagaan Gorge is underlain by undolomitized Taishir succession.

In the Ol Fm, carbonate $\delta^{13}C$ and $\delta^{18}O$ do not covary (Table 3.A3). In the Tsagaan Gorge, where the underlying Taishir Fm is undolomitized, $\delta^{18}O$ varies between -12 and -2‰. However, in the Khongor Range, it varies dramatically between -27 and -5‰. In the Ol Fm sections that overly the dolomitized Taishir Fm carbonates, at the Ikh Goliin Tsakhir and Unkheltseg localities, carbonate $\delta^{13}C$ and $\delta^{18}O$ also do not covary. In general, the $\delta^{18}O$ varies between -7.8 and -1‰ (Table 3.A3).

Carbon isotope values in limestone of Member Sh1 of the Shuurgat Fm gradually increase up-section from -4‰ to -0.3‰ (F708, Figure 3.11). In the variably brecciated, thin-bedded dolo-micrite, nodular-bedded calcisiltite, and grainstone of Sh2, $\delta^{13}C$ values hover between +2 and +4‰. There are no sections of Sh2 preserved as limestone that can be used to assess the degree to which dolomitization has altered the $\delta^{13}C$ values of this interval. In members Sh3 and Sh4, $\delta^{13}C$ values vary between sections preserved as limestone and those that have been dolomitized. In Khunkher Gorge, the western gorge of Tsagaan Gorge, NE Khukh Davaa, Unkheltseg and Ikh Goliin Tsakhir localities, where Sh3 and Sh4 are either dominated by limestone or partially preserved as limestone (described herein as Sh3-4), $\delta^{13}C$ values increase abruptly to +8‰, decline back to +2 to +4‰ and increase again to +8‰ before returning back to ~ + 2‰ at the top of the Shuurgat Fm. However, in Shuurgat Range, Ol Mountain, Khevtee Tsakhir Range and Zuun-Arts locality, where Sh3 and Sh4 are dominated by dolostone, these features of the $\delta^{13}C$ profile are not as well defined and positive peaks are subdued to $\leq$ +6‰ (Figure 3.11).

In the Shuurgat Fm, carbonate $\delta^{13}C$ and $\delta^{18}O$ do not covary (Table 3.A3). In Sh1, $\delta^{18}O$ varies between -15 and -7‰. In members Sh2 and Sh3, $\delta^{18}O$ values become heavier and vary between -16 and +1.5‰. In Sh4, $\delta^{18}O$ values stay enriched between -10 and 1.5‰.

3.5.2. Strontium Isotope Results

Strontium isotopes were measured in both Cryogenian and Ediacaran strata on the Zavkhan Terrane to construct a high-resolution Cryogenian curve and to test if deposition the Shuurgat Fm was restricted to early Ediacaran or extended throughout the Ediacaran. Samples with high Sr concentration and low clay content (0.4-16.5% with an average at 5%, Table 3.A4) were targeted and diagenetic alteration was screened using carbonate content and a cross-plot of $^{87}Sr/^{86}Sr$ vs. Sr concentration (Halverson et al., 2007) for each sample. Values discussed here are selected by a cutoff value of Sr concentration of < 500 ppm (Figure 3.A1). $^{87}Sr/^{86}Sr$ values considered diagenetically altered are included in the Table 3.A4 but are not shown in the plots.

Sr concentration in the analyzed Taishir Fm limestone was > 500 ppm (Table 3.A4) and all analyses were used. The $^{87}Sr/^{86}Sr$ values in finely laminated T1 cap carbonate start at 0.70673 and increase abruptly through T1 until the transition with T2 transgression. Values drop gradually to 0.70704 and eventually increase slightly to as much as 0.70726 through the rest of T2. Values increase again in the lower portion of T3 to 0.70736 where they plateau for the rest of T3 and T4.

Strontium concentration in both the Ol and Shuurgat Fm limestones was between a minimum of 61 and as high as 2250 ppm (Table 3.A4). Of the 52 samples analyzed, six samples were considered diagenetically altered because they yielded Sr concentrations < 121 ppm. The $^{87}Sr/^{86}Sr$ values of the recessive limestone succession of the Ol Fm (U1121, Table 3.A4) start enriched at 0.70756 and increase slightly to 0.70765 through the rest of the Ol Fm limestone. At the start of the transgressive sequence of the basal Shuurgat Fm (U1122, Table 3.A4), Sh1, the $^{87}Sr/^{86}Sr$ values become more radiogenic to as high as 0.70773 and decrease gradually to 0.70757 (Figure 3.11). All of the measured samples in Sh3 and Sh4 of the Shuurgat Fm (U1235, F872 and U1437) yielded $^{87}Sr/^{86}Sr$ values of < 0.70795. In Khunkher Gorge, the values ranged between 0.70765 and 0.70785. Seven samples from stratigraphically equivalent succession (section U1235, Figure 3.11) in the western tributary of Tsagaan Gorge yielded similar values and ranged between 0.70783 and 0.70795.

3.6. DISCUSSION

3.6.1. Depositional Environments

Tectonic setting of the Zavkhan Formation.— The Zavkhan Fm has been previously suggested to record magmatism in either a rift-related setting (e.g. Ilyin, 1990) or on an active continental arc (e.g. Kuzmichev et al., 2001). The former interpretation stems from the bimodal volcanic rock assemblage and the overlying passive margin deposits. The interpretation that the Zavkhan Fm formed as an active continental arc is supported by major and trace elemental analysis (e.g. Levashova et al., 2010), and by correlation with Sarkhoi Volcanics of the Tuva-Mongolia Zone (e.g. Kuzmichev and Larionov, 2011). This is further supported by zircon trace element geochemistry (Yang et al., 2012) with low Nb/Hf and high Th/Nb ratios (sample U1213 in Table 3.A1), which are based on studies that showed depleted Nb content in magmatic arc magmas (e.g. Pearce and Peate, 1995). However, the presence of km-scale fan conglomerate sequences in the lower Zavkhan Fm succeeded by thick, fault confined exposures of continentally-derived sediments of the Khasagt Fm (figures 3.3 and 3.5), culminating in extensive marine deposition throughout the Cryogenian to early Ediacaran Tsagaan-Olom Group is consistent with deposition on a rifted passive margin. Hence, it appears that the Zavkhan Terrane transformed from an active arc and back-arc complex to a rifted ribbon continent with passive margins on both sides, which is typically achieved through the subduction of a ridge (Stampfli and Borel, 2002), analogous to the rifting of Baja, California.

Glacial Facies Associations in the Maikhan-Uul Formation.—Broadly, the Maikhan-Uul Fm consists of two diamictites separated by clast poor siliciclastic strata that prograde southwestward (Macdonald, 2011a) (figures 3.6, 3.15A, B, C, and 3.16A). The lower portions of both diamictite members are interpreted to have been deposited in a sub-glacial environment as lodgement tills in contact with the ice sheet. Features indicative of ice-grounding are particularly common in the lower member, including sedimentary shear fabrics (Figure 3.7C) and blocks with soft-sedimentary folding (Boulton et al., 2001), bullet shaped clasts (Boulton, 1978; Lindsay et al., 1996b), and carbonate concretions along reactivation surfaces at the base of individual diamictite units (Fairchild and Spiro, 1990; Lindsay, 1989;

Macdonald, 2011a).

The middle member has previously been interpreted to represent an interglacial period separating two distinct glacial events (Lindsay et al., 1996b); however, the dearth of laminated diamictite with dropstones characteristic of ice rafted debris in between the lower and upper member is inconsistent with the interpretation of a full, global scale-deglaciation (Macdonald, 2011a). Instead, the contact above the lower member is sharp, succeeded by graded beds of sandstone and shale. West of the Khongor Range, these beds coarsen up to coarse-grained sediment gravity flow facies. These facies are interpreted to reflect local retreat of the ice grounding line without whole-scale deglaciation, and deposition beneath an ice shelf (*c.f.* Domack and Hoffman, 2011) or in a proglacial lake (Benn et al., 2015). Unfortunately, sub-ice shelf facies models are in their infancy and are limited to ice cores retrieved below the Larson ice shelf and Ross Sea (Domack et al., 1998; Domack et al., 1999). At these localities, deposition beneath an ice shelf is marked by turbidite and shale deposition and the lack of diamictite facies. Another possibility is that these facies reflect the development of a waterbelt, as predicted in the Jormungand hypothesis (Abbot et al., 2011) or movement of the ice-line during increased seasonality in the late stages of glaciation (Benn et al., 2015).

At Tsagaan and South Khukh Davaa blocks, dropstones occur in the uppermost meter of the middle Maikhan-Uul Fm, followed by glacial erosion surfaces, concretionary carbonates, and soft sedimentary folding, and provide additional evidence for a second advance of the ice grounding line. In the upper member, these features become less common upward and are succeeded by massive to weakly-bedded, graded diamictite interbedded with graded and channelized beds of cross-stratified sandstone. This facies assemblage (Table 3.2) is interpreted to represent deposition in an ice contact fan in a sub- to pro-glacial environment (Domack and Hoffman, 2011; Powell, 1990).

In South Khukh Davaa block, the upper diamictite culminates with sandstone and siltstone with abundant mudcracks (Macdonald, 2011a) (Figure 3.7E) demonstrating subaerial exposure in a proglacial setting. Finally, the base of the Taishir Fm represents a global deglaciation, flooding of the margin and open water deposition based on its carbonate facies and geochemical signature. Thus, the stratigraphic

succession of the Maikhan-Uul Fm is interpreted to reflect retreat of the ice-grounding line in the middle member, either due to tectonic subsidence or local thinning of a cold based ice sheet (Davis et al., 2006), and a readvance of the grounding line in the upper member (Macdonald, 2011a), potentially by a wet-based glacier during deglaciation. Without further geochronological constraints it is difficult to determine the timescale of the ice-line advance and retreat. Moreover, the complexity of ice advance and retreat documented in the most recent glaciation (Ridge et al., 2012) suggests that we may not have sufficient geochronological resolution (10 Ka – 100 Ka) to sort out advance and retreat in the Cryogenian. Nonetheless, the presence of exposure surfaces in the upper member implies either that, locally, deglaciation and glacio-isostatic rebound occurred before the global glacioeustatic transgression, or that there was a local regression due to ice gravity effects (Creveling et al., 2012).

Concretionary carbonates are present in all of our glacial facies associations. Carbonate is a very minor clast constituent in the diamictites. The matrix and clasts of the Maikhan-Uul Fm are dominated by volcaniclastic material, and consequently, the generation of carbonate alkalinity in subglacial porewater must have been the product of the reaction of CO_2 with the weathered rock. In this setting, precipitation occurs due to relegation processes with pressure melting occurring on the up flow side of protuberances and refreezing on their lee side (Aharon, 1988). Carbonate coatings of shear surfaces and clasts have been previously reported at several other localities and have also been interpreted to have formed through pressure dissolution and reprecipitation (Deynoux, 1985; Fairchild and Spiro, 1990). Subglacial carbonates from section F1216 sampled from the base of the lower Maikhan-Uul at Shivee Tsakhir region, and F1204 sampled from the lower portion of the upper member of the Maikhan-Uul Fm at Khukh Davaa tend to have extremely depleted $\delta^{18}O$ values (mostly between -22 and -20‰) and relatively positive $\delta^{13}C$ (0 to +4‰; Figure 3.6). The oxygen isotopic composition of subglacial rocks is largely dependent on that of local glacier ice (Aharon, 1988; Fairchild and Spiro, 1990) and thus, these data suggest that the isotopic value of the subglacial ice in the Maikhan-Uul Fm ranged from -22 to -20‰. These values are between the $\delta^{18}O$ value of subglacial carbonates in Quebec and Switzerland (Fairchild and Spiro, 1990) and we suggest they in part preserve a primary signature because they are far more

depleted than any values of bulk rock or cements from both underlying and overlying strata.

Carbonate precipitates also occur at the base of the middle member of the Maikhan-Uul Fm, directly above the massive diamictite of the lower member. These beds are all limestone, but aragonite pseudomorphs are present in some samples suggesting an original aragonitic mineralogy and authigenic precipitation at or near the sediment-water interface. Carbonates in sections F1203, F1214 and F1212 have depleted $\delta^{13}C$ values (ranging from -1 to -7.5‰) and depleted $\delta^{18}O$ values (with F1203 and F1214 largely between -25 and -20‰ and F1212 more enriched at -10 to -8‰; Figure 3.6). The wide range of both carbon and oxygen isotope values in these rocks are difficult to explain in a marine setting during a glacio-eustatic transgression and are more consistent with glacial lacustrine values. Like the $\delta^{18}O$ of the subglacial carbonates, the $\delta^{18}O$ values from F1203 and F1214 can be interpreted to reflect the isotopic value of the ice. While the carbonates from sections F1205 and F1214 are composed of limestone, F1212 samples are dolomite, and thus may have also been affected by post-depositional fluids, as most of the carbonates in the overlying Tsagaan-Olom Group have $\delta^{18}O$ values around -10‰. Alkalinity to generate carbonate was likely driven by anaerobic remineralization of organic matter that formed during the lift off of the ice sheet, generating negative $\delta^{13}C$ values. Thus, proglacial carbonates formed below water column that was not in communication with seawater, but it is unclear if this was below an ice-shelf or within a proglacial lake.

Proglacial carbonate concretions in sandstones of the upper member display a spread of $\delta^{13}C$ and $\delta^{18}O$ values between glacial melt water values and extremely enriched values (Figure 3.6), which may reflect a mixture of glacial water and some other reservoir. Within proglacial lakes, evaporation can lead to enrichment in oxygen isotope values and the isotopic value of carbonates can reflect a mixture between an evaporitic and ice end-members (Fairchild and Spiro, 1990). Alternatively, $\delta^{18}O$ enriched cements within Neoproterozoic glacial deposits have been interpreted to reflect methanogenesis (Kennedy et al., 2008).

Diamictite-free facies within Sturtian glacial deposits have previously been interpreted to represent an open water, interglacial period, not only in the Maikhan-Uul Fm of Mongolia (Lindsay et al.,

1996b), but also in the Ghubrah Fm of Oman (Allen and Etienne, 2008), the Sturt of Australia (Le Heron, 2012; Le Heron et al., 2011), the Chuos of Namibia (Le Heron et al., 2013), and the Kingston Peak Fm of Death Valley, California (Le Heron and Busfield, 2015; Le Heron et al., 2014). The presence of diamictite-free facies has been used alternatively to argue that the Sturtian glaciation is globally diachronous and does not represent Snowball conditions (Allen and Etienne, 2008) or that there is an interglacial period within the Sturtian glacial epoch (Le Heron et al., 2014). Instead, our data suggest that these facies reflect either deposition beneath an ice shelf (Domack et al., 1998; Domack et al., 1999), the opening of a waterbelt (Abbot et al., 2011) or movement of the ice-line during increased seasonality in the late stages of glaciation or late stages of glaciation with increased seasonality (Benn et al., 2015), but not a full global deglaciation (Macdonald, 2011a). Moreover, all of these successions lack age constraints within the diamictites, and consequently these successions may largely record deglaciation rather than the tenure of the glaciation.

Carbonate facies assemblages in the Taishir Formation.—The facies patterns of the Taishir Fm are interpreted to represent deposition on an open carbonate ramp (Ahr, 1973) that forms a basin tapering wedge composed of four large-scale stratigraphic sequences that gradually thin to the west-southwest over 100 km with no sharp facies changes (figures 3.15D, 3.16B, and 3.16C). Previous authors have separated carbonate ramps into homoclinal and distally steepened ramps (Burchette and Wright, 1992; Read, 1982), distinguished by a change in slope in the ramp, which results in mass wasting and slump folding in more distal localities. Slump folds are extremely rare, and no evidence has been found for a major break in depositional style in members T1 to T4 up to the faults that bound the Zavkhan Terrane. Consequently, the homoclinal carbonate ramp is preferred as a facies model.

Homoclinal ramps have relatively uniform slopes of less than 1° and within these facies models have distinguished inner-ramp, mid-ramp, outer-ramp, and basinal facies assemblages (Table 3.2), although true basinal facies have proven difficult to identify (Burchette and Wright, 1992). Inner-ramp sediments are deposited above fair weather wave base (FWWB) and are dominated by sand shoals, shoreface deposits, and back-barrier peritidal to intertidal deposits. Periodically restricted and sub-aerially

exposed peritidal to intertidal environments can readily preserve m-scale parasequences capped by exposure surfaces that are prone to early dolomitization. Our inner-ramp facies assemblage consists of nodular-bedded carbonate, grainstone, microbialaminite, and intraclast breccia packaged in well-developed m-scale parasequences (Table 3.2).

Mid-ramp sediments form between FWWB and storm wave base (SWB) and are influenced by frequent storm reworking. Ooid-grainstone shoals and grain flows are also common in this environment, as is seen in the Jurassic Smackover Fm on the US Gulf Coast, which hosts a ~ 100 m thick build-up of ooid and pellet grainstone and oncolitic packstone (e.g. Ahr, 1973). Our mid-ramp facies assemblage includes thin-bedded micritic limestone with heterolithic interbeds, nodular-bedded calcisiltite and grainstone with common graded beds and thick ooid shoals (Table 3.2). Mid-ramp facies is distinguished from inner-ramp facies by the lack of exposure-capped parasequences and a predominance of graded beds in the former.

Outer-ramp environments extend from storm wave base to the basin plain (Burchette and Wright, 1992). Sediments in these environments show little evidence for storm reworking but do include minor distal turbidites and slump folding. Our outer-ramp facies consist of shale, micrite, and calcisiltite with minor graded beds of grainstone. The outer-ramp is distinguished from the mid-ramp facies assemblage by the lack of evidence of wave base and the lack of thick beds of redeposited grain flows. Here, the basinal environments are included with our outer-ramp facies assemblage because of the inability to confidently distinguish between the two.

T1 consists predominantly of thin-bedded micritic limestone and shale, interpreted to represent deposition in an outer-ramp environment (figures 3.8 and 3.15D). The lower 10-20 m of T1 is succeeded by calcisiltite without grainstone flows and is interpreted to represent the maximum flooding surface (MFS) of sequence 1. Up-section, graded beds of carbonate with chert nodules and carbonate clast breccias, interpreted as debris flows, become more common within the background calcisiltite sedimentation, consistent with high-stand (HST) shedding and a transition to a mid-ramp environment. The succession becomes more carbonate rich and resistant upwards, culminating with a silicified bed of

black limestone that marks the top of the T1 HST.

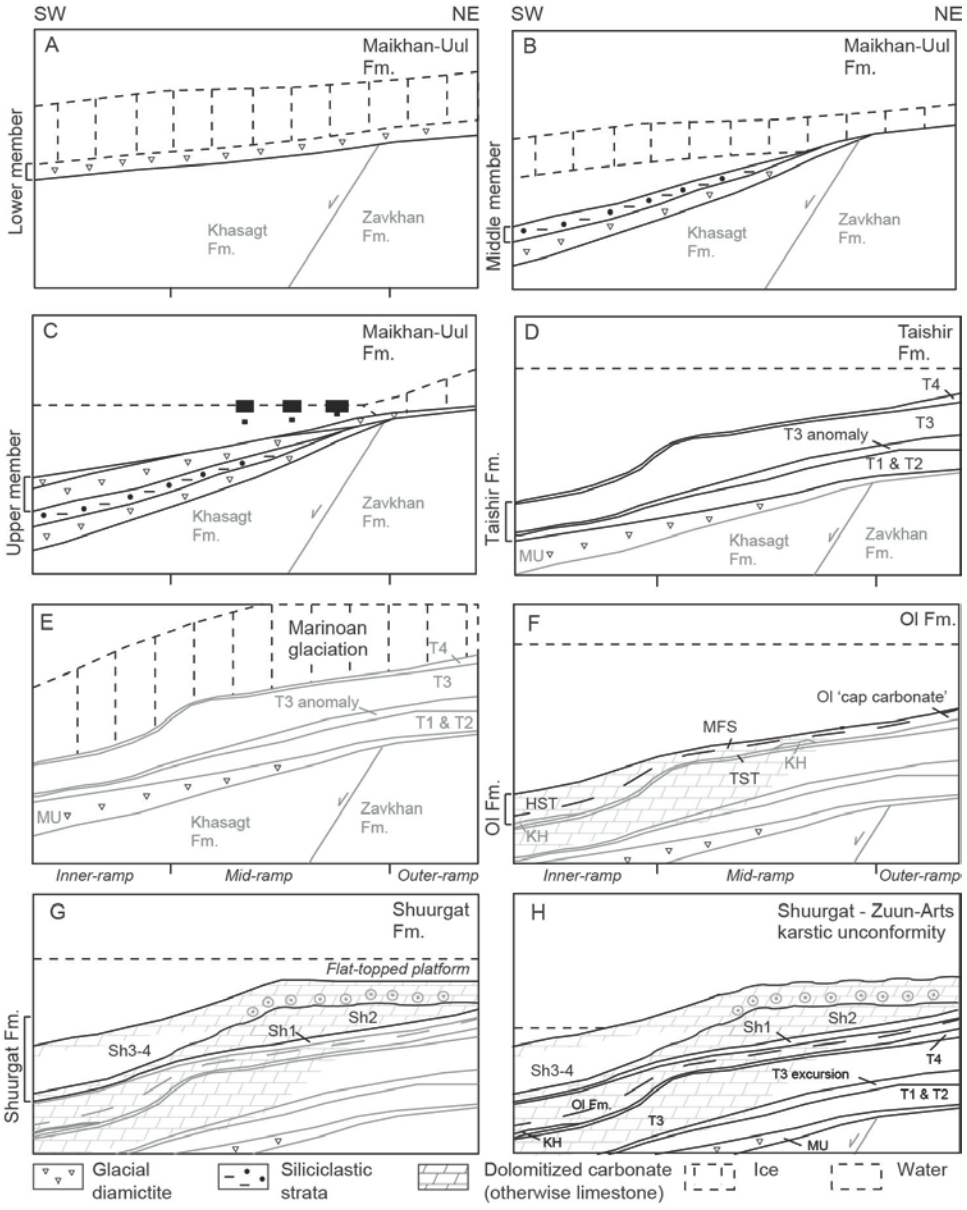

Figure 3.15. Depositional model for the Tsagaan-Olom Group formations
Orientation of transect in present coordinates. (A) Lower member of the Maikhan-Uul Formation. (B) Middle siliciclastic member of the Maikhan-Uul Formation. (C) Upper member of the Maikhan-Uul Formation. In general, the Maikhan-Uul Formation thickens to the southwest in the Zavkhan Terrane. (D) Taishir Formation. Both T1 and T2 thin to the southwest. (E) Marinoan glaciation. Mantling of grounded ice throughout the Marinoan glaciation is preferred. (F) Ol Formation. Khongor (KH) diamictite formed as a rainout deposit during deglaciation filling ice-cut channels. Fluid event responsible for dolomitizing upper Taishir and Ol Formation limestone took place before the deposition of Sh1 of the Shuurgat Formation. (G) Shuurgat Formation. Flat-topped platform formed during Sh2 to Sh3 as a result of progradation of the margin during Ol to Sh2 and consequently, the sharp facies change in Sh3-4 is observed as well as the well-development of carbonate parasequences in Sh4. (H) Exposure of the platform after the deposition of the Shuurgat Formation responsible for eroding and karsting the carbonates of the upper Tsagaan-Olom Group.

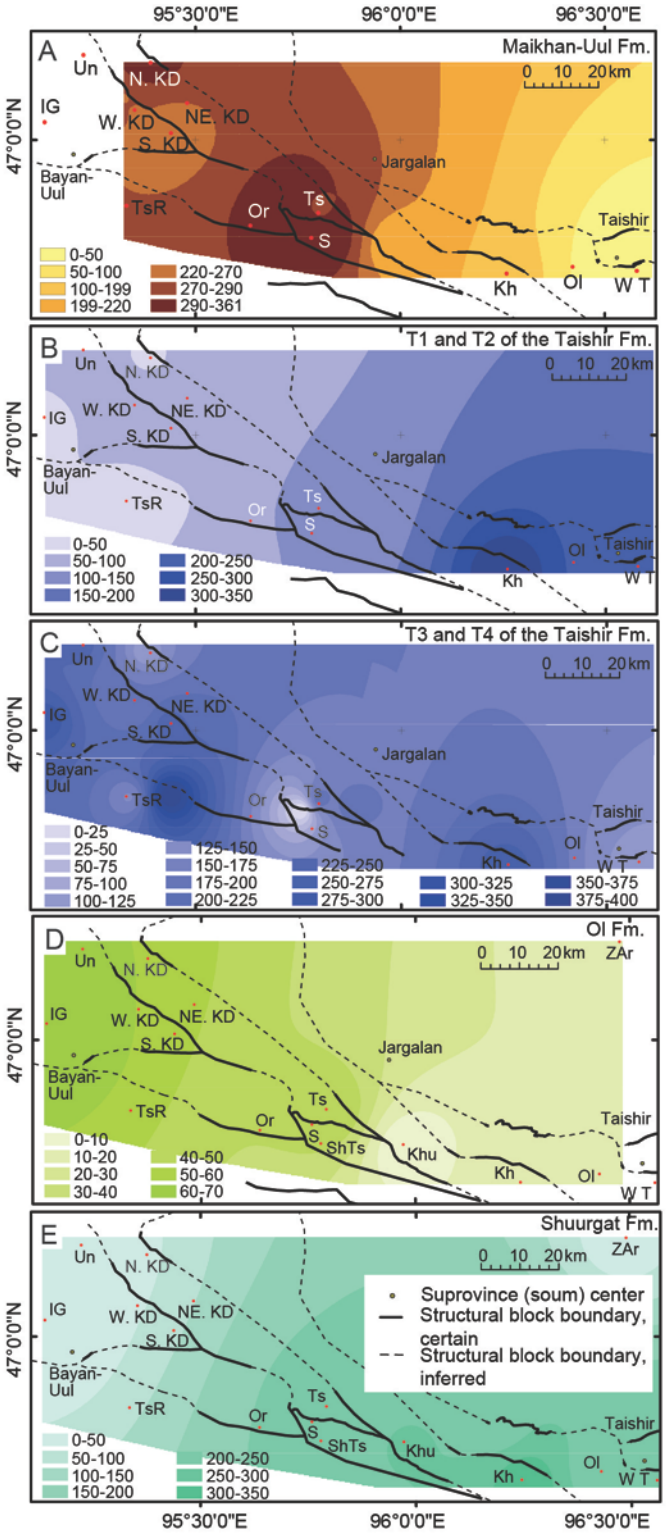

Figure 3.16. Isopach map of the Tsagaan-Olom Group formations

Tectonic block boundaries are traced. Solid lines = certain faults. Dashed lines = inferred faults. Labels on maps are as follows: South Khukh Davaa block = Un – Unkheltseg, IG – Ikh Goliin Tsakhir, S. KD – southern Khukh Davaa, W. KD – western Khukh Davaa; Tsakhir block = TsR – Tsakhir Range; Orlogo block = Or – Orlogo Gorge; Salaa block = S – Salaa Gorge, ShTs – Shivee Tsakhir; ZAr – Zuun-Arts;

Figure 3.16 (Continued) Khunkher block = Kh – Khongor Range, Khu – Khunkher Gorge; Taishir block = W.T – western Taishir, E.T – eastern Taishir, Ol – Ol Mountain; Tsagaan block = N. KD – northern Khukh Davaa, NE. KD – northeastern Khukh Davaa, Ts – Tsagaan Gorge. Each map is color coded according to thickness (m). The extent of our study area is within the structural block boundaries. (A) Maikhan-Uul Formation. (B) T1 and T2 of the Taishir Formation. (C) T3 and T4 of the Taishir Formation. (D) Ol Formation. (E) Shuurgat Formation.

The sequence T2 transgressive sequence tract (TST) begins with thin-bedded micritic limestone and interbedded graded beds of limestone that are commonly recessive. Defining the large-scale MFS is complicated by the presence of multiple smaller scale sequences in sequence T2. The lower 10-50 m of T2 oscillates between outer- and mid-ramp environments before shoaling up to an inner-ramp facies assemblage marked by well-developed exposure-capped parasequences (Figure 3.8, composite sections 8, 10, 12 and 14). The top parasequence is not obviously different from the underlying parasequences and is succeeded by a sharp flooding surface that marks the top of T2.

The basal TST of T3 is a sharp flooding surface of thin-bedded micritic limestone (Figure 3.9B) that corresponds with the onset of the Taishir excursion (Figure 3.8). Within the TST, graded carbonate grainstone beds and carbonate clast breccias are common within the background micritic carbonate sedimentation and are interpreted as sediment gravity flows deposited in a mid- to outer-ramp environment. Black chert beds and nodules are particularly common within the T3 TST. The MFS is marked by the disappearance of graded beds and is succeeded by ~ 100 m of massively bedded, thinly laminated, fetid limestone mudstone. Above, massive to graded grainstone beds become more common in the T3 HST, marking the reappearance of mid-ramp environments. The total thickness of T3 is between 200 and 300 m across the basin. Overall, thickness variations within T3 suggest a topographic high formed during the deposition of T3 (figures 3.15D and 3.16C).

Although T4 is not well-exposed or well-preserved throughout the basin, the thin-bedded micritic limestone overlain by black shale (Figure 3.8, composite section 12) marks another MFS at the base of T4. Hence it is interpreted to document a return to an outer-mid-ramp environment in the basin.

Here the lack of siliciclastic input to the Taishir Fm suggests that it is consistent with deposition on an isolated platform, but that the facies assemblages of the Taishir Fm are more akin to that of a homoclinal carbonate ramp. Traditionally, facies models for isolated platforms and carbonate ramps have

been separated, with models of isolated platforms influenced heavily by the Bahama Banks and distinguished by high relief margins and abundant slope failure (e.g. Read, 1982). The development of a homoclinal carbonate ramp on an isolated platform may reflect the fact that the margin was very mature, having subsided for ~ 150 Ma after rifting at ~ 800 Ma.

The facies architecture of T1 and T2 was heavily influenced by progradation of the margin during deposition of the Maikhan-Uul Fm. The Maikhan-Uul Fm thickens to the southwest (figures 3.6 and 3.16A), controlling the inverse thickening of T1 and T2 to the northeast (figures 3.8 and 3.16B). Additionally, drowning of the margin, both in lower T1 and in lower T3, would have favored the development of ramp morphology (Read, 1982). However, the systematic stacking of the measured sections (figures 3.15D and 3.16C) suggests that during the progradation of T3, the ramp morphology started its initial step towards development of an outer rim.

Glacial facies associations in the Khongor Formation.— The Khongor diamictite is not as well developed as the glacial diamictite in the Maikhan-Uul Fm, potentially due, in part, to the difference in accommodation later in the subsidence history, and also to the shorter duration of the Marinoan glaciation. Thus, the interpretation of its depositional environments is necessarily limited. With the exception of the Khongor Range, eastern tributary of Tsagaan Gorge and Unkheltseg localities, the Khongor diamictite is not preserved, implying that the Zavkhan Terrane was either exposed or mantled by grounded ice throughout the Marinoan glaciation (Figure 3.15E). The presence of striated limestone clasts (Figure 3.10B) and clasts with intense soft-sedimentary folding (Macdonald, 2011a) suggests that grounded ice was at least nearby if not present on the whole of the margin. The distribution of diamictite is similar to that of the Marinoan Ghaub Fm in Namibia where irregular preservation of diamictite on the platform has been interpreted to represent either moraines or channel fills (Hoffman, 2011). Where the Khongor diamictite is preserved, there is no evidence for incision into the underlying Taishir Fm. In fact, in the Khongor Range at the type locality of the Khongor diamictite, more of T4 is preserved than in at other localities. Moreover, the presence of boulder nests (Macdonald, 2011a) and weak lamination in otherwise massive diamictite facies is also more consistent with the interpretation of the Khongor

diamictite as a moraine deposited during ice retreat rather than a channel fill deposit or a wedge of lodgement till. Thus, the most of the Marinoan glaciation and some of the preglacial time are suggested to have been lost at the top contact of the Taishir Fm due to sub-glacial erosion and that the three localities in which the Khongor Fm is well-developed record only the termination of the Marinoan glaciation.

Carbonate facies assemblages in the Ol Formation.— The TST begins with the cap dolostone of the basal Ol Fm, which is exposed throughout the basin with thickness ranging from 10-35 m. The MFS of the Ol Fm is marked by thin-bedded micritic limestone interbedded with shale and nodular-bedded calcisiltite. This sequence is carbonate-dominated in the mid-inner-ramp environment in the eastern part of the exposure area, namely in the Taishir, Ol, and Khongor localities and becomes thinner (Figure 3.16D), more siliciclastic-dominated at the western and southwestern exposures, especially in South Khukh Davaa block and is not present to the north at Zuun-Arts (Figure 3.11). Up-section, the Ol Fm HST sequence is > 10 m thick (with the exception of the Zunn-Arts section) and defined by medium to massively bedded limestone, which is locally dolomitized. At Taishir, Ol, Khongor, Khunkher, and Tsagaan Gorge localities, the thickness of the HST averages ~ 15 m, and the carbonate facies are dominated by massively bedded lime-grainstone. In Khukh Davaa, on the other hand, the sequence becomes as thick as 70 m, and ooids are developed at the top of the sequence.

The fact that thickness and facies change do not vary in the Ol Fm across the Zavkhan Terrane is still suggestive of ramp morphology. Due to an early stage of rim build-up during T3, the thickness of the Ol Fm as a whole increases to the southwest (Figure 3.16D) and at locations, namely in Ikh Goliin Tsakhir, Unkheltseg and NE Khukh Davaa regions, the HST sequence of the Ol Fm becomes thicker with ooids forming at the top, which can be seen as thickened in inner-mid-ramp environment in Figure 3.15F.

Carbonate facies assemblages in the Shuurgat Formation.— In general, the Shuurgat Fm carbonates form two large-scale stratigraphic sequences dominated by TST and HST, separated by an uncomformity (figures 3.11 and 3.12C). Facies changes and thickness variations with general thinning towards the west-southwest are developed throughout the basin (figures 3.11, 3.15G, and 3.16E). Although the depositional environment for these carbonates is interpreted as a carbonate ramp (Read,

1982), stratigraphic patterns suggest a proto-rim formed during the deposition of Sh2 that may have been responsible for the distribution of early dolomitization and the carbonate facies change observed within Sh3 and Sh4 between outer-mid-ramp and mid-inner-ramp depositional environment (e.g. Dunham, 1980) (Figure 3.11, section F872). Due to an absence of slump folding and mass wasting representative of slope facies, and the lack of thick stromatolitic build-ups marking a reef, it is problematic to invoke a depositional environment with a true rimmed margin, so instead a flat-topped platform is envisioned.

Member Sh1 is preserved as limestone and composed of gray weathering, grainstone interbedded with pink calcisiltite with chert lenses and nodules, interpreted to represent deposition in a mid- to outer-ramp depositional environment (figures 3.11, 3.12B, and 3.15G). Sh1 represents the TST of a sequence 1. Up-section, the succession becomes more carbonate rich and dominated by bedded lime-grainstone with thin interbeds of calcisiltite. The transition to Sh2 has been difficult to document due to poor exposure and minor faulting and folding at the top of Sh1.

Overall, both Sh1 and Sh2 thin dramatically to the west and southwest on the margin. Sh2 carbonate strata are dominated by dolo-micrite, nodular-bedded dolostone, and minor ooid grainstone shoals that are variably brecciated and are attributed to later dolomitization. Hence, both members are interpreted to largely represent deposition in a mid- to upper-ramp environment in the HST of sequence 1.

Above the unconformity at the top of Sh2, on the Khunkher, Tsagaan and South Khukh Davaa blocks, limestone-dominated carbonate facies of Sh3 and Sh4 are composed of thin-bedded micritic limestone and nodular-bedded calcisiltite that are interpreted to represent the TST and HST on the mid- to upper-foreslope (Figure 3.15G). On the platform, the TST to HST above Sh2 is represented by dolo-grainstone with ooid shoals. The overlying Sh3-4 displays well-developed parasequences, which are the product of small-scale base-level changes that become well-defined on the flat-topped platform margin. Progradation of the margin during Ol to Sh2 time, followed by exposure at the top of Sh2 is suggested to have led to transformation of the margin from a carbonate ramp to a flat-topped platform, resulting in the sharp facies changes and well-developed parasequences seen in Sh3 and Sh4. In general, the combined thickness of Sh3 and Sh4 varies from place to place due in part to the development of a platform margin

geometry, concomitant facies change, and to the uncomformity (Figure 3.15H) at the top contact of the Shuurgat Fm.

3.6.2. Geochronology

Maximum depositional age within the clastic sediments.— Five clastic samples are discussed and the detrital age spectra of four of these (Figure 3.14) are used to infer provenance of the Zavkhan Terrane basement. The youngest LA-ICPMS dates from the sandstone and the quartzite clast in the conglomerate unit of the Zavkhan Fm are 743 ± 28 Ma ($^{206}Pb/^{238}Pb$) and 1887 ± 78 Ma ($^{207}Pb/^{206}Pb$) respectively, which are broadly taken as maximum depositional ages. However, the CA-ID-TIMS date of 802.11 ± 0.45/0.56/1.0 from a rhyolite flow directly above the sandstone bed demonstrates the limitations of LA-ICPMS ages from individual grains (Condon and Bowring, 2011). CA-ID-TIMS dates from tuffaceous sandstones from the Maikhan-Uul and Taishir fms suggest a detrital population and that the maximum depositional ages are 729.8 ± 1.4 and 768.9 ± 3.2 Ma, respectively. Finally, sandstone from the karsted surface at the top of the Shuurgat Fm yielded a youngest LA-ICPMS date of 692.8 ± 34.7 Ma, which is broadly taken as the maximum age of the sandstone.

Detrital zircon provenance.— The Zavkhan and Baidrag terranes are often lumped into one composite Precambrian terrane (e.g. Levashova et al., 2010). However, the Baidrag Terrane lacks overlap assemblages equivalent with the Zavkhan Fm volcanics and the Tsagaan-Olom Group and hosts Ediacaran metamorphism and magmatism that is absent in the Zavkhan Terrane (Kozakov and others, 2012). Consequently, these terranes were possibly separated until at least the Cambrian and may have separate Proterozoic tectonic and detrital zircon provenance histories. Ruzhentsev and Burashnikov (1996) suggested that the two terranes were part of a rifted portion of western Gondwana. This inference was supported by a paleomagnetic study that yielded a paleolatitude of $47^{+16}_{-12}{}^{o}$ N on Zavkhan Fm rhyolites, consistent with paleomagnetic data from India, South China, Tarim or Australia (Levashova et al., 2010). Rojas-Agramonte and others (2011) proposed that the terranes originated from Tarim due to a detrital and xenocrystic age peaks from Mongolian and Tarim samples that are not present in those from

China or Siberia. However, these data are from Paleozoic samples that formed after many of these basement terranes had accreted with each other and with additional juvenile arc terranes. Alternatively, using the multigrain bulk TIMS date of 755 ± 3 Ma from an alkali granite that intrudes the Zavkhan Fm volcanics (Yarmolyuk et al., 2008b), Wilhem and others (2012) proposed that the Zavkhan and Baidrag terranes experienced the Baikalian Orogeny (Kuzmichev et al., 2001) and were part of a single, ribbon microcontinent that was periodically associated with Siberia. These interpretations suffered from a lack of detailed geological work and from lumping results from the Zavkhan and Baidrag terranes together. We provide evidence that Precambrian basement ages, metamorphic ages, and overlap assemblages of the Zavkhan Terrane that are distinct from those in the Baidrag Terrane, offering strong evidence that these were two separate terranes during the Neoproterozoic.

Recent detrital spectra compilations from Paleozoic strata of Siberia (Rojas-Agramonte et al., 2011 and references therein), display dominant pre-1000 Ma age peaks at 1700-2500, 2350-3100, and 3250-3400 Ma. For Tarim, the spectra peaks are at 900-1100, 1700-1900, and 2450-2700 Ma (Zhang et al., 2013). North China has a broad spectrum that spans 1650-2600 Ma with distinct peaks at 1847 Ma and 2500 Ma (Sun et al., 2012) (Figure 3.14B). Our samples from Neoproterozoic strata on the Zavkhan Terrane (Figure 3.14A) have peaks at 1950-2100 and 2400-2600 Ma that form a broader hump between 1800 and 2800 Ma. These age peaks resemble those from Siberia, Tarim, and North China, but are not a perfect match with any of the proposed source terranes. Another prominent peak in the age spectra from Mongolia is present between 780-810 Ma, which is interpreted to have been sourced from the Zavkhan Fm. Hence it is suggested that the detrital population of the Zavkhan Terrane is locally derived from the underlying basement and that it may have its own distinctive characteristics.

Age of the Zavkhan Formation volcanics.— The first reported age constraint on the Zavkhan Fm was reported by Burashnikov (1990) with $^{207}Pb/^{206}Pb$ TIMS bulk zircon dates of 850 ± 2 and 750 ± 3 Ma (Badarch et al., 2002). Levashova and others (2010) dated rhyolites in the upper Zavkhan Fm near Tsagaan Gorge at 773.5 ± 3.6 Ma and in the lower part of the section near Bayan Gorge of 803.4 ± 8.0 Ma, both with LA-ICPMS $^{206}Pb/^{238}U$ on zircon. The entire Zavkhan Fm is further constrained in this

study with CA-ID-TIMS dates at 802.11 ± 0.45, 797.22 ± 0.56, and 787.45 ± 0.47 Ma. The latter age is obtained from rhyolite that is interpreted to be an olistolith of the Zavkhan Fm that is from a flow that is younger than what is preserved in the uppermost-Zavkhan Fm at the Taishir locality. This interpretation is supported by the discontinuous exposure of the ca. 787 Ma rhyolite, the maximum depositional age of middle Maikhan-Uul Fm of 729.8 ± 1.4 Ma from detrital grains, and the erosional uncomformity at the base of the erosional unconformity at the base of the Maikhan-Uul Fm.

Age of the Maikhan-Uul Formation.— Maximum depositional age constraints for the Sturtian glaciation on the Zavkhan Terrane are provided by our 787.45 ± 0.47/0.58/1.0 Ma date on a rhyolite olistolith near the base of the Maikhan-Uul Fm, and our 729.8 ± 1.4 Ma date on a detrital grain in the tuffaceous sandstone in the middle Maikhan-Uul Fm (figures 3.5 and 3.13D). Globally, the duration of the Sturtian glaciation is bracketed within a ~ 57 Ma window. The 717.4 ± 0.2 Ma date on the Mount Harper Volcanic Complex and the 716.5 ± 0.2 Ma date on the Rapitan Group (both $^{206}Pb/^{238}U$ CA-ID-TIMS single grain zircon dates) in northwestern Canada (Macdonald et al., 2010) and 715.9 ± 2.8 Ma and 716.1 ± 3.4 Ma dates (SIMS weighted mean $^{206}Pb/^{238}U$ zircon date) on a tuffaceous siltstone in the Gongdong Fm in South China (Lan et al., 2014) constrain the onset of the Sturtian glaciation. The 663 ± 4 Ma $^{206}Pb/^{238}U$ TIMS date on combined multi-grain separates of zircon from the Datangpo Fm in South China (Zhou et al., 2004), 659.7 ± 5.3 Ma $^{206}Pb/^{238}U$ SHRIMP date on the Wilyerpa Fm in Australia (although these were reported in an abstract without data) (Fanning and Link, 2008), a Re-Os date of 662.4 ± (3.9/4.6) Ma on the Sturtian-age Twitya cap carbonate in NW Canada (Rooney et al., 2014) and 659.0 ± (3.9/4.5) Ma Re-Os date on the basal Taishir Fm (Rooney et al., 2015) constrain the end of the Sturtian glaciation. The 687.4 ± 1.3 Ma and 685.5 ± 0.4 Ma dates from Idaho (Condon and Bowring, 2011; Keeley et al., 2013) and 711.5 ± 0.3 Ma from Oman (Bowring et al., 2007) (both $^{206}Pb/^{238}U$ CA-ID-TIMS single grain zircon dates) are interpreted to represent syn-glacial depositional ages. Because the middle member of the Maikhan-Uul Fm is interpreted to record local stepback of the ice grounding line during a larger glacial epoch, and not full-scale deglaciation, we correlate the whole of the Maikhan-Uul Fm to the ca. 717-660 Ma Sturtian glacial epoch (Figure 3.17).

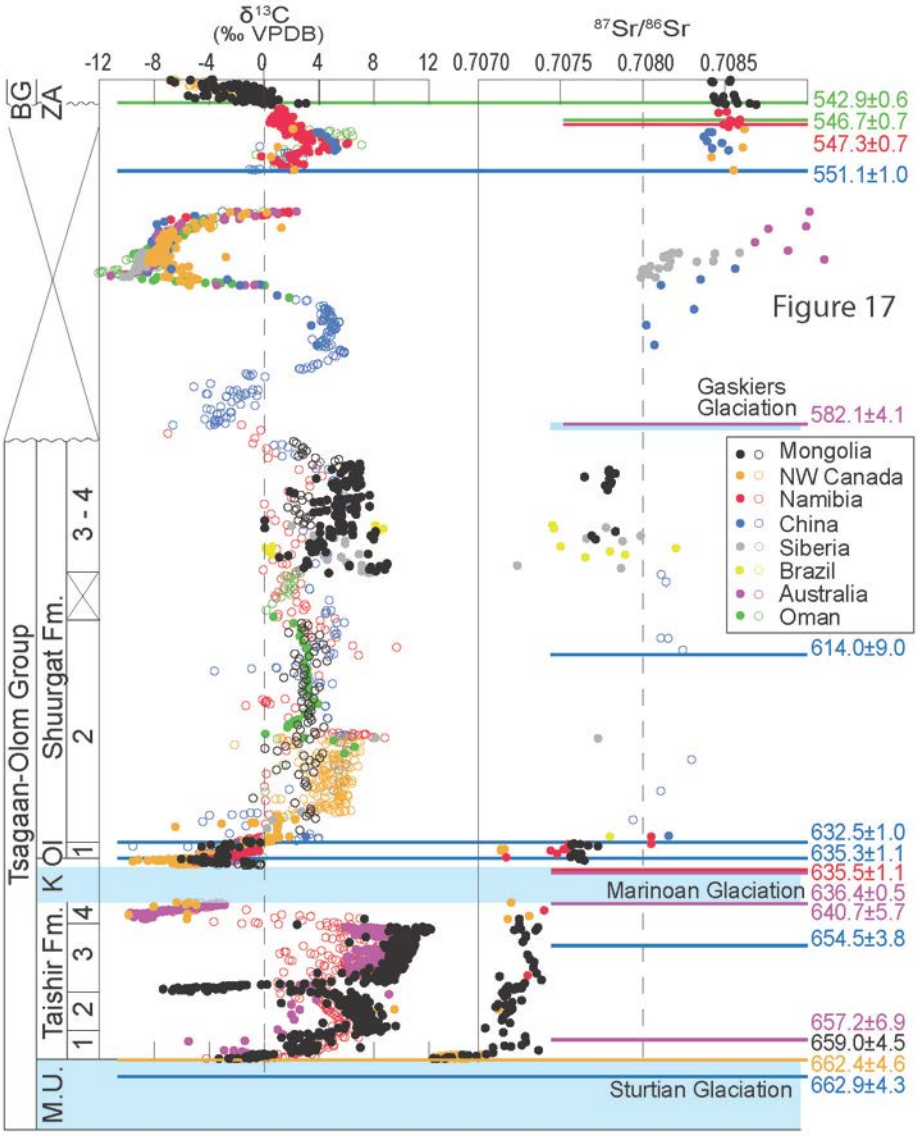

Figure 3.17. Global correlations of Cryogenian strata from key locations with associated isotopic and geochronologic data

All of the data are color coded for geographic location: Black = Mongolia, Purple = Australia, Red = Namibia, Blue = China, Green = Oman, Yellow = Brazil, and Orange = NW Canada. The approximate depositional span of each formation from which the chemostratigraphic data were utilized is shown on right-hand side. Each of these stratigraphic successions contains multiple unconformities of unknown extent, so there are certainly additional intervals in which strata are not present, and this figure is purely meant as an exercise to summarize our current age model for the Cryogenian and Ediacaran. Data from non-dolomitized carbonates are shown by filled and dolomitized by open circles. The $\delta^{13}C$ data is from Mongolia (this paper, Macdonald et al., 2009a), northwestern Canada (Johnston et al., 2012; Macdonald et al., 2013; Rooney et al., 2014), Namibia (Halverson et al., 2005), Australia (McKirdy et al., 2001; Rose et al., 2012; Swanson-Hysell et al., 2010), Oman (Fike et al., 2006), China (Sawaki et al., 2010b; Zhu et al., 2013), Brazil (Misi and Veizer, 1998), and Siberia (Melezhik et al., 2009; Pokrovskii et al., 2006). Strontium isotope data is from Mongolia (this study, Brasier et al., 1996a; Shields et al., 2002), northwestern Canada (Kaufman et al., 1993; Narbonne et al., 1994; Rooney et al., 2014), Namibia (Halverson et al., 2007; Kaufman et al., 1993; Yoshioka et al., 2003), Australia (Calver, 2000), China (Cui et al., 2015; Sawaki et al., 2010b), Brazil (Misi and Veizer, 1998), and Siberia (Melezhik et al., 2009; Pokrovskii et al., 2006). Geochronological constraints are from Mongolia (Rooney et al., 2015),

Figure 3.17 (Continued) Australia (Calver et al., 2013; Calver et al., 2004; Rooney et al., 2014) and others (Schmitz et al., 2012 with references therein). All uncertainties for reported dates include the internal, tracer solution, (where applicable), and decay constant uncertainties for the U-Pb and Re-Os geochronometers.

3.6.3. Chemostratigraphy

Carbon Isotopes.— Limestone successions of the Taishir Fm preserve the post-Sturtian Rasthof $\delta^{13}C$ excursion in the basal T1 TST and the mid-Cryogenian Taishir excursion in the basal T3 TST. In general, within the Taishir Fm, carbonate $\delta^{13}C$ values are more negative in TSTs and more positive in HSTs (Figure 3.8). The oceanic $\delta^{13}C$ signal preserved in carbonate rocks can be obscured by noise from detrital carbon (Johnston et al., 2012; Swart, 2008), restriction (Panchuk et al., 2006), early alteration (Knauth and Kennedy, 2009; Melim et al., 2001), and burial diagenesis (Derry, 2010). In the Taishir Fm, the $\delta^{13}C$ profiles can be correlated for > 100 km across the margin (figures 3.3 and 3.8). The fidelity of the carbonate $\delta^{13}C$ signal is further supported by the tight covariance with organic $\delta^{13}C$ values (Johnston et al., 2012; Shields et al., 2002).

The Cryogenian Trezona $\delta^{13}C$ excursion (Halverson et al., 2005; Rose et al., 2012; Swanson-Hysell et al., 2010), on the other hand, is not well developed in Mongolia. Trend in $\delta^{13}C$ values especially in the Taishir negative $\delta^{13}C$ excursion is comparable with the Trezona, which is further complicated by nonvariable values in $^{87}Sr/^{86}Sr$ (Figure 3.8 and Halverson et al., 2007). However, the removal of T4 in all localities except the Khongor Range, Zuun-Arts, and Ikh Goliin Tsakhir is suggestive of glacial erosion (Macdonald et al., 2009a) that may be responsible for an absence of Trezona excursion. This is further supported by limestone clasts in the Khongor diamictite that yield comparatively depleted $\delta^{13}C$ values (Figure 3.8) distinct from those of the underlying T3.

One of the distinct features of the Cryogenian carbonate record of the Zavkhan Terrane is the prevalence of limestone (Figure 3.8) compared to comparable carbonate dominated records in Namibia (Halverson et al., 2005) and Arctic Alaska (Macdonald et al., 2010). Parallel sections of unaltered and dolomitized successions provide an opportunity to document the $\delta^{13}C$ effects of dolomitization, which reveals variations of up to 8‰ between undolomitized and dolomitized sections (Figure 3.8).

In the Ediacaran strata, the early-Ediacaran Maieberg $\delta^{13}C$ excursion (Halverson et al., 2002; Hoffman and Schrag, 2002) is preserved in the TST and HST of the Ol Fm wherever the underlying Taishir Fm carbonates are preserved as limestone. However, the excursion is absent in localities where the underlying Taishir Fm and upper portion of the Ol Fm are dolomitized (Figure 3.11).

Carbon isotope signatures of Sh1 TST through Sh3 are comparable to other stratigraphically equivalent early Ediacaran strata globally (Calver, 2000; Fike et al., 2006; Macdonald et al., 2013; Misi and Veizer, 1998; Zhu et al., 2013). The return of $\delta^{13}C$ values in Sh4 from +6 to +8‰ back to +2 to +0.5‰ is also recognized from stratigraphically equivalent successions preserved in South China (Zhu et al., 2013), Namibia (Halverson et al., 2005) and NW Canada (Macdonald and others, 2013).

In our correlation framework, there is an up to 5‰ difference between limestone dominated Sh3 and Sh4 preserved in outer-mid-ramp and dolostone dominated Sh3 and Sh4 present in mid-inner-ramp depositional environment. Although $\delta^{13}C$ values can vary by as much as 2‰ between coexisting dolomite-calcite pairs (Degens and Epstein, 1964), the data presented here suggest that evolution of dolomitizing fluid has the potential to drive $\delta^{13}C$ variability within limestone and its dolomitized equivalent as demonstrated in the upper Taishir (T3), Ol, and Shuurgat (Sh3 and Sh4) fms. Due to the correspondence of lateral $\delta^{13}C$ variability with dolomitization fronts, we propose that the replacement and recrystallization of the primary carbonates from dolomitizing fluids played a crucial role in modifying $\delta^{13}C$ profiles. In general, it appears that dolomitization dampens $\delta^{13}C$ variability and shifts the mean values. This phenomenon is not unique to Mongolia. Large lateral $\delta^{13}C$ gradients have also been documented between Ediacaran carbonates deposited in foreslope and platform settings in Namibia (Halverson et al., 2005; Hoffman, 2011; Hoffman et al., 2007). We suggest that these lateral gradients are most easily attributable to differences in the water-rock ratio or the isotopic composition of the fluid during dolomitization rather than seawater isotopic gradients.

Strontium Isotopes.—Because of the long (2.4 Ma, Jones and Jenkyns, 2001) residence time in the ocean, Sr isotopes also provide a correlation tool for Precambrian carbonates that complement $\delta^{13}C$ correlations (Banner, 2004; DePaulo and Ingram, 1985). A cutoff value of Sr concentration of < 500 ppm

was used as a screening method for diagenetic alteration for the selection of $^{87}Sr/^{86}Sr$ values to compare our data with those from NW Canada (Halverson et al., 2007; Narbonne, 1994; Rooney et al., 2014), Namibia (Halverson et al., 2007; Kaufman et al., 1993; Yoshioka et al., 2003), China (Sawaki et al., 2010b), Siberia (Melezhik et al., 2009; Pokrovskii et al., 2006), Brazil (Misi and Veizer, 1998), Australia (Calver, 2000) and Oman (Table 3.A4; figures 3.17 and 3.A1).

The rise in $^{87}Sr/^{86}Sr$ from 0.70673 to 0.70737 in Member T1 of the Taishir Fm is in agreement with values measured previously between 0.70675 to 0.70694 (Brasier et al., 1996b; Shields et al., 2002), which is mirrored in the Rasthof Fm of Namibia (Yoshioka et al., 2003) and the Twitya Fm of NW Canada (Rooney et al., 2014). The carbon isotope chemostratigraphy from these three areas is also very similar, as discussed above. After this dramatic rise in the Sturtian cap carbonate, Sr isotope values are relatively steady through the rest of the Taishir Fm, with a slight rise near the base of T3.

A comparatively elevated $^{87}Sr/^{86}Sr$ value of 0.7091 ± 0.0001 (average value from Liu et al., 2014) was measured in the Ol Fm cap dolostone, which is similar to what Liu and others (2013) reported in Group-II of the Nuccaleena Fm cap dolostone in South Australia and in Member 1 of the Doushantuo Fm from China (Sawaki et al., 2010b). Although these values may be attributed to diagenetic alteration that lowers Sr concentration, elevated $^{87}Sr/^{86}Sr$ values are still persistent in step-leaching treatments, which have been used as evidence for a glacial meltwater plume with a radiogenic $^{87}Sr/^{86}Sr$ composition (Liu et al., 2014). Our single leach $^{87}Sr/^{86}Sr$ measurements of the Ol Fm are from the TST limestone succession, and the values of 0.70756 and 0.70765 (figures 3.11 and 3.17) agree with what Liu and others (2014) reported in the same interval, becoming less radiogenic up-section.

Overall, $^{87}Sr/^{86}Sr$ values increase from the basal Taishir Fm to the top of the Shuurgat Fm, from 0.70673 to 0.70795, excluding the values measured in the Ol cap dolostone (Liu et al., 2014) and are significantly less radiogenic compared to the values of > 0.7083 reported (Brasier et al., 1996b) in the latest Ediacaran-Cambrian Zuun-Arts Fm. Globally, the most reliable $^{87}Sr/^{86}Sr$ values from early to middle Ediacaran sections deposited prior to the Shuram excursions range from 0.7073 to 0.7083 (Figure 3.17) (Halverson et al., 2007; McKirdy et al., 2001; Melezhik et al., 2009; Misi and Veizer, 1998;

Narbonne et al., 1994; Pokrovskii et al., 2006; Rooney et al., 2014; Sawaki et al., 2010a; Sawaki et al., 2010b; Yoshioka et al., 2003). In contrast, limestone strata deposited after the Shuram excursion, in the late Ediacaran between ~ 552 and 541 Ma, have $^{87}Sr/^{86}Sr$ values between 0.7083 and 0.7090 (Brasier et al., 1996b; Halverson et al., 2007; McKirdy et al., 2001; Melezhik et al., 2009; Narbonne et al., 1994; Pokrovsky et al., 2011). Hence, $^{87}Sr/^{86}Sr$ data from the Shuurgat Fm suggest that this unit was likely deposited during the early to middle Ediacaran, prior to the Shuram excursion, and confirm previous suggestions that the karst surface between the Shuurgat and Zuun-Arts Fm represents a major hiatus (Figure 3.17).

Together, our new Cryogenian and Ediacaran $^{87}Sr/^{86}Sr$ compilation (Figure 3.17) suggests that, rather than a gradual rise to more radiogenic values from an increase of continental margins during the rifting of Rodinia (Halverson et al., 2007), the Cryogenian to Ediacaran rise is stepwise, likely reflecting extreme weathering in the aftermath of the Cryogenian Snowball Earth events, and an additional extreme weathering event associated with the Shuram $\delta^{13}C$ excursion.

3.6.4. Construction of an Age Model

The carbon and strontium isotope profiles of the Taishir Fm and a Re-Os age of 659.0 ± (3.9/4.5) (Rooney et al., 2015) obtained from T1 are very similar to the 662.4 ± (3.9/4.6) Ma Twitya Fm in northwest Canada, and consequently, in our age model the base of the Taishir Fm is pinned at 660 Ma. The T1 cap carbonate was previously dated using $^{207}Pb/^{204}Pb$ on carbonate yielding a $^{207}Pb/^{206}Pb$ isochron date of 632 ± 47 Ma (MSWD = 7.3) (Ovchinnikova et al., 2012b). Although this method is neither very precise nor reliable because of the mobility of U and Pb in carbonate (Sumner and Bowring, 1996), this date is within error estimates based on global correlations.

The age of the Taishir Fm is further constrained by correlations of the overlying Khongor Fm diamictite with the Marinoan glaciation and basal Ol Fm with the Marinoan cap carbonate (Macdonald et al., 2009a). This suggests that the underlying Khongor Fm diamictite is an end-Cryogenian glacial deposit, with the termination bracketed by $^{206}Pb/^{238}U$ CA-ID-TIMS dates of 635.5 ± 0.6 Ma and 635.2 ±

0.6 Ma from zircon from China (Condon et al., 2005), 635.5 ± 1.2 Ma from zircon from Namibia (Hoffmann et al., 2004), and 636.4 ± 0.5 Ma from zircon from Australia (Calver et al., 2013). By correlation, these data constrain the age of the Taishir Fm and the Khongor Fm to between 659 and 635 Ma. Assuming that the start of the Marinoan glaciation was ~ 640 Ma and taking into account the absence and erosion of the Trezona excursion in the Zavkhan Terrane, in our age model, the top of the Taishir Fm carbonate is given with a geochemically interpolated age of 643 Ma (Figure 3.17). However, we acknowledge that the Marinoan glaciation may have started earlier and the top of the Taishir Fm is as old as ca. 650 Ma.

There are no absolute ages on the Ol or Shuurgat fms, and thus our age model relies on chemostratigraphic correlation to other Ediacaran successions globally, particularly Namibia (Halverson et al., 2005) and South China (Condon et al., 2005; Zhu et al., 2013) (Figure 3.17). Using $\delta^{13}C$ correlations with South China, the entire Ol Fm and Sh1 of the Shuurgat Fm are bracketed by $^{206}Pb/^{238}U$ CA-ID-TIMS dates of 635.2 ± 0.6 and 632.5 ± 0.5 Ma at the base. The uncomformity at the top of the Sh4 could explain why the Gaskiers glaciation and Shuram $\delta^{13}C$ excursion are not preserved in the Zavkhan Terrane (see Figure. 18, Halverson et al., 2010) and hence a 584 Ma age (Hoffman and Li, 2009) is assigned to the top of the Shuurgat Fm (Figure 3.17). The age of the Shuram $\delta^{13}C$ excursion is constrained between ca. 582 Ma and 551 Ma with the correlation of the Gaskiers glaciation with dropstones in the Bunyeroo Fm (Gostin et al., 2010) and the placement of the placement of the 551 Ma ash in South China in the Miaohe member of the Denying Fm (An et al., 2015), and the duration of the excursion remains poorly constrained.

3.6.5. The Cryogenian and Ediacaran Carbon Cycle

Although $\delta^{13}C$ trends are reproducible in limestone sections across the Zavkhan Terrane, dolomitized sections show large lateral isotopic variability. It is generally accepted that dolomite records a primary seawater signal with minor variations from the equivalent limestone (Degens and Epstein, 1964) due to amount of concentration of carbon in aqueous fluids (Kaufman et al., 1997; Knoll et al.,

1986). However, as discussed previously, this assumption does not hold true for much of the Cryogenian strata in southwest Mongolia, in which ≤ 8‰ variability is present between limestone and coeval dolomitized strata (figures 3.8 and 3.11). Globally, both Cryogenian and Ediacaran carbonate are dominated by dolostone (Halverson et al., 2002; Macdonald et al., 2010) and consequently, most Neoproterozoic $\delta^{13}C$ compilations are based on them (Halverson et al., 2010). The data presented herein underscore the need to use caution when using $\delta^{13}C$ data from dolomites for correlations and compilations. By using data obtained from dolomite, the truly extreme variability of Neoproterozoic $\delta^{13}C$ values preserved in limestone may have been dampened.

In limestone-dominated sections, our correlations suggest that the Taishir $\delta^{13}C$ excursion is preserved, but the Trezona $\delta^{13}C$ excursion is largely removed under the sub-Khongor erosional surface, and the Shuram $\delta^{13}C$ excursion is missing below the karstic surface at the base of the Zuun-Arts Fm (Figure 3.17). The Taishir and Trezona $\delta^{13}C$ excursions present two of the largest perturbations to the carbon cycle in the geological record (Johnston et al., 2012), comparable with the Ediacaran Shuram excursion (Grotzinger et al., 2011). Although the nadir of the Shuram excursion is more negative (-12‰), the Shuram departs from a less enriched background (+2 to +4‰), compared to the Taishir and Trezona excursions that start from a ~ +8 to +10‰ background and plummet to -7‰. Thus, many of the arguments and models for the origin and nature of the Shuram $\delta^{13}C$ excursion (for example Derry, 2010; Grotzinger et al., 2011) are applicable to the Cryogenian $\delta^{13}C$ excursions.

Through comparisons with Pliocene-Pleistocene $\delta^{13}C$ anomalies associated with glacio-eustatic sea level fall and subaerial exposure, and by the covariance between $\delta^{13}C$-$\delta^{18}O$, multiple authors have proposed that the Trezona excursion was driven by meteoric diagenesis and remineralization of a terrestrial biosphere (Knauth and Kennedy, 2009; Swart and Kennedy, 2012). However, it is unlikely that there was a significant terrestrial biosphere during the Cryogenian (Gensel, 2008; Sanderson, 2003; Zimmer et al., 2007) and consequently extensive organic matter remineralization in the uppermost portion of the sediments near these purported exposure surfaces is unlikely. Although exposure surfaces related to the Marinoan glaciation are present directly above the Trezona excursion at all of the locations in which it

has been described, in Mongolia the Trezona excursion is largely absent beneath a sub-glacial erosion surface. However, the Taishir excursion is in a broad TST to HST, and the nearest exposure surface is > 100 m above the excursion. Therefore, meteoric alteration, if it was a driving the Taishir excursion, must have occurred in the lower vadose, phreatic, or mixing zone wedges (Melim et al., 2001) associated with the sub-Khongor Fm exposure surfaces at the top of the Taishir Fm. Moreover, there is no petrographic evidence for large-scale replacement and meteoric cements directly associated with the excursion. Lastly, $\delta^{13}C$ and $\delta^{18}O$ do not covary while $\delta^{13}C_{carb}$ and $\delta^{13}C_{org}$ do covary in the Taishir excursion (Table 3.A3, Johnston et al., 2012). Thus, although meteoric diagenesis may be consistent with some features of the Trezona excursion, it is completely inconsistent with the sequence stratigraphic architecture and geochemistry of the Taishir excursion in Mongolia.

Another feature of the Trezona excursion in Australia (Swanson-Hysell et al., 2010) and Namibia (Johnston et al., 2012) is that $\delta^{13}C_{carb}$ and $\delta^{13}C_{org}$ do not covary. This lack of covariance between $\delta^{13}C_{carb}$ and $\delta^{13}C_{org}$ inspired Rothman and others (2003) to propose the existence of a large Neoproterozoic dissolved organic carbon pool (DOC) that was periodically remineralized, driving dynamic behavior in the isotopic composition of the dissolved inorganic carbon pool (DIC). Moreover, the existence of a large DOC reservoir in Neoproterozoic oceans is inconsistent with $\delta^{13}C$ records from NW Canada and Mongolia that show covariance throughout the Cryogenian period (Johnston et al., 2012). Johnston and others (2012) instead suggested that the lack of covariance in $\delta^{13}C_{carb}$ and $\delta^{13}C_{org}$ in Australia and Namibia could be explained by bulk organic carbon in TOC-lean samples being more prone to masking by detrital and migrated organic matter. Thus, the $\delta^{13}C$ data from Mongolia is inconsistent with driving mechanisms that evoke the remineralization of a large DOC reservoir. Johnston and others (2012) suggested that the Taishir excursion was due to the addition of isotopically light carbon to the ocean/atmosphere through either oxidation of organic matter associated with the uplift and erosion of previously deposited strata (*c.f.* Higgins and Schrag, 2006) or the release of methane Schrag, (2002). These models predict a timescale consistent with the mixing time of the ocean. That is, the excursion should not last more than 100 ka. The average thickness of the Taishir excursion is ~ 30 m. The maximum average sedimentation rate calculated

above suggests a duration of the Taishir excursion of 100 ka to 1 Ma, broadly consistent with these models and perhaps suggestive of increased sedimentation rates. However, these models do not directly address the positive background $\delta^{13}C$ values of the Cryogenian.

Schrag and others (2013) proposed an alternative model whereby both the positive background $\delta^{13}C$ values and the negative excursions are related to changes in a large, isotopically depleted sink of carbon in authigenic carbonate. The precipitation of authigenic carbonate is inhibited by the amount of O_2 in seawater due to the acidity generated via oxidation of reduced compounds (C_{org}, H_2S, Fe^{2+}) (Higgins et al., 2009). During the Taishir excursion, the addition of carbon to the ocean/atmosphere would lead to an increased global production of authigenic carbon, thereby producing a negative feedback on changes to the carbon isotopic composition of the ocean, whereas the addition of oxidants to the ocean, either as free oxygen or other electron acceptors (Fe(III), SO_4^{2-}) could have led to a greater importance of aerobic respiration over anaerobic respiration, further limiting the amount of organic matter delivered to the sediment for anaerobic respiration. Although the ultimate origin of large shifts in the Cryogenian $\delta^{13}C$ composition of the oceans remains enigmatic, our data reinforce the reproducibility and fidelity of these signals (Figure 3.8).

3.7. CONCLUSIONS

With detailed mapping, stratigraphy, sedimentology, geochemistry, the Tsagaan-Olom Group is now confidently correlated with Cryogenian and early-Ediacaran successions around the globe. Moreover, detrital age spectra of the lower Zavkhan, Maikhan-Uul, Taishir and Shuurgat fms provide the first strong evidence for the presence of Proterozoic basement on the Zavkhan Terrane. The age spectra reveal dominant age peaks at 1950-2100 and 2400-2600 Ma. These data have some similarities and some differences from previously reported basement ages from Tarim, North China, Siberia and NE Gondwana and highlight uncertainties related to the origin and travels of the Proterozoic continental fragments that form the core of the CAOB.

The Zavkhan Terrane is mantled with the Zavkhan Fm, dated at 802.11 ± 0.45/0.56/1.0, 797.22 ± 0.56 and 787.45 ± 0.47/0.58/1.0 Ma, and rift-related rocks of the Khasagt Fm. After 729.8 ± 1.4 Ma, the Zavkhan Terrane was covered with ice sheets and lodgement tills of the lower Maikhan-Uul Fm. During this glaciation, the ice-grounding line retreated and readvanced, and coarse siliciclastic turbidite beds were deposited in the middle Maikhan-Uul Fm. Although these strata have previously been interpreted to mark a transgression (Lindsay et al., 1996b), they were not necessarily deposited in open water and could have formed below an ice shelf or in a glacio-lacustrine setting. Deposition of rain-out diamictites in the upper member of the Maikhan-Uul Fm culminated with a local regression and exposure, followed by a laterally extensive transgression and carbonate deposition of Member T1 of the Taishir Fm. This local regression was likely either the product of glacio-isostatic rebound or ice gravity. Carbon and strontium isotope values, along with Re-Os geochronology confirm previous suggestions that at least the upper Maikhan-Uul Fm is correlative with the 717-660 Ma Sturtian glaciation.

The Taishir Fm was deposited on an isolated, passively subsiding homoclinal carbonate ramp in four large-scale sequences. The Taishir $\delta^{13}C$ excursion occurs in the TST of the third sequence. These data are consistent with the input of isotopically light carbon to the ocean, either from the mantle, methane, or organic carbon, or from an oxidation event that lead to the crash of the authigenic carbonate sink—these scenarios are not mutually exclusive. Above the Taishir excursion, $\delta^{13}C$ values become extremely enriched before dropping again prior to deposition of the Khongor Fm diamictite. This downward trend in $\delta^{13}C$ is correlated to the onset of the Trezona excursion. By distinguishing between these excursions, these geochemical records can now be globally integrated together into composite records. The data from Mongolia provide the backbone for understanding the great geochemical, climatic and biological changes that characterize the Cryogenian glacial interlude.

The Khongor Fm, the Marinoan glacial diamictite, is absent at most exposures on the Zavkhan Terrane. Nonetheless, the presence of isolated, thick diamictites on the Khunkher block with striated clasts and soft-sedimentary folding suggest that the Khongor Fm was deposited during deglaciation as a glacial moraine. These glacial deposits are overlain by a cap dolostone of the Ol Fm, which contains

sedimentary features including tubestone stromatolites, giant wave ripples, and both aragonite and barite fans, that are characteristic of the ca. 635 Ma basal Ediacaran cap dolostone. In addition, $^{87}Sr/^{86}Sr$ values obtained from limestone of the upper the Ol Fm match values preserved in limestone that overlies the Marinoan cap dolostone in Australia. Furthermore, the absence of the Shuram excursion in Mongolia, and $^{87}Sr/^{86}Sr$ values of < 0.70795 in the Shuurgat Fm suggest that much of the mid- to late Ediacaran is missing at a karst surface between the Shuurgat and Zuun-Arts fms.

In both Ediacaran and Cryogenian strata, large lateral $\delta^{13}C$ gradients are apparent in dolomitized strata. These data emphasize the importance of building composite $\delta^{13}C$ curves and assessing the nature of the carbon cycle with the least-altered samples, preferably limestones. The $\delta^{13}C$ variability of the Neoproterozoic is dampened in dolomitized strata, and the least-altered samples indicate that both the positive and negative $\delta^{13}C$ excursions in our Cryogenian and Ediacaran composite curve are even greater than what have been depicted in previous compilations. That is, in the most pristinely preserved sections, large carbon isotope excursions are a robust and reproducible feature of Neoproterozoic records.

3.8. ACKNOWLEDGMENTS

We thank: NASA MIT Astrobiology node and NASA Geobiology grant # NNH10ZDA001N-EXO for support; the NSF GRF (to EFS) for support; J.C. Creveling and David Jones for help in the field; Claire Bucholz for discussions and help drafting Figure 3.1; our field assistants Bataa, Erdenebayar Oyun, Tsolmon Adiya, Javkhlan Otgonkhuu, Gerelt Sarantuya, Javzandulam Chuluunbaatar, Munkh-Erdene Delger, Munkh Jugder, Ariunsanaa Dorj, Odbayar Erdenebat, Dan Bradley, Tanya Petach and Sarah Moon; Bayasgalan Amgalan, Altantsetseg Baldandorj, Oyungerel Sambuu, D.Oyun and Lkhagva-Ochir Said for help with logistics; Chuluun Minjin, and D.Dorjnamjaa for valuable scientific input; Greg Eischeid and Sarah Manley for use of and assistance in the Harvard University Laboratory for Paleoceanography.

3.9. REFERENCES

Abbot, D. S., Voigt, A., and Koll, D., 2011, The Jormungand global climate state and implications for Neoproterozoic glaciations: Journal of Geophysical Research, v. 116, no. D18103.

Aharon, P., 1988, Oxygen, carbon and U-seriew isotopes of aragonites from Vestfold Hills Antarctica: clues to geochemical processes in subglacial environments: Geochimica et Cosmochimica Acta, v. 52, p. 2231-2331.

Ahr, W. M., 1973, The carbonate ramp: An alternative to the shelf model: Gulf Coast Association of Geological Societies Transactions, v. 23, p. 221-225.

Aitken, J. D., 1991, The Ice Brook Formation and Post-Rapitan, Late Proterozoic glaciation, Mackenzie Mountains, Northwest Territories: Geological Survey of Canada Bulletin, v. 404, p. 1-43.

Alekseeva, R., Afanasjeva, G., and Shishkina, G., 2001, Lower and Middle Devonian brachiopods of the Far East of Russia and Mongolia: strophomenids and chonetids: Trudy Palaeontological Institute, Russian Academy of Sciences, v. 281, p. 1-132.

Allen, P. A., and Etienne, J. L., 2008, Sedimentary challenge to Snowball Earth: Nature Geoscience, v. 1, p. 817-926.

Álvaro, J. J., Ahlberg, P., Babcock, L. E., Bordonaro, O. L., Choi, D. K., Cooper, R. A., Ergaliev, G. K., Gapp, I. W., Pour, M. G., and Hughes, N. C., 2013, Global Cambrian trilobite palaeobiogeography assessed using parsimony analysis of endemicity: Geological Society, London, Memoirs, v. 38, no. 1, p. 273-296.

An, Z., Jiang, G., Tong, J., Tian, L., Ye, Q., Song, H., and Song, H., 2015, Stratigraphic position of the Ediacaran Miaohe biota and its constrains on the age of the upper Doushantuo δ 13 C anomaly in the Yangtze Gorges area, South China: Precambrian Research, v. 271, p. 243-253.

Atashkin, V. A., 1995, The Cambrian system of the foldbelts of Russia and Mongolia: correlation chart and explanatory notes, International Union of Geological Sciences, v. 32.

Badarch, G., Byamba, J., Mahbadar, Ts., Minjin, Ch., Orolmaa, D., Tomurtogoo, O., and Khosbayar, Ts, 1998, Geological map of Mongolia: Mongolian Academy of Sciences, Mineral Resources Authority of Mongolia.

Badarch, G., Cunningham, W. D., and Windley, B., 2002, A new terrane subdivision for Mongolia: implications for the Phanerozoic crustal growth of Central Asia: Journal of Asian Earth Sciences, v. 21, p. 87-110.

Banner, J. L., 2004, Radiogenic isotopes: systematics and applications to earth surface processes and chemical stratigraphy: Earth-Science Reviews, v. 65, p. 141-194.

Benn, D. I., Le Hir, G., Bao, H., Donnadieu, Y., Dumas, C., Fleming, E. J., Hambrey, M. J., McMillan, E. A., Petronis, M. S., and Ramstein, G., 2015, Orbitally forced ice sheet fluctuations during the Marinoan Snowball Earth glaciation: Nature Geoscience, v. 8, no. 9, p. 704-707.

Bezzubetsev, V. V., 1963, On the Precambrian-Cambrian stratigraphy of the Dzabkhan River Basin: Materials on the Geology of MPR, Gostopotekhizdat, v. 1963, p. 29-42.

Blodgett, R. B., Rohr, D. M., and Boucot, A. J., 2002, Paleozoic links among some Alaskan accreted terranes and Siberia based on megafossils, *in* Miller, E. L., Grantz, A., and Klemperer, S. L., eds., Tectonic Evolution of the Bering Shelf--Chukchi Sea--Arctic Margin and Adjacent Landmasses: Boulder, Colorado, Geological Society of America Special Paper 360, p. 273-290.

Bold, U., Crowley, J. L., Smith, E. F., Sambuu, O., and Macdonald, F. A., submitted, Neoproterozoic to early Paleozoic tectonic evolution of the Zavkhan Terrane of Mongolia: Implications for crustal growth in the Central Asian Orogenic Belt: Lithosphere.

Bold, U., Macdonald, F. A., Smith, E. F., Crowly, J. C., Minjin, C., and Dorjnamjaa.D., 2013, Elevating the Neoproterozoic Tsagaan-Olom Formation to a Group: Mongolian Geoscientist, v. 39, p. 5.

Bold, U., Schrag, D. P., Higgins, J. A., Erdenebayar, J., and Macdonald, F. A., in preparation, Effect of dolomitization on isotopic records from Neoproterozoic carbonates in southwestern Mongolia: Geological Society of America Bulletin.

Bold, U., Smith, E. F., Rooney, A. D., Buchwaldt, R., Ramezani, J., Schrag, D. P., and Macdonald, F. A., 2016, Neoproterozoic stratigraphy of the Zavkhan Terrane of Mongolia: The backbone for Cryogenian and Early Ediacaran chemistratigraphic records: American Journal of Science, v. 316, p. 1-63.

Bosak, T., Lahr, D. J. G., Pruss, S. B., Macdonald, F. A., Dalton, L., and Matys, E., 2011a, Agglutinated tests in post-Sturtian cap carbonates of Namibia and Mongolia: Earth and Planetary Science Letters, v. 308, p. 29-40.

Bosak, T., Lahr, D. J. G., Pruss, S. B., Macdonald, F. A., Gooday, A. J., Dalton, L., and Matys, E., 2012, Possible early foraminiferans in post-Sturtian (716-635 Ma) cap carbonates: Geology, v. 40, no. 1, p. 67-70.

Bosak, T., Macdonald, F. A., Lahr, D. J. G., and Matys, E., 2011b, Putative Cryogenian ciliates from Mongolia: Geology, v. 39, no. 12, p. 1123-1126.

Boulton, G. S., 1978, Boulder shapes and grain-size distribution of debris as indicators of transport paths through a glacier and till genesis: Sedimentology, v. 25, p. 773-799.

Boulton, G. S., Dobbie, K. E., and Zatsepin, S., 2001, Sediment deformation beneath glaciers and its coupling to the sublacial hydraulic system: Quaternary International, v. 86, p. 3-28.

Bowring, J., McLean, N., and Bowring, S., 2011, Engineering cyber infrastructure for U-Pb geochronology: Tripoli and U-Pb_Redux: Geochemistry, Geophysics, Geosystems, v. 12, no. 6.

Bowring, S. A., Grotzinger, J. P., Condon, D. J., Ramezani, J., and Newall, M., 2007, Geochronologic constraints on the chronostratigraphic framework of the Neoproterozoic Huqf Supergroup, Sultanate of Oman: American Journal of Science, v. 307, p. 1097-1145.

Brasier, M. D., Dorjnamjaa, D., and Lindsay, J. F., 1996a, The Neoproterozoic to early Cambrian in southwest Mongolia: an introduction: Geological Magazine, v. 133, no. 4, p. 365-369.

Brasier, M. D., Magaritz, M., Corfield, R., Luo, H., Wu, X., Lin, O., Jiang, Z., Hamdi, B., He, T., and Fraser, A. G., 1990, The carbon- and oxygen-isotope record of the Precambrian-Cambrian

boundary interval in China and Iran and their correlation: Geological Magazine, v. 127, p. 319-332.

Brasier, M. D., Shields, G., Kuleshov, V. N., and Zhegallo, E. A., 1996b, Integrated chemo- and biostratigraphic calibration of early animal evolution: Neoproterozoic -early Cambrian of southwest Mongolia: Geological Magazine, v. 133, no. 4, p. 445-485.

Brown, D., Ryan, P. D., Afonso, J. C., Boutelier, D., Burg, J., Byrne, T., Calvert, A., Cook, F., DeBari, S., and Dewey, J., 2011, Arc–continent collision: the making of an orogen, Springer.

Buchan, C., Cunningham, D., Windley, B., and Tomurhuu, D., 2001, Structural and lithological characteristics of the Bayankhongor Ophiolite Zone, Central Mongolia: Journal of the Geological Society of London, v. 158, p. 445-460.

Bucholz, C. E., Jagoutz, O., Schmidt, M. W., and Sambuu, O., 2014, Phlogopite-and clinopyroxene-dominated fractional crystallization of an alkaline primitive melt: petrology and mineral chemistry of the Dariv Igneous Complex, Western Mongolia: Contributions to Mineralogy and Petrology, v. 167, no. 4, p. 1-28.

Burashnikov, V. V., 1990, Tectonics of the Urgamal zone, Early Calidonides of western Mongolia [Phd: Russian Academy of Sciences, 25 p.

Burchette, T. P., and Wright, V. P., 1992, Carbonate ramp depositional systems: Sedimentary Geology, v. 79, p. 3-57.

Byamba, J., 2011, History of geologic study in Mongolia, Ulaanbaatar, Mongolia, Soyombo printing, Stratigraphy.

Calver, C., Crowley, J., Wingate, M., Evans, D., Raub, T., and Schmitz, M., 2013, Globally synchronous Marinoan deglaciation indicated by U-Pb geochronology of the Cottons Breccia, Tasmania, Australia: Geology, v. 41, no. 10, p. 1127-1130.

Calver, C. R., 2000, Isotope stratigraphy of the Ediacaran (Neoproterozoic III) of the Adelaid Rift Complex, Australia, and the overprint of water column stratification: Precambrian Research, v. 100, p. 121-150.

Calver, C. R., Black, L. P., Everard, J. L., and Seymour, D. B., 2004, U-Pb zircon age constraints on late Neoproterozoic glaciation in Tasmania: Geology, v. 32, no. 10, p. 893-896.

Cocks, L., and Torsvik, T. H., 2007, Siberia, the wandering northern terrane, and its changing geography through the Paleozoic: Earth Science Reviews, v. 82, no. 1-2, p. 29-74.

Cohen, P. A., and Macdonald, F. A., 2015, The proterozoic record of eukaryotes: Paleobiology, v. 41, no. 04, p. 610-632.

Cohen, P. A., Macdonald, F. A., Pruss, S., Matys, E., and Bosak, T., 2015, Fossils of putative marine algae from the Cryogenian glacial interlude of Mongolia: Palaios, v. 30, no. 3, p. 238-247.

Cole, R. B., and Stewart, B. W., 2009, Continental margin volcanism at sites of spreading ridge subduction: examples from southern Alaska and western California: Tectonophysics, v. 464, no. 1, p. 118-136.

Condon, D. J., and Bowring, S. A., 2011, A user's guide to Neoproterozoic geochronology, *in* Arnaud, E., Halverson, G. P., and Shields-Zhou, G., eds., The Geological Record of Neoproterozoic Glaciations, Volume 36: London, Geological Society, p. 135-149.

Condon, D. J., Zhu, M., Bowring, S. A., Wang, W., Yang, A., and Jin, Y., 2005, U-Pb ages from the Neoproterozoic Doushanto Formation, China: Science, v. 308, p. 95-98.

Creveling, J., Mitrovica, J., Chan, N.-H., Latychev, K., and Matsuyama, I., 2012, Mechanisms for oscillatory true polar wander: Nature, v. 491, no. 7423, p. 244-248.

Cui, H., Kaufman, A. J., Xiao, S., Zhu, M., Zhou, C., and Liu, X.-M., 2015, Redox architecture of an Ediacaran ocean margin: Integrated chemostratigraphic (δ 13 C–δ 34 S–87 Sr/86 Sr–Ce/Ce*) correlation of the Doushantuo Formation, South China: Chemical Geology, v. 405, p. 48-62.

Davis, P. T., Briner, J. P., Coulthard, R. D., Finkel, R. W., and Miller, G. H., 2006, Preservation of Arctic landscapes overridden by cold-based ice sheets: Quaternary Research, v. 65, no. 1, p. 156-163.

Degens, E. T., and Epstein, S., 1964, Oxygen and carbon isotope ratios in coexisting calcites and dolomites from recent and ancient sediments: Geochimica et Cosmochimica Acta, v. 28, no. 1, p. 23-44.

Demoux, A., Kroener, A., Badarch, G., Jian, P., Tomurhuu, D., and Wingate, M. T. D., 2009a, Zircon ages from the Baydrag block and the Bayankhongor ophiolite zone: Time constraints on late Neoproterozoic to Cambrian subduction- and accretion-related magmatism in central Mongolia: Journal of Geology, v. 117, p. 377-397.

Demoux, A., Kröner, A., Hegner, E., and Badarch, G., 2009b, Devonian arc-related magmatism in the Tseel terrane of SW Mongolia: chronological and geochemical evidence: Journal of the Geological Society, v. 166, no. 3, p. 459-471.

Demoux, A., Kröner, A., Liu, D., and Badarch, G., 2009c, Precambrian crystalline basement in southern Mongolia as revealed by SHRIMP zircon dating: International Journal of Earth Sciences, v. 98, no. 6, p. 1365-1380.

DePaulo, D. J., and Ingram, B. L., 1985, High-Resolution Stratigraphy with Strontium Isotopes: Science, v. 227, no. 4689, p. 938-941.

Dergunov, A. B., 2001, Tectonics, Magmatism, and Metallogeny of Mongolia, Psychology Press.

Derry, L. A., 2010, A diagenetic origin for the Ediacaran Shuram-Wonoka carbon isotope anomaly: Earth and Planetary Science Letters, v. 294, p. 152-162.

Deynoux, M., 1985, Terrestrial or waterlain glacial diamictites? Three case studies from the Late Precambrian and Late Ordovician glacial drifts in West Africa: Palaeogeography, Palaeoclimatology, Palaeoecology, v. 51, p. 97-141.

Dijkstra, A. H., Brouwer, F. M., Cunningham, W. D., Buchan, C., Badarch, G., and Mason, P. R., 2006, Late Neoproterozoic proto-arc ocean crust in the Dariv Range, Western Mongolia: a supra-subduction zone end-member ophiolite: Journal of the Geological Society, v. 163, no. 2, p. 363-373.

Dobretsov, N. L., and Buslov, M., 2007, Late Cambrian-Ordovician tectonics and geodynamics of Central Asia: Russian Geology and Geophysics, v. 48, no. 1, p. 71-82.

Dobretsov, N. L., Buslov, M. M., and Vernikovsky, V. A., 2003, Neoproterozoic to Early Ordovician evolution of the Paleo-Asian Ocean: implications to the break-up of Rodinia: Gondwana Research, v. 6, no. 2, p. 143-159.

Domack, E., O'Brien, P., Harris, P., Taylor, F., Quilty, P. G., Santis, L. D., and Raker, B., 1998, Late Quaternary sediment facies in Prydz Bay, East Antarctica and their relationship to glacial advance onto the continental shelf: Antarctic Science, v. 10, no. 03, p. 236-246.

Domack, E. W., and Hoffman, P. F., 2011, An ice grounding-line wedge from the Ghaub glaciation (635 Ma) on the distal foreslope of the Otavi carbonate platform, Namibia, and its bearing on the snowball Earth hypothesis: Geological Society of America Bulletin, v. 123, no. 7-8, p. 1448-1477.

Domack, E. W., Jacobson, E. A., Shipp, S., and Anderson, J. B., 1999, Late Pleistocene--Holocene retreat of the West Antarctic Ice-Sheet system in the Ross Sea: Part 2--Sedimentologic and stratigraphic signature: Geological Society of America Bulletin, v. 111, no. 10, p. 1517-1536.

Dorjnamjaa, D., and Enkhbaatar, B., 2011, Classification of flora of the Precambrian and Cambrian periods and their stratigraphic importance, Mongolian Geology and Mineral Resources: Ulaanbaatar, Mongolia, Soyombo printing, p. 12-26.

Dunham, J. B., 1980, Shallow Subsurface Dolomitization of Subtidally Deposited Carbonate Sediments in the Hanson Creek Formanon (Ordovician—Silurian) of Central Nevada.

Edel, J. B., Schulmann, K., Hanžl, P., and Lexa, O., 2014, Palaeomagnetic and structural constraints on 90° anticlockwise rotation in SW Mongolia during the Permo–Triassic: Implications for Altaid oroclinal bending. Preliminary palaeomagnetic results: Journal of Asian Earth Sciences, v. 94, no. 0, p. 157-171.

Erwin, D. H., Laflamme, M., Tweedt, S. M., Sperling, E. A., Pisani, D., and Peterson, K. J., 2011, The Cambrian Conundrum: Early Divergence and Later Ecological Success in the Early History of Animals: Science, v. 334, p. 1091-1097.

Evans, D. A. D., Zhuravlev, A. Y., Budney, C. J., and Kirschvink, J. L., 1996, Palaeomagnetism of the Bayan Gol Formation, western Mongolia: Geological Magazine, v. 133, no. 4, p. 487-496.

Fairchild, I. J., and Spiro, B., 1990, Carbonate minerals in glacial sediments: geochemical clues to palaeoenvironment: Geological Society, London, Special Publications, v. 53, no. 1, p. 201-216.

Fanning, C. M., and Link, P. K., 2008, Age constraints for the Sturtian glaciation: data from the Adelaide Geosyncline, South Australia and Pocatello Formation Idaho, USA: Geological Society of Australia Abstracts, No. 91, Selwyn Symposium 2008, Melbourne, p. 57-62.

Fike, D. A., Grotzinger, J. P., Pratt, L. M., and Summons, R. E., 2006, Oxidation of the Ediacaran Ocean: Nature, v. 444, p. 744-747.

Gensel, P. G., 2008, The earliest land plants: Annual Review of Ecological and Evolutionary Systems, v. 39, p. 459-477.

Gibson, T., Myrow, P., Macdonald, F., Minjin, C., and Gehrels, G., 2013a, Depositional history, tectonics, and detrital zircon geochronology of Ordovician and Devonian strata in southwestern Mongolia: Geological Society of America Bulletin, v. 125, no. 5-6, p. 877-893.

Gibson, T., Myrow, P., Macdonald, F. A., Minjin, C., and Gehrels, G., 2013b, Depositional history, tectonics, and detrital zircon geochronology of Ordovician and Devonian strata in southwestern Mongolia: Geological Society of America Bulletin, v. 125, no. 5-6, p. 877-893.

Gladkochub, D., Stanevich, A., Mazukabzov, A., Donskaya, T., Pisarevsky, S., Nicoll, G., Motova, Z., and Kornilova, T., 2013, Early evolution of the Paleoasian ocean: LA-ICP-MS dating of detrital zircon from Late Precambrian sequences of the southern margin of the Siberian craton: Russian Geology and Geophysics, v. 54, no. 10, p. 1150-1163.

Glorie, S., De Grave, J., Buslov, M., Zhimulev, F., and Safonova, I. Y., 2014, Detrital zircon provenance of early Palaeozoic sediments at the southwestern margin of the Siberian Craton: Insights from U–Pb geochronology: Journal of Asian Earth Sciences, v. 82, p. 115-123.

Goldring, R., and Jensen, S., 1996, Trace fossils and biofabrics at the Precambrian-Cambrian boundary interval in western Mongolia: Geological Magazine, v. 133, no. 4, p. 403-415.

Gostin, V. A., McKirdy, D. M., Webster, L. J., and Williams, G. E., 2010, Ediacaran ice-rafting and coeval asteroid impact, South Australia: insights into the terminal Proterozoic environment: Australian Journal of Earth Sciences, v. 57, no. 7, p. 859-869.

Grotzinger, J. P., Fike, D. A., and Fischer, W. W., 2011, Enigmatic origin of the largest-known carbon isotope excursion in Earth's history: Nature Geoscience, v. 4, p. 285-292.

Guy, A., Schulmann, K., Janoušek, V., Štípská, P., Armstrong, R., Belousova, E., Dolgopolova, A., Seltmann, R., Lexa, O., and Jiang, Y., 2015, Geophysical and geochemical nature of relaminated arc-derived lower crust underneath oceanic domain in southern Mongolia: Tectonics, v. 34, no. 5, p. 1030-1053.

Halverson, G. P., Dudás, F. O., Maloof, A. C., and Bowring, S. A., 2007, Evolution of the $^{87}Sr/^{86}Sr$ composition of Neoproterozoic Seawater: Palaeogeography Palaeoclimatology Palaeoecology, v. 256, p. 103-129.

Halverson, G. P., Hoffman, P. F., Schrag, D. P., and Kaufman, A. J., 2002, A major perturbation of the carbon cycle before the Ghaub glaciation (Neoproterozoic) in Namibia: prelude to snowball Earth?: Geochemistry, Geophysics, Geosystems, v. 3, no. 6, doi: 10.1029/2001GC000244.

Halverson, G. P., Hoffman, P. F., Schrag, D. P., Maloof, A. C., and Rice, A. H. N., 2005, Toward a Neoproterozoic composite carbon-isotope record: Geological Society of America Bulletin, v. 117, no. 9-10, p. 1181-1207.

Halverson, G. P., Wade, B. P., Hurtgen, M. T., and Barovich, K. M., 2010, Neoproterozoic Chemostratigraphy: Precambrian Research, v. 182, no. 4, p. 337-350.

Han, Y., Zhao, G., Sun, M., Eizenhöfer, P. R., Hou, W., Zhang, X., Liu, D., Wang, B., and Zhang, G., 2015, Paleozoic accretionary orogenesis in the Paleo-Asian Ocean: Insights from detrital zircons from Silurian to Carboniferous strata at the northwestern margin of the Tarim Craton: Tectonics, v. 34, no. 2, p. 334-351.

Hanzl, P., Schulmann, K., Janousek, V., Lexa, O., Hrdlickova, K., Jiang, Y., Burianek, D., Altanbaatar, B., Ganchuluun, T., and Erban, V., 2016, Making continental crust: origin of Devonian orthogneisses from SE Mongolian Altai: Journal of GEOsciences, v. 61, no. 1, p. 25-50.

Harper, D. A., Rasmussen, C. M., Liljeroth, M., Blodgett, R. B., Candela, Y., Jin, J., Percival, I. G., Rong, J.-y., Villas, E., and Zhan, R.-b., 2013, Biodiversity, biogeography and phylogeography of Ordovician rhynchonelliform brachiopods: Geological Society, London, Memoirs, v. 38, no. 1, p. 127-144.

Higgins, J. A., Fischer, W. W., and Schrag, D. P., 2009, Oxygenation fo the ocean and sediments: Consequeences for the seafloor carbonate factory: Earth and Planetary Science Letters, v. 284, p. 25-33.

Higgins, J. A., and Schrag, D. P., 2006, Beyond methane: towards a theory for the Paleocene–Eocene thermal maximum: Earth and Planetary Science Letters, v. 245, no. 3, p. 523-537.

Hoffman, P. F., 1991, Did the breakout of Laurentia turn Gondwanaland inside-out?: Science, v. 252, no. 5011, p. 1409-1412.

-, 2011, Strange bedfellows: glacial diamictite and cap carbonate from the Marinoan (635 Ma) glaciation in Namibia: Sedimentology, v. 58, p. 57-119.

Hoffman, P. F., and Halverson, G. P., 2008, Otavi Group of the western Northern Platform, the Eastern Kaoko Zone and the western Northern Margin Zone, *in* Miller, R. M., ed., The Geology of Namibia, vol. 2. Handbook of the Geological Survey of Namibia, Volume 2: Windhoek, p. 13.69-13.136.

Hoffman, P. F., Halverson, G. P., Domack, E. W., Husson, J. M., Higgins, J. A., and Schrag, D. P., 2007, Are basal Ediacaran (635 Ma) post-glacial "cap dolostones" diachronous?: Earth and Planetary Science Letters, v. 258, p. 114-131.

Hoffman, P. F., Kaufman, A. J., Halverson, G. P., and Schrag, D. P., 1998, A Neoproterozoic Snowball Earth: Science, v. 281, p. 1342-1346.

Hoffman, P. F., and Li, Z.-X., 2009, A palaeogeographic context for Neoproterozoic glaciations: Palaeogeography Palaeoclimatology Palaeoecology, v. 277, no. 3-4, p. 158-172.

Hoffman, P. F., Macdonald, F. A., and Halverson, G. P., 2011, Chemical sediments associated with Neoproterozoic glaciation: iron formation, cap carbonate, barite and phosphorite, *in* Arnaud, E., Halverson, G. P., and Shields, G., eds., The Geologic Record of Neoproterozoic Glaciations: London, Geological Society of London.

Hoffman, P. F., and Schrag, D. P., 2002, The snowball Earth hypothesis; testing the limits of global change: Terra Nova, v. 14, no. 3, p. 129-155.

Hoffmann, K. H., Condon, D. J., Bowring, S. A., and Crowley, J. L., 2004, U-Pb zircon date from the Neoproterozoic Ghaub Formation, Namibia: Constraints on Marinoan glaciation: Geology, v. 32, p. 817-820.

Hou, H. F., and Boucot, A. J., 1990, the Balkhash-Mongolia-Okhotsk region of the Old World realm: Geological Society, London, Memoir, v. 12, p. 297-303.

Ilyin, A. V., 1990, Proterozoic supercontinent, its latest Precambrian rifting, breakup, dispersal into smaller continents, and subsidence of their margins: Evidence from Asia: Geology, v. 18, p. 1231-1234.

Jaffey, A., Flynn, K., Glendenin, L., Bentley, W. t., and Essling, A., 1971, Precision measurement of half-lives and specific activities of U 235 and U 238: Physical Review C, v. 4, no. 5, p. 1889.

Jahn, B. M., Litvinovsky, B. A., Zanvilevich, A. N., and Rechow, M., 2009, Peralkaline granitoid magmatism in the Mongolian-Transbaikalian Belt: Evolution, petrogenesis and tectonic significance: Lithos, v. 113, p. 521-539.

Jian, P., Kröner, A., Jahn, B.-m., Windley, B. F., Shi, Y., Zhang, W., Zhang, F., Miao, L., Tomurhuu, D., and Liu, D., 2014, Zircon dating of Neoproterozoic and Cambrian ophiolites in West Mongolia and implications for the timing of orogenic processes in the central part of the Central Asian Orogenic Belt: Earth-Science Reviews, v. 133, p. 62-93.

Johnston, D. T., Macdonald, F. A., Gill, B., Hoffman, P. F., and Schrag, D. P., 2012, Uncovering the Neoproterozoic carbon cycle: Nature, v. 483, p. 320-324.

Jones, C. E., and Jenkyns, H. C., 2001, Seawater strontium isotopes, oceanic anoxic events, and seafloor hydrothermal activity in the Jurassic and Cretaceous: American Journal of Science, v. 301, no. 2, p. 112-149.

Jones, D., 1983, Recognition, Character and Analysis of Tectonostratigraphic Terranes In Western North America: Journal of Geological Education, v. 31, no. 4, p. 295-303.

Kaufman, A. J., Jacobsen, S. B., and Knoll, A. H., 1993, The Vendian record of Sr and C isotopic variations in seawater; implications for tectonics and paleoclimate: Earth and Planetary Science Letters, v. 120, no. 3-4, p. 409-430.

Kaufman, A. J., Knoll, A. H., and Narbonne, G. M., 1997, Isotopes, ice ages, and terminal Proterozoic Earth history: Proceedings of the National Academy of Sciences, v. 95, p. 6600-6605.

Keeley, J. A., Link, P. K., Fanning, C. M., and Schmitz, M. D., 2013, Pre- to synglacial rift-related volcanism in the Neoproterozoic (Cryogenian) Pocatello Formation, SE Idaho: New SHRIMP and CA-ID-TIMS constraints: Lithosphere, v. 5, no. 1, p. 128-150.

Kennedy, M., Mrofka, D., and Von Der Borch, C., 2008, Snowball Earth termination by destabilization of equatorial permafrost methane clathrate: Nature, v. 453, no. 7195, p. 642-645.

Khain, E. V., Bibikova, E. V., Kröner, A., Zhuravlev, D. Z., Sklyarov, E. V., Fedotova, A. A., and Kravchenko-Berezhnoy, I. R., 2002, The most ancient ophiolite of the Central Asian fold belt: U–Pb and Pb–Pb zircon ages for the Dunzhugur Complex, Eastern Sayan, Siberia, and geodynamic implications: Earth and Planetary Science Letters, v. 199, no. 3, p. 311-325.

Khain, E. V., Bibikova, E. V., Salnikova, E. B., Kroener, A., Gibsher, A. S., Didenko, A. N., Degtyarev, K. E., and Fedotova, A. A., 2003, The Palaeo-Asian ocean in the Neoproterozoic and early Palaeozoic: new geochronologic data and palaeotectonic reconstructions: Precambrian Research, v. 122, p. 329-358.

Khain, E. V., Neymark, L. A., and Amelin, Y. V., ISOTOPIC-GEOCHRONOLOGICAL STUDY OF THE GRANITES AND GRANITE-GNEISSIS OF THE GARDAN BLOCK THE EASTERN SAYAN RANGE IN SIBERIA BY PB-PB AND U-PB METHODS ON ZIRCONS AND SM-ND METHOD, *in* Proceedings DOKLADY AKADEMII NAUK1995, Volume 342, MEZHDUNARODNAYA KNIGA 39 DIMITROVA UL., 113095 MOSCOW, RUSSIA, p. 776-780.

Khomentovsky, V. V., and Gibsher, A. S., 1996, The Neoproterozoic-Lower Cambrian in northern Govi-Altai, western Mongolia: Regional setting, lithostratigraphy and biostratigraphy: Geological Magazine, v. 133, p. 371-390.

Kilian, T. M., Swanson-Hysell, N. L., Macdonald, F. A., Bold, U., and Crowley, J. L., in preparation, Paleomagnetism of Ordovician-Silurian Teel basalts from the Zavkhan Terrane - Paleogeography of Mongolia during the Paleozoic.

Kirschvink, J. L., 1992, Late Proterozoic low-latitude global glaciation: the snowball earth, *in* Schopf, J. W., and Klein, C., eds., The Proterozoic Biosphere: Cambridge, Cambridge University Press, p. 51-52.

Knauth, P. L., and Kennedy, M. J., 2009, The late Precambrian greening of the Earth: Nature, v. 460, p. 728-732.

Knoll, A. H., Hayes, J. M., Kaufman, A. J., Swett, K., and Lambert, I. B., 1986, Secular variation in carbon isotope ratios from Upper Proterozoic succesions of Svalbard and East Greenland: Nature, v. 321, p. 832-838.

Knoll, A. H., Javaux, E., Hewitt, D., and Cohen, P. A., 2006, Eukaryotic organisms in Proterozoic oceans: Philosophical Transactions of the Royal Society of London B: Biological Sciences, v. 361, no. 1470, p. 1023-1038.

Kolodner, K., Avigad, D., McWilliams, M., Wooden, J., Weissbrod, T., and Feinstein, S., 2006, Provenance of north Gondwana Cambrian–Ordovician sandstone: U–Pb SHRIMP dating of detrital zircons from Israel and Jordan: Geological Magazine, v. 143, no. 03, p. 367-391.

Korobov, M., 1980, Biostratigrafiya i miomernye trilobity nizhnego kembriya Mongolii [Biostratigraphy and miomerid trilobites from the Lower Cambrian of Mongolia]. The Joint Soviet-Mongolian Scientific-Research Geological Expedition: The Joint Soviet-Mongolian Scientific-Research Geological Expedition, Transactions, v. 26, p. 5-108.

-, 1989, Lower Cambrian biostratigraphy and polymeroid trilobites of Mongolia: Trans. Joint Soviet–Mongolian Research Expedition [in Russian]. Nauka, Moscow, no. 48, p. 186-192.

Kovach, V., Yarmolyuk, V., Kovalenko, V., Kozlovskyi, A., Kotov, A., and Terent'eva, L., 2011, Composition, sources, and mechanisms of formation of the continental crust of the Lake Zone of the Central Asian Caledonides. II. Geochemical and Nd isotope data: Petrology, v. 19, no. 4, p. 399-425.

Kozakov, I., Kotov, A., Sal'nikova, E., Bibikova, E., Kovach, V., Kirnozova, T., Berezhnaya, N., and Lykhin, D., 1999, Metamorphic age of crystalline complexes of the Tuva-Mongolia Massif: the U-Pb geochronology of granitoids: PETROLOGY C/C OF PETROLOGIIA, v. 7, p. 177-191.

Kozakov, I., Sal'nikova, E., Yarmolyuk, V., Kozlovsky, A., Kovach, V., Azimov, P. Y., Anisimova, I., Lebedev, V., Enjin, G., and Erdenejargal, C., 2012a, Convergent boundaries and related igneous and metamorphic complexes in Caledonides of Central Asia: Geotectonics, v. 46, no. 1, p. 16-36.

Kozakov, I., Yarmolyuk, V., Kovach, V., Bibikova, E., Kirnozova, T., Kozlovskii, A., Plotkina, Y. V., Fugzan, M., Lebedev, V., and Erdenezhargal, C., 2012b, The Early Baikalian crystalline complex in the basement of the Dzabkhan microcontinent of the Early Caledonian orogenic area, Central Asia: Stratigraphy and Geological Correlation, v. 20, no. 3, p. 231-239.

Kozakov, I. K., Yarmolyuk, V. V., Kovach, V. P., Bibikova, E. V., Kirnozova, T. I., Kozlovskii, A. M., Plotkina, Y. V., Fugzan, M. M., Lebedev, V. I., and Erdenezhargal, C., 2012c, The early Baikalian crystalline complex in the basement of the Dzabkhan Microcontinent of teh early Caledonian orogenic area, Central Asia: Stratigraphy and Geological Correlation, v. 20, no. 3, p. 231-239.

Kravchinsky, V. A., Konstantinov, K. M., and Cogne, J.-P., 2001, Palaeomagnetic study of Vendian and Early Cambrian of South Siberia and Central Mongolia: was the Siberian platform assembled at this time?: Precambrian Research, v. 110, p. 61-92.

Kravchinsky, V. A., Sklyarov, E. V., Gladkochub, D. P., and Harbert, W. P., 2010, Paleomagnetism of the Precambrian Eastern Sayan rocks: implications for the Ediacaran–Early Cambrian paleogeography of the Tuva-Mongolian composite terrane: Tectonophysics, v. 486, no. 1, p. 65-80.

Kröner, A., Demoux, A., Zack, T., Rojas-Agramonte, Y., Jian, P., Tomurhuu, D., and Barth, M., 2011, Zircon ages for a felsic volcanic rock and arc-related early Palaeozoic sediments on the margin of the Baydrag microcontinent, central Asian orogenic belt, Mongolia: Journal of Asian Earth Sciences, v. 42, no. 5, p. 1008-1017.

Kröner, A., Kovach, V., Belousova, E., Hegner, E., Armstrong, R., Dolgopolova, A., Seltmann, R., Alexeiev, D., Hoffmann, J., and Wong, J., 2014, Reassessment of continental growth during the accretionary history of the Central Asian Orogenic Belt: Gondwana Research, v. 25, no. 1, p. 103-125.

Kröner, A., Lehmann, J., Schulmann, K., Demoux, A., Lexa, O., Tomurhuu, D., Štípská, P., Liu, D., and Wingate, M. T., 2010, Lithostratigraphic and geochronological constraints on the evolution of the Central Asian Orogenic Belt in SW Mongolia: Early Paleozoic rifting followed by late Paleozoic accretion: American Journal of Science, v. 310, no. 7, p. 523-574.

Kruse, P. D., Gandin, A., Debrenne, F., and Wood, R., 1996, Early Cambrian bioconstructions in the Zavkhan Basin of western Mongolia: Geological Magazine, v. 133, no. 4, p. 429-444.

Kuzmichev, A., Bibikova, E. V., and Zhuravlev, D. Z., 2001, Neoproterozoic (~800 Ma) orogeny in the Tuva-Mongolia Massif (Siberia): island arc-continent collision at the northeast Rodinia margin: Precambrian Research, v. 110, p. 109-126.

Kuzmichev, A., Kroener, A., Hegner, E., Dunyi, L., and Yusheng, W., 2005a, The Shishkhid ophiolite, nothern Mongolia: A key to the reconstruction of a Neoproterozoic island-arc system in central Asia: Precambrian Research, v. 138, p. 125-150.

Kuzmichev, A., Kröner, A., Hegner, E., Dunyi, L., and Yusheng, W., 2005b, The Shishkhid ophiolite, northern Mongolia: a key to the reconstruction of a Neoproterozoic island-arc system in central Asia: Precambrian Research, v. 138, no. 1, p. 125-150.

Kuzmichev, A., and Larionov, A., 2011, The Sarkhoi Group in East Sayan: Neoproterozoic (~ 770–800 Ma) volcanic belt of the Andean type: Russian Geology and Geophysics, v. 52, no. 7, p. 685-700.

Kuzmichev, A., Sklyarov, E., Postnikov, A., and Bibikova, E., 2007, The Oka Belt (Southern Siberia and Northern Mongolia): A Neoproterozoic analog of the Japanese Shimanto Belt?: Island Arc, v. 16, no. 2, p. 224-242.

Lamb, M. A., and Badarch, G., 1997, Paleozoic sedimentary basins and volcanic-arc systems of Southern Mongolia: new stratigraphic and sedimentologic constraints: International Geology Review, v. 39, no. 6, p. 542-576.

-, 2001, Paleozoic sedimentary basins and volcanic arc systems of southern Mongolia: new geochemical and petrographic constraints: Geological Society of America Memoirs, v. 194, p. 117-149.

Lan, Z., Li, X., Zhu, M., Chen, Z., Zhang, Q., Li, Q., Lu, D., Liu, Y., and Tang, G., 2014, A rapid and synchronous initiation of the wide spread Cryogenian glaciations: Precambrian Research.

Le Heron, D. P., 2012, The Cryogenian record of glaciation and deglaciation in South Australia: Sedimentary Geology, v. 243-244, p. 57-69.

Le Heron, D. P., and Busfield, M. E., 2015, Pulsed iceberg delivery driven by Sturtian ice sheet dynamics: An example from Death Valley, California: Sedimentology.

Le Heron, D. P., Busfield, M. E., and Kamona, F., 2013, An interglacial on snowball Earth? Dynamic ice behaviour revealed in the Chuos Formation, Namibia: Sedimentology, v. 60, p. 411-427.

Le Heron, D. P., Busfield, M. E., and Prave, A. R., 2014, Neoproterozoic ice sheets and olistoliths: multiple glacial cycles in the Kingston Peak Formation, California: Journal of the Geological Society, p. 2013-2130.

Le Heron, D. P., Cox, G. M., Trundley, A. E., and Collins, A. S., 2011, Sea-ice free conditions during the early Cryogenian (Sturt) glaciation, South Australia: Geology, v. 39, p. 31-34.

Lehmann, J., Schulmann, K., Lexa, O., Corsini, M., Kröner, A., Štípská, P., Tomurhuu, D., and Otgonbator, D., 2010, Structural constraints on the evolution of the Central Asian Orogenic Belt in SW Mongolia: American Journal of Science, v. 310, no. 7, p. 575-628.

Letnikova, E., Kuznetsov, A., Vishnevskaya, I., Veshcheva, S., Proshenkin, A., and Geng, H., 2013, The Vendian passive continental margin in the southern Siberian Craton: geochemical and isotopic (Sr, Sm–Nd) evidence and U–Pb dating of detrital zircons by the LA-ICP-MS method: Russian Geology and Geophysics, v. 54, no. 10, p. 1177-1194.

Levashova, N. M., Kalugin, V. M., Gibsher, A. S., Yff, J., Ryabinin, A. B., Meert, J., and Malone, S. J., 2010, The origin of the Baydaric microcontinent, Mongolia: Constraints from paleomagnetism and geochronology: Tectonophysics, v. 485, no. 1-4, p. 306-320.

Li, H., Xu, Y., Huang, X., He, B., Luo, Z., and Yan, B., 2009, Activation of northern margin of the North China Craton in Late Paleozoic: Evidence from U-Pb dating and Hf isotopes of detrital zircons from the Upper Carboniferous Taiyuan Formation in the Ningwu-Jingle basin: Chinese Science Bulletin, v. 54, no. 4, p. 677-686.

Li, Z. X., Bogdanova, S. V., Collins, A. S., Davidson, A., De Waele, B., Ernst, R. E., Fitzsimons, I. C. W., Fuck, R. A., Gladkochub, D. P., Jacobs, J., Karlstrom, K. E., Lu, S., Natapov, L. M., Pease, V., Pisarevsky, S. A., Thrane, K., and Vernikovsky, V., 2008, Assembly, configuration, and break-up history of Rodinia: A synthesis: Precambrian Research, v. 160, no. 1-2, p. 179-210.

Lindsay, J. F., 1989, Depositional controls on glacial facies associations in a basinal setting, Late Proterozoic, Amadeus Basin, central Australia: Palaeogeography, Palaeoclimatology, Palaeoecology, v. 73, p. 205-232.

Lindsay, J. F., Braiser, M. D., Dorjnamjaa, D., Goldring, R., Kruse, P. D., and Wood, R. A., 1996a, Facies and sequence controls on the appearance of the Cambrian biota in southwestern Mongolia: Implications for the Precambrian-Cambrian boundary: Geological Magazine, v. 133, p. 417-428.

Lindsay, J. F., Brasier, M., Shields, G., Khomentovsky, V. V., and Bat-Ireedui, Y. A., 1996b, Glacial facies associations in a Neoproterozoic back-arc setting, Zavkhan Basin, western Mongolia: Geological Magazine, v. 133, no. 4, p. 391-402.

Liu, C., Wang, Z., and Raub, T. D., 2013, Geochemical constraints on the origin of Marinoan cap dolostones from Nuccaleena Formation, South Australia: Chemical Geology, v. 351, p. 95-104.

Liu, C., Wang, Z., Raub, T. D., Macdonald, F. A., and Evans, D. A., 2014, Neoproterozoic cap-dolostone deposition in stratified glacial meltwater plume: Earth and Planetary Science Letters, v. 404, p. 22-32.

Ludwig, K. R., 2008, User's manual for Isoplot 3.70: A geochronological Toolkit for Microsoft Excel: Berkeley Geochronology Center Special Publication, v. 4.

Macdonald, F. A., 2011a, The Dzabkhan Platform, *in* E., A., Halverson, G. P., and Shields, G., eds., The geological record of Neoproterozoic glaciations: London, Geological Society of London.

-, 2011b, The Tsagaan Oloom Formation, southwestern Mongolia: Geological Society, London, Memoirs, v. 36, no. 1, p. 331-337.

Macdonald, F. A., and Jones, D. S., 2011, The Khubsugul Basin, *in* E., A., Halverson, G. P., and Shields, G., eds., The geological record of Neoproterozoic glaciations: London, Geological Society of London.

Macdonald, F. A., Jones, D. S., and Schrag, D. P., 2009a, Stratigraphic and tectonic implications of a new glacial diamictite-cap carbonate couplet in southwestern Mongolia: Geology, v. 37, p. 123-126.

Macdonald, F. A., McClelland, W. C., Schrag, D. P., and Macdonald, W. P., 2009b, Neoproterozoic glaciation on a carbonate platform margin in Arctic Alaska and the origin of the North Slope subterrane: Geological Society of America Bulletin, v. 121, p. 448-473.

Macdonald, F. A., Ryan-Davis, J., Coish, R., Crowley, J., and Karabinos, P., 2014, A newly identified Gondwanan terrane in the northern Appalachian Mountains: Implications for the Taconic orogeny and closure of the Iapetus Ocean: Geology, v. 42, no. 6, p. 539-542.

Macdonald, F. A., Schmitz, M. D., Crowley, J. L., Roots, C. F., Jones, D. S., Maloof, A. C., Strauss, J. V., Cohen, P. A., Johnston, D. T., and Schrag, D. P., 2010, Calibrating the Cryogenian: Science, v. 327, p. 1241-1243.

Macdonald, F. A., Strauss, J. V., Sperling, E. A., Halverson, G. P., Narbonne, G. M., Johnston, D. T., Kunzmann, M., Schrag, D. P., and Higgins, J. A., 2013, The stratigraphic relationship between the Shuram carbon isotope excursion, the oxygenation of Neoproterozoic oceans, and the first appearance of the Ediacara biota and bilaterian trace fossils in northwestern Canada: Chemical Geology, v. 362, p. 250-272.

Mattinson, J. M., 2005, Zircon U-Pb chemical abrasion ("CA-TIMS") method: combined annealing and multi-step partial dissolution analysis for improved precision and accuracy of zircon ages: Chemical Geology, v. 220, p. 47-66.

McKirdy, D. M., Burgess, J. M., Lemon, N. M., Yu, X., Cooper, A. M., Gostin, V. A., Jenkins, R. J. F., and Both, R. A., 2001, A chemostratigraphic overview of the late Cryogenian interglacial sequence in the Adelaide fold-thrust belt, South Australia: Precambrian Research, v. 106, p. 149-186.

McLean, N., Bowring, J., and Bowring, S., 2011, An algorithm for U-Pb isotope dilution data reduction and uncertainty propagation: Geochemistry, Geophysics, Geosystems, v. 12, no. 6.

Melezhik, V. A., Pokrovskii, B. G., Fallick, A. E., Kuznetsov, A. B., and Bujakaite, M. I., 2009, Constraints on 87Sr/86Sr of Late Ediacaran seawater: insight from Siberian high-Sr limestones: Journal of the Geological Society of London, v. 166, p. 183-191.

Melim, L. A., Swart, P. K., and Maliva, R., 2001, Meteoric and marine burial diagenesis, *in* Ginsberg, R. N., ed., Subsurface geology of a prograding carbonate platform margin, Great Bahama Bank: Results of the Bahamas Drilling Project, Volume 70: Tulsa, SEPM Special Publication.

Misi, A., and Veizer, J., 1998, Neoproterozoic carbonate sequences of the Una Group, Irecê Basin, Brazil: chemostratigraphy, age and correlations: Precambrian Research, v. 89, no. 1, p. 87-100.

Mossakovsky, A., Ruzhentsev, S., Samygin, S., and Kheraskova, T., 1994, Central Asian fold belt: geodynamic evolution and formation history: Geotectonics, v. 27, no. 6, p. 445-474.

Narbonne, G. M., 1994, New Ediacaran (Neoproterozoic) fossils from northwestern Canada: Journal of Paleontology, v. 68, p. 411-416.

Narbonne, G. M., Kaufman, A. J., and Knoll, A. H., 1994, Integrated chemostratigraphy and biostratigraphy of the Windermere Supergroup, northwestern Canada: Implications for Neoproterozoic correlations and the early evolution of animals: Geological Society of America Bulletin, v. 106, p. 1281-1291.

Och, L. M., and Shields-Zhou, G., 2012, The Neoproterozoic oxygenation event: Environmental perturbations and biogeochemical cycling: Earth-Science Reviews, v. 110, p. 26-57.

Ovchinnikova, G., Kuznetsov, A., Vasil'eva, I., Gorokhov, I., Letnikova, E., and Gorokhovskii, B., 2012a, U-Pb age and Sr isotope signature of cap limestones from the Neoproterozoic Tsagaan Oloom Formation, Dzabkhan River Basin, Western Mongolia: Stratigraphy and Geological Correlation, v. 20, no. 6, p. 516-527.

Ovchinnikova, G. V., Kuznetsov, A. B., Vasil'eva, I. M., Gorokhov, I. M., Letnikova, E. F., and Gorokhovskii, B. M., 2012b, U-Pb age and Sr isotope signature of cap limestone from the Neoproterozoic Tsagaan Oloom Formation, Dzabkhan River Basin, Western Mongolia: Stratigraphy and Geological Correlation, v. 20, no. 6, p. 516-527.

Panchuk, K. M., Holmden, C. E., and Leslie, S. A., 2006, Local controls on carbon cycling in the Ordovician midcontienent region of North America, with implications for carbon isotope secular curves: Journal of Sedimentary Research, v. 76, p. 200-211.

Pearce, J. A., and Peate, D. W., 1995, Tectonic implications of the composition of volcanic arc magmas: Annual Review of Earth and Planetary Sciences, v. 23, p. 251-286.

Petrosyan, N., 1967, Stratigraphic importance of the Devonian flora of the USSR.

Planavsky, N. J., Rouxel, O. J., Bekker, A., Lalonde, S. V., Konhauser, K. O., Reinhard, C. T., and Lyons, T. W., 2010, The evolution of the marine phosphate reservoir: Nature, v. 467, p. 1088-1090.

Pojeta Jr, J., 1986, Devonian rocks and Lower and Middle Devonian pelecypods of Guangxi, China, and the Traverse Group of Michigan, 2330-7102.

Pokrovskii, B. G., Melezhik, V. A., and Bujakaite, M. I., 2006, Carbon, Oxygen, Strontium, and Sulfur Isotopic Compositions in Late Precambrian Rocks of the Patom Complex, Central Siberia: Communication 1. Results, Isotope Stratigraphy, and Dating Problems: Lithology and Mineral Resources, v. 41, no. 5, p. 450-474.

Pokrovsky, B. G., Mavromatis, V., and Pokrovsky, O. S., 2011, Co-variation of Mg and C isotopes in late Precambrian carbonates of the Siberian Platform: A new tool for tracing the change in weathering regime?: Chemical Geology, v. 290, no. 1, p. 67-74.

Powell, R. D., 1990, Glacimarine processes at grounding-line fans and their growth to ice-contact deltas, *in* Dowdeswell, J. A., and Scourse, J. D., eds., Glacimarine Environments, Volume 53: London, Geological Society of London Speical Publications, p. 53-73.

Powerman, V., Shatsillo, A., Chumakov, N., Kapitonov, I., and Hourigan, J., 2015, Interaction between the Central Asian Orogenic Belt (CAOB) and the Siberian craton as recorded by detrital zircon suites from Transbaikalia: Precambrian Research, v. 267, p. 39-71.

Pruss, S. B., Bosak, T., Macdonald, F. A., McLane, M., and Hoffman, P. F., 2010, Microbial facies in a Sturtian cap carbonate, the Rasthof Formation, Otavi Group, northern Namibia: Precambrian Research, v. 181, p. 187-198.

Ramezani, J., Hoke, G. D., Fastovsky, D. E., Bowring, S. A., Therrien, F., Dworkin, S. I., Atchley, S. C., and Nordt, L. C., 2011, High-precision U-Pb zircon geochronology of the Late Triassic Chinle Formation, Petrified Forest National Park (Arizona, USA): Temporal constraints on the early evolution of dinosaurs: Geological Society of America Bulletin, v. 123, no. 11-12, p. 2142-2159.

Read, J. F., 1982, Carbonate platforms of passive (extensional) continental margins: types, characteristics and evolution: Tectonophysics, v. 81, p. 195-212.

Ridge, J. C., Balco, G., Bayless, R. L., Beck, C. C., Carter, L. B., Dean, J. L., Voytek, E. B., and Wei, J. H., 2012, The new North American Varve Chronology: A precise record of southeastern Laurentide Ice Sheet deglaciation and climate, 18.2-12.5 kyr BP, and correlations with Greenland ice core records: American Journal of Science, v. 312, no. 7, p. 685-722.

Rizza, M., Ritz, J. F., Prentice, C., Vassallo, R., Braucher, R., Larroque, C., Arzhannikova, A., Arzhannikov, S., Mahan, S., and Massault, M., 2015, Earthquake Geology of the Bulnay Fault (Mongolia): Bulletin of the Seismological Society of America, v. 105, no. 1, p. 72-93.

Rojas-Agramonte, Y., Kröner, A., Demoux, A., Xia, X., Wang, W., Donskaya, T., Liu, D., and Sun, M., 2011, Detrital and xenocrystic zircon ages from Neoproterozoic to Palaeozoic arc terranes of Mongolia: significance for the origin of crustal fragments in the Central Asian Orogenic Belt: Gondwana Research, v. 19, no. 3, p. 751-763.

Rooney, A. D., Macdonald, F. A., Strauss, J. V., Dudás, F. Ö., Hallmann, C., and Selby, D., 2014, Re-Os geochronology and coupled Os-Sr isotope constraints on the Sturtian snowball Earth: Proceedings of the National Academy of Sciences, v. 111, no. 1, p. 51-56.

Rooney, A. D., Strauss, J. V., Brandon, A. D., and Macdonald, F. A., 2015, A Cryogenian chronology: Two long-lasting synchronous Neoproterozoic glaciations: Geology, v. 43, no. 5, p. 459-462.

Rose, C. V., Swanson-Hysell, N. L., Husson, J. M., Poppick, L. N., Cottle, J. M., Schoene, B., and Maloof, A. C., 2012, Constraints on the origin and relative timing of the Trezona δ< sup> 13</sup> C anomaly below the end-Cryogenian glaciation: Earth and Planetary Science Letters, v. 319, p. 241-250.

Rothman, D. H., Hayes, J. M., and Summons, R. E., 2003, Dynamics of the Neoproterozoic carbon cycle: Proceedings of the National Academy of Sciences, v. 100, p. 8124-8129.

Rudnev, S., Izokh, A., Borisenko, A., Shelepaev, R., Orihashi, Y., Lobanov, K., and Vishnevsky, A., 2012, Early Paleozoic magmatism in the Bumbat-Hairhan area of the Lake Zone in western Mongolia (geological, petrochemical, and geochronological data): Russian Geology and Geophysics, v. 53, no. 5, p. 425-441.

Rudnick, R. L., 1995, Making continental crust: Nature, v. 378, no. 6557, p. 571-577.

Ruzhentsev, S. V., and Burashnikov, V. V., 1996, Tectonics of the western Mongolian Salairides: Geotectonics, v. 29, no. 5, p. 379-394.

Ruzhentsev, S. V., and Pospelov, I. I., 1992, The south Mongolian variscan fold system: Geotectonics, v. 26, p. 383-395.

Salnikova, E., Kozakov, I., Kotov, A., Kröner, A., Todt, W., Bibikova, E., Nutman, A., Yakovleva, S., and Kovach, V., 2001, Age of Palaeozoic granites and metamorphism in the Tuvino-Mongolian Massif of the Central Asian Mobile Belt: loss of a Precambrian microcontinent: Precambrian Research, v. 110, no. 1, p. 143-164.

Samozvantsen, B. A., Tsukerik, A. B., Golyakov, B. I., 1981, Report of geological mapping work of scale 1: 200 000 in area Great Lakes deppression to western branches of Hangay Highland, v. 3576.

Sanderson, M. J., 2003, Molecular data from 27 proteins do not support a Precambrian origin of land plants: American Journal of Botany, v. 90, p. 954-956.

Sarg, J., 1988, Carbonate sequence stratigraphy.

Sawaki, Y., Kawai, T., Shibuya, T., Tahata, M., Omori, S., Komiya, T., Yoshida, N., Hirata, T., Ohno, T., Windley, B., and Maruyama, S., 2010a, 87Sr/86Sr chemostratigraphy of Neoproterozoic Dalradian carbonates below the Port Askaig Glaciogenic Formation, Scotland: Precambrian Research, v. 179, p. 150-164.

Sawaki, Y., Ohno, T., Tahata, T., Komiya, T., Hirata, T., Maruyama, S., Windley, B. F., Han, J., Shu, D., and Li, Y., 2010b, The Ediacaran radiogenic Sr isotope excursion in the Doushantuo Formation in the Three Gorges area, South China: Precambrian Research, v. 176, p. 46-64.

Schmitz, M., Gradstein, F., Ogg, J., and Ogg, G., 2012, Appendix 2—Radiometric ages used in GTS2012: The Geologic Time Scale, p. 1045-1082.

Schrag, D. P., Berner, R. A., Hoffman, P. F., and Halverson, G. P., 2002, On the initiation of snowball Earth: Geochemistry, Geophysics, Geosystems, v. 3.

Schrag, D. P., Higgins, J. A., Macdonald, F. A., and Johnston, D. T., 2013, Authigenic carbonate and the history of the global carbon cycle: science, v. 339, no. 6119, p. 540-543.

Schulmann, K., and Paterson, S., 2011, Geodynamics: Asian continental growth: Nature Geoscience, v. 4, p. 827-829.

Sengör, A., Natal'In, B., and Burtman, V., 1993, Evolution of the Altaid tectonic collage and Palaeozoic crustal growth in Eurasia: Nature, v. 364, p. 299-307.

Sengor, A. C., and Natal'in, B. A., 1996, Paleotectonics of Asia: fragments of synthesis, *in* Yin, A., and Harrison, M., eds., The Tectonic Evolution of Asia: Cambridge, Cambridge University Press, p. 486-640.

Serezhnikova, E. A., Ragozina, A. L., Dorjnamjaa, D., and Lyubov'V, Z., 2014, Fossil microbial communities in Neoproterozoic interglacial rocks, Maikhanuul Formation, Zavkhan basin, Western Mongolia: Precambrian Research, v. 245, p. 66-79.

Shields, G., Stille, P., Brasier, M., and Atudorei, N.-V., 1997, Stratified oceans and oxygenation of the late Precambrian environment: a post glacial geochemical record from the Neoproterozoic of W. Mongolia: Terra Nova, v. 9, p. 218-222.

Shields, G. A., Braiser, M. D., Stille, P., and Dorjnamjaa, D., 2002, Factors contributing to high $\delta^{13}C$ values in Cryogenian limestones of western Mongolia: Earth and Planetary Science Letters, v. 196, p. 99-111.

Sláma, J., Košler, J., Condon, D. J., Crowley, J. L., Gerdes, A., Hanchar, J. M., Horstwood, M. S., Morris, G. A., Nasdala, L., and Norberg, N., 2008, Plešovice zircon—a new natural reference material for U–Pb and Hf isotopic microanalysis: Chemical Geology, v. 249, no. 1, p. 1-35.

Smalley, P., Higgins, A., Howarth, R., Nicholson, H., Jones, C., Swinburne, N., and Bessa, J., 1994, Seawater Sr isotope variations through time: a procedure for constructing a reference curve to date and correlate marine sedimentary rocks: Geology, v. 22, no. 5, p. 431-434.

Smith, E. F., Macdonald, F. A., Petach, T. A., Bold, U., and Schrag, D. P., 2015, Integrated stratigraphic, geochemical, and paleontological late Ediacaran to early Cambrian records from southwestern Mongolia: Geological Society of America Bulletin, p. B31248. 31241.

Soejono, I., Burianek, D., Svojtka, M., Zacek, V., Cap, P., and Janousek, V., 2016, Mid-Ordovician and Late Devonian magmatism in the Togtokhinshil Complex: new insight into the formation and accretionary evolution of the Lake Zone (western Mongolia): Journal of GEOsciences, v. 61, no. 1, p. 5-23.

Stampfli, G., and Borel, G., 2002, A plate tectonic model for the Paleozoic and Mesozoic constrained by dynamic plate boundaries and restored synthetic oceanic isochrons: Earth and Planetary Science Letters, v. 196, no. 1, p. 17-33.

Štípská, P., Schulmann, K., Lehmann, J., Corsini, M., Lexa, O., and Tomurhuu, D., 2010, Early Cambrian eclogites in SW Mongolia: evidence that the Palaeo-Asian Ocean suture extends further east than expected: Journal of metamorphic Geology, v. 28, no. 9, p. 915-933.

Sumner, D. Y., and Bowring, S. A., 1996, U-Pb geochronologic constraints on deposition of the Campbellrand Subgroup, Transvaal Supergroup, South Africa: Precambrian Research, v. 79, p. 25-35.

Sun, J.-F., Yang, J.-H., Wu, F.-Y., and Wilde, S. A., 2012, Precambrian crustal evolution of the eastern North China Craton as revealed by U–Pb ages and Hf isotopes of detrital zircons from the Proterozoic Jing'eryu Formation: Precambrian Research, v. 200, p. 184-208.

Swanson-Hysell, N. L., Rose, C. V., Calmet, C. C., Halverson, G. P., Hurtgen, M. T., and Maloof, A. C., 2010, Cryogenian glaciation and the onset of carbon-isotope decoupling: Science, v. 328, p. 608-611.

Swart, P. K., 2008, Global synchronous changes in the carbon isotopic composition of carbonate sediments unrelated to changes in the global carbon cycle: Proceedings of the National Academy of Sciences, v. 105, no. 37, p. 13741-13745.

Swart, P. K., and Kennedy, M. J., 2012, Does the global stratigraphic reproducibility of d13C in Neoproterozoic carbonates require a marine origin? A Pliocene-Pleistocene comparison: Geology, v. 40, no. 1, p. 87-90.

Teraoka, Y., Suzuki, M., Tungalag, F., Ichinnorov, N., and Sakamari, Y., 1996, Tectonic framework of the Bayankhongor area, west Mongolia: BULLETIN-GEOLOGICAL SURVEY JAPAN, v. 47, p. 447-456.

Togtokh, D., Baatarkhuyag, A., and Bayardalai, S., 1995, The report of result of the geological grouppedmapping at scale 1:200000: Ulaanbaatar, Mongolia, p. 1575.

Tomurtogoo, O., 2005, Tectonics and structural evolution of Mongolia: Geodynamics and Metallogeny of Mongolia With a Special Emphasis on Copper and Gold Deposits: IAGOD Guidebook Series, v. 11, p. 5-12.

Tucker, M. E., and Wright, V. P., 1990, Dolomites and dolomitization models: Carbonate sedimentology, p. 365-400.

Ulitina, L., Bondarenko, O., and Minjin, C., 2009, Evolution of the taxonomic diversity of Mongolian Ordovician-Silurian corals: Paleontological Journal, v. 43, no. 5, p. 499-505.

Van der Voo, R., van Hinsbergen, D. J., Domeier, M., Spakman, W., and Torsvik, T. H., 2015, Latest Jurassic–earliest Cretaceous closure of the Mongol-Okhotsk Ocean: A paleomagnetic and seismological-tomographic analysis: Geological Society of America Special Papers, v. 513, p. 589-606.

Vandeginste, V., Sweenen, R., Gleeson, S. A., Ellam, R. M., Osadetz, K., and Roure, F., 2005, Zebra dolomitization as a result of focused fluid flow in the Rocky Mountains Fold and Thrust Belt, Canada: Sedimentology, v. 52, p. 1067-1095.

Wang, C., Li, N., Sun, Y., and Zong, P., 2011, Distribution of Tuvaella brachiopod fauna and its tectonic significance: Journal of Earth Science, v. 22, p. 11-19.

Wang, T., Zheng, Y., Gehrels, G., and Mu, Z., 2001, Geochronological evidence for existence of South Mongolian microcontinent—A zircon U-Pb age of grantoid gneisses from the Yagan-Onch Hayrhan metamorphic core complex: Chinese Science Bulletin, v. 46, no. 23, p. 2005-2008.

Webster, G. D., and Ariunchimeg, Y., 2004, The northern most Emsian crinoids known, a Devonian fauna from the Chuluun Formation, Shine Jinst area, Southern Mongolia: Geobios, v. 37, no. 4, p. 481-487.

Wilhem, C., Windley, B. F., and Stampfli, G. M., 2012, The Altaids of Central Asia: A tectonic and evolutionary innovative review: Earth-Science Reviews, v. 113, no. 3, p. 303-341.

Windley, B. F., Alexeiev, D., Xiao, W., Kroener, A., and Badarch, G., 2007, Tectonic models for accretion of the Central Asian Orogenic Belt: Journal of the Geological Society of London, v. 164, p. 31-47.

Xia, X., Sun, M., Zhao, G., and Luo, Y., 2006, LA-ICP-MS U–Pb geochronology of detrital zircons from the Jining Complex, North China Craton and its tectonic significance: Precambrian Research, v. 144, no. 3, p. 199-212.

Xiao, W., Windley, B. F., Hao, J., and Zhai, M., 2003, Accretion leading to collision and the Permian Solonker suture, Inner Mongolia, China: termination of the central Asian orogenic belt: Tectonics, v. 22, no. 6.

Yakubchuk, A., 2004, Architecture and mineral deposit settings of the Altaid orogenic collage: a revised model: Journal of Asian Earth Sciences, v. 23, no. 5, p. 761-779.

Yang, J.-H., Wu, F.-Y., Shao, J.-A., Wilde, S. A., Xie, L.-W., and Liu, X.-M., 2006, Constraints on the timing of uplift of the Yanshan Fold and Thrust Belt, North China: Earth and Planetary Science Letters, v. 246, no. 3, p. 336-352.

Yang, J., Cawood, P. A., Du, Y., Huang, H., Huang, H., and Tao, P., 2012, Large Igneous Province and magmatic arc sourced Permian–Triassic volcanogenic sediments in China: Sedimentary Geology, v. 261, p. 120-131.

Yarmolyuk, V., Kovach, V., Kovalenko, V., Salnikova, E., Kozlovskii, A., Kotov, A., Yakovleva, S., and Fedoseenko, A., 2011, Composition, sources, and mechanism of continental crust growth in the Lake Zone of the Central Asian Caledonides: I. Geological and geochronological data: Petrology, v. 19, no. 1, p. 55-78.

Yarmolyuk, V., Kovalenko, V., Anisimova, I., Sal'nikova, E., Kovach, V., Kozakov, I., Kozlovsky, A., Kudryashova, E., Kotov, A., and Plotkina, Y. V., Late Riphean alkali granites of the Zabhan microcontinent: evidence for the timing of Rodinia breakup and formation of microcontinents in the Central Asian Fold Belt, *in* Proceedings Doklady Earth Sciences2008a, Volume 420, Springer, p. 583-588.

Yarmolyuk, V., Kovalenko, V., Sal'nikova, E., Kozakov, I., Kotov, A., Kovach, V., Vladykin, N., and Yakovleva, S., 2005, U-Pb-Age of sin-and postmetamorphic granitoids from Southern Mongolia-evidence for the presence of grenvilides in the Central Asian Fold Belt.

Yarmolyuk, V. V., Kovalenko, V. I., Anisimova, I. V., Sal'nikova, E. B., Kovach, V. P., Kozakov, I. K., Kozlovskii, A. M., Kudryashova, E. A., Kotov, A. B., Plotkina, Y. V., Terent'eva, L. B., and Yakovleva, S. Z., 2008b, Late Riphean alkali granites of the Zabhan Microcontinent: Evidence for the timing of Rodinia breakup and formation of microcontinents in the Central Asian Fold Belt: Doklady Earth Sciences, v. 420, no. 4, p. 583-588.

Yoshioka, H., Asahara, Y., Tojo, B., and Kawakami, S., 2003, Systematic variations in C, O, and Sr isotopes and elemental concentrations in Neoproterozoic carbonates in Namibia: implications for a glacial to interglacial transition: Precambrian Research, v. 124, p. 69-85.

Zacek, V., Burianek, D., Pecskay, Z., and Skoda, R., 2016, Astrophyllite-alkali amphibole rhyolite, an evidence of early Permian A-type alkaline volcanism in the western Mongolian Altai: Journal of GEOsciences, v. 61, no. 1, p. 93-103.

Zhang, C.-L., Zou, H.-B., Li, H.-K., and Wang, H.-Y., 2013, Tectonic framework and evolution of the Tarim Block in NW China: Gondwana Research, v. 23, no. 4, p. 1306-1315.

Zhao, Y., Song, B., and Zhang, S. H., The Central Mongolian microcontinent: Its Yangtze affinity and tectonic implications, *in* Proceedings Symposium on continental growth and orogeny in Asia, Taipei, Taiwan, 2006, p. 135-136.

Zhou, C., Tucker, R., Xiao, S., Peng, Z., Yuan, X., and Chen, Z., 2004, New constraints on the ages of Neoproterozoic glaciations in south China: Geology, v. 32, p. 437-440.

Zhu, M., Lu, M., Zhang, J., Zhao, F., Li, G., Aihua, Y., Zhao, X., and Zhao, M., 2013, Carbon isotope chemostratigraphy and sedimentary facies evolution of the Ediacaran Doushantuo Formation in western Hubei, South China: Precambrian Research, v. 225, p. 7-28.

Zimmer, A., Lang, D., Richardt, S., Frank, W., Reski, R., and Rensing, S. A., 2007, Dating the early evolution of plants: detection and molecular clock analyses of orthologs: Molecular genetics and genomics, v. 278, p. 393-402.

Zonenshain, L. P., 1973, The evolution of Central Asiatic geosynclines through sea-floor spreading: Tectonophysics, v. 19, p. 213-232.

Zorin, Y. A., 1999, Geodynamics of the western part of the Mongolia–Okhotsk collisional belt, Trans-Baikal region (Russia) and Mongolia: Tectonophysics, v. 306, no. 1, p. 33-56.

CHAPTER 4. EFFECT OF DOLOMITIZATION ON ISOTOPIC RECORDS FROM NEOPROTEROZOIC CARBONATES IN SOUTHWESTERN MONGOLIA

This chapter is being prepared to be submitted to Geologic Society of America Bulletin: ***Bold, U.****, Schrag, D. P., Higgins, J. A., Erdenebayar, J., and Macdonald, F. A., in preparation, Effect of dolomitization on isotopic records from Neoproterozoic carbonates in southwestern Mongolia: Geological Society of America Bulletin.*

ABSTRACT

Carbon isotope values from carbonate rocks ($\delta^{13}C_{carb}$), including those from many dolomitized successions, are the primary lens through which we interpret the Proterozoic carbon cycle. The $\delta^{13}C_{carb}$ value of carbonates is typically considered to be rock buffered to dolomitizing fluids. However, chemostratigraphic studies have demonstrated large, up to 10‰ differences in $\delta^{13}C_{carb}$ between limestone and dolomitized successions of the Neoproterozoic Tsagaan-Olom Group in southwestern Mongolia. To understand the nature of this geochemical variation, we conducted detailed geological mapping, petrographic, fluid inclusion, clumped isotopic, and geochemical studies of the Taishir, Ol, and Shuurgat formations of the Tsagaan-Olom Group. We suggest that dolomitization and isotopic variation was driven by the circulation of hot, saline, basinal fluids related to orogenesis in the hinterland either prior to or during foreland basin formation (545-525 Ma) that accommodated overlying, undolomitized late Ediacaran and early Cambrian sediments. This model supports homogenization temperature of ~ 110^{o} C recorded in fluid inclusion and clumped-isotopes paleothermometries, and progressive fabric destruction of pre-existing carbonate textures that broadly scales with the degree of isotopic offset. The dolomitizing fluids followed faults and stratigraphic units that were more porous and bound by impermeable seals such as shale and phosphorite deposits. Some dolomitized units that retain sedimentary fabrics also display large isotopic disparity from their undolomitized counterparts. Dolomitization homogenized

Neoproterozoic $\delta^{13}C_{carb}$ records; undolomitized successions show more extreme negative excursions from more positive background values. The $\delta^{13}C_{carb}$ isotopic effect of dolomitization on Phanerozoic rocks may be more difficult to discern where there is less of a difference between the $\delta^{13}C_{carb}$ values of recently deposited sediments and seawater-derived dolomitizing fluids. These results caution against the use of geochemical data from dolomites that do not appear to be early diagenetic to interpret the isotopic composition of Neoproterozoic seawater.

4.1. INTRODUCTION

Proterozoic and Paleozoic platform carbonates are dominated by dolostone (for example Morrow, 1982; Warren, 2000; Zenger et al., 1980). Isotopic records from these dolostone successions are commonly used to interpret the geochemistry of former oceans (for example Halverson et al., 2010; Kaufman and Knoll, 1995). Although there is an immense literature on the process of dolomitization, no consensus exists regarding the prevalence of different modes of dolomitization and the effects on isotopic systems in the preexisting carbonates. Although some experiments suggest environmental changes in temperature and seawater chemistry over geologic time could account for the predominance of dolomite in Proterozoic and Archean carbonates (e.g. Arvidson and Mackenzie, 1999), it is generally agreed that the majority of ancient dolomite is a replacement product (Zenger et al., 1980). Nonetheless, because dolomitizing fluids have abundant oxygen and low carbon (Warren, 2000), oxygen isotopes in dolomite are commonly interpreted to reflect the composition and temperature of dolomitizing fluids whereas carbon isotopes are thought to be rock buffered and reflect the isotopic composition of the precursor carbonate (Tucker and Wright, 1990). Thus, carbon isotope values from dolomites are widely considered as robust recorders of the carbon cycle in Earth history.

Carbon isotope records in dolomite successions have played a particularly important role in the interpretation of Neoproterozoic environmental change. The assumption that $\delta^{13}C_{carb}$ values are rock-buffered has been bolstered by broad regional reproducibility and little variability in $\delta^{13}C_{carb}$ values of different textures in Namibian (Halverson et al., 2002; Kaufman et al., 1991) and Svalbard (Halverson et

al., 2004) dolomites. These records have formed the backbone for the Neoproterozoic composite $\delta^{13}C_{carb}$ curve, which is characterized by extended periods of positive $\delta^{13}C_{carb}$ with negative $\delta^{13}C_{carb}$ excursions (Halverson, 2006; Rose et al., 2012). Along with Namibia (Hoffman, 2011) and Arctic Alaska (Macdonald et al., 2009), Mongolia hosts the only carbonate-dominated Cryogenian non-glacial interlude sequence, and yet, despite the broad geochronological and stratigraphic correlations (e.g. Macdonald et al., 2009b), there are significant differences between the $\delta^{13}C_{carb}$ profiles of these successions. Particularly, background $\delta^{13}C_{carb}$ values from limestone in Mongolia are more isotopically enriched than dolomitized records of Namibia and Arctic Alaska.

Along with differences in $\delta^{13}C_{carb}$ profiles between coeval successions on different margins, $\delta^{13}C_{carb}$ gradients have been observed on individual margins. Under the assumption that dolomites record primary seawater $\delta^{13}C_{carb}$ values, variable $\delta^{13}C_{carb}$ values measured between dolomitized Ediacaran carbonates deposited in platform and foreslope settings in Namibia (Hoffman, 2011) and platform, slope, and basin settings in South China (Jiang et al., 2007) have been attributed to surface-to-deep ocean $\delta^{13}C$ gradient derived from either sinking and remineralization of organic matter or sulfate reduction in anoxic deep oceans respectively. However, a detailed investigation of isotopic effects of progressive dolomitization has not been carried out partly because demonstrably coeval limestone and progressively dolomitized successions in the Neoproterozoic have not been clearly identified.

The Zavkhan Terrane of southwestern Mongolia hosts the Tsagaan-Olom Group, which forms a carbonate ramp that spans the Cryogenian non-glacial interlude (~ 660-643 Ma) and early Ediacaran Period (~ 635-580 Ma) (Bold et al., 2016). The Cryogenian Taishir and Ediacaran Ol and Shuurgat formations (fms) of the Tsagaan-Olom Group are composed of coeval limestone and dolomitized strata that provide an opportunity to document the geochemical effects of dolomitization. Particularly, limestone sections of the Taishir Formation (Fm) tightly covary in $\delta^{13}C_{carb}$ and $\delta^{13}C_{org}$ values (Johnston et al., 2012), which suggests that measured $\delta^{13}C_{carb}$ are primary, whereas the $\delta^{13}C_{carb}$ values of the dolomitized equivalent strata of the Taishir, Ol, and Shuurgat fms record significant variability (Bold et al., 2016). Here we document differences in geochemical proxies preserved in coeval limestone and dolostone

successions in the Tsagaan Olom Group, develop a model for dolomitization, and discuss how these results affect our view on the fidelity of $\delta^{13}C_{carb}$ records obtained from dolostone.

4.1.1. Geologic setting

The Zavkhan Terrane of southwestern Mongolia is a Neoproterozoic ribbon continent that was incorporated into the Central Asian Orogenic Belt (e.g. Windley et al., 2007). The basement gneiss of the Zavkhan Terrane is 1967 ± 13 Ma old and it is in intrusive relationship with 811.36 ± 0.24 Ma Dund-Orthocomplex, which is conformably overlain by volcanics and siliciclastics of the Yargait Fm followed by the Zavkhan Fm (Bold et al., in review). The base of the Zavkhan Fm is characterized by a few tens of meters thick sedimentary strata that are dominated by cobble conglomerate. Up section, felsic volcanic beds with minor volcaniclastic and mafic rocks become prevalent. Rhyolite flows within the Zavkhan Fm have been dated at 802.1 ± 1.0 Ma and 797.2 ± 1.1 Ma with U-Pb chemical abrasion-ion dilution-thermal ionization mass spectrometry (CA-ID-TIMS) on zircon. Above, the Zavkhan Fm is unconformably overlain by the Khasagt Fm, which is composed of 0-1000 m of siltstone, sandstone, and conglomerate, and the Tsagaan-Olom Group (Bold et al., 2016).

The Tsagaan-Olom Group consists of the Cryogenian Maikhan-Uul, Taishir, and Khongor fms, and the Ediacaran Ol and Shuurgat fms (Figure 4.1). Glacial diamictites and siliciclastic rocks of the Maikhan-Uul Fm were deposited during the ~ 717-660 Ma Sturtian glaciation. The base of the overlying Taishir Fm has been dated with Re/Os on organic-rich lime-micrite at 659.0 ± 4.5 Ma, which is indistinguishable from dates on Sturtian cap carbonates at several localities globally (Rooney et al., 2015). The Taishir Fm is a < 600 m thick limestone-dominated succession divided into four members (T1, T2, T3, and T4) that define the major sequence boundaries. The Taishir Fm is succeeded by glacigenic deposits of the Khongor Fm, which ranges from 0 to 15 m thick and is composed of carbonate clasts in weakly stratified shale, siltstone, and calcisiltite matrix. The Cryogenian Taishir and Khongor fms are sharply overlain by the Ol Fm, which hosts sedimentological features characteristic of basal Ediacaran cap dolostones globally (Hoffman, 2011), including pseudomorphed aragonite fans, tubestone

stromatolites (Figure 4.3N), sedimentary barite, and giant wave ripples. The Ol Fm is up to 40 m thick and is composed of buff-colored, finely-laminated micropeloidal dolostone (Ol cap dolostone), overlain by nodular bedded calcisiltite and flat-bedded lime-micrite interbedded with thin beds of shale, and massively bedded lime-grainstone. The Ol Fm is conformably overlain by the Shuurgat Fm, which consists of up to 500 m of dolostone-dominated carbonate strata (figures 4.3K, 4.3L, and 4.3M) that is divided into four mappable members (Sh1, Sh2, Sh3, and Sh4). The karstic surface at the top of the Shuurgat Fm has been interpreted to mark ~ 40 Myr year hiatus spanning the middle to late Ediacaran Period (Bold et al., 2013; Bold et al., 2016; Macdonald et al., 2009a). Above this erosional unconformity, the Shuurgat Fm is overlain by buff- to pink-colored stromatolitic dolostone, phosphatic shale, and thin-bedded limestone of the Zuun-Arts Fm (Smith et al., 2015).

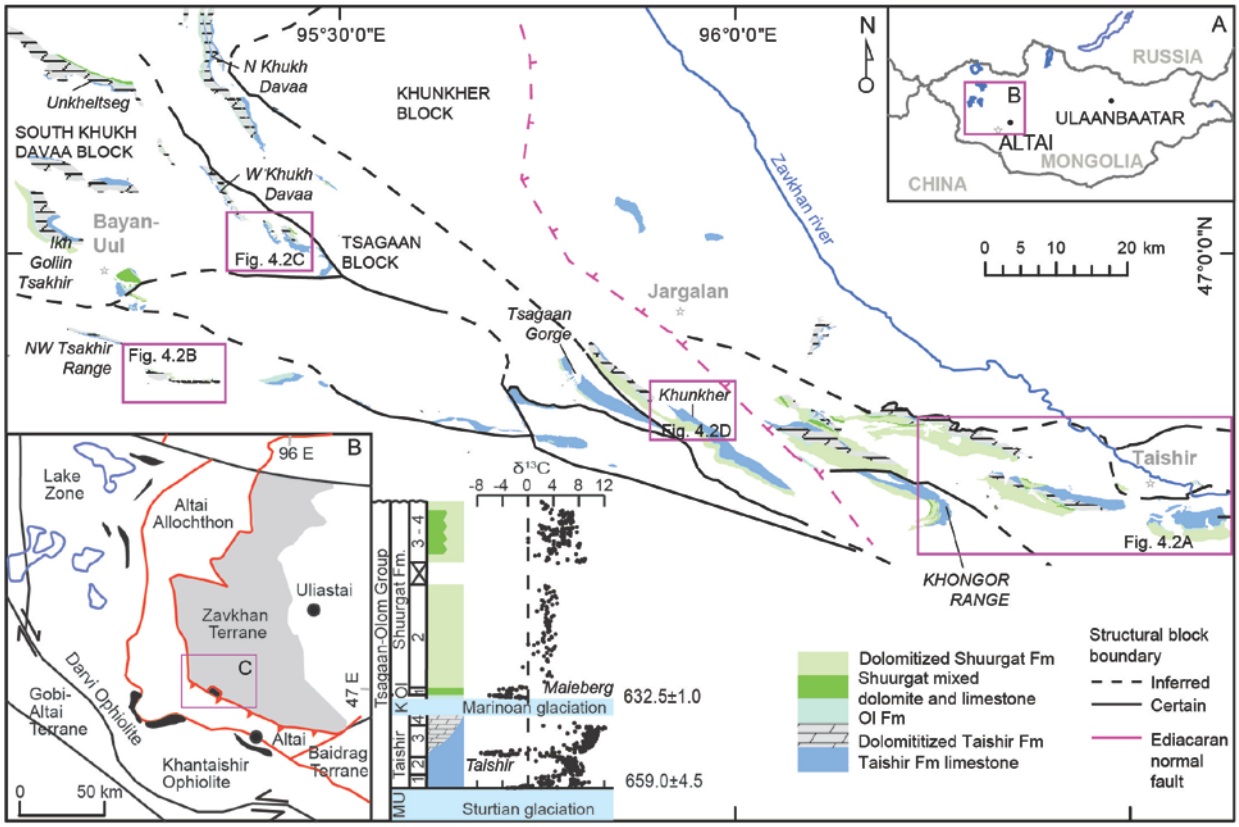

Figure 4.1. Outline map of the Zavkhan Terrane showing the extent of dolomitized carbonates of the Tsagaan-Olom Group

A) Location map of the study area. B) Simplified terrane map of southwestern Mongolia. Extent of inset map C is boxed. C) Simplified geological map of the Zavkhan Terrane. Dolomitized carbonates of the Taishir, Ol, and Shuurgat formations are shown. Extent for figures 4.2A, 4.2B, 4.2C and 4.2D are highlighted by maroon boxes.

During the Ediacaran Period, the southern margin of the Zavkhan Terrane transformed from a passive to an active margin. Ediacaran metamorphism and magmatism are recorded on the northeastern margin of the Baidrag Terrane (Demoux et al., 2009a; Kozakov et al., 2012b), which may represent a collision between the Zavkhan and Baidrag terranes. In the Lake Terrane, the Khantaishir ophiolite was formed at ~ 571 Ma (Jian et al., 2014; Khain et al., 2003), and was presumably obducted onto the Zavkhan Terrane by 545-520 Ma (Štípská et al., 2010). Although there is no sedimentary rock record preserved spanning ~ 580-545 Ma on the Zavkhan Terrane, it hosts a late Ediacaran to early Cambrian foreland basin that accommodated the deposition of Zuun-Arts, Bayangol, Salaagol, and Khairkhan fms (Smith et al., 2015). Accretion continued on the southern margin of the amalgamated Mongolian terranes throughout the Paleozoic and culminated with extensive Permian plutonism (e.g. Jahn et al., 2009).

4.2. METHODS

4.2.1. Mapping of the dolomitization front

To better constrain the geometry and extent of dolomitization, we mapped the distribution of dolomitized carbonates over 100 km along strike (Figure 4.1). Dolomitization of the Taishir Fm was targeted because of the sharp visual contrast between the dark-colored limestone and the light-colored dolomitization fronts. Both vertical and along strike transitions from limestone to dolostone within the Taishir Fm were documented at each of the localities where representative stratigraphic sections of the Taishir Fm were measured in Bold et al. (2016). At selected localities (Figure 4.2), vertical examination of dolomitization front was carried out through the Ol and Shuurgat fms; however, the geometry of dolomitization fronts was more difficult to constrain with map relationships because dolomitization was more complete in the Ol cap dolostone and Shuurgat Fm and equivalent limestone strata is relatively uncommon.

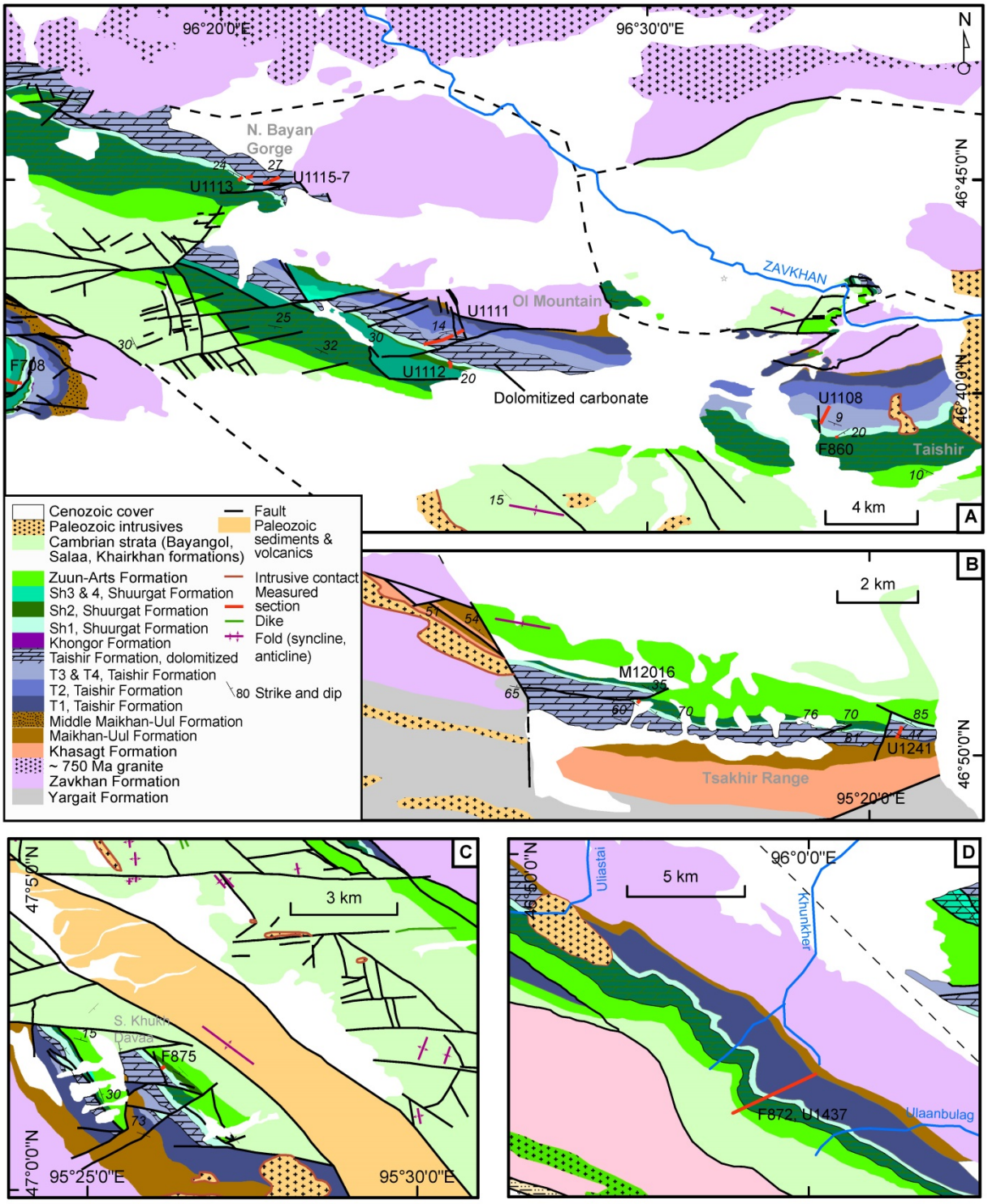

Figure 4.2. Detailed geological map
Geological map of the Taishir, Ol Mountain, and northern Bayan Gorge locality. Mapped dolomitization front is shown by dolomite symbol. Taishir locality hosts non-dolomitized Taishir (except a few meters of partially dolomitized carbonates in the upper T3) and upper Ol Formation carbonates.

Figure 4.2 (Continued) Dolomitization becomes more pervasive to the northeast and the uppermost Taishir and the whole Ol Formation carbonates are dolomitized in the Ol Mountain. The whole T3 including upper T2 of the Taishir Formation as well as the entire Ol Formation is dolomitized at the northern Bayan Gorge locality. B) Geological map of the Tsakhir Range. Taishir Formation carbonates are completely dolomitized here except the basal T1 limestone. Upper Ol Formation carbonates are also dolomitized. C) Geological map of the southern Khukh Davaa locality. Dolomitized carbonates are highlighted. D) Geological map of the Khunkher Gorge. The entire Taishir Formation is non-dolomitized. Member Sh3-4 of the Shuurgat Formation is dominated by limestone.

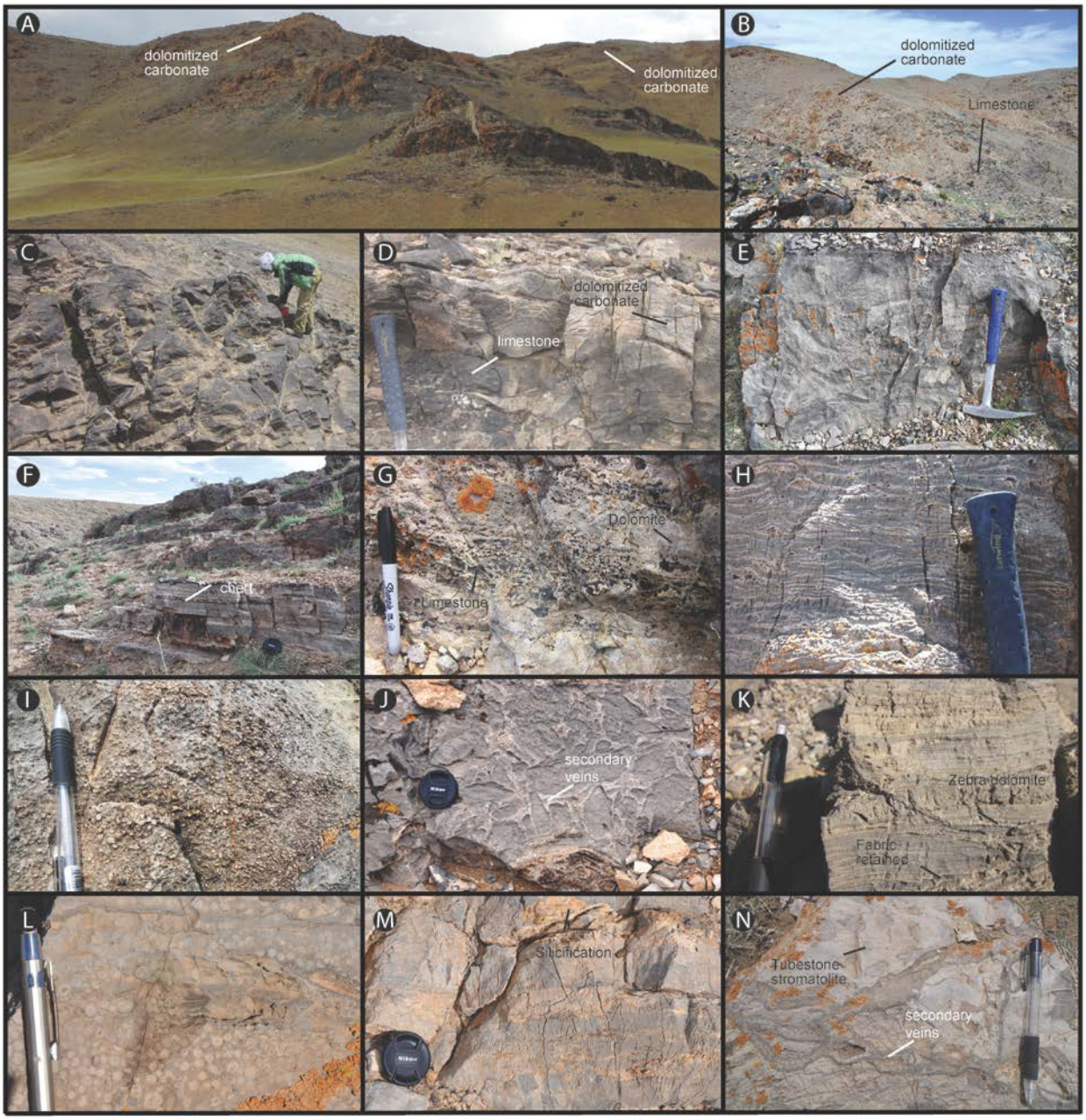

Figure 4.3. Carbonates of the Taishir, Ol, and Shuurgat formations
A) Extent of dolomitization as exposed and preserved in western Khukh Davaa (Figure 4.1). Note the irregular pathway of dolomitizing fluid as expressed by dolomitized carbonates, which are orange brown weathered compared to limestone strata. B) Dolomitized Taishir carbonates as exposed in Unkheltseg Range (Figure 4.1). Boundary with the limestone strata is also irregular. C) Limestone T3 as exposed in northwestern Tsakhir Range (Figure 4.1).

Figure 4.3 (Continued) D) Faintly dolomitized T3 of the Taishir Formation at stratigraphic height of 93.6 m of section U1108 measured at Taishir locality. E) Semi texture destructive dolomite of T3 as preserved in northern Khukh Davaa (Figure 4.1). Geological hammer for scale is 330 mm in length. F) Dolomitized basal T3 (Section U1115; figures 4.2A and 4.4) of the Taishir Formation where in limestone equivalent successions, the Taishir negative $\delta^{13}C_{carb}$ excursion is always preserved. The resistant bed-parallel lenses are chert. Camera lens cap for scale is 52 mm in diameter. G) Very patchily dolomitized carbonate of the T3 of the Taishir Formation as exposed in the southern Khukh Davaa locality. H) Texture destructive dolomite, zebra dolomite, that is intensively recrystallized with abundant bed parallel veins (Section U1115-26m). I) Dolomitized ooid-grainstone of the upper T3 Member. Note the silicification of ooids, which makes them prominent on weathered surface (northern Khukh Davaa, Figure 4.1). Pen for scale is 12 cm in length. J) Extensive veining in the dolomitized T3 as preserved in Ikh Goliin Tsakhir locality (Figure 4.1). Note the weathering resistant veins compared to dolomite matrix. K) Zebra dolomite of Member Sh2 of the Shuurgat Formation as preserved in the Ol Mountain (F708, Figure 4.6). In the lower left, fabric-retained dolomite is preserved and characterized by thinly laminated beds of carbonate. Pencil for scale is 15 cm in length. L) Ooid dolo-grainstone of Member Sh3 of the Shuurgat Formation at Khongor Range (Section F708). Pen for scale is 10 cm in length. M) Massively weathered dolo-micrite of Member Sh4 of the Shuurgat Formation at Khongor Range. N) Ol Formation cap dolostone preserved in the northeastern Khukh Davaa (stratigraphic section U1212 - 8.5 m, Bold et al., 2016). Note the abundant secondary veins present. Tubestone stromatolites are visible. Descriptions of localities of sections where the photos A – C, E, I, and J are taken are included in Bold et al. (2016).

4.2.2. $\delta^{13}C_{carb}$ and $\delta^{18}O$ analysis

In order to fully characterize isotope discrepancy between limestone and dolomitized sections, the Taishir and Ol fms were targeted due to clear and mappable relationships. A total of five localities (Figure 4.2) that preserved composite sections of the Taishir and Ol fms are chosen for detailed isotopic analysis (figures 4.3-4.10). Three of these localities, the Taishir, Ol Mountain, and northern Bayan Gorge sections (Figure 4.2A) are nearly continuously exposed along strike and were specifically chosen to assess transition from all limestone to all dolomitized carbonates of the Taishir and Ol fms (Figure 4.4 and Table 4.A1). The Tsakhir Range (Figure 4.2B) was chosen due to its preservation of a patchy dolomitization pattern, and South Khukh Davaa (Figure 4.2C) was chosen because it preserves the most extreme isotopic variation recorded within the Ol Fm. Two composite sections of the Shuurgat Fm were measured, in Khongor Range (F708, F947, and U1439) and Khunkher Gorge (F872 and U1437), to further assess the significance of this dolomitization event in the rest of the Tsagaan-Olom Group carbonates (figures 4.2A and 4.6).

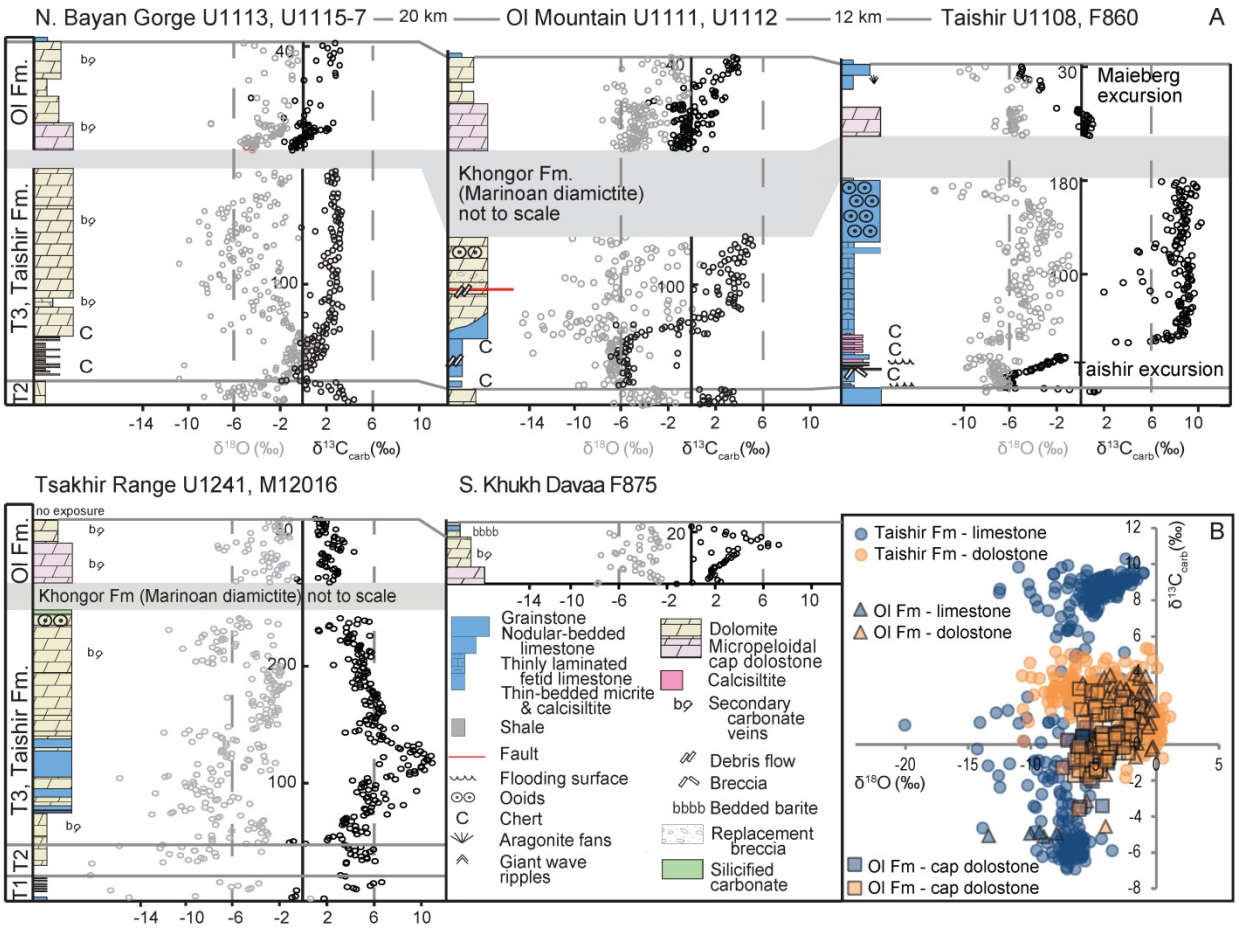

Figure 4.4. Chemostratigraphy of the Taishir and Ol Formation carbonates included in this study
A) Sections measured for comparison in the upper Taishir and Ol fms in northern Bayan Gorge, Ol Mountain, Taishir, Tsakhir Range, and southern Khukh Davaa localities. B) Cross-plot of $\delta^{13}C_{carb}$ and $\delta^{18}O$ is shown including all of the data presented in this study.

Carbonate samples for $\delta^{13}C_{carb}$ and $\delta^{18}O_{carb}$ analysis were sampled at ~ 1 m resolution (Table 4.A1 and Figure 4.4) in each of the selected localities. Powders analyzed were drilled from clean and vein-free carbonates and total of 1362 samples were analyzed. In order to further document small-scale geochemical variability, different macro-textures of selected samples were micro-drilled for $\delta^{13}C_{carb}$ and $\delta^{18}O$ analysis (figures 4.7 and 4.8; Table 4.A2). The analytical technique followed is outlined in Bold et al. (2016). The results are reported in per mil (‰) notation relative to the standard VPDB.

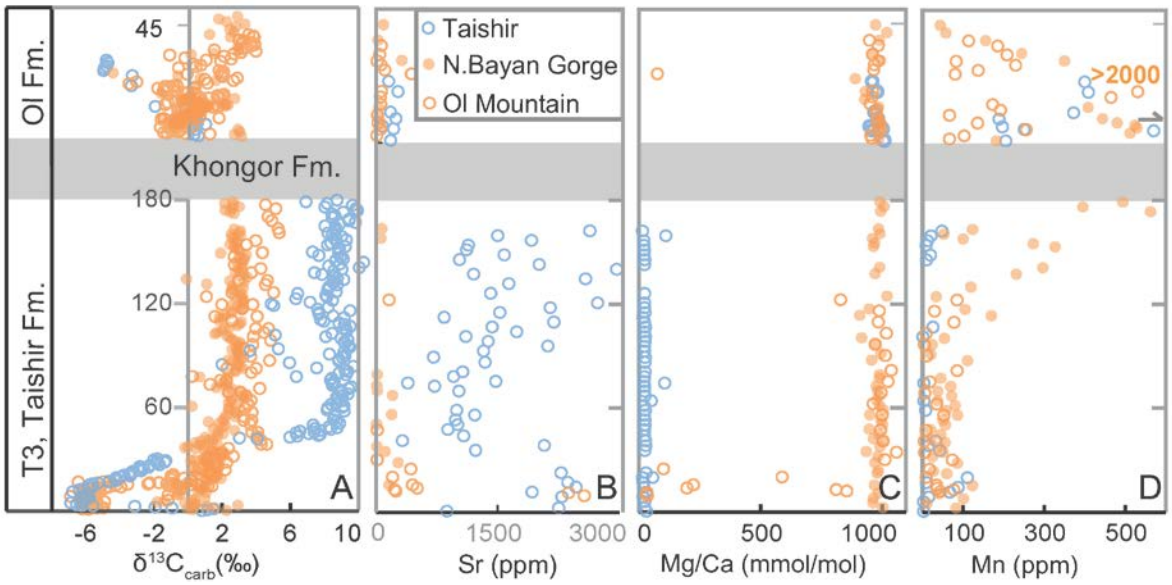

Figure 4.5. Co-plots of $\delta^{13}C_{carb}$ and elemental concentration data of the Taishir and Ol formations
A) Co-plots of $\delta^{13}C_{carb}$ values preserved in northern Bayan Gorge, Ol Mountain, and Taishir localities, concentration (ppm) of Sr (B) and Mn (C), and Mg/Ca ratio (D) in analyzed carbonates in mmol/mol. Thickness of Khongor Formation is not drawn to scale.

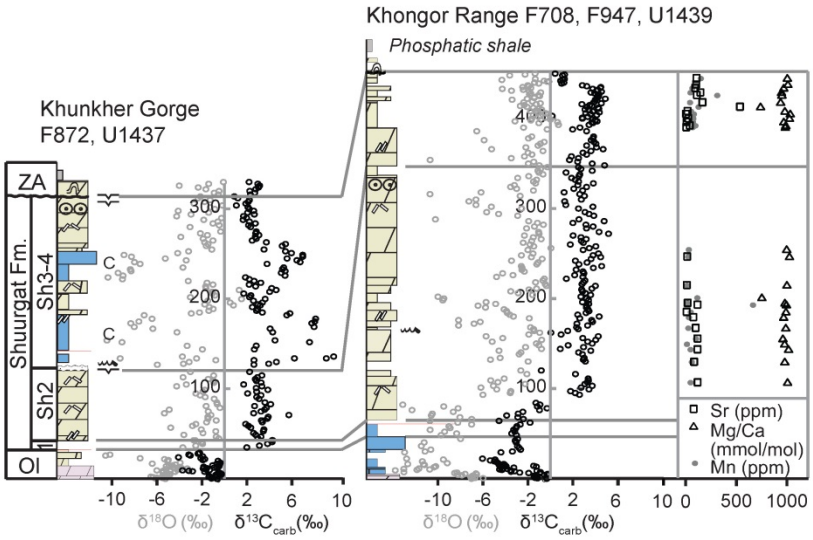

Figure 4.6. Stratigraphic description of the Shuurgat Formation as exposed in the Khongor Range and Khunkher Gorge
Legend for lithology is the same as in Figure 4.4. $\delta^{13}C_{carb}$, $\delta^{18}O$, concentration of Sr, Mn, Mg, and Ca are measured in the Shuurgat Formation.

4.2.3. Petrography

Petrographic examination of carbonates was made on 24 thin sections prepared for optical study. Different textures of dolomitized carbonates are studied in detail and carbonate mineralogy of lime-mudstone, lime-grainstone, and dolomitized equivalents (figures 4.3, 4.9 and 4.10) were studied. Selected

samples were stained by Alizarin red and Potassium Ferricyanide composite (Evamy, 1963; Tamer, 1965) for further differentiation of calcitic and dolomitic fabrics (Figure 4.10).

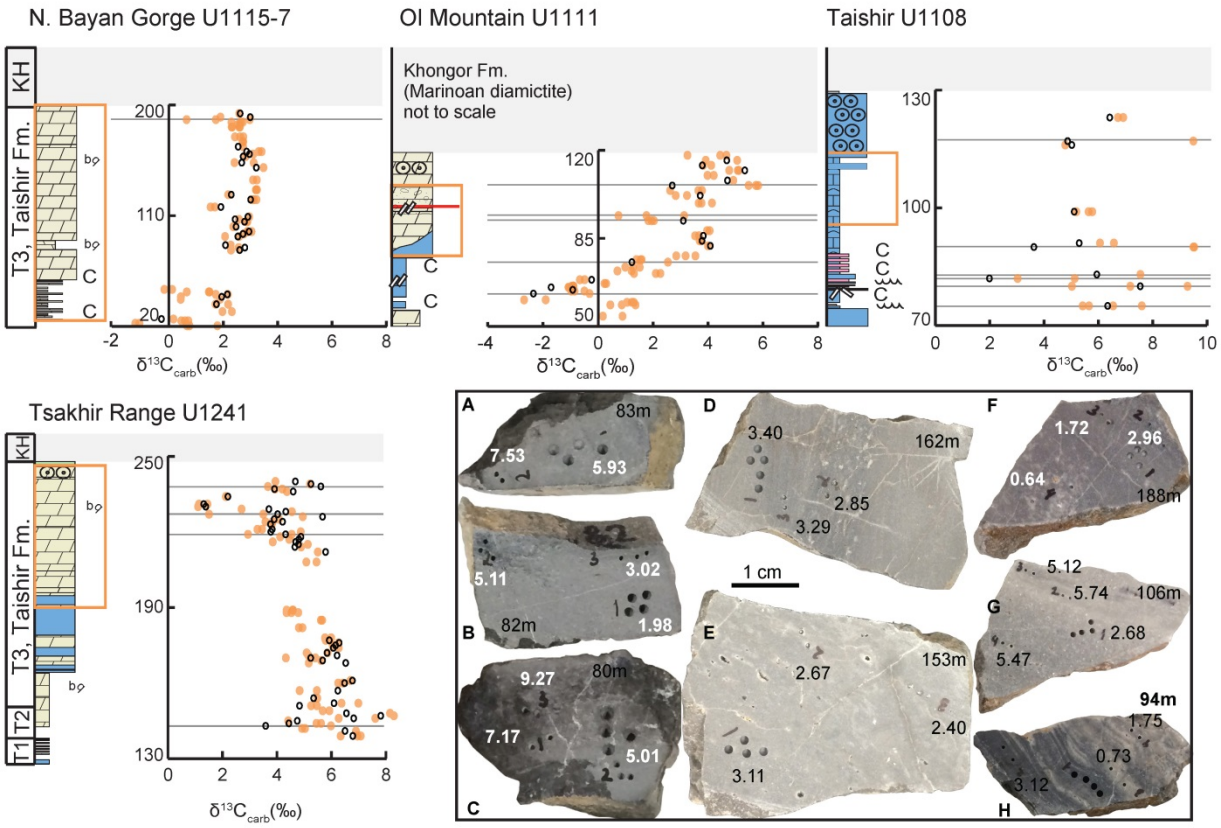

Figure 4.7. Isotopic variability recorded in the Taishir Formation carbonates in hand sample scale Different macro-textures were targeted. Interval of examination is boxed in orange. Black circles denote values included in original $\delta^{13}C_{carb}$ profiles included in Figure 4.3. Orange-filled circles denote macro-textures analyzed in this study to reflect isotopic variability. Intervals with ≥ 2‰ are highlighted by gray horizontal lines. Selection of hand samples that preserved variable isotopic values are shown in the box. A-C – U1108, D-E – U1116, F – U1117, and G-H – U1111. Stratigraphic height of each of the samples is labeled in meter.

4.2.4. Elemental concentration

Concentrations of Mn, Sr, Mg, and Ca (Table 4.A1) were measured on a Thermo Scientific Element 2 inductively coupled plasma mass spectrometer (ICP-MS) at Princeton University. Because the samples were dissolved in a weak acetic acid (0.1 M in concentration), which leaves insoluble sediment to phase out, the elemental compositions are assumed to be carbonate-bound. For the analysis, 25 µL of sample solution was diluted in 1 milliliter (mL) of 2% HNO_3 acid and measured against six in-house

multi-element standards. All of the data are reported in parts per million (ppm) except Mg/Ca, which is reported as mmol/mol.

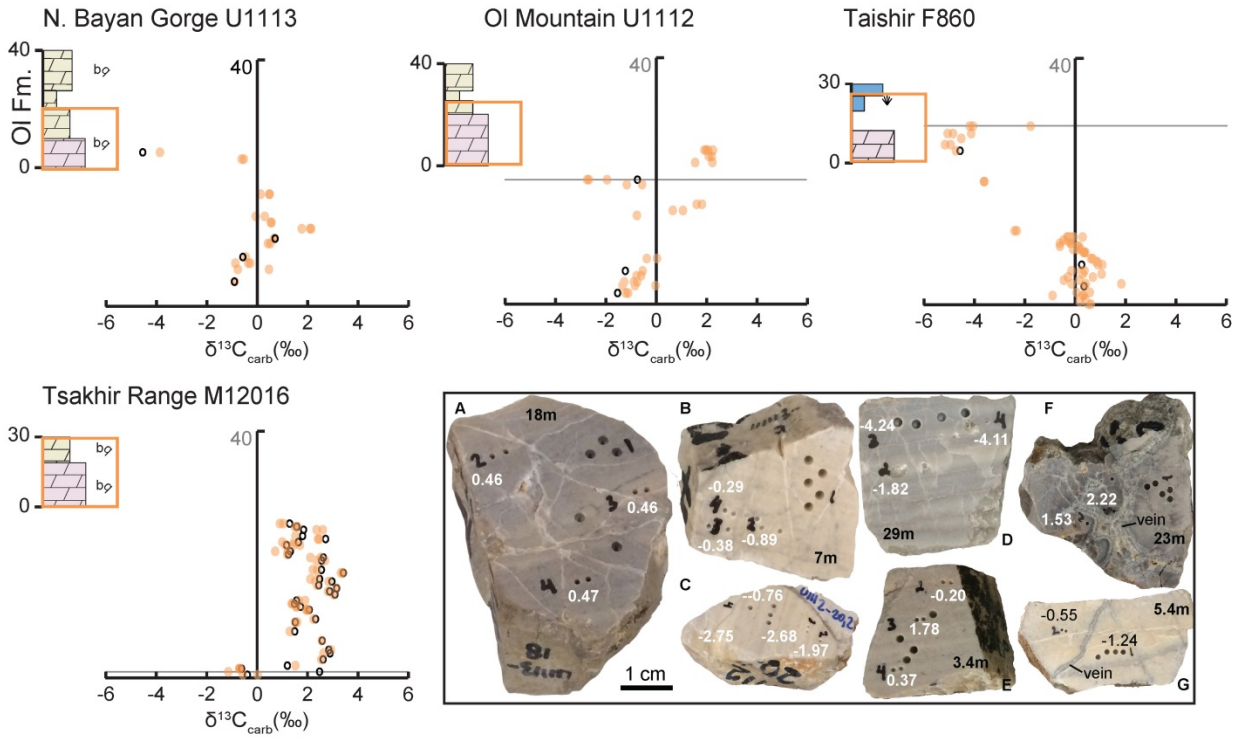

Figure 4.8. Isotopic variability recorded in the Ol Formation carbonates in hand sample scale
Interval of examination is boxed in orange. Black circles denote values included in original $\delta^{13}C_{carb}$ profiles included in Figure 4.3. Orange-filled circles denote macro-textures analyzed in this study to reflect isotopic variability. Intervals with ≥ 2‰ are highlighted by gray horizontal lines. Selection of hand samples that preserved variable isotopic values are shown in the box. A-B – U1113, C and F-G – U1112, and D-E – F860. Stratigraphic height of each of the samples is labeled in meter.

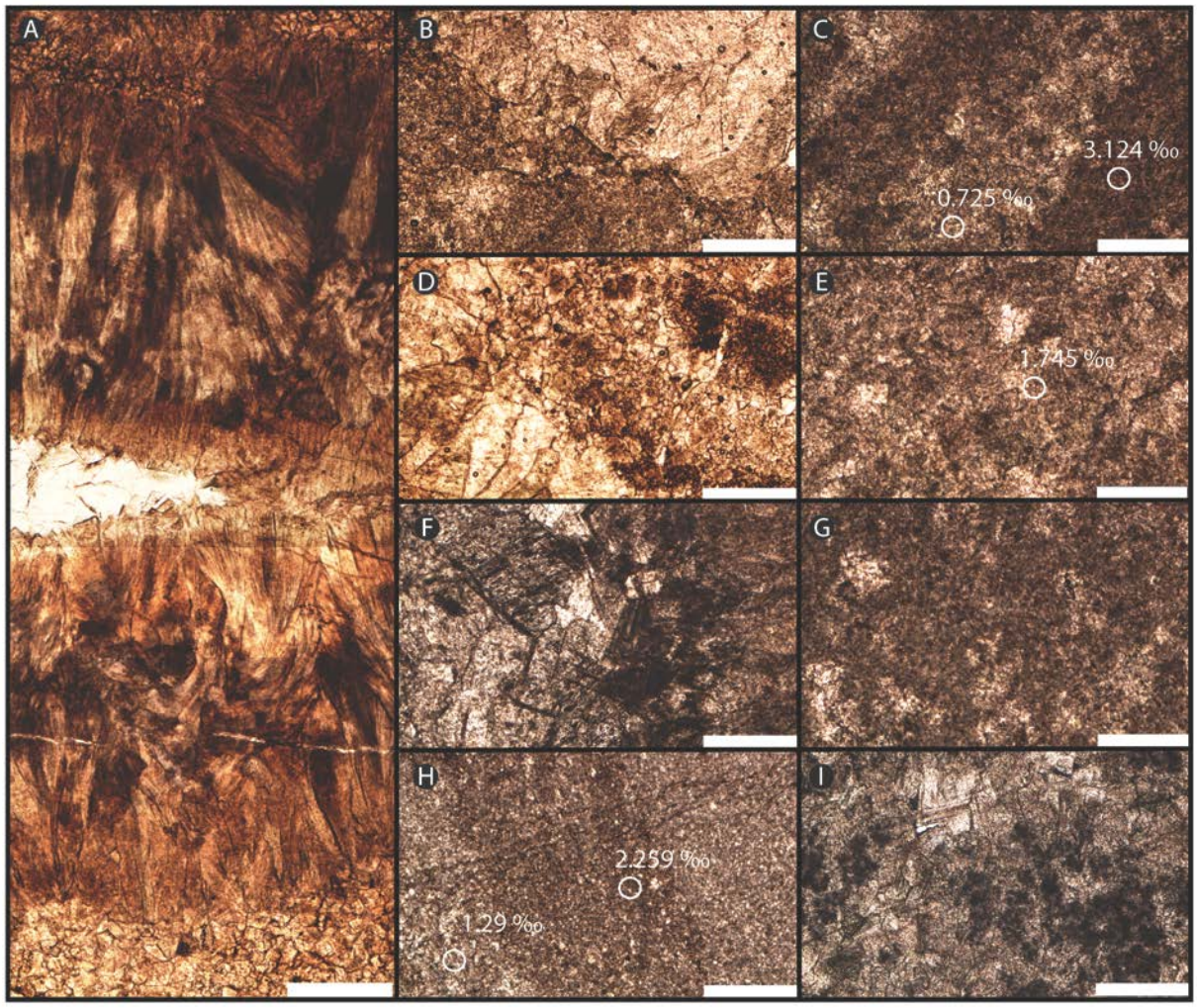

Figure 4.9. Petrography of the Taishir and Ol Formation carbonates

White horizontal bars for scale are 500 μm in length. A, B, D, and F – secondary (dolomite but rarely silicified) veins abundant in the dolomitized carbonates. A) Carbonate vein hosted in Ol cap dolostone at western Khukh Davaa (Figure 4.1). Three generations of crystal growth growing normal to the substrate. It is filled with a first generation of fibrous crystals, then by a continual growth of botryoids and finally blocky crystals that are now silicified. B) Secondary vein filled with blocky cement that consists of coarse grained crystals without preferred orientation in Ol Formation carbonate in Tsagaan Gorge (Figure 4.1). C) Irregularly dolomitized carbonate of T3 of the Taishir Formation as preserved in the Ol Mountain (Section U1111-94, Figure 4.7H). Dark brown anhedral carbonates represent partially dolomitized carbonate. Medium-coarsely crystalline, subhedral, and light grey carbonates represent completely dolomitized carbonate. Note the variable $\delta^{13}C_{carb}$ values preserved respectively. Values are in unit of per mil. D) Secondary vein preserved in upper Ol Formation in Tsagaan Gorge that is filled with preferentially oriented blocky crystals. E) Completely dolomitized carbonate as preserved in U1111-94. Characterized by coarsely crystalline and subhedral to euhedral dolomite. Note the very light $\delta^{13}C_{carb}$ value preserved in this texture. F) Secondary vein characterized by a growth of first generation subhedral to euhedral crystals with well-developed boundary faces and then of blocky crystals as preserved in dolomitized in Ol Formation carbonates (U1112-23 m, Figure 4.4). G) Coarse-crystalline and subhedral dolomite representative of dolomitized T3 as preserved in northern Bayan Gorge (U1117-188 m, Figure 4.4). H) Partially dolomitized carbonate of the upper T3 as preserved in Ol Mountain. Dark brown anhedral carbonates represent partial dolomitization whereas subhedral to anhedral, light grey carbonates represent complete dolomitization (U1111-71 m, Figure 4.4). Note the variable $\delta^{13}C_{carb}$ values preserved. I) Ol Formation cap dolostone as preserved at Taishir locality (F860, Figure 4.4). The carbonates are mm-laminated and composed of interbeds of microcrystalline, anhedral, and cloudy dolomite and subhedral to euhedral, coarse-crystalline, and clear dolomite.

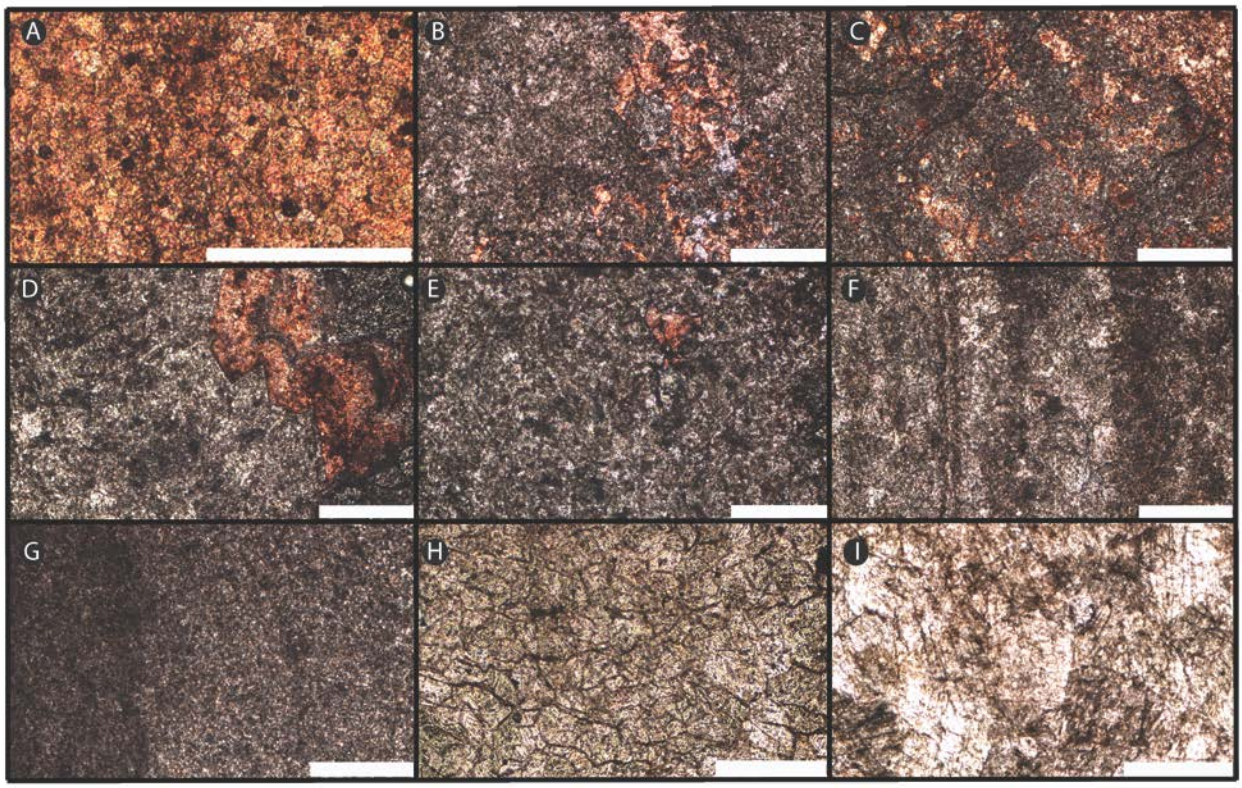

Figure 4.10. Petrography of Alizarin red and Potassium Ferricyanide stained carbonates
White horizontal bars for scale are 500 µm in length. A) A microcrystalline T3 lime-micrite at Taishir locality (U1108-60 m, Figure 4.4). B-E) Irregular dolomitization in the partially dolomitized T3 as preserved in northern Bayan Gorge and Ol Mountain. Residual calcite is stained whereas the dolomite is clear (U1116-162 m, U1111-71 m, 86, U1111-162 m). F-G) Finely crystalline dolomite. An example for microcrystalline dolomite with light and dark colored bands in hand sample (U1111-94 m, T3, Figure 4.7H). Dolomitization may be complete on the right side and sparse on the left. H) A coarsely crystalline, equant, subhedral dolomite (U1216-0.4 m, Ol Formation; Bold et al., 2016). I) A coarsely crystalline, subhedral to euhedral replacement dolomite (U1111-70, T3). The rhombs are mostly clear with rare cloudy cores.

4.2.5. Fluid inclusions

Polished thin sections (100 μm thick) were made from both limestone and dolostone slabs and studied petrographically (figures 4.11A – 4.11D) in both transmitted and reflected lights using Nikon eclipse EL 100N POL microscope. Fluid inclusion microthermometry was undertaken using a Linkam THMS 600 heating-freezing stage (with Olympus 50× long focus lens) at the International Center for Research and Education on Mineral and Energy Resource (ICREMR), Akita University in Japan. The thermocouple for the heating/freezing stage was calibrated using melting temperature of metals and the ice melting temperature of pure water. The homogenization temperature (T_h) has a calibration error of < 1° C, whilst the accuracy of ice melting is ±0.1° C. 1° C/min heating rate was applied to all heating and cooling experiments. Analyzed inclusions were between 2 and 8 microns in length. Fluid inclusion types at room temperature, size of inclusions, T_h, and final ice melting temperature measurements were obtained. Salinity was determined by ice melting and solid melting temperatures (Bodnar, 1993) reported as wt. % (NaCl eq.) (Table 4.A3).

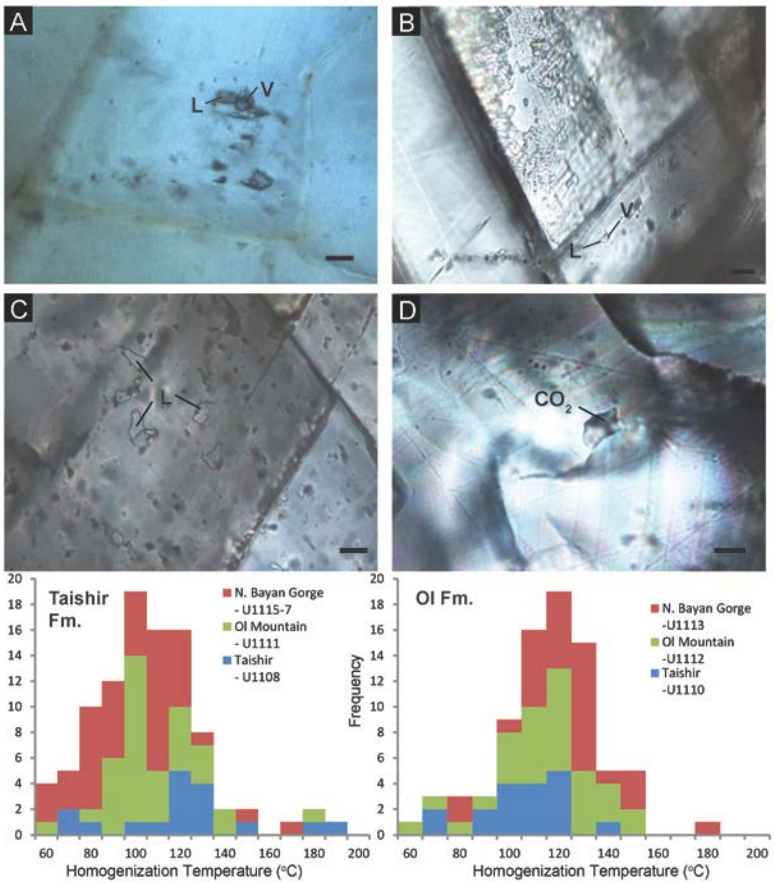

Figure 4.11. Fluid inclusion and scatter plot of homogenization temperatures (T_h)
Black bar for scale is 5 μm in length. L – liquid; V – vapor. a) Liquid rich fluid inclusion type-I of sample U1108-10. b) Liquid rich fluid inclusion type I of sample U1110-5.4 m. c) Liquid fluid inclusion type-II of sample P-1. d) CO_2 fluid inclusion type-III of sample U1112-36.5. e) Scatterplot of homogenization temperatures (T_h) for both the non-dolomitized and dolomitized carbonates of the Taishir Formation measured at Taishir, Ol Mountain, and northern Bayan Gorge localities. f) Scatterplot of homogenization temperatures (T_h) for the Ol Formation carbonates.

4.2.6. Clumped -isotope paleothermometry

As an independent test to constrain recrystallization temperatures of the carbonates, selected samples (both dolostone and limestone) of the Taishir, Ol, and Shuurgat fms (Figure 4.A1) were analyzed for clumped isotope paleothermometry. Five limestone samples were selected from the Taishir Fm from stratigraphic section U1108, two more limestone samples of the Taishir Fm were chosen from section U1111, five dolostone samples were selected from dolomitized Taishir Fm from sections U1115, U1116, and U1117, five Ol Fm carbonate samples (3 dolostone and 2 limestone) from sections F708, F860, and U1113, and three Shuurgat Fm carbonates (2 dolostone and 1 limestone) from sections F708, F872, and

U1439. Approximately 2-4 mg sample powder was used for each sample and analyzed by high-efficiency sample preparation inlet and dual-reservoir measurement technique (Petersen and Schrag, 2014) at Harvard University Laboratory for Geochemical Oceanography. Each measurement was replicated 2-3 times depending on reproducibility of the signature. Detailed description of the analytical technique is outlined in Petersen and Schrag (2015).

Table 4.1. Clumped-isotope paleothermometry data of the Taishir, Ol, and Shuurgat formations

Sample number*	Rock Type	Δ_{47} (‰)	std dev.	Δ_{47}T (°C)†	std dev.	$\delta^{13}C_{carb}$ (‰)	std dev.	δ^{18O}_{carb} (‰)	std dev.	$\delta^{13}C_{carb}$ (‰)	δ^{18O}_{carb} (‰)	Fluid inclusion temperature (°C)	Description§
										Optima			
Shuurgat Formation													
U1439-9.5	Dolomite	0.37	0.01	**431.85**	**27**	3.686	0.02	-0.787	0.1	3.7507	0.0103		Member Sh4, Khongor Range
F872-261	Limestone	0.39	0.05	**352.3**	**163**	7.024	0.01	-8.022	0.05	6.7278	-7.995		Member Sh3-4, Khunkher Gorge
Ol Formation													
F708-33	Dolomite	0.32	0.05	**478.9**	**NA#**	-1.627	0.05	-7.488	0.21	-1.446	-6.916		Cap dolostone, Khongor Range
U1113-32.1	Dolomite	0.51	0.05	**142.75**	**48**	0.467	0.03	-5.604	0.1	0.0863	-4.76	**141.5**	upper Ol, N. Bayan Gorge
F875-33.5	Dolomite	0.55	0.12	**115.6**	**92**	5.541	0.08	-5.094	0.1	6.402	-5.332		upper Ol, with barite, western Khukh Davaa
U1113-9.6	Dolomite	0.57	0.14	**105.15**	**96**	0.4595	0.01	-2.495	0.06	0.428	-2.611	**122**	Cap dolostone, N. Bayan Gorge
F860-26	Limestone	0.49	0.01	**159.55**	**9**	-5.205	0.000	-9.307	0.003	-5.113	-8.961		upper Ol, Taishir
Taishir Formation													
U1108-58	Limestone	0.42	0.001	**253.5**	**1**	8.797	0.08	-2.116	0.004	9.1229	-1.789		upper T3, Taishir
U1108-101	Limestone	0.46	0.02	**193.5**	**26**	9.138	0.03	-4.233	0.12	9.2732	-4.338		upper T3, Taishir
U1115-26	Dolomite	0.49	0.01	**155.8**	**12**	-0.305	0.03	-0.571	0.02	-0.284	-0.431		Taishir excursion T3, N. Bayan Gorge
U1108-10	Limestone	0.52	0.02	**125.05**	**18**	-5.896	0.003	-7.299	0.02	-6.159	-7.495	**126**	Taishir excursion T3, Taishir
U1116-47	Dolomite	0.49	0.03	**162.27**	**36**	2.1197	0.04	-7.491	0.13	2.1681	-6.961	**108**	upper T3, N. Bayan Gorge
U1116-29	Dolomite	0.51	0.05	**142**	**49**	2.872	0.03	-7.428	0.03	2.9421	-7.18		upper T3, N. Bayan Gorge
U1111-56	Limestone	0.49	0.07	**162.1**	**82**	-5.033	0.01	-7.462	0.16	-4.817	-7.26	**113.9**	upper T3, Ol Mountain
U1111-50	Limestone	0.47	0.09	**206.6**	**114**	-5.175	0.02	-6.235	0.1	-5.3	-6.709	**108.0**	Taishir excursion T3, Ol Mountain
U1115-52	Dolomite	0.54	0.07	**119.07**	**62**	1.6143	0.02	-0.751	0.06	-5.202	-5.727	**97.3**	Taishir excursion T3, Taishir
U1108-76	Limestone	0.51	0.13	**162**	**137**	9.036	0.02	-4.475	0.08	9.2472	-4.401		upper T3, Taishir
U1117-44	Dolomite	0.55	0.09	**112.27**	**58**	2.7253	0.03	-5.373	0.11	2.1637	-1.751	**111.4**	upper T3, N. Bayan Gorge

*Stratigraphic section - depth

†Celcius

§Member, Locality

#N.A. = not applicable.

4.3. RESULTS

4.3.1. Extent of dolomitization on the Zavkhan Terrane

At some localities, the whole of the Taishir Fm is preserved as limestone (figures 4.1 and 4.3C), but at others, the upper members are preserved as dolostone (figures 4.1, 4.3A, 4.3B, 4.3E, 4.3H, 4.3I, and 4.3J). The upper Ol Fm, lime-grainstone unit, is dolomitized in many localities on the Zavkhan Terrane, particularly where the underlying Taishir Fm carbonates are dolomitized. Where exposed, this basal unit of the Shuurgat Fm is preserved as limestone (Bold et al., 2016) and minor limestone is preserved in the upper members, Sh3-4. In general, the Shuurgat and Ol fms are more commonly dolomititzed than the Taishir Fm, and dolomitization progressed from the top of the Taishir Fm downwards.

Most of the contacts between limestone and dolostone are gradational with halos of partially dolomitized limestone extending tens of meters around completely dolomitized zones. Some contacts between limestone and dolostone are sharper, such as that at the top of the Ol Fm; however, these correspond with stratigraphic boundaries that correspond with differences in primary porosity. The nature of these transitions is shown in the measured stratigraphic sections (figures 4.3A and 4.3B).

Dolomitization fronts are discontinuous across block bounding faults (Figure 4.1). Many of these are Paleozoic right-lateral faults, and the dolomitization fronts across individual blocks can potentially be used as a piercing point to restore offset. However, some of these faults are likely reactivated Precambrian faults. Particularly, a potential Ediacaran fault on the Zavkhan Terrane is suggested by the erosion of unit Sh4 and the presence of a well-defined sandstone-filled karsted surface at the top of the Shuurgat Fm on the South Khukh Davaa, Tsagaan, and a portion of the Khunkher blocks (Figure 4.1). This boundary also coincides with a jump in the stratigraphic locus of dolomitization from predominantly within Taishir Fm to up into both the Taishir and Shuurgat fms.

With regards to specific localities, in the eastern part of the basin, near the Taishir locality (Figure 4.2A), both the Taishir and upper Ol fms are composed of limestone. Partially dolomitized carbonates of the Taishir Fm are present in stratigraphic section U1108 (figures 4.2 and 4.7). From Taishir, a dolomitization front expands along strike to the northwest and within 11 km, at Ol Mountain

(stratigraphic sections of U1111 and U1112), upper T3 (Figure 4.4) and the upper Ol Fm are completely dolomitized. At Ol Mountain, the basal Ol Fm preserves abundant secondary veins (figures 4.3N, 4.8B, and 4.8G). Along strike, at northern Bayan Gorge, the dolomitization front expands further to replace the upper portion of T2, entirety of T3, and the Ol Fm (figures 4.2, 4.3F, and 4.4). At northern Bayan Gorge, the Ol Fm also contains abundant secondary veins (Figure 4.8B), which are common at the most pervasively dolomitized localities (figures 4.3E, 4.3H, 4.3J, and 4.8F).

Further west and southwest, both the upper Taishir and Ol fms are preserved as dolostone and secondary carbonate veins are present. Transition from limestone to dolostone within the Taishir Fm is irregular but easily traceable in the field due to the color contrast between the dark limestone and light dolostone (figures 4.2B, 4.2C, 4.3A, and 4.3B). At South Khukh Davaa (Figure 4.2C) and the Tsakhir Range (Figure 4.2B), progressive fabric destruction is displayed (figures 4.3G and 4.4), where relict limestone, dark grey in color, is surrounded by pale brown coarse crystalline dolomite. Similarly, in the Tsakhir Range, in stratigraphic section U1241 (Figure 4.4), dolomitization fronts are laterally discontinuous in lenticular bodies, which further allowed us to explore the effect of dolomitization on the isotopic composition of the carbonate strata.

In the Ol Fm, in addition to preserving abundant secondary carbonate veins, dolomitization accompanied the remobilization of barite. At South Khukh Davaa (Figure 4.2C), in stratigraphic section F875 (Figure 4.4), below the < 20 cm thick bedded barite, barite veins are common. Petrographic observations of some of the veins (figures 4.9A, 4.9B, 4.9D, and 4.9F) display multiple generations of crystal growth but are composed of dolomite. Similar veins are found in underlying Taishir Fm (Figure 4.9E) and are also composed of dolomite.

Where exposed, the basal Shuurgat Fm, Sh1, is composed of limestone. It is composed of fine- to medium-bedded lime-micrite interbedded with marly shale and calcisiltite (Figure 4.6). The rest of the Shuurgat Fm is dominated by dolostone (figures 4.3K-M) except Sh3-4 exposed and preserved in Khunkher and Tsagaan gorges (Bold et al., 2016). The limestone Sh1 is nicely exposed in the Khongor Range (figures 4.2A and 4.6); however, the transition from limestone to dolostone is impeded by a small

fault and a few meters of non-exposure. In the Khongor Range, Sh2, Sh3 and Sh4 are all pervasively dolomitized. In contrast, at Khunkher Gorge (figures 4.2D and 4.6) Sh3 and Sh4 are preserved predominantly as limestone and sits on a karstic unconformity present at the top of Sh2 (Bold et al., 2016). Sh2 is distinguished by its common zebra dolomite texture and although it is a useful map unit, it may not represent a correlative sequence stratigraphic unit and may include some of Sh1 or Sh3 at other localities.

Silicification is common in dolomitized carbonate of the Taishir, Ol, and Shuurgat fms. It is prevalent in the upper portion of T3 of the Taishir Fm (Figure 4.4) and displayed in silicified ooids that are resistant to weathering (Figure 4.3I). In the Ol Fm, dolomitized aragonite fans in the Ol Fm are also silicified. Dolomitized Sh3-4 carbonates preserve both primary chert nodules and lenticular beds that are sometimes bedded to lenticular and secondary silicification seams (Figure 4.3M). Karsted surfaces present above Sh2 in Khunkher Gorge (Figure 4.1) and at the top of the Shuurgat Fm are also silicified.

4.3.2. Texture and petrography

An array of paragenetic and diagenetic textures is preserved in dolomitized carbonates (figures 4.9 and 4.10). As mentioned above, texture retentive dolomitization (figures 4.3F and 4.3L) is present in all three formations affected by dolomitization, but particularly in the Taishir Fm, laterally these textures grade into brecciated, fabric destructive dolomite (figures 4.3E and 4.3G) with abundant secondary carbonate veins (Figure 4.9). Dolostones are described as fabric-retentive if primary bedding is visible and composed of fine-crystalline dolomite (figures 4.9H, 4.10F, and 4.10G). Fabric retentive dolostones of the Taishir Fm are best observed in northern Bayan Gorge (Figure 4.3F) where the basal T3 is preserved as dolostone. Fabric is also retained in the Ol cap dolostone (Figure 4.8C) although secondary carbonate veins are common where the underlying strata are the most altered (figures 4.8B and 4.8G).

Where primary fabrics are destroyed, bedding is no longer visible. Instead carbonates are brecciated (figures 4.3E and 4.3G), extensively veined (Figure 4.3J), coarse-crystalline (Figure 4.3I), vuggy (Figure 4.7E), sugary (Figure 4.7G), and sometimes form zebra dolomite (figures 4.3H and 4.3K;

Vandeginste et al., 2005). The sequence of fabric destruction is nicely demonstrated in transitional zones from limestone to dolostone at South Khukh Davaa (Figure 4.3G) where primary textures can be observed from relict limestone. In the upper T3, as dolomitization becomes pervasive, dolostone successions get massively recrystallized and in extreme cases, formed brecciated carbonate (Figure 4.3E) and zebra dolomite (Figure 4.3H; Vandeginste et al., 2005). These are not common in the upper Ol Fm dolostone. Secondary carbonate veins and coarse-crystalline dolomite are the main feature of dolomitized upper Ol Fm.

In Member Sh2 (Figure 4.3K) and upper Sh3-4 (figures 4.3L and 4.3M), fabric retentive dolomitization is common although zebra dolomites are present (Figure 4.3K). Coarse crystalline dolomites are prevalent in massively bedded units of the Shuurgat Fm but vuggy and brecciated textures are almost absent. Nicely preserved thin-bedded dolo-micrite of Sh2, ooid dolo-grainstone of Sh3, and thin- to medium-bedded dolo-micrite and nodular bedded dolostone are characteristic of the Shuurgat Fm dolostones.

Microscopic textures of the Taishir Fm vary from fine-coarse crystalline and subhedral-euhedral dolomite, often associated with variable $\delta^{13}C_{carb}$ values (Section 4.3), to nonplanar, fine crystalline, and anhedral limestone, which preserves the least-altered $\delta^{13}C_{carb}$ values (Figure 4.9). Limestone textures are well-preserved in thin sections of the lower T3 thin-bedded lime-micrite sampled at the Taishir locality (Figure 4.10A), whereas the partially dolomitized (figures 4.10B, 4.10C, 4.10D, 4.10E, 4.9C, and 4.9H) and completely dolomitized (figures 4.9E, 4.9G, 4.10F, 4.10G, and 4.10I) textures are best illustrated in samples from Ol Mountain and northern Bayan Gorge localities.

Carbonate staining of the T3 thin-bedded lime-micrite (Figure 4.10A) reveals that these strata are composed of pure limestone with nonplanar anhedral to subhedral crystals. However, as these strata are partially dolomitized along strike, the abundance of limestone decreases and is irregularly dolomitized, which is illustrated in partially dolomitized Taishir Fm sequences of Ol Mountain and northern Bayan Gorge (figures 4.10B–E). Predictably, the completely dolomitized carbonates at the top of the dolomitized Taishir (figures 4.10F-G, and I) and Ol (Figure 4.10H) fms reveal no change in color when stained.

Saddle dolomite (Radke and Mathis, 1980) that is characteristic of a burial dolomitization regime is not common in the dolomitized carbonates of both Taishir and Ol fms but is preserved at the top of the Taishir Fm at Ol Mountain (Figure 4.10I).

4.3.3. $\delta^{13}C$ and $\delta^{18}O$ results

At the Taishir locality (stratigraphic sections U1108 and F860, Figure 4.4), where the carbonates are preserved primarily as limestone, with the exception of partially dolomitized interval in the middle of upper T3 (stratigraphic heights of 75-125 m, Figure 4.3D) and the Marinoan cap dolostone, the Taishir (> -6‰) and Maieberg (> -5.8‰) excursions are well-expressed and preserved. Similarly, the prolonged positive $\delta^{13}C_{carb}$ values (~ +10‰) recorded above the Taishir negative excursion is well-preserved. At Ol Mountain (stratigraphic sections U1111-12, Figure 4.4), where the uppermost Taishir Fm and the Ol Fm carbonates are dolomitized, the prolonged positive $\delta^{13}C_{carb}$ values reach up to +5‰, which is significantly lower compared to the ~ +10‰ values recorded in equivalent limestone strata at the Taishir locality. In addition, at Ol Mountain, the Maieberg excursion is no longer present in the Ol Fm carbonates. $\delta^{13}C_{carb}$ values start at -2‰ and reach +4‰. In terms of the third parallel section measured at northern Bayan Gorge (stratigraphic sections U1115-17 and U1113, figures 4.4 and 4.3F), where the entire Member T3 (including the Taishir excursion) and the Ol Fm carbonates are dolomitized, the Taishir excursion is barely seen (> -2‰) and the overlying dolomitized carbonate of the upper T3, which should have recorded extended periods of high $\delta^{13}C_{carb}$ values, records $\delta^{13}C_{carb}$ values up to +3‰. The $\delta^{13}C_{carb}$ values of the Ol Fm are similar to the values measured in Ol Mountain and instead of having a pronounced negative anomaly, the values reach ~ +4‰.

In the Tsakhir Range (stratigraphic sections U1241 and M12016, Figure 4.4), because the lower members of the Taishir Fm are partially dolomitized, the effect of progressive dolomitization was documented in detail. Although the carbonate strata that preserved the Taishir excursion is dolomitized, the nadir of the excursion reaches only ~ -2‰ (Figure 4.4). The overlying carbonate strata that are preserved as limestone record a thick succession of high $\delta^{13}C_{carb}$ values, as high as +11‰, but the values

decrease to ~ +4‰ in dolomitized carbonates within the same interval. Interestingly, the Ol Fm carbonates record only positive $\delta^{13}C_{carb}$ values except at the base where values of ~ -0.5‰ preserved. On average, $\delta^{13}C_{carb}$ of the Ol Fm are ~ +2‰. At South Khukh Davaa, the Taishir Fm is dolomitized and the upper T3 record $\delta^{13}C_{carb}$ values of +6‰ (Bold et al., 2016). Carbon isotope values of the Marinoan cap dolostone start negative at ~ -1.5‰ and increase to > +7.2‰ (Figure 4.4).

At Khongor Range, upper Ol Fm and basal Shuurgat Fm (Sh1) are composed of limestone. Maieberg negative $\delta^{13}C_{carb}$ excursion is present (figures 4.2A and 4.6) in the Ol Fm and the values stay negative in the Sh1 but return to ~ +2‰ in dolostone succession of the lower Shuurgat Fm (Figure 4.3K). The rest of the Shuurgat Fm is composed of dolostone and $\delta^{13}C_{carb}$ values stay at ~ +2.96‰ with a minimum at -0.81‰ and maximum at +5.17‰ (figures 4.3L and 4.3M). This signature changes to less enriched values of +1‰ in the basal Zuun-Arts Fm (Smith et al., 2015).

At Khunkher Gorge (Figure 4.6), the exposed Ol Fm is dolomitized and $\delta^{13}C_{carb}$ values of Maieberg excursion reach as negative as -4‰. Above the fault, values stay at ~ +3‰ in the Sh2. However, in Sh3-4, limestone successions preserve very positive values that reach +10‰ while the values return to +3‰ in the dolomitized succession in the middle. Similar to the Khongor Range section, values drop to +1‰ at the top of the Shuurgat Fm and continue through the base of the Zuun-Arts Fm.

In all of the measured sections, the $\delta^{13}C_{carb}$ and $\delta^{18}O$ do not covary systematically (Table 4.A1) except for the Ol Fm sections measured at Khongor Range, Ol Mountain and northern Bayan Gorge localities and Shuurgat Fm at Khongor Range. Corresponding stratigraphy is illustrated in figures 4 and 6 with associated $\delta^{13}C_{carb}$ and $\delta^{18}O$ data. Vertical scale is exaggerated in the illustration of the Ol Fm than the Taishir Fm to highlight sedimentological and stratigraphic features in detail.

Greater than 2‰ variability is thought to be uncommon in co-existing calcite and dolomite (Degens and Epstein, 1964). However, in our partially dolomitized sections, > 2‰ variability in $\delta^{13}C_{carb}$ within hand samples is common. This variability decreases in completely dolomitized carbonates of both the Taishir (Figure 4.7) and Ol (Figure 4.8) fms. > 2‰ variability is present at stratigraphic heights of 75, 80, 82, 83, and 117 m in section U1108 and 29 m in section F860 at Taishir locality and 60.5, 63, 94, 96,

and 106 m in section U1111 and 20.2 m in section U1112 at Ol Mountain. It is also present at stratigraphic height of 188 m in section U1117 in northern Bayan Gorge and 143, 219, 227, and 238 in section U1241 and 1 m in M12016 in Tsakhir Range.

The largest isotopic variability in Member T3 of Taishir Fm is preserved in sample U1108-80 m (Figure 4.7C), which is a partially dolomitized carbonate with $\delta^{13}C_{carb}$ values ranging between +9.27‰ to +5.01‰ in a single hand sample. The most positive value is associated with dark grey lime-micrite whereas the values in coarser crystalline textures become lighter. In terms of completely dolomitized T3 carbonate, the most variable values were preserved in sample U1117-106 m (Figure 4.7G) sampled in northern Bayan Gorge, where they ranged from +5.47‰ to +2.68‰. The lightest value is also associated with coarse-crystalline dolostone, which is sugary in texture. This relationship is supported by petrographic observations of dolomitized carbonates (Figure 4.7). For instance, the heaviest $\delta^{13}C_{carb}$ value of 0.73‰, measured in sample U1111-94 m (Figure 4.7H), is obtained from medium-coarse crystalline and subhedral dolomite, while the fine-crystalline, anhedral, and micritic dolomite preserved a value of 3.12‰. A different view of the same sample is shown in Figure 7E where only medium-coarse crystalline and subhedral-euhedral dolomite texture is displayed with a preserved $\delta^{13}C_{carb}$ value of 1.75‰. Moreover, petrographic observation of sample U1111-71 m equally revealed two different textures, fine-crystalline and anhedral and medium-coarse crystalline and subhedral (Figure 4.9H), where lighter $\delta^{13}C_{carb}$ value is associated with coarser crystalline texture.

Only two samples of the Ol cap dolostone displayed variability of > 2‰ (Figure 4.8). In sample U1112-20.2 m (Figure 4.8C), in the same hand sample, $\delta^{13}C_{carb}$ ranged from -2.75‰ to -0.76‰ and in M12016-1 m, the values ranged from -1.16‰ to 2.46‰. Macro-textures do not vary except color distinction between individual laminae. Additionally, a sample analyzed from upper Ol Fm limestone in section F860 at stratigraphic height of 29 m yielded > 2‰ variability that ranged from -4.24‰ to -1.82‰.

4.3.4. Signatures in the elemental concentration

Concentrations of Mn and Sr differ between limestone dominated and dolomitized sections (Figure 4.5) of the Taishir and Ol fms and stratigraphic patterns are preserved within each measured section. As a whole, the Taishir Fm limestone has high concentration of Sr, which ranges from 320 ppm to 3405 ppm. The sequence that hosts the Taishir excursion and the overlying fetid limestone sequence reach 2286 ppm in Sr concentration. Sr concentration decreases in partially dolomitized interval in middle T3 of the Taishir Fm and increases back in the uppermost lime-grainstone and ooid lime-grainstone sequence of the T3. As expected, Sr levels are low in the dolomitized carbonates of the Taishir Fm (stratigraphic sections measured in Ol Mountain, northern Bayan Gorge, and Tsakhir Range) and reach maximum of 267 ppm.

Mn concentration of the dolomitized Taishir Fm ranges between 10 ppm and 561 ppm, which is at least ~ 10 ppm higher than limestones of the Taishir Fm except in the basal lime-micrite sequence that preserves the Taishir excursion. Interestingly, Mn levels in the dolomitized carbonates gradually increase in the uppermost T3 from 51 ppm to 561 ppm. Conversely, Mn concentration in the Ol Fm cap dolostone measured at Taishir locality is higher than cap dolostone sequence measured at northern Bayan Gorge locality. Mn concentrations begin at 205 ppm and increase to as much as 570 ppm. A similar increase is present in U1113 with concentrations that start at 182 ppm and increase to 529 ppm with three extremely enriched samples that range from 1668 ppm to 4757 ppm. In the rest of the Ol Fm, the concentration averages ~ 43 ppm.

Sr concentrations in the Shuurgat Fm dolostones (Figure 4.6) are low with an average at 102 ppm that range from 0.44 ppm and 534.92 ppm. Only two samples yield > 400 ppm concentration. Mn concentrations range from 9 ppm to 665 ppm with an average at 91 ppm. The highest concentration is measured in Sh3 and represented by one sample at 665 ppm.

Based on Sr and Ca concentrations (Figure 4.5) of the Taishir, Ol, and Shuurgat fms, the Sr/Ca molar ratios (Veizer, 1983) of the dolomitizing fluids were calculated (Table 4.A4) and compared with the modern seawater value of 0.0086. Sr/Ca ratios were calculated using minimum suggested value of

0.015 for distribution coefficient of strontium between fluid and dolomite (Azmy et al., 2009). The Sr/Ca molar ratio for the Ol cap dolostone at Taishir is 0.0141, whereas the cap dolostones within the larger dolomitization fronts (sampled in stratigraphic sections U1112 and U1113) is 0.0045. The latter is similar to dolomitized Taishir Fm, which yielded a, Sr/Ca ratio of 0.0050. This ratio increases in the Shuurgat Fm and become 0.0086.

4.3.5. Fluid inclusion results

A total of 186 fluid inclusions (Table 4.A3) were measured in dolostone and limestone samples of the Taishir and Ol fms sampled at Taishir, Ol Mountain, and northern Bayan Gorge localities. Fluid inclusions in carbonates were classified as liquid (L) or vapor (V) inclusions based on their phase relationships at room temperature. Three main types of fluid inclusions were recognized under microscope and their basic features are described below (Figure 4.11).

Liquid-rich inclusions (type - I) are the most abundant type. They are randomly distributed, colorless, and consist of liquid and vapor phases (two phases, L > V). Shape wise, they are irregular to rounded and up to 5 μm in length, although most are < 3 μm long (no thermometric data was obtained on fluid inclusions < 2 μm long) and phase ratios by volume % range are from L70-90:V30-10. Liquid inclusions were scattered along seams of secondary quartz or formed clusters of inclusions within secondary quartz (figures 4.11A and B). Liquid fluid inclusions (type - II) were also abundant. They have regular shapes, but occasionally exhibit necking-down phenomena. Size ranges from several microns to 8 μm (Figure 4.11C). Finally, CO_2 inclusions (type - III) (VCO_2) are found in dolostone and limestone samples but are not common. They are relatively regular in shape and black in color. T_h of each phase of type - III inclusions were not measured as these are difficult to interpret (Figure 4.11D).

T_h in non-dolomitized limestone of the Taishir Fm ranges between 70° C to 194° C with salinity estimates at 17-29 wt. %, which are similar to values preserved in dolomitized Taishir Fm carbonates (61-187° C and 5-34 wt. % respectively). At the Taishir locality, T_h of the Ol cap dolostone varies between 71° C to 148° C with a salinity of 1-27 wt. %, whereas at Ol Mountain T_h varies from 69° C to 159° C with a

salinity of 21-27 wt. %, and at northern Bayan Gorge T_h varies from 82° C to 151° C with a salinity of 21-26 wt. %. Fluid inclusions of dolomitized upper Ol Fm carbonates at Ol Mountain and northern Bayan Gorge yielded a T_h between 91° C to 189° C with a salinity of 13-29 wt. %.

4.3.6. Clumped-isotope paleothermometry results

Measured clumped-isotope values and corresponding temperature estimates (Table 4.1) did not reveal systematic variability between limestone dominated and dolomitized successions of the Taishir and Ol fms. $\Delta_{47}T$ (°C) estimates of the Taishir Fm limestones ranged from 125° C to 254° C, whereas the Taishir Fm dolostones ranged from 112° C to 162° C. $\Delta_{47}T$ (°C) of the Ol Fm cap dolostones were between 105° C and 317° C, upper Ol limestone was at 160° C, and upper Ol dolostones were between 116° C and 143° C. Both the limestone and dolostone samples of the Shuurgat Fm yielded higher temperatures and ranged between 352° C and 432° C.

4.4. DISCUSSION

4.4.1. Fidelity of fluid inclusion derived homogenization temperatures of carbonate

The use of T_h and fluid composition of fluid inclusions in carbonates to determine the temperature of dolomitizing fluids is based on the assumption that the temperature and composition has not been later reset (Flügel, 2004). However, there are number of ways to alter fluid inclusion data from carbonates. As described by Goldstein (2001), heterogeneous entrapment of fluid, necking down process of irregularly shaped inclusions, nucleation of a bubble, and thermal re-equilibration of fluid inclusions may yield different T_h and salinity. Thermal re-equilibration is explained via thermal expansion of the liquid that causes internal pressure to increase compared to external confining pressure (Goldstein, 1993). In general, spherical shaped (Bodnar, 2003) and smaller sized fluid inclusions (Burruss, 1987; Lacazette, 1990) are more prone to thermal re-equilibration. In the Taishir and Ol fms, fluid inclusions are mostly irregular in shape, but small in size.

In general, T_h of < 50° C and salinity between fresh water and seawater are assumed to be representative of mixing-zone environment whereas T_h between 82° C and > 165° C and salinity between

12 wt. % and 28 wt. % (NaCl eq.) are characteristic of dolomites formed in hydrothermal environment (Braithwaite and Rizzi, 1997; Luczaj, 2006). All of the measured fluid inclusion temperatures are consistent with formation in a hydrothermal environment, as are the salinities, with the exception of the Ol cap dolostone at the Taishir locality. It is possible that this cap dolostone originally formed as primary dolostone or during mixing zone dolomitization and that all of the temperatures have been later re-equilibrated during burial metamorphism. The high temperatures recorded in fluid inclusions from the Taishir limestones are also suggestive that temperatures were reset during burial metamorphism.

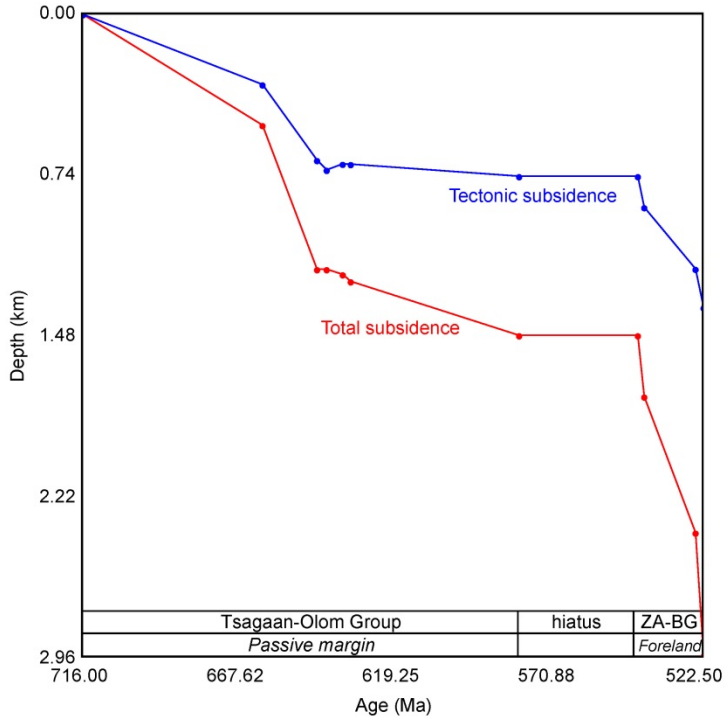

Figure 4.12. Decompaction and backstripping of the Tsagaan-Olom Group and latest Ediacaran and early Cambrian strata exposed and preserved on the Zavkhan Terrane
Subsidence analysis was done using Backstrip v. 4.0 by Nestor Cardozo http://www.ux.uis.no/~nestor/work/programs.html. Backstrip performs 1D Airy backstripping with exponential reduction of porosity, based on Allen and Allen (2013). ZA denotes to the Zuun-Arts Formation and BG to Bayangol Formation (Smith et al., 2015).

However, burial temperatures from subsidence model (Figure 4.12) are low to account for the fluid inclusion temperatures. Instead, it is possible that the fluid inclusions formed during partial dolomitization and that the limestones were saturated with warm fluids during the dolomitization event,

but the fluid flux was lower, limiting pervasive dolomitization. Hence the fluid inclusion temperatures and salinities are more consistent with orogenic/hydrothermal dolomitization.

4.4.2. Use of clumped isotope paleothermometry in diagenetic studies

Clumped isotope paleothermometry has been increasingly used to evaluate diagenesis, paleofluid compositions, and temperatures to interpret geologic history of rocks and fluid flow in the basins related to tectonic, topographic, and structural processes (Huntington and Lechler, 2015). For example, Budd et al. (2013) have used this technique to understand syndepositional fractures in Permian carbonates in Guadalupe Mountains (New Mexico, USA) in association with detailed petrography, fluid inclusion analyses, and stable isotopes to characterize multiple fluid flow events. In order to understand burial diagenetic processes in the Upper Cretaceous Mancos Shale (Colorado, USA), Dale et al. (2014) analyzed carbonate concretions in different shale layers and fracture fills. They demonstrated that shale horizons could act as a barrier to fluid mixing, which shielded carbonate concretions whereas the temperature of the fracture fills were reset to later burial temperature. Recently, burial temperatures of the Nisku Fm (Alberta, Canada) were compared with fluid inclusion and traditional oxygen isotope geothermometry (Millán et al., 2016). In terms of Neoproterozoic carbonates, a clumped-isotope study on secondary calcite veins of the Marinoan cap dolostone in South China yielded temperatures of $> 100^{o}$C, which were interpreted to indicate precipitation under the influence of hydrothermal fluids (Bristow et al., 2011).

For dolomitized carbonates of the Tsagaan-Olom Group, clumped-isotope paleothermometry was used in association with fluid inclusion temperatures to evaluate contrasting models for dolomitization. All of the samples revealed comparable temperature estimates ($> 100^{o}$ C) with fluid inclusion data and further supported importance of high temperature in dolomitization. Interestingly, the Taishir Fm limestone samples preserved higher temperatures than co-existing dolostones, which can be explained through susceptibility of dolomite fabric to subsequent alteration (e.g. Tan and Hudson, 1971).

4.4.3. Orogenic/hydrothermal dolomitization

Sometime after the deposition of the Shuurgat Fm (580 Ma), dolomitization occurred either during or before a foreland basin developed (545-525 Ma) and accommodated ~ 2 km of late Ediacaran and early Cambrian strata (figures 4.12 and 4.13; Smith et al., 2015). Metamorphism and subduction related magmatism in the hinterland between 579 and 537 Ma (Demoux et al., 2009a; Jian et al., 2014) provide evidence for middle Ediacaran orogenesis to the southwest of the Zavkhan Terrane. An analogous setting has been proposed for dolomitization of the Cambro-Ordovician platform in the Canadian Appalachians where enigmatic Early to Middle Ordovician accretionary events drove hot saline fluids along faults and through the platform prior to deposition in the Middle to Late Ordovician foreland basin (Lavoie and Chi, 2010). In the foreland diagenetic zone, orogenesis can trigger carbonate dissolution, dolomitization, and porosity generation in carbonate successions (Heydari, 1997). Due to increased geothermal gradient and nearby heat source from magmatism, hot and saline fluids can migrate upwards through faults (Davies and Smith Jr, 2006) and laterally through permeable units.

Saddle, zebra, and fabric destructive dolomite textures within the Taishir, Ol, and Shuurgat fms are suggestive of high temperature and focused fluid flow. Orogenic dolomitization is further supported by enrichment of Mn in dolomitized successions in the Zavkhan Terrane (Figure 4.5), which is favored in deeply buried fluids with reducing condition (Warren, 2000).

The low Sr/Ca ratio of the Taishir and Ol fms within the dolomitizaiton front compared to modern seawater is consistent with dolomitization with basinal fluids, which typically have much lower Sr/Ca ratios than seawater (Skougstadt and Horr, 1960). The high Sr/Ca ratio of the fluid responsible for forming cap dolostone at Taishir locality can be explained by increased weathering input after Marinoan deglaciation as is also observed by radiogenic $^{87}Sr/^{86}Sr$ value of 0.7091 preserved in the same dolostone (Liu et al., 2014). Sr/Ca molar ratio of the Shuurgat Fm dolostones similar to present-day seawater is interpreted to reflect either the chemical evolution of the fluid as it migrated through the basin and incorporated more Sr as it dolomitized the Taishir Fm or the influence of more seawater stratigraphically higher in the basin. That is, the composition of the fluid likely evolved during its flow path.

During orogenic fluid flow, Mg^{2+} for dolomitization can be sourced by the incorporation of seawater into the system either through direct incorporation or expulsion from thrusting and pore fluid overpressure (Oliver, 1986). Moreover, the approaching volcanic arc could have provided the additional Mg^{2+} during collision either through weathering of mafic rocks (Siever and Woodford, 1979) or groundwater evolution (Ingebritsen et al., 1992). It is unlikely that the thin shaly intervals in the Tsagaan-Olom Group and underlying Khasagt and Zavkhan Fms contributed the necessary Mg^{2+} for burial dolomitization (Tucker and Wright, 1990).

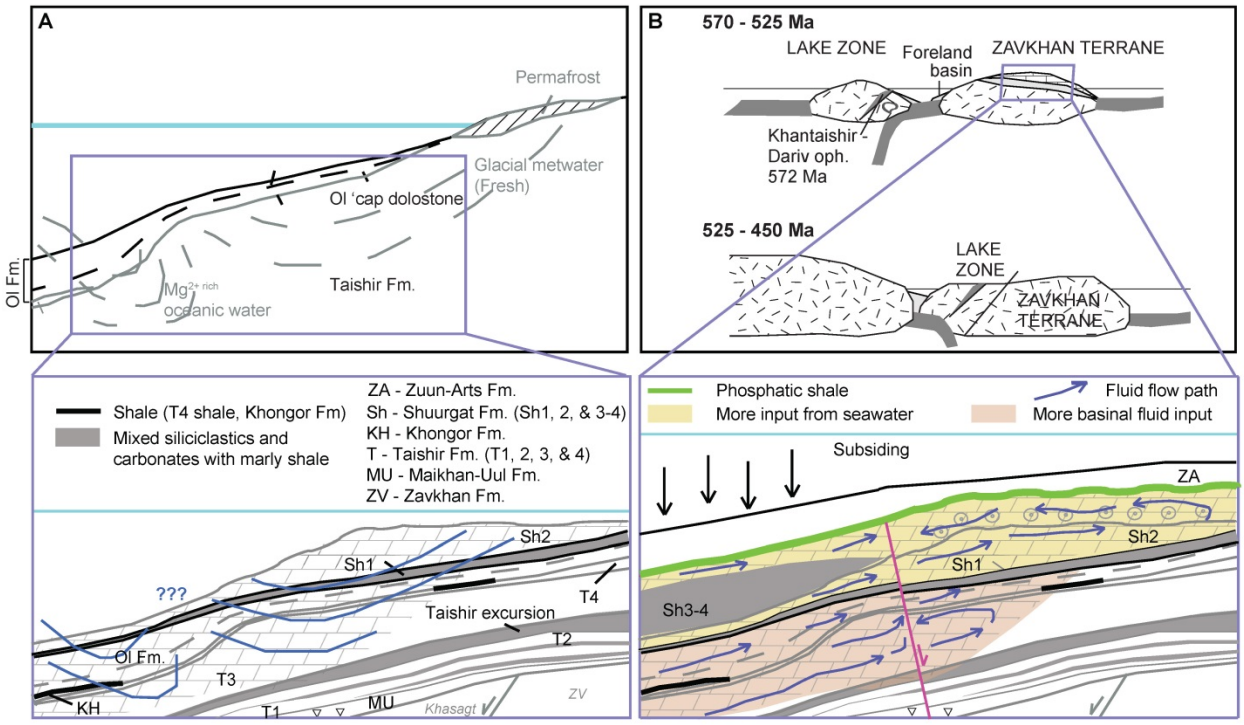

Figure 4.13. Proposed model for dolomitization
A) Potential shallow marine diagenesis responsible for dolomitization of the Ol cap dolostone and possibly parts of the Taishir and Shuurgat formations. B) Orogenic/hydrotectonic dolomitization model proposed for the extent of dolomitization present in the Tsagaan-Olom Group carbonates.

Above the Ol Fm, the basal Shuurgat Fm (Member Sh1) is composed of carbonate strata (when exposed) with interbeds of marly shale and calcisiltite. We suggest that the Sh1 limestone is not dolomitized because it constituted an aquaclude (Figure 4.13B), and the distribution of early dolomitization and overlying shale and calcisiltite represents the stratigraphic control on the flow of dolomitizing fluids rather than a temporal separation of multiple dolomitization events. The latter is

supported by high fluid inclusion temperatures, well above predicted burial temperatures (figures 4.12 and 4.13), and fabric destructive textures in the Taishir, upper Ol, and Shuurgat fms that are suggestive of fluids infiltrated after lithification of these carbonates. Similarly, carbonate successions with interbeds of siliciclastic intervals have been documented to have escaped dolomitization in the upper Carboniferous Cantabrian zone carbonates in Spain (Gasparrini et al., 2006), which may have been the case for Sh1 and parts of Sh3-4.

Coexisting limestone and dolostone within members Sh3-4 of the Shuurgat Fm also display $\delta^{13}C$ variability of ~ 4‰ between limestone and dolostone (Figure 4.6; Bold et al., 2016). This further suggests that the dolomitization event that affected both the Taishir and Ol fms was also responsible for the dolomitization of the Shuurgat Fm. Above, the basal Zuun-Arts Fm is composed of microbial dolostone and phosphatic shale (Smith et al., 2015), and is succeeded by Ediacaran and early Cambrian foreland basin deposits including carbonates that are not dolomitized. The phosphatic shale interval may have acted as an aquaclude that sealed the dolomitizing fluid during foreland development (Figure 4.13B). Similarly, a shaly interval that seals dolomitization has been documented on Cordova Embayment Region of northeastern British Columbia (Morrow et al., 2001) and also on the Anticosti platform represented by Macasty shale (Lavoie and Chi, 2010).

Our data suggest that pervasive fluid flow was the primary driver of dolomitization in the Tsagaan-Olom Group and was responsible for diagenetic textures preserved in associated carbonates, variability in geochemical proxies, fluid inclusion, and clumped-isotope paleothermometry. Consequently, we suggest that dolomitization is related to Ediacaran orogenesis and foreland basin formation (Figure 4.13B). However, we do not exclude the possibility of primary to early stage dolomitization for some of the units (Figure 4.13A), likely in shallow marine (e.g. mixing zone) environment, such as the Ol cap dolostone.

4.4.4. The Ol cap dolostone

Due to its distinctive lithological and sedimentological features, significance in Earth history, and vast distribution and occurrence on many continents, the Marinoan cap carbonate (Hoffman, 2011) is one of the best known sedimentary sequences of any age. The lower few meters of this sequence is typically preserved as dolostone, as is the case for the Ol Fm. Dolomite of the Marinoan cap dolostone has been interpreted as primary (Hoffman, 2011), but this is highly debated (Shields, 2005), and has alternatively been interpreted to be of early diagenetic in origin (Fairchild and Spiro, 1987), in part due to the difficulty in synthesizing dolomite under natural conditions in laboratory (Al-Awadi et al., 2009).

Throughout the Zavkhan Terrane, the Marinoan cap dolostone that is present at the base of the Ol Fm is always preserved as dolostone. Fluid inclusion and Sr/Ca ratios from the cap dolostone at Taishir locality suggests that it formed prior to the dolomitization front that affects the geochemistry of both the Taishir and Ol fms at other localities. Primary or early shallow marine dolomitization (Figure 4.13A) has been proposed for the Ol cap dolostone by Liu et al. (2014) based on magnesium and strontium isotope values. This may have been in effect especially during the Marinoan deglaciation as mixing of strong flows of glacial meltwater and strong greenhouse forcing of surface waters initiated Kohout convection (Kohout et al., 1977).

4.4.5. Effect of dolomitization on geochemical proxy records

One of the first studies on isotopic variability of co-existing calcites and dolomites was done by Degens and Epstein (1964) where they showed that < 2‰ variability existed in $\delta^{13}C_{carb}$ while $\delta^{18}O$ values either stayed the same or became greater in dolomites from the precursor calcite. Variable $\delta^{13}C_{carb}$ (+3.4‰ and -1.6‰) and $\delta^{18}O$ (-5.7‰ and -7.4‰) values were reported in saddle dolostone cements in Pennsylvanian limestone (Wojcik et al., 1997) of Cherokee basin of southeastern Kansas, and were interpreted to have been formed by basin-wide fluid flow event with isotopic variability reflecting the proportion of two components, a host limestone with ^{13}C enrichment and fluids with thermally-derived carbon with depleted ^{13}C, varying with changing water to rock ratios. Similarly, a 9‰ difference in

$\delta^{13}C_{carb}$ and 14‰ in $\delta^{18}O$ values were obtained in co-existing calcite and dolomite in a marbleized contact aureole at the southern end of the Last Chance Mountains of Death Valley, California (Roselle et al., 1999). These authors explained this difference as the product of infiltration of magmatic fluids and suggested that fluids became rich with CO_2 from an unknown source.

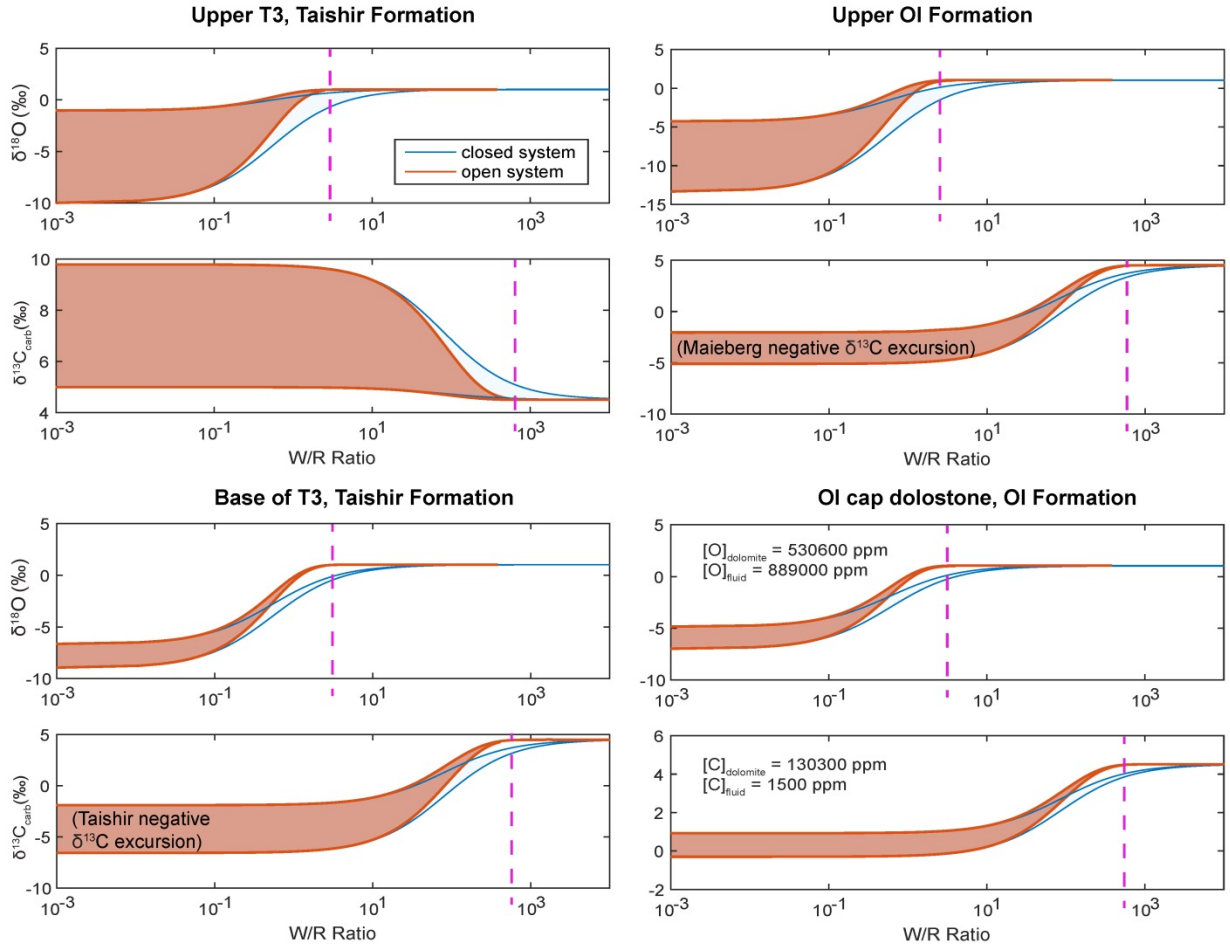

Figure 4.14. Water-rock ratio calculations (Banner and Hanson, 1990; Jacobsen and Kaufman, 1999) required to affect $\delta^{13}C$carb and $\delta^{18}O$ values of a carbonate

Calculations are done for four scenarios, alteration of isotopic values recorded in basal T3 and upper T3 of the Taishir Formation, Ol cap dolostone, and upper Ol Formation. Initial isotopic compositions for the Taishir and Ol formations are derived from stratigraphic sections U1108 and F860 measured at the Taishir locality (Figure 4.4). Groundwater (brine) elemental composition is used where [C] = 1500 ppm and [O] = 889000 ppm (Banner and Hanson, 1990). $[C]_{limestone}$ is 120000 ppm, and $[O]_{limestone}$ is 480000 ppm, which are used in limestone successions of the Taishir and Ol formations. Fractionation factors used for O (Friedman and O'Neil, 1977) is 1.0283 and C (Deines et al., 1974) is 1.0099. $\delta^{13}C$ and $\delta^{18}O$ values of fluid are 3.5‰ and 0‰ respectively. Distribution coefficients used for C and O are 120 and 0.54 (Jacobsen and Kaufman, 1999). Full isotopic reset is denoted by dashed purple line.

In general, $\delta^{13}C_{carb}$ of dolomite is interpreted to preserve initial value of precursor carbonate due to relative insolubility of CO_2 (Land, 1980), which is broadly supported by studies of Cenozoic carbonates, although it is entirely dependent on water to rock ratio at which dolomitization occurs. On the contrary, $\delta^{18}O$ values are expected to change during diagenesis. ^{18}O enrichment in formation waters responsible for dolomitization is usually associated either with evaporative environment or isotopic equilibration with carbonates and silicate minerals in sediments (Murata et al., 1969), whereas more depleted $\delta^{18}O$ values are often ascribed to formation temperature of > 100^{o} C (Warren, 2000).

In Mongolia, $\delta^{18}O$ values are not significantly different in limestone and dolostone sections suggesting that the $\delta^{18}O$ of limestones were reset during the dolomitization event (Figure 4.4). However, $\delta^{13}C_{carb}$ shows great variability between limestone and dolomite successions. Dolomitization homogenized pre-existing $\delta^{13}C_{carb}$ signatures such as the Taishir negative excursion, its overlying prolonged positive values, and the Maieberg negative excursion in the Ol Fm. Differences between individual dolomitized sections could represent the extent of fluid flow or the evolution of the fluid as it reacted with wall-rock along its flow path. High fluid temperatures may have also driven isotopic change (Jones and Xiao, 2005) as well as variability in the initial composition of a mixture of fluids derived from orogenesis, deep basin, and seawater.

A common approach to approximate dolomitizing fluid compositions is to use water-rock interaction calculations (Banner and Hanson, 1990), which is a way to constrain how much fluid is needed to affect isotopic systems in a carbonate rock. Extent of effect depends on initial elemental and isotopic composition of fluid and rock, water-rock distribution coefficient, and water-rock fractionation factor (Jacobsen and Kaufman, 1999) with an assumption that a carbonate rock interacts with fluid at increasing water-rack ratios (Derry, 2010). A simple simulation of this approach is done for Taishir and Ol fms to characterize dolomitizing fluid composition and water-rock ratio that are required to alter primary $\delta^{13}C_{carb}$ and $\delta^{18}O$ preserved in limestone successions to the extent as they are recorded in dolomitized equivalent strata (Figure 4.14). According to these calculations, isotopic variability recorded in co-existing limestone and dolomitized carbonates of the Tsagaan-Olom Group can be explained with a

fluid with $\delta^{13}C_{carb}$ value of +3.5‰ and $\delta^{18}O$ of 0‰, an elemental composition similar to groundwater brine (Banner and Hanson, 1990), and a water-rock ratio of > 10^3 for carbon. A similar ratio was proposed for the Mississipian Burlington-Keokuk dolomites (Banner, 1988) by the same method, which suggests that our estimates are reasonable. However, these calculations do not include any chemical reactions between fluid and rock and predict significant isotopic exchange only at high water-rock ratios (Derry, 2010). Mineralogical change of calcite to form dolomite is also not incorporated, which would involve complex interaction between more elements.

The Cryogenian $\delta^{13}C_{carb}$ profiles from Namibia (Hoffman, 2011), Arctic Alaska (Macdonald et al., 2009), and Mongolia preserve significant differences. The Namibian carbonates of the Rasthof, Gruis, Ombaatjie, and Maieberg fms are dominated by dolomite and record three negative $\delta^{13}C_{carb}$ excursions, namely the Rasthof excursion ($\delta^{13}C_{carb}$ down to -4‰) in the basal Rasthof Formation, the Trezona excursion ($\delta^{13}C_{carb}$ down to -7‰) in the uppermost Ombaatjie Fm, and the Maieberg excursion in the basal Maeiberg Fm (e.g. Halverson et al., 2005). These negative excursions depart from a positive $\delta^{13}C_{carb}$ background of up to +6‰ in the Rasthof Fm and up to +9‰ in the Ombaatjie Fm. The Cryogenian non-glacial interlude of Arctic Alaska is pervasively dolomitized, and preserves the Rasthof excursion, but stratigraphically higher, values are not as enriched as Namibia and instead hover around +5‰ with a downturn at the top that could be correlative with the Trezona excursion (Macdonald et al., 2009a). In Mongolia, limestone-dominated strata the Taishir and Ol fms record the Rasthof and Maieberg excursions along with another negative $\delta^{13}C_{carb}$ excursion referred to as the Taishir excursion ($\delta^{13}C_{carb}$ down to -8‰, Figure 4.1), which is interpreted to not be correlative with the Trezona excursion (Bold et al., 2016). The initial downturn of the Trezona excursion is potentially preserved at the top of the Taishir Fm, but much of it is absent, perhaps due to sub-glacial erosion (Bold et al., 2016). Moreover, background $\delta^{13}C_{carb}$ values from limestone in Mongolia are more isotopically enriched than dolomitized records of Namibia and Arctic Alaska.

Similarly, in Mongolia, dolomitized sections are isotopically homogenized and $\delta^{13}C_{carb}$ profiles resemble those from Arctic Alaska. Dolomitization appears to dampen Cryogenian $\delta^{13}C_{carb}$ variability.

Depending on where the stratigraphic section is measured on the Zavkhan Terrane, 8-10‰ variability is present in $\delta^{13}C_{carb}$. These differences are larger than any of the values proposed for diagenetic alteration. We suggest that this apparent variability is in part due to the extreme $\delta^{13}C_{carb}$ fluctuations in Neoproterozoic seawater (Halverson et al., 2010). These fluctuations are much greater than those in Phanerozoic oceans (Veizer et al., 1999). If dolomitizing fluids have values that average ~ 0‰ and alter rocks that have little isotopic variability to begin with, the effect of dolomitizing fluids on $\delta^{13}C_{carb}$ values will be less apparent.

4.4.6. Isotopic variability in basal Ediacaran cap dolostones

One of the distinguishing characteristics of Marinoan cap carbonate sequence is the $\delta^{13}C_{carb}$ signature that reaches values as negative as -6‰ (Halverson et al., 2005). The most negative values are often associated with carbonates that formed during maximum flooding and highstand system tracts, which is the same for the Ol Fm where the most negative values are in limestone of the middle and upper portions of the formation (Bold et al., 2016).

Variable $\delta^{13}C_{carb}$ values have been reported in Keilberg Member (cap dolostone) of Tsumeb Subgroup of Otavi Platform of Namibia (Hoffman, 2011) between inner platform and outer platform sections. The variability was < 2‰ and values became progressively less negative towards outer platform. This apparent gradient has been related to secular seawater temperature change during diachronous deposition in the glacioeustatic transgression (Hoffman, 2011).

Similarly, in the Ol cap dolostone, large lateral $\delta^{13}C_{carb}$ variability is present between sections but we suggest that it is related to dolomitization. In general, where the underlying Taishir Fm is more dolomitized, the overlying cap dolostone is more isotopically enriched (Figure 4.4). The largest variability in $\delta^{13}C_{carb}$ is recorded in the dolomitized carbonates of the upper Ol Fm (stratigraphic section F875), where there is an extreme positive value of +7.28‰ recorded, while the limestone equivalent strata at Taishir locality (stratigraphic section F860) recorded the Maieberg negative excursion with a nadir at -5.11‰. In all of the samples of the Ol cap dolostone, including F860 (stratigraphic section measured at a

locality where no apparent late dolomitization is documented in the Ol Fm), where different macro-textures were analyzed for isotope variability, close to 2‰ differences have been measured (figures 4.8C, E, and G). Considering < 2‰ variability within a hand sample of F860-3.4 m, one may suggest that this dolomite is a product of diagenesis, however it is possible that the cap dolostone was deposited as a primary dolomite or early dolomitization (Figure 4.13A) and then also strongly altered by later dolomitizing fluids (Figure 4.13B).

In the Ol cap dolostone, it is difficult to envoke diachronous deposition as an explanation for the $\delta^{13}C_{carb}$ variability because the Taishir, Ol Mountain and northern Bayan Gorge localities are located along depositional strike with no apparent facies change between them (figures 4.2 and 4.4). Instead, a later dolomitizing fluid (Figure 4.13B) affected its initial $\delta^{13}C_{carb}$ and $\delta^{18}O$ signatures as it dolomitized and altered isotopic composition of the upper Taishir and the whole Ol Fm carbonates. As a result, the late-stage (Figure 4.13B) dolomitized carbonates of the Taishir and Ol fms record significantly different $\delta^{13}C_{carb}$ values from the earlier phases yielding an apparent isotopic gradient.

4.5. CONCLUSIONS

The Neoproterozoic Tsagaan-Olom Group exposed in the Zavkhan Terrane of southwestern Mongolia hosts coexisting limestone and dolostone successions that span later Cryogenian and earliest Ediacaran. The $\delta^{13}C_{carb}$ values of the dolomitized strata vary significantly from limestone strata that have recorded near primary seawater $\delta^{13}C_{carb}$ signature (Johnston et al., 2012). Along strike, variability of ~ 8‰ in $\delta^{13}C_{carb}$ is preserved between limestone-dominated and dolomitized carbonate successions of the Taishir and Ol fms. The Ol cap dolostone is always preserved as dolostone on the Zavkhan Terrane; however, variable $\delta^{13}C_{carb}$ values are preserved between the Ol cap dolostone at sections where the bounding strata is limestone, and other localities where both underlying Taishir and rest of the Ol Fm carbonates are affected by dolomitization. Map relationships, petrography, geochemistry, fluid inclusions, and clumped-isotopes suggest dolomitization was driven by an Ediacaran orogenic fluid. In general, the $\delta^{13}C_{carb}$ values of the Ol cap dolostone are heavier with progressive dolomitization whereas limestone of

the Taishir Fm becomes lighter, with the exception of the interval that hosts the Taishir excursion. According to calculations after Banner and Hanson (1990); Jacobsen and Kaufman (1999), isotopic variability recorded in co-existing limestone and dolomitized carbonates of the Tsagaan-Olom Group can be accommodated with a fluid with $\delta^{13}C_{carb}$ value of +3.5‰ and $\delta^{18}O$ of 0‰ and a water-rock ratio of > 10^3 for carbon. Although dolomitization broadly resulted in isotopic homogenization to $\delta^{13}C_{carb}$ values near +3.5‰, significant variability is present along strike. These differences may be due in part to focused fluid flow and differential water-rock ratios, but also, the composition of the fluids likely evolved along their flow paths. These results caution against the interpretation of lateral differences in $\delta^{13}C_{carb}$ between dolomitized sections or localities to represent isotopic gradients in seawater.

4.6. ACKNOWLEDGMENTS

We would like to thank the MIT node of the NASA Astrobiology Institute and NASA Astrobiology grant NNH10ZDA001N-EXO for support. We would also like to thank Greg Eischeid and Sarah Manley for help in the laboratory to collect carbon and oxygen isotopes and clumped-isotope paleothermometry data; Elizabeth Lundstrom for help in the laboratory to collect elemental concentration data; Anne-Sofie Crüger Ahm for insightful comments and discussion.

4.7. REFERENCES

Abbot, D. S., Voigt, A., and Koll, D., 2011, The Jormungand global climate state and implications for Neoproterozoic glaciations: Journal of Geophysical Research, v. 116, no. D18103.

Aharon, P., 1988, Oxygen, carbon and U-seriew isotopes of aragonites from Vestfold Hills Antarctica: clues to geochemical processes in subglacial environments: Geochimica et Cosmochimica Acta, v. 52, p. 2231-2331.

Ahr, W. M., 1973, The carbonate ramp: An alternative to the shelf model: Gulf Coast Association of Geological Societies Transactions, v. 23, p. 221-225.

Aitken, J. D., 1991, The Ice Brook Formation and Post-Rapitan, Late Proterozoic glaciation, Mackenzie Mountains, Northwest Territories: Geological Survey of Canada Bulletin, v. 404, p. 1-43.

Al-Awadi, M., Clark, W. J., Moore, W. R., Herron, M., Zhang, T., Zhao, W., Hurley, N., Kho, D., Montaron, B., and Sadooni, F., 2009, Dolomite: perspectives on a perplexing mineral: Oilfield Review, v. 21, no. 3, p. 32-45.

Alekseeva, R., Afanasjeva, G., and Shishkina, G., 2001, Lower and Middle Devonian brachiopods of the Far East of Russia and Mongolia: strophomenids and chonetids: Trudy Palaeontological Institute, Russian Academy of Sciences, v. 281, p. 1-132.

Allen, P. A., and Allen, J. R., 2013, Basin analysis: Principles and application to petroleum play assessment, John Wiley & Sons.

Allen, P. A., and Etienne, J. L., 2008, Sedimentary challenge to Snowball Earth: Nature Geoscience, v. 1, p. 817-926.

Álvaro, J. J., Ahlberg, P., Babcock, L. E., Bordonaro, O. L., Choi, D. K., Cooper, R. A., Ergaliev, G. K., Gapp, I. W., Pour, M. G., and Hughes, N. C., 2013, Global Cambrian trilobite palaeobiogeography assessed using parsimony analysis of endemicity: Geological Society, London, Memoirs, v. 38, no. 1, p. 273-296.

An, Z., Jiang, G., Tong, J., Tian, L., Ye, Q., Song, H., and Song, H., 2015, Stratigraphic position of the Ediacaran Miaohe biota and its constrains on the age of the upper Doushantuo δ 13 C anomaly in the Yangtze Gorges area, South China: Precambrian Research, v. 271, p. 243-253.

Arvidson, R. S., and Mackenzie, F. T., 1999, The dolomite problem; control of precipitation kinetics by temperature and saturation state: American Journal of Science, v. 299, no. 4, p. 257-288.

Atashkin, V. A., 1995, The Cambrian system of the foldbelts of Russia and Mongolia: correlation chart and explanatory notes, International Union of Geological Sciences, v. 32.

Azmy, K., Knight, I., Lavoie, D., and Chi, G., 2009, Origin of dolomites in the Boat Harbour Formation, St. George Group, in western Newfoundland, Canada: implications for porosity development: Bulletin of Canadian Petroleum Geology, v. 57, no. 1, p. 81-104.

Badarch, G., Byamba, J., Mahbadar, Ts., Minjin, Ch., Orolmaa, D., Tomurtogoo, O., and Khosbayar, Ts, 1998, Geological map of Mongolia: Mongolian Academy of Sciences, Mineral Resources Authority of Mongolia.

Badarch, G., Cunningham, W. D., and Windley, B., 2002, A new terrane subdivision for Mongolia: implications for the Phanerozoic crustal growth of Central Asia: Journal of Asian Earth Sciences, v. 21, p. 87-110.

Banner, J. L., 1988, Water-rock interaction history of regionally extensive dolomites of the Burlington-Keokuk Formation (Mississippian): isotopic evidence.

Banner, J. L., 2004, Radiogenic isotopes: systematics and applications to earth surface processes and chemical stratigraphy: Earth-Science Reviews, v. 65, p. 141-194.

Banner, J. L., and Hanson, G. N., 1990, Calculation of simultaneous isotopic and trace element variations during water-rock interaction with application to carbonate diagenesis: Geochimica et Cosmochimica Acta, v. 54, p. 3123-3137.

Benn, D. I., Le Hir, G., Bao, H., Donnadieu, Y., Dumas, C., Fleming, E. J., Hambrey, M. J., McMillan, E. A., Petronis, M. S., and Ramstein, G., 2015, Orbitally forced ice sheet fluctuations during the Marinoan Snowball Earth glaciation: Nature Geoscience, v. 8, no. 9, p. 704-707.

Bezzubetsev, V. V., 1963, On the Precambrian-Cambrian stratigraphy of the Dzabkhan River Basin: Materials on the Geology of MPR, Gostopotekhizdat, v. 1963, p. 29-42.

Blodgett, R. B., Rohr, D. M., and Boucot, A. J., 2002, Paleozoic links among some Alaskan accreted terranes and Siberia based on megafossils, *in* Miller, E. L., Grantz, A., and Klemperer, S. L., eds., Tectonic Evolution of the Bering Shelf--Chukchi Sea--Arctic Margin and Adjacent Landmasses: Boulder, Colorado, Geological Society of America Special Paper 360, p. 273-290.

Bodnar, R. J., 2003, Reequilibration of fluid inclusions: Fluid inclusions: Analysis and interpretation, v. 32, p. 213-230.

Bold, U., Crowley, J. L., Smith, E. F., Sambuu, O., and Macdonald, F. A., in review, Neoproterozoic to early Paleozoic tectonic evolution of the Zavkhan Terrane of Mongolia: Implications for crustal growth in the Central Asian Orogenic Belt: Lithosphere.

Bold, U., Macdonald, F. A., Smith, E. F., Crowly, J. C., Minjin, C., and Dorjnamjaa.D., 2013, Elevating the Neoproterozoic Tsagaan-Olom Formation to a Group: Mongolian Geoscientist, v. 39, p. 5.

Bold, U., Schrag, D. P., Higgins, J. A., Erdenebayar, J., and Macdonald, F. A., in preparation, Effect of dolomitization on isotopic records from Neoproterozoic carbonates in southwestern Mongolia: Geological Society of America Bulletin.

Bold, U., Smith, E. F., Rooney, A. D., Buchwaldt, R., Ramezani, J., Schrag, D. P., and Macdonald, F. A., 2016, Neoproterozoic stratigraphy of the Zavkhan Terrane of Mongolia: The backbone for Cryogenian and Early Ediacaran chemistratigraphic records: American Journal of Science, v. 316, p. 1-63.

Bosak, T., Lahr, D. J. G., Pruss, S. B., Macdonald, F. A., Dalton, L., and Matys, E., 2011a, Agglutinated tests in post-Sturtian cap carbonates of Namibia and Mongolia: Earth and Planetary Science Letters, v. 308, p. 29-40.

Bosak, T., Lahr, D. J. G., Pruss, S. B., Macdonald, F. A., Gooday, A. J., Dalton, L., and Matys, E., 2012, Possible early foraminiferans in post-Sturtian (716-635 Ma) cap carbonates: Geology, v. 40, no. 1, p. 67-70.

Bosak, T., Macdonald, F. A., Lahr, D. J. G., and Matys, E., 2011b, Putative Cryogenian ciliates from Mongolia: Geology, v. 39, no. 12, p. 1123-1126.

Boulton, G. S., 1978, Boulder shapes and grain-size distribution of debris as indicators of transport paths through a glacier and till genesis: Sedimentology, v. 25, p. 773-799.

Boulton, G. S., Dobbie, K. E., and Zatsepin, S., 2001, Sediment deformation beneath glaciers and its coupling to the sublacial hydraulic system: Quaternary International, v. 86, p. 3-28.

Bowring, J., McLean, N., and Bowring, S., 2011, Engineering cyber infrastructure for U-Pb geochronology: Tripoli and U-Pb_Redux: Geochemistry, Geophysics, Geosystems, v. 12, no. 6.

Bowring, S. A., Grotzinger, J. P., Condon, D. J., Ramezani, J., and Newall, M., 2007, Geochronologic constraints on the chronostratigraphic framework of the Neoproterozoic Huqf Supergroup, Sultanate of Oman: American Journal of Science, v. 307, p. 1097-1145.

Braithwaite, C., and Rizzi, G., 1997, The geometry and petrogenesis of hydrothermal dolomites at Navan, Ireland: Sedimentology, v. 44, no. 3, p. 421-440.

Brasier, M. D., Dorjnamjaa, D., and Lindsay, J. F., 1996a, The Neoproterozoic to early Cambrian in southwest Mongolia: an introduction: Geological Magazine, v. 133, no. 4, p. 365-369.

Brasier, M. D., Magaritz, M., Corfield, R., Luo, H., Wu, X., Lin, O., Jiang, Z., Hamdi, B., He, T., and Fraser, A. G., 1990, The carbon- and oxygen-isotope record of the Precambrian-Cambrian boundary interval in China and Iran and their correlation: Geological Magazine, v. 127, p. 319-332.

Brasier, M. D., Shields, G., Kuleshov, V. N., and Zhegallo, E. A., 1996b, Integrated chemo- and biostratigraphic calibration of early animal evolution: Neoproterozoic -early Cambrian of southwest Mongolia: Geological Magazine, v. 133, no. 4, p. 445-485.

Bristow, T. F., Bonifacie, M., Derkowski, A., Eiler, J. M., and Grotzinger, J. P., 2011, A hydrothermal origin for isotopically anomalous cap dolostone cements from south China: Nature, v. 474, no. 7349, p. 68-71.

Brown, D., Ryan, P. D., Afonso, J. C., Boutelier, D., Burg, J., Byrne, T., Calvert, A., Cook, F., DeBari, S., and Dewey, J., 2011, Arc–continent collision: the making of an orogen, Springer.

Buchan, C., Cunningham, D., Windley, B., and Tomurhuu, D., 2001, Structural and lithological characteristics of the Bayankhongor Ophiolite Zone, Central Mongolia: Journal of the Geological Society of London, v. 158, p. 445-460.

Bucholz, C. E., Jagoutz, O., Schmidt, M. W., and Sambuu, O., 2014, Phlogopite-and clinopyroxene-dominated fractional crystallization of an alkaline primitive melt: petrology and mineral chemistry of the Dariv Igneous Complex, Western Mongolia: Contributions to Mineralogy and Petrology, v. 167, no. 4, p. 1-28.

Budd, D. A., Frost, E. L., Huntington, K. W., and Allwardt, P. F., 2013, Syndepositional deformation features in high-relief carbonate platforms: long-lived conduits for diagenetic fluids: Journal of Sedimentary Research, v. 83, no. 1, p. 12-36.

Burashnikov, V. V., 1990, Tectonics of the Urgamal zone, Early Calidonides of western Mongolia [Phd: Russian Academy of Sciences, 25 p.

Burchette, T. P., and Wright, V. P., 1992, Carbonate ramp depositional systems: Sedimentary Geology, v. 79, p. 3-57.

Burruss, R., 1987, Diagenetic palaeotemperatures from aqueous fluid inclusions: re-equilibration of inclusions in carbonate cements by burial heating: Mineralogical Magazine, v. 51, no. 62, p. 477-481.

Byamba, J., 2011, History of geologic study in Mongolia, Ulaanbaatar, Mongolia, Soyombo printing, Stratigraphy.

Calver, C., Crowley, J., Wingate, M., Evans, D., Raub, T., and Schmitz, M., 2013, Globally synchronous Marinoan deglaciation indicated by U-Pb geochronology of the Cottons Breccia, Tasmania, Australia: Geology, v. 41, no. 10, p. 1127-1130.

Calver, C. R., 2000, Isotope stratigraphy of the Ediacaran (Neoproterozoic III) of the Adelaid Rift Complex, Australia, and the overprint of water column stratification: Precambrian Research, v. 100, p. 121-150.

Calver, C. R., Black, L. P., Everard, J. L., and Seymour, D. B., 2004, U-Pb zircon age constraints on late Neoproterozoic glaciation in Tasmania: Geology, v. 32, no. 10, p. 893-896.

Cocks, L., and Torsvik, T. H., 2007, Siberia, the wandering northern terrane, and its changing geography through the Paleozoic: Earth Science Reviews, v. 82, no. 1-2, p. 29-74.

Cohen, P. A., and Macdonald, F. A., 2015, The proterozoic record of eukaryotes: Paleobiology, v. 41, no. 04, p. 610-632.

Cohen, P. A., Macdonald, F. A., Pruss, S., Matys, E., and Bosak, T., 2015, FOSSILS OF PUTATIVE MARINE ALGAE FROM THE CRYOGENIAN GLACIAL INTERLUDE OF MONGOLIA: Palaios, v. 30, no. 3, p. 238-247.

Cole, R. B., and Stewart, B. W., 2009, Continental margin volcanism at sites of spreading ridge subduction: examples from southern Alaska and western California: Tectonophysics, v. 464, no. 1, p. 118-136.

Condon, D. J., and Bowring, S. A., 2011, A user's guide to Neoproterozoic geochronology, *in* Arnaud, E., Halverson, G. P., and Shields-Zhou, G., eds., The Geological Record of Neoproterozoic Glaciations, Volume 36: London, Geological Society, p. 135-149.

Condon, D. J., Zhu, M., Bowring, S. A., Wang, W., Yang, A., and Jin, Y., 2005, U-Pb ages from the Neoproterozoic Doushanto Formation, China: Science, v. 308, p. 95-98.

Creveling, J., Mitrovica, J., Chan, N.-H., Latychev, K., and Matsuyama, I., 2012, Mechanisms for oscillatory true polar wander: Nature, v. 491, no. 7423, p. 244-248.

Cui, H., Kaufman, A. J., Xiao, S., Zhu, M., Zhou, C., and Liu, X.-M., 2015, Redox architecture of an Ediacaran ocean margin: Integrated chemostratigraphic (δ 13 C–δ 34 S–87 Sr/86 Sr–Ce/Ce*) correlation of the Doushantuo Formation, South China: Chemical Geology, v. 405, p. 48-62.

Dale, A., John, C. M., Mozley, P. S., Smalley, P., and Muggeridge, A. H., 2014, Time-capsule concretions: unlocking burial diagenetic processes in the Mancos Shale using carbonate clumped isotopes: Earth and Planetary Science Letters, v. 394, p. 30-37.

Davies, G. R., and Smith Jr, L. B., 2006, Structurally controlled hydrothermal dolomite reservoir facies: An overview: AAPG bulletin, v. 90, no. 11, p. 1641-1690.

Davis, P. T., Briner, J. P., Coulthard, R. D., Finkel, R. W., and Miller, G. H., 2006, Preservation of Arctic landscapes overridden by cold-based ice sheets: Quaternary Research, v. 65, no. 1, p. 156-163.

Degens, E. T., and Epstein, S., 1964, Oxygen and carbon isotope ratios in coexisting calcites and dolomites from recent and ancient sediments: Geochimica et Cosmochimica Acta, v. 28, no. 1, p. 23-44.

Deines, P., Langmuir, D., and Harmon, R. S., 1974, Stable carbon isotope ratios and the existence of a gas phase in the evolution of carbonate ground waters: Geochimica et Cosmochimica Acta, v. 38, no. 7, p. 1147-1164.

Demoux, A., Kroener, A., Badarch, G., Jian, P., Tomurhuu, D., and Wingate, M. T. D., 2009a, Zircon ages from the Baydrag block and the Bayankhongor ophiolite zone: Time constraints on late Neoproterozoic to Cambrian subduction- and accretion-related magmatism in central Mongolia: Journal of Geology, v. 117, p. 377-397.

Demoux, A., Kröner, A., Hegner, E., and Badarch, G., 2009b, Devonian arc-related magmatism in the Tseel terrane of SW Mongolia: chronological and geochemical evidence: Journal of the Geological Society, v. 166, no. 3, p. 459-471.

Demoux, A., Kröner, A., Liu, D., and Badarch, G., 2009c, Precambrian crystalline basement in southern Mongolia as revealed by SHRIMP zircon dating: International Journal of Earth Sciences, v. 98, no. 6, p. 1365-1380.

DePaulo, D. J., and Ingram, B. L., 1985, High-Resolution Stratigraphy with Strontium Isotopes: Science, v. 227, no. 4689, p. 938-941.

Dergunov, A. B., 2001, Tectonics, Magmatism, and Metallogeny of Mongolia, Psychology Press.

Derry, L. A., 2010, A diagenetic origin for the Ediacaran Shuram-Wonoka carbon isotope anomaly: Earth and Planetary Science Letters, v. 294, p. 152-162.

Deynoux, M., 1985, Terrestrial or waterlain glacial diamictites? Three case studies from the Late Precambrian and Late Ordovician glacial drifts in West Africa: Palaeogeography, Palaeoclimatology, Palaeoecology, v. 51, p. 97-141.

Dijkstra, A. H., Brouwer, F. M., Cunningham, W. D., Buchan, C., Badarch, G., and Mason, P. R., 2006, Late Neoproterozoic proto-arc ocean crust in the Dariv Range, Western Mongolia: a supra-subduction zone end-member ophiolite: Journal of the Geological Society, v. 163, no. 2, p. 363-373.

Dobretsov, N. L., and Buslov, M., 2007, Late Cambrian-Ordovician tectonics and geodynamics of Central Asia: Russian Geology and Geophysics, v. 48, no. 1, p. 71-82.

Dobretsov, N. L., Buslov, M. M., and Vernikovsky, V. A., 2003, Neoproterozoic to Early Ordovician evolution of the Paleo-Asian Ocean: implications to the break-up of Rodinia: Gondwana Research, v. 6, no. 2, p. 143-159.

Domack, E., O'Brien, P., Harris, P., Taylor, F., Quilty, P. G., Santis, L. D., and Raker, B., 1998, Late Quaternary sediment facies in Prydz Bay, East Antarctica and their relationship to glacial advance onto the continental shelf: Antarctic Science, v. 10, no. 03, p. 236-246.

Domack, E. W., and Hoffman, P. F., 2011, An ice grounding-line wedge from the Ghaub glaciation (635 Ma) on the distal foreslope of the Otavi carbonate platform, Namibia, and its bearing on the snowball Earth hypothesis: Geological Society of America Bulletin, v. 123, no. 7-8, p. 1448-1477.

Domack, E. W., Jacobson, E. A., Shipp, S., and Anderson, J. B., 1999, Late Pleistocene--Holocene retreat of the West Antarctic Ice-Sheet system in the Ross Sea: Part 2--Sedimentologic and stratigraphic signature: Geological Society of America Bulletin, v. 111, no. 10, p. 1517-1536.

Dorjnamjaa, D., and Enkhbaatar, B., 2011, Classification of flora of the Precambrian and Cambrian periods and their stratigraphic importance, Mongolian Geology and Mineral Resources: Ulaanbaatar, Mongolia, Soyombo printing, p. 12-26.

Dunham, J. B., 1980, Shallow Subsurface Dolomitization of Subtidally Deposited Carbonate Sediments in the Hanson Creek Formanon (Ordovician—Silurian) of Central Nevada.

Edel, J. B., Schulmann, K., Hanžl, P., and Lexa, O., 2014, Palaeomagnetic and structural constraints on 90° anticlockwise rotation in SW Mongolia during the Permo–Triassic: Implications for Altaid oroclinal bending. Preliminary palaeomagnetic results: Journal of Asian Earth Sciences, v. 94, no. 0, p. 157-171.

Erwin, D. H., Laflamme, M., Tweedt, S. M., Sperling, E. A., Pisani, D., and Peterson, K. J., 2011, The Cambrian Conundrum: Early Divergence and Later Ecological Success in the Early History of Animals: Science, v. 334, p. 1091-1097.

Evamy, B., 1963, The application of a chemical staining technique to a study of dedolomitisation: Sedimentology, v. 2, no. 2, p. 164-170.

Evans, D. A. D., Zhuravlev, A. Y., Budney, C. J., and Kirschvink, J. L., 1996, Palaeomagnetism of the Bayan Gol Formation, western Mongolia: Geological Magazine, v. 133, no. 4, p. 487-496.

Fairchild, I. J., and Spiro, B., 1987, Petrological and isotopic implications of some contrasting Late Precambrian carbonates, NE Spitsbergen: Sedimentology, v. 34, no. 6, p. 973-989.

-, 1990, Carbonate minerals in glacial sediments: geochemical clues to palaeoenvironment: Geological Society, London, Special Publications, v. 53, no. 1, p. 201-216.

Fanning, C. M., and Link, P. K., 2008, Age constraints for the Sturtian glaciation: data from the Adelaide Geosyncline, South Australia and Pocatello Formation Idaho, USA: Geological Society of Australia Abstracts, No. 91, Selwyn Symposium 2008, Melbourne, p. 57-62.

Fike, D. A., Grotzinger, J. P., Pratt, L. M., and Summons, R. E., 2006, Oxidation of the Ediacaran Ocean: Nature, v. 444, p. 744-747.

Flügel, E., 2004, Microfacies of carbonate rocks: Analysis, interpretation and application, Berlin, Springer, 976 p.:

Friedman, I., and O'Neil, J. R., 1977, Compilation of stable isotope fractionation factors of geochemical interest, USGPO.

Gasparrini, M., Bechstädt, T., and Boni, M., 2006, Massive hydrothermal dolomites in the southwestern Cantabrian Zone (Spain) and their relation to the Late Variscan evolution: Marine and Petroleum Geology, v. 23, no. 5, p. 543-568.

Gensel, P. G., 2008, The earliest land plants: Annual Review of Ecological and Evolutionary Systems, v. 39, p. 459-477.

Gibson, T., Myrow, P., Macdonald, F., Minjin, C., and Gehrels, G., 2013a, Depositional history, tectonics, and detrital zircon geochronology of Ordovician and Devonian strata in southwestern Mongolia: Geological Society of America Bulletin, v. 125, no. 5-6, p. 877-893.

Gibson, T., Myrow, P., Macdonald, F. A., Minjin, C., and Gehrels, G., 2013b, Depositional history, tectonics, and detrital zircon geochronology of Ordovician and Devonian strata in southwestern Mongolia: Geological Society of America Bulletin, v. 125, no. 5-6, p. 877-893.

Gladkochub, D., Stanevich, A., Mazukabzov, A., Donskaya, T., Pisarevsky, S., Nicoll, G., Motova, Z., and Kornilova, T., 2013, Early evolution of the Paleoasian ocean: LA-ICP-MS dating of detrital zircon from Late Precambrian sequences of the southern margin of the Siberian craton: Russian Geology and Geophysics, v. 54, no. 10, p. 1150-1163.

Glorie, S., De Grave, J., Buslov, M., Zhimulev, F., and Safonova, I. Y., 2014, Detrital zircon provenance of early Palaeozoic sediments at the southwestern margin of the Siberian Craton: Insights from U–Pb geochronology: Journal of Asian Earth Sciences, v. 82, p. 115-123.

Goldring, R., and Jensen, S., 1996, Trace fossils and biofabrics at the Precambrian-Cambrian boundary interval in western Mongolia: Geological Magazine, v. 133, no. 4, p. 403-415.

Goldstein, R. H., 1993, Fluid inclusions as carbonate microfabrics: a petrographic method to determine diagenetic history, Carbonate microfabrics, Springer, p. 279-290.

-, 2001, Fluid inclusions in sedimentary and diagenetic systems: Lithos, v. 55, no. 1, p. 159-193.

Gostin, V. A., McKirdy, D. M., Webster, L. J., and Williams, G. E., 2010, Ediacaran ice-rafting and coeval asteroid impact, South Australia: insights into the terminal Proterozoic environment: Australian Journal of Earth Sciences, v. 57, no. 7, p. 859-869.

Grotzinger, J. P., Fike, D. A., and Fischer, W. W., 2011, Enigmatic origin of the largest-known carbon isotope excursion in Earth's history: Nature Geoscience, v. 4, p. 285-292.

Guy, A., Schulmann, K., Janoušek, V., Štípská, P., Armstrong, R., Belousova, E., Dolgopolova, A., Seltmann, R., Lexa, O., and Jiang, Y., 2015, Geophysical and geochemical nature of relaminated arc-derived lower crust underneath oceanic domain in southern Mongolia: Tectonics, v. 34, no. 5, p. 1030-1053.

Halverson, G. P., 2006, A Neoproterozoic chronology, *in* Xiao, S., and Kaufman, A. J., eds., Neoproterozoic Geobiology and Paleobiology, Volume Topics in Geobiology 27: New York, NY, Springer, p. 231-271.

Halverson, G. P., Dudás, F. O., Maloof, A. C., and Bowring, S. A., 2007, Evolution of the $^{87}Sr/^{86}Sr$ composition of Neoproterozoic Seawater: Palaeogeography Palaeoclimatology Palaeoecology, v. 256, p. 103-129.

Halverson, G. P., Hoffman, P. F., Schrag, D. P., and Kaufman, A. J., 2002, A major perturbation of the carbon cycle before the Ghaub glaciation (Neoproterozoic) in Namibia: prelude to snowball Earth?: Geochemistry, Geophysics, Geosystems, v. 3, no. 6, doi: 10.1029/2001GC000244.

Halverson, G. P., Hoffman, P. F., Schrag, D. P., Maloof, A. C., and Rice, A. H. N., 2005, Toward a Neoproterozoic composite carbon-isotope record: Geological Society of America Bulletin, v. 117, no. 9-10, p. 1181-1207.

Halverson, G. P., Maloof, A. C., and Hoffman, P. F., 2004, The Marinoan glaciation (Neoproterozoic) in northeast Svalbard: Basin Research, v. 16, p. 297-324.

Halverson, G. P., Wade, B. P., Hurtgen, M. T., and Barovich, K. M., 2010, Neoproterozoic Chemostratigraphy: Precambrian Research, v. 182, no. 4, p. 337-350.

Han, Y., Zhao, G., Sun, M., Eizenhöfer, P. R., Hou, W., Zhang, X., Liu, D., Wang, B., and Zhang, G., 2015, Paleozoic accretionary orogenesis in the Paleo-Asian Ocean: Insights from detrital zircons from Silurian to Carboniferous strata at the northwestern margin of the Tarim Craton: Tectonics, v. 34, no. 2, p. 334-351.

Hanzl, P., Schulmann, K., Janousek, V., Lexa, O., Hrdlickova, K., Jiang, Y., Burianek, D., Altanbaatar, B., Ganchuluun, T., and Erban, V., 2016, Making continental crust: origin of Devonian orthogneisses from SE Mongolian Altai: Journal of GEOsciences, v. 61, no. 1, p. 25-50.

Harper, D. A., Rasmussen, C. M., Liljeroth, M., Blodgett, R. B., Candela, Y., Jin, J., Percival, I. G., Rong, J.-y., Villas, E., and Zhan, R.-b., 2013, Biodiversity, biogeography and phylogeography of Ordovician rhynchonelliform brachiopods: Geological Society, London, Memoirs, v. 38, no. 1, p. 127-144.

Heydari, E., 1997, Hydrotectonic models of burial diagenesis in platform carbonates based on formation water geochemistry in North American sedimentary basins.

Higgins, J. A., Fischer, W. W., and Schrag, D. P., 2009, Oxygenation fo the ocean and sediments: Consequeences for the seafloor carbonate factory: Earth and Planetary Science Letters, v. 284, p. 25-33.

Higgins, J. A., and Schrag, D. P., 2006, Beyond methane: towards a theory for the Paleocene–Eocene thermal maximum: Earth and Planetary Science Letters, v. 245, no. 3, p. 523-537.

Hoffman, P. F., 1991, Did the breakout of Laurentia turn Gondwanaland inside-out?: Science, v. 252, no. 5011, p. 1409-1412.

-, 2011, Strange bedfellows: glacial diamictite and cap carbonate from the Marinoan (635 Ma) glaciation in Namibia: Sedimentology, v. 58, p. 57-119.

Hoffman, P. F., and Halverson, G. P., 2008, Otavi Group of the western Northern Platform, the Eastern Kaoko Zone and the western Northern Margin Zone, *in* Miller, R. M., ed., The Geology of Namibia, vol. 2. Handbook of the Geological Survey of Namibia, Volume 2: Windhoek, p. 13.69-13.136.

Hoffman, P. F., Halverson, G. P., Domack, E. W., Husson, J. M., Higgins, J. A., and Schrag, D. P., 2007, Are basal Ediacaran (635 Ma) post-glacial "cap dolostones" diachronous?: Earth and Planetary Science Letters, v. 258, p. 114-131.

Hoffman, P. F., Kaufman, A. J., Halverson, G. P., and Schrag, D. P., 1998, A Neoproterozoic Snowball Earth: Science, v. 281, p. 1342-1346.

Hoffman, P. F., and Li, Z.-X., 2009, A palaeogeographic context for Neoproterozoic glaciations: Palaeogeography Palaeoclimatology Palaeoecology, v. 277, no. 3-4, p. 158-172.

Hoffman, P. F., Macdonald, F. A., and Halverson, G. P., 2011, Chemical sediments associated with Neoproterozoic glaciation: iron formation, cap carbonate, barite and phosphorite, *in* Arnaud, E., Halverson, G. P., and Shields, G., eds., The Geologic Record of Neoproterozoic Glaciations: London, Geological Society of London.

Hoffman, P. F., and Schrag, D. P., 2002, The snowball Earth hypothesis; testing the limits of global change: Terra Nova, v. 14, no. 3, p. 129-155.

Hoffmann, K. H., Condon, D. J., Bowring, S. A., and Crowley, J. L., 2004, U-Pb zircon date from the Neoproterozoic Ghaub Formation, Namibia: Constraints on Marinoan glaciation: Geology, v. 32, p. 817-820.

Hou, H. F., and Boucot, A. J., 1990, the Balkhash-Mongolia-Okhotsk region of the Old World realm: Geological Society, London, Memoir, v. 12, p. 297-303.

Huntington, K. W., and Lechler, A. R., 2015, Carbonate clumped isotope thermometry in continental tectonics: Tectonophysics, v. 647, p. 1-20.

Ilyin, A. V., 1990, Proterozoic supercontinent, its latest Precambrian rifting, breakup, dispersal into smaller continents, and subsidence of their margins: Evidence from Asia: Geology, v. 18, p. 1231-1234.

Ingebritsen, S., Sherrod, D., and Mariner, R., 1992, Rates and patterns of groundwater flow in the Cascade Range volcanic arc, and the effect on subsurface temperatures: Journal of Geophysical Research: Solid Earth (1978–2012), v. 97, no. B4, p. 4599-4627.

Jacobsen, S. B., and Kaufman, A. J., 1999, The Sr, C and O isotopic evolution of Neoproterozoic seawater: Chemical Geology, v. 161, no. 1, p. 37-57.

Jaffey, A., Flynn, K., Glendenin, L., Bentley, W. t., and Essling, A., 1971, Precision measurement of half-lives and specific activities of U 235 and U 238: Physical Review C, v. 4, no. 5, p. 1889.

Jahn, B. M., Litvinovsky, B. A., Zanvilevich, A. N., and Rechow, M., 2009, Peralkaline granitoid magmatism in the Mongolian-Transbaikalian Belt: Evolution, petrogenesis and tectonic significance: Lithos, v. 113, p. 521-539.

Jian, P., Kröner, A., Jahn, B.-m., Windley, B. F., Shi, Y., Zhang, W., Zhang, F., Miao, L., Tomurhuu, D., and Liu, D., 2014, Zircon dating of Neoproterozoic and Cambrian ophiolites in West Mongolia and implications for the timing of orogenic processes in the central part of the Central Asian Orogenic Belt: Earth-Science Reviews, v. 133, p. 62-93.

Jiang, G., Kaufman, A. J., Christie-Blick, N., Zhang, S., and Wu, H., 2007, Carbon isotope variability across the Ediacaran Yangtze platform in South China: Implications for a large surface-to-deep ocean< i> δ</i>< sup> 13</sup> C gradient: Earth and Planetary Science Letters, v. 261, no. 1, p. 303-320.

Johnston, D. T., Macdonald, F. A., Gill, B., Hoffman, P. F., and Schrag, D. P., 2012, Uncovering the Neoproterozoic carbon cycle: Nature, v. 483, p. 320-324.

Jones, C. E., and Jenkyns, H. C., 2001, Seawater strontium isotopes, oceanic anoxic events, and seafloor hydrothermal activity in the Jurassic and Cretaceous: American Journal of Science, v. 301, no. 2, p. 112-149.

Jones, D., 1983, Recognition, Character and Analysis of Tectonostratigraphic Terranes In Western North America: Journal of Geological Education, v. 31, no. 4, p. 295-303.

Jones, G. D., and Xiao, Y., 2005, Dolomitization, anhydrite cementation, and porosity evolution in a reflux system: Insights from reactive transport models: AAPG bulletin, v. 89, no. 5, p. 577-601.

Kaufman, A. J., Hayes, J., Knoll, A. H., and Germs, G. J., 1991, Isotopic compositions of carbonates and organic carbon from upper Proterozoic successions in Namibia: stratigraphic variation and the effects of diagenesis and metamorphism: Precambrian Research, v. 49, no. 3, p. 301-327.

Kaufman, A. J., Jacobsen, S. B., and Knoll, A. H., 1993, The Vendian record of Sr and C isotopic variations in seawater; implications for tectonics and paleoclimate: Earth and Planetary Science Letters, v. 120, no. 3-4, p. 409-430.

Kaufman, A. J., and Knoll, A. H., 1995, Neoproterozoic variations in the C-isotopic composition of seawater; stratigraphic and biogeochemical implications: Neoproterozoic stratigraphy and Earth history, v. 73, no. 1-4, p. 27-49.

Kaufman, A. J., Knoll, A. H., and Narbonne, G. M., 1997, Isotopes, ice ages, and terminal Proterozoic Earth history: Proceedings of the National Academy of Sciences, v. 95, p. 6600-6605.

Keeley, J. A., Link, P. K., Fanning, C. M., and Schmitz, M. D., 2013, Pre- to synglacial rift-related volcanism in the Neoproterozoic (Cryogenian) Pocatello Formation, SE Idaho: New SHRIMP and CA-ID-TIMS constraints: Lithosphere, v. 5, no. 1, p. 128-150.

Kennedy, M., Mrofka, D., and Von Der Borch, C., 2008, Snowball Earth termination by destabilization of equatorial permafrost methane clathrate: Nature, v. 453, no. 7195, p. 642-645.

Khain, E. V., Bibikova, E. V., Kröner, A., Zhuravlev, D. Z., Sklyarov, E. V., Fedotova, A. A., and Kravchenko-Berezhnoy, I. R., 2002, The most ancient ophiolite of the Central Asian fold belt: U–Pb and Pb–Pb zircon ages for the Dunzhugur Complex, Eastern Sayan, Siberia, and geodynamic implications: Earth and Planetary Science Letters, v. 199, no. 3, p. 311-325.

Khain, E. V., Bibikova, E. V., Salnikova, E. B., Kroener, A., Gibsher, A. S., Didenko, A. N., Degtyarev, K. E., and Fedotova, A. A., 2003, The Palaeo-Asian ocean in the Neoproterozoic and early Palaeozoic: new geochronologic data and palaeotectonic reconstructions: Precambrian Research, v. 122, p. 329-358.

Khain, E. V., Neymark, L. A., and Amelin, Y. V., ISOTOPIC-GEOCHRONOLOGICAL STUDY OF THE GRANITES AND GRANITE-GNEISSIS OF THE GARDAN BLOCK THE EASTERN SAYAN RANGE IN SIBERIA BY PB-PB AND U-PB METHODS ON ZIRCONS AND SM-ND METHOD, *in* Proceedings DOKLADY AKADEMII NAUK1995, Volume 342, MEZHDUNARODNAYA KNIGA 39 DIMITROVA UL., 113095 MOSCOW, RUSSIA, p. 776-780.

Khomentovsky, V. V., and Gibsher, A. S., 1996, The Neoproterozoic-Lower Cambrian in northern Govi-Altai, western Mongolia: Regional setting, lithostratigraphy and biostratigraphy: Geological Magazine, v. 133, p. 371-390.

Kilian, T. M., Swanson-Hysell, N. L., Macdonald, F. A., Bold, U., and Crowley, J. L., in preparation, Paleomagnetism of Ordovician-Silurian Teel basalts from the Zavkhan Terrane - Paleogeography of Mongolia during the Paleozoic.

Kirschvink, J. L., 1992, Late Proterozoic low-latitude global glaciation: the snowball earth, *in* Schopf, J. W., and Klein, C., eds., The Proterozoic Biosphere: Cambridge, Cambridge University Press, p. 51-52.

Knauth, P. L., and Kennedy, M. J., 2009, The late Precambrian greening of the Earth: Nature, v. 460, p. 728-732.

Knoll, A. H., Hayes, J. M., Kaufman, A. J., Swett, K., and Lambert, I. B., 1986, Secular variation in carbon isotope ratios from Upper Proterozoic succesions of Svalbard and East Greenland: Nature, v. 321, p. 832-838.

Knoll, A. H., Javaux, E., Hewitt, D., and Cohen, P. A., 2006, Eukaryotic organisms in Proterozoic oceans: Philosophical Transactions of the Royal Society of London B: Biological Sciences, v. 361, no. 1470, p. 1023-1038.

Kohout, F., Henry, H., and Banks, J., 1977, Hydrogeology related to geothermal conditions of the Floridan Plateau: Florida Bureau of Geology Special Publication, no. 21.

Kolodner, K., Avigad, D., McWilliams, M., Wooden, J., Weissbrod, T., and Feinstein, S., 2006, Provenance of north Gondwana Cambrian–Ordovician sandstone: U–Pb SHRIMP dating of detrital zircons from Israel and Jordan: Geological Magazine, v. 143, no. 03, p. 367-391.

Korobov, M., 1980, Biostratigrafiya i miomernye trilobity nizhnego kembriya Mongolii [Biostratigraphy and miomerid trilobites from the Lower Cambrian of Mongolia]. The Joint Soviet-Mongolian Scientific-Research Geological Expedition: The Joint Soviet-Mongolian Scientific-Research Geological Expedition, Transactions, v. 26, p. 5-108.

-, 1989, Lower Cambrian biostratigraphy and polymeroid trilobites of Mongolia: Trans. Joint Soviet–Mongolian Research Expedition [in Russian]. Nauka, Moscow, no. 48, p. 186-192.

Kovach, V., Yarmolyuk, V., Kovalenko, V., Kozlovskyi, A., Kotov, A., and Terent'eva, L., 2011, Composition, sources, and mechanisms of formation of the continental crust of the Lake Zone of the Central Asian Caledonides. II. Geochemical and Nd isotope data: Petrology, v. 19, no. 4, p. 399-425.

Kozakov, I., Kotov, A., Sal'nikova, E., Bibikova, E., Kovach, V., Kirnozova, T., Berezhnaya, N., and Lykhin, D., 1999, Metamorphic age of crystalline complexes of the Tuva-Mongolia Massif: the U-Pb geochronology of granitoids: PETROLOGY C/C OF PETROLOGIIA, v. 7, p. 177-191.

Kozakov, I., Sal'nikova, E., Yarmolyuk, V., Kozlovsky, A., Kovach, V., Azimov, P. Y., Anisimova, I., Lebedev, V., Enjin, G., and Erdenejargal, C., 2012a, Convergent boundaries and related igneous and metamorphic complexes in Caledonides of Central Asia: Geotectonics, v. 46, no. 1, p. 16-36.

Kozakov, I., Yarmolyuk, V., Kovach, V., Bibikova, E., Kirnozova, T., Kozlovskii, A., Plotkina, Y. V., Fugzan, M., Lebedev, V., and Erdenezhargal, C., 2012b, The Early Baikalian crystalline complex in the basement of the Dzabkhan microcontinent of the Early Caledonian orogenic area, Central Asia: Stratigraphy and Geological Correlation, v. 20, no. 3, p. 231-239.

Kozakov, I. K., Yarmolyuk, V. V., Kovach, V. P., Bibikova, E. V., Kirnozova, T. I., Kozlovskii, A. M., Plotkina, Y. V., Fugzan, M. M., Lebedev, V. I., and Erdenezhargal, C., 2012c, The early Baikalian crystalline complex in the basement of the Dzabkhan Microcontinent of teh early Caledonian orogenic area, Central Asia: Stratigraphy and Geological Correlation, v. 20, no. 3, p. 231-239.

Kravchinsky, V. A., Konstantinov, K. M., and Cogne, J.-P., 2001, Palaeomagnetic study of Vendian and Early Cambrian of South Siberia and Central Mongolia: was the Siberian platform assembled at this time?: Precambrian Research, v. 110, p. 61-92.

Kravchinsky, V. A., Sklyarov, E. V., Gladkochub, D. P., and Harbert, W. P., 2010, Paleomagnetism of the Precambrian Eastern Sayan rocks: implications for the Ediacaran–Early Cambrian paleogeography of the Tuva-Mongolian composite terrane: Tectonophysics, v. 486, no. 1, p. 65-80.

Kröner, A., Demoux, A., Zack, T., Rojas-Agramonte, Y., Jian, P., Tomurhuu, D., and Barth, M., 2011, Zircon ages for a felsic volcanic rock and arc-related early Palaeozoic sediments on the margin of the Baydrag microcontinent, central Asian orogenic belt, Mongolia: Journal of Asian Earth Sciences, v. 42, no. 5, p. 1008-1017.

Kröner, A., Kovach, V., Belousova, E., Hegner, E., Armstrong, R., Dolgopolova, A., Seltmann, R., Alexeiev, D., Hoffmann, J., and Wong, J., 2014, Reassessment of continental growth during the accretionary history of the Central Asian Orogenic Belt: Gondwana Research, v. 25, no. 1, p. 103-125.

Kröner, A., Lehmann, J., Schulmann, K., Demoux, A., Lexa, O., Tomurhuu, D., Štípská, P., Liu, D., and Wingate, M. T., 2010, Lithostratigraphic and geochronological constraints on the evolution of the Central Asian Orogenic Belt in SW Mongolia: Early Paleozoic rifting followed by late Paleozoic accretion: American Journal of Science, v. 310, no. 7, p. 523-574.

Kruse, P. D., Gandin, A., Debrenne, F., and Wood, R., 1996, Early Cambrian bioconstructions in the Zavkhan Basin of western Mongolia: Geological Magazine, v. 133, no. 4, p. 429-444.

Kuzmichev, A., Bibikova, E. V., and Zhuravlev, D. Z., 2001, Neoproterozoic (~800 Ma) orogeny in the Tuva-Mongolia Massif (Siberia): island arc-continent collision at the northeast Rodinia margin: Precambrian Research, v. 110, p. 109-126.

Kuzmichev, A., Kroener, A., Hegner, E., Dunyi, L., and Yusheng, W., 2005a, The Shishkhid ophiolite, nothern Mongolia: A key to the reconstruction of a Neoproterozoic island-arc system in central Asia: Precambrian Research, v. 138, p. 125-150.

Kuzmichev, A., Kröner, A., Hegner, E., Dunyi, L., and Yusheng, W., 2005b, The Shishkhid ophiolite, northern Mongolia: a key to the reconstruction of a Neoproterozoic island-arc system in central Asia: Precambrian Research, v. 138, no. 1, p. 125-150.

Kuzmichev, A., and Larionov, A., 2011, The Sarkhoi Group in East Sayan: Neoproterozoic (~ 770–800 Ma) volcanic belt of the Andean type: Russian Geology and Geophysics, v. 52, no. 7, p. 685-700.

Kuzmichev, A., Sklyarov, E., Postnikov, A., and Bibikova, E., 2007, The Oka Belt (Southern Siberia and Northern Mongolia): A Neoproterozoic analog of the Japanese Shimanto Belt?: Island Arc, v. 16, no. 2, p. 224-242.

Lacazette, A., 1990, Application of linear elastic fracture mechanics to the quantitative evaluation of fluid-inclusion decrepitation: Geology, v. 18, no. 8, p. 782-785.

Lamb, M. A., and Badarch, G., 1997, Paleozoic sedimentary basins and volcanic-arc systems of Southern Mongolia: new stratigraphic and sedimentologic constraints: International Geology Review, v. 39, no. 6, p. 542-576.

-, 2001, Paleozoic sedimentary basins and volcanic arc systems of southern Mongolia: new geochemical and petrographic constraints: Geological Society of America Memoirs, v. 194, p. 117-149.

Lan, Z., Li, X., Zhu, M., Chen, Z., Zhang, Q., Li, Q., Lu, D., Liu, Y., and Tang, G., 2014, A rapid and synchronous initiation of the wide spread Cryogenian glaciations: Precambrian Research.

Land, L. S., 1980, The isotopic and trace element geochemistry of dolomite: the state of the art.

Lavoie, D., and Chi, G., 2010, Lower Paleozoic foreland basins in eastern Canada: tectono-thermal events recorded by faults, fluids and hydrothermal dolomites: Bulletin of Canadian Petroleum Geology, v. 58, no. 1, p. 17-35.

Le Heron, D. P., 2012, The Cryogenian record of glaciation and deglaciation in South Australia: Sedimentary Geology, v. 243-244, p. 57-69.

Le Heron, D. P., and Busfield, M. E., 2015, Pulsed iceberg delivery driven by Sturtian ice sheet dynamics: An example from Death Valley, California: Sedimentology.

Le Heron, D. P., Busfield, M. E., and Kamona, F., 2013, An interglacial on snowball Earth? Dynamic ice behaviour revealed in the Chuos Formation, Namibia: Sedimentology, v. 60, p. 411-427.

Le Heron, D. P., Busfield, M. E., and Prave, A. R., 2014, Neoproterozoic ice sheets and olistoliths: multiple glacial cycles in the Kingston Peak Formation, California: Journal of the Geological Society, p. 2013-2130.

Le Heron, D. P., Cox, G. M., Trundley, A. E., and Collins, A. S., 2011, Sea-ice free conditions during the early Cryogenian (Sturt) glaciation, South Australia: Geology, v. 39, p. 31-34.

Lehmann, J., Schulmann, K., Lexa, O., Corsini, M., Kröner, A., Štípská, P., Tomurhuu, D., and Otgonbator, D., 2010, Structural constraints on the evolution of the Central Asian Orogenic Belt in SW Mongolia: American Journal of Science, v. 310, no. 7, p. 575-628.

Letnikova, E., Kuznetsov, A., Vishnevskaya, I., Veshcheva, S., Proshenkin, A., and Geng, H., 2013, The Vendian passive continental margin in the southern Siberian Craton: geochemical and isotopic (Sr, Sm–Nd) evidence and U–Pb dating of detrital zircons by the LA-ICP-MS method: Russian Geology and Geophysics, v. 54, no. 10, p. 1177-1194.

Levashova, N. M., Kalugin, V. M., Gibsher, A. S., Yff, J., Ryabinin, A. B., Meert, J., and Malone, S. J., 2010, The origin of the Baydaric microcontinent, Mongolia: Constraints from paleomagnetism and geochronology: Tectonophysics, v. 485, no. 1-4, p. 306-320.

Li, H., Xu, Y., Huang, X., He, B., Luo, Z., and Yan, B., 2009, Activation of northern margin of the North China Craton in Late Paleozoic: Evidence from U-Pb dating and Hf isotopes of detrital zircons from the Upper Carboniferous Taiyuan Formation in the Ningwu-Jingle basin: Chinese Science Bulletin, v. 54, no. 4, p. 677-686.

Li, Z. X., Bogdanova, S. V., Collins, A. S., Davidson, A., De Waele, B., Ernst, R. E., Fitzsimons, I. C. W., Fuck, R. A., Gladkochub, D. P., Jacobs, J., Karlstrom, K. E., Lu, S., Natapov, L. M., Pease, V., Pisarevsky, S. A., Thrane, K., and Vernikovsky, V., 2008, Assembly, configuration, and break-up history of Rodinia: A synthesis: Precambrian Research, v. 160, no. 1-2, p. 179-210.

Lindsay, J. F., 1989, Depositional controls on glacial facies associations in a basinal setting, Late Proterozoic, Amadeus Basin, central Australia: Palaeogeography, Palaeoclimatology, Palaeoecology, v. 73, p. 205-232.

Lindsay, J. F., Braiser, M. D., Dorjnamjaa, D., Goldring, R., Kruse, P. D., and Wood, R. A., 1996a, Facies and sequence controls on the appearance of the Cambrian biota in southwestern Mongolia: Implications for the Precambrian-Cambrian boundary: Geological Magazine, v. 133, p. 417-428.

Lindsay, J. F., Brasier, M., Shields, G., Khomentovsky, V. V., and Bat-Ireedui, Y. A., 1996b, Glacial facies associations in a Neoproterozoic back-arc setting, Zavkhan Basin, western Mongolia: Geological Magazine, v. 133, no. 4, p. 391-402.

Liu, C., Wang, Z., and Raub, T. D., 2013, Geochemical constraints on the origin of Marinoan cap dolostones from Nuccaleena Formation, South Australia: Chemical Geology, v. 351, p. 95-104.

Liu, C., Wang, Z., Raub, T. D., Macdonald, F. A., and Evans, D. A., 2014, Neoproterozoic cap-dolostone deposition in stratified glacial meltwater plume: Earth and Planetary Science Letters, v. 404, p. 22-32.

Luczaj, J. A., 2006, Evidence against the Dorag (mixing-zone) model for dolomitization along the Wisconsin archA case for hydrothermal diagenesis: AAPG bulletin, v. 90, no. 11, p. 1719-1738.

Ludwig, K. R., 2008, User's manual for Isoplot 3.70: A geochronological Toolkit for Microsoft Excel: Berkeley Geochronology Center Special Publication, v. 4.

Macdonald, F. A., 2011a, The Dzabkhan Platform, *in* E., A., Halverson, G. P., and Shields, G., eds., The geological record of Neoproterozoic glaciations: London, Geological Society of London.

-, 2011b, The Tsagaan Oloom Formation, southwestern Mongolia: Geological Society, London, Memoirs, v. 36, no. 1, p. 331-337.

Macdonald, F. A., and Jones, D. S., 2011, The Khubsugul Basin, *in* E., A., Halverson, G. P., and Shields, G., eds., The geological record of Neoproterozoic glaciations: London, Geological Society of London.

Macdonald, F. A., Jones, D. S., and Schrag, D. P., 2009a, Stratigraphic and tectonic implications of a new glacial diamictite-cap carbonate couplet in southwestern Mongolia: Geology, v. 37, p. 123-126.

Macdonald, F. A., McClelland, W. C., Schrag, D. P., and Macdonald, W. P., 2009, Neoproterozoic glaciation on a carbonate platform margin in Arctic Alaska and the origin of the North Slope subterrane: Geological Society of America Bulletin, v. 121, no. 3-4, p. 448-473.

Macdonald, F. A., McClelland, W. C., Schrag, D. P., and Macdonald, W. P., 2009b, Neoproterozoic glaciation on a carbonate platform margin in Arctic Alaska and the origin of the North Slope subterrane: Geological Society of America Bulletin, v. 121, p. 448-473.

Macdonald, F. A., Ryan-Davis, J., Coish, R., Crowley, J., and Karabinos, P., 2014, A newly identified Gondwanan terrane in the northern Appalachian Mountains: Implications for the Taconic orogeny and closure of the Iapetus Ocean: Geology, v. 42, no. 6, p. 539-542.

Macdonald, F. A., Schmitz, M. D., Crowley, J. L., Roots, C. F., Jones, D. S., Maloof, A. C., Strauss, J. V., Cohen, P. A., Johnston, D. T., and Schrag, D. P., 2010, Calibrating the Cryogenian: Science, v. 327, p. 1241-1243.

Macdonald, F. A., Strauss, J. V., Sperling, E. A., Halverson, G. P., Narbonne, G. M., Johnston, D. T., Kunzmann, M., Schrag, D. P., and Higgins, J. A., 2013, The stratigraphic relationship between the Shuram carbon isotope excursion, the oxygenation of Neoproterozoic oceans, and the first appearance of the Ediacara biota and bilaterian trace fossils in northwestern Canada: Chemical Geology, v. 362, p. 250-272.

Mattinson, J. M., 2005, Zircon U-Pb chemical abrasion ("CA-TIMS") method: combined annealing and multi-step partial dissolution analysis for improved precision and accuracy of zircon ages: Chemical Geology, v. 220, p. 47-66.

McKirdy, D. M., Burgess, J. M., Lemon, N. M., Yu, X., Cooper, A. M., Gostin, V. A., Jenkins, R. J. F., and Both, R. A., 2001, A chemostratigraphic overview of the late Cryogenian interglacial sequence in the Adelaide fold-thrust belt, South Australia: Precambrian Research, v. 106, p. 149-186.

McLean, N., Bowring, J., and Bowring, S., 2011, An algorithm for U-Pb isotope dilution data reduction and uncertainty propagation: Geochemistry, Geophysics, Geosystems, v. 12, no. 6.

Melezhik, V. A., Pokrovskii, B. G., Fallick, A. E., Kuznetsov, A. B., and Bujakaite, M. I., 2009, Constraints on 87Sr/86Sr of Late Ediacaran seawater: insight from Siberian high-Sr limestones: Journal of the Geological Society of London, v. 166, p. 183-191.

Melim, L. A., Swart, P. K., and Maliva, R., 2001, Meteoric and marine burial diagenesis, *in* Ginsberg, R. N., ed., Subsurface geology of a prograding carbonate platform margin, Great Bahama Bank: Results of the Bahamas Drilling Project, Volume 70: Tulsa, SEPM Special Publication.

Millán, M. I., Machel, H., and Bernasconi, S. M., 2016, Constraining Temperatures of Formation and Composition of Dolomitizing Fluids In the Upper Devonian Nisku Formation (Alberta, Canada) With Clumped Isotopes: Journal of Sedimentary Research, v. 86, no. 2, p. 107-112.

Misi, A., and Veizer, J., 1998, Neoproterozoic carbonate sequences of the Una Group, Irecê Basin, Brazil: chemostratigraphy, age and correlations: Precambrian Research, v. 89, no. 1, p. 87-100.

Morrow, D. W., 1982, Diagenesis 1. Dolomite-Part 1: The chemistry of dolomitization and dolomite precipitation: Geoscience Canada, v. 9, no. 1.

Morrow, D. W., Stasiuk, L. D., and Zhao, M., 2001, Dolomitization and Burial Diagenesis of Devonian Slave Point and Keg River Formations in the Cordova Embayment Region of Northeast British Columbia, Canada.

Mossakovsky, A., Ruzhentsev, S., Samygin, S., and Kheraskova, T., 1994, Central Asian fold belt: geodynamic evolution and formation history: Geotectonics, v. 27, no. 6, p. 445-474.

Murata, K. J., Friedman, I., and Madsen, B. M., 1969, Isotopic composition of diagenetic carbonates in marine Miocene formations of California and Oregon, 2330-7102.

Narbonne, G. M., 1994, New Ediacaran (Neoproterozoic) fossils from northwestern Canada: Journal of Paleontology, v. 68, p. 411-416.

Narbonne, G. M., Kaufman, A. J., and Knoll, A. H., 1994, Integrated chemostratigraphy and biostratigraphy of the Windermere Supergroup, northwestern Canada: Implications for Neoproterozoic correlations and the early evolution of animals: Geological Society of America Bulletin, v. 106, p. 1281-1291.

Och, L. M., and Shields-Zhou, G., 2012, The Neoproterozoic oxygenation event: Environmental perturbations and biogeochemical cycling: Earth-Science Reviews, v. 110, p. 26-57.

Oliver, J., 1986, Fluids expelled tectonically from orogenic belts: their role in hydrocarbon migration and other geologic phenomena: Geology, v. 14, no. 2, p. 99-102.

Ovchinnikova, G., Kuznetsov, A., Vasil'eva, I., Gorokhov, I., Letnikova, E., and Gorokhovskii, B., 2012a, U-Pb age and Sr isotope signature of cap limestones from the Neoproterozoic Tsagaan Oloom Formation, Dzabkhan River Basin, Western Mongolia: Stratigraphy and Geological Correlation, v. 20, no. 6, p. 516-527.

Ovchinnikova, G. V., Kuznetsov, A. B., Vasil'eva, I. M., Gorokhov, I. M., Letnikova, E. F., and Gorokhovskii, B. M., 2012b, U-Pb age and Sr isotope signature of cap limestone from the Neoproterozoic Tsagaan Oloom Formation, Dzabkhan River Basin, Western Mongolia: Stratigraphy and Geological Correlation, v. 20, no. 6, p. 516-527.

Panchuk, K. M., Holmden, C. E., and Leslie, S. A., 2006, Local controls on carbon cycling in the Ordovician midcontienent region of North America, with implications for carbon isotope secular curves: Journal of Sedimentary Research, v. 76, p. 200-211.

Pearce, J. A., and Peate, D. W., 1995, Tectonic implications of the composition of volcanic arc magmas: Annual Review of Earth and Planetary Sciences, v. 23, p. 251-286.

Petersen, S., and Schrag, D., 2015, Antarctic ice growth before and after the Eocene-Oligocene transition: New estimates from clumped isotope paleothermometry: Paleoceanography, v. 30, no. 10, p. 1305-1317.

Petersen, S. V., and Schrag, D. P., 2014, Clumped isotope measurements of small carbonate samples using a high-efficiency dual-reservoir technique: Rapid Communications in Mass Spectrometry, v. 28, no. 21, p. 2371-2381.

Petrosyan, N., 1967, Stratigraphic importance of the Devonian flora of the USSR.

Planavsky, N. J., Rouxel, O. J., Bekker, A., Lalonde, S. V., Konhauser, K. O., Reinhard, C. T., and Lyons, T. W., 2010, The evolution of the marine phosphate reservoir: Nature, v. 467, p. 1088-1090.

Pojeta Jr, J., 1986, Devonian rocks and Lower and Middle Devonian pelecypods of Guangxi, China, and the Traverse Group of Michigan, 2330-7102.

Pokrovskii, B. G., Melezhik, V. A., and Bujakaite, M. I., 2006, Carbon, Oxygen, Strontium, and Sulfur Isotopic Compositions in Late Precambrian Rocks of the Patom Complex, Central Siberia: Communication 1. Results, Isotope Stratigraphy, and Dating Problems: Lithology and Mineral Resources, v. 41, no. 5, p. 450-474.

Pokrovsky, B. G., Mavromatis, V., and Pokrovsky, O. S., 2011, Co-variation of Mg and C isotopes in late Precambrian carbonates of the Siberian Platform: A new tool for tracing the change in weathering regime?: Chemical Geology, v. 290, no. 1, p. 67-74.

Powell, R. D., 1990, Glacimarine processes at grounding-line fans and their growth to ice-contact deltas, *in* Dowdeswell, J. A., and Scourse, J. D., eds., Glacimarine Environments, Volume 53: London, Geological Society of London Speical Publications, p. 53-73.

Powerman, V., Shatsillo, A., Chumakov, N., Kapitonov, I., and Hourigan, J., 2015, Interaction between the Central Asian Orogenic Belt (CAOB) and the Siberian craton as recorded by detrital zircon suites from Transbaikalia: Precambrian Research, v. 267, p. 39-71.

Pruss, S. B., Bosak, T., Macdonald, F. A., McLane, M., and Hoffman, P. F., 2010, Microbial facies in a Sturtian cap carbonate, the Rasthof Formation, Otavi Group, northern Namibia: Precambrian Research, v. 181, p. 187-198.

Radke, B. M., and Mathis, R. L., 1980, On the formation and occurrence of saddle dolomite: Journal of Sedimentary Research, v. 50, no. 4.

Ramezani, J., Hoke, G. D., Fastovsky, D. E., Bowring, S. A., Therrien, F., Dworkin, S. I., Atchley, S. C., and Nordt, L. C., 2011, High-precision U-Pb zircon geochronology of the Late Triassic Chinle Formation, Petrified Forest National Park (Arizona, USA): Temporal constraints on the early evolution of dinosaurs: Geological Society of America Bulletin, v. 123, no. 11-12, p. 2142-2159.

Read, J. F., 1982, Carbonate platforms of passive (extensional) continental margins: types, characteristics and evolution: Tectonophysics, v. 81, p. 195-212.

Ridge, J. C., Balco, G., Bayless, R. L., Beck, C. C., Carter, L. B., Dean, J. L., Voytek, E. B., and Wei, J. H., 2012, The new North American Varve Chronology: A precise record of southeastern Laurentide Ice Sheet deglaciation and climate, 18.2-12.5 kyr BP, and correlations with Greenland ice core records: American Journal of Science, v. 312, no. 7, p. 685-722.

Rizza, M., Ritz, J. F., Prentice, C., Vassallo, R., Braucher, R., Larroque, C., Arzhannikova, A., Arzhannikov, S., Mahan, S., and Massault, M., 2015, Earthquake Geology of the Bulnay Fault (Mongolia): Bulletin of the Seismological Society of America, v. 105, no. 1, p. 72-93.

Rojas-Agramonte, Y., Kröner, A., Demoux, A., Xia, X., Wang, W., Donskaya, T., Liu, D., and Sun, M., 2011, Detrital and xenocrystic zircon ages from Neoproterozoic to Palaeozoic arc terranes of

Mongolia: significance for the origin of crustal fragments in the Central Asian Orogenic Belt: Gondwana Research, v. 19, no. 3, p. 751-763.

Rooney, A. D., Macdonald, F. A., Strauss, J. V., Dudás, F. Ö., Hallmann, C., and Selby, D., 2014, Re-Os geochronology and coupled Os-Sr isotope constraints on the Sturtian snowball Earth: Proceedings of the National Academy of Sciences, v. 111, no. 1, p. 51-56.

Rooney, A. D., Strauss, J. V., Brandon, A. D., and Macdonald, F. A., 2015, A Cryogenian chronology: Two long-lasting synchronous Neoproterozoic glaciations: Geology, v. 43, no. 5, p. 459-462.

Rose, C. V., Swanson-Hysell, N. L., Husson, J. M., Poppick, L. N., Cottle, J. M., Schoene, B., and Maloof, A. C., 2012, Constraints on the origin and relative timing of the Trezona δ< sup> 13</sup> C anomaly below the end-Cryogenian glaciation: Earth and Planetary Science Letters, v. 319, p. 241-250.

Roselle, G. T., Baumgartner, L. P., and Valley, J. W., 1999, Stable isotope evidence of heterogeneous fluid infiltration at the Ubehebe Peak contact aureole, Death Valley National Park, California: American Journal of Science, v. 299, no. 2, p. 93-138.

Rothman, D. H., Hayes, J. M., and Summons, R. E., 2003, Dynamics of the Neoproterozoic carbon cycle: Proceedings of the National Academy of Sciences, v. 100, p. 8124-8129.

Rudnev, S., Izokh, A., Borisenko, A., Shelepaev, R., Orihashi, Y., Lobanov, K., and Vishnevsky, A., 2012, Early Paleozoic magmatism in the Bumbat-Hairhan area of the Lake Zone in western Mongolia (geological, petrochemical, and geochronological data): Russian Geology and Geophysics, v. 53, no. 5, p. 425-441.

Rudnick, R. L., 1995, Making continental crust: Nature, v. 378, no. 6557, p. 571-577.

Ruzhentsev, S. V., and Burashnikov, V. V., 1996, Tectonics of the western Mongolian Salairides: Geotectonics, v. 29, no. 5, p. 379-394.

Ruzhentsev, S. V., and Pospelov, I. I., 1992, The south Mongolian variscan fold system: Geotectonics, v. 26, p. 383-395.

Salnikova, E., Kozakov, I., Kotov, A., Kröner, A., Todt, W., Bibikova, E., Nutman, A., Yakovleva, S., and Kovach, V., 2001, Age of Palaeozoic granites and metamorphism in the Tuvino-Mongolian Massif of the Central Asian Mobile Belt: loss of a Precambrian microcontinent: Precambrian Research, v. 110, no. 1, p. 143-164.

Samozvantsen, B. A., Tsukerik, A. B., Golyakov, B. I., 1981, Report of geological mapping work of scale 1: 200 000 in area Great Lakes deppression to western branches of Hangay Highland, v. 3576.

Sanderson, M. J., 2003, Molecular data from 27 proteins do not support a Precambrian origin of land plants: American Journal of Botany, v. 90, p. 954-956.

Sarg, J., 1988, Carbonate sequence stratigraphy.

Sawaki, Y., Kawai, T., Shibuya, T., Tahata, M., Omori, S., Komiya, T., Yoshida, N., Hirata, T., Ohno, T., Windley, B., and Maruyama, S., 2010a, 87Sr/86Sr chemostratigraphy of Neoproterozoic

Dalradian carbonates below the Port Askaig Glaciogenic Formation, Scotland: Precambrian Research, v. 179, p. 150-164.

Sawaki, Y., Ohno, T., Tahata, T., Komiya, T., Hirata, T., Maruyama, S., Windley, B. F., Han, J., Shu, D., and Li, Y., 2010b, The Ediacaran radiogenic Sr isotope excursion in the Doushantuo Formation in the Three Gorges area, South China: Precambrian Research, v. 176, p. 46-64.

Schmitz, M., Gradstein, F., Ogg, J., and Ogg, G., 2012, Appendix 2—Radiometric ages used in GTS2012: The Geologic Time Scale, p. 1045-1082.

Schrag, D. P., Berner, R. A., Hoffman, P. F., and Halverson, G. P., 2002, On the initiation of snowball Earth: Geochemistry, Geophysics, Geosystems, v. 3.

Schrag, D. P., Higgins, J. A., Macdonald, F. A., and Johnston, D. T., 2013, Authigenic carbonate and the history of the global carbon cycle: science, v. 339, no. 6119, p. 540-543.

Schulmann, K., and Paterson, S., 2011, Geodynamics: Asian continental growth: Nature Geoscience, v. 4, p. 827-829.

Sengör, A., Natal'In, B., and Burtman, V., 1993, Evolution of the Altaid tectonic collage and Palaeozoic crustal growth in Eurasia: Nature, v. 364, p. 299-307.

Sengor, A. C., and Natal'in, B. A., 1996, Paleotectonics of Asia: fragments of synthesis, *in* Yin, A., and Harrison, M., eds., The Tectonic Evolution of Asia: Cambridge, Cambridge University Press, p. 486-640.

Serezhnikova, E. A., Ragozina, A. L., Dorjnamjaa, D., and Lyubov'V, Z., 2014, Fossil microbial communities in Neoproterozoic interglacial rocks, Maikhanuul Formation, Zavkhan basin, Western Mongolia: Precambrian Research, v. 245, p. 66-79.

Shields, G., 2005, Neoproterozoic cap carbonates: a critical appraisal of existing models and the plumeworld hypothesis: Terra Nova, v. 17, no. 4, p. 299-310.

Shields, G., Stille, P., Brasier, M., and Atudorei, N.-V., 1997, Stratified oceans and oxygenation of the late Precambrian environment: a post glacial geochemical record from the Neoproterozoic of W. Mongolia: Terra Nova, v. 9, p. 218-222.

Shields, G. A., Braiser, M. D., Stille, P., and Dorjnamjaa, D., 2002, Factors contributing to high $\delta^{13}C$ values in Cryogenian limestones of western Mongolia: Earth and Planetary Science Letters, v. 196, p. 99-111.

Siever, R., and Woodford, N., 1979, Dissolution kinetics and the weathering of mafic minerals: Geochimica et Cosmochimica Acta, v. 43, no. 5, p. 717-724.

Skougstadt, M., and Horr, C. A., 1960, Occurrence of strontium in natural water: US Geol. Survey, Circ, v. 420, p. 6.

Sláma, J., Košler, J., Condon, D. J., Crowley, J. L., Gerdes, A., Hanchar, J. M., Horstwood, M. S., Morris, G. A., Nasdala, L., and Norberg, N., 2008, Plešovice zircon—a new natural reference material for U–Pb and Hf isotopic microanalysis: Chemical Geology, v. 249, no. 1, p. 1-35.

Smalley, P., Higgins, A., Howarth, R., Nicholson, H., Jones, C., Swinburne, N., and Bessa, J., 1994, Seawater Sr isotope variations through time: a procedure for constructing a reference curve to date and correlate marine sedimentary rocks: Geology, v. 22, no. 5, p. 431-434.

Smith, E. F., Macdonald, F. A., Petach, T. A., Bold, U., and Schrag, D. P., 2015, Integrated stratigraphic, geochemical, and paleontological late Ediacaran to early Cambrian records from southwestern Mongolia: Geological Society of America Bulletin, p. B31248. 31241.

Soejono, I., Burianek, D., Svojtka, M., Zacek, V., Cap, P., and Janousek, V., 2016, Mid-Ordovician and Late Devonian magmatism in the Togtokhinshil Complex: new insight into the formation and accretionary evolution of the Lake Zone (western Mongolia): Journal of GEOsciences, v. 61, no. 1, p. 5-23.

Stampfli, G., and Borel, G., 2002, A plate tectonic model for the Paleozoic and Mesozoic constrained by dynamic plate boundaries and restored synthetic oceanic isochrons: Earth and Planetary Science Letters, v. 196, no. 1, p. 17-33.

Štípská, P., Schulmann, K., Lehmann, J., Corsini, M., Lexa, O., and Tomurhuu, D., 2010, Early Cambrian eclogites in SW Mongolia: evidence that the Palaeo-Asian Ocean suture extends further east than expected: Journal of metamorphic Geology, v. 28, no. 9, p. 915-933.

Sumner, D. Y., and Bowring, S. A., 1996, U-Pb geochronologic constraints on deposition of the Campbellrand Subgroup, Transvaal Supergroup, South Africa: Precambrian Research, v. 79, p. 25-35.

Sun, J.-F., Yang, J.-H., Wu, F.-Y., and Wilde, S. A., 2012, Precambrian crustal evolution of the eastern North China Craton as revealed by U–Pb ages and Hf isotopes of detrital zircons from the Proterozoic Jing'eryu Formation: Precambrian Research, v. 200, p. 184-208.

Swanson-Hysell, N. L., Rose, C. V., Calmet, C. C., Halverson, G. P., Hurtgen, M. T., and Maloof, A. C., 2010, Cryogenian glaciation and the onset of carbon-isotope decoupling: Science, v. 328, p. 608-611.

Swart, P. K., 2008, Global synchronous changes in the carbon isotopic composition of carbonate sediments unrelated to changes in the global carbon cycle: Proceedings of the National Academy of Sciences, v. 105, no. 37, p. 13741-13745.

Swart, P. K., and Kennedy, M. J., 2012, Does the global stratigraphic reproducibility of d13C in Neoproterozoic carbonates require a marine origin? A Pliocene-Pleistocene comparison: Geology, v. 40, no. 1, p. 87-90.

Tamer, A., 1965, CHEMICAL STAINING METHODS USED IN THE IDENTIFICATION OF CARBONATE MINERALS.

Tan, F., and Hudson, J., 1971, Carbon and oxygen isotopic relationships of dolomites and co-existing calcites, Great Estuarine Series (Jurassic), Scotland: Geochimica et Cosmochimica Acta, v. 35, no. 8, p. 755-767.

Teraoka, Y., Suzuki, M., Tungalag, F., Ichinnorov, N., and Sakamari, Y., 1996, Tectonic framework of the Bayankhongor area, west Mongolia: BULLETIN-GEOLOGICAL SURVEY JAPAN, v. 47, p. 447-456.

Togtokh, D., Baatarkhuyag, A., and Bayardalai, S., 1995, The report of result of the geological grouppedmapping at scale 1:200000: Ulaanbaatar, Mongolia, p. 1575.

Tomurtogoo, O., 2005, Tectonics and structural evolution of Mongolia: Geodynamics and Metallogeny of Mongolia With a Special Emphasis on Copper and Gold Deposits: IAGOD Guidebook Series, v. 11, p. 5-12.

Tucker, M. E., and Wright, V. P., 1990, Dolomites and dolomitization models: Carbonate sedimentology, p. 365-400.

Ulitina, L., Bondarenko, O., and Minjin, C., 2009, Evolution of the taxonomic diversity of Mongolian Ordovician-Silurian corals: Paleontological Journal, v. 43, no. 5, p. 499-505.

Van der Voo, R., van Hinsbergen, D. J., Domeier, M., Spakman, W., and Torsvik, T. H., 2015, Latest Jurassic–earliest Cretaceous closure of the Mongol-Okhotsk Ocean: A paleomagnetic and seismological-tomographic analysis: Geological Society of America Special Papers, v. 513, p. 589-606.

Vandeginste, V., Sweenen, R., Gleeson, S. A., Ellam, R. M., Osadetz, K., and Roure, F., 2005, Zebra dolomitization as a result of focused fluid flow in the Rocky Mountains Fold and Thrust Belt, Canada: Sedimentology, v. 52, p. 1067-1095.

Veizer, J., 1983, Chemical diagenesis of carbonates: theory and application of trace element technique.

Veizer, J., Ala, D., Azmy, K., Bruckschen, P., Buhl, D., Bruhn, F., Carden, G. A. F., Diener, A., Ebneth, S., Godderis, Y., Jasper, T., Korte, C., Pawelleck, F., Podlaha, O. G., and Stauss, H., 1999, $^{87}Sr/^{86}Sr$, $d^{13}C$ and $d^{18}O$ evolution of Phanerozoic seawater: Chemical Geology, v. 161, p. 59-88.

Wang, C., Li, N., Sun, Y., and Zong, P., 2011, Distribution of Tuvaella brachiopod fauna and its tectonic significance: Journal of Earth Science, v. 22, p. 11-19.

Wang, T., Zheng, Y., Gehrels, G., and Mu, Z., 2001, Geochronological evidence for existence of South Mongolian microcontinent—A zircon U-Pb age of grantoid gneisses from the Yagan-Onch Hayrhan metamorphic core complex: Chinese Science Bulletin, v. 46, no. 23, p. 2005-2008.

Warren, J., 2000, Dolomite: occurrence, evolution and economically important associations: Earth-Science Reviews, v. 52, no. 1, p. 1-81.

Webster, G. D., and Ariunchimeg, Y., 2004, The northern most Emsian crinoids known, a Devonian fauna from the Chuluun Formation, Shine Jinst area, Southern Mongolia: Geobios, v. 37, no. 4, p. 481-487.

Wilhem, C., Windley, B. F., and Stampfli, G. M., 2012, The Altaids of Central Asia: A tectonic and evolutionary innovative review: Earth-Science Reviews, v. 113, no. 3, p. 303-341.

Windley, B. F., Alexeiev, D., Xiao, W., Kroener, A., and Badarch, G., 2007, Tectonic models for accretion of the Central Asian Orogenic Belt: Journal of the Geological Society of London, v. 164, p. 31-47.

Wojcik, K. M., Goldstein, R. H., and Walton, A. W., 1997, Regional and local controls of diagenesis driven by basin-wide flow system: Pennsylvanian sandstones and limestones, Cherokee basin, southeastern Kansas.

Xia, X., Sun, M., Zhao, G., and Luo, Y., 2006, LA-ICP-MS U–Pb geochronology of detrital zircons from the Jining Complex, North China Craton and its tectonic significance: Precambrian Research, v. 144, no. 3, p. 199-212.

Xiao, W., Windley, B. F., Hao, J., and Zhai, M., 2003, Accretion leading to collision and the Permian Solonker suture, Inner Mongolia, China: termination of the central Asian orogenic belt: Tectonics, v. 22, no. 6.

Yakubchuk, A., 2004, Architecture and mineral deposit settings of the Altaid orogenic collage: a revised model: Journal of Asian Earth Sciences, v. 23, no. 5, p. 761-779.

Yang, J.-H., Wu, F.-Y., Shao, J.-A., Wilde, S. A., Xie, L.-W., and Liu, X.-M., 2006, Constraints on the timing of uplift of the Yanshan Fold and Thrust Belt, North China: Earth and Planetary Science Letters, v. 246, no. 3, p. 336-352.

Yang, J., Cawood, P. A., Du, Y., Huang, H., Huang, H., and Tao, P., 2012, Large Igneous Province and magmatic arc sourced Permian–Triassic volcanogenic sediments in China: Sedimentary Geology, v. 261, p. 120-131.

Yarmolyuk, V., Kovach, V., Kovalenko, V., Salnikova, E., Kozlovskii, A., Kotov, A., Yakovleva, S., and Fedoseenko, A., 2011, Composition, sources, and mechanism of continental crust growth in the Lake Zone of the Central Asian Caledonides: I. Geological and geochronological data: Petrology, v. 19, no. 1, p. 55-78.

Yarmolyuk, V., Kovalenko, V., Anisimova, I., Sal'nikova, E., Kovach, V., Kozakov, I., Kozlovsky, A., Kudryashova, E., Kotov, A., and Plotkina, Y. V., Late Riphean alkali granites of the Zabhan microcontinent: evidence for the timing of Rodinia breakup and formation of microcontinents in the Central Asian Fold Belt, *in* Proceedings Doklady Earth Sciences2008a, Volume 420, Springer, p. 583-588.

Yarmolyuk, V., Kovalenko, V., Sal'nikova, E., Kozakov, I., Kotov, A., Kovach, V., Vladykin, N., and Yakovleva, S., 2005, U-Pb-Age of sin-and postmetamorphic granitoids from Southern Mongolia-evidence for the presence of grenvilides in the Central Asian Fold Belt.

Yarmolyuk, V. V., Kovalenko, V. I., Anisimova, I. V., Sal'nikova, E. B., Kovach, V. P., Kozakov, I. K., Kozlovskii, A. M., Kudryashova, E. A., Kotov, A. B., Plotkina, Y. V., Terent'eva, L. B., and Yakovleva, S. Z., 2008b, Late Riphean alkali granites of the Zabhan Microcontinent: Evidence for the timing of Rodinia breakup and formation of microcontinents in the Central Asian Fold Belt: Doklady Earth Sciences, v. 420, no. 4, p. 583-588.

Yoshioka, H., Asahara, Y., Tojo, B., and Kawakami, S., 2003, Systematic variations in C, O, and Sr isotopes and elemental concentrations in Neoproterozoic carbonates in Namibia: implications for a glacial to interglacial transition: Precambrian Research, v. 124, p. 69-85.

Zacek, V., Burianek, D., Pecskay, Z., and Skoda, R., 2016, Astrophyllite-alkali amphibole rhyolite, an evidence of early Permian A-type alkaline volcanism in the western Mongolian Altai: Journal of GEOsciences, v. 61, no. 1, p. 93-103.

Zenger, D., Dunham, J., and Ethington, R. L., 1980, Concepts and models of dolomitization.

Zhang, C.-L., Zou, H.-B., Li, H.-K., and Wang, H.-Y., 2013, Tectonic framework and evolution of the Tarim Block in NW China: Gondwana Research, v. 23, no. 4, p. 1306-1315.

Zhao, Y., Song, B., and Zhang, S. H., The Central Mongolian microcontinent: Its Yangtze affinity and tectonic implications, *in* Proceedings Symposium on continental growth and orogeny in Asia, Taipei, Taiwan, 2006, p. 135-136.

Zhou, C., Tucker, R., Xiao, S., Peng, Z., Yuan, X., and Chen, Z., 2004, New constraints on the ages of Neoproterozoic glaciations in south China: Geology, v. 32, p. 437-440.

Zhu, M., Lu, M., Zhang, J., Zhao, F., Li, G., Aihua, Y., Zhao, X., and Zhao, M., 2013, Carbon isotope chemostratigraphy and sedimentary facies evolution of the Ediacaran Doushantuo Formation in western Hubei, South China: Precambrian Research, v. 225, p. 7-28.

Zimmer, A., Lang, D., Richardt, S., Frank, W., Reski, R., and Rensing, S. A., 2007, Dating the early evolution of plants: detection and molecular clock analyses of orthologs: Molecular genetics and genomics, v. 278, p. 393-402.

Zonenshain, L. P., 1973, The evolution of Central Asiatic geosynclines through sea-floor spreading: Tectonophysics, v. 19, p. 213-232.

Zorin, Y. A., 1999, Geodynamics of the western part of the Mongolia–Okhotsk collisional belt, Trans-Baikal region (Russia) and Mongolia: Tectonophysics, v. 306, no. 1, p. 33-56.

APPENDICES

APPENDIX 2.1. SUPPLEMENT TO CHAPTER 2: TABLES

Table 2.A1. U-Pb isotopic CA-ID-TIMS data

							Radiogenic Isotope Ratios		
Sample	$\frac{Th}{U}$	$^{206}Pb^*$ x10^{-13} mol	mol % $^{206}Pb^*$	$\frac{Pb^*}{Pb_c}$	Pb_c (pg)	$\frac{^{206}Pb}{^{204}Pb}$	$\frac{^{208}Pb}{^{206}Pb}$	$\frac{^{207}Pb}{^{206}Pb}$	% err
(a)	(b)	(c)	(c)	(c)	(c)	(d)	(e)	(e)	(f)
DS34									
z2	0.500	0.3340	99.20%	38	0.22	2265	0.156	0.057619	0.199
z5b	0.448	0.3434	99.15%	35	0.25	2113	0.140	0.057375	0.216
z1	0.678	0.7252	99.66%	93	0.20	5343	0.212	0.057534	0.122
z3	0.547	2.5747	99.92%	370	0.18	21897	0.171	0.057484	0.071
z4	0.332	1.3657	99.76%	122	0.27	7645	0.104	0.057555	0.088
z5a	0.382	0.7385	99.63%	79	0.23	4894	0.120	0.057474	0.121
z9	0.093	1.8699	99.85%	174	0.24	11678	0.029	0.057464	0.076
z8	0.032	0.5888	99.59%	65	0.20	4429	0.010	0.057318	0.149
z6	0.036	0.2075	98.97%	25	0.18	1747	0.011	0.057406	0.382
F1128A									
z1	1.175	0.6966	99.19%	44	0.47	2233	0.369	0.055769	0.257
z2	0.808	0.5119	99.21%	41	0.34	2272	0.254	0.055681	0.212
z3	0.836	0.5654	98.99%	32	0.48	1785	0.262	0.055661	0.264
z4	1.141	0.4229	98.97%	34	0.37	1746	0.358	0.055619	0.305
z5	0.846	0.4930	99.06%	35	0.39	1918	0.265	0.055609	0.303
z6	0.819	0.1889	96.23%	8	0.61	479	0.257	0.055551	0.841
z7	0.877	0.3968	98.87%	29	0.38	1594	0.275	0.055755	0.356
TS08									
z1	1.341	8.4153	99.91%	403	0.64	19528	0.412	0.066102	0.065
z2	0.782	14.4847	99.98%	###	0.28	77171	0.241	0.066109	0.061
z3	0.922	8.3621	99.97%	962	0.24	51572	0.284	0.066172	0.063
z4	1.294	4.4624	99.94%	613	0.22	30320	0.398	0.066202	0.065
z5	0.943	1.5140	99.84%	217	0.20	11624	0.290	0.066197	0.079
z6	0.913	0.9161	99.76%	137	0.19	7392	0.281	0.066142	0.099
z7	0.774	1.7251	99.45%	58	0.81	3182	0.238	0.066245	0.093
U12001									
z1	0.629	0.1443	97.10%	10	0.36	622	0.197	0.057448	0.751
z3	0.419	0.2716	98.77%	24	0.28	1468	0.131	0.057303	0.313
z4	0.405	0.5432	99.10%	32	0.41	2005	0.127	0.057310	0.248
z6	0.014	0.0692	94.25%	4	0.35	314	0.005	0.057966	1.883
U1340A									
z1	1.297	2.8710	99.81%	188	0.46	9234	0.400	0.064855	0.073
z2	1.201	2.8931	99.86%	258	0.33	12953	0.370	0.064942	0.070
z3	1.277	3.3146	99.85%	239	0.42	11814	0.394	0.064948	0.070
z5	1.272	2.3194	99.86%	249	0.28	12367	0.392	0.064975	0.072
z6	1.233	1.3749	99.72%	128	0.32	6424	0.380	0.064867	0.083

U-Pb isotopic CA-ID-TIMS data continued.

	Radiogenic Isotope Ratios						Isotopic Dates					
	$\frac{^{207}Pb}{^{235}U}$		$\frac{^{206}Pb}{^{238}U}$		corr.		$\frac{^{207}Pb}{^{206}Pb}$		$\frac{^{207}Pb}{^{235}U}$		$\frac{^{206}Pb}{^{238}U}$	
Sample		% err		% err	coef.			±		±		±
(a)	(e)	(f)	(e)	(f)			(g)	(f)	(g)	(f)	(g)	(f)
DS34												
z2	0.653864	0.254	0.082304	0.083	0.750		515.30	4.38	510.85	1.02	509.86	0.41
z5b	0.650822	0.271	0.082269	0.094	0.705		505.98	4.75	508.98	1.09	509.65	0.46
z1	0.652586	0.181	0.082264	0.076	0.857		512.08	2.68	510.07	0.72	509.62	0.37
z3	0.651529	0.134	0.082203	0.069	0.958		510.14	1.55	509.42	0.54	509.26	0.34
z4	0.651761	0.150	0.082130	0.071	0.933		512.86	1.94	509.56	0.60	508.83	0.35
z5a	0.650788	0.175	0.082123	0.075	0.830		509.77	2.65	508.96	0.70	508.78	0.36
z9	0.649909	0.140	0.082026	0.070	0.954		509.39	1.68	508.42	0.56	508.21	0.34
z8	0.646914	0.207	0.081856	0.078	0.825		503.80	3.28	506.58	0.82	507.19	0.38
z6	0.647386	0.441	0.081791	0.114	0.617		507.17	8.39	506.87	1.76	506.80	0.56
F1128A												
z1	0.545207	0.315	0.070904	0.118	0.631		443.18	5.71	441.85	1.13	441.60	0.50
z2	0.544822	0.266	0.070966	0.085	0.733		439.65	4.72	441.60	0.95	441.97	0.36
z3	0.545145	0.320	0.071032	0.097	0.682		438.89	5.88	441.81	1.15	442.37	0.41
z4	0.544717	0.363	0.071031	0.106	0.648		437.17	6.79	441.53	1.30	442.37	0.45
z5	0.545527	0.357	0.071149	0.105	0.624		436.80	6.74	442.06	1.28	443.07	0.45
z6	0.543618	0.921	0.070974	0.166	0.557		434.48	18.72	440.81	3.30	442.02	0.71
z7	0.545735	0.404	0.070990	0.104	0.560		442.64	7.92	442.20	1.45	442.11	0.45
TS08												
z1	1.220623	0.129	0.133927	0.068	0.964		809.60	1.37	810.06	0.72	810.23	0.52
z2	1.222770	0.126	0.134148	0.068	0.973		809.82	1.28	811.04	0.70	811.49	0.52
z3	1.223621	0.127	0.134113	0.069	0.969		811.82	1.31	811.43	0.71	811.29	0.52
z4	1.221976	0.129	0.133871	0.068	0.968		812.79	1.36	810.68	0.72	809.91	0.52
z5	1.224591	0.141	0.134169	0.070	0.940		812.61	1.65	811.87	0.79	811.61	0.54
z6	1.222667	0.162	0.134069	0.078	0.895		810.88	2.07	810.99	0.91	811.04	0.59
z7	1.225027	0.155	0.134119	0.074	0.911		814.13	1.95	812.07	0.87	811.32	0.56
U12001												
z1	0.651145	0.835	0.082206	0.173	0.568		508.76	16.50	509.18	3.34	509.28	0.85
z3	0.650610	0.374	0.082346	0.098	0.702		503.22	6.89	508.85	1.50	510.11	0.48
z4	0.649477	0.306	0.082193	0.102	0.683		503.47	5.45	508.16	1.22	509.20	0.50
z6	0.658908	2.016	0.082442	0.358	0.448		528.49	41.26	513.95	8.13	510.68	1.76
U1340A												
z1	1.134270	0.137	0.126845	0.069	0.958		769.63	1.54	769.79	0.74	769.84	0.50
z2	1.136297	0.134	0.126900	0.070	0.964		772.47	1.47	770.75	0.73	770.16	0.50
z3	1.136561	0.133	0.126919	0.070	0.958		772.64	1.46	770.88	0.72	770.27	0.51
z5	1.137682	0.136	0.126991	0.069	0.955		773.54	1.52	771.41	0.73	770.68	0.50
z6	1.135683	0.146	0.126980	0.072	0.934		770.01	1.75	770.46	0.79	770.61	0.52

(a) z1, z2, etc. are labels for analyses composed of single zircon grains that were annealed and chemically abraded (Mattinson, 2005). Labels in bold denote those used in weighted mean calculations.
(b) Model Th/U ratio calculated from radiogenic $^{208}Pb/^{206}Pb$ ratio and $^{207}Pb/^{235}U$ date.
(c) Pb* and Pbc are radiogenic and common Pb, respectively. mol % ^{206}Pb* is with respect to radiogenic and blank Pb.
(d) Measured ratio corrected for spike and fractionation only. Fractionation correction is 0.18 ± 0.03 (1 sigma) %/amu (atomic mass unit) for single-collector
Daly analyses, based on analysis of EARTHTIME ^{202}Pb-^{205}Pb tracer solution.
(e) Corrected for fractionation, spike, common Pb, and initial disequilibrium in $^{230}Th/^{238}U$. Common Pb in analyses was assigned to the zircon with a composition determined
by Stacey and Kramers (1975), except for 0.3 pg that was assigned to laboratory blank with a composition of $^{206}Pb/^{204}Pb = 18.04 \pm 0.61\%$; $^{207}Pb/^{204}Pb = 15.54 \pm 0.52\%$;
$^{208}Pb/^{204}Pb = 37.69 \pm 0.63\%$ (1 sigma). $^{206}Pb/^{238}U$ and $^{207}Pb/^{206}Pb$ ratios corrected for initial disequilibrium in $^{230}Th/^{238}U$ using Th/U [magma] = 3.0 ± 0.3 (1 sigma).
(f) Errors are 2 sigma, propagated using algorithms of Schmitz and Schoene (2007) and Crowley et al. (2007).
(g) Calculations based on the decay constants of Jaffey et al. (1971). $^{206}Pb/^{238}U$ and $^{207}Pb/^{206}Pb$ dates corrected for initial disequilibrium in $^{230}Th/^{238}U$ using Th/U [magma] = 3.0 ± 0.3 (1 sigma).

Table 2.A2. U-Pb isotopic LA-ICPMS data of magmatic samples

LA-ICPMS data from sample DS24

		Corrected isotope ratios							Apparent ages (Ma)						
		207Pb*	±2s	206Pb*	±2s	error	207Pb*	±2s	207Pb*	±2s	207Pb*	±2s	206Pb*	±2s	%
Analysis	Th/U	235U*	(%)	238U	(%)	corr.	206Pb*	(%)	206Pb*	(Ma)	235U	(Ma)	238U*	(Ma)	disc.
DS24 S 302	0.52	9.585394	5.145	0.431047	4.888	0.95	0.161281	1.606	2469	27	2396	47	2310	95	6
DS24 L 121	0.25	9.274254	4.666	0.417422	4.044	0.86	0.161139	2.327	2468	39	2365	43	2249	77	9
DS24 L 122	0.23	9.526908	3.725	0.432848	2.972	0.78	0.159 63	2.245	2452	38	2390	34	2319	58	5
DS24 S 307	1.15	9.595588	3.652	0.439388	2.775	0.75	0.158388	2.375	2439	40	2397	34	2348	55	4
DS24 L 117	0.36	8.933763	3.994	0.419922	3.313	0.82	0.1543	2.229	2394	38	2331	36	2260	63	6
DS24 M 300	0.43	8.073086	4.137	0.380444	3.895	0.94	0.153903	1.395	2390	24	2239	37	2078	69	13
DS24 M 290	0.45	8.821252	4.374	0.415763	4.181	0.95	0.153 88	1.284	2389	22	2320	40	2241	79	6
DS24 XS 316	0.03	8.421402	4.345	0.402081	3.725	0.85	0.151904	2.237	2367	38	2277	39	2179	69	8
DS24 XS 313	1.37	8.883886	5.159	0.431538	4.701	0.91	0.149308	2.125	2338	36	2326	47	2313	91	1
DS24 XS 314	1.36	8.756924	4.216	0.431542	3.879	0.91	0.147173	1.653	2313	28	2313	38	2313	75	0
DS24 S 310	0.8	8.090275	4.39	0.407255	3.206	0.72	0.144077	2.999	2277	52	2241	40	2202	60	3
DS24 S 303	0.45	6.983884	4.913	0.363937	4.668	0.95	0.139178	1.531	2217	27	2109	44	2001	80	10
DS24 S 306	1.26	7.279357	6.815	0.384104	6.307	0.92	0.137449	2.58	2195	45	2146	61	2095	113	5
DS24 M 299	0.44	6.933683	7.98	0.367688	7.296	0.91	0.136768	3.234	2187	56	2103	71	2019	126	8
DS24 L 118	0.21	6.077558	4.823	0.355029	4.368	0.9	0.124155	2.047	**2017**	**36**	1987	42	1959	74	3
DS24 L 116	1.52	5.973729	7.447	0.351532	6.751	0.9	0.123248	3.145	**2004**	**56**	1972	65	1942	113	3
DS24 M 292	1.43	5.809157	3.903	0.343316	3.434	0.87	0.122721	1.854	**1996**	**33**	1948	34	1903	57	5
DS24 L 115	1.34	5.768801	5.516	0.341991	5.129	0.92	0.122 34	2.03	**1991**	**36**	1942	48	1896	84	5
DS24 L 120	0.13	6.081185	5.687	0.361128	4.487	0.78	0.122131	3.493	**1988**	**62**	1988	50	1988	77	0
DS24 L 114	0.91	5.506 09	6.28	0.327102	5.913	0.94	0.122084	2.117	**1987**	**38**	1902	54	1824	94	8
DS24 M 294	2.33	5.833617	6.19	0.347 07	5.431	0.87	0.121904	2.971	**1984**	**53**	1951	54	1921	90	3
DS24 M	0.2	6.340	5.4	0.378	5.0	0.9	0.121	2.2	**1979**	**40**	2024	48	2069	89	-5

289	8	52	93	342	05	1	546	64							
DS24 S 305	1.3	5.960 961	5.4 12	0.355 762	4.7 98	0.8 8	0.121 522	2.5 04	**1979**	**45**	1970	47	1962 .1	81	1
DS24 L 112	1.4	5.693 881	6.6 68	0.340 752	6.0 47	0.9	0.121 19	2.8 11	**1974**	**50**	1930	58	1890	99	4
DS24 L 113	1.2 1	5.766 841	6.2 4	0.345 399	5.9 01	0.9 4	0.121 092	2.0 28	**1972**	**36**	1941	54	1913	98	3
DS24 S 308	0.7	5.864 259	3.9 73	0.351 315	3.3 8	0.8 4	0.121 064	2.0 88	**1972**	**37**	1956	34	1941	57	2
DS24 L 123	2.7 8	6.008 89	6.1 63	0.360 491	5.3 04	0.8 6	0.120 892	3.1 38	**1969**	**56**	1977	54	1984	91	-1
DS24 M 291	1.7 2	5.955 332	4.7 45	0.357 307	4.2 91	0.9	0.120 882	2.0 25	**1969**	**36**	1969	41	1969	73	0
DS24 M 295	2.8 3	5.888 464	4.7 13	0.353 525	4.2 3	0.8 9	0.120 804	2.0 77	**1968**	**37**	1960	41	1951	71	1
DS24 M 296	1.6 7	5.752 675	3.6 19	0.346 61	3.2 07	0.8 8	0.120 372	1.6 78	**1962**	**30**	1939	31	1918	53	2
DS24 L 110	1.2 9	5.693 541	6.8 02	0.343 158	5.8 03	0.8 5	0.120 334	3.5 5	**1961**	**63**	1930	59	1902	96	3
DS24 L 108	2.2 7	5.652 428	5.2 52	0.340 844	4.7 22	0.8 9	0.120 276	2.2 98	**1960**	**41**	1924	45	1891	77	4
DS24 L 111	0.5 9	5.682 328	5.0 42	0.343 221	4.8 39	0.9 5	0.120 075	1.4 17	**1957**	**25**	1929	44	1902	80	3
DS24 L 107	0.9 1	5.807 258	4.2 68	0.351 614	3.5 61	0.8 2	0.119 785	2.3 53	**1953**	**42**	1947	37	1942	60	1
DS24 S 311	2.2 4	5.990 751	5.4 98	0.362 925	4.4 38	0.8	0.119 719	3.2 45	**1952**	**58**	1975	48	1996	76	-2
DS24 M 298	0.5	5.466 74	4.0 06	0.331 807	3.7 55	0.9 3	0.119 493	1.3 96	**1949**	**25**	1895	34	1847	60	5
DS24 S 309	0.5 1	5.413 964	5.7 85	0.330 258	5.3 34	0.9 2	0.118 894	2.2 4	**1940**	**40**	1887	50	1840	85	5
DS24 L 119	1.7	5.573 56	6.6 12	0.341 653	5.4 86	0.8 3	0.118 317	3.6 9	**1931**	**66**	1912	57	1895	90	2
DS24 L 109	1.9 7	5.737 99	5.1 76	0.353 034	4.3 03	0.8 2	0.117 881	2.8 77	**1924**	**52**	1937	45	1949	72	-1
DS24 S 304	1.4 6	5.605 028	5.1 33	0.346 064	4.6 07	0.8 9	0.117 468	2.2 64	**1918**	**41**	1917	44	1916	76	0
DS24 M 297	0.6 5	4.641 654	4.4 86	0.291 472	4.2 67	0.9 5	0.115 498	1.3 85	1888	25	1757	37	1649	62	13

Experiment 10 -3/6/2014

Isotope ratios and ages are NOT corrected for initial common Pb.
Isotope ratio and apparent age errors do not include systematic calibration errors of 3.71892869152324% ($^{208}Pb/^{232}Th$), 0.285029107243422% ($^{207}Pb/^{206}Pb$), 2.01285858976754% ($^{206}Pb/^{238}U$) (all 1-sigma).

Trace element concentrations in ppm, calculated using mean count rate method.

Sweep-by-sweep downhole fractionation of U/Pb ratios NOT corrected via Si/Zr fractionation factor.

Backgrounds were monitored between sweeps 10 to 20. Sample counts were integrated from sweeps 28 to 54.

Ablation used a laser spot size of 25 microns, and a laser firing repetition rate of 10 Hz.

Experiment 3 - 2/28/2014

Isotope ratios and ages are NOT corrected for initial common Pb.
Isotope ratio and apparent age errors do not include systematic calibration errors of 5.31771810566801% ($^{208}Pb/^{232}Th$), 0.307507508903004% ($^{207}Pb/^{206}Pb$), 1.69318032221799% ($^{206}Pb/^{238}U$) (all 1-sigma).

Trace element concentrations in ppm, calculated using mean count rate method.

Sweep-by-sweep downhole fractionation of U/Pb ratios NOT corrected via Si/Zr fractionation factor.

Backgrounds were monitored between sweeps 10 to 20. Sample counts were integrated from sweeps 28 to 54.
Ablation used a laser spot size of 25 microns, and a laser firing repetition rate of 10 Hz.

LA-ICPMS data from sample DS24 continued.

	Concentrations (ppm)																					
Analysis	P	Ti	Y	Zr	Nb	Ce	Pr	Nd	Sm	Eu	Gd	Tb	Dy	Ho	Er	Tm	Yb	Lu	Hf	Ta	Th	U	T(°C)
DS24S 302	195.365	9.2043	384.255	470182	1.3001	7.5061	0.5189	3.9677	3.9042	0.8636	13.2632	3.5183	41.0224	13.648	56.6838	13.9461	168.994	18.8632	8791.6	1.0512	63.1355	121.216	788
DS24L 121	228.647	5.8903	425.146	519515	1.3686	3.8418	0.0704	1.1060	1.2900	0.7079	8.5304	3.5082	40.2643	14.5462	59.4434	15.5894	188.439	22.1282	8328.96	1.1322	50.2619	202.654	744
DS24L 122	252.01	8.3415	416.597	522966	1.2378	6.1832	0.3567	1.6399	1.4876	0.2478	8.5026	3.1682	38.5554	12.8892	60.1385	16.9479	198.267	21.23	8221.94	1.1490	54.3747	232.943	778
DS24S 307	250.101	6.7522	517.153	472864	1.0937	9.1201	0.0296	1.5585	3.0145	0.2498	14.837	4.8649	57.8147	19.0545	74.3311	18.6409	206.814	21.192	8110.43	0.6053	100.444	87.6047	757
DS24L 117	359.551	5.8509	727.716	528576	2.1721	4.5493		0.3497	2.3307	0.1212	15.428	5.3829	70.6619	22.9477	97.41	26.0178	318.792	33.5465	8572.94	1.6811	91.7854	257.698	744
DS24M 290	506.515	8.9123	160.594	559310	4.9549	6.3239	0.0355	1.4309	5.1499	0.2857	35.068	11.808	153.98	54.483	249.012	62.9845	682.863	92.2284	113.741	3.5761	224.139	495.438	784
DS24XS 316	68.361	7.4025	248.866	590416	0.5873	1.0137	0.0761	0.3825	0.4796	0.3095	3.3604	1.3168	18.719	7.5131	34.4439	9.2734	102.303	14.7967	130.837	0.1512	10.2145	310.24	766
DS24XS 313	215.887	5.0051	642.518	606946	1.2406	8.8182	0.0452	1.1931	2.7649	0.3773	15.950	5.4995	62.2016	22.2299	91.1447	21.6023	218.463	31.7497	113.553	0.6113	107.714	78.6775	729
DS24XS 314	198.444	3.9464	561.452	616023	0.6802	6.9969	0.0501	0.7058	2.8354	0.3070	14.386	4.8388	53.2889	19.2474	83.5146	20.1084	193.876	27.3552	119.046	0.3859	78.6133	57.6827	708
DS24S 310	201.267	5.3949	403.521	473801	0.9554	6.6609	0.0295	0.5385	2.3711	0.2368	9.9087	3.9547	42.646	14.3633	59.0639	15.2232	172.228	17.8814	828.46	0.4853	74.8156	93.6268	736
DS24S 303	599.128	5.6996	128.318	470279	2.7643	6.4099	0.0820	1.6547	5.4806	0.3222	31.719	10.270	127.42	46.176	191.614	49.6235	584.903	63.6857	9025.94	1.7818	200.502	446.426	741

DS24 S 306	278.435	6.2332	487.709	473822	0.8341	7.4508 2	0.0342 9	1.0871 4	3.3222 8	0.2045 2	15.329 5	4.8444 9	53.550 2	17.669 7	63.190 5	15.911 1	175.55 7	18.387 3	812 7.8 2	0.3243 1	77.379 3	61.561 8	749
DS24 L 118	89.796 6	7.2207 9	157.90 3	515279	1.4603	4.7927 1		0.0373 2	1.8777 6	0.5790 5	7.3176 9	2.2577	20.236 7	5.3718 5	15.181 1	2.8234 9	26.251 5	2.5078 2	766 8.7 1	0.5732 7	19.05	92.269 6	764
DS24 L 115	247.73 8	7.7161 8	509.40 4	511846	1.9070 6	13.321 7	0.0536 5	1.5679 8	5.5675 1	0.4196	16.886 9	5.9312 1	59.138	16.365 5	58.402 8	14.037 1	149.96 8	14.129 9	718 2.7 8	0.8337 7	126.25 2	93.868 5	770
DS24 L 120	74.310 6	4.8113	43.453 7	552111	1.0262 9	1.6718 5			0.0354 9	0.1721 6	1.1907 8	0.8152	5.1684 3	1.4800 8	3.4691 4	0.6686	4.8989 8	0.3599 8	860 1.7 9	0.5591 8	9.1351 4	68.110 2	726
DS24 M 294	174.58 8	8.0876 8	331.31	531970	0.7487 7	6.5652 6	0.0358	0.8024 8	2.7478 4	0.2056 6	13.071 5	3.657	41.043 3	12.289 1	43.508	8.9299	97.185 9	11.085 4	100 14. 1	0.2413 3	106.58	45.700 6	775
DS24 M 289	80.866 6	7.0815 8	142.45 7	569668	1.0057 5	1.7375 8		0.1204 4	0.7490 3	0.4897	4.9347 6	1.8488 1	19.334 6	5.5265 2	15.437	2.1058 8	15.358 4	1.5253 2	113 61. 7	0.3859	14.538 5	51.822 8	762
DS24 S 305	194.22 6	5.9487 9	271.02 1	465097	1.0864 1	6.2116		0.3319 1	1.4121 4	0.2190 9	8.3442	2.9265 4	29.603 4	10.235 1	37.645 8	9.1876 7	109.71 2	11.598 9	877 1.0 9	0.5031 1	55.300 6	42.396 3	745
DS24 L 112	258.59 2	7.8260 6	594.04	555445	1.1636 9	14.898 2	0.0830 3	2.5150 3	7.4235 5	0.4018 4	24.011	6.8353 2	68.606 7	18.021	68.484 6	15.487 9	157.56 8	14.664	824 3.1 7	0.4886 8	146.05 1	104.68 8	771
DS24 S 308	174.80 1	6.5565 5	289.54 8	464200	1.1916	6.5751 6	0.0176 6	0.6099 5	1.8604 4	0.0561 2	8.8502 7	2.9249 7	30.276 7	9.6918	38.134 7	9.4152 5	103.85 7	10.896 6	893 6.6 5	0.5754 9	56.536 6	80.385 6	754
DS24 L 123	248.19 8	7.8581 7	498.81 5	550874	2.7185 9	10.097 1	0.049	0.9398 1	2.541	0.1278 2	14.417 5	4.7191 9	47.774 8	16.866 8	58.859 9	13.246 9	143.14 2	14.642 4	869 8.7 1	1.1894 7	137.94 7	49.596 7	772
DS24 M 291	196.90 3	8.2602	484.08 8	567488	1.5377 8	14.189 8	0.0086 6	1.5976	3.5230 2	0.4084 7	17.000 3	5.2378 5	54.462 4	17.498	65.457	14.383 2	145.78	16.875 3	110 57. 1	0.9288 9	142.16 9	82.845 2	777
DS24 M 295	170.13	9.3197 3	289.44 6	523849	0.7197 7	7.1587	0.0717 4	1.2595 3	2.4158	0.1826 1	12.902	3.6706	37.045 6	10.444 9	40.025	8.7263 4	82.940 7	9.6681 2	100 53	0.2316 1	117.66 5	41.581 4	789
DS24 M 296	228.97 6	8.3330 6	557.22 2	521810	2.2475 2	13.029 5	0.0843 2	1.6559 7	3.8938 8	0.3904 3	20.207 6	6.4340 3	63.909 6	19.787 4	73.543 7	16.742 6	168.20 6	19.119 6	983 7.4	0.8986 5	151.03	90.440 7	778

DS24 L 110	235.761	9.2516 4	371.24 1	558 169	0.7382 9	7.7420 7	0.0387 4	0.8146 6	2.5581 2	0.1985 4	13.173 7	3.7586 3	39.335 7	12.493 5	42.345 1	10.315 3	103.77 5	10.374 6	8305.96	0.4003	73.836 8	57.174	78 8
DS24 L 108	223.37 7	7.2495 2	390.88 3	548 333	0.4619 8	7.9445 4	0.0885 4	0.6739 4	3.0437 1	0.1183 3	14.558 7	4.0912 1	40.670 6	13.192 5	47.385 5	11.823 9	113.81 8	11.554 3	8094.65	0.1565 5	122.51 8	53.951 7	76 4
DS24 L 111	353.63 6	8.7320 3	935.60 8	539 495	3.3318 7	14.184 6	0.0696 8	0.8372 4	3.9059 9	0.3203 8	22.839 2	8.3180 1	91.958 9	31.086 1	111.91	23.461 1	236.20 8	23.768	9056.74	1.5541 8	154.31 9	263.69 4	78 2
DS24 L 107	266.49 2	7.0547 4	381.32 7	550 898	1.6785 2	12.174 3	0.0531 6	0.8769 5	2.3486 7	0.1496 7	11.250 9	3.8834 6	41.287	12.802 3	47.607 6	11.206 9	123.43	12.332 1	8408.96	0.7926 9	98.725 5	108.69 6	76 1
DS24 S 311	218.97 8	7.4140 3	378.64 1	475 239	0.6096 9	7.3540 6	0.0338 8	1.0567 5	3.7094 9	0.2537 7	13.704 5	4.5284 6	45.222 7	14.104 4	52.329 8	12.424 5	134.96 6	14.270 8	8618.61	0.2794 7	105.58 2	47.087 5	76 6
DS24 M 298	192.63 8	6.588	352.74 3	501 074	1.4677 6	9.4627 5	0.0200 6	1.1193 5	2.3456 9	0.2297 2	9.9416 2	3.0954 3	38.615 2	13.19	49.124 1	12.278 7	127.44	14.218 2	9840.86	1.1189 8	83.477 7	166.79 1	75 5
DS24 S 309	214.32 1	8.3254 8	487.57 1	478 801	1.6141 5	13.410 3	0.0315	1.1281 1	3.0193 3	0.2663 3	14.075 7	4.8199 3	49.729 7	17.367 6	68.027 8	17.562 5	193.87 9	21.63	8034.86	0.7535 6	175.88 8	342.51 7	77 8
DS24 L 119	202.64 6	7.0256 3	284.40 6	546 457	1.0145 5	6.4081 9		0.8777 5	1.9687 3	0.2081 5	10.087 4	2.7408 3	29.391 7	9.1915 3	31.703 2	8.0237	77.547 9	7.4674 1	8261.28	0.3133 4	78.116 1	45.893 7	76 1
DS24 L 109	256.81 6	7.6297 2	323.81	554 585	0.9536 7	6.6441	0.0047 7	0.8344 1	2.3779 3	0.2269 7	9.8439 4	3.2590 1	35.544 6	10.735 2	38.383 6	8.7948 2	99.145 9	10.550 1	7838.31	0.2838 5	82.607	41.947 9	76 9
DS24 S 304																							77 5
DS24 M 297	231.00 7	7.9617 6	604.34 1	516 726	2.2253 2	13.574 1	0.0394 2	1.0985 9	4.2633 2	0.4726 4	19.412 3	6.7492 2	68.460 1	21.793 6	82.571 8	19.169 3	192.56 6	22.180 1	9914.94	1.5993	152.68 4	234.84	77 3

LA-ICPMS data from sample US10

		Corrected isotope ratios							Apparent ages (Ma)						
		207Pb*	±2s	206Pb*	±2s	error	207Pb*	±2s	207Pb*	±2s	207Pb*	±2s	206Pb*	±2s	%
Analysis	Th/U	235U*	(%)	238U	(%)	corr.	206Pb*	(%)	206Pb*	(Ma)	235U	(Ma)	238U*	(Ma)	disc.
US10 L 215	1.38	9.733085	4.895	0.397952	3.832	0.78	0.177386	3.046	2629	51	2410	45	2160	70	18
US10 L 212	1.88	11.42347	4.09	0.478803	3.632	0.88	0.173037	1.881	2587	31	2558	38	2522	76	3
US10 M 228	2.07	10.04585	5.001	0.422897	4.075	0.81	0.172286	2.899	2580	48	2439	46	2274	78	12
US10 S 253	0.14	8.462776	4.771	0.367017	4.467	0.93	0.167234	1.676	2530	28	2282	43	2015	77	20
US10 S 249	0.77	9.99265	3.71	0.441542	2.565	0.68	0.164138	2.681	2499	45	2434	34	2358	51	6
US10 L 220	0.1	7.581447	5.326	0.352819	5.182	0.97	0.155847	1.228	2411	21	2183	48	1948	87	19
US10 M 234	0.53	7.812121	7.176	0.379579	6.501	0.9	0.149268	3.038	2338	52	2210	65	2074	115	11
US10 S 245	1.12	4.932794	8.353	0.29874	7.001	0.84	0.119756	4.557	1953	81	1808	71	1685	104	14
US10 S 247	1.01	4.367077	7.493	0.270779	6.071	0.81	0.11697	4.392	1910	79	1706	62	1545	83	19
US10 M 229	1.22	5.163773	5.612	0.320443	4.711	0.84	0.116873	3.048	1909	55	1847	48	1792	74	6
US10 L 224	0.76	3.833052	4.482	0.257908	4.273	0.95	0.10779	1.351	1762	25	1600	36	1479	56	16
US10 S 250	0.66	3.900534	4.956	0.263018	3.319	0.66	0.107557	3.681	1758	67	1614	40	1505	45	14
US10 L 217	0.75	3.482517	6.404	0.239323	4.176	0.65	0.105538	4.856	1724	89	1523	51	1383	52	20
US10 S 251	0.09	3.630937	10.93	0.25943	9.999	0.91	0.101507	4.404	1652	82	1556	87	1487	133	10
US10 M 239	0.46	3.170932	10.72	0.229969	10.07	0.94	0.100004	3.671	1624	68	1450	83	1334	121	18
US10 L 209	2.83	1.288138	9.906	0.13636	5.29	0.53	0.068513	8.376	884	173	840	57	*824*	*41*	7
US10 L 216	0.55	1.18259	9.392	0.133126	4.993	0.53	0.064427	7.955	756	168	793	52	*806*	*38*	-7
US10 L 206	1.11	1.162998	12.08	0.132103	5.656	0.47	0.06385	10.68	737	226	783	66	*800*	*43*	-9
US10 L 210	0.74	1.216146	4.542	0.131717	3.818	0.83	0.066964	2.461	837	51	808	25	*798*	*29*	5
US10 M 235	0.56	1.176605	11.84	0.126986	5.941	0.5	0.0672	10.24	844	213	790	65	*771*	*43*	9
US10 S 254	0.2	1.498055	14.14	0.115477	10.6	0.75	0.094087	9.366	1510	177	930	86	704	71	53
US10 M 242	0.04	0.725509	8.785	0.087138	6.274	0.71	0.060386	6.148	617	133	554	38	**539**	**32**	13
US10 M 236	0.03	0.687935	7.607	0.084311	5.488	0.72	0.059178	5.268	574	115	532	31	**522**	**28**	9

Notes: 3/8/2014

Isotope ratios and ages are NOT corrected for initial common Pb.
Isotope ratio and apparent age errors do NOT include systematic calibration errors of 0.233081391786937% ($^{207}Pb/^{206}Pb$), 0.63501720787273% ($^{206}Pb/^{23}8U$) (all 1-sigma).
Isotope ratios and ages corrected using a measured linear secondary standard age bias - ^{206}Pb count rate relationship.

Trace element concentrations in ppm, calculated using mean count rate method.

Sweep-by-sweep downhole fractionation of U/Pb ratios NOT corrected via Si/Zr fractionation factor.

Backgrounds were monitored between sweeps 10 to 20. Sample counts were integrated from sweeps 28 to 48.

Ablation used a laser spot size of 25 microns, and a laser firing repetition rate of 10 Hz.

LA-ICPMS data from sample US10 continued.

	Concentrations (ppm)																					
Analysis	P	Ti	Y	Zr	Nb	Ce	Pr	Nd	Sm	Eu	Gd	Tb	Dy	Ho	Er	Tm	Yb	Lu	Hf	Ta	Th	U	T(°C)
US10 L 212	334.245	8.7534	856.982	558810	2.0967 2	25.834 4	0.1671 8	2.3239 1	6.0299 5	0.7181 7	27.952 5	8.3154 6	95.218	32.1543	126.613	30.4757	317.327	35.8967	911 3.08	0.6600 7	182.081	96.7562	783
US10 M 228	177.496	9.0977 7	432.994	530098	1.8848 9	31.290 7	0.0954 3	1.6436 8	3.6638 8	0.2440 2	13.019 4	3.9972 5	43.028 9	14	62.4069	17.8144	198.583	23.1806	919 6.25	0.8101 5	114.99	55.654	787
US10 S 253	218.504	11.6606	585.815	644315	20.2898	3.5209		0.1907 9	0.5005 4	0.1192 3	5.5821 5	2.6355 9	43.903 5	20.1337	103.981	31.5322	406.556	59.9145	141 61.55	39.1221	58.5819	406.405	812
US10 S 249	304.19	7.4896 8	105 2.61	685535	3.1578 2	23.068 4	3.6473 6	33.042 1	18.761 3	1.5046 5	33.194 1	8.7104 7	101.10 9	36.0916	163.545	40.7427	391.283	55.0083	145 76.29	2.0572 9	126.864	165.662	767
US10 L 220	112.972	7.2096 7	303.802	576617	1.3441 8	3.2098 5		0.2739 9	0.9167 2	0.2156 1	8.6839 3	2.7260 6	32.719 1	10.249	39.8302	9.2343 9	90.335 3	11.1369	114 93.66	1.9403 6	19.6181	196.558	763
US10 S 245	156.373	11.573	385.076	646795	0.9619 8	11.908 2	0.0827 8	1.6111 8	2.5484 5	0.8002	13.447 9	4.0892 8	41.585	14.641	52.9428	12.5238	123.558	15.957	101 57.99	0.4951 7	11.6425	10.434 2	812
US10	178.	6.1	446	680	0.5	10.	0.0	0.8	2.2	0.5	13.	3.5	45.	15.	62.	15.	159	22.	131	0.2	167	166	74

S 247	478	328 2	.68 2	380	143 8	963 3	524 2	635 4	042 8	22	608 4	249 2	176 2	629 6	929 8	199 6	.94 6	575 2	58. 9	220 7	.77 6	.07 6	8
US10 M 229	128. 648	11. 714 9	218 .67 8	561 170	0.7 835 8	6.9 961 6	0.0 072 1	0.6 703 1	1.3 073 4	0.6 617 5	7.8 016 9	2.3 121 6	26. 118 4	7.9 787 7	31. 104 7	7.7 226 8	84. 494 7	9.2 880 3	896 3.5	0.6 581 1	112 .25 5	91. 919 6	81 3
US10 L 224	115. 994	8.9 461 1	159 .07 1	647 917	1.0 271 1	19. 724 8	0.0 746 2	2.2 314 6	3.6 740 5	1.2 125 8	11. 608 4	2.5 362 4	21. 603 3	5.2 632 7	18. 302 3	3.8 866 6	34. 078 9	3.6 671 9	102 50. 7	0.7 069 1	124 .06 1	162 .25 3	78 5
US10 S 250	178. 678	8.5 912 8	408 .51 2	672 238	0.7 432	8.2 647 9	0.0 226 9	0.5 111 2	1.3 657 3	0.2 856 9	8.8 403 6	3.6 318 6	39. 768 6	14. 598 4	63. 978 5	15. 406 1	.28	21. 324 8	130 79. 4	0.2 855 2	52. 248 4	79. 712 3	78 1
US10 L 217	144. 159	5.5 158 3	240 .43	568 424	1.6 791 5	20. 690 6	0.0 371 6	1.0 586 4	1.0 580 2	0.4 285 6	7.1 389 6	2.0 741	25. 826 2	8.1 262 7	36. 960 5	10. 008 1	117 .87 6	14. 212	980 6.3 1	0.9 251 9	29. 359 2	39. 024 9	73 8
US10 S 251	80.9 332	3.0 651 4	101 .83 5	687 690	0.5 461	1.2 052 2			0.4 697 2	0.1 118 9	2.5 561 1	0.7 206 4	9.5 252 5	3.1 070 2	12. 090 4	2.7 709 7	25. 207 2	3.9 293	134 51. 9	0.2 690 7	7.5 323 1	87. 272 5	68 6
US10 M 239	76.7 019	10. 914 7	77. 693	545 700	0.4 600 4	11. 653 4	0.0 381 4	0.7 761	1.3 875 4	0.5 460 7	4.3 772 2	1.2 188 6	10. 997 2	3.0 089 6	9.4 088 6	3.0 542 6	28. 852 5	3.6 224 2	915 3.7	0.2 884 8	65. 434	141 .72	80 5
US10 L 209	250. 171	38. 644 7	188 .59 6	630 198	0.8 551 9	1.4 004 2	0.0 188 7	1.0 120 1	2.3 599 6	0.1 022 1	9.3 399 7	2.4 960 6	23. 100 4	6.9 534 5	24. 555 4	5.2 325 6	47. 386 7	5.7 581 6	107 78. 2	0.3 623 7	32. 961 8	11. 655 2	95 7
US10 L 216	131. 563	6.7 899	194 .89 7	556 178	0.5 134 4	5.3 535 7		0.3 937 1	1.4 033 2	0.5 668 1	5.2 632 1	1.7 785 4	19. 637 1	6.4 090 6	28. 149	7.8 258 5	90. 485 3	10. 624 4	857 8.0 4	0.4 619 5	21. 238 3	38. 859 7	75 8
US10 L 206	158. 404	9.1 790 7	360 .21 7	615 448	0.6 536 5	8.4 982 8	0.0 448 6	0.8 622 7	1.6 505 7	0.4 367 1	6.5 797	2.3 819 9	32. 989 3	12. 010 5	55. 865	14. 193 8	159 .34	21. 513 7	970 0.0 6	0.1 803 1	9.7 828 2	8.8 432 6	78 7
US10 L 210	243. 574	1.7 796 9	809 .46 4	609 027	3.8 679 2	15. 941 1		0.6 318 5	1.5 603 8	0.2 381 6	10. 066 7	4.9 931 1	66. 357 2	28. 331 9	133 .15 3	36. 983 5	404 .27 7	55. 467	136 07. 8	3.7 159	223 .99 7	303 .80 1	64 3
US10 M 235	198. 3	6.5 428 9	389 .35	573 884	0.7 361 1	8.3 472 5		0.5 453 8	1.9 077	0.4 090 9	14. 803	5.2 844 8	47. 566 5	12. 949 4	40. 121	8.0 663 6	78. 830 7	7.6 498	101 72	0.5 077 6	8.4 335 2	15. 019 5	75 4
US10 S 254	148. 045	6.1 943	493 .29 3	623 248	1.9 542 1	40. 032	6.1 755	38. 436 9	19. 562 5	2.3 239 8	21. 135	4.6 064	43. 551 5	16. 812 2	78. 118 6	20. 627 1	230 .99 4	31. 301 4	115 83. 6	0.8 474 6	35. 671 5	180 .77 5	74 9
US10	77.2	2.0	326	516	2.5	2.2	0.0	1.1	1.3	0.4	3.7	1.4	24.	11.	51.	14.	193	24.	100	1.2	12.	338	65

M 242	687	026 5	.08 5	414	249 1	615 1	950 7	056 5	428 7	038 8	675 1	284 3	679 1	286 3	739 3	273 3	.84 4	151 4	40. 5	195 9	525 5	.32 9	2
US10 M 236	69.8 54	1.2 152 6	135 .43 4	556 975	1.2 976 5	0.6 372				0.0 749 6	0.5 557 1	0.7 599 3	9.5 923 5	4.8 992 4	23. 157 4	7.1 824 1	87. 105 4	12. 200 7	109 14. 8	0.6 967	4.1 520 1	157 .27 2	61 5

LA-ICPMS data from sample US11

		Corrected isotope ratios							Apparent ages (Ma)						
		207Pb*	±2s	206Pb*	±2s	error	207Pb*	±2s	207Pb*	±2s	207Pb*	±2s	206Pb*	±2s	%
Analysis	Th/U	235U*	(%)	238U	(%)	corr.	206Pb*	(%)	206Pb*	(Ma)	235U	(Ma)	238U*	(Ma)	disc.
US11 S 298	0.56	0.689881	5.811	0.087619	3.84	0.66	0.057105	4.361	496	96	533	24	541	20	-9
US11 M 290	0.91	0.680544	5.527	0.085889	3.665	0.66	0.057467	4.137	510	91	527	23	531	19	-4
US11 M 283	0.54	0.678628	7.845	0.085627	6.252	0.79	0.05748	4.738	510	104	526	32	530	32	-4
US11 M 291	1.01	0.709132	5.579	0.084205	4.563	0.81	0.061079	3.21	642	69	544	24	**521**	**23**	19
US11 S 300	0.69	0.664323	5.312	0.083295	3.806	0.71	0.057844	3.706	524	81	517	22	**516**	**19**	2
US11 M 284	0.87	0.634139	5.386	0.082891	4.515	0.83	0.055485	2.936	432	65	499	21	**513**	**22**	-19
US11 S 295	0.6	0.656058	7.636	0.082687	5.312	0.69	0.057544	5.485	512	121	512	31	**512**	**26**	0
US11 M 289	0.92	0.665406	5.558	0.082596	3.759	0.67	0.058429	4.095	546	89	518	23	**512**	**18**	6
US11 L 260	0.43	0.628553	6.37	0.082158	5.561	0.87	0.055487	3.107	432	69	495	25	**509**	**27**	-18
US11 L 262	0.54	0.638797	5.682	0.08209	3.681	0.64	0.056438	4.329	470	96	502	22	**509**	**18**	-8
US11 S 296	0.93	0.638211	4.887	0.081764	3.573	0.72	0.056611	3.334	476	74	501	19	**507**	**17**	-6
US11 L 266	0.81	0.638336	5.227	0.081577	3.872	0.73	0.056752	3.512	482	78	501	21	**506**	**19**	-5
US11 M 287	0.89	0.62835	5.477	0.081553	3.824	0.69	0.055881	3.921	448	87	495	21	**505**	**19**	-13
US11 S 297	1.2	0.621282	7.638	0.08123	5.815	0.76	0.055472	4.952	431	110	491	30	**503**	**28**	-17
US11 M 282	0.66	0.643393	6.503	0.080885	4.577	0.7	0.057691	4.62	518	101	504	26	**501**	**22**	3
US11 L 273	0.61	0.671752	5.401	0.080788	3.657	0.67	0.060306	3.974	615	86	522	22	**501**	**18**	19
US11 L 271	0.49	0.636842	4.918	0.080642	3.093	0.62	0.057276	3.824	502	84	500	19	**500**	**15**	0
US11 L 268	0.77	0.632892	5.058	0.080547	3.583	0.7	0.056987	3.571	491	79	498	20	**499**	**17**	-2
US11 L 281	0.55	0.63509	5.683	0.080527	3.729	0.65	0.057199	4.288	499	94	499	22	**499**	**18**	0
US11 L 269	0.75	0.656663	6.14	0.080417	4.874	0.79	0.059224	3.734	575	81	513	25	**499**	**23**	13

US11 M 285	0.79	0.632948	7.443	0.080102	6.458	0.87	0.057309	3.7	503	81	498	29	**497**	**31**	1
US11 L 275	0.78	0.63438	5.242	0.080067	4.283	0.81	0.057464	3.023	509	66	499	21	**497**	**20**	3
US11 L 261	0.9	0.62908	4.295	0.079869	3.035	0.7	0.057125	3.04	496	67	496	17	**495**	**14**	0
US11 L 277	0.79	0.628967	5.59	0.079794	4.495	0.8	0.057169	3.323	498	73	495	22	**495**	**21**	1
US11 L 259	0.84	0.626218	4.631	0.079749	3.67	0.79	0.056951	2.825	490	62	494	18	**495**	**17**	-1
US11 L 265	0.41	0.631779	5.639	0.079721	3.289	0.58	0.057477	4.58	510	101	497	22	**494**	**16**	3
US11 L 270	0.56	0.625095	6.687	0.079698	4.38	0.65	0.056885	5.054	487	112	493	26	**494**	**21**	-1
US11 M 288	0.95	0.622796	5.927	0.079629	4.003	0.67	0.056725	4.372	481	97	492	23	**494**	**19**	-3
US11 L 267	0.6	0.635957	5.896	0.079543	4.455	0.75	0.057986	3.862	529	85	500	23	**493**	**21**	7
US11 L 278	0.6	0.604827	5.315	0.079238	3.014	0.56	0.05536	4.378	427	98	480	20	**492**	**14**	-15
US11 L 264	0.72	0.596415	6.255	0.079212	4.487	0.71	0.054608	4.358	396	98	475	24	**491**	**21**	-24
US11 M 286	0.86	0.644643	6.789	0.078961	5.379	0.79	0.059211	4.142	575	90	505	27	**490**	**25**	15
US11 M 294	0.83	0.641738	5.647	0.078782	4.301	0.76	0.059079	3.66	570	80	503	22	**489**	**20**	14
US11 M 293	0.77	0.604999	7.811	0.078581	6.436	0.82	0.055839	4.426	446	98	480	30	**488**	**30**	-9
US11 S 299	0.67	0.6254	6.089	0.078528	4.36	0.71	0.057761	4.251	521	93	493	24	**487**	**20**	6
US11 L 258	0.65	0.642483	6.386	0.07842	4.208	0.65	0.05942	4.803	582	104	504	25	**487**	**20**	16
US11 L 263	0.8	0.615766	4.331	0.078345	3.684	0.84	0.057004	2.278	492	50	487	17	**486**	**17**	1
US11 L 276	0.79	0.611522	5.3	0.078268	3.643	0.68	0.056666	3.85	479	85	485	20	**486**	**17**	-1
US11 L 279	0.79	0.612582	4.611	0.078228	3.065	0.66	0.056794	3.444	484	76	485	18	**486**	**14**	0
US11 L 280	0.65	0.617189	4.486	0.077991	2.947	0.65	0.057395	3.382	507	74	488	17	**484**	**14**	4
US11 L 272	0.8	0.593834	5.726	0.076871	4.578	0.8	0.056028	3.438	453	76	473	22	**477**	**21**	-5
US11 L 274	0.88	0.598862	4.466	0.076621	3.833	0.85	0.056687	2.292	479	51	477	17	**476**	**18**	1

Notes: 3/8/2014

Isotope ratios and ages are NOT corrected for initial common Pb.

Isotope ratio and apparent age errors do NOT include systematic calibration errors of 0.233081391786937% (207Pb/206Pb), 0.63501720787273% ($^{206}Pb/^{238}U$) (all 1-sigma).

Isotope ratios and ages corrected using a measured linear secondary standard age bias - ^{206}Pb count rate relationship.

Trace element concentrations in ppm, calculated using mean count rate method.

Sweep-by-sweep downhole fractionation of U/Pb ratios NOT corrected via Si/Zr fractionation factor.

Backgrounds were monitored between sweeps 10 to 20. Sample counts were integrated from sweeps 28 to 48.

Ablation used a laser spot size of 25 microns, and a laser firing repetition rate of 10 Hz.

LA-ICPMS data from sample US11 continued.

	Concentrations (ppm)																						
Analysis	P	Ti	Y	Zr	Nb	La	Ce	Pr	Nd	Sm	Eu	Gd	Tb	Dy	Ho	Er	Tm	Yb	Lu	Hf	Ta	Th	U	T(°C)
US11S 298	120.975	8.3407.15	245.445	52796	0.56037		3.5888.2	0.0309.3	0.5831.3	1.4375.8	0.3221.3	4.9239.9	2.1831.7	26.990.5	9.073	38.813.3	9.4326.9	108.686	12.332	7705.39	0.3896.6	33.868.4	60.067.2	778
US11M 290	145.037	4.6010.5	110 8.43	539862	1.4039	0.13898	8.5746.6	0.5022.8	8.4542.9	11.895.6	3.2461.2	40.288.1	11.880.9	123.439	38.6302	160.533	42.341.9	464.349	49.2647	6249.39	1.0482.4	177.601	194.731	722
US11M 283	122.326	6.3918.2	376.924	518061	0.6937.2		4.5124.9	0.0386.6	1.475	2.4822.7	0.3714	10.478.5	3.9698	42.051.6	13.82	57.343.4	15.719.4	171.698	18.4488	7615.78	0.5664.1	45.481.1	84.368.6	752
US11M 291	166.182	4.0492.5	952.876	530388	2.5680.3	0.07999	10.644.9	0.3395.4	5.6949.8	8.4253.3	1.8635	29.885.6	9.7823.1	105.038	33.9036	139.179	33.070.6	393.933	43.9219	6185.84	1.3162.9	214.005	211.664	710
US11S 300	144.833	7.7922.7	463.834	584898	1.6089.6		7.0594.9	0.0599.6	0.9037.4	2.6943.8	0.4665.9	10.891.4	4.2103.9	48.999.3	17.093	68.868.3	17.298.8	203.061	24.0845	9111.32	0.9849.6	81.774.8	118.585	771
US11M 284	138.008	4.6959.5	844.881	530027	1.2252.5	0.03501	6.867	0.2530.4	5.5369.6	9.1565.4	1.7345.6	28.637.4	9.4084	97.856	31.5813	125.2	31.1603	332.457	36.6568	722 8.1	0.6796.5	132.174	152.761	723
US11S 295	124.892	12.3088.2	276.841	537939	0.7838.2		4.3428.9	0.0381.7	0.8137.5	2.4542.3	0.4697.8	9.4201.1	2.6303.8	32.209.6	10.7303	40.799.8	9.8820.3	120.042	12.9475	7259.02	0.4905.8	41.321.8	68.750.8	818
US11M 289	130.062	8.8790.5	992.419	525855	0.9555.1	0.08884	4.9235.5	0.4274.5	6.9432.7	9.1379.1	2.6502.8	33.398.6	9.8980.2	107.145	33.2599	135.014	34.943.1	385.747	43.3009	5795.98	0.8576.9	142.924	154.774	784
US11L 260	108.903	7.6692	218.054	522081	0.6987.7		4.2261.8	0.0079.8	0.3788.7	0.9255.8	0.1803.9	4.9505.5	1.732	21.238	7.96889	33.016.1	9.1297.4	108.994	12.7268	791 1.6	0.6412.7	37.957.4	88.046.2	769
US11L 262	112.674	7.4658.5	382.423	514503	0.6763.8		4.1292.2	0.0443.2	1.6035.9	2.3823.4	0.5529.3	11.597.6	3.1239.2	39.686	14.2127	57.670.6	15.112.2	171.413	17.9332	6576.2	0.5216.9	48.426	88.880.1	767

	163	10.		53	1.9	0.1	8.4		9.9	12.	2.6		17.	196		249	62.	674	71.		1.7	295	315	
US11	.93	661	173	88	556	772	263	0.7	893	562	218	54.	812	.36	65.2	.37	107	.65	517	697	993	.15	.88	80
S 296	5	1	7.7	98	6	9	8	809	9	6	4	143	6	9	314	8	6	8	3	2.2	1	3	7	3
	164	12.	121	49	1.4	0.0	6.9	0.6	9.3	15.		53.	13.	151		169	42.	481	46.	582	1.2	168	207	
US11	.05	456	1.6	62	383	528	467	138	015	284	3.4	830	643	.18	45.2	.28	546	.77	375	5.1	115	.92	.93	81
L 266	8	3	5	63	5	7	8	5	8	8	126	8	7	7	158	8	2	9	8	4	4	8	4	9
US11		10.		52	1.1		7.7		9.7	12.	2.0	47.		163		204	50.	520		756	1.0	241	272	
M	156	640	139	31	214	0.0	406	0.5	809	154	325	553	13.	.96	52.1	.74	578	.73	56.	0.5	360	.68	.26	80
287	.58	1	7.1	64	4	556	3	606	1	4	6	2	465	9	38	9	2	7	281	4	1	2	7	3
		4.8	112	54	2.1	0.0		0.3	6.4	12.	3.6	37.	11.	124			40.	436	48.		0.8	220	184	
US11	161	890	5.9	98	736	316	7.2	313	345	919	708	903	519	.60	42.3	162	534	.29	553	624	726	.75	.50	72
S 297	.51	4	4	73	7	2	273	1	4	6	1	9	6	7	74	.35	1	2	8	2.7	2	9	4	7
US11	122	4.6	506	50	0.9		4.8	0.0	1.5	4.0	1.0	15.	4.8	55.		76.	19.	217	22.	656	0.6	65.	98.	
M	.78	026	.88	29	130		298	257	925	899	377	387	567	146	18.8	566	456	.52	970	1.6	823	276	717	72
282	1	2	2	54	6		2	5	4	5	8	5	6	1	251	2	2	8	4	1	3	4	5	2
	151	12.	387	48	0.8		5.1	0.0	2.0	3.6		13.	4.3	44.		57.		165	15.	610	0.5	48.	79.	
US11	.12	793	.52	67	185		318	995	877	356	0.9	978	382	312	14.7	205	14.	.94	997	1.7	301	385	781	82
L 273	9	3	5	93	4		1	9	7	4	112	2	9	3	327	8	067	9	6	1	1	2	6	2
	99.	7.6	342	49	0.5		4.0	0.0	1.2		0.2	9.9		37.		52.	13.	158	15.	725	0.4	42.	87.	
US11	301	727	.29	07	044		939	457	312	2.4	583	093	3.2	180	12.2	487	550	.91	842	6.8	016	477	135	77
L 271	2	8	3	86	9		6	1	3	101	4	5	912	4	458	9	4	5	1	4	2	5	5	0
	170	4.6	883	48	1.2		7.7	0.3	6.1	7.6	2.3	34.	10.			133	35.	387	37.	548	1.0	145	189	
US11	.98	487	.49	86	119	0.0	378	384	976	737	096	263	040	106	32.7	.01	155	.67	611	8.8	408	.58	.51	72
L 268	9	4	6	55	6	657	4	3	5	7	8	4	9	.01	003	6	6	1	4	6	5	5	3	2
			364	53	0.8		3.8	0.0	1.2	2.8	0.6	9.2		39.		55.	14.	175	18.	661	0.8	45.	83.	
US11	144	8.4	.35	27	220		657	659	835	006	304	082	3.3	147	13.4	415	555	.48	696	5.6	101	848	915	77
L 281	.59	577	5	89	7		5	9	8	7	8	5	333	6	087	1	7	4	7	6	5	4	9	9
	140	8.6	915	50	1.0	0.0	5.8	0.5	6.8	9.8	2.6	37.	10.			128	33.	364	37.	591	0.9	123	164	
US11	.93	057	.90	58	594	577	724	292	211	668	358	097	919	110	34.9	.39	090	.88	449	4.4	466	.44	.40	78
L 269	7	6	8	33	1	5	6	2	3	7	4	4	4	.18	248	9	8	5	2	3	7	1	2	1
US11	105	9.8		54	1.1		5.9	0.3	5.1	6.9	1.3	28.	9.2	95.		124		325	35.	694	0.6		141	
M	.46	372	887	48	164		610	357	704	956	703	147	454	792	32.1	.07	29.	.09	752	9.9	736	112	.62	79
285	8	1	.48	53	7		1	9	8	6	7	9	2	7	264	6	619	2	5	8	9	.29	1	5
	138	9.1	106	48	1.1	0.1	7.8	0.6	9.9	11.	2.2	40.	11.	124		152		417		593	0.6	162	207	
US11	.27	045	1.6	87	526	694	500	062	811	403	427	442	855	.83	39.3	.62	38.	.95	40.	6.5	877	.30	.05	78
L 275	3	2	3	31	2	3	3	8	1	8	9	6	4	8	874	8	087	6	037	8	1	4	7	7
	205	9.9	170	50		0.1	7.4	0.7	9.2	15.		67.	19.	204		252	60.	658	66.	577	1.7	274	305	
US11	.42	049	3.8	94	2.4	134	471	572	662	912	4.0	713	250	.14	64.7	.72	487	.62	062	0.6	479	.39	.31	79
L 261	1	9	7	38	334	1	4	1	3	7	562	9	1	8	701	8	3	2	6	6	4	1	8	5

	159			50	1.5	0.0	9.1	0.4	9.3		2.3	37.	12.	135		171	43.	464		678	0.9	196	249	
US11	.24	5.2	118	96	159	731	780	701	596	10.	402	788	942	.89	42.7	.59	107	.19	44.	5.1	506	.55	.83	73
L 277	3	218	0.6	68	6	9	2	3	8	712	5	7	5	3	147	7	3	9	946	7	2	1	6	3
	174	8.9	114	51		0.0	7.0	0.5	10.	12.		46.	12.	137		170	41.	454	44.	695	0.8	179	212	
US11	.53	132	0.0	92	1.4	013	283	149	333	470	2.2	302	896	.25	44.4	.53	319	.14	990	5.8	115	.58	.91	78
L 259	4	9	5	56	336	8	3	7	1	5	675	4	4	6	92	9	6	4	5	9	8	7	1	4
	170	9.4	502	49	1.3		5.3	0.1	2.9	3.4	0.9	15.	4.2	53.		80.	21.	271	29.	626	1.0	73.	180	
US11	.88	609	.06	93	971		124	595	500	342	617	543	265	482	18.4	122	874	.95	937	7.5	644	321	.24	79
L 265	7	5	6	50	2		3	2	7	4	9	9	5	6	953	8	1	8	8	3	6	1	4	1
	110		443	49	0.7		4.6	0.0		3.4	0.9	14.	5.0	52.		66.	17.	204	19.	677	0.5	59.	105	
US11	.23	6.9	.54	20	241		335	022	1.5	817	277	697	589	456	17.7	562	068	.76	304	9.4	654	647	.98	76
L 270	1	36	8	05	2		1	3	874	8	7	8	2	3	465	6	8	2	9	3	6	6	1	0
US11	125	7.8	117	54	1.0		7.6	0.4	8.5	11.	1.3	43.	13.			166	39.	415	43.	755	0.7	189	199	
M	.28	169	7.5	98	014		292	423	916	721	369	451	257	141	42.6	.41	648	.99	458	1.7	612	.34	.78	77
288	6	8	9	95	2		9	8	9	4	7	2	4	.58	387	9	7	3	7	1	4	8	3	1
	175	10.	407	51			9.3	0.0	1.7	2.9	0.3	13.	4.1	46.		61.	15.	177	17.	725	0.8	105	175	
US11	.45	687	.87	18	1.7		590	465	774	279	766	682	057	461	14.1	184	919	.80	956	0.3	904	.91	.21	80
L 267	1	9	7	32	766		9	4	4	2	2	5	5	7	877	3	1	7	8	3	4	9	6	3
	128		379	51	0.6		3.7	0.0	1.4	3.2		13.	4.5	45.		55.	14.	161	16.	635	0.4	45.	75.	
US11	.96	8.5	.75	94	996		357	502	089	032	0.8	082	641	894	13.5	162	716	.97	549	6.3	343	409	871	78
L 278	9	846	8	60	3		5	1	7	4	579	7	2	8	882	1	9	4	6	4	3	4	6	1
	117	8.0	640	50	0.7	0.0	4.5	0.2	5.2	7.6	2.0	24.	7.3	80.		95.	23.	270		569		73.	102	
US11	.78	367	.42	16	601	393	788	520	491	105	359	128	350	364	24.0	599	238	.67	27.	3.2	0.5	630	.43	77
L 264	3	7	4	61	9	3	8	3	4	6	7	3	8	3	167	4	8	9	093	2	227	7	7	4
US11	150	8.6	840	53			5.9		5.6	8.4	1.2	30.	8.2	94.		122	29.	326	34.	647		115	133	
M	.22	902	.91	89	0.9	0.0	774	0.3	062	235	708	559	581	270	30.4	.56	944	.50	428	7.9	0.7	.20	.58	78
286	2	3	7	01	82	76	1	74	8	7	3	5	6	3	868	9	8	4	8	3	179	7	9	2
US11	139	4.1	943	52	1.2	0.0	7.3	0.4	7.2	10.	1.6	35.	10.	118		138	32.	356	36.	606	0.6	142		
M	.23	846	.14	14	682	298	373	172	291	471	137	457	902	.64	34.7	.64	832	.99	350	3.7	769	.48	170	71
294	1	2	1	08	9	4	2	2	6	9	1	4	6	4	867	3	7	5	9	7	7	1	.81	3
US11	136	11.	685	54	0.4		5.0	0.3	6.1	8.6	1.2	28.	7.6	77.		94.	21.	228	22.	651	0.3	71.		
M	.91	313	.05	26	763		891	323	383	296	681	681	529	523	24.2	001	744	.58	005	4.0	293	945	93.	80
293	2	4	9	26	4		5	2	9	7	2	8	6	5	838	1	3	6	4	3	2	4	555	9
	163	10.	853	56	1.6	0.0	6.4	0.2	4.3	7.6	1.1	26.	8.2	85.			31.	355	40.		1.1	116	175	
US11	.88	155	.57	37	356	446	724	521	216	664	201	120	010	123	30.1	129	675	.07	742	707	326	.98	.69	79
S 299	2	5	6	35	7	8	1	3	1	6	5	1	3	7	257	.52	5	8	7	9.8	5	2	8	8
	127	8.9	514	52	0.5	0.0	4.1		2.8		1.4	19.	5.7	61.		76.		218	23.	637	0.6	58.	89.	
US11	.38	789	.61	93	788	308	952	0.1	640	4.5	730	240	925	210	18.8	167	19.	.18	466	5.4	605	218	266	78
L 258	8	5	3	02	5	5	9	619	6	902	5	4	1	6	699	6	791	2	4	7	2	3	8	5

US11 L 263	180.476	5.4733 9	134 6.8 7	49 27 70	1.9 515 6	0.0 955 2	9.2 126 5	0.5 603 2	9.2 107 1	13. 221 4	2.3 366 3	52. 384 1	14. 912 3	159 .62 4	51.0 056	197 .00 3	49. 140 4	533 .88 2	51. 014 5	628 8.2 1	1.1 939 8	246 .32 6	308 .42 5	737
US11 L 276	150.721	9.7557 4	107 0.2 4	49 25 99	1.1 192 2	0.0 395 2	7.9 619 7	0.5 209 7	7.6 485 3	12. 407 7	1.8 166 3	38. 154 7	12. 146 8	134 .54 2	41.0 396	147 .01 2	38. 348 7	403 .61 3	37. 49	604 2.1 5	0.4 996 4	170 .08 1	215 .22 3	794
US11 L 279	154.699	10. 343 2	848 .8	51 01 00	0.9 784 6	0.3 150 3	6.2 498 1	0.4 048 2	5.6 571 7	9.8 423 9	2.1 328 1	34. 359 7	9.7 482 8	96. 583 8	30.2 503	118 .20 7	30. 252 9	336 .67 4	32. 415 6	656 1.0 9	0.6 993 3	115 .93 9	147 .27 2	800
US11 L 280	129.051	12. 663 1	335 .69 7	52 37 48	0.8 850 2		6.4 236 7	0.0 399 7	1.6 145 3	3.0 325 2	0.5 240 8	11. 575 8	3.1 103 4	38. 268 9	11.6 983	50. 170 9	13. 272 4	146 .67 6	14. 366 4	685 3.3 7	0.6 929 6	67. 974 5	104 .44 6	821
US11 L 272	157.371	11. 991 5	121 7.5 7	49 61 85	1.2 346 2	0.0 780 3	6.7 244 2	0.5 838 1	8.8 385 2	14. 641 7	2.5 563 6	46. 919 5	14. 998 5	153 .25	46.0 5	173 .01 5	42. 198 1	438 .34 8	43. 256 6	573 4.7 4	0.9 075	175 .56 9	219 .28 5	815
US11 L 274	179.763	10. 771	160 4.4 2	50 91 77	2.0 033 3	0.1 949 8	9.9 105 2	0.7 907 9	10. 706 8	14. 594 7	4.1 223 3	57. 767 5	19. 054 7	195 .75 4	60.8 085	248 .47 3	58. 372 2	649 .11 6	62. 956 2	567 6	1.5 326 1	290 .37 2	330 .62 9	804

LA-ICPMS data from sample U1520

		Corrected isotope ratios							Apparent ages (Ma)						
		207Pb*	±2s	206Pb*	±2s	error	207Pb*	±2s	207Pb*	±2s	207Pb*	±2s	206Pb*	±2s	%
Analysis	Th/U	235U*	(%)	238U	(%)	corr.	206Pb*	(%)	206Pb*	(Ma)	235U	(Ma)	238U*	(Ma)	disc.
U1520 M 53	0.18	1.353252	3.886	0.147402	3.328	0.86	0.066585	2.007	825	42	869	23	886	28	-7
U1520 S 168	0.43	1.389691	4.202	0.145774	3.832	0.91	0.069141	1.723	903	36	885	25	**877**	**31**	3
U1520 M 43	0.23	1.397144	4.658	0.145615	4.156	0.89	0.069588	2.103	916	43	888	28	**876**	**34**	4
U1520 S 124	0.39	1.341845	3.515	0.145009	3.086	0.88	0.067113	1.682	841	35	864	20	**873**	**25**	-4
U1520 S 138	0.56	1.296036	4.345	0.144798	2.747	0.63	0.064916	3.367	772	71	844	25	872	22	-13
U1520 S 157	0.55	1.391848	4.673	0.144737	3.795	0.81	0.069745	2.726	921	56	885	28	**871**	**31**	5
U1520 S 152	0.76	1.415947	3.61	0.143731	3.046	0.84	0.071449	1.938	970	40	896	21	**866**	**25**	11
U1520 S 155	0.62	1.368758	3.776	0.143348	3.521	0.93	0.069252	1.365	906	28	876	22	**864**	**28**	5
U1520 S 164	0.55	1.348133	4.069	0.14267	3.803	0.93	0.068533	1.447	885	30	867	24	**860**	**31**	3
U1520 S 123	0.52	1.297855	3.73	0.142467	3.469	0.93	0.066071	1.369	809	29	845	21	**859**	**28**	-6
U1520 S 134	0.61	1.330192	3.38	0.141544	2.789	0.83	0.068159	1.909	873	40	859	20	**853**	**22**	2

U1520 S 160	0.58	1.329009	4.463	0.141379	3.855	0.86	0.068177	2.249	874	47	858	26	**852**	**31**	2
U1520 M 44	0.44	1.325638	4.339	0.141358	4.053	0.93	0.068015	1.549	869	32	857	25	**852**	**32**	2
U1520 S 163	0.48	1.378327	4.513	0.141324	4.273	0.95	0.070735	1.453	950	30	880	27	**852**	**34**	10
U1520 S 154	0.87	1.316237	4.572	0.14099	4.25	0.93	0.067709	1.686	860	35	853	26	**850**	**34**	1
U1520 S 162	0.52	1.331048	4.277	0.14085	4.024	0.94	0.068539	1.449	885	30	859	25	**849**	**32**	4
U1520 S 135	0.74	1.305307	3.649	0.14058	3.285	0.9	0.067342	1.588	848	33	848	21	**848**	**26**	0
U1520 M 41	0.44	1.322113	3.138	0.140075	2.546	0.81	0.068455	1.834	882	38	855	18	**845**	**20**	4
U1520 S 149	0.3	1.33605	4.539	0.140048	4.299	0.95	0.06919	1.456	904	30	862	26	**845**	**34**	7
U1520 S 147	0.71	1.326292	4.338	0.139867	3.864	0.89	0.068774	1.97	892	41	857	25	**844**	**31**	5
U1520 S 137	0.68	1.313995	4.409	0.139257	4.221	0.96	0.068435	1.275	882	26	852	25	**840**	**33**	5
U1520 S 143	0.65	1.340893	2.961	0.139138	2.536	0.86	0.069895	1.528	925	31	864	17	**840**	**20**	9
U1520 S 165	0.65	1.312321	4.315	0.138957	4.148	0.96	0.068495	1.189	884	25	851	25	**839**	**33**	5
U1520 M 51	0.47	1.302825	3.49	0.138952	3.283	0.94	0.068002	1.184	869	25	847	20	**839**	**26**	3
U1520 S 170	0.5	1.331384	3.402	0.138891	3.016	0.89	0.069523	1.573	914	32	859	20	**838**	**24**	8
U1520 M 52	0.48	1.305216	3.367	0.138879	3.161	0.94	0.068163	1.159	874	24	848	19	**838**	**25**	4
U1520 S 140	0.49	1.296167	5.605	0.138706	5.242	0.94	0.067774	1.983	862	41	844	32	**837**	**41**	3
U1520 M 48	0.52	1.303712	4.262	0.138679	4.05	0.95	0.068182	1.326	874	27	847	24	**837**	**32**	4
U1520 M 42	0.28	1.351851	3.468	0.138373	2.951	0.85	0.070856	1.821	953	37	868	20	**835**	**23**	12
U1520 M 46	0.4	1.306506	3.395	0.138252	2.985	0.88	0.068539	1.617	885	33	849	20	**835**	**23**	6
U1520 S 158	0.57	1.331089	4.433	0.13775	4.196	0.95	0.070083	1.432	931	29	859	26	**832**	**33**	11
U1520 S 151	0.81	1.312929	3.86	0.137687	3.458	0.9	0.069159	1.714	903	35	851	22	**832**	**27**	8
U1520 S 16	0.47	1.323901	4.46	0.13768	4.304	0.97	0.06974	1.169	921	24	856	26	**832**	**34**	10
U1520 M 40	0.24	1.28806	3.845	0.137639	3.69	0.96	0.067872	1.079	865	22	840	22	**831**	**29**	4
U1520 S 156	0.68	1.312193	3.873	0.13744	3.6	0.93	0.069244	1.428	906	29	851	22	**830**	**28**	8
U1520 S 161	0.61	1.304958	3.538	0.137427	3.244	0.92	0.068869	1.411	895	29	848	20	**830**	**25**	7
U1520 M 49	0.27	1.296471	3.752	0.137182	3.391	0.9	0.068543	1.606	885	33	844	22	**829**	**26**	6
U1520 S 132	0.8	1.285096	4.009	0.137171	3.755	0.94	0.067947	1.404	867	29	839	23	**829**	**29**	4
U1520 S 126	0.31	1.265459	5.56	0.136995	5.428	0.98	0.066995	1.203	838	25	830	32	**828**	**42**	1
U1520 S 130	0.31	1.346621	4.172	0.136966	3.655	0.88	0.071307	2.012	966	41	866	24	**827**	**28**	14
U1520 S 166	0.39	1.329475	5.318	0.136934	4.541	0.85	0.070415	2.767	940	57	859	31	**827**	**35**	12

U1520 S 125	0.76	1.262702	4.302	0.136843	4.097	0.95	0.066923	1.31	835	27	829	24	**827**	**32**	1
U1520 S 153	0.75	1.314306	3.69	0.136745	3.324	0.9	0.069708	1.603	920	33	852	21	**826**	**26**	10
U1520 S 145	0.49	1.302235	3.455	0.13664	3.172	0.92	0.069121	1.37	902	28	847	20	**826**	**25**	9
U1520 S 141	0.3	1.30903	4.32	0.136553	3.989	0.92	0.069526	1.66	914	34	850	25	**825**	**31**	10
U1520 S 127	0.61	1.247831	4.467	0.136553	4.124	0.92	0.066275	1.714	815	36	822	25	**825**	**32**	-1
U1520 S 142	0.63	1.290144	4.99	0.136541	4.802	0.96	0.068529	1.354	885	28	841	29	**825**	**37**	7
U1520 S 171	0.27	1.294688	4.997	0.136432	4.839	0.97	0.068825	1.247	893	26	843	29	**824**	**37**	8
U1520 S 150	0.48	1.348624	4.042	0.13639	3.796	0.94	0.071715	1.388	978	28	867	24	**824**	**29**	16
U1520 S 144	0.66	1.261277	3.763	0.13622	3.462	0.92	0.067153	1.476	843	31	828	21	**823**	**27**	2
U1520 M 39	0.21	1.288671	4.061	0.135637	3.606	0.89	0.068907	1.868	896	39	841	23	**820**	**28**	8
U1520 S 129	0.7	1.255024	4.374	0.135368	4.056	0.93	0.067241	1.637	845	34	826	25	**818**	**31**	3
U1520 S 131	0.47	1.27042	3.498	0.135356	3.248	0.93	0.068072	1.298	871	27	833	20	**818**	**25**	6
U1520 S 128	0.69	1.249643	4.4	0.135302	3.666	0.83	0.066985	2.434	837	51	823	25	**818**	**28**	2
U1520 S 172	0.52	1.289374	4.811	0.135252	4.561	0.95	0.069141	1.532	903	32	841	28	**818**	**35**	9
U1520 S 136	0.74	1.270842	4.526	0.135074	4.24	0.94	0.068237	1.583	876	33	833	26	**817**	**33**	7
U1520 S 159	0.19	1.277821	4.263	0.133804	3.989	0.94	0.069263	1.505	907	31	836	24	810	30	11
U1520 S 133	0.35	1.251436	4.454	0.133762	4.297	0.96	0.067854	1.172	864	24	824	25	809	33	6
U1520 S 139	0.76	1.33049	5.269	0.132147	4.909	0.93	0.073022	1.913	1015	39	859	31	800	37	21
U1520 S 146	0.68	1.281826	4.428	0.131996	4.262	0.96	0.070432	1.2	941	25	838	25	799	32	15
U1520 S 169	0.53	1.253747	4.073	0.131264	3.876	0.95	0.069273	1.252	907	26	825	23	795	29	12

Notes: 1/13/2016

Isotope ratios and ages are NOT corrected for initial common Pb.
Isotope ratio and apparent age errors include systematic calibration errors of 0.260377558504708% ($^{207}Pb/^{206}Pb$), 0.625201237497987% ($^{206}Pb/^{238}U$) (all 1-sigma).
Isotope ratios and ages corrected using a measured linear secondary standard age bias - ^{206}Pb count rate relationship.

Trace element concentrations in ppm, calculated using mean count rate method.

Sweep-by-sweep downhole fractionation of U/Pb ratios NOT corrected via Si/Zr fractionation factor.

Backgrounds were monitored between sweeps 12 to 24. Sample counts were integrated from sweeps 35 to 60.

Ablation used a laser spot size of 25 microns, and a laser firing repetition rate of 10 Hz.

Notes: 1/13/2016

Isotope ratios and ages are NOT corrected for initial common Pb.
Isotope ratio and apparent age errors include systematic calibration errors of 0.216544516652568% ($^{207}Pb/^{206}Pb$), 0.7623573901163 19% ($^{206}Pb/^{238}U$) (all 1-sigma).
Isotope ratios and ages corrected using a measured linear secondary standard age bias - ^{206}Pb count rate relationship.

Trace element concentrations in ppm, calculated using mean count rate method.

Sweep-by-sweep downhole fractionation of U/Pb ratios NOT corrected via Si/Zr fractionation factor.

Backgrounds were monitored between sweeps 12 to 24. Sample counts were integrated from sweeps 35 to 60.

Ablation used a laser spot size of 25 microns, and a laser firing repetition rate of 10 Hz.

LA-ICPMS data from sample U1520 continued.

	Concentrations (ppm)																						
Analysis	P	Ti	Y	Zr	Nb	La	Ce	Pr	Nd	Sm	Eu	Gd	Tb	Dy	Ho	Er	Tm	Yb	Lu	Hf	Ta	Th	U	T(°C)
U1520 M53	215.947	1.9416	543.576	50.7974	30.0325		4.6559			0.3381		4.7132	3.0260	49.630	19.633	99.382	31.654	358.219	43.666	159.177	23.009	59.2214	325.81	628
U1520 S168	311.876	2.7808	191.445	51.9195	18.2127		15.485	0.0881	2.1949	5.9769	0.4955	39.618	16.595	207.646	78.228	318.909	77.090	797.807	92.220	104.667	9.7454	154.701	361.716	655
U1520 M43	373.364	2.3420	113.46.49	50.1721	43.356 7	43.7064	73.1169	18.5275	94.2862	39.709 5	0.9780 7	44.3103	13.025	128.839	43.533 3	206.937	54.795 5	605.391	74.740 1	153.153	27.611 8	127.57	547.471	642
U1520 S124	673.143	2.0894 4	217.17.1	54.4808	7.6134 9		8.7087 7	0.0194 3	0.6393 3	5.4192 8	0.2382	43.157 6	16.466 7	218.589	85.579 8	355.864	84.703 3	816.802	102.493	109.486	2.9226 4	112.391	291.814	634
U1520 S138	325.742	3.8849 7	236.15.7	60.7655	16.745 2		13.2651	0.0311 8	1.7031 9	8.0837 2	1.1017 4	51.364	18.966 1	238.227	91.589	382.464	83.793 2	780.821	114.291	134.649	6.4580 8	126.684	225.616	682
U1520 S157	392.444	3.2314 6	244.8.02	60.6741	10.1051		11.2129	0.0743 4	2.4698 3	6.9763 9	0.6599 9	54.369 7	18.628 3	240.882	91.595	388.819	84.408 2	775.233	111.837	124.733	4.0328 3	118.957	215.232	667

U152 0 S 152	410 .13 9	3.1 224 2	486 4.0 1	62 42 38	13. 840 7		19. 463 4	0.2 540 3	6.8 986 1	14. 384 8	1.0 474 3	107 .61 4	38. 503 4	482 .48 8	182 .32 2	752 .86 8	153 .91 7	131 5.4 2	205 .95 3	135 47. 6	5.2 573 7	286 .27 9	377 .03 1	66 5
U152 0 S 155	408 .01 6	1.9 205 2	329 7.9	63 27 12	7.8 112 7	0.7 077	17. 598 2	0.6 419 7	4.4 518 1	11. 617 4	0.4 634 5	71. 616 5	26. 261 5	340 .48 4	128 .56 1	559 .08 2	120 .84 3	106 1.8 5	159 .50 4	138 76. 3	4.1 417 8	269 .91 6	435 .52 7	62 7
U152 0 S 164	583 .66 4	2.3 13	480 8.1 9	52 55 02	21. 956 9	1.8 631 2	23. 653 3	0.6 760 2	8.2 906 3	12. 818 9	0.4 240 2	100 .12 3	38. 868 4	498 .97 2	181 .70 4	764 .31 2	172 .39 7	164 0.3 8	199 .28 6	112 02. 4	6.7 954	404 .01 4	736 .69 3	64 1
U152 0 S 123	450 .91 5	2.9 245 8	404 7.6 4	54 19 96	16. 18	2.2 769	20. 617 4	0.7 307 9	4.5 259 5	12. 264 7	0.3 273 3	86. 466	33. 574 2	435 .93 9	160 .71 9	649 .73 7	148 .68 3	137 8.0 8	170 .63 4	118 92. 7	6.2 872 2	297 .25 5	575 .45 3	65 9
U152 0 S 134	343 .12 1	2.4 360 6	462 0.8 8	60 61 09	19. 472 9	0.9 257 6	19. 220 5	0.5 616 2	6.0 820 9	13. 203 8	0.2 411 6	89. 839 9	36. 764 3	465 .86 2	174 .22 1	744 .47 3	158 .03 5	135 0.4 5	206 .55 8	160 72. 9	11. 000 8	361 .41 3	590 .27 5	64 5
U152 0 S 160	515 .69 7	2.4 674 5	363 3.9 6	55 37 22	8.4 374 7	0.2 646 9	15. 583 6	0.2 424 7	4.7 565 3	10. 429 2	0.6 289 9	77. 271 7	29. 139 9	364 .88 5	140 .88 2	582 .28 6	133 .27 1	121 0.3 3	159 .85 5	117 73. 5	3.8 371 5	286 .05	495 .10 9	64 6
U152 0 M 44	111 1.8 6	1.8 904 2	365 0.5 4	50 62 65	18. 436 9	0.0 108 6	11. 786 8	0.0 370 9	1.9 177 1	8.5 351 1	0.2 078 7	67. 587 3	28. 739 6	383 .50 7	148 .28 2	618 .42 6	151 .18 8	141 8.5 2	165 .78 5	105 78. 4	6.1 960 5	372 .77	847 .07	62 6
U152 0 S 163	433 .96 6	2.3 226 8	360 6.7 5	53 70 79	31. 340 5	2.7 752 2	24. 947 2	0.8 522 1	6.5 579 6	10. 253 1	0.3 623 8	75. 53	30. 136 2	373 .25 4	139 .33	596 .26 6	139 .10 2	131 5.2	159 .67 9	119 91	13. 111 8	345 .11 1	717 .67 6	64 2
U152 0 S 154	655 .28 1	4.1 601	649 8.5 3	64 48 99	11. 540 5	9.9 101 8	50. 770 2	7.5 359 7	57. 004 1	50. 441 2	1.7 014 4	190 .09 9	58. 356 3	682 .8	247 .00 8	994 .50 3	196 .64 2	162 3.8 3	256 .83 3	132 61. 1	4.3 051 4	389 .22 9	444 .85 5	68 8
U152 0 S 162	644 .24 3	1.6 095 8	409 3.5 9	54 52 70	23. 874 2		17. 856 5	0.0 923 4	2.6 206 4	9.3 909	0.2 661 8	72. 010 3	30. 817 3	413 .83 5	155 .08 5	674 .26 6	152 .08 6	141 8.7 9	181 .68 4	122 85. 4	8.2 214 8	392 .41 5	754 .48 2	61 5
U152 0 S 135	473 .90 8	2.6 209 3	629 9.8 9	62 29 86	14. 103 6	0.9 967 5	24. 855 3	0.7 203 2	9.5 668 4	22. 153 8	0.7 458 7	132 .57 6	48. 610 4	619 .95 8	233 .12 3	988 .01 8	212 .38 5	175 5.5 1	266 .77 4	135 19. 4	4.7 307 9	503 .51 6	678 .65 3	65 1
U152 0 M 41	395 .03 1	2.4 721 2	280 8.9 5	51 56 27	28. 449 1	0.1 860 6	18. 977 5	0.1 167 5	2.5 515 9	8.5 634 2	0.2 207 7	56. 239	23. 399 5	310 .51 7	112 .93 2	472 .24 5	108 .26 6	109 2.5	121 .97 3	109 89. 6	10. 862 1	247 .90 2	564 .52 4	64 6
U152 0 S 149	259 .77 1	1.7 791 1	170 5.0 3	60 46 75	57. 684	0.1 230 8	9.3 003 6	0.0 982 9	0.6 064 4	2.0 658		14. 645	8.0 88	132 .60 2	58. 103	309 .94 6	83. 517 3	923 .51 2	155 .26 7	224 92. 2	31. 875 6	223 .94 4	751 .32 3	62 2

U152 0 S 147	444 .35 8	4.1 631 1	371 5.2	59 60 85	8.1 758 3	5.3 015 7	25. 356 1	2.7 960 5	24. 793 4	20. 255 2	1.6 087 9	96. 599 3	33. 968 6	403 .58 1	145 .78 3	603 .47 2	128 .69 3	115 7.2 8	157 .53 7	110 67. 8	3.0 479 8	209 .71 5	297 .27 3	68 8
U152 0 S 137	507 .52	3.0 653 1	558 4.6 5	61 59 06	12. 501	0.0 501 9	20. 049 8	0.2 543 6	5.9 744 1	17. 019 7	0.6 598 1	125 .08 1	44. 108 2	564 .34 6	211 .60 7	882 .12 2	189 .23 9	164 4.0 7	235 .44 2	133 54. 8	4.5 904	401 .09 6	592 .90 8	66 3
U152 0 S 143																								68 3
U152 0 S 165	511 .24 2	3.2 319 3	520 7.9	52 00 58	21. 346 5	0.4 476 6	31. 153 7	0.3 157 2	6.5 405	16. 792 9	0.4 903	112 .77 9	42. 761 5	556 .99	203 .61 4	830 .38 1	183 .06 9	168 3.3 9	205 .15 2	105 54. 5	8.1 093 6	489 .46 5	751 .31 1	66 7
U152 0 M 51	470 .78 2	2.2 446 9	321 8.7 3	50 65 42	27. 333 1	0.0 016 4	22. 294 3	0.0 316	1.9 144	7.5 270 9	0.2 000 4	61. 522 6	26. 336 7	342 .64 6	125 .22 9	524 .19 5	121 .31 3	116 5.5 3	131 .39 6	107 61. 4	9.8 564 2	328 .97 9	702 .20 5	63 9
U152 0 S 170	425 .07	2.5 960 2	386 7.9 9	52 15 66	24. 941 3	0.1 928 8	27. 821 8	0.1 293 2	3.6 494 5	11. 415 7	0.5 160 9	86. 457 3	30. 728 1	410 .96 3	151 .07 8	632 .03 4	142 .60 4	132 7.3 2	159 .20 1	111 84. 2	10. 444 3	309 .47 1	622 .47 3	65 0
U152 0 M 52	519 .33 3	3.2 992 8	337 0.9 2	51 72 13	24. 190 5	25. 081 7	86. 89	10. 950 1	73. 459 3	28. 732 8	1.1 165 8	97. 558 1	31. 120 6	378 .55 4	132 .60 5	548 .28 7	124 .89 9	118 7.9 8	133 .66 6	102 32. 2	9.4 380 4	242 .63 1	505 .85 2	66 9
U152 0 S 140	302 .02 9	1.7 714 3	264 2.3 4	57 88 57	29. 551 9	1.0 481 2	12. 756 1	0.4 316 1	5.0 906 9	9.2 544 8	0.6 253 6	61. 088 2	20. 676 4	266 .12 9	100 .74 4	422 .36	97. 250 6	905 .74 5	130 .76 3	124 89. 3	12. 259 9	201 .93 7	414 .21 3	62 2
U152 0 M 48	483 .74 4	2.6 618 3	528 1.6 9	51 97 56	22. 334 5	0.7 721 7	21. 530 7	0.2 808 6	5.5 355 1	14. 292 5	0.2 859 3	106 .96 1	43. 449 3	565 .01 5	210 .12	883 .37 5	198 .08	183 8.3 3	213 .62	117 79. 4	7.1 249	441 .49 9	848 .52 2	65 2
U152 0 M 42	437 .38 1	1.6 959	224 6.3 4	48 94 52	43. 628 9	25. 893 2	45. 935 9	6.2 437 8	40. 004 1	23. 979 3	0.7 684 3	64. 108 8	20. 271 5	248 .04 2	86. 011 9	380 .15 3	96. 038 6	982 .81 5	117 .80 8	140 68. 8	28. 723 1	215 .03 6	770 .28 5	61 8
U152 0 M 46	335 .34 6	3.2 288 4	247 4.2 2	51 77 59	30. 366 6	1.5 009 3	20. 902 4	0.8 664 9	8.0 725 4	10. 102 8	0.2 350 8	54. 101 8	21. 719 8	269 .79 6	98. 555 5	420 .56 9	99. 031 3	950 .45 7	113 .62 2	129 60. 1	15. 136 8	226 .16 6	560 .50 2	66 7
U152 0 S 158	402 .77 3	2.6 414 4	399 5.0 4	59 47 87	17. 023 5	1.3 803 4	27. 781 8	0.5 971 2	9.7 782 7	14. 415	0.5 508 9	91. 507 3	34. 514 7	427 .69	155 .11 2	651 .71 3	141 .81 9	129 3.0 7	187 .81 7	147 18. 8	29. 326 6	327 .84 6	571 .02 6	65 1
U152 0 S 151	564 .84 5	2.3 539 5	533 8.9 8	62 15 22	20. 485 1	3.7 846 8	29. 931	1.6 090 5	13. 213 5	17. 123 4	0.5 403 2	113 .73 5	41. 032 5	524 .14 8	201 .95 8	843 .47 2	178 .79	153 5.1 1	238 .57 2	142 33. 1	7.8 960 6	646 .56 5	798 .70 6	64 3

U152 0 S 16	392 .95 5	4.1 216 3	379 6.8 2	51 23 49	16. 537 5	0.0 575 6	15. 412 1	0.1 027 6	2.6 627 1	9.2 913 7	0.3 716 4	76. 951 5	29. 743 3	403 .78 6	147 .94	625 .65 7	148 .04 4	144 6.4 7	158 .30 3	120 73. 4	6.6 665 4	286 .32 3	613 .37 2	68 7
U152 0 M 40	365 .42 4	2.2 431	139 7.4 3	50 29 49	89. 732	1.1 668	11. 592 2	0.7 095 2	4.5 925 4	4.6 013	0.1 149 7	20. 738 8	8.9 989 3	124 .77 7	50. 697 2	253 .04 9	71. 955 6	866 .34 8	108 .89 8	175 59. 5	56. 714 6	279 .95 1	117 6.2 1	63 9
U152 0 S 156	487 .67	2.3 016 8	428 6.0 2	60 93 42	35. 325 7	1.2 838 1	29. 040 9	0.6 182 8	4.6 422 6	11. 149 7	0.5 860 9	87. 668 2	33. 012 7	439 .52	165 .62 9	685 .11 3	146 .09 8	131 6.5 5	184 .41 9	143 97	12. 798	443 .03 6	651 .13 5	64 1
U152 0 S 161	488 .73 6	2.0 218 1	499 6.8 3	55 12 42	15. 401 2		20. 512 2	0.2 316 4	5.0 949 4	13. 872 5	0.4 042 2	104 .72 5	39. 457	514 .41 7	191 .21 3	793 .73 1	177 .70 2	158 2.5 8	202 .76	117 17. 6	5.5 820 1	394 .18 5	646 .44 2	63 1
U152 0 M 49	357 .90 3	2.1 239 5	156 0.6	51 19 14	88. 523 1	0.0 585 8	11. 193 2	0.0 463	0.1 984 8	1.6 604 8		17. 715 8	8.5 279	129 .61 7	54. 696 9	286 .03 1	81. 573 9	926 .44	119 .18 7	172 90. 3	55. 254 1	299 .54 2	108 9.8 7	63 5
U152 0 S 132	553 .42 4	2.8 073 5	486 4.3	61 88 73	21. 630 4	2.2 447 2	35. 606 5	1.3 109 1	12. 122 3	18. 248 8	0.5 499 9	106 .56 1	39. 119 2	491 .57 1	185 .65 7	763 .32 2	162 .86 5	140 6.4 8	201 .92 3	129 19. 1	7.6 756 1	499 .83 7	624 .95	65 6
U152 0 S 126	377 .18	2.9 251 5	194 8.7 1	54 33 71	90. 706 2	0.1 196 8	12. 426 9	0.1 433 7	1.0 251 9	3.1 300 3	0.0 343 3	23. 801 6	11. 787 1	169 .38 9	70. 830 7	351 .09 1	100 .07 5	107 3.9	153 .34 7	184 64. 4	50. 773 3	335 .24 3	107 3.1 5	65 9
U152 0 S 130	335 .76 6	3.0 487 4	188 5.6 6	60 04 00	96. 174 7	6.7 042 3	16. 777 9	2.2 632 7	15. 569 3	10. 519 9	0.4 274 5	37. 445 7	15. 592 9	198 .87 2	74. 165 4	349 .30 8	91. 993 1	950 .34 8	147 .68 1	218 40. 8	48. 987 7	266 .87 1	871 .81 5	66 3
U152 0 S 166	499 .50 1	1.7 591 9	228 4.4 9	50 02 29	12. 838 6	1.6 117 1	14. 907 5	1.0 076 5	6.2 871 8	11. 186 4	0.3 779 5	52. 220 4	18. 966 5	244 .53 4	89. 328 9	382 .14 4	90. 460 8	927 .96 2	104 .49 2	101 52. 9	11. 710 6	173 .86 7	444 .42 4	62 1
U152 0 S 125																								66 5
U152 0 S 153	630 .76 6	6.5 344 5	610 8.0 4	61 78 12	14. 028 1	0.8 961	25. 156 4	0.6 689 9	6.3 839 1	16. 676 1	0.5 668 3	129 .38 1	48. 720 5	626 .15 1	232 .39 6	963 .17 1	201 .6	169 8.4 3	263 .53 9	142 83	5.0 034 8	527 .32 8	704 .89 7	72 7
U152 0 S 145	459 .82 5	4.9 284 7	510 2.8	55 58 71	30. 699 2	2.1 926 2	18. 369 7	1.3 005 3	8.6 806 3	14. 768 1	0.3 981 5	94. 082 9	36. 895 1	495 .90 6	192 .76	829 .78 9	191 .81 1	178 3.2 5	241 .65 4	154 00. 9	13. 832 6	461 .49 3	940 .88 7	70 2
U152 0 S 141	345 .19 8	2.3 461 1	186 2.5 4	55 74 26	86. 016	2.2 471 4	30. 945 1	0.8 605 1	7.8 973 3	8.5 782 6	0.2 089 6	26. 757 4	12. 715 2	171 .79 8	65. 374	320 .44 1	87. 329 5	979 .79 9	138 .71 2	191 44. 4	50. 336 8	290 .48 7	967 .07 9	64 2

U152 0 S 127	505 .39 9	3.0 271 2	434 8.1 8	56 11 77	22. 655 2	0.0 840 9	32. 575 5	0.1 309 5	3.9 839	12. 150 2	0.5 614 4	91. 296 3	35. 726 6	455 .96 7	170 .47 8	701 .26 5	157 .09 2	144 5.5 7	186 .95 5	116 03. 6	8.3 206 4	375 .01 7	610 .43 7	66 2
U152 0 S 142	534 .54 4	2.4 598 7	465 0.5 8	54 72 30	17. 598 7	1.4 226	28. 541 7	1.1 753 1	10. 095 5	19. 930 8	0.6 304	108 .63 5	38. 352 2	490 .06 2	178 .99 6	732 .05 3	164 .72 3	153 1.1 6	192 .08 4	115 35	7.2 577 9	439 .16 1	701 .03 5	64 6
U152 0 S 171	296 .03	2.4 891 1	168 9.6	51 55 99	65. 164	0.4 148 6	12. 518 2	0.1 263 4	1.2 472	2.9 796 4	0.0 11	20. 235 1	9.7 582	144 .46 7	59. 070 4	298 .48 4	86. 942 3	101 8.6	126 .00 7	164 52. 1	33. 671 2	244 .97 7	903 .68 4	64 7
U152 0 S 150	406 .89	2.2 497 4	414 4.7 1	60 46 15	41. 173 5	9.9 890 7	35. 754 7	5.6 801 2	39. 128 1	29. 759 3	1.1 423 1	109 .23 4	38. 901 6	448 .66 2	159 .02 7	659 .13 9	145 .62 4	130 0.2 9	207 .71	185 94. 3	30. 816 1	386 .83 2	801 .76 3	63 9
U152 0 S 144	436 .44 8	3.4 334 7	503 6.2 9	56 23 85	10. 675 1		18. 044 6	0.2 581 3	5.9 782 1	17. 366 7	1.0 458 8	115 .67 4	41. 736 2	536 .78 1	193 .61 3	796 .85 1	176 .23 5	159 4.3 6	205 .05 8	111 36. 7	3.9 545 5	324 .19 1	492 .34 5	67 2
U152 0 M 39	279 .06 8	1.7 281 1	108 2.9 3	49 53 82	71. 988 5	0.3 438 3	9.7 538 5	0.2 966 1	1.9 530 8	2.2 874 4		10. 703 6	6.5 260 2	90. 443 7	38. 673 7	197 .89	57. 593 2	714 .37 5	87. 691 1	173 40. 6	47. 505 7	186 .72 6	869 .95 2	62 0
U152 0 S 129	489 .38 3	2.6 306 5	430 9.4 1	59 46 27	28. 720 5		29. 100 4	0.0 457	3.3 555 6	10. 617	0.4 118 7	85. 990 2	33. 347 5	440 .39 4	165 .51	683 .56 1	149 .67 7	130 0.9 4	180 .72 8	135 36. 5	11. 547 9	512 .35 4	731 .01 8	65 1
U152 0 S 131	437 .94 8	2.2 121 2	499 9.0 9	61 49 55	42. 461 7		23. 859 2	0.0 533 6	1.7 557 6	9.8 058 9	0.2 702 7	88. 116 8	37. 806 8	488 .62 4	188 .25 6	814 .2	180 .39 4	159 3.3 7	233 .09 3	149 44. 1	13. 554 6	397 .05	838 .42 5	63 8
U152 0 S 128	422 .58 8	3.0 141 1	556 9.5 6	60 93 38	13. 793 5	1.4 496 1	22. 875 9	0.5 649 6	8.6 924 1	21. 406 8	1.0 521 2	130 .95 6	47. 512 3	582 .05 2	216 .23 5	881 .59 9	186 .72 5	160 1.4 2	228 .52 9	130 06. 8	5.2 561 5	319 .02 6	463 .95 4	66 2
U152 0 S 172	648 .15 2	2.3 669 2	458 2.3 4	50 97 86	15. 301 7	0.5 854 4	19. 923 7	0.6 630 7	7.3 428 2	15. 157 4	0.4 518 9	103 .43 7	38. 981 6	492 .13 9	180 .91 3	733 .23 1	170 .44	170 9.9 6	187 .58 5	107 04. 7	5.3 271 6	388 .28 8	742 .07 2	64 3
U152 0 S 136	507 .95 9	2.8 318 9	541 6.3	60 81 03	24. 178 9	16. 340 7	71. 918 5	7.0 786 6	52. 591 2	31. 421 4	0.7 981 1	128 .31	45. 376 3	550 .51 8	206 .97 2	839 .82	176 .81 1	155 2.4	225 .02 9	135 87. 3	9.5 240 1	513 .27 5	693 .29 4	65 7
U152 0 S 159	243 .34 7	2.1 436	112 3.1 9	57 07 36	63. 457 3	11. 207	31. 119 9	5.5 249 8	31. 873 8	18. 35	0.4 566 3	32. 046	10. 915 7	125 .96 3	45. 403 8	220 .83 4	62. 550 6	705 .85 2	113 .09 1	202 48. 3	78. 349 4	160 .94 4	835 .23	63 6
U152 0 S 133	383 .25 6	2.7 792 4	222 7.5 9	59 42 59	97. 431 5	0.0 114 8	13. 590 8		0.3 363 9	2.9 028 5		21. 977 4	11. 347 6	183 .24 7	77. 850 1	393 .62 4	107 .39 6	114 1.8 4	186 .08 3	214 28	56. 480 4	405 .48 2	116 8.9	65 5

U152 0 S 139	682 .54 6	3.2 535 2	655 7.4 7	60 18 64	25. 227 2	6.1 864 4	63. 483 7	4.2 070 8	29. 702 7	37. 181 7	0.9 761	163 .51 8	56. 957 1	709 .37	247 .23 4	101 2.5 6	219 .27 5	193 7.9 1	268 .23 7	130 20. 1	8.7 645	678 .87 1	897 .41	66 8
U152 0 S 146	520 .78 9	2.8 694 8	596 3.6 8	57 13 12	21. 676 4	2.7 656 8	24. 176 2	1.1 794 4	11. 929 8	20. 844 8	0.7 294 3	130 .77 9	50. 726 2	640 .52 1	233 .43 2	959 .13 9	207 .57 6	186 5.0 3	251 .76 1	136 21. 3	7.8 673 3	597 .76 3	875 .11 4	65 8
U152 0 S 169	485 .07 9	2.3 213 2	440 2.1	53 29 28	28. 316 7	0.5 215 2	27. 734 2	0.6 129 6	5.7 018 2	14. 403 6	0.3 395 8	92. 199 2	36. 390 3	476 .82 8	173 .81 4	710 .51 1	164 .51 3	155 9.9 5	182 .57 5	114 21. 7	9.9 375 9	442 .46 9	827 .77 4	64 2

LA-ICPMS data from sample U1519

		Corrected isotope ratios							Apparent ages (Ma)						
		207Pb*	±2s	206Pb*	±2s	error	207Pb*	±2s	207Pb*	±2s	207Pb*	±2s	206Pb*	±2s	%
Analysis	Th/U	235U*	(%)	238U	(%)	corr.	206Pb*	(%)	206Pb*	(Ma)	235U	(Ma)	238U*	(Ma)	disc.
Inherited core															
U1519 M 63	1.18	9.031352	2.697	0.393466	1.938	0.72	0.166473	1.875	2523	31	2341	25	2139	35	15
U1519 M 73	0.58	6.5983	3.744	0.346495	3.061	0.82	0.138113	2.155	2204	37	2059	33	1918	51	13
U1519 S 179	0.27	6.407044	7.704	0.318252	7.092	0.92	0.146011	3.008	2300	52	2033	68	1781	110	23
U1519 S 181	0.40	7.92542	10.95	0.381378	10.46	0.96	0.150718	3.248	2354	55	2223	99	2083	186	12
Metamorphic growth															
U1519 M 54	0.03	1.35418	4.161	0.142277	3.444	0.83	0.06903	2.335	900	48	869	24	858	28	5
U1519 M 55	0.12	1.401553	4.287	0.148612	3.307	0.77	0.0684	2.729	881	56	890	25	893	28	-1
U1519 M 57	0.01	1.367964	3.645	0.149732	2.838	0.78	0.066261	2.287	815	48	875	21	899	24	-10
U1519 M 59	0.02	1.380155	3.433	0.145566	3.016	0.88	0.068765	1.638	892	34	881	20	876	25	2
U1519 M 62	0.05	1.343866	6.306	0.146451	6.085	0.96	0.066552	1.657	824	35	865	37	881	50	-7
U1519 M 75	0.01	1.350345	4.513	0.135629	2.971	0.66	0.072209	3.397	992	69	868	26	820	23	17
U1519 M 76	0.01	1.412273	4.348	0.150763	4.056	0.93	0.067939	1.567	867	32	894	26	905	34	-4
U1519 M 83	0.02	1.285316	4.622	0.138596	4.276	0.93	0.06726	1.753	846	36	839	26	837	34	1
U1519 M 84	0.01	1.304253	4.345	0.1376	4.002	0.92	0.068745	1.693	891	35	848	25	831	31	7
U1519 M 85	0.02	1.341704	4.012	0.141375	3.742	0.93	0.068831	1.447	894	30	864	23	852	30	5
U1519 M 88	0.04	1.390331	4.168	0.148681	2.686	0.64	0.067821	3.188	863	66	885	25	894	22	-4

U1519 M 89	0.02	1.338851	3.536	0.144342	3.084	0.87	0.067273	1.731	846	36	863	21	869	25	-3
U1519 M 90	0.01	1.298813	4.035	0.139675	3.22	0.8	0.067441	2.432	851	51	845	23	843	25	1
U1519 M 92	0.03	1.375868	4.292	0.144866	3.959	0.92	0.068883	1.656	895	34	879	25	872	32	3
U1519 S 185	0.04	1.348527	4.776	0.140403	3.026	0.63	0.06966	3.696	918	76	867	28	847	24	8
U1519 S 18	0.02	1.369285	4.76	0.143703	4.494	0.94	0.069108	1.569	902	32	876	28	866	36	4
U1519 S 191	0.00	1.386008	5.104	0.145474	4.752	0.93	0.0691	1.863	902	38	883	30	876	39	3
Magmatic population															
U1519 M 58	1.63	1.432964	4.32	0.152299	2.903	0.67	0.06824	3.2	876	66	903	26	914	25	-4
U1519 M 61	0.71	1.459821	4.715	0.154896	3.757	0.8	0.068353	2.848	879	59	914	28	928	32	-6
U1519 M 65	0.60	1.501069	6.261	0.143102	4.879	0.78	0.076077	3.924	1097	79	931	38	862	39	21
U1519 M 70	1.03	1.383455	4.212	0.147175	3.65	0.87	0.068176	2.103	874	44	882	25	885	30	-1
U1519 M 72	0.56	1.433431	5.188	0.148659	4.291	0.83	0.069934	2.915	926	60	903	31	893	36	4
U1519 M 74	0.63	1.383355	3.902	0.14703	3.248	0.83	0.068238	2.164	876	45	882	23	884	27	-1
U1519 M 77	1.13	1.389899	4.2	0.144568	3.033	0.72	0.069729	2.905	920	60	885	25	870	25	5
U1519 M 79	0.63	1.526797	4.928	0.150398	3.801	0.77	0.073627	3.136	1031	63	941	30	903	32	12
U1519 M 87	0.90	1.590199	5.605	0.156412	4.44	0.79	0.073736	3.42	1034	69	966	35	937	39	9
U1519 M 91	0.73	1.324633	4.057	0.140441	3.477	0.86	0.068407	2.091	881	43	857	23	847	28	4
U1519 S 175	1.11	1.35947	4.558	0.142731	4.127	0.91	0.06908	1.936	901	40	872	27	860	33	5
U1519 S 177	1.07	1.593119	4.561	0.156203	4.153	0.91	0.07397	1.886	1041	38	968	28	936	36	10
U1519 S 178	0.29	1.336363	4.778	0.135824	3.933	0.82	0.071359	2.713	968	55	862	28	821	30	15
U1519 S 187	1.05	1.499697	4.668	0.156309	4.155	0.89	0.069586	2.129	916	44	930	28	936	36	-2
U1519 S 190	0.78	1.404378	5.197	0.14786	4.319	0.83	0.068886	2.889	895	60	891	31	889	36	1
U1519 S 192	1.43	1.360874	4.321	0.145233	3.741	0.87	0.06796	2.162	867	45	872	25	874	31	-1
U1519 S 193	0.69	1.382269	3.486	0.14114	2.886	0.83	0.07103	1.955	958	40	881	21	851	23	11
U1519 S 194	1.43	1.379969	3.904	0.147057	2.77	0.71	0.068058	2.75	870	57	880	23	884	23	-2
U1519 S 195	0.34	1.392809	4.054	0.140881	3.398	0.84	0.071703	2.212	978	45	886	24	850	27	13
U1519 S 196	0.73	1.402169	3.995	0.145142	3.219	0.81	0.070066	2.366	930	49	890	24	874	26	6
U1519 S 199	0.60	1.565902	6.008	0.151871	3.419	0.57	0.07478	4.94	1063	99	957	37	911	29	14
Metamorphic growth															
U1519 M 78	0.04	1.476558	5.807	0.12787	4.068	0.7	0.083749	4.143	1287	81	921	35	776	30	40

U1519 M 82	0.14	1.492526	5.663	0.126253	3.957	0.7	0.085739	4.051	1332	78	927	34	766	29	42							
U1519 M 60	0.01	1.265676	4.276	0.12306	3.485	0.82	0.074594	2.477	1058	50	830	24	748	25	29							
U1519 M 80	0.28	1.734074	9.888	0.118945	2.132	0.22	0.105736	9.655	1727	177	1021	64	724	15	58							

LA-ICPMS data from sample U1519 continued.

	Concentrations (ppm)																						
Analysis	P	Ti	Y	Zr	Nb	La	Ce	Pr	Nd	Sm	Eu	Gd	Tb	Dy	Ho	Er	Tm	Yb	Lu	Hf	Ta	Th	U	T(°C)
Inherited core																								
U1519 M 63	245.36	6.5326	997.33	62 48 12	0.8378 5		16.239 7	0.3452 1	4.4975 3	7.2301 4	2.1180 5	26.511 3	9.5340 2	103.80 8	37.165 3	153.11 9	35.327 5	328.41 4	50.486 5	993 0.8 8	0.5038 6	80.070 6	67.829 7	727
U1519 M 73	273.29 6	9.9650 2	998.71 4	58 76 18	6.8668 8		18.175 3	0.0248 7	0.9038	2.6304 9	0.1653	19.366 8	7.2531 4	88.73	36.068 2	162.22 5	40.864 4	391.60 7	56.403 5	116 37. 8	3.1885 6	120.79 7	208.21 3	767
U1519 S 179	341.63 8	6.3505	799.68 9	62 06 67	0.9650 7		6.9035 5	0.0402 5	1.0154	3.5520 4	0.4942 5	14.485 3	5.2114 4	69.623 6	25.603 3	122.37 5	30.311 9	292.57 8	47.099 7	132 37. 6	0.7298 5	65.346 6	246.14 2	725
U1519 S 181	172.11 2	81.181 6	372.39 3	62 44 39	1.4765 8		8.5680 1	0.0464 6	0.4804 5	1.1418 3	0.3667 3	5.9961 5	2.5897 6	29.787 8	11.335 8	56.989 8	15.135 3	152.02 7	29.413 2	138 16. 3	1.5386 2	101.57 1	251.33 3	1023
Metamorphic growth																								
U1519 M 54	76.877 5	1.0403 6	238.16 1	54 89 95	0.8714 3	0.0650 2	1.4192 4	0.0936 1	0.5801 1	0.6039 8	0.1851 7	1.8564 9	1.1873 9	16.676 7	7.0705 9	39.226 5	12.659 9	146.85 3	23.536 9	109 26. 4	0.7401 2	13.213 6	416.98 8	585
U1519 M 55	80.266 6	1.2452	273.27 4	56 30 91	0.5525 2		2.1489 5			0.2247 6	0.1324 2	2.3455 2	1.6282 8	20.363 8	8.8397 3	44.498 7	12.000 7	145.71	23.457 9	129 26. 9	0.4417 5	25.751 9	206.36 1	597
U1519 M 57	91.669 4	1.1332 8	139.09 5	55 94 12	0.6078 5	0.2471 8	1.2744 3	0.1406 6	1.1132 5	0.3673 7	0.1892 2	1.1375 5	0.4985 8	9.2897 4	4.1648	23.964 1	7.3270 8	92.036 8	16.249 3	113 75. 2	0.6794 9	3.3485 4	257.40 6	590
U1519 M 59	72.906 3	1.2143	282.85 3	58 07 45	1.0391 1		1.1451				0.0828 7	2.7103 7	1.1975 7	20.738 1	8.6407	47.366 6	14.056 2	165.09 9	28.534 6	118 61. 4	0.8743 1	8.6405 8	448.19 9	595
U1519	106	1.1	323	59	0.6	0.1	2.3	0.1	0.6	0.8	0.4	4.1	1.5	22.	9.7	53.	14.	171	31.	134	0.4	20.	392	59

9 M 62	.127	8371	.841	6224	5907	2651	0276	4972	1724	0037	1081	0314	5457	5682	6781	0423	3836	.406	8089	65.5	5712	4889	.747	3
U1519 M 75	79.8912	0.8615	107.799	59 78 87	0.3647 6	0.1519 4	1.0663 6	0.0905 2	0.8697 9	0.2388 4	0.0968 5	0.6829 9	0.4179	6.0942 9	2.8496	17.2801	5.9526 3	88.1035	20.3138	127 77.9	0.2063 9	3.3805 3	385.016	572
U1519 M 76	82.1913	0.8571 4	192.398	59 37 67	0.8558 6	0.0706 2	1.4184 2	0.1016 7	0.7875 9	0.656	0.2053	1.6490 2	0.7939 5	12.0497	5.8657 9	35.9555	10.6406	131.478	24.1823	124 86.4	0.7953 1	2.8059 5	326.992	572
U1519 M 83	61.6073	0.3409 4	183.828	61 33 22	0.4202 3		0.9127 9				0.0792 6	1.3060 5	0.6351 7	10.7255	5.3652 4	29.7812	9.1821	104.436	21.8774	142 69.5	0.3386 1	5.9152 1	381.899	516
U1519 M 84	101.794	0.5080 1	259.29	61 98 75	0.6880 4	0.0429	0.9706 6	0.0686 1	0.4928 4	0.2349 5	0.2250 5	2.0752 9	1.0531 4	16.4034	7.7462 3	42.8386	13.0875	152.384	30.9481	129 77.6	0.7289 5	4.9673 8	391.704	539
U1519 M 85	104.975	2.0854 3	290.386	62 37 46	1.2562 7	0.4418 7	3.0074 8	0.2904	2.7370 9	1.1135 7	0.4273 5	3.1566 5	1.3871 3	20.387	8.2078 7	46.201	12.723	152.108	27.8196	128 94.7	1.3464 2	10.7272	624.27	634
U1519 M 88	112.626	0.6929 7	126.685	59 15 20	0.5602 8		0.9576 3				0.0818	0.3048 4	0.5340 4	7.9145 6	3.8468 8	20.3119	6.1130 4	73.8283	12.1411	118 83.8	0.6599 4	5.1868 5	138.68	558
U1519 M 89	83.2086	1.2006 4	215.822	57 65 47	0.9509 2	0.0207 1	1.1985 5	0.0552 5	0.5255 1	0.1443	0.1457 3	2.0426 4	1.0385 6	14.2431	6.6328 8	34.9188	11.2081	132.934	23.0096	115 20.5	1.098	8.2951 5	549.917	594
U1519 M 90	85.011	0.2114 7	162.302	56 95 00	0.6181 2		0.3434 7				0.0643 8	1.0427 3	0.5522 5	9.9365 5	5.0230 2	29.1613	9.1081 3	119.857	20.3716	111 97.5	0.6948 2	1.6541 9	269.069	490
U1519 M 92	72.3517	0.8840 4	295.375	56 07 18	0.8594	0.0644	1.8962 7	0.0174 5	0.2987 6	0.1777 5	0.1408 5	1.9625 5	1.4620 3	21.1013	9.3464 9	50.6772	14.4402	173.658	27.3374	120 60.6	0.7045	15.0108	447.07	574
U1519 S 185	50.8142	0.8121	81.7755	63 72 67	0.0684 6		0.5886 3			0.0579 8	0.1959 8	1.6685 2	0.7817 3	6.5559 5	2.2267 1	9.908	2.1557 7	25.8595	6.0522 2	120 19.2		3.6931 9	89.4855	574
U1519 S 18	85.326	0.7705	231.218	60 51 41	0.7523 6		0.9608 4			0.3513 7	0.0932 4	1.3720 6	0.9226 6	14.3865	6.6441 6	37.7106	11.1032	131.95	25.9137	132 41.4	0.8500 6	10.6079	484.489	565
U1519 S 191	58.3182	1.0772 4	264.121	54 55 45	0.8309 6		0.3202 3		0.0795	0.1059 8	0.1050 3	0.9277 1	0.9535 1	17.6598	8.2911 2	44.8646	14.8253	196.289	31.5266	108 38.4	0.9131 8	1.3882 9	394.103	587
Magmatic population																								

U151 9 M 58	220 .63 2	15. 183 5	846 .63	56 75 88	0.6 557	0.0 534 7	27. 880 9	0.3 895 7	5.5 513 1	8.1 030 6	1.9 260 4	27. 688 5	7.9 596	90. 655 7	29. 868 4	124 .86 1	29. 686 2	277 .39 7	37. 947 4	912 6.2 3	0.5 075 9	195 .33	119 .85 5	81 0
U151 9 M 61	182 .94 4	6.1 655 3	465 .39 5	60 23 15	0.7 891 6		12. 183 9	0.0 585 9	1.0 716 7	2.0 442	0.8 777 7	10. 608 2	3.5 748 8	42. 235 5	15. 710 9	73. 536 4	19. 461 3	195 .92 3	30. 270 7	924 2.7 4	0.3 000 4	75. 966 5	106 .38 5	72 2
U151 9 M 65	282 .84 5	14. 459 7	117 4.5 4	62 04 77	1.8 254 9	2.9 879	26. 354 5	1.9 720 4	12. 985 4	10. 723 4	3.8 823 8	34. 839 7	9.7 005 1	113 .37 7	40. 293 7	171 .57 5	40. 186 1	379 .95 5	62. 021	107 28. 4	0.4 058 7	195 .67 5	326 .19 8	80 5
U151 9 M 70	137 .10 1	3.8 568	362 .93 1	61 44 04	0.5 885 9		22. 755 4	0.0 248 5	0.5 234 6	1.3 315 7	0.4 629 7	8.0 595 5	2.7 117 1	29. 753 8	11. 738 4	55. 033 6	15. 145 8	158 .46 1	27. 374 9	114 26. 8	0.4 357 6	211 .91	206 .07 2	68 2
U151 9 M 72	223 .88 7	5.2 396 2	495 .13 8	61 42 57	0.4 791 9		8.5 759 4		0.7 948 2	1.9 144 8	0.7 540 5	8.2 297 8	2.9 069 2	37. 302 9	15. 488 1	76. 863 9	21. 964	244 .16 6	43. 103 4	987 9.1 8	0.1 987 2	74. 983 2	133 .85	70 8
U151 9 M 74	269 .40 5	8.7 770 2	123 7.0 8	60 25 92	1.5 698		19. 680 4	0.0 767 5	2.1 340 8	2.4 895 4	1.7 257 6	23. 399 6	8.7 987 1	105 .20 4	43. 174 7	192 .23 5	46. 992 4	476 .36 5	75. 832 1	935 5.7 3	0.6 553 2	169 .38	266 .92 8	75 5
U151 9 M 77	158 .40 4	4.8 593	327 .97 6	60 12 94	0.6 142 9		20. 564 9	0.0 373 1	1.0 237 9	1.4 056 1	0.4 960 5	7.8 951 3	2.4 741 8	29. 500 4	11. 094 8	50. 117 7	13. 293 3	149 .75 9	25. 622 2	105 06. 5	0.4 364 5	146 .87 3	130 .31 1	70 1
U151 9 M 79	236 .19 1	4.3 131 9	743 .09 6	59 52 76	0.8 958 3	3.1 579 8	18. 821 8	1.5 41	9.5 399 2	7.9 004 2	2.8 974 5	24. 003 2	6.7 761 2	72. 360 5	25. 260 2	101 .81 1	24. 632 9	246 .11	38. 844 1	102 33. 9	0.3 349 4	133 .39 6	212 .03 2	69 1
U151 9 M 87	148 .89 3	4.7 901	199 .68 9	63 14 19	0.4 052 4		15. 118 5	0.0 325 3	0.1 318	0.8 664 7	0.3 212	3.5 565 3	1.4 337 7	16. 386 9	6.4 377	31. 457 2	8.7 443 1	97. 374 7	17. 308 2	112 50. 3	0.3 355 9	85. 853 5	95. 518 2	70 0
U151 9 M 91	272 .74 5	10. 498 6	101 7.6 6	57 30 74	1.8 990 9	0.0 099 6	15. 719 5	0.0 430 6	2.1 686 7	2.9 613 3	1.3 803 2	20. 435 4	7.2 243	92. 767 9	35. 232 9	158 .76 2	39. 280 2	398 .10 7	58. 700 3	814 2.4 3	0.5 893 7	178 .67 9	243 .97 6	77 2
U151 9 S 175	165 .08 8	4.8 450 7	550 .07 9	56 08 36	1.0 805 2		22. 904	0.0 274	1.6 563 4	3.3 332 7	0.9 098 1	11. 607 8	3.7 066 3	45. 543 6	17. 604 6	82. 596 4	22. 203 4	263 .73 9	41. 545 1	896 2.5 2	0.5 248 2	240 .08 8	216 .58 5	70 1
U151 9 S 177	128 .97 8	3.8 394 5	455 .15 9	59 73 41	0.9 321 3	0.5 387 5	23. 558 2	0.4 685 8	4.0 47	4.0 472 1	1.1 887 2	12. 194 3	3.0 320 5	39. 666 7	14. 759 8	68. 486	19. 092 6	205 .30 7	37. 618 9	111 26. 2	0.3 847 2	198 .76 7	186 .27 7	68 1
U151 9 S 178	130 .71 3	3.1 921 5	107 5.3 3	61 39 58	3.1 477 2	0.3 866 3	17. 912 2	0.3 755 4	2.7 597 8	2.9 857 5	1.4 641 3	18. 269 4	6.5 606 9	88. 571 9	34. 901 3	164 .78 6	41. 757 4	429 .67 1	71. 955 8	132 58. 7	1.4 540 9	143 .73	500 .34	66 6

U151 9 S 187	111 .60 4	3.5 932 6	280 .52 3	62 03 94	0.5 299 1		14. 809 5		0.6 815 6	0.8 932 6	0.4 084 4	5.7 791	1.7 536 5	22. 272 4	8.5 058 4	42. 671 3	10. 542 1	128 .67 5	23. 477 9	115 68. 8	0.3 098 7	131 .69 1	125 .33 1	67 6
U151 9 S 190	263 .50 3	6.6 822 2	990 .71 4	58 33 28	0.8 694 7		11. 838 2	0.1 082 8	1.7 907	3.6 695 1	1.4 422 6	20. 662 1	7.1 421 9	88. 242 4	33. 105 7	159 .22 5	39. 573 8	416 .30 8	68. 807 7	835 9.6 7	0.3 530 8	149 .55 5	192 .41 4	72 9
U151 9 S 192	466 .96 4	16. 093 5	319 5.6 9	61 79 26	3.4 657 3	0.7 462 1	56. 377 7	2.0 857 2	28. 150 1	38. 321 7	16. 863 9	152 .93 7	39. 153 7	373 .29 4	112 .47 1	407 .11 4	85. 064 8	742 .45 6	112 .43 4	939 6.1 8	0.7 139	592 .63 8	414 .91 4	81 6
U151 9 S 193	231 .39 5	5.5 309 5	977 .61 3	61 38 80	1.1 086 5	0.7 059	18. 069 4	0.7 321 8	6.6 701 8	5.5 283 7	2.2 852 1	26. 916 3	8.4 722 3	87. 310 4	33. 380 1	138 .81 9	32. 007 8	316 .02 1	57. 098 8	103 72. 5	0.5 574	192 .39 5	279 .26 8	71 2
U151 9 S 194	160 .30 7	3.7 459 5	494 .33 5	62 35 76	0.8 078 6		23. 004	0.0 588	1.3 758 6	2.0 436 6	0.7 759 3	10. 499 8	3.4 640 3	41. 022 5	15. 645 2	77. 060 4	19. 351 4	206 .95 8	39. 710 3	117 05. 1	0.4 704 3	232 .96 6	162 .96 1	67 9
U151 9 S 195	215 .66 7	9.0 832 3	144 7.4 1	61 62 06	3.2 975 3	3.6 694 2	30. 909 4	2.9 569 5	18. 827 3	12. 046 6	4.9 379 2	34. 012	10. 437 4	122 .79 7	45. 853 6	209 .39 2	51. 940 5	520 .22 8	90. 766 4	126 27. 6	1.3 616 9	173 .29 1	517 .13 9	75 8
U151 9 S 196	152 .65 7	2.5 418 8	513 .17 7	62 75 23	0.7 730 5		18. 237 8	0.0 313 1	0.4 464 5	2.7 423 4	0.5 877 8	10. 830 8	3.7 659 4	44. 624 9	17. 341 8	78. 806 6	18. 194 9	188 .91 8	33. 088 2	124 17. 1	0.4 055 8	170 .61 7	234 .78 1	64 8
U151 9 S 199	215 .48 9	7.9 202 7	741 .89 2	57 70 75	1.0 074 1	0.5 052	14. 983 2	0.4 720 6	3.3 224 1	5.7 097 5	1.6 759 4	16. 609 2	5.4 954	67. 621 8	25. 197 9	110 .97 7	27. 649 7	293 .64 9	46. 647 2	890 5.8 3	0.3 420 5	112 .57 7	186 .87 2	74 5
Metamorphic growth																								
U151 9 M 78	99. 327 9	4.7 272 6	335 .09 5	59 70 51	0.7 901 3	2.1 234 8	11. 271	1.6 301 7	12. 442	6.0 067 2	2.5 915 7	10. 747	2.8 009 5	29. 272 2	9.7 494 9	49. 089 5	13. 673 3	164 .95 2	32. 407 7	128 81. 9	0.5 179	23. 706 1	554 .69 4	69 9

Notes: 1/13/2016

Isotope ratios and ages are NOT corrected for initial common Pb.

Isotope ratio and apparent age errors include systematic calibration errors of 0.216544516652568% ($^{207}Pb/^{206}Pb$), 0.7623573901163l9% ($^{206}Pb/^{238}U$) (all 1-sigma).

Isotope ratios and ages corrected using a measured linear secondary standard age bias - ^{206}Pb count rate relationship.

Trace element concentrations in ppm, calculated using mean count rate method.

Sweep-by-sweep downhole fractionation of U/Pb ratios NOT corrected via Si/Zr fractionation factor.

Backgrounds were monitored between sweeps 12 to 24. Sample counts were integrated from sweeps 35 to 60.
Ablation used a laser spot size of 25 microns, and a laser firing repetition rate of 10 Hz.

Notes: 1/13/2016

Isotope ratios and ages are NOT corrected for initial common Pb.
Isotope ratio and apparent age errors include systematic calibration errors of 0.2603775585047 08% ($^{207}Pb/^{206}Pb$), 0.625201237497987% ($^{206}Pb/^{238}U$) (all 1-sigma).
Isotope ratios and ages corrected using a measured linear secondary standard age bias - ^{206}Pb count rate relationship.
Trace element concentrations in ppm, calculated using mean count rate method.
Sweep-by-sweep downhole fractionation of U/Pb ratios NOT corrected via Si/Zr fractionation factor.
Backgrounds were monitored between sweeps 12 to 24. Sample counts were integrated from sweeps 35 to 60.
Ablation used a laser spot size of 25 microns, and a laser firing repetition rate of 10 Hz.

LA-ICPMS data from sample U1340A

		Corrected isotope ratios							Apparent ages (Ma)						
		207Pb*	±2s	206Pb*	±2s	error	207Pb*	±2s	207Pb*	±2s	207Pb*	±2s	206Pb*	±2s	%
Analysis	Th/U	235U*	(%)	238U	(%)	corr.	206Pb*	(%)	206Pb*	(Ma)	235U	(Ma)	238U*	(Ma)	disc.
LA-ICPMS data from samples that are further analyzed by CA-ID-TIMS method															
U1340A S 205	1.32	1.430711	8.363	0.133888	2.9	0.34	0.077501	7.844	1134	156	902	50	810	22	29
U1340A S 204	1.67	1.140576	6.438	0.127247	4.364	0.67	0.065009	4.733	775	100	773	35	772	32	0
U1340A S 203	1.47	1.180408	4.455	0.1293	2.842	0.63	0.066212	3.432	813	72	792	24	784	21	4
U1340A S 202	1.23	1.131276	5.859	0.125938	3.765	0.64	0.065149	4.49	779	94	768	32	765	27	2
U1340A S 200	1.87	1.039707	8.248	0.120954	5.528	0.67	0.062343	6.122	686	131	724	43	736	38	-7
U1340A S 199	1.84	1.159212	4.929	0.126894	3.75	0.75	0.066255	3.199	814	67	782	27	770	27	5
U1340A S 198	1.36	1.131495	5.717	0.125195	3.648	0.63	0.065549	4.401	792	92	768	31	760	26	4
U1340A S 197	1.79	1.152114	5.591	0.123221	4.214	0.75	0.067812	3.674	863	76	778	30	749	30	13
U1340A M 196	1.01	1.180063	5.095	0.131068	3.595	0.7	0.065299	3.611	784	76	791	28	794	27	-1
U1340A M 195	1.47	1.606051	14.58	0.144929	3.82	0.26	0.080371	14.07	1206	277	973	91	872	31	28
U1340A M 194	1.07	1.131308	7.408	0.122882	5.906	0.79	0.066772	4.471	831	93	768	40	747	42	10

U1340A M 193	1.18	1.160181	6.709	0.123225	4.632	0.69	0.068285	4.853	877	100	782	37	749	33	15
U1340A M 192	1.24	1.100697	6.491	0.123536	4.415	0.68	0.064621	4.759	762	100	754	35	751	31	1
U1340A M 191	1	1.096886	7.834	0.125014	5.069	0.64	0.063636	5.973	730	127	752	42	759	36	-4
U1340A M 190	1.17	1.15009	5.296	0.119809	3.991	0.75	0.069621	3.482	917	72	777	29	729	28	20
U1340A M 188	2.22	1.205258	8.207	0.125391	5.567	0.68	0.069713	6.031	920	124	803	46	762	40	17
U1340A M 186	1.3	1.147147	5.519	0.12793	4.122	0.74	0.065035	3.669	775	77	776	30	776	30	0
U1340A M 185	0.92	1.158525	7.809	0.125605	5.146	0.66	0.066895	5.874	835	122	781	43	763	37	9
U1340A L 184	1.58	2.076278	10.37	0.125282	4.538	0.44	0.120198	9.324	1959	166	1141	71	761	33	61
U1340A L 183	1.81	1.07267	7.479	0.117004	3.879	0.51	0.066491	6.394	822	134	740	39	713	26	13
U1340A L 18	1.91	1.089914	5.205	0.123385	3.85	0.73	0.064066	3.503	744	74	748	28	750	27	-1
U1340A L 181	1.04	1.651318	6.181	0.132966	4.295	0.69	0.090072	4.444	1427	85	990	39	805	32	44
U1340A L 180	1.01	1.113387	6.714	0.127187	3.691	0.54	0.063489	5.608	725	119	760	36	772	27	-7
U1340A L 179	0.95	1.201022	15.16	0.12149	4.716	0.31	0.071698	14.41	977	294	801	84	739	33	24
U1340A L 178	1.64	1.593891	10.41	0.124928	2.066	0.19	0.092533	10.2	1478	193	968	65	759	15	49
U1340A L 177	0.95	1.09178	6.505	0.122144	3.806	0.58	0.064828	5.275	769	111	749	34	743	27	3
U1340A L 176	1.55	1.136991	6.518	0.122099	4.731	0.72	0.067537	4.483	854	93	771	35	743	33	13
U1340A L 175	0.88	1.102144	6.16	0.121904	4.947	0.8	0.065572	3.671	793	77	754	33	742	35	6
U1340A L 174	1.72	1.113192	4.633	0.122663	3.789	0.81	0.06582	2.665	801	56	760	25	746	27	7
U1340A L 173	1.67	1.107168	6.212	0.124535	4.292	0.69	0.064479	4.491	757	95	757	33	757	31	0
U1340A L 172	1.27	1.083571	6.547	0.121123	4.476	0.68	0.064883	4.777	771	101	745	35	737	31	4
U1340A L 171	1.12	1.44974	8.497	0.109517	4.848	0.57	0.096008	6.978	1548	131	910	51	670	31	57

Notes: 3/8/2014

Isotope ratios and ages are NOT corrected for initial common Pb.
Isotope ratio and apparent age errors do NOT include systematic calibration errors of 0.233081391786937% ($^{207}Pb/^{206}Pb$), 0.63501720787273% ($^{206}Pb/^{238}U$) (all 1-sigma).
Isotope ratios and ages corrected using a measured linear secondary standard age bias - ^{206}Pb count rate relationship.

Trace element concentrations in ppm, calculated using mean count rate method.

Sweep-by-sweep downhole fractionation of U/Pb ratios NOT corrected via Si/Zr fractionation factor.

Backgrounds were monitored between sweeps 10 to 20. Sample counts were integrated from sweeps 28 to 48.
Ablation used a laser spot size of 25 microns, and a laser firing repetition rate of 10 Hz.

LA-ICPMS data from sample U1340A continued.

	Concentrations (ppm)																						
Analysis	P	Ti	Y	Zr	Nb	La	Ce	Pr	Nd	Sm	Eu	Gd	Tb	Dy	Ho	Er	Tm	Yb	Lu	Hf	Ta	Th	U	T(°C)
LA-ICPMS data from samples that are further analyzed by CA-ID-TIMS method																								
U1340 A S 205	726.18 1	3.4 001 4	286 2.5 5	54 46 85	3.9 997 6		71. 971 3	0.1 550 4	2.5 332 2	7.8 655	3.3 446 9	53. 340 8	23. 085	284 .50 8	107 .78 5	466 .95 8	112 .3	115 2.7 6	128 .68 4	527 2.5 9	0.9 635 1	102 .86 2	77. 865 5	69 5
U1340 A S 204	521 .79 2	3.7 917 1	418 9.8 4	53 52 96	3.8 556 4		101 .60 8	0.2 332 4	8.4 184 9	25. 366 6	8.9 402 6	114 .50 7	41. 166 1	480 .61 4	168 .48 7	646 .03 5	149 .47 3	145 5.0 7	149 .51 5	555 2.3	1.0 327 6	148 .85 1	89. 146 2	70 5
U1340 A S 203	611 .86 1	4.9 974	383 6.3 5	55 27 85	12. 415 6		156 .97 4	0.1 35	3.4 596 3	13. 613	5.6 239 3	93. 278 6	34. 898 6	431 .31 7	152 .62 8	616 .34	139 .68 3	142 5.4 1	151 .05 5	566 4.8 8	3.2 030 7	251 .78 1	170 .81 8	72 9
U1340 A S 202	637 .80 2	5.3 616 3	235 2.2 2	53 33 20	5.7 577 7	0.0 135 9	76. 667 2	0.1 914 6	2.3 211 6	9.5 313 2	3.4 055 7	56. 143 7	20. 775 2	264 .18 9	92. 478	378 .20 4	90. 962 7	946 .93 5	102 .77 4	585 2.7 9	1.2 010 3	77. 593 5	63. 011 6	73 5
U1340 A S 200	415 .54 9	7.0 276 2	267 5.9 5	58 86 87	1.6 332 7	0.0 138 5	58. 095 3	0.5 583 4	8.0 671 9	16. 369 5	6.3 559 4	80. 284 4	27. 723 2	307 .57 5	101 .23 9	418 .74 3	98. 088 2	102 5.7 1	117 .01 6	671 8.8	0.6 869 5	88. 581 9	47. 265	76 1
U1340 A S 199	668 .33 8	5.7 815 6	326 0.0 6	62 56 60	6.7 05		97. 113	0.1 528 5	2.5 129 8	13. 518 8	4.7 761 7	78. 037	29. 752 3	366 .13 5	126 .04 7	501 .74 7	116 .54 8	111 7.8 2	131 .82 1	721 2.1 8	1.9 231 1	162 .46 5	88. 385 8	74 2
U1340 A S 198	904 .57 1	3.6 610 4	325 2.7 5	65 88 58	5.7 154 1		64. 955 3	0.0 919 7	1.9 355 6	7.4 648 8	4.0 609 2	64. 671 9	25. 798 9	328 .12 6	118 .99 3	512 .33 1	119 .42 5	115 2.8 5	145 .04 9	750 6.2 7	1.2 892 3	96. 030 3	70. 757	70 2
U1340 A S 197	488 .30 8	5.6 639 1	279 6.9 8	64 11 39	5.7 634 7		95. 088	0.1 826 2	2.9 645 4	12. 24	4.2 762	71. 270 1	25. 743 3	308 .10 7	111 .04 1	443 .14 7	97. 019 8	941 .02 7	116 .37 7	750 3.8 4	1.8 332 8	150 .22 3	83. 955	74 1
U1340 A M 196	501 .33 5	6.2 285 4	266 5.6 7	52 79 83	9.5 313 1		106 .85	0.1 484 8	3.1 683 1	8.5 334 6	4.0 361 3	57. 989 3	20. 742 1	278 .02 5	103 .24 9	429 .37 9	108 .69 1	115 2.2 3	115 .44 9	519 2.5 2	1.7 160 2	77. 716 1	77. 214 9	74 9
U1340	439	7.8	193	50	1.6	0.7	48.	0.4	7.4	13.	5.6	58.	19.	222	77.	301	71.	780	79.	546	0.4	55.	37.	77

A M 195	.82 2	628 5	2.9 3	58 45	978 1	011 2	411 4	032	743 6	965 9	843 2	585 4	060 8	.47 7	639 8	.57	009 3	.72 4	450 3	0.9 8	679 9	424 2	790 2	2
U1340 A M 194	596 .76 2	6.9 073 2	245 1.9 1	48 67 16	6.4 782 3		96. 385 9	0.1 681 7	3.7 335 4	9.5 529 2	4.3 350 2	57. 914 1	21. 266 4	265 .82 2	93. 277 2	393 .58 6	100 .85 7	108 5.1 4	111 .13	505 0.5 4	1.6 613 4	73. 662 3	69. 005 4	75 9
U1340 A M 193	554 .96 8	7.0 894 7	255 7.0 3	48 68 69	7.3 606 4		104 .06 5	0.1 291 9	3.7 122 2	12. 680 3	4.8 754 4	63. 332 4	23. 692 2	278 .29 2	98. 896 1	404 .00 3	102 .99 1	108 2.7 5	109 .11 9	521 1.5 2	1.4 730 4	92. 782 6	78. 593 5	76 2
U1340 A M 192	514 .34 1	6.1 458 7	220 9.7 5	47 07 62	6.6 360 5		87. 756 9	0.0 993	2.2 280 6	8.0 904 2	3.7 166 6	53. 184 8	20. 159 2	245 .57 8	87. 776 9	347 .08 1	85. 661 8	934 .16 4	92. 777 6	472 3.8 7	1.5 265 7	100 .97	81. 666 1	74 8
U1340 A M 191	455 .61 7	5.5 526 2	261 7.7	49 28 80	13. 123 6		121 .79 3	0.1 093 3	1.5 662 6	7.8 447 2	3.1 634 3	44. 579 5	18. 888 1	262 .02 6	102 .34 1	460 .05 9	113 .75 1	127 9.9 5	130 .52 7	512 4.5 4	1.8 913 9	113 .39 1	113 .25 2	73 9
U1340 A M 190	585 .16 9	4.6 592 8	351 0.6	48 53 18	14. 919 7	0.0 132 6	184 .54 1	0.1 234 2	2.8 565 6	13. 093	5.1 932 3	74. 742 1	27. 697 6	367 .06 8	129 .79 2	554 .13 7	138 .37 5	147 9.2 3	144 .01 6	474 3.1 6	2.9 738 1	224 .78 9	191 .46 6	72 3
U1340 A M 188	158 1.8 2	6.4 860 2	190 2.6 3	51 88 99	4.6 629 8	277 7.6 1	350 7.0 6	363 .11 8	138 8.9 2	176 .05 8	20. 302 8	129 .66 3	21. 643 1	211 .58 8	73. 481 5	303 .75 2	72. 709 9	782 .47 2	81. 939 9	563 8.4 6	1.3 744 9	122 .26 5	55. 108	75 3
U1340 A M 186	638 .45 6	5.9 086 9	273 9.3 5	52 82 44	7.0 416 8	0.4 112 1	117 .59 5	0.3 537 7	4.7 452 1	14. 054 6	5.4 686 4	78. 057 1	27. 520 9	328 .23 1	110 .68 9	434 .62 1	101 .47 1	104 5.3 3	98. 193	511 1.9 4	1.6 426 3	128 .76 6	99. 109 3	74 4
U1340 A M 185	475 .58 7	5.5 372 6	234 1.0 1	50 67 76	8.8 332 4		84. 584 5	0.0 805 1	1.6 092 1	9.1 473 2	3.2 295	49. 392 1	17. 925 6	243 .67 1	89. 169 7	381 .78 1	95. 828 2	106 2.0 5	105 .98 7	533 2.6 3	2.2 189 4	76. 341 7	83. 350 6	73 8
U1340 A L 184	569 .36 3	7.7 350 7	376 2.9 1	61 01 46	10. 487 3	0.1 992 6	123 .99 4	0.3 068 1	5.1 339 2	15. 217 2	5.6 650 2	86. 977 8	31. 648	390 .22 2	145 .66 1	609 .46 7	143 .29 6	146 4.2 8	174 .13 4	690 3.6 6	2.2 779 2	131 .79 2	83. 168 3	77 0
U1340 A L 183	591 .98 2	4.7 995	266 0.0 8	61 58 82	2.2 720 6	0.0 263 3	54. 564 6	0.1 818 7	5.2 796	13. 316 6	7.5 087 8	89. 079 6	28. 621 8	319 .65 5	102 .52 1	408 .81 5	95. 276 9	929 .02 2	103 .54 2	673 4.2 5	0.7 123 8	74. 511 2	41. 258 7	72 5
U1340 A L 18	530 .61 9	4.7 867 4	406 1.5 9	58 22 95	2.9 295 8		94. 507 6	0.3 533 8	9.0 997 7	23. 953 2	9.8 161 9	123 .36 9	40. 209 8	474 .81 2	162 .7	634 .33 8	139 .17 1	138 2.0 8	151 .29 5	629 2.9 2	0.9 689 4	138 .69 3	72. 461 2	72 5
U1340 A L 181	492 .51	6.1 762 9	238 8.5 1	54 98 54	6.8 384 6	0.0 936 6	83. 664 6	0.0 879	2.1 863 2	8.2 269 6	3.7 609 6	53. 882 5	19. 954 1	250 .28 6	92. 795 7	391 .46 2	93. 570 3	103 3.2 3	114 .61 3	596 6.4 4	1.4 083	64. 635 1	61. 852 7	74 9
U1340 A L	582 .08	5.8 891	237 2.7	54 77	7.6 213	4.1 484	94. 078	2.0 398	7.9 898	9.3 768	3.9 942	54. 197	19. 643	252 .03	91. 950	395 .84	98. 591	103 8.5	111 .22	579 8.7	1.7 227	62. 295	61. 773	74 4

180	8	7	2	84	8	6	3	6	6	9	4	9	3	1	1		6	3	4	7	1	9	8	
U1340 A L 179	419.1	4.3846	246 8.8 8	55 04 29	8.9 697 4	0.0 440 5	87. 152 5	0.1 125 5	1.4 724 3	6.5 493 4	3.4 533 5	46. 706 1	20. 036 6	257 .72 2	95. 362 9	408 .53	98. 285 3	106 7.9 4	106 .87 7	553 4.0 6	1.5 894	66. 203	69. 977 9	71 7
U1340 A L 178	596 .53 3	5.9 982 5	278 1.2 8	53 37 90	5.8 925 2	0.0 013 4	117 .62 6	0.2 797 2	4.6 440 5	12. 227 1	5.0 458 6	79. 576 9	26. 731 3	326 .06 4	112 .04 8	425 .96 8	103 .18 2	102 5.3 9	101 .90 9	588 1.5	2.1 428 3	180 .08	109 .52 4	74 6
U1340 A L 177	513 .19 3	6.6 071 8	234 6.2 7	52 17 93	7.4 503 2		87. 071 6	0.1 109 9	2.0 436 2	9.4 058 7	3.6 296 1	55. 556 3	19. 697 3	249 .86 5	91. 305 6	383 .96 4	99. 734 3	107 0.7	114 .85 9	538 5.9 8	1.5 674	63. 660 8	66. 922	75 5
U1340 A L 176	505 .29 1	5.3 054 2	316 8.9	52 50 70	3.5 174 7		86. 025 3	0.3 476 8	8.4 224 1	19. 523 8	7.4 385 7	96. 312 2	31. 495	370 .45 3	127 .50 2	498 .15 5	114 .11 9	118 9.2 7	117 .20 5	543 3.2 5	0.8 656 1	107 .59 2	69. 418 4	73 4
U1340 A L 175	465 .49 8	5.1 929 1	249 9.9 3	51 92 24	11. 836 4		90. 106 2	0.0 526 6	1.6 596 9	6.5 453 9	2.4 379 1	45. 221 7	19. 39	240 .53 4	94. 156 3	406 .03 4	104 .04 5	117 4.5 1	123 .90 5	632 9.7	2.5 532 9	86. 030 8	97. 365 2	73 3
U1340 A L 174	626 .84 8	7.0 623 2	297 8.0 1	54 54 65	7.4 068 8		122 .93 1	0.1 085 3	3.9 756 4	13. 505 9	5.3 028 3	82. 167 4	29. 921 3	345 .33	119 .95 9	472 .82 4	111 .08 4	110 6.0 9	115 .19 4	567 8.1 3	2.0 296 3	210 .07 8	122 .30 3	76 1
U1340 A L 173	559 .06 1	5.9 373 8	302 5.7 2	58 37 74	5.4 362 6		97. 360 8	0.2 020 9	5.1 410 4	15. 699 4	6.1 655 3	80. 459 2	28. 591 5	338 .91 8	118 .41 7	479 .08 8	109 .33 6	106 3.2 5	119 .86 2	649 5.3 6	1.4 673 3	127 .48 5	76. 424 9	74 5
U1340 A L 172	727 .74 8	4.5 518 4	295 9.3 5	57 99 20	4.2 400 6	0.1 762 2	77. 173 9	0.1 873 1	3.5 528	11. 713 9	4.3 028 7	59. 202 9	23. 936 5	301 .62 2	109 .33 5	465 .43 7	110 .04 5	113 8.9 5	126 .09 8	603 7.4 8	1.3 056 8	112 .30 9	88. 380 9	72 1
U1340 A L 171	524 .94 2	3.7522	140 0.7	61 86 51	3.1 346 5	0.2 326 1	27. 131 5	0.2 614	2.5 916 9	5.7 786 3	2.1 49	28. 938 9	11. 325 8	140 .65 7	55. 178 7	233 .57 8	55. 798	581 .60 5	74. 797 1	752 8.4 4	0.8 061 4	32. 540 4	29. 081 5	70 4

LA-ICPMS data from sample DS34

		Corrected isotope ratios							Apparent ages (Ma)						
		207Pb*	±2s	206Pb*	±2s	error	207Pb*	±2s	207Pb*	±2s	207Pb*	±2s	206Pb*	±2s	%
Analysis	Th/U	235U*	(%)	238U	(%)	corr.	206Pb*	(%)	206Pb*	(Ma)	235U	(Ma)	238U*	(Ma)	disc.
DS34 S 23	0.79	14.97618	6.264	0.519133	5.316	0.85	0.209229	3.313	2900	54	2814	60	2696	117	7
DS34 S 24	0.21	1.229024	5.007	0.134227	4.492	0.89	0.066408	2.211	819	46	814	28	812	34	1
DS34 M 9	1.57	1.415643	7.277	0.130567	5.001	0.68	0.078636	5.286	1163	105	896	43	791	37	32
DS34 S 37	0.35	0.891969	16.15	0.109076	15.57	0.96	0.059309	4.272	578	93	647	77	667	99	-15
DS34 S 27	0.7	0.889335	7.599	0.106279	6.317	0.83	0.06069	4.224	628	91	646	36	651	39	-4
DS34 M 10	0.03	0.873184	13.56	0.104983	12.87	0.95	0.060323	4.282	615	92	637	64	644	79	-5
DS34 S 22	0.82	0.869084	15.41	0.101082	14.28	0.93	0.062357	5.776	686	123	635	73	621	85	10
DS34 S 17	0.39	0.802105	13.03	0.091284	11.8	0.9	0.063729	5.526	733	117	598	59	563	64	23
DS34 L 3	0.42	0.879781	6.808	0.089247	2.69	0.39	0.071496	6.254	972	128	641	32	551	14	43
DS34 S 25	0.54	0.718071	5.529	0.088397	4.822	0.87	0.058915	2.704	564	59	550	23	546	25	3
DS34 S 28	1.19	0.709155	5.835	0.087615	4.971	0.85	0.058703	3.056	556	67	544	25	541	26	3
DS34 S 20	0.48	0.701858	5.651	0.086224	4.019	0.71	0.059036	3.972	568	86	540	24	533.2	21	6
DS34 L 1	0.54	0.680802	5.467	0.08615	4.264	0.78	0.057314	3.421	504	75	527	22	533	22	-6
DS34 M 6	0.28	0.769974	16.12	0.08586	13.89	0.86	0.065041	8.18	776	172	580	71	531	71	32
DS34 M 12	0.54	0.710818	6.678	0.085503	5.719	0.85	0.060294	3.447	614	74	545	28	529	29	14
DS34 L 2	0.35	0.666051	6.931	0.084778	3.348	0.48	0.05698	6.068	491	134	518	28	525	17	-7
DS34 M 7	0.29	0.707537	11.21	0.08445	7.157	0.64	0.060764	8.623	631	186	543	47	523	36	17
DS34 S 29	0.56	0.647392	4.689	0.083871	3.659	0.77	0.055983	2.933	452	65	507	19	519	18	-15
DS34 M 4	0.45	0.699097	7.735	0.083681	7.429	0.96	0.060591	2.154	625	46	538	32	518	37	17
DS34 S 26	0.1	0.674783	4.946	0.083234	3.956	0.79	0.058798	2.97	560	65	524	20	515	20	8
DS34 M 14	0.07	0.65313	9.031	0.082692	7.838	0.87	0.057284	4.486	503	99	510	36	512	39	-2
DS34 M 8	0.35	0.670514	6.006	0.082622	5.279	0.88	0.058858	2.864	562	62	521	24	512	26	9
DS34 S 21	0.54	0.669916	4.887	0.082106	3.463	0.7	0.059176	3.448	574	75	521	20	509	17	11
DS34 S 34	0.6	0.63536	5.902	0.081696	5.623	0.95	0.056405	1.794	468	40	499	23	506	27	-8
DS34 S 31	0.67	0.642366	4.654	0.081567	3.645	0.78	0.057117	2.894	496	64	504	18	505	18	-2
DS34 S 30	0.82	0.641793	4.399	0.081329	3.841	0.87	0.057234	2.144	501	47	503	17	504	19	-1

DS34 S 32	0.44	0.619657	6.77	0.08104	5.077	0.75	0.055456	4.478	431	100	490	26	502	25	-17
DS34 S 38	0.49	0.653206	6.237	0.079953	5.319	0.85	0.059254	3.257	576	71	510	25	496	25	14
DS34 M 13	0.57	0.639557	5.165	0.079048	4.38	0.84	0.05868	2.737	555	60	502	20	490	21	12
DS34 M 16	0.03	0.749375	7.911	0.076898	5.7	0.72	0.070678	5.487	948	112	568	34	478	26	50
DS34 S 39	0.39	0.599328	4.605	0.076252	3.014	0.65	0.057005	3.482	492	77	477	18	474	14	4
DS34 S 33	0.14	0.641276	4.588	0.07551	3.683	0.8	0.061594	2.735	660	59	503	18	469	17	29
DS34 S 19	0.2	0.601739	4.783	0.074159	3.861	0.8	0.05885	2.823	562	62	478	18	461	17	18

LA-ICPMS data from sample DS34 continued.

	Concentrations (ppm)																						
Analysis	P	Ti	Y	Zr	Nb	La	Ce	Pr	Nd	Sm	Eu	Gd	Tb	Dy	Ho	Er	Tm	Yb	Lu	Hf	Ta	Th	U	T(°C)
DS34 S 23	278.199	5.6171	165 0.6	69 85 65	1.1 431 5	0.1 410 6	15. 209	0.1 585 8	2.3 158	7.4 106 6	1.9 535 2	41. 036 7	13. 676 1	170 .32 3	61. 219 6	251 .61 6	61. 979 2	628 .04 5	83. 717 2	113 43. 8	0.8 281 4	59. 003 3	74. 934 4	740
DS34 S 24	122 .08 2	9.4 002 5	326 .80 9	69 01 11	1.0 713 7		5.7 235 8		0.6 336 7	2.1 789 8	1.2 985 8	16. 078	4.4 198 5	39. 649 7	10. 323 7	35. 685 6	6.5 769 6	60. 690 7	8.1 577 2	114 38. 8	0.8 595 5	35. 291	170 .27 9	790
DS34 S 27	275 .37 9	8.6 897 4	107 0.4 9	66 97 56	1.2 188 9	0.0 142 5	13. 589 6	0.0 699 1	1.6 540 3	4.3 728 1	1.1 840 6	21. 607 9	8.0 767 9	101 .49 2	36. 574 8	167 .40 8	41. 813 8	441 .70 9	63. 653 2	104 00. 3	0.3 959 3	113 .43 2	162 .35 8	782
DS34 M 10	295 .06 1	15. 235	493 .71 7	46 27 21	2.4 434 1	10. 171 2	34. 292 5	8.7 262 7	55. 570 3	16. 567 7	4.4 028 8	17. 356	4.2 268 9	45. 400 7	17. 261 8	69. 287 6	18. 027 2	207 .73 9	23. 489 1	899 1.3 2	2.0 706 2	30. 462	876 .30 5	842
DS34 S 22	230 .54 7	20. 675 7	515 .08 6	66 37 74	1.0 505 9	0.5 889	19. 296 2	0.7 260 6	8.7 783 3	8.6 690 2	3.3 284 6	26. 632 2	7.0 180 2	63. 653 1	17. 231 1	65. 091 6	13. 678 3	131 .19 1	16. 843 2	790 0.2 3	0.2 231 2	87. 833 4	106 .89 6	877
DS34 S 17	246 .95 9	12. 028 3	522 .10 9	60 30 63	0.7 095 9	1.7 284	8.4 981 4	1.4 412 9	6.9 040 3	9.3 37	1.5 334 1	28. 512 2	6.6 643 1	64. 311 3	17. 999	62. 206 2	13. 004 1	128 .45 8	13. 694 1	824 3.2 8	0.3 084	88. 695 9	229 .34	816
DS34 L 3	133 .30 9	12. 71	352 .06 3	63 34 68	1.1 052 4	0.4 633 2	8.0 288 8	0.8 136 2	6.4 294 8	6.6 020 3	2.6 776 7	21. 672 5	5.0 485 1	45. 628 7	13. 283 3	47. 502 3	9.2 193 3	87. 365 2	10. 077 9	882 4.3 7	0.3 599 4	103 .46 7	245 .86 5	822
DS34 S	250 .01	21. 696	839 .04	68 58	1.0 382	0.6 370	14. 136	0.9 435	15. 489	22. 797	5.8 305	55. 533	13. 478	114 .08	31. 300	97. 677	16. 097	146 .71	17. 640	880 5.9	0.3 731	367 .90	310 .28	883

28	2	7		82	6	3	1	6	3	9	3	7	5	3	5		5	6	3		1	9	6	
DS3 4 S 20	140 .62 5	9.6 889 5	288 .78 3	64 57 54	0.6 663 2		4.4 576 9	0.1 894 5	2.4 449 2	4.0 742 6	1.0 461 5	13. 135 5	3.6 403	36. 309	10. 186 6	37. 778 3	8.7 393 2	81. 255 8	9.8 300 8	962 6.4 5	0.2 486 3	83. 936 8	173 .11 5	79 3
DS3 4 L 1	138 .79 3	11. 782 3	345 .54	62 68 97	0.9 147 8		4.2 869	0.0 707 9	1.3 322 8	4.6 074 1	1.4 359 8	16. 427 5	3.9 188 1	41. 618 6	12. 523	46. 511 8	10. 559	105 .50 2	12. 697 3	861 3.0 3	0.3 084 8	79. 151 5	145 .70 8	81 3
DS3 4 M 6	351 .43 1	30. 927 8	607 .83 7	52 68 71	2.9 106 8	5.8 259 5	47. 996 9	8.3 910 4	76. 587 2	24. 222	4.9 788 6	35. 406 4	7.8 475 8	67. 745 7	20. 379 2	74. 762 3	18. 523 1	189 .11 1	19. 929	675 1.8 2	0.6 077 8	115 .76 6	408 .69 6	92 7
DS3 4 M 12	147 .25 9	12. 151 5	294 .05 6	52 37 83	0.4 305 6		4.6 591 9	0.1 799 6	2.8 957 7	6.1 035 7	2.0 235	15. 005 7	4.4 452 2	39. 563 5	10. 607 5	35. 597 1	8.2 052	85. 142 2	8.5 303	630 2.1 7	0.1 702 5	77. 952 8	143 .96 3	81 7
DS3 4 L 2	111 .08 1	7.1 132 2	182 .13 7	63 59 97	0.4 820 2	1.5 246 4	9.2 640 1	1.4 937 6	8.7 418 9	2.4 425 5	0.7 773 1	7.4 583 5	2.1 578 7	19. 418 1	6.3 324	24. 716	5.4 969 9	53. 761 9	7.1 293 1	904 3.2 7	0.1 088 6	36. 400 2	104 .00 9	76 2
DS3 4 M 7	120 .90 1	8.3 082 1	178 .52 8	53 41 86	0.6 091 9	0.8 053 1	7.6 709 9	0.9 629 3	7.5 714 7	5.0 105 6	1.5 746 8	9.1 622 2	2.4 029 8	21. 531 4	6.2 198 3	23. 948 9	5.5 256 9	58. 016	6.1 382	727 5.9 9	0.1 774 4	41. 536 7	143 .15 8	77 7
DS3 4 S 29	142 .41 5	9.7 132 3	496 .85 4	69 99 62	0.8 501 1	0.0 523 8	5.6 044 6	0.1 713 2	3.8 208 6	7.9 259	1.7 914 5	23. 427 5	6.5 834 4	59. 301 8	17. 098 1	63. 349 7	13. 701 3	130 .84 9	16. 025 4	938 7.8 8	0.4 167 9	97. 081 2	172 .03 9	79 3
DS3 4 M 4	207 .67 2	12. 304 8	355 .45 5	52 32 02	0.4 890 1	0.0 023 4	4.5 447 5	0.1 616	3.4 455 4	5.6 683 2	1.4 196 9	18. 777 8	4.7 433 4	44. 004 4	11. 591 4	43. 347 6	10. 080 4	108 .36	10. 881 7	623 8.0 5	0.1 367 4	77. 664 8	172 .64 8	81 8
DS3 4 S 26	167 .02 5	18. 446 1	347 .15 7	67 47 46	0.9 224 4	1.6 669 2	6.7 656 7	0.6 255 9	3.2 982 3	2.6 062 3	1.1 504 5	11. 006 9	2.7 955 2	35. 784 7	11. 750 2	43. 508 8	8.9 796 9	93. 417 1	11. 734 3	122 48. 1	0.7 120 1	53. 263 8	509 .41 8	86 4
DS3 4 M 14	133 .77 4	2.9 086 9	606 .99 1	46 34 82	1.9 596 8	1.2 353 4	7.7 088	1.1 091	9.9 524 3	3.8 060 1	1.2 888 2	16. 287 9	5.5 196 7	73. 985	22. 641	76. 441 8	18. 337 4	200 .12 2	17. 938	111 47	0.9 359 3	63. 747 1	971 .82 6	68 2
DS3 4 M 8	153 .31 8	10. 488 4	266 .22 7	52 18 43	0.7 102 3		3.5 023 1	0.1 171 8	1.8 101 4	3.2 604 1	1.0 359	12. 413	2.9 377 8	31. 662 7	9.1 673	32. 809 6	8.3 174 4	88. 402 3	9.1 243 2	646 5.3 9	0.3 009	57. 768 2	162 .85	80 1
DS3 4 S 21	154 .21 3	11. 686 3	386 .39 6	66 11 03	0.9 254 3	0.6 422 5	7.9 936 2	0.3 675 8	4.6 981 5	6.5 602 1	1.6 789 6	21. 082 1	5.3 641 9	47. 497 2	12. 909 3	47. 683 2	10. 168 7	96. 737 4	10. 894 9	870 7.7 6	0.4 268 2	94. 849 7	175 .41 1	81 3
DS3 4 S	218 .82	17. 514	575 .50	65 20	1.0 386		6.4 562	0.2 369	5.6 870	7.8 349	2.0 239	29. 701	7.4 226	70. 700	20. 008	73. 289	15. 803	143 .32	16. 580	817 7.8	0.2 184	163 .08	272 .31	85 8

34	6	5	3	93	6		1	2	9	6	3	1		2	6	6	7	1	9	8	2	7	8	
DS3	299	33.	179	67	1.3			0.2		17.	6.1	96.	26.	234	64.	203	39.	342		814	0.2	287		
4 S	.99	113	1.2	87	890		8.8	964	6.0	986	935	237	556	.30	724	.52	472	.22	37.	1.7	808	.41	427	93
31	7	3	8	32	3		194	7	762	6	4	9	6	7	9	6	4	6	216	8	4	2	.57	6
DS3	262	25.	173	68	4.7	0.5	25.	0.7	10.	19.	4.4	77.	21.	205	58.	213	45.		51.	977	1.2	639	774	
4 S	.16	737	2.9	28	931	093	948	326	997	158	638	760	598	.36	877	.99	111	411	648	8.5	269	.03	.65	90
30	5	5	8	23	2	5	9	5	8	6	4	9	3	9	6	1	9	.37	1	4	5	2	5	4
DS3	167	11.	315	65	0.5		3.3	0.0	2.3	5.3	1.1	20.	6.1	46.	10.	33.	6.0	52.	5.4	818	0.1	49.	110	
4 S	.41	683	.02	38	687		275	685	484	745	289	556	580	410	669	272	388	388	860	4.5	641	004	.27	81
32	2	4	5	70	2		4	8	4	8	2	7	5	5	7	4	2	8	8	3	4	3	7	3
DS3	188	9.4	491	59	0.9		3.9	0.1	1.7	4.5	1.4	18.	5.9			68.	15.	160		807	0.1	132		
4 S	.15	031	.43	77	519		233	457	103	828	915	921	807	56.	18.	302	298	.73	17.	3.4	612	.46	267	79
38	1	8	8	79	3		7	1	8	9	2	3	1	225	718	7	6	3	62	8	9	7	.65	0
DS3	179	11.	342	58	0.4	0.0	4.5		7.0	10.	2.2	32.	8.1	53.	11.	34.	5.7	51.	4.9	778	0.2	84.	219	
4 S	.02	202	.74	27	119	570	869	0.5	004	611	857	902	127	988	381	508	772	029	909	6.3	668	966	.41	80
39	5	2	6	01	6	1	4	806	1	3	9	6	9	5	8	8	1	5	3	7	8	2	7	8

Notes: 3/7/2014

Isotope ratios and ages are NOT corrected for initial common Pb.

Isotope ratio and apparent age errors do NOT include systematic calibration errors of 0.233081391786937% ($^{207}Pb/^{206}Pb$), 0.63501720787273% ($^{206}Pb/^{238}U$) (all 1-sigma).

Isotope ratios and ages corrected using a measured linear secondary standard age bias - ^{206}Pb count rate relationship.

Trace element concentrations in ppm, calculated using mean count rate method.

Sweep-by-sweep downhole fractionation of U/Pb ratios NOT corrected via Si/Zr fractionation factor.

Backgrounds were monitored between sweeps 10 to 20. Sample counts were integrated from sweeps 28 to 48.

Ablation used a laser spot size of 25 microns, and a laser firing repetition rate of 10 Hz.

LA-ICPMS data from sample TS08

		Corrected isotope ratios							Apparent ages (Ma)						
		207Pb*	±2s	206Pb*	±2s	error	207Pb*	±2s	207Pb*	±2s	207Pb*	±2s	206Pb*	±2s	%
Analysis	Th/U	235U*	(%)	238U	(%)	corr.	206Pb*	(%)	206Pb*	(Ma)	235U	(Ma)	238U*	(Ma)	disc.
TS08 S 101	1.4	1.426603	5.624	0.144792	4.238	0.75	0.071459	3.696	971	75	900	34	872	35	10
TS08 S 109	1.49	1.456158	7.688	0.144402	4.76	0.62	0.073136	6.037	1018	122	912	46	870	39	15
TS08 M 24	0.86	1.299951	6.032	0.143503	5.21	0.86	0.0657	3.04	797	64	846	35	864	42	-8
TS08 S 97	0.91	1.430852	7.72	0.142808	3.527	0.46	0.072667	6.867	1005	139	902	46	861	28	14
TS08 M 29	0.77	1.34906	5.598	0.14177	4.092	0.73	0.069015	3.821	899	79	867	33	855	33	5
TS08 M 22	1.4	1.278741	3.935	0.140272	3.509	0.89	0.066117	1.78	810	37	836	22	846	28	-4
TS08 M 31	0.74	1.412076	10.57	0.140156	4.723	0.45	0.073071	9.458	1016	192	894	63	846	37	17
TS08 S 103	1.15	1.274878	4.836	0.13904	3.648	0.75	0.066501	3.175	822	66	835	28	839	29	-2
TS08 M 20	0.7	1.204182	6.365	0.138859	4.256	0.67	0.062895	4.732	705	101	803	35	838	33	-19
TS08 M 17	1	1.417974	4.498	0.137895	3.754	0.83	0.074579	2.479	1057	50	897	27	833	29	21
TS08 S 108	1.03	1.271598	4.943	0.13783	3.827	0.77	0.066912	3.129	835	65	833	28	832	30	0
TS08 M 19	1.02	1.257098	5.009	0.137671	4.15	0.83	0.066226	2.805	813	59	827	28	831	32	-2
TS08 S 96	1	1.209112	5.747	0.136786	4.637	0.81	0.06411	3.396	745	72	805	32	826	36	-11
TS08 M 30	1.29	1.249538	4.601	0.136705	3.843	0.84	0.066293	2.531	816	53	823	26	826	30	-1
TS08 S 114	1.02	1.221146	7.917	0.136607	4.034	0.51	0.064832	6.812	769	143	810	44	825	31	-7
TS08 M 13	0.96	1.680546	10.81	0.136443	3.579	0.33	0.08933	10.2	1411	195	1001	69	825	28	42
TS08 M 25	0.94	1.242637	4.49	0.136347	2.904	0.65	0.066099	3.425	810	72	820	25	824	22	-2
TS08 M 16	0.84	1.216883	3.476	0.135867	2.644	0.76	0.064958	2.257	773	47	808	19	821	20	-6
TS08 M 38	0.65	1.311286	7.407	0.135834	4.534	0.61	0.070015	5.856	929	120	851	43	821	35	12
TS08 M 36	1.08	1.220422	5.231	0.135557	4.437	0.85	0.065296	2.771	784	58	810	29	819	34	-5
TS08 S 115	0.99	1.1343	7.223	0.135473	4.432	0.61	0.060726	5.704	630	123	770	39	819	34	-30
TS08 M 34	1.56	1.303767	5.376	0.135463	3.023	0.56	0.069804	4.446	923	91	847	31	819	23	11
TS08 L 11	0.87	1.275733	4.502	0.135413	3.665	0.81	0.068328	2.615	879	54	835	26	819	28	7
TS08 M 18	1.02	1.427446	9.603	0.134957	5.323	0.55	0.076712	7.992	1114	160	900	57	816	41	27
TS08 S 112	1.46	1.249905	4.921	0.134622	4.107	0.83	0.067338	2.71	848	56	823	28	814	31	4
TS08 S 111	1.15	1.214889	6.39	0.134498	4.147	0.65	0.065512	4.862	791	102	807	36	813	32	-3

TS08 M 23	0.96	1.232896	4.504	0.134391	3.613	0.8	0.066536	2.689	823	56	816	25	813	28	1
TS08 L 3	1.02	1.211088	6.563	0.134262	3.719	0.57	0.065422	5.408	788	114	806	37	812	28	-3
TS08 S 117	1.06	1.214605	5.38	0.134115	4.138	0.77	0.065683	3.438	796	72	807	30	811	32	-2
TS08 S 113	1.19	1.349425	6.583	0.133984	4.527	0.69	0.073046	4.78	1015	97	867	38	811	34	20
TS08 L 6	0.87	1.251731	4.767	0.133929	4.274	0.9	0.067785	2.112	862	44	824	27	810	33	6
TS08 S 107	1.17	1.213471	5.739	0.133647	4.916	0.86	0.065852	2.962	802	62	807	32	809	37	-1
TS08 M 12	0.79	1.259571	5.396	0.133633	3.746	0.69	0.068361	3.884	880	80	828	31	809	28	8
TS08 L 9	0.75	1.239966	5.22	0.133589	3.391	0.65	0.067319	3.969	848	83	819	29	808	26	5
TS08 S 110	1.4	1.314671	5.925	0.133527	3.863	0.65	0.071408	4.493	969	92	852	34	808	29	17
TS08 M 26	1.29	1.307739	4.652	0.13341	3.55	0.76	0.071093	3.006	960	61	849	27	807	27	16
TS08 M 21	1.12	1.178679	4.714	0.133248	4.148	0.88	0.064155	2.24	747	47	791	26	806	31	-8
TS08 M 37	1.06	1.163362	8.05	0.133089	5.035	0.63	0.063398	6.282	722	133	784	44	805	38	-12
TS08 L 10	0.86	1.227908	5.114	0.133042	3.69	0.72	0.066939	3.541	836	74	813	29	805	28	4
TS08 M 28	0.63	1.235982	4.472	0.132995	4.064	0.91	0.067403	1.866	850	39	817	25	805	31	5
TS08 S 98	1.08	1.227844	4.456	0.132978	4.072	0.91	0.066967	1.808	837	38	813	25	805	31	4
TS08 M 35	0.83	1.193233	4.753	0.132892	4.059	0.85	0.065122	2.473	778	52	797	26	804	31	-3
TS08 M 27	1	1.232851	4.563	0.132746	3.778	0.83	0.067358	2.559	849	53	816	26	804	29	5
TS08 S 99	1.36	1.194909	4.901	0.132683	3.749	0.76	0.065316	3.157	785	66	798	27	803	28	-2
TS08 M 33	0.81	1.209279	3.953	0.1322	3.219	0.81	0.066343	2.294	817	48	805	22	800	24	2
TS08 L 4	1.1	1.221164	6.455	0.131875	4.471	0.69	0.06716	4.656	843	97	810	36	799	34	5
TS08 S 102	0.99	1.152436	5.362	0.131273	4.046	0.75	0.063671	3.519	731	75	778	29	795	30	-9
TS08 M 32	1.48	1.197131	4.502	0.131179	3.197	0.71	0.066187	3.17	812	66	799	25	795	24	2
TS08 L 8	1.05	1.306089	6.224	0.131065	4.528	0.73	0.072275	4.269	994	87	848	36	794	34	20
TS08 L 5	0.96	1.228382	6.738	0.130847	4.135	0.61	0.068088	5.32	871	110	814	38	793	31	9
TS08 S 121	0.93	1.191399	4.814	0.130789	3.495	0.73	0.066067	3.311	808	69	797	27	792	26	2
TS08 M 15	1.35	1.277006	4.26	0.130724	3.701	0.87	0.070849	2.109	953	43	836	24	792	28	17
TS08 M 14	1.66	1.284336	4.439	0.130586	2.869	0.65	0.071331	3.387	967	69	839	25	791	21	18
TS08 S 118	0.91	1.170521	5.38	0.129311	4.254	0.79	0.065651	3.294	795	69	787	29	784	31	1
TS08 S 120	1.26	1.188864	5.14	0.129165	4.496	0.87	0.066755	2.49	830	52	795	28	783	33	6
TS08 S 119	1.24	1.189774	5.633	0.12875	4.373	0.78	0.067022	3.551	838	74	796	31	781	32	7

TS08 S 116	1.18	1.188065	4.393	0.128044	3.151	0.72	0.067294	3.061	847	64	795	24	777	23	8							
TS08 S 104	1.26	1.144594	5.968	0.123447	5.454	0.91	0.067247	2.425	845	50	775	32	750	39	11							
TS08 S 105	1.06	1.218212	5.598	0.123426	4.336	0.77	0.071584	3.541	974	72	809	31	750	31	23							

LA-ICPMS data from sample TS08 continued.

	Concentrations (ppm)																						
Analysis	P	Ti	Y	Zr	Nb	La	Ce	Pr	Nd	Sm	Eu	Gd	Tb	Dy	Ho	Er	Tm	Yb	Lu	Hf	Ta	Th	U	T(°C)
TS08 S 101	130.468	1.9299 4	320.297	64 5800	0.1 5269	0.0 227	4.9 8297	0.2 0729	2.4 3127	2.5 3768	1.1 5635	9.7 2652	2.6 7002	29. 8735	10. 9153	48. 042	12. 94	131.445	26. 7522	645 4.01	0.0 6235	320.418	228.425	628
TS08 S 109																								693
TS08 M 24	110.46	1.7 395	121.053	61 9281	0.0 7218		2.9 7745	0.0 2305	0.2 5538	0.4 9662	0.1 8238	3.1 954	0.7 3527	9.4 8226	3.8 9371	19. 4471	5.3 3858	69. 9251	13. 6015	640 4.34	0.1 8127	123.994	144.6	620
TS08 S 97	136.444	4.5 9046	188.825	62 7730	0.3 8156		5.9 9386		0.1 5512	0.4 799	0.1 8611	2.9 3468	1.2 0121	15. 1916	5.6 5363	30. 5716	7.9 3483	84. 3885	16. 0208	919 3.17	0.2 3715	88. 5623	96. 8155	696
TS08 M 29	78. 6097	1.4 2955	57. 2586	61 4759	0.0 2454		2.1 4926		0.1 6694		0.1 5972	0.2 1491	0.4 1916	4.3 3034	1.9 4065	9.9 6413	3.0 9699	33. 332	7.3 7249	559 8.01	0.0 4811	75. 1089	96. 9708	606
TS08 M 22	143.347	1.6 1751	398.247	57 7494	0.0 8317	0.0 313	4.3 6242	0.1 4272	1.7 2013	2.1 4339	1.4 2063	10. 6875	3.1 9871	35. 9996	13. 6494	63. 9892	16. 3599	182.625	31. 0118	401 8.56	0.1 1886	448.202	320.984	615
TS08 M 31	150.01	7.1 4196	240.947	58 7074	0.3 2503		6.3 2937		0.3 6378	0.9 1381	0.3 1474	3.4 5522	1.9 0899	20. 4633	7.7 4287	39. 6337	10. 5116	123.607	19. 4875	104 57.3	0.1 7409	28. 785	38. 8546	735
TS08 S 103	160.832	1.9 064	315.797	63 8805	0.1 4585		5.0 324	0.0 2082	0.3 1994	0.7 8314	0.5 4414	3.5 815	1.8 1222	21. 5955	9.9 3504	50. 9671	14. 1388	158.646	33. 4585	461 5.15	0.0 1985	382.759	333.371	627
TS08 M 20	71. 9071	2.2 4097	57. 2689	57 2939			2.5 0286			0.1 2835	0.2 0491	1.1 0851	0.4 5044	4.8 4455	1.8 6189	9.8 2613	2.9 0386	35. 6291	6.0 3049	619 0.38	0.0 3248	34. 5747	49. 3123	639

TS08M 17	111.266	2.32864	169.257	55 7214	0.0653 5	0.08839	4.4511 6	0.04852	0.8846 6	1.0491 4	0.5988 7	4.1880 8	1.1931 2	13.2856	5.8854 6	27.3215	7.4645 9	89.777	14.6358	517 5.5	0.1248 7	183.406	184.32	642
TS08S 108	108.126	2.47178	156.655	63 1123	0.0533 9		2.7976 7	0.0061	0.2698 3	0.7056 4	0.2779 3	3.4800 2	0.9884 3	12.2928	4.9372 2	23.4776	6.1078 1	73.2123	14.0388	6573.09	0.0275	133.148	128.916	646
TS08M 19	88.2741	2.03409	103.096	56 2485	0.1444		3.0053 3		0.1800 8	0.5142 6	0.2696 7	3.0798 3	0.8739	10.3813	3.5353	17.7848	4.8095 1	53.9647	9.0969 1	5391.72	0.0860 3	118.828	116.862	632
TS08S 96	157.617	7.19821	196.438	60 8501	0.2339 2		4.8196 9	0.03731	0.7984	1.0450 2	0.6102	6.0246 4	1.7269 3	16.5868	6.8124 4	32.5658	9.1045 7	102.21 1	20.0971	7912.36	0.6415 2	119.692	119.375	736
TS08M 30	204.567	9.93627	532.454	62 7449	1.5671 3		13.6225	0.05314	1.4455 3	2.2272 1	0.7559 7	13.0353	4.2515 6	48.3437	17.9713	80.4378	19.9952	193.671	33.0327	11702.2	1.3728 5	193.462	149.409	767
TS08S 114	283.439	8.2125	621.505	64 8018	1.4576 2		11.1614	0.0147	0.8361 6	1.2713 1	0.3483 3	9.9573 2	3.7372	48.943	19.9263	100.151	25.6822	252.374	46.7679	12527	0.9117 9	43.6134	42.7772	748
TS08M 13	176.946	7.06363	508.438	53 6096	1.7090 5		12.817		0.8257 9	1.5085 3	0.6577 8	10.3899	3.594	46.4406	17.9006	82.0799	21.9517	245.198	33.719	9563.38	0.7600 2	54.135	56.586	734
TS08M 25	78.1965	3.07459	97.7927	62 2793	0.1436 1		3.1229 1			0.2390 6	0.1854 2	1.5633 3	0.5009 6	7.0674 8	3.3409 5	16.5307	4.1642 6	51.6806	9.7916 1	6451.54	0.0605 7	100.23 3	106.517	663
TS08M 16	147.814	2.61997	133.657	55 6164	0.1401 1		3.0503	0.01836	0.2163 2	0.3393	0.3253 8	2.8775 5	0.9464 5	11.5832	4.8295 6	22.4836	6.5021 4	77.8393	12.7187	4838.6	0.0619 2	125.638	149.797	651
TS08M 38	103.652	2.82504	37.9419	52 2830	0.0716 4		2.3420 9		0.0860 6		0.0485 7	0.6722	0.2526 8	3.2579 5	1.2254 4	6.1379 7	1.7337 6	23.1553	3.4921 7	6007.42	0.0560 6	35.410 4	54.860 4	657
TS08M 36	134.582	4.56552	151.654	54 5948	0.2653 5		4.5712 4		0.6642 5	1.2294 9	0.4150 7	4.7736 4	1.2320 4	13.4376	5.0127 8	23.5493	6.2188	72.2152	11.2786	557 8.65	0.184	127.215	117.482	696
TS08S 115	193.649	7.05636	524.852	65 5220	1.6295 8		13.8375		0.5752 9	1.6976 3	0.2765 3	8.6462 6	3.5378	43.8288	17.9406	81.0792	20.5849	212.931	38.2167	12671.6	0.9194 9	48.918 4	49.539 6	734
TS08M 34	154.223	7.28633	631.877	55 5576	0.5536 4	0.02692	12.5419	0.11618	2.4406 8	5.5915 8	1.4986	21.3561	6.2326 3	67.2751	22.3013	92.89	22.2867	226.055	32.3388	9273.91	0.7837 8	336.232	214.985	737

TS08 L 11	238.775	7.0354 2	426.513	50 72 54	0.8007 1		9.8343 4	0.0752 5	1.3193 8	1.9048 4	0.8033 1	10.765 7	3.5668 7	41.534 4	14.810 5	65.612 1	16.678 2	199.35	25.409 8	817 1.2 5	0.9601 6	107.59 1	123.07	73 4
TS08 S 112	239.434	9.6305 3	961.089	62 95 37	1.5633 7	0.0109 7	15.179 8	0.1430 1	2.7941 9	4.5602 9	1.3788	24.749 9	7.4817 9	85.755 2	32.353	142.21 1	33.769	335.83 7	56.844 1	118 76. 9	1.4071 5	245.12 5	168.13 4	76 4
TS08 S 111	225.327	8.4186 8	617.32	62 62 71	1.9878 8		15.794 6	0.0190 4	0.6430 6	1.4423 5	0.5332	9.4457 8	3.9845 7	50.603 5	20.137 2	95.813 4	23.656 3	238.78	42.066 8	119 54. 9	0.9635 7	68.222 5	59.238	75 1
TS08 M 23	137.603	1.3070 3	110.27 8	60 84 82	0.0348 5		3.2771 5		0.1703 9	0.6335 7	0.2047 5	2.3533 2	0.9380 3	10.286 2	3.5875 7	17.672 6	4.7935 5	54.294 5	9.6625 5	534 3.6 2	0.0192 1	141.02 7	147.23 2	60 0
TS08 L 3	220.883	9.3019	579.67 5	58 22 63	1.3359 4		13.507		0.9594 7	1.5374 4	0.5995 5	11.713 3	3.8739	50.084 1	18.985 4	97.208 9	24.276 7	265.47 6	40.748 2	106 66. 7	0.9938 8	47.769 7	46.842 5	76 0
TS08 S 117	131.466	4.7339 2	147.26 3	63 82 06	0.1280 2	0.0016 4	3.6060 7	0.0253 5	0.3911 6	0.5688 7	0.3702 6	3.5318 9	1.1779 7	11.677 2	4.7365 4	23.352 4	5.9733 7	68.258 1	13.057 9	703 8.5 2	0.1540 3	151.03 6	141.89 5	69 9
TS08 S 113	265.554	6.8364 3	736.85 4	64 58 40	1.3216 7		12.830 5	0.0352 5	1.8269 9	3.2629 2	0.9391 5	15.551 4	5.3119 9	61.849 4	23.374 1	112.96 2	28.591 6	277.57 2	50.983 2	112 88. 4	0.9490 8	109.33 2	91.903 3	73 1
TS08 L 6	86.9753	1.7126 9	92.982 2	52 91 02	0.1132 7		3.5541 8		0.0774 5	0.2658 3	0.2010 3	1.3085 2	0.8090 3	8.7631 3	3.2323 7	15.925 3	4.4259 8	53.047 2	7.7932 6	520 5.1	0.0763 3	172.54 9	199.47 4	61 9
TS08 S 107	106.92	3.5472 1	136.48 8	63 61 17	0.1958 4		3.7530 8		0.1841 1	0.4101 1	0.2867 4	2.9274 5	1.1325	11.040 7	4.2890 8	21.325 1	5.8852 9	63.530 3	12.453 2	616 3.9 2	0.1039 5	174.59 7	149.70 6	67 5
TS08 M 12	119.01 3	7.8303 5	226.67 9	52 33 47	0.9392 9		8.8018		0.3304 5	0.7712 8	0.4460 2	4.1102 1	1.7464 6	19.394 4	7.3751 1	36.523	9.8068	108.38 7	14.862 9	981 9.7 1	0.4994 6	73.522 6	92.512 8	74 4
TS08 L 9	114.80 1	1.4470 2	93.460 9	52 88 20	0.0270 6		2.5101 6			0.2098 7	0.2441 7	1.8296 6	0.6048 8	7.6584 2	2.8572	15.323 7	4.4660 7	58.09	8.8104 6	473 1.5 4	0.0473 8	93.769	125.56 7	60 7
TS08 S 110	151.67	2.8997 5	460.47 6	64 20 35	0.1478 5	0.0940 6	6.6016 2	0.2284 1	2.5669 1	3.2929 7	1.5384 6	12.538 3	3.8518 5	40.806 7	15.232 8	72.883 7	18.184 5	196.41 6	38.229 7	652 1.9 6	0.2763 7	430.74 4	308.22 3	65 9
TS08 M 26	188.84 7	6.7668 3	452.70 8	62 02 03	1.0214 9		15.180 5	0.0009 4	0.9312 5	1.6195 1	0.5487 7	9.4112 3	3.2671 3	40.343 1	15.173 2	68.790 3	17.116 6	178.83 3	29.910 6	121 46. 7	0.9722 7	134.88	104.63 9	73 0

TS08 M 37	247.735	8.7084	617.839	54 04 24	1.8439		14.2756	0.0126 1	0.5813 2	2.7174 3	0.7254 3	13.372 3	4.7879 3	62.890 4	21.758 4	100.41 7	26.427 7	292.06 4	38.801 3	909 5.52	0.9103 9	56.631 8	53.352	754
TS08 L 10	177.128	7.5598 8	457.33 4	51 64 44	1.1699 3		11.9041		0.6441 6	1.5050 2	0.4588 7	7.9550 9	3.1417 5	41.254 7	15.735 2	74.562 4	20.652 4	240.55 7	32.390 9	893 3.05	0.7637 8	41.938 2	49.026 1	741
TS08 M 28	120.694	1.6274 1	274.05 1	60 10 90	0.1853 2		4.0929 7		0.4240 6	0.8380 5	0.4276 3	3.7961 2	1.6253 4	18.556 8	9.0059 8	48.183 1	14.004 4	167.87 3	33.195 1	533 7.46	0.161	234.04 9	370.89 5	615
TS08 S 98	112.097	1.1125 5	98.158 4	62 89 82	0.0911 3		3.0864 3	0.0120 3	0.0426 5	0.2945	0.3426 2	1.6418 4	0.6217 3	7.8812 2	3.229	15.490 1	4.5260 4	48.729 4	9.8232 1	493 8.65	0.0806 2	235.87 5	218.04 5	589
TS08 M 35	129.228	1.1412 6	150.30 7	56 58 58	0.0231 7		3.6040 5	0.0275 7	0.1887 7	0.6551 4	0.3266 6	3.3576 3	0.8277 1	11.200 8	4.7884 2	23.359 3	7.1857 1	87.044 3	14.649 8	433 7.69	0.0512 4	214.78 7	259.91 5	591
TS08 M 27	158.578	1.6810 3	132.62 3	61 86 59	0.0540 2		3.9539 4	0.0061 7	0.2031 4	0.4028 6	0.3163 7	3.4489 4	0.9864 4	10.809 9	4.5813 2	20.850 1	5.5883 6	64.261 5	11.266 8	538 0.28	0.0091 9	198.22 3	197.27 3	618
TS08 S 99	202.549	8.8469 2	539.61 8	63 84 37	1.2546 7		11.262	0.0326 2	1.3877 3	1.5411 7	0.7890 2	12.501 8	4.0600 1	43.821 9	17.545 9	80.673 5	19.655 9	199.53 7	32.827 1	119 44.5	1.2633 1	120.83 6	89.159 2	755
TS08 M 33	133.46	2.0057 7	131.57 4	56 35 83	0.1310 6		3.4076		0.6187 2	0.7362 1	0.4303 6	2.4992 3	0.9973 8	12.045 5	4.0435 3	21.053 3	6.5535 5	85.794 6	16.485 2	517 7.51	0.3267 9	195.32 9	242.6	631
TS08 L 4	240.91	9.1242 4	614.82 5	58 74 22	1.8055 3		16.3805		0.6408 5	2.2399 8	0.7046 4	13.060 9	4.6413 9	53.539 2	21.681 6	100.48 3	25.688 8	266.44 7	41.071 2	106 65.3	0.9654 8	71.101 6	64.831	758
TS08 S 102	191.04 5	9.2760 3	414.76 1	65 50 36	1.3417 4		11.361	0.0278 6	0.2752 2	1.2051 3	0.5159 3	7.6680 4	2.6641 2	31.367 2	13.663 2	65.057 3	16.359 2	167.81 5	30.542 2	130 14.3	0.7576 6	79.535 2	80.465 2	760
TS08 M 32	248.91 5	8.1464 3	116 9.75	59 08 11	1.1227 5		16.7303	0.1947 3	3.7226 4	7.5245 5	1.7769 5	36.787 9	10.010 5	116.63	38.810 2	171.65 2	42.840 5	434.28 4	62.993 3	102 41.1	0.7255	122.05 7	82.332 9	748
TS08 L 8	227.28 9	8.4857 4	605.66 1	53 76 87	1.6811 1		15.1728	0.0378 4	1.5173 9	2.2331 6	0.5749	12.930 8	4.4303	55.461 2	20.075 6	95.448 4	25.983 8	281.36 7	38.014 8	931 6.4	0.8297	59.445 9	56.456 4	751
TS08 L 5	196.54 5	9.0798 4	531.04 8	55 46 99	1.5899 3		14.841	0.0259	0.9414 1	1.5922 2	0.4767 3	10.659 4	3.6362	47.771 5	17.803 8	89.542 5	23.770 6	254.42 4	36.694 7	966 2.31	0.8539 9	51.173 4	53.098	758

TS08S121	126.523	1.0046	117.692	62 64 36	0.1372		2.7269			0.3204	0.2480	2.2853	0.8781	9.2825	3.9795	18.6116	5.2633	62.9187	11.7277	653 1.1 9	0.0627	132.73	142.02	582
TS08M15	155.061	9.2177	601.32	53 31 92	1.0126		11.0227	0.1682	3.4342	5.1848	1.7397	21.750	5.3485	59.718	20.587	93.933 7	23.688 2	238.39 5	33.296 3	981 8.6 4	1.1098 6	262.94 7	194.84 5	759
TS08M14	145.83	1.0327	321.58 5	53 28 08	0.1188 2		5.5692 8	0.1592 4	2.0106 9	2.0309 7	1.4853 8	9.5007 7	2.8425 3	30.373 4	11.123	50.404 9	13.063 2	154.17 9	23.407 7	360 6.1 2	0.0525 6	570.83 4	344.32 9	584
TS08S118	151.871	5.4863 4	217.39 2	63 68 10	0.3126 7		5.8074 1		0.3489 9	0.5270 6	0.1449 4	4.3408 1	1.3833 3	18.225 9	7.0303 2	33.605 3	9.0584 5	96.473	17.832 8	877 4.9 3	0.1560 1	150.17 7	165.31 6	712
TS08S120	178.097	7.2741 5	390.75 3	62 93 19	0.4565 1		7.1877 9	0.0805 5	1.4279 9	1.9216 6	0.6024 8	10.625 3	3.0587 5	32.564 1	12.619 4	61.223 9	15.437 4	153.15 6	29.083 6	931 4.7 6	0.5381 4	226.00 1	179.75 2	737
TS08S119	195.081	6.9295 6	389.29 2	61 98 18	0.908		10.575 9	0.0536 4	1.0612 7	1.8719 3	0.5650 6	10.577 1	3.2727 8	34.095 3	13.326 5	55.442 2	13.430 5	132.40 1	22.779 7	131 27. 1	1.3040 5	301.77 6	244.14 7	733
TS08S116	116.539	4.2872 6	127.32 5	65 13 14	0.0935 4		2.9155 2	0.0256 4	0.2029 4	0.6278 3	0.3277 6	2.0827 9	0.5779 8	10.329 9	3.9332 6	20.644 4	5.3887 5	60.028 6	11.567 9	639 8.3 7	0.0668 4	129.30 5	109.43 1	690
TS08S104	127.323	3.6248 4	370.24 2	64 29 28	0.1373 7	0.0742 4	5.6561 5	0.1896	2.4422 6	2.2105 6	1.3046 2	9.7610 9	2.8061 2	30.596 2	11.942 7	60.861 1	14.908 4	168.88 2	34.404 6	644 6.1 5	0.1963 3	414.66 6	328.05 1	677
TS08S105	95.9974	2.3787 7	129.73 1	63 92 79	0.0973 2	0.02	3.9360 7	0.0118 6	0.4504 3	0.8361	0.3031 1	2.5248 7	0.7947	10.895 3	4.4317 6	22.349 3	5.6583 5	66.712 5	13.164	636 2.5 7	0.0529 8	226.86 1	214.92 8	643

Notes: 1/13/2016

Isotope ratios and ages are NOT corrected for initial common Pb.

Isotope ratio and apparent age errors include systematic calibration errors of 0.2603775585047 08% ($^{207}Pb/^{206}Pb$), 0.625201237497987% ($^{206}Pb/^{238}U$) (all 1-sigma).

Isotope ratios and ages corrected using a measured linear secondary standard age bias - ^{206}Pb count rate relationship.

Trace element concentrations in ppm, calculated using mean count rate method.

Sweep-by-sweep downhole fractionation of U/Pb ratios NOT corrected via Si/Zr fractionation factor.

Backgrounds were monitored between sweeps 12 to 24. Sample counts were integrated from sweeps 35 to 60.

Ablation used a laser spot size of 25 microns, and a laser firing repetition rate of 10 Hz.

LA-ICPMS data from sample U12001

		Corrected isotope ratios							Apparent ages (Ma)						
		207Pb*	±2s	206Pb*	±2s	error	207Pb*	±2s	207Pb*	±2s	207Pb*	±2s	206Pb*	±2s	%
Analysis	Th/U	235U*	(%)	238U	(%)	corr.	206Pb*	(%)	206Pb*	(Ma)	235U	(Ma)	238U*	(Ma)	disc.
U12001 L 80	0.18	4.683143	4.472	0.248126	2.953	0.65	0.136888	3.359	2188	58	1764	37	1429	38	35
U12001 L 81	1.02	1.130798	5.668	0.130394	4.071	0.71	0.062896	3.943	705	84	768	31	790	30	-12
U12001 L 82	0.49	5.261268	4.662	0.310953	3.34	0.7	0.122714	3.253	1996	58	1863	40	1745	51	13
U12001 L 83	0.65	1.083277	7.005	0.112417	3.856	0.54	0.069889	5.848	925	120	745	37	687	25	26
U12001 L 84	1.54	1.171728	7.263	0.125363	3.687	0.5	0.067789	6.258	862	130	787	40	761	26	12
U12001 M 169	0.73	1.057617	9.45	0.121784	6.805	0.72	0.062985	6.556	708	139	733	49	741	48	-5
U12001 M 170	0.43	1.075069	8.807	0.103303	6.593	0.75	0.075479	5.839	1081	117	741	46	634	40	41
U12001 M 171	0.38	0.79315	12.06	0.087564	11.12	0.92	0.065695	4.657	797	98	593	54	541	58	32
U12001 M 172	0.31	0.730158	9.093	0.073077	7.996	0.88	0.072466	4.329	999	88	557	39	455	35	54
U12001 M 173	0.2	3.579011	14.53	0.172676	12.84	0.88	0.150325	6.806	2350	116	1545	115	1027	122	56
U12001 M 174	0.07	0.627685	9.815	0.066805	8.603	0.87	0.068144	4.725	873	98	495	38	417	35	52
U12001 M 175	0.94	0.948355	11	0.089897	8.431	0.76	0.076511	7.064	1108	141	677	54	555	45	50
U12001 M 176	0.57	0.461868	13.43	0.060024	13.11	0.98	0.055807	2.913	445	65	386	43	376	48	15
U12001 M 177	0.69	0.734863	9.054	0.079572	8.086	0.89	0.06698	4.074	837	85	559	39	494	38	41
U12001 M 178	0.49	0.63057	6.394	0.078311	4.381	0.68	0.058399	4.657	545	102	496	25	486	21	11
U12001 M 179	0.02	0.730233	7.668	0.051373	6.082	0.79	0.103092	4.671	1681	86	557	33	323	19	81
U12001 M 180	0.38	0.662891	7.154	0.079094	6.208	0.86	0.060786	3.555	632	77	516	29	491	29	22
U12001 S 207	0.3	0.734412	7.447	0.072787	5.175	0.69	0.073179	5.355	1019	108	559	32	453	23	56
U12001 S 208	1.46	0.655381	6.188	0.081159	3.48	0.55	0.058567	5.117	551	112	512	25	503	17	9
U12001 S 209	0.33	0.880813	12.5	0.077156	11.61	0.93	0.082797	4.655	1264	91	641	59	479	54	62
U12001 S 210	0.02	0.917246	6.493	0.080768	4.59	0.7	0.082366	4.592	1254	90	661	32	501	22	60
U12001 S 211	1.8	1.196251	5.743	0.129321	4.372	0.75	0.067089	3.723	841	78	799	32	784	32	7
U12001 S 212	0.76	1.127108	12.23	0.115319	7.401	0.6	0.070887	9.74	954	199	766	66	704	49	26

U12001/U1341 S 678	0.3	5.083239	3.936	0.306728	3.443	0.86	0.120195	1.906	1959	34	1833	33	1725	52	12
U12001/U1341 XS 683	1.31	1.191461	6.975	0.133816	4.873	0.69	0.064576	4.991	761	105	797	39	810	37	-6
U12001/U1341 S 673	1.91	1.21071	7.67	0.131114	6.584	0.86	0.066971	3.934	837	82	806	43	794.2	49	5
U12001/U1341 S 669	1.52	1.166356	8.384	0.130694	5.949	0.71	0.064725	5.907	765	124	785	46	792	44	-3
U12001/U1341 S 658	1.15	1.471412	11.47	0.128949	5.591	0.48	0.082759	10.02	1264	196	919	69	782	41	38
U12001/U1341 S 675	1.46	1.400862	7.223	0.128348	5.359	0.74	0.07916	4.842	1176	96	889	43	778	39	34
U12001/U1341 XS 685	0.96	1.67558	8.392	0.12781	6.712	0.8	0.095082	5.037	1530	95	999	53	775	49	49
U12001/U1341 S 656	1.08	1.156858	7.22	0.127546	6.28	0.87	0.065783	3.561	799	75	780	39	774	46	3
U12001/U1341 S 676	1.34	1.204886	6.057	0.126562	5.375	0.88	0.069046	2.793	900	58	803	34	768	39	15
U12001/U1341 S 672	1.16	1.233059	6.278	0.123758	5.013	0.79	0.072262	3.779	993	77	816	35	752	36	24
U12001/U1341 S 679	1.11	1.79342	8.659	0.122215	5.608	0.64	0.106428	6.597	1739	121	1043	56	743	39	57
U12001/U1341 S 681	1.16	1.04478	6.153	0.121602	5.782	0.94	0.062313	2.104	685	45	726	32	740	40	-8
U12001/U1341 S 665	0.75	1.120609	10.95	0.120583	5.153	0.47	0.067401	9.666	850	201	763	59	734	36	14
U12001/U1341 S 680	1.1	1.067247	6.982	0.118202	4.865	0.69	0.065484	5.008	790	105	737	37	720	33	9
U12001/U1341 S 664	0.63	1.03803	7.927	0.114713	5.423	0.68	0.065629	5.781	795	121	723	41	700	36	12
U12001/U1341 S 661	0.51	1.268794	11.29	0.113867	7.904	0.7	0.080815	8.066	1217	159	832	64	695	52	43
U12001/U1341 S 670	0.83	0.985792	8.486	0.109777	7.197	0.85	0.065129	4.496	778	95	697	43	671	46	14
U12001/U1341 S 659	0.59	1.128384	12.56	0.102729	10.62	0.84	0.079664	6.707	1189	132	767	68	630	64	47
U12001/U1341 S 655	0.13	0.864108	13.24	0.101289	11.25	0.85	0.061873	6.981	670	149	632	62	622	67	7
U12001/U1341 S 657	0.01	0.842497	8.907	0.087994	7.413	0.83	0.06944	4.937	912	102	621	41	544	39	40
U12001/U1341 S 662	0.01	0.690311	8.409	0.087376	7.789	0.92	0.0573	3.17	503	70	533	35	540	40	-7
U12001/U1341 S 668	0.16	0.71914	8.08	0.086927	6.38	0.79	0.060001	4.957	604	107	550	34	537	33	11
U12001/U1341 S 671	0.01	0.651426	6.575	0.08251	6.046	0.92	0.057261	2.582	502	57	509	26	511	30	-2
U12001/U1341 XS 684	0.01	0.665009	8.376	0.079184	7.689	0.92	0.06091	3.321	636	71	518	34	491	36	23
U12001/U1341 S 667	0.01	0.741242	9.344	0.078447	4.596	0.49	0.06853	8.136	885	168	563	40	487	22	45
U12001/U1341 S 663	0.01	0.652983	5.815	0.076792	5.052	0.86	0.061672	2.88	663	62	510	23	477	23	28

LA-ICPMS data from sample U12001 continued.

	Concentrations (ppm)																			

Analysis	P	Ti	Y	Zr	Nb	La	Ce	Pr	Nd	Sm	Eu	Gd	Tb	Dy	Ho	Er	Tm	Yb	Lu	Hf	Ta	Th	U	T(°C)
U12001 L80	488.205	13.56	15 69.6	55 59.39	4.6 90.63	3.9 15	22.73 02	4.4 00.49	30.50 04	20.98 37	9.081 53	49.39 58	15.37 12	17 1.219	56.01 73	21 3.936	48.20 02	48 1.464	49.93 89	13 18 8.9	5.6 98 45	12 8.637	72 3.178	829
U12001 L81	569.398	6.522	13 64.93	56 08.73	4.4 55.56	28.39 94	77.41 19	6.847 86	34.69	12.32 62	1.185 56	38.88 51	12.69 36	14 4.389	54.03 43	22 2.914 2	54.28	57 1.318 14	70.18 13	92 06.37	2.0 61 28	17 0.434	16 6.822	754
U12001 L82	364.49	14.46	91 3.174	55 19.22	5.9 27 9		10.84 75	0.2 08.05	3.7 59.03	6.717	0.1 44.48	28.46 02	9.471 57	10 9.532	34.19 79	13 6.574	32.75 25	31 3.431	33.76 59	10 38 7.2	3.0 17 38	29.45 49	60.29 36	836
U12001 L83	500.102	7.679	19 07.54	56 85.28	3.1 29.01	0.3 83.32	25.85 97	0.3 90.2	4.1 32.4	8.339 36	3.194 23	43.95 9	15.48 44	19 1.938	75.08 67	33 3.475	80.78 96	86 2.512	10 4.218	83 94.15	1.5 36.24	85.31 92	13 0.544	770
U12001 L84	540.474	12.81	26 33.47	57 03.27	3.0 22.53	0.4 68.9	46.64 67	0.4 41	7.4 78.12	15.88 34	4.376 84	71.30 36	24.54 75	28 7.987	10 6.042	41 9.615	10 3.97	10 08.45	12 5.015	84 95.54	1.2 53 24	22 7.898	14 7.625	823
U12001 M 169	294.806	8.829	10 46.72	49 31.25	2.0 71.95	0.0 51.65	15.58 42	0.0 32.27	1.6 21.23	3.207 32	1.500 22	18.11 53	6.917 26	86.40 27	35.27 65	16 9.148	47.12 23	55 9.383	71.20 12	70 05.93	0.8 48.34	69.18 23	95.32 25	784
U12001 M 173	260.801	18.04	94 7.259	49 12.10	3.6 32.96	7.0 45.03	33.87	6.611 69.09	41.94	28.21 5	13.60 17	49.52 45	13.07 21	11 7.89	30.95 61	11 0.684	26.28 47	27 3.366	32.31 84	94 25.8	2.0 00.37	72.70 34	35 9.917	861
U12001 M 176	175.647	10.72	26 55.13	47 26.93	20.10 29	0.3 16.41	60.22 36	1.3 22.41	17.64 87	23.65 61	5.632 87	84.91 66	23.84 4	24 3.053	77.15 55	31 8.454	87.47 61	94 1.905	10 5.892	48 81.13	3.0 83.57	15 14.29	26 71.8	804
U12001 M 177	168.237	6.796	97 3.521	50 47.34	7.3 64.47	1.5 82.71	50.55 02	1.5 46.56	10.65 23	10.62 12	4.832 36	32.91 33	9.414 28	93.83 57	29.58 82	12 3.272	30.60 16	33 1.007	39.09 66	50 43.44	1.0 18.12	35 8.081	52 0.284	758
U12001 M 178	149.814	10.24	54 2.481	52 02.16	2.3 67.54	0.0 47.69	6.597 66	0.1 97.14	3.3 20.94	4.883 07	1.450 59	19.55 22	5.056 09	54.33 63	17.37 48	71.17 81	19.25 6	20 3.677	25.50 24	61 79.3	0.9 22.21	10 1.38	20 6.152	799
U12001 M 180	151.526	15.51	12 78.72	51 72.84	4.7 29.31	4.0 60.04	41.85	4.179 62	30.72 21	25.36 32	10.23 9	55.03 12	16.04 28	13 9.989	38.38 74	14 0.531	32.02 61	33 4.074	34.74 69	75 93	0.9 12.51	20 9.298	55 4.138	844
U12001 S210	359.989	4.464	12 06.17	60 95.66	4.9 03.19	30.98 01	74.72 35	23.14 35	15 0.484	67.46 27	30.98 41	79.55 1	16.27 6	13 5.922	38.08 93	15 1.535	35.34 85	35 1.521	53.45 33	15 47 7.6	13.61 14	15.12 14	64 7.76	719

	29	6.3	18	63	2.3	3.1	20.	1.9	16.	14.	5.0	55.	18.	19	66.	28	64.	59	94.	99	0.8	69.	91.	
U12001 S	6.3	42	80.	07	48	27	43	03	41	69	68	33	41	8.0	51	2.7	21	6.2	29	42.	11	52	18	75
212	77	74	5	11	02	56	36	37	81	55	83	31	99	18	73	02	72	71	7	35	78	11	81	1
U12001/U	14	8.5	43	53	3.7	0.1	26.	0.0	1.8	3.6	1.1	14.	4.1	48.	15.	66.	16.	18	21.	82	1.9	96.	31	
1341 S	5.8	23	3.8	01	31	72	04	82	92	91	48	44	95	43	64	99	43	3.7	47	42.	17	76	8.9	78
678	16	15	99	45	99	58	26	74	71	98	03	47	53	31	07	04	6	32	55	66	63	99	9	0
U12001/U	49	11.	14	49	1.9		34.	0.0	2.0	6.0	1.9	31.	11.	14	54.	24		66	71.	74	0.9	11	83.	
1341 XS	4.7	26	59.	00	01		02	51	58	34	42	65	76	4.1	26	4.7	60.	7.8	88	91.	47	0.1	76	80
683	17	96	16	73	8		61	99	91	93	89	49	34	25	21	62	3	19	61	9	7	33	44	9
U12001/U	61	6.2	20	50	3.1	0.0	53.	0.1	3.2	7.9	2.9	46.	17.	21	76.	32	80.	87	91.	75	1.2	16	10	
1341 S	3.3	40	77.	50	07	06	75	08	69	12	65	04	61	1.5	40	5.1	89	5.3	67	36.	63	1.1	5.9	75
669	45	98	69	34	16	67	04	15	95	7	31	92	97	98	84	48	22	22	99	08	02	39	38	0
U12001/U	58	6.0	16	43	1.6	0.0	21.	0.1	4.0	7.8	2.5	38.	13.	17	61.	27	70.	79	81.	60	0.6	82.	71.	
1341 S	1.7	62	48.	30	10	85	34	83	99	04	13	89	54	1.3	37	1.0	62	5.2	64	05.	26	48	56	74
658	46	26	91	12	12	83	12	6	22	32	31	11	07	29	73	6	65	36	25	74	87	31	01	7
U12001/U	66	9.7	31	51	3.3	1.6	45.	1.1	12.	18.	6.0		29.	33	12	48	11	12	14	73	1.3	21	14	
1341 S	8.7	44	08.	79	50	00	51	98	31	76	70	83.	56	2.2	0.2	5.7	9.0	77.	1.1	47.	93	3.0	6.2	79
675	96	96	52	62	28	52	41	21	79	12	95	91	99	22	17	52	08	65	26	01	54	86	1	4
U12001/U	57	8.5	20	48	1.5	1.7	24.	1.8	16.	13.	5.7	55.	17.	20	73.	30	77.	81	88.	68	0.6	64.	66.	
1341 XS	5.6	53	34.	58	02	91	22	94	08	62	84	14	15	9.9	21	6.2	47	1.1	24	28.	19	43	95	78
685	12	33	92	53	61	02	26	45	71	48	83	32	96	21	21	52	38	33	79	71	81	66	22	0
U12001/U	62	16.	22	46	3.2	0.1	29.	0.3	5.2	11.	4.8	48.	17.	22	83.	34	88.	99	10	55	0.7	86.	79.	
1341 S	5.1	66	58.	15	17	43	19	56	19	56	94	65	43	2.5	73	6.4	22	2.8	4.5	94.	93	43	71	85
656	3	69	81	00	65	97	62	46	04	52	51	27	69	72	78	66	54	09	86	93	45	16	1	2
U12001/U	50	9.9	16	53	1.7		28.	0.1	2.5	7.1	2.3	37.	12.		61.	26	69.	76	86.	76	0.7	10	79.	
1341 S	8.0	00	98.	90	96		92	00	25	82	67	02	46	16	98	8.7	10	2.2	15	21.	37	6.2	39	79
676	65	97	79	03	3		43	2	6	32	48	82	97	1.8	54	18	1	65	74	01	02	33	11	5
U12001/U	45	9.1	18	51	4.0	0.0	47.	0.1	3.6	8.3	3.1	38.	14.	17	67.	30	80.	88	10	73	1.0	12	10	
1341 S	6.0	37	72.	47	63	98	10	40	75	91	11	01	91	5.4	56	5.0	05	1.5	1.4	83.	68	6.0	8.7	78
672	12	26	53	24	54	05	14	2	26	03	47	02	04	42	64	94	13	29	19	06	54	57	59	7
U12001/U	98	5.4	25	54	2.4	2.9	37.	2.1	18.	20.	5.9	63.	22.	25	92.	40	10	10	12	79	0.8	11	10	
1341 S	0.2	01	43.	35	51	42	69	58	63	14	24	31	33	5.2	81	3.0	1.1	68.	8.9	26.	02	2.3	1.5	73
679	24	69	03	08	46	09	68	9	49	11	28	49	98	84	09	28	62	59	99	93	37	29	67	6
U12001/U	68	7.7	27	56	2.9	0.3	33.	0.3	4.4	11.	3.6	54.	20.	25	99.	42	10	10	13	81	0.9	12	10	
1341 S	7.0	73	27.	95	51	80	03	41	10	66	71	95	22	7.0	46	0.7	3.4	78.	5.5	01.	26	2.7	6.2	77
681	14	66	18	56	84	11	64	08	29	69	24	66	05	27	62	03	92	13	02	53	78	83	28	1
U12001/U	40	14.	10	48	0.9		10.	0.0	2.0	5.6	2.5	25.	8.8	10	39.	17	42.	48	55.	58	0.4	23.	31.	
1341 S	2.3	50	92.	06	55		58	93	01	75	81	73	39	4.3	66	0.2	46	6.6	64	43.	34	82	75	83
665	63	01	58	24	2		58	09	32	84	79	95	2	48	31	73	25	47	46	94	87	51	11	6

U12001/U	42	5.8	14	55	3.0		36.	0.1	2.1	5.5	1.8	25.	11.	13	51.	22	58.	63	74.	92	1.0	11	10	
1341 S	4.2	63	29.	24	09		61	78	18	27	03	26	00	1.3	25	6.1	05	2.6	63	93.	08	7.7	7.3	74
680	21	64	9	70	81		59	25	41	27	88	8	66	38	61	28	36	66	69	53	88	56	37	4
U12001/U	41	7.5	11	46	1.5			0.0	1.5	4.1	1.3	22.	8.5	10	41.	17	46.	55	60.	69	0.8	52.	83.	
1341 S	9.1	03	58.	94	29		20.	95	58	57	47	02	22	7.2	85	6.5	75	5.0	59	06.	01	62	04	76
664	04	69	87	90	95		25	28	42	92	65	78	81	08	2	89	41	42	3	41	84	65	99	7
U12001/U	53	9.5	13	46	2.2	1.5	24.	1.1	8.5	9.3	3.3	33.	11.	14	51.	22	60.	65	69.	71	0.7	56.	11	
1341 S	3.0	21	72.	27	01	25	24	18	48	48	77	83	69	2.6	74	3.2	15	8.4	61	39.	34	70	2.0	79
661	5	83	21	75	05	53	19	39	05	15	51	19	87	21	64	72	78	72	9	45	88	57	98	1
U12001/U	56	9.3	16	45	3.2	1.8	43.	1.4	13.	11.	3.6	39.	13.	15	56.	23	66.	74	80.	72	1.6	88.	15	
1341 S	4.8	60	45.	91	73	04	45	99	66	42	59	44	90	9.9	18	0.3	64	3.4	14	19.	07	77	0.7	78
659	4	46	59	92	74	16	46	99	64	58	53	68	02	99	46	07	71	67	81	09	57	59	74	9
U12001/U	49	2.8	88	42	1.6	5.8	6.9	2.7	12.	5.2	6.6	11.	5.0	76.	28.	10	23.	23	19.	87	1.5	5.7	47	
1341 S	9.8	71	5.5	87	03	28	86	75	84	53	04	18	65	55	33	3.5	25	7.1	10	71.	74	31	9.3	68
657	34	57	88	92	72	75	12	93	72	6	82	23	99	74	09	6	88	53	84	41	98	33	03	1
U12001/U	43	1.4	77	45	1.8	0.0	0.2		0.1	0.6	0.0	5.2	3.7	63.	25.	11	27.	28	24.	95	1.4	5.6	85	
1341 S	3.5	53	9.4	32	28	42	63		04	13	71	72	43	86	82	2.8	85	6.8	26	80.	86	17	9.3	62
662	77	98	7	34	58	82	17		35	15	09	86	34	54	87	77	89	09	96	54	93	55	65	8
U12001/U	55	2.1	11	51	0.9	0.0	0.6	0.1	1.1	1.0	0.4	8.5	5.5	95.	35.	15	38.	38	35.	11	0.5	4.3	58	
1341 S	5.7	59	14.	30	67	29	94	39	01	68	82	15	88	70	71	5.8	30	3.7	16	77	57	39	4.7	65
671	34	08	72	72	34	47	83	23	13	93	7	11	07	85	51	05	6	3	72	9.4	36	16	48	8

Notes: 3/1/2014

Isotope ratios and ages are NOT corrected for initial common Pb.

Isotope ratio and apparent age errors do NOT include systematic calibration errors of 0.283223964862561% ($^{207}Pb/^{206}Pb$), 0.514114561642605% ($^{206}Pb/^{238}U$) (all 1-sigma).

Isotope ratios and ages corrected using a measured linear secondary standard age bias - ^{206}Pb count rate relationship.

Trace element concentrations in ppm, calculated using mean count rate method.

Sweep-by-sweep downhole fractionation of U/Pb ratios NOT corrected via Si/Zr fractionation factor.

Backgrounds were monitored between sweeps 10 to 20. Sample counts were integrated from sweeps 28 to 45.

Ablation used a laser spot size of 25 microns, and a laser firing repetition rate of 10 Hz.

Notes: 12/17/2012

Isotope ratios and ages are NOT corrected for initial common Pb.

Isotope ratio and apparent age errors do NOT include systematic calibration errors of 0.303809498288358%

($^{207}Pb/^{206}Pb$), 0.6605775737474 85% ($^{206}Pb/^{238}U$) (all 1-sigma).

Isotope ratios and ages corrected using a measured linear secondary standard age bias - ^{206}Pb count rate relationship.

Trace element concentrations in ppm, calculated using mean count rate method.

Sweep-by-sweep downhole fractionation of U/Pb ratios NOT corrected via Si/Zr fractionation factor.

Backgrounds were monitored between sweeps 17 to 27. Sample counts were integrated from sweeps 39 to 68.

Ablation used a laser spot size of 25 microns, and a laser firing repetition rate of 10 Hz.

LA-ICPMS data from sample F1128A

		Corrected isotope ratios							Apparent ages (Ma)						
		207Pb*	±2s	206Pb*	±2s	error	207Pb*	±2s	207Pb*	±2s	207Pb*	±2s	206Pb*	±2s	%
Analysis	Th/U	235U*	(%)	238U	(%)	corr.	206Pb*	(%)	206Pb*	(Ma)	235U	(Ma)	238U*	(Ma)	disc.
F1128A S 230	1.03	0.609713	7.791	0.071402	6.094	0.78	0.061932	4.854	672	104	483	30	445	26	34
F1128A S 238	1.01	0.67689	11.15	0.070886	3.572	0.32	0.069256	10.56	906	218	525	46	441	15	51
F1128A XS 97	1.26	0.529891	7.312	0.070685	5.817	0.79	0.054369	4.43	386	100	432	26	440	25	-14
F1128A S 235	1.07	0.613434	9.818	0.070496	7.907	0.8	0.063111	5.819	712	124	486	38	439	34	38
F1128A XS 100	1.13	0.557685	7.616	0.070162	4.656	0.61	0.057648	6.027	516	132	450	28	437	20	15
F1128A S 226	1.49	0.570303	4.974	0.069908	3.465	0.69	0.059167	3.568	573	78	458	18	436	15	24
F1128A XS 101	1.48	0.715268	14.9	0.069831	5.107	0.34	0.074288	13.99	1049	282	548	63	435	21	59
F1128A S 231	1.08	0.535997	5.286	0.069712	4.185	0.79	0.055764	3.229	443	72	436	19	434	18	2
F1128A S 232	0.91	0.547791	5.545	0.069652	3.877	0.69	0.05704	3.965	493	87	444	20	434	16	12
F1128A S 233	0.95	0.542052	4.95	0.069279	4.096	0.82	0.056747	2.779	482	61	440	18	432	17	10
F1128A S 234	1.11	0.501638	6.398	0.068898	5.725	0.89	0.052806	2.855	320	65	413	22	430	24	-34
F1128A S 240	1.12	0.560517	3.575	0.068209	2.632	0.72	0.059599	2.419	589	52	452	13	425	11	28
F1128A S 228	1.81	0.533235	4.377	0.068196	3.593	0.81	0.05671	2.499	480	55	434	15	425	15	11
F1128A XS 99	1.33	0.55357	6.826	0.068131	5.255	0.77	0.058929	4.356	564	95	447	25	425	22	25
F1128A XS 105	1.4	0.52588	5.351	0.067971	4.577	0.85	0.056113	2.772	457	62	429	19	424	19	7
F1128A XS 106	1.04	0.686623	9.315	0.067902	5.743	0.61	0.073339	7.334	1023	148	531	39	424	24	59
F1128A XS 96	1.3	0.510614	6.325	0.067552	3.452	0.54	0.054822	5.3	405	119	419	22	421	14	-4
F1128A S 225	1.16	0.522271	3.697	0.067445	3.097	0.83	0.056162	2.019	459	45	427	13	421	13	8

F1128A XS 107	1.2	0.647523	5.882	0.067415	4.53	0.76	0.069662	3.751	918	77	507	23	421	18	54
F1128A XS 104	1.91	0.550166	6.11	0.067245	4.123	0.67	0.059338	4.51	580	98	445	22	420	17	28
F1128A S 237	0.81	0.555564	5.05	0.066903	3.847	0.75	0.060227	3.272	612	71	449	18	417	16	32
F1128A S 229	1.18	0.663747	9.882	0.066843	5.888	0.59	0.072019	7.937	986	162	517	40	417	24	58
F1128A S 236	1.05	0.515488	4.811	0.066436	3.616	0.74	0.056275	3.173	463	70	422	17	414.6	15	10
F1128A S 227	0.96	0.518211	4.153	0.06608	3.561	0.85	0.056877	2.136	487	47	424	14	412	14	15
F1128A XS 108	1.4	0.484677	6.838	0.064316	5.17	0.75	0.054655	4.476	398	100	401	23	402	20	-1
F1128A XS 98	1.3	0.535682	7.902	0.059932	5.475	0.69	0.064825	5.698	769	120	436	28	375	20	51
F1128A XS 103	1.16	0.797841	6.877	0.059332	3.823	0.55	0.097527	5.717	1577	107	596	31	372	14	76

Notes: 5/11/2012

Isotope ratios and ages are not corrected for initial common Pb.
Isotope ratio and apparent age errors include systematic calibration errors of 3.451217236438 98% ($^{208}Pb/^{232}Th$), 0.404994411934365% ($^{207}Pb/^{206}Pb$), 0.544150160013833% (206Pb/238U).

Trace element concentrations in ppm, calculated using mean count rate method.

Backgrounds were monitored between sweeps 17 to 27. Sample counts were integrated from sweeps 36 to 65.

Notes: 5/14/2012

Isotope ratios and ages are not corrected for initial common Pb.
Isotope ratio and apparent age errors include systematic calibration errors of 1.571508975397 05% ($^{208}Pb/^{232}Th$), 0.608900802129852% ($^{207}Pb/^{206}Pb$), 0.474447761622307% ($^{206}Pb/^{238}U$).

Trace element concentrations in ppm, calculated using mean count rate method.

Backgrounds were monitored between sweeps 17 to 27. Sample counts were integrated from sweeps 36 to 65.

LA-ICPMS data from sample F1128A continued.

	Concentrations (ppm)																						
Analysis	P	Ti	Y	Zr	Nb	La	Ce	Pr	Nd	Sm	Eu	Gd	Tb	Dy	Ho	Er	Tm	Yb	Lu	Hf	Ta	Th	U	T(°C)
F1128A S238	531.158	32.7257	1616.96	5087.37	2.9623	0.24523	25.8409	0.31468	4.77074	9.16507	4.19606	43.3357	14.7739	171.506	60.2381	254.645	62.7485	684.292	77.1794	5779.63	1.13425	47.6599	46.9576	935
F1128A XS97	594.91	8.6033	2301.83	4751.85	9.6054		86.4867	0.2233	3.53723	8.68372	1.84598	43.8829	16.8246	206.897	81.4655	372.992	96.6301	1042.35	133.891	8637.67	3.44969	451.388	358.488	781
F1128A XS100	361.162	11.8114	1375.07	5129.16	4.4569	0.17724	48.7146	0.19181	2.56226	4.57268	1.43478	27.7004	9.45899	124.848	45.9835	212.288	56.8371	620.784	81.6598	7932.07	1.91731	170.905	151.882	814
F1128A S226	607.621	14.0256	2604.56	5096.91	9.2643		101.813	0.21743	5.66658	11.9351	4.10601	59.8059	21.5636	260.089	95.7646	406.808	103.031	1158.68	125.183	6498.54	2.72919	266.212	178.742	832
F1128A XS101	325.959	15.7903	1452.5	4300.70	5.1643	0.40209	54.9826	1.25675	12.3169	15.7281	4.30522	47.9297	14.0804	150.256	54.0138	226.54	57.7203	609.159	84.0137	7128.74	1.96986	267.591	180.261	846
F1128A S231	381.077	6.73289	1774.07	5440.31	9.6249	0.11219	60.7255	0.28663	3.81026	6.77865	1.51328	32.4668	12.4258	161.97	62.2447	277.374	74.9144	872.253	103.292	8795	3.76686	333.671	308.361	757
F1128A S232	305.202	11.6987	1419.57	5300.54	4.7663		43.8194	0.13165	2.35678	5.21052	1.57708	26.4505	9.80871	126.957	47.6438	225.701	62.0964	722.477	84.7565	6985.99	1.81458	110.308	121.57	813
F1128A S234	370.512	6.54813	1556.8	5461.47	8.7741		58.6278	0.07222	1.7753	4.94037	0.8353	27.9302	11.3861	147.848	55.4714	258.041	69.7327	812.447	98.1756	9429.05	3.47768	365.191	327.754	754
F1128A S228	738.86	17.8578	4403.86	5144.16	10.7829	1.77998	164.892	1.23611	18.2865	27.4083	9.33449	127.641	42.7829	486.133	162.971	659.046	159.492	1722.32	180.402	6255.59	2.82756	448.795	248.212	860
F1128A XS99	569.319	8.1471	2197.71	4900.67	9.4132	0.13215	75.1005	0.44767	5.61632	8.42903	2.28506	42.6308	16.0953	205.207	77.5085	352.903	90.4455	971.056	129.347	7990.3	2.84665	502.666	378.615	775
F1128A XS96	381.103	10.4842	1480.4	4784.54	4.8692	0.02292	67.184	0.17176	3.40533	6.63602	2.26293	33.3422	11.637	142.178	52.8032	222.747	55.5361	613.78	76.4371	7368.36	1.66145	195.667	151.059	801
F1128A XS107	539.051	8.58568	1958.04	4931.72	5.3281	0.11829	57.0932	0.48515	6.81928	10.6923	2.83742	43.0702	14.6743	182.937	70.5423	309.932	80.2008	875.311	121.751	7977.22	2.0008	251.723	210.587	781
F1128A XS104	382.613	20.7028	1634.52	5004.86	3.7502	0.19347	55.8052	0.17782	4.01319	7.20942	2.94379	38.1491	12.3773	160.313	60.5132	265.125	63.6908	667.382	94.8625	7248.17	1.30173	350.353	183.525	877
F1128A S237	692.756	7.37858	1821.12	5077.08	6.2696	12.3603	55.2932	1.67083	9.41592	9.27853	1.95933	34.2695	12.7515	165.584	63.0066	294.12	80.9016	923.3	107.291	8237.91	2.28163	218.751	268.909	766
F1128A S229	415.624	7.93999	1777.29	5209.95	8.2543	1.07632	63.5954	1.75758	16.0983	14.3232	3.23985	43.1835	14.1449	175.073	63.8467	286.392	78.408	882.088	101.399	7457.82	2.50301	279.874	236.569	773
F1128A S227	485.642	5.9733	1951.48	4960.24	10.5459	0.05185	62.2383	0.16363	2.55668	6.87018	1.0832	32.699	13.3696	173.044	65.5827	293.58	82.2913	956.16	107.992	7887.25	3.45754	318.386	330.524	745
F1128A XS98	365.736	15.5333	1689.96	4797.79	6.6197	1.92087	69.3449	4.00923	33.7187	36.5757	8.01873	68.8623	18.2163	183.135	62.0443	273.793	71.3289	786.862	102.659	7875.35	2.02818	428.939	329.703	844

F1128A XS 103	496.8 32	18.89 27	2452. 07	5248 14	11.88 51	7.572 16	118.3 52	8.359 4	68.36 72	54.82 41	12.43 38	105.8 95	29.83 32	277.8 85	88.61 02	377.0 42	96.93 92	1032. 71	145.8 98	1042 8.5	4.609 81	672.9 14	578.8 97	866

Table 2.A3. U-Pb isotopic LA-ICPMS data of detrital samples

LA-ICPMS data from sample from E1336-41

		Corrected isotope ratios							Dates (Ma)						
		207Pb*	±2s	206Pb*	±2s	error	207Pb*	±2s	207Pb*	±2s	207Pb*	±2s	206Pb*	±2s	%
Analysis	Th/U	235U*	(%)	238U	(%)	corr.	206Pb*	(%)	206Pb*	(Ma)	235U	(Ma)	238U*	(Ma)	disc.
E1336-41 4	0.50	17.27369	7.037	0.56696	6.212	0.88	0.22097	3.306	2988	53	2950	68	2895	145	3
E1336-41 68	0.61	12.83967	4.488	0.50236	3.331	0.74	0.18537	3.008	2701	50	2668	42	2624	72	3
E1336-41 21	0.53	11.65476	8.777	0.50412	7.397	0.84	0.16767	4.724	2535	79	2577	82	2631	160	-4
E1336-41 97	0.45	10.42733	6.742	0.46749	5.376	0.80	0.16177	4.069	2474	69	2473	62	2473	110	0
E1336-41 61	0.68	9.91378	6.258	0.45150	4.946	0.79	0.15925	3.834	2448	65	2427	58	2402	99	2
E1336-41 31	0.25	10.49085	5.739	0.48685	5.025	0.88	0.15628	2.772	2416	47	2479	53	2557	106	-6
E1336-41 67	1.34	7.93468	10.345	0.41449	7.592	0.73	0.13884	7.028	2213	122	2224	93	2235	143	-1
E1336-41 100	0.32	7.76342	8.084	0.40931	6.392	0.79	0.13756	4.948	2197	86	2204	73	2212	120	-1
E1336-41 13	0.55	7.93595	8.153	0.42126	5.770	0.71	0.13663	5.761	2185	100	2224	74	2266	110	-4
E1336-41 41	1.87	5.95637	5.664	0.35181	4.621	0.82	0.12279	3.274	1997	58	1969	49	1943	78	3
E1336-41 59	0.80	5.02550	7.361	0.31465	5.531	0.75	0.11584	4.857	1893	87	1824	62	1764	85	7
E1336-41 92	0.99	5.25790	5.793	0.33111	4.544	0.78	0.11517	3.594	1883	65	1862	49	1844	73	2
E1336-41 116	0.92	4.76885	7.970	0.31888	6.456	0.81	0.10846	4.673	1774	85	1779	67	1784	101	-1
E1336-41 53	0.33	3.71558	11.154	0.25510	9.748	0.87	0.10564	5.421	1725	100	1575	89	1465	128	15
E1336-41 51	0.50	3.77302	11.550	0.27806	8.565	0.74	0.09841	7.749	1594	145	1587	93	1582	120	1
E1336-41 98	0.22	2.23945	14.915	0.19395	11.965	0.80	0.08374	8.906	1287	173	1193	105	1143	125	11
E1336-41 117	0.72	1.58390	12.441	0.16588	5.973	0.48	0.06925	10.913	906	225	964	77	989	55	-9
E1336-41 2	0.93	1.52131	9.284	0.16443	6.739	0.73	0.06710	6.385	841	133	939	57	981	61	-17
E1336-41 8	0.04	1.53894	15.758	0.16283	8.256	0.52	0.06855	13.422	885	277	946	97	972	75	-10
E1336-41 52	0.33	1.53438	7.727	0.16014	5.564	0.72	0.06949	5.362	913	110	944	48	958	50	-5
E1336-41 45	0.41	1.60726	9.711	0.15965	6.204	0.64	0.07302	7.471	1014	151	973	61	955	55	6

E1336-41 105	1.91	1.39164	34.138	0.15954	10.138	0.30	0.06326	32.598	717	692	885	202	954	90	-33
E1336-41 109	1.28	1.56235	6.205	0.15949	3.615	0.58	0.07104	5.043	959	103	955	38	954	32	0
E1336-41 11	0.00	1.39304	20.799	0.15894	7.571	0.36	0.06357	19.373	727	411	886	123	951	67	-31
E1336-41 19	0.66	1.53478	10.134	0.15803	6.110	0.60	0.07044	8.085	941	166	944	62	946	54	-1
E1336-41 39	1.08	1.39128	12.872	0.15781	7.400	0.57	0.06394	10.533	740	223	885	76	945	65	-28
E1336-41 63	1.20	1.55460	8.738	0.15732	4.900	0.56	0.07167	7.235	977	147	952	54	942	43	4
E1336-41 70	0.80	1.48248	6.587	0.15686	4.777	0.73	0.06854	4.536	885	94	923	40	939	42	-6
E1336-41 85	1.50	1.51613	9.915	0.15498	6.885	0.69	0.07095	7.134	956	146	937	61	929	60	3
E1336-41 9	0.52	1.39752	7.801	0.15465	5.791	0.74	0.06554	5.227	792	110	888	46	927	50	-17
E1336-41 87	1.03	1.45810	13.231	0.15373	7.671	0.58	0.06879	10.781	892	223	913	80	922	66	-3
E1336-41 47	0.28	1.72387	11.925	0.15352	6.427	0.54	0.08144	10.045	1232	197	1017	77	921	55	25
E1336-41 72	0.51	1.52266	6.773	0.15320	4.755	0.70	0.07209	4.824	988	98	940	42	919	41	7
E1336-41 56	0.45	1.45661	8.693	0.15268	7.190	0.83	0.06919	4.886	905	101	913	52	916	61	-1
E1336-41 74	1.36	1.33292	10.384	0.15248	5.457	0.53	0.06340	8.834	722	187	860	60	915	47	-27
E1336-41 83	0.89	1.38537	13.373	0.15180	7.390	0.55	0.06619	11.146	812	233	883	79	911	63	-12
E1336-41 17	0.91	1.50109	13.329	0.15145	7.455	0.56	0.07189	11.050	983	225	931	81	909	63	7
E1336-41 58	0.93	1.43048	9.653	0.15102	5.506	0.57	0.06870	7.929	890	164	902	58	907	47	-2
E1336-41 25	0.57	1.33346	16.013	0.15068	8.338	0.52	0.06418	13.671	748	289	860	93	905	70	-21
E1336-41 1	0.93	1.37277	9.528	0.15025	6.098	0.64	0.06627	7.320	815	153	877	56	902	51	-11
E1336-41 111	1.12	1.40631	13.120	0.14888	6.758	0.52	0.06851	11.246	884	233	892	78	895	56	-1
E1336-41 10	0.72	1.16102	15.610	0.14882	7.336	0.47	0.05658	13.778	475	305	782	85	894	61	-88
E1336-41 115	0.42	1.53584	7.462	0.14839	5.120	0.69	0.07506	5.428	1070	109	945	46	892	43	17
E1336-41 34	1.66	1.53311	8.683	0.14813	6.357	0.73	0.07506	5.915	1070	119	944	53	890	53	17
E1336-41 90	0.82	1.35598	10.277	0.14779	6.121	0.60	0.06654	8.256	824	172	870	60	889	51	-8
E1336-41 71	0.57	1.40100	14.346	0.14778	6.529	0.46	0.06876	12.775	892	264	889	85	888	54	0
E1336-41 38	0.74	1.37700	12.356	0.14767	6.504	0.53	0.06763	10.505	857	218	879	73	888	54	-4
E1336-41 20	0.81	1.37592	8.485	0.14725	6.396	0.75	0.06777	5.575	862	116	879	50	886	53	-3
E1336-41 80	2.12	1.26088	30.462	0.14714	9.830	0.32	0.06215	28.832	679	616	828	172	885	81	-30
E1336-41 35	0.71	1.34975	12.354	0.14713	5.649	0.46	0.06654	10.987	823	229	867	72	885	47	-7
E1336-41 66	1.03	1.43722	6.537	0.14687	4.256	0.65	0.07097	4.961	957	101	905	39	883	35	8

E1336-41 82	0.77	1.44647	8.250	0.14653	5.663	0.69	0.07160	6.000	974	122	908	50	881	47	10
E1336-41 27	0.93	1.54293	12.787	0.14615	6.697	0.52	0.07657	10.892	1110	218	948	79	879	55	21
E1336-41 96	0.53	1.70469	8.299	0.14562	5.472	0.66	0.08490	6.239	1313	121	1010	53	876	45	33
E1336-41 26	0.55	1.43666	13.358	0.14538	8.790	0.66	0.07167	10.059	977	205	904	80	875	72	10
E1336-41 28	0.98	1.41850	14.332	0.14496	7.820	0.55	0.07097	12.010	957	246	897	85	873	64	9
E1336-41 23	1.24	1.33902	7.992	0.14495	6.189	0.77	0.06700	5.057	838	105	863	46	873	51	-4
E1336-41 113	0.94	1.29636	12.284	0.14381	6.186	0.50	0.06538	10.613	787	223	844	70	866	50	-10
E1336-41 69	0.90	1.43804	8.062	0.14379	6.086	0.75	0.07253	5.288	1001	107	905	48	866	49	13
E1336-41 12	1.14	1.36469	14.151	0.14238	8.260	0.58	0.06952	11.490	914	236	874	83	858	66	6
E1336-41 29	0.91	1.30678	11.701	0.14137	7.417	0.63	0.06704	9.050	839	188	849	67	852	59	-2
E1336-41 54	0.50	1.43666	10.162	0.14035	6.401	0.63	0.07424	7.893	1048	159	904	61	847	51	19
E1336-41 22	0.66	1.15287	15.047	0.14021	8.335	0.55	0.05963	12.528	590	272	779	82	846	66	-43
E1336-41 46	0.77	1.40125	11.527	0.13959	5.966	0.52	0.07280	9.863	1009	200	889	68	842	47	16
E1336-41 120	0.70	1.30483	13.668	0.13943	8.838	0.65	0.06787	10.426	865	216	848	79	841	70	3
E1336-41 79	0.92	1.42014	7.521	0.13939	5.405	0.72	0.07389	5.229	1039	106	897	45	841	43	19
E1336-41 37	0.48	1.14951	13.082	0.13855	8.498	0.65	0.06017	9.946	610	215	777	71	836	67	-37
E1336-41 108	1.11	1.30040	9.236	0.13770	6.575	0.71	0.06849	6.486	884	134	846	53	832	51	6
E1336-41 16	0.76	1.28531	10.663	0.13748	6.740	0.63	0.06781	8.262	863	171	839	61	830	53	4
E1336-41 3	0.72	1.33992	16.931	0.13711	8.795	0.52	0.07088	14.467	954	296	863	98	828	68	13
E1336-41 107	1.07	1.26788	14.367	0.13428	9.006	0.63	0.06848	11.194	883	231	831	82	812	69	8
E1336-41 101	0.92	1.21236	9.400	0.13314	4.839	0.51	0.06604	8.058	808	169	806	52	806	37	0
E1336-41 103	0.56	1.26527	20.335	0.13313	8.532	0.42	0.06893	18.459	897	381	830	115	806	65	10
E1336-41 6	0.97	1.09919	14.698	0.13302	7.057	0.48	0.05993	12.893	601	279	753	78	805	53	-34
E1336-41 65	0.90	1.20531	8.463	0.13288	4.762	0.56	0.06579	6.996	800	147	803	47	804	36	-1
E1336-41 36	1.16	1.00298	15.466	0.13285	6.802	0.44	0.05476	13.890	402	311	705	79	804	51	-100
E1336-41 78	0.91	1.19824	9.413	0.13270	5.275	0.56	0.06549	7.796	790	164	800	52	803	40	-2
E1336-41 112	1.35	1.22205	8.229	0.13180	4.260	0.52	0.06724	7.040	845	146	811	46	798	32	6
E1336-41 43	1.06	1.13026	16.280	0.13156	8.827	0.54	0.06231	13.679	685	292	768	88	797	66	-16
E1336-41 60	0.75	1.12157	7.908	0.13107	5.138	0.65	0.06206	6.011	676	129	764	42	794	38	-17
E1336-41 49	0.73	1.17877	8.411	0.13098	6.040	0.72	0.06527	5.853	783	123	791	46	793	45	-1

E1336-41 57	0.91	1.11938	7.810	0.13067	5.151	0.66	0.06213	5.871	679	125	763	42	792	38	-17
E1336-41 76	0.77	1.15958	10.330	0.12980	6.136	0.59	0.06479	8.310	768	175	782	56	787	45	-2
E1336-41 30	0.75	1.06548	15.231	0.12961	8.439	0.55	0.05962	12.679	590	275	737	80	786	62	-33
E1336-41 62	1.00	1.00516	15.336	0.12935	5.536	0.36	0.05636	14.302	467	317	706	78	784	41	-68
E1336-41 99	1.38	1.25101	9.286	0.12928	6.955	0.75	0.07018	6.153	934	126	824	52	784	51	16
E1336-41 14	1.08	0.80327	38.755	0.12914	8.835	0.23	0.04511	37.734	-50	918	599	175	783	65	1679
E1336-41 110	1.06	1.12205	8.198	0.12855	4.957	0.60	0.06331	6.529	719	139	764	44	780	36	-8
E1336-41 106	1.05	1.28989	6.627	0.12803	5.618	0.85	0.07307	3.514	1016	71	841	38	777	41	24
E1336-41 84	0.91	1.20112	12.099	0.12744	7.255	0.60	0.06835	9.682	879	200	801	67	773	53	12
E1336-41 86	0.74	1.19088	9.071	0.12732	5.258	0.58	0.06784	7.392	864	153	796	50	773	38	11
E1336-41 55	0.79	1.25004	8.966	0.12714	6.356	0.71	0.07131	6.324	966	129	823	51	772	46	20
E1336-41 102	1.00	1.20275	10.300	0.12706	5.457	0.53	0.06865	8.736	888	180	802	57	771	40	13
E1336-41 42	0.65	1.10455	13.162	0.12666	6.417	0.49	0.06325	11.492	717	244	756	70	769	47	-7
E1336-41 81	0.72	1.24999	8.138	0.12651	5.190	0.64	0.07166	6.269	976	128	823	46	768	38	21
E1336-41 50	1.17	1.08082	11.184	0.12643	5.731	0.51	0.06200	9.603	674	205	744	59	767	41	-14
E1336-41 88	1.31	1.16997	9.503	0.12628	7.180	0.76	0.06720	6.225	844	130	787	52	767	52	9
E1336-41 32	0.76	1.19652	11.638	0.12599	6.163	0.53	0.06888	9.872	895	204	799	64	765	44	15
E1336-41 75	1.06	1.18198	10.791	0.12582	5.177	0.48	0.06813	9.469	873	196	792	59	764	37	12
E1336-41 95	0.82	1.14130	8.338	0.12557	4.545	0.55	0.06592	6.990	804	146	773	45	763	33	5
E1336-41 93	1.39	1.25090	7.720	0.12441	4.523	0.59	0.07292	6.256	1012	127	824	44	756	32	25
E1336-41 44	0.94	0.94310	18.169	0.12439	6.753	0.37	0.05499	16.867	412	377	675	90	756	48	-84
E1336-41 48	1.13	1.01459	13.192	0.12423	6.650	0.50	0.05923	11.393	576	248	711	67	755	47	-31
E1336-41 119	0.83	1.16687	12.780	0.12378	5.511	0.43	0.06837	11.530	880	239	785	70	752	39	15
E1336-41 104	0.73	0.98589	17.592	0.12321	7.250	0.41	0.05804	16.029	531	351	697	89	749	51	-41
E1336-41 91	1.16	1.10974	10.885	0.12265	7.068	0.65	0.06562	8.278	794	174	758	58	746	50	6
E1336-41 73	0.51	0.99563	13.024	0.12178	4.609	0.35	0.05930	12.181	578	265	702	66	741	32	-28
E1336-41 40	1.22	1.07231	11.965	0.12093	6.037	0.50	0.06431	10.330	752	218	740	63	736	42	2
E1336-41 77	0.72	1.08734	11.778	0.12075	4.013	0.34	0.06531	11.073	784	233	747	62	735	28	6
E1336-41 15	0.72	0.81082	26.452	0.11886	11.536	0.44	0.04947	23.804	170	556	603	120	724	79	-325
E1336-41 89	0.87	1.00779	12.212	0.11852	4.762	0.39	0.06167	11.245	663	241	708	62	722	33	-9

E1336-41 33	0.69	0.95895	17.207	0.11844	7.124	0.41	0.05872	15.663	557	342	683	86	722	49	-30						

LA-ICPMS data from sample from E1336-41 continued.

	Concentrations (ppm)																					
Analysis	P	Ti	Y	Nb	La	Ce	Pr	Nd	Sm	Eu	Gd	Tb	Dy	Ho	Er	Tm	Yb	Lu	Hf	Ta	Th	U	T(°C)
E1336-414	526	5.38	1422	3.47		7.00		1.22	3.75	0.25	23.93	9.37	118.7	48.49	232.1	57.6	583	93.5	9256	1.38	76.1	153	736
E1336-4168	268	5.38	1253	6.23		15.74		1.84	4.21	0.28	23.84	8.52	123.5	46.64	196.3	43.4	379	61.2	10658	3.85	117.5	194	736
E1336-4121	215	6.14	550	2.22		10.87		0.79	2.78	0.15	10.65	3.58	48.7	18.57	83.0	19.1	181	23.7	7681	0.87	47.5	89	748
E1336-4197	237	2.82	520	0.49		5.10	0.05		1.51	0.62	9.51	3.44	42.9	16.83	82.0	19.1	210	43.8	10665	0.33	21.4	48	680
E1336-4161	305	6.11	1069	2.02		11.68	0.07	1.85	4.36	0.66	19.56	7.71	101.7	36.75	166.2	38.6	364	57.3	8891	1.29	130.7	193	748
E1336-4131	845	0.83	1366	2.77	0.07	5.76	0.09	1.12	3.75	0.36	20.54	8.27	119.6	43.01	200.6	52.3	581	80.2	9635	1.37	101.3	408	588
E1336-4167	233	2.75	787	3.01		15.96		1.00	2.86	0.26	16.73	5.58	71.7	26.57	129.5	28.9	271	52.7	11767	0.81	48.3	36	677
E1336-41100	127	1.18	218	0.62		2.66	0.03		0.88	0.21	4.22	1.26	17.2	8.04	36.0	9.0	97	15.7	10187	0.38	25.1	80	613
E1336-4113	45	5.41	467	2.44		12.16		0.79	1.62	0.24	14.05	4.33	49.3	15.94	63.4	12.9	125	20.5	6202	0.87	45.4	83	736
E1336-4159	284	7.21	744	4.24		9.78		0.58	2.89	0.89	15.27	6.02	73.3	27.08	111.3	26.6	250	35.5	9284	0.98	31.1	39	764
E1336-4192	338	7.56	1511	8.08	0.03	20.00	0.13	3.29	7.30	0.08	34.94	11.72	151.7	52.66	233.7	49.0	420	66.4	11361	2.87	163.2	165	768
E1336-4153	299	20.16	566	3.06		11.90		0.73	1.08	0.35	11.16	3.50	60.9	19.44	82.2	17.1	175	23.7	10196	1.72	75.4	227	874
E1336-4198	102	0.82	172	2.35		1.18	0.02	0.32	0.66		3.51	1.19	13.2	5.79	19.6	4.0	45	7.1	11551	1.11	16.5	74	588
E1336-41117	564	5.31	2800	2.43		8.10		0.34	3.64	0.62	39.78	18.15	235.8	99.45	478.7	107.4	970	172.6	11219	0.80	49.6	69	735
E1336-412	162	5.36	153	0.36		15.05			1.00	0.57	5.34	0.98	14.4	3.98	23.0	6.1	75	12.4	7926	0.34	88.8	95	735

E1336-418	118	3.08	87	1.16		0.89						0.02	3.4	2.57	15.2	5.7	79	15.4	10924	1.44	1.2	31	687
E1336-4152	120	2.10	242	1.48		7.69					3.57	1.17	17.5	7.64	42.7	11.1	129	21.1	9506	1.17	60.0	182	656
E1336-4145	146	1.37	513	0.32		0.87			1.05	0.83	4.16	2.50	35.5	16.11	81.2	24.0	312	59.1	5695		34.8	85	624
E1336-41105	300	28.43	583	0.27		70.21	0.09	3.87	4.56	1.85	28.18	6.51	64.9	22.82	83.3	21.6	215	33.6	6288		27.6	14	916
E1336-41109	220	12.01	611	0.83		21.86	0.08	1.45	2.56	1.10	14.80	4.90	60.3	19.91	95.4	21.0	224	35.4	8759	0.14	143.5	112	816
E1336-4111	121	2.13	66	0.60								0.12	2.0	1.74	11.1	5.8	86	18.3	10450	1.03	0.0	23	657
E1336-4119	70	6.23	410	0.41		14.11	0.04	0.42	0.50	0.96	6.18	2.20	29.5	10.75	59.9	16.7	206	34.5	6166	0.20	59.3	90	749
E1336-4139	166	12.39	512	0.73		17.89	0.10	1.66	1.93	0.93	13.24	4.03	48.5	17.56	70.4	16.3	165	23.9	6708	0.26	95.8	89	819
E1336-4163	235	23.69	506	0.87		19.58	0.11	1.53	3.76	0.55	15.34	4.51	49.1	18.61	79.1	17.7	158	27.2	8508	0.21	157.6	132	894
E1336-4170	285	3.90	1268	10.69		28.99	0.05	0.84	1.26	0.56	15.70	5.47	93.7	39.10	207.8	54.0	582	104.9	11186	4.61	174.2	217	707
E1336-4185	355	4.94	1342	1.55		28.65	0.10	2.51	6.52	2.54	30.57	10.22	124.9	44.00	196.4	47.0	486	76.1	9022	0.51	162.7	108	728
E1336-419	103	3.18	389	0.52		21.80	0.06	1.59	3.16	1.68	18.37	4.05	38.4	12.74	52.4	12.0	128	23.0	10878	0.38	108.2	209	690
E1336-4187	142	9.13	458	0.54		8.92		0.47	1.96	0.87	9.76	2.88	34.9	15.43	75.6	18.8	216	35.0	7626	0.27	36.9	36	787
E1336-4147	80	2.39	64	0.37		1.03						0.22	3.7	1.63	8.2	1.9	22	2.8	9556	0.99	8.3	29	666
E1336-4172	275	4.20	1014	3.55		21.89		1.18	2.16	0.92	19.21	5.82	85.9	33.57	168.3	40.5	405	68.9	9781	1.92	75.3	147	713
E1336-4156	142	3.68	864	2.38	0.70	22.76	0.51	4.20	2.83	1.45	14.93	4.81	59.8	25.55	128.9	39.3	465	96.7	10688	0.63	161.5	361	702
E1336-4174	205	8.29	1161	0.40		17.31	0.28	4.86	5.09	2.11	23.33	8.51	96.8	37.52	183.1	47.0	461	93.3	10374	0.33	133.2	98	777
E1336-4183	140	8.31	408	0.26		9.07	0.05	0.81	1.57	0.93	6.71	2.63	31.3	13.47	69.0	17.5	221	39.2	7667	0.25	45.6	51	777
E1336-4117	217	2.42	658	2.33		14.43		0.62	2.94	0.76	12.63	4.34	63.7	21.53	106.2	25.4	259	37.6	7579	0.60	45.1	49	667
E1336-41	26	15.	48	0.9		20.7		0.8	1.8	0.2	12.	3.7	46.	14.	72.	16.	15	25.	898	0.3	79.	85	845

58	2	63	0	8		5		2	1	1	94	9	6	58	6	4	3	8	1	0	4		
E1336-41 25	316	2.04	673	0.58		9.81		0.76	2.33	0.58	11.24	3.93	49.7	20.16	101.3	25.3	277	45.8	7499	0.24	34.2	60	654
E1336-41 1	176	8.95	413	1.03		16.01	0.01	0.13	1.01	0.42	7.72	3.08	36.2	13.91	57.1	15.3	169	25.4	6959	0.46	68.2	73	785
E1336-41 111	287	23.30	483	1.14		21.07		1.82	3.04	0.99	13.81	4.67	47.8	17.46	76.9	16.4	169	24.7	8960	0.84	70.2	63	892
E1336-41 10	171	7.03	848	0.22		4.01	0.02	0.68	2.82	0.33	17.51	6.40	79.4	29.79	134.5	30.3	285	43.9	9196	0.14	34.0	47	761
E1336-41 115	200	1.41	718	2.19		9.56			1.41	0.90	9.77	3.64	55.7	22.92	116.4	25.0	271	48.9	13849	1.26	59.9	142	626
E1336-41 34	242	25.44	855	1.22		26.91	0.56	7.00	9.15	1.31	31.19	9.88	93.5	28.90	106.5	25.3	229	32.3	7195	0.22	219.3	132	902
E1336-41 90	388	11.42	1151	1.62		9.69		0.32	1.23	0.46	15.61	6.98	103.1	40.14	178.8	45.8	448	61.5	10581	0.43	82.0	100	810
E1336-41 71	319	14.17	806	0.71		8.24		0.81	2.32	0.50	15.19	5.38	73.8	26.49	132.7	30.3	300	49.2	10177	0.83	21.6	38	834
E1336-41 38	66	4.94	180	0.23		4.41			1.30	0.82	5.41	1.18	14.9	5.05	23.4	6.0	67	10.2	6405	0.14	42.6	57	728
E1336-41 35	195	10.52	415	0.43		7.62			1.05	0.16	8.91	2.86	41.8	15.04	63.1	14.3	154	21.3	7786	0.18	37.2	53	801
E1336-41 66	248	7.06	559	1.24		36.24		0.80	2.96	0.88	16.06	4.21	54.8	19.23	85.4	18.9	184	32.8	10896	0.81	228.9	221	761
E1336-41 82	223	12.07	320	1.58	0.08	26.45		0.35	1.39	0.40	6.84	1.81	25.7	11.08	45.9	10.3	123	19.0	9771	0.96	118.3	153	816
E1336-41 27	261	13.17	832	0.47		9.70	0.04	1.89	4.45	0.93	21.98	6.30	76.4	28.01	115.1	27.3	267	34.1	7561	0.31	51.8	55	826
E1336-41 96	78	2.86	770	0.88	0.24	19.85	0.10	1.16	2.20	0.67	13.20	3.86	57.7	22.07	118.0	33.2	371	84.8	12110	0.20	88.3	168	681
E1336-41 26	127	3.69	434	1.83		8.86		0.73	0.89	0.48	5.59	2.94	36.9	15.31	66.5	16.0	176	25.8	6603	0.41	23.8	44	702
E1336-41 28	219	13.57	374	0.86		16.22		1.10	0.54	0.73	6.71	2.79	33.6	13.23	54.6	14.6	147	20.1	6925	0.46	47.8	49	829
E1336-41 23	407	13.83	1057	3.93	0.16	57.83	0.26	5.86	5.24	1.44	26.54	7.16	101.6	36.42	152.1	36.1	377	50.6	6658	1.70	168.8	136	831
E1336-41 113	160	9.20	477	0.54		8.78	0.08	0.66	0.80	0.69	7.03	2.78	34.6	14.89	74.9	21.1	232	49.1	8294	0.41	56.0	59	788
E1336-41 69	179	4.37	957	2.50	0.41	28.39	0.17	1.17	4.43	1.59	16.60	6.52	75.2	31.23	156.5	37.7	409	78.4	11446	0.72	190.6	212	717

E1336-41 12	229	14.61	511	0.97		15.55	0.06	0.64	2.35	0.76	15.38	4.19	46.3	16.30	70.2	17.2	175	29.9	7369	0.51	47.5	42	837
E1336-41 29	227	8.70	948	0.23		9.34		1.09	4.06	0.52	23.85	8.06	83.5	29.44	126.8	29.8	310	41.2	8385	0.26	76.1	84	782
E1336-41 54	277	9.08	786	0.83		7.96		0.63	1.24	0.45	14.72	3.75	65.4	25.29	130.3	33.7	381	63.8	9469	0.55	43.7	87	786
E1336-41 22	212	10.00	479	0.50		8.65			0.92	0.08	5.98	2.73	41.7	18.10	69.7	17.9	169	26.3	8170	0.25	36.5	55	796
E1336-41 46	221	11.57	541	0.74		9.96		1.06	1.55	0.23	9.64	3.58	44.7	16.35	80.5	19.1	182	26.3	7968	0.27	44.3	57	812
E1336-41 120	328	9.04	637	0.61		9.12		0.73	2.03	0.39	12.63	4.43	58.7	22.55	105.9	25.8	263	39.9	8737	0.27	41.4	59	786
E1336-41 79	188	2.27	872	5.23		44.67	0.02	1.51	2.71	0.74	14.65	5.85	74.9	31.46	141.5	35.3	347	58.8	10501	2.12	241.0	263	662
E1336-41 37	238	8.55	637	0.93		6.25		0.90	1.78	0.71	10.35	3.85	51.3	21.12	94.7	23.2	260	41.5	7240	0.56	53.6	112	780
E1336-41 16	271	12.24	530	0.69		10.63			0.91	0.43	9.45	3.86	48.3	18.02	84.0	18.9	198	26.1	8314	0.22	47.1	62	818
E1336-41 101	270	4.18	654	1.54		18.09			1.43	0.59	10.20	4.37	52.7	22.89	103.2	26.1	299	51.2	10597	0.72	142.5	154	713
E1336-41 103	256	8.07	838	0.55		8.25	0.04	0.40	1.29	0.34	12.31	4.82	70.6	27.50	145.5	37.7	415	66.6	7796	0.31	31.2	55	775
E1336-41 6	190	7.23	826	0.49		9.61		1.34	3.31	1.01	19.81	6.26	73.5	24.90	112.5	26.9	283	44.1	8847	0.20	49.4	51	764
E1336-41 65	463	5.23	1535	5.76	0.45	41.45	0.11	2.05	1.92	0.50	19.35	8.56	118.0	52.45	261.5	67.3	709	139.3	11468	1.85	162.6	180	733
E1336-41 36	336	15.03	1097	0.59		13.37	0.14	5.17	5.32	0.44	28.51	8.76	96.9	35.04	154.7	36.9	346	51.1	8068	0.22	79.4	68	840
E1336-41 78	232	4.86	629	0.40		10.40	0.05	0.93	1.57	0.70	13.29	3.96	50.4	20.88	104.3	26.7	269	54.5	11815	0.41	97.7	108	727
E1336-41 112	278	6.27	1814	1.85		34.76	0.22	3.18	6.64	1.35	33.29	11.45	158.8	62.29	300.3	72.3	750	133.6	10888	0.93	228.4	170	750
E1336-41 43	217	9.12	934	0.24		14.43	0.05	1.32	4.15	0.77	19.15	7.33	86.3	31.55	135.1	30.1	311	42.6	7918	0.02	66.1	63	787
E1336-41 49	340	4.15	1028	5.63	0.67	38.27	0.25	1.70	1.67	0.19	11.24	4.88	70.7	32.71	157.1	47.4	504	81.8	9449	2.66	133.1	183	712
E1336-41 57	360	7.26	1299	1.96		21.68		1.83	1.90	0.67	23.13	7.23	105.5	42.41	205.6	55.1	595	104.4	9203	0.78	270.1	297	764
E1336-41	29	10.	10	1.4		16.8	0.0	0.6	2.1	0.6	18.	5.8	80.	33.	163	41.	39	78.	106	0.7	99.	13	797

76	5	03	36	0		4	4	2	0	7	00	1	8	86	.2	2	8	2	75	5	7	0	
E1336-41 30	24 3	8.5 7	52 7	0.5 8		16.2 5		0.7 7	1.1 0	0.2 9	11. 19	3.7 9	42. 9	16. 90	78. 7	19. 0	19 4	26. 1	767 2	0.2 6	41. 3	55	781
E1336-41 62	25 2	14. 92	58 9	0.4 9		12.4 5		0.9 4	1.4 4	0.2 0	11. 89	4.0 0	51. 5	19. 85	86. 5	19. 3	19 0	31. 0	979 5	0.5 1	47. 7	48	839
E1336-41 14	28 4	14. 29	72 1	0.4 6		10.1 2		0.1 4	1.6 9	0.2 3	13. 91	4.5 1	59. 8	23. 58	105 .2	25. 6	26 3	38. 0	700 4	0.2 6	21. 6	20	834
E1336-41 86	29 9	10. 87	90 9	1.1 8		13.5 9	0.0 4	1.1 5	3.1 2	0.4 8	17. 98	6.2 5	76. 5	31. 25	143 .3	35. 1	36 4	57. 2	889 7	0.5 2	76. 2	10 4	805
E1336-41 55	16 5	3.5 2	43 5	0.9 5		17.1 8		0.9 9	1.2 2	0.4 7	5.3 2	2.2 2	33. 6	14. 61	68. 0	19. 1	21 0	37. 8	987 9	0.3 5	142 .0	17 9	698
E1336-41 102	31 1	13. 27	93 9	0.6 3		10.2 5	0.0 7	2.3 0	4.8 3	0.8 4	23. 65	6.9 0	90. 8	31. 80	148 .8	35. 1	34 0	49. 5	896 1	0.4 5	80. 2	80	826
E1336-41 81	23 9	9.1 8	66 4	1.0 8		8.90	0.0 3		0.6 8	0.7 1	5.2 6	3.0 1	47. 5	20. 38	111 .9	28. 7	32 1	59. 5	683 2	0.4 0	121 .1	16 8	788
E1336-41 50	25 6	8.5 8	14 74	0.8 9		18.8 8	0.1 9	4.1 8	8.1 0	1.4 6	35. 99	10. 78	131 .4	48. 27	213 .8	48. 9	52 0	72. 0	804 2	0.1 7	128 .8	11 0	781
E1336-41 88	32 5	10. 23	18 51	0.9 0		19.3 2	0.1 8	3.7 4	8.0 9	1.6 9	50. 71	14. 70	189 .9	65. 06	277 .0	64. 7	60 6	90. 8	888 4	0.3 6	213 .7	16 3	799
E1336-41 32	28 7	12. 33	60 1	0.6 6		11.8 2		0.6 5	1.4 0	0.2 6	12. 50	4.6 8	54. 2	20. 16	79. 8	20. 7	21 3	30. 7	719 9	0.3 6	55. 8	74	818
E1336-41 75	17 3	8.3 7	89 4	0.6 5		18.0 5		1.1 5	4.4 5	0.8 7	18. 59	6.6 9	79. 7	29. 59	140 .8	32. 7	32 5	60. 0	127 18	0.4 1	138 .6	13 1	778
E1336-41 95	23 9	7.5 7	85 6	0.8 6		14.1 3		0.6 6	1.8 2	0.4 9	9.9 0	4.0 5	67. 0	26. 61	143 .4	37. 9	39 6	83. 1	104 98	0.5 4	107 .4	13 0	768
E1336-41 93	55 9	12. 36	87 61	12. 56	10. 43	106. 69	6.9 2	46. 28	27. 75	9.2 8	74. 74	26. 81	273 .3	97. 17	428 .9	102 .2	96 7	180 .9	126 36	4.0 3	774 .8	55 9	819
E1336-41 48	31 5	10. 87	13 08	0.8 3		15.8 1	0.1 1	4.1 5	4.7 4	0.6 8	25. 22	9.9 4	123 .3	44. 39	187 .8	43. 8	43 7	64. 5	767 5	0.4 7	118 .4	10 4	805
E1336-41 119	31 1	10. 71	81 4	0.8 8		11.6 2	0.1 5	1.1 9	4.3 1	0.9 8	17. 88	6.5 0	80. 8	28. 99	126 .7	29. 1	32 8	46. 9	801 0	0.2 2	74. 0	89	803
E1336-41 104	26 5	6.7 9	55 5	0.7 9		10.7 6		0.1 3	1.9 6	0.1 2	11. 63	4.3 0	52. 2	18. 93	78. 8	21. 2	21 8	29. 8	929 3	0.1 5	44. 1	61	758
E1336-41 91	32 9	15. 72	11 36	0.7 2		16.9 4	0.1 4	4.6 0	7.1 8	1.0 3	30. 59	9.3 1	113 .9	42. 00	175 .3	39. 6	38 1	57. 8	852 5	0.4 3	98. 1	85	845
E1336-41 73	24 6	8.1 4	81 6	0.9 2		8.41	0.0 2	0.5 6	1.5 8	0.6 4	11. 02	4.2 7	67. 7	27. 58	143 .8	36. 3	38 0	75. 3	984 9	0.6 0	34. 9	68	775
E1336-41 40	29 2	9.3 2	14 47	0.9 2		16.2 0	0.2 2	5.8 3	6.5 2	1.6 0	32. 68	11. 70	143 .5	48. 62	215 .1	46. 1	46 3	65. 2	730 4	0.2 9	120 .6	99	789

E1336-41 77	285	9.67	935	0.92		8.86		0.36	1.17	0.44	14.26	5.21	72.7	30.41	157.6	41.5	391	84.9	10248	0.18	41.3	58	793
E1336-41 15	250	8.82	518	0.19		4.71		0.81	0.18	0.40	9.82	3.08	45.0	15.37	76.2	17.6	195	28.7	7639	0.17	14.0	19	783
E1336-41 89	300	14.29	570	1.02		16.34		0.59	2.60	0.40	11.53	3.94	53.2	20.67	86.7	19.3	201	29.4	9372	0.53	56.2	64	834
E1336-41 33	234	11.14	445	0.10		9.74			0.77	0.13	8.64	2.64	35.7	13.56	61.3	16.3	162	24.3	7501	0.11	36.5	53	807

December 31, 2014 - January 1, 2015
Isotope ratio and date errors include systematic calibration errors of 1.02% ($^{207}Pb/^{206}Pb$), 0.98% ($^{206}Pb/^{238}U$) (2 sigma).
Trace element concentrations were deleted from analyses known to have intersected inclusions of other minerals based on P and Ti.

Ablation used a laser spot size of 25 microns, and a laser firing repetition rate of 10 Hz.
Activity of TiO_2 for Ti-in-Zircon temperature calculation is 0.8.

LA-ICPMS data from sample from E1105-35

		Corrected isotope ratios							Dates (Ma)						
		207Pb*	±2s	206Pb*	±2s	error	207Pb*	±2s	207Pb*	±2s	207Pb*	±2s	206Pb*	±2s	%
Analysis	Th/U	235U*	(%)	238U	(%)	corr.	206Pb*	(%)	206Pb*	(Ma)	235U	(Ma)	238U*	(Ma)	disc.
E1105-35 33	1.56	8.90777	4.578	0.41712	4.338	0.95	0.15488	1.462	2401	25	2329	42	2247	82	6
E1105-35 67	0.88	6.85733	4.102	0.39489	3.818	0.93	0.12595	1.500	2042	27	2093	36	2145	70	-5
E1105-35 61	1.10	4.74133	7.485	0.28553	3.911	0.52	0.12043	6.382	1963	114	1775	63	1619	56	18
E1105-35 16	1.35	4.98457	4.515	0.32080	4.050	0.90	0.11269	1.996	1843	36	1817	38	1794	63	3
E1105-35 37	0.76	1.74257	9.042	0.15661	3.495	0.39	0.08070	8.339	1214	164	1024	58	938	31	23
E1105-35 19	1.08	1.37384	5.975	0.15186	4.145	0.69	0.06561	4.304	794	90	878	35	911	35	-15
E1105-35 3	1.64	1.63360	12.813	0.15170	5.473	0.43	0.07810	11.585	1150	230	983	81	910	46	21
E1105-35 50	1.16	1.54390	7.991	0.15120	5.283	0.66	0.07406	5.996	1043	121	948	49	908	45	13
E1105-35 27	0.95	1.52491	11.853	0.15037	6.217	0.52	0.07355	10.092	1029	204	940	73	903	52	12
E1105-35 39	1.33	1.52035	6.663	0.14947	3.738	0.56	0.07377	5.516	1035	111	939	41	898	31	13
E1105-35 5	0.78	1.42657	5.447	0.14801	4.409	0.81	0.06990	3.199	925	66	900	33	890	37	4
E1105-35 42	0.78	1.34876	5.736	0.14745	4.301	0.75	0.06634	3.794	817	79	867	33	887	36	-9

E1105-35 64	0.64	1.39932	3.439	0.14737	2.840	0.83	0.06887	1.940	895	40	889	20	886	24	1
E1105-35 66	1.13	1.30545	5.473	0.14662	3.052	0.56	0.06458	4.543	761	96	848	31	882	25	-16
E1105-35 18	1.48	1.34628	4.225	0.14659	3.338	0.79	0.06661	2.591	826	54	866	25	882	28	-7
E1105-35 13	1.98	1.35000	6.388	0.14646	4.845	0.76	0.06685	4.163	833	87	868	37	881	40	-6
E1105-35 24	1.91	1.45164	6.356	0.14628	5.214	0.82	0.07197	3.634	985	74	911	38	880	43	11
E1105-35 8	0.79	1.35425	6.317	0.14456	4.853	0.77	0.06794	4.044	867	84	869	37	870	40	0
E1105-35 53	0.63	1.24331	6.780	0.14440	4.173	0.62	0.06245	5.344	690	114	820	38	869	34	-26
E1105-35 10	0.71	1.32681	6.185	0.14439	4.802	0.78	0.06665	3.898	827	81	857	36	869	39	-5
E1105-35 65	1.39	1.37101	5.231	0.14423	3.458	0.66	0.06894	3.925	897	81	877	31	869	28	3
E1105-35 28	1.29	1.31993	4.941	0.14178	4.510	0.91	0.06752	2.017	854	42	854	29	855	36	0
E1105-35 40	0.92	1.32233	7.951	0.14104	3.575	0.45	0.06800	7.102	869	147	856	46	851	28	2
E1105-35 25	1.03	1.31210	5.358	0.13834	4.372	0.82	0.06879	3.097	893	64	851	31	835	34	6
E1105-35 31	0.87	1.23043	4.506	0.13367	3.291	0.73	0.06676	3.079	830	64	815	25	809	25	3
E1105-35 1	2.01	1.23312	5.678	0.13272	4.780	0.84	0.06739	3.064	850	64	816	32	803	36	5
E1105-35 36	0.87	1.17273	4.155	0.13192	3.068	0.74	0.06447	2.802	757	59	788	23	799	23	-5
E1105-35 60	1.57	1.13977	5.167	0.13037	3.509	0.68	0.06341	3.792	722	80	772	28	790	26	-9
E1105-35 20	2.65	1.18335	5.149	0.12654	3.798	0.74	0.06782	3.476	863	72	793	28	768	27	11
E1105-35 22	1.98	1.10367	6.883	0.12533	4.742	0.69	0.06387	4.988	737	106	755	37	761	34	-3
E1105-35 26	0.59	0.67978	4.579	0.08617	3.516	0.77	0.05721	2.933	500	65	527	19	533	18	-7

March 31, 2012

Isotope ratio and date errors include systematic calibration errors of 0.14% ($^{207}Pb/^{206}Pb$), 0.98% ($^{206}Pb/^{238}U$) (2 sigma).

Trace element concentrations were deleted from analyses known to have intersected inclusions of other minerals based on P and Ti.

Ablation used a laser spot size of 25 microns, and a laser firing repetition rate of 10 Hz.

Activity of TiO_2 for Ti-in-Zircon temperature calculation is 0.8.

LA-ICPMS data from sample from E1105-35 continued.

	Concentrations																				

	(ppm)																						
Analysis	P	Ti	Y	Nb	La	Ce	Pr	Nd	Sm	Eu	Gd	Tb	Dy	Ho	Er	Tm	Yb	Lu	Hf	Ta	Th	U	T(°C)
E1105-35 33	182	6.11	1352	4.29	0.26	49.33	0.10	0.87	3.58	0.68	25.45	8.62	114.7	47.48	219.2	57.8	649	82.4	12949	2.72	306.0	196	748
E1105-35 67	221	9.59	1212	4.24	0.05	16.92	0.31	4.94	8.47	0.28	35.23	11.98	136.4	47.33	197.9	48.4	502	59.0	9877	1.78	113.4	129	792
E1105-35 61	241	2218.76	1122	27.31	0.46	6.70	0.29	5.22	9.58	2.12	37.76	12.67	133.9	44.00	178.3	40.5	415	51.5	9090	4.85	51.5	47	1967
E1105-35 37	155	4.14	296	0.32		4.53	0.01	0.22	1.04	0.36	3.84	2.07	25.0	9.65	50.5	14.5	183	28.4	11317	0.18	29.5	39	712
E1105-35 19	128	18.33	331	1.37		21.26		0.94	2.06	0.66	10.23	3.10	31.3	11.53	47.4	12.5	137	18.8	12127	0.88	89.7	83	863
E1105-35 3	176	29.79	1000	1.40		25.03	0.60	8.29	11.65	3.35	37.11	11.71	117.7	37.08	145.1	34.3	361	44.0	10223	0.82	171.1	104	923
E1105-35 27	201	6.52	650	1.48	0.02	10.66	0.02	1.76	2.97	0.94	12.26	4.12	54.7	21.83	107.0	30.9	388	58.5	10407	0.76	185.0	195	754
E1105-35 39	175	21.84	430	1.67	1.31	26.77	0.43	1.65	2.09	0.79	13.04	4.01	46.2	14.98	65.4	16.8	188	24.2	9735	1.11	102.1	77	884
E1105-35 5	171	11.63	683	1.05	0.14	11.04	0.18	2.62	3.19	0.75	17.13	5.87	67.7	24.12	109.8	27.0	288	36.5	10618	1.01	141.0	180	812
E1105-35 42	161	4.96	590	1.11		14.17	0.05	1.49	3.07	0.80	12.64	3.95	51.0	20.09	95.6	28.2	363	48.8	10246	0.51	101.5	130	728
E1105-35 66	195	18.80	432	1.79	0.19	26.05	0.09	1.09	2.63	0.98	10.28	3.79	46.9	15.97	67.0	17.8	199	25.1	11070	1.27	89.5	79	866
E1105-35 18	200	22.82	626	1.97	0.58	26.55	0.19	1.97	3.99	1.11	18.43	6.02	62.9	21.57	94.6	22.8	248	33.2	11368	1.56	130.3	88	889
E1105-35 13	218	5.91	1096	1.23	0.07	20.87	0.36	2.64	5.25	2.00	27.69	8.74	101.4	37.99	174.6	44.9	513	77.4	12244	0.57	160.5	81	744
E1105-35 24	206	32.37	1013	1.52	0.28	33.18	0.59	10.44	15.39	3.54	45.88	12.42	122.7	37.68	155.1	36.0	393	48.2	10685	1.06	201.2	105	933
E1105-35 53	231	9.86	751	2.18	0.37	5.60	0.19	1.06	1.13	0.40	11.93	5.19	66.7	24.99	113.0	28.7	332	36.6	7151	0.99	40.3	64	795
E1105-35 10	182	7.43	970	2.02		9.45		2.04	3.88	0.54	24.16	8.77	99.7	36.17	151.2	35.3	361	47.6	10194	1.17	60.9	86	766
E1105-35 65	150	4.22	533	1.22	0.53	16.48		1.59	1.73	0.97	10.60	4.00	49.4	18.50	88.3	25.4	308	45.3	11540	0.59	107.0	77	714
E1105-35 28	193	5.92	834	1.52		20.93	0.24	3.02	4.24	1.78	17.11	6.24	76.7	29.53	134.2	36.9	439	63.3	10897	0.75	175.1	136	745

E1105-35 40	11 2	3.99	658	0.4 7		11. 97	0. 04	1.5 4	3.4 6	2. 12	17.5 1	6.1 5	73. 0	25.3 1	105. 0	26. 3	29 1	35. 8	820 2	0. 19	26. 5	29	709
E1105-35 25	14 6	4.28	115 4	2.0 7		12. 85	0. 02	2.9 4	4.3 5	1. 02	24.3 9	8.9 0	103 .2	41.7 0	189. 6	52. 5	62 0	89. 3	118 49	1. 53	248 .8	24 2	715
E1105-35 31	14 9	6.57	513	1.6 3	0. 27	20. 74	0. 20	1.5 2	2.6 6	1. 01	13.0 5	4.0 7	47. 1	18.3 0	80.6	22. 2	25 2	34. 2	114 22	1. 01	187 .5	21 6	755
E1105-35 36	22 6	9.12	107 0	2.2 0	0. 18	14. 57		1.7 7	3.9 7	0. 99	22.9 7	9.0 9	107 .6	39.7 4	176. 2	44. 6	48 9	63. 8	103 16	0. 99	134 .8	15 5	787
E1105-35 20	88 4	20.11	532 2	4.8 3	0. 62	87. 93	1. 13	17. 17	28. 16	8. 74	149. 17	49. 28	577 .8	207. 69	842. 9	191 .8	19 23	242 .4	101 83	1. 51	363 .2	13 7	874
E1105-35 26	46 4	8.16	623 9	1.0 1	0. 21	6.6 6	0. 40	8.2 9	25. 93	6. 86	165. 87	57. 33	698 .4	246. 15	101 0.6	235 .9	23 68	292 .7	896 1	0. 42	84. 1	14 2	776

LA-ICPMS data from sample from F1121-25

		Corrected isotope ratios							Dates (Ma)						
		207Pb*	±2s	206Pb*	±2s	error	207Pb*	±2s	207Pb*	±2s	207Pb*	±2s	206Pb*	±2s	%
Analysis	Th/U	235U*	(%)	238U	(%)	corr.	206Pb*	(%)	206Pb*	(Ma)	235U	(Ma)	238U*	(Ma)	disc.
F1121-25 131	0.73	8.68432	5.278	0.40225	4.155	0.79	0.15658	3.255	2419	55	2305	48	2179	77	10
F1121-25 112	1.03	4.71579	5.646	0.30040	4.881	0.86	0.11386	2.838	1862	51	1770	47	1693	73	9
F1121-25 120	1.43	5.04896	4.984	0.32749	4.076	0.82	0.11181	2.868	1829	52	1828	42	1826	65	0
F1121-25 128	0.89	2.17249	4.800	0.19256	3.480	0.73	0.08182	3.306	1241	65	1172	33	1135	36	9
F1121-25 118	0.95	1.38244	4.702	0.15049	3.533	0.75	0.06662	3.103	826	65	881	28	904	30	-9
F1121-25 141	1.09	1.37634	4.595	0.14553	3.310	0.72	0.06859	3.186	886	66	879	27	876	27	1
F1121-25 113	0.55	1.36379	6.052	0.14488	5.285	0.87	0.06827	2.948	877	61	874	35	872	43	1
F1121-25 119	1.74	1.35178	4.720	0.14408	3.670	0.78	0.06805	2.969	870	62	868	28	868	30	0
F1121-25 117	0.70	1.33121	4.562	0.14259	3.467	0.76	0.06771	2.964	860	62	859	26	859	28	0
F1121-25 139	1.13	1.34569	5.546	0.14002	3.307	0.60	0.06970	4.452	920	92	866	32	845	26	8
F1121-25 133	1.83	1.43332	6.096	0.13970	3.802	0.62	0.07441	4.765	1053	96	903	36	843	30	20
F1121-25 143	0.73	1.38238	5.414	0.13941	3.419	0.63	0.07192	4.198	984	85	881	32	841	27	14
F1121-25 142	1.04	1.32519	5.375	0.13919	3.040	0.57	0.06905	4.433	900	91	857	31	840	24	7
F1121-25 116	1.30	1.26314	5.307	0.13819	4.338	0.82	0.06629	3.058	816	64	829	30	834	34	-2
F1121-25 124	1.19	1.32011	7.602	0.13782	6.700	0.88	0.06947	3.592	913	74	855	44	832	52	9

F1121-25 134	1.10	1.49606	9.164	0.13740	3.417	0.37	0.07897	8.503	1171	168	929	56	830	27	29
F1121-25 146	1.24	1.54244	8.937	0.13615	5.113	0.57	0.08217	7.329	1250	143	947	55	823	40	34
F1121-25 132	0.90	1.23299	6.283	0.13559	3.205	0.51	0.06595	5.404	805	113	816	35	820	25	-2
F1121-25 115	0.93	1.16246	4.998	0.13129	3.891	0.78	0.06422	3.137	749	66	783	27	795	29	-6
F1121-25 144	0.90	1.22723	5.431	0.13024	4.617	0.85	0.06834	2.860	879	59	813	30	789	34	10
F1121-25 121	1.83	1.18347	6.590	0.12964	4.124	0.63	0.06621	5.140	813	107	793	36	786	31	3
F1121-25 140	1.20	1.19334	7.147	0.12963	2.433	0.34	0.06677	6.720	831	140	798	39	786	18	5
F1121-25 127	0.84	1.18304	5.799	0.12878	4.143	0.71	0.06663	4.057	826	85	793	32	781	30	5
F1121-25 110	2.21	1.14906	6.173	0.12564	4.581	0.74	0.06633	4.138	817	86	777	34	763	33	7
F1121-25 125	1.65	1.14762	6.092	0.12473	4.968	0.82	0.06673	3.527	829	74	776	33	758	36	9
F1121-25 129	2.38	1.10662	6.932	0.12407	4.904	0.71	0.06469	4.899	764	103	757	37	754	35	1
F1121-25 114	1.63	1.09720	9.590	0.12333	6.352	0.66	0.06452	7.184	759	152	752	51	750	45	1
F1121-25 126	1.64	1.04391	6.074	0.11861	3.587	0.59	0.06383	4.901	736	104	726	31	723	25	2
F1121-25 147	1.31	1.20939	5.136	0.11839	2.773	0.54	0.07409	4.323	1044	87	805	29	721	19	31

June 15, 2012

Isotope ratio and date errors include systematic calibration errors of 0.24% ($^{207}Pb/^{206}Pb$), 0.75% ($^{206}Pb/^{238}U$) (2 sigma).

Trace element concentrations were deleted from analyses known to have intersected inclusions of other minerals based on P and Ti.

Ablation used a laser spot size of 25 microns, and a laser firing repetition rate of 10 Hz.

Activity of TiO_2 for Ti-in-Zircon temperature calculation is 0.8.

LA-ICPMS data from sample from F1121-25 continued.

	Concentrations (ppm)																					
Analysis	P	Ti	Y	Nb	La	Ce	Pr	Nd	Sm	Eu	Gd	Tb	Dy	Ho	Er	Tm	Yb	Lu	Hf	Ta	Th	U	T(°C)
F1121-25 131	160	9.28	735	2.53	0.29	7.02	0.06	1.86	3.95	0.29	21.98	7.20	83.6	27.91	110.1	26.3	272	31.5	10560	1.06	30.4	42	789
F1121-25 112	309	13.41	1260	3.91	0.09	8.71	0.16	4.33	8.65	1.42	37.80	12.52	140.2	47.48	184.7	46.3	494	50.4	7450	1.94	52.2	51	827
F1121-25 120	275	19.41	2466	3.73	0.07	6.80	0.63	11.69	20.68	2.40	82.33	25.78	295.4	94.96	370.2	85.6	851	90.7	8970	1.75	63.9	45	870
F1121-25 128	574	17.67	1329	1.86	1.81	9.95	0.83	6.99	9.57	1.07	38.84	12.79	152.7	50.43	208.3	47.0	499	57.2	11040	1.19	91.5	102	859
F1121-25 141	377	8.65	1322	1.29	0.02	14.43	0.01	2.67	5.60	1.91	31.00	11.14	129.9	49.99	211.3	54.7	598	72.6	9296	0.70	76.5	70	781
F1121-25 113	240	3.06	841	2.43	0.11	15.08	0.06	0.74	2.18	0.64	14.18	5.01	73.3	28.59	135.9	39.8	513	62.1	9895	1.88	89.1	161	686

F1121-25 119	186	26.38	767	1.99		28.03	0.29	6.09	8.37	2.33	30.13	8.20	86.8	27.91	105.5	27.4	289	33.3	9653	1.05	105.6	61	907
F1121-25 117	244	14.10	1499	0.69		5.83	0.25	3.33	7.80	1.28	29.92	10.85	134.6	54.84	240.8	62.1	673	77.8	8203	0.65	95.2	136	833
F1121-25 139	166	22.70	452	1.77	0.01	21.39	0.01	1.27	2.36	0.72	11.47	3.77	43.4	16.11	68.3	18.5	202	23.9	10560	1.42	73.0	64	888
F1121-25 143	315	15.67	1101	1.12	0.02	9.60	0.08	1.91	5.02	1.04	21.91	8.49	104.7	39.38	174.4	44.3	507	61.3	8810	0.92	73.9	101	845
F1121-25 142	184	9.38	1229	0.51		9.67	0.07	2.06	5.72	1.20	27.07	9.71	123.5	44.54	191.8	49.4	550	66.9	10772	0.32	47.4	45	790
F1121-25 116	504	9.97	2158	5.05	0.10	47.21	0.20	3.59	7.45	2.54	42.12	16.91	218.8	83.66	357.1	93.1	1043	113.8	8848	1.42	151.8	116	796
F1121-25 146	214	3.61	622	2.10	1.65	35.55	0.43	2.93	3.84	1.45	16.40	5.40	60.1	21.31	90.0	25.4	316	38.7	9656	0.70	257.5	208	700
F1121-25 132	239	4.88	1035	1.01		9.60	0.05	0.85	4.37	1.65	25.34	8.70	102.4	36.75	156.5	39.7	451	63.0	10406	0.33	34.4	38	727
F1121-25 115	238	6.85	1005	3.01	0.15	22.13		0.49	2.81	0.75	19.26	7.04	94.0	35.74	162.7	45.2	516	59.4	8696	1.24	68.9	74	759
F1121-25 144	186	8.28	991	3.17	0.27	12.01	0.11	2.06	4.28	1.16	19.76	7.40	92.3	36.52	155.9	42.3	504	58.7	7433	1.21	137.8	153	777
F1121-25 121	368	11.00	3185	2.00		29.65	0.34	8.07	15.46	5.49	90.19	28.28	349.4	124.13	505.2	123.0	1278	154.8	8944	0.79	158.2	86	806
F1121-25 140	160	7.56	998	0.30	0.01	4.76	0.16	2.54	5.28	2.57	25.29	8.57	101.5	35.40	159.7	43.9	512	68.3	8044	0.25	84.1	70	768
F1121-25 127	158	4.24	1244	3.50		32.19		2.42	5.05	2.64	28.99	10.28	125.0	44.32	190.5	50.2	567	70.2	10658	0.89	150.8	179	714
F1121-25 110	272	15.86	1784	1.25	0.01	32.57	0.38	6.93	14.77	5.57	52.82	17.13	194.4	65.80	255.5	64.5	728	76.0	6947	0.53	212.6	96	846
F1121-25 125	302	5.39	1150	0.85	0.19	18.88	0.26	3.12	5.89	1.89	26.19	9.04	107.1	40.35	186.1	49.5	619	82.7	10135	0.53	166.9	101	736
F1121-25 129	214	6.55	1397	1.59	0.06	29.35	0.18	3.91	6.57	1.68	30.89	10.22	130.0	50.23	219.9	57.1	678	89.0	10022	0.84	214.9	90	754
F1121-25 114	267	20.05	1832	0.96		18.28	0.10	4.66	12.39	4.23	54.69	18.73	212.6	73.01	290.9	70.1	739	77.7	7757	0.44	45.0	28	873
F1121-25 126	227	7.76	1669	1.83	0.07	28.96	0.19	3.79	8.05	2.58	45.33	15.19	180.6	63.83	256.9	61.2	650	74.9	10913	0.96	115.2	70	771

LA-ICPMS data from sample from E1326

		Corrected isotope ratios							Dates (Ma)						
		207Pb*	±2s	206Pb*	±2s	error	207Pb*	±2s	207Pb*	±2s	207Pb*	±2s	206Pb*	±2s	%
Analysis	Th/U	235U*	(%)	238U	(%)	corr.	206Pb*	(%)	206Pb*	(Ma)	235U	(Ma)	238U*	(Ma)	disc.
E1326 106	1.55	8.42881	4.712	0.38946	3.349	0.71	0.15696	3.315	2423	56	2278	43	2120	61	12
E1326 82	0.56	7.72946	6.028	0.38534	5.345	0.89	0.14548	2.787	2293	48	2200	54	2101	96	8
E1326 67	0.50	7.23344	7.856	0.38824	6.332	0.81	0.13513	4.651	2166	81	2141	70	2115	114	2
E1326 79	2.50	5.58097	5.598	0.33014	5.136	0.92	0.12261	2.228	1994	40	1913	48	1839	82	8
E1326 83	2.35	5.90749	7.429	0.35609	6.253	0.84	0.12032	4.012	1961	72	1962	65	1964	106	0
E1326 100	0.74	4.72482	7.415	0.30118	6.114	0.82	0.11378	4.196	1861	76	1772	62	1697	91	9

E1326 134	1.10	4.97050	6.533	0.32534	4.941	0.76	0.11080	4.275	1813	78	1814	55	1816	78	0
E1326 88	0.79	4.58263	6.213	0.30293	5.206	0.84	0.10972	3.391	1795	62	1746	52	1706	78	5
E1326 73	1.10	4.48656	6.400	0.29955	5.744	0.90	0.10863	2.821	1777	51	1728	53	1689	85	5
E1326 86	0.78	4.62302	7.746	0.31209	5.942	0.77	0.10743	4.970	1756	91	1753	65	1751	91	0
E1326 122	0.61	4.12869	9.691	0.28758	8.003	0.83	0.10412	5.464	1699	101	1660	79	1629	115	4
E1326 129	0.40	3.42362	5.464	0.24617	4.156	0.76	0.10087	3.548	1640	66	1510	43	1419	53	14
E1326 102	0.16	1.95805	14.802	0.17628	13.713	0.93	0.08056	5.573	1211	110	1101	99	1047	132	14
E1326 120	0.08	1.49251	6.872	0.15715	5.980	0.87	0.06888	3.386	895	70	927	42	941	52	-5
E1326 131	3.40	1.52033	10.512	0.15361	6.372	0.61	0.07178	8.360	980	170	939	64	921	55	6
E1326 95	0.24	1.45181	5.657	0.15183	3.417	0.60	0.06935	4.508	909	93	911	34	911	29	0
E1326 113	0.00	1.45145	7.929	0.15088	6.222	0.78	0.06977	4.915	922	101	910	48	906	53	2
E1326 115	0.01	1.45167	6.969	0.14983	6.241	0.90	0.07027	3.102	936	64	911	42	900	52	4
E1326 110	1.03	1.43415	6.024	0.14870	5.241	0.87	0.06995	2.970	927	61	903	36	894	44	4
E1326 116	0.75	1.37059	6.408	0.14862	4.186	0.65	0.06688	4.852	834	101	876	38	893	35	-7
E1326 103	0.67	1.37326	7.689	0.14716	3.947	0.51	0.06768	6.599	859	137	878	45	885	33	-3
E1326 71	0.85	1.39878	4.311	0.14711	3.649	0.85	0.06896	2.294	898	47	888	26	885	30	1
E1326 125	0.99	1.38785	9.935	0.14405	8.015	0.81	0.06988	5.872	925	121	884	59	868	65	6
E1326 76	1.59	1.38576	5.496	0.14400	4.580	0.83	0.06980	3.038	922	62	883	32	867	37	6
E1326 108	1.00	1.31078	8.625	0.14313	7.132	0.83	0.06642	4.852	820	101	850	50	862	58	-5
E1326 84	2.58	1.18064	18.756	0.14282	10.047	0.54	0.05996	15.838	602	343	792	103	861	81	-43
E1326 118	1.35	1.35169	8.019	0.14207	6.537	0.82	0.06900	4.645	899	96	868	47	856	52	5
E1326 80	0.71	1.31703	8.431	0.14204	6.197	0.73	0.06725	5.717	846	119	853	49	856	50	-1
E1326 89	0.89	1.31947	6.045	0.14103	5.005	0.83	0.06786	3.390	864	70	854	35	850	40	2
E1326 111	0.55	1.32849	8.057	0.14069	5.823	0.72	0.06849	5.569	883	115	858	47	849	46	4
E1326 81	1.10	1.33089	6.837	0.14051	5.892	0.86	0.06870	3.467	890	72	859	40	848	47	5
E1326 77	1.12	1.30925	5.259	0.14027	2.895	0.55	0.06770	4.390	859	91	850	30	846	23	2
E1326 91	0.56	1.28568	10.554	0.14018	5.448	0.52	0.06652	9.038	823	189	839	60	846	43	-3
E1326 133	0.41	1.32536	6.153	0.13991	4.775	0.78	0.06870	3.880	890	80	857	36	844	38	5
E1326 65	0.65	1.34910	9.413	0.13977	7.345	0.78	0.07000	5.887	928	121	867	55	843	58	9
E1326 70	0.79	1.27119	7.656	0.13973	4.802	0.63	0.06598	5.963	806	125	833	44	843	38	-5

E1326 112	0.64	1.31365	6.564	0.13962	4.743	0.72	0.06824	4.538	876	94	852	38	843	37	4
E1326 78	1.27	1.30648	8.734	0.13903	6.120	0.70	0.06815	6.232	873	129	849	50	839	48	4
E1326 96	0.85	1.31001	6.510	0.13845	5.420	0.83	0.06863	3.606	887	75	850	37	836	42	6
E1326 90	1.07	1.36818	7.612	0.13800	6.372	0.84	0.07191	4.163	983	85	875	45	833	50	15
E1326 87	0.70	1.23182	7.593	0.13758	5.546	0.73	0.06494	5.185	772	109	815	43	831	43	-8
E1326 105	0.64	1.31790	6.701	0.13720	4.425	0.66	0.06967	5.032	919	103	854	39	829	34	10
E1326 114	0.96	1.30082	7.544	0.13634	5.477	0.73	0.06920	5.187	905	107	846	43	824	42	9
E1326 123	0.92	1.19746	9.719	0.13564	6.684	0.69	0.06403	7.055	743	149	799	54	820	51	-10
E1326 72	0.83	1.22920	10.538	0.13501	6.750	0.64	0.06603	8.092	807	169	814	59	816	52	-1
E1326 124	0.88	1.16091	7.831	0.13181	6.589	0.84	0.06388	4.232	738	90	782	43	798	49	-8
E1326 93	0.98	1.21580	6.684	0.13040	5.091	0.76	0.06762	4.331	857	90	808	37	790	38	8
E1326 94	0.86	1.14722	5.414	0.12971	4.585	0.85	0.06415	2.881	746	61	776	29	786	34	-5
E1326 92	1.18	1.12552	7.778	0.12942	4.326	0.56	0.06307	6.464	711	137	766	42	785	32	-10
E1326 98	0.84	1.19856	7.640	0.12926	5.122	0.67	0.06725	5.668	845	118	800	42	784	38	7
E1326 119	0.70	1.13486	8.126	0.12859	6.111	0.75	0.06401	5.356	742	113	770	44	780	45	-5
E1326 66	0.46	1.24250	8.006	0.12833	5.644	0.70	0.07022	5.679	935	116	820	45	778	41	17
E1326 107	0.67	1.20786	7.848	0.12777	5.554	0.71	0.06856	5.545	886	115	804	44	775	41	12
E1326 128	0.88	1.13450	5.746	0.12620	3.313	0.58	0.06520	4.695	781	99	770	31	766	24	2
E1326 104	1.27	1.23350	9.475	0.12599	8.460	0.89	0.07101	4.267	958	87	816	53	765	61	20
E1326 97	1.17	1.07792	6.829	0.12578	4.213	0.62	0.06216	5.374	680	115	743	36	764	30	-12
E1326 136	0.94	1.21786	10.158	0.12508	6.558	0.65	0.07062	7.757	946	159	809	57	760	47	20
E1326 117	0.63	1.10907	8.013	0.12504	6.526	0.81	0.06433	4.650	753	98	758	43	759	47	-1
E1326 137	1.04	1.10044	7.582	0.12481	6.728	0.89	0.06395	3.496	740	74	754	40	758	48	-2
E1326 68	0.78	1.13766	7.320	0.12440	5.203	0.71	0.06633	5.149	817	108	771	40	756	37	7
E1326 101	1.18	1.19734	7.183	0.12343	4.536	0.63	0.07035	5.569	939	114	799	40	750	32	20
E1326 99	1.07	1.06345	6.926	0.12202	5.561	0.80	0.06321	4.128	715	88	736	36	742	39	-4
E1326 75	1.33	1.11727	4.467	0.12173	3.415	0.76	0.06657	2.879	824	60	762	24	741	24	10
E1326 127	1.20	1.08086	6.537	0.12144	4.968	0.76	0.06455	4.248	760	90	744	34	739	35	3
E1326 85	0.83	1.06970	7.368	0.12115	6.256	0.85	0.06404	3.893	743	82	739	39	737	44	1
E1326 126	1.14	1.04539	6.522	0.12045	4.120	0.63	0.06295	5.055	706	108	727	34	733	29	-4

E1326 130	1.20	1.03363	6.731	0.11859	5.240	0.78	0.06321	4.224	715	90	721	35	722	36	-1							
E1326 74	1.09	1.01048	6.905	0.11402	5.977	0.87	0.06427	3.458	751	73	709	35	696	39	7							
E1326 109	0.66	1.00197	7.066	0.11381	5.797	0.82	0.06385	4.040	737	86	705	36	695	38	6							

LA-ICPMS data from sample from E1326 continued.

	Concentrations (ppm)																					
Analysis	P	Ti	Y	Nb	La	Ce	Pr	Nd	Sm	Eu	Gd	Tb	Dy	Ho	Er	Tm	Yb	Lu	Hf	Ta	Th	U	T(°C)
E1326 82	226	7.38	602	3.22		10.35	0.03	0.66	2.84	0.26	12.06	4.61	57.5	21.27	94.6	21.9	221	30.6	9194	1.58	47.2	84	766
E1326 67	155	7.55	548	2.70		9.89	0.05	1.02	2.36	0.08	13.67	4.89	54.9	19.91	85.0	19.6	197	24.8	7856	1.22	49.5	99	768
E1326 79	248	11.50	1029	1.87	0.45	69.74	1.94	25.39	25.55	7.28	68.76	15.52	137.8	39.69	134.6	26.8	236	30.6	8013	0.89	264.5	106	811
E1326 83	212	23.03	346	0.76	0.05	34.17	0.54	5.96	8.21	2.40	20.12	4.85	42.3	12.83	46.8	9.9	96	12.5	6802	0.34	98.3	42	890
E1326 134	384	5.30	1860	3.81	0.17	17.54	0.65	9.82	14.19	0.82	58.02	18.28	201.5	68.27	272.5	60.8	565	70.4	8344	2.22	157.8	144	734
E1326 73	278	8.97	2275	4.25	0.21	17.16	1.63	19.24	25.53	2.19	98.22	24.73	255.3	86.09	321.9	67.0	607	80.9	8678	2.52	109.4	100	785
E1326 122	168	10.64	645	4.41		10.02	0.02	0.97	2.22	0.05	16.82	5.15	64.3	23.61	102.7	25.2	238	29.8	8881	2.14	40.7	67	803
E1326 129	168	5.81	450	2.50		7.74	0.04	0.64	1.30	0.15	9.61	3.22	42.5	16.52	70.4	16.6	161	24.9	10425	1.64	34.7	86	743
E1326 102	137	2.77	524	6.98	0.04	8.06	0.08	1.32	1.73	0.37	15.53	3.89	53.7	20.39	83.9	21.9	231	35.8	10256	4.63	42.6	275	678
E1326 120	85	15.18	416	28.07		6.97	0.02	0.16	1.37	0.80	9.12	3.28	37.5	13.88	56.9	12.7	134	17.8	9257	13.97	34.6	408	841
E1326 95	125	3.75	635	1.88		2.04		0.08	0.87	0.23	9.29	3.55	50.6	20.76	102.3	24.9	284	51.9	9272	1.19	33.3	139	703
E1326 113	61	1.58	295	3.63		0.03				0.03	0.34	0.50	13.3	8.43	51.4	16.9	233	33.9	13722	2.81	0.1	75	634
E1326 115	41	2.02	277	6.76		0.36					0.84	0.73	14.0	7.52	45.0	13.1	149	22.7	10435	5.46	0.9	139	653
E1326 110	203	12.50	408	2.37	0.04	34.88	0.14	1.63	4.07	1.52	14.25	4.29	40.3	13.18	53.5	12.7	128	21.0	9612	1.07	229.5	224	820

E1326116	180	3.77	681	1.47		17.64	0.04	1.12	2.75	1.01	11.33	4.22	59.7	22.11	105.3	29.8	336	56.0	9037	0.61	121.2	162	704
E1326071	284	10.02	638	2.91	0.13	30.58	0.29	4.62	5.15	2.27	24.13	6.26	69.7	21.90	90.6	22.1	230	34.6	9126	1.40	206.6	244	796
E1326125	229	27.56	407	1.39	0.02	23.10	0.05	1.32	2.77	0.61	11.25	3.28	38.2	13.59	56.1	13.2	140	19.3	8167	0.82	82.4	83	912
E1326076	287	21.88	1272	1.51	0.25	31.78	0.74	10.58	10.88	2.23	47.59	12.16	133.5	44.70	183.1	39.4	350	54.9	9372	0.85	180.2	114	884
E1326108	237	15.79	448	1.79		20.17	0.06	1.17	1.77	0.96	12.46	3.76	43.2	16.14	69.1	16.2	175	22.9	7613	0.85	81.1	81	846
E1326080	232	6.81	723	0.51		9.36	0.03	0.97	2.96	0.46	14.47	4.51	62.2	24.40	105.5	27.9	296	43.2	11056	0.56	58.0	81	758
E1326089	253	10.74	1175	0.55		12.40	0.16	3.41	6.42	1.28	29.18	8.85	113.3	39.86	179.3	39.7	429	55.6	9333	0.32	95.9	108	804
E1326111	203	9.67	661	0.69		7.09		0.68	1.55	0.36	10.83	4.75	57.3	22.56	100.8	23.1	247	38.6	10489	0.35	36.2	66	793
E1326081	170	14.10	379	1.20		26.69	0.14	2.09	3.80	0.95	13.77	3.91	37.8	12.20	49.9	11.5	118	18.0	8472	0.62	140.3	128	833
E1326077	246	11.70	1591	0.63		13.25	0.22	4.63	7.81	1.48	37.90	12.13	148.6	55.57	241.7	54.8	523	84.4	10120	0.32	119.2	106	813
E1326091	402	7.17	770	0.41		6.54		0.37	1.92	0.38	10.49	4.46	62.0	27.23	127.2	33.8	381	56.7	9437	0.18	15.0	27	763
E1326133	99	1.75	391	0.46		12.37		0.29	0.37	0.63	5.82	1.97	24.3	11.67	58.2	17.2	227	43.4	9176	0.05	37.8	93	642
E1326065	215	10.18	491	0.59		9.65	0.00	0.30	1.15	0.35	9.83	3.27	44.8	16.75	74.0	20.2	209	28.7	8258	0.29	43.2	66	798
E1326070	263	13.17	1234	0.65		7.81	0.19	3.43	7.04	0.88	31.81	10.19	125.5	44.76	186.2	41.4	389	54.5	8531	0.38	59.5	76	825
E1326112	166	6.98	537	0.55		9.81		0.23	0.99	0.29	8.16	3.19	40.1	17.08	79.3	20.7	238	37.2	10798	0.33	45.5	72	760
E1326078	249	22.00	540	0.29		16.78	0.06	1.59	3.05	1.64	13.63	4.96	52.7	19.59	85.1	19.4	196	30.6	7295	0.16	47.0	37	885
E1326096	212	8.80	793	0.77		10.37	0.03	0.80	1.91	0.47	13.59	5.19	69.6	25.79	122.4	29.5	291	50.5	11457	0.35	57.2	67	783
E1326090	751	15.85	2201	8.38		69.35	0.07	2.32	8.08	0.54	54.40	19.17	258.6	85.47	330.8	73.5	681	87.7	10487	3.56	196.0	184	846
E1326087	219	10.54	1207	0.38		8.16	0.13	3.36	6.25	1.37	32.44	10.35	127.8	44.14	186.7	44.7	444	59.5	8611	0.26	54.8	78	802
E1326	296	9.17	583	0.6		8.5		0.7	1.6	0.2	11.	3.4	50.	19.	89.	22.	22	34.	991	0.3	41.	65	787

105				2		9		0	6	9	78	9	3	83	6	5	9	1	0	3	6		
E1326 114	224	11.40	1154	0.45		10.95	0.23	3.76	6.34	1.15	31.63	9.60	112.7	39.67	169.6	38.6	384	54.3	9295	0.21	84.7	88	810
E1326 123	168	4.57	634	0.47		11.54	0.18	2.02	3.99	0.81	15.83	4.55	60.9	21.84	97.0	27.3	316	48.5	9312	0.24	92.2	101	721
E1326 124	1146	16.84	2383	1.57		9.39	0.28	6.45	9.81	1.90	58.22	20.54	242.0	90.24	376.5	86.8	882	116.5	8610	0.79	84.8	97	853
E1326 93	221	6.22	629	1.19		18.93		0.82	2.52	1.56	12.48	4.13	48.5	18.55	95.9	24.4	277	47.0	9959	0.77	159.0	162	749
E1326 92	211	11.51	1184	0.49		13.27	0.17	3.28	7.30	1.43	32.10	10.00	115.3	41.44	178.2	40.4	387	54.7	8822	0.34	82.0	70	811
E1326 98	240	12.86	665	0.80		11.62	0.10	1.03	2.54	0.64	16.71	4.89	63.4	23.01	104.3	24.0	253	40.7	9285	0.48	43.0	51	823
E1326 66	88	2.31	444	0.72	0.09	13.03	0.13	1.49	2.40	1.36	9.45	2.76	33.4	13.59	68.8	20.3	249	40.8	9501	0.17	64.4	140	664
E1326 107	176	8.26	537	0.80		9.98		0.44	1.10	0.30	9.77	3.04	39.7	16.38	76.7	20.3	210	29.7	9548	0.46	57.7	86	777
E1326 128	274	10.75	1797	0.79		5.50	0.19	3.32	7.70	1.30	40.47	13.29	175.0	68.42	282.8	60.9	575	86.2	8484	0.53	107.7	122	804
E1326 104	259	15.09	438	3.14	0.09	33.80	0.31	3.32	3.31	1.06	11.38	3.54	41.2	14.67	63.6	16.1	165	23.3	9494	1.33	182.4	144	841
E1326 97	260	10.93	1018	0.40	0.01	13.61	0.11	2.06	4.45	1.02	24.81	8.24	97.4	35.81	154.9	34.2	320	50.7	10208	0.39	72.2	62	806
E1326 136	239	6.75	729	1.30	0.05	20.72	0.06	1.29	2.40	1.02	12.03	4.63	59.8	23.37	117.4	31.2	382	58.8	8766	0.59	180.8	193	757
E1326 117	251	9.76	723	1.16		13.72	0.02	0.61	3.12	0.65	16.25	5.08	66.1	25.68	120.4	31.0	352	49.6	8411	0.92	60.2	95	794
E1326 68	182	10.82	414	0.81		11.64	0.02	0.37	1.09	0.37	9.45	3.13	36.8	14.81	66.0	17.0	174	24.8	8825	0.37	65.6	85	805
E1326 101	196	11.95	1276	0.40		14.30	0.19	4.34	7.90	1.51	38.13	11.03	126.4	45.70	195.4	44.1	417	60.6	9010	0.32	92.3	79	815
E1326 99	263	8.86	1098	0.70		12.73	0.17	2.12	4.88	1.21	25.33	7.70	97.9	37.31	165.7	39.1	399	65.6	9825	0.40	107.3	100	784
E1326 75	252	9.71	1806	0.90		16.72	0.34	5.77	9.47	1.68	48.98	15.09	174.6	65.35	282.9	62.8	595	93.9	9491	0.57	203.6	153	793
E1326 127	236	9.03	1423	0.76		16.70	0.22	4.06	8.09	2.01	38.11	11.07	135.7	49.89	215.3	48.9	482	73.3	8939	0.45	132.3	110	786
E1326 85	299	7.71	940	0.84		9.57	0.10	1.07	3.36	1.56	20.08	6.27	84.2	33.16	154.4	40.6	471	70.5	7292	0.40	79.7	96	770

E1326 126	223	13.00	1121	0.45		14.62	0.16	4.13	5.54	1.53	32.60	10.07	116.0	41.29	169.5	39.5	377	52.8	8998	0.39	81.6	72	824
E1326 130	253	8.22	1300	0.46		14.42	0.10	2.66	5.80	1.25	28.85	10.19	120.5	44.82	198.1	44.3	431	68.0	10025	0.27	124.7	104	776
E1326 109	274	5.17	504	0.36		9.29	0.01	0.55	1.23	0.55	7.77	3.32	38.5	16.67	82.7	23.1	285	46.4	7878	0.34	62.9	96	732

January 4, 2015

Isotope ratio and date errors include systematic calibration errors of 0.31% ($^{207}Pb/^{206}Pb$), 0.76% ($^{206}Pb/^{238}U$) (2 sigma).

Trace element concentrations were deleted from analyses known to have intersected inclusions of other minerals based on P and Ti.

Ablation used a laser spot size of 25 microns, and a laser firing repetition rate of 10 Hz.

Activity of TiO_2 for Ti-in-Zircon temperature calculation is 0.8.

LA-ICPMS data from sample from DS69

		Corrected isotope ratios							Dates (Ma)						
		207Pb*	±2s	206Pb*	±2s	error	207Pb*	±2s	207Pb*	±2s	207Pb*	±2s	206Pb*	±2s	%
Analysis	Th/U	235U*	(%)	238U	(%)	corr.	206Pb*	(%)	206Pb*	(Ma)	235U	(Ma)	238U*	(Ma)	disc.
DS69 210	1.47	6.37669	5.624	0.37648	5.420	0.96	0.12284	1.498	1998	27	2029	49	2060	96	-3
DS69 110	1.07	1.35692	8.854	0.14616	6.761	0.76	0.06733	5.717	848	119	871	52	879	56	-4
DS69 216	1.36	1.23102	8.597	0.14290	5.017	0.58	0.06248	6.981	691	149	815	48	861	40	-25
DS69 66	1.20	1.53884	21.127	0.14144	9.771	0.46	0.07891	18.732	1170	371	946	130	853	78	27
DS69 207	1.57	1.25885	6.372	0.13971	4.256	0.67	0.06535	4.742	786	100	827	36	843	34	-7
DS69 57	1.21	1.22501	9.180	0.13862	6.177	0.67	0.06409	6.791	745	144	812	51	837	48	-12
DS69 48	1.38	2.53738	17.950	0.13795	6.739	0.38	0.13340	16.637	2143	291	1283	131	833	53	61
DS69 212	2.03	1.59407	8.169	0.13672	4.101	0.50	0.08456	7.065	1306	137	968	51	826	32	37
DS69 211	0.99	1.29297	8.413	0.13632	6.039	0.72	0.06879	5.857	892	121	843	48	824	47	8
DS69 106	1.80	1.36217	14.175	0.13616	5.112	0.36	0.07256	13.221	1002	268	873	83	823	39	18
DS69 117	1.76	1.26364	12.194	0.13566	5.690	0.47	0.06756	10.785	855	224	830	69	820	44	4
DS69 80	1.14	1.19890	6.709	0.13543	4.355	0.65	0.06420	5.103	748	108	800	37	819	33	-9

DS69 119	1.27	1.20802	6.678	0.13540	5.256	0.79	0.06471	4.120	765	87	804	37	819	40	-7
DS69 63	1.19	1.51169	17.650	0.13411	7.174	0.41	0.08175	16.126	1240	316	935	108	811	55	35
DS69 82	1.30	1.24085	5.673	0.13390	3.900	0.69	0.06721	4.120	844	86	819	32	810	30	4
DS69 96	1.35	1.21451	6.792	0.13378	4.252	0.63	0.06584	5.296	801	111	807	38	809	32	-1
DS69 217	1.49	1.18912	5.501	0.13371	4.562	0.83	0.06450	3.073	758	65	796	30	809	35	-7
DS69 94	1.38	1.95228	7.694	0.13359	4.234	0.55	0.10599	6.424	1732	118	1099	52	808	32	53
DS69 208	1.37	1.66140	6.851	0.13342	3.565	0.52	0.09031	5.851	1432	112	994	43	807	27	44
DS69 203	2.60	1.30701	5.883	0.13341	3.899	0.66	0.07105	4.405	959	90	849	34	807	30	16
DS69 83	3.03	1.18353	10.239	0.13314	5.507	0.54	0.06447	8.632	757	182	793	56	806	42	-6
DS69 205	1.04	1.12378	6.810	0.13295	4.468	0.66	0.06130	5.140	650	110	765	37	805	34	-24
DS69 94	2.58	1.20899	5.003	0.13287	3.608	0.72	0.06599	3.467	806	73	805	28	804	27	0
DS69 91	1.61	1.20981	8.151	0.13258	4.811	0.59	0.06618	6.579	812	138	805	45	803	36	1
DS69 103	2.01	1.24823	6.741	0.13164	3.584	0.53	0.06877	5.709	892	118	823	38	797	27	11
DS69 71	0.99	1.32101	13.728	0.13162	5.250	0.38	0.07279	12.685	1008	257	855	79	797	39	21
DS69 74	1.02	1.20337	9.075	0.13151	7.328	0.81	0.06636	5.353	818	112	802	50	796	55	3
DS69 85	0.80	1.30423	11.105	0.13124	4.596	0.41	0.07208	10.109	988	206	848	64	795	34	20
DS69 54	1.06	1.19061	8.305	0.13070	6.499	0.78	0.06607	5.172	809	108	796	46	792	48	2
DS69 215	1.35	1.15294	5.432	0.13069	4.290	0.79	0.06398	3.332	741	70	779	30	792	32	-7
DS69 89	1.04	1.20507	7.031	0.13056	5.099	0.73	0.06694	4.841	836	101	803	39	791	38	5
DS69 68	0.77	1.24082	8.611	0.13032	6.850	0.80	0.06905	5.218	900	108	819	48	790	51	12
DS69 213	1.46	1.10065	5.208	0.13030	3.841	0.74	0.06126	3.518	648	76	754	28	790	29	-22
DS69 50	0.92	1.15502	9.473	0.13002	5.873	0.62	0.06443	7.433	756	157	780	52	788	44	-4
DS69 99	1.35	1.17848	6.895	0.12971	5.682	0.82	0.06590	3.906	803	82	791	38	786	42	2
DS69 86	1.87	1.20024	8.657	0.12945	6.126	0.71	0.06725	6.117	845	127	801	48	785	45	7
DS69 100	1.32	1.16359	5.915	0.12915	3.737	0.63	0.06534	4.586	785	96	784	32	783	28	0
DS69 88	0.82	1.19758	5.314	0.12868	4.220	0.79	0.06750	3.230	853	67	799	29	780	31	9
DS69 107	1.39	1.24022	11.670	0.12845	8.024	0.69	0.07003	8.474	929	174	819	66	779	59	16
DS69 101	1.97	1.17603	7.365	0.12780	3.976	0.54	0.06674	6.199	830	129	789	40	775	29	7
DS69 204	2.26	1.17417	6.654	0.12773	4.110	0.62	0.06667	5.232	828	109	789	36	775	30	6
DS69 51	0.87	1.12425	7.755	0.12714	5.583	0.72	0.06413	5.382	746	114	765	42	772	41	-3

DS69 49	1.00	1.14560	7.739	0.12649	5.469	0.71	0.06569	5.476	796	115	775	42	768	40	4
DS69 47	1.40	1.09244	10.483	0.12628	5.938	0.57	0.06274	8.639	700	184	750	56	767	43	-10
DS69 81	1.54	1.16137	7.248	0.12608	4.772	0.66	0.06681	5.456	832	114	783	40	765	34	8
DS69 43	1.34	1.17968	6.848	0.12588	6.002	0.88	0.06797	3.297	868	68	791	38	764	43	12
DS69 79	1.83	1.15631	5.527	0.12561	3.856	0.70	0.06676	3.960	830	83	780	30	763	28	8
DS69 214	1.53	1.10000	5.139	0.12559	3.648	0.71	0.06353	3.620	726	77	753	27	763	26	-5
DS69 65	1.35	1.10323	5.299	0.12532	3.911	0.74	0.06385	3.574	737	76	755	28	761	28	-3
DS69 112	1.29	1.11158	7.139	0.12401	5.314	0.74	0.06501	4.767	775	100	759	38	754	38	3
DS69 109	1.27	1.16749	6.906	0.12278	4.906	0.71	0.06897	4.860	898	100	785	38	747	35	17
DS69 45	0.76	1.05817	6.918	0.12251	5.472	0.79	0.06265	4.232	696	90	733	36	745	39	-7
DS69 46	0.94	1.10331	5.596	0.12238	4.272	0.76	0.06539	3.615	787	76	755	30	744	30	5
DS69 76	1.22	1.12513	5.945	0.12144	4.367	0.73	0.06720	4.033	844	84	765	32	739	30	12
DS69 40	1.56	1.06644	6.838	0.12048	4.906	0.72	0.06420	4.764	748	101	737	36	733	34	2

March 7, 2014
Isotope ratio and date errors include systematic calibration errors of 0.23% ($^{207}Pb/^{206}Pb$), 0.66% ($^{206}Pb/^{238}U$) (2 sigma).
Trace element concentrations were deleted from analyses known to have intersected inclusions of other minerals based on P and Ti.
Ablation used a laser spot size of 25 microns, and a laser firing repetition rate of 10 Hz.
Activity of TiO_2 for Ti-in-Zircon temperature calculation is 0.8.

January 13, 2016
Isotope ratio and date errors include systematic calibration errors of 0.22% ($^{207}Pb/^{206}Pb$), 0.76% ($^{206}Pb/^{238}U$) (2 sigma).
Trace element concentrations were deleted from analyses known to have intersected inclusions of other minerals based on P and Ti.
Ablation used a laser spot size of 25 microns, and a laser firing repetition rate of 10 Hz.
Activity of TiO_2 for Ti-in-Zircon temperature calculation is 0.8.

LA-ICPMS data from sample from DS69 continued.

	Concentrations (ppm)																					
Analysis	P	Ti	Y	Nb	La	Ce	Pr	Nd	Sm	Eu	Gd	Tb	Dy	Ho	Er	Tm	Yb	Lu	Hf	Ta	Th	U	T(°C)
DS69210	178	17.19	937	3.54	0.01	33.07	0.21	4.26	7.39	1.05	31.58	9.73	105.7	35.44	140.8	31.1	280	41.9	11639	1.43	179.1	122	823
DS69110	202	7.48	717	1.51		16.42	0.03	0.39	2.07	0.38	12.28	4.61	60.7	24.69	116.3	30.2	335	46.3	10123	0.74	49.6	47	767
DS69216	322	13.96	1376	1.17		19.37	0.11	2.01	4.01	2.68	28.99	9.80	126.3	48.20	214.2	47.5	451	77.7	10011	0.48	43.3	32	801
DS69 66	310	18.77	1252	1.58		14.37	0.10	1.72	5.35	2.92	25.86	10.11	113.4	43.95	198.1	49.5	526	66.9	7809	0.50	36.7	31	866
DS69207	447	22.21	2178	1.33		22.80	0.16	3.93	7.72	4.07	44.39	15.02	195.8	77.02	345.7	75.7	705	122.4	9174	0.65	66.3	42	852
DS69 57	316	11.81	1392	1.62		19.97	0.13	2.66	5.71	2.20	35.87	11.66	145.6	52.12	223.9	57.5	652	72.2	7691	0.72	63.1	52	814
DS69212	485	13.96	4112	3.67	0.02	63.74	0.53	9.32	16.41	6.50	99.97	32.22	408.9	152.88	650.5	142.4	1311	206.6	9446	1.09	250.8	123	801
DS69211	392	15.80	1343	1.76	0.30	15.66	0.20	2.47	4.78	2.38	28.51	9.94	123.4	50.24	225.3	54.2	533	88.4	9155	0.75	41.8	42	814
DS69106	231	10.61	1724	1.03		19.11	0.22	4.36	10.28	4.14	54.26	17.13	191.8	65.94	265.6	62.2	630	78.2	8956	0.43	67.1	37	802
DS69117	340	9.65	2894	2.00	0.05	26.79	0.38	6.28	15.41	4.17	79.85	25.78	313.2	104.82	446.9	101.8	1010	129.9	9555	0.56	151.6	86	793
DS69 80	441	9.87	1341	1.62		18.39	0.06	1.75	4.40	1.49	25.75	9.29	116.8	47.52	221.8	55.5	609	84.3	10387	0.82	63.2	56	795
DS69119	259	12.81	1262	1.65		19.49	0.06	2.18	3.16	1.60	18.31	7.64	99.1	39.64	199.9	58.1	701	101.5	8820	0.65	127.5	101	823
DS69 63	365	16.82	1136	1.28		16.36	0.11	1.53	4.02	1.75	24.19	8.74	108.1	38.94	180.8	47.8	512	65.5	8446	0.65	37.5	31	853
DS69 82	319	11.04	1407	2.50	0.12	22.68	0.13	2.33	3.45	0.99	27.10	9.62	129.6	52.59	231.0	56.1	622	94.1	10319	1.02	90.8	70	807
DS69 96	463	8.39	1504	2.81		49.24	0.10	2.48	6.21	3.28	35.43	12.51	149.2	57.13	243.5	58.7	638	74.4	8486	0.99	88.9	66	778
DS69217	273	6.69	1196	1.91		24.32	0.07	1.14	1.98	0.61	18.93	7.20	99.5	40.23	191.4	45.7	455	83.2	11918	0.99	158.8	107	729
DS69 94	407	11.21	2107	3.76		29.97	0.32	4.28	8.99	2.52	52.45	15.91	205.1	78.55	349.8	84.8	933	120.6	9887	1.28	121.8	88	808

DS69208	426	15.07	2258	2.49		30.54	0.07	3.27	6.09	3.00	40.26	15.01	192.0	81.70	370.0	86.6	810	140.2	9369	0.80	93.4	68	809
DS69203	424	11.99	3019	1.49	0.17	62.72	0.64	13.84	20.43	9.43	105.83	29.76	337.4	116.78	476.1	102.8	914	142.7	10115	0.78	166.3	64	785
DS6983	271	25.28	1886	0.51		21.04	0.42	9.85	16.53	6.19	66.10	19.87	216.8	73.41	278.7	60.1	569	82.5	9825	0.27	61.5	20	902
DS69205	224	6.78	1118	1.78		16.11	0.04	1.27	2.44	0.65	17.47	7.00	93.8	37.73	183.6	45.2	458	84.3	11825	0.99	61.7	59	731
DS6994	574	17.13	4333	2.00	0.14	64.60	1.00	18.61	33.73	17.46	160.57	47.47	528.1	170.96	654.0	153.0	1624	172.5	6329	0.50	197.3	76	855
DS6991	329	18.80	2018	0.66	0.03	18.22	0.29	6.66	15.10	8.05	63.89	19.72	222.6	76.91	299.3	72.2	747	83.2	6780	0.37	52.6	33	866
DS6971	255	8.31	932	1.66		18.07	0.03	1.67	3.31	1.72	19.05	7.81	92.8	34.90	148.3	36.9	430	50.5	8044	0.70	35.1	36	777
DS6974	280	6.50	1236	0.89		17.47	0.08	2.29	3.98	1.24	27.06	9.44	120.3	46.32	196.7	50.8	573	63.1	8068	0.63	69.6	68	753
DS6985	228	3.69	2198	8.44	0.02	23.15	0.11	3.20	6.61	0.89	43.85	16.91	220.2	81.10	341.1	80.5	763	96.2	9745	2.84	144.8	180	702
DS6954	330	11.44	1681	1.83		21.80	0.08	3.44	7.47	2.41	34.36	13.53	167.4	63.15	270.5	72.4	840	89.0	7684	0.95	87.2	82	810
DS69215	451	6.75	3626	2.91	0.01	28.10	0.40	7.78	18.22	4.45	99.70	31.32	382.4	139.35	575.3	124.4	1130	186.2	10639	1.25	201.3	149	730
DS6989	285	10.14	1274	2.05		21.27	0.11	1.19	4.08	1.23	22.05	8.28	105.7	41.29	202.7	55.0	604	82.0	9316	0.79	88.3	85	798
DS6968	280	2.82	3141	9.06	0.04	30.00	0.18	4.89	14.39	1.52	75.72	28.45	343.5	122.28	496.1	115.8	1214	132.4	8403	2.93	224.7	293	680
DS69213	409	5.87	2389	2.16		33.29	0.26	6.61	12.20	4.01	62.82	20.13	241.9	86.82	364.9	79.9	764	122.9	10643	0.94	129.4	89	718
DS6950	288	11.61	786	0.91		15.96	0.00	0.80	2.55	0.70	14.93	5.48	72.7	29.09	130.5	33.7	411	47.8	8174	0.52	45.4	49	812
DS6999	260	8.14	1744	1.15	0.04	18.67	0.16	2.84	7.56	1.82	41.92	14.58	174.0	66.08	281.4	68.0	691	87.7	10320	0.49	88.7	66	775
DS6986	312	19.44	2166	1.37	0.04	18.49	0.41	8.00	14.30	7.09	60.32	20.07	236.1	84.20	348.9	77.0	792	103.1	8275	0.33	77.1	41	870
DS69100	410	13.82	2617	4.53		33.82	0.20	3.41	6.76	2.55	48.79	17.90	236.5	92.12	426.8	104.4	1114	145.2	9114	1.32	143.1	108	831
DS69107	246	14.53	989	0.46		13.73	0.10	1.71	3.55	2.80	25.39	8.30	100.8	38.04	160.6	37.6	380	52.1	9546	0.24	22.7	16	836
DS69	43	20.8	264	1.6		25.	0.2	5.6	12.	6.4	69.0	22.	273	101.	410	93.	95	130	841	0.5	96.	49	878

101	8	4	1	6		69	8	6	89	9	9	30	.9	67	.6	4	7	.1	2	9	6		
DS69204	437	16.81	3719	1.38	0.27	34.44	0.40	10.07	17.66	9.05	112.31	34.35	382.9	138.70	565.5	120.4	1069	170.2	9442	0.53	143.6	64	821
DS6951	220	7.10	751	1.96	0.04	17.64	0.04	0.52	1.61	0.48	12.36	4.59	67.6	25.99	122.6	33.4	412	49.8	9244	0.84	52.0	60	762
DS6947	253	24.32	1074	0.44		11.88	0.09	2.69	7.83	4.57	34.23	11.33	124.7	43.00	166.1	41.9	455	47.2	6236	0.10	27.3	19	897
DS6981	351	11.32	1985	1.51		20.87	0.21	4.08	8.92	2.02	43.54	15.65	201.4	75.22	314.3	79.1	884	121.2	9403	0.52	109.0	71	809
DS6943	387	11.22	1500	3.45		33.93	0.06	2.21	5.22	2.01	28.91	12.52	144.2	54.74	243.7	62.2	708	78.8	8065	1.22	160.9	120	808
DS6979	327	12.81	2243	1.14		32.70	0.19	5.99	10.81	5.76	62.21	21.52	232.3	85.88	347.4	78.4	815	100.6	9420	0.45	80.3	44	822
DS69214	334	13.64	1942	1.32		19.35	0.20	3.82	8.15	2.08	43.73	14.43	177.7	69.82	311.1	73.2	701	116.5	10231	0.59	105.8	69	799
DS6965	379	15.82	2340	3.62	0.03	27.14	0.14	3.29	7.70	2.87	42.36	15.47	213.2	86.85	379.3	99.1	1073	135.8	8189	0.97	129.1	95	846
DS69112	435	13.22	1751	2.87	0.51	34.24	0.23	4.16	8.13	3.94	42.63	13.92	172.6	65.75	286.6	70.7	732	89.4	8822	0.79	69.0	53	826
DS69109	312	8.21	1184	0.99		20.14	0.04	1.45	4.34	1.56	25.13	9.44	116.5	43.29	186.1	46.3	490	67.9	9414	0.62	47.3	37	776
DS6945																							
DS6946	322	10.06	1110	1.91		19.77	0.09	1.64	4.28	1.52	21.95	7.70	109.0	39.91	179.4	49.0	580	60.8	7427	0.95	73.6	78	797
DS6976	237	7.24	1391	2.15		23.45	0.02	1.57	4.41	0.65	25.11	9.60	131.4	49.12	222.2	55.9	636	80.0	9778	0.98	103.6	85	764
DS6940	395	13.83	1358	2.85	0.12	31.79	0.10	2.61	5.80	1.45	32.61	10.71	134.7	49.54	223.2	54.9	633	75.7	8498	0.94	109.8	70	831

LA-ICPMS data from sample F1128B

		Corrected isotope ratios							Dates (Ma)						
		207Pb*	±2s	206Pb*	±2s	error	207Pb*	±2s	207Pb*	±2s	207Pb*	±2s	206Pb*	±2s	%
Analysis	Th/U	235U*	(%)	238U	(%)	corr.	206Pb*	(%)	206Pb*	(Ma)	235U	(Ma)	238U*	(Ma)	disc.
F1128B 79	0.51	8.50376	4.593	0.37201	3.845	0.84	0.16579	2.513	2516	42	2286	42	2039	67	19
F1128B 65	0.76	9.09674	4.663	0.41124	4.155	0.89	0.16043	2.117	2460	36	2348	43	2221	78	10
F1128B 76	0.49	8.86502	6.862	0.40445	6.268	0.91	0.15897	2.791	2445	47	2324	63	2190	116	10
F1128B 73	0.23	8.48121	4.765	0.39546	4.382	0.92	0.15554	1.872	2408	32	2284	43	2148	80	11
F1128B 72	0.33	7.99928	3.964	0.40409	3.544	0.89	0.14357	1.776	2271	31	2231	36	2188	66	4
F1128B 123	2.28	6.45972	5.462	0.34310	4.666	0.85	0.13655	2.839	2184	49	2040	48	1902	77	13
F1128B 71	0.48	5.78698	3.972	0.34107	3.688	0.93	0.12306	1.476	2001	26	1944	34	1892	60	5
F1128B 83	1.73	5.57318	5.077	0.32903	4.259	0.84	0.12285	2.764	1998	49	1912	44	1834	68	8
F1128B 70	0.31	5.49601	4.078	0.33044	3.189	0.78	0.12063	2.541	1966	45	1900	35	1841	51	6
F1128B 129	0.09	5.57414	3.772	0.33603	3.283	0.87	0.12031	1.857	1961	33	1912	32	1868	53	5
F1128B 87	0.06	4.71976	4.481	0.28790	4.053	0.90	0.11890	1.912	1940	34	1771	38	1631	58	16
F1128B 86	1.23	4.91925	3.807	0.30257	2.969	0.78	0.11792	2.383	1925	43	1806	32	1704	44	11
F1128B 124	1.31	5.33525	5.291	0.32994	3.971	0.75	0.11728	3.496	1915	63	1875	45	1838	64	4
F1128B 125	0.69	5.07380	4.424	0.32039	3.814	0.86	0.11485	2.241	1878	40	1832	38	1792	60	5
F1128B 67	0.67	4.66205	4.134	0.29479	3.472	0.84	0.11470	2.245	1875	40	1760	35	1665	51	11
F1128B 128	0.20	4.17274	4.768	0.26440	3.376	0.71	0.11446	3.367	1871	61	1669	39	1512	46	19
F1128B 22	1.96	3.99193	7.388	0.26720	6.813	0.92	0.10835	2.856	1772	52	1633	60	1527	93	14
F1128B 127	0.86	2.12068	11.942	0.18315	9.627	0.81	0.08398	7.067	1292	137	1156	82	1084	96	16
F1128B 21	2.19	1.66854	16.650	0.13660	5.199	0.31	0.08859	15.818	1395	303	997	106	825	40	41
F1128B 24	2.28	1.29329	5.880	0.13104	3.885	0.66	0.07158	4.414	974	90	843	34	794	29	19
F1128B 82	1.07	1.20474	4.391	0.12648	3.603	0.82	0.06908	2.510	901	52	803	24	768	26	15
F1128B 20	1.63	1.15138	6.599	0.12377	5.304	0.80	0.06747	3.926	852	82	778	36	752	38	12
F1128B 75	1.26	1.19268	4.539	0.13028	3.665	0.81	0.06640	2.678	819	56	797	25	789	27	4
F1128B 165	1.14	1.18515	5.583	0.13055	4.287	0.77	0.06584	3.577	801	75	794	31	791	32	1
F1128B 85	0.64	1.09187	6.264	0.12401	3.917	0.63	0.06386	4.888	737	103	749	33	754	28	-2
F1128B 126	1.67	1.16370	11.651	0.13343	5.720	0.49	0.06325	10.150	717	216	784	64	807	43	-13

F1128B 78	1.12	0.60533	6.789	0.07506	3.859	0.57	0.05849	5.585	548	122	481	26	467	17	15
F1128B 84	0.51	0.61801	6.639	0.07705	4.413	0.66	0.05817	4.960	536	109	489	26	479	20	11
F1128B 80	1.20	0.61765	4.935	0.07724	4.195	0.85	0.05799	2.599	529	57	488	19	480	19	9
F1128B 163	0.61	0.62983	4.649	0.07945	3.330	0.72	0.05749	3.244	510	71	496	18	493	16	3
F1128B 68	0.86	1.10136	19.953	0.13901	5.185	0.26	0.05746	19.268	509	424	754	106	839	41	-65
F1128B 81	0.68	0.60555	6.131	0.07658	4.019	0.66	0.05735	4.630	505	102	481	23	476	18	6
F1128B 74	0.49	0.61477	5.429	0.07782	4.352	0.80	0.05730	3.246	503	71	487	21	483	20	4
F1128B 69	0.86	0.55665	7.703	0.07488	3.320	0.43	0.05392	6.950	368	157	449	28	465	15	-27

LA-ICPMS data from sample F1128B continued.

	Concentrations (ppm)																					
Analysis	P	Ti	Y	Nb	La	Ce	Pr	Nd	Sm	Eu	Gd	Tb	Dy	Ho	Er	Tm	Yb	Lu	Hf	Ta	Th	U	T(°C)
F1128B 79	152	13.18	272	0.47	0.00	7.73	0.06	0.66	1.61	0.36	6.29	2.17	26.4	9.70	48.0	14.3	194	25.4	8420	0.17	53.3	104	826
F1128B 65	200	7.87	686	1.34		18.17	0.15	2.12	5.04	1.20	19.75	5.91	66.4	22.80	100.6	27.1	292	43.2	10542	1.08	92.2	121	772
F1128B 76	299	9.90	624	0.91	0.03	15.11	0.02	1.31	2.78	0.74	14.66	4.96	60.9	22.38	94.1	26.3	317	36.0	8218	0.60	65.0	133	795
F1128B 73	100	10.17	362	1.04	0.02	5.09	0.05	0.51	1.34	0.43	11.27	3.25	37.0	12.94	54.5	14.9	183	22.9	8963	0.99	32.6	139	798
F1128B 72	111	10.51	186	0.37	0.02	5.12	0.03	0.11	0.75	0.31	4.39	1.31	18.9	6.51	29.4	8.5	105	13.3	9987	0.41	42.7	130	801
F1128B 123	225	28.90	718	2.74	0.10	31.24	0.19	2.27	5.81	1.49	24.64	7.57	78.8	26.79	101.3	22.4	221	30.0	10129	1.04	103.0	45	919
F1128B 83	249	12.04	604	7.39		16.18	0.10	1.53	6.64	0.19	32.19	10.37	92.3	22.72	66.9	12.5	99	10.2	11270	1.71	65.8	38	816
F1128B 70	86	6.03	221	0.22	0.04	6.62	0.01	0.98	2.62	1.23	10.21	2.56	25.3	8.45	34.8	8.5	94	10.9	9905	0.18	21.8	70	746
F1128B 129	69	5.36	24	0.20	0.01	6.10	0.01	0.62	1.24	0.71	2.49	0.59	3.9	0.89	2.2	0.5	3	0.4	11852	0.02	12.2	137	735
F1128B 87	62	9.28	22	0.22		5.61	0.02	0.83	1.67	1.17	3.39	0.54	3.4	0.77	2.4	0.3	4	0.4	11320	0.05	9.5	154	789
F1128B 86	161	8.69	388	0.71	0.04	18.26	0.05	2.02	2.88	0.44	12.54	3.86	43.4	14.39	59.0	15.4	155	18.8	10744	0.37	60.5	49	782
F1128B 125	82	36.43	33	0.28	0.03	2.10	0.04	1.14	1.34	0.50	2.71	0.58	5.0	1.25	4.2	0.8	9	1.1	11035	0.09	33.9	49	949
F1128B 67	117	7.07	284	2.04		16.81		0.58	1.58	0.07	6.48	2.63	30.5	10.13	41.6	10.5	111	14.0	12218	0.92	94.8	142	762
F1128B 128	71	14.02	31	0.19	0.02	4.02	0.05	0.33	1.10	0.42	2.89	0.63	4.4	1.14	3.7	0.9	8	1.6	12230	0.11	10.1	51	832
F1128B 22	172	4.95	683	1.59	0.24	38.53	0.10	0.88	3.29	0.36	16.97	5.85	65.7	24.09	96.9	22.6	228	29.2	9183	0.70	200.3	102	728
F1128B 127	147	5.12	453	0.76		7.28	0.05	0.58	1.56	0.18	9.32	3.11	42.0	16.25	70.9	17.6	184	26.0	12966	0.41	26.3	31	731
F1128B 24	177	11.47	1458	0.91	0.02	37.13	0.48	9.38	16.25	5.25	54.77	15.72	165.7	56.32	222.9	52.1	529	68.2	6272	0.35	115.4	51	811

F1128B 165	181	3.52	656	2.16		21.38	0.01	0.74	2.22	0.41	13.66	4.72	57.7	22.14	102.5	28.5	330	37.9	9472	1.19	75.7	66	698
F1128B 85	139	9.48	353	0.63		10.60	0.03	0.88	2.31	1.13	11.03	3.03	35.8	12.49	51.8	13.7	153	19.6	9877	0.76	29.4	46	791
F1128B 126	149	13.97	378	0.77	0.06	8.81	0.07	0.69	1.43	0.49	8.26	2.96	34.3	12.77	58.2	14.0	145	21.1	10682	0.26	16.4	10	832
F1128B 78	124	22.58	348	2.05		27.52	0.05	1.86	2.79	0.98	10.65	3.66	37.4	12.29	53.7	14.8	167	18.9	7152	1.24	94.8	85	888
F1128B 84	62	3.53	284	0.77		15.17	0.07	0.76	1.46	0.88	7.58	2.48	27.4	10.17	46.4	12.4	152	18.4	9485	0.32	42.5	83	698
F1128B 80	157	5.95	966	5.22	0.04	81.07	0.20	3.92	6.91	1.89	27.19	9.46	107.6	36.60	149.1	37.9	422	41.8	8984	2.08	405.9	339	745
F1128B 163	107	3.90	505	1.24		23.33	0.13	1.62	2.69	1.49	13.52	3.93	47.0	16.07	73.7	21.5	267	31.9	7418	0.64	90.8	149	707
F1128B 68	138	14.84	246	0.54		9.87	0.09	0.85	2.24	0.75	9.13	2.94	28.5	9.07	32.8	8.5	89	9.8	9376	0.15	4.1	5	839
F1128B 81	81	7.35	202	1.47		22.16	0.01		0.86	0.30	3.95	1.38	18.5	6.46	31.9	8.9	116	14.2	8737	0.72	49.4	72	765
F1128B 74																							
F1128B 69	176	31.03	614	1.47	0.16	20.91	0.27	4.00	6.31	1.46	18.89	4.97	56.8	20.70	94.4	27.6	326	42.2	6334	0.98	54.5	63	928

May 10, 2012

Isotope ratio and date errors include systematic calibration errors of 0.38% ($^{207}Pb/^{206}Pb$), 0.84% ($^{206}Pb/^{238}U$) (2 sigma).

Trace element concentrations were deleted from analyses known to have intersected inclusions of other minerals based on P and Ti.

Ablation used a laser spot size of 25 microns, and a laser firing repetition rate of 10 Hz.

Activity of TiO_2 for Ti-in-Zircon temperature calculation is 0.8.

May 15, 2012

Isotope ratio and date errors include systematic calibration errors of 0.11% ($^{207}Pb/^{206}Pb$), 0.46% ($^{206}Pb/^{238}U$) (2 sigma).

Trace element concentrations were deleted from analyses known to have intersected inclusions of other minerals based on P and Ti.

Ablation used a laser spot size of 25 microns, and a laser firing repetition rate of 10 Hz.

Activity of TiO_2 for Ti-in-Zircon temperature calculation is 0.8.

May 11, 2012

Isotope ratio and date errors include systematic calibration errors of 0.26% ($^{207}Pb/^{206}Pb$), 0.54% ($^{206}Pb/^{238}U$) (2 sigma).

Trace element concentrations were deleted from analyses known to have intersected inclusions of other minerals based on P and Ti.

Ablation used a laser spot size of 25 microns, and a laser firing repetition rate of 10 Hz.

Activity of TiO_2 for Ti-in-Zircon temperature calculation is 0.8.

May 14, 2012

Isotope ratio and date errors include systematic calibration errors of 0.27% ($^{207}Pb/^{206}Pb$), 0.71% ($^{206}Pb/^{238}U$) (2 sigma).

Trace element concentrations were deleted from analyses known to have intersected inclusions of other minerals based on P and Ti.

Ablation used a laser spot size of 25 microns, and a laser firing repetition rate of 10 Hz.

Activity of TiO_2 for Ti-in-Zircon temperature calculation is 0.8.

LA-ICPMS data from sample U1127-1

		Corrected isotope ratios							Dates (Ma)						
		207Pb*	±2s	206Pb*	±2s	error	207Pb*	±2s	207Pb*	±2s	207Pb*	±2s	206Pb*	±2s	%
Analysis	Th/U	235U*	(%)	238U	(%)	corr.	206Pb*	(%)	206Pb*	(Ma)	235U	(Ma)	238U*	(Ma)	disc.
U1127-1 13	1.17	4.88165	5.338	0.31064	3.643	0.68	0.11397	3.901	1864	70	1799	45	1744	56	6
U1127-1 21	0.81	4.62070	5.594	0.32204	3.492	0.62	0.10406	4.370	1698	81	1753	47	1800	55	-6
U1127-1 4	1.09	1.29890	4.926	0.14437	3.846	0.78	0.06525	3.078	783	65	845	28	869	31	-11
U1127-1 5	1.47	1.30284	5.126	0.13737	2.873	0.56	0.06879	4.245	892	88	847	29	830	22	7
U1127-1 40	0.80	1.16838	5.411	0.13125	4.131	0.76	0.06456	3.496	760	74	786	30	795	31	-5
U1127-1 36	0.91	1.16563	5.680	0.12881	4.908	0.86	0.06563	2.859	795	60	785	31	781	36	2
U1127-1 30	1.00	1.14699	7.648	0.12865	6.634	0.87	0.06466	3.805	763	80	776	41	780	49	-2
U1127-1 35	0.40	1.13576	4.454	0.12801	3.306	0.74	0.06435	2.986	753	63	770	24	777	24	-3
U1127-1 42	1.60	1.17367	4.547	0.12758	3.685	0.81	0.06672	2.665	829	56	788	25	774	27	7
U1127-1 34	0.29	1.16157	5.658	0.12702	4.570	0.81	0.06632	3.336	817	70	783	31	771	33	6
U1127-1 12	0.93	1.21003	7.416	0.12612	5.501	0.74	0.06959	4.974	916	102	805	41	766	40	16
U1127-1 6	0.79	1.08210	4.928	0.12424	3.440	0.70	0.06317	3.529	714	75	745	26	755	25	-6
U1127-1 42	0.98	1.12000	4.434	0.12286	3.850	0.87	0.06611	2.200	810	46	763	24	747	27	8
U1127-1 10	1.17	1.07128	4.213	0.12275	2.707	0.64	0.06330	3.229	718	69	739	22	746	19	-4
U1127-1 3	1.36	1.09205	4.573	0.12216	3.965	0.87	0.06484	2.278	769	48	749	24	743	28	3
U1127-1 9	1.20	1.02639	5.335	0.12117	3.537	0.66	0.06143	3.995	654	86	717	27	737	25	-13
U1127-1 28	0.98	1.09968	5.153	0.12061	3.451	0.67	0.06613	3.827	810	80	753	27	734	24	9
U1127-1 39	0.98	0.99613	6.106	0.11901	3.661	0.60	0.06071	4.887	629	105	702	31	725	25	-15
U1127-1 2	1.16	1.05717	6.057	0.11894	4.274	0.71	0.06446	4.292	757	91	732	32	724	29	4
U1127-1 14	1.04	1.11337	5.629	0.11777	3.887	0.69	0.06856	4.071	886	84	760	30	718	26	19
U1127-1 41	0.26	0.96770	6.689	0.10823	5.755	0.86	0.06485	3.410	769	72	687	33	662	36	14
U1127-1 9	0.41	0.68247	4.388	0.08791	3.702	0.84	0.05631	2.355	464	52	528	18	543	19	-17
U1127-1 15	0.79	0.67102	5.627	0.08681	4.962	0.88	0.05606	2.654	455	59	521	23	537	26	-18

U1127-1 1	1.16	0.67663	5.730	0.08494	4.937	0.86	0.05777	2.908	521	64	525	23	526	25	-1
U1127-1 25	0.67	0.67021	5.339	0.08481	3.417	0.64	0.05732	4.103	504	90	521	22	525	17	-4
U1127-1 28	0.52	0.66696	6.810	0.08464	5.106	0.75	0.05715	4.506	497	99	519	28	524	26	-5
U1127-1 2	0.73	0.66777	5.184	0.08432	4.057	0.78	0.05744	3.227	508	71	519	21	522	20	-3
U1127-1 26	0.59	0.66553	5.261	0.08371	4.271	0.81	0.05766	3.072	517	67	518	21	518	21	0
U1127-1 38	0.32	0.69917	5.780	0.08371	5.180	0.90	0.06058	2.565	624	55	538	24	518	26	17
U1127-1 21	0.49	0.65739	6.201	0.08297	4.077	0.66	0.05747	4.673	510	103	513	25	514	20	-1
U1127-1 38	0.41	0.63767	4.476	0.08293	3.099	0.69	0.05577	3.231	443	72	501	18	514	15	-16
U1127-1 12	0.46	0.66734	5.393	0.08265	3.369	0.62	0.05856	4.212	551	92	519	22	512	17	7
U1127-1 8	0.42	0.63385	4.023	0.08215	2.951	0.73	0.05596	2.735	451	61	498	16	509	14	-13
U1127-1 43	0.39	0.62908	5.844	0.08209	3.877	0.66	0.05558	4.373	436	97	496	23	509	19	-17
U1127-1 17	0.47	0.66794	5.450	0.08196	3.796	0.70	0.05911	3.910	571	85	519	22	508	19	11
U1127-1 17	0.84	0.66765	9.540	0.08190	8.097	0.85	0.05912	5.045	572	110	519	39	507	40	11
U1127-1 23	0.35	0.62335	4.364	0.08174	2.659	0.61	0.05531	3.461	425	77	492	17	506	13	-19
U1127-1 33	0.46	0.65597	6.617	0.08167	4.341	0.66	0.05826	4.994	539	109	512	27	506	21	6
U1127-1 24	1.04	0.63928	5.784	0.08145	3.253	0.56	0.05692	4.783	489	106	502	23	505	16	-3
U1127-1 16	0.30	0.61279	5.123	0.08094	3.733	0.73	0.05491	3.508	409	78	485	20	502	18	-23
U1127-1 6	0.47	0.64276	5.863	0.08075	5.026	0.86	0.05773	3.020	520	66	504	23	501	24	4
U1127-1 7	0.90	0.61504	3.764	0.08053	3.163	0.84	0.05539	2.040	428	45	487	15	499	15	-17
U1127-1 16	0.61	0.62372	4.625	0.08048	3.212	0.69	0.05621	3.327	461	74	492	18	499	15	-8
U1127-1 33	0.64	0.62039	4.952	0.08024	4.037	0.82	0.05608	2.868	455	64	490	19	498	19	-9
U1127-1 8	1.40	0.60299	4.317	0.08018	3.212	0.74	0.05454	2.884	394	65	479	16	497	15	-26
U1127-1 14B	0.62	0.64964	4.504	0.08008	2.918	0.65	0.05884	3.430	561	75	508	18	497	14	11
U1127-1 37	0.72	0.64306	5.010	0.07973	4.352	0.87	0.05850	2.481	548	54	504	20	494	21	10
U1127-1 10	0.90	0.63229	6.769	0.07965	5.248	0.78	0.05757	4.276	513	94	498	27	494	25	4
U1127-1 39	0.42	0.63150	5.193	0.07951	4.096	0.79	0.05760	3.193	515	70	497	20	493	19	4
U1127-1 31	0.48	0.62016	5.641	0.07951	5.197	0.92	0.05657	2.193	475	48	490	22	493	25	-4
U1127-1 27	0.57	0.61849	5.407	0.07925	4.001	0.74	0.05660	3.637	476	80	489	21	492	19	-3
U1127-1 32	0.77	0.64457	4.306	0.07919	3.383	0.79	0.05903	2.664	568	58	505	17	491	16	14
U1127-1 3	1.47	0.62436	5.084	0.07911	3.359	0.66	0.05724	3.816	501	84	493	20	491	16	2

U1127-1 11	0.42	0.62386	4.894	0.07906	3.367	0.69	0.05723	3.552	500	78	492	19	491	16	2
U1127-1 31	0.37	0.59470	5.350	0.07896	3.843	0.72	0.05463	3.722	397	83	474	20	490	18	-23
U1127-1 29	0.65	0.61519	5.182	0.07892	3.691	0.71	0.05653	3.636	473	80	487	20	490	17	-3
U1127-1 29	0.37	0.64029	8.208	0.07887	7.282	0.89	0.05888	3.788	563	83	502	33	489	34	13
U1127-1 40	1.20	0.59676	5.278	0.07880	3.489	0.66	0.05492	3.961	409	89	475	20	489	16	-20
U1127-1 41	0.62	0.63239	4.266	0.07880	3.323	0.78	0.05821	2.675	538	59	498	17	489	16	9
U1127-1 37	0.57	0.62264	4.819	0.07870	3.283	0.68	0.05738	3.527	506	78	491	19	488	15	3
U1127-1 23	1.01	0.62780	4.812	0.07852	3.093	0.64	0.05799	3.687	529	81	495	19	487	15	8
U1127-1 36	0.43	0.61549	4.827	0.07827	3.576	0.74	0.05703	3.241	493	71	487	19	486	17	1
U1127-1 35	0.44	0.60760	4.607	0.07825	2.740	0.59	0.05631	3.704	465	82	482	18	486	13	-5
U1127-1 32	0.35	0.60695	4.399	0.07791	3.577	0.81	0.05650	2.560	472	57	482	17	484	17	-2
U1127-1 4	0.54	0.63267	5.742	0.07784	4.428	0.77	0.05895	3.655	565	80	498	23	483	21	14
U1127-1 30	0.63	0.59771	4.798	0.07784	3.283	0.68	0.05569	3.498	440	78	476	18	483	15	-10
U1127-1 18	0.63	0.59816	5.681	0.07782	3.873	0.68	0.05575	4.156	442	92	476	22	483	18	-9
U1127-1 5	0.67	0.65130	6.684	0.07781	5.324	0.80	0.06071	4.041	629	87	509	27	483	25	23
U1127-1 34	0.48	0.60484	4.924	0.07762	3.934	0.80	0.05651	2.960	473	65	480	19	482	18	-2
U1127-1 20	0.63	0.62053	7.299	0.07762	3.848	0.53	0.05798	6.202	529	136	490	28	482	18	9
U1127-1 20	0.65	0.59428	6.881	0.07752	5.540	0.81	0.05560	4.081	437	91	474	26	481	26	-10
U1127-1 18	1.00	0.64176	11.223	0.07691	9.023	0.80	0.06052	6.674	622	144	503	45	478	42	23
U1127-1 15B	0.84	0.61094	6.594	0.07671	3.093	0.47	0.05776	5.824	521	128	484	25	476	14	8
U1127-1 24	0.68	0.62918	4.350	0.07656	3.383	0.78	0.05960	2.734	589	59	496	17	476	16	19
U1127-1 22	1.32	0.62301	6.342	0.07632	4.283	0.68	0.05921	4.678	575	102	492	25	474	20	18
U1127-1 1	1.91	0.66112	11.682	0.07512	3.691	0.32	0.06383	11.083	736	235	515	47	467	17	37
U1127-1 13	0.59	0.64176	7.164	0.07301	6.137	0.86	0.06375	3.696	733	78	503	28	454	27	38
U1127-1 27	0.75	0.58056	9.664	0.06989	8.691	0.90	0.06025	4.225	613	91	465	36	435	37	29
U1127-1 11	0.66	0.51038	5.511	0.06936	4.377	0.79	0.05337	3.347	345	76	419	19	432	18	-25
U1127-1 25	0.67	0.50902	6.374	0.05758	5.792	0.91	0.06411	2.661	745	56	418	22	361	20	52

May 10, 2012

Isotope ratio and date errors include systematic calibration errors of 0.38% ($^{207}Pb/^{206}Pb$), 0.84% ($^{206}Pb/^{238}U$) (2 sigma).
Trace element concentrations were deleted from analyses known to have intersected inclusions of other minerals based on P and Ti.

Ablation used a laser spot size of 25 microns, and a laser firing repetition rate of 10 Hz.

Activity of TiO_2 for Ti-in-Zircon temperature calculation is 0.8.

May 15, 2012
Isotope ratio and date errors include systematic calibration errors of 0.11% ($^{207}Pb/^{206}Pb$), 0.46% ($^{206}Pb/^{238}U$) (2 sigma).
Trace element concentrations were deleted from analyses known to have intersected inclusions of other minerals based on P and Ti.

Ablation used a laser spot size of 25 microns, and a laser firing repetition rate of 10 Hz.
Activity of TiO_2 for Ti-in-Zircon temperature calculation is 0.8.

LA-ICPMS data from sample U1127-1 continued.

	Concentrations (ppm)																						
Analysis	P	Ti	Y	Nb	La	Ce	Pr	Nd	Sm	Eu	Gd	Tb	Dy	Ho	Er	Tm	Yb	Lu	Hf	Ta	Th	U	T(°C)
U1127-1 13	181	19.86	419	1.47		11.35	0.14	1.51	3.32	0.35	13.69	3.94	46.3	15.14	63.4	16.6	178	20.1	8349	0.46	23.5	20	872
U1127-1 21	101	3.01	279	2.22		2.52	0.06	0.99	1.85	0.35	7.35	2.71	31.2	10.73	46.6	12.9	169	25.2	8532	0.93	15.4	19	685
U1127-1 4	227	13.13	755	2.56		25.82	0.04	1.41	3.43	0.63	15.93	6.07	74.4	26.92	117.3	29.4	316	38.6	11227	1.41	114.2	105	825
U1127-1 5	197	19.98	808	1.09	0.04	17.30	0.18	2.58	4.06	0.97	21.95	7.22	83.2	29.51	117.6	29.2	290	35.9	10634	0.53	64.3	44	873
U1127-1 40	208	11.99	1004	0.91	0.10	10.74	0.10	2.14	4.15	1.61	20.23	7.73	93.1	34.46	155.0	41.1	499	58.3	6955	0.33	47.9	60	815
U1127-1 36	178	8.25	642	0.61		10.60	0.08	1.89	4.06	1.00	19.23	5.46	65.3	23.69	100.6	26.2	306	35.3	8023	0.35	56.1	62	777
U1127-1 30	261	12.86	1080	1.35		16.50	0.15	2.54	5.90	1.03	28.14	8.59	105.8	40.14	175.0	43.6	497	63.1	8254	0.82	104.1	104	823
U1127-1 35	230	8.48	1145	0.95		3.10	0.06	1.97	4.90	0.62	26.12	9.62	121.2	45.06	183.7	46.4	527	58.7	7589	0.69	40.8	103	779
U1127-1 34	560	11.18	1398	1.20		1.80	0.09	1.47	4.94	0.36	30.25	10.90	150.6	51.86	216.7	54.1	598	67.9	9279	0.70	40.8	142	808

U1127-112	1102	12.53	2593	1.44	5.18	21.74	1.48	8.87	10.45	1.85	58.09	21.46	259.3	94.12	397.0	99.3	1093	119.8	9281	0.92	134.6	145	820
U1127-16	199	8.72	729	1.13	0.01	12.24	0.08	0.62	2.86	0.55	15.98	5.46	66.0	25.25	119.9	31.8	369	49.3	10404	0.90	71.2	90	782
U1127-142	277	7.60	1031	2.64	0.01	16.96	0.12	2.57	5.23	1.94	27.46	8.60	103.7	36.95	150.9	39.3	459	54.7	7807	1.08	96.1	98	769
U1127-13	137	7.30	832	0.61	0.11	15.83	0.12	2.04	5.04	1.42	19.11	6.28	73.9	27.56	126.8	35.5	417	61.1	11732	0.41	154.4	114	765
U1127-139	197	11.43	661	0.66	0.03	9.67	0.02	0.86	2.43	0.61	13.77	5.08	62.9	23.28	101.3	26.3	290	37.6	10044	0.53	44.1	45	810
U1127-12	186	15.46	741	0.89	0.01	12.03	0.05	1.46	3.38	0.54	14.81	5.90	72.6	26.39	117.0	29.3	307	42.7	11270	0.72	50.5	43	843
U1127-114	255	8.43	997	0.78	0.01	15.66	0.11	2.32	5.33	1.16	24.94	8.75	100.7	35.45	150.2	38.4	424	45.9	7888	0.44	80.5	78	779
U1127-141	163	4.25	386	0.51	0.10	6.08	0.11	0.59	1.36	0.48	6.22	2.53	35.0	13.10	64.4	17.9	222	28.4	9127	0.45	23.4	89	715
U1127-19	147	6.14	662	1.21	0.01	8.68	0.03	0.92	2.81	0.65	12.36	4.21	54.9	22.13	104.3	30.0	380	45.9	7759	0.72	72.8	177	748
U1127-11	263	10.84	1524	1.33		13.81	0.21	3.26	7.40	1.56	41.59	14.13	167.2	58.92	236.3	58.3	633	66.5	7463	0.74	132.7	115	805
U1127-125	262	5.01	755	2.61	0.19	15.25	0.03	0.54	2.18	0.91	13.34	5.62	71.5	27.92	122.9	36.2	445	52.5	8689	1.07	121.2	180	729
U1127-128	189	9.66	794	1.04	0.00	8.15	0.06	1.39	3.95	0.67	19.19	6.38	82.1	29.81	130.8	32.9	380	45.4	8387	0.61	68.0	130	793
U1127-12	168	8.76	965	0.72	0.05	11.01	0.16	2.61	5.09	0.87	24.87	8.20	93.8	33.96	140.3	35.5	393	43.7	8065	0.53	119.1	163	783
U1127-126	148	3.74	459	1.25	0.05	11.42	0.02	0.48	1.49	0.35	7.08	2.67	35.8	15.03	76.5	22.5	282	39.0	9989	1.01	109.6	186	703
U1127-138	156	4.81	547	2.48	0.04	19.78	0.01	0.51	1.72	0.28	9.85	3.49	47.2	19.37	90.1	25.3	299	40.3	11650	1.55	114.9	280	726
U1127-143	119	13.60	284	0.88	0.08	4.12	0.01	0.56	1.46	0.15	6.06	2.07	26.4	9.68	42.1	11.7	143	16.2	7024	0.51	46.6	120	829
U1127-117	109	3.98	280	1.36		11.19		0.29	0.81	0.43	5.27	1.48	23.1	9.22	46.3	14.0	186	24.6	10745	0.87	67.3	142	709
U1127-133	174	6.79	556	1.20		7.20	0.05	0.76	2.02	0.55	9.77	3.70	50.3	19.20	92.5	26.9	331	40.7	9157	0.92	42.0	90	758
U1127-124	277	6.88	777	2.19		18.80	0.04	1.64	3.04	1.63	17.26	5.58	76.6	28.98	130.8	36.8	461	55.2	7226	0.80	93.4	90	759
U1127-1	198	5.9	633	0.5		4.7	0.0	1.5	2.5	0.3	11.	4.3	55.	20.	98.	28.	354	42.	822	0.4	54.	17	745

16		2		1		7	8	8	5	6	81	2	7	66	3	9		0	7	0	1	8	
U1127-16	121	5.26	2084	7.06	0.03	11.91	0.49	7.98	15.70	0.17	67.74	22.26	247.3	83.45	329.1	75.6	733	74.8	6127	2.37	179.3	382	734
U1127-17	208	22.25	2139	1.72	0.07	9.29	0.54	8.88	14.76	1.12	65.57	20.26	228.1	77.93	317.1	75.6	758	88.4	8203	0.90	369.4	410	886
U1127-116	286	4.77	1029	3.20	0.10	15.89	0.03	1.00	3.12	1.04	19.17	7.22	96.9	37.31	167.3	46.5	553	73.1	9850	1.52	118.3	195	725
U1127-133	223	3.59	772	2.68	0.07	16.61	0.08	1.28	2.40	0.67	14.46	5.05	67.8	26.69	127.3	35.4	441	58.1	9459	1.69	218.8	344	700
U1127-18	422	9.64	1927	3.98		42.85	0.17	2.55	6.29	2.66	37.11	13.61	177.5	68.87	314.4	85.0	964	122.2	9237	1.24	293.0	209	793
U1127-114B	197	6.84	666	1.97	0.07	15.14	0.13	1.27	2.15	0.92	11.97	4.06	57.4	22.53	108.1	32.2	420	54.2	8971	1.00	113.6	182	758
U1127-137	160	13.56	1347	1.00	0.05	10.27	0.46	7.33	11.53	0.85	41.95	12.44	140.9	48.89	194.1	48.8	518	57.1	7702	0.75	269.8	374	829
U1127-110	309	12.35	1279	3.41	0.07	38.32	0.13	2.69	5.66	2.25	26.94	9.33	121.2	45.53	204.9	55.8	635	75.0	6372	1.25	83.4	92	819
U1127-139	136	5.70	377	0.77	0.03	7.67	0.05	0.57	1.23	0.30	7.36	2.44	32.0	13.00	59.2	16.6	200	24.7	8379	0.45	55.9	133	741
U1127-131	348	6.43	659	2.30	0.67	22.39	0.25	2.05	2.82	0.56	12.82	4.39	58.1	22.74	103.8	29.0	344	43.7	8991	1.03	125.0	258	752
U1127-127	207	11.52	759	0.88	0.10	9.02	0.07	1.34	3.74	0.60	19.61	6.46	73.5	26.92	115.7	30.0	328	35.9	8526	0.60	70.8	124	811
U1127-132	226	8.17	843	1.97		19.16	0.08	1.23	2.82	0.82	16.25	5.53	74.0	28.95	136.9	37.7	448	56.9	8450	1.21	136.4	178	776
U1127-13	388	6.81	1029	3.51	0.11	24.16	0.13	1.78	4.29	1.17	20.56	7.19	92.8	35.95	159.6	45.6	519	61.5	7715	1.39	143.4	97	758
U1127-131	241	4.59	273	0.61	1.06	7.84	0.29	1.60	0.85	0.18	4.61	1.78	24.2	9.30	44.9	13.5	164	19.9	9467	0.40	47.8	128	721
U1127-129	174	7.74	506	1.41		19.01		0.50	2.12	0.54	8.83	3.30	42.8	17.37	82.0	23.3	299	35.0	8559	1.00	103.6	160	770
U1127-129	102	5.74	254	0.69		6.13		0.36	0.59	0.10	3.08	1.59	20.6	8.49	40.2	11.7	143	18.0	9798	0.40	34.5	93	742
U1127-140	258	12.85	1620	0.86		14.70	0.15	4.87	9.62	1.73	45.10	14.75	176.0	63.04	255.1	60.0	594	74.2	11066	0.74	141.0	117	823
U1127-141	150	7.33	967	1.05	0.37	13.25	0.39	6.11	8.24	2.11	31.71	9.00	101.5	34.29	138.8	34.2	349	45.7	10303	0.81	141.7	229	765
U1127-137	209	12.23	615	0.93		11.64	0.07	1.44	2.88	0.66	14.49	5.12	60.2	21.74	96.8	25.5	293	35.4	9440	0.68	98.6	172	818

U1127-123	136	5.63	675	0.71		8.31	0.11	2.33	4.75	1.65	16.71	5.96	68.1	25.35	106.7	29.1	334	42.1	8585	0.43	81.3	80	740
U1127-136	253	11.27	926	1.22		9.90	0.12	1.28	4.16	0.64	21.73	7.30	89.7	32.35	142.3	37.3	410	48.7	8912	0.74	92.0	216	809
U1127-135	129	15.80	375	1.22		4.79		0.81	2.03	0.23	8.61	2.92	36.4	12.72	56.9	15.4	178	21.0	8075	0.63	73.6	166	846
U1127-132	166	4.73	597	1.79	0.00	10.78	0.00	1.19	2.76	0.51	13.53	4.49	55.8	21.36	93.0	26.3	306	34.9	8114	1.08	148.1	425	724
U1127-130	246	7.60	869	2.61	0.10	16.94	0.01	0.98	2.86	0.56	16.27	6.48	79.6	30.39	142.8	40.2	472	53.9	9007	1.75	107.5	170	769
U1127-134	230	9.23	646	1.56		13.34	0.10	0.88	2.97	0.65	15.08	5.27	65.2	23.51	101.9	29.2	332	39.1	8791	0.97	113.0	235	788
U1127-120	182	12.99	656	0.70		7.61	0.01	1.60	3.34	0.57	16.24	5.25	66.1	24.01	100.7	26.8	284	30.8	8690	0.47	56.1	89	824
U1127-120	87	13.48	970	1.29	0.12	3.60	0.32	5.31	9.29	0.41	33.72	10.76	113.5	35.58	150.1	35.9	361	41.7	5910	0.50	54.6	85	828
U1127-118	345	11.63	1198	1.01		9.48	0.10	1.97	4.98	1.23	28.55	9.72	112.3	41.66	178.8	43.8	488	55.9	7694	0.67	46.0	46	812
U1127-15B	283	9.52	931	1.37	0.02	8.75	0.07	1.53	2.87	1.27	17.46	6.82	90.8	33.85	150.4	41.8	490	59.4	7973	0.62	41.9	50	791
U1127-124	313	7.07	1716	4.35	0.07	19.00	0.17	2.07	6.64	1.79	33.11	12.79	159.7	62.49	279.5	74.7	865	108.0	8185	1.58	189.2	277	762
U1127-122	233	43.56	1193	1.27	0.03	25.21	0.34	6.83	12.00	4.21	41.85	11.89	132.5	43.40	175.6	43.7	487	60.7	6810	0.48	133.9	101	974
U1127-113	610	69.48	1813	2.59	0.15	17.99	0.34	5.13	10.61	4.24	53.67	17.38	195.0	65.10	269.6	68.9	800	95.6	7366	1.00	126.0	212	1043
U1127-111	228	10.68	1778	1.30	0.09	6.30	0.20	4.56	10.89	3.16	54.08	17.69	208.3	71.13	283.4	66.5	707	76.4	6903	0.48	63.8	97	803
U1127-125	502	11.16	1803	5.08	0.31	38.01	0.44	4.47	11.26	4.59	46.32	17.20	192.0	61.02	254.8	69.0	760	98.5	9867	2.22	266.8	396	808

LA-ICPMS data from sample U1121-17.5

		Corrected isotope ratios							Dates (Ma)						
		207Pb*	±2s	206Pb*	±2s	error	207Pb*	±2s	207Pb*	±2s	207Pb*	±2s	206Pb*	±2s	%
Analysis	Th/U	235U*	(%)	238U	(%)	corr.	206Pb*	(%)	206Pb*	(Ma)	235U	(Ma)	238U*	(Ma)	disc.
U1121-17.5 38	1.03	12.20046	5.056	0.50062	3.713	0.73	0.17675	3.431	2623	57	2620	47	2616	80	0
U1121-17.5 53	0.61	11.54308	4.531	0.48616	3.870	0.85	0.17220	2.356	2579	39	2568	42	2554	82	1
U1121-17.5 183	0.56	10.73462	3.045	0.46865	2.790	0.92	0.16613	1.221	2519	21	2500	28	2478	57	2
U1121-17.5 93	1.16	10.38129	8.363	0.46220	7.884	0.94	0.16290	2.788	2486	47	2469	77	2449	161	1
U1121-17.5 44	1.81	9.30553	4.055	0.43003	3.378	0.83	0.15694	2.243	2423	38	2369	37	2306	65	5
U1121-17.5 78	0.64	7.46838	4.738	0.39697	4.081	0.86	0.13645	2.406	2183	42	2169	42	2155	75	1
U1121-17.5 25	0.54	5.40971	4.737	0.30318	4.371	0.92	0.12941	1.825	2090	32	1886	41	1707	66	18
U1121-17.5 181	1.49	6.08715	3.395	0.34783	3.005	0.89	0.12692	1.579	2056	28	1988	30	1924	50	6
U1121-17.5 74	1.79	6.36128	5.034	0.36656	4.769	0.95	0.12586	1.611	2041	28	2027	44	2013	82	1
U1121-17.5 28	0.20	6.05272	3.959	0.35063	3.495	0.88	0.12520	1.860	2032	33	1983	34	1938	58	5
U1121-17.5 180	1.62	6.07353	5.666	0.35500	4.939	0.87	0.12408	2.777	2016	49	1986	49	1958	83	3
U1121-17.5 92	1.35	5.66051	4.510	0.33433	3.821	0.85	0.12279	2.397	1997	43	1925	39	1859	62	7
U1121-17.5 91	0.71	1.47457	9.051	0.15372	6.857	0.76	0.06957	5.909	916	122	920	55	922	59	-1
U1121-17.5 46	1.62	1.35181	7.003	0.14029	4.600	0.66	0.06989	5.279	925	108	868	41	846	36	9
U1121-17.5 29	0.84	1.20094	7.943	0.13889	5.193	0.65	0.06271	6.009	698	128	801	44	838	41	-20
U1121-17.5 39	0.87	1.28693	3.717	0.13750	2.365	0.64	0.06788	2.867	865	59	840	21	830	18	4
U1121-17.5 43	0.82	1.24663	5.387	0.13728	4.219	0.78	0.06586	3.350	802	70	822	30	829	33	-3
U1121-17.5 35	0.93	1.21791	3.500	0.13525	2.700	0.77	0.06531	2.227	784	47	809	20	818	21	-4
U1121-17.5 54	0.69	1.23482	4.923	0.13398	4.038	0.82	0.06684	2.815	833	59	817	28	811	31	3
U1121-17.5 48	0.81	1.23951	4.341	0.13388	2.985	0.69	0.06715	3.152	842	66	819	24	810	23	4
U1121-17.5 31	0.84	1.22639	3.894	0.13361	3.052	0.78	0.06657	2.419	824	50	813	22	808	23	2
U1121-17.5 50	0.99	1.20689	3.266	0.13313	2.711	0.83	0.06575	1.820	798	38	804	18	806	21	-1
U1121-17.5 67	1.56	1.22682	7.465	0.13265	5.303	0.71	0.06707	5.254	840	109	813	42	803	40	4
U1121-17.5 41	0.76	1.22334	5.979	0.13259	3.685	0.62	0.06692	4.708	835	98	811	33	803	28	4
U1121-17.5 37	1.51	1.21256	7.648	0.13228	5.444	0.71	0.06648	5.371	822	112	806	43	801	41	3
U1121-17.5 42	1.66	1.18746	4.681	0.13210	3.087	0.66	0.06519	3.518	781	74	795	26	800	23	-2

U1121-17.5 33	0.91	1.18375	3.837	0.13163	3.268	0.85	0.06523	2.012	782	42	793	21	797	25	-2
U1121-17.5 57	0.67	1.18494	4.455	0.13104	3.606	0.81	0.06558	2.616	793	55	794	25	794	27	0
U1121-17.5 52	1.02	1.17063	4.392	0.13099	3.841	0.87	0.06481	2.130	768	45	787	24	794	29	-3
U1121-17.5 85	0.72	1.16765	4.718	0.13028	4.247	0.90	0.06500	2.056	774	43	786	26	789	32	-2
U1121-17.5 27	1.18	1.17261	5.295	0.13015	3.869	0.73	0.06535	3.615	786	76	788	29	789	29	0
U1121-17.5 32	1.23	1.20512	5.506	0.12997	3.854	0.70	0.06725	3.932	845	82	803	31	788	29	7
U1121-17.5 80	2.12	1.17948	6.189	0.12951	4.185	0.68	0.06605	4.560	808	95	791	34	785	31	3
U1121-17.5 76	0.96	1.17079	3.873	0.12910	3.458	0.89	0.06577	1.744	799	37	787	21	783	25	2
U1121-17.5 88	1.52	1.20127	7.300	0.12880	6.247	0.86	0.06765	3.777	858	78	801	40	781	46	9
U1121-17.5 30	0.94	1.17869	13.367	0.12873	5.609	0.42	0.06641	12.133	819	253	791	73	781	41	5
U1121-17.5 65	1.01	1.18580	5.050	0.12823	4.810	0.95	0.06707	1.539	840	32	794	28	778	35	7
U1121-17.5 89	1.35	1.22548	10.452	0.12801	4.718	0.45	0.06943	9.327	912	192	812	58	776	35	15
U1121-17.5 36	1.57	1.15073	5.154	0.12720	2.922	0.57	0.06561	4.245	794	89	778	28	772	21	3
U1121-17.5 71	0.89	1.15162	4.831	0.12662	4.237	0.88	0.06596	2.319	805	49	778	26	769	31	5
U1121-17.5 56a	1.24	1.19657	7.404	0.12649	5.527	0.75	0.06861	4.927	887	102	799	41	768	40	13
U1121-17.5 82	1.83	1.14569	5.992	0.12649	5.190	0.87	0.06569	2.995	797	63	775	32	768	38	4
U1121-17.5 45	1.78	1.12499	4.771	0.12623	3.300	0.69	0.06464	3.445	763	73	765	26	766	24	0
U1121-17.5 79	0.69	1.06244	8.076	0.12602	4.861	0.60	0.06115	6.449	644	139	735	42	765	35	-19
U1121-17.5 55	1.38	1.13240	5.290	0.12566	3.151	0.60	0.06536	4.249	786	89	769	29	763	23	3
U1121-17.5 62	0.61	1.12965	6.039	0.12548	4.770	0.79	0.06530	3.704	784	78	768	33	762	34	3
U1121-17.5 84	1.67	1.14638	5.469	0.12537	3.341	0.61	0.06632	4.330	816	90	776	30	761	24	7
U1121-17.5 51	2.09	1.12857	5.446	0.12526	4.143	0.76	0.06535	3.534	786	74	767	29	761	30	3
U1121-17.5 75	1.54	1.14162	7.129	0.12480	5.912	0.83	0.06634	3.983	817	83	773	39	758	42	7
U1121-17.5 58	1.46	1.24069	9.011	0.12403	4.936	0.55	0.07255	7.539	1001	153	819	51	754	35	25
U1121-17.5 47	0.86	1.13955	4.008	0.12400	3.463	0.86	0.06665	2.017	827	42	772	22	754	25	9
U1121-17.5 86	0.81	1.14563	4.523	0.12394	3.739	0.83	0.06704	2.546	839	53	775	25	753	27	10
U1121-17.5 49	1.13	1.33560	8.658	0.12357	4.421	0.51	0.07839	7.444	1157	148	861	50	751	31	35
U1121-17.5 73	0.99	1.11843	7.025	0.12348	5.200	0.74	0.06569	4.723	796	99	762	38	751	37	6
U1121-17.5 26	1.14	1.07651	6.356	0.12339	4.317	0.68	0.06327	4.666	718	99	742	33	750	31	-5
U1121-17.5 64	0.81	1.12216	4.488	0.12333	4.060	0.90	0.06599	1.911	806	40	764	24	750	29	7

U1121-17.5 61	1.58	1.07671	6.631	0.12328	4.087	0.62	0.06334	5.222	720	111	742	35	749	29	-4
U1121-17.5 95	0.98	1.16804	4.879	0.12304	4.256	0.87	0.06885	2.386	894	49	786	27	748	30	16
U1121-17.5 94	0.96	1.04169	5.314	0.11973	3.549	0.67	0.06310	3.956	712	84	725	28	729	24	-2
U1121-17.5 59	0.80	1.17647	5.384	0.11947	3.773	0.70	0.07142	3.841	969	78	790	30	728	26	25
U1121-17.5 68	0.83	1.21167	7.445	0.11894	5.012	0.67	0.07389	5.506	1038	111	806	41	724	34	30
U1121-17.5 72	1.30	1.12455	5.862	0.11890	5.121	0.87	0.06860	2.852	887	59	765	32	724	35	18
U1121-17.5 69	2.37	1.08572	7.020	0.11825	4.622	0.66	0.06659	5.284	825	110	746	37	721	32	13
U1121-17.5 70	1.93	1.07542	6.671	0.11782	5.329	0.80	0.06620	4.013	813	84	741	35	718	36	12
U1121-17.5 60a	0.70	1.07356	5.954	0.11655	5.119	0.86	0.06681	3.041	832	63	740	31	711	34	15
U1121-17.5 81	3.24	1.06538	6.146	0.11266	3.648	0.59	0.06859	4.946	886	102	736	32	688	24	22
U1121-17.5 63	1.82	1.00293	6.058	0.10541	3.746	0.62	0.06901	4.761	899	98	705	31	646	23	28

LA-ICPMS data from sample U1121-17.5 continued.

	Concentrations (ppm)																					
Analysis	P	Ti	Y	Nb	La	Ce	Pr	Nd	Sm	Eu	Gd	Tb	Dy	Ho	Er	Tm	Yb	Lu	Hf	Ta	Th	U	T(°C)
U1121-17.5 38	200	6.10	669	1.06	0.04	20.40	0.32	6.68	6.80	2.05	25.51	7.82	76.99	25.88	98.8	22.1	206	30.5	9056	0.53	45.2	44	747
U1121-17.5 53	187	4.54	876	2.05	0.19	3.89	0.06	2.21	4.65	1.25	24.54	8.24	94.9	31.50	128.3	28.5	271	37.7	8928	0.87	19.2	31	720
U1121-17.5 183	200	19.32	590	3.27		7.13	0.07	1.57	3.41	0.07	15.75	5.17	59.4	20.93	87.5	22.0	235	25.6	8106	1.45	147.6	266	869
U1121-17.5 44	271	6.14	772	1.12	0.16	14.07	0.11	2.08	3.89	0.26	23.38	6.95	76.6	27.78	114.8	26.1	239	35.5	11534	0.36	94.4	52	748
U1121-17.5 181	193	16.21	337	2.94	0.14	37.39	0.21	3.75	5.89	1.12	18.69	4.95	46.0	12.30	43.9	9.8	98	9.7	7730	0.96	204.2	137	849
U1121-17.5 74	186	15.91	810	2.12	0.12	40.65	0.51	8.13	12.50	2.87	39.59	10.26	95.4	29.44	110.8	24.3	226	31.6	10142	1.15	250.4	140	847
U1121-17.5 28	205	6.19	353	2.00		3.69	0.02	0.48	3.04	0.12	18.40	6.02	54.0	12.87	34.0	5.8	45	5.1	11846	1.83	42.8	216	749
U1121-17.5 180	186	31.26	798	2.06		27.69	0.51	8.09	12.95	2.84	44.52	11.25	104.0	30.30	106.4	25.0	257	25.8	7771	0.84	84.0	52	929
U1121-17.5 92	77	7.10	384	1.29	0.14	28.71	0.51	6.18	7.85	1.49	21.75	5.29	49.5	14.24	49.6	10.0	104	13.4	9344	0.42	150.8	112	762

U1121-17.5 91	411	6.53	1405	1.77		12.88	0.06	1.10	2.66	0.56	21.27	8.10	106.0	47.53	234.4	62.0	704	101.2	9102	0.72	51.1	71	754
U1121-17.5 29	180	6.28	724	0.88	0.06	12.64	0.10	1.31	3.77	0.98	16.41	5.41	64.2	25.27	118.0	29.9	323	47.1	8781	0.39	39.5	47	750
U1121-17.5 43	168	5.97	1585	2.56	0.02	6.89	0.23	4.31	7.31	0.73	40.69	14.10	159.8	58.84	242.0	54.6	503	72.6	7900	1.45	84.2	103	745
U1121-17.5 54	195	6.74	1234	2.71	0.42	7.59	0.26	3.71	6.01	0.60	30.95	10.71	126.7	47.35	198.2	44.9	440	59.9	8169	1.44	69.5	101	757
U1121-17.5 41	192	14.85	1449	1.21		5.56	0.22	3.11	5.53	1.46	35.38	10.65	131.1	48.09	210.8	48.4	480	75.4	8786	0.73	65.6	87	839
U1121-17.5 37	318	8.62	2064	1.46		26.77	0.30	4.56	10.45	3.26	50.38	17.22	204.0	76.41	325.3	75.2	745	109.9	10154	0.63	111.4	74	781
U1121-17.5 42	338	5.91	2245	1.77		45.37	0.12	2.39	7.31	2.41	48.67	17.03	201.9	79.52	352.5	85.2	805	124.2	10933	0.83	154.6	93	744
U1121-17.5 57	190	5.08	1927	3.74	0.12	8.48	0.29	4.02	8.72	0.94	46.11	16.57	193.4	72.36	305.2	72.1	721	89.8	7570	1.68	172.4	257	730
U1121-17.5 85	267	4.47	2245	11.90	0.34	23.83	0.34	4.66	8.85	0.79	49.39	18.92	234.6	84.41	346.1	82.9	766	98.6	9450	4.11	232.0	324	719
U1121-17.5 27	453	12.39	1524	2.11	0.43	23.04	0.26	3.20	5.71	2.31	32.70	12.25	151.9	57.43	250.7	62.3	658	86.3	6472	0.75	71.7	61	819
U1121-17.5 32	683	10.82	2152	2.43	0.08	33.14	0.17	4.02	8.50	3.00	47.43	16.81	207.8	80.32	338.9	80.0	810	111.2	8689	1.00	74.1	60	805
U1121-17.5 76	424	4.73	4575	11.54	8.25	45.68	2.89	24.34	21.98	2.29	109.10	40.28	445.5	164.46	723.4	153.4	1341	187.6	10083	3.83	430.6	447	724
U1121-17.5 30	320	13.18	832	0.86	0.04	11.63	0.07	0.33	2.36	0.89	16.11	5.83	78.1	29.71	133.0	35.1	376	52.1	8540	0.40	27.3	29	826
U1121-17.5 65	166	3.80	476	2.25	0.54	22.84	0.17	1.37	2.31	0.61	9.86	3.16	40.7	15.69	77.4	20.9	255	38.6	10033	1.56	211.3	209	705
U1121-17.5 56a	370	9.93	2113	2.22	0.11	37.44	0.25	4.09	10.25	3.28	49.40	17.05	215.4	81.50	350.5	83.0	835	115.8	8999	0.88	116.3	94	796
U1121-17.5 45	660	15.95	3000	4.52		51.33	0.17	4.21	9.65	3.16	57.38	20.79	277.8	111.36	477.5	113.4	1172	183.1	9055	1.47	289.2	162	847
U1121-17.5 79	211	9.16	995	1.08		3.95	0.03	1.08	3.44	1.43	19.72	7.34	86.8	35.44	160.6	39.0	390	65.0	8386	0.35	27.3	39	787
U1121-17.5 51	876	18.63	2299	3.51	2.51	54.51	1.08	9.11	10.09	4.12	52.85	17.47	222.5	87.74	370.8	85.8	869	124.4	8136	1.09	263.0	126	865
U1121-17.5 47	578	12.18	3553	11.43	8.33	55.97	2.77	19.45	16.45	1.50	81.79	29.26	363.0	134.84	557.3	120.2	1105	155.1	9455	3.33	355.5	414	817
U1121-	14	7.8	15	0.3	0.0	4.5	0.1	2.7	7.8	1.4	36.7	12.	151	57.3	247	57.	55	73.	927	0.1	97.	12	771

17.5 86	9	2	75	1	4	1	4	4	0	8	0	80	.7	2	.0	3	3	9	0	8	0	0	
U1121-17.5 49	233	37.45	866	1.26	0.02	15.11	0.10	1.84	3.84	1.05	17.46	6.39	82.4	31.64	137.4	34.8	355	51.2	9366	0.68	43.0	38	953
U1121-17.5 73	275	11.85	905	1.05	0.06	17.39	0.06	1.45	2.44	1.02	17.94	6.91	85.0	33.47	150.2	38.2	394	56.7	8894	0.50	40.6	41	814
U1121-17.5 26	301	9.02	950	2.12	0.12	28.51	0.10	1.53	3.07	0.97	19.11	6.60	86.7	35.49	156.9	39.8	441	58.0	8558	0.91	104.0	91	786
U1121-17.5 64	312	9.22	2608	4.99	2.25	14.00	0.94	9.53	13.55	0.99	71.82	23.97	286.2	102.56	414.4	91.2	890	105.5	6802	1.66	373.2	464	788
U1121-17.5 95	421	5.70	1475	6.24	0.38	51.63	0.24	2.32	4.96	1.22	25.89	9.69	130.4	53.90	241.5	62.3	707	93.5	9631	2.00	187.7	192	741
U1121-17.5 94	271	8.09	874	2.13		21.66	0.06	0.87	2.83	0.73	17.47	6.53	80.3	32.08	149.5	37.7	414	56.1	8439	0.72	72.7	76	775
U1121-17.5 69	458	22.18	3136	2.36	0.04	58.31	0.58	10.78	16.84	8.55	89.72	28.15	336.8	119.72	503.5	115.4	1166	151.5	7382	0.67	227.7	96	886
U1121-17.5 70	266	20.38	1891	0.84	0.09	23.27	0.41	7.51	14.70	5.69	64.85	19.56	210.8	71.99	289.2	64.6	631	83.6	7548	0.42	133.6	69	875
U1121-17.5 60a	313	8.45	1614	3.90	0.06	18.13	0.24	2.55	5.59	0.95	31.26	11.02	151.9	55.70	250.3	65.9	691	91.1	7747	1.73	195.3	278	779

May 11, 2012
Isotope ratio and date errors include systematic calibration errors of 0.26% ($^{207}Pb/^{206}Pb$), 0.54% ($^{206}Pb/^{238}U$) (2 sigma).
Trace element concentrations were deleted from analyses known to have intersected inclusions of other minerals based on P and Ti.

Ablation used a laser spot size of 25 microns, and a laser firing repetition rate of 10 Hz.

Activity of TiO_2 for Ti-in-Zircon temperature calculation is 0.8.

May 14, 2012
Isotope ratio and date errors include systematic calibration errors of 0.27% ($^{207}Pb/^{206}Pb$), 0.71% ($^{206}Pb/^{238}U$) (2 sigma).
Trace element concentrations were deleted from analyses known to have intersected inclusions of other minerals based on P and Ti.

Ablation used a laser spot size of 25 microns, and a laser firing repetition rate of 10 Hz.

Activity of TiO_2 for Ti-in-Zircon temperature calculation is 0.8.

LA-ICPMS data from sample U1331

		Corrected isotope ratios							Dates (Ma)						
		207Pb*	±2s	206Pb*	±2s	error	207Pb*	±2s	207Pb*	±2s	207Pb*	±2s	206Pb*	±2s	%
Analysis	Th/U	235U*	(%)	238U	(%)	corr.	206Pb*	(%)	206Pb*	(Ma)	235U	(Ma)	238U*	(Ma)	disc.
U1331 363	0.87	15.61128	8.528	0.49326	7.847	0.92	0.22954	3.340	3049	53	2853	81	2585	167	15
U1331 312	0.33	15.45599	8.647	0.52577	7.475	0.86	0.21320	4.348	2930	70	2844	82	2724	166	7
U1331 377	0.64	12.70710	5.578	0.51015	4.792	0.86	0.18065	2.855	2659	47	2658	53	2657	104	0
U1331 412	1.23	12.00946	3.969	0.50258	3.803	0.96	0.17331	1.137	2590	19	2605	37	2625	82	-1
U1331 344	0.78	9.73291	4.553	0.44403	3.985	0.88	0.15898	2.202	2445	37	2410	42	2369	79	3
U1331 360	0.43	9.05672	5.679	0.41799	4.555	0.80	0.15714	3.392	2425	58	2344	52	2251	87	7
U1331 342	0.46	9.72239	4.581	0.45058	3.905	0.85	0.15650	2.396	2418	41	2409	42	2398	78	1
U1331 381	1.77	8.80019	3.805	0.40925	3.409	0.90	0.15596	1.691	2412	29	2318	35	2211	64	8
U1331 345	0.74	9.13517	4.957	0.42800	4.357	0.88	0.15480	2.364	2400	40	2352	45	2297	84	4
U1331 330	0.43	8.04994	3.421	0.40551	3.201	0.94	0.14397	1.207	2276	21	2237	31	2194	60	4
U1331 333	0.82	8.32169	3.660	0.42879	3.284	0.90	0.14076	1.615	2237	28	2267	33	2300	64	-3
U1331 314	0.64	8.09649	8.502	0.42117	7.711	0.91	0.13942	3.580	2220	62	2242	77	2266	147	-2
U1331 390	0.84	6.82131	5.225	0.35498	4.937	0.94	0.13937	1.710	2219	30	2088	46	1958	83	12
U1331 368	0.75	7.47410	4.102	0.40200	3.921	0.96	0.13484	1.203	2162	21	2170	37	2178	72	-1
U1331 365	0.48	7.34231	4.526	0.39898	3.178	0.70	0.13347	3.222	2144	56	2154	40	2164	58	-1
U1331 309	0.55	5.58213	5.068	0.31149	4.378	0.86	0.12997	2.552	2098	45	1913	44	1748	67	17
U1331 327	1.14	6.52265	5.919	0.36876	5.717	0.97	0.12829	1.532	2075	27	2049	52	2024	99	2
U1331 398	1.40	6.59566	4.879	0.38135	4.388	0.90	0.12544	2.134	2035	38	2059	43	2083	78	-2
U1331 403	0.12	6.42375	4.714	0.37795	4.346	0.92	0.12327	1.826	2004	32	2036	41	2067	77	-3
U1331 354	0.25	5.85359	4.331	0.35182	3.914	0.90	0.12067	1.855	1966	33	1954	38	1943	66	1
U1331 384	1.27	5.49216	3.407	0.33192	2.695	0.79	0.12001	2.084	1956	37	1899	29	1848	43	6
U1331 407	1.28	5.64550	7.832	0.34570	7.407	0.95	0.11844	2.545	1933	46	1923	68	1914	123	1
U1331 402	0.67	4.95810	3.587	0.30528	3.039	0.85	0.11779	1.906	1923	34	1812	30	1717	46	11
U1331 316	1.01	5.59880	4.767	0.34828	4.245	0.89	0.11659	2.167	1905	39	1916	41	1926	71	-1
U1331 310	0.79	5.62697	11.298	0.35623	10.887	0.96	0.11456	3.021	1873	54	1920	97	1964	184	-5
U1331 302	0.62	5.12698	4.012	0.32550	3.611	0.90	0.11424	1.749	1868	32	1841	34	1817	57	3

U1331 378	1.31	5.20856	4.680	0.33088	4.439	0.95	0.11417	1.482	1867	27	1854	40	1843	71	1
U1331 313	0.72	5.30367	7.203	0.33906	6.462	0.90	0.11345	3.180	1855	57	1869	62	1882	105	-1
U1331 341	0.73	4.71800	7.127	0.30455	6.137	0.86	0.11236	3.624	1838	66	1770	60	1714	92	7
U1331 334	1.06	5.04195	3.600	0.32876	2.704	0.75	0.11123	2.377	1820	43	1826	31	1832	43	-1
U1331 332	0.97	4.65646	4.135	0.30425	2.907	0.70	0.11100	2.940	1816	53	1759	35	1712	44	6
U1331 397	0.71	4.87279	5.285	0.31850	4.159	0.79	0.11096	3.261	1815	59	1798	45	1782	65	2
U1331 348	0.81	5.28837	6.006	0.34683	5.587	0.93	0.11059	2.204	1809	40	1867	51	1919	93	-6
U1331 417	0.88	5.06233	4.528	0.33242	3.653	0.81	0.11045	2.676	1807	49	1830	38	1850	59	-2
U1331 355	1.10	5.21297	7.449	0.34291	5.383	0.72	0.11026	5.149	1804	94	1855	63	1901	89	-5
U1331 305	1.39	4.18285	8.506	0.27517	7.748	0.91	0.11025	3.509	1803	64	1671	70	1567	108	13
U1331 393	1.11	5.10137	6.026	0.33601	5.133	0.85	0.11011	3.156	1801	57	1836	51	1867	83	-4
U1331 331	0.87	4.65812	3.666	0.30906	3.069	0.84	0.10931	2.005	1788	37	1760	31	1736	47	3
U1331 357	0.68	4.13482	9.264	0.28555	8.941	0.97	0.10502	2.424	1715	45	1661	76	1619	128	6
U1331 405	1.27	4.46602	6.742	0.31741	4.724	0.70	0.10205	4.811	1662	89	1725	56	1777	73	-7
U1331 379	0.92	3.63665	4.742	0.26116	3.700	0.78	0.10099	2.967	1642	55	1558	38	1496	49	9
U1331 385	0.38	3.27025	6.898	0.24421	4.906	0.71	0.09712	4.849	1570	91	1474	54	1409	62	10
U1331 371	0.06	2.79094	5.030	0.21524	3.756	0.75	0.09404	3.346	1509	63	1353	38	1257	43	17
U1331 325	1.00	1.84211	13.160	0.17804	12.618	0.96	0.07504	3.739	1070	75	1061	87	1056	123	1
U1331 347	0.36	1.85646	6.762	0.18123	5.745	0.85	0.07429	3.566	1049	72	1066	45	1074	57	-2
U1331 410	0.03	1.62416	11.136	0.17010	10.741	0.96	0.06925	2.938	906	61	980	70	1013	101	-12
U1331 380	0.01	1.91052	13.927	0.16719	5.497	0.39	0.08288	12.797	1266	250	1085	93	997	51	21
U1331 388	1.04	1.66387	4.325	0.16418	3.885	0.90	0.07350	1.900	1028	38	995	27	980	35	5
U1331 391	1.01	1.57692	4.286	0.16320	3.935	0.92	0.07008	1.700	931	35	961	27	975	36	-5
U1331 413	0.03	1.57579	5.963	0.16308	5.199	0.87	0.07008	2.919	931	60	961	37	974	47	-5
U1331 400	1.17	1.48523	6.837	0.16166	6.088	0.89	0.06663	3.111	826	65	924	41	966	55	-17
U1331 362	0.44	1.48089	4.825	0.15966	4.155	0.86	0.06727	2.452	846	51	923	29	955	37	-13
U1331 364	2.41	1.73970	17.778	0.15874	11.952	0.67	0.07948	13.162	1184	260	1023	115	950	106	20
U1331 317	0.90	1.67070	17.205	0.15842	14.478	0.84	0.07649	9.294	1108	186	997	109	948	128	14
U1331 372	1.98	1.44939	7.746	0.15752	4.763	0.61	0.06673	6.108	830	127	910	47	943	42	-14
U1331 306	0.63	1.42367	7.632	0.15641	6.861	0.90	0.06602	3.343	807	70	899	46	937	60	-16

U1331 346	0.53	1.57233	4.856	0.15638	3.504	0.72	0.07292	3.362	1012	68	959	30	937	31	7
U1331 337	0.00	1.51273	4.780	0.15620	3.677	0.77	0.07024	3.054	935	63	936	29	936	32	0
U1331 409	0.44	1.51581	5.601	0.15594	5.185	0.93	0.07050	2.118	943	43	937	34	934	45	1
U1331 308	0.87	1.43631	7.622	0.15586	4.276	0.56	0.06684	6.310	833	132	904	46	934	37	-12
U1331 318	0.29	1.52081	6.547	0.15573	5.429	0.83	0.07083	3.659	952	75	939	40	933	47	2
U1331 396	0.53	1.46615	7.021	0.15504	6.150	0.88	0.06859	3.387	886	70	917	42	929	53	-5
U1331 366	0.58	1.45097	5.911	0.15442	4.980	0.84	0.06815	3.185	873	66	910	36	926	43	-6
U1331 369	0.75	1.44019	5.131	0.15369	4.220	0.82	0.06796	2.918	867	60	906	31	922	36	-6
U1331 416	1.40	1.46187	5.512	0.15367	4.786	0.87	0.06900	2.734	899	56	915	33	921	41	-3
U1331 340	0.66	1.42116	7.158	0.15364	5.157	0.72	0.06709	4.963	840	103	898	43	921	44	-10
U1331 386	0.66	1.44773	4.331	0.15303	3.951	0.91	0.06861	1.775	887	37	909	26	918	34	-3
U1331 389	1.01	1.46250	5.385	0.15226	4.691	0.87	0.06966	2.643	918	54	915	32	914	40	1
U1331 320	0.52	1.47335	6.393	0.15154	5.675	0.89	0.07051	2.944	943	60	920	39	910	48	4
U1331 406	1.00	1.45210	6.406	0.15152	5.242	0.82	0.06951	3.683	914	76	911	39	909	44	0
U1331 370	1.60	1.39773	4.445	0.15143	3.641	0.82	0.06694	2.550	836	53	888	26	909	31	-9
U1331 338	0.03	1.40604	4.905	0.15133	3.247	0.66	0.06739	3.676	850	76	891	29	908	28	-7
U1331 358	0.88	1.45407	5.470	0.15126	4.340	0.79	0.06972	3.330	920	68	912	33	908	37	1
U1331 359	0.86	1.37065	5.200	0.15052	4.244	0.82	0.06604	3.005	808	63	876	31	904	36	-12
U1331 392	0.00	1.43988	4.222	0.15041	3.378	0.80	0.06943	2.533	912	52	906	25	903	28	1
U1331 321	0.40	1.43705	8.110	0.14996	6.902	0.85	0.06950	4.259	914	88	904	49	901	58	1
U1331 319	0.11	1.41772	5.379	0.14951	4.624	0.86	0.06877	2.747	892	57	896	32	898	39	-1
U1331 376	0.69	1.41314	5.188	0.14940	4.548	0.88	0.06860	2.496	887	52	894	31	898	38	-1
U1331 350	0.82	1.37975	7.115	0.14923	6.230	0.88	0.06706	3.436	840	72	880	42	897	52	-7
U1331 336	0.75	1.38560	4.551	0.14800	3.355	0.74	0.06790	3.075	866	64	883	27	890	28	-3
U1331 408	0.64	1.47140	8.806	0.14776	6.440	0.73	0.07222	6.006	992	122	919	53	888	53	10
U1331 361	0.63	1.35763	5.075	0.14726	3.613	0.71	0.06687	3.564	834	74	871	30	886	30	-6
U1331 374	1.09	1.38367	5.540	0.14704	4.217	0.76	0.06825	3.592	876	74	882	33	884	35	-1
U1331 323	0.32	1.37622	6.747	0.14654	6.121	0.91	0.06811	2.839	872	59	879	40	882	50	-1
U1331 387	0.56	1.45297	5.089	0.14646	4.643	0.91	0.07195	2.084	985	42	911	31	881	38	11
U1331 335	0.80	1.33777	3.685	0.14635	2.924	0.79	0.06630	2.243	816	47	862	21	880	24	-8

U1331 411	0.52	1.39781	4.227	0.14621	3.852	0.91	0.06934	1.741	909	36	888	25	880	32	3
U1331 343	0.64	1.46257	7.670	0.14561	3.996	0.52	0.07285	6.547	1010	133	915	46	876	33	13
U1331 303	0.00	1.45957	6.103	0.14526	3.022	0.50	0.07288	5.302	1011	107	914	37	874	25	13
U1331 349	0.53	1.39717	5.521	0.14516	4.724	0.86	0.06981	2.857	923	59	888	33	874	39	5
U1331 329	0.90	1.35565	5.354	0.14513	3.314	0.62	0.06775	4.205	861	87	870	31	874	27	-1
U1331 352	0.50	1.38268	5.694	0.14489	4.510	0.79	0.06921	3.476	905	72	882	34	872	37	4
U1331 301	0.61	1.36435	5.941	0.14412	4.701	0.79	0.06866	3.633	889	75	874	35	868	38	2
U1331 375	0.69	1.32146	5.606	0.14342	4.917	0.88	0.06682	2.694	832	56	855	32	864	40	-4
U1331 401	1.02	1.28371	4.066	0.14318	3.522	0.87	0.06503	2.033	775	43	839	23	863	28	-11
U1331 339	0.74	1.32894	4.436	0.14267	3.138	0.71	0.06756	3.136	855	65	858	26	860	25	-1
U1331 367	1.01	1.35503	8.958	0.14263	5.191	0.58	0.06890	7.301	896	151	870	52	860	42	4
U1331 307	1.04	1.29779	11.000	0.14193	10.162	0.92	0.06632	4.211	816	88	845	63	856	81	-5
U1331 395	1.08	1.46887	7.733	0.14159	6.157	0.80	0.07524	4.679	1075	94	918	47	854	49	21
U1331 324	0.59	1.40613	4.782	0.14156	3.838	0.80	0.07204	2.852	987	58	892	28	853	31	14
U1331 373	0.90	1.35847	4.346	0.14148	3.200	0.74	0.06964	2.941	918	60	871	25	853	26	7
U1331 326	0.69	1.28592	4.407	0.13969	3.723	0.84	0.06676	2.358	830	49	839	25	843	29	-2
U1331 328	1.47	1.27301	6.946	0.13806	5.124	0.74	0.06688	4.689	834	98	834	39	834	40	0
U1331 399	1.26	1.22877	5.912	0.13759	4.024	0.68	0.06477	4.331	767	91	814	33	831	31	-8
U1331 383	1.48	1.30066	9.185	0.13735	7.921	0.86	0.06868	4.650	889	96	846	53	830	62	7
U1331 304	0.42	1.31384	6.328	0.13603	5.090	0.80	0.07005	3.759	930	77	852	36	822	39	12
U1331 404	0.59	1.16619	5.204	0.13553	3.847	0.74	0.06241	3.504	688	75	785	28	819	30	-19
U1331 415	1.78	1.20660	6.310	0.13538	4.190	0.66	0.06464	4.718	763	99	804	35	818	32	-7
U1331 356	1.17	1.23556	6.313	0.13306	4.106	0.65	0.06734	4.796	848	100	817	35	805	31	5
U1331 382	1.31	1.19826	6.260	0.13181	4.315	0.69	0.06593	4.535	804	95	800	35	798	32	1
U1331 414	3.30	1.18962	5.700	0.12941	3.994	0.70	0.06667	4.067	828	85	796	31	784	29	5
U1331 351	0.82	1.15489	7.572	0.12825	4.990	0.66	0.06531	5.695	784	120	780	41	778	37	1

LA-ICPMS data from sample U1331 continued.

	Concentrations (ppm)																						
Analysis	P	Ti	Y	Nb	La	Ce	Pr	Nd	Sm	Eu	Gd	Tb	Dy	Ho	Er	Tm	Yb	Lu	Hf	Ta	Th	U	T(°C)
U1331 363	190	7.41	509	1.40	0.02	9.49	0.05	1.56	2.47	0.85	14.06	4.80	52.8	18.088	74.7	18.4	194	22.1	7669	0.71	29.8	34	766
U1331 312	394	5.13	799	2.46	0.04	4.25	0.02	0.70	3.41	0.27	18.12	6.09	78.1	27.78	120.8	30.5	364	37.9	7793	1.58	96.3	295	731
U1331 377	168	7.58	690	2.99	0.15	8.66	0.11	1.12	1.41	0.14	11.84	4.57	62.7	23.00	104.6	27.0	265	36.1	11037	2.27	53.4	84	768
U1331 412	175	5.79	660	2.10		38.03	0.05	2.22	4.15	1.18	17.22	5.98	62.3	21.49	97.1	25.4	277	37.1	8858	1.11	114.9	93	743
U1331 344	158	5.09	408	0.74		16.90	0.06	1.14	3.32	0.79	14.12	4.03	40.9	13.76	59.4	15.5	186	19.5	7833	0.61	114.5	148	731
U1331 360	136	3.91	667	0.88		1.80		0.47	1.73	0.45	12.20	4.56	65.6	24.79	116.2	32.1	367	42.9	7200	0.45	26.3	60	707
U1331 342	65	3.96	239	1.21		15.57	0.02	0.17	0.72	0.66	4.04	1.91	22.4	7.57	35.8	11.0	142	17.6	9837	0.74	64.6	140	708
U1331 381	265	4.48	1685	3.67	0.29	41.61	1.13	17.82	27.85	8.21	82.94	22.79	210.8	64.84	227.3	52.3	537	57.9	7098	1.25	178.6	101	719
U1331 345	197	6.89	652	2.12		31.30	0.10	1.42	4.14	0.41	16.92	5.64	62.7	21.58	100.3	26.6	323	35.8	9446	1.51	239.0	321	759
U1331 330	490	5.86	1330	2.50		8.25	0.06	1.34	4.62	0.88	26.80	11.18	138.4	46.46	180.0	41.5	421	54.4	11294	1.79	103.9	242	744
U1331 333	127	8.26	952	3.40		10.93	0.05	2.03	6.60	0.25	28.11	8.89	105.5	35.89	144.0	32.4	309	38.3	9629	0.96	84.5	103	777
U1331 314	68	8.05	161	2.03		6.76		0.29	0.50	0.30	3.33	1.32	14.9	5.72	25.2	6.7	83	8.2	5423	0.40	40.2	63	774
U1331 390	200	6.31	558	2.27	0.01	9.80	0.07	1.31	3.42	0.16	12.97	4.40	53.2	19.67	85.4	20.7	214	27.8	10461	1.04	82.3	98	751
U1331 368	282	7.88	1403	4.20		6.65	0.05	2.21	5.08	0.53	31.00	11.87	142.3	52.90	226.1	53.1	529	66.5	10128	2.64	113.5	152	772
U1331 365	168	6.80	163	0.41		6.89	0.03	1.48	1.55	1.07	8.16	1.89	18.99	5.96	18.99	4.0	39	4.3	7849	0.11	21.8	45	758
U1331 309	195	8.13	489	2.07	0.07	14.25	0.06	1.07	3.27	0.37	12.57	4.67	54.1	18.12	73.6	18.9	230	23.5	7358	1.25	124.9	227	775
U1331 327	188	4.86	1185	1.09	0.03	9.48	0.22	3.79	7.15	0.95	31.27	10.49	117.1	44.61	188.4	42.6	470	59.6	9729	0.70	176.1	155	727

U1331398	194	9.23	688	2.36		29.02	0.12	2.58	5.29	0.84	22.49	7.36	76.7	25.39	102.3	25.1	269	28.1	8037	1.31	145.5	104	788
U1331403	75	1.13	159	0.77	0.22	1.22	0.06	0.20	0.10	0.09	2.55	1.16	13.7	5.85	24.1	7.3	91	9.4	8847	0.69	23.3	198	610
U1331354	522	9.65	1301	12.88		9.75	0.08	0.88	4.33	0.07	21.17	9.88	128.2	45.52	195.6	48.6	535	53.3	11645	7.99	153.2	611	793
U1331384	125	7.55	422	3.12		20.88	0.03	0.46	2.30	0.24	8.37	3.01	39.2	14.31	65.0	16.3	186	25.8	11670	1.53	141.5	112	768
U1331407	94	9.16	312	2.41	0.51	31.71	0.24	1.83	1.85	0.79	9.17	2.82	29.1	10.00	44.3	12.0	138	18.8	9562	1.03	378.6	296	787
U1331402	356	6.22	1117	4.92	2.54	18.45	0.71	6.30	6.95	0.75	25.35	9.56	109.1	41.80	187.8	50.5	600	66.7	7386	2.64	135.3	201	749
U1331316	88	5.41	664	3.44	0.06	39.36	0.10	1.03	3.72	0.25	14.67	5.09	55.8	20.24	95.9	29.3	360	40.0	8417	1.15	455.9	450	736
U1331310	271	6.16	1673	9.25	0.07	15.95	0.20	2.78	6.80	0.35	37.87	13.88	172.8	62.36	266.0	64.1	626	64.6	7857	4.35	121.7	154	748
U1331302	234	6.14	2289	8.79		14.61	0.15	3.70	8.80	0.26	44.86	17.89	227.7	85.33	344.4	87.7	911	82.3	9879	5.55	229.1	372	748
U1331378	292	4.75	2452	9.67	0.06	24.13	0.49	8.86	15.72	0.75	72.07	23.81	266.2	94.59	382.6	83.6	829	95.5	10995	5.98	208.1	158	724
U1331313	211	8.25	703	6.61		10.52	0.06	0.68	2.28	0.21	15.45	5.27	69.6	25.51	111.7	28.1	314	31.6	7851	2.71	44.6	62	777
U1331341	180	6.01	577	4.97	0.01	7.60	0.03	1.00	2.20	0.30	13.47	4.86	60.8	21.24	87.1	23.7	261	28.0	8307	2.49	32.3	44	746
U1331334	213	8.44	1210	8.65		13.70	0.09	1.12	3.96	0.16	25.64	9.20	117.4	44.39	191.7	45.2	432	57.8	12225	3.44	71.9	68	779
U1331332	187	4.97	920	3.90		7.94	0.02	0.86	3.30	0.26	19.23	7.21	88.7	33.51	145.5	34.6	345	45.1	10030	1.72	46.9	48	728
U1331397	158	6.02	1053	7.15	0.08	10.62	0.18	2.54	6.52	0.11	26.52	8.96	107.0	38.08	166.5	39.0	411	40.3	7691	4.80	95.1	134	746
U1331417	287	7.22	1042	11.52	1.02	18.28	0.41	3.65	4.99	0.29	23.61	8.28	99.4	37.94	164.3	39.0	383	53.7	11553	6.98	101.6	116	764
U1331355	220	28.08	507	1.64		8.88	0.07	1.96	3.35	0.37	13.96	4.41	54.2	17.75	74.4	19.1	209	22.0	7401	0.68	18.4	17	915
U1331305	325	4.74	1943	5.26	0.06	16.92	0.60	9.50	13.09	0.29	55.13	18.61	205.7	70.11	278.3	71.9	718	68.5	7451	2.06	316.8	227	724
U1331393	214	4.66	1565	3.33		9.63	0.27	5.09	9.57	0.54	47.74	15.74	179.3	62.24	242.9	53.9	546	59.0	8978	1.46	79.9	72	723
U1331	21	11.	10	7.8		10.	0.1	2.1	4.6	0.2	25.6	9.2	106	37.8	157	36.	34	42.	114	3.2	70.	80	813

331	3	78	47	6		90	0	2	9	0	4	0	.4	2	.3	1	5	5	12	8	2		
U1331357	241	8.41	1892	9.87		12.64	0.29	4.37	9.13	0.83	45.57	16.13	198.2	70.72	291.9	71.1	749	72.7	8732	4.53	141.1	207	779
U1331405	210	9.00	939	2.20	0.04	6.39	0.18	3.90	7.04	0.38	30.80	9.75	112.8	34.54	138.6	32.2	333	34.8	7518	0.77	37.5	30	785
U1331379	223	5.30	993	3.05		6.23	0.11	3.43	6.46	0.23	30.67	9.57	107.3	37.13	147.2	35.1	356	38.8	9006	1.38	45.1	49	734
U1331385	96	2.58	338	2.56	0.02	4.49	0.04	0.90	1.03	0.17	6.76	2.46	31.0	11.97	56.1	15.7	185	31.4	13770	1.51	36.1	96	672
U1331371	61	2.37	173	3.42		1.18			0.13		1.57	1.01	12.2	5.47	24.8	7.1	81	13.4	17181	3.55	12.2	207	665
U1331325	100	1.25	416	1.54	2.82	17.92	0.56	2.71	1.21	0.87	4.94	2.30	32.0	13.11	66.6	20.7	289	50.2	10326	0.37	185.1	185	617
U1331347	126	8.22	105	0.45		3.92	0.02	0.42	0.87	0.34	4.75	1.52	14.6	3.73	11.6	3.1	34	3.5	9456	0.47	24.7	68	776
U1331380	68	0.54	78	5.45								0.03	1.8	1.96	22.6	14.0	301	52.4	10777	5.88	0.1	5	561
U1331388	241	11.57	968	1.80	1.46	34.84	1.23	8.04	8.84	3.23	27.91	9.02	97.3	32.75	134.8	32.6	323	44.6	9566	0.59	291.4	280	812
U1331391	158	2.46	771	2.39		22.17	0.03	0.85	2.71	0.75	15.85	5.87	67.7	26.44	120.6	31.3	347	48.7	11304	0.92	199.8	199	669
U1331413	74	8.63	56	0.38	0.02	1.47	0.04	0.16	0.39	0.27	3.71	0.73	5.4	1.61	6.5	1.9	19	3.0	12845	0.21	4.9	160	781
U1331362	160	1.88	744	4.80	0.12	9.98	0.03	0.65	2.07	0.48	11.79	4.35	63.7	25.63	127.2	38.8	462	56.2	8177	3.31	105.1	242	647
U1331364	770	12.36	3442	3.06	0.19	67.11	0.45	8.48	16.37	5.68	82.46	30.04	348.1	126.97	543.7	128.8	1267	171.0	6691	1.12	152.9	63	819
U1331372	272	14.80	1053	1.10		48.45	0.07	2.14	6.86	1.50	32.31	10.05	115.3	39.33	163.2	38.2	355	52.8	9761	0.55	52.9	27	838
U1331306	164	5.13	566	2.03	0.01	25.70	0.01	0.47	1.98	0.56	11.81	4.49	56.6	21.22	92.8	24.6	295	34.0	8653	1.27	71.0	112	731
U1331346	124	3.51	963	8.07	4.02	54.57	1.95	12.66	9.21	2.87	25.77	8.35	97.4	33.17	142.1	39.2	460	53.7	7883	4.10	154.3	290	698
U1331337	40	0.81	249	25.41		0.24					0.34	0.46	9.6	6.42	57.6	21.2	280	43.8	14882	21.97	0.5	96	587
U1331409	99	3.20	617	2.33	1.52	27.66	0.83	3.75	3.33	1.42	12.28	4.24	55.9	20.09	92.2	28.4	364	53.8	10804	0.69	153.5	349	690
U1331318	175	3.31	589	1.19	0.04	7.25	0.03	0.42	2.33	1.67	14.82	4.80	55.3	21.41	83.8	21.8	250	26.2	8143	0.40	47.7	166	693

U1331396	95	1.42	480	1.31	0.20	20.11	0.11	1.23	1.70	0.85	6.61	3.03	39.6	15.85	73.9	22.5	303	44.1	9318	0.39	112.8	215	626
U1331366	66	0.37	390	2.02	0.05	11.94		0.16	0.81	0.38	4.57	1.96	27.8	10.25	60.8	19.5	264	42.5	12379	0.53	112.9	194	538
U1331369	118	7.09	320	0.66	0.01	11.51	0.04	0.44	1.37	0.50	6.66	2.45	29.9	10.63	50.8	13.7	161	21.5	10980	0.43	84.5	113	762
U1331416	247	3.51	1525	3.24		33.93	0.22	3.85	7.16	1.06	39.49	13.24	162.6	57.59	238.8	55.0	541	74.2	11584	1.74	239.8	171	698
U1331340	95	1.71	264	1.01		15.18		0.29	1.14	0.28	4.64	1.73	21.4	9.05	41.7	12.7	163	20.9	9318	0.54	37.5	57	640
U1331386	178	3.34	1251	8.51		22.06	0.02	0.80	3.51	0.32	17.61	7.06	96.2	40.67	205.1	57.6	684	103.8	12387	7.09	334.0	507	694
U1331389	130	5.12	612	0.92		16.21	0.08	1.56	2.76	0.80	16.09	5.01	55.2	20.74	91.3	22.7	260	38.5	10823	0.45	155.2	154	731
U1331320	121	6.85	188	0.62		10.51	0.03	0.43	0.78	0.16	5.50	1.36	19.1	7.07	28.0	7.8	93	10.6	8256	0.45	63.3	121	758
U1331406	202	15.11	528	0.56		13.01	0.10	1.81	4.68	1.08	17.76	5.25	56.7	18.58	77.9	19.2	210	23.8	7721	0.33	63.9	64	841
U1331370	299	11.13	1220	2.15		27.41	0.07	2.59	5.19	1.16	26.56	8.95	111.6	42.32	186.1	47.2	501	69.0	11430	1.53	227.0	142	807
U1331338	71	1.38	212	11.06		0.27					0.12	0.27	8.5	5.66	49.5	20.9	331	60.1	13069	5.87	2.0	64	625
U1331358	209	9.90	535	0.39		12.58	0.08	1.86	4.45	1.21	17.77	5.61	60.8	20.48	80.9	20.4	226	25.3	6679	0.24	66.0	75	795
U1331359	147	3.44	782	1.42	0.06	27.35	0.07	1.26	2.43	1.48	17.77	6.02	72.4	27.65	119.7	33.2	413	52.6	8194	0.29	93.6	109	696
U1331392	85	6.18	195	4.51							0.58	0.48	9.2	5.30	41.4	15.4	211	25.7	13616	1.02	0.1	221	749
U1331321	42	1.84	460	1.75	0.13	14.58	0.11	0.85	0.96	0.59	4.98	2.22	31.0	13.71	73.5	26.1	358	51.3	9278	0.50	162.7	403	646
U1331319	70	2.30	236	4.21	6.78	4.56	0.72	3.23	0.89	0.38	2.28	1.34	16.3	7.54	38.9	13.9	180	22.1	8033	2.71	26.8	254	663
U1331376	107	1.97	629	1.69	0.15	19.32	0.10	0.84	3.02	1.10	14.69	4.82	55.4	20.56	91.6	26.6	316	43.6	12328	0.64	100.1	145	651
U1331350	157	4.54	465	1.38		20.01	0.03	0.71	2.19	0.55	7.98	3.25	39.2	15.64	73.6	21.6	284	33.3	8421	0.51	59.3	73	720
U1331336	74	2.86	273	1.15	0.02	21.62	0.05	0.84	0.93	0.39	6.14	1.91	22.4	9.03	39.3	10.6	134	23.7	13399	0.52	165.0	219	681
U1331	93	3.4	17	0.6		10.		0.1	0.4	0.3	2.46	1.0	13.	5.90	30.	9.0	11	15.	948	0.4	22.	35	696

408		2	3	0		56		8	5	3		3	8		8		3	6	1	0	3		
U1331361	195	3.63	525	1.01	0.86	22.83	0.17	1.84	2.47	0.87	10.92	3.70	46.9	18.26	82.5	22.9	279	36.3	9565	0.67	87.8	140	701
U1331374	147	8.12	1316	1.71		24.96	0.07	2.29	6.30	3.00	36.49	12.10	139.6	48.79	190.3	43.8	447	65.3	10007	0.46	76.2	70	775
U1331323	90	2.23	673	1.12	0.13	18.15	0.07	1.24	1.70	0.85	12.33	3.88	54.9	21.55	100.9	28.2	395	53.8	9631	0.28	67.7	213	661
U1331335	91	2.67	498	0.90		18.66		0.60	1.19	0.52	8.15	3.14	42.5	16.70	76.4	21.4	240	39.3	13357	0.79	132.4	166	675
U1331411	101	2.70	1139	2.79	0.92	30.70	0.38	2.61	4.38	1.53	23.40	7.91	99.2	37.44	168.2	45.6	540	76.8	12701	0.76	170.5	330	676
U1331343	170	5.24	491	0.80	2.75	21.53	1.43	6.08	5.89	2.78	15.27	5.18	54.4	17.09	69.9	20.9	231	29.5	8737	0.44	90.4	142	733
U1331303	60	1.28	33	0.19		0.07							0.9	0.77	7.5	5.2	135	23.0	8923	0.11	0.1	46	619
U1331349	233	7.88	871	1.97		15.72	0.07	1.32	2.95	1.61	15.22	6.46	79.3	30.02	131.5	35.4	440	49.0	6458	0.61	150.9	285	772
U1331329	167	8.27	544	0.44		13.42	0.03	0.55	2.07	0.46	11.02	4.27	53.4	18.70	80.9	21.0	219	30.3	10519	0.35	46.8	52	777
U1331352	124	5.11	168	0.65		10.62		0.18	0.65	0.29	3.23	1.11	14.8	4.86	23.7	7.2	95	11.0	8023	0.29	53.3	106	731
U1331301	167	11.01	365	1.49		17.73	0.04	0.84	1.77	0.49	6.77	2.67	34.6	12.51	53.6	14.8	182	19.6	7602	0.98	48.7	80	806
U1331375	92	1.92	581	1.15		21.13	0.01	0.71	1.67	0.87	13.27	4.10	51.0	19.29	84.7	24.0	289	41.6	12102	0.38	94.2	137	649
U1331401	168	4.43	781	0.65		18.72	0.08	2.07	3.76	1.33	18.61	6.30	74.6	26.76	123.4	34.9	448	54.1	7749	0.36	190.4	186	718
U1331339	137	3.95	724	1.27	0.05	22.49	0.02	1.18	3.06	1.27	16.17	4.99	63.9	24.29	108.3	29.3	332	45.5	10160	0.40	96.5	131	708
U1331367	117	11.24	127	0.08		6.00	0.02	0.27	0.94	0.22	2.55	1.20	11.7	4.21	19.0	5.4	58	8.6	9662	0.02	19.4	19	808
U1331307	177	7.53	749	0.63	0.74	16.11	0.21	1.78	3.62	0.87	19.84	6.01	73.9	27.09	121.1	31.3	353	39.6	7545	0.45	98.8	95	768
U1331395	252	8.34	1519	1.34	3.49	62.87	3.65	29.84	32.56	13.24	74.72	20.47	210.9	56.08	213.0	49.0	521	58.9	9725	0.39	303.5	281	778
U1331324	289	3.41	1342	1.72	0.27	12.86	0.20	3.16	6.83	1.63	30.63	10.47	133.0	49.93	214.2	56.4	644	76.1	9839	0.88	98.1	166	696
U1331373	82	2.36	456	0.86		19.76	0.00	0.59	1.68	0.54	8.84	3.19	38.3	14.86	69.0	18.0	199	31.9	13184	0.50	159.6	177	665

U1331 328	18 6	7.3 6	13 16	0.4 8	0.0 2	12. 17	0.2 4	3.9 5	8.5 2	2.2 9	45.1 5	13. 23	148 .2	49.1 7	189 .6	42. 6	42 6	53. 6	969 9	0.3 5	95. 6	65	765
U1331 399	47 5	13. 35	25 68	2.1 5		23. 83	0.3 4	5.5 4	12. 39	4.7 6	63.9 3	22. 30	272 .6	98.0 5	411 .2	103 .0	11 50	118 .9	622 6	0.8 0	123 .5	98	827
U1331 383	43 7	6.9 4	20 18	2.3 5	0.6 4	36. 97	0.3 2	2.8 0	6.9 5	2.1 2	41.0 1	15. 76	205 .1	76.1 4	322 .5	78. 0	80 8	102 .3	961 0	0.9 1	84. 5	57	760
U1331 304	11 2	1.2 9	44 9	1.5 3		12. 08	0.0 2		0.7 1	0.4 7	6.46	2.0 9	32. 7	13.5 1	70. 4	22. 4	31 4	41. 8	803 1	0.4 3	62. 0	14 9	619
U1331 415	49 0	29. 18	21 75	1.2 7		18. 99	0.3 0	4.9 3	10. 13	4.6 9	51.8 1	16. 99	216 .0	81.3 0	345 .0	85. 3	82 4	118 .6	862 6	0.4 9	77. 5	43	920
U1331 356	43 8	18. 00	16 22	1.8 4	0.2 1	21. 21	0.1 5	2.5 7	6.5 3	2.9 6	31.4 8	11. 64	160 .5	59.7 1	265 .7	68. 6	77 2	83. 7	564 6	0.5 6	58. 4	50	861
U1331 382	41 4	18. 67	13 06	1.3 4	1.4 7	20. 53	0.2 9	4.6 5	5.9 1	2.2 2	30.9 9	10. 02	126 .1	46.5 4	214 .6	51. 2	55 2	71. 1	877 0	0.6 2	51. 4	39	865
U1331 414	51 5	10. 86	35 22	1.8 4	0.0 7	71. 02	1.0 6	17. 89	26. 69	10. 65	114. 68	34. 09	383 .2	129. 30	530 .5	128 .3	12 79	168 .0	877 5	0.6 9	276 .8	84	805
U1331 351	40 7	18. 46	10 87	0.9 4		12. 65	0.0 4	1.0 2	4.2 0	1.7 8	22.1 7	8.1 1	108 .5	39.3 0	176 .2	48. 4	58 7	60. 3	628 2	0.4 6	20. 6	25	864

March 8, 2014

Isotope ratio and date errors include systematic calibration errors of 0.24% ($^{207}Pb/^{206}Pb$), 0.58% ($^{206}Pb/^{238}U$) (2 sigma).

Trace element concentrations were deleted from analyses known to have intersected inclusions of other minerals based on P and Ti.

Ablation used a laser spot size of 25 microns, and a laser firing repetition rate of 10 Hz.

Activity of TiO_2 for Ti-in-Zircon temperature calculation is 0.8.

APPENDIX 2.2. SUPPLEMENT TO CHAPTER 2: FIGURES

Figure 2.A1. Cathodoluminescence images of zircon grains dated by U-Pb LA-ICPMS from sample DS24.

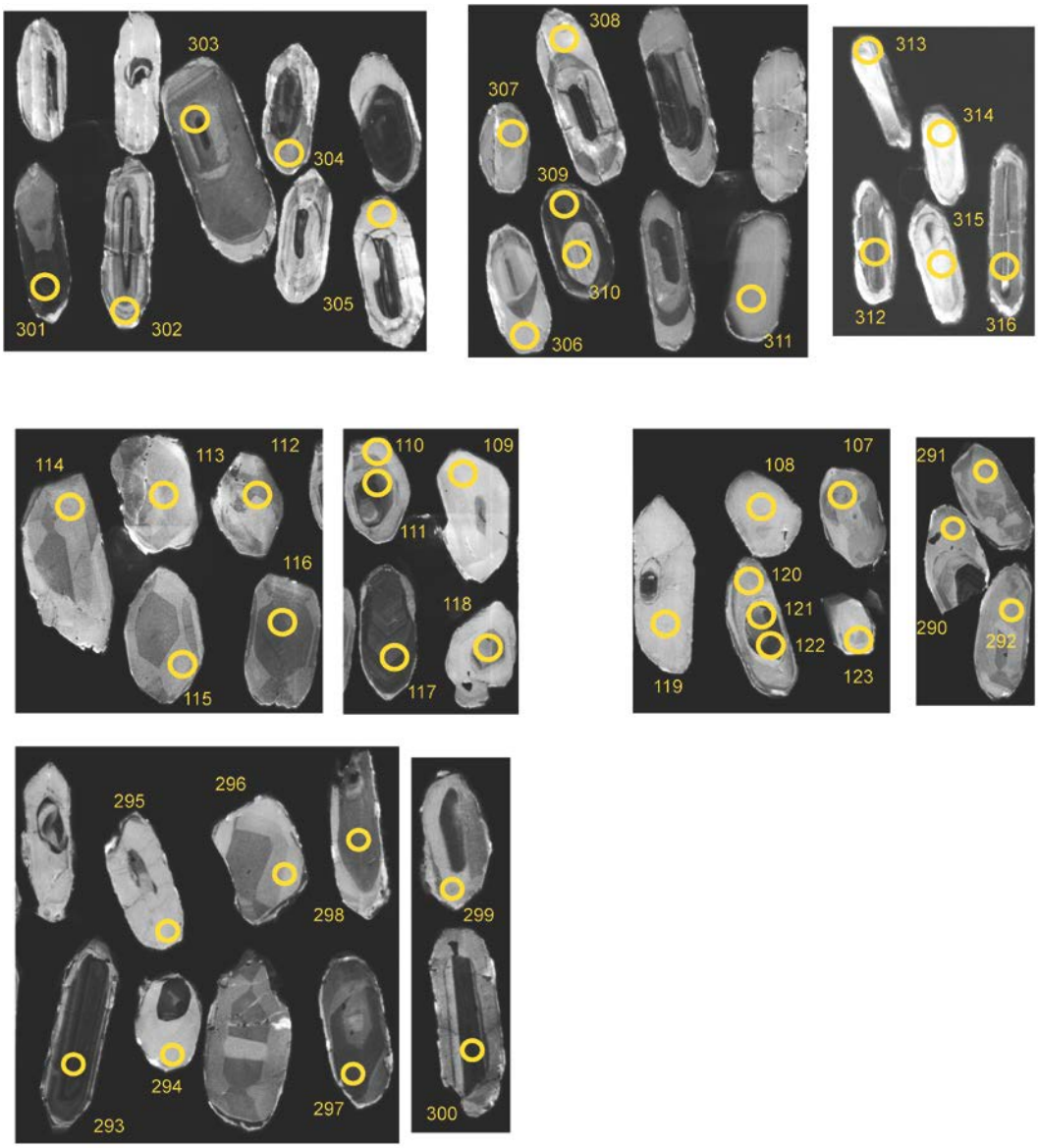

Figure 2.A2. Cathodoluminescence images of zircon grains dated by U-Pb LA-ICPMS from sample U1519.

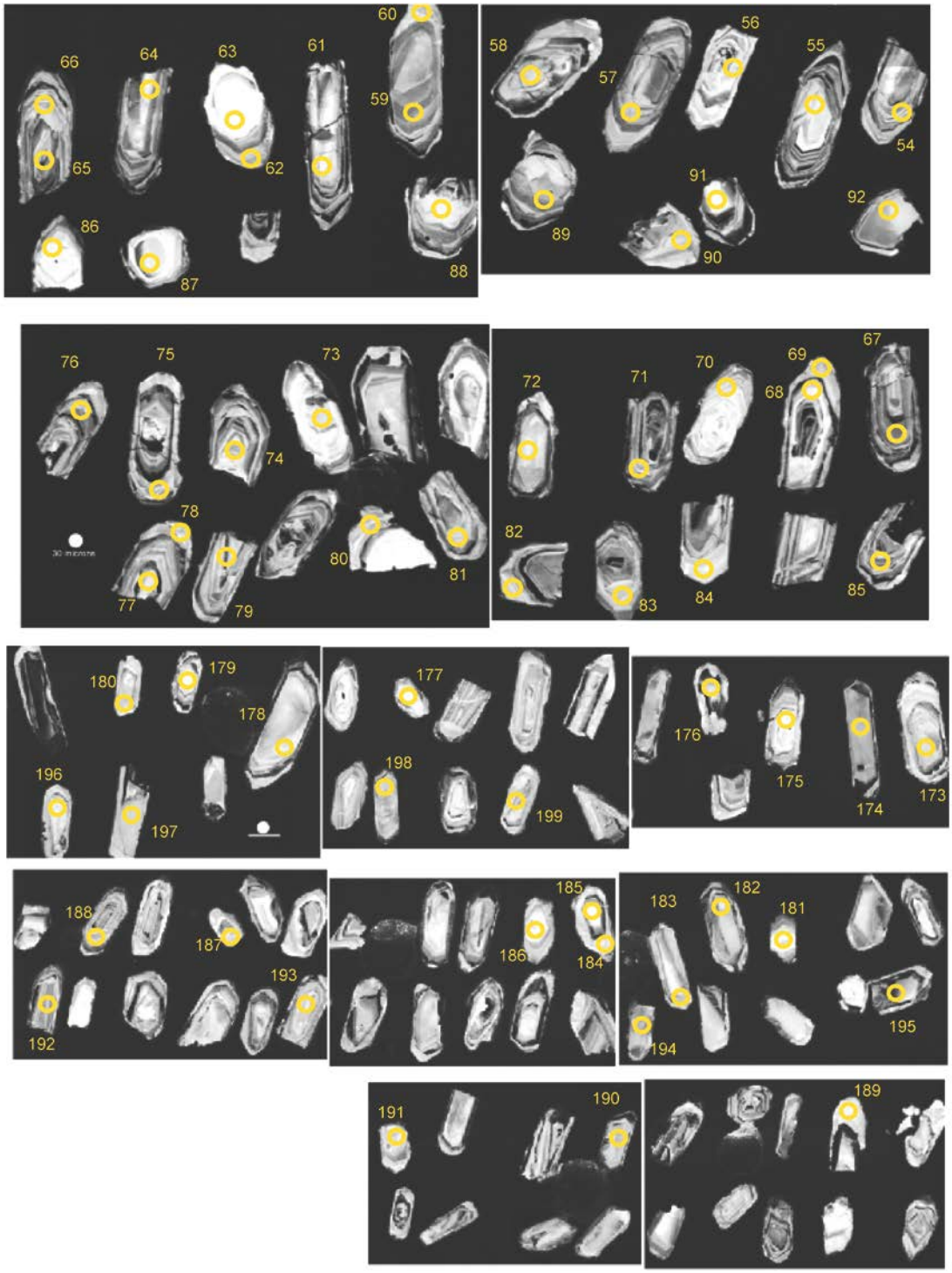

Figure 2.A3. Cathodoluminescence images of zircon grains dated by U-Pb LA-ICPMS from sample U1520.

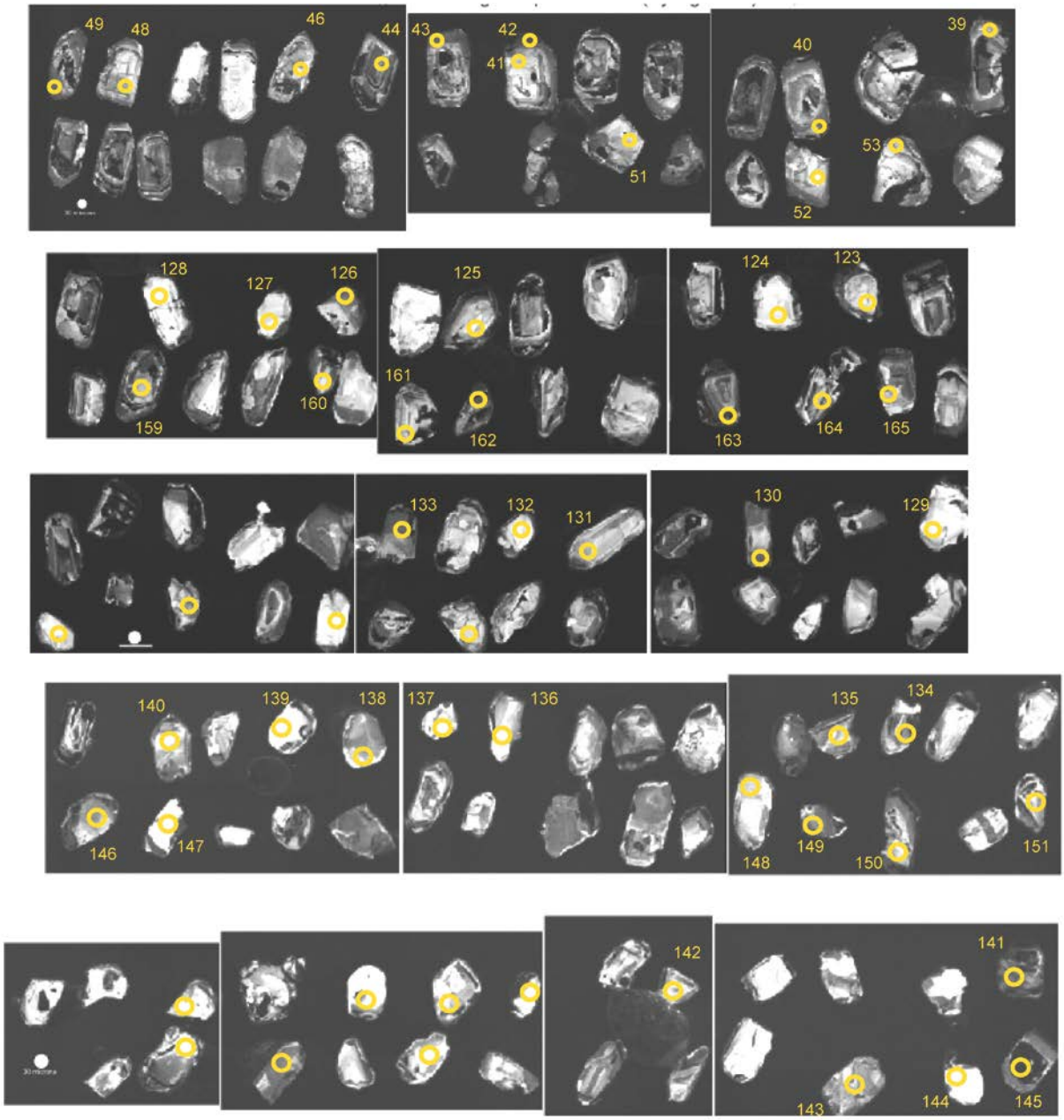

Figure 2.A4. Cathodoluminescence images of zircon grains dated by U-Pb LA-ICPMS from sample TS08.

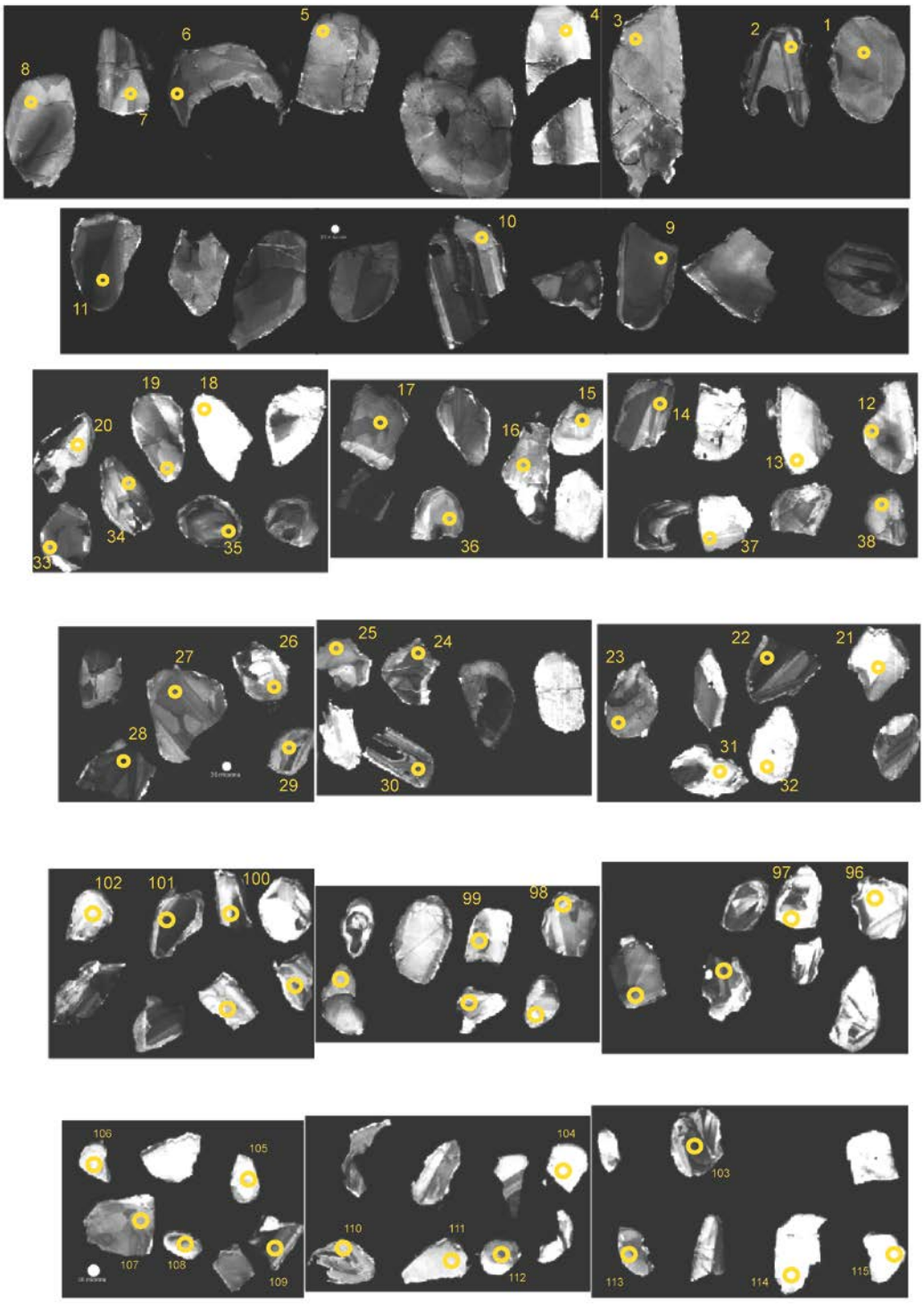

Figure 2A5. Cathodoluminescence images of zircon grains dated by U-Pb LA-ICPMS from sample U1331.

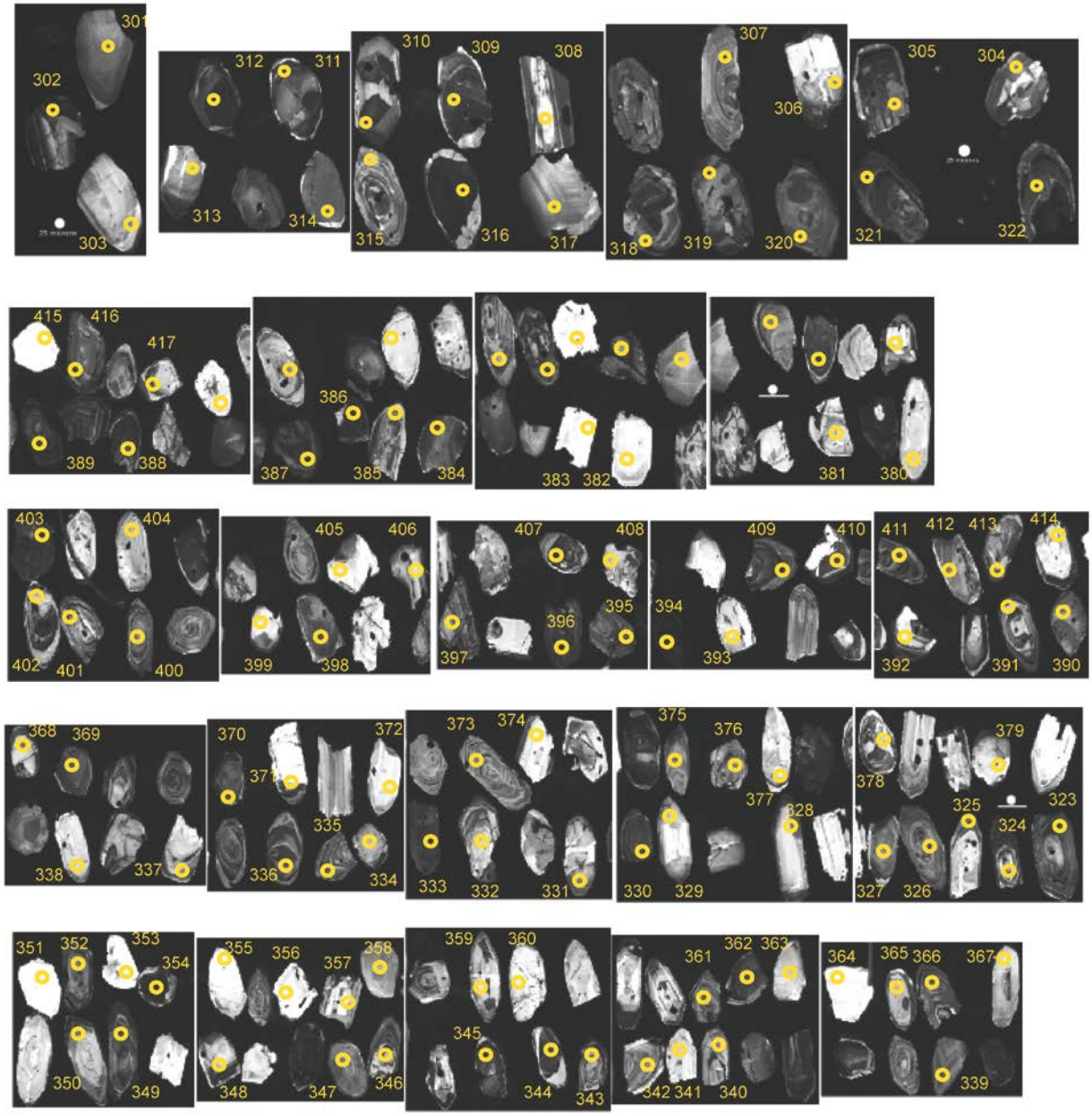

Figure 2.A6. Cathodoluminescence images of zircon grains dated by U-Pb LA-ICPMS from sample U1340A.

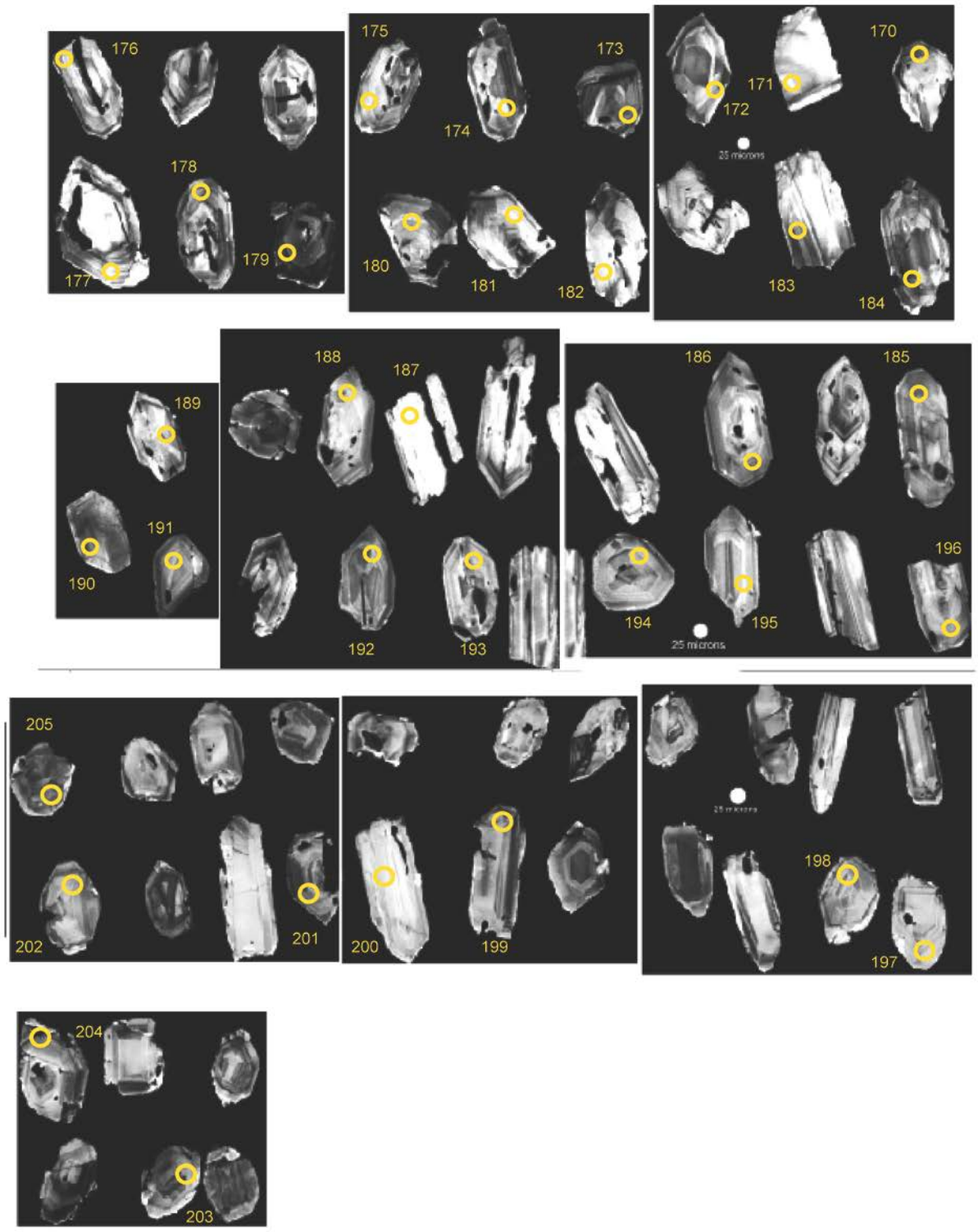

Figure 2.A7. Cathodoluminescence images of zircon grains dated by U-Pb LA-ICPMS from sample DS69.

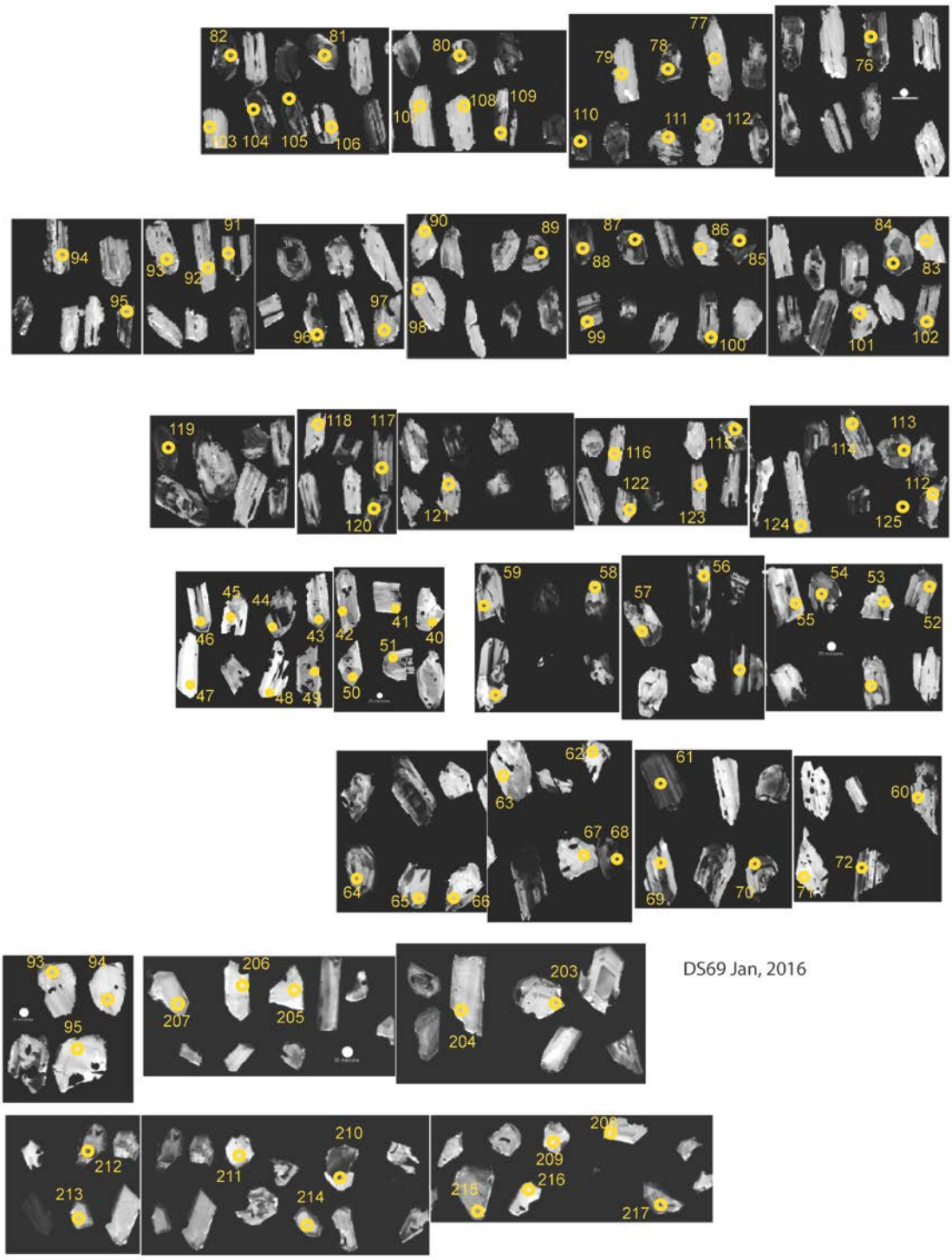

Figure 2.A8. Cathodoluminescence images of zircon grains dated by U-Pb LA-ICPMS from sample U1121-17.5.

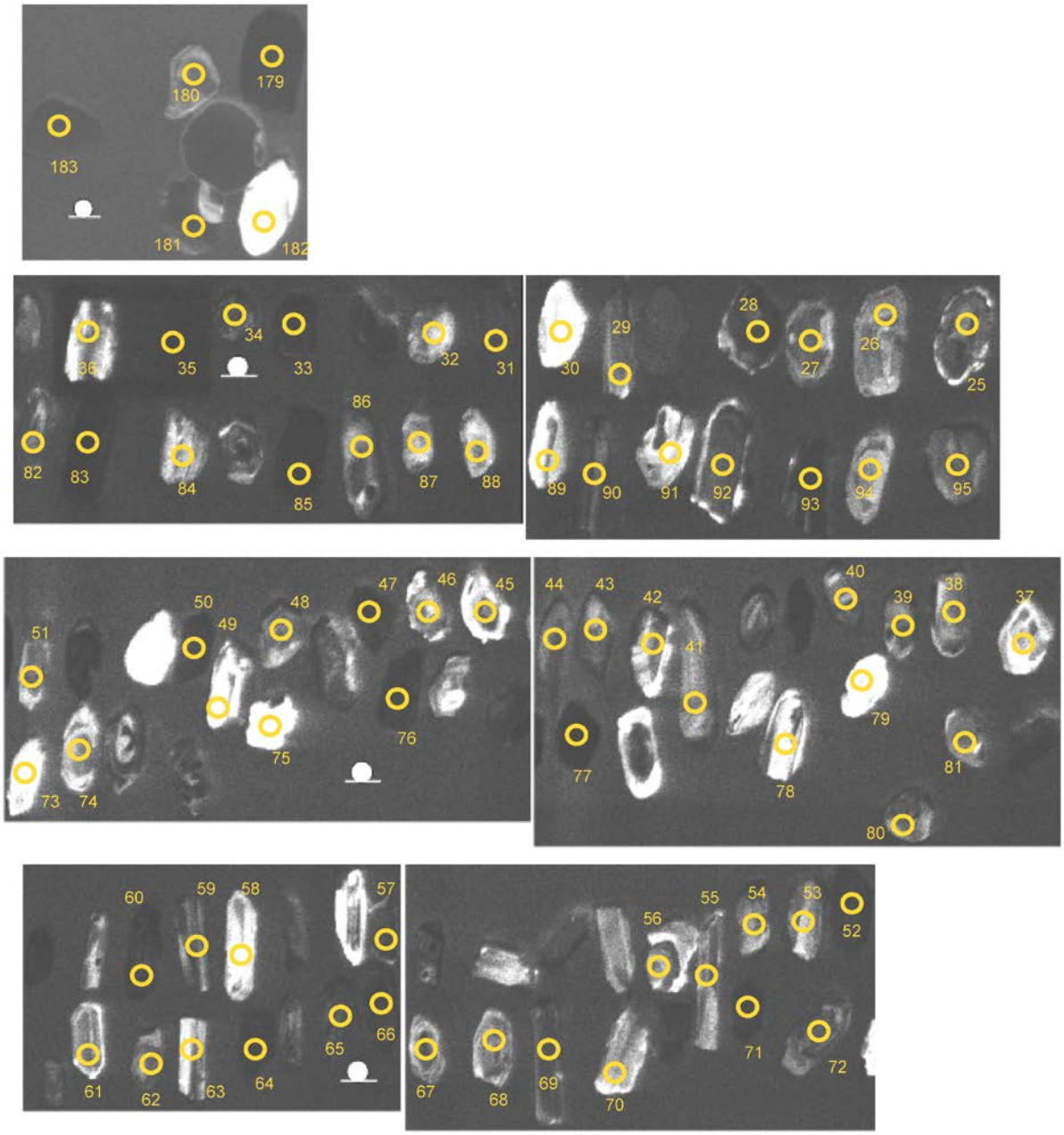

Figure 2.A9. Cathodoluminescence images of zircon grains dated by U-Pb LA-ICPMS from sample E1105-35.

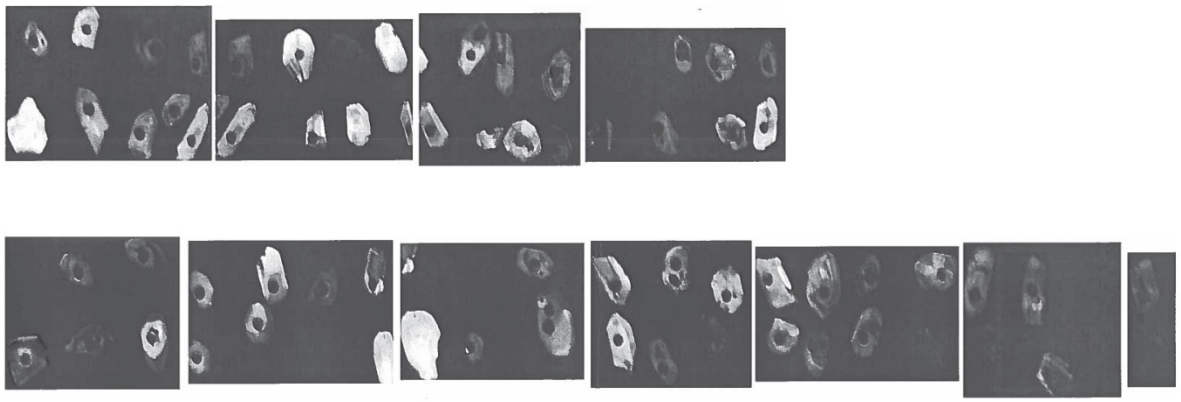

Figure 2.A10. Cathodoluminescence images of zircon grains dated by U-Pb LA-ICPMS from sample F1121-25.

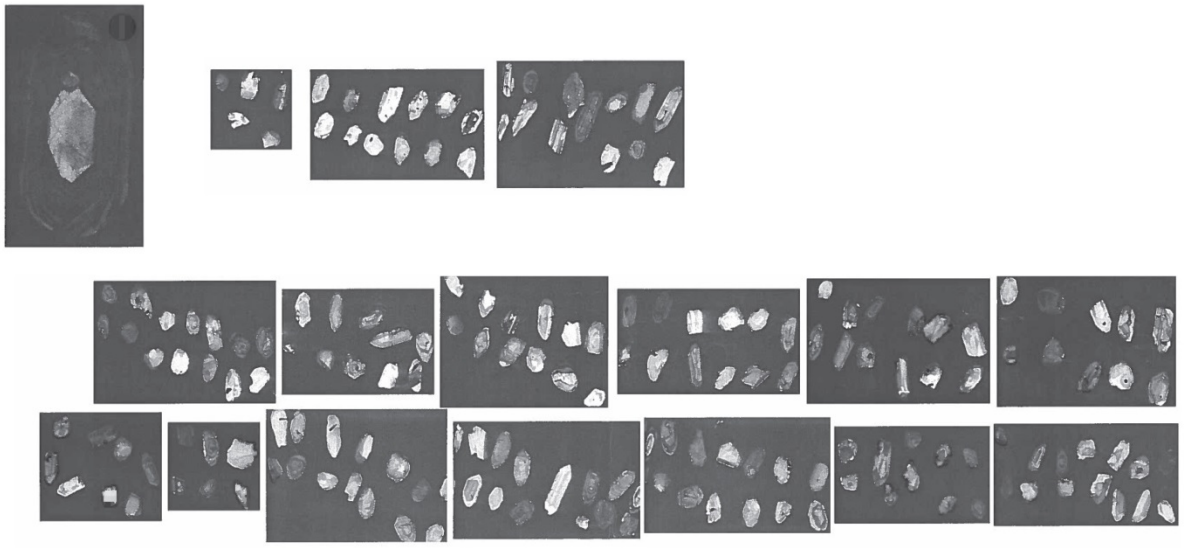

Figure 2.A11. Cathodoluminescence images of zircon grains dated by U-Pb LA-ICPMS from sample E1326.

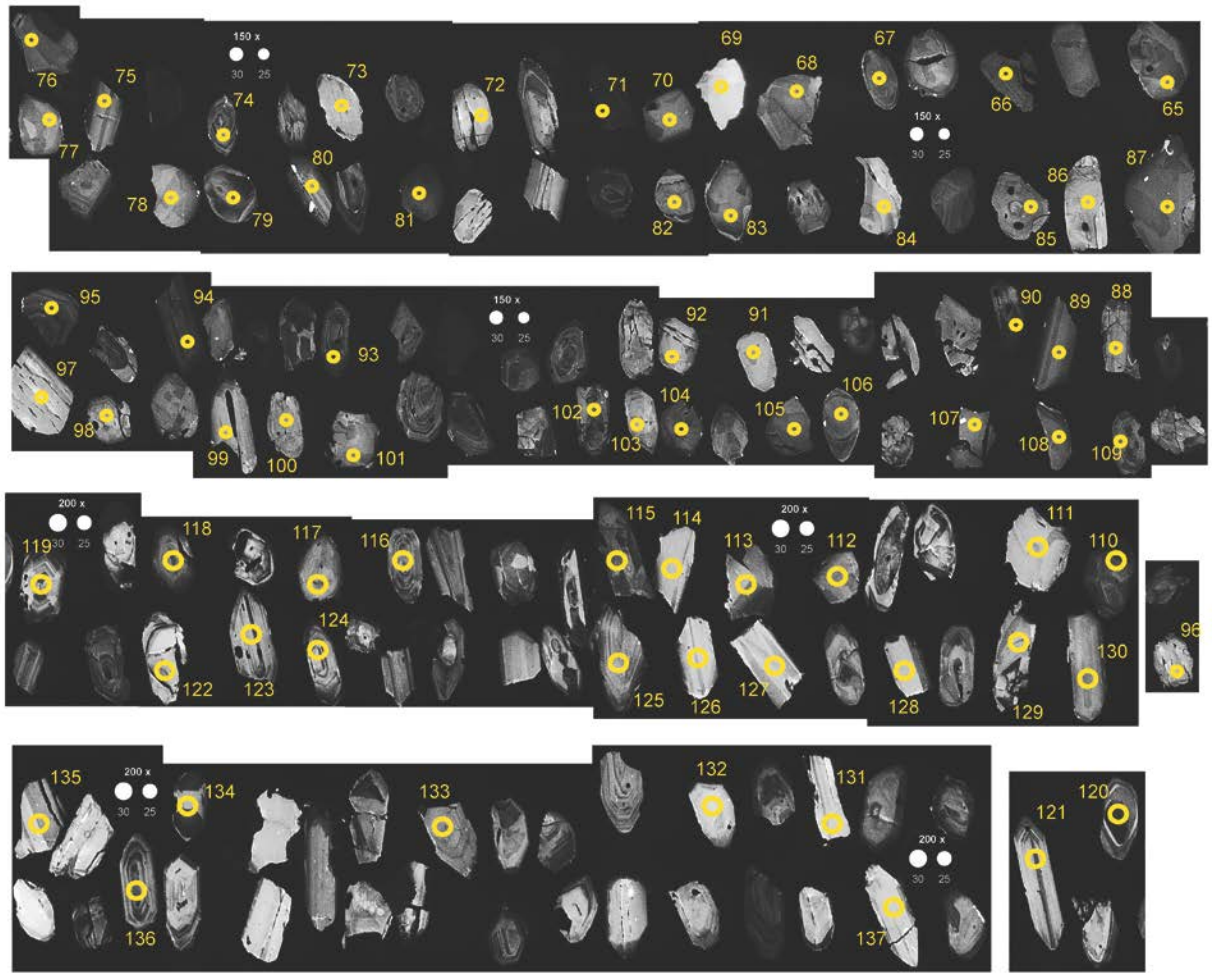

Figure 2.A12. Cathodoluminescence images of zircon grains dated by U-Pb LA-ICPMS from sample E1336-46.

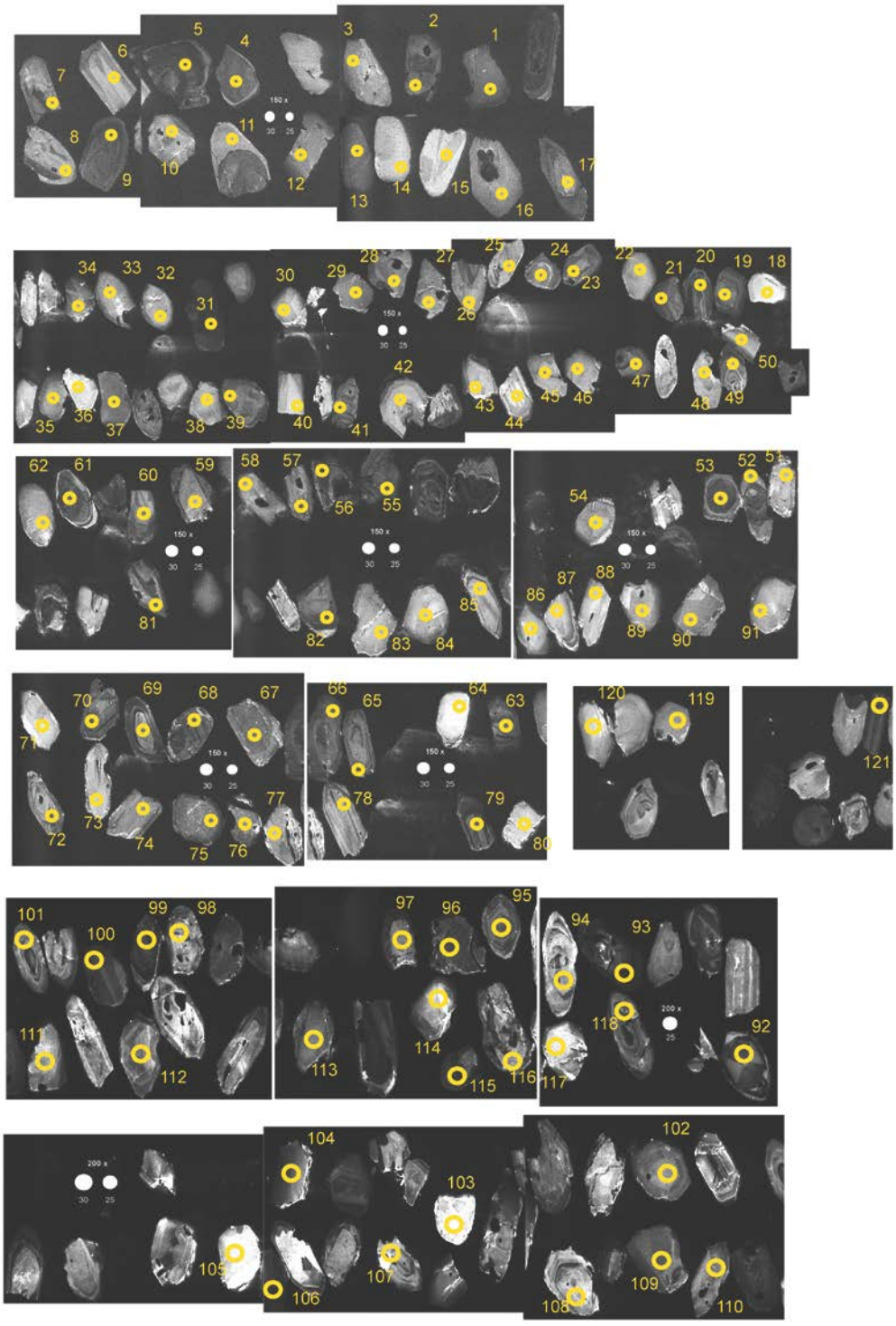

Figure 2.A13. Cathodoluminescence images of zircon grains dated by U-Pb LA-ICPMS from sample DS05.

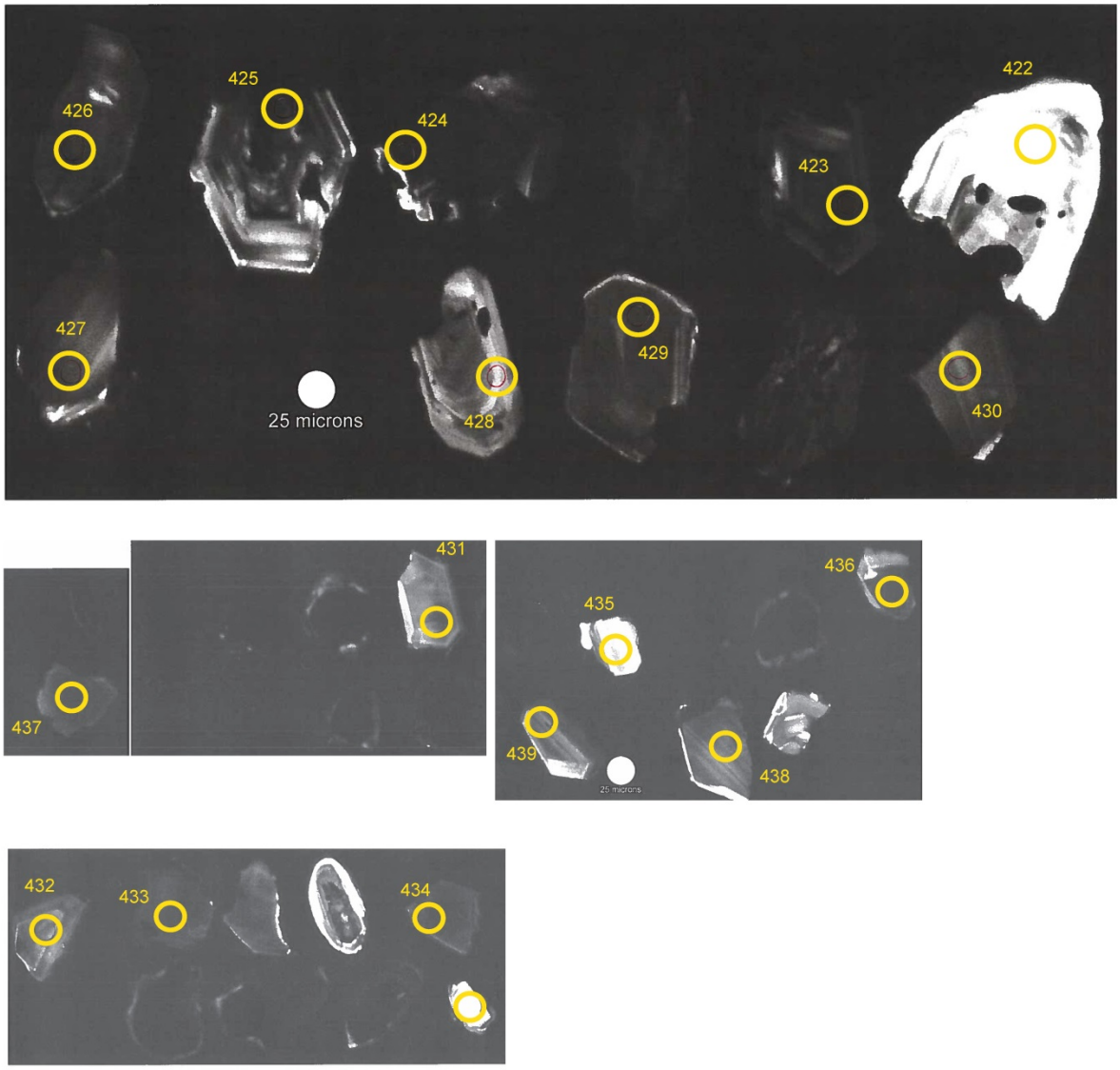

Figure 2.A14. Cathodoluminescence images of zircon grains dated by U-Pb LA-ICPMS from sample US10.

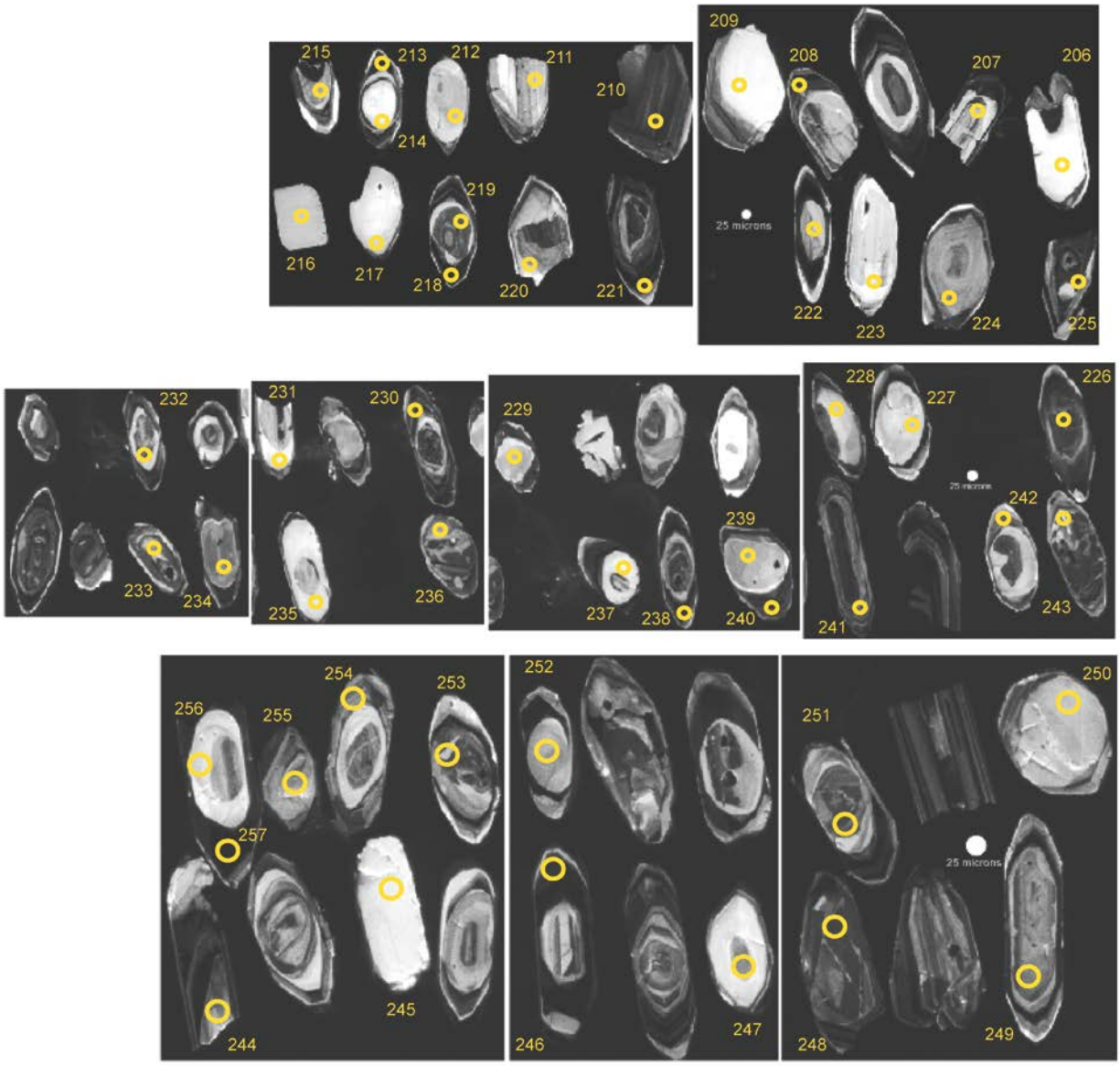

Figure 2.A15. Cathodoluminescence images of zircon grains dated by U-Pb LA-ICPMS from sample DS34.

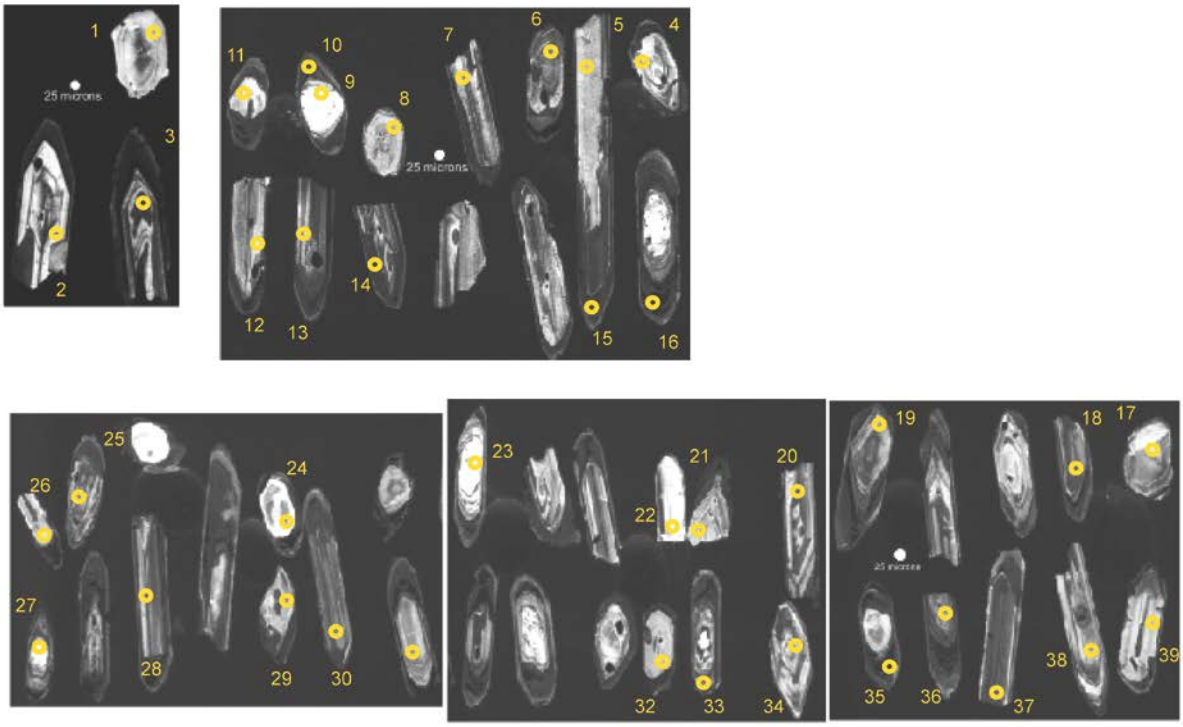

Figure 2.A16. Cathodoluminescence images of zircon grains dated by U-Pb LA-ICPMS from sample U12001.

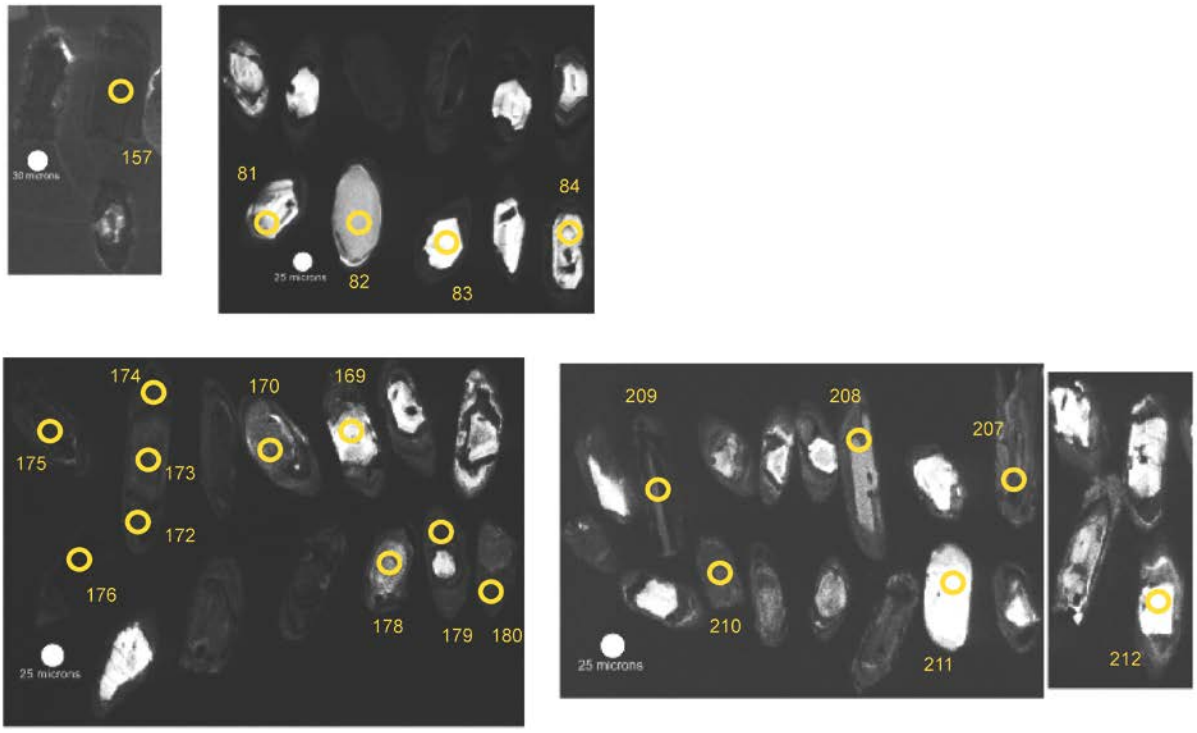

Figure 2.A17. Cathodoluminescence images of zircon grains dated by U-Pb LA-ICPMS from sample US11.

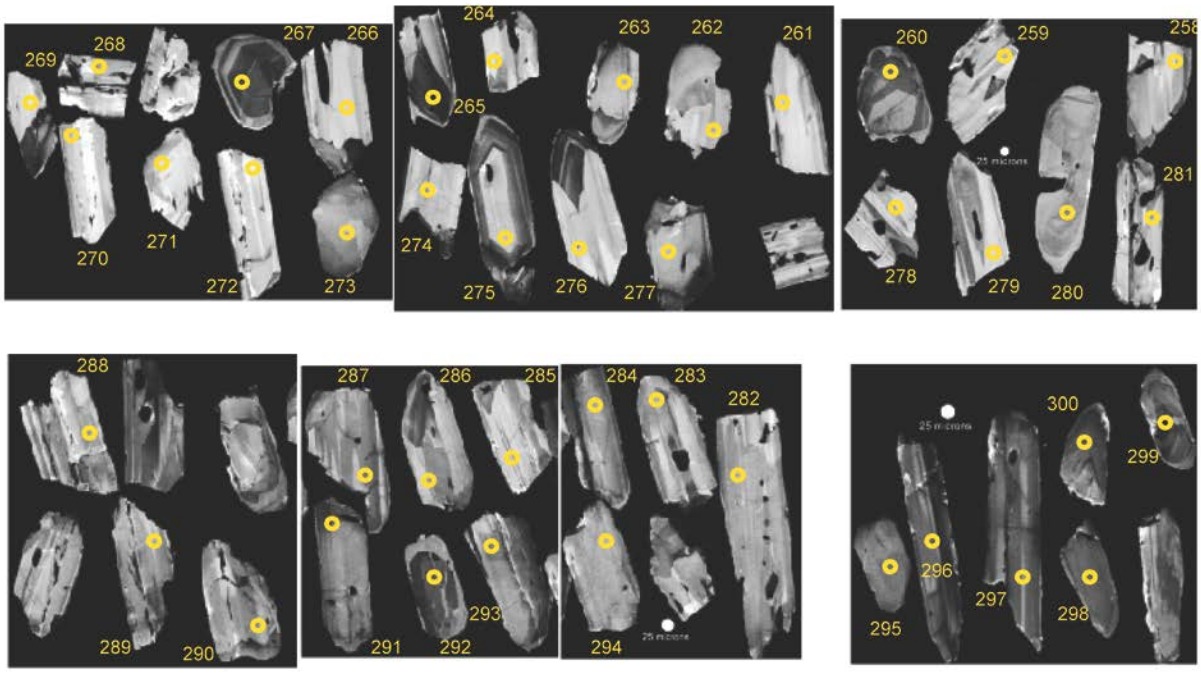

Figure 2.A18. Cathodoluminescence images of zircon grains dated by U-Pb LA-ICPMS from sample F1128B.

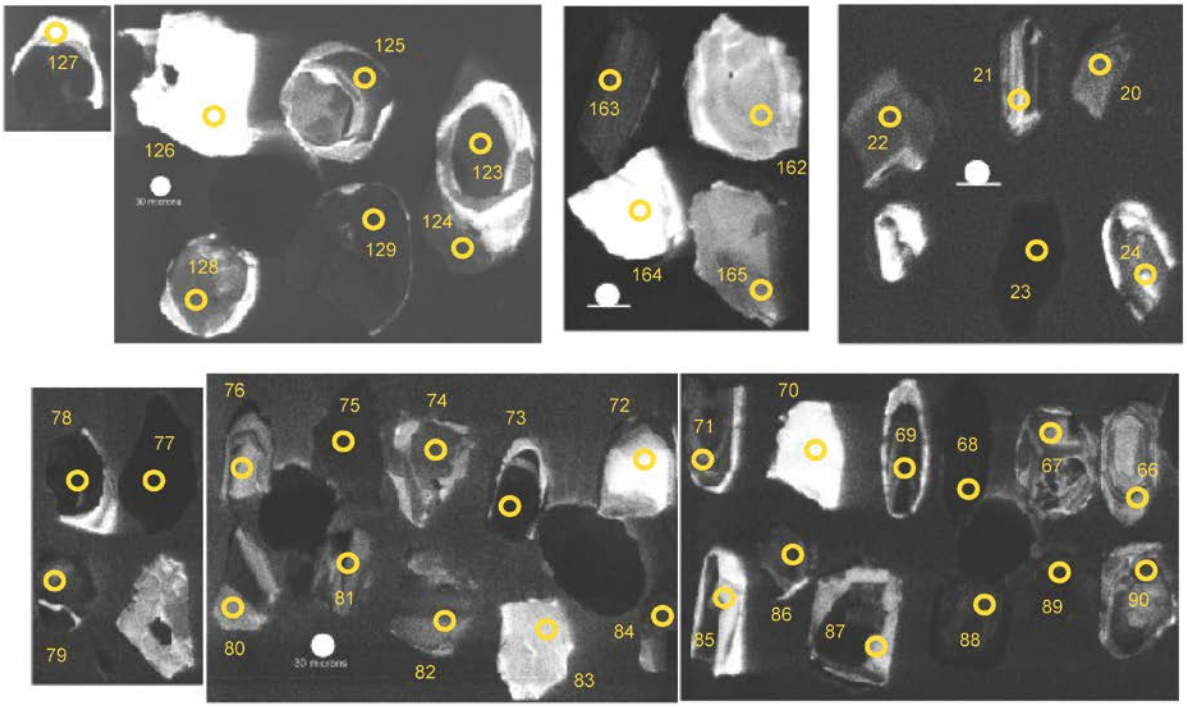

Figure 2.A19. Cathodoluminescence images of zircon grains dated by U-Pb LA-ICPMS from sample F1128A.

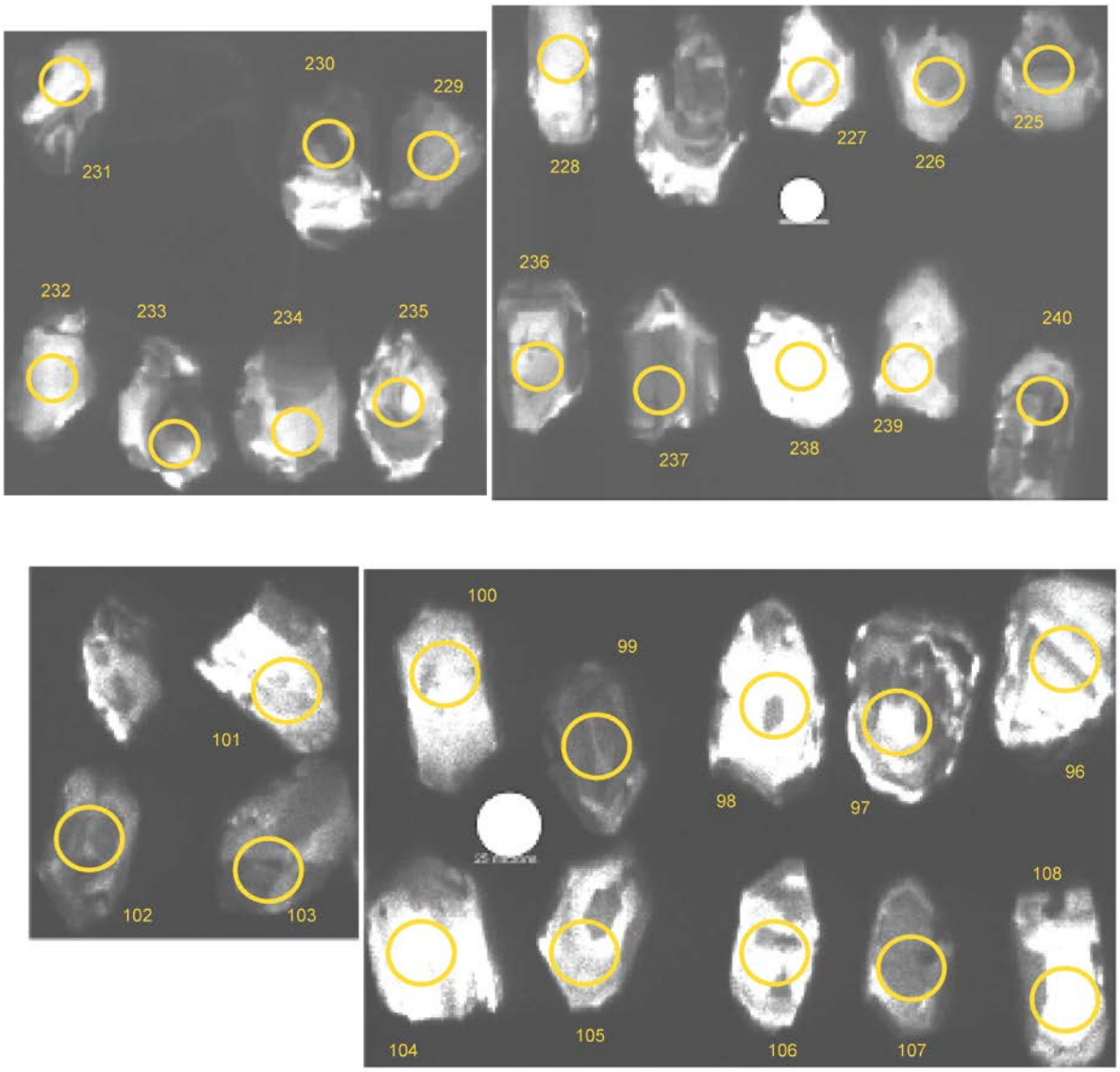

Figure 2.A20. Cathodoluminescence images of zircon grains dated by U-Pb LA-ICPMS from sample U1127-1.

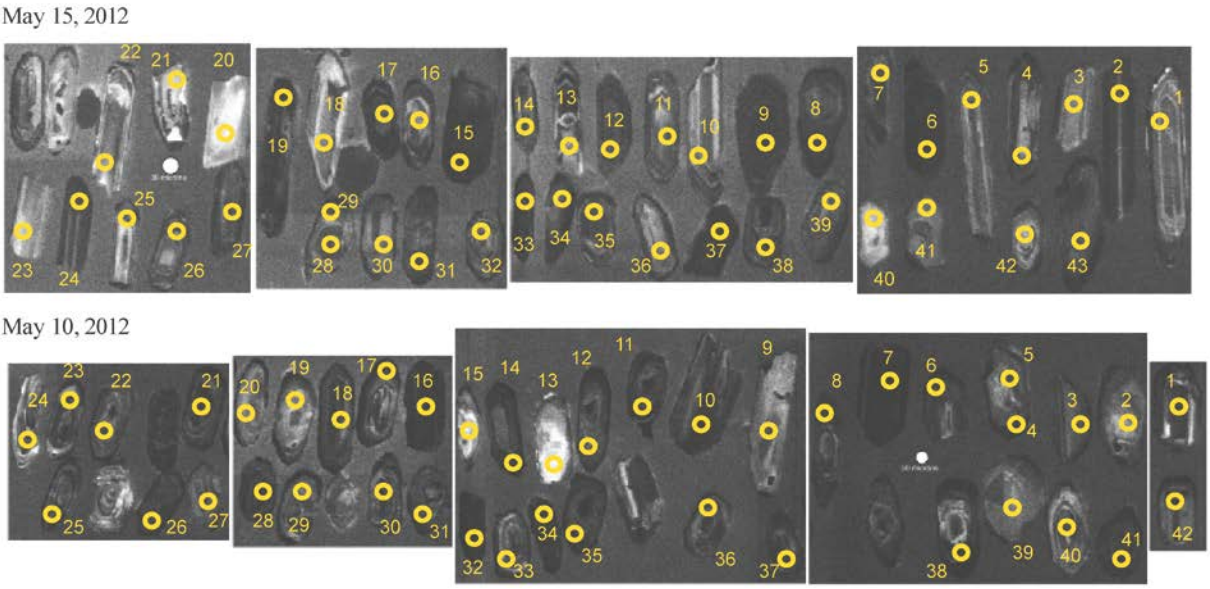

Figure 2.A21. Zircon trace element chemistry of the magmatic samples of the Zavkhan Terrane.
Th/U versus Nb/Hf and Th/Nb versus Hf/Th diagrams. Ratios of concentrations of Hf, Th, and Nb were compared with predefined regions for within-plate/anorogenic and arc-related/orogenic setting (Yang et al., 2012). The Dund-Orthocomplex (TS08) and Zavkhan Fm volcanics are plotted on arc-related/orogenic setting.

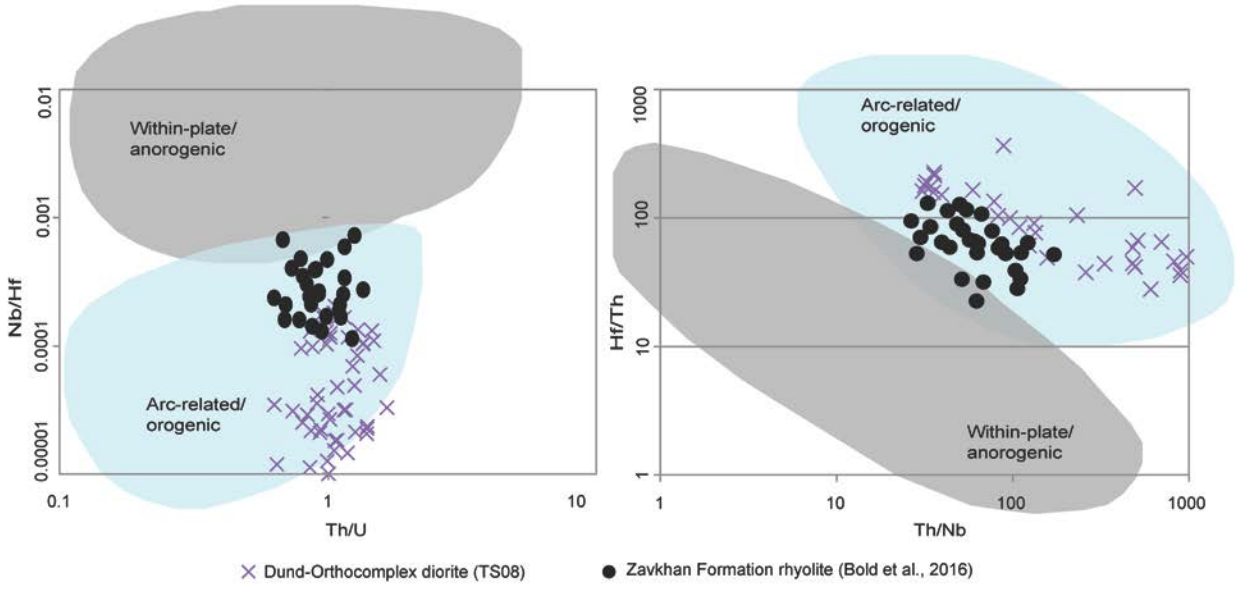

APPENDIX 3.1. SUPPLEMENT TO CHAPTER 3: METHODS

3.1.1. LA-ICPMS method

Zircon grains were separated from rocks using standard techniques, including crushing, pulverizing, washing, magnetic separation, heavy liquids, and hand picking, and annealed at 900^{o}C for 60 hours in a muffle furnace. Annealed zircon grains were directly poured into a petri dish, agitated, and divided into quarters. Depending on the number of zircons separated from each sample, all of the zircons from one quarter were selected. Grains that suit the requirements for analysis were analyzed. These randomly selected grains were mounted in epoxy and polished until their centers were exposed. Cathodoluminescence (CL) images were obtained with a JEOL JSM-1300 scanning electron microscope and Gatan MiniCL. Zircon was analyzed by laser ablation inductively coupled plasma mass spectrometry (LA-ICPMS) using a ThermoElectron X-Series II quadrupole ICPMS and New Wave Research UP-213 Nd:YAG UV (213 nm) laser ablation system at the Boise State University. In-house analytical protocols, standard materials, and data reduction software were used for acquisition and calibration of U-Pb dates and a suite of high field strength elements (HFSE) and rare earth elements (REE) (Paces and Miller 1993, Norman, Pearson et al. 1996, Black, Kamo et al. 2003, Sláma, Košler et al. 2008). Zircon was ablated with a laser spot of 25 or 30 μm wide using fluence and pulse rates of 5 J/cm2 and 10 Hz, respectively, during a 45 second analysis (15 sec gas blank, 30 sec ablation) that excavated a pit ~ 25 μm deep. Ablated material was carried by a 1.2 L/min He gas stream to the nebulizer flow of the plasma. Quadrupole dwell times were 5 ms for Si and Zr, 200 ms for ^{49}Ti and ^{207}Pb, 80 ms for ^{206}Pb, 40 ms for ^{202}Hg, ^{204}Pb, ^{208}Pb, ^{232}Th, and ^{238}U and 10 ms for all other HFSE and REE; total sweep duration is 950 ms. Background count rates for each analyte were obtained prior to each spot analysis and subtracted from the raw count rate for each analyte. For concentration calculations, background-subtracted count rates for each analyte were internally normalized to ^{29}Si and calibrated with respect to NIST SRM-610 and -612 glasses as the primary standards. Ablations pits that appear to have intersected glass or mineral inclusions were identified based on Ti and P signal excursions, and associated sweeps were discarded. U-Pb dates from

these analyses are considered valid if the U-Pb ratios appear to have been unaffected by the inclusions. Signals at mass 204 were normally indistinguishable from zero following subtraction of mercury backgrounds measured during the gas blank (< 1000 cps ^{202}Hg), and thus dates are reported without common Pb correction. Rare analyses that appear contaminated by common Pb were rejected based on mass 204 greater than baseline.

Data were collected in seven experiments in December 2012, May 2013, and December 2014. For U-Pb and ^{207}Pb/^{206}Pb dates, instrumental fractionation of the background-subtracted ratios was corrected and dates were calibrated with respect to interspersed measurements of zircon standards and reference materials. The primary standard Plešovice zircon (Sláma et al., 2008) was used to monitor time-dependent instrumental fractionation based on two analyses for every 10 analyses of unknown zircon. A polynomial fit to the standard analyses yields each sample-specific fractionation factor. A secondary correction to ^{206}Pb/^{238}U of 1.3-3.3% (dependent upon experiment) was made based upon the bias indicated by weighted mean dates from the zircon standards Temora (418 Ma) and FC1 (1098 Ma), which were treated as unknowns and measured once for every 10 analyses of unknown zircon. The secondary correction is thought to mitigate matrix-dependent variations due to contrasting compositions and ablation characteristics between the Plešovice zircon and other standards (and unknowns); because all primary and secondary standards are chemically abraded, bias between standards is not considered to be due to Pb loss.

Radiogenic isotope ratio and age error propagation for all analyses includes uncertainty contributions from counting statistics and background subtraction. Because the detrital zircon analyses are interpreted individually, uncertainties from the standard calibrations are propagated into the errors on each date. These uncertainties are the local standard deviations of the polynomial fits to the interspersed primary standard measurements versus time for the time-dependent, relatively larger U-Pb fractionation factor, and the standard errors of the means of the consistently time-invariant and smaller ^{207}Pb/^{206}Pb fractionation factor. These uncertainties are 1.1-1.6% (2σ) for ^{206}Pb/^{23}8U and 0.5-0.9% (2σ) for ^{207}Pb/^{206}Pb.

Age interpretations are based on $^{207}Pb/^{206}Pb$ dates for analyses with $^{207}Pb/^{206}Pb$ dates > 1000 Ma. Analyses with > 20% positive discordance and > 10% negative discordance are not considered. The $^{206}Pb/^{238}U$ dates are used for analyses with $^{207}Pb/^{206}Pb$ dates < 1000 Ma. Errors on the dates from individual analyses are given at 2σ.

3.1.2. CA-ID-TIMS U-Pb Geochronology Method

Zircons were separated from all samples using standard crushing, magnetic, and high-density liquid separations. Individually selected zircon grains were analyzed by the U-Pb isotope dilution thermal-ionization mass spectrometry (ID-TIMS) technique following the detailed procedures described in Ramezani and others (2011). All zircons were pre-treated by a chemical abrasion (CA-ID-TIMS) method modified after Mattinson (2005) to mitigate the effects of radiation-induced Pb loss, and spiked with the EARTHTIME ET535 mixed ^{205}Pb-^{233}U-^{235}U tracer prior to dissolution and chemical separation of U and Pb. All isotopic measurements were made on a Sector 54 mass spectrometer instrument at the Massachusetts Institute of Technology. Uranium and lead isotopic data reduction, date calculation and propagation of uncertainties were carried out using computer applications and algorithms of Bowring and others (2011) and McLean and others (2011).

Sample dates representing the best estimate for the zircon crystallization age – and interpreted as the volcanic eruption and/or maximum depositional age – are derived from weighted mean $^{206}Pb/^{238}U$ date of a statistically coherent cluster of the youngest zircon analyses from each sample, provided that there are at least three precise analyses to form a cluster. Uncertainties on weighted mean dates are reported at 95% confidence level and follow the notation ± x/y/z Ma, where x is the internal (analytical) uncertainty in the absence of all external errors, y incorporates the U-Pb tracer calibration error and z includes the latter as well as the decay constant errors of Jaffey and others (1971). Total uncertainties (z) are necessary for comparison of dates from different isotopic chronometers (for example U-Pb versus $^{40}Ar/^{39}Ar$ or Re-Os).

3.1.3. Carbonate Carbon and Oxygen Isotope Methods

All carbonate samples were cut perpendicular to bedding, revealing internal textures. Between 5-60 mg of powder were microdrilled from the matrix, avoiding veining, fractures, and siliciclastic components. Carbonate $\delta^{13}C$ and $\delta^{18}O$ isotopic data were acquired simultaneously on a VG Optima dual inlet mass spectrometer attached to a VG Isocarb preparation device (Micromass, Milford, MA) in the Harvard University Laboratory for Geochemical Oceanography. ~ 1 mg micro-drilled samples were reacted in a common, purified H_3PO_4 bath at 90°C. Evolved CO_2 was collected cryogenically and analyzed using an in-house reference gas. External error (1σ) from standards was better than ± 0.1‰ for both $\delta^{13}C$ and $\delta^{18}O$. Samples were calibrated to VPDB (Value of the Pee-Dee Belemnite) using the Cararra marble standard. Potential memory effect resulting from the common acid-bath system was minimized by increasing the reaction time to ten minutes for dolostone samples. Memory effect is estimated at < 0.1‰ based on variability of standards run after dolostone samples. Carbon ($\delta^{13}C$) and oxygen ($\delta^{18}O$) isotopic results are reported in per mil notation of $^{13}C/^{12}C$ and $^{18}O/^{16}O$, respectively, relative to the standard VPDB.

3.1.4. Strontium Isotope Methods

Strontium isotopic analyses were performed on the same aliquots of powders used for carbon and oxygen isotopic analyses. Here we report $^{87}Sr/^{86}Sr$ measurements of 14 samples of the Ol Fm, 11 samples of Sh1 of the Shuurgat Fm, 16 samples of the basal Sh3a and 15 samples of the Sh3b of the Shuurgat Fm analyzed using a ThermoScientific Neptune multicollector inductively-coupled-plasma mass spectrometer (MC-ICPMS) at Woods Hole Oceanographic Institute (WHOI) (Table 3.A4). Forty-four 44 samples of the Taishir Fm were analyzed using an Isotopix 396 IsoProbe T™ in the MIT Radiogenic Isotope Laboratory. In order to test the fidelity of the $^{87}Sr/^{86}Sr$ measurements by ICPMS, three, Sr-rich (> 500 ppm) lime-micrite horizons (F949 – 148, 164, and 184) of the T1 cap carbonate of the Taishir Fm were analyzed with a minimum of 5 duplicates each. On average, these "standards" yielded values of 0.70726, 0.70732, and 0.70741, respectively, displaying variation only in the 4th and 5th decimal place compared to

data obtained using TIMS (0.70722, 0.707273, and 0.70739, respectively; Table 3.A4).

MC-ICPMS Sr analyses: For all analyses, 50 ± 2 mg of powder was dissolved in 15 ml Falcon tubes with an initial washing step using 2 ml of a 1:1 methanol water solution (all steps had 3 cycles intersperced with ~ 15 min sonication). The second step involved adding 1 ml 0.2 N ammonium acetate and the final washing is with deionized water prior to final digestion using 5 ml of 0.5 N acetic acid. Duplicates were created for a subset of samples and 3 ml of the 5 ml acetic acid solution was transferred to a clean tube for major and minor element concentrations, and 1 ml to another clean tube for Sr column chemistry.

Strontium column chemistry was performed on 1 ml of sample to isolate Sr from coexisting matrix elements. The samples, previously dissolved in acetic acid, were dried and redissolved in 3N HNO_3. This step was repeated three times to ensure that all the acetic acid was evaporated. The solution was then loaded onto a preconditioned Sr Spec column. After three consecutive loadings of 0.25 ml 3N HNO_3, to ensure that other elements had been removed, Sr was eluted by 1 reservoir loading (~ 1ml) of ultrapure water. $^{87}Sr/^{86}Sr$ values were generated using ThermoScientific Neptune MC-ICPMS. The measurements were performed with typical ^{88}Sr beam intensities from 30 to 50 volts. $^{87}Sr/^{86}Sr$ ratios were corrected for Kr and Rb, and normalized using the exponential law. The standard NBS 987 was analyzed frequently between samples to monitor the consistency of the measured values and on average, yielded a value of 0.7102719 compared to data reported using TIMS (Smalley et al., 1994).

TIMS Sr analyses: For all analyses, 15 mg of sample powder was used. Initial washing step was 1:1 methanol rinse to remove suspended clays, which is followed by leaching and dissolution steps. Samples were leached three times in 0.2N ammonium acetate and then rinsed three times with MQH_2O. Calcite fraction of each sample was dissolved in 0.5N acetic acid, separated from the insoluble fraction in 3N HNO_3. Sr was separed from the matrix following standard Sr chromatography procedures and measured on an Isotopix IsoProbe T™ in dynamic mode, with target intensity of 3V ^{88}Sr. All data were corrected to $^{86}Sr/^{88}Sr = 0.1194$ for internal mass bias. Each analysis represents a minimum of 60 ratio measurements, with internal precision of better than 0.001% (1σ). Analyses were referenced against NBS

SRM 987 (0.71025), with a long-term average of 0.71024 and 2-σ external precision of 0.000014; no bias correction was made.

APPENDIX 3.2. SUPPLEMENT TO CHAPTER 3: TABLES

Table 3.A1. U-Pb LA-ICPMS geochronological data from the Zavkhan Fm and Tsagaan-Olom Group.

LA-ICPMS data from U1213

		Corrected isotope ratios							Apparent ages (Ma)						
		207Pb*	±2s	206Pb*	±2s	error	207Pb*	±2s	207Pb*	±2s	207Pb*	±2s	206Pb*	±2s	%
Analysis	Th/U	235U*	(%)	238U	(%)	corr.	206Pb*	(%)	206Pb*	(Ma)	235U	(Ma)	238U*	(Ma)	disc.
U1213 L 30		1.223	5.8	0.132	4.0	0.7	0.068	4.2	874	87	811	32	799	30	9
U1213 L 23		1.195	6.0	0.131	3.9	0.6	0.067	4.6	841	96	798	33	794	29	6
U1213 L 12		1.156	4.7	0.131	3.4	0.7	0.065	3.2	780	67	780	25	791	25	-1
U1213 L 8		1.121	5.1	0.130	3.9	0.8	0.064	3.4	728	72	764	27	787	29	-8
U1213 L 10		1.163	5.4	0.130	3.9	0.7	0.066	3.7	806	77	783	29	786	29	2
U1213 L 19		1.146	6.2	0.130	3.3	0.5	0.065	5.2	776	110	775	34	786	25	-1
U1213 L 18		1.152	5.7	0.130	3.8	0.7	0.065	4.2	788	89	778	31	786	28	0
U1213 L 21		1.180	5.9	0.130	4.1	0.7	0.067	4.3	839	89	791	33	785	30	6
U1213 L 2		1.155	6.2	0.129	5.0	0.8	0.066	3.6	797	76	780	34	785	37	2
U1213 L 20		1.245	6.8	0.129	3.5	0.5	0.071	5.9	956	121	821	39	783	26	18
U1213 L 22		1.173	6.6	0.129	3.9	0.6	0.067	5.4	842	111	788	36	780	29	7
U1213 L 32		1.102	7.4	0.128	3.6	0.5	0.063	6.5	718	138	754	39	777	26	-8
U1213 L 11		1.206	6.5	0.128	4.6	0.7	0.069	4.7	909	96	803	36	777	34	15
U1213 L 17		1.219	5.4	0.128	3.4	0.6	0.070	4.2	932	86	809	30	776	25	17
U1213 L 28		1.144	5.5	0.128	3.6	0.7	0.066	4.1	801	87	774	30	776	26	3
U1213 L 34		1.147	5.8	0.128	4.0	0.7	0.066	4.3	812	89	776	32	774	29	5
U1213 L 29		1.164	4.9	0.127	3.9	0.8	0.067	3.0	849	63	784	27	772	28	9
U1213 L 27		1.098	5.8	0.127	3.9	0.7	0.064	4.2	737	90	752	31	768	28	-4
U1213 L 7		1.194	6.2	0.126	4.4	0.7	0.070	4.3	920	89	798	34	766	32	17
U1213 L 24		1.122	6.0	0.126	3.5	0.6	0.066	4.9	794	103	764	32	764	25	4
U1213 L 13		1.123	5.8	0.126	3.6	0.6	0.066	4.6	800	97	765	31	763	26	5
U1213 L 15		1.111	6.4	0.126	3.7	0.6	0.065	5.2	779	109	759	34	762	27	2
U1213 L 25		1.017	7.2	0.125	4.1	0.6	0.060	5.9	593	128	712	37	761	29	-28
U1213 L 35		1.097	7.6	0.125	4.2	0.6	0.065	6.3	761	133	752	40	759	30	0
U1213 L 1		1.094	5.9	0.125	3.8	0.6	0.064	4.5	757	95	750	31	759	27	0
U1213 L 36		1.095	5.6	0.125	4.5	0.8	0.065	3.3	759	69	751	30	759	32	0
U1213 L 3		1.066	5.4	0.125	3.3	0.6	0.063	4.2	707	90	737	28	757	24	-7

U1213 L 5		1.070	6.6	0.124	3.7	0.6	0.063	5.5	719	117	739	35	756	26	-5
U1213 L 31		1.163	5.7	0.124	3.1	0.5	0.069	4.8	897	99	783	31	755	22	16
U1213 L 26		1.125	4.8	0.124	3.1	0.6	0.067	3.6	829	76	766	26	755	22	9
U1213 L 16		1.141	5.8	0.124	3.5	0.6	0.068	4.7	859	97	773	32	754	25	12
U1213 L 4		1.123	5.7	0.123	3.6	0.6	0.067	4.5	849	93	764	31	746	26	12
U1213 L 14		1.106	5.4	0.123	4.8	0.9	0.066	2.5	818	51	756	29	746	34	9
U1213 L 9		1.041	5.5	0.122	3.5	0.6	0.063	4.2	707	89	724	28	740	25	-5
U1213 L 33		1.157	5.5	0.121	3.5	0.6	0.070	4.3	942	87	780	30	735	24	22

LA-ICPMS data from U1213 continued.

	Concentrations (ppm)																					
Analysis	P	Ti	Y	Nb	La	Ce	Pr	Nd	Sm	Eu	Gd	Tb	Dy	Ho	Er	Tm	Yb	Lu	Hf	Ta	Th	U
U1213 L 30	262	7	1413	2	0	20	0	3	8	2	32	11	134	54	238	66	754	97	8877	1	133	145
U1213 L 23	262	6	1638	1	0	23	0	6	11	4	44	13	170	63	273	72	790	96	8157	1	159	130
U1213 L 12	390	5	1360	3	0	32	0	2	6	2	26	9	126	50	224	61	690	88	8654	1	311	271
U1213 L 8	-	-	-	-	-	-	-	-	-	-	-	-	-	-	-	-	-	-	-	-	-	-
U1213 L 10	420	6	1303	3	0	30	0	3	4	1	22	8	108	46	227	64	748	104	8709	1	149	168
U1213 L 19	303	6	1042	2		16	0	2	4	2	20	8	93	38	180	50	605	79	8451	1	75	109
U1213 L 18	379	11	1684	4	0	32	0	2	5	2	28	11	142	61	289	81	950	123	7656	1	110	140
U1213 L 21	350	10	1191	2	0	30	0	2	5	2	23	9	108	45	205	55	649	79	7713	1	200	177
U1213 L 2	351	9	1214	2	0	24	0	2	4	2	24	8	105	44	210	59	658	94	8629	1	109	128
U1213 L 20	-	-	-	-	-	-	-	-	-	-	-	-	-	-	-	-	-	-	-	-	-	-
U1213 L 22	262	7	1403	1	0	20	0	4	8	2	32	11	139	53	238	62	749	90	8511	0	134	142
U1213 L 32	333	9	1143	2		25	0	2	4	1	23	8	101	43	206	56	655	87	9373	1	106	122
U1213 L 11	502	7	1128	1		15	0	0	4	1	20	8	105	41	194	54	646	86	8020	1	64	82
U1213 L 17	310	9	1507	1	0	20	0	5	9	3	45	14	157	59	259	65	750	91	7844	1	127	116
U1213 L 28	488	6	1901	6	2	41	1	5	5	2	30	11	152	68	326	91	1102	135	9193	2	176	261
U1213 L 34	265	6	1039	2		25	0	2	5	1	21	7	91	37	181	50	586	79	9956	1	191	222
U1213 L 29	426	4	1060	3	3	36	1	4	4	1	17	7	95	39	180	50	570	72	10007	1	190	229
U1213 L 27	398	9	1394	3		27	0	2	4	2	25	10	122	51	250	70	817	110	8493	1	101	126
U1213 L 7	376	8	1369	1	0	22	0	2	6	2	31	10	127	51	226	60	687	92	8626	1	110	99
U1213 L 24	478	9	1782	2	1	27	0	4	7	3	37	12	170	67	300	82	913	112	7672	1	122	135
U1213 L 13	326	9	1319	3		26	0	2	4	1	23	8	110	49	225	67	780	107	8627	1	92	126

U1213 L 15	-	-	-	-	-	-	-	-	-	-	-	-	-	-	-	-	-	-	-	-	-	-	-
U1213 L 25	407	4	1136	1	0	16	0	1	4	2	24	8	103	41	197	56	662	84	8958	1	78	114
U1213 L 35	329	8	1139	2	0	27	0	2	4	2	23	8	103	43	198	53	606	77	9100	1	158	143
U1213 L 1	-	-	-	-	-	-	-	-	-	-	-	-	-	-	-	-	-	-	-	-	-	-
U1213 L 36	550	10	2917	6	0	53	0	3	10	4	53	20	261	104	476	121	1347	175	8145	2	367	294
U1213 L 3	406	8	2459	2	0	35	0	8	15	4	68	19	244	93	396	100	1102	148	8687	1	262	195
U1213 L 5	475	12	2134	5	0	46	0	2	8	2	40	13	189	80	378	106	1111	151	8317	1	253	220
U1213 L 31	351	8	1172	2		27	0	1	4	1	22	8	106	44	205	58	640	85	8944	1	138	150
U1213 L 26	335	6	1649	2	1	27	0	6	10	3	38	13	159	61	279	77	869	107	9064	1	171	175
U1213 L 16	365	8	1262	3	0	29	0	2	5	1	25	9	111	45	220	61	720	91	8566	2	134	149
U1213 L 4	-	-	-	-	-	-	-	-	-	-	-	-	-	-	-	-	-	-	-	-	-	-
U1213 L 14	371	4	1287	4	18	55	2	10	5	1	25	10	122	48	220	60	664	84	9187	1	294	298
U1213 L 9	303	5	939	2	1	18	0	2	3	1	16	5	74	32	161	46	571	80	8673	1	67	108
U1213 L 33	314	8	938	1	0	23	0	1	4	1	17	7	81	33	159	43	503	67	9173	1	86	99

Experiment on December 17, 2012

Isotope ratio and date errors include systematic calibration errors of 0.61% ($^{207}Pb/^{206}Pb$) and 1.32% ($^{206}Pb/^{238}U$) (2 sigma).

Trace element concentrations were deleted from analyses known to have intersected inclusions of other minerals based on P and Ti.

Backgrounds were monitored between sweeps 10 to 20. Sample counts were integrated from sweeps 28 to 54.

Ablation used a laser spot size of 30 microns, and a laser firing repetition rate of 10 Hz.

Activity of TiO_2 for Ti-in-Zircon temperature calculation is 0.8.

LA-ICPMS data from U1333

		Corrected isotope ratios							Dates (Ma)						
		207Pb*	±2s	206Pb*	±2s	error	207Pb*	±2s	207Pb*	±2s	207Pb*	±2s	206Pb*	±2s	%
Analysis	Th/U	235U*	(%)	238U	(%)	corr.	206Pb*	(%)	206Pb*	(Ma)	235U	(Ma)	238U*	(Ma)	disc.
U1333 L 136	1.7	25.985	4.6	0.672	3.8	0.8	0.280	2.6	3366	40	3346	45	3313	98	2
U1333 M 214	0.1	21.104	7.0	0.620	6.2	0.9	0.247	3.2	3164	51	3143	68	3111	153	2
U1333 M 166	0.4	16.279	5.4	0.541	4.7	0.9	0.218	2.5	2969	40	2893	51	2786	107	6
U1333 M 165	0.8	16.050	13.1	0.545	10.3	0.8	0.214	8.2	2933	133	2880	126	2804	233	4
U1333 M 163	0.6	12.687	3.8	0.495	3.1	0.8	0.186	2.3	2706	37	2657	36	2592	65	4
U1333 S 261	1.0	12.054	7.2	0.473	6.2	0.9	0.185	3.8	2696	62	2609	68	2498	127	7
U1333 M 226	0.5	13.121	7.1	0.516	6.1	0.9	0.184	3.5	2692	58	2688	67	2683	134	0
U1333 S 235	0.3	12.993	5.4	0.514	5.0	0.9	0.183	2.2	2684	36	2679	51	2672	109	0
U1333 M 216	0.7	12.136	8.5	0.487	7.3	0.9	0.181	4.3	2660	71	2615	80	2557	155	4
U1333 M 159	0.8	11.264	4.2	0.457	3.9	0.9	0.179	1.5	2643	24	2545	39	2424	79	8
U1333 S 257	0.4	10.652	8.9	0.436	7.5	0.8	0.177	4.9	2626	82	2493	83	2334	146	11
U1333 S 236	0.7	11.117	4.4	0.462	3.7	0.8	0.174	2.4	2601	39	2533	41	2449	75	6
U1333 M 187	0.4	12.041	12.3	0.501	10.1	0.8	0.174	7.1	2598	119	2608	116	2620	217	-1
U1333 M 181	0.8	11.157	6.1	0.465	5.3	0.9	0.174	3.0	2597	50	2536	57	2461	108	5
U1333 M 200	0.4	12.077	7.5	0.503	7.0	0.9	0.174	2.6	2597	43	2610	70	2628	151	-1
U1333 M 161	1.1	11.787	4.4	0.492	3.8	0.9	0.174	2.3	2593	38	2588	41	2581	81	0
U1333 L 134	1.0	11.890	5.6	0.499	3.8	0.7	0.173	4.1	2585	68	2596	52	2610	82	-1
U1333 M 168	0.6	10.726	4.2	0.451	3.5	0.8	0.172	2.4	2582	40	2500	39	2400	70	7
U1333 S 240	0.8	10.599	7.0	0.453	6.3	0.9	0.170	3.0	2554	50	2489	65	2409	127	6
U1333 L 149	0.8	10.235	6.4	0.438	5.5	0.9	0.169	3.2	2551	54	2456	59	2343	109	8
U1333 M 184	0.8	10.113	6.8	0.434	5.1	0.8	0.169	4.4	2548	74	2445	63	2323	100	9
U1333 S 251	0.6	10.509	5.3	0.452	4.5	0.9	0.168	2.7	2543	46	2481	49	2406	91	5
U1333 M 219	1.0	9.253	7.4	0.399	6.2	0.8	0.168	4.0	2540	67	2363	67	2164	114	15
U1333 S 232	0.3	10.742	5.5	0.464	4.3	0.8	0.168	3.5	2539	58	2501	51	2455	88	3
U1333 S 238	0.8	9.691	8.4	0.418	6.4	0.8	0.168	5.4	2538	91	2406	77	2253	122	11
U1333 M 170	1.2	10.121	5.3	0.437	4.4	0.8	0.168	2.9	2536	49	2446	49	2339	86	8
U1333 M 164	0.4	10.665	5.0	0.464	4.5	0.9	0.167	2.2	2527	36	2494	47	2455	93	3
U1333 L 147	0.9	10.795	6.9	0.472	5.9	0.9	0.166	3.5	2517	60	2506	64	2491	121	1
U1333 S 237	1.0	9.695	6.5	0.425	5.5	0.9	0.165	3.3	2512	56	2406	59	2283	106	9
U1333 L 151	0.9	10.363	6.3	0.454	5.1	0.8	0.165	3.7	2512	61	2468	58	2415	102	4
U1333 M 199	0.7	10.312	6.9	0.453	5.3	0.8	0.165	4.4	2510	74	2463	64	2407	107	4

U1333 M 227	0.7	10.204	8.7	0.448	7.6	0.9	0.165	4.2	2509	70	2453	80	2386	151	5
U1333 M 180	0.6	10.635	6.2	0.468	5.7	0.9	0.165	2.5	2505	43	2492	58	2476	117	1
U1333 M 223	0.6	10.317	7.0	0.456	5.7	0.8	0.164	4.1	2500	69	2464	65	2420	114	3
U1333 L 150	2.0	10.697	5.7	0.473	4.7	0.8	0.164	3.2	2496	54	2497	53	2498	97	0
U1333 L 133	1.3	10.673	5.1	0.473	4.2	0.8	0.164	2.9	2495	48	2495	47	2495	87	0
U1333 L 138	1.6	10.832	5.5	0.481	4.1	0.8	0.163	3.6	2492	60	2509	51	2529	86	-1
U1333 M 175	0.9	10.130	5.0	0.449	3.9	0.8	0.163	3.0	2492	51	2447	46	2393	78	4
U1333 L 142	0.8	9.732	6.1	0.432	5.6	0.9	0.163	2.4	2490	41	2410	56	2315	109	7
U1333 M 160	2.0	10.441	4.5	0.464	3.7	0.8	0.163	2.6	2490	43	2475	42	2456	77	1
U1333 M 224	0.6	9.818	6.7	0.436	5.9	0.9	0.163	3.1	2489	53	2418	61	2334	115	6
U1333 M 201	1.4	9.684	6.5	0.433	5.8	0.9	0.162	3.0	2480	51	2405	60	2318	113	7
U1333 M 222	0.2	10.125	5.4	0.453	4.5	0.8	0.162	2.9	2479	50	2446	50	2407	91	3
U1333 S 245	1.0	10.488	7.6	0.469	6.8	0.9	0.162	3.6	2477	60	2479	71	2481	139	0
U1333 S 244	0.7	10.510	5.8	0.472	5.4	0.9	0.162	2.2	2472	36	2481	54	2492	111	-1
U1333 M 209	0.5	9.643	9.1	0.433	7.3	0.8	0.161	5.4	2471	90	2401	83	2320	142	6
U1333 M 167	0.9	9.416	6.8	0.424	6.0	0.9	0.161	3.3	2467	55	2379	62	2279	114	8
U1333 M 203	0.6	9.401	6.7	0.426	5.8	0.9	0.160	3.4	2455	57	2378	62	2289	112	7
U1333 L 144	1.3	8.605	7.6	0.391	7.0	0.9	0.160	2.9	2453	50	2297	69	2126	127	13
U1333 S 234	0.1	10.089	5.4	0.458	4.6	0.9	0.160	2.8	2453	47	2443	50	2431	93	1
U1333 L 143	0.4	9.414	5.2	0.428	4.9	0.9	0.160	1.8	2452	30	2379	48	2296	94	6
U1333 M 177	0.5	10.072	3.7	0.458	3.0	0.8	0.159	2.1	2450	36	2441	34	2431	61	1
U1333 M 174	1.2	9.630	5.1	0.442	4.6	0.9	0.158	2.2	2436	37	2400	47	2358	91	3
U1333 L 132	0.7	9.822	4.3	0.451	4.0	0.9	0.158	1.8	2434	30	2418	40	2400	79	1
U1333 L 148	0.4	9.972	6.6	0.465	6.1	0.9	0.156	2.4	2409	41	2432	60	2461	125	-2
U1333 M 191	0.6	9.981	7.6	0.465	6.9	0.9	0.156	3.3	2408	57	2433	70	2463	140	-2
U1333 XS 35	0.7	9.311	7.0	0.441	5.9	0.8	0.153	3.8	2380	64	2369	64	2356	116	1
U1333 M 186	1.3	8.570	7.0	0.418	6.2	0.9	0.149	3.3	2332	56	2293	64	2250	118	4
U1333 M 202	1.3	8.225	6.6	0.405	5.7	0.9	0.147	3.4	2315	58	2256	60	2192	105	5
U1333 M 183	1.3	8.429	6.4	0.417	5.3	0.8	0.146	3.6	2305	61	2278	58	2249	101	2
U1333 M 213	1.1	7.513	7.6	0.373	6.8	0.9	0.146	3.3	2302	57	2175	68	2042	119	11
U1333 S 258	0.8	8.171	7.4	0.406	6.8	0.9	0.146	2.9	2299	50	2250	67	2197	126	4
U1333 S 243	1.4	7.887	7.2	0.393	6.1	0.8	0.146	3.8	2295	66	2218	65	2136	110	7
U1333 L 135	1.1	8.645	6.5	0.432	5.6	0.9	0.145	3.3	2288	56	2301	59	2316	110	-1
U1333 L 137	0.8	8.456	4.5	0.426	3.5	0.8	0.144	2.8	2277	49	2281	41	2285	68	0
U1333 S 248	0.1	8.027	6.7	0.404	5.8	0.9	0.144	3.3	2277	57	2234	60	2188	108	4

U1333 S 247	0.5	7.610	11.6	0.383	9.4	0.8	0.144	6.8	2275	117	2186	104	2092	168	8
U1333 M 217	1.1	7.625	7.3	0.385	5.8	0.8	0.144	4.3	2273	74	2188	65	2098	105	8
U1333 M 173	1.6	8.059	7.3	0.408	5.8	0.8	0.143	4.4	2267	75	2238	66	2206	108	3
U1333 M 182	0.7	7.941	7.6	0.403	6.7	0.9	0.143	3.6	2261	62	2224	68	2185	123	3
U1333 S 239	0.7	7.996	7.6	0.409	6.7	0.9	0.142	3.5	2248	61	2231	68	2211	125	2
U1333 M 178	0.4	7.742	4.3	0.398	3.9	0.9	0.141	1.7	2239	30	2202	39	2161	72	3
U1333 L 153	0.2	7.866	4.4	0.405	3.7	0.8	0.141	2.4	2239	41	2216	39	2191	68	2
U1333 M 192	0.5	7.945	7.8	0.409	6.9	0.9	0.141	3.7	2238	64	2225	71	2210	129	1
U1333 L 139	0.7	7.917	4.4	0.409	3.8	0.9	0.141	2.2	2234	37	2222	40	2208	71	1
U1333 M 211	0.1	7.459	7.7	0.385	6.9	0.9	0.140	3.4	2232	59	2168	69	2101	124	6
U1333 L 145	0.6	7.267	5.4	0.375	5.0	0.9	0.140	2.0	2232	34	2145	48	2055	88	8
U1333 M 162	1.0	7.343	9.4	0.380	5.6	0.6	0.140	7.6	2229	131	2154	84	2076	100	7
U1333 L 146	0.4	7.561	6.9	0.393	6.0	0.9	0.140	3.3	2222	58	2180	62	2136	110	4
U1333 S 254	0.8	7.447	8.6	0.388	7.4	0.9	0.139	4.5	2218	78	2167	77	2113	133	5
U1333 M 208	0.5	7.151	6.7	0.373	5.9	0.9	0.139	3.1	2217	54	2130	60	2042	104	8
U1333 M 220	1.0	7.359	9.0	0.385	7.3	0.8	0.139	5.3	2212	91	2156	80	2098	131	5
U1333 L 152	0.5	7.414	4.2	0.389	3.7	0.9	0.138	2.0	2205	34	2163	37	2118	67	4
U1333 M 225	1.2	7.560	8.6	0.397	7.7	0.9	0.138	3.7	2204	64	2180	77	2155	142	2
U1333 M 157	1.0	6.547	6.1	0.344	4.8	0.8	0.138	3.6	2202	63	2052	53	1906	80	13
U1333 M 207	0.5	7.143	7.0	0.376	6.6	0.9	0.138	2.5	2199	43	2129	63	2058	116	6
U1333 M 156	0.7	7.459	5.4	0.395	4.3	0.8	0.137	3.2	2190	56	2168	48	2145	78	2
U1333 M 197	0.7	7.901	6.9	0.420	6.0	0.9	0.136	3.4	2182	60	2220	63	2261	115	-4
U1333 M 212	0.6	6.753	7.6	0.361	6.3	0.8	0.136	4.2	2172	73	2080	67	1987	108	9
U1333 S 255	1.1	6.603	9.4	0.355	7.8	0.8	0.135	5.3	2162	92	2060	83	1959	132	9
U1333 M 188	0.5	6.669	7.6	0.359	7.0	0.9	0.135	2.9	2161	50	2068	67	1976	119	9
U1333 M 205	0.5	6.718	7.6	0.363	6.2	0.8	0.134	4.3	2152	76	2075	67	1998	106	7
U1333 M 198	0.5	6.474	8.5	0.352	6.9	0.8	0.133	5.0	2141	88	2042	75	1946	116	9
U1333 M 185	0.3	6.707	4.8	0.366	4.0	0.8	0.133	2.7	2139	47	2074	43	2009	69	6
U1333 M 204	0.9	6.510	6.9	0.356	6.3	0.9	0.133	2.9	2134	51	2047	61	1962	106	8
U1333 M 215	0.4	7.334	8.9	0.404	8.1	0.9	0.132	3.8	2122	67	2153	80	2186	149	-3
U1333 S 230	0.9	6.296	5.5	0.348	4.6	0.8	0.131	3.0	2116	53	2018	48	1923	76	9
U1333 M 176	0.9	6.622	5.0	0.366	4.7	0.9	0.131	1.9	2116	33	2062	44	2009	81	5
U1333 S 233	0.7	6.581	6.7	0.366	5.8	0.9	0.130	3.4	2103	59	2057	59	2011	100	4
U1333 S 259	0.9	5.884	7.1	0.331	5.7	0.8	0.129	4.2	2085	74	1959	62	1842	92	12
U1333 S 249	0.5	6.395	7.2	0.361	6.7	0.9	0.129	2.5	2079	45	2032	63	1985	114	5

U1333 S 246	0.4	6.234	8.2	0.353	7.9	1.0	0.128	2.2	2072	39	2009	72	1948	132	6
U1333 M 171	0.4	6.496	5.0	0.368	4.4	0.9	0.128	2.3	2072	41	2045	44	2019	77	3
U1333 L 141	1.6	6.538	6.2	0.371	5.6	0.9	0.128	2.8	2068	49	2051	55	2034	97	2
U1333 M 195	1.5	6.167	8.3	0.352	7.0	0.8	0.127	4.5	2060	80	2000	73	1943	117	6
U1333 S 252	1.7	5.750	8.2	0.328	6.7	0.8	0.127	4.7	2058	83	1939	71	1829	107	11
U1333 L 140	0.6	6.364	5.0	0.364	4.6	0.9	0.127	1.9	2055	34	2027	44	2000	79	3
U1333 S 229	0.0	6.558	7.5	0.375	7.0	0.9	0.127	2.7	2053	47	2054	66	2054	123	0
U1333 M 194	1.1	6.454	6.3	0.371	5.2	0.8	0.126	3.6	2044	64	2040	56	2035	90	0
U1333 S 262	0.3	6.867	9.1	0.396	8.4	0.9	0.126	3.5	2040	62	2094	81	2150	154	-5
U1333 S 228	1.5	5.998	8.4	0.346	6.5	0.8	0.126	5.3	2040	93	1976	73	1915	107	6
U1333 M 193	1.9	5.872	8.5	0.340	7.0	0.8	0.125	4.7	2034	84	1957	74	1885	115	7
U1333 M 189	0.5	6.305	8.3	0.366	7.2	0.9	0.125	4.1	2029	73	2019	72	2009	124	1
U1333 S 241	1.2	6.060	9.6	0.354	7.8	0.8	0.124	5.7	2017	101	1985	84	1954	131	3
U1333 M 179	0.9	5.874	6.2	0.344	5.3	0.8	0.124	3.3	2015	59	1957	54	1904	87	6
U1333 S 250	1.0	5.748	6.8	0.336	6.1	0.9	0.124	2.9	2014	52	1939	59	1869	99	7
U1333 S 231	0.6	5.995	6.2	0.351	5.8	0.9	0.124	2.4	2011	43	1975	54	1941	97	3
U1333 M 155	2.1	5.673	8.1	0.333	5.9	0.7	0.123	5.6	2006	99	1927	70	1855	95	7
U1333 S 256	1.2	5.885	8.3	0.357	6.0	0.7	0.120	5.7	1949	102	1959	72	1969	102	-1
U1333 S 242	0.4	4.873	7.1	0.298	5.6	0.8	0.119	4.4	1938	78	1798	60	1679	83	13
U1333 S 260	0.8	5.808	7.8	0.361	6.5	0.8	0.117	4.3	1905	78	1948	67	1988	111	-4
U1333 S 260	0.8	5.722	8.9	0.360	7.8	0.9	0.115	4.3	1887	78	1935	77	1980	134	-5

	Concentrations (ppm)																					
Analysis	P	Ti	Y	Nb	La	Ce	Pr	Nd	Sm	Eu	Gd	Tb	Dy	Ho	Er	Tm	Yb	Lu	Hf	Ta	Th	U
U1333 L 136	371	9	1377	4		26	0	1	5	1	28	10	130	48	211	45	401	70	10881	2	120	71
U1333 M 214	107	1	220	0		0				0	2	1	16	8	41	13	175	29	9492	1	18	218
U1333 M 166	229	6	663	1	0	10	0	4	6	2	19	6	61	22	103	26	251	39	9898	1	94	243
U1333 M 165	166	7	581	9		13	0	1	2	0	11	4	60	21	96	23	212	32	10271	4	5	6
U1333 M 163	278	3	964	5		18		1	3	0	21	8	99	35	153	34	334	50	12259	3	170	279
U1333 S 261	194	16	525	2		6	0	1	2	0	11	5	57	20	83	20	217	25	8072	1	36	37
U1333 M 226	168	9	734	4		7		1	2	0	19	6	75	30	119	28	279	40	9554	2	63	117
U1333 S 235	135	7	467	6		11		0	1	0	7	3	49	18	88	24	270	32	11082	4	90	271
U1333 M 216	189	4	663	1		6	0	3	3	0	22	7	69	26	109	26	277	37	8008	1	34	50
U1333 M 159	393	9	1174	4	0	23	1	7	9	2	35	10	132	42	176	36	335	51	11985	2	296	365

U1333 S 257	117	3	418	0		3	0	3	5	2	23	5	59	15	56	12	113	12	7913	0	22	56
U1333 S 236	170	13	868	3		7	0	3	8	0	30	10	113	37	148	33	336	38	8799	1	61	91
U1333 M 187	98	6	153	0		7	0	0	1	1	4	1	13	5	23	7	86	15	9721	0	45	129
U1333 M 181	147	4	484	1		11		1	1	0	9	3	43	17	80	22	219	31	9642	1	79	102
U1333 M 200	127	2	287	0		6			1	0	8	2	26	9	40	12	135	17	10637	1	37	103
U1333 M 161																						
U1333 L 134	103	7	431	1		15		1	2	0	10	3	36	14	65	15	139	29	12033	0	60	57
U1333 M 168	226	5	569	3		8	0	0	2	0	9	4	48	20	96	22	219	33	10086	1	47	80
U1333 S 240	148	10	524	1		15	0	3	5	1	21	6	69	22	90	22	237	29	9251	0	49	63
U1333 L 149	187	8	598	1	0	10	0	1	1	0	13	4	56	21	95	21	193	35	12823	0	49	62
U1333 M 184	112	9	297	0		10	0	1	3	1	13	3	36	11	45	10	113	16	9316	0	30	37
U1333 S 251	233	4	1126	0		5	0	2	5	1	29	10	123	43	190	46	510	64	8743	1	64	108
U1333 M 219	167	18	663	1	0	24	1	16	18	3	45	10	81	25	92	20	195	23	7170	1	304	293
U1333 S 232	210	13	459	1		4	0	1	3	1	17	5	53	18	74	19	210	28	7755	1	24	71
U1333 S 238	152	5	417	1		20	0	2	2	1	12	3	46	16	73	18	213	28	7478	0	14	18
U1333 M 170	138	7	345	2		45	0	2	3	1	16	4	36	10	43	11	98	16	8403	1	84	71
U1333 M 164	130	3	838	0		4	0	3	6	2	21	8	87	30	135	32	303	50	9059	0	67	160
U1333 L 147	83	10	171	0		8		1	1	0	5	1	16	5	27	5	60	10	11101	0	40	44
U1333 S 237	168	6	494	1	0	13		1	4	1	13	5	60	20	85	22	232	26	8638	0	67	69
U1333 L 151	117	9	254	1		20	0	0	1	0	8	2	25	7	36	8	79	15	11406	0	51	54
U1333 M 199	169	14	349	1		11	0	1	2	0	9	3	35	13	62	15	162	23	9214	0	46	62
U1333 M 227	214	4	816	1	0	12	0	2	4	0	28	8	91	32	131	29	290	41	10623	0	43	59
U1333 M 180	137	11	329	1		14		1	2	0	11	3	36	12	51	13	117	17	9866	1	74	118
U1333 M 223	148	10	244	1		14		0	2	0	6	2	25	9	38	9	89	14	9050	0	28	49
U1333 L 150	158	22	1029	0	0	47	1	21	22	5	61	14	125	37	145	28	253	45	9492	0	223	109
U1333 L 133	134	8	546	1		30	0	2	5	1	22	5	57	17	75	14	142	23	10821	0	99	77
U1333 L 138	148	13	359	1		30	0	3	3	1	17	4	35	12	49	9	91	16	9409	0	76	48
U1333 M 175	170	14	545	1	0	15	0	2	2	0	15	5	56	20	84	20	192	34	11480	1	57	63
U1333 L 142	213	9	797	1		17	0	3	6	1	26	8	77	29	121	28	282	44	9996	1	70	87
U1333 M 160	396	10	1475	6		37	0	3	6	1	35	13	147	54	245	54	472	75	11877	3	319	161
U1333 M 224	435	4	985	1		7	0	1	4	1	17	7	95	37	166	42	433	68	9321	0	71	115
U1333 M 201	253	6	1091	1		14	0	3	7	1	35	12	134	45	182	40	419	51	9726	0	115	82
U1333 M 222	127	2	462	2		3			0		5	3	37	14	69	22	217	34	9501	2	52	228
U1333 S 245	120	3	310	0	0	17	0	1	2	1	8	3	36	13	56	14	155	21	9520	0	72	72
U1333 S 244	152	12	261	1		17	0	0	2	1	11	3	30	10	42	10	113	14	9603	1	91	132

U1333 M 209	100	4	569	0		2	0	1	3	1	13	5	60	23	96	22	240	32	7556	0	27	51
U1333 M 167	191	6	808	1		13	0	5	6	2	25	7	78	27	132	33	341	56	7972	0	74	79
U1333 M 203	115	3	262	0		6		0	2	0	8	2	27	9	43	11	128	19	9286	0	37	58
U1333 L 144	152	23	745	1	0	12	1	8	10	2	31	8	78	26	111	24	231	36	9283	0	204	159
U1333 S 234	72	1	73	0		1			0	0	3	1	9	3	11	3	30	3	12734	0	25	172
U1333 L 143	147	6	238	1		8		1	3	0	13	3	29	8	28	6	53	8	13615	0	69	162
U1333 M 177	210	3	774	2		7		1	2	0	22	8	79	28	115	25	239	38	11896	2	127	264
U1333 M 174	133	4	389	2		11		0	1	0	9	3	38	13	56	15	135	25	11768	1	101	84
U1333 L 132	177	3	645	2		23		1	2	0	13	5	60	22	99	24	224	37	13160	1	104	152
U1333 L 148	111	3	172	1		7		0	0	0	3	2	18	6	29	7	62	13	13691	1	33	91
U1333 M 191	174	5	349	0		2		0	2	0	9	3	35	13	63	15	161	22	7712	0	25	43
U1333 XS 35	195	13	1109	1		3	0	6	10	3	46	12	129	40	165	34	296	45	8490	1	22	33
U1333 M 186	190	5	1620	2	0	21	1	20	26	1	79	21	209	63	248	51	457	57	9245	2	221	174
U1333 M 202	339	12	1012	3		38	0	4	7	2	32	10	113	39	167	41	429	54	9681	2	132	104
U1333 M 183	224	6	441	2		21	0	2	1	0	13	4	50	17	74	16	162	23	10521	1	112	85
U1333 M 213	591	9	1340	3		12	0	2	6	0	29	12	137	52	216	51	522	67	9631	2	170	161
U1333 S 258	250	8	497	1		4	0	1	4		18	6	62	20	75	19	183	20	10007	0	97	129
U1333 S 243	220	10	402	2		29	0	1	3	0	14	5	49	16	67	16	184	24	10195	1	157	114
U1333 L 135	194	11	433	1		19		1	2	0	11	4	40	16	69	15	129	24	11648	0	96	86
U1333 L 137	434	14	1663	3		9	0	1	2	1	30	11	153	59	277	63	597	106	10732	1	67	82
U1333 S 248	216	10	252	1		3	0	2	6	1	28	7	46	9	25	4	27	3	11729	1	17	115
U1333 S 247	198	9	344	0		6		1	0	0	8	3	32	12	62	16	177	25	8834	0	34	68
U1333 M 217	217	9	448	3		21		1	1	0	11	3	40	17	73	20	222	30	8079	1	70	66
U1333 M 173	165	26	465	1		10	0	3	4	1	21	5	52	17	68	14	122	22	8124		33	22
U1333 M 182	208	14	710	7	0	26	0	1	3	0	17	7	69	26	123	28	287	40	10696	2	74	107
U1333 S 239	197	8	502	3		12	0	2	3	0	15	5	60	21	87	23	233	28	10152	1	106	145
U1333 M 178	126	3	735	9		13	0	1	3		17	6	71	28	130	30	295	40	11956	5	98	272
U1333 L 153	441	1	1117	4		3			3	0	17	8	98	37	176	39	398	65	14309	2	57	252
U1333 M 192	422	10	799	2		3	0	0	3	0	24	11	112	28	83	11	76	6	10178	2	61	125
U1333 L 139	185	14	434	3		31		1	2	0	12	3	40	14	69	16	151	27	11436	1	167	223
U1333 M 211	112	3	128	1	1	4	0	1	3	3	8	2	17	5	20	4	48	6	9339	1	8	83
U1333 L 145	172	11	807	2		5	0	2	3	0	17	6	78	29	129	27	261	44	12001	1	165	295
U1333 M 162	125	3	193	0	0	3	0	0	1	1	6	2	19	7	31	6	64	13	5833	0	14	14
U1333 L 146	148	9	326	1		2		1	1	0	8	3	36	11	47	10	98	17	12086	1	41	96
U1333 S 254	146	13	414	2		9	0	1	3	0	16	5	53	17	71	17	180	23	7944	1	43	56

U1333 M 208	163	7	385	1		10			2	0	9	3	40	13	61	14	145	19	9783	1	66	143
U1333 M 220	153	14	1458	2	0	18	1	16	19	1	65	19	193	58	224	49	479	59	7800	1	131	133
U1333 L 152	119	17	462	1		7	0	2	2	0	14	4	48	16	72	15	151	25	9360	1	125	230
U1333 M 225	174	5	999	2	0	15	0	7	9	1	36	10	108	39	160	36	346	50	9329	1	188	152
U1333 M 157	172	9	556	3	0	52	0	4	5	1	18	5	51	18	83	20	203	32	12078	1	288	275
U1333 M 207	486	7	1007	4		11	0	3	5	0	24	8	108	38	166	39	401	51	10674	2	126	247
U1333 M 156	257	13	681	1		8	0	2	3	0	17	5	64	25	108	26	253	42	8525	0	69	102
U1333 M 197	166	9	442	1		9		1	1	1	10	4	47	15	71	17	178	24	8267	1	118	180
U1333 M 212	161	8	585	3		13		1	3	0	15	5	67	23	103	25	252	32	8606	1	82	130
U1333 S 255	155	10	544	4	0	35	0	4	4	1	18	6	65	23	95	24	242	31	9733	2	227	213
U1333 M 188	147	3	512	2	0	16	0	3	4	1	15	5	56	20	83	19	181	24	10995	1	148	314
U1333 M 205	149	9	351	0		6		1	2	0	8	3	36	12	60	14	161	22	8480	0	37	75
U1333 M 198	238	6	781	5	5	29	2	10	5	0	20	7	80	29	129	31	304	40	8889	2	54	103
U1333 M 185	280	9	486	1		2	0	1	2	0	18	5	55	19	64	16	160	21	9894	1	78	304
U1333 M 204	184	12	400	1		11	0	1	4	0	11	3	43	15	68	18	180	25	8006	0	67	70
U1333 M 215	120	6	253	1		6		0	1	0	7	2	26	9	38	10	102	14	9780	0	39	96
U1333 S 230	371	18	493	0		3	0	5	10	1	34	8	69	19	68	15	154	15	8348	0	86	96
U1333 M 176	143	5	1061	0		14	0	3	8	2	35	9	106	36	167	41	391	72	12630	0	231	256
U1333 S 233	250	19	578	2		23	0	3	5	1	24	6	75	26	102	25	265	33	8214	1	48	68
U1333 S 259	171	15	487	5		33	0	2	5	1	16	6	58	18	74	18	185	23	8069	2	65	69
U1333 S 249	80	2	461	0		3	0	2	3	1	13	4	45	18	85	24	292	41	7791	0	102	192
U1333 S 246	313	20	287	1		3	0	4	9	0	39	8	58	11	27	4	28	2	11255	0	145	369
U1333 M 171	282	6	572	1		10	0	2	4	1	21	6	60	20	89	20	197	32	10136	1	103	230
U1333 L 141	148	12	603	4		37	0	4	6	1	19	6	65	22	83	20	178	26	9709	1	195	126
U1333 M 195	267	27	643	5		42	0	4	7	1	26	7	79	26	103	24	248	31	8641	2	146	100
U1333 S 252	236	39	633	1		26	1	10	14	3	39	10	94	27	94	22	214	25	7727	0	50	30
U1333 L 140	132	2	450	2		12		0	2	0	10	3	48	15	64	14	136	22	13067	1	137	236
U1333 S 229	79	4	30	0	0	1		0	1	1	4	1	5	1	2	0	3	1	10002	0	4	325
U1333 M 194	154	7	351	2		27	0	1	3	1	13	3	41	12	53	13	124	15	9508	1	112	104
U1333 S 262	240	9	171	0		0	0		3		18	4	30	6	18	4	41	5	11743	1	52	191
U1333 S 228	232	24	467	4		56	0	2	4	1	14	5	55	19	75	19	188	23	8244	1	42	29
U1333 M 193	101	30	464	1	0	28	1	10	9	4	33	7	64	18	70	16	152	18	7666	0	120	64
U1333 M 189	212	5	1762	2		14	0	8	15	2	64	20	225	66	260	56	509	61	8881	2	163	305
U1333 S 241	185	34	365	1		25	0	3	4	1	14	4	49	14	56	13	142	17	8786	1	37	30
U1333 M 179																						

U1333 S 250	167	15	587	3		28	0	2	3	1	22	6	68	24	101	23	237	28	9399	1	196	187
U1333 S 231	174	9	539	8		31	0	2	4	0	13	5	60	21	93	25	281	35	10085	4	144	248
U1333 M 155	239	36	1088	1		28	0	8	12	3	49	13	132	41	150	31	274	42	9497	1	71	33
U1333 S 256	197	39	494	1		22	0	4	6	2	26	6	67	19	82	18	195	23	8753	1	40	33
U1333 S 242	138	14	366	4		6	0	1	2	0	8	3	41	14	63	16	151	19	9620	2	47	109
U1333 S 260	174	14	325	4		28	0	2	3	0	11	3	35	13	57	15	157	19	9263	2	108	130
U1333 S 260	174	14	325	4		28	0	2	3	0	11	3	35	13	57	15	157	19	9263	2	108	130

Experiment 12 - 18 December 2014

Isotope ratio and date errors include systematic calibration errors of 0.91% ($^{207}Pb/^{206}Pb$) and 1.59% ($^{206}Pb/^{238}U$) (all 2-sigma).

Trace element concentrations were deleted from analyses known to have intersected inclusions of non-zircon minerals based on P and Ti.

Ablation used a laser spot size of 25 microns and a laser firing repetition rate of 10 Hz.

Activity of TiO_2 for T-in-Zircon temperature calculation is 0.8

Experiment 10 - 15 December 2014

Isotope ratio and date errors include systematic calibration errors of 0.64% ($^{207}Pb/^{206}Pb$) and 1.41% ($^{206}Pb/^{238}U$) (all 2-sigma).

Trace element concentrations were deleted from analyses known to have intersected inclusions of non-zircon minerals based on P and Ti.

Ablation used a laser spot size of 25 microns and a laser firing repetition rate of 10 Hz.

Activity of TiO_2 for T-in-Zircon temperature calculation is 0.8

LA-ICPMS data from U1214

		Corrected isotope ratios							Dates (Ma)						
		207Pb*	±2s	206Pb*	±2s	error	207Pb*	±2s	207Pb*	±2s	207Pb*	±2s	206Pb*	±2s	%
Analysis	Th/U	235U*	(%)	238U	(%)	corr.	206Pb*	(%)	206Pb*	(Ma)	235U	(Ma)	238U*	(Ma)	disc.
U1214 L 269	0.7	36.264	4.1	0.755	3.8	0.9	0.348	1.5	3699	22	3674	40	3628	106	2
U1214 M 327	0.8	25.578	5.8	0.664	5.4	0.9	0.279	2.1	3359	32	3331	56	3283	138	2
U1214 S 336	0.8	23.617	4.3	0.631	3.7	0.8	0.271	2.4	3315	37	3253	42	3153	91	5
U1214 S 347	0.9	20.996	5.8	0.632	5.5	1.0	0.241	1.7	3125	26	3138	56	3159	139	-1
U1214 M 321	0.9	18.017	7.9	0.578	7.0	0.9	0.226	3.7	3023	59	2991	76	2942	166	3
U1214 M 304	0.6	16.653	5.6	0.559	4.3	0.8	0.216	3.6	2952	58	2915	54	2861	100	3

U1214 M 314	0.7	17.632	6.5	0.597	5.9	0.9	0.214	2.8	2939	45	2970	63	3016	143	-3
U1214 M 309	1.0	12.929	7.7	0.490	6.7	0.9	0.191	3.9	2753	65	2674	73	2572	141	7
U1214 M 296	0.7	13.076	6.6	0.497	6.2	0.9	0.191	2.2	2750	36	2685	62	2600	134	5
U1214 M 292	0.7	12.438	6.3	0.474	5.1	0.8	0.190	3.6	2743	60	2638	59	2503	107	9
U1214 S 365	0.7	13.443	5.9	0.515	5.3	0.9	0.189	2.6	2735	43	2711	56	2679	116	2
U1214 M 281	0.7	13.167	7.0	0.508	6.0	0.9	0.188	3.5	2725	58	2692	66	2648	130	3
U1214 S 333	0.9	13.295	5.8	0.522	5.5	0.9	0.185	1.8	2696	30	2701	55	2708	121	0
U1214 M 285	0.6	12.778	5.3	0.502	4.5	0.9	0.184	2.8	2694	46	2663	50	2624	98	3
U1214 S 353	1.0	12.440	6.4	0.489	5.4	0.8	0.184	3.5	2693	57	2638	60	2567	114	5
U1214 S 339	0.6	13.209	4.5	0.529	3.9	0.9	0.181	2.2	2662	36	2695	42	2739	87	-3
U1214 M 291	0.1	11.335	8.0	0.457	6.1	0.8	0.180	5.2	2653	87	2551	75	2425	122	9
U1214 M 283	0.6	12.258	7.7	0.496	6.6	0.9	0.179	4.0	2645	66	2624	72	2598	141	2
U1214 M 311	0.4	12.350	6.2	0.510	5.6	0.9	0.176	2.5	2612	41	2631	58	2656	123	-2
U1214 M 316	1.2	11.965	6.7	0.497	6.2	0.9	0.175	2.7	2601	45	2602	63	2602	132	0
U1214 S 372	1.0	10.417	8.0	0.433	7.5	0.9	0.174	2.8	2600	47	2473	74	2320	145	11
U1214 S 340	0.7	11.579	7.3	0.482	6.5	0.9	0.174	3.2	2599	54	2571	68	2535	136	2
U1214 L 265	0.8	11.602	5.3	0.489	4.5	0.8	0.172	2.8	2577	47	2573	50	2568	95	0
U1214 M 312	0.7	10.393	6.0	0.440	5.3	0.9	0.171	2.7	2572	45	2470	55	2349	105	9
U1214 L 266	1.0	11.305	6.2	0.481	4.8	0.8	0.171	4.0	2563	67	2549	58	2530	100	1
U1214 M 322	0.7	11.105	5.9	0.476	5.1	0.9	0.169	2.8	2549	47	2532	55	2511	107	1
U1214 S 361	1.3	10.587	8.0	0.455	6.8	0.9	0.169	4.2	2547	70	2488	74	2416	137	5
U1214 M 298	0.3	10.989	8.0	0.472	6.4	0.8	0.169	4.7	2546	79	2522	74	2492	133	2
U1214 M 300	0.5	11.006	7.4	0.474	7.0	1.0	0.168	2.3	2541	38	2524	69	2502	145	2
U1214 S 346	1.0	10.034	5.5	0.434	5.2	0.9	0.168	1.9	2536	32	2438	51	2322	101	8
U1214 M 310	1.5	10.668	6.4	0.462	5.8	0.9	0.167	2.8	2532	47	2495	60	2449	118	3
U1214 S 352	0.5	11.140	6.2	0.483	5.3	0.9	0.167	3.3	2530	55	2535	58	2541	112	0
U1214 S 348	3.0	10.545	6.7	0.460	6.0	0.9	0.166	3.2	2519	53	2484	63	2441	121	3
U1214 M 277	0.7	10.667	6.1	0.467	5.3	0.9	0.166	3.1	2513	51	2495	57	2472	109	2
U1214 L 268	1.0	10.177	3.7	0.446	2.9	0.8	0.165	2.3	2511	39	2451	35	2379	58	5
U1214 M 320	0.4	10.530	5.7	0.462	5.2	0.9	0.165	2.5	2510	41	2483	53	2449	106	2
U1214 M 330	0.7	10.781	7.9	0.474	7.2	0.9	0.165	3.2	2506	53	2504	73	2503	150	0
U1214 M 301	1.0	9.773	6.6	0.430	6.4	1.0	0.165	1.9	2506	33	2414	61	2306	123	8
U1214 S 338	0.6	10.155	6.3	0.448	6.0	1.0	0.164	1.9	2500	33	2449	58	2388	120	4
U1214 S 337	0.8	10.079	6.2	0.447	6.1	1.0	0.164	1.4	2494	24	2442	58	2380	121	5
U1214 M 326	1.0	10.753	6.5	0.477	5.5	0.8	0.164	3.5	2492	59	2502	60	2514	114	-1

U1214 M 273	0.6	10.640	6.4	0.472	5.5	0.9	0.163	3.3	2492	55	2492	59	2493	113	0
U1214 M 279	0.7	10.307	7.5	0.458	6.5	0.9	0.163	3.8	2491	64	2463	69	2429	131	3
U1214 S 359	1.1	10.918	7.5	0.485	6.7	0.9	0.163	3.3	2489	55	2516	70	2550	142	-2
U1214 M 305	0.7	10.117	5.4	0.450	4.8	0.9	0.163	2.5	2487	41	2446	50	2396	96	4
U1214 S 349	0.6	10.786	3.9	0.480	3.5	0.9	0.163	1.7	2487	29	2505	36	2527	73	-2
U1214 M 286	0.7	10.936	6.8	0.487	6.1	0.9	0.163	3.0	2485	50	2518	63	2558	129	-3
U1214 M 325	0.5	10.628	6.3	0.474	5.5	0.9	0.162	3.1	2481	52	2491	59	2503	115	-1
U1214 M 272	0.9	10.059	6.1	0.450	5.8	0.9	0.162	1.9	2478	33	2440	56	2395	116	3
U1214 M 295	0.2	10.342	10.2	0.464	9.6	0.9	0.162	3.7	2475	62	2466	95	2455	195	1
U1214 S 370	1.1	9.241	7.2	0.414	6.8	0.9	0.162	2.4	2475	41	2362	66	2234	128	10
U1214 M 331	0.6	10.762	8.7	0.483	8.1	0.9	0.161	3.1	2471	52	2503	81	2542	171	-3
U1214 M 319	1.1	9.672	7.6	0.436	6.3	0.8	0.161	4.2	2466	71	2404	70	2332	123	5
U1214 M 275	0.6	10.426	6.6	0.470	5.8	0.9	0.161	3.2	2463	54	2473	61	2486	120	-1
U1214 M 294	0.6	9.698	10.0	0.438	9.1	0.9	0.161	4.0	2461	68	2407	92	2343	179	5
U1214 S 358	0.3	10.116	5.5	0.461	4.9	0.9	0.159	2.3	2445	39	2445	50	2446	101	0
U1214 M 278	0.6	8.890	6.3	0.406	5.3	0.8	0.159	3.4	2442	58	2327	58	2198	99	10
U1214 M 323	0.5	10.134	6.0	0.463	5.5	0.9	0.159	2.4	2441	41	2447	56	2454	112	-1
U1214 M 282	1.3	9.522	8.4	0.436	6.7	0.8	0.158	5.1	2437	86	2390	77	2335	132	4
U1214 M 306	1.1	9.450	7.3	0.434	6.7	0.9	0.158	3.0	2433	51	2383	67	2324	130	4
U1214 M 303	0.2	8.879	5.7	0.410	5.1	0.9	0.157	2.6	2425	43	2326	52	2214	96	9
U1214 S 351	1.2	9.237	4.5	0.427	4.1	0.9	0.157	1.9	2424	31	2362	41	2290	79	6
U1214 L 267	1.0	10.025	5.4	0.466	4.7	0.9	0.156	2.7	2414	46	2437	50	2465	95	-2
U1214 S 362	0.5	10.296	5.5	0.481	4.9	0.9	0.155	2.4	2404	41	2462	51	2532	104	-5
U1214 M 332	0.6	9.383	6.0	0.439	5.6	0.9	0.155	2.0	2402	34	2376	55	2346	111	2
U1214 S 355	0.7	8.085	12.3	0.379	12.0	1.0	0.155	2.6	2400	45	2241	111	2070	213	14
U1214 M 315	0.4	8.781	7.0	0.420	6.1	0.9	0.152	3.5	2363	61	2315	64	2262	116	4
U1214 M 317	1.3	8.257	5.4	0.399	4.6	0.9	0.150	2.8	2347	48	2260	48	2164	84	8
U1214 M 280	0.8	8.790	6.3	0.427	5.6	0.9	0.149	2.9	2338	49	2316	57	2293	108	2
U1214 S 368	0.3	7.992	6.0	0.394	3.3	0.6	0.147	5.0	2313	85	2230	54	2141	61	7
U1214 M 271	0.8	7.978	8.3	0.402	6.9	0.8	0.144	4.7	2277	81	2228	75	2176	127	4
U1214 M 290	0.6	7.733	6.1	0.390	5.0	0.8	0.144	3.5	2274	61	2200	55	2123	90	7
U1214 M 324	1.4	7.585	8.6	0.383	7.7	0.9	0.144	3.8	2273	66	2183	77	2089	138	8
U1214 S 367	0.7	7.150	6.1	0.369	4.6	0.8	0.140	4.0	2232	69	2130	54	2027	81	9
U1214 S 350	1.1	7.979	6.0	0.413	5.3	0.9	0.140	2.8	2229	48	2229	54	2229	100	0
U1214 M 329	1.2	7.765	9.4	0.402	8.5	0.9	0.140	4.0	2228	70	2204	84	2178	157	2

U1214 M 318	0.1	7.418	5.7	0.385	5.1	0.9	0.140	2.6	2222	45	2163	51	2102	92	5
U1214 M 297	0.5	6.797	10.7	0.354	10.2	0.9	0.139	3.4	2217	59	2085	95	1955	171	12
U1214 S 334	0.7	7.725	4.4	0.403	3.9	0.9	0.139	2.2	2213	37	2199	40	2185	72	1
U1214 S 371	1.0	7.124	6.5	0.386	5.9	0.9	0.134	2.7	2149	48	2127	58	2104	105	2
U1214 M 313	0.7	6.615	6.1	0.362	5.2	0.9	0.133	3.1	2133	54	2061	54	1990	89	7
U1214 S 356	1.2	6.203	6.4	0.349	5.1	0.8	0.129	3.8	2084	68	2005	56	1929	85	7
U1214 M 299	0.6	6.311	7.2	0.356	6.4	0.9	0.128	3.4	2077	59	2020	64	1964	109	5
U1214 S 363	0.7	6.693	6.9	0.379	5.8	0.8	0.128	3.8	2073	67	2072	61	2070	103	0
U1214 L 264	0.8	6.595	4.8	0.374	4.5	0.9	0.128	1.6	2069	29	2059	42	2048	79	1
U1214 S 341	2.0	6.512	7.9	0.370	6.9	0.9	0.128	3.9	2066	69	2048	70	2030	119	2
U1214 S 344	0.9	6.292	6.3	0.358	5.2	0.8	0.127	3.6	2064	64	2017	56	1972	89	4
U1214 M 274	1.4	6.256	7.0	0.357	5.6	0.8	0.127	4.1	2060	73	2012	61	1966	95	5
U1214 S 369	0.4	6.482	5.6	0.370	4.8	0.9	0.127	2.9	2057	51	2043	49	2030	84	1
U1214 L 270	0.4	6.123	8.4	0.351	5.6	0.7	0.127	6.3	2051	111	1994	73	1939	93	5
U1214 S 345	0.9	6.415	4.5	0.370	3.9	0.9	0.126	2.1	2040	37	2034	39	2029	68	1
U1214 S 342	1.5	6.329	5.9	0.366	5.5	0.9	0.125	2.1	2036	37	2023	51	2010	95	1
U1214 M 284	0.9	5.948	6.9	0.345	5.4	0.8	0.125	4.2	2032	74	1968	60	1908	90	6
U1214 S 360	1.5	6.131	7.6	0.356	6.7	0.9	0.125	3.5	2029	62	1995	66	1962	113	3
U1214 M 328	1.3	6.117	6.4	0.355	5.3	0.8	0.125	3.5	2027	63	1993	56	1960	90	3
U1214 M 276	0.6	6.571	6.8	0.382	5.8	0.9	0.125	3.6	2024	63	2055	60	2087	103	-3
U1214 M 307	0.5	6.327	7.0	0.369	6.2	0.9	0.124	3.3	2020	58	2022	62	2024	108	0
U1214 S 335	1.5	6.084	4.3	0.355	3.3	0.8	0.124	2.7	2019	48	1988	37	1958	56	3
U1214 L 263	1.5	6.315	5.8	0.370	4.6	0.8	0.124	3.5	2011	62	2021	51	2029	80	-1
U1214 S 354	1.0	6.089	5.8	0.357	5.0	0.9	0.124	3.0	2010	53	1989	51	1968	84	2
U1214 M 302	0.8	5.988	6.4	0.355	5.4	0.8	0.122	3.4	1988	60	1974	56	1960	92	1
U1214 M 308	2.3	6.104	9.1	0.363	7.2	0.8	0.122	5.5	1986	99	1991	79	1996	123	-1
U1214 M 287	0.2	5.972	7.4	0.355	6.6	0.9	0.122	3.3	1985	59	1972	65	1959	112	1
U1214 S 343	1.3	6.095	7.3	0.364	6.3	0.9	0.121	3.7	1976	66	1989	64	2002	108	-1
U1214 S 364	1.4	6.145	6.1	0.367	5.2	0.9	0.121	3.2	1976	57	1997	54	2017	90	-2
U1214 M 289	1.8	5.916	10.8	0.367	7.5	0.7	0.117	7.9	1912	141	1964	94	2013	129	-5

LA-ICPMS data from U1214 continued.

	Concentrations (ppm)																					
Analysis	P	Ti	Y	Nb	La	Ce	Pr	Nd	Sm	Eu	Gd	Tb	Dy	Ho	Er	Tm	Yb	Lu	Hf	Ta	Th	U
U1214 L 269	157	3	566	1		7	0	1	3	0	11	5	55	20	85	20	180	30	10627	1	111	169
U1214 M 327	302	6	1002	6		19	0	1	3	1	23	8	105	39	171	41	414	59	10184	3	55	72
U1214 S 347	230	4	869	1		15	0	5	7	1	28	9	95	35	147	33	297	47	10747	1	119	133
U1214 M 321	166	7	915	1		13		0	3	1	19	7	86	34	149	36	384	49	9060	1	74	82
U1214 M 304	140	8	437	1		7		0	1	0	8	3	41	15	72	17	194	25	8921	0	17	31
U1214 M 314	396	6	2017	2		13	0	3	7	3	45	17	212	80	336	85	868	107	9186	1	95	134
U1214 M 309	228	17	1435	1	0	6	0	6	10	2	58	15	171	55	213	47	446	53	7985	1	48	47
U1214 M 296	284	6	681	1		7	0	2	3	1	15	6	68	25	111	26	289	38	7573	0	50	68
U1214 M 292	229	16	726	3		12	0	1	4	1	17	6	75	25	100	24	246	31	7712	1	73	109
U1214 S 365	159	7	587	1		15	0	1	4	1	16	5	64	23	103	25	253	36	9168	1	105	151
U1214 M 281	206	17	515	2		9		1	2	0	11	3	50	18	76	18	184	23	8059	0	41	60
U1214 S 333	160	8	983	2		11	0	4	8	0	33	11	111	39	151	31	280	43	10078	1	159	175
U1214 M 285	241	6	523	2		18		1	3	0	10	4	52	18	76	20	212	26	8835	1	133	223
U1214 S 353	117	2	186	1		13				0	3	1	15	7	33	9	115	18	12163	1	72	75
U1214 S 339	218	9	739	6		11	0	1	2	0	15	5	64	26	129	30	273	44	12695	4	84	144
U1214 M 291	174	5	307	1		3		0	1	0	6	2	30	11	51	13	142	18	9087	0	4	26
U1214 M 283	353	12	824	2		7		1	3	0	15	6	77	30	128	32	336	44	8510	1	37	65
U1214 M 311	114	3	242	1		7	0	0	1	0	4	2	24	9	38	9	105	13	9454	0	74	172
U1214 M 316	342	4	1656	2		23	0	8	17	1	68	18	204	67	261	59	546	67	8933	1	275	227
U1214 S 372	239	19	761	3	5	108	12	120	49	12	53	11	95	28	103	25	257	36	10657	1	261	255
U1214 S 340	188	15	686	3		6	0	2	2	0	16	6	69	26	108	25	227	32	10570	1	44	65
U1214 L 265	147	6	651	1		6	0	2	5	1	17	5	60	22	93	24	230	42	9576	0	109	137
U1214 L 266	133	9	757	1		9		1	2	0	17	5	71	26	108	24	206	33	10820	0	41	43
U1214 M 322	141	11	939	0		4	0	2	5	1	22	9	105	37	158	38	393	50	8490	0	35	53
U1214 S 361	187	13	1121	2	0	6	0	7	9	1	38	11	132	42	167	37	359	43	8554	1	64	49
U1214 M 298	104	4	208	1		7		0	1	0	4	1	18	6	30	7	84	11	9134	0	35	116
U1214 M 310	299	6	994	2		13	0	3	8	0	37	11	121	38	150	32	331	38	10138	0	324	218
U1214 S 352	161	7	549	1	0	6		1	2	0	12	4	54	20	86	22	218	34	8966	1	34	69
U1214 S 348	228	15	707	2		18	0	1	2	0	17	6	70	28	121	27	247	40	13389	1	224	76
U1214 M 277	151	14	866	1		5	0	2	4	1	26	7	87	30	123	28	270	36	8547	1	99	148
U1214 L 268	189	8	696	1		22	0	2	4	1	21	6	68	22	102	25	236	42	10440	1	200	208

U1214 M 320	108	2	191	0		13		0	1	0	5	1	17	6	32	8	105	16	10493	0	45	110
U1214 M 330	169	8	683	2	0	19		2	2	1	16	5	71	26	111	26	272	41	10436	1	165	226
U1214 M 301	255	10	1487	1	0	13	0	7	8	3	55	15	161	54	207	48	487	57	7608	1	188	194
U1214 S 338	173	5	408	0		10		2	3	1	14	4	43	15	60	15	145	23	10379	0	44	77
U1214 S 337	329	4	922	1	1	12	1	5	5	1	23	7	94	35	152	36	355	65	11818	1	131	166
U1214 M 326	163	11	390	1	0	22	0	2	3	1	15	4	43	14	58	14	145	19	8611	0	82	85
U1214 M 273	157	4	272	0	0	13		0	1	0	6	2	22	9	44	11	134	23	10620	0	50	77
U1214 M 279	165	7	692	6		12	0	1	3	0	14	5	71	24	107	25	253	33	8774	3	77	118
U1214 S 359	210	5	774	1		36	0	3	4	2	23	7	79	27	114	29	309	44	7679	0	149	140
U1214 S 349	190	12	647	26		12		1	2	0	11	5	65	23	108	27	258	42	14356	22	86	147
U1214 M 286	141	7	267	1		20		1	2	0	7	2	27	8	34	9	107	14	8691	0	41	56
U1214 M 325	385	28	1056	8		18	0	2	5		26	11	128	44	165	37	327	40	10791	5	116	257
U1214 M 272	263	2	495	2	1	41	0	4	3	1	11	4	49	16	78	22	259	41	11418	1	141	165
U1214 M 295	166	7	352	2		11			1	0	7	2	30	12	54	15	171	22	7845	1	18	81
U1214 M 331	126	5	351	1		10	0	1	2	0	11	3	37	12	52	14	147	22	9611	1	109	184
U1214 M 319	223	8	367	1		15	0	1	4	0	13	4	45	15	57	13	131	16	9602	1	167	151
U1214 M 275	200	7	961	10		18	0	1	3	0	22	9	93	35	146	34	320	44	10857	4	154	250
U1214 M 294	236	5	887	4		36		2	6	1	19	6	80	27	129	32	364	49	7495	1	64	111
U1214 S 358	236	14	617	18		17	0	1	3	0	14	5	64	24	105	26	245	33	10139	10	68	260
U1214 M 278	79	7	174	1	0	3		0	1	0	4	1	18	6	24	5	51	6	8415	0	109	192
U1214 M 323	233	2	577	1		9		0	1	0	9	4	52	20	95	24	301	42	11987	1	89	166
U1214 M 282	222	5	1202	1	0	30	1	12	15	2	51	14	135	42	152	37	337	41	7190	1	231	182
U1214 M 303	73	9	354	4	0	9	0	1	3	1	10	3	35	12	53	14	166	23	11641	3	51	213
U1214 S 351	154	8	822	4	0	57	1	4	5	1	20	7	79	29	127	31	304	50	11067	2	216	187
U1214 L 267	296	23	409	1		3	0	3	7		31	8	63	15	38	6	35	4	12338	1	102	106
U1214 S 362	130	3	479	5		11	0	2	2	0	11	4	51	20	76	20	197	25	9637	3	81	159
U1214 M 332	188	7	642	2		12		1	2	0	15	6	63	24	103	25	254	35	10316	1	69	106
U1214 M 315	194	9	403	2		8		1	2	0	10	3	40	15	62	17	172	20	8889	2	46	106
U1214 M 317	141	5	920	2	0	24	0	8	9	4	37	9	95	31	137	35	384	47	6958	0	113	89
U1214 M 280	170	2	727	2		10	0	3	3	0	24	6	69	27	111	24	226	30	8218	1	67	79
U1214 S 368	489	2	1265	3		11	0	1	3	0	20	9	122	47	210	50	525	67	12812	2	85	293
U1214 M 271	347	18	1090	2		10		0	2	1	20	7	104	39	176	43	443	65	10056	1	24	32
U1214 M 290	187	9	536	2		8	0	1	3	0	16	4	55	18	76	18	186	24	7040	1	59	102
U1214 S 367	134	9	332	2		12	0	3	5	0	14	4	41	14	56	13	145	23	7594	0	29	45
U1214 S 350	244	8	667	1		22	0	2	5	1	21	6	67	23	98	22	213	36	11094	1	117	102

U1214 M 329	164	13	636	3		36	0	2	4	1	17	6	67	23	101	26	280	39	11475	2	144	119
U1214 M 318	148	6	121	0		1		0	1	0	9	2	19	5	14	3	28	3	11027	0	32	219
U1214 S 334	154	12	454	1		10	0	1	2	0	12	3	44	16	71	17	161	27	11134	1	120	165
U1214 S 371	195	5	1572	2	0	13	1	12	18	2	77	21	194	61	226	52	445	58	8138	1	272	280
U1214 M 313	188	6	463	1		13	0	0	2	1	11	4	45	17	75	20	203	27	8196	0	125	171
U1214 S 356	187	25	537	3		33	0	3	4	1	17	6	62	20	83	21	215	28	9939	2	49	41
U1214 M 299	132	8	455	3		45	0	1	2	1	7	4	41	16	66	16	176	21	8147	1	67	112
U1214 S 363	158	4	245	0		12	0	2	3	1	16	4	35	9	32	7	62	6	10518	0	48	67
U1214 L 264	256	10	956	4		9	0	3	6	0	25	9	94	34	142	32	308	48	10792	1	183	237
U1214 S 344	108	8	269	1		9	0	1	1	0	5	2	28	9	44	10	105	15	11807	0	61	68
U1214 M 274	207	23	481	2		22	0	3	3	1	15	5	55	18	72	17	167	24	9826	1	62	43
U1214 S 369	281	4	919	4		13		1	3	0	20	7	95	35	153	40	417	57	12100	4	79	192
U1214 L 270	179	16	314	1		13	0	1	2	1	10	3	33	11	48	11	115	18	9796	0	19	45
U1214 S 345	175	11	481	4		35	0	1	2	0	11	3	47	16	77	22	224	34	11949	2	196	210
U1214 S 342	209	14	1547	2		27	1	21	25	2	77	21	214	66	261	56	483	65	10589	1	348	227
U1214 M 284	74	3	227	0	1	7	0	1	1	1	6	2	22	6	31	9	97	13	8308		69	75
U1214 S 360	219	8	556	7	0	40	1	8	5	1	12	4	46	17	85	22	219	28	8017	2	204	132
U1214 M 328	156	13	600	3	0	28	0	2	4	1	17	6	61	22	98	24	234	33	11004	1	138	107
U1214 M 276	165	18	646	0	0	7	0	3	6	1	26	7	69	25	99	23	210	27	9626	0	34	53
U1214 M 307	197	13	485	1		7	0	1	3	0	11	4	51	17	78	18	186	24	8851	1	76	167
U1214 L 263	185	17	828	2		17	0	3	6	1	25	8	87	30	125	27	261	36	10948	1	149	97
U1214 S 354	114	12	486	4		40	0	1	3	1	10	4	47	17	83	23	295	45	11539	1	174	166
U1214 M 302	181	10	432	2		20		1	1	0	10	3	46	15	71	17	184	24	9883	1	87	108
U1214 M 308	223	12	491	4	0	36	0	2	2	0	12	4	51	16	74	17	186	23	9742	1	124	54
U1214 M 287	95	7	201	2	0	9		1	1	1	4	2	20	6	20	6	56	6	9606	3	55	261
U1214 S 364	197	11	530	2		39	0	1	3	1	17	5	62	21	83	21	222	28	11072	1	182	126
U1214 M 289	249	32	534	3		49	0	3	4	1	18	6	60	18	74	17	195	22	7578	1	37	21

Experiment 13 - 17 December 2014

Isotope ratio and date errors include systematic calibration errors of 0.74% ($^{207}Pb/^{206}Pb$) and 1.63% ($^{206}Pb/^{238}U$) (all 2-sigma).

Trace element concentrations were deleted from analyses known to have intersected inclusions of non-zircon minerals based on P and Ti.

Ablation used a laser spot size of 25 microns and a laser firing repetition rate of 10 Hz.

Activity of TiO_2 for T-in-Zircon temperature calculation is 0.8

LA-ICPMS data from U1214 continued.

		Corrected isotope ratios							Dates (Ma)						
		207Pb*	±2s	206Pb*	±2s	error	207Pb*	±2s	207Pb*	±2s	207Pb*	±2s	206Pb*	±2s	%
Analysis	Th/U	235U*	(%)	238U	(%)	corr.	206Pb*	(%)	206Pb*	(Ma)	235U	(Ma)	238U*	(Ma)	disc.
U1214 M 139	0.3	27.081	5.6	0.693	4.3	0.8	0.283	3.6	3382	74	3386	72	3394	114	0
U1214 L 46	0.7	25.678	4.0	0.638	3.4	0.9	0.292	2.1	3428	75	3334	71	3181	86	9
U1214 S 227	1.1	16.461	5.1	0.549	4.2	0.8	0.217	2.9	2962	69	2904	68	2821	96	6
U1214 M 137	0.4	14.575	6.2	0.539	5.3	0.9	0.196	3.2	2793	89	2788	83	2781	120	1
U1214 L 44	0.5	15.788	7.1	0.524	6.1	0.9	0.219	3.6	2970	91	2864	89	2716	135	10
U1214 S 238	0.9	15.948	5.4	0.497	5.1	0.9	0.233	1.8	3070	58	2874	69	2601	109	19
U1214 S 232	0.9	12.979	3.6	0.497	2.7	0.8	0.189	2.4	2737	65	2678	57	2600	58	6
U1214 M 147	1.1	11.745	7.1	0.496	6.2	0.9	0.172	3.3	2576	76	2584	80	2595	133	1
U1214 M 142	0.6	11.421	8.7	0.490	8.0	0.9	0.169	3.4	2549	78	2558	93	2570	169	1
U1214 M 151	0.7	10.892	7.9	0.486	7.2	0.9	0.163	3.3	2483	76	2514	86	2552	151	3
U1214 S 230	0.6	12.236	3.7	0.486	2.9	0.8	0.183	2.3	2678	65	2623	57	2552	60	6
U1214 M 136	1.1	10.448	11.3	0.478	9.4	0.8	0.158	6.3	2439	130	2475	119	2519	196	4
U1214 M 132	0.7	9.628	10.3	0.471	8.8	0.8	0.148	5.5	2326	121	2400	110	2488	181	8
U1214 M 122	1.2	10.476	8.3	0.459	7.6	0.9	0.166	3.4	2513	93	2478	96	2435	155	4
U1214 M 140	0.8	9.674	6.3	0.455	5.6	0.9	0.154	2.8	2394	71	2404	73	2417	113	1
U1214 S 241	0.9	7.825	6.3	0.401	4.9	0.8	0.142	4.0	2248	88	2211	72	2172	91	4
U1214 M 130	0.7	7.727	6.1	0.385	4.7	0.8	0.146	3.9	2296	101	2200	77	2098	84	10
U1214 S 242	1.6	7.562	7.5	0.382	6.5	0.9	0.144	3.8	2271	85	2180	80	2085	115	10
U1214 M 141	0.4	6.419	8.2	0.370	6.9	0.8	0.126	4.5	2039	97	2035	84	2031	120	0
U1214 M 152	1.3	5.808	8.5	0.360	7.7	0.9	0.117	3.4	1910	84	1948	85	1983	132	4
U1214 M 146	0.7	6.578	7.6	0.359	6.4	0.9	0.133	3.9	2137	88	2056	79	1977	110	9
U1214 M 124	0.7	6.170	8.0	0.359	7.4	0.9	0.125	3.0	2025	94	2000	88	1977	126	3
U1214 S 239	2.0	6.009	5.0	0.356	3.6	0.7	0.122	3.5	1992	84	1977	61	1963	61	2
U1214 S 240	1.9	6.536	6.6	0.351	3.8	0.6	0.135	5.4	2165	109	2051	72	1939	64	12
U1214 L 37	1.7	5.728	6.0	0.344	4.5	0.8	0.121	3.9	1966	104	1936	74	1908	75	3
U1214 S 236	2.7	5.675	3.6	0.333	2.7	0.8	0.124	2.4	2011	70	1928	52	1851	44	9
U1214 L 40	2.6	5.539	6.3	0.331	4.2	0.7	0.121	4.7	1978	115	1907	76	1842	67	8
U1214 S 228	0.1	5.303	4.4	0.311	4.0	0.9	0.124	1.8	2013	65	1869	56	1743	61	15
U1214 M 134	0.8	1.314	14.4	0.148	12.6	0.9	0.064	6.9	758	172	852	90	888	105	18

U1214 M 150	0.9	1.211	8.0	0.139	6.4	0.8	0.063	4.9	718	123	806	52	838	50	18
U1214 M 135	0.5	1.210	10.1	0.137	8.1	0.8	0.064	6.1	740	160	805	66	829	63	13
U1214 M 143	0.8	1.200	8.4	0.136	6.1	0.7	0.064	5.8	733	139	800	53	825	47	13
U1214 S 233	0.8	1.216	4.3	0.133	3.0	0.7	0.066	3.1	817	92	808	36	805	23	2
U1214 M 126	0.5	1.203	6.7	0.132	5.5	0.8	0.066	3.8	813	121	802	50	798	41	2
U1214 M 149	0.7	1.139	10.1	0.131	6.8	0.7	0.063	7.5	710	173	772	61	794	51	12
U1214 M 119	0.7	1.223	7.9	0.130	7.3	0.9	0.068	3.0	876	111	811	56	788	54	11
U1214 M 123	1.0	1.207	5.8	0.130	4.8	0.8	0.067	3.3	849	114	804	47	788	36	8
U1214 S 234	1.0	1.174	6.3	0.130	3.8	0.6	0.066	5.0	793	124	788	44	787	28	1
U1214 L 39	0.8	1.204	8.3	0.130	4.8	0.6	0.067	6.8	848	167	803	57	786	36	8
U1214 M 129	0.9	1.180	6.9	0.128	4.9	0.7	0.067	4.9	827	138	792	51	779	36	6
U1214 L 43	0.5	1.128	6.6	0.128	4.0	0.6	0.064	5.3	732	146	767	48	779	29	7
U1214 M 127	0.6	1.142	8.9	0.128	7.4	0.8	0.065	4.8	762	137	774	58	777	55	2
U1214 M 128	0.6	1.169	7.3	0.128	5.6	0.8	0.066	4.6	818	133	786	52	775	41	6
U1214 L 41	0.5	1.145	4.9	0.127	3.7	0.8	0.065	3.2	780	113	775	42	773	27	1
U1214 M 121	1.1	1.166	6.9	0.127	5.4	0.8	0.066	4.3	821	128	785	50	772	39	6
U1214 M 131	1.1	1.191	7.0	0.127	3.9	0.6	0.068	5.8	865	151	796	51	772	29	11
U1214 S 235	1.5	1.164	4.3	0.127	3.1	0.7	0.066	2.9	821	90	784	35	771	23	7
U1214 S 229	0.8	1.100	7.9	0.126	4.8	0.6	0.063	6.3	713	149	753	49	767	35	8
U1214 M 148	1.0	1.175	9.1	0.126	7.2	0.8	0.068	5.6	856	133	789	57	765	52	11
U1214 L 42	0.5	1.106	6.4	0.125	3.8	0.6	0.064	5.1	740	143	756	47	762	27	3
U1214 M 145	0.6	1.183	9.1	0.125	8.1	0.9	0.068	4.2	882	109	793	57	761	58	15
U1214 M 120	0.7	1.082	8.0	0.125	6.9	0.9	0.063	4.1	706	128	745	53	758	49	8
U1214 L 45	0.7	1.093	8.3	0.124	4.8	0.6	0.064	6.8	745	170	750	54	752	34	1
U1214 M 125	0.5	1.158	9.3	0.124	8.2	0.9	0.068	4.4	867	130	781	61	751	58	14
U1214 L 47	0.5	1.124	7.1	0.122	3.5	0.5	0.067	6.1	826	157	765	50	744	25	10
U1214 S 231	1.0	1.174	6.5	0.122	3.9	0.6	0.070	5.2	919	125	789	45	743	28	20

	Concentrations (ppm)																					
Analysis	P	Ti	Y	Nb	La	Ce	Pr	Nd	Sm	Eu	Gd	Tb	Dy	Ho	Er	Tm	Yb	Lu	Hf	Ta	Th	U
U1214 M 139	82	1	137	1		2		0		0	2	1	11	4	22	6	87	11	8660	1	9	35
U1214 L 46	144	2	1011	1	0	4	0	1	2	1	21	8	99	39	164	40	410	48	7945	0	41	61
U1214 S 227	147	14	705	1	0	17	0	4	4	2	19	6	68	22	99	26	302	45	10092	0	111	99

U1214 M 137	200	8	808	1		6		1	3	1	15	6	80	30	138	38	416	47	6813	1	66	182
U1214 L 44	188	7	678	1	0	16	0	4	5	2	21	6	69	24	102	27	310	41	9539	1	61	125
U1214 S 238	254	7	1180	6	0	21	1	5	6	2	29	10	119	41	177	39	361	51	11407	3	155	170
U1214 S 232	199	14	1487	1	0	10	0	6	10	2	49	14	152	51	209	45	403	62	10907	1	90	102
U1214 M 147	213	15	617	1		14	0	3	4	1	24	7	69	20	87	23	233	22	7020	0	83	78
U1214 M 142	166	11	318	1	0	11	0	1	2	0	11	3	33	11	46	12	139	16	6400	0	52	81
U1214 M 151	181	6	656	0	0	9	0	2	5	1	24	7	68	23	95	25	267	33	7360	0	65	94
U1214 S 230	530	7	1665	3		4	0	1	3	0	24	10	138	55	258	64	624	97	10866	2	73	116
U1214 M 136	190	14	531	1		11		2	3	1	18	5	63	20	77	21	228	25	6691	0	40	37
U1214 M 132	340	9	944	2	0	5	0	1	5	1	27	8	95	33	144	32	318	37	9662	1	49	72
U1214 M 122	316	7	1484	4	0	31	0	9	15	2	54	16	185	62	218	52	532	59	7318	2	309	254
U1214 M 140	219	4	945	3	0	9	0	3	7	0	28	9	103	35	127	33	354	34	6667	1	93	113
U1214 S 241	151	12	866	2		8	0	3	7	0	28	9	91	30	126	28	270	36	9403	1	59	64
U1214 M 130	141	16	892	2	0	6	0	6	9	1	38	11	110	35	129	30	297	31	6571	1	43	61
U1214 S 242	168	13	1448	1	0	9	1	16	18	2	63	19	171	54	213	48	466	59	6292	0	84	53
U1214 M 141	259	16	600	4	0	5	0	1	3		12	5	63	23	94	26	274	27	7858	3	33	78
U1214 M 152	135	14	703	2	0	24	0	1	4	1	21	7	70	24	102	26	255	27	8510	1	122	94
U1214 M 146	168	10	427	1		14	0	1	2	0	8	4	43	14	67	19	221	24	6674	0	48	64
U1214 M 124	689	23	361	2	21	56	5	27	9	1	16	4	49	15	54	14	146	17	8012	1	44	60
U1214 S 239	209	30	505	2		18	0	3	4	1	16	6	53	17	70	17	153	22	9662	1	48	24
U1214 S 240	126	372	393	2		16	0	2	3	1	14	4	43	14	59	13	117	17	7985	1	55	29
U1214 L 37	237	47	1352	2	0	38	2	22	26	5	73	19	181	52	187	42	418	46	8633	1	127	73
U1214 S 236	372	18	1575	3	7	56	1	15	17	4	67	17	181	56	216	46	401	59	10511	1	329	120
U1214 L 40	335	36	1131	2	0	45	1	12	19	5	63	15	150	44	162	39	360	41	8771	1	56	22
U1214 S 228	182	15	225	0	0	2	0	0	2	0	14	4	28	7	24	6	62	10	12893	1	34	562
U1214 M 134	215	3	1145	2	1	23	0	4	4	1	22	8	88	33	168	50	492	70	10495	1	185	242
U1214 M 150	354	7	1517	1	0	13	0	6	8	3	39	13	154	51	236	63	665	78	6590	0	137	158
U1214 M 135	332	4	820	2		9	0	1	2	0	13	5	70	28	130	37	468	57	8463	1	65	135
U1214 M 143	282	5	1445	2	1	18	0	5	8	1	33	12	137	47	224	58	664	72	7175	1	141	173
U1214 S 233	266	6	1554	4	0	14	0	2	4	1	27	9	114	50	248	63	654	111	10982	2	185	246
U1214 M 126	193	6	594	1	1	13	0	1	2	0	10	3	46	19	95	29	365	44	8952	1	70	134
U1214 M 149	215	10	672	1	0	12	0	1	3	1	13	5	64	24	105	29	339	39	6730	0	51	75
U1214 M 119	302	3	1263	6	2	46	1	3	5	1	20	8	107	45	209	58	747	104	9257	3	433	578
U1214 M 123	328	5	2053	8	0	21	0	3	8	2	45	16	209	78	352	88	944	108	8316	2	430	422
U1214 S 234	267	11	1212	1	1	15	0	3	5	1	22	8	99	38	189	44	441	76	11227	1	82	82

U1214 L 39	3329	13	787	1	40	85	11	57	16	2	27	7	78	29	130	34	340	46	8381	1	61	77
U1214 M 129	613	16	2977	6	0	46	0	4	9	3	55	21	281	110	490	122	1345	151	7704	2	290	332
U1214 L 43	145	3	532	1		9	0	1	2	0	7	3	45	19	90	27	313	41	9481	1	52	96
U1214 M 127	3824	5	428	1	42	90	8	43	7	1	12	4	42	15	70	22	273	35	8221	1	87	144
U1214 M 128	198	3	533	2		19	0	1	2	0	9	3	44	19	90	25	318	42	9440	1	157	248
U1214 L 41	178	4	919	3		12	0	1	3	0	17	6	81	33	159	42	469	62	10272	2	102	194
U1214 M 121	274	10	1678	1	0	15	0	6	10	4	48	15	172	60	255	68	752	89	7174	0	179	170
U1214 M 131	18557	9	2187	2	196	480	53	241	53	9	80	23	218	80	346	92	1033	121	6952	1	306	276
U1214 S 235	319	20	3362	1	0	16	1	10	19	7	101	31	330	117	510	112	1011	171	9113	0	211	142
U1214 S 229	208	10	794	1	0	9	0	1	3	1	17	6	72	26	124	32	310	46	9192	1	45	53
U1214 M 148	130	7	640	0	0	8	0	3	4	1	15	4	53	20	100	28	353	46	7043	0	63	65
U1214 L 42	229	1	1011	4	0	8		1	3	1	18	7	94	38	178	46	511	64	10648	2	111	210
U1214 M 145	5450	14	550	2	72	137	15	76	15	1	18	5	52	18	88	25	325	43	6675	1	100	168
U1214 M 120	215	3	1042	2	0	30	0	2	4	2	18	7	92	36	180	49	597	83	9876	1	186	262
U1214 L 45	1156	5	955	1	19	46	4	24	7	1	22	8	91	35	161	40	448	58	9799	1	77	115
U1214 M 125	1052	4	502	2	15	37	3	13	3	1	9	3	43	17	82	28	389	52	8625	1	131	240
U1214 L 47	346	4	393	1	3	13	0	2	1	0	6	2	29	13	67	19	245	34	9459	0	64	121
U1214 S 231	824	5	1993	2	12	36	3	15	10	2	44	14	164	62	296	74	752	118	10623	1	250	253

17 December, 2012

Isotope ratios and ages are not corrected for initial common Pb.

Isotope ratio and apparent age errors do not include systematic calibration errors of 1.81026298055907% ($^{208}Pb/^{232}Th$), 0.773493715556818% ($^{207}Pb/^{206}Pb$), 0.747942531690396% ($^{206}Pb/^{238}U$).

Trace element concentrations in ppm, calculated using mean count rate method.

Backgrounds were monitored between sweeps 17 to 27. Sample counts were integrated from sweeps 39 to 68.

LA-ICPMS data from F1206-146.1

		Corrected isotope ratios							Dates (Ma)						
		207Pb*	±2s	206Pb*	±2s	error	207Pb*	±2s	207Pb*	±2s	207Pb*	±2s	206Pb*	±2s	%
Analysis	Th/U	235U*	(%)	238U	(%)	corr.	206Pb*	(%)	206Pb*	(Ma)	235U	(Ma)	238U*	(Ma)	disc.
F1206-146.1 M 206	0.1	1.633	20.9	0.160	7.9	0.7	0.074	7.5	1049.00	151.48	983.17	68.88	953.78	70.45	9.00
F1206-146.1 M 216	0.1	1.164	5.9	0.129	5.4	0.9	0.065	2.3	785.00	48.95	783.88	32.40	783.57	40.24	0.00
F1206-146.1 M 227	0.1	1.221	7.9	0.135	6.7	0.9	0.066	4.1	792.00	85.45	810.18	44.04	816.44	51.81	-3.00
F1206-146.1 M 209	0.1	1.110	6.0	0.125	5.1	0.9	0.065	3.1	762.47	65.87	758.13	32.20	756.65	36.80	1.00

F1206-146.1 M 223	0.2	1.164	6.5	0.129	5.9	0.9	0.066	2.9	795.00	60.10	783.79	35.79	779.92	43.30	2.00
F1206-146.1 L 36	0.2	1.145	7.5	0.130	6.7	0.9	0.064	3.3	734.00	69.14	774.65	40.65	788.75	50.13	-7.00
F1206-146.1 M 195	0.2	1.161	6.9	0.128	5.7	0.8	0.066	3.9	798.81	82.10	782.24	37.64	776.43	41.56	3.00
F1206-146.1 M 194	0.2	1.203	6.1	0.132	5.4	0.9	0.066	2.8	812.00	58.84	802.16	33.92	798.62	40.80	2.00
F1206-146.1 M 192	0.3	5.633	6.5	0.330	5.8	0.9	0.124	2.9	2013.00	51.77	1921.21	55.98	1837.01	92.70	9.00
F1206-146.1 M 229	0.3	1.266	8.4	0.129	6.8	0.8	0.071	5.0	970.76	102.28	830.74	47.98	779.37	50.00	20.00
F1206-146.1 M 208	0.3	1.183	6.9	0.132	6.3	0.9	0.065	2.9	767.00	61.25	792.74	38.07	801.75	47.33	-4.00
F1206-146.1 M 201	0.3	1.125	5.9	0.125	5.2	0.9	0.065	2.8	786.29	59.78	765.46	31.90	758.33	37.26	4.00
F1206-146.1 M 211	0.4	1.356	7.6	0.146	6.5	0.8	0.067	4.0	848.00	83.77	870.34	44.50	878.76	53.06	-4.00
F1206-146.1 M 222	0.4	1.229	5.9	0.134	5.3	0.9	0.067	2.6	830.00	53.91	813.87	32.87	807.83	40.02	3.00
F1206-146.1 M 214	0.4	1.200	5.6	0.135	3.9	0.7	0.064	3.9	754.00	82.85	800.71	30.96	817.35	30.55	-8.00
F1206-146.1 M 220	0.4	1.303	5.4	0.143	4.8	0.9	0.066	2.4	808.00	50.81	846.91	30.88	861.53	38.67	-7.00
F1206-146.1 L 41	0.4	1.394	9.3	0.145	6.7	0.7	0.070	6.5	916.00	132.67	886.45	55.11	874.32	55.01	5.00
F1206-146.1 L 23	0.5	1.359	7.3	0.140	5.6	0.8	0.070	4.7	939.00	96.99	871.32	43.03	844.88	44.60	10.00
F1206-146.1 L 46	0.5	1.207	8.8	0.134	5.4	0.6	0.065	6.9	785.00	145.72	803.61	48.81	810.14	41.10	-3.00
F1206-146.1 L 43	0.5	1.137	6.9	0.120	5.6	0.8	0.069	4.2	886.15	85.83	770.87	37.60	731.69	38.65	17.00
F1206-146.1 L 22	0.5	1.308	7.1	0.134	4.9	0.7	0.071	5.2	948.00	105.85	849.35	40.92	811.88	37.22	14.00
F1206-146.1 M 191	0.5	1.374	7.5	0.148	5.9	0.8	0.068	4.5	853.00	94.41	877.66	43.91	887.09	49.17	-4.00
F1206-146.1 M 226	0.5	1.478	7.9	0.151	7.0	0.9	0.071	3.7	955.00	75.54	921.43	47.89	907.18	59.16	5.00
F1206-146.1 L 31	0.5	1.308	5.9	0.140	5.1	0.9	0.068	2.9	856.00	60.62	849.02	34.10	846.07	40.90	1.00
F1206-146.1 M 225	0.5	1.244	7.4	0.134	6.3	0.8	0.067	4.0	848.00	82.92	820.63	41.79	810.30	47.69	5.00
F1206-146.1 L 21	0.6	1.237	5.5	0.130	4.8	0.9	0.069	2.9	906.00	59.03	817.30	31.21	784.92	35.20	13.00
F1206-146.1 M 200	0.6	1.150	7.2	0.127	5.8	0.8	0.066	4.3	798.56	89.65	777.22	38.98	769.80	41.82	4.00
F1206-146.1 L 42	0.6	1.294	5.2	0.139	4.3	0.8	0.068	2.9	855.00	60.87	843.01	30.08	838.08	34.25	2.00
F1206-146.1 M 219	0.6	1.371	5.5	0.147	3.9	0.7	0.068	3.9	863.00	81.85	876.65	32.53	881.91	32.05	-2.00
F1206-146.1 L 47	0.6	1.228	5.8	0.134	4.7	0.8	0.067	3.4	824.00	70.40	813.57	32.57	809.70	36.07	2.00
F1206-146.1 L 44	0.6	1.311	5.7	0.139	5.0	0.9	0.068	2.8	880.00	57.58	850.71	33.15	839.24	39.63	5.00
F1206-146.1 L 49	0.6	1.252	5.5	0.133	4.3	0.8	0.068	3.2	882.00	66.90	824.39	31.27	803.06	33.95	9.00
F1206-146.1 M 197	0.6	1.314	7.9	0.135	6.8	0.9	0.070	4.0	940.00	82.39	851.69	45.72	817.89	52.51	13.00
F1206-146.1 L 40	0.6	1.374	7.8	0.137	6.2	0.8	0.073	4.7	1005.00	94.22	877.98	45.73	828.33	48.53	18.00
F1206-146.1 M 224	0.6	1.244	6.5	0.134	5.5	0.9	0.067	3.4	845.00	70.74	820.58	36.67	811.34	42.37	4.00
F1206-146.1 M 189	0.7	1.309	7.4	0.138	5.9	0.8	0.069	4.6	896.00	94.69	849.64	42.91	831.75	45.84	7.00
F1206-146.1 L 39	0.7	4.253	7.0	0.286	6.0	0.9	0.108	3.7	1766.00	66.75	1684.29	57.63	1619.33	85.67	8.00
F1206-146.1 M 204	0.7	1.397	6.6	0.145	5.9	0.9	0.070	2.9	927.00	60.30	887.54	39.15	871.57	48.33	6.00
F1206-146.1 M 185	0.7	4.638	8.5	0.304	7.5	0.9	0.111	3.9	1812.00	70.50	1756.13	70.86	1708.97	113.24	6.00

F1206-146.1 L 24	0.7	1.001	6.4	0.113	5.3	0.8	0.064	3.5	741.83	74.83	704.47	32.33	692.81	34.74	7.00
F1206-146.1 M 228	0.7	1.408	9.5	0.149	8.3	0.9	0.069	4.7	891.00	97.28	892.17	56.55	892.48	69.01	0.00
F1206-146.1 L 51	0.7	1.189	7.4	0.126	5.6	0.8	0.069	4.8	884.81	98.54	795.25	40.67	763.66	40.54	14.00
F1206-146.1 M 203	0.7	1.376	7.2	0.143	6.6	0.9	0.070	2.7	919.00	56.37	878.76	42.25	862.84	53.64	6.00
F1206-146.1 L 30	0.7	1.286	5.6	0.132	4.7	0.8	0.070	3.0	941.00	60.86	839.46	31.95	801.38	35.72	15.00
F1206-146.1 L 52	0.7	1.268	7.3	0.136	5.6	0.8	0.068	4.7	852.00	97.10	831.48	41.48	823.45	43.42	3.00
F1206-146.1 M 199	0.8	1.202	8.7	0.131	7.3	0.8	0.067	4.8	823.00	99.37	801.31	48.43	793.43	54.71	4.00
F1206-146.1 M 213	0.8	1.210	8.3	0.137	6.0	0.7	0.064	5.8	751.00	121.91	805.10	46.29	824.78	46.46	-10.00
F1206-146.1 L 26	0.8	1.257	5.4	0.138	4.5	0.8	0.066	3.0	814.00	62.69	826.48	30.46	830.81	34.89	-2.00
F1206-146.1 M 205	0.8	1.110	6.3	0.122	5.6	0.9	0.066	3.0	803.09	63.43	758.18	33.90	743.03	39.14	7.00
F1206-146.1 M 210	0.8	1.203	7.1	0.127	5.9	0.8	0.069	4.0	886.18	81.73	801.82	39.25	771.78	42.72	13.00
F1206-146.1 M 215	0.8	5.247	5.7	0.334	4.5	0.8	0.114	3.2	1864.00	57.82	1860.30	48.45	1856.11	75.66	0.00
F1206-146.1 L 33	0.8	1.287	6.8	0.137	5.9	0.9	0.068	3.2	875.00	66.08	839.92	38.79	826.43	46.47	6.00
F1206-146.1 L 28	0.8	1.302	5.9	0.140	4.5	0.8	0.067	3.9	847.00	81.01	846.78	34.10	846.33	35.53	0.00
F1206-146.1 L 45	0.8	1.226	5.9	0.131	4.5	0.8	0.068	3.8	873.00	78.96	812.41	32.97	790.53	33.46	9.00
F1206-146.1 M 221	0.8	1.356	6.3	0.143	5.5	0.9	0.069	3.1	885.00	64.79	870.27	36.81	864.20	44.17	2.00
F1206-146.1 L 34	0.8	1.248	6.4	0.137	5.8	0.9	0.066	2.7	809.00	55.48	822.53	36.06	827.23	45.19	-2.00
F1206-146.1 M 187	0.9	1.336	9.2	0.147	7.7	0.8	0.066	5.0	802.00	103.76	861.54	53.45	884.50	64.11	-10.00
F1206-146.1 M 193	0.9	1.074	6.4	0.122	6.0	0.9	0.064	2.4	738.80	50.06	740.89	33.93	741.58	42.05	0.00
F1206-146.1 M 207	0.9	1.233	6.6	0.135	5.6	0.8	0.066	3.6	818.00	74.58	815.52	37.12	814.47	42.67	0.00
F1206-146.1 M 198	0.9	1.383	7.3	0.149	6.2	0.8	0.068	3.9	854.00	81.06	881.84	43.16	892.88	51.67	-5.00
F1206-146.1 L 35	0.9	1.267	5.8	0.132	5.2	0.9	0.070	2.6	921.00	53.72	831.22	33.29	798.03	39.41	13.00
F1206-146.1 M 19	0.9	1.278	9.0	0.134	8.5	0.9	0.069	2.9	904.00	59.56	835.81	51.27	810.19	64.90	10.00
F1206-146.1 M 202	0.9	1.357	6.9	0.145	5.7	0.8	0.068	3.9	861.00	80.18	870.77	40.28	874.36	46.64	-1.00
F1206-146.1 M 218	1.0	1.363	6.6	0.143	5.6	0.9	0.069	3.4	898.00	70.30	873.27	38.62	863.31	45.60	4.00
F1206-146.1 M 196	1.1	1.262	6.3	0.139	4.8	0.8	0.066	4.1	802.00	85.03	828.74	35.48	838.59	37.50	-5.00
F1206-146.1 L 27	1.1	1.257	6.9	0.132	4.8	0.7	0.069	5.0	894.00	102.73	826.46	39.28	801.41	36.52	10.00
F1206-146.1 L 25	1.1	1.410	6.1	0.145	5.6	0.9	0.071	2.6	950.00	52.53	893.27	36.49	870.43	45.43	8.00
F1206-146.1 M 217	1.1	1.406	5.7	0.147	4.9	0.9	0.069	2.9	904.00	59.03	891.45	33.93	886.28	40.99	2.00
F1206-146.1 M 212	1.1	1.301	6.7	0.140	5.8	0.9	0.067	3.3	848.00	69.59	846.35	38.46	845.64	45.98	0.00
F1206-146.1 L 38	1.3	1.194	6.7	0.130	6.0	0.9	0.067	3.0	823.00	62.63	798.02	37.12	789.12	44.63	4.00
F1206-146.1 L 50	1.4	1.276	5.3	0.135	4.8	0.9	0.069	2.4	888.00	48.88	835.23	30.51	815.43	36.83	8.00

LA-ICPMS data from F1206-146.1 continued.

	Concentrations (ppm)																					
Analysis	P	Ti	Y	Nb	La	Ce	Pr	Nd	Sm	Eu	Gd	Tb	Dy	Ho	Er	Tm	Yb	Lu	Hf	Ta	Th	U
F1206-146.1 M 206	57	2	195	8	0	1			0	0	1	1	12	6	30	9	108	10	8392	10	3	30
F1206-146.1 M 216	967	5	2004	1	0	2	0	0	3	0	23	11	171	69	332	98	1237	122	8886	1	28	225
F1206-146.1 M 227	801	5	1733	1	0	2	0	1	2	0	17	10	149	59	298	81	1001	101	8836	1	19	150
F1206-146.1 M 209	637	7	1377	1		2	0	1	2	0	16	8	114	47	227	65	798	83	8315	1	32	215
F1206-146.1 M 223	1050	7	2282	1		2	0	1	3	0	29	14	200	80	368	100	1169	116	8345	1	30	191
F1206-146.1 L 36	794	6	2016	3	0	4	0	3	8	0	47	19	216	74	270	70	738	67	7849	2	85	349
F1206-146.1 M 195	946	8	2059	1		3	0	1	4	0	27	12	175	68	310	85	986	98	8062	1	45	184
F1206-146.1 M 194	982	8	2099	1	0	2	0	1	4	0	26	13	179	68	321	90	1037	99	8373	1	31	127
F1206-146.1 M 192	70	4	86	7	0	6	0	1	3	1	7	2	14	3	9	2	16	2	6258	6	35	117
F1206-146.1 M 229	945	12	2241	1	0	1	0	2	7	0	42	17	210	73	315	78	799	80	7843	1	42	127
F1206-146.1 M 208	761	6	1714	1		3	0	1	3	0	24	11	156	60	278	73	811	85	8620	1	47	141
F1206-146.1 M 201	333	7	1330	4	0	8	0	1	3	1	23	9	119	45	210	57	691	76	7179	2	99	292
F1206-146.1 M 211	89	3	138	0		4		0	0	0	1	1	10	4	22	8	115	16	8781	0	68	183
F1206-146.1 M 222	798	7	1762	1		3	0	1	5	0	30	12	172	65	282	74	824	83	8260	1	63	156
F1206-146.1 M 214	622	17	1125	1		1	0	2	7	0	36	11	130	38	147	36	375	34	8210	1	47	111
F1206-146.1 M 220	154	3	371	1		17	0	1	2	1	8	3	33	13	56	16	216	24	7938	0	59	136
F1206-146.1 L 41	125	6	254	0		5	0	1	2	1	4	2	23	9	40	13	170	21	8179	0	14	32
F1206-146.1 L 23	204	11	401	1		5	0	0	1	0	7	3	37	14	66	19	220	24	8582	0	15	32
F1206-146.1 L 46	143	5	259	0	0	6	0	0	1	0	6	2	24	9	41	12	157	19	7833	0	14	30
F1206-146.1 L 43	125	5	118	0	0	5		0	0	0	2	1	10	4	19	6	77	9	7798	0	18	38
F1206-146.1 L 22	207	7	856	1		6	0	0	2	1	15	6	83	31	144	41	460	51	8021	1	24	48
F1206-146.1 M 191	130	7	320	1	0	8	0	1	1	0	6	2	29	11	50	14	169	19	7132	0	28	55
F1206-146.1 M 226	121	4	517	4		17	0	0	2	1	9	4	46	18	80	23	272	29	6387	1	157	311
F1206-146.1 L 31	187	7	350	1		10		0	1	0	6	2	30	12	59	17	233	28	7371	1	62	116
F1206-146.1 M 225	513	7	1420	1		12	0	1	4	1	24	9	126	50	221	58	686	68	7363	1	58	106
F1206-146.1 L 21	141	4	359	1		10		0	1	0	6	2	30	12	60	18	246	32	9228	1	60	108
F1206-146.1 M 200	1299	25	3304	2	1	9	0	5	11	1	63	24	313	115	500	130	1424	139	7240	1	121	217
F1206-146.1 L 42	196	7	530	1	0	8	0	1	2	1	10	3	48	18	87	27	346	39	6996	0	57	101
F1206-146.1 M 219	325	4	238	0	2	11	0	2	2	0	6	2	21	8	37	11	150	17	7606	0	34	59
F1206-146.1 L 47	129	4	212	1	0	13	0	0	1	0	5	2	19	7	33	11	136	17	8608	0	52	92
F1206-146.1 L 44	156	6	259	1		9	0	0	1	0	4	2	23	9	43	13	179	20	7792	0	63	109
F1206-146.1 L 49	1338	3	586	1	9	33	3	13	5	1	13	5	57	20	93	26	333	37	9155	1	78	132

F1206-146.1 M 197	184	11	421	1		9	0	1	2	0	11	3	42	14	60	16	187	19	7213	0	47	77
F1206-146.1 L 40	248	12	590	2	2	14	0	3	3	1	12	4	54	21	96	28	339	37	7361	1	85	134
F1206-146.1 M 224	834	15	2070	1	0	3	0	4	11	1	55	18	214	74	297	73	783	78	7438	1	74	117
F1206-146.1 M 189	327	12	1005	1		7	0	1	3	1	20	7	94	35	147	37	405	42	7216	0	28	43
F1206-146.1 L 39	250	8	557	4	0	8	0	2	4	0	17	5	64	21	87	23	242	23	7038	2	27	41
F1206-146.1 M 204	225	20	609	1	0	10	0	2	2	0	12	4	56	20	91	25	273	30	7611	1	41	61
F1206-146.1 M 185	218	6	757	4		7	0	2	3	0	20	6	82	29	118	28	317	31	6436	2	32	48
F1206-146.1 L 24	275	5	1204	3	0	25	0	1	3	1	17	7	107	42	198	58	686	82	8645	1	82	118
F1206-146.1 M 228	192	5	349	1	1	12	0	1	1	0	6	2	28	11	54	17	218	27	7757	1	76	109
F1206-146.1 L 51	1391	12	1184	1	6	32	2	13	8	2	28	9	114	42	184	51	565	65	7280	0	43	59
F1206-146.1 M 203	143	9	581	1	0	9	0	1	3	0	15	5	56	20	78	21	239	24	7820	0	63	86
F1206-146.1 L 30	167	8736	704	24	1	17	0	1	2	1	12	4	63	25	117	36	475	57	6933	3	156	211
F1206-146.1 L 52	175	8	908	0	0	5	0	3	5	3	23	8	89	32	144	41	489	61	6422	0	51	68
F1206-146.1 M 199	241	8	842	4	0	25	0	2	5	1	22	8	92	35	136	35	403	41	5977	1	51	67
F1206-146.1 M 213	167	7	488	0	0	11	0	1	3	2	15	5	49	17	73	19	227	24	5486	0	24	32
F1206-146.1 L 26	129	3	397	2		21	0	0	2	1	8	3	35	14	62	20	240	30	8459	1	140	184
F1206-146.1 M 205	203	8	606	1	0	12	0	1	3	1	12	4	51	20	89	28	359	42	7536	0	58	75
F1206-146.1 M 210	242	30	748	3	0	20	0	1	4	1	15	6	72	27	116	32	366	35	5969	1	57	73
F1206-146.1 M 215	234	31	570	3	0	5	0	1	4	0	16	5	62	20	84	20	224	22	6643	1	17	21
F1206-146.1 L 33	142	5	211	0		10	0	1	1	0	4	2	19	7	33	10	130	15	7574	0	72	87
F1206-146.1 L 28	189	12	527	1		15	0	1	5	1	20	6	61	20	81	20	214	21	7330	0	71	86
F1206-146.1 L 45	317	18	1025	3	0	21	0	3	7	2	25	8	106	38	171	46	569	59	6405	1	68	82
F1206-146.1 M 221	172	5	589	1	0	18	0	6	8	3	22	6	62	19	76	21	253	29	6965	0	79	95
F1206-146.1 L 34	221	10	1060	0		12	0	2	6	1	31	10	121	41	162	40	442	42	7854	0	66	78
F1206-146.1 M 187	176	12	420	1	0	10	0	1	3	1	11	3	39	14	60	17	193	22	5921	0	34	40
F1206-146.1 M 193	788	4	1273	2	2	29	1	4	4	1	26	9	112	43	199	54	669	74	7488	1	116	134
F1206-146.1 M 207	263	11	1211	2	0	11	0	4	6	1	31	10	122	44	185	48	530	55	6859	1	84	97
F1206-146.1 M 198	102	6	337	0		20	0	2	4	2	13	3	33	10	43	13	166	18	6621	0	101	116
F1206-146.1 L 35	306	11	1235	1		13	0	3	6	2	30	11	130	45	193	53	603	61	6678	0	105	116
F1206-146.1 M 19	230	10	1484	1		13	0	3	6	2	37	12	138	49	202	51	566	57	6217	1	83	92
F1206-146.1 M 202	231	15	1252	1	0	11	0	3	6	1	30	11	126	45	183	46	514	51	6707	1	120	128
F1206-146.1 M 218	154	5	789	1	0	20	0	3	6	3	23	7	80	27	113	31	365	36	5533	0	54	54
F1206-146.1 M 196	152	6	501	1	0	22	0	1	2	1	13	4	49	16	77	22	275	29	7109	0	88	82
F1206-146.1 L 27	203	5	523	1	0	13	0	1	3	1	13	4	49	18	80	24	302	34	7314	0	63	58
F1206-146.1 L 25	140	10	191	1		26	0	1	2	1	6	2	21	7	29	7	91	10	7166	0	108	100

F1206-146.1 M 217	250	17	1115	3	2	47	1	6	8	2	30	10	116	39	169	44	508	49	6119	1	204	183
F1206-146.1 M 212	180	6	759	2	0	27	0	4	6	2	22	6	75	26	115	32	406	44	7005	0	101	89
F1206-146.1 L 38	245	21	1558	2	0	17	1	8	11	2	42	14	167	60	237	60	645	65	6340	1	307	238
F1206-146.1 L 50	113	4	478	2		44	0	2	4	2	15	4	46	16	68	19	232	27	8510	1	297	210

2 May, 2013

Isotope ratios and ages are NOT corrected for initial common Pb.

Isotope ratio and apparent age errors do not include systematic calibration errors of 3.37001023234556% ($^{208}Pb/^{232}Th$), 0.283867945906847% ($^{207}Pb/^{206}Pb$), 2.11018041496079% ($^{206}Pb/^{238}U$) (all 1-sigma).

Trace element concentrations in ppm, calculated using mean count rate method.

Sweep-by-sweep downhole fractionation of U/Pb ratios NOT corrected via Si/Zr fractionation factor.

Backgrounds were monitored between sweeps 10 to 20. Sample counts were integrated from sweeps 28 to 53.

Ablation used a laser spot size of 25 microns, and a laser firing repetition rate of 10 Hz.

LA-ICPMS data from F1203-272.1

		Corrected isotope ratios							Dates (Ma)						
		207Pb*	±2s	206Pb*	±2s	error	207Pb*	±2s	207Pb*	±2s	207Pb*	±2s	206Pb*	±2s	%
Analysis	Th/U	235U*	(%)	238U	(%)	corr.	206Pb*	(%)	206Pb*	(Ma)	235U	(Ma)	238U*	(Ma)	disc.
F1203-272.1 M 158	0.6	9.341	9.6	0.404	9.0	0.9	0.168	3.3	2534	55	2372	88	2188	167	14
F1203-272.1 L 67	0.6	9.277	6.5	0.429	5.8	0.9	0.157	3.0	2423	50	2366	60	2300	113	5
F1203-272.1 L 52	1.4	8.714	6.7	0.407	5.5	0.8	0.155	3.9	2406	66	2309	61	2200	103	9
F1203-272.1 S 220	0.8	1.292	6.3	0.141	5.3	0.9	0.067	3.3	826	69	842	36	848	42	-3
F1203-272.1 M 159	0.8	1.291	10.0	0.140	9.2	0.9	0.067	3.9	839	82	842	57	843	73	0
F1203-272.1 M 155	0.6	1.256	10.0	0.137	7.1	0.7	0.066	7.1	821	148	826	57	828	55	-1
F1203-272.1 S 223	1.3	1.284	6.7	0.137	5.1	0.8	0.068	4.2	872	88	839	38	826	40	5
F1203-272.1 M 156	0.6	1.178	8.7	0.129	7.3	0.8	0.066	4.9	816	102	790	48	781	53	4
F1203-272.1 L 59	1.3	1.208	7.5	0.128	5.8	0.8	0.068	4.6	874	96	804	41	779	43	11
F1203-272.1 L 56	1.2	1.160	6.2	0.128	5.6	0.9	0.066	2.7	794	56	782	34	777	41	2
F1203-272.1 M 162	1.1	1.188	10.3	0.127	9.5	0.9	0.068	4.0	856	83	795	57	774	69	10
F1203-272.1 L 60	0.9	1.158	9.8	0.127	5.8	0.6	0.066	7.9	815	165	781	53	769	42	6
F1203-272.1 L 55	1.0	1.162	6.7	0.126	5.4	0.8	0.067	4.0	830	83	783	37	766	39	8
F1203-272.1 S 222	2.3	1.117	7.0	0.126	5.6	0.8	0.064	4.2	748	88	762	37	766	40	-2
F1203-272.1 L 58	1.1	1.095	8.1	0.125	5.9	0.7	0.063	5.6	718	118	751	43	762	43	-6
F1203-272.1 L 64	1.0	1.108	8.0	0.124	5.9	0.7	0.065	5.4	761	113	757	43	756	42	1

F1203-272.1 M 160	1.5	1.116	9.9	0.124	8.6	0.9	0.065	4.9	777	103	761	53	756	61	3
F1203-272.1 M 15	1.4	1.112	10.7	0.124	7.5	0.7	0.065	7.6	770	160	759	57	755	54	2
F1203-272.1 L 54	1.0	1.080	8.2	0.124	6.1	0.7	0.063	5.4	711	115	744	43	755	44	-6
F1203-272.1 M 157	2.3	1.110	11.7	0.124	9.6	0.8	0.065	6.6	773	140	758	62	753	68	3
F1203-272.1 M 154	1.0	1.115	7.2	0.124	5.8	0.8	0.065	4.2	788	87	760	38	751	41	5
F1203-272.1 L 63	0.7	1.131	6.0	0.123	5.0	0.8	0.067	3.3	831	70	768	32	747	35	10
F1203-272.1 L 65	0.8	1.087	7.3	0.122	5.3	0.7	0.065	5.0	767	106	747	39	740	37	4
F1203-272.1 L 49	0.8	1.083	9.1	0.121	6.1	0.7	0.065	6.7	779	142	745	48	734	42	6
F1203-272.1 S 221	1.5	1.037	6.9	0.120	5.6	0.8	0.063	4.1	695	87	723	36	732	39	-5
F1203-272.1 L 62	0.9	0.998	16.7	0.119	6.8	0.4	0.061	15.3	635	329	703	85	725	47	-14
F1203-272.1 S 219	1.3	1.069	7.8	0.119	5.6	0.7	0.065	5.4	788	113	738	41	722	38	8
F1203-272.1 L 51	0.9	1.016	9.9	0.118	5.2	0.5	0.063	8.4	695	179	712	51	717	35	-3
F1203-272.1 L 61	1.8	1.063	6.1	0.117	4.9	0.8	0.066	3.7	796	77	735	32	715	33	10
F1203-272.1 L 50	1.2	1.032	7.5	0.114	5.2	0.7	0.065	5.4	788	113	720	38	698	34	11
F1203-272.1 L 66	1.4	1.025	6.8	0.114	5.3	0.8	0.065	4.3	789	90	716	35	694	35	12
F1203-272.1 L 57	1.5	0.998	6.4	0.113	5.2	0.8	0.064	3.7	745	78	703	32	689	34	7

LA-ICPMS data from F1203-272.1 continued.

	Concentrations (ppm)																					
Analysis	P	Ti	Y	Nb	La	Ce	Pr	Nd	Sm	Eu	Gd	Tb	Dy	Ho	Er	Tm	Yb	Lu	Hf	Ta	Th	U
F1203-272.1 M 158	2266	19	1130	3	87	137	15	66	16	2	38	11	105	39	161	44	518	60	8687	1	354	636
F1203-272.1 L 67	131	14	264	0	0	10	0	1	2	1	5	2	24	9	42	12	137	20	9852	0	70	116
F1203-272.1 L 52	205	8	764	1	0	24	0	6	11	3	33	10	94	30	114	26	267	30	8515	1	35	26
F1203-272.1 S 220	195	2	1092	2		33	0	2	4	1	25	9	93	33	162	41	422	69	11240	1	167	202
F1203-272.1 M 159	228	6	888	2	0	12	0	1	3	0	13	5	78	30	136	38	463	52	8005	1	104	132
F1203-272.1 M 155	243	11	844	1		4	0	1	4	1	18	7	85	32	132	34	385	42	5958	0	22	38
F1203-272.1 S 223	172	5	834	2		21		1	3	1	16	5	65	26	127	34	344	65	11546	1	118	93
F1203-272.1 M 156	294	4	2370	4	0	9	0	5	9	2	61	22	272	91	387	93	951	96	7093	1	52	83
F1203-272.1 L 59	116	4	469	3	0	31	0	1	2	1	12	3	44	16	75	21	250	35	9303	1	228	176
F1203-272.1 L 56	1292	8	1382	6	14	69	4	19	11	4	36	12	137	49	216	56	642	87	8759	2	445	375
F1203-272.1 M 162	235	6	906	1	0	24	0	3	5	1	18	6	81	29	138	39	498	59	7197	1	253	224
F1203-272.1 L 60	201	8	733	1	0	20		1	2	1	16	6	78	28	119	32	369	46	9666	1	35	41
F1203-272.1 L 55	600	4	566	2	6	22	1	8	3	1	12	4	54	19	92	25	307	42	9310	1	222	227
F1203-272.1 S 222	553	19	3323	2	0	51	1	7	15	7	85	28	335	119	507	113	1037	157	9127	1	201	89

F1203-272.1 L 58	2462	11	1088	2	44	110	11	54	15	2	30	8	102	41	177	48	535	67	9205	1	123	111
F1203-272.1 L 64	466	11	1881	4	0	41	0	3	8	2	36	14	178	70	323	83	918	114	8926	1	117	115
F1203-272.1 M 160	410	11	2543	3		33	0	6	13	4	62	21	250	87	379	88	920	100	6513	1	193	129
F1203-272.1 M 15	237	12	1543	1	0	26	0	5	8	3	36	13	141	52	224	56	617	68	6941	1	155	109
F1203-272.1 L 54	175	4	941	2	0	12	0	3	5	2	26	8	94	34	145	41	469	61	9252	1	194	188
F1203-272.1 M 157	318	14	1977	1	0	32	0	8	16	4	58	18	217	73	300	79	879	96	5900	1	201	87
F1203-272.1 M 154	314	6	2185	5		23	0	3	7	2	48	17	204	78	356	90	968	110	7311	1	206	210
F1203-272.1 L 63	755	3	408	2	5	21	1	5	3	1	10	3	36	15	67	19	236	33	10421	2	204	293
F1203-272.1 L 65	306	9	1491	2		8	0	3	5	1	30	11	146	57	246	61	654	84	7934	1	131	166
F1203-272.1 L 49	1127	14	928	1	9	26	2	12	5	2	21	7	90	34	158	40	430	54	8229	0	57	71
F1203-272.1 S 221	338	5	2025	5	0	60	0	3	5	1	37	12	167	68	332	82	831	133	11534	2	437	289
F1203-272.1 L 62	456	25	1104	1	0	11	0	2	5	3	31	10	117	45	183	45	461	56	7267	0	25	27
F1203-272.1 S 219	348	3	2088	3	0	33	0	2	4	1	37	14	166	68	329	85	891	141	9934	1	276	205
F1203-272.1 L 51	501	9	909	2	3	36	1	5	4	0	15	7	84	35	151	43	463	58	10279	1	68	73
F1203-272.1 L 61	231	13	952	1	0	37	0	2	4	1	22	7	91	35	153	41	457	59	8970	1	547	306
F1203-272.1 L 50	532	11	1969	1	0	25	0	2	7	3	44	15	197	75	327	82	875	113	8137	1	172	138
F1203-272.1 L 66	623	15	2010	2	4	27	1	10	10	4	47	18	218	79	326	78	798	95	7290	1	212	150
F1203-272.1 L 57	1013	10	4174	2	0	56	0	7	16	8	100	36	434	166	701	169	1778	230	7291	1	500	334

17 December, 2012

Isotope ratios and ages are not corrected for initial common Pb.

Isotope ratio and apparent age errors do not include systematic calibration errors of 1.810262980559 07% ($^{208}Pb/^{232}Th$), 0.773493715556818% ($^{207}Pb/^{206}Pb$), 0.7479425316903 96% ($^{206}Pb/^{238}U$).

Trace element concentrations in ppm, calculated using mean count rate method.

Backgrounds were monitored between sweeps 17 to 27. Sample counts were integrated from sweeps 39 to 68.

Table 3.A2. U-Pb CA-ID-TIMS geochronological data from the Zavkhan Fm and Tsagaan-Olom Group.

	Composition					Ratios[5]						Age (Ma)				
Sample	Pb_c[2]	Pb*[2]	Th	^{206}Pb[3]	^{208}Pb[4]	^{206}Pb	err	^{207}Pb	err	^{207}Pb	err	^{206}Pb	err	^{207}Pb	^{207}Pb	corr.
Fraction[1]	(pg)	Pb_c	U	^{204}Pb	^{206}Pb	^{238}U	(2σ%)	^{235}U	(2σ%)	^{206}Pb	(2σ%)	^{238}U	(2σ)	^{235}U	^{206}Pb	coef.
F718: Rhyolite, upper Zavkhan Formation																
z3	0.4	22.5	0.73	1275.0	0.224	0.131929	(.20)	1.19485	(.68)	0.06572	(.63)	798.9	1.5	798.2	796	0.37
z4	0.4	81.0	0.82	4444.2	0.251	0.131641	(.07)	1.19320	(.23)	0.06577	(.21)	**797.22**	**0.56**	797.4	798.1	0.37
z5	0.7	20.9	0.99	1115.8	0.303	0.132112	(.15)	1.20245	(.75)	0.06604	(.71)	799.9	1.1	801.7	807	0.37
F701-14.5: Rhyolite (olistolith ?), lower Maikhan-Uul Formation																
z1	0.6	21.2	1.38	1040.1	0.423	0.129765	(.17)	1.17564	(.81)	0.06574	(.76)	**786.5**	**1.3**	789.3	797	0.37
z2	0.5	36.9	1.24	1849.1	0.382	0.129964	(.10)	1.17340	(.46)	0.06551	(.44)	**787.66**	**0.74**	788.2	789.9	0.34
z3	0.6	27.8	1.59	1301.5	0.489	0.130036	(.19)	1.17689	(.65)	0.06567	(.60)	**788.1**	**1.4**	789.9	795	0.40
z4	0.5	31.4	1.36	1538.6	0.416	0.129877	(.13)	1.17247	(.55)	0.06550	(.51)	**787.17**	**0.94**	787.8	790	0.40
z5	0.4	44.8	1.32	2210.7	0.405	0.130001	(.20)	1.17273	(.45)	0.06546	(.38)	**787.9**	**1.5**	787.9	788.1	0.55
F1203-272.1: Tuffaceous sandstone, middle Maikhan-Uul Formation																
z49	1.1	21.6	0.76	1215.8	0.234	0.126299	(.57)	1.13424	(.92)	0.06516	(.70)	766.7	4.1	769.8	779	0.65
z50	0.5	49.5	0.73	2781.8	0.224	0.122738	(.86)	1.07970	(.92)	0.06383	(.30)	746.3	6.1	743.5	735.0	0.95
z57	0.3	71.9	0.93	3849.1	0.286	0.119875	(.20)	1.05714	(.30)	0.06399	(.21)	**729.8**	**1.4**	732.4	740.3	0.71
z61	0.4	80.6	0.87	4367.6	0.268	0.128763	(.15)	1.15829	(.25)	0.06527	(.19)	780.8	1.1	781.1	782.1	0.66
z62	0.3	25.1	0.96	1346.2	0.294	0.130774	(.28)	1.18078	(.68)	0.06552	(.60)	792.3	2.1	791.7	790	0.48
z65	0.6	41.9	0.62	2418.6	0.190	0.130679	(.13)	1.18385	(.35)	0.06573	(.31)	791.7	1.0	793.1	797.0	0.47
z66	0.8	13.8	1.10	727.0	0.339	0.120897	(.30)	1.07450	(1.12)	0.06449	(1.05)	735.7	2.1	740.9	757	0.34
F868-64: Tuffaceous sandstone, lower Taishir Formation																
z2	1.0	21.4	0.66	1234.1	0.203	0.131650	(.18)	1.19583	(.66)	0.06591	(.61)	797.3	1.4	798.7	803	0.39
z3	0.8	48.3	0.64	2771.3	0.196	0.134284	(2.04)	1.22492	(2.06)	0.06619	(.31)	812	16	812	811.4	0.99
z4	0.5	21.6	1.53	1027.3	0.470	0.130633	(.23)	1.18171	(.83)	0.06564	(.78)	791.5	1.7	792.1	794	0.32

z5	0.5	8.2	0.21	520.9	0.061	0.310145	(.38)	4.58232	(1.02)	0.10720	(.91)	1741.4	5.8	1746.1	1752	0.45
z7	0.3	15.7	0.68	902.0	0.209	0.132213	(.21)	1.19514	(1.02)	0.06559	(.97)	800.5	1.6	798.3	792	0.34
z10	0.4	9.8	0.69	571.9	0.211	0.126678	(.44)	1.11134	(1.52)	0.06366	(1.41)	**768.9**	**3.2**	758.8	729	0.38
U1213: Rhyolite, lower Zavkhan Formation																
z3	0.4	91.9	0.72	5151.2	0.221	0.132451	(.08)	1.20456	(.19)	0.06599	(.15)	**801.83**	**0.62**	802.7	805.1	0.58
z4	0.2	142.7	0.74	7956.0	0.227	0.132516	(.15)	1.20449	(.20)	0.06595	(.11)	**802.2**	**1.1**	802.7	803.9	0.83
z7	0.2	64.0	0.89	3451.6	0.275	0.132650	(.27)	1.20821	(.37)	0.06609	(.24)	**803.0**	**2.0**	804.4	808.2	0.75
z9	0.3	162.6	0.75	9038.9	0.231	0.132613	(.15)	1.20418	(.19)	0.06589	(.10)	**802.8**	**1.1**	802.5	801.8	0.84
z31	0.6	69.6	0.80	3840.5	0.244	0.132471	(.20)	1.20439	(.29)	0.06597	(.20)	**801.9**	**1.5**	802.6	804.5	0.73

Notes: Corr. coef. = correlation coefficient. Age calculations are based on the decay constants of Jaffey et al. (1971).

[1] All analyses are single zircon grains and pre-treated by the thermal annealing and acid leaching (CA-ID-TIMS) technique. Data used in age calculations are in **bold**.

[2] Pb_c is total common Pb in analysis. Pb* is radiogenic Pb concentration.

[3] Measured ratio corrected for U-Pb tracer and fractionation only.

[4] Radiogenic Pb ratio.

[5] Corrected for fractionation, tracer, blank, and initial Th/U disequilibrium in magma. All common Pb is assumed to be blank. Total procedural blank was less than 0.1pg for U. Blank isotopic composition: $^{206}Pb/^{204}Pb = 18.20 \pm 0.45$, $^{207}Pb/^{204}Pb = 15.29 \pm 0.24$, $^{208}Pb/^{204}Pb = 37.16 \pm 0.77$.

Table 3.A3. Carbonate carbon and oxygen isotope data from the Tsagaan-Olom Group.

Khongor Range	N 46 10.803'	E 96 16.50'			
Section	**height**	**δ^{13}Ccarb**	**δ^{18}Ocarb**	**Unit**	**Lithology**
F701	103.5	-1.45	1.31	MU	l
F701	127.5	-2.14	-2.82	MU	l
F701	170.0	-2.14	-11.73	MU	l
F701	176.1	-3.06	-17.83	T1	l
F701	176.6	-2.09	-10.23	T1	l
F701	178.0	-2.40	-12.49	T1	l
F701	179.0	-1.94	-12.25	T1	l
F701	180.0	-1.30	-15.27	T1	l
F701	181.0	-1.03	-14.78	T1	l
F701	182.0	-1.61	-17.38	T1	l
F701	183.0	-0.56	-13.64	T1	l
F701	184.0	-1.60	-15.63	T1	l
F701	185.0	0.43	-10.55	T1	l

Khongor Range	N 46 10'48.2	E 96 16'29.9"			
Section	**height**	**δ^{13}Ccarb**	**δ^{18}Ocarb**	**Unit**	**Lithology**
F702	0.0	-2.58	-18.12	T1	l
F702	1.0	-1.10	-16.46	T1	l
F702	3.0	-1.32	-15.55	T1	l
F702	4.0	-0.58	-15.36	T1	l
F702	5.0	-1.30	-15.89	T1	l
F702	6.0	-0.73	-14.40	T1	l
F702	7.0	-0.80	-14.99	T1	l
F702	8.0	-0.45	-14.46	T1	l
F702	9.0	-0.92	-13.83	T1	l
F702	10.0	-0.68	-13.07	T1	l
F702	11.0	-0.23	-12.93	T1	l
F702	12.0	-0.09	-11.31	T1	l
F702	13.0	0.23	-8.65	T1	l
F702	14.0	-0.68	-13.53	T1	l
F702	15.0	-0.47	-12.11	T1	l
F702	16.0	-0.55	-8.93	T1	l
F702	17.0	-0.15	-12.96	T1	l
F702	18.0	-0.24	-12.73	T1	l
F702	19.0	-0.35	-15.03	T1	l
F702	21.0	-0.01	-9.73	T1	l
F702	36.0	3.47	-8.83	T1	l
F702	38.0	3.77	-7.84	T1	l
F702	40.0	3.29	-8.17	T1	l
F702	42.0	2.41	-5.63	T1	l

Khongor Range	N 46 10'48.2	E 96 16'29.9"			
Section	**height**	**δ^{13}Ccarb**	**δ^{18}Ocarb**	**Unit**	**Lithology**
F703	0.0	4.64	-6.90	T2	l

F703	2.0	2.01	-5.57	T2	l
F703	4.0	3.51	-7.30	T2	l
F703	6.0	4.54	-13.15	T2	l
F703	12.0	6.64	-9.40	T2	l
F703	25.0	7.48	-6.04	T2	l
F703	28.0	8.47	-3.48	T2	l
F703	32.0	7.03	-7.28	T2	l
F703	34.0	7.06	-7.09	T2	l
F703	36.0	7.72	-10.57	T2	l
F703	38.0	8.60	-3.54	T2	l
F703	40.0	6.77	-9.63	T2	l
F703	42.0	8.32	-5.86	T2	l
F703	44.0	8.59	-3.75	T2	l
F703	46.0	6.91	-9.72	T2	l
F703	48.0	7.18	-9.51	T2	l
F703	50.0	8.90	-5.50	T2	l
F703	52.0	9.58	-3.98	T2	l
F703	54.0	7.78	-8.40	T2	l
F703	56.0	7.46	-6.48	T2	l
F703	58.0	6.82	-8.59	T2	l
F703	60.0	7.53	-8.52	T2	l
F703	62.0	7.11	-9.73	T2	l
F703	64.0	7.76	-8.53	T2	l
F703	66.0	7.52	-10.05	T2	l
F703	68.0	7.84	-8.65	T2	l
F703	74.0	7.32	-9.84	T2	l
F703	76.0	6.74	-10.24	T2	l
F703	78.0	6.99	-9.07	T2	l

Khongor Range **N46 41'58.0"** **E 96 14'54.9"**

Section	**height**	**δ^{13}Ccarb**	**δ^{18}Ocarb**	**Unit**	**Lithology**
F704	122.0	4.14	-4.80	T1	l
F704	124.0	7.76	-7.27	T1	l
F704	126.0	6.28	-5.04	T1	l
F704	128.0	4.03	-6.31	T1	l
F704	146.0	6.60	-6.98	T2	l
F704	148.0	7.99	-6.09	T2	l
F704	150.0	6.90	-8.57	T2	l
F704	152.0	7.60	-7.56	T2	l
F704	154.0	8.33	-3.76	T2	l
F704	156.0	8.65	-5.26	T2	l
F704	158.0	8.14	-4.98	T2	l
F704	160.0	5.93	-8.41	T2	l
F704	162.0	7.03	-7.13	T2	l
F704	166.0	5.65	-7.18	T2	l
F704	168.0	7.61	-6.91	T2	l
F704	170.0	6.56	-8.37	T2	l
F704	172.0	7.85	-4.51	T2	l

F704	174.0	6.90	-7.80	T2	1
F704	176.0	7.43	-10.89	T2	1
F704	178.0	7.34	-8.95	T2	1
F704	180.0	6.65	-8.65	T2	1
F704	182.0	7.49	-7.88	T2	1
F704	184.0	6.66	-7.86	T2	1
F704	186.0	7.02	-6.59	T2	1
F704	188.0	6.52	-7.52	T2	1
F704	192.0	7.00	-6.95	T2	1
F704	194.0	7.22	-6.41	T2	1
F704	196.0	7.01	-7.11	T2	1
F704	200.0	7.47	-7.93	T2	1
F704	202.0	8.55	-10.13	T2	1
F704	204.0	6.57	-8.88	T2	1
F704	206.0	6.14	-7.63	T2	1
F704	208.0	5.95	-7.47	T2	1
F704	210.0	7.26	-8.92	T2	1
F704	214.0	6.38	-9.05	T2	1
F704	216.0	6.56	-9.57	T2	1
F704	218.0	7.09	-7.19	T2	1
F704	220.0	7.41	-5.87	T2	1
F704	222.0	7.50	-7.01	T2	1
F704	224.0	7.29	-8.33	T2	1
F704	226.0	7.05	-8.38	T2	1
F704	228.0	6.68	-6.60	T2	1
F704	230.0	6.64	-13.87	T2	1
F704	232.0	6.84	-12.01	T2	1
F704	236.0	6.07	-11.75	T2	1
F704	238.0	5.81	-10.83	T2	1
F704	240.0	5.49	-11.67	T2	1
F704	242.0	5.54	-15.57	T2	1
F704	244.0	7.09	-8.71	T2	1
F704	246.0	5.87	-19.93	T2	1
F704	248.0	4.57	-14.57	T2	1
F704	250.0	1.24	-18.38	T2	1
F704	252.0	6.96	-20.50	T2	1
F704	254.0	6.73	-11.37	T2	1
F704	256.0	7.24	-13.96	T2	1
F704	258.0	7.07	-11.30	T2	1
F704	260.0	5.40	-13.15	T2	1
F704	264.0	5.88	-12.30	T2	1
F704	266.0	5.55	-9.97	T2	1
F704	268.0	7.33	-6.94	T2	1
F704	270.0	6.43	-7.55	T2	1
F704	272.0	6.79	-10.37	T2	1
F704	274.0	7.40	-7.11	T2	1
F704	278.0	5.35	-8.93	T2	1
F704	280.0	6.59	-8.25	T2	1

F704	282.0	5.25	-8.51	T2	1
F704	284.0	5.43	-8.77	T2	1
F704	286.0	6.62	-5.15	T2	1
F704	288.0	4.71	-8.58	T2	1
F704	290.0	5.01	-7.72	T2	1
F704	292.0	4.53	-8.59	T2	1
F704	294.0	3.93	-8.62	T2	1
F704	298.0	3.94	-7.67	T2	1
F704	300.0	3.39	-8.60	T2	1
F704	302.0	1.92	-6.88	T2	1
F704	310.0	-5.38	-18.35	T2	1
F704	312.0	-4.15	-19.66	T2	1
F704	314.0	-5.33	-12.89	T2	1
F704	316.0	-6.69	-13.79	T3	1
F704	318.0	-6.19	-6.60	T3	1
F704	320.0	-5.78	-10.85	T3	1
F704	322.0	-5.98	-14.72	T3	1
F704	324.0	-5.46	-8.15	T3	1
F704	326.0	-7.37	-11.22	T3	1
F704	328.0	-6.58	-9.53	T3	1
F704	330.0	-5.74	-8.30	T3	1
F704	332.0	-5.44	-9.27	T3	1
F704	334.0	-6.29	-11.69	T3	1
F704	336.0	-5.11	-11.78	T3	1
F704	338.0	-4.94	-9.90	T3	1
F704	340.0	-4.33	-11.94	T3	1
F704	346.0	-2.41	-11.08	T3	1
F704	348.0	-2.67	-7.51	T3	1
F704	350.0	-2.60	-13.10	T3	1
F704	352.0	-1.29	-17.74	T3	1
F704	354.0	-1.29	-8.14	T3	1
F704	356.0	0.20	-17.50	T3	1
F704	360.0	1.13	-11.94	T3	1
F704	362.0	3.83	-14.02	T4	1
F704	364.0	7.27	-12.12	T4	1
F704	366.0	8.79	-6.33	T4	1
F704	368.0	7.37	-6.82	T4	1
F704	370.0	6.16	-5.87	T4	1
F704	372.0	8.82	-5.43	T4	1
F704	374.0	9.09	-5.27	T4	1
F704	376.0	9.49	-4.64	T4	1
F704	378.0	8.08	-6.56	T4	1
F704	380.0	7.55	-7.55	T4	1
F704	382.0	7.51	-9.83	T4	1
F704	384.0	8.04	-5.42	T4	1
F704	386.0	9.21	-5.43	T4	1
F704	388.0	8.75	-8.74	T4	1
F704	392.0	9.56	-9.78	T4	1

F704	396.0	8.93	-6.67	T4	1
F704	398.0	9.13	-5.46	T4	1
F704	400.0	5.66	-5.97	T4	1
F704	402.0	7.27	-8.96	T4	1
F704	404.0	7.45	-11.23	T4	1
F704	406.0	9.35	-9.78	T4	1
F704	412.0	9.21	-6.31	T4	1
F704	414.0	8.70	-7.00	T4	1
F704	416.0	9.57	-4.56	T4	1
F704	418.0	7.67	-7.74	T4	1
F704	420.0	9.65	-4.36	T4	1
F704	424.0	8.97	-7.02	T4	1
F704	426.0	9.35	-4.73	T4	1
F704	428.0	8.90	-4.75	T4	1
F704	430.0	9.71	-2.66	T4	1
F704	432.0	10.02	-2.51	T4	1
F704	436.0	8.62	-5.40	T4	1
F704	438.0	10.09	-3.06	T4	1
F704	442.0	9.22	-4.81	T4	1
F704	446.0	9.93	-2.85	T4	1
F704	450.0	9.41	-4.55	T4	1
F704	456.0	9.51	-3.80	T4	1
F704	462.0	9.88	-1.59	T4	1
F704	466.0	9.10	-6.25	T4	1
F704	470.0	9.57	-3.57	T4	1
F704	474.0	9.45	-3.10	T4	1
F704	478.0	9.46	-4.27	T4	1
F704	482.0	9.76	-3.30	T4	1
F704	486.0	9.46	-4.89	T4	1
F704	490.0	8.83	-5.82	T4	1
F704	494.0	9.00	-4.99	T4	1
F704	498.0	8.96	-2.88	T4	1
F704	502.0	8.69	-10.22	T4	1
F704	506.0	9.51	-3.22	T4	1
F704	510.0	6.20	-5.22	T4	1
F704	514.0	9.86	-2.62	T4	1
F704	518.0	9.34	-3.06	T4	1
F704	522.0	9.72	-2.74	T4	1
F704	526.0	9.77	-3.07	T4	1
F704	530.0	9.85	-3.70	T4	1
F704	534.0	9.89	-4.51	T4	1
F704	538.0	9.69	-3.18	T4	1
F704	542.0	9.74	-3.97	T4	1
F704	546.0	9.70	-3.34	T4	1
F704	550.0	9.08	-4.36	T4	1
F704	554.0	9.96	-3.32	T4	1
F704	558.0	10.35	-3.93	T4	1
F704	562.0	11.02	-2.98	T4	1

F704	566.0	11.54	-3.55	T4	l

Khongor Range **N46 39'45.4"** **E95 49'06.3"**

Section	height	δ^{13}Ccarb	δ^{18}Ocarb	Unit	Lithology
F708	0.0	10.02	-6.74	T4	l
F708	1.0	10.36	-4.42	T4	l
F708	2.5	9.61	-5.02	T4	l
F708	4.0	9.05	-7.95	T4	l
F708	5.0	9.95	-4.57	T4	l
F708	6.0	10.04	-3.98	T4	l
F708	7.0	7.70	-14.03	T4	l
F708	7.5	8.04	-14.79	T4	l
F708	8.0	4.99	-13.77	T4	l

Taishir **N46 40'59.9"** **E96 33'50.3"**

Section	height	δ^{13}Ccarb	δ^{18}Ocarb	Unit	Lithology
F713	81.7	-3.13	-16.96	T1	l
F713	83.0	-2.03	-13.55	T1	l
F713	84.0	-1.49	-13.56	T1	l
F713	85.0	-1.35	-14.34	T1	l
F713	86.0	-0.45	-9.46	T1	l
F713	87.0	-0.33	-10.08	T1	l
F713	88.0	-0.85	-9.81	T1	l
F713	89.0	-0.65	-9.40	T1	l
F713	90.5	-0.74	-8.76	T1	l
F713	92.0	-1.09	-6.98	T1	l
F713	94.0	-0.47	-7.56	T1	l
F713	96.0	-1.18	-11.25	T1	l
F713	98.0	-0.62	-7.76	T1	l
F713	100.0	-1.23	-11.29	T1	l

Tsagaan Gorge **N46 49'01.1** **E95 49'06.3"**

Section	height	δ^{13}Ccarb	δ^{18}Ocarb	Unit	Lithology
F723	-2.0	10.80	-9.21	T	l
F723	-1.0	9.89	-9.14	T	l
F723	0.0	10.68	-6.50	T	l
F723	24.1	-0.28	-4.61		
F723	25	-0.77	-5.58		
F723	26	-0.58	-5.15		
F723	27	-0.58	-6.05		
F723	28	0.28	-4.91		
F723	29	1.01	-4.89		
F723	30	0.71	-3.99		
F723	31	-0.23	-3.83		
F723	32	2.20	-4.03		
F723	33	1.81	-3.87		
F723	34	1.39	-4.09		
F723	35	1.52	-4.29		

F723	36	1.24	-3.60		
F723	37	1.66	-4.10		
F723	38	0.98	-4.14		
F723	39	0.34	-4.46		
F723	41	-0.78	-3.32		
F723	43	-0.69	-4.69		
F723	45	-1.69	-3.71		
F723	47	-1.15	-12.35		
F723	49	-1.81	-10.52		
F723	51	-1.37	-10.76		
F723	53	-2.30	-11.78		
F723	55	1.04	-6.30		
F723	57	1.17	-6.43		
F723	59	0.95	-6.41		
F723	61	1.76	-6.36		
F723	63	-0.39	-5.79		
F723	65	-1.37	-6.22		
F723	67	-1.46	-5.94		
F723	71	-0.91	-2.49		
F723	73	-0.39	-1.75		
F723	75	0.45	-2.59		
F723	77	1.11	-2.15		
F723	79	1.85	-3.82		
F723	81	2.48	-3.70		

Taishir	**N46 40.162'**	**E95 34.032"**			
Section	**height**	**δ^{13}Ccarb**	**δ^{18}Ocarb**	**Unit**	**Lithology**
F864	79.0	7.74	-7.28	T2	l
F864	81.0	7.00	-8.21	T2	l
F864	83.0	7.04	-8.70	T2	l
F864	85.0	6.48	-11.42	T2	l
F864	87.0	6.36	-15.11	T2	l
F864	89.0	6.19	-12.94	T2	l
F864	95.0	5.60	-9.12	T2	l
F864	97.0	6.29	-9.18	T2	l
F864	99.0	4.58	-15.03	T2	l
F864	101.0	5.68	-8.23	T2	l
F864	103.0	6.25	-10.69	T2	l
F864	105.0	6.74	-15.10	T2	l
F864	107.0	4.33	-14.03	T2	l
F864	109.0	6.41	-9.26	T2	l
F864	111.0	5.23	-13.98	T2	l
F864	113.0	6.12	-8.38	T2	l
F864	115.0	3.09	-9.50	T2	l
F864	117.0	2.78	-9.11	T2	l
F864	119.0	2.09	-7.19	T2	l
F864	121.0	1.69	-7.98	T2	l
F864	123.0	1.32	-7.87	T2	l

F864	125.0	1.65	-9.33	T2	l
F864	127.0	1.35	-7.26	T2	l
F864	129.0	0.02	-8.76	T2	l
F864	131.0	-0.88	-24.67	T2	l
F864	132.0	-3.52	-13.92	T3	l
F864	136.0	-5.39	-10.45	T3	l
F864	137.0	-5.38	-11.20	T3	l
F864	138.0	-6.21	-9.24	T3	l
F864	139.0	-6.01	-9.66	T3	l
F864	140.0	-5.79	-8.20	T3	l
F864	141.0	-4.19	-15.35	T3	l
F864	142.0	-4.44	-12.55	T3	l
F864	143.0	-3.13	-15.66	T3	l
F864	144.0	-4.13	-12.98	T3	l
F864	145.0	-5.73	-8.63	T3	l
F864	146.0	-5.09	-11.87	T3	l
F864	149.0	-5.23	-11.12	T3	l
F864	150.0	-5.98	-8.20	T3	l
F864	151.0	-4.77	-12.73	T3	l
F864	152.0	-5.32	-8.29	T3	l
F864	153.0	-5.05	-18.97	T3	l
F864	154.0	-4.55	-6.92	T3	l
F864	155.0	-4.01	-7.88	T3	l
F864	156.0	-3.71	-8.90	T3	l
F864	157.0	-3.25	-11.07	T3	l
F864	158.0	-2.89	-9.44	T3	l
F864	159.0	-3.22	-7.83	T3	l
F864	160.0	-2.29	-10.37	T3	l
F864	161.0	-2.51	-9.43	T3	l
F864	162.0	-1.80	-13.12	T3	l
F864	163.0	-1.10	-15.92	T3	l
F864	164.0	-1.29	-14.89	T3	l
F864	167.0	-1.78	-13.45	T3	l
F864	168.0	-1.82	-15.23	T3	l
F864	169.0	-2.29	-10.53	T3	l
F864	170.0	-0.47	-18.11	T3	l
F864	171.0	5.75	-11.06	T4	l

Taishir

Section	Height	δ^{13}Ccarb	δ^{18}Ocarb	Unit	Lithology
F864	0	8.38	-6.08	T2	l
F864	2	7.73	-8.60	T2	l
F864	4	8.75	-3.45	T2	l
F864	6	8.18	-4.57	T2	l
F864	8	8.01	-7.06	T2	l
F864	10	8.13	-5.02	T2	l
F864	12	8.53	-7.20	T2	l
F864	14	8.36	-3.70	T2	l

F864	16	8.65	-3.23	T2	l
F864	18	8.04	-5.93	T2	l
F864	20	8.37	-4.02	T2	l
F864	22	7.23	-6.32	T2	l
F864	24	7.12	-3.70	T2	l
F864	26	7.67	-6.51	T2	l
F864	28	7.29	-4.51	T2	l
F864	30	8.96	-3.31	T2	l
F864	32	7.09	-8.08	T2	l
F864	34	7.97	-5.80	T2	l
F864	36	4.75	-17.08	T2	l
F864	38	7.60	-8.57	T2	l
F864	42	7.13	-8.28	T2	l
F864	44	8.54	-5.70	T2	l
F864	46	8.51	-8.53	T2	l
F864	48	8.67	-6.71	T2	l
F864	50	9.06	-5.76	T2	l
F864	52	8.17	-7.74	T2	l
F864	54	8.46	-6.05	T2	l
F864	56	8.69	-5.69	T2	l
F864	58	7.97	-7.27	T2	l
F864	60	8.02	-7.15	T2	l
F864	62	7.99	-7.06	T2	l
F864	64	8.14	-6.72	T2	l
F864	67	3.61	-17.11	T2	l
F864	69	6.40	-8.91	T2	l
F864	71	6.26	-9.76	T2	l
F864	73	7.09	-11.00	T2	l
F864	75	7.42	-8.48	T2	l
F864	77	8.82	-7.42	T2	l
F864	79	8.14	-7.22	T2	l

Taishir	**N46 40.488'**	**E95 34.163"**			
Section	**Height**	**δ^{13}Ccarb**	**δ^{18}Ocarb**	**Unit**	**Lithology**
F863	104	6.68	-8.47	T2	l
F863	108	6.75	-9.37	T2	l
F863	112	6.73	-9.91	T2	l
F863	117.5	7.18	-8.11	T2	l
F863	122	8.02	-5.98	T2	l
F863	126	6.77	-8.50	T2	l
F863	130	7.40	-7.52	T2	l
F863	134	7.82	-9.53	T2	l
F863	138	8.07	-7.05	T2	l
F863	142	5.74	-18.20	T2	l
F863	146	7.31	-8.08	T2	l
F863	150	8.44	-5.52	T2	l
F863	154	8.10	-5.94	T2	l
F863	158	8.09	-6.53	T2	l

F863	162	8.47	-9.88	T2	1
F863	166	8.54	-8.50	T2	1
F863	170	8.39	-7.39	T2	1
F863	174	7.42	-6.60	T2	1
F863	178	8.59	-5.89	T2	1
F863	182	9.23	-5.55	T2	1
F863	32	7.09	-8.08	T2	1
F863	34	7.97	-5.80	T2	1
F863	36	4.75	-17.08	T2	1
F863	38	7.60	-8.57	T2	1
F863	42	7.13	-8.28	T2	1
F863	44	8.54	-5.70	T2	1
F863	46	8.51	-8.53	T2	1
F863	48	8.67	-6.71	T2	1
F863	50	9.06	-5.76	T2	1
F863	52	8.17	-7.74	T2	1
F863	54	8.46	-6.05	T2	1
F863	56	8.69	-5.69	T2	1
F863	58	7.97	-7.27	T2	1
F863	60	8.02	-7.15	T2	1
F863	62	7.99	-7.06	T2	1
F863	64	8.14	-6.72	T2	1
F863	67	3.61	-17.11	T2	1
F863	69	6.40	-8.91	T2	1
F863	71	6.26	-9.76	T2	1
F863	73	7.09	-11.00	T2	1
F863	75	7.42	-8.48	T2	1
F863	77	8.82	-7.42	T2	1
F863	79	8.14	-7.22	T2	1
F863	79	7.74	-7.28	T2	1
F863	81	7.00	-8.21	T2	1
F863	83	7.04	-8.70	T2	1
F863	85	6.48	-11.42	T2	1
F863	87	6.36	-15.11	T2	1
F863	89	6.19	-12.94	T2	1
F863	95	5.60	-9.12	T2	1
F863	97	6.29	-9.18	T2	1
F863	99	4.58	-15.03	T2	1
F863	101	5.68	-8.23	T2	1
F863	103	6.25	-10.69	T2	1
F863	105	6.74	-15.10	T2	1
F863	107	4.33	-14.03	T2	1
F863	109	6.41	-9.26	T2	1
F863	111	5.23	-13.98	T2	1
F863	113	6.12	-8.38	T2	1
F863	115	3.09	-9.50	T2	1
F863	117	2.78	-9.11	T2	1
F863	119	2.09	-7.19	T2	1

F863	121	1.69	-7.98	T2	l
F863	123	1.32	-7.87	T2	l
F863	125	1.65	-9.33	T2	l
F863	127	1.35	-7.26	T2	l
F863	129	0.02	-8.76	T2	l
F863	131	-0.88	-24.67	T3	l
F863	132	-3.52	-13.92	T3	l
F863	136	-5.39	-10.45	T3	l
F863	137	-5.38	-11.20	T3	l
F863	138	-6.21	-9.24	T3	l
F863	139	-6.01	-9.66	T3	l
F863	140	-5.79	-8.20	T3	l
F863	141	-4.19	-15.35	T3	l
F863	142	-4.44	-12.55	T3	l
F863	143	-3.13	-15.66	T3	l
F863	144	-4.13	-12.98	T3	l
F863	145	-5.73	-8.63	T3	l
F863	146	-5.09	-11.87	T3	l
F863	149	-5.23	-11.12	T3	l
F863	150	-5.98	-8.20	T3	l
F863	151	-4.77	-12.73	T3	l
F863	152	-5.32	-8.29	T3	l
F863	153	-5.05	-18.97	T3	l
F863	154	-4.55	-6.92	T3	l
F863	155	-4.01	-7.88	T3	l
F863	156	-3.71	-8.90	T3	l
F863	157	-3.25	-11.07	T3	l
F863	158	-2.89	-9.44	T3	l
F863	159	-3.22	-7.83	T3	l
F863	160	-2.29	-10.37	T3	l
F863	161	-2.51	-9.43	T3	l
F863	162	-1.80	-13.12	T3	l
F863	163	-1.10	-15.92	T3	l
F863	164	-1.29	-14.89	T3	l
F863	167	-1.78	-13.45	T3	l
F863	168	-1.82	-15.23	T3	l
F863	169	-2.29	-10.53	T3	l
F863	170	-0.47	-18.11	T3	l
F863	171	5.75	-11.06	T3	l

Taishir	**N46 39.754'**	**E96 34.333'**			
Section	**height**	**δ^{13}Ccarb**	**δ^{18}Ocarb**	**Unit**	**Lithology**
F865	0.0	-5.96	-7.07	T3	l
F865	1.0	-6.83	-8.84	T3	l
F865	2.0	-6.24	-10.76	T3	l
F865	3.0	-6.43	-7.40	T3	l
F865	4.0	-5.77	-10.03	T3	l
F865	5.0	-6.07	-7.15	T3	l

F865	6.0	-5.63	-7.47	T3	l
F865	7.0	-5.76	-6.48	T3	l
F865	8.0	-6.40	-7.23	T3	l
F865	9.0	-6.17	-8.27	T3	l
F865	10.0	-6.60	-7.03	T3	l
F865	11.0	-6.49	-7.65	T3	l
F865	12.0	-5.94	-7.06	T3	l
F865	15.0	-4.13	-6.56	T3	l
F865	16.0	-4.23	-6.79	T3	l
F865	20.0	-5.18	-6.94	T3	l
F865	21.0	-4.57	-6.89	T3	l
F865	22.0	-4.45	-7.47	T3	l
F865	23.0	-4.15	-6.30	T3	l
F865	24.0	-3.64	-7.47	T3	l
F865	25.0	-3.49	-7.42	T3	l
F865	26.0	-3.08	-7.55	T3	l
F865	27.0	-3.16	-6.99	T3	l
F865	28.0	-2.64	-6.41	T3	l
F865	29.0	-2.83	-11.16	T3	l
F865	30.0	-3.01	-11.00	T3	l
F865	31.0	-1.03	-13.69	T3	l
F865	32.0	-2.60	-10.69	T3	l
F865	33.0	-1.77	-10.28	T3	l
F865	34.0	-1.98	-14.26	T3	l

S. Khukh Davaa **N47 01.773'** **E95 26.198'**

Section	height	δ^{13}Ccarb	δ^{18}Ocarb	Unit	Lithology
F875	0.1	6.50	-6.13	T3	d
F875	1.0	6.10	-2.63	T3	d
F875	2.0	5.10	-2.51	T3	d
F875	3.0	4.94	-6.54	T3	d
F875	4.0	5.72	-3.02	T3	d
F875	5.0	5.29	-4.01	T3	d

Uliastai Gorge **N47 49.492'** **E95 49.327'**

Section	height	δ^{13}Ccarb	δ^{18}Ocarb	Unit	Lithology
F949	0.1	-2.10	-14.78	T1	l
F949	0.6	-1.94	-12.40	T1	l
F949	1.0	-2.39	-10.62	T1	l
F949	2.0	-1.45	-10.09	T1	l
F949	3.0	-0.63	-11.21	T1	l
F949	4.0	-0.38	-11.06	T1	l
F949	5.0	-0.20	-8.73	T1	l
F949	6.0	0.49	-12.32	T1	l
F949	7.0	0.52	-12.15	T1	l
F949	8.0	0.23	-12.15	T1	l
F949	9.0	-0.87	-13.57	T1	l
F949	13.0	2.00	-4.70	T1	l

F949	15.0	2.07	-10.95	T1	1
F949	16.0	2.52	-13.08	T1	1
F949	18.0	2.73	-12.08	T1	1
F949	19.0	2.52	-11.92	T1	1
F949	21.0	2.70	-9.46	T1	1
F949	22.0	1.86	-10.65	T1	1
F949	23.0	3.27	-10.27	T1	1
F949	24.0	2.71	-10.17	T1	1
F949	27.0	1.67	-10.64	T1	1
F949	29.0	3.76	-12.21	T1	1
F949	31.0	2.10	-8.32	T1	1
F949	33.0	2.96	-9.05	T1	1
F949	36.0	3.14	-10.40	T1	1
F949	37.0	3.23	-10.40	T1	1
F949	39.0	2.04	-11.65	T1	1
F949	44.0	2.52	-12.49	T1	1
F949	45.0	1.26	-10.79	T1	1
F949	47.0	1.94	-13.05	T1	1
F949	48.0	2.43	-11.58	T1	1
F949	49.0	4.04	-7.13	T1	1
F949	50.0	4.87	-4.07	T1	1
F949	51.0	2.62	-9.82	T1	1
F949	52.0	2.20	-12.30	T1	1
F949	53.0	3.19	-10.34	T1	1
F949	54.0	4.57	-10.43	T1	1
F949	55.0	4.72	-11.75	T1	1
F949	56.0	4.01	-7.04	T1	1
F949	57.0	4.92	-13.01	T1	1
F949	58.0	7.05	-3.21	T2	1
F949	60.0	7.73	-10.34	T2	1
F949	61.0	7.82	-10.62	T2	1
F949	62.0	8.01	-8.23	T2	1
F949	63.0	8.36	-6.34	T2	1
F949	64.0	5.83	-6.04	T2	1
F949	65.0	5.39	-6.73	T2	1
F949	66.0	6.75	-8.76	T2	1
F949	67.0	8.03	-9.91	T2	1
F949	72.0	5.95	-9.61	T2	1
F949	73.0	6.78	-10.00	T2	1
F949	74.0	6.81	-10.16	T2	1
F949	75.0	8.04	-10.62	T2	1
F949	76.0	4.28	-9.15	T2	1
F949	78.0	8.33	-4.66	T2	1
F949	80.0	7.60	-13.05	T2	1
F949	82.0	7.98	-6.01	T2	1
F949	84.0	7.12	-7.29	T2	1
F949	86.0	6.87	-9.55	T2	1
F949	88.0	7.33	-6.15	T2	1

F949	90.0	7.19	-8.75	T2	1
F949	92.0	8.62	-2.51	T2	1
F949	94.0	6.18	-9.49	T2	1
F949	96.0	7.80	-6.98	T2	1
F949	98.0	7.64	-9.62	T2	1
F949	100.0	7.50	-14.46	T2	1
F949	102.0	7.15	-10.81	T2	1
F949	104.0	7.63	-9.79	T2	1
F949	106.0	6.88	-9.94	T2	1
F949	108.0	7.10	-6.66	T2	1
F949	110.0	8.35	-5.85	T2	1
F949	112.0	7.44	-4.49	T2	1
F949	114.0	6.73	-7.95	T2	1
F949	116.0	6.87	-6.38	T2	1
F949	117.0	6.19	-9.76	T2	1
F949	118.0	5.70	-9.84	T2	1
F949	120.0	7.66	-8.40	T2	1
F949	122.0	6.67	-18.39	T2	1
F949	124.0	5.53	-10.69	T2	1
F949	126.0	6.32	-11.23	T2	1
F949	128.0	6.22	-8.24	T2	1
F949	130.0	6.44	-8.10	T2	1
F949	132.0	5.12	-9.22	T2	1
F949	134.0	5.37	-7.14	T2	1
F949	136.0	4.89	-9.27	T2	1
F949	138.0	5.12	-7.54	T2	1
F949	140.0	5.15	-8.40	T2	1
F949	142.0	6.32	-9.87	T2	1
F949	144.0	4.26	-8.41	T2	1
F949	145.0	2.69	-8.20	T2	1
F949	146.0	2.19	-9.14	T2	1
F949	147.0	-2.98	-9.16	T3	1
F949	148.0	-4.26	-10.62	T3	1
F949	149.0	-3.52	-10.84	T3	1
F949	150.0	-4.30	-7.96	T3	1
F949	151.0	-3.40	-8.37	T3	1
F949	152.0	-3.67	-9.71	T3	1
F949	153.0	-3.45	-9.36	T3	1
F949	154.0	-3.29	-11.20	T3	1
F949	155.0	-3.73	-8.53	T3	1
F949	156.0	-4.39	-9.01	T3	1
F949	157.0	-4.07	-9.43	T3	1
F949	158.0	-4.25	-7.82	T3	1
F949	159.0	-1.80	-16.75	T3	1
F949	160.0	-2.48	-10.02	T3	1
F949	161.0	-2.98	-15.25	T3	1
F949	162.0	-2.05	-13.90	T3	1
F949	163.0	-2.32	-19.51	T3	1

F949	164.0	-1.74	-11.25	T3	1
F949	165.0	-1.59	-10.99	T3	1
F949	166.0	-0.21	-10.91	T3	1
F949	167.0	1.89	-9.10	T4	1
F949	168.0	2.89	-8.42	T4	1
F949	170.0	2.97	-12.71	T4	1
F949	172.0	4.22	-11.63	T4	1
F949	174.0	3.77	-12.57	T4	1
F949	176.0	7.33	-10.07	T4	1
F949	178.0	4.89	-11.00	T4	1
F949	180.0	8.27	-9.35	T4	1
F949	182.0	8.64	-7.05	T4	1
F949	184.0	8.33	-7.43	T4	1
F949	186.0	8.50	-8.60	T4	1
F949	188.0	8.82	-8.88	T4	1
F949	190.0	8.94	-10.84	T4	1
F949	191.0	9.02	-11.32	T4	1
F949	193.0	8.25	-6.64	T4	1
F949	195.0	6.55	-15.46	T4	1
F949	197.0	8.70	-8.30	T4	1
F949	200.0	7.40	-12.42	T4	1
F949	202.0	8.58	-13.00	T4	1
F949	204.0	6.65	-16.89	T4	1
F949	206.0	8.16	-11.94	T4	1
F949	208.0	8.22	-9.59	T4	1
F949	210.0	9.09	-11.90	T4	1
F949	212.0	3.88	-30.26	T4	1
F949	214.0	8.53	-10.18	T4	1
F949	216.0	9.61	-8.73	T4	1
F949	218.0	9.45	-7.03	T4	1
F949	220.0	8.32	-9.19	T4	1
F949	222.0	9.75	-6.26	T4	1
F949	224.0	9.68	-5.57	T4	1
F949	226.0	9.64	-6.91	T4	1
F949	228.0	10.09	-6.15	T4	1
F949	230.0	9.27	-5.90	T4	1
F949	232.0	9.19	-9.78	T4	1
F949	235.0	9.74	-5.31	T4	1
F949	237.0	9.71	-5.01	T4	1
F949	239.0	10.22	-2.25	T4	1
F949	241.0	10.14	-2.73	T4	1
F949	243.0	9.89	-4.04	T4	1
F949	245.0	10.02	-3.23	T4	1
F949	247.0	9.68	-6.25	T4	1
F949	249.0	9.63	-4.84	T4	1
F949	252.0	10.05	-4.03	T4	1
F949	254.0	10.17	-3.17	T4	1
F949	256.0	9.86	-8.72	T4	1

F949	258.0	9.87	-4.66	T4	1
F949	260.0	10.18	-1.55	T4	1
F949	264.0	9.33	-6.69	T4	1
F949	266.0	10.48	-2.39	T4	1
F949	268.0	10.38	-1.70	T4	1
F949	270.0	10.21	-3.88	T4	1
F949	272.0	9.07	-6.87	T4	1
F949	274.0	10.37	-1.42	T4	1
F949	276.0	10.31	-2.99	T4	1
F949	278.0	10.43	-1.72	T4	1
F949	280.0	9.62	-9.36	T4	1
F949	282.0	10.56	-2.25	T4	1
F949	284.0	10.62	-1.58	T4	1
F949	286.0	9.83	-4.22	T4	1
F949	288.0	10.23	-3.26	T4	1
F949	290.0	9.75	-6.47	T4	1
F949	292.0	10.77	-0.91	T4	1
F949	294.0	10.38	-3.36	T4	1
F949	296.0	10.25	-1.52	T4	1
F949	298.0	10.23	-2.10	T4	1
F949	300.0	10.61	-5.10	T4	1
F949	302.0	10.45	-3.34	T4	1
F949	304.0	10.18	-4.79	T4	1
F949	308.0	10.88	-0.94	T4	1
F949	310.0	10.80	-2.39	T4	1
F949	312.0	10.69	-1.29	T4	1
F949	315.0	10.00	-5.02	T4	1
F949	317.0	10.67	-2.49	T4	1
F949	319.0	10.73	-2.69	T4	1
F949	321.0	10.99	-2.38	T4	1
F949	324.0	10.89	-3.18	T4	1
F949	327.0	10.95	-2.01	T4	1
F949	328.0	10.69	-3.62	T4	1
F949	330.0	10.66	-3.78	T4	1
F949	332.0	10.40	-2.26	T4	1
F949	334.0	10.56	-4.26	T4	1
F949	336.0	10.77	-3.27	T4	1
F949	338.0	10.62	-3.32	T4	1
F949	340.0	10.59	-4.01	T4	1
F949	342.0	10.73	-3.24	T4	1
F949	344.0	10.80	-3.16	T4	1
F949	346.0	10.67	-3.24	T4	1
F949	348.0	11.08	-3.46	T4	1
F949	350.0	10.55	-3.22	T4	1
F949	352.0	10.86	-3.19	T4	1
F949	354.0	10.68	-4.10	T4	1
F949	356.0	10.38	-4.38	T4	1
F949	358.0	10.43	-4.98	T4	1

F949	360.0	10.82	-4.95	T4	l
F949	362.0	10.65	-5.68	T4	l
F949	364.0	10.64	-5.12	T4	l
F949	368.0	10.86	-5.62	T4	l
F949	370.0	11.70	-3.15	T4	l
F949	372.0	11.81	-2.96	T4	l
F949	376.0	11.26	-4.15	T4	l
F949	378.0	11.76	-3.86	T4	l
F949	380.0	12.13	-4.58	T4	l
F949	382.0	11.11	-5.47	T4	l
F949	384.0	11.95	-4.17	T4	l
F949	386.0	11.96	-4.56	T4	l
F949	387.0	11.05	-5.47	T4	l
F949	388.0	9.66	-7.85	T4	l
F949	389.0	9.20	-9.67	T4	l

Taishir	**N46 39.713'**	**E96 34.251'**			
Section	**height**	**δ^{13}Ccarb**	**δ^{18}Ocarb**	**Unit**	**Lithology**
U1108	0.2	-5.60	-6.96	T3	l
U1108	0.6	-6.25	-8.16	T3	l
U1108	1	-6.57	-6.89	T3	l
U1108	1.5	-6.36	-7.74	T3	l
U1108	2	-6.91	-7.11	T3	l
U1108	2.5	-6.36	-7.22	T3	l
U1108	3	-6.28	-6.79	T3	l
U1108	3.5	-6.15	-7.13	T3	l
U1108	4	-6.13	-6.79	T3	l
U1108	4.5	-5.91	-6.65	T3	l
U1108	5	-5.82	-6.66	T3	l
U1108	5.5	-5.85	-6.56	T3	l
U1108	6	-5.96	-6.84	T3	l
U1108	6.7	-6.06	-6.72	T3	l
U1108	7	-6.08	-7.31	T3	l
U1108	7.5	-6.03	-7.10	T3	l
U1108	8	-5.99	-8.30	T3	l
U1108	8.5	-6.80	-7.15	T3	l
U1108	9.5	-6.41	-7.29	T3	l
U1108	10	-6.16	-7.49	T3	l
U1108	11	-5.87	-6.94	T3	l
U1108	11.5	-5.60	-6.52	T3	l
U1108	12	-5.71	-7.13	T3	l
U1108	12.5	-5.80	-7.76	T3	l
U1108	13	-5.64	-7.24	T3	l
U1108	13.5	-5.31	-7.41	T3	l
U1108	14	-4.65	-6.14	T3	l
U1108	14.5	-4.64	-7.05	T3	l
U1108	15	-4.23	-7.76	T3	l
U1108	15.5	-4.31	-7.47	T3	l

U1108	16	-4.24	-7.03	T3	1
U1108	16.5	-4.26	-6.32	T3	1
U1108	17	-3.99	-6.65	T3	1
U1108	17.5	-3.43	-9.75	T3	1
U1108	18	-3.77	-7.53	T3	1
U1108	18.5	-3.50	-9.59	T3	1
U1108	19	-3.33	-6.67	T3	1
U1108	19.5	-3.28	-7.49	T3	1
U1108	20	-3.30	-7.01	T3	1
U1108	20.5	-2.77	-9.13	T3	1
U1108	21	-2.76	-7.63	T3	1
U1108	21.5	-2.86	-7.19	T3	1
U1108	22	-2.62	-7.70	T3	1
U1108	22.5	-2.35	-7.18	T3	1
U1108	23	-2.85	-5.29	T3	1
U1108	23.5	-2.31	-5.60	T3	1
U1108	24	-1.70	-8.51	T3	1
U1108	25	-1.83	-8.97	T3	1
U1108	25.5	-1.40	-9.50	T3	1
U1108	26	-1.89	-8.29	T3	1
U1108	26.5	-1.34	-6.95	T3	1
U1108	27	-2.03	-8.65	T3	1
U1108	27.5	-1.82	-7.78	T3	1
U1108	39	4.04	-7.58	T3	1
U1108	39.5	3.00	-6.89	T3	1
U1108	40	5.96	-7.97	T3	1
U1108	40.5	6.38	-7.73	T3	1
U1108	41	7.63	-9.44	T3	1
U1108	41.5	7.72	-6.88	T3	1
U1108	42	7.08	-7.58	T3	1
U1108	42.5	6.31	-7.03	T3	1
U1108	43	7.38	-4.73	T3	1
U1108	43.5	6.55	-6.87	T3	1
U1108	44	7.75	-5.27	T3	1
U1108	44.5	8.35	-6.13	T3	1
U1108	45	7.43	-8.61	T3	1
U1108	45.5	8.74	-5.13	T3	1
U1108	46	8.26	-5.26	T3	1
U1108	47	7.33	-6.97	T3	1
U1108	48	8.88	-2.44	T3	1
U1108	49	8.70	-5.31	T3	1
U1108	50	8.51	-4.84	T3	1
U1108	52	8.57	-4.22	T3	1
U1108	53	8.56	-3.73	T3	1
U1108	55	9.13	-6.83	T3	1
U1108	55.7	8.14	-4.84	T3	1
U1108	57	8.17	-4.38	T3	1
U1108	57.1	9.03	-2.27	T3	1

U1108	58	9.12	-1.79	T3	1
U1108	59	8.39	-8.10	T3	1
U1108	60	8.70	-3.38	T3	1
U1108	61	8.98	-5.21	T3	1
U1108	62	8.72	-8.04	T3	1
U1108	63	8.69	-5.94	T3	1
U1108	64	9.02	-3.45	T3	1
U1108	65	9.36	-3.90	T3	1
U1108	66	8.99	-4.30	T3	1
U1108	67	8.96	-6.90	T3	1
U1108	68	9.39	-3.68	T3	1
U1108	69	9.55	-2.80	T3	1
U1108	70	8.45	-4.54	T3	1
U1108	71	8.43	-4.81	T3	1
U1108	72	8.55	-5.05	T3	1
U1108	73	8.34	-4.93	T3	1
U1108	74	8.42	-4.79	T3	1
U1108	75	6.33	-7.11	T3	1
U1108	76	9.25	-4.40	T3	1
U1108	77	8.84	-4.74	T3	1
U1108	78	9.35	-3.91	T3	1
U1108	79	9.18	-2.67	T3	1
U1108	80	7.53	-5.31	T3	1
U1108	81	9.68	-1.77	T3	1
U1108	82	1.98	-4.90	T3	1
U1108	83	5.93	-5.40	T3	1
U1108	84	8.83	-5.50	T3	1
U1108	85	8.84	-6.12	T3	1
U1108	86	9.04	-4.34	T3	1
U1108	87	9.18	-5.96	T3	1
U1108	88	8.27	-5.14	T3	1
U1108	89	9.13	-2.44	T3	1
U1108	90	3.62	-4.57	T3	1
U1108	91	5.28	-5.67	T3	1
U1108	92	9.48	-2.07	T3	1
U1108	93	9.39	-2.44	T3	1
U1108	94	9.19	-4.68	T3	1
U1108	95	9.15	-4.72	T3	1
U1108	96	9.36	-5.58	T3	1
U1108	97.1	8.96	-3.15	T3	1
U1108	98	8.06	-4.19	T3	1
U1108	99	5.10	-2.53	T3	1
U1108	100	8.43	-3.52	T3	1
U1108	101	9.27	-4.34	T3	1
U1108	102	9.27	-1.78	T3	1
U1108	103	9.14	-2.13	T3	1
U1108	104	9.50	-1.05	T3	1
U1108	105.1	9.16	-2.49	T3	1

U1108	106	8.84	-1.99	T3	1
U1108	107	7.95	-5.68	T3	1
U1108	108	7.76	-5.72	T3	1
U1108	109	9.13	-1.54	T3	1
U1108	110	8.49	-4.60	T3	1
U1108	111	7.66	-5.13	T3	1
U1108	112	7.67	-5.19	T3	1
U1108	113	9.49	-1.04	T3	1
U1108	114	7.59	-4.62	T3	1
U1108	115	8.20	-3.65	T3	1
U1108	116	5.01	-6.34	T3	1
U1108	117	4.86	-6.47	T3	1
U1108	118	7.14	-5.01	T3	1
U1108	119	8.46	-3.78	T3	1
U1108	120	6.30	-6.28	T3	1
U1108	121	8.13	-5.30	T3	1
U1108	122	8.06	-4.72	T3	1
U1108	123	6.41	-6.96	T3	1
U1108	124	8.67	-3.50	T3	1
U1108	125	8.17	-3.12	T3	1
U1108	126	8.20	-5.01	T3	1
U1108	127	8.27	-3.20	T3	1
U1108	128	8.75	-3.68	T3	1
U1108	129	8.51	-3.42	T3	1
U1108	130	8.51	-2.98	T3	1
U1108	131	9.11	-1.93	T3	1
U1108	132	8.75	-3.62	T3	1
U1108	133	8.60	-2.99	T3	1
U1108	134	7.84	-4.86	T3	1
U1108	135	7.40	-5.29	T3	1
U1108	136	8.53	-3.50	T3	1
U1108	137	9.01	-2.49	T3	1
U1108	138	10.03	-1.78	T3	1
U1108	139	8.24	-4.33	T3	1
U1108	140	8.89	-3.28	T3	1
U1108	141	10.29	-2.43	T3	1
U1108	142	8.64	-3.14	T3	1
U1108	143	9.08	-2.65	T3	1
U1108	144	8.95	-3.56	T3	1
U1108	145	7.66	-4.98	T3	1
U1108	146	8.81	-4.29	T3	1
U1108	147	7.29	-4.81	T3	1
U1108	148	8.81	-3.64	T3	1
U1108	149	8.88	-2.68	T3	1
U1108	150	9.20	-2.87	T3	1
U1108	151	8.16	-4.20	T3	1
U1108	152	8.37	-4.37	T3	1
U1108	153	8.70	-4.39	T3	1

U1108	154	9.27	-4.03	T3	l
U1108	155	8.54	-3.45	T3	l
U1108	156	9.00	-4.34	T3	l
U1108	157	8.45	-4.47	T3	l
U1108	158	8.19	-5.58	T3	l
U1108	159	8.64	-4.49	T3	l
U1108	160	8.60	-3.24	T3	l
U1108	161	8.66	-7.07	T3	l
U1108	162	8.01	-6.40	T3	l
U1108	163	8.86	-10.19	T3	l
U1108	164.1	9.80	-7.56	T3	l
U1108	165	9.42	-8.17	T3	l
U1108	166	9.45	-8.18	T3	l
U1108	167	8.44	-10.05	T3	l
U1108	167.9	8.61	-12.47	T3	l
U1108	169	8.42	-12.52	T3	l
U1108	170	9.09	-4.95	T3	l
U1108	171	9.92	-7.05	T3	l
U1108	172	9.82	-10.97	T3	l
U1108	173	8.01	-9.61	T3	l
U1108	174	9.63	-5.53	T3	l
U1108	175	8.14	-5.93	T3	l
U1108	176	6.90	-6.69	T3	l
U1108	177	8.73	-5.43	T3	l

Northern Bayan Gorge **N46 50' 13.8"** **E96 20' 21.7"**

Section	**height**	**δ^{13}Ccarb**	**δ^{18}Ocarb**	**Unit**	**Lithology**
U1241	1	1.78	0.64	T1	l
U1241	2	-0.93	-14.73	T1	l
U1241	3	-0.65	-9.11	T1	l
U1241	8	-0.55	-16.29	T1	l
U1241	9	4.51	-4.60	T1	l
U1241	10	4.28	-4.40	T1	l
U1241	11	3.76	-6.07	T1	l
U1241	12	5.71	-5.50	T1	l
U1241	14	5.97	-3.75	T1	l
U1241	15	6.67	-7.05	T1	l
U1241	20	3.58	-20.84	T1	l
U1241	21	3.18	-18.00	T2	l
U1241	31	3.66	-17.88	T2	l
U1241	32	3.68	-11.85	T2	l
U1241	33	6.11	-8.95	T2	l
U1241	34	5.00	-9.71	T2	l
U1241	35	5.42	-8.42	T2	l
U1241	36	5.40	-8.64	T2	l
U1241	37	4.93	-7.37	T2	l
U1241	38	4.40	-10.38	T2	l
U1241	39	4.04	-11.32	T2	l

U1241	40	5.31	-7.46	T2	l
U1241	41	5.67	-3.53	T2	l
U1241	42	4.42	-9.15	T2	l
U1241	42	4.38	-9.20	T2	l
U1241	43	5.97	-7.93	T2	l
U1241	44	3.86	-12.11	T2	l
U1241	45	4.89	-10.24	T2	l
U1241	46	3.77	-15.56	T2	l
U1241	47	3.50	-11.87	T2	l
U1241	48	0.21	-4.80	T3	l
U1241	49	-1.14	-3.80	T3	l
U1241	50	-0.81	-7.69	T3	l
U1241	51	2.07	-3.18	T3	l
U1241	52	3.31	-7.70	T3	l
U1241	53	2.18	-6.22	T3	l
U1241	54	2.55	-8.87	T3	l
U1241	55	3.13	-7.74	T3	l
U1241	56	4.59	-2.99	T3	d
U1241	57	5.43	-3.50	T3	d
U1241	58	4.92	-3.07	T3	d
U1241	59	4.41	-6.02	T3	d
U1241	60	4.50	-4.64	T3	d
U1241	61	3.99	-4.14	T3	d
U1241	62	5.31	-3.50	T3	d
U1241	63	4.45	-3.71	T3	d
U1241	64	3.35	-7.40	T3	d
U1241	65	3.53	-3.70	T3	d
U1241	66	3.62	-4.37	T3	d
U1241	67	4.10	-3.42	T3	d
U1241	68	3.43	-3.33	T3	d
U1241	69	3.54	-7.68	T3	d
U1241	70	3.66	-7.25	T3	d
U1241	71	4.32	-7.07	T3	d
U1241	72	5.16	-5.27	T3	d
U1241	73	7.13	-12.79	T3	d
U1241	74	5.42	-11.19	T3	l
U1241	75	5.76	-11.01	T3	l
U1241	76	5.69	-9.97	T3	l
U1241	77	5.33	-7.83	T3	l
U1241	78	5.21	-9.50	T3	d
U1241	79	5.79	-8.29	T3	d
U1241	80	7.50	-10.32	T3	l
U1241	81	8.51	-6.67	T3	l
U1241	82	5.91	-4.50	T3	l
U1241	83	6.38	-8.26	T3	d
U1241	84	5.54	-6.16	T3	d
U1241	85	6.12	-7.38	T3	d
U1241	86	7.00	-7.21	T3	d

U1241	87	5.37	-5.48	T3	d
U1241	88	5.51	-5.92	T3	d
U1241	89	5.96	-7.81	T3	l
U1241	90	5.09	-8.93	T3	l
U1241	91	6.87	-12.51	T3	l
U1241	92	4.57	-8.42	T3	l
U1241	93	9.62	-7.91	T3	l
U1241	94	5.55	-9.08	T3	l
U1241	95	6.10	-8.41	T3	l
U1241	96	4.94	-9.51	T3	l
U1241	97	5.18	-9.87	T3	d
U1241	98	6.16	-7.24	T3	d
U1241	99	5.03	-9.24	T3	d
U1241	100	5.20	-9.99	T3	d
U1241	101	5.53	-9.30	T3	d
U1241	102	4.19	-6.95	T3	d
U1241	103	7.83	-7.76	T3	d
U1241	104	5.46	-15.53	T3	d
U1241	105	7.10	-11.69	T3	d
U1241	106	7.42	-11.43	T3	d
U1241	107	9.03	-9.00	T3	l
U1241	108	9.49	-6.37	T3	l
U1241	109	9.04	-7.63	T3	l
U1241	110	9.45	-3.56	T3	l
U1241	111	10.28	-2.77	T3	l
U1241	112	8.30	-7.82	T3	l
U1241	113	10.01	-4.99	T3	l
U1241	114	10.03	-4.99	T3	l
U1241	115	8.91	-6.99	T3	l
U1241	116	6.46	-8.92	T3	l
U1241	117	10.94	-2.34	T3	l
U1241	118	10.27	-3.19	T3	l
U1241	119	10.59	-4.55	T3	l
U1241	120	10.46	-4.71	T3	l
U1241	121	8.52	-6.12	T3	l
U1241	122	6.82	-6.48	T3	l
U1241	123	10.85	-3.31	T3	l
U1241	124	9.65	-6.39	T3	l
U1241	125	10.22	-6.06	T3	l
U1241	126	9.11	-6.93	T3	l
U1241	127	9.94	-6.75	T3	l
U1241	128	9.32	-6.90	T3	l
U1241	129	8.24	-4.43	T3	d
U1241	130	8.09	-3.70	T3	d
U1241	131	9.34	-3.38	T3	d
U1241	132	8.86	-6.49	T3	l
U1241	133	9.81	-3.81	T3	l
U1241	134	7.48	-6.51	T3	l

U1241	135	6.07	-9.38	T3	d
U1241	136	7.12	-5.65	T3	d
U1241	137	6.62	-5.89	T3	d
U1241	138	5.72	-6.84	T3	d
U1241	139	6.77	-6.97	T3	d
U1241	140	6.70	-8.78	T3	d
U1241	141	6.49	-7.36	T3	d
U1241	142	5.53	-10.01	T3	d
U1241	143	3.57	-11.78	T3	d
U1241	144	4.42	-8.31	T3	d
U1241	145	4.73	-9.64	T3	d
U1241	146	6.80	-4.20	T3	d
U1241	147	7.80	-3.98	T3	d
U1241	148	6.54	-6.33	T3	d
U1241	149	5.91	-2.95	T3	d
U1241	150	5.52	-2.17	T3	d
U1241	151	4.81	-2.93	T3	d
U1241	152	6.08	-3.63	T3	d
U1241	153	5.33	-2.75	T3	d
U1241	154	5.33	-4.32	T3	d
U1241	155	6.14	-3.14	T3	d
U1241	156	5.85	-2.99	T3	d
U1241	157	6.22	-3.72	T3	d
U1241	158	5.64	-2.35	T3	d
U1241	159	6.38	-3.16	T3	d
U1241	160	6.47	-2.42	T3	d
U1241	161	6.76	-2.38	T3	d
U1241	162	6.60	-2.09	T3	d
U1241	163	6.44	-3.10	T3	d
U1241	164	6.37	-2.15	T3	d
U1241	165	6.70	-2.57	T3	d
U1241	166	5.77	-4.18	T3	d
U1241	167	5.35	-3.61	T3	d
U1241	168	6.51	-4.32	T3	d
U1241	169	5.66	-2.72	T3	d
U1241	170	5.23	-4.27	T3	d
U1241	171	6.19	-2.63	T3	d
U1241	172	5.83	-3.10	T3	d
U1241	173	6.29	-6.40	T3	d
U1241	174	6.06	-3.36	T3	d
U1241	175	6.14	-2.25	T3	d
U1241	176	6.27	-4.58	T3	d
U1241	177	5.91	-2.49	T3	d
U1241	178	5.87	-2.29	T3	d
U1241	179	5.87	-2.09	T3	d
U1241	179	5.85	-2.16	T3	d
U1241	180	5.66	-1.93	T3	d
U1241	181	4.40	-2.83	T3	d

U1241	182	4.87	-1.74	T3	d
U1241	183	5.22	-1.85	T3	d
U1241	184	4.85	-2.31	T3	d
U1241	185	5.73	-1.22	T3	d
U1241	186	4.21	-2.49	T3	d
U1241	187	5.20	-3.02	T3	d
U1241	188	4.69	-2.67	T3	d
U1241	189	4.54	-4.32	T3	d
U1241	190	5.05	-2.93	T3	d
U1241	191	5.16	-2.89	T3	d
U1241	192	4.90	-2.01	T3	d
U1241	193	4.68	-2.98	T3	d
U1241	194	5.45	-2.02	T3	d
U1241	195	5.26	-1.84	T3	d
U1241	196	5.41	-2.34	T3	d
U1241	197	4.37	-3.33	T3	d
U1241	198	5.06	-2.01	T3	d
U1241	199	5.10	-2.31	T3	d
U1241	200	4.55	-1.90	T3	d
U1241	201	2.58	-4.77	T3	d
U1241	202	5.14	-7.64	T3	d
U1241	202	5.10	-7.67	T3	d
U1241	203	4.76	-8.04	T3	d
U1241	204	4.42	-9.08	T3	d
U1241	205	5.14	-8.52	T3	d
U1241	206	3.85	-6.69	T3	d
U1241	207	5.02	-7.65	T3	d
U1241	208	5.75	-3.93	T3	d
U1241	209	5.32	-2.97	T3	d
U1241	210	4.69	-4.15	T3	d
U1241	211	4.97	-3.96	T3	d
U1241	212	5.77	-7.04	T3	d
U1241	213	5.64	-6.75	T3	d
U1241	214	4.65	-7.24	T3	d
U1241	215	4.78	-10.18	T3	d
U1241	216	4.68	-7.67	T3	d
U1241	217	4.79	-5.79	T3	d
U1241	218	4.87	-2.51	T3	d
U1241	219	4.30	-5.69	T3	d
U1241	220	3.76	-8.85	T3	d
U1241	221	3.81	-7.31	T3	d
U1241	222	3.18	-6.91	T3	d
U1241	223	3.75	-6.66	T3	d
U1241	224	4.19	-6.82	T3	d
U1241	225	3.89	-8.55	T3	d
U1241	226	5.66	-2.74	T3	d
U1241	227	4.01	-8.36	T3	d
U1241	228	4.31	-5.80	T3	d

U1241	229	3.69	-7.28	T3	d
U1241	230	1.38	-6.73	T3	d
U1241	231	1.30	-11.36	T3	d
U1241	232	2.61	-7.54	T3	d
U1241	233	3.67	-5.23	T3	d
U1241	234	2.19	-4.59	T3	d
U1241	235	2.26	-5.55	T3	d
U1241	236	4.58	-2.10	T3	d
U1241	237	3.90	-4.75	T3	d
U1241	238	5.60	-2.95	T3	d
U1241	239	5.24	-6.19	T3	d
U1241	240	4.66	-5.26	T3	d
U1241	241	3.16	-5.41	T3	d

Salaa Gorge **N 46 48.297'** **E 95 45.48'**

Section	**Height**	**δ^{13}Ccarb**	**δ^{18}Ocarb**	**Unit**	**Lithology**
F1132	0.1	-3.55	-17.78	T1	l
F1132	0.5	-2.49	-12.30	T1	l
F1132	1	-1.74	-16.27	T1	l
F1132	1.6	-1.63	-16.49	T1	l
F1132	2	-1.62	-16.56	T1	l
F1132	2.5	-1.12	-16.14	T1	l
F1132	3	-0.82	-13.81	T1	l
F1132	3.5	-0.54	-10.38	T1	l
F1132	4	-0.80	-15.26	T1	l
F1132	4.5	0.01	-15.08	T1	l
F1132	5	-0.19	-10.14	T1	l
F1132	5.5	0.08	-14.62	T1	l
F1132	6	-0.84	-16.81	T1	l
F1132	6.5	-1.33	-18.03	T1	l
F1132	7	-1.59	-13.71	T1	l
F1132	9	-1.59	-7.24	T1	l
F1132	10	1.11	-3.09	T1	l
F1132	11	3.52	-1.76	T1	l
F1132	12	3.56	-0.83	T1	l
F1132	15	3.72	-3.61	T1	l
F1132	17	3.56	-15.55	T1	l
F1132	19	2.38	-9.80	T1	l
F1132	32	3.47	-10.69	T2	l
F1132	34	5.77	-11.39	T2	l
F1132	36	6.01	-12.33	T2	l
F1132	38	6.64	-11.17	T2	l
F1132	40	7.14	-10.95	T2	l
F1132	42	8.24	-2.41	T2	l
F1132	46	7.42	-10.18	T2	l
F1132	48	7.44	-7.90	T2	l
F1132	50	6.72	-6.22	T2	l
F1132	52	7.48	-8.28	T2	l

F1132	54	7.67	-7.50	T2	1
F1132	55	8.56	-12.57	T2	1
F1132	56	6.37	-13.97	T2	1
F1132	57	6.91	-13.42	T2	1
F1132	58	6.64	-12.47	T2	1
F1132	59	5.24	-13.55	T2	1
F1132	60	8.20	-7.89	T2	1
F1132	62	8.59	-6.65	T2	1
F1132	64	8.17	-9.65	T2	1
F1132	68	6.96	-6.72	T2	1
F1132	72	8.28	-14.85	T2	1
F1132	76	7.76	-14.51	T2	1
F1132	80	7.55	-10.53	T2	1
F1132	84	8.31	-12.62	T2	1
F1132	88	8.29	-14.65	T2	1
F1132	92	8.89	-12.61	T2	1
F1132	96	7.81	-12.72	T2	1
F1132	100	7.17	-14.22	T2	1
F1132	104	6.68	-6.41	T2	1
F1132	105.5	6.99	-14.57	T2	1
F1132	110	8.03	-10.35	T2	1
F1132	112.6	5.30	-2.81	T2	1
F1132	114.5	5.14	-2.96	T2	1
F1132	117	-6.83	-14.81	T3	1
F1132	119	-1.41	-9.44	T3	1
F1132	120	0.40	-7.66	T3	1
F1132	121	-0.87	-8.91	T3	1
F1132	122	-3.79	-11.80	T3	1
F1132	123	-6.71	-14.69	T3	1
F1132	124	-6.67	-7.84	T3	1
F1132	125	-6.73	-7.72	T3	1
F1132	126	-7.26	-11.65	T3	1
F1132	127	-7.94	-8.75	T3	1
F1132	128	-7.95	-8.37	T3	1
F1132	129	-8.15	-6.40	T3	1
F1132	130	-8.18	-8.03	T3	1
F1132	131	-8.13	-7.94	T3	1
F1132	132	-7.27	-11.97	T3	1
F1132	133	-7.21	-8.70	T3	1
F1132	135	-6.22	-11.93	T3	1
F1132	136	-5.94	-8.96	T3	1
F1132	137	-6.04	-11.30	T3	1
F1132	138	-5.35	-11.06	T3	1
F1132	139	-4.94	-7.58	T3	1
F1132	140	-4.41	-8.13	T3	1
F1132	141	-4.43	-7.03	T3	1
F1132	142	-3.62	-7.40	T3	1
F1132	143	-3.27	-8.86	T3	1

F1132	144	-3.49	-9.83	T3	l
F1132	145	-1.94	-20.11	T3	l
F1132	147	-1.80	-15.65	T3	l
F1132	149	1.24	-25.30	T3	l
F1132	152	3.61	-24.55	T3	l
F1132	156	7.11	-22.42	T3	l
F1132	160	7.46	-20.08	T3	l
F1132	164	8.62	-18.20	T3	l
F1132	168	8.90	-22.92	T3	l
F1132	172	7.79	-17.39	T3	l
F1132	176	8.85	-12.10	T3	l
F1132	180	7.87	-19.57	T3	l
F1132	184	6.93	-11.31	T3	l
F1132	188	7.35	-26.73	T3	l
F1132	192	9.01	-17.28	T3	l
F1132	196	6.51	-13.76	T3	l
F1132	200	9.65	-9.41	T3	l
F1132	204	9.90	-5.97	T3	l
F1132	208	9.87	-9.18	T3	l
F1132	212	8.70	-8.56	T3	l
F1132	216	9.45	-8.88	T3	l
F1132	220	10.12	-4.60	T3	l
F1132	224	10.30	-2.34	T3	l
F1132	228	10.26	-3.01	T3	l
F1132	236	10.29	-10.06	T3	l

Uliastai Gorge	**N 46 50.929'**	**E 96 48.423'**			
Section	**Height**	**δ^{13}Ccarb**	**δ^{18}Ocarb**	**Unit**	**Lithology**
F948	326.1	-2.86	-12.46	T1	l
F948	326.6	-1.80	-9.82	T1	l
F948	327.2	-2.20	-11.23	T1	l
F948	327.5	-1.26	-8.17	T1	l
F948	328.2	-1.66	-13.44	T1	l
F948	328.7	-1.05	-12.77	T1	l
F948	329.2	-0.35	-11.26	T1	l
F948	330	-0.40	-13.38	T1	l
F948	331	-0.25	-11.62	T1	l
F948	332	-0.68	-10.74	T1	l
F948	333	-0.91	-5.99	T1	l
F948	334	0.02	-11.18	T1	l
F948	335	-0.84	-13.65	T1	l
F948	336	-0.23	-11.97	T1	l
F948	337	-1.07	-7.65	T1	l
F948	338	0.00	-11.54	T1	l
F948	339	-0.80	-14.35	T1	l
F948	340	-0.24	-9.38	T1	l
F948	341	-0.11	-11.86	T1	l
F948	342	-0.01	-9.42	T1	l

F948	343	1.57	-7.98	T1	l
F948	344	-0.61	-10.01	T1	l
F948	345	-0.52	-11.52	T1	l

Khongor Range	**N46 39'45.4"**	**E96 15'18.6"**			
Section	**height**	**δ^{13}Ccarb**	**δ^{18}Ocarb**	**Unit**	**Lithology**
F708	29.7	-0.32	-7.02	Ol	d
F708	30.2	-1.14	-5.99	Ol	d
F708	30.5	-1.31	-6.70	Ol	d
F708	31.0	-1.41	-6.95	Ol	d
F708	31.5	-1.30	-7.08	Ol	d
F708	32.0	-1.38	-6.67	Ol	d
F708	33.0	-1.45	-6.92	Ol	d
F708	33.5	-1.23	-7.87	Ol	d
F708	34.0	-0.54	-8.22	Ol	d
F708	34.5	-0.31	-6.56	Ol	d
F708	35.0	-0.24	-7.59	Ol	d
F708	35.5	-0.96	-6.62	Ol	d
F708	36.0	-1.93	-8.52	Ol	d
F708	36.5	-2.73	-8.31	Ol	d
F708	37.0	-0.89	-13.03	Ol	d
F708	37.5	-3.50	-17.21	Ol	d
F708	38.0	-3.19	-19.10	Ol	d
F708	38.5	-1.20	-27.94	Ol	d
F708	39.0	-3.52	-13.80	Ol	d
F708	39.5	-4.31	-11.87	Ol	d
F708	40.0	-4.52	-10.74	Ol	d
F708	40.5	-3.83	-13.04	Ol	d
F708	41.0	-4.21	-11.70	Ol	d
F708	42.0	-3.25	-15.45	Ol	d
F708	42.5	-4.44	-10.35	Ol	d
F708	43.0	-1.25	-24.32	Ol	d
F708	43.5	-3.94	-10.20	Ol	d
F708	44.0	-1.49	-22.74	Ol	d
F708	45.0	-4.05	-11.20	Ol	d
F708	45.5	-4.58	-11.29	Ol	d
F708	46.0	-4.15	-12.69	Ol	d
F708	47.0	-4.66	-9.17	Ol	d
F708	48.0	-4.76	-14.69	Ol	d
F708	49.0	-4.98	-11.39	Ol	d
F708	50.0	-5.35	-14.40	Ol	l
F708	51.0	-4.92	-9.52	Ol	l
F708	52.0	-6.04	-12.79	Ol	l
F708	59.0	-4.40	-12.97	Ol	l
F708	60.0	-3.38	-11.15	Ol	l
F708	62.0	-2.65	-10.64	Ol	l
F708	64.0	-2.79	-16.88	Ol	l
F708	66.0	-2.94	-11.48	Ol	l

F708	70.0	-3.04	-11.23	Ol	1
F708	72.0	-3.13	-15.04	Ol	1
F708	74.0	-2.92	-7.99	Ol	1
F708	78.0	-3.02	-9.73	Ol	1
F708	80.0	-3.44	-8.34	Ol	1
F708	82.0	-3.17	-9.41	Ol	1
F708	84.0	-3.27	-10.70	Ol	1
F708	86.0	-3.07	-8.92	Ol	1
F708	88.0	-2.98	-9.02	Ol	1
F708	90.0	-2.68	-7.01	Ol	1
F708	92.0	-1.81	-8.24	Sh1	1
F708	94.0	-4.57	-10.71	Sh1	1
F708	96.0	-2.40	-7.00	Sh1	1
F708	98.0	-2.90	-8.05	Sh1	1
F708	100.0	-3.89	-10.59	Sh1	1
F708	102.0	-2.86	-10.50	Sh1	1
F708	104.0	-2.45	-8.64	Sh1	1
F708	106.0	-0.97	-12.31	Sh1	1
F708	108.0	-0.30	-8.21	Sh1	1
F708	110.0	-1.16	-9.49	Sh1	1
F708	112.0	-0.93	-13.13	Sh1	1
F708	114.0	-1.29	-15.03	Sh1	1
F708	123.0	2.59	-6.00	Sh2	1
F708	125.0	2.21	-3.57	Sh2	1
F708	127.0	1.79	-3.52	Sh2	1
F708	129.0	3.43	-4.77	Sh2	1
F708	131.0	2.73	-6.18	Sh2	1
F708	133.0	3.72	-5.07	Sh2	1
F708	135.0	3.07	-2.24	Sh2	1
F708	137.0	3.29	-4.67	Sh2	1
F708	139.0	3.39	-5.31	Sh2	1
F708	141.0	3.36	-4.11	Sh2	1
F708	146.0	2.23	-2.09	Sh2	1
F708	150.0	-0.81	-2.63	Sh2	1
F708	160.0	3.11	-1.98	Sh2	1
F708	162.0	2.93	-5.33	Sh2	1
F708	164.0	3.00	-4.47	Sh2	1
F708	168.0	2.85	-2.78	Sh2	1
F708	170.0	2.51	-2.62	Sh2	1
F708	172.0	3.59	-4.57	Sh2	1
F708	174.0	0.88	-0.79	Sh2	1
F708	176.0	2.95	-2.21	Sh2	1
F708	178.0	1.58	-1.03	Sh2	1
F708	180.0	3.72	-1.25	Sh2	1
F708	182.0	3.32	-5.18	Sh2	1
F708	184.0	4.03	-0.78	Sh2	1
F708	186.0	2.88	-4.24	Sh2	1
F708	188.0	4.26	-5.72	Sh2	1

F708	190.0	0.95	-1.92	Sh2	l
F708	192.0	0.05	-0.95	Sh2	l
F708	194.0	1.54	-1.44	Sh2	d
F708	196.0	2.48	-1.50	Sh2	d
F708	198.0	2.33	-1.77	Sh2	d
F708	200.0	3.31	-8.17	Sh2	d
F708	202.0	2.36	-6.79	Sh2	d
F708	204.0	3.75	-6.24	Sh2	d
F708	206.0	3.67	-8.17	Sh2	d
F708	208.0	2.61	-1.88	Sh2	d
F708	210.0	4.34	-3.29	Sh2	d
F708	212.0	2.43	-3.62	Sh2	d
F708	214.0	3.17	-3.83	Sh2	d
F708	216.0	3.43	-3.90	Sh2	d
F708	218.0	3.34	-4.12	Sh2	d
F708	220.0	3.20	-5.77	Sh2	d
F708	222.0	3.21	-6.44	Sh2	d
F708	224.0	3.41	-4.87	Sh2	d
F708	226.0	2.85	-5.72	Sh2	d
F708	228.0	3.39	-9.57	Sh2	d
F708	230.0	3.21	-9.48	Sh2	d
F708	232.0	2.71	-10.00	Sh2	d
F708	234.0	3.58	-1.58	Sh2	d
F708	236.0	3.12	-2.87	Sh2	d
F708	238.0	2.86	-3.53	Sh2	d
F708	240.0	2.78	-1.91	Sh2	d
F708	241.0	3.69	-1.23	Sh2	d
F708	244.0	4.00	-0.35	Sh2	d
F708	246.0	2.81	-0.46	Sh2	d
F708	248.0	2.94	-1.32	Sh2	d
F708	250.0	3.08	-0.67	Sh2	d
F708	252.0	1.42	-0.54	Sh2	d
F708	254.0	2.89	-4.79	Sh2	d
F708	256.0	2.16	-3.33	Sh2	d
F708	258.0	2.98	-4.25	Sh2	d
F708	260.0	2.90	-2.32	Sh2	d
F708	262.0	2.29	-2.54	Sh2	d
F708	264.0	3.82	-2.52	Sh2	d
F708	266.0	4.56	-2.59	Sh2	d
F708	268.0	2.54	-1.21	Sh2	d
F708	270.0	3.26	-1.10	Sh2	d
F708	272.0	2.22	-3.46	Sh2	d
F708	274.0	3.62	-0.73	Sh2	d
F708	276.0	4.47	-1.69	Sh2	d
F708	278.0	3.79	-2.58	Sh2	d
F708	280.0	4.28	-1.55	Sh2	d
F708	284.0	2.91	-2.00	Sh2	d
F708	286.0	3.46	0.05	Sh2	d

F708	288.0	4.04	-1.48	Sh2	d
F708	290.0	1.77	-1.80	Sh2	d
F708	292.0	2.93	-2.42	Sh2	d
F708	294.0	2.76	-1.66	Sh2	d
F708	296.0	3.19	-0.82	Sh2	d
F708	298.0	2.72	-1.52	Sh2	d
F708	300.0	2.02	-2.31	Sh2	d
F708	302.0	5.17	-1.01	Sh2	d
F708	304.0	4.33	-1.05	Sh2	d
F708	308.0	3.21	-2.12	Sh2	d
F708	310.0	3.80	-1.42	Sh2	d
F708	312.0	3.16	-0.62	Sh2	d
F708	314.0	2.00	-1.15	Sh2	d
F708	316.0	4.78	-1.93	Sh2	d
F708	318.0	2.54	-10.23	Sh2	d
F708	322.0	3.86	-2.91	Sh2	d
F708	324.0	3.44	-4.61	Sh2	d
F708	326.0	3.08	-5.67	Sh2	d
F708	330.0	2.50	-2.56	Sh2	d
F708	332.0	3.78	-5.25	Sh2	d
F708	334.0	1.37	-6.62	Sh2	d
F708	338.0	1.27	-7.25	Sh2	d
F708	340.0	2.75	-6.62	Sh3	d
F708	344.0	3.03	-2.69	Sh3	d
F708	346.0	2.61	-10.71	Sh3	d
F708	348.0	1.22	-6.17	Sh3	d
F708	350.0	2.87	-1.51	Sh3	d
F708	352.0	2.08	-3.00	Sh3	d
F708	354.0	3.22	-3.54	Sh3	d
F708	356.0	2.44	-3.20	Sh3	d
F708	358.0	3.82	-1.32	Sh3	d
F708	360.0	2.51	-1.50	Sh3	d
F708	362.0	2.21	-1.23	Sh3	d
F708	364.0	1.89	-2.91	Sh3	d
F708	366.0	2.54	-1.93	Sh3	d
F708	368.0	2.62	-0.66	Sh3	d
F708	370.0	1.39	-1.02	Sh3	d
F708	372.0	3.72	-1.11	Sh3	d
F708	374.0	2.71	-0.88	Sh3	d
F708	376.0	2.50	-0.27	Sh3	d
F708	378.0	4.82	-0.99	Sh3	d
F708	380.0	3.72	-1.96	Sh3	d
F708	382.0	2.42	-1.48	Sh3	d
F708	384.0	1.70	-10.70	Sh3	d
F708	386.0	2.50	-3.48	Sh3	d
F708	388.0	1.87	-2.31	Sh3	d
F708	390.0	3.22	-1.64	Sh3	d
F708	392.0	2.90	-1.99	Sh3	d

F708	394.0	3.61	-0.66	Sh3	d
F708	396.0	4.69	-5.23	Sh3	d
F708	398.0	4.10	-2.18	Sh3	d
F708	400.0	3.22	-1.10	Sh3	d
F708	402.0	4.05	-0.89	Sh3	d
F708	404.0	3.88	-0.55	Sh3	d
F708	406.0	3.63	-5.90	Sh3	d
F708	408.0	3.79	-1.95	Sh3	d
F708	410.0	3.84	-1.66	Sh3	d
F708	416.0	3.22	-6.55	Sh3	d
F708	418.0	1.98	-0.29	Sh3	d
F708	420.0	2.63	-2.39	Sh3	d
F708	422.0	2.97	-0.61	Sh3	d
F708	424.0	2.52	-2.08	Sh3	d
F708	426.0	2.93	-0.84	Sh3	d
F708	428.0	3.08	-0.68	Sh3	d
F708	430.0	3.48	-3.11	Sh3	d
F708	432.0	4.12	-0.73	Sh3	d
F708	434.0	4.23	-0.79	Sh3	d
F708	436.0	4.27	-0.93	Sh3	d
F708	438.0	3.63	-1.02	Sh3	d
F708	442.0	4.01	-3.69	Sh3	d
F708	444.0	3.80	-2.21	Sh3	d
F708	446.0	3.71	-2.17	Sh3	d
F708	448.0	3.49	-1.82	Sh3	d
F708	450.0	3.73	-2.08	Sh3	d
F708	452.0	3.00	-1.44	Sh3	d
F708	454.0	2.95	-0.66	Sh3	d
F708	456.0	3.58	-0.37	Sh3	d
F708	458.0	4.42	-1.94	Sh3	d
F708	460.0	3.65	-3.28	Sh3	d
F708	462.0	3.82	-5.47	Sh3	d
F708	464.0	2.89	-0.96	Sh3	d
F708	466.0	2.69	-1.36	Sh3	d
F708	468.0	3.41	-1.67	Sh3	d
F708	470.0	3.59	-0.12	Sh3	d
F708	472.0	3.75	-0.09	Sh3	d
F708	474.0	3.40	-2.63	Sh3	d
F708	476.0	2.96	-0.42	Sh3	d
F708	478.0	3.49	-2.27	Sh3	d
F708	480.0	2.63	0.17	Sh3	d
F708	482.0	3.58	-0.85	Sh3	d
F708	484.0	3.48	-5.04	Sh3	d
F708	486.0	3.54	0.13	Sh3	d
F708	488.0	3.61	-2.59	Sh3	d
F708	490.0	3.38	-1.70	Sh3	d
F708	492.0	3.25	-1.34	Sh3	d
F708	495.0	1.61	0.14	Sh3	d

F708	498.0	1.75	-1.83	Sh3	d
F708	502.0	3.60	-1.02	Sh3	d
F708	506.0	0.97	0.20	Sh3	d
F708	510.0	3.32	-1.31	Sh3	d
F708	512.0	4.14	-1.54	Sh3	d
F708	514.0	3.99	-0.95	Sh3	d
F708	518.0	3.99	-1.04	Sh3	d
F708	526.0	4.56	-1.07	Sh3	d
F708	530.0	4.01	-1.41	Sh3	d
F708	534.0	4.45	-1.36	Sh3	d
F708	538.0	5.05	-1.84	Sh3	d
F708	542.0	3.85	-2.94	Sh3	d
F708	546.0	3.12	-1.62	Sh3	d
F708	550.0	0.72	-0.23	ZA	d
F708	554.0	0.77	-2.48	ZA	d
F708	558.0	0.80	-1.61	ZA	d
F708	562.0	1.18	-4.96	ZA	d
F708	566.0	1.14	-0.93	ZA	d
F708	576.0	0.52	-3.35	ZA	d
F708	580.0	-0.04	-2.18	ZA	d
F708	582.0	0.55	-0.85	ZA	d
F708	584.0	2.50	-0.60	ZA	d
F708	586.0	3.06	-0.96	ZA	d

Khevtee Tsakhir Range **N46 40'04.8"** **E96 49'22.2"**

Section	**height**	**δ^{13}Ccarb**	**δ^{18}Ocarb**	**Unit**	**Lithology**
F710	109.7	-0.91	-6.54	Ol	d
F710	111.0	-0.96	-7.38	Ol	d
F710	112.0	-1.47	-6.51	Ol	d
F710	113.0	-0.78	-7.89	Ol	d
F710	114.0	-1.15	-8.12	Ol	d
F710	115.0	-0.63	-7.48	Ol	d
F710	116.0	-0.21	-7.76	Ol	d
F710	117.0	-0.21	-6.17	Ol	d
F710	118.0	-1.97	-6.75	Ol	d
F710	119.0	-2.62	-6.31	Ol	d
F710	119.7	-2.96	-8.20	Ol	d
F710	122.0	-1.79	-7.84	Ol	d
F710	123.0	-2.37	-8.21	Ol	d
F710	124.0	-0.35	-8.25	Ol	d
F710	125.0	-0.61	-6.85	Ol	d
F710	126.0	-2.04	-12.10	Ol	d
F710	127.0	-3.80	-13.76	Ol	d
F710	129.5	-3.47	-10.75	Ol	d
F710	135.0	-5.29	-27.26	Ol	d
F710	136.0	-5.18	-28.72	Ol	d
F710	137.0	-5.11	-19.99	Ol	d
F710	138.0	-4.99	-16.12	Ol	d

F710	139.0	-4.47	-9.10	Ol	d
F710	140.0	-4.98	-11.37	Ol	l
F710	141.0	-4.85	-11.13	Ol	l
F710	142.0	-5.00	-15.55	Ol	l
F710	143.0	-5.53	-20.22	Ol	l
F710	144.0	-4.09	-18.84	Ol	l
F710	156.0	-3.06	-11.79	Ol	l
F710	158.0	-3.14	-8.85	Ol	l
F710	160.0	-3.24	-18.00	Ol	l
F710	162.0	-2.85	-17.66	Ol	l
F710	164.0	-3.00	-12.09	Ol	l
F710	168.0	-2.98	-11.81	Ol	l
F710	172.0	-2.29	-10.69	Ol	l
F710	176.0	-2.41	-8.11	Ol	l
F710	180.0	-2.90	-13.11	Ol	l
F710	182.0	-3.27	-11.69	Ol	l
F710	184.0	-2.35	-7.68	Ol	l
F710	186.0	-2.85	-7.15	Ol	l
F710	189.0	-1.23	-7.02	Ol	l

Tsagaan Gorge W. **N46 51'53.9"** **E95 46'50.7"**

Section	**height**	**δ^{13}Ccarb**	**δ^{18}Ocarb**	**Unit**	**Lithology**
F724	2.0	-1.39	-5.13	Ol	d
F724	3.0	0.07	-5.32	Ol	d
F724	4.0	1.01	-4.50	Ol	d
F724	5.0	0.82	-5.23	Ol	d
F724	6.0	0.96	-4.49	Ol	d
F724	7.0	1.20	-3.76	Ol	d
F724	8.0	1.48	-3.30	Ol	d
F724	10.0	1.25	-3.02	Ol	d
F724	12.0	1.21	-2.98	Ol	d
F724	14.0	0.06	-2.43	Ol	d
F724	16.0	0.94	-6.40	Ol	d
F724	20.0	1.28	-4.88	Ol	d
F724	24.0	1.31	-1.96	Ol	d
F724	28.0	0.18	-5.91	Ol	d
F724	34.0	0.89	-2.63	Ol	d
F724	48.0	2.18	-2.57	Ol	d
F724	52.0	2.36	-1.67	Ol	d
F724	56.0	3.56	-2.41	Sh1	l
F724	60.0	3.79	-1.73	Sh1	l
F724	64.0	3.56	-2.95	Sh1	l
F724	68.0	4.82	-1.30	Sh2	d
F724	72.0	4.27	-1.45	Sh2	d
F724	76.0	3.92	-3.32	Sh2	d
F724	80.0	3.68	-6.10	Sh2	d
F724	84.0	3.64	-2.53	Sh2	d
F724	88.0	4.33	-2.33	Sh2	d

F724	92.0	4.94	-1.52	Sh2	d
F724	96.0	4.95	-2.85	Sh2	d
F724	100.0	4.39	-2.40	Sh2	d
F724	104.0	4.52	-1.64	Sh2	d
F724	108.0	4.40	-1.89	Sh2	d
F724	112.0	1.55	-3.54	Sh2	d
F724	116.0	3.87	-2.42	Sh2	d
F724	120.0	3.78	-5.64	Sh2	d
F724	124.0	0.39	-2.51	Sh2	d
F724	134.0	7.55	-5.81	Sh3-4	d
F724	148.0	8.45	-6.42	Sh3-4	l
F724	152.0	8.53	-7.09	Sh3-4	l
F724	156.0	6.44	-6.33	Sh3-4	l
F724	160.0	2.82	-1.29	Sh3-4	l
F724	164.0	3.15	-3.01	Sh3-4	l
F724	168.0	1.93	-1.73	Sh3-4	d
F724	172.0	4.42	-7.86	Sh3-4	d
F724	178.0	-1.79	-3.24	Sh3-4	l
F724	183.0	5.47	-5.93	Sh3-4	l
F724	194.0	5.29	-6.59	Sh3-4	l
F724	198.0	6.86	-4.78	Sh3-4	l
F724	205.0	5.76	-5.53	Sh3-4	l
F724	210.0	6.99	-5.71	Sh3-4	l
F724	214.0	6.07	-6.37	Sh3-4	l
F724	218.0	4.58	-3.05	Sh3-4	l
F724	224.0	7.53	-6.77	Sh3-4	l
F724	228.0	3.89	-6.96	Sh3-4	l
F724	264.0	8.13	-6.57	Sh3-4	l
F724	266.0	7.03	-8.83	Sh3-4	l
F724	270.0	7.04	-8.95	Sh3-4	l
F724	274.0	6.77	-10.64	Sh3-4	l
F724	280.0	4.69	-2.31	Sh3-4	l
F724	284.0	4.16	-1.66	Sh3-4	l
F724	288.0	3.33	0.12	Sh3-4	d
F724	292.0	1.84	0.12	Sh3-4	d
F724	296.0	1.86	-2.35	ZA	d
F724	300.0	1.41	-0.99	ZA	d

Khunkher Gorge **N46 44.413'** **E95 58.814'**

Section	**height**	**δ^{13}Ccarb**	**δ^{18}Ocarb**	**Unit**	**Lithology**
F872	20.0	-0.66	-5.25	Ol	d
F872	20.5	-1.15	-6.12	Ol	d
F872	21.0	-0.98	-5.49	Ol	d
F872	21.5	-1.18	-6.01	Ol	d
F872	22.0	-1.38	-6.34	Ol	d
F872	22.5	-0.86	-6.54	Ol	d
F872	23.0	-0.70	-5.50	Ol	d
F872	23.5	-1.37	-5.40	Ol	d

F872	24.0	-0.66	-5.45	Ol	d
F872	24.5	-0.77	-4.86	Ol	d
F872	25.0	-0.27	-5.23	Ol	d
F872	25.5	-0.27	-4.90	Ol	d
F872	26.0	-0.33	-5.09	Ol	d
F872	26.5	-0.38	-5.11	Ol	d
F872	27.0	-0.47	-5.47	Ol	d
F872	27.5	-0.53	-5.16	Ol	d
F872	28.0	-1.77	-4.40	Ol	d
F872	28.5	-2.84	-4.83	Ol	d
F872	29.0	-3.17	-5.45	Ol	d
F872	29.5	-3.73	-6.01	Ol	d
F872	30.0	-1.32	-4.19	Ol	d
F872	30.5	-1.66	-4.06	Ol	d
F872	31.0	-1.62	-5.19	Ol	d
F872	31.5	-1.89	-3.30	Ol	d
F872	32.0	-1.57	-3.83	Ol	d
F872	32.5	-0.93	-4.44	Ol	d
F872	33.0	-0.68	-4.06	Ol	d
F872	33.5	-1.85	-4.00	Ol	d
F872	34.0	-0.48	-5.19	Ol	d
F872	34.5	-0.47	-4.93	Ol	d
F872	35.0	-1.05	-4.63	Ol	d
F872	36.0	-0.44	-4.35	Ol	d
F872	37.0	-0.66	-6.42	Ol	d
F872	38.0	-0.37	-3.94	Ol	d
F872	40.0	-0.57	-5.07	Ol	d
F872	41.0	-1.92	-4.99	Ol	d
F872	42.0	-1.75	-5.33	Ol	d
F872	43.0	-2.10	-7.50	Ol	d
F872	44.0	-4.09	-12.77	Ol	d
F872	45.0	-1.93	-15.19	Ol	d
F872	46.0	-3.04	-10.57	Ol	d
F872	47.0	-3.17	-10.18	Ol	d
F872	48.0	-2.35	-16.25	Ol	l
F872	49.0	-2.21	-13.47	Ol	l
F872	55.0	1.99	-3.70	Sh2	d
F872	57.0	3.11	-2.55	Sh2	d
F872	59.0	3.83	-1.94	Sh2	d
F872	61.0	4.23	-2.04	Sh2	d
F872	63.0	4.25	-2.73	Sh2	d
F872	61.0	4.24	-1.99	Sh2	d
F872	63.0	4.29	-2.61	Sh2	d
F872	65.0	2.98	-0.51	Sh2	d
F872	67.0	3.25	-0.73	Sh2	d
F872	69.0	2.77	-3.61	Sh2	d
F872	71.0	2.59	-1.91	Sh2	d
F872	73.0	3.46	-0.77	Sh2	d

F872	75.0	3.51	-2.06	Sh2	d
F872	77.0	2.34	-4.78	Sh2	d
F872	79.0	2.13	-2.84	Sh2	d
F872	81.0	1.89	-2.54	Sh2	d
F872	83.0	3.37	-1.59	Sh2	d
F872	85.0	3.29	-0.73	Sh2	d
F872	87.0	3.81	-1.46	Sh2	d
F872	89.0	3.89	-1.47	Sh2	d
F872	91.0	5.73	-1.20	Sh2	d
F872	93.0	2.60	-5.34	Sh2	d
F872	95.0	3.25	-1.44	Sh2	d
F872	97.0	3.58	-4.91	Sh2	d
F872	99.0	3.73	-0.40	Sh2	d
F872	101.0	2.68	-1.63	Sh2	d
F872	103.0	4.11	-0.64	Sh2	d
F872	105.0	3.60	-0.68	Sh2	d
F872	109.0	3.08	-0.91	Sh2	d
F872	111.0	2.87	-1.71	Sh2	d
F872	113.0	3.25	-2.16	Sh2	d
F872	115.0	2.06	-2.54	Sh2	d
F872	117.0	2.86	-1.91	Sh2	d
F872	119.0	3.86	-1.74	Sh2	d
F872	121.0	2.82	-13.44	Sh2	d
F872	123.0	3.33	-4.25	Sh2	d
F872	125.0	1.71	-3.39	Sh2	d
F872	127.0	3.26	-0.94	Sh2	d
F872	129.0	2.84	-0.98	Sh2	d
F872	131.0	2.75	-1.44	Sh2	d
F872	133.0	2.94	-3.68	Sh2	d
F872	135.0	3.33	-0.96	Sh2	d
F872	139.0	2.24	-3.03	Sh2	d
F872	147.0	2.62	-5.97	Sh2	d
F872	148.0	4.65	-3.39	Sh2	l
F872	150.0	4.70	-0.81	Sh2	l
F872	152.0	8.13	-5.43	Sh3-4	l
F872	154.0	8.78	-4.59	Sh3-4	l
F872	154.0	7.65	-1.36	Sh3-4	l
F872	156.0	2.88	-1.96	Sh3-4	l
F872	160.0	3.22	-2.28	Sh3-4	l
F872	164.0	3.09	-5.15	Sh3-4	l
F872	168.0	1.10	-1.33	Sh3-4	l
F872	170.0	1.75	-1.46	Sh3-4	l
F872	172.0	7.57	-9.11	Sh3-4	l
F872	174.0	4.50	-10.45	Sh3-4	l
F872	183.0	4.29	-4.22	Sh3-4	l
F872	187.0	4.06	-6.37	Sh3-4	l
F872	189.0	7.97	-8.02	Sh3-4	l
F872	193.0	7.77	-8.33	Sh3-4	l

F872	195.0	8.04	-7.61	Sh3-4	l
F872	198.0	8.11	-6.44	Sh3-4	l
F872	202.0	5.55	-7.14	Sh3-4	l
F872	204.0	5.82	-2.95	Sh3-4	d
F872	205.0	3.37	-2.22	Sh3-4	d
F872	207.0	2.85	-1.39	Sh3-4	d
F872	209.0	2.95	-1.00	Sh3-4	d
F872	211.0	2.48	-1.34	Sh3-4	d
F872	213.0	3.19	0.80	Sh3-4	d
F872	214.0	2.98	-1.75	Sh3-4	d
F872	216.0	3.37	0.51	Sh3-4	d
F872	218.0	2.58	-1.49	Sh3-4	d
F872	220.0	3.62	1.52	Sh3-4	d
F872	222.0	2.23	-3.03	Sh3-4	d
F872	224.0	2.35	-0.84	Sh3-4	d
F872	226.0	1.72	-1.08	Sh3-4	d
F872	228.0	4.02	-1.10	Sh3-4	d
F872	230.0	4.60	1.31	Sh3-4	d
F872	232.0	4.20	-1.65	Sh3-4	d
F872	234.0	2.77	-1.67	Sh3-4	d
F872	236.0	2.20	-1.02	Sh3-4	d
F872	238.0	3.23	-1.55	Sh3-4	d
F872	240.0	2.64	-3.22	Sh3-4	d
F872	242.0	2.21	-9.07	Sh3-4	l
F872	244.0	1.87	-10.36	Sh3-4	l
F872	246.0	5.39	-9.02	Sh3-4	l
F872	249.0	5.06	-9.46	Sh3-4	l
F872	251.0	5.40	-8.30	Sh3-4	l
F872	253.0	5.16	-8.37	Sh3-4	l
F872	255.0	5.27	-3.69	Sh3-4	l
F872	259.0	3.79	-7.50	Sh3-4	l
F872	261.0	6.73	-8.00	Sh3-4	l
F872	263.0	6.44	-3.40	Sh3-4	l
F872	265.0	5.57	-5.26	Sh3-4	l
F872	267.0	6.96	-8.27	Sh3-4	l
F872	269.0	6.96	-8.93	Sh3-4	l
F872	271.0	5.96	-4.16	Sh3-4	l
F872	273.0	5.43	-3.19	Sh3-4	d
F872	275.0	3.52	-1.12	Sh3-4	d
F872	279.0	5.14	-1.62	Sh3-4	d
F872	281.0	5.43	-1.46	Sh3-4	d
F872	283.0	3.73	-1.76	Sh3-4	d
F872	285.0	2.47	-1.02	Sh3-4	d
F872	287.0	2.83	-1.89	Sh3-4	d
F872	289.0	2.74	-3.88	Sh3-4	d
F872	291.0	3.06	-1.51	Sh3-4	d
F872	293.0	2.78	-2.14	Sh3-4	d
F872	295.0	2.83	-0.34	Sh3-4	d

F872	300.0	2.33	-3.06	Sh3-4	d
F872	302.0	2.14	-0.47	Sh3-4	d
F872	304.0	2.75	-1.02	Sh3-4	d
F872	306.0	2.22	-0.59	Sh3-4	d
F872	308.0	1.66	-1.84	ZA	d
F872	310.0	1.97	-0.26	ZA	d
F872	312.0	1.70	-4.25	ZA	d
F872	314.0	2.66	-2.97	ZA	d
F872	316.0	2.06	-1.40	ZA	d
F872	318.0	2.60	-4.11	ZA	d
F872	320.0	2.21	-0.85	ZA	d
F872	322.0	2.09	-1.26	ZA	d
F872	324.0	1.06	-0.18	ZA	d
F872	326.0	1.90	-2.70	ZA	d
F872	328.0	2.11	-1.77	ZA	d
F872	330.0	2.22	-1.28	ZA	d
F872	332.0	1.19	-2.34	ZA	d
F872	334.0	0.87	-2.14	ZA	d
F872	336.0	2.31	-0.55	ZA	d
F872	338.0	2.69	-0.91	ZA	d
F872	340.0	2.25	-0.48	ZA	d
F872	342.0	2.78	-1.65	ZA	d
F872	344.0	3.03	-2.33	ZA	d
F872	346.0	3.13	-4.02	ZA	d
F872	348.0	2.97	-1.40	ZA	d
F872	350.0	2.19	-0.09	ZA	d

Khongor Range	**N46 39'47.2"**	**E96 15'19.9"**			
Section	**height**	**δ^{13}Ccarb**	**δ^{18}Ocarb**	**Unit**	**Lithology**
F947	38.1	-3.79	-13.28	Ol	d
F947	38.5	-4.15	-12.14	Ol	d
F947	39.0	-4.62	-7.45	Ol	d
F947	39.5	-4.96	-15.88	Ol	d
F947	40.0	-4.89	-16.69	Ol	d
F947	40.5	-5.04	-11.09	Ol	d
F947	41.0	-5.24	-10.56	Ol	d
F947	41.5	-4.68	-8.62	Ol	l
F947	42.5	-4.19	-10.76	Ol	l
F947	43.0	-4.41	-10.47	Ol	l
F947	78.5	-2.11	-8.65	Ol	l
F947	79.5	-3.46	-10.69	Ol	l
F947	80.5	-0.96	-5.36	Ol	l
F947	82.0	-1.91	-9.81	Ol	l
F947	83.0	-0.85	-8.01	Ol	l
F947	84.0	-1.58	-11.04	Ol	l
F947	85.0	-1.06	-9.13	Ol	l
F947	86.0	-0.56	-12.91	Ol	l
F947	87.0	-0.57	-8.51	Ol	l

F947	88.0	-0.69	-10.04	Ol	l
F947	89.0	0.08	-9.37	Ol	l
F947	91.0	-0.98	-11.62	Ol	l
F947	92.0	-0.49	-10.36	Ol	l
F947	97.0	0.05	-8.32	Ol	l
F947	99.0	-1.48	-11.52	Ol	l
F947	100.5	-0.29	-11.71	Ol	l
F947	102.0	-0.99	-9.29	Ol	l
F947	103.0	0.78	-9.61	Ol	l
F947	104.0	3.59	-13.90	Ol	l
F947	105.0	1.17	-19.32	Ol	l
F947	105.5	-0.34	-16.15	Sh1	d
F947	106.6	3.87	-3.01	Sh1	d

Khukh Davaa NE. **N 47 5.526'** **E 95 28.843'**

Section	**height**	**δ^{13}Ccarb**	**δ^{18}Ocarb**	**Unit**	**Lithology**
F1206	0.2	4.15	-1.42	Sh3-4	d
F1206	3.8	3.94	-5.05	Sh3-4	d
F1206	6.3	4.96	-4.98	Sh3-4	d
F1206	8	7.78	-3.00	Sh3-4	d
F1206	9	8.43	-2.85	Sh3-4	d
F1206	10.3	6.21	-2.97	Sh3-4	l
F1206	12.4	8.96	-3.78	Sh3-4	l
F1206	14.1	7.75	-5.38	Sh3-4	l
F1206	16.3	7.63	-1.86	Sh3-4	d
F1206	17	6.96	-2.69	Sh3-4	d
F1206	18	2.88	-1.46	Sh3-4	d
F1206	19	3.00	-3.97	Sh3-4	d
F1206	20	3.29	-1.27	Sh3-4	d
F1206	21	3.47	-0.14	Sh3-4	d
F1206	22	3.20	-1.51	Sh3-4	d
F1206	23	3.17	-1.71	Sh3-4	d
F1206	24	2.00	-0.81	Sh3-4	d
F1206	25	2.75	-1.81	Sh3-4	d
F1206	26	2.28	-0.58	Sh3-4	d
F1206	27	2.04	-0.73	Sh3-4	d
F1206	28	2.32	-2.48	Sh3-4	d
F1206	29	1.73	-1.31	Sh3-4	d
F1206	30	2.36	-4.48	Sh3-4	d
F1206	31	3.49	-4.36	Sh3-4	d
F1206	32	3.75	-27.11	Sh3-4	d
F1206	33	3.89	-1.75	Sh3-4	l
F1206	34	2.46	-2.53	Sh3-4	d
F1206	35	2.47	-1.29	Sh3-4	d
F1206	36	3.78	-1.75	Sh3-4	d
F1206	37	3.79	-14.52	Sh3-4	d
F1206	38	3.32	-3.82	Sh3-4	l
F1206	39	4.04	-0.86	Sh3-4	l

F1206	40	3.10	-1.77	Sh3-4	d
F1206	42	2.47	-0.72	Sh3-4	d
F1206	43	2.37	-2.73	Sh3-4	d
F1206	44	0.90	-2.68	Sh3-4	d
F1206	45	1.94	-1.39	Sh3-4	d
F1206	46	1.90	-1.82	Sh3-4	d
F1206	47	4.81	-20.02	Sh3-4	d
F1206	48	4.26	-18.57	Sh3-4	d
F1206	50.5	4.99	-16.27	Sh3-4	d
F1206	52.3	1.71	-5.06	Sh3-4	d
F1206	53.4	4.97	-12.86	Sh3-4	d
F1206	55.5	4.78	-3.82	Sh3-4	d
F1206	56.6	6.46	-14.12	Sh3-4	d
F1206	60	4.07	-12.37	Sh3-4	l
F1206	61	6.39	-10.66	Sh3-4	l
F1206	62	5.78	-11.30	Sh3-4	l
F1206	63	5.44	-12.19	Sh3-4	l
F1206	64	5.53	-11.31	Sh3-4	d
F1206	65	5.57	-12.63	Sh3-4	d
F1206	66	5.63	-12.93	Sh3-4	l
F1206	67	0.05	-11.80	Sh3-4	l
F1206	70.7	1.55	-7.15	Sh3-4	d
F1206	82	5.64	-9.17	Sh3-4	d
F1206	84	5.27	-8.99	Sh3-4	l
F1206	85	5.67	-9.15	Sh3-4	l
F1206	86	5.18	-10.16	Sh3-4	l
F1206	87	6.71	-11.62	Sh3-4	l
F1206	89	6.64	-9.80	Sh3-4	l
F1206	90	3.61	-6.45	Sh3-4	l
F1206	91	4.07	-7.95	Sh3-4	l
F1206	92	5.63	-8.77	Sh3-4	l
F1206	93	4.57	-8.06	Sh3-4	l
F1206	94	5.36	-8.16	Sh3-4	l
F1206	95	6.29	-8.24	Sh3-4	l
F1206	96	6.75	-9.71	Sh3-4	l
F1206	96.9	5.28	-7.65	Sh3-4	l
F1206	98	7.07	-10.17	Sh3-4	d
F1206	99	7.69	-7.76	Sh3-4	d
F1206	100	6.61	-6.49	Sh3-4	d
F1206	101	7.44	-10.63	Sh3-4	d
F1206	102	7.02	-13.25	Sh3-4	d
F1206	103	4.69	-13.75	Sh3-4	d
F1206	106	4.74	-12.03	Sh3-4	d
F1206	108	6.15	-11.28	Sh3-4	d
F1206	110	6.02	-10.02	Sh3-4	l
F1206	111	5.51	-10.44	Sh3-4	l
F1206	112	6.96	-11.46	Sh3-4	l
F1206	113	7.07	-12.42	Sh3-4	l

F1206	114	6.50	-11.60	Sh3-4	d
F1206	115	7.20	-11.99	Sh3-4	d
F1206	116	7.62	-11.99	Sh3-4	d
F1206	117	6.99	-11.52	Sh3-4	d
F1206	119	7.08	-11.17	Sh3-4	d
F1206	120	7.38	-10.56	Sh3-4	d
F1206	122	6.87	-13.46	Sh3-4	d
F1206	123	6.96	-13.08	Sh3-4	d
F1206	124	6.23	-14.32	Sh3-4	d
F1206	125	6.45	-14.11	Sh3-4	d
F1206	127	6.76	-12.70	Sh3-4	l
F1206	128	6.97	-12.36	Sh3-4	l
F1206	129	5.29	-11.79	Sh3-4	l
F1206	131	5.80	-10.08	Sh3-4	l
F1206	132	4.95	-8.93	Sh3-4	l
F1206	133	7.01	-11.93	Sh3-4	l
F1206	134	6.51	-8.64	Sh3-4	l
F1206	135	6.65	-11.93	Sh3-4	l
F1206	136	5.91	-11.93	Sh3-4	l
F1206	137	6.37	-10.67	Sh3-4	l
F1206	138	6.29	-12.50	Sh3-4	l
F1206	139	6.97	-11.39	Sh3-4	l
F1206	142	4.90	-2.65	Sh3-4	l
F1206	143	3.50	-2.40	Sh3-4	l
F1206	144	2.60	-3.02	Sh3-4	l
F1206	145	1.66	-1.24	Sh3-4	l
F1206	146	0.95	-0.94	Sh3-4	l
F1206	147	1.12	-2.07	ZA	d
F1206	148	2.35	-1.66	ZA	d
F1206	149	2.26	-1.57	ZA	d
F1206	150	2.81	-0.81	ZA	d
F1206	151	2.65	-1.33	ZA	d
F1206	152	2.06	0.50	ZA	d
F1206	153	1.73	-1.63	ZA	d
F1206	154	2.12	-3.39	ZA	d
F1206	155	1.74	-3.32	ZA	d
F1206	157	1.68	-2.33	ZA	d
F1206	158	1.89	-3.28	ZA	d
F1206	159	1.76	-2.55	ZA	d
F1206	160	1.56	-1.88	ZA	d
F1206	165	2.42	-1.92	ZA	d
F1206	166	0.64	-2.06	ZA	d
F1206	167	3.05	-1.08	ZA	d
F1206	168	2.72	0.10	ZA	d
F1206	169	3.66	-0.03	ZA	d
F1206	170	3.06	-0.93	ZA	d
F1206	171	3.38	-0.30	ZA	d
F1206	172	3.40	-0.47	ZA	d

F1206	174	-1.14	-6.34	ZA	d
F1206	175	-1.54	-4.11	ZA	d
F1206	175.5	-2.38	-1.64	ZA	d

Khevtee Tsakhir Range	**N46 39'10.6"**	**E96 48'41.8"**			
Section	**height**	**δ^{13}Ccarb**	**δ^{18}Ocarb**	**Unit**	**Lithology**
U1225	0	-2.25	-8.43	Sh1	l
U1225	0.5	-1.51	-12.46	Sh1	l
U1225	1	-0.41	-20.03	Sh1	l
U1225	1.5	-2.45	-10.51	Sh1	l
U1225	2	-0.57	-18.11	Sh1	l
U1225	2.5	-1.49	-15.26	Sh1	l
U1225	3	0.27	-23.43	Sh1	l
U1225	3.5	-0.46	-24.94	Sh1	l
U1225	4	-0.48	-19.13	Sh1	l
U1225	4.5	-2.10	-11.07	Sh1	l
U1225	5	-2.44	-8.92	Sh1	l
U1225	5.5	-2.90	-7.76	Sh1	l
U1225	6	-2.67	-9.07	Sh1	l
U1225	6.5	-2.14	-10.75	Sh1	l
U1225	7	-2.75	-11.71	Sh1	l
U1225	7.5	-1.24	-17.32	Sh1	l
U1225	8	-2.48	-9.66	Sh1	l
U1225	8.5	-2.62	-8.93	Sh1	l
U1225	9	-2.72	-9.01	Sh1	l
U1225	9.5	-1.67	-12.93	Sh1	l
U1225	10	-1.33	-18.69	Sh1	l
U1225	10.5	-0.33	-20.03	Sh1	l
U1225	11	-2.41	-9.51	Sh1	l
U1225	11.5	-0.40	-19.07	Sh1	l
U1225	12.5	-2.69	-7.84	Sh1	l
U1225	13	-2.40	-12.96	Sh1	l
U1225	13.5	-2.52	-9.15	Sh1	l
U1225	14	-2.11	-11.87	Sh1	l
U1225	14.5	-0.91	-19.02	Sh1	l
U1225	15	-1.76	-16.06	Sh1	l
U1225	15.5	-0.57	-17.55	Sh1	l
U1225	16	-0.95	-16.50	Sh1	l
U1225	16.5	0.10	-22.89	Sh1	l
U1225	17	0.21	-19.76	Sh1	l
U1225	17.5	0.24	-21.09	Sh1	l
U1225	18	-2.18	-14.65	Sh1	l
U1225	18.5	-2.60	-7.36	Sh1	l
U1225	19	-1.83	-9.70	Sh1	l
U1225	19.5	-2.15	-8.25	Sh1	l
U1225	20.5	-2.53	-8.95	Sh1	l
U1225	21	-2.37	-9.87	Sh1	l
U1225	21.5	-1.36	-12.30	Sh1	l

U1225	22	-1.58	-16.78	Sh1	1
U1225	22.5	-2.46	-8.82	Sh1	1
U1225	23	-2.13	-8.62	Sh1	1
U1225	23.5	-2.01	-9.25	Sh1	1
U1225	24	-1.53	-9.36	Sh1	1
U1225	24.5	-2.13	-8.46	Sh1	1
U1225	25	0.10	-19.72	Sh1	1
U1225	25.5	0.39	-21.23	Sh1	1
U1225	26	-0.56	-18.48	Sh1	1
U1225	26.5	-2.07	-11.07	Sh1	1
U1225	27.5	-1.89	-8.48	Sh1	1
U1225	28	-2.44	-7.92	Sh1	1
U1225	28.5	-2.50	-8.12	Sh1	1
U1225	29	-2.40	-8.69	Sh1	1
U1225	30	-2.56	-8.25	Sh1	1
U1225	30.5	-2.46	-7.90	Sh1	1
U1225	31	-2.64	-7.73	Sh1	1
U1225	31.5	-3.17	-10.28	Sh1	1
U1225	32	-2.59	-7.46	Sh1	1
U1225	32.5	-1.20	-15.35	Sh1	1
U1225	33	-1.49	-16.28	Sh1	1
U1225	33.5	-2.38	-10.08	Sh1	1
U1225	34.5	-2.42	-13.23	Sh1	1
U1225	35	-2.77	-9.85	Sh1	1
U1225	35.5	-3.01	-14.38	Sh1	1
U1225	36	-3.14	-11.53	Sh1	1
U1225	36.5	-2.82	-8.98	Sh1	1
U1225	37	-2.78	-10.77	Sh1	1
U1225	40.5	-2.61	-17.60	Sh1	1
U1225	61.5	-0.92	-28.98	Sh1	1
U1225	62.5	-1.10	-27.86	Sh1	1
U1225	63.5	-0.89	-30.72	Sh1	1
U1225	64.5	-1.02	-29.76	Sh1	1
U1225	65.5	-0.84	-12.99	Sh1	1
U1225	67	-0.40	-10.04	Sh1	1
U1225	68	-0.54	-26.80	Sh1	1
U1225	69	-0.68	-15.50	Sh1	1
U1225	70	-0.63	-29.09	Sh1	1
U1225	71	-0.58	-21.23	Sh1	1
U1225	72	-0.37	-27.68	Sh1	1
U1225	74	-1.21	-28.16	Sh1	1
U1225	75	-0.60	-20.92	Sh1	1
U1225	76	-0.54	-21.13	Sh1	1
U1225	77.5	-0.37	-20.12	Sh1	1
U1225	78.5	-0.51	-9.70	Sh1	1
U1225	79.5	-1.33	-29.69	Sh1	1
U1225	80.5	-0.90	-17.44	Sh1	1
U1225	81.5	-0.09	-20.92	Sh1	1

U1225	82.5	-0.20	-19.43	Sh1	l
U1225	84.5	-0.52	-27.40	Sh1	l
U1225	86.5	-0.09	-19.01	Sh1	l
U1225	88.5	0.49	-10.25	Sh1	l
U1225	89.5	0.33	-9.35	Sh1	l
U1225	90.5	1.30	-16.08	Sh1	l
U1225	91.5	0.54	-10.07	Sh1	l
U1225	92.5	0.14	-12.43	Sh1	l
U1225	93.5	0.44	-11.29	Sh1	l
U1225	95.5	0.59	-15.84	Sh1	l
U1225	96.5	1.21	-12.99	Sh1	l
U1225	97.5	-0.25	-12.69	Sh1	l
U1225	98.5	0.82	-12.19	Sh1	l
U1225	99.5	0.38	-14.07	Sh1	l
U1225	100.5	-0.45	-13.68	Sh1	l
U1225	101.5	0.29	-12.65	Sh1	l
U1225	103	0.14	-15.13	Sh1	l
U1225	104	0.17	-14.77	Sh1	l
U1225	105	0.17	-19.63	Sh1	l
U1225	106	2.92	-13.36	Sh1	l
U1225	107	2.50	-9.91	Sh1	l
U1225	108	0.63	-14.57	Sh1	l
U1225	109	1.07	-13.02	Sh1	l
U1225	110	0.61	-11.17	Sh1	l
U1225	111	0.46	-10.98	Sh1	l
U1225	112	0.30	-11.82	Sh1	l
U1225	113	0.35	-7.88	Sh1	l
U1225	114	0.69	-13.21	Sh1	l
U1225	115	1.30	-13.01	Sh1	l
U1225	116	1.16	-14.76	Sh1	l
U1225	117	0.99	-9.20	Sh1	l
U1225	118	0.98	-17.89	Sh1	l
U1225	119	0.23	-14.08	Sh1	l
U1225	120	1.72	-20.12	Sh1	l
U1225	121	3.12	-14.56	Sh1	l
U1225	123	4.65	-6.84	Sh1	d

Tsagaan Gorge W. **N46 49.46'** **E95 48.14'**

Section	**height**	**δ^{13}Ccarb**	**δ^{18}Ocarb**	**Unit**	**Lithology**
U1235	79	6.31	-6.51	Sh3-4	l
U1235	80	6.72	-9.38	Sh3-4	l
U1235	81	6.41	-8.27	Sh3-4	l
U1235	82	5.63	-8.67	Sh3-4	l
U1235	83	5.27	-9.08	Sh3-4	l
U1235	85	5.62	-8.79	Sh3-4	l
U1235	86	3.49	-9.50	Sh3-4	l
U1235	87	6.03	-8.44	Sh3-4	l
U1235	89	2.93	-7.88	Sh3-4	l

U1235	90	6.16	-8.80	Sh3-4	l
U1235	91	6.05	-7.64	Sh3-4	l
U1235	93	5.52	-8.46	Sh3-4	l
U1235	94	7.40	-7.50	Sh3-4	l
U1235	104	7.98	-7.15	Sh3-4	l
U1235	105	6.95	-6.92	Sh3-4	l
U1235	106	7.24	-7.28	Sh3-4	l
U1235	107	4.38	-6.15	Sh3-4	l
U1235	109	4.98	-6.19	Sh3-4	l
U1235	110	7.21	-6.81	Sh3-4	l
U1235	111	7.64	-6.70	Sh3-4	l
U1235	112	7.14	-7.04	Sh3-4	l
U1235	113	5.80	-6.40	Sh3-4	l
U1235	114	6.76	-6.64	Sh3-4	l
U1235	115	7.30	-6.88	Sh3-4	l
U1235	116	7.57	-7.37	Sh3-4	l
U1235	117	4.26	-6.88	Sh3-4	l
U1235	118	4.15	-8.07	Sh3-4	l
U1235	119	1.92	-16.90	Sh3-4	l
U1235	143	5.80	-8.52	Sh3-4	l
U1235	144	4.82	-7.36	Sh3-4	l
U1235	145	5.24	-8.13	Sh3-4	l

Shuurgat Range **N46 47.76'** **E96 11.45'**

Section	**height**	**δ^{13}Ccarb**	**δ^{18}Ocarb**	**Unit**	**Lithology**
U1240	0	3.22	-5.08	Sh2	d
U1240	1	3.12	-4.60	Sh2	d
U1240	2	3.03	-4.45	Sh2	d
U1240	3	2.71	-4.60	Sh2	d
U1240	4	3.15	-4.26	Sh2	d
U1240	5	3.24	-4.64	Sh2	d
U1240	6	3.33	-3.93	Sh2	d
U1240	7	3.07	-3.92	Sh2	d
U1240	8	3.55	-2.74	Sh2	d
U1240	9	2.36	-7.43	Sh2	d
U1240	10	3.09	-3.98	Sh2	d
U1240	11	3.58	-1.06	Sh2	d
U1240	12	3.24	-1.03	Sh2	d
U1240	13	2.38	-4.81	Sh2	d
U1240	14	2.52	-5.90	Sh2	d
U1240	15	3.36	-2.60	Sh2	d
U1240	16	3.53	-3.35	Sh2	d
U1240	17	3.26	-3.40	Sh2	d
U1240	18	3.44	-2.87	Sh2	d
U1240	19	3.05	-4.72	Sh2	d
U1240	20	3.19	-3.56	Sh2	d
U1240	21	3.49	-2.68	Sh2	d
U1240	22	2.89	-3.21	Sh2	d

U1240	23	2.77	-5.16	Sh2	d
U1240	24	3.18	-5.63	Sh2	d
U1240	25	2.54	-5.85	Sh2	d
U1240	26	2.75	-5.97	Sh2	d
U1240	27	2.88	-3.57	Sh2	d
U1240	28	2.99	-6.41	Sh2	d
U1240	29	2.49	-9.47	Sh2	d
U1240	30	3.00	-5.11	Sh2	d
U1240	31	2.81	-7.03	Sh2	d
U1240	32	2.99	-4.91	Sh2	d
U1240	33	2.34	-8.59	Sh2	d
U1240	34	2.54	-9.78	Sh2	d
U1240	35	3.03	-5.43	Sh2	d
U1240	36	2.98	-6.07	Sh2	d
U1240	37	2.71	-9.70	Sh2	d
U1240	38	3.24	-5.64	Sh2	d
U1240	39	2.78	-5.27	Sh2	d
U1240	40	2.61	-7.72	Sh2	d
U1240	41	2.34	-2.54	Sh2	d
U1240	42	2.79	-5.65	Sh2	d
U1240	43	3.22	-6.37	Sh2	d
U1240	44	3.14	-4.85	Sh2	d
U1240	45	2.88	-3.99	Sh2	d
U1240	46	3.04	-2.09	Sh2	d
U1240	47	2.93	-2.65	Sh2	d
U1240	48	2.57	-7.11	Sh2	d
U1240	49	2.73	-7.33	Sh2	d
U1240	50	2.98	-7.07	Sh2	d
U1240	51	2.55	-5.58	Sh2	d
U1240	52	2.72	-7.02	Sh2	d
U1240	53	2.37	-4.16	Sh2	d
U1240	54	2.80	-5.11	Sh2	d
U1240	56	2.94	-5.29	Sh2	d
U1240	57	4.15	-5.58	Sh2	d
U1240	58	4.02	-3.66	Sh2	d
U1240	59	4.45	-4.56	Sh2	d
U1240	60	3.87	-1.34	Sh2	d
U1240	61	3.76	0.02	Sh2	d
U1240	62	3.92	-1.41	Sh2	d
U1240	63	4.99	-1.21	Sh2	d
U1240	64	4.93	-2.02	Sh2	d
U1240	65	4.67	-2.49	Sh2	d
U1240	66	4.46	-1.47	Sh2	d
U1240	67	4.78	-0.92	Sh2	d
U1240	68	4.79	-1.07	Sh2	d
U1240	69	4.82	-1.12	Sh2	d
U1240	70	4.97	-0.74	Sh2	d
U1240	71	4.75	-0.84	Sh2	d

U1240	72	4.88	-0.57	Sh2	d
U1240	73	4.28	-1.68	Sh2	d
U1240	74	4.53	-3.24	Sh2	d
U1240	75	4.49	-0.94	Sh2	d
U1240	76	4.41	-3.04	Sh2	d
U1240	77	3.85	-1.60	Sh2	d
U1240	78	4.37	-0.97	Sh2	d
U1240	79	4.28	-2.69	Sh2	d
U1240	80	4.82	-1.45	Sh2	d
U1240	81	4.48	-1.17	Sh2	d
U1240	82	3.27	-1.74	Sh2	d
U1240	83	5.09	-1.16	Sh2	d
U1240	84	4.29	-0.90	Sh2	d
U1240	85	4.45	-1.35	Sh2	d
U1240	86	4.27	-1.20	Sh2	d
U1240	87	4.48	-0.89	Sh2	d
U1240	88	4.13	-2.14	Sh2	d
U1240	89	4.69	-1.32	Sh2	d
U1240	90	4.21	-1.81	Sh2	d
U1240	91	3.66	-2.06	Sh2	d
U1240	92	3.53	-5.14	Sh2	d
U1240	93	2.82	-4.45	Sh2	d
U1240	94	2.95	-3.69	Sh2	d
U1240	95	1.77	-1.41	Sh2	d
U1240	96	2.86	-4.93	Sh2	d
U1240	97	2.78	-4.83	Sh2	d
U1240	98	2.62	-5.06	Sh2	d
U1240	99	1.93	-1.86	Sh2	d
U1240	100	2.01	-4.05	Sh2	d
U1240	101	3.00	-0.21	Sh2	d
U1240	105	2.16	-3.20	Sh2	d
U1240	106	2.95	-0.65	Sh2	d
U1240	108	3.23	-1.01	Sh2	d
U1240	109	4.00	-0.34	Sh2	d
U1240	110	2.71	-0.81	Sh2	d
U1240	111	2.93	-4.42	Sh2	d
U1240	112	2.65	-3.67	Sh2	d
U1240	113	2.69	-1.30	Sh2	d
U1240	114	2.07	-4.43	Sh2	d
U1240	115	3.19	-1.03	Sh2	d
U1240	116	2.17	-2.45	Sh2	d
U1240	117	2.55	-0.70	Sh2	d
U1240	118	1.38	-4.24	Sh2	d
U1240	119	3.95	-0.06	Sh2	d
U1240	120	4.57	-1.19	Sh2	d
U1240	121	1.31	-0.69	Sh2	d
U1240	122	3.84	-5.12	Sh2	d
U1240	123	1.98	-6.21	Sh2	d

U1240	124	1.43	-0.28	Sh2	d
U1240	125	3.83	-0.73	Sh2	d
U1240	126	2.15	-0.92	Sh2	d
U1240	127	3.33	-0.86	Sh2	d
U1240	128	1.42	-1.10	Sh2	d
U1240	129	2.06	-1.25	Sh2	d
U1240	130	1.95	-1.65	Sh2	d
U1240	131	3.01	-0.75	Sh2	d
U1240	132	3.23	-4.48	Sh2	d
U1240	133	2.15	-5.67	Sh2	d
U1240	134	2.50	-5.35	Sh2	d
U1240	135	2.30	-2.35	Sh2	d
U1240	136	2.83	-5.29	Sh2	d
U1240	137	2.34	-4.24	Sh2	d
U1240	138	2.80	0.22	Sh2	d
U1240	139	2.80	-2.90	Sh2	d
U1240	140	4.60	-1.20	Sh2	d
U1240	141	3.81	-1.51	Sh2	d
U1240	142	2.01	-1.89	Sh2	d
U1240	143	0.41	-2.93	Sh2	d
U1240	144	4.42	-0.67	Sh2	d
U1240	145	2.70	0.46	Sh2	d
U1240	146	2.85	-1.29	Sh2	d
U1240	147	3.33	-0.57	Sh2	d
U1240	148	4.31	-0.38	Sh2	d
U1240	149	3.42	-0.19	Sh2	d
U1240	150	2.72	-0.87	Sh2	d
U1240	151	2.78	-1.42	Sh2	d
U1240	152	4.20	-0.41	Sh2	d
U1240	153	0.23	-0.84	Sh2	d
U1240	154	2.57	-1.77	Sh2	d
U1240	155	2.21	-6.16	Sh2	d
U1240	155	2.17	-6.21	Sh2	d
U1240	156	2.06	-1.09	Sh2	d
U1240	157	3.31	0.26	Sh2	d
U1240	158	3.12	-4.58	Sh2	d
U1240	159	2.95	-2.50	Sh2	d
U1240	160	4.43	-0.40	Sh2	d
U1240	161	-0.11	-0.49	Sh2	d
U1240	162	-1.30	-6.82	Sh2	d
U1240	163	2.54	-5.01	Sh3	d
U1240	164	3.50	-1.89	Sh3	d
U1240	165	3.36	-5.05	Sh3	d
U1240	166	2.80	-1.46	Sh3	d
U1240	167	3.69	0.37	Sh3	d
U1240	168	1.57	-0.26	Sh3	d
U1240	169	3.65	-0.90	Sh3	d
U1240	170	3.22	-1.37	Sh3	d

U1240	171	3.06	-0.98	Sh3	d
U1240	172	3.22	-1.13	Sh3	d
U1240	173	2.64	-0.23	Sh3	d
U1240	174	2.74	-1.75	Sh3	d
U1240	175	3.62	-1.32	Sh3	d
U1240	176	3.67	-0.75	Sh3	d
U1240	177	3.49	-0.24	Sh3	d
U1240	178	3.69	-0.82	Sh3	d
U1240	179	3.42	-0.49	Sh3	d
U1240	180	3.48	-0.62	Sh3	d
U1240	181	3.62	-0.39	Sh3	d
U1240	182	3.86	-0.47	Sh3	d
U1240	183	2.87	-2.52	Sh3	d
U1240	184	3.62	-2.95	Sh3	d
U1240	185	3.31	-0.73	Sh3	d
U1240	186	3.66	-0.63	Sh3	d
U1240	187	4.07	-0.47	Sh3	d
U1240	188	3.60	-1.19	Sh3	d
U1240	189	4.12	-0.50	Sh3	d
U1240	190	3.64	-1.66	Sh3	d
U1240	191	3.90	-1.72	Sh3	d
U1240	192	3.86	-2.45	Sh3	d
U1240	195	4.01	-1.88	Sh3	d
U1240	196	3.73	-2.30	Sh3	d
U1240	197	3.99	-2.11	Sh3	d
U1240	198	4.28	-1.31	Sh3	d
U1240	199	4.55	-1.70	Sh3	d
U1240	200	4.97	-1.08	Sh3	d
U1240	201	4.55	-2.08	Sh3	d
U1240	202	4.32	-1.89	Sh3	d
U1240	203	4.15	-1.33	Sh3	d
U1240	204	4.63	-1.77	Sh3	d
U1240	205	4.30	-2.10	Sh3	d
U1240	206	4.37	-1.23	Sh3	d
U1240	207	4.26	-2.69	Sh3	d
U1240	208	4.10	-2.74	Sh3	d
U1240	209	4.83	-1.62	Sh3	d
U1240	210	4.29	-1.10	Sh3	d
U1240	211	4.23	-2.97	Sh3	d
U1240	212	2.99	-0.75	Sh3	d
U1240	213	4.13	-2.93	Sh3	d
U1240	214	2.54	-0.12	Sh3	d
U1240	217	3.73	-0.81	Sh3	d
U1240	218	3.34	-0.80	Sh3	d
U1240	219	3.51	-0.93	Sh3	d
U1240	220	3.99	-3.29	Sh3	d
U1240	221	2.97	-1.69	Sh3	d
U1240	222	3.75	-1.57	Sh3	d

U1240	224	4.14	-2.70	Sh3	d
U1240	225	4.11	-1.30	Sh3	d
U1240	227	4.19	-0.14	Sh3	d
U1240	228	4.43	-0.44	Sh3	d
U1240	229	4.16	-1.03	Sh3	d
U1240	230	4.42	-1.23	Sh3	d
U1240	240	3.66	-1.59	Sh3	d
U1240	232	3.59	-1.71	Sh3	d
U1240	233	4.12	0.28	Sh3	d
U1240	234	3.98	-0.40	Sh3	d
U1240	235	3.56	-1.63	Sh3	d
U1240	236	4.01	-0.90	Sh3	d
U1240	237	3.85	0.11	Sh3	d
U1240	238	2.85	0.12	Sh3	d
U1240	239	4.08	-1.11	Sh3	d
U1240	240	4.43	-1.21	Sh3	d
U1240	241	4.38	-1.71	Sh3	d
U1240	242	4.59	-2.11	Sh3	d
U1240	243	3.67	-1.23	Sh3	d
U1240	244	4.47	-0.97	Sh3	d
U1240	245	3.25	-1.00	Sh3	d
U1240	246	4.47	-0.77	Sh3	d
U1240	247	3.47	-0.81	Sh3	d
U1240	248	3.90	-0.73	Sh3	d
U1240	249	3.84	-0.67	Sh3	d
U1240	250	3.74	-0.80	Sh3	d
U1240	251	4.40	-1.04	Sh3	d
U1240	252	0.75	0.08	Sh4	d
U1240	253	1.04	-0.08	Sh4	d
U1240	254	1.05	0.41	Sh4	d
U1240	255	1.24	0.25	Sh4	d
U1240	256	0.63	-0.03	Sh4	d
U1240	257	1.80	-0.20	Sh4	d
U1240	258	1.24	0.00	Sh4	d
U1240	259	0.72	0.32	Sh4	d
U1240	260	-0.08	-0.10	Sh4	d
U1240	261	0.47	-0.69	Sh4	d

Khevtee Tsakhir Range **N 46 39.046'** **E 96 51.69'**

Section	**height**	**δ^{13}Ccarb**	**δ^{18}Ocarb**	**Unit**	**Lithology**
F1208	1	4.24	-4.81	Sh2	d
F1208	20	3.86	-4.73	Sh2	d
F1208	41	5.16	-6.23	Sh2	d
F1208	60	3.84	-3.92	Sh2	d
F1208	80	1.77	-0.63	Sh3	d
F1208	104	3.40	-4.85	Sh3	d
F1208	120	4.17	-1.32	Sh3	d
F1208	140	3.34	-3.92	Sh3	d

F1208	150	5.11	-4.88	Sh3	d
F1208	160	3.69	-0.63	Sh3	d
F1208	170	4.83	-1.20	Sh3	d
F1208	170	4.77	-1.22	Sh3	d
F1208	180	4.79	-4.21	Sh3	d
F1208	190	2.86	-1.15	Sh3	d
F1208	198	4.25	-1.20	Sh3	d
F1208	210	3.55	-0.59	Sh3	d
F1208	220	3.16	-0.49	Sh3	d
F1208	230	2.59	-1.02	Sh4	d
F1208	240	2.80	-0.39	Sh4	d
F1208	250	2.70	-1.33	Sh4	d
F1208	260	2.86	-3.14	Sh4	d
F1208	270	3.27	-2.38	Sh4	d
F1208	286	0.69	-0.54	Sh4	d
F1208	296	2.51	-2.06	Sh4	d
F1208	300	2.81	-1.10	Sh4	d
F1208	304	3.54	-1.76	Sh4	d
F1208	308	3.74	-1.27	Sh4	d
F1208	312	2.59	-2.66	Sh4	d
F1208	316	1.90	-3.09	Sh4	d
F1208	320	2.15	-2.30	Sh4	d
F1208	324	1.71	-3.03	Sh4	d
F1208	328	1.13	-2.30	Sh4	d
F1208	332	1.57	-1.09	Sh4	d
F1208	336	1.88	-1.51	Sh4	d
F1208	340	2.16	-2.14	Sh4	d
F1208	344	2.70	-1.19	Sh4	d
F1208	348	2.97	-0.31	Sh4	d
F1208	352	2.53	0.44	Sh4	d
F1208	356	2.23	0.14	Sh4	d
F1208	360	1.03	-1.40	Sh4	d
F1208	364	1.38	-2.72	Sh4	d
F1208	372	2.34	0.31	Sh4	d
F1208	374	2.42	-3.98	Sh4	d
F1208	376	1.98	-2.05	Sh4	d
F1208	380	2.49	-4.49	Sh4	d
F1208	384	1.74	-3.60	Sh4	d
F1208	388	0.52	-0.46	ZA	d
F1208	389	1.16	-1.76	ZA	d
F1208	392	-0.06	-0.36	ZA	d
F1208	396	0.02	-1.38	ZA	d
F1208	398	0.47	-1.77	ZA	d
F1208	406	-0.59	-1.78	ZA	d
F1208	414	0.23	-1.74	ZA	d
F1208	418	0.77	-2.12	ZA	d
F1208	432	0.72	-2.68	ZA	d

Orlogo Gorge	N46 47.39'	E95 37.94'			
Section	**height**	**δ^{13}Ccarb**	**δ^{18}Ocarb**	**Unit**	**Lithology**
U1202	111	1.03	-6.49	Ol	d
U1202	111.2	1.49	-6.06	Ol	d
U1202	111.4	1.40	-6.90	Ol	d
U1202	111.6	1.72	-6.00	Ol	d
U1202	111.8	2.07	-5.73	Ol	d
U1202	112	2.31	-5.61	Ol	d
U1202	112.2	2.02	-5.69	Ol	d
U1202	112.4	2.23	-5.31	Ol	d
U1202	112.6	2.20	-5.49	Ol	d
U1202	112.8	2.01	-5.52	Ol	d
U1202	113	2.43	-5.86	Ol	d
U1202	113.2	2.00	-4.72	Ol	d
U1202	113.4	2.28	-5.94	Ol	d
U1202	113.6	2.30	-6.25	Ol	d
U1202	113.8	2.50	-5.82	Ol	d
U1202	114	2.48	-6.35	Ol	d
U1202	116	2.33	-5.35	Ol	d
U1202	116.2	2.33	-4.08	Ol	d
U1202	116.4	2.61	-3.40	Ol	d
U1202	116.6	2.51	-2.92	Ol	d
U1202	116.8	2.76	-3.68	Ol	d
U1202	117	4.61	-4.84	Ol	d
U1202	117.2	2.54	-4.61	Ol	d
U1202	117.4	4.23	-4.01	Ol	d
U1202	117.6	3.78	-4.30	Ol	d
U1202	117.8	2.72	-3.07	Ol	d
U1202	118	3.23	-4.80	Ol	d
U1202	118.2	2.72	-4.03	Ol	d
U1202	118.4	2.91	-5.48	Ol	d
U1202	118.6	2.07	-4.39	Ol	d
U1202	118.8	3.03	-5.88	Ol	d
U1202	119	0.61	-4.77	Ol	d
U1202	119.2	2.69	-5.43	Ol	d
U1202	119.4	2.40	-4.16	Ol	d
U1202	119.6	3.83	-4.73	Ol	d
U1202	119.8	4.15	-3.96	Ol	d
U1202	120	2.39	-2.45	Ol	d
U1202	120.2	2.40	-4.49	Ol	d

Orlogo Gorge	N46 47.43'	E95 38.91'			
Section	**height**	**δ^{13}Ccarb**	**δ^{18}Ocarb**	**Unit**	**Lithology**
U1201	0	-3.47	-18.66	T1	l
U1201	1	-1.34	-15.92	T1	l
U1201	2	-0.82	-14.75	T1	l
U1201	3.8	-0.48	-14.46	T1	l
U1201	5	-0.87	-15.07	T1	l

U1201	6.1	-0.55	-10.93	T1	l
U1201	7.2	-0.16	-7.08	T1	l
U1201	8	-0.25	-8.44	T1	l

Zuun-Arts Mountain	**N46 14.243'**	**E96 29.243'**			
Section	**height**	**δ^{13}Ccarb**	**δ^{18}Ocarb**	**Unit**	**Lithology**
U1329	0	3.22	-2.18	T3	d
U1329	2	4.26	-1.71	T3	d
U1329	4	3.41	-3.12	T3	d
U1329	8	3.27	-3.76	T3	d
U1329	10	3.25	-3.79	T3	d
U1329	12	3.17	-3.41	T3	d
U1329	14	2.73	-4.04	T3	d
U1329	16	1.72	-4.86	T3	d
U1329	18	1.89	-5.05	T3	d
U1329	20	2.07	-3.01	T3	d
U1329	22	2.22	-3.03	T3	d
U1329	24	2.50	-2.82	T3	d
U1329	26	2.73	-2.83	T3	d
U1329	28	1.81	-4.21	T3	d
U1329	30	1.00	-4.63	T3	d
U1329	32	1.32	-2.72	T3	d
U1329	34	3.92	-3.64	T3	d
U1329	36	4.21	-3.02	T3	d
U1329	38	4.38	-3.39	T3	d
U1329	40	4.02	-3.28	T3	d
U1329	42	3.88	-2.83	T3	d
U1329	48	3.31	-2.83	T3	d
U1329	50	2.70	-5.45	T3	d
U1329	52	3.88	-4.65	T3	d
U1329	54	2.83	-3.48	T3	d
U1329	56	2.81	-3.42	T3	d
U1329	72	0.18	-20.45	T3	d
U1329	74	1.04	-3.96	T3	d
U1329	76	1.06	-4.42	T3	d
U1329	80	0.45	-4.33	T3	d
U1329	82	1.04	-3.13	T3	d
U1329	84	0.85	-5.41	T3	d
U1329	86	0.43	-6.27	T3	d
U1329	88	2.55	-3.50	T3	d
U1329	90	3.85	-1.72	T3	d
U1329	92	3.48	-2.91	T3	d
U1329	94	3.87	-4.27	T3	d
U1329	96	1.29	-3.02	T3	d
U1329	98	1.50	-6.64	T3	d
U1329	100	2.25	-3.23	T3	d
U1329	102	3.10	-4.21	T4	d
U1329	104	3.41	-3.57	T4	d

U1329	106	3.55	-2.17	T4	d
U1329	108	1.96	-5.23	T4	d
U1329	110	2.39	-3.55	T4	d
U1329	112	3.10	-3.48	T4	d
U1329	114	3.26	-3.22	T4	d
U1329	116	2.71	-1.73	T4	d
U1329	118	2.48	-2.05	T4	d
U1329	120	3.14	-2.15	T4	d
U1329	122	0.70	-2.44	T4	d
U1329	124	2.52	-1.96	T4	d
U1329	126	3.28	-1.56	T4	d
U1329	128	2.50	-3.59	T4	d
U1329	130	2.69	-3.02	T4	d
U1329	132	1.98	-5.09	T4	d
U1329	134	1.82	-6.02	T4	d
U1329	136	0.79	-7.69	T4	d
U1329	138	0.01	-6.01	T4	d
U1329	140	-0.31	-3.12	T4	d
U1329	142	0.47	-5.67	T4	d
U1329	144	-0.05	-7.34	T4	d
U1329	146	-1.15	-7.15	T4	d
U1329	148	-1.56	-2.33	T4	d
U1329	150	-0.68	-4.37	T4	d
U1329	152	-1.59	-4.08	T4	d
U1329	154	-0.52	-8.64	T4	d
U1329	156	-1.63	-11.43	T4	d
U1329	160	-2.26	-9.48	T4	d
U1329	162	-2.35	-15.22	T4	d
U1329	164	-2.88	-6.73	T4	d
U1329	166	-1.22	-4.80	T4	d

Ikh Goliin Tsakhir **N47 02.61'** **E95 08.32'**

Section	**height**	**δ^{13}Ccarb**	**δ^{18}Ocarb**	**Unit**	**Lithology**
U1432	0	-3.93	-12.78	T1	l
U1432	1	-2.36	-12.01	T1	l
U1432	2	-1.17	-11.01	T1	l
U1432	3	-1.45	-11.49	T1	l
U1432	4	-1.35	-14.73	T1	l
U1432	5	-0.76	-11.82	T1	l
U1432	6	-1.54	-14.20	T1	l
U1432	7	-1.35	-9.90	T1	l
U1432	8	-1.52	-8.94	T1	l
U1432	9	0.38	-3.92	T1	l
U1432	10	2.41	-4.58	T1	l
U1432	11	0.84	-6.35	T1	l
U1432	12	3.64	-3.22	T1	l
U1432	13	4.63	-1.74	T1	l
U1432	14	3.88	-0.24	T1	l

U1432	15	1.42	-4.75	T1	1
U1432	16	2.00	-7.39	T1	1
U1432	17	2.57	-7.69	T1	1
U1432	18	-2.73	-11.61	T1	1
U1432	18.9	0.86	-7.94	T1	1
U1432	22	4.59	-5.42	T1	1
U1432	23.5	7.92	-2.19	T2	1
U1432	25	8.24	-4.90	T2	1
U1432	26	3.08	-8.40	T2	1
U1432	27	4.31	-7.26	T2	1
U1432	28	5.73	-5.34	T2	1
U1432	29	5.91	-7.58	T2	1
U1432	30	6.41	-5.29	T2	1
U1432	31	7.81	-3.30	T2	1
U1432	33	7.19	-4.43	T2	1
U1432	34	6.56	-3.92	T2	1
U1432	35	5.99	-4.88	T2	1
U1432	36	7.48	-4.01	T2	1
U1432	37	7.79	-5.62	T2	1
U1432	38	4.88	-6.70	T2	1
U1432	39	4.26	-7.32	T2	1
U1432	40	7.56	-6.96	T2	1
U1432	41	6.80	-7.52	T2	1
U1432	42	5.54	-7.25	T2	1
U1432	43	5.08	-6.44	T2	1
U1432	44	4.75	-6.78	T2	1
U1432	45	2.72	-6.61	T2	1
U1432	46	2.43	-6.05	T2	1
U1432	47	2.73	-6.49	T2	1
U1432	49	-0.63	-7.07	T3	1
U1432	50	-0.36	-6.55	T3	1
U1432	51	-0.46	-8.30	T3	1
U1432	53	1.61	-9.31	T3	1
U1432	54	2.22	-11.97	T3	1
U1432	55	2.37	-7.82	T3	1
U1432	56	2.65	-9.68	T3	1
U1432	57	3.22	-15.03	T3	1
U1432	58	3.65	-11.65	T3	1
U1432	59	3.61	-12.81	T3	1
U1432	60	4.25	-6.58	T3	1
U1432	61	4.26	-8.90	T3	1
U1432	62	6.91	-7.40	T3	1
U1432	63	4.34	-16.94	T3	1
U1432	64	6.05	-12.65	T3	1
U1432	65	8.29	-8.46	T3	1
U1432	66	7.71	-15.52	T3	1
U1432	67	6.76	-7.25	T3	1
U1432	68	8.14	-11.28	T3	1

U1432	69	5.73	-10.97	T3	l
U1432	70	8.66	-4.60	T3	l
U1432	71	8.99	-6.48	T3	l
U1432	72	9.06	-3.59	T3	l
U1432	73	9.36	-4.60	T3	l
U1432	74	9.15	-4.92	T3	l
U1432	75	9.20	-4.08	T3	l
U1432	76	7.52	-10.64	T3	l
U1432	77	8.67	-7.84	T3	l
U1432	78	7.37	-8.43	T3	l
U1432	79	6.16	-8.82	T3	l
U1432	80	8.89	-5.38	T3	l
U1432	81	7.15	-8.67	T3	l
U1432	82	8.63	-4.21	T3	l
U1432	83	7.22	-8.48	T3	l
U1432	84	9.09	-6.32	T3	l
U1432	85	9.05	-8.36	T3	l
U1432	86	8.80	-7.90	T3	l

Ikh Goliin Tsakhir **N47 0.96'** **E95 09.45'**

Section	**height**	**δ^{13}Ccarb**	**δ^{18}Ocarb**	**Unit**	**Lithology**
U1436	0	4.77	-3.27	T4	d
U1436	4	4.53	-5.42	T4	d
U1436	8	4.86	-2.61	T4	d
U1436	12	4.61	-2.44	T4	d
U1436	16	4.94	-2.27	T4	d
U1436	20	4.46	-5.18	T4	d
U1436	24	5.14	-6.22	T4	d
U1436	28	5.22	-2.74	T4	d
U1436	32	5.34	-4.38	T4	d
U1436	36	4.80	-7.25	T4	d
U1436	40	5.51	-5.30	T4	d
U1436	44	5.79	-6.23	T4	d
U1436	48	5.76	-6.50	T4	d
U1436	52	5.31	-7.43	T4	d
U1436	56	6.43	-2.85	T4	d
U1436	60	5.41	-6.83	T4	d
U1436	64	5.83	-5.20	T4	d
U1436	68	5.52	-6.72	T4	d
U1436	72	5.39	-6.01	T4	d

Khukh Davaa S. **N 47 1.755'** **E 95 25.582'**

Section	**height**	**δ^{13}Ccarb**	**δ^{18}Ocarb**	**Unit**	**Lithology**
F1125	4	-1.09	-14.77	T1	l
F1125	5	1.08	0.48	T1	l
F1125	5.5	4.10	-1.47	T1	l
F1125	6	1.85	-0.10	T1	l
F1125	6.5	2.94	0.15	T1	l

F1125	7	3.15	-1.22	T1	l
F1125	7.5	3.26	-0.08	T1	l
F1125	8.1	5.63	0.25	T1	l
F1125	8.5	3.85	-1.23	T1	l
F1125	9.5	5.21	-1.13	T1	l
F1125	10	5.49	2.10	T1	l
F1125	10.5	4.68	-2.15	T1	l
F1125	11	5.58	-0.95	T2	l
F1125	29.5	5.23	-4.13	T2	l
F1125	30.7	5.18	-7.11	T2	l
F1125	31.7	6.82	-14.01	T2	l
F1125	34	6.29	-11.52	T2	l
F1125	36	5.70	-14.89	T2	l
F1125	38	5.90	-6.05	T2	l
F1125	40	4.76	-8.02	T2	l
F1125	41	5.54	-5.52	T2	l
F1125	42	5.64	-11.88	T2	l
F1125	44	5.19	-14.84	T2	l
F1125	44.5	2.25	-1.57	T2	l
F1125	46	5.81	-6.22	T2	l
F1125	47	6.03	-15.96	T2	l
F1125	48.5	6.48	-9.31	T2	l
F1125	48.6	6.12	-9.03	T2	l
F1125	50	7.16	-13.51	T2	l
F1125	51	7.39	-14.09	T2	l
F1125	52	7.24	-11.36	T2	l
F1125	52.5	5.97	-9.75	T2	l
F1125	53.5	8.31	-15.40	T2	l
F1125	54.5	6.32	-10.01	T2	l
F1125	55	6.51	-12.84	T2	l
F1125	56.3	6.45	-8.77	T2	l
F1125	57	4.28	-15.69	T2	l
F1125	58	7.49	-9.15	T2	l
F1125	59.4	6.62	-9.16	T2	l
F1125	60.5	7.49	-8.12	T2	l
F1125	62	7.58	-8.98	T2	l
F1125	63	7.70	-18.28	T2	l
F1125	64	7.19	-11.13	T2	l
F1125	65	4.82	-17.63	T2	l
F1125	66	7.93	-5.70	T2	l
F1125	67	5.37	-5.42	T2	l
F1125	68	8.74	-3.57	T2	l
F1125	69	9.30	-5.28	T2	l

Unkheltseg **N47 12.31'** **E95 13.24'**

Section	**height**	**δ^{13}Ccarb**	**δ^{18}Ocarb**	**Unit**	**Lithology**
U1426	0	4.45	-0.33	T1	l
U1426	1	-3.54	-19.37	T1	l

U1426	2	-0.75	-11.44	T1	l
U1426	3	-1.16	-12.80	T1	l
U1426	4	-0.67	-7.70	T1	l
U1426	5	-0.60	-10.61	T1	l
U1426	6.5	-0.59	-12.11	T1	l
U1426	7.5	-0.44	-11.90	T1	l
U1426	8.5	-0.62	-12.41	T1	l
U1426	9.5	-0.34	-13.42	T1	l
U1426	10.5	-1.90	-11.64	T1	l
U1426	11.5	-1.04	-11.75	T1	l
U1426	13.1	-1.51	-10.26	T1	l
U1426	14	-2.06	-9.52	T1	l
U1426	18	2.27	-11.07	T2	d
U1426	19	4.40	-0.09	T2	d
U1426	28	2.90	-10.46	T2	l
U1426	29	2.80	-11.39	T2	l
U1426	30	1.61	-10.49	T2	l
U1426	31	2.63	-6.04	T2	l
U1426	32	-0.92	-11.96	T2	l
U1426	33	1.71	-7.72	T2	l
U1426	34	2.28	-9.07	T2	l
U1426	35	2.38	-10.41	T2	l
U1426	36	2.58	-10.44	T2	l
U1426	38	1.98	-8.39	T2	l
U1426	40	2.30	-5.19	T2	l
U1426	41.5	1.95	-8.82	T2	l
U1426	42.5	1.90	-5.96	T2	l
U1426	43.5	2.16	-4.64	T2	l
U1426	45.5	3.75	-8.98	T2	l
U1426	47	3.56	-8.39	T2	l
U1426	48	3.61	-8.17	T2	l
U1426	49	3.58	-11.35	T2	l
U1426	50	2.72	-10.50	T2	l
U1426	52	3.68	-10.27	T2	l
U1426	53	3.42	-10.27	T2	l
U1426	54	3.02	-10.60	T2	l
U1426	55	2.74	-8.08	T2	l
U1426	56	3.47	-4.94	T2	l
U1426	57	2.34	-8.62	T2	l
U1426	58	2.39	-10.26	T2	l
U1426	59.5	3.11	-8.97	T2	l
U1426	60.5	2.22	-10.78	T2	l
U1426	61.5	1.61	-6.80	T2	l
U1426	62.5	2.59	-11.94	T2	l
U1426	63.5	3.18	-10.67	T2	l
U1426	64.5	2.54	-11.59	T2	l
U1426	65.5	2.54	-6.56	T2	l
U1426	66.5	1.83	-10.20	T2	l

U1426	67.5	1.81	-4.14	T2	l
U1426	68.5	1.75	-11.21	T2	l
U1426	69.5	1.40	-11.36	T2	l
U1426	71	1.74	-5.13	T2	l
U1426	72	1.42	-3.24	T2	d
U1426	73	2.09	-4.67	T2	d
U1426	74	2.08	-5.23	T2	d
U1426	75	2.48	-6.26	T2	d
U1426	76	2.44	-10.51	T2	d
U1426	77	2.58	-4.44	T2	d
U1426	78	3.16	-6.01	T2	d
U1426	79	3.14	-8.45	T2	d
U1426	80	2.03	-16.47	T2	l
U1426	81	0.99	-12.27	T2	l
U1426	82	2.19	-10.14	T2	l
U1426	83	1.52	-17.77	T2	l
U1426	84	1.23	-15.94	T2	l
U1426	85	1.70	-13.82	T2	l
U1426	87	2.05	-14.35	T2	l
U1426	89	1.93	-16.00	T2	d
U1426	90	1.67	-12.75	T2	d
U1426	91	2.08	-9.49	T2	d
U1426	92	2.04	-7.66	T2	d
U1426	93	4.78	-4.58	T2	d
U1426	94	6.52	-3.20	T2	d
U1426	95	6.99	-0.13	T2	d
U1426	96	7.51	-1.92	T2	d
U1426	98.1	2.73	-21.79	T2	d
U1426	99	5.55	-21.58	T2	d
U1426	99.9	6.03	-15.54	T2	d
U1426	101	4.70	-23.94	T2	d
U1426	102	3.59	-25.62	T2	d

Unkheltseg	**N47 13.06'**	**E95 11.27'**			
Section	**height**	**δ^{13}Ccarb**	**δ^{18}Ocarb**	**Unit**	**Lithology**
U1427	72	2.26	-4.80	T2	d
U1427	76	4.63	-2.44	T2	d
U1427	80	1.91	-2.89	T2	d
U1427	84	5.09	-2.68	T2	d
U1427	88	3.72	-5.56	T2	d
U1427	92	2.36	-5.66	T2	d
U1427	96	2.67	-2.37	T2	d
U1427	100	2.04	-7.14	T2	d
U1427	104	2.24	-8.76	T2	d
U1427	108	3.33	-3.73	T2	d
U1427	112	1.48	-1.58	T2	d
U1427	116	6.88	-2.15	T2	d
U1427	120	2.16	-2.52	T2	d

U1427	124	3.40	-1.63	T2	d
U1427	128	1.72	-2.46	T2	d
U1427	132	1.66	-1.77	T2	d
U1427	138	2.09	-2.12	T2	d
U1427	21	3.91	-5.97	T2	d
U1427	25	2.46	-7.91	T2	d
U1427	29	2.37	-7.68	T2	d
U1427	33	3.09	-4.68	T2	d
U1427	37	2.09	-6.39	T2	d
U1427	42.8	2.54	-6.56	T2	d
U1427	47	-1.83	-3.11	T3	d
U1427	52	0.82	-5.91	T3	d
U1427	56	-0.76	-2.50	T3	d
U1427	60	2.39	-3.24	T3	d
U1427	64	2.57	-1.65	T3	d
U1427	68	2.59	-4.02	T3	d

Unkheltseg **N47 13.45'** **E95 11.10'**

Section	height	δ^{13}Ccarb	δ^{18}Ocarb	Unit	Lithology
U1428	0	4.41	-6.10	T3	d
U1428	8	4.54	-2.71	T3	d
U1428	16	3.94	-5.56	T3	d
U1428	22	2.54	-5.38	T3	d
U1428	28	3.43	-5.67	T3	d
U1428	32	2.89	-6.72	T3	d
U1428	38	4.40	-6.50	T3	d
U1428	46	4.85	-3.46	T3	d
U1428	58	3.96	-5.89	T3	d
U1428	62	2.33	-6.20	T3	d
U1428	72	4.49	-2.51	T3	d
U1428	78	0.70	-8.23	T3	d
U1428	82	3.06	-6.30	T3	d
U1428	88	1.56	-9.24	T3	d
U1428	102	3.23	-5.77	T3	d
U1428	108	3.41	-5.68	T3	d
U1428	112	2.73	-4.92	T3	d
U1428	118	2.68	-6.70	T3	d
U1428	126	3.48	-2.63	T3	d
U1428	137.5	4.93	-6.24	T3	d
U1428	143.5	2.67	-4.68	T3	d

Khukh Davaa NE **N47 11.14'** **E95 22.99'**

Section	height	δ^{13}Ccarb	δ^{18}Ocarb	Unit	Lithology
U1210	5	-1.52	-6.37	T1	l
U1210	9	-0.39	-12.61	T1	l
U1210	12	-1.14	-6.45	T1	l
U1210	13	0.45	-3.77	T1	l
U1210	14	3.56	0.10	T1	l

U1210	15	4.98	-0.26	T2	d
U1210	16	4.83	0.00	T2	d
U1210	17	2.12	0.35	T2	d
U1210	18	1.86	-1.67	T2	d
U1210	19	1.57	-2.12	T2	d
U1210	54	0.21	-6.83	T3	d
U1210	55.5	1.25	-6.80	T3	d
U1210	56.5	1.37	-7.74	T3	d
U1210	59	1.31	-11.93	T3	d
U1210	64	2.93	-2.96	T3	d
U1210	65	3.48	-4.04	T3	d
U1210	66.5	4.72	-3.92	T3	d
U1210	67.5	5.74	-2.78	T3	d
U1210	68.5	3.25	-1.70	T3	d
U1210	71	4.40	-17.07	T3	l
U1210	72	5.01	-20.09	T3	l
U1210	73	5.00	-6.33	T3	l

Khongor Range	**N46 40.38'**	**E96 14.88'**			
Section	**height**	**δ^{13}Ccarb**	**δ^{18}Ocarb**	**Unit**	**Lithology**
U1439	3	3.44	0.72	Sh4	d
U1439	5	3.79	-1.03	Sh4	d
U1439	6	3.68	0.64	Sh4	d
U1439	7	4.15	-3.15	Sh4	d
U1439	8	3.98	-1.73	Sh4	d
U1439	9	3.75	0.01	Sh4	d
U1439	10	2.85	-1.65	Sh4	d
U1439	11	2.84	-0.47	Sh4	d
U1439	12	3.32	-1.06	Sh4	d
U1439	13	0.15	-0.86	Sh4	d
U1439	14	4.13	-1.54	Sh4	d
U1439	15	3.58	-0.20	Sh4	d
U1439	16	3.14	-0.42	Sh4	d
U1439	17	4.36	-1.16	Sh4	d
U1439	18	3.76	-1.74	Sh4	d
U1439	19	3.44	-1.26	Sh4	d
U1439	20	3.08	-0.79	Sh4	d
U1439	21	4.31	-1.08	Sh4	d
U1439	22	4.24	-1.52	Sh4	d
U1439	23	3.26	-2.08	Sh4	d
U1439	24	3.70	-2.68	Sh4	d
U1439	27	4.53	-0.90	Sh4	d
U1439	28	3.85	-2.38	Sh4	d
U1439	25	3.50	-2.33	Sh4	d
U1439	26	2.80	-1.26	Sh4	d
U1439	29	3.95	-1.61	Sh4	d
U1439	31	3.99	-3.40	Sh4	d
U1439	32	4.89	-2.06	Sh4	d

U1439	33	4.21	-1.44	Sh4	d
U1439	34	4.24	-1.44	Sh4	d
U1439	35	4.30	-0.96	Sh4	d
U1439	36	4.22	-1.05	Sh4	d
U1439	37	4.33	-1.86	Sh4	d
U1439	38	3.94	-1.75	Sh4	d
U1439	39	3.61	-0.86	Sh4	d
U1439	40	4.54	-1.87	Sh4	d
U1439	41	4.11	-3.46	Sh4	d
U1439	42	4.22	-2.41	Sh4	d
U1439	43	3.77	-4.28	Sh4	d
U1439	44	4.45	-1.75	Sh4	d
U1439	45	4.48	-2.46	Sh4	d
U1439	46	3.24	-1.91	Sh4	d
U1439	47	2.84	-2.00	Sh4	d
U1439	49	1.00	-1.04	Sh4	d
U1439	50	1.20	-1.41	Sh4	d
U1439	51	-0.16	-0.28	Sh4	d
U1439	52	0.91	-0.56	Sh4	d
U1439	53	1.10	-4.31	Sh4	d
U1439	54	1.25	-1.34	Sh4	d
U1439	58	1.08	-3.62	Sh4	d
U1439	59	1.26	-2.25	Sh4	d
U1439	60	0.42	-1.36	Sh4	d

Ol Mountain	**N46 41.938'**	**E96 22.287'**			
Section	**height**	**δ^{13}Ccarb**	**δ^{18}Ocarb**	**Unit**	**Lithology**
U1337	0	-0.82	-4.45	Ol	d
U1337	2	-0.70	-3.88	Ol	d
U1337	4	-0.57	-2.99	Ol	d
U1337	6	-3.56	-5.79	Ol	d
U1337	14.1	1.28	-2.15	Ol	d
U1337	16	1.09	-1.64	Ol	d
U1337	19	1.31	-1.79	Ol	d
U1337	21	0.87	-1.47	Ol	d
U1337	23	1.23	-4.48	Ol	d
U1337	25	2.56	-4.98	Ol	d
U1337	27	2.35	-5.20	Ol	d
U1337	29	2.55	-6.45	Ol	d
U1337	31	2.31	-4.62	Ol	d
U1337	33	2.03	-2.33	Ol	d
U1337	35	1.94	-3.35	Ol	d
U1337	37	2.70	-6.55	Ol	d
U1337	39	2.61	-5.19	Ol	d
U1337	41	1.02	-2.76	Ol	d
U1337	43	1.49	-2.82	Ol	d
U1337	45	1.67	-4.70	Ol	d
U1337	47	1.58	-2.04	Ol	d

U1337	94	2.25	-1.39	Sh2	d
U1337	96	2.39	-3.97	Sh2	d
U1337	98	2.25	-3.50	Sh2	d
U1337	100	2.38	-4.52	Sh2	d
U1337	102	2.00	-1.17	Sh2	d
U1337	104	1.61	-0.52	Sh2	d
U1337	106	2.46	-1.43	Sh2	d
U1337	108	1.98	-1.82	Sh2	d
U1337	110	2.73	-0.78	Sh2	d
U1337	112	2.52	-1.60	Sh2	d
U1337	114	1.78	-0.61	Sh2	d
U1337	116	2.30	-3.10	Sh2	d
U1337	118	2.32	-0.61	Sh2	d
U1337	120	3.04	-0.58	Sh2	d
U1337	122	3.11	-0.94	Sh2	d
U1337	124	3.09	0.02	Sh2	d
U1337	126	0.85	-0.52	Sh2	d
U1337	128	3.01	0.16	Sh2	d
U1337	130	2.88	-2.66	Sh2	d
U1337	132	2.00	-1.01	Sh2	d
U1337	134	3.11	-0.87	Sh2	d
U1337	136	2.43	-0.57	Sh2	d
U1337	138	2.69	-1.73	Sh2	d
U1337	140	2.34	-2.15	Sh2	d
U1338	142	2.67	0.01	Sh2	d
U1338	144	3.43	0.87	Sh2	d
U1338	146	2.82	-1.23	Sh2	d
U1338	148	2.75	0.90	Sh2	d
U1338	150	2.76	0.10	Sh2	d
U1338	152	2.49	0.26	Sh2	d
U1338	154	2.75	0.31	Sh2	d
U1338	156	2.99	0.05	Sh2	d
U1338	158	2.37	-0.36	Sh2	d
U1338	160	3.20	-0.39	Sh2	d
U1338	162	3.26	0.30	Sh2	d
U1338	164	3.85	0.14	Sh2	d
U1338	166	2.23	-0.44	Sh2	d
U1338	168	2.17	-3.00	Sh2	d
U1338	170	3.50	0.37	Sh2	d
U1338	172	2.60	-8.14	Sh2	d
U1338	174	2.85	0.16	Sh2	d
U1338	176	2.56	0.43	Sh2	d
U1338	178	1.91	-2.38	Sh2	d
U1338	180	1.55	-1.26	Sh2	d
U1338	182	1.99	-0.24	Sh2	d
U1338	184	3.01	0.04	Sh2	d
U1338	186	1.44	-0.93	Sh2	d
U1338	188	2.46	0.36	Sh2	d

U1338	190	2.74	-0.22	Sh2	d
U1338	192	2.22	-1.59	Sh2	d
U1338	194	2.60	-4.30	Sh2	d
U1338	196	2.03	-1.34	Sh2	d
U1338	198	1.74	-2.30	Sh2	d
U1338	201	2.20	-0.60	Sh2	d
U1338	203	2.40	-1.49	Sh2	d
U1338	205	1.76	-0.09	Sh2	d
U1338	207	2.55	-2.39	Sh2	d
U1338	209	3.31	-4.83	Sh2	d
U1338	211	3.31	-0.70	Sh2	d
U1338	213	3.66	1.54	Sh2	d
U1338	215	3.20	-1.00	Sh2	d
U1338	217	2.96	-1.75	Sh2	d
U1338	219	2.68	-4.29	Sh2	d
U1338	221	2.82	-2.52	Sh2	d
U1338	223	0.05	-0.96	Sh3	d
U1338	225	2.05	-1.72	Sh3	d
U1338	227	2.31	-1.63	Sh3	d
U1338	229	3.21	-0.93	Sh3	d
U1338	231	1.92	-1.81	Sh3	d
U1338	233	2.21	-1.55	Sh3	d
U1338	235	2.96	-1.49	Sh3	d
U1338	237	3.28	-4.48	Sh3	d
U1338	239	3.92	-1.86	Sh3	d
U1338	241	3.09	-1.83	Sh3	d
U1338	242	2.67	-1.07	Sh3	d
U1339	244	2.57	-1.64	Sh3	d
U1339	246	3.71	-0.22	Sh3	d
U1339	248	3.37	-0.17	Sh3	d
U1339	250	3.55	-1.45	Sh3	d
U1339	252	2.50	-0.96	Sh3	d
U1339	254	3.94	-2.87	Sh3	d
U1339	256	3.53	-2.93	Sh3	d
U1339	258	3.90	-4.02	Sh3	d
U1339	260	3.75	-4.10	Sh3	d
U1339	262	3.40	0.20	Sh3	d
U1339	264	4.02	-1.78	Sh3	d
U1339	266	3.34	-2.34	Sh3	d
U1339	268	3.58	-5.03	Sh3	d
U1339	270	4.70	-0.19	Sh3	d
U1339	272	3.31	-0.25	Sh3	d
U1339	274	4.15	-1.64	Sh3	d
U1339	277	4.68	0.31	Sh3	d
U1339	279	3.23	-3.47	Sh3	d
U1339	281	2.62	-0.24	Sh3	d
U1339	283	4.66	-4.27	Sh3	d
U1339	285	4.64	-2.39	Sh3	d

U1339	287	4.41	-3.29	Sh3	d
U1339	289	4.27	0.30	Sh3	d
U1339	291	4.33	-1.30	Sh3	d
U1339	293	4.64	-1.28	Sh3	d
U1339	295	3.28	-1.23	Sh3	d
U1339	297	3.57	-1.44	Sh3	d
U1339	299	3.65	-0.67	Sh3	d
U1339	301	3.41	-0.98	Sh3	d
U1339	303	2.22	-0.24	Sh4	d
U1339	305	3.10	-0.34	Sh4	d
U1339	307	2.71	-1.73	Sh4	d
U1339	309	1.56	-2.97	Sh4	d
U1339	311	2.22	-0.59	Sh4	d
U1339	313	0.70	0.01	Sh4	d
U1339	315	3.58	-0.60	Sh4	d
U1339	317	2.68	-1.22	Sh4	d
U1339	319	1.10	0.09	Sh4	d
U1339	321	1.27	-0.16	Sh4	d
U1339	323	2.01	-1.68	Sh4	d
U1339	325	1.26	-1.08	Sh4	d
U1339	327	0.28	-0.14	Sh4	d
U1339	329	0.71	-2.31	Sh4	d
U1339	331	1.35	-0.63	Sh4	d
U1339	333	-1.68	-0.69	Sh4	d
U1339	335	-0.50	-0.03	Sh4	d
U1339	337	-1.30	-0.71	Sh4	d
U1339	339	0.95	-0.05	Sh4	d
U1339	341	-0.78	-0.64	Sh4	d
U1339	343	2.52	-1.19	Sh4	d

Khevtee Tsakhir Range	**N46 38.975'**	**E96 51.752'**			
Section	**height**	**δ^{13}Ccarb**	**δ^{18}Ocarb**	**Unit**	**Lithology**
U1341	0	3.39	-1.46	Sh2	d
U1341	2	3.50	-0.71	Sh2	d
U1341	4	1.99	-1.01	Sh2	d
U1341	6	4.23	-3.35	Sh2	d
U1341	8	4.15	-4.27	Sh2	d
U1341	10	3.32	-1.98	Sh2	d
U1341	12	3.66	-1.16	Sh2	d
U1341	14	3.23	-1.03	Sh2	d
U1341	16	4.23	-4.58	Sh2	d
U1341	18	4.50	-1.46	Sh2	d
U1341	20	4.43	-4.27	Sh2	d
U1341	22	3.95	-2.13	Sh2	d
U1341	24	3.73	-0.71	Sh2	d
U1341	26	4.08	-0.63	Sh2	d
U1341	28	4.64	-2.79	Sh2	d
U1341	30	3.66	-5.43	Sh2	d

U1341	32	2.40	-1.17	Sh2	d
U1341	34	1.79	-1.97	Sh2	d
U1341	36	2.80	-8.89	Sh2	d
U1341	38	2.01	-2.98	Sh2	d
U1341	40	2.90	-1.19	Sh2	d
U1341	42	5.63	-0.51	Sh2	d
U1341	44	4.08	-1.56	Sh2	d
U1341	46	3.84	0.22	Sh2	d
U1341	48	3.09	-0.78	Sh2	d
U1341	50	2.93	-3.04	Sh2	d
U1341	52	2.35	-3.78	Sh2	d
U1341	54	3.46	-5.91	Sh2	d
U1341	56	4.31	-1.74	Sh2	d
U1341	58	4.12	-2.51	Sh2	d
U1341	60	4.05	-0.92	Sh2	d
U1341	62	4.00	-0.80	Sh3	d
U1341	64	2.79	-2.39	Sh3	d
U1341	66	3.70	-1.44	Sh3	d
U1341	68	4.18	-1.44	Sh3	d
U1341	70	3.90	-0.80	Sh3	d
U1341	72	4.25	-0.22	Sh3	d
U1341	74	3.76	-5.08	Sh3	d
U1341	76	3.99	-2.08	Sh3	d
U1341	78	4.04	-1.58	Sh3	d
U1341	80	3.67	-2.52	Sh3	d
U1341	82	3.63	0.00	Sh3	d
U1341	84	3.46	-1.60	Sh3	d
U1341	86	5.18	0.05	Sh3	d
U1341	88	4.76	-0.07	Sh3	d
U1341	90	4.69	-1.35	Sh3	d
U1341	92	4.78	-3.06	Sh3	d
U1341	94	4.47	-6.72	Sh3	d
U1341	98	4.80	-1.94	Sh3	d
U1341	100	4.39	-3.77	Sh3	d
U1341	102	4.83	-1.79	Sh3	d
U1341	104	4.62	-1.23	Sh3	d
U1341	106	5.34	-3.95	Sh3	d
U1341	108	4.50	-1.17	Sh3	d
U1341	111	5.81	-0.44	Sh3	d
U1341	113	4.78	-3.08	Sh3	d
U1341	115	6.08	-0.83	Sh3	d
U1341	117	3.16	-1.44	Sh3	d
U1341	119	4.37	-3.70	Sh3	d
U1341	121	4.07	-0.84	Sh3	d
U1341	123	4.62	-0.57	Sh3	d
U1341	125	4.32	-0.40	Sh3	d
U1341	127	4.55	1.71	Sh3	d
U1341	129	4.77	-0.21	Sh3	d

U1341	131	3.09	-0.28	Sh3	d
U1341	133	4.41	-0.28	Sh3	d
U1341	135	4.02	-0.87	Sh3	d
U1341	137	4.12	-0.12	Sh3	d
U1341	140	3.21	-2.68	Sh3	d
U1341	143	4.48	-0.23	Sh3	d
U1341	145	3.98	-1.07	Sh3	d
U1341	147	4.15	-0.29	Sh3	d
U1341	149	4.84	-0.56	Sh3	d
U1341	151	4.62	-0.63	Sh3	d
U1341	153	5.72	-1.21	Sh3	d
U1341	155	5.08	-0.53	Sh3	d
U1341	157	2.33	-0.52	Sh3	d
U1341	159	2.63	-0.99	Sh3	d
U1341	161	2.82	-1.62	Sh3	d
U1341	163	3.75	-1.21	Sh3	d
U1341	165.3	4.09	-0.18	Sh4	d
U1341	167.5	3.18	-2.27	Sh4	d
U1341	169.5	3.05	-0.12	Sh4	d
U1341	171.5	3.55	-0.43	Sh4	d
U1341	173.5	3.71	-0.44	Sh4	d
U1341	175.5	4.62	-2.10	Sh4	d
U1341	177.5	3.40	-1.73	Sh4	d
U1341	179.5	3.26	-1.03	Sh4	d
U1341	181.5	2.73	-0.34	Sh4	d
U1341	183.5	3.23	-0.32	Sh4	d
U1341	185.5	3.07	-1.32	Sh4	d
U1341	187.5	4.80	-2.69	Sh4	d
U1341	189.5	3.69	-0.33	Sh4	d
U1341	191.5	2.45	-0.50	Sh4	d
U1341	193.5	3.42	-0.58	Sh4	d
U1341	195.5	3.06	-3.07	Sh4	d
U1341	197.5	2.77	-0.75	Sh4	d
U1341	199.5	2.68	-1.76	Sh4	d

Zuun-Arts Mountain **N47 14.243'** **E96 29.243'**

Section	**height**	**δ^{13}Ccarb**	**δ^{18}Ocarb**	**Unit**	**Lithology**
U1329	0	3.22	-2.18	Sh2	d
U1329	2	4.26	-1.71	Sh2	d
U1329	4	3.41	-3.12	Sh2	d
U1329	8	3.27	-3.76	Sh2	d
U1329	10	3.25	-3.79	Sh2	d
U1329	12	3.17	-3.41	Sh2	d
U1329	14	2.73	-4.04	Sh2	d
U1329	16	1.72	-4.86	Sh2	d
U1329	18	1.89	-5.05	Sh2	d
U1329	20	2.07	-3.01	Sh2	d
U1329	22	2.22	-3.03	Sh2	d

U1329	24	2.50	-2.82	Sh2	d
U1329	26	2.73	-2.83	Sh2	d
U1329	28	1.81	-4.21	Sh2	d
U1329	30	1.00	-4.63	Sh2	d
U1329	32	1.32	-2.72	Sh2	d
U1329	34	3.92	-3.64	Sh2	d
U1329	36	4.21	-3.02	Sh2	d
U1329	38	4.38	-3.39	Sh2	d
U1329	40	4.02	-3.28	Sh2	d
U1329	42	3.88	-2.83	Sh2	d
U1329	48	3.31	-2.83	Sh2	d
U1329	50	2.70	-5.45	Sh2	d
U1329	52	3.88	-4.65	Sh2	d
U1329	54	2.83	-3.48	Sh2	d
U1329	56	2.81	-3.42	Sh2	d
U1329	72	0.18	-20.45	Sh2	d
U1329	74	1.04	-3.96	Sh2	d
U1329	76	1.06	-4.42	Sh2	d
U1329	80	0.45	-4.33	Sh2	d
U1329	82	1.04	-3.13	Sh2	d
U1329	84	0.85	-5.41	Sh2	d
U1329	86	0.43	-6.27	Sh2	d
U1329	88	2.55	-3.50	Sh2	d
U1329	90	3.85	-1.72	Sh3	d
U1329	92	3.48	-2.91	Sh3	d
U1329	94	3.87	-4.27	Sh3	d
U1329	96	1.29	-3.02	Sh3	d
U1329	98	1.50	-6.64	Sh3	d
U1329	100	2.25	-3.23	Sh3	d
U1329	102	3.10	-4.21	Sh3	d
U1329	104	3.41	-3.57	Sh3	d
U1329	106	3.55	-2.17	Sh3	d
U1329	108	1.96	-5.23	Sh3	d
U1329	110	2.39	-3.55	Sh3	d
U1329	112	3.10	-3.48	Sh3	d
U1329	114	3.26	-3.22	Sh3	d
U1329	116	2.71	-1.73	Sh3	d
U1329	118	2.48	-2.05	Sh3	d
U1329	120	3.14	-2.15	Sh3	d
U1329	122	0.70	-2.44	Sh3	d
U1329	124	2.52	-1.96	Sh3	d
U1329	126	3.28	-1.56	Sh3	d
U1329	128	2.50	-3.59	Sh3	d
U1329	130	2.69	-3.02	Sh3	d
U1329	132	1.98	-5.09	Sh3	d
U1329	134	1.82	-6.02	Sh3	d
U1329	136	0.79	-7.69	Sh4	d
U1329	138	0.01	-6.01	Sh4	d

U1329	140	-0.31	-3.12	Sh4	d
U1329	142	0.47	-5.67	Sh4	d
U1329	144	-0.05	-7.34	Sh4	d
U1329	146	-1.15	-7.15	Sh4	d
U1329	148	-1.56	-2.33	Sh4	d
U1329	150	-0.68	-4.37	Sh4	d
U1329	152	-1.59	-4.08	Sh4	d
U1329	154	-0.52	-8.64	Sh4	d
U1329	156	-1.63	-11.43	Sh4	d
U1329	160	-2.26	-9.48	Sh4	d
U1329	162	-2.35	-15.22	Sh4	d
U1329	164	-2.88	-6.73	Sh4	d
U1329	166	-1.22	-4.80	Sh4	d

Ikh Goliin Tsakhir **N47 01.22'** **E95 08.33'**

Section	**height**	**δ^{13}Ccarb**	**δ^{18}Ocarb**	**Unit**	**Lithology**
U1433	72	-0.76	-7.02	Sh1-2	l
U1433	73	-0.52	-8.14	Sh1-2	l
U1433	74	-0.34	-4.89	Sh1-2	l
U1433	75	2.42	-6.05	Sh1-2	l
U1433	76	1.75	-6.38	Sh1-2	l
U1433	77	2.89	-5.96	Sh1-2	l
U1433	78	-0.94	-4.08	Sh1-2	l
U1433	79	4.01	-5.27	Sh1-2	l
U1433	80	2.24	-4.44	Sh1-2	l
U1433	86	6.18	-4.68	Sh1-2	l
U1433	87	5.80	-6.47	Sh1-2	l
U1433	89	5.86	-6.13	Sh1-2	l
U1433	90	6.80	-4.80	Sh3-4	l
U1433	91	7.24	-4.80	Sh3-4	l
U1433	92	7.17	-5.22	Sh3-4	l
U1433	93	6.66	-6.12	Sh3-4	l
U1433	94	6.82	-8.01	Sh3-4	l
U1433	95	6.90	-3.31	Sh3-4	l
U1433	96	0.12	-19.00	Sh3-4	l
U1433	97	7.18	-4.71	Sh3-4	l
U1433	98	7.58	-4.70	Sh3-4	l
U1433	99	8.03	-4.05	Sh3-4	l
U1433	103	7.12	-8.29	Sh3-4	d
U1433	104	5.86	-9.11	Sh3-4	d
U1433	105	4.94	-9.46	Sh3-4	d
U1433	106	4.15	-12.41	Sh3-4	d
U1433	107	6.39	-3.10	Sh3-4	d
U1433	108	4.25	-1.48	Sh3-4	d
U1433	109	3.62	-1.08	Sh3-4	d
U1433	110	5.03	0.11	Sh3-4	d
U1433	111	4.77	-0.85	Sh3-4	d
U1433	112	4.81	-0.23	Sh3-4	d

U1433	113	3.43	-0.81	Sh3-4	d
U1433	114	3.65	-0.75	Sh3-4	d
U1433	115	5.21	-1.33	Sh3-4	d
U1433	116	6.61	-1.38	Sh3-4	d
U1433	117	6.96	-1.65	Sh3-4	d
U1433	118	6.27	-1.53	Sh3-4	d
U1433	119	5.33	-1.75	Sh3-4	d
U1433	120	5.58	-1.03	Sh3-4	d
U1433	121	4.01	-0.64	Sh3-4	d
U1433	122	4.03	-1.74	Sh3-4	d
U1433	123	4.61	-0.12	Sh3-4	d
U1433	124	3.85	-0.26	Sh3-4	d
U1433	125	3.59	-2.03	Sh3-4	d
U1433	126	2.85	0.02	Sh3-4	d
U1433	128	3.10	-0.53	Sh3-4	d
U1433	130	4.77	-0.93	Sh3-4	d
U1433	132	4.47	-1.81	Sh3-4	d
U1433	134	4.77	-0.46	Sh3-4	d
U1433	136	4.51	-2.61	Sh3-4	d
U1433	138	4.03	-0.13	Sh3-4	d
U1433	140	3.86	-1.44	Sh3-4	d
U1433	142	4.38	-0.76	Sh3-4	d
U1433	144	3.54	-2.05	Sh3-4	d
U1433	146	2.95	-0.37	Sh3-4	d
U1433	148	4.29	-0.55	Sh3-4	d
U1433	150	3.89	-0.34	Sh3-4	d
U1433	152	3.11	-1.46	Sh3-4	d
U1433	154	3.46	-0.60	Sh3-4	d
U1433	156	3.67	-2.58	Sh3-4	d
U1433	158	4.36	-2.46	Sh3-4	d
U1433	160	4.01	-0.58	Sh3-4	d
U1433	162	4.18	-0.47	Sh3-4	d
U1433	164	3.54	-1.54	Sh3-4	d
U1433	166	2.90	-0.33	Sh3-4	d
U1433	171	1.53	-2.84	ZA	l
U1433	173	1.84	0.20	ZA	l
U1433	175	2.19	-0.03	ZA	l
U1433	177	1.67	-0.56	ZA	l
U1433	179	2.70	-0.83	ZA	l
U1433	181	1.96	-1.69	ZA	l
U1433	183	1.62	-1.43	ZA	l
U1433	25	-0.76	-5.43	Ol	d
U1433	27	-0.18	-4.72	Ol	d
U1433	29	0.31	-2.10	Ol	d
U1433	31	1.12	-3.34	Ol	d
U1433	33	1.34	-1.54	Ol	d
U1433	35	1.73	-1.62	Ol	d
U1433	37	3.25	-1.26	Ol	d

U1433	39	2.99	-1.05	Ol	d
U1433	32	2.75	-3.59	Ol	d
U1433	43	3.40	-7.31	Ol	d
U1433	44	2.62	-5.90	Ol	d
U1433	46	2.41	-2.69	Ol	d
U1433	48	2.62	-4.33	Ol	d
U1433	50	1.60	-3.78	Ol	d
U1433	52	2.42	-6.94	Ol	d
U1433	54	2.39	-1.95	Ol	d
U1433	56	2.39	-2.39	Ol	d
U1433	58	2.37	-2.27	Ol	d
U1433	60	2.37	-1.92	Ol	d
U1433	62	2.39	-1.30	Ol	d
U1433	64	2.54	-1.69	Ol	d
U1433	66	2.46	-1.95	Ol	d
U1433	68	-0.12	-1.80	Ol	d

Unkheltseg **N47 12.93'** **E95 13.37'**

Section	**height**	**δ^{13}Ccarb**	**δ^{18}Ocarb**	**Unit**	**Lithology**
U1429	0	0.87	-1.81	Ol	d
U1429	2	0.88	-1.70	Ol	d
U1429	4	0.77	-3.03	Ol	d
U1429	6	0.84	-3.61	Ol	d
U1429	8	0.54	-1.89	Ol	d
U1429	10	1.78	-2.45	Ol	d
U1429	12	1.54	-3.11	Ol	d
U1429	14	0.82	-2.93	Ol	d
U1429	16	0.69	-4.59	Ol	d
U1429	18	1.11	-3.00	Ol	d
U1429	20	2.07	-5.91	Ol	d
U1429	22	1.05	-1.89	Ol	d
U1429	25	3.69	-6.83	Ol	d
U1429	27	3.14	-5.90	Ol	d
U1429	30	2.09	-6.36	Ol	d
U1429	32	2.57	-2.06	Ol	d
U1429	34	2.78	-1.95	Ol	d
U1429	36	1.77	-1.54	Ol	d
U1429	38	1.06	-1.84	Ol	d
U1429	40	1.05	-1.67	Ol	d
U1429	42	3.41	-2.85	Ol	d
U1429	46	2.90	-2.73	Ol	d
U1429	48	2.61	-2.81	Ol	d
U1429	50	2.61	-3.02	Ol	d
U1429	52	3.45	-1.71	Ol	d
U1429	54	3.11	-0.63	Ol	d
U1429	56	3.04	-3.26	Ol	d
U1429	58	2.54	-2.18	Ol	d
U1429	60	1.97	-1.75	Ol	d

U1429	97.5	5.89	-7.01	Sh3-4	l
U1429	98.5	5.50	-13.85	Sh3-4	l
U1429	100.5	7.72	-17.57	Sh3-4	l
U1429	101.5	7.28	-18.80	Sh3-4	l
U1429	102.5	6.66	-20.70	Sh3-4	l
U1429	103.5	6.39	-21.38	Sh3-4	l
U1429	104.5	5.85	-20.21	Sh3-4	l
U1429	105.6	6.24	-22.41	Sh3-4	l
U1429	106.5	6.41	-23.80	Sh3-4	l
U1429	108	4.99	-6.68	Sh3-4	l
U1429	109	5.16	-8.21	Sh3-4	d
U1429	110	4.17	-11.36	Sh3-4	d
U1429	112	4.18	-4.95	Sh3-4	d
U1429	114	5.45	-2.10	Sh3-4	d
U1429	115	6.19	-4.04	Sh3-4	d
U1429	116	5.07	-4.53	Sh3-4	d
U1429	117	5.20	-2.71	Sh3-4	d
U1429	119	5.17	-5.28	Sh3-4	l
U1429	120	6.24	-3.08	Sh3-4	d
U1429	124	8.09	-5.25	Sh3-4	d
U1429	125	6.67	-3.16	Sh3-4	d
U1429	126	7.18	-2.60	Sh3-4	d
U1429	127	6.51	-2.17	Sh3-4	d
U1429	128	7.77	-1.89	Sh3-4	d
U1429	129	6.31	-2.99	Sh3-4	d
U1429	130	5.54	-2.53	Sh3-4	d
U1429	131	5.95	-3.09	Sh3-4	d
U1429	132	5.39	-2.68	Sh3-4	d
U1429	133	5.83	-2.27	Sh3-4	d
U1429	134	5.51	-2.96	Sh3-4	d
U1429	135	5.35	-2.07	Sh3-4	d
U1429	136	5.82	-3.56	Sh3-4	d
U1429	137	7.86	-3.01	Sh3-4	d
U1429	138	8.02	-5.23	Sh3-4	d
U1429	139	8.38	-2.73	Sh3-4	d
U1429	140	8.17	-3.50	Sh3-4	d
U1429	141	8.65	-2.23	Sh3-4	d
U1429	143	6.88	-3.44	Sh3-4	d
U1429	144	5.93	-2.03	Sh3-4	d
U1429	147	4.21	-0.97	Sh3-4	d
U1429	148	4.14	-1.37	Sh3-4	d

South Khukh Davaa **N 47 1.774'** **E 95 25.909'**

Section	**height**	**δ^{13}Ccarb**	**δ^{18}Ocarb**	**Unit**	**Lithology**
F1126	4	4.99	-2.22	T3	l
F1126	8	10.08	-7.12	T3	l
F1126	12	10.36	-6.28	T3	l
F1126	16	9.19	-18.42	T3	l

F1126	20	10.47	-9.54	T3	l
F1126	24	10.70	-14.91	T3	l
F1126	28	10.46	-16.42	T3	l
F1126	32	10.74	-13.12	T3	l
F1126	36	10.75	-11.99	T3	l
F1126	40	10.33	-19.79	T3	l
F1126	44	10.59	-7.42	T3	l
F1126	48	10.58	-11.40	T3	l
F1126	52	10.09	-13.23	T3	l
F1126	56	10.36	-13.26	T3	l
F1126	60	10.80	-7.07	T3	l
F1126	64	10.20	-13.72	T3	l
F1126	68	10.15	-14.32	T3	l
F1126	72	10.10	-15.62	T3	l
F1126	76	10.61	-15.33	T3	l
F1126	80	11.00	-10.22	T3	l
F1126	84	11.01	-2.64	T3	l
F1126	88	10.79	-1.24	T3	l
F1126	92	10.46	-6.91	T3	l
F1126	96	9.84	-15.57	T3	l
F1126	100	7.93	-6.61	T3	l
F1126	102	6.70	-7.19	T3	l
F1126	104	9.90	-5.99	T3	l

Khongor Range	**N 46 42.267'**	**E 96 14.435'**			
F867	4	1.74	-8.86	MU-upper	d
F867	9.7	1.05	-6.26	MU-upper	d
F867	65	-1.27	-1.96	MU-upper	d
F867	71	-3.38	-1.94	MU-upper	d
F867	71.5	-3.14	-5.06	MU-upper	d

Salaa Gorge					
F950	188.7	3.21	1.06	MU-upper	d
F950	188.8	3.96	4.38	MU-upper	d
F950	189	2.90	0.31	MU-upper	d
F950	189.2	2.47	-1.26	MU-upper	d
F950	189.4	-1.28	-13.69	MU-upper	d
F950	189.6	-4.15	-16.67	MU-upper	l

S. Khukh Davaa	**N 47 0.788'**	**E 95 25.933'**			
F880	0.3	-4.87	-22.46	MU-upper	l

N. Khukh Davaa	**N 47 10.433'**	**E 95 25.526'**			
F1204	58	1.20	-22.04	MU-upper	l
F1204	58.05	1.57	-21.91	MU-upper	l
F1204	58.1	1.58	-21.84	MU-upper	l
F1204	58.15	1.59	-21.79	MU-upper	l
F1204	58.35	0.88	-21.23	MU-upper	l
F1204	58.4	0.25	-21.44	MU-upper	l

F1204	58.55	0.48	-21.42	MU-upper	l
F1204	58.6	0.49	-21.51	MU-upper	l
F1204	58.7	0.58	-17.68	MU-upper	l
F1204	58.9	2.39	-21.22	MU-upper	l
F1204	76.1	0.50	-20.07	MU-upper	l
F1204	76.2	2.88	-19.88	MU-upper	l
F1204	76.45	1.52	-20.32	MU-upper	l
F1204	76.55	1.37	-20.39	MU-upper	l
F1204	76.6	1.24	-20.96	MU-upper	l

N. Khukh Davaa **N 47 11.23'** **E 95 23.758'**

F1203	272.11	-5.30	-23.43	MU-middle	l
F1203	272.13	-6.51	-24.01	MU-middle	l
F1203	272.15	-7.13	-23.08	MU-middle	l
F1203	272.17	-6.39	-22.44	MU-middle	l
F1203	272.19	-6.09	-22.77	MU-middle	l
F1203	272.21	-7.20	-22.66	MU-middle	l
F1203	272.23	-6.82	-22.93	MU-middle	l
F1203	272.25	-4.89	-22.96	MU-middle	l
F1203	272.29	-4.81	-23.48	MU-middle	l
F1203	272.31	-4.68	-22.84	MU-middle	l
F1203	272.35	-4.15	-23.33	MU-middle	l
F1203	272.39	-4.19	-23.14	MU-middle	l
F1203	272.43	-4.77	-23.48	MU-middle	l
F1203	272.45	-3.98	-23.46	MU-middle	l
F1203	272.47	-5.23	-23.34	MU-middle	l
F1203	272.51	-4.22	-24.35	MU-middle	l
F1203	272.53	-3.60	-20.43	MU-middle	l
F1203	272.55	-3.84	-23.48	MU-middle	l
F1203	272.7	-4.73	-23.87	MU-middle	l
F1203	272.72	-4.38	-23.11	MU-middle	l
F1203	272.91	-4.08	-24.80	MU-middle	l
F1203	272.95	-4.83	-24.01	MU-middle	l
F1203	272.97	-4.63	-24.36	MU-middle	l
F1203	272.99	-5.54	-24.51	MU-middle	l
F1203	273.27	-4.71	-23.97	MU-middle	l

Salaa Gorge

F1212	42.1	-3.50	-9.23	MU-middle	d
F1212	56.5	-1.82	-10.41	MU-middle	d
F1212	56.6	-1.50	-8.68	MU-middle	d
F1212	56.63	-1.63	-8.67	MU-middle	d
F1212	56.75	-1.78	-8.98	MU-middle	d
F1212	56.8	-1.75	-8.20	MU-middle	d

Shivee Tsakhir **N 46 46.417'** **E 95 47.858'**

F1214	0.01	-3.76	-7.10	MU-middle	l
F1214	0.05	-5.95	-20.30	MU-middle	l
F1214	0.1	-5.70	-20.34	MU-middle	l

F1214	0.15	-6.09	-20.31	MU-middle	l
F1214	0.2	-6.54	-20.48	MU-middle	l
F1214	0.25	-6.80	-20.34	MU-middle	l
F1214	0.37	-6.37	-20.44	MU-middle	l
F1214	0.4	-6.41	-20.45	MU-middle	l

Shivee Tsakhir	**N 46 46.417'**	**E 95 47.858'**			
F1216	5.3	1.14	-20.05	MU-lower	l
F1216	5.8	3.71	-21.30	MU-lower	l
F1216	8	5.15	-8.22	MU-lower	d
F1216	13	0.04	-15.18	MU-lower	d
F1216	17	3.47	-22.44	MU-lower	l
F1216	19	3.40	-22.52	MU-lower	l
F1216	26	3.62	-21.41	MU-lower	l
F1216	29	0.90	-14.43	MU-lower	d

Shivee Tsakhir	**N 46 46.417'**	**E 95 47.858'**			
F1215	3.1	5.13	-6.32	MU-lower	d

Table 3.A4. Composite data table for Sr isotope ratios and elemental concentration.
Cryogenian and Ediacaran carbonates (used in Figure 3.17). Data considered altered are striked through.

Sample Name	Height	Unit	Location	Model Age	87Sr/86Sr	Sr(ppm)	Mn/Sr	Rb/Sr	%carb	Method	Period	Reference
Yd1	1	Doushantuo	Yangjiaping section, China		0.7081	681	0.13	0.0074	68.1	TIMS	Ediacaran	Cui et al., 2015
Yd2	4	Doushantuo	Yangjiaping section, China		0.70812	520	0.15	0.0154	69.3	TIMS	Ediacaran	Cui et al., 2015
~~Yd3~~	~~8~~	~~Doushantuo~~	~~Yangjiaping section, China~~	-	~~0.70811~~	~~491~~	~~0.18~~	~~0.0138~~	~~62.3~~	~~TIMS~~	~~Ediacaran~~	~~Cui et al., 2015~~
~~Yd5~~	~~16~~	~~Doushantuo~~	~~Yangjiaping section, China~~	-	~~0.70805~~	~~394~~	~~0.12~~	~~0.0063~~	~~70.1~~	~~TIMS~~	~~Ediacaran~~	~~Cui et al., 2015~~
~~Yd6~~	~~20~~	~~Doushantuo~~	~~Yangjiaping section, China~~	-	~~0.7081~~	~~385~~	~~0.16~~	~~0.011~~	~~81~~	~~TIMS~~	~~Ediacaran~~	~~Cui et al., 2015~~
~~Yd8~~	~~28~~	~~Doushantuo~~	~~Yangjiaping section, China~~	-	~~0.7079~~	~~286~~	~~0.03~~	~~0.0009~~	~~97.2~~	~~TIMS~~	~~Ediacaran~~	~~Cui et al., 2015~~
Yd9	32	Doushantuo	Yangjiaping section, China		0.70793	1353	0.01	0.0002	97.6	TIMS	Ediacaran	Cui et al., 2015
Yd10	36	Doushantuo	Yangjiaping section, China		0.708	775	0.04	0.0028	94.4	TIMS	Ediacaran	Cui et al., 2015
Yd11	40	Doushantuo	Yangjiaping section, China		0.70801	558	0.13	0.0072	76.6	TIMS	Ediacaran	Cui et al., 2015
Yd12	44	Doushantuo	Yangjiaping section, China		0.70803	899	0.11	0.0038	96.7	TIMS	Ediacaran	Cui et al., 2015
Yd13	49	Doushantuo	Yangjiaping section, China		0.70796	697	0.03	0.0003	95.2	TIMS	Ediacaran	Cui et al., 2015

Yd14	53	Doushantuo	Yangjiaping section, China		0.70791	689	0.02	0.0002	96.2	TIMS	Ediacaran	Cui et al., 2015
Yd15	56	Doushantuo	Yangjiaping section, China		0.70799	1119	0.03	0.0012	97.6	TIMS	Ediacaran	Cui et al., 2015
Yd16	60	Doushantuo	Yangjiaping section, China		0.70794	1483	0.01	0.0002	97.3	TIMS	Ediacaran	Cui et al., 2015
Yd17	65	Doushantuo	Yangjiaping section, China		0.70794	612	0.01	0.0006	98.7	TIMS	Ediacaran	Cui et al., 2015
Yd18	70	Doushantuo	Yangjiaping section, China		0.70799	578	0.03	0.0007	98.4	TIMS	Ediacaran	Cui et al., 2015
Yd19	75	Doushantuo	Yangjiaping section, China		0.70794	850	0.02	0.0008	98.9	TIMS	Ediacaran	Cui et al., 2015
Yd20	79	Doushantuo	Yangjiaping section, China	-572.3	0.70807	559	0.05	0.0006	97.5	TIMS	Ediacaran	Cui et al., 2015
Yd21	84	Doushantuo	Yangjiaping section, China	-569.9	0.70802	831	0.03	0.0003	73.9	TIMS	Ediacaran	Cui et al., 2015
Yd22	88	Doushantuo	Yangjiaping section, China	-567.9	0.70831	586	0.15	0.0024	91.3	TIMS	Ediacaran	Cui et al., 2015
Yd24	96	Doushantuo	Yangjiaping section, China	-565.0	0.70811	964	0.04	0.0002	98.7	TIMS	Ediacaran	Cui et al., 2015
Yd25	98	Doushantuo	Yangjiaping section, China	-564.3	0.70835	893	0.05	0.0003	84.3	TIMS	Ediacaran	Cui et al., 2015
Yd26	103.4	Doushantuo	Yangjiaping section, China	-563.0	0.70856	1662	0.02	0.0016	59	TIMS	Ediacaran	Cui et al., 2015
-	-	~~Dengying~~	~~China~~	~~-543.1~~	~~0.708456~~	~~389~~	-	-	-	~~MC-ICPMS~~	~~Ediacaran~~	~~Sawaki et al., 2010~~

		Dengying	China	-546.4	0.708403	1014				MC-ICPMS	Ediacaran	Sawaki et al., 2010
		Dengying	China	-546.4	0.708415	3729				MC-ICPMS	Ediacaran	Sawaki et al., 2010
		Dengying	China	-547.0	0.708371	11034				MC-ICPMS	Ediacaran	Sawaki et al., 2010
		Dengying	China	-547.5	0.708390	3241				MC-ICPMS	Ediacaran	Sawaki et al., 2010
		Dengying	China	-547.7	0.708481	3011				MC-ICPMS	Ediacaran	Sawaki et al., 2010
		Dengying	China	-548.4	0.708421	672				MC-ICPMS	Ediacaran	Sawaki et al., 2010
		Dengying	China	-548.6	0.708518	518				MC-ICPMS	Ediacaran	Sawaki et al., 2010
-	-	~~Member 3~~	~~China~~	~~-577.1~~	~~0.708129~~	~~293~~	-	-	-	~~MC-ICPMS~~	~~Ediacaran~~	~~Sawaki et al., 2010~~
-	-	~~Member 2~~	~~China~~	~~-589.3~~	~~0.707772~~	~~383~~	-	-	-	~~MC-ICPMS~~	~~Ediacaran~~	~~Sawaki et al., 2010~~
-	-	~~Member 2~~	~~China~~	~~-595.9~~	~~0.708116~~	~~369~~	-	-	-	~~MC-ICPMS~~	~~Ediacaran~~	~~Sawaki et al., 2010~~
-	-	~~Member 2~~	~~China~~	~~-598.1~~	~~0.708040~~	~~430~~	-	-	-	~~MC-ICPMS~~	~~Ediacaran~~	~~Sawaki et al., 2010~~
-	-	~~Member 2~~	~~China~~	~~-598.9~~	~~0.708179~~	~~434~~	-	-	-	~~MC-ICPMS~~	~~Ediacaran~~	~~Sawaki et al., 2010~~
		Member 2	China	-600.2	0.708111	572				MC-ICPMS	Ediacaran	Sawaki et al., 2010
		Member 2	China	-601.1	0.708140	524				MC-ICPMS	Ediacaran	Sawaki et al., 2010
-	-	~~Member 2~~	~~China~~	~~-606.3~~	~~0.708119~~	~~474~~	-	-	-	~~MC-ICPMS~~	~~Ediacaran~~	~~Sawaki et al., 2010~~
		Member 2	China	-607.9	0.708109	659				MC-ICPMS	Ediacaran	Sawaki et al., 2010
		Member 2	China	-607.9	0.708153	517				MC-ICPMS	Ediacaran	Sawaki et al., 2010
		Member 2	China	-609.3	0.708242	534				MC-ICPMS	Ediacaran	Sawaki et al., 2010
-	-	~~Member 2~~	~~China~~	~~-612.3~~	~~0.707982~~	~~487~~	-	-	-	~~MC-ICPMS~~	~~Ediacaran~~	~~Sawaki et al., 2010~~
-	-	~~Member 2~~	~~China~~	-	~~0.70~~	~~249~~	-	-	-	~~MC-ICPMS~~	~~Ediac~~	~~Sawaki et al., 2010~~

				613.9	8284						aran	
-	-	Member 2	China	-615.6	0.708091	385	-	-	-	MC-ICPMS	Ediacaran	Sawaki et al., 2010
-	-	Member 2	China	-615.9	0.708062	475	-	-	-	MC-ICPMS	Ediacaran	Sawaki et al., 2010
-	-	Member 2	China	-618.8	0.708189	384	-	-	-	MC-ICPMS	Ediacaran	Sawaki et al., 2010
		Member 2	China	-622.6	0.708295	537				MC-ICPMS	Ediacaran	Sawaki et al., 2010
		Member 2	China	-626.4	0.708109	645				MC-ICPMS	Ediacaran	Sawaki et al., 2010
		Member 2	China	-630.0	0.707940	500				MC-ICPMS	Ediacaran	Sawaki et al., 2010
		Member 2	China	-631.9	0.708157	736				MC-ICPMS	Ediacaran	Sawaki et al., 2010
-	-	Member 2	China	-632.0	0.708019	296	-	-	-	MC-ICPMS	Ediacaran	Sawaki et al., 2010
-	-	Member 2	China	-634.1	0.708184	436	-	-	-	MC-ICPMS	Ediacaran	Sawaki et al., 2010
MD2	-	Buah	Oman	-552.0	0.70871	471	0.51	-	-	5 collector VG Sector instrument	Ediacaran	Burns et al., 1994
WS9	-	Shuram	Oman	-554.0	0.70867	491	0.62	-	-	5 collector VG Sector instrument	Ediacaran	Burns et al., 1994
WS2	-	Shuram	Oman	-556.0	0.70874	474	0.51	-	-	5 collector VG Sector instrument	Ediacaran	Burns et al., 1994
5.36		Wonoka Fm.	South Australia	556.9	0.70910	577	1.15				Ediacaran	Calver, 2000
5.41		Wonoka Fm.	South Australia	555.8	0.70888	717	0.54				Ediacaran	Calver, 2000
5.44		Wonoka Fm.	South Australia	554.8	0.70868	921	0.63				Ediacaran	Calver, 2000
5.52		Wonoka Fm.	South Australia	553.1	0.70876	1420	0.24				Ediacaran	Calver, 2000
5.54		Wonoka Fm.	South	552.8	0.70	1064	0.42				Ediac	Calver, 2000

			Australia		899						aran	
~~6.12~~	-	Wonoka Fm.	South Australia	~~551.0~~	~~0.70 901~~	~~429~~	~~0.63~~	-	-	-	Ediac aran	Calver, 2000
~~VML-8~~	-	~~Salitre Fm.~~	~~Irecê basin (Brazil)~~	~~-619.5~~	~~0.70 769~~	~~461~~	~~0.03~~	-	-	~~MC-ICPMS~~	~~Ediac aran~~	~~Misi and Vizer, 1998~~
VML--8bc		Salitre Fm.	Irecê basin (Brazil)	-594.6	0.70 746	1220	0.01			MC-ICPMS	Ediac aran	Misi and Vizer, 1998
JC--54		Salitre Fm.	Irecê basin (Brazil)	-594.2	0.70 745	792	0.02			MC-ICPMS	Ediac aran	Misi and Vizer, 1998
IR--AM--11		Salitre Fm.	Irecê basin (Brazil)	-596.8	0.70 75	2380	0.03			MC-ICPMS	Ediac aran	Misi and Vizer, 1998
VML--6a		Salitre Fm.	Irecê basin (Brazil)	-597.0	0.70 82	896	0.01			MC-ICPMS	Ediac aran	Misi and Vizer, 1998
VML--6b		Salitre Fm.	Irecê basin (Brazil)	-597.4	0.70 78	790	0.01			MC-ICPMS	Ediac aran	Misi and Vizer, 1998
VML--6c		Salitre Fm.	Irecê basin (Brazil)	-597.8	0.70 789	963	0.09			MC-ICPMS	Ediac aran	Misi and Vizer, 1998
VML--7b		Salitre Fm.	Irecê basin (Brazil)	-598.1	0.70 765	1430	0.01			MC-ICPMS	Ediac aran	Misi and Vizer, 1998
VML--3		Salitre Fm.	Irecê basin (Brazil)	-632.0	0.70 78	1720	0.02			MC-ICPMS	Ediac aran	Misi and Vizer, 1998
C46--84.2		Maieberg	Namibia	-632.0	0.70 805	894	0.19			TIMS	Ediac aran	Halverson et al., 2007
C46--74.4		Maieberg	Namibia	-632.9	0.70 805	1230	0.14			TIMS	Ediac aran	Halverson et al., 2007
P1012X--187.6		Maieberg	Namibia	-632.9	0.70 755	690	0.03			TIMS	Ediac aran	Halverson et al., 2007
P1012X--158.5		Maieberg	Namibia	-633.5	0.70 752	1900	0.02			TIMS	Ediac aran	Halverson et al., 2007
P1012X--151.2		Maieberg	Namibia	-633.7	0.70 756	4270	0			TIMS	Ediac aran	Halverson et al., 2007
P1012		Maieberg	Namibia	-	0.70	942	0.11			TIMS	Ediac	Halverson et al.,

X--150.2				633.7	744						aran	2007
P1012X--105.2		Maieberg	Namibia	-633.9	0.70756	1280				TIMS	Ediacaran	Halverson et al., 2007
P1012X--96.2		Maieberg	Namibia	-634.1	0.70748	1360	0.03			TIMS	Ediacaran	Halverson et al., 2007
P1012X--87.9		Maieberg	Namibia	-634.1	0.70758	1170	0.07			TIMS	Ediacaran	Halverson et al., 2007
C46--20.2		Maieberg	Namibia	-635.0	0.70717	1790	0.06			TIMS	Ediacaran	Halverson et al., 2007
		Nama	Namibia	-539.0	0.70870	1512				TIMS	Ediacaran	Kaufman et al., 1993
SS17		Nama	Namibia	-543.9	0.70851	1591	0.04	0.12		TIMS	Ediacaran	Kaufman et al., 1993
SH12		Nama	Namibia	-544.0	0.70846	3336	0.05	0.51		TIMS	Ediacaran	Kaufman et al., 1993
NG91		Nama	Namibia	-544.9	0.70859	1886	0.22	0.04		TIMS	Ediacaran	Kaufman et al., 1993
SH43		Nama	Namibia	-544.9	0.70853	1520	0.02	0.06		TIMS	Ediacaran	Kaufman et al., 1993
NG90		Nama	Namibia	-545.1	0.70857	1493	0.08	0.08		TIMS	Ediacaran	Kaufman et al., 1993
NG87		Nama	Namibia	-545.3	0.70857	2093	0.06	0.03		TIMS	Ediacaran	Kaufman et al., 1993
SH49		Nama	Namibia	-545.4	0.70849	1979	0.03	0.07		TIMS	Ediacaran	Kaufman et al., 1993
NG85		Nama	Namibia	-545.5	0.70858	1029	0.07	0.09		TIMS	Ediacaran	Kaufman et al., 1993
NG83		Nama	Namibia	-545.7	0.70852	1856	0.1	0.09		TIMS	Ediacaran	Kaufman et al., 1993
		Nama	Namibia	-550.0	0.70840	3596				TIMS	Ediacaran	Kaufman et al., 1993
P4006-346.6		Ombaatjie	Namibia	-641.0	0.70735	1100	0.31			TIMS	Cryogenian	Halverson et al., 2007
P1012-292		Ombaatje	Namibia	-648.9	0.70725	868	0.03			TIMS	Cryogenian	Halverson et al., 2007

11.97		Rasthof	Namibia	-658.6	0.70699	1340	0.58			Thermionic Quadrupole MS	Cryogenian	Yoshioka et al., 2003
9.94		Rasthof	Namibia	-658.7	0.70698	1430	0.62			Thermionic Quadrupole MS	Cryogenian	Yoshioka et al., 2003
5.96		Rasthof	Namibia	-658.8	0.70689	1720	0.51			Thermionic Quadrupole MS	Cryogenian	Yoshioka et al., 2003
4.95		Rasthof	Namibia	-658.9	0.70685	1460	0.65			Thermionic Quadrupole MS	Cryogenian	Yoshioka et al., 2003
3.99		Rasthof	Namibia	-658.9	0.70697	790	0.38			Thermionic Quadrupole MS	Cryogenian	Yoshioka et al., 2003
M14-172		Hayhook	NW Canada	-633.5	0.70714					TIMS	Ediacaran	Halverson et al., 2007
M14-1.7		Hayhook	NW Canada	-633.5	0.70716	3010	0.07			TIMS	Ediacaran	Halverson et al., 2007
G11-1.53		Hayhook	NW Canada	-633.5	0.70716	2960	0.08			TIMS	Ediacaran	Halverson et al., 2007
G11-0.14		Hayhook	NW Canada	-633.7	0.70714					TIMS	Ediacaran	Halverson et al., 2007
P7-12.4		Keele	NW Canada	-640.0	0.70720					TIMS	Cryogenian	Halverson et al., 2007
P7-4.1		Keele	NW Canada	-641.6	0.70731					TIMS	Cryogenian	Halverson et al., 2007
P7-2.2		Keele	NW Canada	-642.0	0.70718					TIMS	Cryogenian	Halverson et al., 2007
P10H-3		Keele	NW Canada	-653.0	0.70718					TIMS	Cryogenian	Halverson et al., 2007
		Middle Keele	NW Canada	-653.0	0.70712					TIMS	Cryogenian	Narbonne et al., 1994

F1173	0.1	Twitya	NW Canada	-659.0	0.70693	641	0.70114822		96.1	TIMS	Cryogenian	Rooney et al., 2014
F1173	1	Twitya	NW Canada	-659.0	0.70690	-	-		-	TIMS	Cryogenian	Rooney et al., 2014
F1173	1.6	Twitya	NW Canada	-659.0	0.70686	-	-		-	TIMS	Cryogenian	Rooney et al., 2014
F1173	2	Twitya	NW Canada	-659.0	0.70678	-	-		-	TIMS	Cryogenian	Rooney et al., 2014
F1173	2.6	Twitya	NW Canada	-659.0	0.70681	-	-		-	TIMS	Cryogenian	Rooney et al., 2014
F1173	3.1	Twitya	NW Canada	-658.9	0.70672	2763	0.06230072 7		98	TIMS	Cryogenian	Rooney et al., 2014
F1173	3.7	Twitya	NW Canada	-658.9	0.70675	-	-		-	TIMS	Cryogenian	Rooney et al., 2014
F1173	4.9	Twitya	NW Canada	-658.9	0.70682	-	-		-	TIMS	Cryogenian	Rooney et al., 2014
F1173	5.5	Twitya	NW Canada	-658.9	0.70681	-	-		-	TIMS	Cryogenian	Rooney et al., 2014
F1173	6	Twitya	NW Canada	-658.9	0.70680	2825	0.14914649 2		96	TIMS	Cryogenian	Rooney et al., 2014
F1173	7.5	Twitya	NW Canada	-658.9	0.70676	3345	0.06126779 3		98	TIMS	Cryogenian	Rooney et al., 2014
F1173	8	Twitya	NW Canada	-658.9	0.70676	3052	0.06876892 9		100	TIMS	Cryogenian	Rooney et al., 2014
F1173	9.5	Twitya	NW Canada	-658.8	0.70674	3808	0.03522714 8		98	TIMS	Cryogenian	Rooney et al., 2014

F1173	10.5	Twitya	NW Canada	-658.8	0.70682	2248	0.331882126		98	TIMS	Cryogenian	Rooney et al., 2014
F1173	11	Twitya	NW Canada	-658.8	0.70685	2082	0.224705662		100	TIMS	Cryogenian	Rooney et al., 2014
F1173	11.5	Twitya	NW Canada	-658.8	0.70677	3007	0.198497035		100	TIMS	Cryogenian	Rooney et al., 2014
F1173	12	Twitya	NW Canada	-658.8	0.70681	2761	0.209712921		100	TIMS	Cryogenian	Rooney et al., 2014
F1173	14	Twitya	NW Canada	-658.8	0.70676	3512	0.347419975		100	TIMS	Cryogenian	Rooney et al., 2014
F1173	14.5	Twitya	NW Canada	-658.8	0.70679	2240	0.327376299		100	TIMS	Cryogenian	Rooney et al., 2014
F1173	16.5	Twitya	NW Canada	-658.7	0.70681	3084	0.205995995		95.9	TIMS	Cryogenian	Rooney et al., 2014
F1173	17	Twitya	NW Canada	-658.7	0.70692	2924	0.296948773		96	TIMS	Cryogenian	Rooney et al., 2014
F1173	17.5	Twitya	NW Canada	-658.7	0.70677	3340	0.386900006		98	TIMS	Cryogenian	Rooney et al., 2014
F1173	19	Twitya	NW Canada	-658.7	0.70679	2372	0.201905739		94.1	TIMS	Cryogenian	Rooney et al., 2014
F1173	19.5	Twitya	NW Canada	-658.7	0.70683	2594	0.222941333		94.1	TIMS	Cryogenian	Rooney et al., 2014
F1173	20.5	Twitya	NW Canada	-658.7	0.70684					TIMS	Cryogenian	Rooney et al., 2014
F1173	21	Twitya	NW Canada	-658.6	0.70692	3240	0.200074831		98	TIMS	Cryogenian	Rooney et al., 2014

F1173	22	Twitya	NW Canada	-658.6	0.70686					TIMS	Cryogenian	Rooney et al., 2014
F1173	23	Twitya	NW Canada	-658.6	0.70681	-	-		-	TIMS	Cryogenian	Rooney et al., 2014
F1173	25.5	Twitya	NW Canada	-658.6	0.70683	-	-		-	TIMS	Cryogenian	Rooney et al., 2014
F1173	27	Twitya	NW Canada	-658.5	0.70684	-	-		-	TIMS	Cryogenian	Rooney et al., 2014
F1173	27.5	Twitya	NW Canada	-658.5	0.70687	1513	0.44634208 4		96.1	TIMS	Cryogenian	Rooney et al., 2014
F1173	28	Twitya	NW Canada	-658.5	0.70701	2898	0.15369165 8		98	TIMS	Cryogenian	Rooney et al., 2014
F1173	29.5	Twitya	NW Canada	-658.5	0.70692	-	-		-	TIMS	Cryogenian	Rooney et al., 2014
F949	0.6	T1	Mongolia (Uliastai Gorge)	659.0	0.706727	2363	0.11251888 4	0.00025063 7		TIMS	Cryogenian	This study
F949	3	T1	Mongolia (Uliastai Gorge)	658.8	0.706814	1326	0.11182714	0.00040947 2		TIMS	Cryogenian	This study
F949	8	T1	Mongolia (Uliastai Gorge)	658.5	0.706904	1281	0.03362134 5	0.00058706 8		TIMS	Cryogenian	This study
F949	18	T1	Mongolia (Uliastai Gorge)	658.0	0.707367	1198	0.21905488 8	0.00105465 1		TIMS	Cryogenian	This study
F949	29	T2	Mongolia (Uliastai Gorge)	657.3	0.707265	2916	0.04208353 4	0.00019165 4		TIMS	Cryogenian	This study
F949	47	T2	Mongolia (Uliastai	656.3	0.707286	3574	0.03695662	0.0001924		TIMS	Cryogenia	This study

			Gorge)				4				n	
F949	56	T2	Mongolia (Uliastai Gorge)	655.8	0.707153					TIMS	Cryogenian	This study
F949	65	T2	Mongolia (Uliastai Gorge)	655.3	0.707043	874	0.00823981	0.00037846	2	TIMS	Cryogenian	This study
F949	76	T2	Mongolia (Uliastai Gorge)	654.7	0.707193					TIMS	Cryogenian	This study
F949	82	T2	Mongolia (Uliastai Gorge)	654.3	0.707144					TIMS	Cryogenian	This study
F949	88	T2	Mongolia (Uliastai Gorge)	654.0	0.707151	590	0.00555216	0.00059434	9	TIMS	Cryogenian	This study
F949	96	T2	Mongolia (Uliastai Gorge)	653.5	0.707171					TIMS	Cryogenian	This study
F949	102	T2	Mongolia (Uliastai Gorge)	653.2	0.707195					TIMS	Cryogenian	This study
F949	106	T2	Mongolia (Uliastai Gorge)	652.9	0.707208					TIMS	Cryogenian	This study
F949	110	T2	Mongolia (Uliastai Gorge)	652.7	0.707107					TIMS	Cryogenian	This study
F949	114	T2	Mongolia (Uliastai Gorge)	652.5	0.707167					TIMS	Cryogenian	This study
F949	116	T2	Mongolia (Uliastai Gorge)	652.4	0.707122	566	0.013582599	0.00040501	2	TIMS	Cryogenian	This study
F949	120	T2	Mongolia (Uliastai Gorge)	652.1	0.707206					TIMS	Cryogenian	This study
F949	124	T2	Mongolia (Uliastai	651.9	0.707264					TIMS	Cryogenia	This study

			Gorge)								n	
F949	132	T2	Mongolia (Uliastai Gorge)	651.5	0.707161					TIMS	Cryogenian	This study
F949	136	T2	Mongolia (Uliastai Gorge)	651.2	0.707175					TIMS	Cryogenian	This study
F949	140	T2	Mongolia (Uliastai Gorge)	651.0	0.707147	744	0.06137235 7	0.00095515 2	97.350410 5	TIMS	Cryogenian	This study
F949	144	T2	Mongolia (Uliastai Gorge)	650.8	0.707159	547	0.09417390 1	0.00102191 9	95.164191 8	TIMS	Cryogenian	This study
F949	148	T3	Mongolia (Uliastai Gorge)	650.6	0.707217				98.034825 9	TIMS	Cryogenian	This study
F949	150	T3	Mongolia (Uliastai Gorge)	650.5	0.707170				98.446534 7	TIMS	Cryogenian	This study
F949	151	T3	Mongolia (Uliastai Gorge)		0.707213	649	0.173601574	0.000 6086	96.496517 4	TIMS	Cryogenian	This study
F949	153	T3	Mongolia (Uliastai Gorge)	650.4	0.707264	538	0.300 94959	0.000591815	94.839024 4	TIMS	Cryogenian	This study
F949	155	T3	Mongolia (Uliastai Gorge)	650.3	0.707228				83.5	TIMS	Cryogenian	This study
F949	157	T3	Mongolia (Uliastai Gorge)	650.3	0.707237				88.032682 9	TIMS	Cryogenian	This study
F949	160	T3	Mongolia (Uliastai Gorge)	650.2	0.707183				98.355113 6	TIMS	Cryogenian	This study
F949	164	T3	Mongolia (Uliastai Gorge)	650.1	0.707273	595	0.063502234	0.000704093	87.862318 8	TIMS	Cryogenian	This study
F949	172	T3	Mongolia (Uliastai	649.8	0.707283	2577	0.00351230	0.00014458	99.594923	TIMS	Cryogenia	This study

			Gorge)				4	9	9		n	
F949	184	T3	Mongolia (Uliastai Gorge)	649.4	0.70 7385	1212	0.015 95684 7	0.000 33773 2	98.93 3	TIMS	Cryo genia n	This study
F949	210	T3	Mongolia (Uliastai Gorge)	648.6	0.70 7355	1530	0.015 75158 3	0.000 24945 8		TIMS	Cryo genia n	This study
F949	210	T3	Mongolia (Uliastai Gorge)		0.70 7363					TIMS	Cryo genia n	This study
F949	232	T3	Mongolia (Uliastai Gorge)	647.9	0.70 7335	1199	0.011 6575	0.000 29856 6		TIMS	Cryo genia n	This study
F949	264	T3	Mongolia (Uliastai Gorge)	646.9	0.70 7315	1264	0.002 31705 4	0.000 29815		TIMS	Cryo genia n	This study
F949	282	T3	Mongolia (Uliastai Gorge)	646.4	0.70 7300	2436	0.000 58357 2	0.000 16528 2		TIMS	Cryo genia n	This study
F949	332	T3	Mongolia (Uliastai Gorge)	644.8	0.70 7272	1292	0.002 20006 4	0.000 31290 7		TIMS	Cryo genia n	This study
F949	358	T3	Mongolia (Uliastai Gorge)	644.0	0.70 7289	1074	0.007 99434 5	0.000 31421 5		TIMS	Cryo genia n	This study
F949	378	T3	Mongolia (Uliastai Gorge)	643.3	0.70 7221	1173	0.020 04763 2	0.000 30201 3		TIMS	Cryo genia n	This study
F949	382	T3	Mongolia (Uliastai Gorge)	643.2	0.70 7259	1303	0.037 45975 4	0.000 28967 9		TIMS	Cryo genia n	This study
F949	388	T4	Mongolia (Uliastai Gorge)	643.0	0.70 7363	558	0.723 05902	0.000 90007 7		TIMS	Cryo genia n	This study
96TST 1A	0.1	T1	Mongolia(Ts agaan Gorge)	659.0	0.70 6754	2900	0.077 58620 7		95.2		Cryo genia n	Brasier et al., 1996; Shields et al., 2002
96TST	1.5	T1	Mongolia(Ts	659.0	0.70	1350	0.224		96.5		Cryo	Brasier et al., 1996;

3			agaan Gorge)		6796		44444 4				genia n	Shields et al., 2002
96TST 6	7.5	T1	Mongolia(Ts agaan Gorge)	658.9	0.70 6840				97.1		Cryo genia n	Brasier et al., 1996; Shields et al., 2002
96TST 13	18	T1	Mongolia(Ts agaan Gorge)	658.7	0.70 6990	960	0.129 16666 7		97.6		Cryo genia n	Brasier et al., 1996; Shields et al., 2002
96TST 16	22.5	T1	Mongolia(Ts agaan Gorge)	658.6	0.70 6944	1500	0.093 33333 3		98.2		Cryo genia n	Brasier et al., 1996; Shields et al., 2002
96TST 21	30	T2	Mongolia(Ts agaan Gorge)	658.5	0.70 7050	1060	0.148 11320 8		97.5		Cryo genia n	Brasier et al., 1996; Shields et al., 2002
96TST 24	38	T2	Mongolia(Ts agaan Gorge)	658.3	0.70 7094	1500	0.104		90.1		Cryo genia n	Brasier et al., 1996; Shields et al., 2002
96TST 31	67	T2	Mongolia(Ts agaan Gorge)	657.6	0.70 7090				97.7		Cryo genia n	Brasier et al., 1996; Shields et al., 2002
96TST 33	73	T2	Mongolia(Ts agaan Gorge)	657.5	0.70 7200	650	0.023 07692 3		99		Cryo genia n	Brasier et al., 1996; Shields et al., 2002
96TST 35	77	T2	Mongolia(Ts agaan Gorge)	657.4	0.70 7164				99.7		Cryo genia n	Shields et al., 2002
96TST 37	97	T2	Mongolia(Ts agaan Gorge)	657.0	0.70 7290				99.9		Cryo genia n	Shields et al., 2002
96TST 42	147	T3	Mongolia(Ts agaan Gorge)	649.0	0.70 7130				99.5		Cryo genia n	Shields et al., 2002
96TST 55	210	T3	Mongolia(Ts agaan Gorge)	647.3	0.70 7340				99.7		Cryo genia n	Shields et al., 2002
96TST 66	320	T3	Mongolia(Ts agaan Gorge)	644.2	0.70 7290				98.8		Cryo genia n	Shields et al., 2002
96TST 69	350	T3	Mongolia(Ts agaan Gorge)	643.4	0.70 7345	934			97		Cryo genia	Shields et al., 2002

											n	
96TST 71	375	T3	Mongolia(Ts agaan Gorge)	642.7	0.70 7247	1110			91.7		Cryo genia n	Shields et al., 2002
~~96TST 75~~	~~400~~	~~T3~~	~~Mongolia(Ts agaan Gorge)~~	~~642.0~~	~~0.70 7253~~	~~60~~	~~-~~	~~-~~	~~95~~		~~Cryo genia n~~	~~Shields et al., 2002~~
~~U1121~~	~~0.5~~	~~Ol~~	~~Mongolia(Ts agaan Gorge)~~	~~-635.2~~	~~0.70 8713~~	~~121~~	~~-~~	~~-~~	~~-~~	~~MC-ICPMS~~	~~Ediac aran~~	~~this study~~
~~U1121~~	~~12~~	~~Ol~~	~~Mongolia(Ts agaan Gorge)~~	~~-634.8~~	~~0.70 7556~~	~~483~~	~~-~~	~~-~~	~~-~~	~~MC-ICPMS~~	~~Ediac aran~~	~~this study~~
U1121	18.5	Ol	Mongolia(Ts agaan Gorge)	-634.5	0.70 7562	861				MC-ICPMS	Ediac aran	this study
U1121	32	Ol	Mongolia(Ts agaan Gorge)	-634.0	0.70 7586	689				MC-ICPMS	Ediac aran	this study
U1121	23.5	Ol	Mongolia(Ts agaan Gorge)	-634.3	0.70 7588	660				MC-ICPMS	Ediac aran	this study
U1121	21	Ol	Mongolia(Ts agaan Gorge)	-634.4	0.70 7598	572				MC-ICPMS	Ediac aran	this study
U1121	27	Ol	Mongolia(Ts agaan Gorge)	-634.2	0.70 7604	626				MC-ICPMS	Ediac aran	this study
U1121	16	Ol	Mongolia(Ts agaan Gorge)	-634.7	0.70 7615	686				MC-ICPMS	Ediac aran	this study
U1121	29.5	Ol	Mongolia(Ts agaan Gorge)	-634.1	0.70 7625	802				MC-ICPMS	Ediac aran	this study
~~U1121~~	~~39.5~~	~~Ol~~	~~Mongolia(Ts agaan Gorge)~~	~~-633.6~~	~~0.70 7644~~	~~309~~	~~-~~	~~-~~	~~-~~	~~MC-ICPMS~~	~~Ediac aran~~	~~this study~~
U1121	9.2	Ol	Mongolia(Ts agaan Gorge)	-634.9	0.70 7645	532				MC-ICPMS	Ediac aran	this study
~~U1121~~	~~4~~	~~Ol~~	~~Mongolia(Ts agaan Gorge)~~	~~-635.1~~	~~0.70 7718~~	~~197~~	~~-~~	~~-~~	~~-~~	~~MC-ICPMS~~	~~Ediac aran~~	~~this study~~
~~U1121~~	~~8~~	~~Ol~~	~~Mongolia(Ts agaan Gorge)~~	~~-634.9~~	~~0.70 7760~~	~~212~~	~~-~~	~~-~~	~~-~~	~~MC-ICPMS~~	~~Ediac aran~~	~~this study~~
~~U1122~~	~~12~~	~~Sh1~~	~~Mongolia(Ts agaan Gorge)~~	~~-633.3~~	~~0.70 7978~~	~~353~~	~~-~~	~~-~~	~~-~~	~~MC-ICPMS~~	~~Ediac aran~~	~~this study~~
~~U1122~~	~~14.5~~	~~Sh1~~	~~Mongolia(Ts agaan Gorge)~~	~~-633.2~~	~~0.70 7605~~	~~445~~	~~-~~	~~-~~	~~-~~	~~MC-ICPMS~~	~~Ediac aran~~	~~this study~~
U1122	16	Sh1	Mongolia(Ts	-	0.70	631				MC-ICPMS	Ediac	this study

			agaan Gorge)	633.1	7727						aran	
U1122	19	Sh1	Mongolia(Ts agaan Gorge)	-633.1	0.70 7668	564				MC-ICPMS	Ediac aran	this study
U1122	21.5	Sh1	Mongolia(Ts agaan Gorge)	-633.0	0.70 7565	835				MC-ICPMS	Ediac aran	this study
U1122	22.5	Sh1	Mongolia(Ts agaan Gorge)	-632.9	0.70 7619	635				MC-ICPMS	Ediac aran	this study
U1122	26.5	Sh1	Mongolia(Ts agaan Gorge)	-632.9	0.70 7582	807				MC-ICPMS	Ediac aran	this study
~~U1122~~	~~30.5~~	~~Sh1~~	~~Mongolia(Ts agaan Gorge)~~	~~-632.7~~	~~0.70 8453~~	~~105~~	-	-	-	~~MC-ICPMS~~	~~Ediac aran~~	~~this study~~
U1235	143	Sh3a	Mongolia(Ts agaan Gorge)	-588.5	0.70 7951	1470				MC-ICPMS	Ediac aran	this study
~~U1235~~	~~118~~	~~Sh3a~~	~~Mongolia(Ts agaan Gorge)~~	~~-592.6~~	~~0.70 8004~~	~~475~~	-	-	-	~~MC-ICPMS~~	~~Ediac aran~~	~~this study~~
U1235	111	Sh3a	Mongolia(Ts agaan Gorge)	-598.1	0.70 7893	669				MC-ICPMS	Ediac aran	this study
U1235	104	Sh3a	Mongolia(Ts agaan Gorge)	-599.0	0.70 7836	1800				MC-ICPMS	Ediac aran	this study
U1235	94	Sh3a	Mongolia(Ts agaan Gorge)	-600.3	0.70 7825	2230				MC-ICPMS	Ediac aran	this study
U1235	86	Sh3a	Mongolia(Ts agaan Gorge)	-600.5	0.70 7883	817				MC-ICPMS	Ediac aran	this study
U1235	79	Sh3a	Mongolia(Ts agaan Gorge)	-602.7	0.70 7826	1020				MC-ICPMS	Ediac aran	this study
~~F872~~	~~172~~	~~Sh3a~~	~~Mongolia(Ts agaan Gorge)~~	~~-602.7~~	~~0.70 7959~~	~~115~~			-	~~MC-ICPMS~~	~~Ediac aran~~	~~this study~~
F872	189	Sh3a	Mongolia(Ts agaan Gorge)	-600.3	0.70 7713	1190				MC-ICPMS	Ediac aran	this study
F872	193	Sh3a	Mongolia(Ts agaan Gorge)	-599.7	0.70 7690	1650				MC-ICPMS	Ediac aran	this study
F872	198	Sh3a	Mongolia(Ts agaan Gorge)	-599.0	0.70 7834	786				MC-ICPMS	Ediac aran	this study
~~F872~~	~~204~~	~~Sh3a~~	~~Mongolia(Ts agaan Gorge)~~	~~-598.1~~	~~0.70 8466~~	~~61~~				~~MC-ICPMS~~	~~Ediac aran~~	~~this study~~
~~F872~~	~~242~~	~~Sh3b~~	~~Mongolia(Ts agaan Gorge)~~	~~-592.6~~	~~0.70 8036~~	~~155~~				~~MC-ICPMS~~	~~Ediac aran~~	~~this study~~
~~F872~~	~~244~~	~~Sh3b~~	~~Mongolia(Ts agaan Gorge)~~	~~-592.3~~	~~0.70 7931~~	~~278~~				~~MC-ICPMS~~	~~Ediac aran~~	~~this study~~

F872	246	Sh3b	Mongolia(Tsagaan Gorge)	-592.1	0.707786	1700				MC-ICPMS	Ediacaran	this study
F872	249	Sh3b	Mongolia(Tsagaan Gorge)	-591.6	0.707784	1750				MC-ICPMS	Ediacaran	this study
F872	251	Sh3b	Mongolia(Tsagaan Gorge)	-591.3	0.707772	2250				MC-ICPMS	Ediacaran	this study
F872	252	Sh3b	Mongolia(Tsagaan Gorge)	-591.2	0.707852	587				MC-ICPMS	Ediacaran	this study
F872	253	Sh3b	Mongolia(Tsagaan Gorge)	-591.1	0.707803	886				MC-ICPMS	Ediacaran	this study
F872	255	Sh3b	Mongolia(Tsagaan Gorge)	-590.8	0.707809	750				MC-ICPMS	Ediacaran	this study
F872	259	Sh3b	Mongolia(Tsagaan Gorge)	-590.2	0.707797	1900				MC-ICPMS	Ediacaran	this study
F872	261	Sh3b	Mongolia(Tsagaan Gorge)	-589.9	0.707646	1970				MC-ICPMS	Ediacaran	this study
~~F872~~	~~263~~	~~Sh3b~~	~~Mongolia(Tsagaan Gorge)~~	~~-589.6~~	~~0.707899~~	~~292~~				~~MC-ICPMS~~	~~Ediacaran~~	~~this study~~
F872	265	Sh3b	Mongolia(Tsagaan Gorge)	-589.3	0.707833	988				MC-ICPMS	Ediacaran	this study
F872	267	Sh3b	Mongolia(Tsagaan Gorge)	-589.0	0.707793	2000				MC-ICPMS	Ediacaran	this study
F872	269	Sh3b	Mongolia(Tsagaan Gorge)	-588.7	0.707795	1590				MC-ICPMS	Ediacaran	this study
~~F872~~	~~271~~	~~Sh3b~~	~~Mongolia(Tsagaan Gorge)~~	~~-588.5~~	~~0.708460~~	~~96~~	~~-~~		~~-~~	~~MC-ICPMS~~	~~Ediacaran~~	~~this study~~
~~U1437~~	~~90~~	~~Sh3a~~	~~Mongolia(Tsagaan Gorge)~~	~~-605.6~~	~~0.707876~~	~~190~~	-		-	~~MC-ICPMS~~	~~Ediacaran~~	~~this study~~
~~U1437~~	~~93~~	~~Sh3a~~	~~Mongolia(Tsagaan Gorge)~~	~~-605.3~~	~~0.707842~~	~~182~~	-		-	~~MC-ICPMS~~	~~Ediacaran~~	~~this study~~
~~U1437~~	~~99~~	~~Sh3a~~	~~Mongolia(Tsagaan Gorge)~~	~~-605.0~~	~~0.708462~~	~~111~~	-		-	~~MC-ICPMS~~	~~Ediacaran~~	~~this study~~
F949	148	T3	Mongolia (Khongor Range)	-652.6	0.707279					MC-ICPMS	Ediacaran	this study
F949	164	T3	Mongolia (Khongor Range)	-651.8	0.707331					MC-ICPMS	Ediacaran	this study
F949	184	T3	Mongolia	-	0.70					MC-ICPMS	Ediac	this study

			(Khongor Range)	650.8	7411						aran	
Bay S1a*	~~596~~	~~ZA~~	~~Mongolia (Bayan Gorge)~~	~~-540.0~~	~~0.708641~~	~~122~~	-	-	-	~~MC-ICPMS~~	Ediacaran	Brasier et al., 1996
Bay S0	598	ZA	Mongolia (Bayan Gorge)	-540.0	0.708530	990				MC-ICPMS	Ediacaran	Brasier et al., 1996
Tsag. 20	618	ZA	Mongolia(Tsagaan Gorge)	-540.2	0.708417	2300				MC-ICPMS	Ediacaran	Brasier et al., 1996
Bay S4	618	ZA	Mongolia (Bayan Gorge)	-540.2	0.708527	620				MC-ICPMS	Ediacaran	Brasier et al., 1996
Bay S5	623	ZA	Mongolia (Bayan Gorge)	-540.3	0.708425	755				MC-ICPMS	Ediacaran	Brasier et al., 1996
Tsag. 24	780	ZA	Mongolia(Tsagaan Gorge)	-541.8	0.708553	1080				MC-ICPMS	Ediacaran	Brasier et al., 1996
Bay. By O2	800	ZA	Mongolia (Bayan Gorge)	-542.0	0.708430	550				MC-ICPMS	Ediacaran	Brasier et al., 1996
Bay. Bd14*	800	ZA	Mongolia (Bayan Gorge)	-542.0	0.708487	510				MC-ICPMS	Ediacaran	Brasier et al., 1996
Bay 2*	837	ZA	Mongolia (Bayan Gorge)	-542.4	0.708562	520				MC-ICPMS	Ediacaran	Brasier et al., 1996
Bay 4*	847	ZA	Mongolia (Bayan Gorge)	-542.5	0.708439	1090				MC-ICPMS	Ediacaran	Brasier et al., 1996
Bay 33	870	ZA	Mongolia (Bayan Gorge)	-542.7	0.708458	620				MC-ICPMS	Ediacaran	Brasier et al., 1996
Tsag. 25*	~~870~~	~~ZA~~	~~Mongolia(Tsagaan Gorge)~~	~~-542.7~~	~~0.708478~~	~~284~~	-	-	-	~~MC-ICPMS~~	Ediacaran	Brasier et al., 1996
Bay 40*	880	ZA	Mongolia (Bayan Gorge)	-542.8	0.708574	1120				MC-ICPMS	Ediacaran	Brasier et al., 1996

Bay 42*	882	ZA	Mongolia (Bayan Gorge)	-542.9	0.708648	1520				MC-ICPMS	Ediacaran	Brasier et al., 1996
Bay 44*	890	ZA	Mongolia (Bayan Gorge)	-542.9	0.708500	1500				MC-ICPMS	Ediacaran	Brasier et al., 1996
Tsag. 26*	895	ZA	Mongolia(Tsagaan Gorge)	-543.0	0.708687	980				MC-ICPMS	Ediacaran	Brasier et al., 1996
110-03	357	Torginskaya Fm.	Siberia (Chara)	-556.0	0.708250	810				TIMS	Ediacaran	Melezhik et al., 2009
~~116-03~~	~~336~~	~~Torginskaya Fm.~~	~~Siberia (Chara)~~	~~-556.2~~	~~0.708240~~	~~382~~	-		-	TIMS	Ediacaran	Melezhik et al., 2010
~~081-03~~	~~282~~	~~Torginskaya Fm.~~	~~Siberia (Chara)~~	~~-556.6~~	~~0.708590~~	~~315~~	-		-	TIMS	Ediacaran	Melezhik et al., 2011
~~084-03~~	~~267~~	~~Torginskaya Fm.~~	~~Siberia (Chara)~~	~~-556.8~~	~~0.708290~~	~~298~~	-		-	TIMS	Ediacaran	Melezhik et al., 2012
~~105-03~~	~~259~~	~~Torginskaya Fm.~~	~~Siberia (Chara)~~	~~-556.8~~	~~0.708290~~	~~302~~	-		-	TIMS	Ediacaran	Melezhik et al., 2013
~~085-03~~	~~251~~	~~Torginskaya Fm.~~	~~Siberia (Chara)~~	~~-556.9~~	~~0.708270~~	~~355~~	-		-	TIMS	Ediacaran	Melezhik et al., 2014
089-03	233	Torginskaya Fm.	Siberia (Chara)	-557.0	0.708200	812				TIMS	Ediacaran	Melezhik et al., 2015
~~094-03~~	~~198~~	~~Torginskaya Fm.~~	~~Siberia (Chara)~~	~~-557.3~~	~~0.708220~~	~~249~~	-		-	TIMS	Ediacaran	Melezhik et al., 2016
~~062-03~~	~~124.5~~	~~Torginskaya Fm.~~	~~Siberia (Chara)~~	~~-558.0~~	~~0.708340~~	~~393~~	-		-	TIMS	Ediacaran	Melezhik et al., 2017
~~063-03~~	~~121.5~~	~~Torginskaya Fm.~~	~~Siberia (Chara)~~	~~-558.0~~	~~0.708220~~	~~361~~	-		-	TIMS	Ediacaran	Melezhik et al., 2018
~~064-03~~	~~118.5~~	~~Torginskaya Fm.~~	~~Siberia (Chara)~~	~~-558.0~~	~~0.708200~~	~~436~~	-		-	TIMS	Ediacaran	Melezhik et al., 2019
~~073-03~~	~~10~~	~~Torginskaya Fm.~~	~~Siberia (Chara)~~	~~-558.9~~	~~0.708300~~	~~320~~	-		-	TIMS	Ediacaran	Melezhik et al., 2020
~~075-03~~	~~0~~	~~Torginskaya Fm.~~	~~Siberia (Chara)~~	~~-559.0~~	~~0.708400~~	~~318~~	-		-	TIMS	Ediacaran	Melezhik et al., 2021
72-04	1095	Cnenchinskaya Fm.	Siberia (Zhuya West)	-556.0	0.708210	3300				TIMS	Ediacaran	Melezhik et al., 2022
74-04	1084	Cnenchinskaya Fm.	Siberia (Zhuya West)	-556.1	0.708250	3670				TIMS	Ediacaran	Melezhik et al., 2023

75-04	1077	Cnenchinskaya Fm.	Siberia (Zhuya West)	-556.1	0.708210	6590				TIMS	Ediacaran	Melezhik et al., 2024
77-04	1066	Cnenchinskaya Fm.	Siberia (Zhuya West)	-556.2	0.708200	4430				TIMS	Ediacaran	Melezhik et al., 2025
79-04	1040	Cnenchinskaya Fm.	Siberia (Zhuya West)	-556.3	0.708180	4440				TIMS	Ediacaran	Melezhik et al., 2026
80-04	1030	Cnenchinskaya Fm.	Siberia (Zhuya West)	-556.4	0.708190	11870				TIMS	Ediacaran	Melezhik et al., 2027
81-04	1015	Cnenchinskaya Fm.	Siberia (Zhuya West)	-556.4	0.708160	3990				TIMS	Ediacaran	Melezhik et al., 2028
82-04	1003	Cnenchinskaya Fm.	Siberia (Zhuya West)	-556.5	0.708180	3640				TIMS	Ediacaran	Melezhik et al., 2029
83-04	986	Cnenchinskaya Fm.	Siberia (Zhuya West)	-556.6	0.708160	2530				TIMS	Ediacaran	Melezhik et al., 2030
89-04	790	Cnenchinskaya Fm.	Siberia (Zhuya West)	-557.7	0.708080	3190				TIMS	Ediacaran	Melezhik et al., 2031
94-04	725	Cnenchinskaya Fm.	Siberia (Zhuya West)	-558.0	0.708040	7050				TIMS	Ediacaran	Melezhik et al., 2032
95-04	710	Cnenchinskaya Fm.	Siberia (Zhuya West)	-558.1	0.708040	1520				TIMS	Ediacaran	Melezhik et al., 2033
96-04	690	Cnenchinskaya Fm.	Siberia (Zhuya West)	-558.2	0.708030	3620				TIMS	Ediacaran	Melezhik et al., 2034
100-04	540	Nikol'skaya Fm.	Siberia (Zhuya West)	-559.0	0.708020	2190				TIMS	Ediacaran	Melezhik et al., 2035
80-05	763	Kholychskaya Fm.	Siberia (Bol'shoy Patom)	-556.0	0.708620	6875				TIMS	Ediacaran	Melezhik et al., 2036
83-05	741	Kholychskaya Fm.	Siberia (Bol'shoy Patom)	-556.1	0.708470	7690				TIMS	Ediacaran	Melezhik et al., 2037
90-05	523	Alyanchskaya Fm.	Siberia (Bol'shoy Patom)	-557.0	0.708460	4670				TIMS	Ediacaran	Melezhik et al., 2038
91-05	508	Alyanchskaya Fm.	Siberia (Bol'shoy Patom)	-557.1	0.708360	25800				TIMS	Ediacaran	Melezhik et al., 2039
98-05	375	Alyanchskaya Fm.	Siberia (Bol'shoy Patom)	-557.7	0.708190	2505				TIMS	Ediacaran	Melezhik et al., 2040

100-05	360	Alyanchskaya Fm.	Siberia (Bol'shoy Patom)	-557.7	0.708190	6280				TIMS	Ediacaran	Melezhik et al., 2041
101-05	353	Alyanchskaya Fm.	Siberia (Bol'shoy Patom)	-557.8	0.708180	4508				TIMS	Ediacaran	Melezhik et al., 2042
104-05	318	Alyanchskaya Fm.	Siberia (Bol'shoy Patom)	-557.9	0.708130	782				TIMS	Ediacaran	Melezhik et al., 2043
123-05	146	Nikol'skaya Fm.	Siberia (Bol'shoy Patom)	-558.6	0.708070	18950				TIMS	Ediacaran	Melezhik et al., 2044
114-05	62	Nikol'skaya Fm.	Siberia (Bol'shoy Patom)	-559.0	0.708110	2730				TIMS	Ediacaran	Melezhik et al., 2045
35/93	1550	Valyukhta Fm.	Siberia (Ura)	-595.5	0.708020	653	0.09	0.0006			Ediacaran	Vinogradov et al., 1996
20/93	1450	Valyukhta Fm.	Siberia (Ura)	-595.8	0.707690	1989	0.08	0.0003			Ediacaran	Vinogradov et al., 1996
19/93	1350	Valyukhta Fm.	Siberia (Ura)	-596.1	0.707910	645	0.1	0.0008			Ediacaran	Vinogradov et al., 1996
18/93	1250	Valyukhta Fm.	Siberia (Ura)	-594.4	0.707810	1824	0.03	0.0051			Ediacaran	Vinogradov et al., 1996
75/93	450	Barakun Fm.	Siberia (Ura)	-599.1	0.707270	875	0.22	0.0015			Ediacaran	Vinogradov et al., 1996
73/93	350	Barakun Fm.	Siberia (Ura)	-599.4	0.707900	2526	0.04	0.0012			Ediacaran	Vinogradov et al., 1996
50/93	70	Barakun Fm.	Siberia (Ura)	-620.0	0.707760	1396		0.001		TIMS	Ediacaran	Pokrovskii et al., 2006
48/93	50	Barakun Fm.	Siberia (Ura)	-630.8						TIMS	Ediacaran	Pokrovskii et al., 2006
47/93	30	Barakun Fm.	Siberia (Ura)	-631.7						TIMS	Ediacaran	Pokrovskii et al., 2006
46/93	20	Barakun Fm.	Siberia (Ura)	-632.1						TIMS	Ediacaran	Pokrovskii et al., 2006
45/93	10	Barakun Fm.	Siberia (Ura)	-632.5						TIMS	Ediacaran	Pokrovskii et al., 2006
37/05	-1	Dzhemkukan (Bol'shoi Patom)	Siberia (Ura)	-633.0						TIMS	Ediacaran	Pokrovskii et al., 2006

		Fm.										
35/05	-2	Dzhemkukan (Bol'shoi Patom) Fm.	Siberia (Ura)	-633.0						TIMS	Ediacaran	Pokrovskii et al., 2006
N91-23A	1942	Blueflower	NW Canada	-551.0	0.708551	791		0.0016		TIMS		Narbonne et al., 1994
N91-23F	2010	Blueflower	NW Canada		0.708416	1410		0.0012		TIMS		Narbonne et al., 1994
N91-23H	2060	Blueflower	NW Canada		0.708607	1249		0.001		TIMS		Narbonne et al., 1994
N91-23K	2155	Blueflower	NW Canada	-546.0	0.708616	1467		0.0006		TIMS		Narbonne et al., 1994
-	~~868~~	~~Buah~~	~~Oman~~	~~-551.3~~	~~0.708830~~	~~23~~	-	-	-	~~5 collector VG Sector instrument~~	~~Ediacaran~~	~~Burns et al., 1994~~
-	~~864~~	~~Buah~~	~~Oman~~	~~-551.4~~	~~0.708940~~	~~34~~	-	-	-	~~5 collector VG Sector instrument~~	~~Ediacaran~~	~~Burns et al., 1994~~
-	~~840~~	~~Buah~~	~~Oman~~	~~-551.8~~	~~0.708669~~	~~491~~	~~0.62~~	-	-	~~5 collector VG Sector instrument~~	~~Ediacaran~~	~~Burns et al., 1994~~
-	~~832~~	~~Buah~~	~~Oman~~	~~-552.0~~	~~0.708708~~	~~471~~	~~0.51~~	-	-	~~5 collector VG Sector instrument~~	~~Ediacaran~~	~~Burns et al., 1994~~
-	~~732~~	~~Shuram~~	~~Oman~~	~~-553.9~~	~~0.708741~~	~~474~~	~~0.51~~	-	-	~~5 collector VG Sector instrument~~	~~Ediacaran~~	~~Burns et al., 1994~~
-	~~674~~	~~Shuram~~	~~Oman~~	~~-555.0~~	~~0.708788~~	~~327~~	-	-	-	~~5 collector VG Sector instrument~~	~~Ediacaran~~	~~Burns et al., 1994~~
-	~~654~~	~~Shuram~~	~~Oman~~	~~-555.4~~	~~0.708557~~	~~201~~	-	-	-	~~5 collector VG Sector instrument~~	~~Ediacaran~~	~~Burns et al., 1994~~
-	~~404~~	~~Khufai~~	~~Oman~~	~~-562.4~~	~~0.708553~~	~~39~~	-	-	-	~~5 collector VG Sector instrument~~	~~Ediacaran~~	~~Burns et al., 1994~~
-	~~388~~	~~Khufai~~	~~Oman~~	~~-~~	~~0.70~~	~~118~~	-	-	-	~~5 collector VG~~	~~Ediac~~	~~Burns et al., 1994~~

				566.4	8510					Sector instrument	aran	
-	274	Khufai	Oman	-589.9	0.708554	78	-	-	-	5 collector VG Sector instrument	Ediacaran	Burns et al., 1994
-	224	Khufai	Oman	-597.9	0.708411	39	-	-	-	5 collector VG Sector instrument	Ediacaran	Burns et al., 1994
-	200	Khufai	Oman	-601.7	0.708279	29	-	-	-	5 collector VG Sector instrument	Ediacaran	Burns et al., 1994
-	194	Khufai	Oman	-602.6	0.708047	31	-	-	-	5 collector VG Sector instrument	Ediacaran	Burns et al., 1994
-	184	Khufai	Oman	-604.2	0.708533	35	-	-	-	5 collector VG Sector instrument	Ediacaran	Burns et al., 1994
-	176	Khufai	Oman	-605.5	0.708556	28	-	-	-	5 collector VG Sector instrument	Ediacaran	Burns et al., 1994
-	172	M. Bay	Oman	-606.1	0.708502	44	-	-	-	5 collector VG Sector instrument	Ediacaran	Burns et al., 1994
Harvard rock "standards"												
F949	148 (*n=18*)	T3	Mongolia (Khongor Range)		0.707260	2σ uncert. = 0.00005				MC-ICPMS		
					0.707217					TIMS		
F949	164 (*n=5*)	T3	Mongolia (Khongor Range)		0.707323	2σ uncert. = 0.00003				MC-ICPMS		
					0.707273					TIMS		
F949	184 (*n=6*)	T3	Mongolia (Khongor Range)		0.707411	2σ uncert. = 0.00001				MC-ICPMS		

APPENDIX 3.3. SUPPLEMENT TO CHAPTER 3: FIGURES

Figure 3.A1. Sr isotope values of the Tsagaan-Olom Group carbonates plotted against Sr concentration.
Concentration cut-off is shown. Screening method follows Halverson and others (2007).

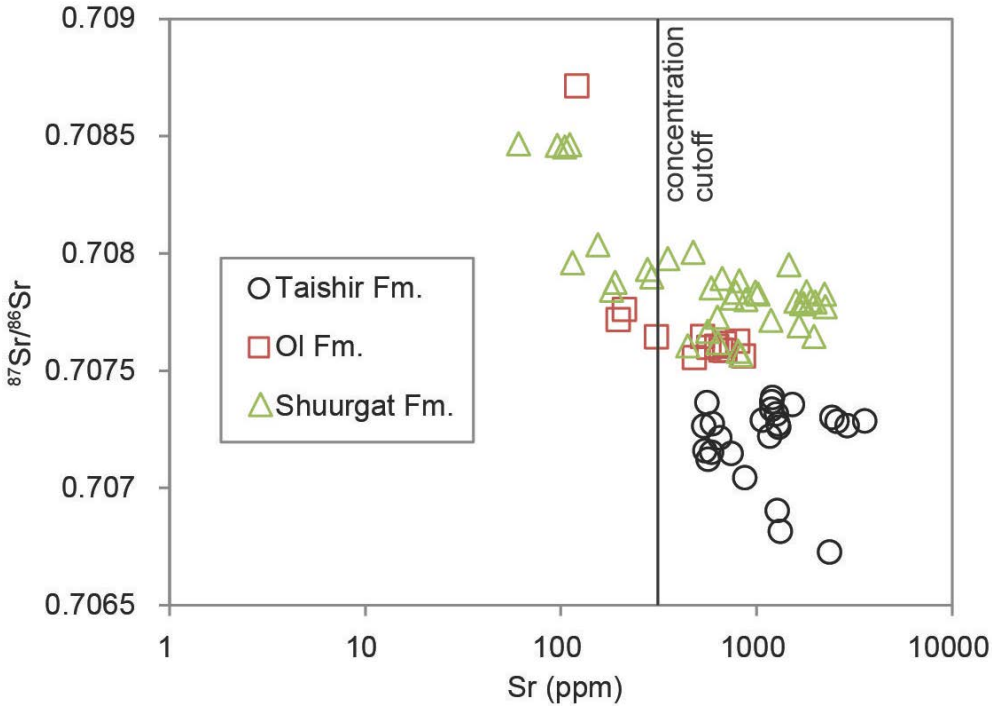

Figure 3.A2. Cathodoluminescence images of zircon grains dated by U-Pb LA-ICPMS from sample U1333.

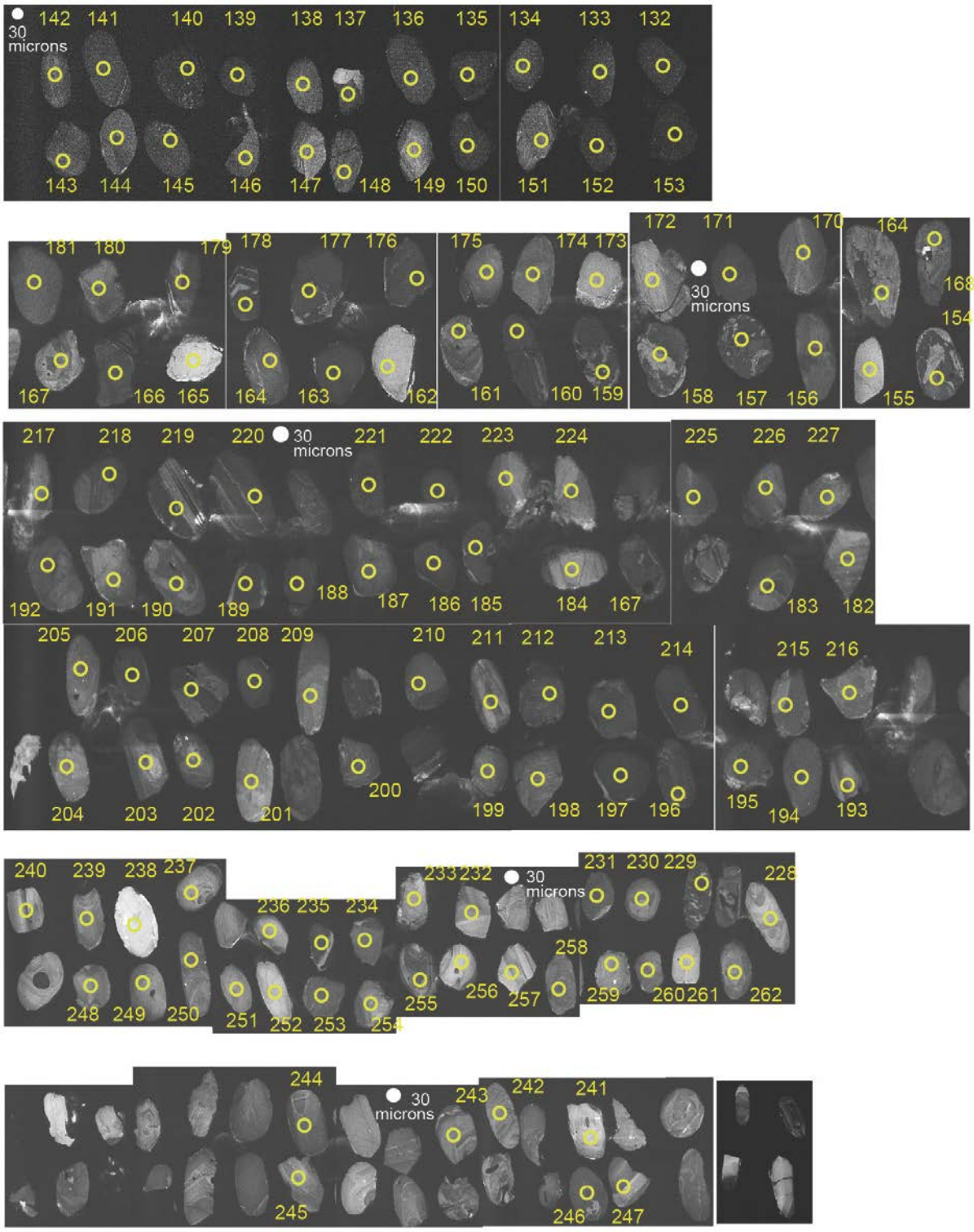

Figure 3.A3. Cathodoluminescence images of zircon grains dated by U-Pb LA-ICPMS from sample U1214.

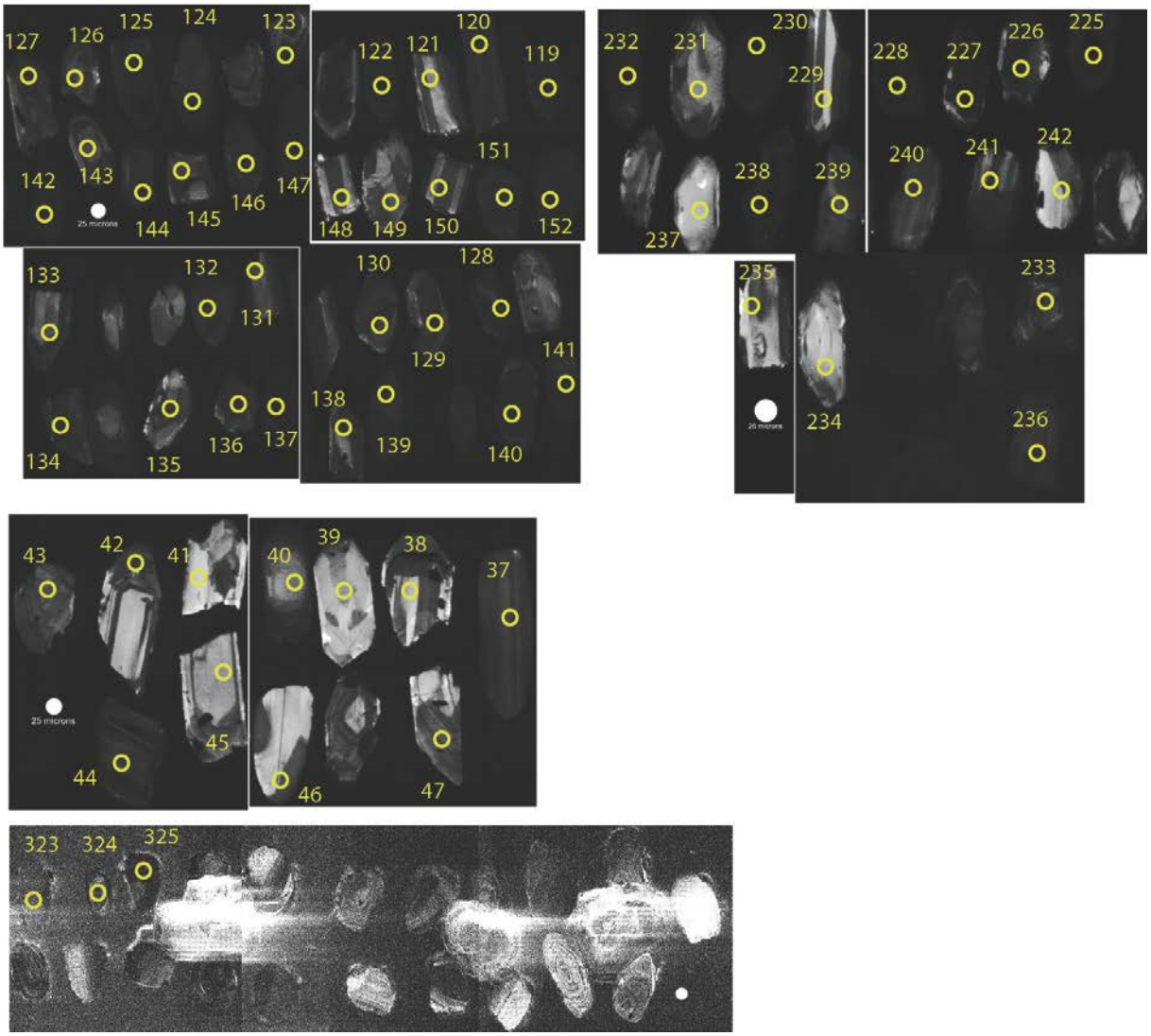

Figure 3.A4. Cathodoluminescence images of zircon grains dated by U-Pb LA-ICPMS from sample F1203-272.1.

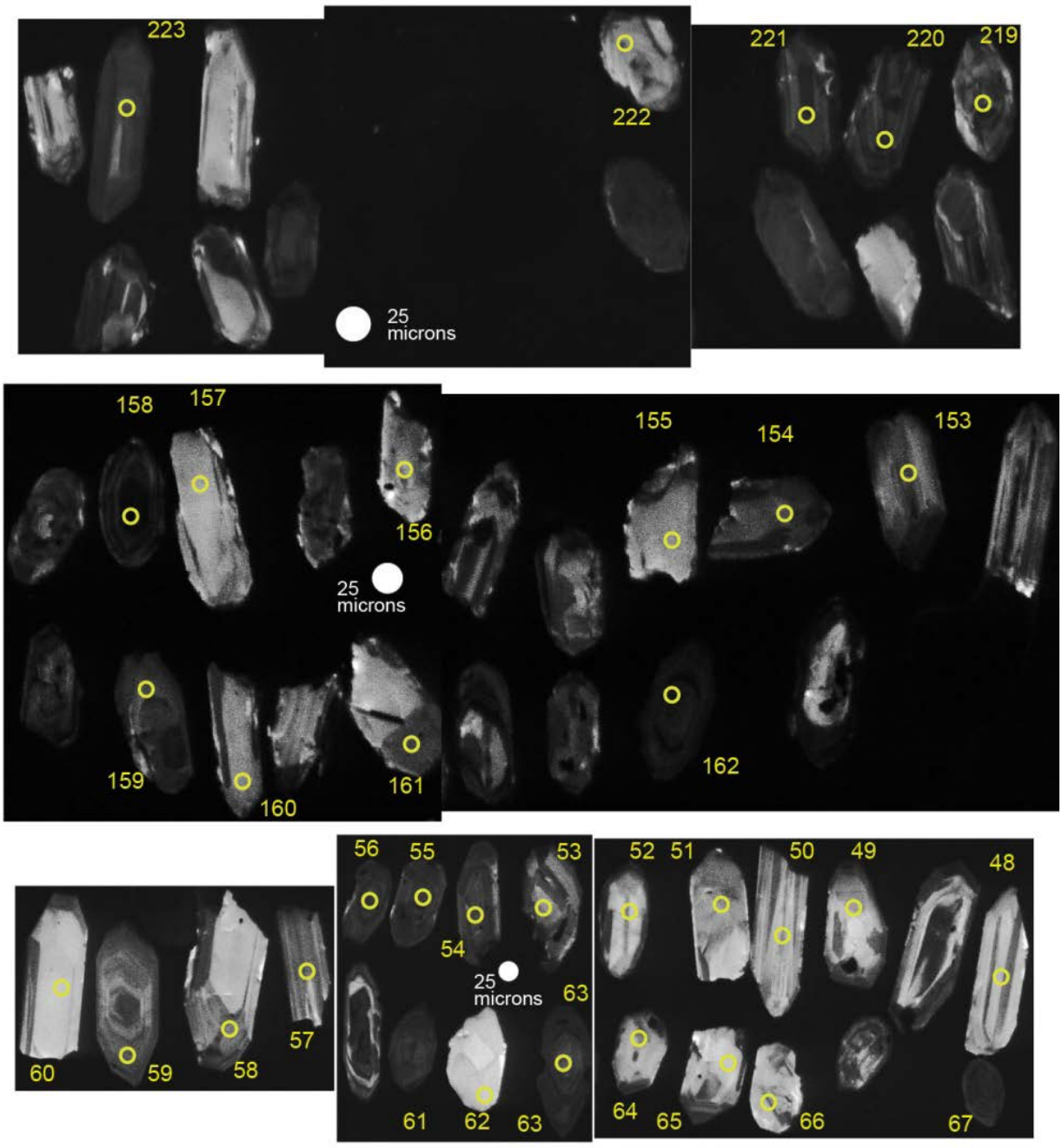

Figure 3.A5. Cathodoluminescence images of zircon grains dated by U-Pb LA-ICPMS from sample F1206-146.1.

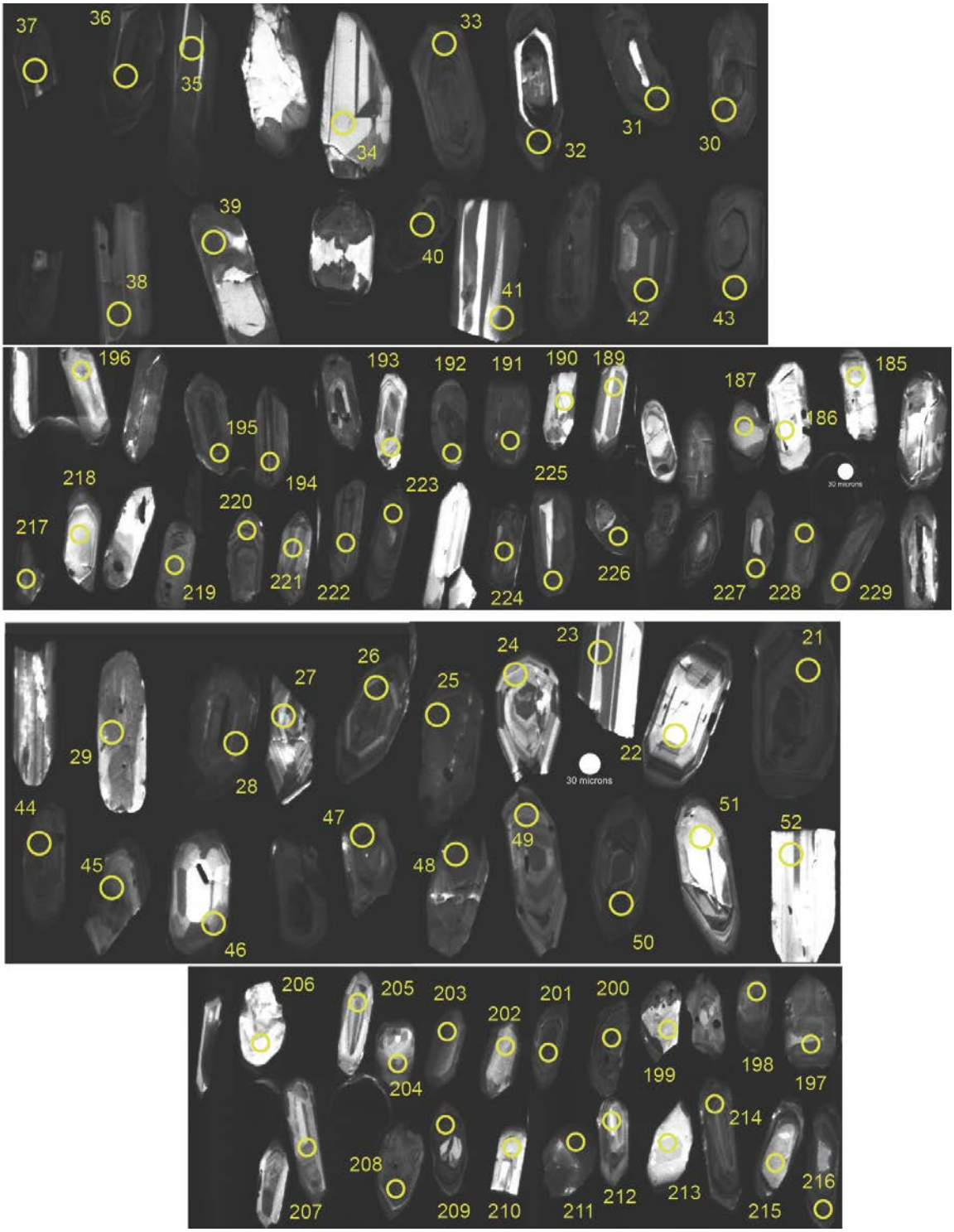

APPENDIX 4.1. SUPPLEMENT TO CHAPTER 4: TABLES

Table 4.A1. $\delta^{13}C_{carb}$ and $\delta^{18}O$ data

The Taishir and Ol formations sampled at Taishir, Ol Mountain, northern Bayan Gorge, Tsakhir Range, and South Khukh Davaa localities and Shuurgat formation at Khongor Range and Khunkher Gorge.

	Depth	Adjusted depth	$d^{18}O$	$d^{13}C$	Fe/[Ca+Mg]	Mg/Ca	Mn/[Ca+Mg]	Sr/[Ca+Mg]	Mn	Sr	Lithology
	(m)	(m)	(‰)	(‰)	(µmol/mol)	(mmol/mol)	(µmol/mol)	(mmol/mol)	ppm	ppm	
Taishir locality				**E 96°34.251'**		**N 46°39.713'**					
Taishir Fm.											
u1108-1	1		-6.89	-6.57	-0.1577	28.8375	0.0112	0.8642	1.89	867.07	limestone
u1108-3	3		-6.79	-6.28	-0.1085	20.8276	-0.0100	2.5592		2285.89	limestone
U1108-7	7		-7.31	-6.08	0.0297	21.5871	0.0366	1.5202	1.55	1365.21	limestone
u1108-10	10		-7.49	-6.16	-0.1276	15.5179	0.0377	2.3799	14.26	2113.25	limestone
u1108-13	13		-7.24	-5.64	-0.0168	26.5923	0.1586	1.5152	66.20	1378.22	limestone
u1108-16	16		-7.03	-4.24	-0.1364	17.8958	0.1615	1.2301	86.90	1100.80	limestone
u1108-19	19		-6.67	-3.33	-0.1855	15.3162	0.0234	1.9458	8.73	1728.59	limestone
u1108-22	22		-7.70	-2.62	-0.1046	13.0344	0.2048	1.6092	110.00	1426.56	limestone
U1108-25	25		-8.97	-1.83	-0.1001	26.7966	0.0132	2.4288		2187.02	limestone
u1108-39	39		-7.58	4.04	-0.0552	21.6356	0.0717	0.9104	41.91	833.40	limestone
u1108-42	42		-7.58	7.08	-0.0278	25.9605	0.0316	1.6803	14.68	1521.32	limestone
u1108-45	45		-8.61	7.43	-0.0229	9.5697	0.0630	2.4278	31.83	2142.90	limestone
u1108-48	48		-2.44	8.88	-0.1712	6.3752	-0.0171	2.1789		1917.90	limestone
U1108-52	52		-4.22	8.57	-0.1918	6.1996	-0.0080	3.0994		2726.05	limestone
u1108-55	55		-6.83	9.13	-0.1907	7.4609	-0.0184	1.5473		1363.54	limestone
U1108-58	58		-1.79	9.12	-0.1317	7.1367	-0.0009	1.8023		1586.52	limestone
U1108-61	61		-5.21	8.98	-0.1872	4.7495	-0.0039	2.8828		2532.72	limestone
U1108-64	64		-3.45	9.02	-0.1064	8.9947	0.0311	1.3060	6.62	1151.82	limestone

U1108-67	67		-6.90	8.96	-0.1875	3.1958	-0.0003	3.3238		2916.83	limestone
U1108-70	70		-4.54	8.45	-0.1870	48.3767	0.0232	2.0469	2.68	2006.03	limestone
U1108-73	73		-4.93	8.34	-0.1565	7.0476	0.0084	1.1635		1024.29	limestone
U1108-76	76		-4.40	9.25	-0.1764	5.6914	-0.0030	2.7989		2460.74	limestone
U1108-79	79		-2.67	9.18	-0.1864	6.1066	0.0022	1.7903		1574.60	limestone
U1108-81	81		-1.77	9.68	-0.1395	103.7738	0.0261	1.3194	2.37	1111.40	limestone
U1108-82	82		-4.90	1.98	-0.1138	19.3430	0.0112	1.2633		1132.35	limestone
U1108-85	85		-6.12	8.84	-0.1098	6.1985	0.0011	2.1725		1910.80	limestone
U1108-88	88		-5.14	8.27	-0.1078	7.6910	0.0167	1.6974		1494.95	limestone
U1108-94	94		-4.68	9.19	-0.0510	7.1305	-0.0001	2.9893		2631.07	limestone
u1108-97.1	97.1		-3.15	8.96	-0.0995	8.6759	0.0002	2.6753		2359.37	limestone
u1108-101	101		-4.34	9.27	-0.0625	6.1312	-0.0095	3.8700		3405.31	limestone
u1108-104	104		-1.05	9.50	-0.1378	4.9562	-0.0178	2.5887		2275.90	limestone
U1108-107	107		-5.68	7.95	-0.1125	8.0902	0.0080	2.5497		2245.99	limestone
U1108-110	110		-4.60	8.49	-0.1525	8.6479	0.0192	1.3844	0.02	1220.50	limestone
u1108-113	113		-1.04	9.49	-0.1447	4.9832	-0.0101	2.3533		2069.01	limestone
u1108-116	116		-6.34	5.01	-0.1772	9.5988	0.0597	0.3585	24.90	320.08	limestone
u1108-119	119		-3.78	8.46	-0.1603	5.7460	-0.0031	1.2203		1073.79	limestone
u1108-122	122		-4.72	8.06	-0.1354	14.9657	-0.0025	0.9867		880.13	limestone
U1108-125	125		-3.12	8.17	-0.0221	7.5771	0.0080	1.1370		1001.48	limestone
U1108-128	128		-3.68	8.75	0.1642	6.0195	0.0112	1.1089		975.29	limestone
U1108-131	131		-1.93	9.11	0.0814	5.6059	-0.0031	1.3779		1211.38	limestone
U1108-137	137		-2.49	9.01	0.1140	5.7725	-0.0084	1.1241		988.97	limestone
u1108-143	143		-2.65	9.08							limestone
U1108-146	146		-4.29	8.81							limestone
U1108-149	149		-2.68	8.88							limestone
U1108-152	152		-4.37	8.37							limestone
U1108-155	155		-3.45	8.54	-0.0133	5.6409	0.0148	1.1565		1016.84	limestone

u1108-158	158		-5.58	8.19	-0.0600	6.5709	0.0328	0.8121	9.10	715.39	limestone
u1108-161	161		-7.07	8.66	-0.0616	4.4037	0.0393	0.4403	18.67	387.07	limestone
U1108-164.1	164.1		-7.56	9.80	-0.1713	4.8828	0.0084	1.6730		1469.95	limestone
u1108-167	167		-10.05	8.44	-0.1700	3.3233	0.0172	1.0829	7.82	950.82	limestone
u1108-170	170		-4.95	9.09	-0.1601	2.7966	0.0193	1.2104	11.51	1062.32	limestone
U1108-173	173		-9.61	8.01	0.5855	108.6294	0.0713	1.6090	20.22	1338.82	limestone
u1108-176	176		-6.69	6.90	-0.0926	12.4678	0.0865	0.7908	47.17	703.28	limestone
U1108	0.2		-6.96	-5.60							limestone
U1108	0.6		-8.16	-6.25							limestone
U1108	1.5		-7.74	-6.36							limestone
U1108	2		-7.11	-6.91							limestone
U1108	2.5		-7.22	-6.36							limestone
U1108	3.5		-7.13	-6.15							limestone
U1108	4		-6.79	-6.13							limestone
U1108	4.5		-6.65	-5.91							limestone
U1108	5		-6.66	-5.82							limestone
U1108	5.5		-6.56	-5.85							limestone
U1108	6		-6.84	-5.96							limestone
U1108	6.7		-6.72	-6.06							limestone
U1108	7.5		-7.10	-6.03							limestone
U1108	8		-8.30	-5.99							limestone
U1108	8.5		-7.15	-6.80							limestone
U1108	9.5		-7.29	-6.41							limestone
U1108	11		-6.94	-5.87							limestone
U1108	11.5		-6.52	-5.60							limestone
U1108	12		-7.13	-5.71							limestone
U1108	12.5		-7.76	-5.80							limestone
U1108	13.5		-7.41	-5.31							limestone

U1108	14		-6.14	-4.65							limestone
U1108	14.5		-7.05	-4.64							limestone
U1108	15		-7.76	-4.23							limestone
U1108	15.5		-7.47	-4.31							limestone
U1108	16.5		-6.32	-4.26							limestone
U1108	17		-6.65	-3.99							limestone
U1108	17.5		-9.75	-3.43							limestone
U1108	18		-7.53	-3.77							limestone
U1108	18.5		-9.59	-3.50							limestone
U1108	19.5		-7.49	-3.28							limestone
U1108	20		-7.01	-3.30							limestone
U1108	20.5		-9.13	-2.77							limestone
U1108	21		-7.63	-2.76							limestone
U1108	21.5		-7.19	-2.86							limestone
U1108	22.5		-7.18	-2.35							limestone
U1108	23		-5.29	-2.85							limestone
U1108	23.5		-5.60	-2.31							limestone
U1108	24		-8.51	-1.70							limestone
U1108	25.5		-9.50	-1.40							limestone
U1108	26		-8.29	-1.89							limestone
U1108	26.5		-6.95	-1.34							limestone
U1108	27		-8.65	-2.03							limestone
U1108	27.5		-7.78	-1.82							limestone
U1108	39.5		-6.89	3.00							limestone
U1108	40		-7.97	5.96							limestone
U1108	40.5		-7.73	6.38							limestone
U1108	41		-9.44	7.63							limestone
U1108	41.5		-6.88	7.72							limestone

U1108	42.5		-7.03	6.31							limestone
U1108	43		-4.73	7.38							limestone
U1108	43.5		-6.87	6.55							limestone
U1108	44		-5.27	7.75							limestone
U1108	44.5		-6.13	8.35							limestone
U1108	45.5		-5.13	8.74							limestone
U1108	46		-5.26	8.26							limestone
U1108	47		-6.97	7.33							limestone
U1108	49		-5.31	8.70							limestone
U1108	50		-4.84	8.51							limestone
U1108	53		-3.73	8.56							limestone
U1108	55.7		-4.84	8.14							limestone
U1108	57		-4.38	8.17							limestone
U1108	57.1		-2.27	9.03							limestone
U1108	59		-8.10	8.39							limestone
U1108	60		-3.38	8.70							limestone
U1108	62		-8.04	8.72							limestone
U1108	63		-5.94	8.69							limestone
U1108	65		-3.90	9.36							limestone
U1108	66		-4.30	8.99							limestone
U1108	68		-3.68	9.39							limestone
U1108	69		-2.80	9.55							limestone
U1108	71		-4.81	8.43							limestone
U1108	72		-5.05	8.55							limestone
U1108	74		-4.79	8.42							limestone
U1108	75		-7.11	6.33							limestone
U1108	77		-4.74	8.84							limestone
U1108	78		-3.91	9.35							limestone

U1108	80		-5.31	7.53							limestone
U1108	83		-5.40	5.93							limestone
U1108	84		-5.50	8.83							limestone
U1108	86		-4.34	9.04							limestone
U1108	87		-5.96	9.18							limestone
U1108	89		-2.44	9.13							limestone
U1108	90		-4.57	3.62							limestone
U1108	91		-5.67	5.28							limestone
U1108	92		-2.07	9.48							limestone
U1108	93		-2.44	9.39							limestone
U1108	95		-4.72	9.15							limestone
U1108	96		-5.58	9.36							limestone
U1108	98		-4.19	8.06							limestone
U1108	99		-2.53	5.10							limestone
U1108	100		-3.52	8.43							limestone
U1108	102		-1.78	9.27							limestone
U1108	103		-2.13	9.14							limestone
U1108	105.1		-2.49	9.16							limestone
U1108	106		-1.99	8.84							limestone
U1108	108		-5.72	7.76							limestone
U1108	109		-1.54	9.13							limestone
U1108	111		-5.13	7.66							limestone
U1108	112		-5.19	7.67							limestone
U1108	114		-4.62	7.59							limestone
U1108	115		-3.65	8.20							limestone
U1108	117		-6.47	4.86							limestone
U1108	118		-5.01	7.14							limestone
U1108	120		-6.28	6.30							limestone

U1108	121		-5.30	8.13							limestone
U1108	123		-6.96	6.41							limestone
U1108	124		-3.50	8.67							limestone
U1108	126		-5.01	8.20							limestone
U1108	127		-3.20	8.27							limestone
U1108	129		-3.42	8.51							limestone
U1108	130		-2.98	8.51							limestone
U1108	132		-3.62	8.75							limestone
U1108	133		-2.99	8.60							limestone
U1108	134		-4.86	7.84							limestone
U1108	135		-5.29	7.40							limestone
U1108	136		-3.50	8.53							limestone
U1108	138		-1.78	10.03							limestone
U1108	139		-4.33	8.24							limestone
U1108	140		-3.28	8.89							limestone
U1108	141		-2.43	10.29							limestone
U1108	142		-3.14	8.64							limestone
U1108	144		-3.56	8.95							limestone
U1108	145		-4.98	7.66							limestone
U1108	147		-4.81	7.29							limestone
U1108	148		-3.64	8.81							limestone
U1108	150		-2.87	9.20							limestone
U1108	151		-4.20	8.16							limestone
U1108	153		-4.39	8.70							limestone
U1108	154		-4.03	9.27							limestone
U1108	156		-4.34	9.00							limestone
U1108	157		-4.47	8.45							limestone
U1108	159		-4.49	8.64							limestone

U1108	160		-3.24	8.60							limestone
U1108	162		-6.40	8.01							limestone
U1108	163		-10.19	8.86							limestone
U1108	165		-8.17	9.42							limestone
U1108	166		-8.18	9.45							limestone
U1108	167.9		-12.47	8.61							limestone
U1108	169		-12.52	8.42							limestone
U1108	171		-7.05	9.92							limestone
U1108	172		-10.97	9.82							limestone
U1108	174		-5.53	9.63							limestone
U1108	175		-5.93	8.14							limestone
U1108	177		-5.43	8.73							limestone
Taishir locality				**E 96°34.356'**		**N 46°39.010'**					
Ol Fm.											
f860-0.5	0.5		-4.90	0.50							dolomite
f860-1	1		-5.53	0.26	0.8547	1008.4161	0.5176	0.0957	204.77	174.97	dolomite
f860-3-2	3		-5.47	0.33							dolomite
F860-5-3	5		-5.59	0.94	1.3107	959.8818	0.4490	0.5993	570.50		dolomite
f860-5p5	5.5		-5.90	0.46	1.0520	1001.0203	0.5733	0.1165	250.72	212.19	dolomite
f860-6p5-2	6.5		-7.07	0.24	2.3121	949.1278	0.5496	0.0851	196.52	74.46	dolomite
f860-9-2	9		-5.87	0.45							dolomite
f860-9p5	9.5		-5.92	0.10	1.0602	982.0572	0.4944	0.1336	188.24	240.96	dolomite
f860-11-2	11		-5.91	-0.26							dolomite
f860-12	12		-5.09	-2.04	1.8892	968.3504	0.9548	0.0968	372.41	173.39	dolomite
f860-20	20		-6.07	-3.46	6.6499	978.8473	0.9580	0.1480	409.28	266.57	dolomite
f860-24	24		-4.30	-3.40	5.8081	959.1550	1.0324	0.0843	400.35	150.30	dolomite
f860-26	26		-8.96	-5.11							limestone

f860-27	27		-13.36	-5.06							limestone
f860-27.8	27.8		-10.03	-4.93							limestone
f860-29	29		-9.31	-4.86							limestone
f860-30	30		-7.95	-4.94							limestone
N. Bayan Gorge				**E 96°21.380'**		**N 46°45.064'**					
Taishir Fm.											
u1115-3	3		-4.93	2.98	0.6849	1000.3791	0.1006	0.0346	81.73	30.27	dolomite
U1115-6	6		-3.23	3.45					9.90		dolomite
u1115-9	9		-6.02	3.17	0.2367	961.4423	0.1095	0.0416	100.02	36.42	dolomite
u1115-12	12		-3.63	3.31	0.2298	981.8984	0.0602	0.0076	39.27	6.68	dolomite
u1115-17	17		-3.91	0.40	0.9630	965.9978	0.1391	0.1761	121.82	153.64	dolomite
u1115-24p5	24.5		-1.21	0.58	0.6522	976.6300	0.0638		58.83		dolomite
u1115-26	26		-0.43	-0.28	0.4968	982.1482	0.0476		26.33		dolomite
u1115-31	31		-10.19	1.25	1.4322	967.5054	0.1419	0.3074	84.89	267.31	dolomite
U1115-35	35		-0.57	1.21	0.5908	980.3547	0.1042		23.57		dolomite
u1115-38	38		-1.41	1.74	0.8311	932.0874	0.0685	0.1200	49.10	104.80	dolomite
u1115-41	41		0.13	1.77	0.4000	988.7085	0.0591	0.0044	38.36	3.83	dolomite
u1115-44	44		0.22	1.93	0.4922	1000.2383	0.0747		54.13		dolomite
U1115-46	46		-0.74	2.14	0.4888	961.7289	0.0933		19.43		dolomite
u1115-49	49		0.41	0.92	0.3333	983.5332	0.0607		44.02		dolomite
U1115-52	52		-0.56	1.69	0.1605	944.2496	0.0840		19.27		dolomite
u1115-55	55		0.21	1.43	0.2489	998.9902	0.0774	0.0012	55.21	1.04	dolomite
u1115-58	58		-0.23	2.02	0.3764	992.4723	0.0756		49.57		dolomite
u1115-61	61		-6.81	1.48	0.4115	946.9438	0.1020	0.2147	85.20	187.11	dolomite
u1115-64	64		-1.19	1.79	0.5082	1002.1439	0.0776		57.24		dolomite
u1115-67	67		-1.64	2.12	0.4963	986.2754	0.0933		79.38		dolomite
u1115-70	70		-1.48	2.83	0.2002	974.2442	0.0544		36.64		dolomite

u1115-73	73		-7.90	2.36	0.7692	986.6273	0.0916	0.2282	70.62	198.79	dolomite
u1115-76	76		-3.45	2.36	0.7787	979.0574	0.0582	0.0102	36.84	8.97	dolomite
u1115-79	79		-2.82	3.26	0.4884	973.7463	0.0824	0.0042	68.63	3.69	dolomite
U1115	3.5		-6.63	3.60							dolomite
U1115	4		-8.47	2.92							dolomite
U1115	4.5		-6.33	3.48							dolomite
U1115	5		-2.98	2.92							dolomite
U1115	5.5		-5.28	3.49							dolomite
U1115	6.5		-4.13	3.42							dolomite
U1115	7		-4.80	3.42							dolomite
U1115	7.5		-6.39	3.13							dolomite
U1115	8		-6.14	3.23							dolomite
U1115	8.5		-5.51	1.56							dolomite
U1115	9.5		-7.09	2.47							dolomite
U1115	10		-4.24	3.43							dolomite
U1115	10.5		-5.06	3.40							dolomite
U1115	11		-2.16	0.36							dolomite
U1115	11.5		-5.90	2.43							dolomite
U1115	12.5		-5.44	3.24							dolomite
U1115	13		-5.12	3.23							dolomite
U1115	13.5		-3.52	2.23							dolomite
U1115	14		-7.26	0.25							dolomite
U1115	14.5		-3.31	-0.05							dolomite
U1115	15		-4.39	1.54							dolomite
U1115	15.5		-3.42	0.34							dolomite
U1115	16		-1.84	1.07							dolomite
U1115	16.5		-1.44	2.90							dolomite
U1115	17.5		-1.71	0.41							dolomite

U1115	18		-2.11	-0.22							dolomite
U1115	18.5		-2.44	-1.84							dolomite
U1115	19		-2.35	-1.42							dolomite
U1115	19.5		-10.62	0.19							dolomite
U1115	20		-3.00	0.36							dolomite
U1115	20.5		-2.89	0.96							dolomite
U1115	22.5		-1.62	-0.68							dolomite
U1115	23		-1.11	-0.51							dolomite
U1115	24		-1.41	1.04							dolomite
U1115	25		-1.13	-0.46							dolomite
U1115	25.5		-3.21	0.72							dolomite
U1115	26.5		-0.39	0.64							dolomite
U1115	27		-2.32	0.97							dolomite
U1115	27.5		-0.21	0.73							dolomite
U1115	28		-0.67	1.08							dolomite
U1115	28.5		-0.92	-0.62							dolomite
U1115	29		-2.27	-0.14							dolomite
U1115	29.5		0.52	-0.77							dolomite
U1115	30		0.07	-0.02							dolomite
U1115	30.5		0.38	0.27							dolomite
U1115	31.5		-0.49	1.00							dolomite
U1115	32		-1.11	1.92							dolomite
U1115	32.5		-0.11	1.55							dolomite
U1115	33		-0.21	1.60							dolomite
U1115	33.5		0.42	0.68							dolomite
U1115	34		-1.55	1.70							dolomite
U1115	34.5		-1.32	1.70							dolomite
U1115	35.5		-0.04	1.10							dolomite

U1115	36		-0.99	0.86							dolomite
U1115	36.5		-0.86	0.48							dolomite
U1115	37		-0.07	0.22							dolomite
U1115	37.5		0.08	1.23							dolomite
U1115	38.5		-0.90	1.56							dolomite
U1115	39		-0.37	1.18							dolomite
U1115	39.5		-0.92	0.93							dolomite
U1115	40		-0.29	1.19							dolomite
U1115	40.5		-1.43	1.22							dolomite
U1115	41.5		-0.76	1.26							dolomite
U1115	42		-0.33	0.93							dolomite
U1115	42.5		-0.96	0.14							dolomite
U1115	43		-0.69	0.32							dolomite
U1115	43.5		0.26	0.82							dolomite
U1115	44.5		-1.20	0.94							dolomite
U1115	45		-0.88	1.15							dolomite
U1115	45.5		-1.19	1.90							dolomite
U1115	46.5		-0.75	1.67							dolomite
U1115	47		0.47	1.97							dolomite
U1115	47.5		1.09	1.54							dolomite
U1115	48		0.66	1.41							dolomite
U1115	48.5		0.14	1.29							dolomite
U1115	49.5		0.29	0.41							dolomite
U1115	50		-0.10	-0.21							dolomite
U1115	50.5		-0.21	-0.03							dolomite
U1115	51		-0.63	0.95							dolomite
U1115	51.5		-3.36	0.64							dolomite
U1115	53		-0.02	0.43							dolomite

U1115	53.5		-0.17	1.44							dolomite
U1115	54		0.16	0.75							dolomite
U1115	54.5		-0.17	1.20							dolomite
U1115	56		-0.41	0.99							dolomite
U1115	57		-0.21	1.72							dolomite
U1115	59		-0.31	1.72							dolomite
U1115	60		-4.59	2.70							dolomite
U1115	62		-0.88	2.05							dolomite
U1115	63		-1.02	2.17							dolomite
U1115	65		-0.98	1.17							dolomite
U1115	66		-6.17	2.01							dolomite
U1115	68		-1.37	2.75							dolomite
U1115	69		-1.62	2.23							dolomite
U1115	71		-2.90	2.72							dolomite
U1115	72		-5.11	2.38							dolomite
U1115	74		-3.43	0.21							dolomite
U1115	75		-1.45	2.81							dolomite
U1115	77		-1.97	2.51							dolomite
U1115	78		-4.23	2.51							dolomite
				E 96°21.151'		**N 46°44.959'**					dolomite
u1116-4	84		-1.87	2.55	0.3269	987.5281	0.0634	0.5966	44.11		dolomite
u1116-6	86		-3.96	2.26	0.3420	987.2817	0.0602	0.5985		9.00	dolomite
u1116-15p1	95.1		-4.98	2.74		954.3262	0.1277	0.5976	110.14		dolomite
u1116-19	99		-2.01	2.89	-0.0230	992.4020	0.0475	0.5965	19.72		dolomite
u1116-25	105		-5.75	2.87	-0.0629	970.5936	0.0417	0.5977	22.39		dolomite
u1116-29	109		-7.18	2.94	-0.0416	913.3002	0.0756	0.5992	52.89		dolomite
u1116-43	123		-5.95	3.11	0.6049	905.5109	0.1732	0.5987	169.22		dolomite
u1116-47	127		-6.96	2.17	0.6504	944.5743	0.1473	0.6019	104.21		dolomite

u1116-55	135		-5.52	3.21	0.8441	1017.5359	0.1597	0.5998	33.02		dolomite
U1116-61	141		-6.40	2.64					118.26		dolomite
u1116-69	149		-5.22	3.47	-0.0321	968.9377	0.2315	0.5983	230.44		dolomite
u1116-73	153		-1.70	3.11	0.0097	987.7162	0.3109	0.5967	295.65		dolomite
u1116-86	166		-6.40	2.72	0.0376	962.0217	0.3127	0.5978	326.23		dolomite
U1116	80		-2.51	3.09							dolomite
U1116	81		-1.69	3.39							dolomite
U1116	82		-4.23	2.27							dolomite
U1116	83		-1.32	2.99							dolomite
U1116	85		-4.40	1.64							dolomite
U1116	87		-1.92	1.90							dolomite
U1116	88		-2.21	2.13							dolomite
U1116	89		-2.46	2.28							dolomite
U1116	91		-3.64	0.65							dolomite
U1116	93		-8.17	2.37							dolomite
U1116	94		-2.95	2.73							dolomite
U1116	96		-4.02	3.21							dolomite
U1116	97		-8.22	3.03							dolomite
U1116	98		-6.37	2.91							dolomite
U1116	100		-8.29	2.56							dolomite
U1116	101		-8.63	2.36							dolomite
U1116	102		-2.20	2.99							dolomite
U1116	103		-3.30	2.96							dolomite
U1116	104		-6.77	2.99							dolomite
U1116	106		-7.90	2.86							dolomite
U1116	107		-5.53	2.56							dolomite
U1116	108		-7.13	2.78							dolomite
U1116	110		-4.72	3.05							dolomite

U1116	111		-2.01	3.03							dolomite
U1116	112		-2.10	2.72							dolomite
U1116	113		-5.38	2.54							dolomite
U1116	114		-1.89	2.42							dolomite
U1116	115		-4.28	2.26							dolomite
U1116	116		-3.93	1.55							dolomite
U1116	117		-6.87	1.68							dolomite
U1116	118		-10.63	1.95							dolomite
U1116	119		-2.03	2.11							dolomite
U1116	120		-5.95	2.39							dolomite
U1116	121		-4.51	2.88							dolomite
U1116	122		-6.17	3.00							dolomite
U1116	124		-3.61	1.82							dolomite
U1116	125		-6.31	2.01							dolomite
U1116	126		-5.12	1.83							dolomite
U1116	128		-5.26	2.48							dolomite
U1116	129		-4.49	2.55							dolomite
U1116	130		-4.96	3.12							dolomite
U1116	131		-6.30	3.22							dolomite
U1116	132		-3.09	2.86							dolomite
U1116	133		-3.12	2.58							dolomite
U1116	134		-2.48	3.24							dolomite
U1116	136		-8.07	3.23							dolomite
U1116	137		-6.52	3.12							dolomite
U1116	138		-9.77	2.74							dolomite
U1116	139		-5.99	3.17							dolomite
U1116	140		-0.36	3.00							dolomite
U1116	142		-4.05	2.58							dolomite

U1116	143		-8.02	3.21							dolomite
U1116	144		-5.67	2.58							dolomite
U1116	145		-5.68	1.07							dolomite
U1116	146		-6.21	3.24							dolomite
U1116	147		-5.18	2.44							dolomite
U1116	148		-4.67	-0.12							dolomite
U1116	150		-8.18	3.00							dolomite
U1116	151		-2.35	3.26							dolomite
U1116	152		-5.82	2.73							dolomite
U1116	154		-8.90	2.91							dolomite
U1116	156		-4.62	3.09							dolomite
U1116	157		-6.78	3.17							dolomite
U1116	158		-1.47	2.81							dolomite
U1116	159		-3.94	3.25							dolomite
U1116	160		-5.00	3.27							dolomite
U1116	161		-7.23	2.97							dolomite
U1116	162		-6.54	3.40							dolomite
U1116	163		-8.43	1.90							dolomite
	164		-4.53	3.00							dolomite
	165		-6.99	2.92							dolomite
				E 96°20.744'		**N 46°45.087'**					dolomite
u1117-18	168		-3.72	2.45	1.1000	966.6259	0.2169	0.5986	272.08		dolomite
u1117-21	171		-2.38	2.66	0.7360	957.8916	0.1271	0.0609	99.38	53.33	dolomite
u1117-24	174		-3.21	2.52	0.6635	988.4920	0.2186	0.5984	51.37		dolomite
u1117-27	177		-2.98	2.68	0.9214	982.8862	0.1953	0.5994	122.42	64.19	dolomite
u1117-38	188		-1.75	2.16	0.1316	991.5268	0.4797	0.5968	561.37		dolomite
u1117-41	191		-1.83	2.65	0.2382	1004.7250	0.3217	0.5964	394.47		dolomite
u1117-44	194		-1.75	2.16	0.1330	988.7006	0.4335	0.0760	493.17	66.42	dolomite

U1117	167		-2.78	2.67							dolomite
U1117	168		-3.72	2.45							dolomite
U1117	169		-2.14	2.81							dolomite
U1117	170		-5.95	2.88							dolomite
U1117	171		-2.38	2.66							dolomite
U1117	172		-5.17	2.55							dolomite
U1117	173		-4.00	3.05							dolomite
U1117	174		-3.21	2.52							dolomite
U1117	175		-3.54	2.96							dolomite
U1117	176		-4.00	3.06							dolomite
U1117	177		-2.98	2.68							dolomite
U1117	186		-1.79	2.67							dolomite
U1117	187		-1.95	2.45							dolomite
U1117	188		-1.75	2.16							dolomite
U1117	189		-1.50	2.57							dolomite
U1117	190		-3.30	2.98							dolomite
U1117	191		-1.83	2.65							dolomite
U1117	192		-1.13	2.13							dolomite
U1117	193		-2.43	2.61							dolomite
U1117	194		-5.50	2.80							dolomite
U1117	195		-3.79	2.48							dolomite
U1117	196		-2.39	2.85							dolomite
N. Bayan Gorge				**E 96°20.462'**		**N 46°45.138'**					
Ol Fm.											
u1113-1	1		-2.62	2.64	0.1263	984.8009	0.1888	0.5971	181.76		dolomite
u1113-4	4		-4.43	-0.92	0.7388	1001.1119	0.3823	0.5981	512.02		dolomite
u1113-6	6		-4.24	-0.76	0.3510	980.6649	0.4076	0.5981	528.99		dolomite
u1113-7	7		-4.60	-0.61	0.4336	999.7686	0.4043	0.0630	523.94	55.13	dolomite

u1113-8	8		-4.37	-0.59	0.5415	993.4743	0.3528	0.0574	480.19	50.26	dolomite
u1113-9p6	9.6		-2.61	0.43	0.5492	988.5133	0.3479	0.0287	443.83	25.13	dolomite
u1113-11	11		-1.94	0.69							dolomite
u1113-14	14		-2.80	0.01	0.6814	986.3536	0.3929	0.0338	408.48	29.63	dolomite
u1113-17	17		-4.02	-1.67	2.7084	972.9091	1.7420	0.0425	2029.72	37.18	dolomite
u1113-20	20		-3.29	0.40	0.6819	974.8626	2.9579	0.5969	4756.79		dolomite
u1113-25	25		-4.04	-4.56	0.1698	934.3952	1.3732	0.0710	1668.19	62.10	dolomite
u1113-32p1	32.1		-4.76	0.09	0.6840	993.8205	0.5790	0.3598	349.88	313.18	dolomite
u1113-35	35		-3.40	2.86	2.0493	963.0499	0.2445	0.5987	244.10		dolomite
u1113-40	40		-0.46	1.18	0.6022	987.9689	0.1226	0.0219	155.06	19.21	dolomite
u1113-43	43		-0.61	2.74	0.2227	1019.0051	0.0653	-0.0046	56.73		dolomite
u1113-46	46		-4.25	1.73	0.4325	972.7757	0.0505	0.0980	42.94	85.70	dolomite
u1113	0.1		-6.14	3.08							dolomite
u1113	2		-5.18	2.99							dolomite
u1113	2.9		-4.68	2.87							dolomite
u1113	5		-4.40	-0.54							dolomite
u1113	5.2		-4.98	-1.02							dolomite
u1113	5.4		-4.26	-0.69							dolomite
u1113	5.6		-4.50	-0.86							dolomite
u1113	5.8		-4.11	-0.33							dolomite
u1113	6.2		-4.33	-0.80							dolomite
u1113	6.4		-3.10	0.18							dolomite
u1113	6.6		-5.21	-0.58							dolomite
u1113	6.8		-4.92	-0.59							dolomite
u1113	7.2		-4.91	-0.93							dolomite
u1113	7.4		-5.46	-1.62							dolomite
u1113	7.6		-4.09	-0.31							dolomite
u1113	7.8		-3.67	-0.25							dolomite

u1113	8.2		-4.49	-0.36							dolomite
u1113	8.4		-5.10	-0.20							dolomite
u1113	8.6		-4.04	0.08							dolomite
u1113	8.8		-4.01	-0.09							dolomite
u1113	9		-4.83	-0.18							dolomite
u1113	9.2		-3.22	0.32							dolomite
u1113	9.4		-2.80	0.72							dolomite
u1113	9.8		-3.89	0.59							dolomite
u1113	10		-2.57	0.21							dolomite
u1113	10.2		-2.48	0.28							dolomite
u1113	10.4		-1.96	0.23							dolomite
u1113	10.6		-2.28	0.17							dolomite
u1113	11.2		-2.01	0.26							dolomite
u1113	11.4		-2.08	0.94							dolomite
u1113	11.6		-2.01	1.09							dolomite
u1113	11.8		-1.85	2.05							dolomite
u1113	12		-1.91	0.97							dolomite
u1113	12.2		-1.84	1.58							dolomite
u1113	12.4		-2.79	2.27							dolomite
u1113	12.6		-1.74	2.19							dolomite
u1113	12.8		-1.40	2.11							dolomite
u1113	13		-2.24	1.02							dolomite
u1113	13.2		-1.68	0.52							dolomite
u1113	13.4		-3.40	0.56							dolomite
u1113	13.6		-1.96	0.49							dolomite
u1113	13.8		-3.01	-0.47							dolomite
u1113	14.2		-3.31	0.52							dolomite
u1113	14.4		-3.70	0.24							dolomite

u1113	14.6			-0.21							dolomite
u1113	14.8			-0.30							dolomite
u1113	15		-3.88	2.67							dolomite
u1113	15.8		-1.52	0.07							dolomite
u1113	18		-1.96	0.10							dolomite
u1113	19										dolomite
u1113	22		-1.26	1.56							dolomite
u1113	23		-3.24	0.63							dolomite
u1113	23.9		-1.63	-0.70							dolomite
u1113	32.5		-0.93	1.46							dolomite
u1113	34		-0.96	2.88							dolomite
u1113	38.1		-0.97	3.23							dolomite
u1113	39		-1.26	2.43							dolomite
u1113	41		-2.46	2.62							dolomite
u1113	42		-1.10	2.40							dolomite
u1113	44		-3.47	3.28							dolomite
u1113	45		-1.05	2.18							dolomite
u1113	47		-5.20	2.84							dolomite
Ol Mountain				**E 96°25.672'**		**N 46°41.452'**					
Taishir Fm.											
U1111 11	11		-2.77	3.63					279.40		limestone
u1111	11.5		-3.75	2.89							limestone
u1111	12		-2.90	2.88							limestone
u1111	12.5		-3.10	2.60							limestone
u1111	13		-3.17	0.71							limestone
u1111	16	0	-9.54	-5.88							limestone
u1111	16.5	0.1568627	-9.08	-6.22							limestone
u1111	17	0.3137255	-7.38	-5.82							limestone

u1111	18	0.627451	-6.25	-5.40							limestone
u1111	18.5	0.7843137	-6.11	-4.98							limestone
u1111	19	0.9411765	-6.03	-5.46							limestone
u1111	19.5	1.0980392	-5.97	-5.12							limestone
u1111	20	1.254902	-6.54	-5.33							limestone
u1111	20.5	1.4117647	-7.03	-5.52							limestone
u1111	24	2.5098039	-6.74	-5.33							limestone
u1111	25	2.8235294	-6.66	-5.47							limestone
u1111	25.5	2.9803922	-5.91	-5.36							limestone
u1111	26	3.1372549	-6.40	-5.56							limestone
u1111	26.5	3.2941176	-6.80	-5.81							limestone
u1111	27	3.4509804	-5.82	-5.40							limestone
u1111	27.5	3.6078431	-6.01	-6.14							limestone
u1111	28	3.7647059	-5.27	-5.41							limestone
u1111	28.5	3.9215686	-6.90	-5.54							limestone
u1111	29	4.0784314	-6.76	-5.40							limestone
u1111	30	4.3921569	-6.51	-4.93							limestone
u1111	30.5	4.5490196	-6.93	-5.47							limestone
u1111	31	4.7058824	-6.10	-5.36							limestone
u1111	31.5	4.8627451	-5.84	-5.37							limestone
u1111	32	5.0196078	-6.82	-5.50							limestone
u1111	32.5	5.1764706	-6.40	-5.52							limestone
u1111	33	5.3333333	-8.13	-1.21							limestone
u1111	34	5.6470588	-7.15	-5.93							limestone
u1111	34.5	5.8039216	-6.27	-5.54							limestone
u1111	36	6.2745098	-6.22	-6.08							limestone
u1111	36.5	6.4313725	-5.76	-5.72							limestone
u1111	37	6.5882353	-6.70	-6.09							limestone

u1111	37.5	6.745098	-6.08	-5.54							limestone
u1111	38	6.9019608	-6.44	-6.32							limestone
u1111	38.5	7.0588235	-6.65	-6.05							limestone
u1111	39.5	7.372549	-5.86	-6.06							limestone
u1111	40	7.5294118	-6.47	-6.92							limestone
u1111	40.5	7.6862745	-6.26	-6.29							limestone
u1111	41	7.8431373	-3.51	-5.90							limestone
u1111	41.5	8	-5.78	-6.05							limestone
u1111	42	8.1568627	-5.94	-6.29							limestone
u1111	43	8.4705882	-13.41	-1.18							limestone
u1111	43.5	8.627451	-6.46	-5.67							limestone
u1111	44	8.7843137	-6.79	-6.04							limestone
u1111	44.5	8.9411765	-6.98	-6.31							limestone
u1111	45	9.0980392	-5.89	-6.22							limestone
u1111	45.5	9.254902	-6.04	-5.44							limestone
u1111	46	9.4117647	-6.02	-5.41							limestone
u1111	46.5	9.5686274	-4.36	-5.24							limestone
u1111	47	9.7254902	-6.90	-5.46							limestone
u1111	47.5	9.8823529	-6.76	-5.29							limestone
u1111	48	10.039216	-6.80	-5.57							limestone
u1111	48.5	10.196078	-6.10	-5.15							limestone
u1111	49	10.352941	-6.26	-5.38							limestone
u1111	49.5	10.509804	-6.61	-5.67							limestone
U1111 50	50	10.666667	-6.71	-5.30	-0.1557	17.0655		2.7847		2561.81	limestone
u1111	50.5	10.823529	-6.87	-5.53							limestone
u1111	51	10.980392	-6.79	-5.26							limestone
u1111	51.5	11.137255	-6.78	-5.41							limestone
u1111	52	11.294118	-5.73	-5.20							limestone

u1111	52.5	11.45098	-6.02	-5.59							limestone
u1111 53	53	11.607843	-6.31	-5.93	-0.1920	12.6889	0.0057	2.8964			dolomite
u1111	53.5	11.764706	-6.32	-5.35							limestone
u1111	54	11.921569	-8.71	-5.46							limestone
u1111	54.5	12.078431	-6.34	-5.47							limestone
u1111	55	12.235294	-7.82	-5.38							limestone
U1111 56	56	12.54902	-7.26	-4.82	-0.1631	16.2444	0.0031	2.6640		2368.98	limestone
u1111	56.5	12.705882	-7.56	-5.23							limestone
u1111	57	12.862745	-9.67	-4.85							limestone
u1111	57.5	13.019608	-7.44	-3.96							limestone
u1111	58	13.176471	-13.85	-4.64							limestone
u1111	58.5	13.333333	-11.69	-1.08							limestone
U1111 59	59	13.490196	-8.19	1.38	0.0297	837.0744	0.1551	0.2750	43.56	239.31	limestone
u1111	59.5	13.647059	-10.95	1.16							limestone
u1111	60.5	13.960784	-9.19	-4.27							limestone
u1111	61	14.117647	-9.19	0.10							limestone
u1111	61.5	14.27451	-6.00	0.14							limestone
u1111 62	62	14.431373	-5.93	0.55	0.2586	793.4006	0.2493	0.2543	76.28	221.62	limestone
u1111	62.5	14.588235	-5.64	-3.57							limestone
u1111	63	14.745098	-12.47	-2.38							limestone
u1111	63.5	14.901961	-4.92	-1.27							limestone
u1111	64	15.058824	-7.18	-1.10							limestone
u1111	64.5	15.215686	-7.92	-0.94							limestone
U1111 65	65	15.372549	-10.25	-2.27	0.0049	179.9327	0.0771	0.5808	35.00	500.71	limestone
u1111	65.5	15.529412	-12.58	-1.73							limestone
u1111	66.5	15.843137	-5.69	-6.47							limestone
u1111	67	16	-7.59	-4.99							limestone
u1111	67.5	16.692308	-10.55	0.16							limestone

U1111 68	68	17.384615	-8.83	-1.00	-0.0944	206.6771	0.1084	0.5136	33.76	443.82	limestone
u1111	68.5	18.076923	-14.28	-0.25							limestone
u1111	69	18.769231	-9.71	-0.92							limestone
u1111	69.5	19.461538	-9.64	-1.01							limestone
u1111	70	20.153846	-9.38	-0.89							limestone
u1111	70.5	20.846154	-7.42	1.16							limestone
U1111 71P5	71.5	22.230769	-8.58	1.23	-0.0687	571.3775	0.0583	0.2278	8.52	198.40	limestone
u1111	71.5	22.230769	-8.58	1.23							limestone
u1111	72	22.923077	-1.85	2.16							limestone
u1111	72.5	23.615385	-7.80	0.65							limestone
u1111	73	24.307692	-6.76	0.26							limestone
u1111	73.5	25	-12.75	1.75							limestone
u1111	74	26.160305	-10.34	1.47							limestone
U1111 74P5	74.5	27.320611	-6.92	2.25	-0.1468	83.7722	0.0527	0.4890	16.28	421.79	limestone
u1111	75	28.480916	-20.06	1.07							limestone
u1111	75.5	29.641221	-14.06	1.21							limestone
u1111	76	30.801527	-10.27	2.62							limestone
u1111	76.5	31.961832	-11.82	1.88							limestone
u1111 77	77	33.122137	-3.83	1.98	-0.0685	993.6288	0.2328	0.0094	72.57	8.19	dolomite
u1111	78	35.442748	-2.00	2.34							dolomite
U1111 133	79	37.763359	-2.49	4.60	-0.1309	1041.0206	0.0560		4.28		dolomite
u1111	79	37.763359	-1.10	4.27							dolomite
u1111	80	40.083969	0.08	4.25							dolomite
u1111	81	42.40458	-4.84	4.03							dolomite
U1111 136	82	44.725191	-8.25	4.07	-0.0863	986.2146	0.0545		3.44		dolomite
u1111	82	44.725191	-8.11	3.73							dolomite
u1111	84	49.366412	-2.00	3.63							dolomite
U1111 139	85	51.687023	-9.97	3.71	0.0252	975.7342	0.0685	0.0107	7.80	9.40	dolomite

u1111	85	51.687023	-0.67	3.25							dolomite
u1111	86	54.007634	-7.29	3.24							dolomite
u1111	87	56.328244	-1.91	3.73							dolomite
u1111	88	58.648855	-5.91	3.33							dolomite
u1111 143	89	60.969466	-6.99	3.46	0.0557	982.4186	0.1702		51.79		dolomite
u1111	89	60.969466	-6.28	3.54							dolomite
u1111	90	63.290076	-6.89	3.68							dolomite
u1111	91	65.610687	-7.06	3.39							dolomite
u1111 146	92	67.931298	-6.62	3.09	0.2951	945.6751	0.1244		34.21		dolomite
u1111	92	67.931298	-4.40	2.37							dolomite
u1111	93	70.251908	-6.43	4.19							dolomite
u1111	94	72.572519	-5.32	1.27							dolomite
U1111 149	95	74.89313	-1.98	1.87	0.5718	977.7261	0.0628		4.52		dolomite
u1111	95	74.89313	-1.75	2.23							dolomite
u1111	96	77.21374	-1.75	0.23							dolomite
u1111	97	79.534351	-3.14	3.69							dolomite
U1111 152	98	81.854962	-5.23	3.98	0.2145	1006.1036	0.0950		17.48		dolomite
u1111	98	81.854962	-6.35	2.27							dolomite
u1111	100	86.496183	-3.99	4.76							dolomite
U1111 155	101	88.816794	-4.49	3.20	1.3326	1019.7161	0.2381		84.40		dolomite
u1111	101	88.816794	-9.32	3.66							dolomite
u1111	103	93.458015	-6.75	3.25							dolomite
u1111	104	95.778626	-3.17	3.77							dolomite
U1111 159	105	98.099237	-5.74	4.83	-0.0335	995.0778	0.0729		9.76		dolomite
u1111	106	100.41985	-10.68	3.82							dolomite
u1111	107	102.74046	-6.45	4.43							dolomite
U1111 162	108	105.06107	-0.30	4.70	-0.0057	953.9250	0.0560		3.72		dolomite
u1111	108	105.06107	-6.77	3.95							dolomite

u1111	110	109.70229	-6.95	2.54							dolomite
u1111 165	111	112.0229	-3.27	4.03	-0.0048	999.7907	0.0622		8.18		dolomite
u1111	111	112.0229	-5.59	1.55							dolomite
u1111	113	116.66412	-5.58	3.17							dolomite
u1111 168	114	118.98473	-6.74	3.78	0.4729	966.8835	0.2359		76.76		dolomite
u1111	114	118.98473	-4.55	1.96							dolomite
u1111	116	123.62595	-1.17	1.05							dolomite
u1111 171	117	125.94656	-6.83	5.00	0.2508	970.7359	0.1234		28.89		dolomite
u1111	117	125.94656	0.76	2.56							dolomite
u1111	119	130.58779	-4.17	4.52							dolomite
u1111 174	120	132.9084	-5.57	4.63	0.1740	811.6446	0.2333	0.1769	84.32	154.38	dolomite
u1111	120	132.9084	-6.44	2.94							dolomite
u1111	122	137.54962	-7.85	3.70							dolomite
u1111	123	139.87023	-3.39	4.24							dolomite
u1111	124	142.19084	-5.80	2.70							dolomite
u1111	126	146.83206	-5.54	2.68							dolomite
u1111	127	149.15267	-1.63	4.34							dolomite
u1111	129	153.79389	-2.98	3.41							dolomite
u1111	130	156.1145	-3.73	3.95							dolomite
u1111	132	160.75573	-0.79	5.33							dolomite
u1111	133	163.07634	-0.52	5.27							dolomite
u1111	135	167.71756	-6.31	4.89							dolomite
u1111	136	170.03817	-7.59	4.67							dolomite
u1111	138	174.67939	-8.01	5.14							dolomite
u1111	139	177	-10.06	4.52							dolomite
Ol Mountain				**E 96°25.671'**		**N 46°41.462'**					
Ol Fm.											
u1112 11	11		-4.77	-0.55	0.5837	974.4309	0.2010	0.0155	64.57	13.62	dolomite

u1112 15p2	15.2		-4.80	1.12	1.3458	950.7169	0.4089	0.0611	171.29	53.48	dolomite
u1112 1p8	1.8		-5.47	-1.55	1.4999	956.8725	0.1996		64.45		dolomite
u1112 27	27		-7.12	-0.67	-0.0337	73.8863	0.1781	0.5000	78.67	432.30	dolomite
u1112 28p5	28.5		-6.46	0.21	0.2659	965.4131	0.3493	0.1192	135.63	104.14	dolomite
u1112 3	3		-4.49	-1.13	0.5547	952.5722	0.3635	0.0054	101.08	4.72	dolomite
u1112 32	32		-0.78	-1.18	0.4790	984.0383	0.2422	0.0114	81.13	9.95	dolomite
u1112 34p5	34.5		-3.09	3.16	3.0344	959.8553	0.4900	0.0451	206.77	39.51	dolomite
u1112 40	40		-1.70	3.51	9.0530	947.8580	0.3446		111.95		dolomite
u1112 8	8		-4.23	-0.14	0.4376	980.7663	0.3594	0.0218	134.11	19.12	dolomite
u1112-5p4	5.4		-5.16	-1.24	0.3229	983.8115	0.2133	0.0559	254.50	48.94	dolomite
u1112-13	13		-6.31	-0.33	0.6445	978.0564	0.1839	0.5991	190.66		dolomite
u1112-18	18		-5.22	-1.55	0.6265	959.3020	0.3971	0.0569	464.04	49.79	dolomite
u1112-20p2	20.2		-5.60	-0.76	0.6968	961.2665	0.4280	0.0711	529.85	62.19	dolomite
u1112-30p5	30.5		-1.12	2.47	2.3632	968.0188	0.2125	0.0644	228.14	56.36	dolomite
u1112-38	38		-1.65	2.92	0.3135	984.4785	0.1804	0.0681	183.88	59.57	dolomite
u1112	1.2		-5.77	1.20							dolomite
u1112	1.4		-5.16	-0.28							dolomite
u1112	1.6		-4.97	-1.33							dolomite
u1112	2		-4.57	-0.72							dolomite
u1112	2.2		-3.86	-1.02							dolomite
u1112	2.4		-6.29	-0.58							dolomite
u1112	2.6		-5.84	-0.94							dolomite
u1112	2.8		-4.92	-0.90							dolomite
u1112	3.2		-5.14	-0.93							dolomite
u1112	3.4		-5.46	-1.25							dolomite
u1112	3.6		-5.01	-0.27							dolomite
u1112	3.8		-6.54	-1.73							dolomite
u1112	4		-4.75	0.11							dolomite

u1112	4.2		-5.89	-0.64							dolomite
u1112	4.4		-4.59	0.18							dolomite
u1112	4.6		-4.29	-0.75							dolomite
u1112	4.8		-3.54	-0.20							dolomite
u1112	5		-4.50	-1.12							dolomite
u1112	5.2		-2.23	-0.48							dolomite
u1112	5.6		-3.93	-0.87							dolomite
u1112	5.8		-5.01	-0.58							dolomite
u1112	6		-4.87	-0.15							dolomite
u1112	6.2		-4.25	-0.21							dolomite
u1112	6.4		-6.01	-0.97							dolomite
u1112	6.6		-4.46	-0.99							dolomite
u1112	6.8		-3.89	-0.53							dolomite
u1112	7		-5.58	-1.69							dolomite
u1112	7.2		-5.55	-1.52							dolomite
u1112	7.4		-2.22	1.75							dolomite
u1112	7.6		-3.89	-0.08							dolomite
u1112	7.8		-2.56	0.62							dolomite
u1112	8.2		-5.23	-0.68							dolomite
u1112	8.4		-4.02	0.23							dolomite
u1112	8.8		-4.53	0.02							dolomite
u1112	9		-4.71	0.00							dolomite
u1112	9.2		-3.93	0.43							dolomite
u1112	9.4		-4.89	-0.68							dolomite
u1112	9.6		-4.63	-0.23							dolomite
u1112	9.8		-4.55	-0.22							dolomite
u1112	10		-5.16	-0.49							dolomite
u1112	10.2		-4.92	-0.24							dolomite

u1112	10.4		-4.73	-0.58							dolomite
u1112	10.8		-5.94	-0.71							dolomite
u1112	11.2		-3.73	-0.48							dolomite
u1112	11.4		-3.36	0.51							dolomite
u1112	11.6		-3.06	1.40							dolomite
u1112	11.8		-3.96	1.69							dolomite
u1112	12		-4.39	0.52							dolomite
u1112	12.2		-2.04	0.99							dolomite
u1112	12.4		-2.60	-0.16							dolomite
u1112	12.6		-6.20	-1.46							dolomite
u1112	12.8		-5.10	-1.45							dolomite
u1112	13.2		-6.01	-0.40							dolomite
u1112	13.4		-7.47	-1.29							dolomite
u1112	13.6		-6.50	-0.84							dolomite
u1112	14		-4.55	-0.09							dolomite
u1112	14.2		-4.53	-0.83							dolomite
u1112	14.4		-3.95	-0.45							dolomite
u1112	14.6		-4.38	-0.47							dolomite
u1112	14.8		-3.68	-0.16							dolomite
u1112	15		-3.07	0.58							dolomite
u1112	15.4		-4.32	0.65							dolomite
u1112	15.6		-4.04	1.64							dolomite
u1112	15.8		-3.25	1.73							dolomite
u1112	16		-2.23	1.79							dolomite
u1112	16.2		-4.59	1.65							dolomite
u1112	16.4		-5.99	1.94							dolomite
u1112	16.6		-4.85	2.04							dolomite
u1112	16.8		-4.29	0.27							dolomite

u1112	17		-3.29	0.35							dolomite
u1112	17.2		-4.24	-0.15							dolomite
u1112	17.4		-6.17	-0.10							dolomite
u1112	17.6		-5.17	-0.92							dolomite
u1112	17.8		-3.80	-0.72							dolomite
u1112	18.2		-5.59	-0.86							dolomite
u1112	18.4		-4.81	-1.34							dolomite
u1112	18.6		-4.48	-1.49							dolomite
u1112	19		-5.29	-1.89							dolomite
u1112	19.2		-4.30	0.28							dolomite
u1112	19.4		-3.77	-0.70							dolomite
u1112	19.6		-4.79	-1.50							dolomite
u1112	19.8		-4.79	-1.38							dolomite
u1112	20		-3.98	-0.94							dolomite
u1112	20.8		-6.18	-3.60							dolomite
u1112	21		-2.67	1.06							dolomite
u1112	21.5		-5.55	-3.15							dolomite
u1112	22		-1.91	2.60							dolomite
u1112	22.5		-2.86	0.90							dolomite
u1112	23		-1.00	2.83							dolomite
u1112	23.5		-0.54	2.01							dolomite
u1112	24		-0.66	1.88							dolomite
u1112	24.5		-0.27	-0.14							dolomite
u1112	25		-0.31	1.90							dolomite
u1112	25.5		-5.65	2.01							dolomite
u1112	26		-3.66	1.75							dolomite
u1112	27.5		-6.19	0.37							dolomite
u1112	28		-5.79	0.66							dolomite

u1112	29.5		-2.75	1.85							dolomite
u1112	30		-0.66	0.98							dolomite
u1112	30.9		-0.36	-0.28							dolomite
u1112	31.5		-1.32	2.05							dolomite
u1112	32.5		-1.37	2.63							dolomite
u1112	33		-2.40	3.07							dolomite
u1112	33.5		-1.68	3.93							dolomite
u1112	34		-1.16	1.47							dolomite
u1112	35		-5.85	3.40							dolomite
u1112	35.5		-1.31	3.66							dolomite
u1112	36		-1.33	3.87							dolomite
u1112	36.5		-2.40	3.06							dolomite
u1112	37		-4.15	3.70							dolomite
u1112	37.5		-2.87	3.16							dolomite
u1112	39		-3.67	3.84							dolomite
u1112	39.5		-0.86	3.78							dolomite
Khongor Range				**E 96°15.310'**		**N 46°39.757'**					
Shuurgat Fm.											
F708 29.7	29.7	0	-7.02	-0.32							dolomite
F708 30.20	30.2	0.5	-5.99	-1.14							dolomite
F708	30.5	0.8	-6.70	-1.31							dolomite
F708	31.0	1.3	-6.95	-1.41							dolomite
F708	31.5	1.8	-7.08	-1.30							dolomite
F708 32	32	2.3	-6.67	-1.38							dolomite
F708 33	33	3.3	-6.92	-1.45							dolomite
F708	33.5	3.8	-7.87	-1.23							dolomite
F708 34	34	4.3	-8.22	-0.54							dolomite
F708	34.5	4.8	-6.56	-0.31							dolomite

F708 35	35	5.3	-7.59	-0.24							dolomite
F708	35.5	5.8	-6.62	-0.96							dolomite
F708	36.0	6.3	-8.52	-1.93							dolomite
F708 36.5	36.5	6.8	-8.31	-2.73							dolomite
F708	37.0	7.3	-13.03	-0.89							dolomite
F708	37.5	7.8	-17.21	-3.50							dolomite
F708	38.0	8.3	-19.10	-3.19							dolomite
F708	38.5	8.8	-27.94	-1.20							dolomite
F708	39.0	9.3	-13.80	-3.52							dolomite
F708	39.5	9.8	-11.87	-4.31							dolomite
F708	40.0	10.3	-10.74	-4.52							dolomite
F708	40.5	10.8	-13.04	-3.83							dolomite
F708	41.0	11.3	-11.70	-4.21							dolomite
F708	42.0	12.3	-15.45	-3.25							dolomite
F708	42.5	12.8	-10.35	-4.44							dolomite
F708	43.0	13.3	-24.32	-1.25							dolomite
F708	43.5	13.8	-10.20	-3.94							dolomite
F708	44.0	14.3	-22.74	-1.49							dolomite
F708	45.0	15.3	-11.20	-4.05							dolomite
F708	45.5	15.8	-11.29	-4.58							dolomite
F708	46.0	16.3	-12.69	-4.15							dolomite
F708	47.0	17.3	-9.17	-4.66							dolomite
F708	48.0	18.3	-14.69	-4.76							dolomite
F708	49.0	19.3	-11.39	-4.98							dolomite
F708	50.0	20.3	-14.40	-5.35							limestone
F708	51.0	21.3	-9.52	-4.92							limestone
F708	52.0	22.3	-12.79	-6.04							limestone
F708	59.0	29.3	-12.97	-4.40							limestone

F708	60.0	30.3	-11.15	-3.38							limestone
F708	62.0	32.3	-10.64	-2.65							limestone
F708	64.0	34.3	-16.88	-2.79							limestone
F708	66.0	36.3	-11.48	-2.94							limestone
F708	70.0	40.3	-11.23	-3.04							limestone
F708	72.0	42.3	-15.04	-3.13							limestone
F708	74.0	44.3	-7.99	-2.92							limestone
F708	78.0	48.3	-9.73	-3.02							limestone
F708	80.0	50.3	-8.34	-3.44							limestone
F708	82.0	52.3	-9.41	-3.17							limestone
F708	84.0	54.3	-10.70	-3.27							limestone
F708	86.0	56.3	-8.92	-3.07							limestone
F708	88.0	58.3	-9.02	-2.98							limestone
F708	90.0	60.3	-7.01	-2.68							limestone
F708	92.0	62.3	-8.24	-1.81							limestone
F708	94.0	64.3	-10.71	-4.57							limestone
F708	96.0	66.3	-7.00	-2.40							limestone
F708	98.0	68.3	-8.05	-2.90							limestone
F708	100.0	70.3	-10.59	-3.89							limestone
F708	102.0	72.3	-10.50	-2.86							limestone
F708	104.0	74.3	-8.64	-2.45							limestone
F708	106.0	76.3	-12.31	-0.97							limestone
F708	108.0	78.3	-8.21	-0.30							limestone
F708	110.0	80.3	-9.49	-1.16							limestone
F708	112.0	82.3	-13.13	-0.93							limestone
F708	114.0	84.3	-15.03	-1.29							limestone
F708-121	121	91									dolomite
F708	123.0	93.3	-6.00	2.59							limestone

F708-125	125	95.3	-3.57	2.21							dolomite
F708	127.0	97.3	-3.52	1.79							limestone
F708	129.0	99.3	-4.77	3.43							limestone
F708	131.0	101.3	-6.18	2.73							limestone
F708	133.0	103.3	-5.07	3.72							limestone
F708	135.0	105.3	-2.24	3.07							limestone
f708-137	137	107.3	-4.67	3.29	1.9187	1008.8619	0.1895	0.0874	44.55	159.79	dolomite
F708	139.0	109.3	-5.31	3.39							limestone
F708	141.0	111.3	-4.11	3.36							limestone
F708	146.0	116.3	-2.09	2.23							limestone
F708	150.0	120.3	-2.63	-0.81							limestone
f708-160	160	130.3	-1.98	3.11	1.0775	981.1285	0.2176	0.0536	57.22	96.63	dolomite
F708	162.0	132.3	-5.33	2.93							limestone
F708	164.0	134.3	-4.47	3.00							limestone
F708	168.0	138.3	-2.78	2.85							limestone
F708-170	170	140.3	-2.62	2.51							dolomite
F708	172.0	142.3	-4.57	3.59							limestone
f708-174	174	144.3	-0.79	0.88	0.3985	1018.8230	0.1712	0.0787	44.39	144.64	dolomite
F708	176.0	146.3	-2.21	2.95							limestone
F708	178.0	148.3	-1.03	1.58							limestone
F708 180	180	150.3	-1.25	3.72	0.4012	980.0102	0.0660		8.84		dolomite
F708	182.0	152.3	-5.18	3.32							limestone
F708	184.0	154.3	-0.78	4.03							limestone
f708-186	186	156.3	-4.24	2.88	3.8613	962.6275	0.3038	0.0833	98.74	148.81	dolomite
F708	188.0	158.3	-5.72	4.26							limestone
F708-190	190	160.3	-1.92	0.95							dolomite
F708	192.0	162.3	-0.95	0.05							limestone
F708	194.0	164.3	-1.44	1.54							dolomite

F708	196.0	166.3	-1.50	2.48							dolomite
f708-198	198	168.3	-1.77	2.33	1.1682	991.5181	0.1154	0.0610	22.55	110.63	dolomite
F708	200.0	170.3	-8.17	3.31							dolomite
F708	202.0	172.3	-6.79	2.36							dolomite
F708	204.0	174.3	-6.24	3.75							dolomite
F708-206	206	176.3	-8.17	3.67							dolomite
F708	208.0	178.3	-1.88	2.61							dolomite
f708-210	210	180.3	-3.29	4.34	0.5695	969.9943	0.1061	0.0843	28.81	151.04	dolomite
F708	212.0	182.3	-3.62	2.43							dolomite
F708	214.0	184.3	-3.83	3.17							dolomite
f708-216	216	186.3	-3.90	3.43	0.4865	992.9321	0.1921	0.0502	46.09	90.99	dolomite
F708	218.0	188.3	-4.12	3.34							dolomite
F708	220.0	190.3	-5.77	3.20							dolomite
F708	222.0	192.3	-6.44	3.21							dolomite
f708-224	224	194.3	-4.87	3.41	3.4150	997.1896	1.3909	0.0811	664.63	147.48	dolomite
F708 226	226	196.3	-5.72	2.85	1.1655	982.7034	0.0972	0.1351	15.52	117.96	dolomite
F708	228.0	198.3	-9.57	3.39							dolomite
F708	230.0	200.3	-9.48	3.21							dolomite
f708-232	232	202.3	-10.00	2.71	0.5298	753.4993	0.2523	0.3665	111.61	581.87	dolomite
F708	234.0	204.3	-1.58	3.58							dolomite
F708	236.0	206.3	-2.87	3.12							dolomite
F708	238.0	208.3	-3.53	2.86							dolomite
F708	240.0	210.3	-1.91	2.78							dolomite
F708	241.0	211.3	-1.23	3.69							dolomite
F708	244.0	214.3	-0.35	4.00							dolomite
f708-246	246	216.3	-0.46	2.81	0.2531	1002.2271	0.0727	0.0397	9.78	72.45	dolomite
F708	248.0	218.3	-1.32	2.94							dolomite
F708-250	250	220.3	-0.67	3.08							dolomite

F708	252.0	222.3	-0.54	1.42							dolomite
F708	254.0	224.3	-4.79	2.89							dolomite
F708	256.0	226.3	-3.33	2.16							dolomite
F708	258.0	228.3	-4.25	2.98							dolomite
F708	260.0	230.3	-2.32	2.90							dolomite
F708	262.0	232.3	-2.54	2.29							dolomite
F708	264.0	234.3	-2.52	3.82							dolomite
F708	266.0	236.3	-2.59	4.56							dolomite
F708	268.0	238.3	-1.21	2.54							dolomite
F708	270.0	240.3	-1.10	3.26							dolomite
F708	272.0	242.3	-3.46	2.22							dolomite
F708	274.0	244.3	-0.73	3.62							dolomite
F708	276.0	246.3	-1.69	4.47							dolomite
f708-278	278	248.3	-2.58	3.79	0.5314	1027.5528	0.1049	0.0434	21.95	80.19	dolomite
F708	280.0	250.3	-1.55	4.28							dolomite
F708	284.0	254.3	-2.00	2.91							dolomite
f708-286	286	256.3	0.05	3.46	0.1499	999.9360	0.0811		27.40		dolomite
F708	288.0	258.3	-1.48	4.04							dolomite
F708	290.0	260.3	-1.80	1.77							dolomite
F708	292.0	262.3	-2.42	2.93							dolomite
F708	294.0	264.3	-1.66	2.76							dolomite
F708	296.0	266.3	-0.82	3.19							dolomite
F708	298.0	268.3	-1.52	2.72							dolomite
F708	300.0	270.3	-2.31	2.02							dolomite
F708	302.0	272.3	-1.01	5.17							dolomite
F708	304.0	274.3	-1.05	4.33							dolomite
F708	308.0	278.3	-2.12	3.21							dolomite
F708	310.0	280.3	-1.42	3.80							dolomite

F708	312.0	282.3	-0.62	3.16							dolomite
F708	314.0	284.3	-1.15	2.00							dolomite
F708	316.0	286.3	-1.93	4.78							dolomite
F708	318.0	288.3	-10.23	2.54							dolomite
F708	322.0	292.3	-2.91	3.86							dolomite
F708	324.0	294.3	-4.61	3.44							dolomite
F708	326.0	296.3	-5.67	3.08							dolomite
F708	330.0	300.3	-2.56	2.50							dolomite
F708	332.0	302.3	-5.25	3.78							dolomite
F708	334.0	304.3	-6.62	1.37							dolomite
F708	338.0	308.3	-7.25	1.27							dolomite
F708	340.0	310.3	-6.62	2.75							dolomite
F708	344.0	314.3	-2.69	3.03							dolomite
F708	346.0	316.3	-10.71	2.61							dolomite
F708	348.0	318.3	-6.17	1.22							dolomite
F708	350.0	320.3	-1.51	2.87							dolomite
F708	352.0	322.3	-3.00	2.08							dolomite
F708	354.0	324.3	-3.54	3.22							dolomite
F708	356.0	326.3	-3.20	2.44							dolomite
F708	358.0	328.3	-1.32	3.82							dolomite
F708	360.0	330.3	-1.50	2.51							dolomite
F708	362.0	332.3	-1.23	2.21							dolomite
F708	364.0	334.3	-2.91	1.89							dolomite
F708	366.0	336.3	-1.93	2.54							dolomite
F708	368.0	338.3	-0.66	2.62							dolomite
F708	370.0	340.3	-1.02	1.39							dolomite
F708	372.0	342.3	-1.11	3.72							dolomite
F708	374.0	344.3	-0.88	2.71							dolomite

F708	376.0	346.3	-0.27	2.50							dolomite
F708	378.0	348.3	-0.99	4.82							dolomite
F708	380.0	350.3	-1.96	3.72							dolomite
F708	382.0	352.3	-1.48	2.42							dolomite
F708	384.0	354.3	-10.70	1.70							dolomite
F708	386.0	356.3	-3.48	2.50							dolomite
F708	388.0	358.3	-2.31	1.87							dolomite
F708	390.0	360.3	-1.64	3.22							dolomite
F708	392.0	362.3	-1.99	2.90							dolomite
F708	394.0	364.3	-0.66	3.61							dolomite
F708	396.0	366.3	-5.23	4.69							dolomite
F708	398.0	368.3	-2.18	4.10							dolomite
F708	400.0	370.3	-1.10	3.22							dolomite
F708	402.0	372.3	-0.89	4.05							dolomite
F708	404.0	374.3	-0.55	3.88							dolomite
F708	406.0	376.3	-5.90	3.63							dolomite
F708	408.0	378.3	-1.95	3.79							dolomite
F708	410.0	380.3	-1.66	3.84							dolomite
F708	416.0	386.3	-6.55	3.22							dolomite
F708	418.0	388.3	-0.29	1.98							dolomite
F708	420.0	390.3	-2.39	2.63							dolomite
u1439-3p5	3.5	393.3	0.72	3.44	1.7128	986.1769	0.2228	0.0589	65.08	51.52	dolomite
u1439-5p5	5.5	395.3	-1.03	3.79	1.0990	990.6390	0.1665	0.0568	93.04	49.66	dolomite
u1439-6	6.0	396.3	0.64	3.68							dolomite
u1439-7	7.0	397.3	-3.15	4.15							dolomite
u1439-8	8.0	398.3	-1.73	3.98							dolomite
u1439-9p5	9.5	399.3	0.01	3.75	1.0084	971.0792	0.0877		68.61		dolomite
u1439-10	10.0	400.3	-1.65	2.85							dolomite

u1439-11	11.0	401.3	-0.47	2.84							dolomite
u1439-12	12.0	402.3	-1.06	3.32							dolomite
u1439-13p5	13.5	403.3	-0.86	0.15	1.1229	1027.6330	0.1344	0.0301	72.75	26.36	dolomite
u1439-14	14.0	404.3	-1.54	4.13							dolomite
u1439-15	15.0	405.3	-0.20	3.58							dolomite
u1439-16	16.0	406.3	-0.42	3.14							dolomite
u1439-17	17.0	407.3	-1.16	4.36							dolomite
u1439-18p5	18.5	408.3	-1.74	3.76	1.5867	1035.9235	0.1408		78.48		dolomite
u1439-19	19.0	409.3	-1.26	3.44							dolomite
u1439-20	20.0	410.3	-0.79	3.08							dolomite
u1439-21p5	21.5	411.3	-1.08	4.31	1.2035	982.3899	0.0963	0.0078	49.85	6.83	dolomite
u1439-22	22.0	412.3	-1.52	4.24							dolomite
u1439-23	23.0	413.3	-2.08	3.26							dolomite
u1439-24	24.0	414.3	-2.68	3.70							dolomite
u1439-25	25.0	415.3	-2.33	3.50							dolomite
u1439-26p5	26.5	416.3	-1.26	2.80	1.5393	740.5590	0.2059	0.3098	123.81	488.04	dolomite
u1439-27	27.0	417.3	-0.90	4.53							dolomite
u1439-28	28.0	418.3	-2.38	3.85							dolomite
u1439-29	29.0	419.3	-1.61	3.95							dolomite
u1439-31p5	31.5	421.3	-3.40	3.99	1.0517	939.9492	0.1418	0.1136	39.51	200.42	dolomite
u1439-32	32.0	422.3	-2.06	4.89							dolomite
u1439-33	33.0	423.3	-1.44	4.21							dolomite
u1439-34	34.0	424.3	-1.44	4.24							dolomite
u1439-35	35.0	425.3	-0.96	4.30							dolomite
u1439-36	36.0	426.3	-1.05	4.22							dolomite
u1439-37	37.0	427.3	-1.86	4.33							dolomite
u1439-38	38.0	428.3	-1.75	3.94							dolomite
u1439-39	39.0	429.3	-0.86	3.61	2.2862	952.4925	0.7392	0.0768	309.28	136.36	dolomite

u1439-40	40.0	430.3	-1.87	4.54							dolomite
u1439-41	41.0	431.3	-3.46	4.11							dolomite
u1439-42p5	42.5	432.3	-2.41	4.22	0.7598	948.1166	0.1610	0.1018	43.71	180.33	dolomite
u1439-43	43.0	433.3	-4.28	3.77							dolomite
u1439-44	44.0	434.3	-1.75	4.45							dolomite
u1439-45	45.0	435.3	-2.46	4.48							dolomite
u1439-46	46.0	436.3	-1.91	3.24							dolomite
u1439-47	47.0	437.3	-2.00	2.84	1.5285	971.0563	0.2139	0.0596	61.64	106.90	dolomite
u1439-49	49.0	439.3	-1.04	1.00							dolomite
u1439-50	50.0	440.3	-1.41	1.20							dolomite
u1439-51	51.0	441.3	-0.28	-0.16	0.5307	1011.9003	0.3304	0.0751	100.03	137.55	dolomite
u1439-52	52.0	442.3	-0.56	0.91							dolomite
u1439-53	53.0	443.3	-4.31	1.10							dolomite
u1439-54	54.0	444.3	-1.34	1.25							dolomite
u1439-58	58.0	448.3	-3.62	1.08	2.3344	1006.4566	0.4691	0.0848	146.63	154.92	dolomite
u1439-59	59.0	449.3	-2.25	1.26							dolomite
u1439-60	60.0	450.3	-1.36	0.42							dolomite
Tsakhir Range				**E 95°20.362'**		**N 46°50.230'**					
Taishir Fm.											
U1241	1		0.64	1.78							limestone
U1241	2		-14.73	-0.93							limestone
U1241	3		-9.11	-0.65							dolomite
U1241	8		-16.29	-0.55							dolomite
U1241	9		-4.60	4.51							dolomite
U1241	10		-4.40	4.28							dolomite
U1241	11		-6.07	3.76							dolomite
U1241	12		-5.50	5.71							dolomite
U1241	14		-3.75	5.97							dolomite

U1241	15		-7.05	6.67							dolomite
U1241	20		-20.84	3.58							limestone
U1241	21		-18.00	3.18							limestone
U1241	31		-17.88	3.66							dolomite
U1241	32		-11.85	3.68							dolomite
U1241	33		-8.95	6.11							dolomite
U1241	34		-9.71	5.00							dolomite
U1241	35		-8.42	5.42							dolomite
U1241	36		-8.64	5.40							dolomite
U1241	37		-7.37	4.93							dolomite
U1241	38		-10.38	4.40							dolomite
U1241	39		-11.32	4.04							dolomite
U1241	40		-7.46	5.31							dolomite
U1241	41		-3.53	5.67							dolomite
U1241	42		-9.15	4.42							dolomite
U1241	42		-9.20	4.38							dolomite
U1241	43		-7.93	5.97							dolomite
U1241	44		-12.11	3.86							dolomite
U1241	45		-10.24	4.89							dolomite
U1241	46		-15.56	3.77							dolomite
U1241	47		-11.87	3.50							dolomite
U1241	48		-4.80	0.21							dolomite
U1241	49		-3.80	-1.14							dolomite
U1241	50		-7.69	-0.81							dolomite
U1241	51		-3.18	2.07							dolomite
U1241	52		-7.70	3.31							dolomite
U1241	53		-6.22	2.18							dolomite
U1241	54		-8.87	2.55							dolomite

U1241	55		-7.74	3.13							dolomite
U1241	56		-2.99	4.59							dolomite
U1241	57		-3.50	5.43							dolomite
U1241	58		-3.07	4.92							dolomite
U1241	59		-6.02	4.41							dolomite
U1241	60		-4.64	4.50							dolomite
U1241	61		-4.14	3.99							dolomite
U1241	62		-3.50	5.31							dolomite
U1241	63		-3.71	4.45							dolomite
U1241	64		-7.40	3.35							dolomite
U1241	65		-3.70	3.53							dolomite
U1241	66		-4.37	3.62							dolomite
U1241	67		-3.42	4.10							dolomite
U1241	68		-3.33	3.43							dolomite
U1241	69		-7.68	3.54							dolomite
U1241	70		-7.25	3.66							dolomite
U1241	71		-7.07	4.32							dolomite
U1241	72		-5.27	5.16							dolomite
U1241	73		-12.79	7.13							dolomite
U1241	74		-11.19	5.42							limestone
U1241	75		-11.01	5.76							limestone
U1241	76		-9.97	5.69							limestone
U1241	77		-7.83	5.33							dolomite
U1241	78		-9.50	5.21							limestone
U1241	79		-8.29	5.79							limestone
U1241	80		-10.32	7.50							limestone
U1241	81		-6.67	8.51							limestone
U1241	82		-4.50	5.91							limestone

U1241	83		-8.26	6.38							dolomite
U1241	84		-6.16	5.54							dolomite
U1241	85		-7.38	6.12							dolomite
U1241	86		-7.21	7.00							dolomite
U1241	87		-5.48	5.37							dolomite
U1241	88		-5.92	5.51							limestone
U1241	89		-7.81	5.96							limestone
U1241	90		-8.93	5.09							limestone
U1241	91		-12.51	6.87							limestone
U1241	92		-8.42	4.57							limestone
U1241	93		-7.91	9.62							limestone
U1241	94		-9.08	5.55							limestone
U1241	95		-8.41	6.10							limestone
U1241	96		-9.51	4.94							dolomite
U1241	97		-9.87	5.18							dolomite
U1241	98		-7.24	6.16							dolomite
U1241	99		-9.24	5.03							dolomite
U1241	100		-9.99	5.20							dolomite
U1241	101		-9.30	5.53							limestone
U1241	102		-6.95	4.19							limestone
U1241	103		-7.76	7.83							limestone
U1241	104		-15.53	5.46							limestone
U1241	105		-11.69	7.10							limestone
U1241	106		-11.43	7.42							limestone
U1241	107		-9.00	9.03							limestone
U1241	108		-6.37	9.49							limestone
U1241	109		-7.63	9.04							limestone
U1241	110		-3.56	9.45							limestone

U1241	111		-2.77	10.28							limestone
U1241	112		-7.82	8.30							limestone
U1241	113		-4.99	10.01							limestone
U1241	114		-4.99	10.03							limestone
U1241	115		-6.99	8.91							limestone
U1241	116		-8.92	6.46							limestone
U1241	117		-2.34	10.94							limestone
U1241	118		-3.19	10.27							limestone
U1241	119		-4.55	10.59							limestone
U1241	120		-4.71	10.46							limestone
U1241	121		-6.12	8.52							limestone
U1241	122		-6.48	6.82							limestone
U1241	123		-3.31	10.85							limestone
U1241	124		-6.39	9.65							limestone
U1241	125		-6.06	10.22							limestone
U1241	126		-6.93	9.11							limestone
U1241	127		-6.75	9.94							limestone
U1241	128		-6.90	9.32							dolomite
U1241	129		-4.43	8.24							dolomite
U1241	130		-3.70	8.09							dolomite
U1241	131		-3.38	9.34							dolomite
U1241	132		-6.49	8.86							limestone
U1241	133		-3.81	9.81							limestone
U1241	134		-6.51	7.48							limestone
U1241	135		-9.38	6.07							dolomite
U1241	136		-5.65	7.12							dolomite
U1241	137		-5.89	6.62							dolomite
U1241	138		-6.84	5.72							dolomite

U1241	139		-6.97	6.77							dolomite
U1241	140		-8.78	6.70							dolomite
U1241	141		-7.36	6.49							dolomite
U1241	142		-10.01	5.53							dolomite
U1241	143		-11.78	3.57							dolomite
U1241	144		-8.31	4.42							dolomite
U1241	145		-9.64	4.73							dolomite
U1241	146		-4.20	6.80							dolomite
U1241	147		-3.98	7.80							dolomite
U1241	148		-6.33	6.54							dolomite
U1241	149		-2.95	5.91							dolomite
U1241	150		-2.17	5.52							dolomite
U1241	151		-2.93	4.81							dolomite
U1241	152		-3.63	6.08							dolomite
U1241	153		-2.75	5.33							dolomite
U1241	154		-4.32	5.33							dolomite
U1241	155		-3.14	6.14							dolomite
U1241	156		-2.99	5.85							dolomite
U1241	157		-3.72	6.22							dolomite
U1241	158		-2.35	5.64							dolomite
U1241	159		-3.16	6.38							dolomite
U1241	160		-2.42	6.47							dolomite
U1241	161		-2.38	6.76							dolomite
U1241	162		-2.09	6.60							dolomite
U1241	163		-3.10	6.44							dolomite
U1241	164		-2.15	6.37							dolomite
U1241	165		-2.57	6.70							dolomite
U1241	166		-4.18	5.77							dolomite

U1241	167		-3.61	5.35							dolomite
U1241	168		-4.32	6.51							dolomite
U1241	169		-2.72	5.66							dolomite
U1241	170		-4.27	5.23							dolomite
U1241	171		-2.63	6.19							dolomite
U1241	172		-3.10	5.83							dolomite
U1241	173		-6.40	6.29							dolomite
U1241	174		-3.36	6.06							dolomite
U1241	175		-2.25	6.14							dolomite
U1241	176		-4.58	6.27							dolomite
U1241	177		-2.49	5.91							dolomite
U1241	178		-2.29	5.87							dolomite
U1241	179		-2.09	5.87							dolomite
U1241	179		-2.16	5.85							dolomite
U1241	180		-1.93	5.66							dolomite
U1241	181		-2.83	4.40							dolomite
U1241	182		-1.74	4.87							dolomite
U1241	183		-1.85	5.22							dolomite
U1241	184		-2.31	4.85							dolomite
U1241	185		-1.22	5.73							dolomite
U1241	186		-2.49	4.21							dolomite
U1241	187		-3.02	5.20							dolomite
U1241	188		-2.67	4.69							dolomite
U1241	189		-4.32	4.54							dolomite
U1241	190		-2.93	5.05							dolomite
U1241	191		-2.89	5.16							dolomite
U1241	192		-2.01	4.90							dolomite
U1241	193		-2.98	4.68							dolomite

U1241	194		-2.02	5.45							dolomite
U1241	195		-1.84	5.26							dolomite
U1241	196		-2.34	5.41							dolomite
U1241	197		-3.33	4.37							dolomite
U1241	198		-2.01	5.06							dolomite
U1241	199		-2.31	5.10							dolomite
U1241	200		-1.90	4.55							dolomite
U1241	201		-4.77	2.58							dolomite
U1241	202		-7.64	5.14							dolomite
U1241	202		-7.67	5.10							dolomite
U1241	203		-8.04	4.76							dolomite
U1241	204		-9.08	4.42							dolomite
U1241	205		-8.52	5.14							dolomite
U1241	206		-6.69	3.85							dolomite
U1241	207		-7.65	5.02							dolomite
U1241	208		-3.93	5.75							dolomite
U1241	209		-2.97	5.32							dolomite
U1241	210		-4.15	4.69							dolomite
U1241	211		-3.96	4.97							dolomite
U1241	212		-7.04	5.77							dolomite
U1241	213		-6.75	5.64							dolomite
U1241	214		-7.24	4.65							dolomite
U1241	215		-10.18	4.78							dolomite
U1241	216		-7.67	4.68							dolomite
U1241	217		-5.79	4.79							dolomite
U1241	218		-2.51	4.87							dolomite
U1241	219		-5.69	4.30							dolomite
U1241	220		-8.85	3.76							dolomite

U1241	221		-7.31	3.81							dolomite
U1241	222		-6.91	3.18							dolomite
U1241	223		-6.66	3.75							dolomite
U1241	224		-6.82	4.19							dolomite
U1241	225		-8.55	3.89							dolomite
U1241	226		-2.74	5.66							dolomite
U1241	227		-8.36	4.01							dolomite
U1241	228		-5.80	4.31							dolomite
U1241	229		-7.28	3.69							dolomite
U1241	230		-6.73	1.38							dolomite
U1241	231		-11.36	1.30							dolomite
U1241	232		-7.54	2.61							dolomite
U1241	233		-5.23	3.67							dolomite
U1241	234		-4.59	2.19							dolomite
U1241	235		-5.55	2.26							dolomite
U1241	236		-2.10	4.58							dolomite
U1241	237		-4.75	3.90							dolomite
U1241	238		-2.95	5.60							dolomite
U1241	239		-6.19	5.24							dolomite
U1241	240		-5.26	4.66							dolomite
U1241	241		-5.41	3.16							dolomite
Tsakhir Range				**E 95°16.887'**		**N 46°50.703'**					
Ol Fm.											
M12016	0		-2.96	2.16							dolomite
M12016	0.5		-5.86	-0.40							dolomite
M12016	1		-1.44	2.46							dolomite
M12016	1.5		-5.45	-0.63							dolomite
M12016	2		-3.01	1.19							dolomite

M12016	2.5		-0.93	1.85							dolomite
M12016	3		-2.24	2.60							dolomite
M12016	3.5		-2.52	2.82							dolomite
M12016	4		-4.27	2.88							dolomite
M12016	4.5		-5.05	2.83							dolomite
M12016	5		-3.50	2.86							dolomite
M12016	5.5		-2.33	2.42							dolomite
M12016	6		-1.96	2.57							dolomite
M12016	6.5		-3.00	1.91							dolomite
M12016	7		-2.06	1.79							dolomite
M12016	7.5		-1.84	1.48							dolomite
M12016	8		-1.52	1.30							dolomite
M12016	8.5		-3.04	1.76							dolomite
M12016	9		-3.58	1.50							dolomite
M12016	9.5		-2.55	2.31							dolomite
M12016	10		-2.45	1.88							dolomite
M12016	10.5		-2.82	2.03							dolomite
M12016	11		-3.22	2.05							dolomite
M12016	11.5		-2.32	1.71							dolomite
M12016	12		-3.45	1.46							dolomite
M12016	12.5		-2.85	1.55							dolomite
M12016	13		-5.08	4.26							dolomite
M12016	13.5		-6.87	3.07							dolomite
M12016	14		-4.78	2.86							dolomite
M12016	14.5		-7.35	3.14							dolomite
M12016	15		-6.66	2.43							dolomite
M12016	15.6		-7.42	2.95							dolomite
M12016	16		-4.86	2.47							dolomite

M12016	16.5		-3.51	2.01							dolomite
M12016	17		-5.84	3.41							dolomite
M12016	17.5		-2.05	2.54							dolomite
M12016	18		-4.55	3.25							dolomite
M12016	18.5		-2.30	2.87							dolomite
M12016	19		-1.26	2.55							dolomite
M12016	19.5		-1.74	2.61							dolomite
M12016	20		-1.41	1.23							dolomite
M12016	20.5		-1.91	1.30							dolomite
M12016	21		-4.61	1.81							dolomite
M12016	21.5		-2.10	1.16							dolomite
M12016	22		-2.44	1.62							dolomite
M12016	22.5		-2.07	2.70							dolomite
M12016	23		-3.34	1.79							dolomite
M12016	23.5		-2.55	1.32							dolomite
M12016	24		-2.50	1.83							dolomite
M12016	24.5		-2.09	1.56							dolomite
M12016	25		-2.23	1.28							dolomite
M12016	25.5		-3.06	1.88							dolomite
M12016	26		-2.27	1.62							dolomite
M12016	26.5		-1.22	1.45							dolomite
M12016	27		-1.79	0.93							dolomite
S. Khukh Davaa				**E 95°26.195'**		**N 47°01.773'**					
Ol Fm.											
F875	18		-7.82	-1.20							dolomite
F875	18.5		-7.71	0.09							dolomite
F875	18.8		-2.69	2.46							dolomite
F875	19.5		-2.92	2.21							dolomite

F875	20		-2.45	1.42							dolomite
F875	20.5		-3.37	1.59							dolomite
F875	21		-2.79	1.60							dolomite
F875	21.5		-3.16	1.96							dolomite
F875	22		-4.09	1.77							dolomite
F875	22.5		-3.39	1.73							dolomite
F875	23		-4.64	1.68							dolomite
F875	23.5		-5.60	1.70							dolomite
F875	24		-5.68	1.95							dolomite
F875	24.5		-6.69	1.92							dolomite
F875	25		-4.63	2.33							dolomite
F875	25.5		-4.06	2.44							dolomite
F875	26		-4.28	2.71							dolomite
F875	26.5		-3.14	2.78							dolomite
F875	27		-2.91	2.90							dolomite
F875	27.5		-4.71	0.21							dolomite
F875	28		-5.07	3.33							dolomite
F875	28.5		-3.41	3.13							dolomite
F875	29		-7.48	3.58							dolomite
F875	29.5		-6.20	3.78							dolomite
F875	30		-6.35	1.68							dolomite
F875	30.5		-5.69	3.54							dolomite
F875	31		-4.26	3.12							dolomite
F875	31.5		-3.08	3.88							dolomite
F875	32		-2.55	5.77							dolomite
F875	32.5		-1.92	6.39							dolomite
F875	33		-4.30	7.28							dolomite
F875	33.5		-5.33	6.40							dolomite

F875	34		-2.81	0.80							dolomite
F875	34.5		-2.68	4.97							dolomite
F875	35		-3.36	5.51							dolomite
F875	35.5		-2.86	4.57							dolomite
F875	36		-4.18	5.82							dolomite
F875	36.5		-6.39	3.48							dolomite
F875	37		-2.98	2.83							dolomite
F875	37.5		-6.78	4.41							dolomite
F875	38		-3.23	2.91							dolomite
F875	39		-3.31	1.92							dolomite
F875	39.5		-4.36	0.65							dolomite
F875	40		-4.06	0.04							dolomite
Khunkher Gorge				**E 95°58.814'**		**N 46°44.413'**					
Ol Fm and Shuurgat Fm.											
F872	20	0	-5.25	-0.66							dolomite
F872	20.5	0.5	-6.12	-1.15							dolomite
F872	21	1	-5.49	-0.98							dolomite
F872	21.5	1.5	-6.01	-1.18							dolomite
F872	22	2	-6.34	-1.38							dolomite
F872	22.5	2.5	-6.54	-0.86							dolomite
F872	23	3	-5.50	-0.70							dolomite
F872	23.5	3.5	-5.40	-1.37							dolomite
F872	24	4	-5.45	-0.66							dolomite
F872	24.5	4.5	-4.86	-0.77							dolomite
F872	25	5	-5.23	-0.27							dolomite
F872	25.5	5.5	-4.90	-0.27							dolomite
F872	26	6	-5.09	-0.33							dolomite
F872	26.5	6.5	-5.11	-0.38							dolomite

F872	27	7	-5.47	-0.47							dolomite
F872	27.5	7.5	-5.16	-0.53							dolomite
F872	28	8	-4.40	-1.77							dolomite
F872	28.5	8.5	-4.83	-2.84							dolomite
F872	29	9	-5.45	-3.17							dolomite
F872	29.5	9.5	-6.01	-3.73							dolomite
F872	30	10	-4.19	-1.32							dolomite
F872	30.5	10.5	-4.06	-1.66							dolomite
F872	31	11	-5.19	-1.62							dolomite
F872	31.5	11.5	-3.30	-1.89							dolomite
F872	32	12	-3.83	-1.57							dolomite
F872	32.5	12.5	-4.44	-0.93							dolomite
F872	33	13	-4.06	-0.68							dolomite
F872	33.5	13.5	-4.00	-1.85							dolomite
F872	34	14	-5.19	-0.48							dolomite
F872	34.5	14.5	-4.93	-0.47							dolomite
F872	35	15	-4.63	-1.05							dolomite
F872	36	16	-4.35	-0.44							dolomite
F872	37	17	-6.42	-0.66							dolomite
F872	38	18	-3.94	-0.37							dolomite
F872	40	20	-5.07	-0.57							dolomite
F872	41	21	-4.99	-1.92							dolomite
F872	42	22	-5.33	-1.75							dolomite
F872	43	23	-7.50	-2.10							dolomite
F872	44	24	-12.77	-4.09							dolomite
F872	45	25	-15.19	-1.93							dolomite
F872	46	26	-10.57	-3.04							dolomite
F872	47	27	-10.18	-3.17							dolomite

F872	48	28	-16.25	-2.35							dolomite
F872	49	29	-13.47	-2.21							dolomite
F872	55	35	-3.70	1.99							dolomite
F872	57	37	-2.55	3.11							dolomite
F872	59	39	-1.94	3.83							dolomite
F872	61	41	-2.04	4.23							dolomite
F872	63	43	-2.73	4.25							dolomite
F872	61	41	-1.99	4.24							dolomite
F872	63	43	-2.61	4.29							dolomite
F872	65	45	-0.51	2.98							dolomite
F872	67	47	-0.73	3.25							dolomite
F872	69	49	-3.61	2.77							dolomite
F872	71	51	-1.91	2.59							dolomite
F872	73	53	-0.77	3.46							dolomite
F872	75	55	-2.06	3.51							dolomite
F872	77	57	-4.78	2.34							dolomite
F872	79	59	-2.84	2.13							dolomite
F872	81	61	-2.54	1.89							dolomite
F872	83	63	-1.59	3.37							dolomite
F872	85	65	-0.73	3.29							dolomite
F872	87	67	-1.46	3.81							dolomite
F872	89	69	-1.47	3.89							dolomite
F872	91	71	-1.20	5.73							dolomite
F872	93	73	-5.34	2.60							dolomite
F872	95	75	-1.44	3.25							dolomite
F872	97	77	-4.91	3.58							dolomite
F872	99	79	-0.40	3.73							dolomite
F872	101	81	-1.63	2.68							dolomite

F872	103	83	-0.64	4.11							dolomite
F872	105	85	-0.68	3.60							dolomite
F872	109	89	-0.91	3.08							dolomite
F872	111	91	-1.71	2.87							dolomite
F872	113	93	-2.16	3.25							dolomite
F872	115	95	-2.54	2.06							dolomite
F872	117	97	-1.91	2.86							dolomite
F872	119	99	-1.74	3.86							dolomite
F872	121	101	-13.44	2.82							dolomite
F872	123	103	-4.25	3.33							dolomite
F872	125	105	-3.39	1.71							dolomite
F872	127	107	-0.94	3.26							dolomite
F872	129	109	-0.98	2.84							dolomite
F872	131	111	-1.44	2.75							dolomite
F872	133	113	-3.68	2.94							dolomite
F872	135	115	-0.96	3.33							dolomite
F872	139	119	-3.03	2.24							dolomite
F872	147	127	-5.97	2.62							limestone
F872	148	128	-3.39	4.65							limestone
F872	150	130	-0.81	4.70							limestone
F872	152	132	-5.43	8.13							limestone
F872	154	134	-4.59	8.78							limestone
F872	154	134	-1.36	7.65							limestone
F872	156	136	-1.96	2.88							limestone
F872	160	140	-2.28	3.22							limestone
F872	164	144	-5.15	3.09							limestone
F872	168	148	-1.33	1.10							limestone
F872	170	150	-1.46	1.75							limestone

F872	172	152	-9.11	7.57							limestone
F872	174	154	-10.45	4.50							limestone
F872	183	163	-4.22	4.29							limestone
F872	187	167	-6.37	4.06							limestone
F872	189	169	-8.02	7.97							limestone
F872	193	173	-8.33	7.77							limestone
F872	195	175	-7.61	8.04							limestone
F872	198	178	-6.44	8.11							limestone
F872	202	182	-7.14	5.55							limestone
F872	204	184	-2.95	5.82							limestone
F872	205	185	-2.22	3.37							dolomite
F872	207	187	-1.39	2.85							dolomite
F872	209	189	-1.00	2.95							dolomite
F872	211	191	-1.34	2.48							dolomite
F872	213	193	0.80	3.19							dolomite
F872	214	194	-1.75	2.98							dolomite
F872	216	196	0.51	3.37							dolomite
F872	218	198	-1.49	2.58							dolomite
F872	220	200	1.52	3.62							dolomite
F872	222	202	-3.03	2.23							dolomite
F872	224	204	-0.84	2.35							dolomite
F872	226	206	-1.08	1.72							dolomite
F872	228	208	-1.10	4.02							dolomite
F872	230	210	1.31	4.60							limestone
F872	232	212	-1.65	4.20							limestone
F872	234	214	-1.67	2.77							limestone
F872	236	216	-1.02	2.20							limestone
F872	238	218	-1.55	3.23							limestone

F872	240	220	-3.22	2.64							limestone
F872	242	222	-9.07	2.21							limestone
F872	244	224	-10.36	1.87							limestone
F872	246	226	-9.02	5.39							limestone
F872	249	229	-9.46	5.06							limestone
F872	251	231	-8.30	5.40							limestone
F872	253	233	-8.37	5.16							limestone
F872	255	235	-3.69	5.27							limestone
F872	259	239	-7.50	3.79							limestone
F872	261	241	-8.00	6.73							limestone
F872	263	243	-3.40	6.44							limestone
F872	265	245	-5.26	5.57							limestone
F872	267	247	-8.27	6.96							limestone
F872	269	249	-8.93	6.96							limestone
F872	271	251	-4.16	5.96							limestone
F872	273	253	-3.19	5.43							limestone
F872	275	255	-1.12	3.52							dolomite
F872	279	259	-1.62	5.14							dolomite
F872	281	261	-1.46	5.43							dolomite
F872	283	263	-1.76	3.73							dolomite
F872	285	265	-1.02	2.47							dolomite
F872	287	267	-1.89	2.83							dolomite
F872	289	269	-3.88	2.74							dolomite
F872	291	271	-1.51	3.06							dolomite
F872	293	273	-2.14	2.78							dolomite
F872	295	275	-0.34	2.83							dolomite
F872	300	280	-3.06	2.33							dolomite
F872	302	282	-0.47	2.14							dolomite

F872	304	284	-1.02	2.75							dolomite
F872	306	286	-0.59	2.22							dolomite
F872	308	288	-1.84	1.66							dolomite
F872	310	290	-0.26	1.97							dolomite
F872	312	292	-4.25	1.70							dolomite
F872	314	294	-2.97	2.66							dolomite
F872	316	296	-1.40	2.06							dolomite
F872	318	298	-4.11	2.60							dolomite
F872	320	300	-0.85	2.21							dolomite
F872	322	302	-1.26	2.09							dolomite
F872	324	304	-0.18	1.06							dolomite
F872	326	306	-2.70	1.90							dolomite
F872	328	308	-1.77	2.11							dolomite
F872	330	310	-1.28	2.22							dolomite
F872	332	312	-2.34	1.19							dolomite
F872	334	314	-2.14	0.87							dolomite
F872	336	316	-0.55	2.31							dolomite
F872	338	318	-0.91	2.69							dolomite
F872	340	320	-0.48	2.25							dolomite
F872	342	322	-1.65	2.78							dolomite
F872	344	324	-2.33	3.03							dolomite
F872	346	326	-4.02	3.13							dolomite
F872	348	328	-1.40	2.97							dolomite
F872	350	330	-0.09	2.19							dolomite

Table 4.A2. $\delta^{13}C_{carb}$ and $\delta^{18}O$ data of the macro-textures of selected samples of the Taishir and Ol Formation carbonates.

Macro-texture*	U1108	$\delta^{13}C_{carb}$	$\delta^{18}O$	Description
1	70	8.45317	-4.54004	T3, Taishir Locality
1	71	8.43117	-4.80532	T3, Taishir Locality
1	72	8.55017	-5.05081	T3, Taishir Locality
1	73	8.33717	-4.93499	T3, Taishir Locality
1	74	8.41717	-4.79246	T3, Taishir Locality
1	75	6.33017	-7.10871	T3, Taishir Locality
1	76	9.24717	-4.40146	T3, Taishir Locality
1	77	8.84417	-4.74494	T3, Taishir Locality
1	78	9.34917	-3.90654	T3, Taishir Locality
1	79	9.18117	-2.67021	T3, Taishir Locality
1	80	7.53017	-5.31312	T3, Taishir Locality
1	81	9.67717	-1.77142	T3, Taishir Locality
1	82	1.97917	-4.90431	T3, Taishir Locality
1	83	5.93217	-5.39528	T3, Taishir Locality
1	84	8.83217	-5.49921	T3, Taishir Locality
1	85	8.84417	-6.11787	T3, Taishir Locality
1	86	9.04417	-4.33811	T3, Taishir Locality
1	87	9.18417	-5.9585	T3, Taishir Locality
1	88	8.27417	-5.14088	T3, Taishir Locality
1	89	9.13317	-2.44254	T3, Taishir Locality
1	90	3.61617	-4.57172	T3, Taishir Locality
1	91	5.28317	-5.67046	T3, Taishir Locality
1	92	9.47717	-2.06937	T3, Taishir Locality
1	93	9.39417	-2.44353	T3, Taishir Locality
1	94	9.19017	-4.68258	T3, Taishir Locality
1	95	9.14517	-4.72119	T3, Taishir Locality
1	96	9.36217	-5.58038	T3, Taishir Locality
1	97.1	8.95617	-3.14732	T3, Taishir Locality
1	98	8.05817	-4.1926	T3, Taishir Locality
1	99	5.09817	-2.5346	T3, Taishir Locality
1	100	8.43117	-3.52346	T3, Taishir Locality
1	101	9.27317	-4.33811	T3, Taishir Locality
1	102	9.27117	-1.78132	T3, Taishir Locality
1	103	9.14317	-2.12975	T3, Taishir Locality
1	104	9.50217	-1.05378	T3, Taishir Locality
1	105.1	9.15517	-2.48511	T3, Taishir Locality
1	106	8.84217	-1.98919	T3, Taishir Locality
1	107	7.94617	-5.68134	T3, Taishir Locality

1	108	7.76417	-5.72094	T3, Taishir Locality
1	109	9.13417	-1.54178	T3, Taishir Locality
1	110	8.49317	-4.60141	T3, Taishir Locality
1	111	7.66117	-5.12901	T3, Taishir Locality
1	112	7.67114	-5.19174	T3, Taishir Locality
1	113	9.48614	-1.03931	T3, Taishir Locality
1	114	7.58514	-4.61565	T3, Taishir Locality
1	115	8.20114	-3.65351	T3, Taishir Locality
1	116	5.01114	-6.33799	T3, Taishir Locality
1	117	4.85614	-6.47261	T3, Taishir Locality
1	118	7.14414	-5.00961	T3, Taishir Locality
1	119	8.45914	-3.78318	T3, Taishir Locality
1	120	6.30014	-6.28058	T3, Taishir Locality
1	121	8.12814	-5.3036	T3, Taishir Locality
1	122	8.06414	-4.72255	T3, Taishir Locality
1	123	6.40814	-6.95962	T3, Taishir Locality
1	124	8.67214	-3.49513	T3, Taishir Locality
1	125	8.16514	-3.11701	T3, Taishir Locality
2	75	5.415	-6.29911	T3, Taishir Locality
2	80	9.274	-3.14048	T3, Taishir Locality
2	82	3.02	-4.89648	T3, Taishir Locality
2	90	9.491	-1.39042	T3, Taishir Locality
2	91	6.052	-6.02294	T3, Taishir Locality
2	99	5.632	-2.54261	T3, Taishir Locality
2	123	6.908	-6.60794	T3, Taishir Locality
3	75	6.525	-6.35454	T3, Taishir Locality
3	80	5.006	-5.78537	T3, Taishir Locality
3	82	5.11	-5.02121	T3, Taishir Locality
3	83	7.528	-4.90737	T3, Taishir Locality
3	90	9.508	-1.62304	T3, Taishir Locality
3	91	6.552	-5.65372	T3, Taishir Locality
3	99	5.169	-2.99794	T3, Taishir Locality
3	116	4.763	-6.45946	T3, Taishir Locality
3	117	9.477	-1.94672	T3, Taishir Locality
3	123	6.703	-6.61388	T3, Taishir Locality
4	75	5.644		T3, Taishir Locality
4	80	7.165	-5.46763	T3, Taishir Locality
5	75	7.591	-4.40948	T3, Taishir Locality
5	99	5.768	-2.79601	T3, Taishir Locality
	U1111			

1	59	1.38267	-8.19359	T3, Ol Mountain
1	61	0.104667	-9.19137	T3, Ol Mountain
1	61.5	0.140667	-5.99612	T3, Ol Mountain
1	62	0.549667	-5.92881	T3, Ol Mountain
1	62.5	-3.56833	-5.64175	T3, Ol Mountain
1	63	-2.37633	-12.4737	T3, Ol Mountain
1	63.5	-1.27033	-4.92213	T3, Ol Mountain
1	64.5	-0.94233	-7.9194	T3, Ol Mountain
1	65	-2.27233	-10.2525	T3, Ol Mountain
1	65.5	-1.73233	-12.5767	T3, Ol Mountain
1	66.5	-6.4662	-5.68794	T3, Ol Mountain
1	67.5	0.160667	-10.5534	T3, Ol Mountain
1	68	-0.99733	-8.8271	T3, Ol Mountain
1	68.5	-0.25433	-14.2812	T3, Ol Mountain
1	69	-0.91933	-9.71203	T3, Ol Mountain
1	69.5	-1.00633	-9.6368	T3, Ol Mountain
1	70	-0.89133	-9.37548	T3, Ol Mountain
1	70.5	1.15667	-7.41557	T3, Ol Mountain
1	71.5	1.22567	-8.58162	T3, Ol Mountain
1	72.5	0.645667	-7.79765	T3, Ol Mountain
1	73	0.257667	-6.76424	T3, Ol Mountain
1	74	1.47367	-10.3436	T3, Ol Mountain
1	74.5	2.24567	-6.91866	T3, Ol Mountain
1	75	1.07367	-20.057	T3, Ol Mountain
1	75.5	1.21167	-14.0605	T3, Ol Mountain
1	76	2.62467	-10.2743	T3, Ol Mountain
1	77	1.9778	-3.82801	T3, Ol Mountain
1	79	4.599	-2.49121	T3, Ol Mountain
1	80	4.764	-3.98589	T3, Ol Mountain
1	81	3.658	-9.31625	T3, Ol Mountain
1	82	4.072	-8.25216	T3, Ol Mountain
1	83	3.253	-6.75451	T3, Ol Mountain
1	84	3.771	-3.1653	T3, Ol Mountain
1	85	3.712	-9.96659	T3, Ol Mountain
1	86	3.816	-10.6823	T3, Ol Mountain
1	87	4.425	-6.4536	T3, Ol Mountain
1	89	3.464	-6.99208	T3, Ol Mountain
1	90	2.5368	-6.95298	T3, Ol Mountain
1	91	1.5548	-5.58599	T3, Ol Mountain
1	92	3.0858	-6.6194	T3, Ol Mountain
1	93	3.1678	-5.57609	T3, Ol Mountain

1	95	1.8738	-1.97995	T3, Ol Mountain
1	96	1.0528	-1.17124	T3, Ol Mountain
1	98	3.9758	-5.22766	T3, Ol Mountain
1	100	2.9368	-6.43924	T3, Ol Mountain
1	101	3.2048	-4.48626	T3, Ol Mountain
1	102	3.7028	-7.85275	T3, Ol Mountain
1	103	4.2418	-3.39445	T3, Ol Mountain
1	105	4.8328	-5.7414	T3, Ol Mountain
1	106	2.68425	-5.54095	T3, Ol Mountain
1	107	4.33725	-1.62608	T3, Ol Mountain
1	108	4.69625	-0.30462	T3, Ol Mountain
1	109	3.40825	-2.97624	T3, Ol Mountain
1	111	4.03225	-3.27418	T3, Ol Mountain
1	112	5.32825	-0.79262	T3, Ol Mountain
1	113	5.26525	-0.51843	T3, Ol Mountain
1	114	3.77925	-6.73966	T3, Ol Mountain
1	115	4.89225	-6.31403	T3, Ol Mountain
1	116	4.67125	-7.59094	T3, Ol Mountain
1	117	5.00325	-6.82677	T3, Ol Mountain
1	119	4.52225	-10.0616	T3, Ol Mountain
1	120	4.63025	-5.57065	T3, Ol Mountain
2	58.5	0.427	-7.81853	T3, Ol Mountain
2	54	0.87	-0.03164	T3, Ol Mountain
2	59.5	1.285	-9.98037	T3, Ol Mountain
2	60.5	-2.716	-8.07293	T3, Ol Mountain
2	64	-0.877	-6.60398	T3, Ol Mountain
2	65.5	-1.075	-12.0541	T3, Ol Mountain
2	66	-0.97	-12.3857	T3, Ol Mountain
2	67	0.276	-10.8604	T3, Ol Mountain
2	68.5	-0.685	-8.26595	T3, Ol Mountain
2	71	2.08471	-6.15855	T3, Ol Mountain
2	72	0.684714	-8.20854	T3, Ol Mountain
2	73.5	1.49871	-12.0026	T3, Ol Mountain
2	76.5	1.56771	-12.0729	T3, Ol Mountain
2	78	3.52771	-4.88263	T3, Ol Mountain
2	84	3.74971	-2.33078	T3, Ol Mountain
2	86	3.51371	-10.7633	T3, Ol Mountain
2	88	3.95071	-6.54063	T3, Ol Mountain
2	92	1.93071	-4.77077	T3, Ol Mountain
2	94	0.724714	-5.18651	T3, Ol Mountain
2	99	3.64471	-4.94895	T3, Ol Mountain

2	102	2.80871	-6.5238	T3, Ol Mountain
2	104	3.63171	-5.7141	T3, Ol Mountain
2	106	5.81471	-1.15682	T3, Ol Mountain
2	110	4.19671	-4.48965	T3, Ol Mountain
2	112	5.10871	-1.41517	T3, Ol Mountain
2	114	3.80871	-7.47307	T3, Ol Mountain
2	116	5.05	-8.09993	T3, Ol Mountain
2	118	4.431	-8.60575	T3, Ol Mountain
3	58.5	0.844	-7.3246	T3, Ol Mountain
3	59.5	1.034	-9.75469	T3, Ol Mountain
3	64	-0.518	-6.81185	T3, Ol Mountain
3	65.5	-0.985	-7.47703	T3, Ol Mountain
3	66	-1.017	-11.8383	T3, Ol Mountain
3	71	1.28971	-7.48099	T3, Ol Mountain
3	73.5	1.25371	-11.4463	T3, Ol Mountain
3	78	3.16871	-5.75469	T3, Ol Mountain
3	92	2.01471	-5.05882	T3, Ol Mountain
3	94	1.74471	-4.38077	T3, Ol Mountain
3	99	4.13071	-5.07763	T3, Ol Mountain
3	104	3.76871	-4.47778	T3, Ol Mountain
3	106	5.46771	-1.8507	T3, Ol Mountain
3	112	5.07071	-1.29342	T3, Ol Mountain
3	118	3.239	-12.9542	T3, Ol Mountain
4	54	0.162	0.534561	T3, Ol Mountain
4	58.5	1.352	-8.77176	T3, Ol Mountain
4	59.5	1.218	-9.94672	T3, Ol Mountain
4	60.5	-1.922	-13.7685	T3, Ol Mountain
4	63	-0.324	-9.95761	T3, Ol Mountain
4	64	-0.991	-6.2219	T3, Ol Mountain
4	65.5	-1.094	-10.3298	T3, Ol Mountain
4	66	-0.922	-9.84279	T3, Ol Mountain
4	67	0.221	-10.0398	T3, Ol Mountain
4	68.5	-0.501	-7.10881	T3, Ol Mountain
4	71	2.25971	-5.59631	T3, Ol Mountain
4	72	1.20871	-10.6475	T3, Ol Mountain
4	73.5	0.976714	-9.07961	T3, Ol Mountain
4	74.5	0.978714	-20.9173	T3, Ol Mountain
4	75.5	2.53271	-9.96553	T3, Ol Mountain
4	76.5	1.38571	-11.6334	T3, Ol Mountain
4	78	2.83671	-7.0702	T3, Ol Mountain
4	82	3.99371	-7.64531	T3, Ol Mountain

4	84	3.68971	-2.45946	T3, Ol Mountain
4	86	3.66771	-10.0705	T3, Ol Mountain
4	88	4.05571	-7.23452	T3, Ol Mountain
4	92	1.82071	-4.73811	T3, Ol Mountain
4	94	3.12371	-1.6369	T3, Ol Mountain
4	96	3.92871	-5.59532	T3, Ol Mountain
4	97	4.38371	-7.64135	T3, Ol Mountain
4	99	3.75971	-6.58122	T3, Ol Mountain
4	102	3.22771	-7.36617	T3, Ol Mountain
4	104	2.61371	-5.03803	T3, Ol Mountain
4	106	5.74271	-0.75988	T3, Ol Mountain
4	108	4.91671	-1.08357	T3, Ol Mountain
4	110	3.97571	-4.96676	T3, Ol Mountain
4	112	4.76771	-2.35454	T3, Ol Mountain
4	114	4.11271	-7.7928	T3, Ol Mountain
4	116	3.91071	-4.53915	T3, Ol Mountain
4	118	4.664	-9.30855	T3, Ol Mountain
	U1115-7			
1	24.5	0.58	-1.20744	T3, N.Bayan Gorge
1	26	-0.284	-0.43139	T3, N.Bayan Gorge
1	38	1.738	-1.4064	T3, N.Bayan Gorge
1	44	1.93067	0.219175	T3, N.Bayan Gorge
1	46	2.13971	-0.73726	T3, N.Bayan Gorge
1	82	2.58971	-4.03503	T3, N.Bayan Gorge
1	84	2.782	-1.76982	T3, N.Bayan Gorge
1	86	2.07	-4.10389	T3, N.Bayan Gorge
1	93	2.524	-9.51345	T3, N.Bayan Gorge
1	95.1	2.71271	-6.11471	T3, N.Bayan Gorge
1	97	2.93571	-8.68041	T3, N.Bayan Gorge
1	99	2.90771	-2.57697	T3, N.Bayan Gorge
1	101	2.459	-8.39689	T3, N.Bayan Gorge
1	105	2.769	-6.31523	T3, N.Bayan Gorge
1	107	2.42271	-5.11694	T3, N.Bayan Gorge
1	109	2.89271	-7.70838	T3, N.Bayan Gorge
1	117	1.902	-3.72379	T3, N.Bayan Gorge
1	121	2.824	-4.75126	T3, N.Bayan Gorge
1	123	2.99371	-6.1553	T3, N.Bayan Gorge
1	127	2.28271	-6.3691	T3, N.Bayan Gorge
1	135	3.218	-2.75769	T3, N.Bayan Gorge
1	149	3.20371	-5.74748	T3, N.Bayan Gorge

1	153	2.668	-1.5669	T3, N.Bayan Gorge
1	158	2.71871	-3.81528	T3, N.Bayan Gorge
1	160	2.953	-4.98387	T3, N.Bayan Gorge
1	162	2.84771	-5.73164	T3, N.Bayan Gorge
1	166	2.53671	-6.47502	T3, N.Bayan Gorge
1	190	2.98167	-3.30306	T3, N.Bayan Gorge
1	193	2.61067	-2.42604	T3, N.Bayan Gorge
2	82	2.27171	-4.22946	T3, N.Bayan Gorge
2	84	2.55271	-1.87361	T3, N.Bayan Gorge
2	86	2.26214	-3.95938	T3, N.Bayan Gorge
2	95.1	2.73814	-4.97893	T3, N.Bayan Gorge
2	97	3.02914	-8.21674	T3, N.Bayan Gorge
2	99	2.89314	-2.00639	T3, N.Bayan Gorge
2	101	2.35614	-8.6305	T3, N.Bayan Gorge
2	105	2.87214	-5.74507	T3, N.Bayan Gorge
2	107	2.55914	-5.53324	T3, N.Bayan Gorge
2	109	2.94214	-7.18036	T3, N.Bayan Gorge
2	117	1.68014	-6.8745	T3, N.Bayan Gorge
2	123	3.11014	-5.947	T3, N.Bayan Gorge
2	127	2.16814	-6.96061	T3, N.Bayan Gorge
2	135	3.20814	-5.52038	T3, N.Bayan Gorge
2	149	3.46525	-5.21826	T3, N.Bayan Gorge
2	153	3.10625	-1.69933	T3, N.Bayan Gorge
2	158	2.81225	-1.46572	T3, N.Bayan Gorge
2	162	3.39625	-6.53674	T3, N.Bayan Gorge
2	166	2.71625	-6.39816	T3, N.Bayan Gorge
2	174	2.72471	-3.87269	T3, N.Bayan Gorge
2	182	2.59857	-6.87266	T3, N.Bayan Gorge
2	186	2.63757	-2.28468	T3, N.Bayan Gorge
2	188	0.637571	-1.09488	T3, N.Bayan Gorge
3	20.5	1.778	-6.87846	T3, N.Bayan Gorge
3	24.5	0.447	-1.62827	T3, N.Bayan Gorge
3	48	1.463	0.627608	T3, N.Bayan Gorge
3	131	3.231	-5.31944	T3, N.Bayan Gorge
3	170	2.70257	-6.65588	T3, N.Bayan Gorge
3	174	2.42271	-3.50843	T3, N.Bayan Gorge
3	182	2.31757	-3.71997	T3, N.Bayan Gorge
3	186	2.29457	-1.80757	T3, N.Bayan Gorge
3	188	1.71857	-1.10676	T3, N.Bayan Gorge
4	20.5	0.654	-2.77155	T3, N.Bayan Gorge
4	22.5	-1.094	-0.9621	T3, N.Bayan Gorge

4	24.5	0.704	-3.52681	T3, N.Bayan Gorge
4	26	0.157	-2.24396	T3, N.Bayan Gorge
4	32	1.958	-1.18778	T3, N.Bayan Gorge
4	38	2.167	-1.75893	T3, N.Bayan Gorge
4	42	0.423	-0.67603	T3, N.Bayan Gorge
4	44	0.43	-1.14126	T3, N.Bayan Gorge
4	46	2.153	-6.19942	T3, N.Bayan Gorge
4	48	1.481	-1.5768	T3, N.Bayan Gorge
4	50	0.107	-0.11082	T3, N.Bayan Gorge
4	93	2.568	-7.93265	T3, N.Bayan Gorge
4	97	2.87471	-8.46661	T3, N.Bayan Gorge
4	123	3.20871	-5.81578	T3, N.Bayan Gorge
4	131	3.191	-6.49637	T3, N.Bayan Gorge
4	139	3.224	-5.59066	T3, N.Bayan Gorge
4	170	2.72357	-6.01049	T3, N.Bayan Gorge
4	174	2.60471	-5.21098	T3, N.Bayan Gorge
4	182	2.29957	-7.97239	T3, N.Bayan Gorge
4	184	2.52257	-0.8979	T3, N.Bayan Gorge
4	186	2.70857	-2.16887	T3, N.Bayan Gorge
4	188	2.96057	-3.19832	T3, N.Bayan Gorge
4	190	1.88571	-2.05532	T3, N.Bayan Gorge
4	193	2.57557	-1.68483	T3, N.Bayan Gorge
4	195	2.35057	-1.71552	T3, N.Bayan Gorge
5	20.5	0.747	-4.81659	T3, N.Bayan Gorge
5	22.5	-1.246	-0.51963	T3, N.Bayan Gorge
5	24.5	0.578	-0.89776	T3, N.Bayan Gorge
5	32	2.305	-2.12716	T3, N.Bayan Gorge
5	38	1.703	-4.39788	T3, N.Bayan Gorge
5	42	1.865	-2.05688	T3, N.Bayan Gorge
5	46	1.712	-5.20956	T3, N.Bayan Gorge
5	48	0.648	0.428647	T3, N.Bayan Gorge
5	50	-0.178	0.190092	T3, N.Bayan Gorge
5	93	2.055	-11.8089	T3, N.Bayan Gorge
5	97	2.89471	-8.26171	T3, N.Bayan Gorge
5	105	2.842	-5.9668	T3, N.Bayan Gorge
5	117	1.522	-6.31919	T3, N.Bayan Gorge
5	121	2.825	-5.11849	T3, N.Bayan Gorge
5	123	3.03971	-5.94446	T3, N.Bayan Gorge
5	131	3.193	-6.5419	T3, N.Bayan Gorge
5	139	3.083	-5.29469	T3, N.Bayan Gorge
5	153	2.40071	-2.37504	T3, N.Bayan Gorge

5	160	3.094	-4.95319	T3, N.Bayan Gorge
5	162	3.29171	-6.32951	T3, N.Bayan Gorge
5	184	2.59357	-2.01643	T3, N.Bayan Gorge
5	182	2.57457	-6.77565	T3, N.Bayan Gorge
	U1241			
1	130	8.08967	-3.69817	T3, Tsakhir Range
1	131	9.33767	-3.37548	T3, Tsakhir Range
1	132	8.86267	-6.49055	T3, Tsakhir Range
1	133	9.80667	-3.81102	T3, Tsakhir Range
1	134	7.47667	-6.50837	T3, Tsakhir Range
1	136	7.12467	-5.64818	T3, Tsakhir Range
1	137	6.61967	-5.8907	T3, Tsakhir Range
1	138	5.72067	-6.83601	T3, Tsakhir Range
1	139	6.77267	-6.97459	T3, Tsakhir Range
1	140	6.69567	-8.78107	T3, Tsakhir Range
1	141	6.48567	-7.35766	T3, Tsakhir Range
1	143	3.57267	-11.7813	T3, Tsakhir Range
1	144	4.42467	-8.31089	T3, Tsakhir Range
1	145	4.73267	-9.63532	T3, Tsakhir Range
1	146	6.80367	-4.19607	T3, Tsakhir Range
1	147	7.79667	-3.98028	T3, Tsakhir Range
1	148	6.53667	-6.33019	T3, Tsakhir Range
1	150	5.52067	-2.17281	T3, Tsakhir Range
1	151	4.81467	-2.93301	T3, Tsakhir Range
1	152	6.08167	-3.63383	T3, Tsakhir Range
1	153	5.32767	-2.75187	T3, Tsakhir Range
1	154	5.33367	-4.31782	T3, Tsakhir Range
1	155	6.13767	-3.13989	T3, Tsakhir Range
1	156	5.84867	-2.98746	T3, Tsakhir Range
1	157	6.22167	-3.71599	T3, Tsakhir Range
1	158	5.63867	-2.35395	T3, Tsakhir Range
1	159	6.38467	-3.15672	T3, Tsakhir Range
1	160	6.46967	-2.41532	T3, Tsakhir Range
1	161	6.75767	-2.3787	T3, Tsakhir Range
1	162	6.60367	-2.08669	T3, Tsakhir Range
1	163	6.43567	-3.10228	T3, Tsakhir Range
1	164	6.37067	-2.15004	T3, Tsakhir Range
1	165	6.70067	-2.57271	T3, Tsakhir Range
1	167	5.34667	-3.61106	T3, Tsakhir Range
1	168	6.51067	-4.31881	T3, Tsakhir Range

1	169	5.66467	-2.71723	T3, Tsakhir Range
1	170	5.22667	-4.27031	T3, Tsakhir Range
1	171	6.19367	-2.63408	T3, Tsakhir Range
1	172	5.82567	-3.10129	T3, Tsakhir Range
1	173	6.29167	-6.40344	T3, Tsakhir Range
1	174	6.05567	-3.36459	T3, Tsakhir Range
1	175	6.13967	-2.25101	T3, Tsakhir Range
1	176	6.26967	-4.57518	T3, Tsakhir Range
1	177	5.90767	-2.49154	T3, Tsakhir Range
1	211	4.96717	-3.96461	T3, Tsakhir Range
1	212	5.77217	-7.03513	T3, Tsakhir Range
1	213	5.64117	-6.75105	T3, Tsakhir Range
1	214	4.64517	-7.24498	T3, Tsakhir Range
1	215	4.77617	-10.1809	T3, Tsakhir Range
1	216	4.67717	-7.66567	T3, Tsakhir Range
1	217	4.79017	-5.79386	T3, Tsakhir Range
1	218	4.86817	-2.50853	T3, Tsakhir Range
1	219	4.30317	-5.69289	T3, Tsakhir Range
1	220	3.75917	-8.85251	T3, Tsakhir Range
1	221	3.81317	-7.30734	T3, Tsakhir Range
1	222	3.18317	-6.91437	T3, Tsakhir Range
1	223	3.74917	-6.65503	T3, Tsakhir Range
1	224	4.19317	-6.81836	T3, Tsakhir Range
1	225	3.88617	-8.55357	T3, Tsakhir Range
1	226	5.66017	-2.7362	T3, Tsakhir Range
1	227	4.01317	-8.36055	T3, Tsakhir Range
1	228	4.31117	-5.80376	T3, Tsakhir Range
1	229	3.69117	-7.2826	T3, Tsakhir Range
1	230	1.37517	-6.72531	T3, Tsakhir Range
1	231	1.29917	-11.3618	T3, Tsakhir Range
1	232	2.60717	-7.53996	T3, Tsakhir Range
1	233	3.67317	-5.23459	T3, Tsakhir Range
1	234	2.18617	-4.58822	T3, Tsakhir Range
1	235	2.25617	-5.55332	T3, Tsakhir Range
1	236	4.58317	-2.10467	T3, Tsakhir Range
1	237	3.89717	-4.7456	T3, Tsakhir Range
1	238	5.59817	-2.94902	T3, Tsakhir Range
1	239	5.23517	-6.1898	T3, Tsakhir Range
1	240	4.66217	-5.25538	T3, Tsakhir Range
1	241	3.15617	-5.4088	T3, Tsakhir Range
2	135	6.18114	-9.63888	T3, Tsakhir Range

2	139	6.32514	-6.63071	T3, Tsakhir Range
2	141	6.88714	-7.26125	T3, Tsakhir Range
2	142	5.01914	-10.1318	T3, Tsakhir Range
2	143	5.96814	-7.64234	T3, Tsakhir Range
2	144	5.60514	-6.7485	T3, Tsakhir Range
2	145	4.39914	-10.31	T3, Tsakhir Range
2	146	6.25314	-3.43051	T3, Tsakhir Range
2	147	8.27914	-3.74034	T3, Tsakhir Range
2	148	8.13714	-5.31816	T3, Tsakhir Range
2	149	5.66614	-3.56117	T3, Tsakhir Range
2	151	5.23914	-1.93781	T3, Tsakhir Range
2	152	6.97514	-4.14123	T3, Tsakhir Range
2	154	5.46714	-4.16399	T3, Tsakhir Range
2	157	4.81914	-5.82992	T3, Tsakhir Range
2	160	6.23614	-2.25258	T3, Tsakhir Range
2	161	6.68114	-2.49609	T3, Tsakhir Range
2	168	5.15414	-6.21299	T3, Tsakhir Range
2	169	5.61014	-2.31198	T3, Tsakhir Range
2	170	5.39614	-2.89599	T3, Tsakhir Range
2	171	5.14314	-5.53395	T3, Tsakhir Range
2	172	5.07614	-4.54212	T3, Tsakhir Range
2	174	6.25414	-2.43076	T3, Tsakhir Range
2	175	6.03314	-2.32385	T3, Tsakhir Range
2	176	6.24814	-4.56785	T3, Tsakhir Range
2	177	5.77714	-1.75964	T3, Tsakhir Range
2	178	5.75114	-2.67723	T3, Tsakhir Range
2	180	5.43014	-2.35454	T3, Tsakhir Range
2	181	4.02114	-6.56241	T3, Tsakhir Range
2	182	4.79114	-2.54261	T3, Tsakhir Range
2	183	5.11014	-2.66535	T3, Tsakhir Range
2	184	4.86514	-2.41987	T3, Tsakhir Range
2	185	5.59914	-2.61982	T3, Tsakhir Range
2	187	5.23214	-3.43546	T3, Tsakhir Range
2	188	4.51914	-3.88683	T3, Tsakhir Range
2	189	4.56714	-3.19379	T3, Tsakhir Range
2	190	3.76714	-7.07204	T3, Tsakhir Range
2	191	5.11914	-3.48283	T3, Tsakhir Range
2	193	3.74414	-6.78498	T3, Tsakhir Range
2	200	4.48614	-2.13762	T3, Tsakhir Range
2	204	4.65114	-8.3054	T3, Tsakhir Range
2	206	3.77914	-7.12747	T3, Tsakhir Range

2	208	5.44014	-4.17375	T3, Tsakhir Range
2	209	4.98514	-3.17202	T3, Tsakhir Range
2	210	4.20914	-6.40884	T3, Tsakhir Range
2	212	5.48714	-6.4811	T3, Tsakhir Range
2	214	4.87414	-6.88001	T3, Tsakhir Range
2	215	5.12014	-9.34772	T3, Tsakhir Range
2	216	3.83414	-10.1574	T3, Tsakhir Range
2	217	4.44014	-6.9295	T3, Tsakhir Range
2	218	4.10614	-4.5489	T3, Tsakhir Range
2	219	2.92314	-10.3039	T3, Tsakhir Range
2	220	4.86114	-5.4566	T3, Tsakhir Range
2	221	3.26814	-8.73896	T3, Tsakhir Range
2	223	3.79614	-6.34648	T3, Tsakhir Range
2	224	3.56414	-6.68204	T3, Tsakhir Range
2	226	4.93414	-4.53604	T3, Tsakhir Range
2	227	1.49414	-15.4908	T3, Tsakhir Range
2	228	4.30514	-5.55757	T3, Tsakhir Range
2	229	2.68814	-9.35465	T3, Tsakhir Range
2	230	1.09314	-5.1834	T3, Tsakhir Range
2	231	1.12614	-12.5826	T3, Tsakhir Range
2	233	3.67514	-4.69441	T3, Tsakhir Range
2	234	2.11114	-4.35786	T3, Tsakhir Range
2	236	4.35514	-1.77335	T3, Tsakhir Range
2	237	3.91414	-4.20246	T3, Tsakhir Range
2	238	3.65514	-6.98098	T3, Tsakhir Range
2	239	5.20414	-6.81468	T3, Tsakhir Range
2	240	3.93114	-6.09011	T3, Tsakhir Range
3	139	7.06314	-6.99596	T3, Tsakhir Range
3	142	4.90614	-9.08852	T3, Tsakhir Range
3	144	5.43814	-8.46887	T3, Tsakhir Range
3	146	7.59514	-3.85516	T3, Tsakhir Range
3	149	5.91114	-2.92964	T3, Tsakhir Range
3	151	5.45114	-1.3825	T3, Tsakhir Range
3	152	6.35814	-3.69084	T3, Tsakhir Range
3	157	5.45114	-3.65719	T3, Tsakhir Range
3	160	6.41714	-2.85838	T3, Tsakhir Range
3	170	4.31314	-7.07515	T3, Tsakhir Range
3	172	5.84214	-3.38498	T3, Tsakhir Range
3	177	5.93414	-2.37137	T3, Tsakhir Range
3	178	5.97814	-2.10906	T3, Tsakhir Range
3	182	4.92314	-2.70594	T3, Tsakhir Range

3	185	5.64614	-1.92989	T3, Tsakhir Range
3	186	4.42714	-3.12762	T3, Tsakhir Range
3	188	4.77014	-2.65051	T3, Tsakhir Range
3	189	4.57314	-3.73524	T3, Tsakhir Range
3	200	4.48014	-2.1297	T3, Tsakhir Range
3	208	5.06514	-2.46823	T3, Tsakhir Range
3	219	4.52714	-4.65284	T3, Tsakhir Range
3	221	3.44214	-7.39078	T3, Tsakhir Range
3	224	3.83014	-7.55608	T3, Tsakhir Range
3	225	4.06214	-9.06363	T3, Tsakhir Range
3	227	3.48514	-8.98543	T3, Tsakhir Range
3	228	4.53614	-5.02205	T3, Tsakhir Range
3	231	1.43714	-14.1	T3, Tsakhir Range
3	237	4.18414	-3.60755	T3, Tsakhir Range
3	244	3.48514	-4.10347	T3, Tsakhir Range
4	139	6.93914	-7.12465	T3, Tsakhir Range
4	188	4.34114	-3.21458	T3, Tsakhir Range
4	189	4.34214	-3.7689	T3, Tsakhir Range
	F860			
1	3	0.331667	-5.46523	Ol, Taishir Locality
1	6.5	0.241667	-7.06978	Ol, Taishir Locality
1	25	-4.58286	-9.90967	Ol, Taishir Locality
2	0.1	0.568333	-5.3438	Ol, Taishir Locality
2	0.5	0.126	-5.47414	Ol, Taishir Locality
2	1	0.140333	-6.20102	Ol, Taishir Locality
2	1.5	0.238333	-6.04264	Ol, Taishir Locality
2	2	0.529	-6.61841	Ol, Taishir Locality
2	3	0.324	-5.89878	Ol, Taishir Locality
2	3.4	-0.199	-5.99381	Ol, Taishir Locality
2	4	-0.50367	-10.4376	Ol, Taishir Locality
2	4.5	0.651	-5.22865	Ol, Taishir Locality
2	5.5	-0.19767	-5.72787	Ol, Taishir Locality
2	6.5	1.028	-5.54244	Ol, Taishir Locality
2	7	0.769	-5.04652	Ol, Taishir Locality
2	7.5	0.576333	-5.24185	Ol, Taishir Locality
2	8.5	0.306333	-5.90109	Ol, Taishir Locality
2	9	0.169	-6.44914	Ol, Taishir Locality
2	9.5	-0.65667	-5.44873	Ol, Taishir Locality
2	10	-0.22667	-6.06145	Ol, Taishir Locality
2	10.5	-0.353	-4.68522	Ol, Taishir Locality

2	11	-0.216	-5.59688	Ol, Taishir Locality
2	11	-0.36667	-4.92906	Ol, Taishir Locality
2	12	-2.458	-6.36401	Ol, Taishir Locality
2	20	-3.671	-6.14229	Ol, Taishir Locality
2	25	-4.78067	-14.2792	Ol, Taishir Locality
2	26	-5.216	-8.38431	Ol, Taishir Locality
2	27	-4.57067	-13.4547	Ol, Taishir Locality
2	27.8	-4.17567	-9.08248	Ol, Taishir Locality
2	29	-1.82067	-5.5398	Ol, Taishir Locality
2	43	-0.32067	-7.67887	Ol, Taishir Locality
3	1.5	0.278333	-5.8318	Ol, Taishir Locality
3	3.4	0.37	-5.31972	Ol, Taishir Locality
3	5	0.261	-5.20094	Ol, Taishir Locality
3	5.5	0.175333	-6.35148	Ol, Taishir Locality
3	8.5	0.286333	-7.46506	Ol, Taishir Locality
3	9	-0.129	-5.46127	Ol, Taishir Locality
3	9.5	0.041333	-5.81596	Ol, Taishir Locality
3	10	-0.25567	-5.69817	Ol, Taishir Locality
3	10.5	-0.515	-5.20786	Ol, Taishir Locality
3	11	0.246	-2.89952	Ol, Taishir Locality
3	27.8	-5.11167	-8.74989	Ol, Taishir Locality
3	29	-4.10467	-8.59251	Ol, Taishir Locality
4	0.1	0.471333	-4.87956	Ol, Taishir Locality
4	0.5	0.37	-5.07621	Ol, Taishir Locality
4	1	0.348333	-6.04165	Ol, Taishir Locality
4	1.5	-0.94867	-6.61874	Ol, Taishir Locality
4	2	0.003	-5.91462	Ol, Taishir Locality
4	3.4	1.78	-5.17916	Ol, Taishir Locality
4	4	0.115333	-6.40196	Ol, Taishir Locality
4	4.5	-0.34	-5.72457	Ol, Taishir Locality
4	5	0.997	-5.18312	Ol, Taishir Locality
4	5.5	0.321333	-6.01789	Ol, Taishir Locality
4	6.5	0.855	-5.4385	Ol, Taishir Locality
4	7	0.830333	-5.31807	Ol, Taishir Locality
4	7.5	0.638333	-5.00131	Ol, Taishir Locality
4	8.5	0.357333	-5.30223	Ol, Taishir Locality
4	9	0.058	-5.67409	Ol, Taishir Locality
4	9.5	0.098333	-6.16241	Ol, Taishir Locality
4	9.5	0.068333	-6.21884	Ol, Taishir Locality
4	10	-0.65267	-5.39528	Ol, Taishir Locality
4	10.5	-0.253	-5.30883	Ol, Taishir Locality

4	11	-0.329	-5.51967	Ol, Taishir Locality
4	11	-0.11067	-6.16142	Ol, Taishir Locality
4	12	-2.371	-6.51249	Ol, Taishir Locality
4	20	-3.656	-6.06211	Ol, Taishir Locality
4	26	-4.994	-9.13956	Ol, Taishir Locality
4	27.8	-4.89567	-9.14979	Ol, Taishir Locality
4	29	-4.23667	-8.24804	Ol, Taishir Locality
	U1112			
1	1.8	-1.54775	-5.46671	Ol, Ol Mountain
1	5.4	-1.2418	-5.15857	Ol, Ol Mountain
1	20.2	-0.76129	-5.59801	Ol, Ol Mountain
2	3	-0.85229	-4.46364	Ol, Ol Mountain
2	3.6	-0.89843	-5.61851	Ol, Ol Mountain
2	20.2	-2.74843	-5.8343	Ol, Ol Mountain
2	25	2.04757	-0.12086	Ol, Ol Mountain
3	1.8	-1.12143	-4.57224	Ol, Ol Mountain
3	3	-1.35029	-5.12189	Ol, Ol Mountain
3	3.6	-1.27743	-6.36783	Ol, Ol Mountain
3	4.6	-0.60843	-4.62569	Ol, Ol Mountain
3	7.4	0.019714	-3.85982	Ol, Ol Mountain
3	15.2	0.647571	-6.4688	Ol, Ol Mountain
3	16.2	1.80371	-5.50793	Ol, Ol Mountain
3	19.4	-0.56843	-3.46459	Ol, Ol Mountain
3	20.2	-2.68343	-5.61257	Ol, Ol Mountain
3	23	2.21471	-3.40845	Ol, Ol Mountain
3	25	1.90257	-0.27429	Ol, Ol Mountain
4	1.8	-1.22343	-5.04638	Ol, Ol Mountain
4	3	-0.04429	-3.86873	Ol, Ol Mountain
4	3.6	-0.77443	-5.66108	Ol, Ol Mountain
4	4.6	-0.79643	-3.92388	Ol, Ol Mountain
4	5.4	-0.55329	-4.46364	Ol, Ol Mountain
4	7.4	-0.39029	-4.25973	Ol, Ol Mountain
4	14.4	-0.78229	-4.37455	Ol, Ol Mountain
4	15.2	1.04557	-3.75561	Ol, Ol Mountain
4	16.2	1.58871	-6.59776	Ol, Ol Mountain
4	19.4	-1.18543	-3.39035	Ol, Ol Mountain
4	20.2	-1.96643	-5.12359	Ol, Ol Mountain
4	23	1.52871	-4.00137	Ol, Ol Mountain
4	24	2.06857	-0.59203	Ol, Ol Mountain
4	25	1.96457	-0.49305	Ol, Ol Mountain

5	25	2.23757	-0.7613	Ol, Ol Mountain
6	24	2.19257	-0.54353	Ol, Ol Mountain
	U1113			
1	4	-0.923	-4.43366	Ol, N. Bayan Gorge
1	8	-0.589	-4.37427	Ol, N. Bayan Gorge
1	11	0.691	-1.94021	Ol, N. Bayan Gorge
1	25	-4.56071	-4.03644	Ol, N. Bayan Gorge
2	7	-0.29243	-3.83678	Ol, N. Bayan Gorge
2	12.6	2.12571	-2.4186	Ol, N. Bayan Gorge
2	18.2	0.473714	-1.88507	Ol, N. Bayan Gorge
3	7	-0.37543	-4.17531	Ol, N. Bayan Gorge
3	12.6	2.07371	-2.14144	Ol, N. Bayan Gorge
3	13.6	0.526571	-2.00654	Ol, N. Bayan Gorge
3	14.6	-0.07929	-2.43641	Ol, N. Bayan Gorge
3	18.2	0.463714	-2.8472	Ol, N. Bayan Gorge
3	23.9	-0.63729	-1.93753	Ol, N. Bayan Gorge
3	10.2	0.407571	-2.47177	Ol, N. Bayan Gorge
4	4	-0.91243	-4.93848	Ol, N. Bayan Gorge
4	6	0.448571	-2.44009	Ol, N. Bayan Gorge
4	7	-0.88643	-4.92561	Ol, N. Bayan Gorge
4	8	-0.47143	-4.62668	Ol, N. Bayan Gorge
4	11	0.656571	-2.01544	Ol, N. Bayan Gorge
4	12.6	1.74871	-2.43542	Ol, N. Bayan Gorge
4	13.6	0.546571	-1.96694	Ol, N. Bayan Gorge
4	14.6	0.281714	-2.23745	Ol, N. Bayan Gorge
4	18.2	0.118714	-2.48393	Ol, N. Bayan Gorge
4	23.9	-0.54929	-1.76331	Ol, N. Bayan Gorge
4	25	-3.87643	-4.97709	Ol, N. Bayan Gorge
4	10.2	0.500571	-2.24806	Ol, N. Bayan Gorge
	M12016			
1	0	2.16456	-2.96376	Ol, Tsakhir Range
1	0.5	-0.40244	-5.86007	Ol, Tsakhir Range
1	1	2.46256	-1.44037	Ol, Tsakhir Range
1	1.5	-0.63344	-5.44829	Ol, Tsakhir Range
1	2	1.18656	-3.00632	Ol, Tsakhir Range
1	2.5	1.84956	-0.92961	Ol, Tsakhir Range
1	3	2.60356	-2.23918	Ol, Tsakhir Range
1	3.5	2.82456	-2.52228	Ol, Tsakhir Range
1	4	2.87856	-4.2664	Ol, Tsakhir Range

1	4.5	2.82856	-5.04542	Ol, Tsakhir Range
1	5	2.86156	-3.49729	Ol, Tsakhir Range
1	5.5	2.42456	-2.33421	Ol, Tsakhir Range
1	6	2.56856	-1.96103	Ol, Tsakhir Range
1	6.5	1.90856	-2.99741	Ol, Tsakhir Range
1	7	1.79256	-2.05507	Ol, Tsakhir Range
1	7.5	1.47756	-1.84225	Ol, Tsakhir Range
1	8	1.30056	-1.51857	Ol, Tsakhir Range
1	8.5	1.75756	-3.03898	Ol, Tsakhir Range
1	9	1.50156	-3.5834	Ol, Tsakhir Range
1	9.5	2.30556	-2.55	Ol, Tsakhir Range
1	10	1.88256	-2.45101	Ol, Tsakhir Range
1	10.5	2.03456	-2.82419	Ol, Tsakhir Range
1	11	2.05156	-3.21716	Ol, Tsakhir Range
1	11.5	1.70656	-2.32431	Ol, Tsakhir Range
1	12	1.46456	-3.45076	Ol, Tsakhir Range
1	12.5	1.54956	-2.84992	Ol, Tsakhir Range
1	13	4.26456	-5.08303	Ol, Tsakhir Range
1	13.5	3.07356	-6.87467	Ol, Tsakhir Range
1	14	2.86156	-4.77519	Ol, Tsakhir Range
1	14.5	3.14056	-7.34584	Ol, Tsakhir Range
1	15	2.42856	-6.6569	Ol, Tsakhir Range
1	15.6	2.95256	-7.42206	Ol, Tsakhir Range
1	16	2.46556	-4.86131	Ol, Tsakhir Range
1	16.5	2.01356	-3.51213	Ol, Tsakhir Range
1	17	3.40956	-5.83928	Ol, Tsakhir Range
1	17.5	2.53756	-2.04814	Ol, Tsakhir Range
1	18	3.24756	-4.55445	Ol, Tsakhir Range
1	18.5	2.86956	-2.29956	Ol, Tsakhir Range
1	19	2.54656	-1.26319	Ol, Tsakhir Range
1	19.5	2.61256	-1.7403	Ol, Tsakhir Range
1	20	1.22756	-1.41265	Ol, Tsakhir Range
1	20.5	1.30256	-1.90659	Ol, Tsakhir Range
1	21	1.81156	-4.61285	Ol, Tsakhir Range
1	21.5	1.15556	-2.09565	Ol, Tsakhir Range
1	22	1.62256	-2.43913	Ol, Tsakhir Range
1	22.5	2.70256	-2.06596	Ol, Tsakhir Range
1	23	1.78956	-3.34485	Ol, Tsakhir Range
1	23.5	1.31556	-2.54802	Ol, Tsakhir Range
1	24	1.82856	-2.50248	Ol, Tsakhir Range
1	24.5	1.55556	-2.08971	Ol, Tsakhir Range

1	25	1.27656	-2.22829	Ol, Tsakhir Range
1	25.5	1.8845	-3.06446	Ol, Tsakhir Range
1	26	1.6165	-2.26961	Ol, Tsakhir Range
1	26.5	1.4455	-1.22333	Ol, Tsakhir Range
1	27	0.9345	-1.78557	Ol, Tsakhir Range
2	0.5	0.007143	-5.17336	Ol, Tsakhir Range
2	1	-1.15886	-5.88705	Ol, Tsakhir Range
2	1.5	-0.71186	-5.32184	Ol, Tsakhir Range
2	2	1.50214	-1.82073	Ol, Tsakhir Range
2	3	2.53014	-2.34634	Ol, Tsakhir Range
2	4	2.62014	-4.15678	Ol, Tsakhir Range
2	4.5	2.91314	-2.22954	Ol, Tsakhir Range
2	6	2.54914	-1.32976	Ol, Tsakhir Range
2	7.5	1.28514	-1.71085	Ol, Tsakhir Range
2	9	1.49114	-3.75193	Ol, Tsakhir Range
2	9.5	2.22414	-2.31862	Ol, Tsakhir Range
2	11	1.99714	-2.97786	Ol, Tsakhir Range
2	11.5	1.53914	-2.12857	Ol, Tsakhir Range
2	12	1.35514	-3.66086	Ol, Tsakhir Range
2	12.5	1.89014	-2.44433	Ol, Tsakhir Range
2	13.5	3.01714	-6.74822	Ol, Tsakhir Range
2	14	2.79514	-3.61038	Ol, Tsakhir Range
2	14.5	3.13314	-7.57079	Ol, Tsakhir Range
2	15	2.36314	-6.85314	Ol, Tsakhir Range
2	15.6	2.29714	-5.6475	Ol, Tsakhir Range
2	16	2.36914	-5.23572	Ol, Tsakhir Range
2	17	3.30914	-4.2914	Ol, Tsakhir Range
2	17.5	2.19314	-2.20578	Ol, Tsakhir Range
2	19	2.67714	-1.65344	Ol, Tsakhir Range
2	19.5	2.51414	-2.27408	Ol, Tsakhir Range
2	20	1.18114	-1.21197	Ol, Tsakhir Range
2	20.5	0.704143	-1.63166	Ol, Tsakhir Range
2	21.5	1.15614	-1.1308	Ol, Tsakhir Range
2	21.5	1.11214	-1.17534	Ol, Tsakhir Range
2	22	1.45214	-3.47576	Ol, Tsakhir Range
2	22.5	2.40014	-3.72322	Ol, Tsakhir Range
2	23	1.50714	-2.67596	Ol, Tsakhir Range
2	24	2.59214	-5.29709	Ol, Tsakhir Range
2	24.5	1.48214	-2.77212	Ol, Tsakhir Range
2	25	1.02814	-1.34673	Ol, Tsakhir Range
3	0.5	-0.57386	-5.8326	Ol, Tsakhir Range

3	1.5	-0.69386	-5.69006	Ol, Tsakhir Range
3	9	1.57314	-3.48269	Ol, Tsakhir Range
3	11	1.97914	-2.56906	Ol, Tsakhir Range
3	11.5	1.55314	-2.41563	Ol, Tsakhir Range
3	12	1.38714	-3.3352	Ol, Tsakhir Range
3	12.5	1.64014	-2.14738	Ol, Tsakhir Range
3	15.6	2.82614	-7.21939	Ol, Tsakhir Range
3	16	2.10014	-4.84671	Ol, Tsakhir Range
3	17	3.38314	-5.56138	Ol, Tsakhir Range
3	17.5	2.36914	-1.73263	Ol, Tsakhir Range
3	19	2.34114	-1.08625	Ol, Tsakhir Range
3	19.5	2.09914	-1.0041	Ol, Tsakhir Range
3	21.5	1.42414	-1.47824	Ol, Tsakhir Range
3	20.5	1.20214	-2.11273	Ol, Tsakhir Range
3	22	0.984143	-1.93654	Ol, Tsakhir Range
3	22.5	2.44914	-2.91154	Ol, Tsakhir Range
3	24	2.34214	-5.53678	Ol, Tsakhir Range
3	24.5	1.58714	-2.50189	Ol, Tsakhir Range
3	25	0.890143	-1.3784	Ol, Tsakhir Range
4	1.5	-0.72286	-5.79004	Ol, Tsakhir Range
4	11	1.92114	-2.84423	Ol, Tsakhir Range
4	21.5	1.68314	-3.16396	Ol, Tsakhir Range

*1 – Figure 4.1; from 2-5 – various macro-textures

Table 4.A3. Fluid inclusion data of the Taishir and Ol Formation carbonates.

Sample number	Tim last	T_h	Salinity	Mineral/Rock	$\delta^{18}0$	$\delta^{13}C$	T_h mean
Member T3, Taishir Fm, dolomite, N. Bayan Gorge							
U1117-36-1	-21		23	Dolomite	-1.790558	2.6736667	111.44545
2	-27	74.4	27				
3	-19	68.7	22				
4	-21	86.9	23				
5	-32	109	30	vopar rich			
6	-26		26				
7	-21	113.4	23				
8	-23.9	110.1	25				
9	-28.9	179.8	28				
10	-24.2	110.7	25				
11	-19	110	22				
12	-22.4	129.9	24				
13	-28.2	133	28				
Member T3, Taishir Fm, dolomite, N. Bayan Gorge							
U1116-82-1	-26	123	26	Dolomite	-6.536743	3.39625	108.09333
2	-18	116	21				
3	-19.8	86.9	22				
4	-4.2	159.7	7				
5	-10.7	68.7	15				
6	-22.7	86.9	24				
7	-2.8	129.4	5				
8	-7	86.9	15				
9	-21.5	113.4	23				
10	-25.9	110.1	26				
11	-12.2	68.7	16				
12	-28.1	86.9	27				
13	-23.9	128.8	25				
14	-28.9	128	28				
15	-24.2	128	25				
Member T3, basal unit, Taishir Fm, limestone, Taishir							
U1108-10-1	-19	72.5	21	Limestone	-7.494922	-6.15875	126.18235
2	-19	136	22				
3		116					
4		194					
5		128					
6	-13	128	17				
7	-23	137	24				
8	-16	225	19	quartz cement			

9	-21	189	23				
10	-31	223	29	quartz cement			
11	-21	124	23				
12		133.8					
13	-21.9	120.5	24				
14	-24.3	129.9	25				
15	-21.4	103.5	23				
16	-21.6	152.9	23				
17	-18.4	86.9	21				
18	-23.4	69.8	25				
19	-20.1	123.3	22				
Member T3, Taishir Fm, dolomite, Ol Mountain							
U1111-172-1	-23.6	140	25	Dolomite	-8.013606	5.13525	113.94211
2	-23	133.8	24				
3	-23.1	120.5	24				
4	-22.8	86.9	24				
5	-21.3	90.8	23				
6	-19.9	123.5	22				
7	-23.6	107	25				
8	-20.2	147.6	23				
9	-24.5	114.8	25				
10	-18.6	113.4	21				
11	-8.4	98.7	12				
12	-7.4	92.3	11				
13	-11.6	130.3	16				
14	-23.8	105.7	25				
15	-10.7	128	15				
16		128	-				
17		100.7	-				
18	-7.3	100.7	11				
19	-16.8	102.2	20				
Member T3, Taishir Fm, dolomite, N. Bayan Gorge							
U1115-81-1	-27.5	87.9	27	Dolomite	-6.56255	3.3497143	97.342105
2	-27.6	113.4	27				
3	-18.6	98.7	21				
4	-23.3	101.8	25				
5	-18.6	75.6	21				
6	-23.7	113.4	25				
7	-25.6	98.7	26				
8	-25.5	96.1	26				
9	-9.8	103.5	14				

10	-26.2	112.4	26				
11	-28.7	83	28				
12	-19.6		22				
13	-27.5	100.8	27				
14	-27.6	91.7	27				
15	-21.7	119	24				
16	-25.7	103.4	26				
17	-25.7	89	26				
18	-22.6	74.1	24				
19		96	-				
20	-23	91	24				
Member T3, Taishir Fm, dolomite, Ol Mountain							
U1111-65-1	-13.4		17	Dolomite	-10.25249	-2.272333	108.30588
2	-21.1	104.4	23				
3	-22.9	126.6	24				
4	-19	90.9	22				
5	-22.3	132.4	22				
6	-24.7	98.3	25				
7	-23	111.2	24				
8	-37.3	94.8	34				
9	-28	103.5	27				
10	-37.2	99.8	34				
11	-12.4	186.6	16				
12	-24.5	107.9	25				
13	-29	111.1	28				
14	-23.5	107.2	25				
15	-26	100.1	26				
16	-36.5	99.5	33				
17	-3.8	60.6	6				
18	-26.3	106.3	21				
Ol Fm cap dolostone, N. Bayan Gorge							
U1113-8.8-1	-23	88.6	22	Dolomite	-4.00703	-0.089	122.51667
2	-21	81.9	23				
3	-23.8	128.8	25				
4	-24.8	131.5	25				
5	-25.6	150.9	26				
6	-23	138.3	24				
7	-24	138.4	25				
8	-25.2	130.6	26				
9	-23.3	107	25				
10	-24.3	127	25				

11	-25.4	113.4	26				
12	-23.8	110.1	25				
13	-24.4	123.3	25				
14	-18.1	140.1	21				
15	-23.4	131.5	25				
16	-24.9	116.9	21				
17	-20.7	111.4	23				
18	-24.2	135.6	25				
Upper Ol Fm, dolomite, N. Bayan Gorge							
u1113-43	-31	189	29	Dolomite	-0.614518	2.7412857	141.45385
2	-26	210	26				
3	-23.8	128.8	25				
4	-24.8	131.5	25				
5	-25.6	150.9	26				
6	-23	138.3	24				
7	-24	138.4	25				
8	-25.2	130.6	26				
9	-23.3	122.8	25				
10	-24.3	115	25				
11	-25.4	150.2	26				
12	-23.8	110.1	25				
13	-24.4	123.3	25				
Ol Fm cap dolostone, Ol Mountain							
u1112-14.6	-18.1	140.1	21	Dolomite	-4.378565	-0.4718	119.31154
2	-23.4	131.5	25				
3	-24.9	116.9	26				
4	-20.7	111.4	23				
5	-24.2	135.6	25				
6	-24.2	140	25				
7	-27.2	149.35	27				
8	-26.6	158.7	27				
9	-22.1	74.4	24				
10	-23.6	68.7	25				
11	-22.7	86.9	24				
12	-24.3	109	25				
13		128.5					
Ol Fm cap dolostone, Taishir							
F860 (U1110)-5.5-1	-13.3	147.5	17	Dolomite	-5.903732	0.4566667	109.33889
2	-	128					
3	-23.3	120.2	25				
4		106.8					

5	-17.8	101.2	21				
6	-12.6	101.2	17				
7	-19.6	109.2	22				
8	-8.4	120.3	12				
9	-14.9	97.6	19				
10	-19.2	113.2	22				
11	-11.3	115.8	15				
12	-17.4	111.7	21				
13	-18.4	122.1	21				
14	-0.7	120.3	1				
15	-3.4	97.6	6				
16	-28	113.2	27				
17	-22.8	71.1	24				
18	-22.9	71.1	24				
Upper Ol Fm, dolomite, Ol Mountain							
U1112-36.5-1	-22.7	114.4	24	Dolomite	-2.39781	3.0597143	120.84211
2	-22.3	122.8	24				
3	-22.8		24				
4	-23.5	112.9	25				
5	-21.5	91.1	23				
6	-22.6	110.2	24				
7	-23.7	127.1	25				
8	-22.9	125.9	24				
9	-9	105.1	13				
10	-24.4	127.9	25				
11	-13.4	125.2	17				
12	-18.3	104.2	21				
13	-17.2	122.7	20				
14	-21.4	131.5	23				
15	-15.3	150.9	19				
16	-24	138.3	25				
17	-17.9	138.4	21				
18	-19.9	107	22				
19	-22.4	127	24				
20	-18.7	113.4	21				

Table 4.A4. Calculated Sr/Ca ratio of fluid responsible for dolomitization of the Taishir, Ol and Shuurgat formations.

	min	*max*	*Ave*		
	molar Sr/Ca fluid	molar Sr/Ca fluid	Sr (ppm)	D_{sr} min	D_{sr} max
Taishir Fm - U1115-17	0.0057	0.0014	74.71	0.015	0.06
Taishir Fm - U1111	0.0044	0.0011	57.32	0.015	0.06
Taishir Fm dolomite	0.0050	0.0013			
Ol cap dolostone F860	0.0141	0.0035	184.69	0.015	0.06
Ol Fm U1112	0.0033	0.0008	43.47	0.015	0.06
Ol Fm U1113	0.0057	0.0014	75.28	0.015	0.06
Ol Fm	0.0045	0.0011			
Shuurgat Fm	0.0086	0.0022	112.92	0.015	0.06

APPENDIX 4.2. SUPPLEMENT TO CHAPTER 4: FIGURE

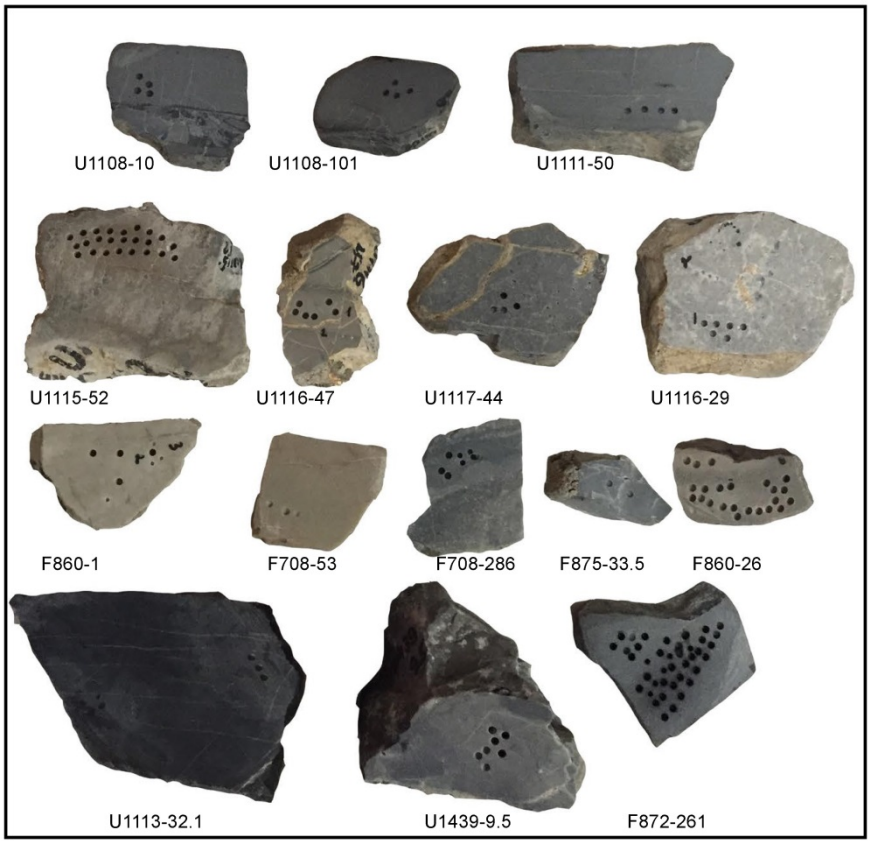

Figure 4.A1. Representative carbonate samples analyzed for clumped-isotope paleothermometry. Limestone: Taishir Fm - U1108-10, U1108-101, and U1111-50; Ol Fm – U1113-32.1 and F860-26; Shuurgat Fm – F872-261. Dolostone: Taishir Fm – U1115-52, U1116-47, U1117-44, and U1116-29; Ol Fm – F860-1, F875-33.5, and F708-53; Shuurgat Fm – F708-286 and U1439-9.5.